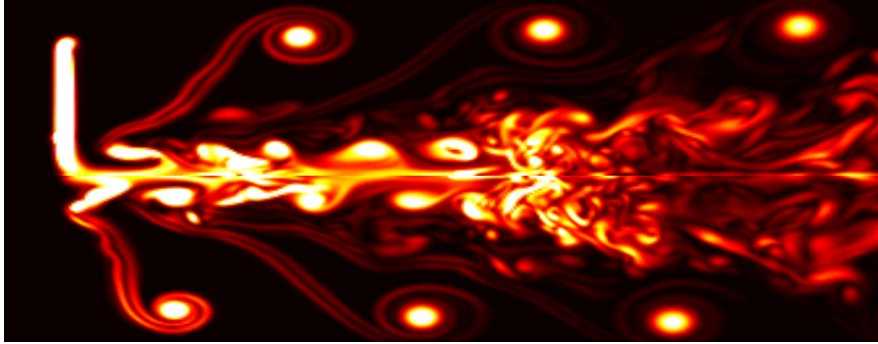
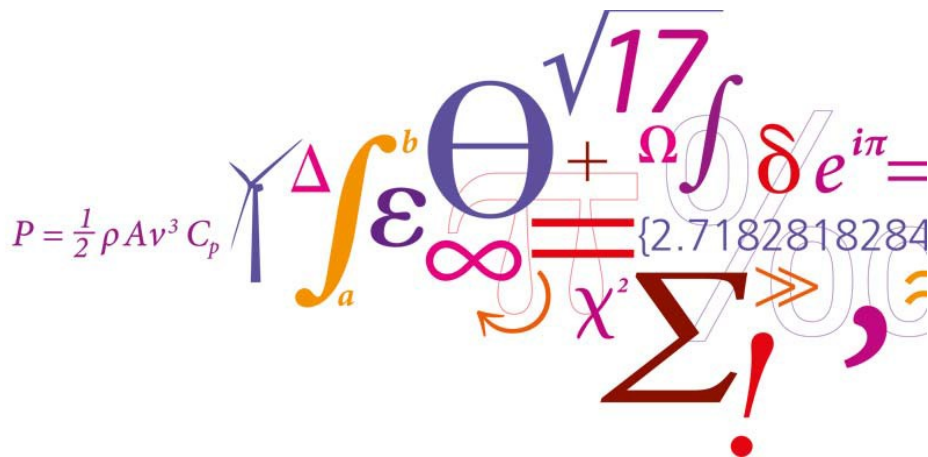


EFMC10 - DTU COPENHAGEN 2014



BOOK OF ABSTRACTS



EFMC10 – European Fluid Mechanics Conference 10
Technical University of Denmark, Lyngby
September 15th – 18th, 2014

Preface

The 10th European Fluid Mechanics Conference (EFMC10) is held at the Technical University of Denmark in Copenhagen (Lyngby) during September 14-18, 2014. This conference is the 10th in the series started in Cambridge in 1991 and continued in Warsaw (1994), Göttingen (1997), Eindhoven (2000), Toulouse (2003), Stockholm (2006), Manchester (2008), München (2010), and Rome (2012). The conference aims at covering the whole field of Fluid Dynamics, comprising from most fundamental aspects to recent applications. It provides a world-wide forum for scientists to meet each other and exchange information of all aspects of fluid mechanics, including instability, swirl flows, aerodynamics, transition, acoustics, turbulence, multi-phase flows, non-Newtonian flows, bio-fluid mechanics, reacting and compressible flows, as well as various applications.

This volume of abstracts comprises all presentations of the conference, including eight plenary lectures, and nearly 500 contributed papers, presented in either oral sessions or during five mini-symposia. The abstracts are sorted chronologically after the day of presentation, corresponding to the way they appear in the conference programme. At the end of the book you will find a list of presenting authors, listed alphabetically, and the page number where their abstract appear.

I like to thank the EFMC committee and the local organizing committee for their work with the evaluation and selection process. In particular, I thank Marianne Hjorthede Arbirk for her invaluable help in preparing the conference and this book of abstracts.

Jens N. Sørensen, chairman EFMC10

Euromech Fluid Mechanics Lecturer

Prosperetti, A.

Simulating particulate flows

Invited Lecturers

Nepf, H.

Vegetation Hydrodynamics at the Blade and Canopy Scale

Succi, S.

Lattice Boltzmann simulations of complex flows across scales of motion

Peinke, J.

Wind Energy and the Need to Understand Turbulence

Iaccarino, G.

Uncertainty Quantification in Flow Simulations - Challenges and Opportunities

Kjørboe, T.

The Fluid Mechanical Constraints of Planktonic Life in the Ocean

Snoeijer, J.

Soft Wetting: Liquid drops on elastic solids

Rieutord, M.

Recent progress and new challenges in Astrophysical Fluid Dynamics

Simulating particulate flows

Andrea Prosperetti^a

Situations in which particles are suspended in a fluid medium occur very frequently in Nature and technology. Examples include sediment transport, sand storms, fluidized beds, suspensions and many others. Problems of this type are usually treated on the basis of very simplified models of uncertain physical realism. Furthermore, some averaged equations models even suffer from mathematical pathologies. Progress requires a better understanding of the microphysics which, in turn, must be based on a detailed resolution of the fluid-particles interaction. Computationally this requirement is very difficult to meet as the particles represent a complex, time-dependent internal boundary for the fluid domain. The immersed boundary method has proven effective in dealing with the problem. A physics-based, related, but different, method - Physalis - is described in this talk and its capabilities illustrated with a variety of examples.

[Supported by NSF grant CBET 1258398]

^a Department of Mechanical Engineering, Johns Hopkins University, Baltimore USA & Department of Applied Science, University of Twente, Enschede, The Netherlands

Vegetation Hydrodynamics at the Blade and Canopy Scale

H.M. Nepf^a and J.T. Rominger^b

The presence of coral, seagrass, kelp and other macrophytes influences the velocity field across several scales, ranging from individual elements, such as branches, blades, and polyps, to the community of elements, called the canopy or meadow. In the first part of this talk, I will discuss plant-flow interaction at the blade-scale, which is relevant to the uptake of nutrients and the blade-scale drag. In the second part of this talk, I will describe flow at the canopy scale, focusing on the obstructed shear-layer that forms at the top of a meadow and how its structure dictates the flow and transport within the canopy.

At the blade-scale, we consider how changes in blade flexural rigidity impact both the drag on the blade and the mass flux to the blade surface. Many species of kelp change their blade morphology in response to the local flow environment. In regions of high current and waves the blades increase their thickness and develop corrugations running parallel to the long axis of the blade. These morphological changes increase the blade's rigidity and thus change its response to flow. In this first case study, model blades are constructed from sheets of high- and low-density polyethylene and placed in flume. A lateral bar is used to produce a von Karman vortex street. The vortex street provides a single scale of periodic turbulence that enables simpler interpretation of the blade motion. The blades are mounted on a load sensor to record drag in the streamwise direction. Mass flux to the blades is measured by dosing the flume with dibromochloromethane, exposing the blades for specific durations of time, and measuring the mass accumulation within the blade through chemical analyses. Finally, the blade motion is recorded and analyzed using digital video. The study considers six different blades of different thickness that represent a six decade variation in blade flexural rigidity. As the blade rigidity increases, the blade motion in response to the passing vortices decreases, the mean and peak instantaneous drag decreases, and the mass flux to the blade decreases.

At the canopy-scale, we consider how canopy-generated turbulence impacts transport and sediment resuspension. The drag-discontinuity at the top of a submerged canopy creates a shear layer, which in turn generates coherent vortices that control exchange between the vegetation and the overflowing open water. Unlike free-shear-layers, the vortices in this obstructed-shear-layer do not grow continuously downstream, but reach and maintain a finite scale determined by a balance between shear-production and canopy dissipation. This balance defines the length-scale of vortex penetration into the canopy, δ_e , which is inversely related to the stem density. Over this length-scale vertical turbulent transport strongly influences the canopy flow dynamics. Deeper within canopy, however, the turbulence scales are constrained and flow is diminished. The penetration length-scale defines two possible flow regimes. Consider a submerged canopy of height h . In sparse canopies, $\delta_e/h = 1$ and the shear-layer turbulence penetrates through the entire canopy down to the bed. Turbulence within the canopy is elevated, relative to adjacent bare-bed conditions, promoting resuspension of material within the bed. In dense canopies, $\delta_e/h < 1$ and the shear-layer turbulence does not penetrate through the entire canopy, so that the near-bed conditions have diminished mean and turbulent velocities, relative to adjacent bare-bed, which promotes sediment deposition and retention. Using a few cases studies, we show how the ratio δ_e/h , which can be predicted from canopy morphology, predicts shifts in resuspension and deposition observed in real and model systems.

^a Dep. Civil and Environmental Engineering, MIT, 77 Massachusetts Ave., Cambridge, MA, USA

^b Dep. Civil and Environmental Engineering, MIT, 77 Massachusetts Ave., Cambridge, MA, USA

Lattice Boltzmann simulations of complex flows across scales of motion

Sauro Succi,
IAC-CNR, Rome, Italy and IACS Harvard, Cambridge USA,

May 4, 2014

Abstract

In the last two decades, the Lattice Boltzmann (LB) method has attracted major interest as an efficient computational scheme for the numerical simulation of complex fluid problems across a broad range of scales, from fully-developed turbulence in complex geometries, to multiphase microflows, all the way down to biopolymer translocation in nanopores and lately relativistic flows in quark-gluon plasmas.. In this talk, after a brief introduction to the main ideas behind the LB method, we shall illustrate recent applications to fluid turbulence, multi-scale hemodynamics, soft-glass rheology and, as time allows, shock propagation in quark-gluon plasmas. Future developments and major challenges ahead will also be briefly touched upon.

Wind Energy and the Need to Understand Turbulence

Joachim Peinke

Wind energy has become one of the cheapest energy sources that can be used for our human energy demand. Thus more and more wind turbines are installed preferably in regions with high wind speeds and so they are operating under highly turbulent working conditions. Wind turbines can be considered as the largest turbulence machines we construct nowadays. For the design of wind turbines several aspects of the features of the turbulent wind conditions are taken into account. In this contribution we will discuss how far this standard wind characterization is sufficient. We will discuss which aspects of the advanced understanding of turbulence are relevant for the wind energy conversion process and where we see new challenging research topics related to turbulence and wind energy.

Uncertainty Quantification in Flow Simulations

Challenges and Opportunities

Gianluca Iaccarino & Michael Emory

Mechanical Engineering, Stanford University

Computational fluid dynamics (CFD) is widely used in a range of engineering applications. Despite its ability to produce comprehensive and detailed information, a rigorous characterization of the prediction accuracy is typically difficult and often limited by the availability of physical measurements. Even for cases in which experimental data are available a meaningful assessment of the simulation quality might be affected by inconsistencies in the operating scenario, the boundary conditions, or the geometrical configuration, or imprecise measurements. In general, these differences are sources of uncertainties but should not affect the intrinsic quality of CFD simulations; on the other hand, they can lead to large discrepancies if not accounted for in the comparisons between measurements and predictions. If all the uncertainties in the measurements can be identified and estimated, they can be effectively propagated in CFD simulations (typically within a probabilistic framework) and properly quantified leading to a fair, albeit statistical, validation assessment. Unfortunately the uncertainties described above, are not the only ones potentially reducing the prediction abilities of CFD simulations, especially in the context of turbulent flows. RANS closures typically used in industry introduce uncertainty into simulations because of assumptions and intrinsic limitations in general related to the form of the model itself. To date there is no well-established framework to quantify the effect of this further uncertainty on the resulting predictions. In the last few years we have introduced a novel approach to construct uncertainty estimates related to RANS models borrowing ideas from error estimates in numerical analysis. The driving principle is that, in general terms, it might be easier to define bounds for a quantity instead of characterizing it precisely: bounds can be based on theoretical reasoning or fundamental properties and can be defined even without a detailed knowledge of the underlying physical process. In the present context, we start by identifying the basic hypotheses used in the model formulation and to construct local sensors based on computable quantities to track their validity: in the absence of violations the computations can be considered valid and free from model-form uncertainties. On the other hand, the identification of flow conditions not consistent with the initial assumptions must trigger the injection of uncertainty. These will negatively affect the confidence in the end results. The presentation will illustrate the basic ideas and the analysis tools we developed: specifically the concept of eigenvalue perturbations and error markers. The proposed approach provides also insight into the importance of modeling assumption and how simple closures can actually be modified to increase their accuracy. The present methodology has been applied to a variety of problems, from simple turbulent flow in channels and ducts, to more complex physical situations involving flow separation and shock/boundary layer interactions, but also to extremely complex three-dimensional simulations of high-speed combustion chambers.

THE FLUID MECHANICAL CONSTRAINTS OF PLANKTONIC LIFE IN THE OCEAN

Thomas Kiørboe, Centre for Ocean Life, DTU Aqua

Marine zooplankton, sub-mm-sized, blind organisms, swim and feed in a nutritionally dilute and viscous environment. To get enough food they have daily to collect microscopic phytoplankton particles from a volume of sticky water that corresponds to about 10^6 times their own body volume. And when swimming and feeding they generate far extending fluid disturbances that attract their predators. I will describe how these small organisms manage the fundamental dilemma of simultaneously being predator and a prey in a low Re fluid environment that is fundamentally different from the environment in which we live. I will show high-speed videos of their feeding and swimming, visualize the flow they generate using PIV, describe how they can swim in ways that minimize the fluid disturbance that they generate, and present simple analytical as well as CFD models that we use to understand how these small organisms optimize the tradeoffs associated with feeding and swimming.

Soft Wetting: Liquid drops on elastic solids

Jacco Snoeijer^a

The wetting of a liquid on a solid usually assumes the substrate to be perfectly rigid. However, this is no longer appropriate when the substrate is very soft: capillary forces can induce substantial elastic deformations, as has been demonstrated e.g. for drops on elastomers. In this talk we discuss the fundamentals of elasto-capillary interactions. Experiments,¹ theory² and simulations³ reveal the surprising nature of capillary forces, which turn out to be different from anything proposed in the literature. This is due to the “Shuttleworth effect”: while for liquid interfaces the surface free energy is equivalent to the surface stress, this is no longer the case when one of the phases is elastic.⁴ A remarkable consequence is that the elastic displacements below a droplet (Fig. 1a) differ from those below a bubble (Fig. 1b), even for a 90 degrees contact angle.³ We work out droplet shapes on very soft substrates⁵ and establish how the contact angle differs from Young's law owing to elastic effects.

^a Physics of Fluids Group, Faculty of Science and Technology, University of Twente, 7500 AE Enschede, The Netherlands & Department of Applied Physics, Eindhoven University of Technology, PO Box 513, 5600 MB Eindhoven, The Netherlands

¹ A. Marchand, S. Das, J.H. Snoeijer and B. Andreotti, *Phys. Rev. Lett.* **108**, 094301 (2012).

² A. Marchand, S. Das, J.H. Snoeijer and B. Andreotti, *Phys. Rev. Lett.* **109**, 236101 (2012).

³ J.H. Weijs, B. Andreotti and J.H. Snoeijer, *Soft Matter* **9**, 8494 (2013).

⁴ R. Shuttleworth, *Proc. Phys. Soc., London Sect. A*, “The surface tension of solids”, **63**, 444-457 (1950).

⁵ L.A. Lubbers, J.H. Weijs, L. Botto, S. Das, B. Andreotti and J.H. Snoeijer, *J. Fluid Mech.* **747**, R1 (2014)

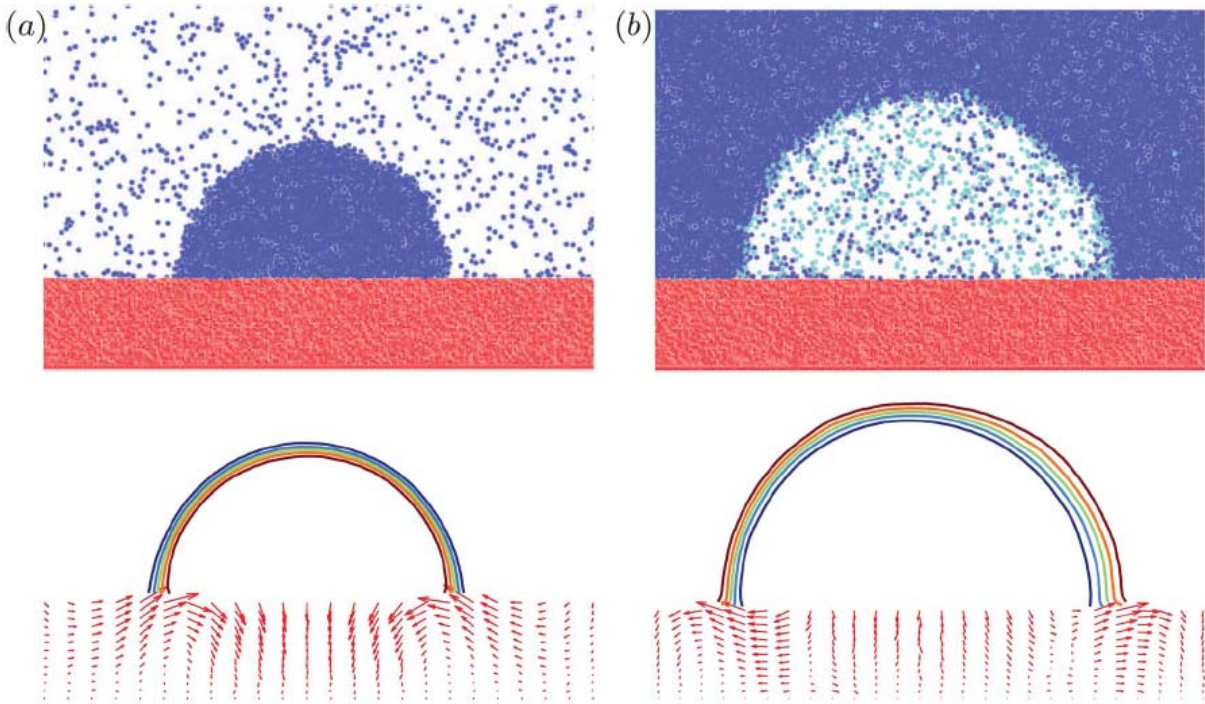


Figure 1: Molecular dynamics simulations of a drop (a) and a bubble (b) on a deformable substrate, both with a contact angle of 90 degrees. Top: snapshot, blue particles are liquid atoms, red particles are solid atoms, cyan particles are gas atoms. Bottom: local displacement (red arrows) of the solid due to the presence of the drop/bubble (shown by liquid isodensity contours). Note that the tangential displacement near the contact line is different from both situations: in the drop case the solid is pulled inwards whereas in the bubble case the solid is pulled outwards.

Recent progress and new challenges in Astrophysical Fluid Dynamics

Michel Rieutord

Astrophysical objects like giant planets, stars, accretion discs, interstellar clouds, galaxies or clusters of galaxies are the scenes of a large variety of fluid flows that control the dynamics of these objects.

Even though these objects are extreme by their size and physical nature, the fluids that are to be dealt with are no more different than the usual newtonian fluids, except that they are often ionized gases and thus conductors of electricity. As a consequence, magnetic fields are important and the dynamics is governed by magnetohydrodynamics equations. But the extreme size of the object implies extreme values in the nondimensional numbers that characterize the flows. For instance, typical Reynolds numbers in the Sun easily reach 10^{12} . It is therefore expected (and observed!) that turbulence plays a central part in most of the astrophysical fluid dynamics problems. Turbulence hindered much of the progress of the field until computers have been able to simulate, not unrealistically, typical astrophysical situations, a step that has been accomplished in the last decade.

In this lecture, I shall review some of the acute problems that astrophysicists are facing as far as fluid dynamics is concerned. I'll therefore present the challenges that are faced when one wishes to understand the formation of stars in a gravitationally collapsing interstellar cloud or the fall of matter into a gravitational well (a young star, a white dwarf, a black hole...) through the so-called accretion discs. I'll also discuss the challenges that our Sun prompts to us either as a star or as the object controlling the space weather that affects the close environment of the Earth. Wandering among the stars, I'll review the recent progresses that have been made about the role of rotation on the internal baroclinic flows and on the eigenmodes that are observed but yet unidentified. Finally, I'll end this lecture with a short review of the recent progresses made in the simulation of one of the most violent event in the Universe, namely the explosion of a supernovae, underlining the fluid dynamics problems that have to be challenged.

M O N D A Y

15th September 2014

Mini Symposia: Cellular Flows

Flagellar locomotion: A mechanical optimum

Christophe Eloy^a, Eric Lauga^b

From algae to vertebrates, numerous eukaryotic cells use flagella or cilia to produce flows or self-propel. The structure of these organelles, called the axoneme, is generally made of nine peripheral doublet microtubules whose relative sliding produces bending (Fig. 1a). Although this internal structure has been highly conserved throughout evolution, the reason of this particular arrangement has so far proven elusive. Another open problem is the following: given the mechanical properties of the axoneme, what is the optimal flagellar waveform among all possible shapes? Here, these questions are examined from a mechanical perspective.

To address the optimal number of doublet microtubules in the axoneme, we suppose that this optimum results from a balance between two opposite effects: a too small number of microtubules yields energetic losses because the structure cannot fully align with arbitrary bending directions; and conversely, a too large number tends to increase the energy needed to produce flow by increasing the organelle radius. With these arguments, it is found that the optimal number of doublet microtubules is nine, in agreement with experimental observations.

The question of the optimal flagellar beat pattern is addressed by computing the optimal shape of an infinite flagellum deforming as a travelling wave. The optimal shape is here the waveform leading to a prescribed swimming speed with minimum energetic cost, which is itself calculated by considering the irreversible internal power expended by the internal motors bending the flagellum. It is important to note that only a portion of this power ends up dissipated in the fluid, the rest being dissipated internally because of the irreversibility of the molecular motors producing bending moments. This optimisation approach allows us to derive a family of shapes depending on a single dimensionless number quantifying the relative importance of elastic to viscous effects: the Sperm number (Fig. 1c). The computed optimal shapes are found to agree with the waveforms observed on spermatozoon of marine organisms¹ (Fig. 1b).

These studies suggest that the structure of the axoneme and the observed flagellar beat pattern are consistent with selection of the lowest energetic costs.

^a Aix Marseille University, CNRS, Centrale Marseille, IRPHE, 13384 Marseille, France

^b DAMTP, University of Cambridge, Centre for Mathematical Sciences, Cambridge CB3 0WA, UK

¹ Lauga and Eloy, *J. Fluid Mech.* **730**, R1 (2013)

² Brennen and Winet, *Ann. Rev. Fluid Mech.* **9**, 339 (1977)

³ Brokaw, *J. Exp. Biol.* **43**, 155 (1965)

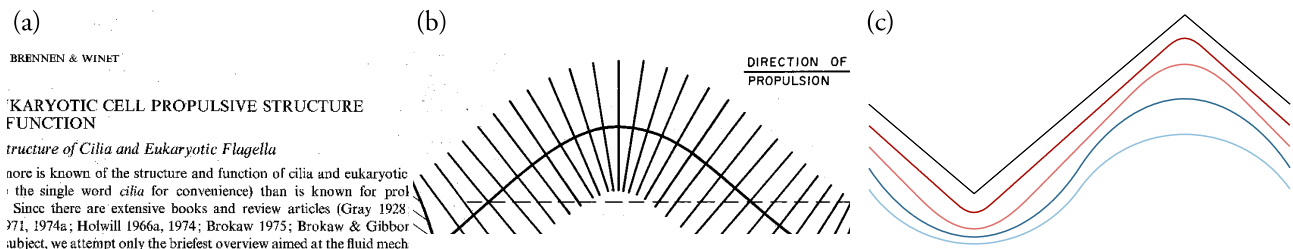


Figure 1: (a) Axoneme structure². (b) Stroboscopic photographs of a swimming tunicate spermatozoon³. (c) Optimal shapes of an infinite flagellum for different rigidities¹ (most flexible at the top).

Characterization of Intracellular Streaming Flows and Traction Forces in Migrating *Physarum Plasmodia*

Shun Zhang^a, Ruedi Meili^{a,b}, Robert D. Guy^c, Juan C. Lasheras^{a,d}, Juan C. del Álamo^a

Physarum plasmodium is a large ($\sim 200\ \mu\text{m}$) amoeba that is used as model organism for microscopic soft adhesive locomotion. It moves by periodically contracting its body, leading to strong traction stresses at the interface between its ventral surface and the substrate, as well as fast intracellular streaming. The aim of this study was to experimentally characterize the relation between traction stresses and intracellular streaming flows, in order to better understand amoeboid cell migration and to enable the design of soft biomimetic robots.

To this end, single plasmodia allowed to move on polyacrylamide gels of known linear elastic properties containing fluorescent microspheres. Joint time-lapse sequences of intracellular streaming and gel deformation were acquired respectively in the bright and fluorescent fields of an inverted microscope at high time resolution. These image sequences were analyzed using particle image velocimetry to determine intracellular flow speed and the deformation of the underlying gel. The traction stresses applied by the plasmodium were computed by solving the elastostatic equation for the gel using the measured gel deformation as boundary conditions¹.

The results reveal a remarkable temporal periodicity in intracellular flow, contact area, cell speed and traction stresses ($T \sim 60\ \text{s}$). Different modes of locomotion were found and characterized in terms of the spatiotemporal coordination of these quantities. In the most prevalent mode, traction stress waves of strength $\sim 100\ \text{Pa}$ propagated from the tail to the cell front in each cycle. The traction stresses were spatially distributed at the cell boundaries, suggesting that they are generated by the contraction of the cell's outer shell (Fig. 1). During these contraction waves, backward streaming flow was observed (Fig. 1a) while forward flow occurred during the relaxation phase of the waves (Fig. 1b). These measurements provide, for the first time, a joint characterization of intracellular mass transport and the forces applied on the substrate of motile amoeboid cells.

^a Mechanical and Aerospace Engineering Department, University of California San Diego, La Jolla, CA

^b Cell and Developmental Biology, University of California San Diego, La Jolla, CA

^c Math Department, University of California Davis, Davis, CA.

^d Bioengineering Department, University of California San Diego, La Jolla, CA

¹ Del Alamo et al, *Proc. Nat. Acad. Sci.* **104**(33) 13343-13348.

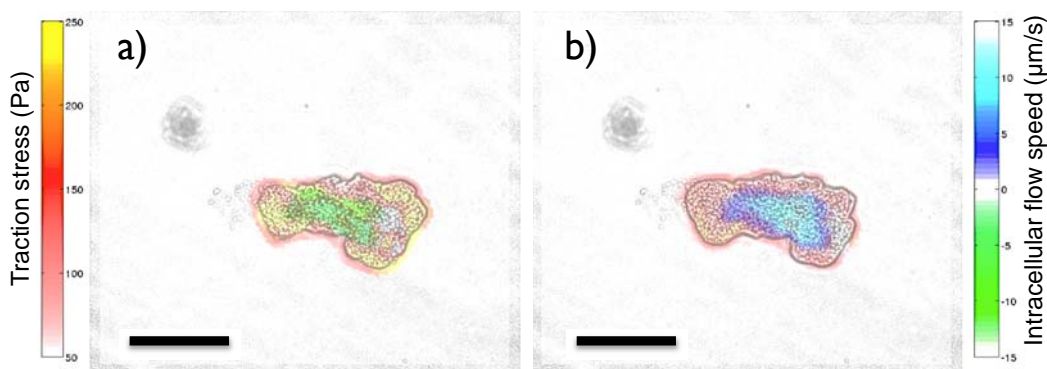


Figure 1. Traction stresses (hot colormap) and intracellular flow speeds (cold colormap with blue indicating forward and green indicating backward) in a *physarum* plasmodium during contraction (a) and relaxation (b).

Flagellar synchronisation through direct hydrodynamic interactions

Douglas Brumley¹, Kirsty Wan², Marco Polin³ and Raymond Goldstein²

Microscale fluid flows generated by ensembles of beating eukaryotic flagella are crucial to fundamental processes such as development, motility and sensing. Despite significant experimental and theoretical progress, the underlying physical mechanisms behind this striking coordination remain unclear. We describe a novel series of experiments in which the flagellar dynamics of two micropipette-held somatic cells of *Volvox carteri*, with measurably different intrinsic beating frequencies, are studied by high-speed imaging as a function of their mutual separation and orientation (Fig. 1a). From analysis of beating time series, we find that the interflagellar coupling, which is constrained by the lack of chemical and mechanical connections between the cells to be purely hydrodynamical, exhibits a spatial dependence that is consistent with theoretical predictions. At close spacings it produces robust synchrony which can prevail for thousands of flagellar beats, while at increasing separations this synchrony is systematically degraded by stochastic processes. Manipulation of the relative cell orientation reveals the existence of both in-phase and antiphase synchronised states, consistent with dynamical theories. Through dynamic flagellar tracking with exquisite precision, we quantify the associated waveforms and show that they are significantly different in the synchronised state (Fig. 1b,c). This study unequivocally reveals that flagella coupled only through a fluid medium are capable of exhibiting robust synchrony despite significant differences in their intrinsic properties.

¹ Department of Civil and Environmental Engineering, MIT, 77 Massachusetts Ave., Cambridge, MA, USA

² DAMTP, University of Cambridge, Wilberforce road., Cambridge, UK

³ Department of Physics, University of Warwick, Gibbet Hill road., Coventry, UK

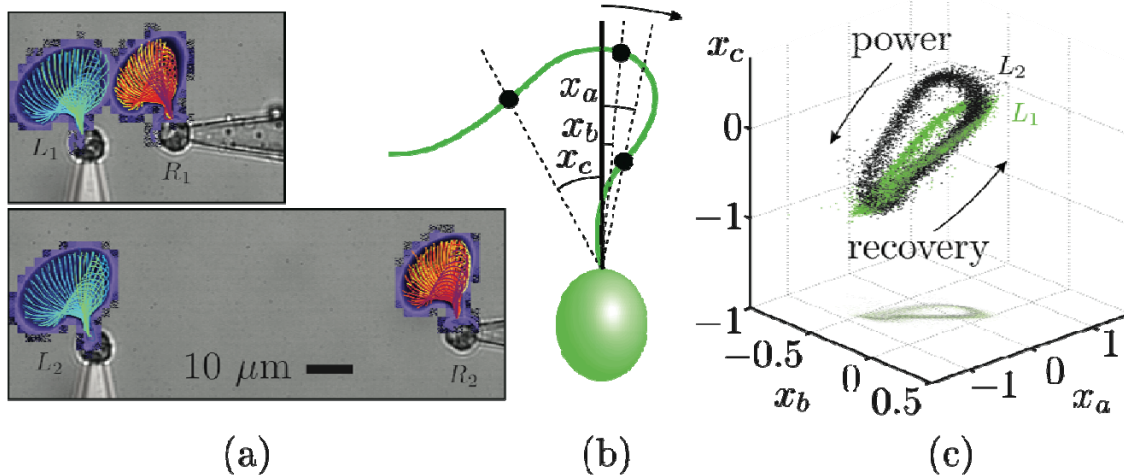


Figure 1: Flagellar waveform changes as two cells are brought to close proximity. (a) Logarithmically-scaled residence time plots of the entire flagella. The tracked waveforms correspond to 1 ms time intervals over 3 successive flagellar beats. (b) Angles x_a , x_b , x_c (in radians) measured and (c) their characteristic 3D trajectories over 8000 frames. Results are shown for the left cell in the closely (green) and widely (black) separated regimes..

Active Gel Model of Contractility-based Cell Polarization and Shape Change

A. Callan-Jones^a and R. Voituriez^{b,c}

Cell polarization, migration, and shape change are required for large-scale movements during embryo development and cancer metastasis. We present theoretical work based on experiments using zebrafish embryos during gastrulation as a model system to understand cell polarization and migration during early development¹. Experimentally, there is now evidence of a novel polarization and migration phenotype for cells within the gastrula that is dependent on cortical acto-myosin contractility. This polarized state is also obtained in cells in-vitro through up-regulation of myosin II activity, in which initially quasi-spherical, immobile cells undergo a cortical instability to a polarized state. The polarized cell is characterized by a high cortical density at the cell rear, persistent cortical actin flows, and a distinctive pear-shape morphology. Using active gel theory², we are able to account for these three signatures of the polarized state. Firstly, a contractile instability of the initially uniform acto-myosin cortex occurs beyond a threshold myosin activity, leading to density inhomogeneities. Secondly, persistent cortical flows in the nonlinear steady state occur as a result of cortical tension, friction between the cortex and its surroundings, and filament turnover. Finally, cortical tension in the polarized cell results in stresses on the cell bulk, treated here as linearly elastic cytoplasm, leading to deformation. Using a weakly nonlinear analysis, we find that, generically, coupling between the two first cortical modes leads to cortical tension anisotropy, favoring cell deformation consistent with the shapes observed experimentally.

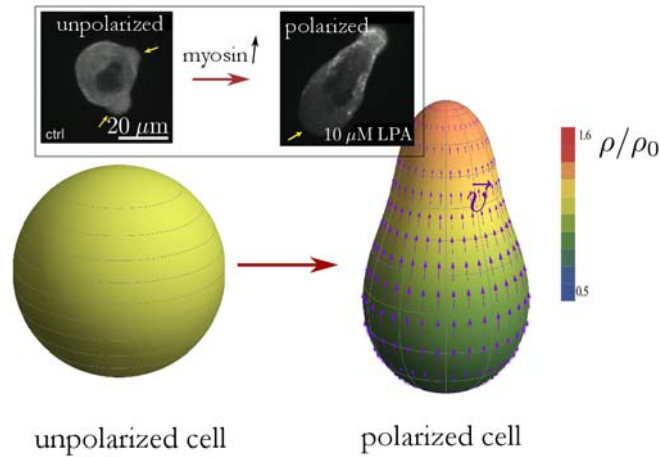


Figure 1: Contractility-driven cell polarization. Experimentally (inset), myosin up-regulation by lysophosphatidic acid (LPA) causes cortical instability and polarization. These features are captured by our model, which predicts cortical flow (\mathbf{V}), density gradients (ρ), and shape change.

^a Laboratoire Matière et Systèmes Complexes, CNRS/Université Paris-Diderot, UMR 7057, 75205 Paris Cedex 13, France

^b Laboratoire Jean Perrin, CNRS Fédération Recherche en Évolution 3231, Université Pierre et Marie Curie, 75005 Paris, France

^c Laboratoire de Physique Théorique de la Matière Condensée, CNRS UMR 7600, Université Pierre et Marie Curie, 75005 Paris, France

¹ Ruprecht et al., "Increasing cortical contractility triggers the emergence of a novel amoeboid migration mode in zebrafish embryonic progenitor cells" (in preparation)

² Kruse et al., *Eur. Phys. J. E* **16**, 5 (2005)

Cytoplasm Rheology and Its Role Cellular Blebbing Dynamics

Robert D. Guy¹, Wanda Strychalski², Calina A. Copos^a

Blebbing occurs when the cytoskeleton detaches from the cell membrane, resulting in the pressure-driven flow of cytosol towards the area of detachment and the local expansion of the cell membrane. Recent experiments involving blebbing cells have led to conflicting hypotheses regarding the time scale of intracellular pressure propagation. The interpretation of one set of experiments supports a poroelastic cytoplasmic model which leads to slow pressure equilibration when compared to the time scale of bleb expansion¹. A different study concludes that pressure equilibrates faster than the timescale of bleb expansion². To address this, we develop a dynamic computational model of the cell that includes mechanics of and the interactions between the intracellular fluid, the actin cortex, the cell membrane, and the cytoskeleton. Results show the relative importance of cytoskeletal elasticity and drag in bleb expansion dynamics. We also show that relatively fast pressure equilibration as a result of cytoskeletal poroelasticity combined with dynamic membrane-cortex adhesion explain recent experiment results.

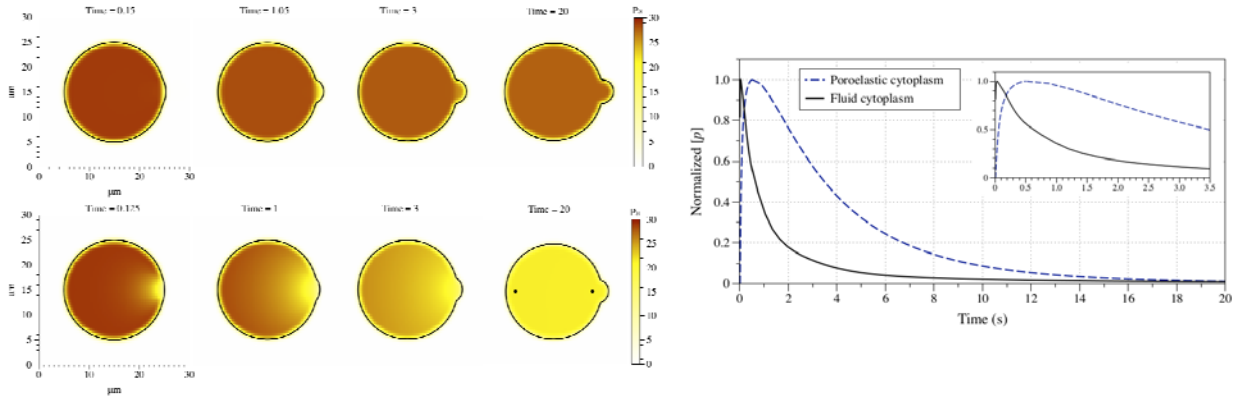


Figure 1: Left: Membrane position and pressure in the bleb model at several time values for both the fluid cytoplasm (top) and poroelastic cytoplasm (bottom). Right: Pressure difference across the cell as a function of time.

¹ Dep. Mathematics, University of California Davis, Davis, CA 95616, USA

² Dep. Mathematics, Case Western Reserve University, Cleveland OH 44106, USA

¹ Charras et al., *Nature*, 435, **365** (2005).

² Tinevez et al., *Proc. Natl. Acad. Sci. USA* **106**, 18581 (2009).

Elasticity on the edge of stability: controlling the mechanics of intra/extracellular networks

F. C. MacKintosh^a

Much like the bones in our bodies, the *cytoskeleton* consisting of filamentous proteins largely determines the mechanical response and stability of cells. Unlike passive materials, however, living cells are kept far out of equilibrium by metabolic processes and energy-consuming molecular motors that generate forces to drive the machinery behind various cellular processes. Inspired by such networks, we describe recent advances in our theoretical understanding of fiber networks, as well as experiments on reconstituted *in vitro* acto-myosin networks and living cells. We show that these exhibit a unique state of highly responsive matter near the isostatic point first studied by Maxwell^{1,2}. We show how such internal force generation by motors can control the mechanics and organization of networks, and even switch floppy or fluid-like and solid-like states^{3,4}. We also show how internal force generation in cellular networks can give rise to diffusive-like motion^{5,6}.

^a Dep. Physics and Astronomy, FEW, VU University, De Boelelaan 1081, 1081HV Amsterdam, THE NETHERLANDS

¹ Maxwell, *Philos Mag*, **27**, 294 (1864).

² Broedersz et al, *Nat Phys*, **7**, 983 (2011).

³ Sheinman et al, *Phys Rev Lett*, **109**, 238101 (2012).

⁴ Alvarado et al., *Nat Phys*, **9**, 591 (2013).

⁵ Brangwynne et al., *J Cell Biol* **183**, 583 (2008).

⁶ MacKintosh and Schmidt, *Curr Op in Cell Biol* **22**, 29 (2010).

Blood Cells in Microfluidic Flows

D.A. Fedosov^a and G. Gompper^a

The flow behavior of vesicles and blood cells is important in many applications in biology and medicine. For example, the flow properties of blood in micro-vessels are determined by the rheological properties of red blood cells (RBCs). Blood flow is therefore strongly affected by diseases such as malaria or diabetes, where RBC deformability is strongly reduced. Furthermore, microfluidic devices have been developed recently, which allow the manipulation of small amounts of suspensions of particles or cells.

Of fundamental interest is here the relation between the flow behavior and the elasticity and deformability of the blood cells, their long-range hydrodynamic interactions in microchannels, and thermal membrane undulations¹. We study these mechanisms by combination of particle-based mesoscale simulation techniques for the fluid hydrodynamics with triangulated-surface models^{1,2} for the membrane. The essential control parameters are the volume fraction of RBCs (tube hematocrit), the flow velocity, and the capillary radius.

In narrow channels, single red blood cells in capillary flow show a transition from the biconcave disk shape at low flow velocities to a parachute shape at high flow velocities^{1,3}. For somewhat wider channels, other shapes such as slippers intervene between these states⁴. At higher volume fractions, hydrodynamic interactions are responsible for a strong deformation-mediated clustering tendency at low hematocrits, as well as several distinct flow phases at higher hematocrits, such as a zig-zag arrangement of slipper shapes³. For large vessels, blood behaves like a continuum fluid, which displays a strong shear-thinning behavior; our simulations show quantitatively how this behavior arises due to RBC deformability and cell-cell attraction⁵.

The dynamics of RBCs has also a very strong influence on other particles and cells flowing in microvessels. For example, RBCs at sufficiently high hematocrit and flow rate lead to a margination of white blood cells (WBC), i.e., a motion to the vessel wall^{6,7}. See below for an illustration^b. This behaviour is closely related to the hydrodynamic lift force, which pushes non-spherical, tank-treading cells away from a wall; this causes RBCs to move to the capillary center, thereby pushing WBCs and other near-spherical cells to the wall. This process is important for WBC adhesion to the vascular endothelium, e.g. in inflammation.

^a Institute of Complex Systems and Institute for Advanced Simulation, Forschungszentrum Jülich, 52425 Jülich, Germany

¹ Fedosov, Noguchi, Gompper. *Biomech. Model. Mechanobiol.*, advance online publication (2013). DOI: 10.1007/s10237-013-0497-9.

² Gompper and Kroll. In *Statistical Mechanics of Membranes and Surfaces*, 2nd edition, edited by Nelson, Piran and Weinberg (World Scientific, Singapore, 2004).

³ McWhirter, Noguchi, and Gompper. *Proc. Natl. Acad. Sci. USA* **106**, 6039 (2009).

⁴ Fedosov, Peltomäki, and Gompper. *Soft Matter*, submitted (2014).

⁵ Fedosov, et al., *Proc. Natl. Acad. Sci. USA* **108**, 11772 (2011).

⁶ Fedosov, Fornleitner, and Gompper. *Phys. Rev. Lett.* **108**, 028104 (2012).

⁷ Fedosov and Gompper. *Soft Matter*, advance online publication (2014). DOI: 10.1039/C3SM52860J.

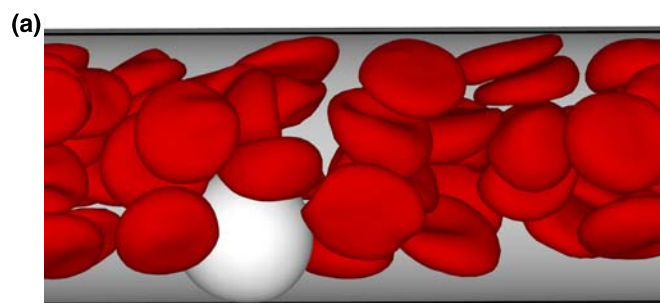


Figure 1: (a) Snapshot of the margination of a white blood cell in microchannel flow at hematocrit $H_T=0.3$.

A hydrodynamic instability in tumor formation

T. Risler^a, M. Basan^{ab}, J.-F. Joanny^{ac} and J. Prost^a

Most tumors originate from epithelia, which are under constant cell renewal. The interface between the epithelium and the connective tissue often presents different degrees of undulation, which are typically more pronounced in pre-malignant and malignant tissues where more layers of dividing cells are present. On long timescales, cellular rearrangements lead to a fluid-like behavior of the tissue^{de}. We propose that the observed undulations may originate from a mechanical instability due to differential cell flows in the epithelium^{fg}. The tissue properties that favor this instability match known characteristics of cancerous tissues. When coupled to the reaction-diffusion equation of metabolites brought by blood vessels located in the connective tissue, the instability of the cellular flow in the epithelium tissue is enhanced via a mechanism reminiscent of the Mullins-Sekerka instability in single-diffusion processes of crystal growth^g.

^a Laboratoire Physicochimie Curie, Institut Curie UMR 168 (UPMC Univ Paris 06, CNRS), 26 rue d'Ulm, F-75005, Paris, France

^b ETH Zürich, Institute of Molecular Systems Biology, Zürich, Switzerland

^c ESPCI ParisTech, F-75005, Paris, France

^d Basan et al., *HFSP J.* **3**, 265 (2009)

^e Ranft et al., *PNAS* **49**, 20863 (2010)

^f Basan et al., *Phys. Rev. Lett.* **106**, 158101 (2011)

^g Risler and Basan, *New J. Phys.*, **15**, 065011 (2013)

Mini Symposia:
Particle-laden turbulent flows

Dispersion of particles from localized sources in turbulence

R. Scatamacchia^{a,b}, L. Biferale^b, A. S. Lanotte^c and F. Toschi^{a,d,e}

We present a detailed investigation of particles relative separation in homogeneous isotropic turbulence. We use data from a 3D direct numerical simulations with 1024^3 collocation points and $Re_\lambda=300$ following the evolution of a large number of passive tracers and heavy inertial particles, with Stokes numbers in the range $St \in [0.5, 5]$. Many studies^{1,2,3} have focused on the subject, including extensions to the case of particles with inertia⁴. In particular, our simulation aims to investigate extreme events characterizing the distribution of relative dispersion in turbulent flows. To do that, we seed the flow with hundred millions of particles emitted from localized sources in time and in space. Thanks to such huge statistics, we are able, for the first time, to assess in a quantitative way deviations from Richardson's prediction for tracers. Furthermore, we present the same kind of measures for heavy particles to understand how the inertia affects the pair separation statistics. We also show that the intermittent corrections to the Richardson prediction are well reproduced by a multifractal prediction for the scaling behaviours of relative separation moments of tracer pairs. Finally, to disentangle the effects of different turbulent scales, we present measurements based on the exit time statistics for tracer particles.

^a Dep. of Physics, Eindhoven Univ. of Technology, 5600 MB, Eindhoven, The Netherlands.

^b Dep. of Physics and INFN, Univ. of Tor Vergata, Via della ricerca scientifica 1, 00133, Rome, Italy.

^c CNR-ISAC and INFN, Str. Prov Lecce-Monteroni, 73100, Lecce, Italy.

^d Dep. of Mathematics and Computer Science, Eindhoven Univ. of Technology, 5600 MB, Eindhoven, The Netherlands.

^e CNR-IAC, Via dei Taurini 19, 00185, Rome, Italy.

¹ L. Biferale et al., *Phys. Fluids* **17**, 115101 (2005).

² F. Nicolleau and J. C. Vassilicos., *Phys. Rev. Lett.* **90**, 024503 (2003)

³ N. Ouellette et al., *New J. Phys.* **8**, 109 (2006).

⁴ J. Bec et al., *J. Fluid Mech.* **645**, 497 (2010)

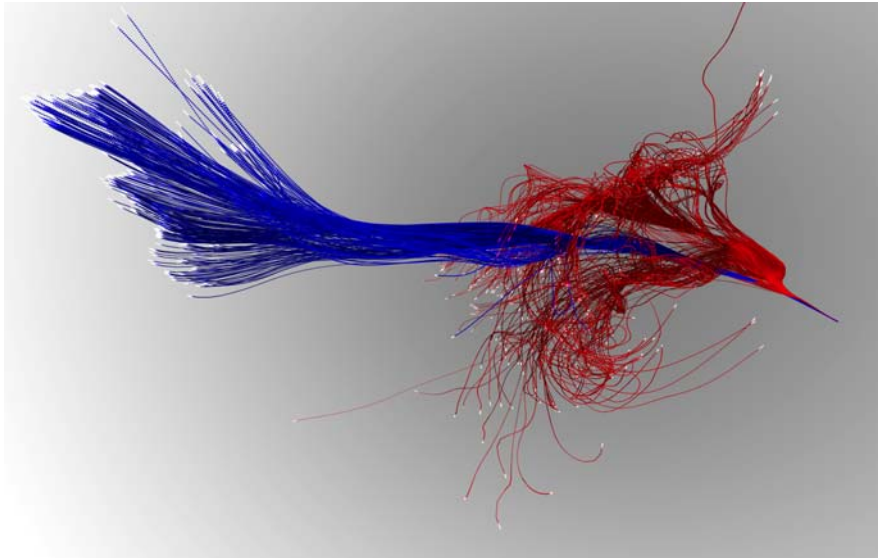


Figure 1: An ensemble of particles with $St = 0$ (red) and heavy particles with $St = 5$ (blue) simultaneously emitted from a source of size comparable to the Kolmogorov scale, η . Trajectories are recorded from the emission time, up to time $t = 75\tau_\eta$ after the emission.

Making droplets glow in turbulence: preferential concentration

H. Bocanegra Evans^a, W. van de Water^a, and N.J. Dam^b

A cloud of monodisperse droplets (with Stokes number of order 1) is churned by homogeneous isotropic turbulence. The turbulent flow is stirred by 8 loudspeaker-driven synthetic jets inside a turbulent cloud chamber with sides 0.4 m. The Taylor Reynolds number is large, $\text{Re}_\lambda \cong 450$. The droplets are made of a phosphorescent Europium solution, and are made to glow after illumination with a strong UV laser (Nd:YAG at 355nm). The concentration of glowing droplets is tracked in time using a fast (500 Hz) intensified camera.

By using a planar laser sheet, we prepare an initial distribution as a thin (1 mm thick) sheet. The evolution of the density field inside this sheet is followed during a few Kolmogorov times. Because of the droplets' inertia, this density $n(\mathbf{x}, t)$ makes a compressible field with moments $n^m(\mathbf{x}, t)$, $m > 1$ increasing in time. This is indeed verified by the experimental results shown in the Figure. The choice of the experimental parameters, namely Stokes numbers of order one, and the focus on the shortest turbulence times and the smallest turbulence length scales, is such that the effects of preferential concentration are strongest.

Selectively tagging droplets and making them glow makes a unique diagnostic for the dynamical behaviour of droplets in turbulence. Other observations concern the dynamics of clusters, and the dispersion of tiny tagged clouds of droplets.

^a Dep. Applied Physics, Eindhoven University of Technology, Eindhoven, The Netherlands

^b Dep. Mechanical Engineering, Eindhoven University of Technology, Eindhoven, The Netherlands

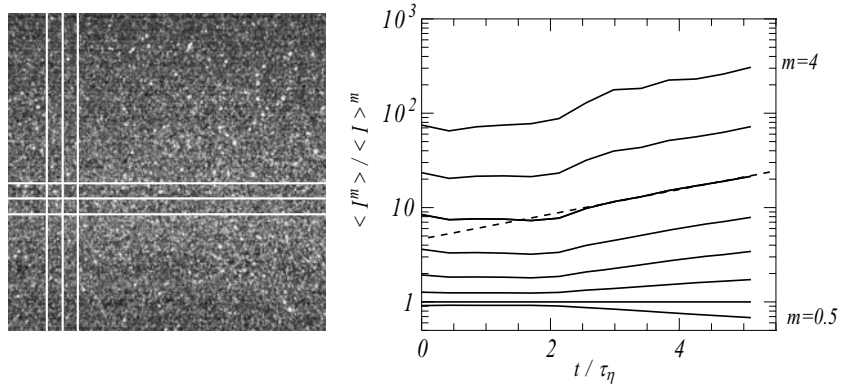


Figure: Left: droplet concentration field inside a tagged sheet of droplets. We compute the moments of the concentration summed in small boxes with size 6.4η , with η the Kolmogorov length. Right: moments $n^m(\mathbf{x}, t)$ increase exponentially with time for $m > 1$.

Super-clustering of inertial particles in turbulent flow

M. Bourgoïn^a, M. Obligado^b

The tendency of inertial particles to clusterize is one of the most remarkable properties of turbulence-particles interactions. Possible clustering mechanisms rely on preferential concentration effects, where particles preferentially sample specific structures of the carrier turbulent field (for instance, heavy particles are centrifugated out from turbulent eddies, while light particles move toward the center of the eddies). The main parameter controlling the clustering efficiency is the particle Stokes number St (ratio of particle viscous relaxation time τ_p to the turbulent dissipation time τ_η , $St = \tau_p / \tau_\eta$). In the present work, we propose an experimental study, where a new approach for the reconstruction of the concentration field of water droplets dispersed in active-grid generated turbulence, allows to investigate clustering properties at scales much larger than previously available data. This new method shows that particles not only form clusters, but that clusters themselves tend to assemble in super-clusters.

Our experiment runs in a low speed windtunnel where turbulence is generated downstream an active-grid. An array of injectors seeds the flow with small water droplets (50 μ m in diameter typically). When varying the mean velocity of the wind, we change the Reynolds number of the flow (between 230 and 400, based on Taylor micro-scale) as well as its dissipation time-scale τ_η , what results in a variation of particles Stokes number between 2 and 10. Particles are visualized using a high-speed camera in a laser sheet parallel to the mean flow. In a previous work we have shown that a Voronoi tessellation analysis of the recorded images reveals a significant level of droplets clustering¹ (much intense than what was previously reported in experiments at lower Reynolds numbers for the same range of Stokes numbers²). Here, we propose a new analysis of this data, based on a “linear camera” reconstruction combined to a Taylor hypothesis (common in wind-tunnel experiments). This allows us to reconstruct the particle concentration field over wide range of scales (from dissipative to metric scales), as shown in figure 1. Using the Voronoi tessellation analysis we first identify clusters of particles. We then iterate the Voronoi analysis to investigate the clustering properties of the center of mass of the identified clusters. Our results show the clear tendency of clusters to form super-clusters with typical dimensions within inertial range scales. Trends of super-clustering with Stokes and Reynolds numbers will be discussed.

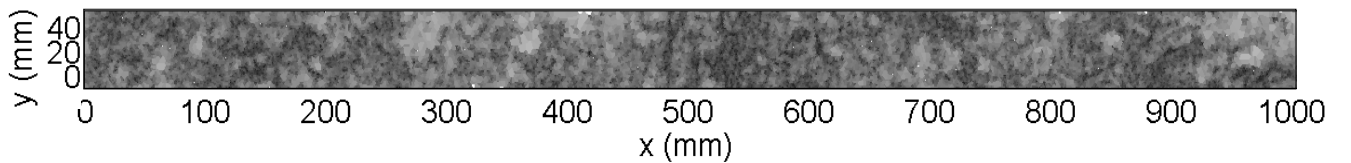


Figure 1: Reconstruction of a one-meter long particles concentration field, covering more than five times the integral scale of the carrier flow. The image shows Voronoi cells, colour coded according to their areas (small darker cells indicate high local concentration).

^a LEGI/CNRS, University of Grenoble, BP53, 38041 Grenoble Cedex 9, France

^b Dep. of Aeronautics, Imperial College London, London SW7 2AZ, United Kingdom

¹ M. Obligado *et al.*, *J. Physics : Conference Series* **312**, 052015 (2011).

² R. Monchaux *et al.*, *Phys. Fluids* **22**, 103304 (2010)

Particles in homogeneous shear turbulence

M. A. T. van Hinsberg^a, H.J.H. Clercx^a and F. Toschi^a

Turbulent flows occur in various industrial and natural phenomena. In many of these cases, turbulent fluctuations are coupled to a large-scale flow. Homogeneous shear turbulence is the first step in understanding how the mean flow influences turbulent fluctuations. The flow is homogeneous but anisotropic. To highlight the difference between homogeneous-isotropic and homogeneous-shear turbulence, in Figure 1 we show the dispersion of particles from a line source. It is clear that the presence of shear introduces an additional dispersion mechanism in the system. More strikingly, a recent study¹ has shown that for inertial particles anisotropic behaviour occurs even at scales where the carrier flow is already isotropic. Thus to understand particle dynamics, the influence of both the small and the large scales of turbulence must be investigated.

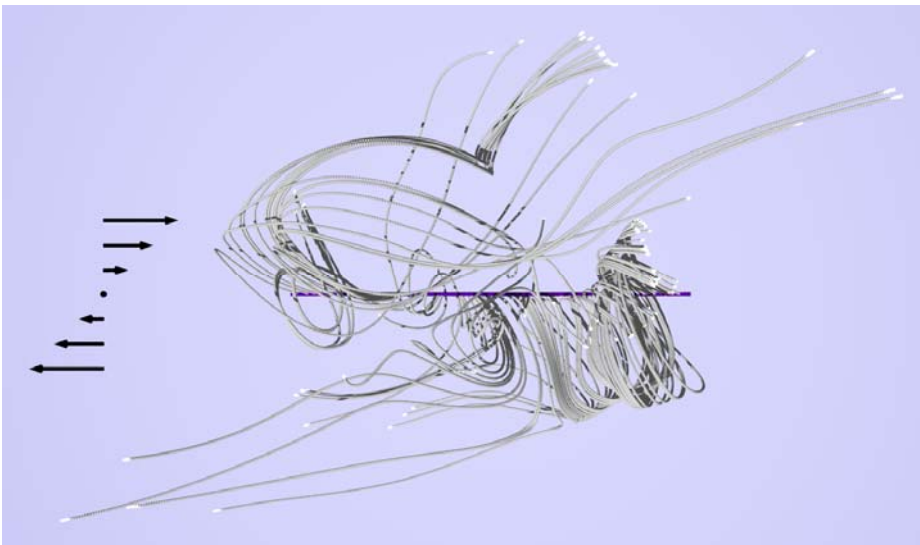


Figure 1: Trajectories of tracers in a homogeneous shear flow. All tracers started from the purple line and the mean flow is shown on the right hand side.

We examine the dynamics of the system by an Eulerian-Lagrangian model. The flow is simulated by an Eulerian approach using a pseudospectral code. We employ the classic Rogallo scheme to numerically integrate homogeneous shear turbulence². Here, the frame of reference moves with the mean flow. The particles are simulated by a Lagrangian approach using the Maxey-Riley equations. For the heavy particles we use a simplified version of the equations consisting of the Stokes drag and the gravity force. For the almost neutral buoyant particles we use the full equations.

We started with investigating the settling velocity. For homogeneous isotropic turbulence it is well known that the settling velocity can increase due to the presence of turbulence. We are interested in how shear will affect this behaviour and what the consequences are for real life applications. First results show interesting new phenomena. When the shear is directed like in Figure 1 and gravity is directed in the positive horizontal direction a vertical drift velocity of the particles is measured in downward direction.

^a Dep. of Physics, Eindhoven University of Technology, 5600MB, The Netherlands

¹ Gualtieri et al., *J. Fluid Mech* **629**, 25 (2009)

² Rogallo. *NASA report*, (1981)

Turbulent channel flow laden with finite-size particles at high volume fractions

F. Picano^{a,c}, W.-P. Breugem^b and L. Brandt^c

Suspensions are found in several processes and applications, e.g. sediment transport in the environment and pharmaceutical engineering. The laminar regime in the semi-dilute or dense regimes, non-vanishing volume fraction, is usually characterized by peculiar rheological properties induced by the suspended phase, such as shear-thickening and jamming. Much less is known about dissipation and mixing in the turbulent regime.

The main aim of the present work is to investigate the turbulent channel flow of a Newtonian fluid laden with neutrally-buoyant rigid spherical particles at fixed bulk Reynolds number $Re = U_0 h/\nu = 2800$ with U_0 the bulk velocity, h the half channel height and ν the fluid kinematic viscosity. The particle radius is selected to be 18 times smaller than the channel half-width, h . Fully-resolved Direct Numerical Simulations with particle tracking and coupling by the Immersed Boundary Method^{1,2} are presented for values of the volume fraction up to $\Phi = 0.2$; Fig 1a) displays an instantaneous snapshot of the densest case. The mean velocity profiles in inner units $U^+ = U/u^*$ vs the wall normal distance $y^+ = y/(\nu/u^*)$ are shown in the right panel of figure 1, where u^* is the friction velocity. The higher the particle concentration the higher is the overall drag as shown by the decrease of the mean velocity profiles in inner units when increasing Φ . For the lowest volume fraction here considered, $\Phi = 0.05$, the particles do not significantly alter the shape of the mean profile though the overall drag is increased. Further increasing the volume fraction Φ , the mean velocity profile deeply changes. In particular, the buffer layer disappears and the log-layer region, though still present, shows increasing slopes. The interaction between a fluctuating shear-rate field and the particle dynamics in dense regimes^{2,3} may lead to these strong modifications. We will show that, although the overall drag increases at the higher particle volume fractions, the turbulent activity and the corresponding turbulent induced drag is reduced by the presence of particles.

A complete analysis of the fluid and particle statistics revealing the mutual interactions between fluid and solid phases will be presented at the conference.

^a Industrial Engineering Dep., University of Padova, Padova, Italy

^b Laboratory for Aero & Hydrodynamics, TU-Delft, Delft, The Netherlands

^c Linné FLOW Centre and SeRC, KTH Mechanics, Stockholm, Sweden

¹ Breugem, *J. Comp Phys.* **231**, 4469 (2012).

² Picano et al., *Phys. Rev. Lett.* **111**, 098302 (2013)

³ Guazzelli & Morris, *Cambr. Univ. Press* (2011)

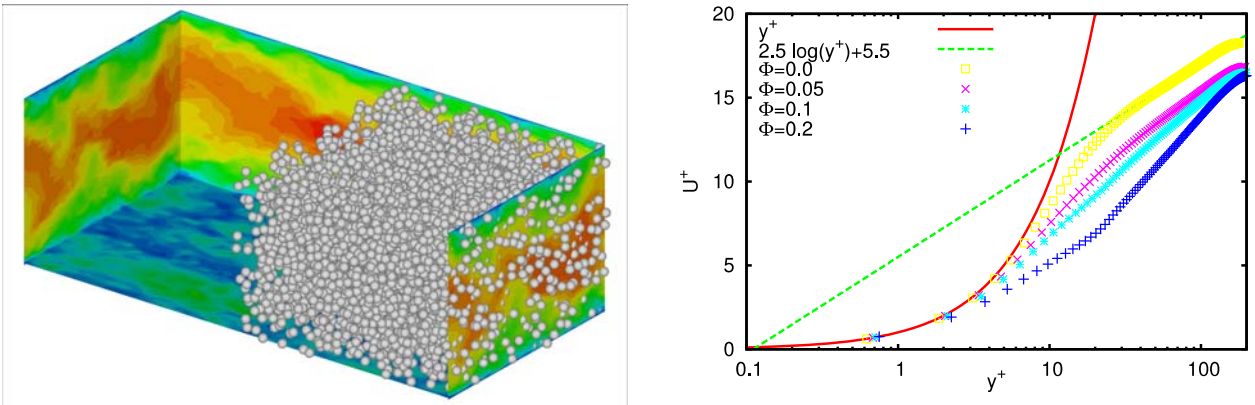


Figure 1: Left: streamwise velocity contours and rigid particle displayed on one half of the domain at volume fraction $\Phi = 0.2$. (b) Mean velocity profiles vs the wall normal direction in inner units for different Φ .

Inertial Particles in Turbulent Curved Pipe Flow

A. Noorani^a, G. Sardina^b, L. Brandt^a and P. Schlatter^a

Turbulent flow in bent geometries, such as pipes, is frequently occurring in a variety of engineering but also biological situations. The curvature leads to an imbalance of the pressure gradient and centrifugal forces which creates a secondary flow inside a cross-stream plane. Depending on the value of the curvature κ , usually defined as the ratio of the pipe diameter and the diameter of the curve, straight, mildly and strongly bent pipes can be distinguished. The strength of the secondary flow can be as strong as 10% of the axial velocity, and has been denoted as Prandtl's skew-induced secondary flow of first kind. Both numerical as well as experimental studies of bent pipes are quite rare, in particular compared to the canonical case of a straight pipe. Recently, we have investigated the changes occurring for the turbulence statistics at a moderate Reynolds numbers for three curvature values.¹ It is interesting to understand the non-trivial behaviour of the in-plane velocity in the statistically steady state, see Fig. 1 (left). A pair of clear Dean vortices can be observed, however squeezed towards the side wall, together with a nearly laminar region close to the lower stagnation point.

Given the importance, but also the flow complexity of the present geometry, it is our goal to study the behaviour of Lagrangian particles released in such a bent pipe. For that purpose, we extended our chosen numerical method, the code Nek5000,² with a module to treat point particles subject to Stokes drag and elastic wall collisions. We simulate turbulence in bent pipes at $Re_b=12000$ (corresponding to $Re_\tau=360$), together with 7 populations of particles with Stokes numbers St^+ (based on inner units) ranging from 0 to 100. We study both the transient development of the particle distribution, but focus on the final statistically steady state.

As expected, the particles are heavily influenced by the secondary motion; the heaviest particles turn out to be excellent markers for the Dean vortices. Instantaneous snapshots are shown in Fig. 1 for straight, mild and strong curvature, with particles at $St^+=50$. A typical particle trajectory is now helicoidal, i.e. the particle moves along the sidewalls down towards the lower stagnation point. Once there, the particle is ejected from the wall region, and rises up towards the outer stagnation point passing through the pipe centre. A number of interesting observations can be made; first, the turbophoresis, i.e. the tendency of particles to remain close to the wall, is in competition with both centrifugal and Dean acceleration forces; this leads to a clear modification of the accumulation patterns in the near-wall region. Further, the intense particle-wall collision at the outer stagnation point leads to a clearly visible reflection layer. Finally, depending on the curvature, there are regions in the flow which are essentially void of particles. This inhomogeneity is in particular important when considering mixing, or concentrate measurements in chemical systems. The final contribution will concentrate on a complete description of the particle dispersion in bent pipes, both from an instantaneous and statistical point of view.

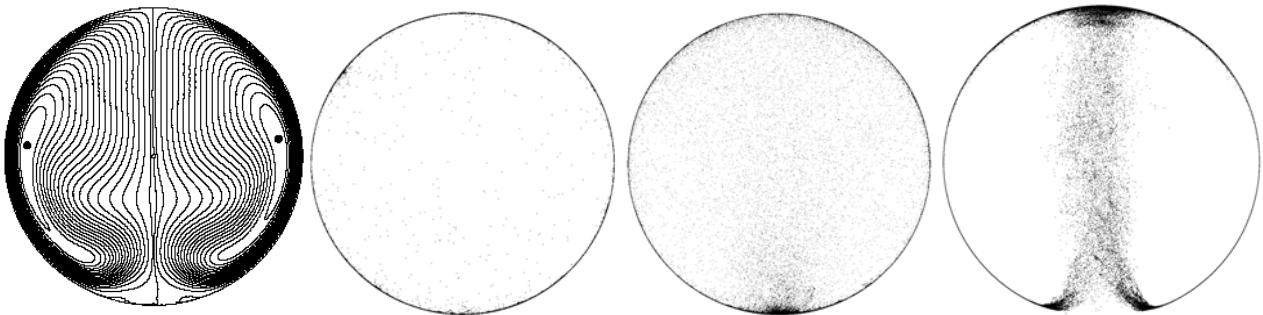


Figure 1: (Left) Stream function for strongly curved pipe. Instantaneous particle locations in fully developed turbulent pipe flow in curved pipes: (From left to right) straight pipe $\kappa=0$, mild curvature $\kappa=0.01$, strong curvature $\kappa=0.1$.

^a Swedish e-Science Research Centre (SeRC) and Linné FLOW Centre, KTH Mechanics, SE-100 44 Stockholm, Sweden.

^b Department of Meteorology, Stockholm University, SE-106 91 Stockholm, Sweden.

¹ Noorani et al., *Int. J. Heat Fluid Flow* **41**, 16-26 (2013).

² Fischer et al., <http://nek5000.mcs.anl.gov>.

Lattice Boltzmann simulations of turbulent fibre suspensions in a channel

M. Do-Quang¹, G. Brethouwer^a, G. Amberg^a and A.V. Johansson^a

Direct numerical simulations of a suspension of rigid finite-size fibres or rods in turbulent plane channel flow at $Re_\tau=180$ have been performed using the lattice Boltzmann method. The interactions between the fibres and fluid as well as the fibre-fibre and fibre-wall interactions are all accounted for and the simulations have been thoroughly validated. We have considered heavy and almost neutrally bouyant fibres, like cellulose fibres in water, with a diameter of 1.6 and lengths from 3.2 to 36 in terms of viscous wall units. The longest fibres considered are thus of the same order as the smaller near-wall turbulent structures and the thickness of the buffer layer.

Figure 1 shows a visualization of an instantaneous flow field with the turbulent structures and fibres. The Lattice Boltzmann simulations showed that near the wall nearly neutrally bouyant fibres tend to accumulate in high-speed turbulent streaks¹. As a result, the fibres have a higher mean velocity than the fluid near the wall. This accumulation is stronger for long fibres and caused by interactions between the solid channel wall and the rigid fibres. Fibres close to the wall have on average a different orientation and motion than the ones further away from the wall. The fibres, especially the longer ones, do affect the turbulence in the channel, but at the relatively low fibre volume fractions considered this does not lead yet to a change in the mean flow drag. Simulations with heavier fibres as well as with higher fibre volume fractions when the fibres reduce the flow drag are ongoing and the results will be presented.

We conclude that the lattice Boltzmann method is a versatile method to investigate turbulent suspensions of finite-size particles and that our results for finite-size fibres differ essentially from previous simulation results for infinitely small elongated particles².

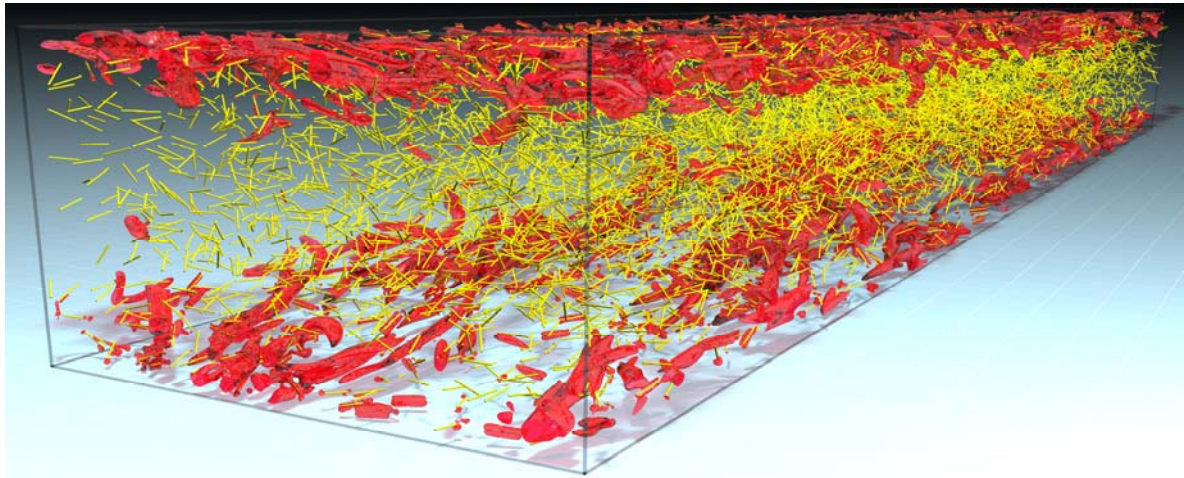


Figure 1: Visualization of the fibres (yellow) and turbulent vortices (red) in an instantaneous velocity field of a lattice Boltzmann channel flow simulation.

¹ Linné FLOW Centre, KTH Mechanics, SE-100 44 Stockholm, Sweden

¹ Do-Quang et al., *Phys. Rev. E*, **89**, 013006 (2014).

² Marchioli et al., *Phys. Fluids* **22**, 033301 (2010).

Transition to turbulence in the presence of finite size particles

L. Brandt^a, I. Lashgari^a, F. Picano^b, and W.-P. Breugem^c

We study the process of transition from the laminar to the turbulent regime in a channel flow suspended with finite-size neutrally buoyant particles via numerical simulations. A fixed ratio of 1/10 between the particle diameter and channel height is considered. The study is conducted in the range of Reynolds numbers $500 \leq Re \leq 5000$ (defined using the bulk velocity and the channel half width) and particle volume fractions $0.001 \leq \phi \leq 0.3$ (see visualization in the figure below).

The simulations reported are performed using the Immersed Boundary solver with second order spatial accuracy developed by Breugem¹. The code couples the uniform Eulerian fixed mesh for the fluid phase with a uniform Lagrangian mesh for the solid phase. The Lagrangian mesh is used to represent the moving surface of the particles in the fluid. Lubrication forces and soft-sphere collision models have been implemented to address the near field interactions (below one grid cell), see also Ref. 2.

We find a non-monotonic behaviour of the critical conditions for transition when increasing the volume fraction as in previous experiments³.

To quantify the behaviour of the flow in different regimes we examine the perturbation kinetic energy budget once the mean quantities are statistically converged. The volume-averaged fluctuation kinetic energy is depicted versus Reynolds number for different volume fractions in the figure, right panel.

For low volume fractions, $\phi \leq 0.05$, the transition threshold is evident through a sharp jump of the average kinetic energy. Interestingly, the critical Reynolds number for the onset of turbulence is decreasing when increasing the particle volume fraction.

For $0.05 \leq \phi \leq 0.3$, the level of the fluctuations increases already at low Reynolds number and the transition becomes smoother. For $\phi=0.3$, it is indeed difficult to identify a transitional Reynolds number and the perturbation kinetic energy only slightly increases with the flow inertia. In this case the level of fluctuations does not reach the one of the single-phase turbulent flows even at high Reynolds numbers. At the same time, we record an increase of the wall friction and a decrease of the turbulent Reynolds stresses. This can be explained by an additional dissipation mechanism at high volume fractions, not connected to classic turbulence. The wall friction increases with the Reynolds number (inertial effects) while the turbulent transport is unaffected, as in a state of intense inertial shear-thickening.

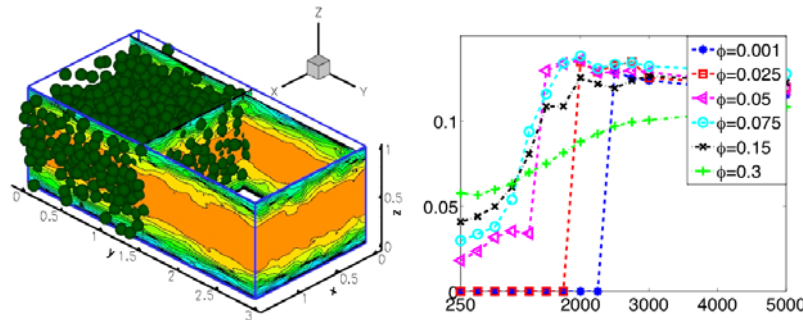


Figure 1. Left: Instantaneous flow field from the simulation with $Re=2500$ and $\phi=0.3$. The rigid particles are displayed only on one half of the domain. Right: Average kinetic energy in the domain versus the Reynolds number for different volume fractions (See legend).

^a Linné FLOW Centre and SeRC, KTH Mechanics, Stockholm, Sweden

^b Industrial Engineering Dep., University of Padova, Padova, Italy

^c Laboratory for Aero & Hydrodynamics, TU-Delft, Delft, The Netherlands

¹ Breugem, *J. Comp Phys.* **231**, 4469 (2012).

² Picano et al., *Phys. Rev. Lett.* **111**, 098302 (2013)

³ Matas et al., *Phys. Rev. Lett.* **90**, 014501 (2003)

Particles settling in a cellular flow field at low Stokes number

D. Lopez^a, L. Bergougnoux^a, G. Bouchet^a and E. Guazzelli^a

The transport of particles in a turbulent environment is relevant to many industrial and natural processes. Very often, the sedimentation of particles is a dominant phenomenon, which is important to understand in a fundamental way. Examples include fluidized-bed reactors, the treatment of waste materials in clarifiers, the transport of sediment in rivers and estuaries, pyroclastic flows from volcanic eruptions, and bioconvection of planktons. Based on the model proposed by Gatignol¹ and Maxey & Riley², multiple numerical studies have been performed on the sedimentation of particles in vortical flows, generally modelled by Taylor-Green vortices. In the model, particle motion is driven by different contributions whose intensity depends on various parameters, in particular the Stokes number, scaling the particle response time with respect to the timescale of the background flow. Yet, the competition between these different terms has never been addressed experimentally.

We present a jointed experimental and numerical study examining the influence of vortical structures on the settling of solid particles under the action of gravity at low Stokes numbers. The two-dimensional model experiment uses electro-convection to generate a two-dimensional array of controlled vortices, which mimics a simplified vortical flow³. At very low Reynolds number, the generated flow is accurately modelled by Taylor-Green vortices. As the Reynolds number increases, the vortices deform but remain stationary in the range of interest. Using Particle Image Velocimetry and Particle Tracking, we determine the motion of settling particles within this vortical flow.

We investigate the role of inertia on the settling rate as well as trajectories, for small spherical particles and slender rods. In the latter, drag anisotropy yields chaotic motion even at negligible inertia. The experimental results (see Figure 1) will then be compared to the theoretical model, testing the influence of the different forces acting on the particle motion.

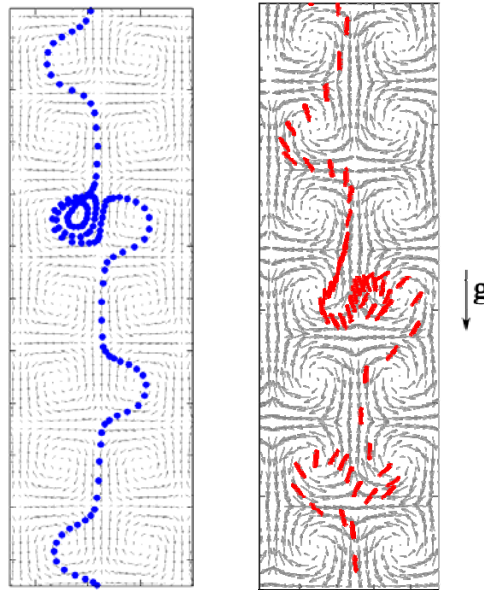


Figure 1: (a) Rigid sphere and (b) rigid fibre settling in a vortical flow.

^a Aix Marseille Université, CNRS, IUSTI UMR 7343, 13013 Marseille, France

¹ R. Gatignol, "The Faxen formulae for a rigid particle in an unsteady non-uniform Stokes flow," J. Méca. Théo. Appli. 2, 143 (1983).

² M. R. Maxey and J. J. Riley, "Equation of Motion for a Small Rigid Sphere in a Nonuniform Flow," Phys. Fluids 26, 883 (1983).

³ L. Rossi, J. C. Vassilicos and Y. Hardalupas, "Electromagnetically controlled multi-scale flows," J. Fluid Mech. 558, 207-242 (2006).

Geophysical

Predicting Nocturnal Boundary Layer Regimes: An Observational Study

I.G.S. van Hooijdonk^a, 3rd Author^a, F.C. Bosveld^b, A.F. Moene^c, H.J.H. Clerx^a and B.J.H. van de Wiel^a

Field observations and theoretical analysis are used to investigate the appearance of different nocturnal boundary layer regimes. Recent theoretical findings predict the appearance of two different regimes: The continuously turbulent (weakly stable) boundary layer and the 'quiet' (very stable) boundary layer. A large number of nights (approx. 4500 in total) are analysed using an ensemble averaging technique. From this it appears that indeed two fundamentally different regimes exist: Weakly stable (turbulent) nights rapidly reach a steady state (within 2-3 hours). In contrast, very stable nights reach a steady state much later after a transition period (2-6 hours). During this period turbulence is weak and non-stationary. A new parameter is introduced that appears to separate the regimes clearly. This parameter does not only facilitate a regime division but also opens up opportunities for a theoretical description of the very stable regime.

^a Fluid Dynamics Laboratory, Eindhoven University of Technology, Den Dolech 2, Eindhoven, Netherlands

^b Royal Netherlands Meteorological Institute, De Bilt, 3730 AE, Netherlands

^c Meteorology and Air Quality Group, Wageningen University, Wageningen, 6701 AP, Netherlands

Global stability of internal wave

G.Lerisson¹, J-M.Chomaz

Internal gravity waves are important in the ocean, they transfer energy to turbulence contributing to the deep ocean mixing and so influencing the thermohaline circulation. Gravity waves are generated by different mechanisms, interaction of currents or tides with topography, or coupling with waves at the thermocline. Plane internal wave of small amplitude are known to be unstable through triadic resonance¹, leading at small scale to the so-called parametric subharmonic instability (PSI). Larger amplitude wave have also been shown to be unstable using linear Floquet analysis². The subharmonic instability has been observed experimentally³ and its nonlinear evolution studied numerically⁴ showing that PSI indeed leads to turbulence. Very recently⁵ a novel camshaft wave generator was used producing a finite size propagating internal wave in a still fluid and observed the appearance of a global instability that they identify being due to the triadic instability. Amazingly Sutherland⁶ generates a wave of similar extend, amplitude, Reynolds and Froude numbers towing a rigid sinusoidal topography and observed no instabilities. In the present work we set a numerical simulation that, by varying both the mean advection velocity and the frequency imposed at the upper wall by a penalization method allows us to compute the stability of a family of flow where the frequency in the fluid frame stay constant for all simulation. When the mean velocity is null the simulation reproduces the tidal flow and the result of Bourget et al. are recovered whereas when the forcing frequency is zero the simulation corresponds to the lee wave flow of a sinusoidal mountain. We show that the global stability properties of these different flows differ strongly with the mean advection. All the flows have the same lateral confinement of the primary beam and correspond to the same unstable wave in the middle of the beam but the flows are globally unstable for small value of the mean advection in the tidal régime (fig1.c) but globally stable for intermediate values of the advection (fig1.b) and become again unstable for large values of the advection velocity in the lee régime (fig1.a). The tidal and the lee unstable domain of the advection velocity involve two different instability modes, involving small scales in the tidal régime and large scales in the lee régime. We show that this two global instability modes correspond to two different branches of the triadic resonance respectively larger and smaller wave vectors than the base flow wave vector. We propose that this change in the global stability property with respect solely to the advection velocity is linked to changes from absolute to convective local instability. In the lee wave unstable domain the small scale local PSI branch is convectively unstable but the large scale triadic instability branch is absolute whereas in the tidal domain this is the other way around. In the stable domain for intermediate advection velocities both local instabilities are convective.

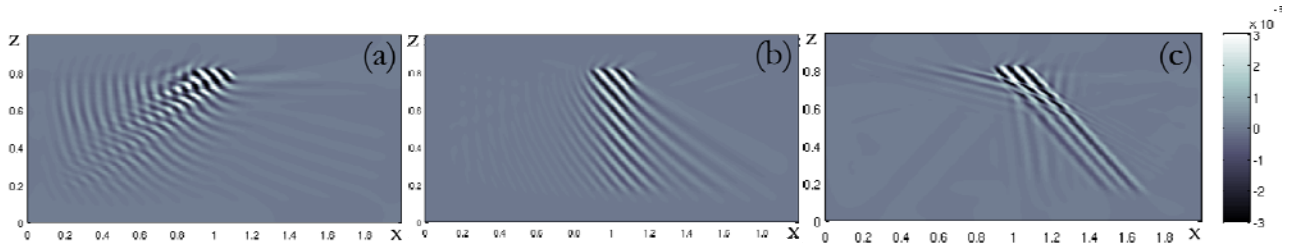


Figure 1: Density perturbation field of 2D numerical simulation for different values of the mean velocity. In (c) the velocity is null, in (a), it compensates the horizontal phase speed of the wave and (b) shows an intermediate value.

-
- ¹ LadHyX, École Polytechnique-CNRS, Palaiseau, , FRANCE
 - ¹ Phillips, The dynamic of the upper ocean, *Cambridge university press* (1966)
 - ² Lombard and Riley, *Phys. Fluids* **8**, 3271 (1996)
 - ³ Benielli & Sommeria, *J. Fluid Mech.* **374**, 117 (1998)
 - ⁴ Koudella & Staquet, *J. Fluid Mech.* **548**, 54 (2005)
 - ⁵ Bourget et al., *J. Fluid Mech.* **723**, 1 (2013)
 - ⁶ Aguilar et al., *Deep-Sea Research II* **53**, 96 (2006)

Regular and chaotic advection around the perturbed steady states of three quasi-geostrophic vortex in a two-layer fluid.

K.V. Koshel^{a,b}, M.A. Sokolovskiy^c, J. Verron^d

We study fluid-particle motion in the velocity field induced by a quasi-stationary point vortex structure consisting of one upper-layer vortex and two identical vortices in the bottom layer of a rotating two-layer fluid¹. The initial vortex configuration shown on figure 1. The regular regimes are investigated, and the possibility of chaotic regimes (chaotic advection) under the effect of quite small non-stationary disturbances of stationary configurations has been shown. Examples of different scenarios are given for the origin and development of chaos. We analyze the role played by the stochastic layer in the processes of mixing and in the capture of fluid particles within a vortex area. We also study the influence of stratification on these effects. It is shown that regular and chaotic advection situations exhibit significant differences in the two layers, see figure 2.

^a Pacific Oceanological Institute, Russian Academy of Sciences, Far East Branch, Vladivostok, Russia

^b Far Eastern Federal University, Vladivostok, Russia

^c Water Problems Institute, RAS, Moscow, Russia

^d Laboratoire des Ecoulements Géophysiques et Industriels, CNRS, BP 52, 38041, Grenoble, CEDEX 9, France

¹ Sokolovskiy et al., *J. Fluid Mech.* 717, 232 (2013).

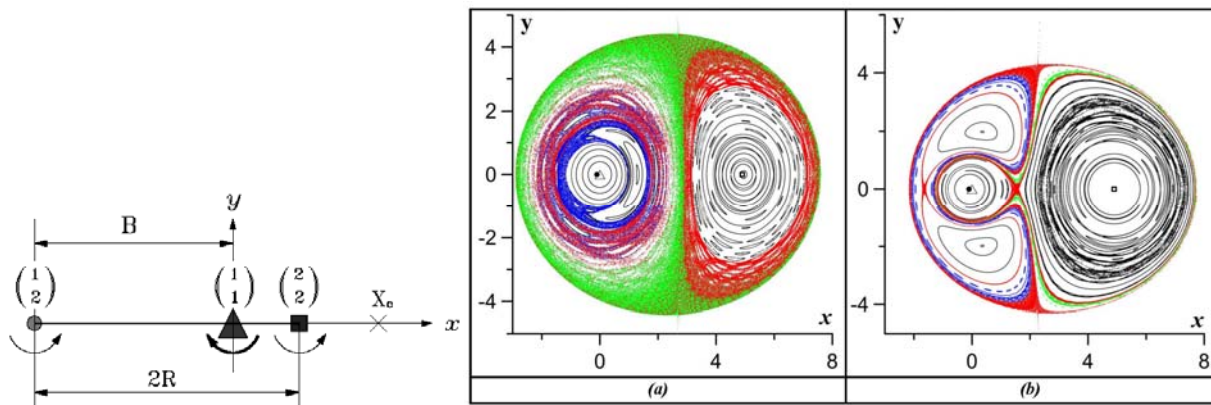


Figure 1: (Left) Scheme of the initial collinear layout of vortices for the case $B > R$. The triangle marks the position of the top-layer vortex and the circle and square mark the positions of the bottom-layer vortices; X_c is the position of the center of rotation given by (3.4) in work¹. The size of each symbol is proportional to the absolute value of the intensity of the vortex. The arc arrows show the cyclonic or anticyclonic directions of vortices. (a) Velocity distribution in time. (Right) Poincaré sections for the top (a) and bottom (b) layers. The figures correspond to perturbed behaviour of the “triton” stationary configurations.

Can rotational breaking of symmetry be observed at small-scales in atmospheric flows?

Enrico Deusebio^a and Erik Lindborg^b

We discuss the breaking of reflectional symmetry in rotating flows, with a particular focus on the implications for geophysical flows. Atmospheric flows at very large scales are strongly affected by rotation, which breaks the parity of the Navier-Stokes equations in the horizontal plane. However, it is not clear whether such symmetry breaking can also be observed at smaller scales, at which the influence of rotation is of secondary importance.

We focus on helicity, defined as the scalar product of velocity and vorticity, $H = \mathbf{u} \cdot \boldsymbol{\omega}$, as a proxy to measure the breaking of symmetry of the flow. Helicity is an inviscidly conserved quantity in a barotropic fluid. In flows that are parity invariant, positive and negative helicity events occur with the same probability, thus giving an overall zero mean helicity. On the other hand, system rotation breaks parity invariance and has therefore the potential of giving rise to non-zero mean helicity.

We have recently carried out direct numerical simulations of the Ekman boundary layer¹, that is the flow developing close to the ground in atmospheric and oceanic flows affected by a system rotation. For such a class of flow, we study the helicity dynamics and find that there is a preference for cyclonic helicity in the lower part of the Ekman layer and anticyclonic helicity in the uppermost part, where H is said to be cyclonic/anticyclonic if $\boldsymbol{\Omega} \cdot \mathbf{e}_y H$ is positive/negative, with $\boldsymbol{\Omega}$ being the rotation vector and \mathbf{e}_y the wall normal unit vector. We derive evolution equations for the mean field helicity and the mean turbulent helicity and show that pressure flux injects cyclonic helicity into the mean field at a rate $2\Omega G^2$ over the total depth of the Ekman layer, where G is the geostrophic wind far from the wall. A substantial part of the mean field helicity is transferred to turbulent helicity and dissipated at small scales by viscosity.

Energy and helicity spectra (Figure 1) show remarkable similarities and suggest that, beside the well-known energy cascade, there also exist a direct turbulent helicity cascade in the atmospheric boundary layer, which transfers helicity from the large-scale flow to the very small scales of motion. Therefore, because of the cascade, a signature of the symmetry breaking observed at large scales propagates downscale and can be observed all the way down to the Kolmogorov scale. We conclude by outlining a possible method to carry out measurements of the helicity dynamics in the atmosphere to be compared with our findings.

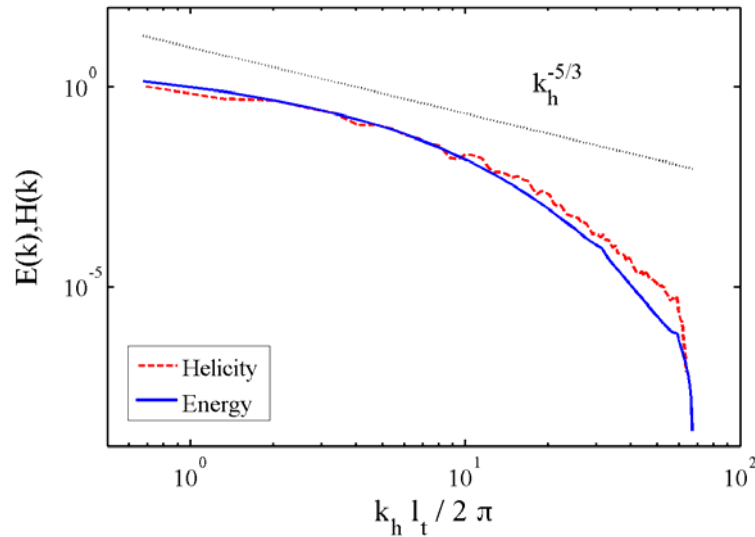


Figure 1. Energy and helicity spectrum. The x-axis is normalised by $2\pi/l_t$, with $l_t = K^{3/2}/\varepsilon$. The energy spectrum is normalised by $\varepsilon^{2/3} l_t^{5/3} / (2\pi)^{5/3}$ and the helicity spectrum is normalised by $\varepsilon_h l_t^{5/3} / \varepsilon^{1/3} (2\pi)^{5/3}$. Dotted line: $10 \cdot (k_h l_t / 2\pi)^{-5/3}$.

^a Department of Applied Mathematics and Theoretical Physics, University of Cambridge, Cambridge

^b Department of Mechanics, Royal Institute of Technology, Stockholm

¹ Deusebio *et al.*, *J. Fluid Mech.* In revision (2014).

Use of Gaussian Process Emulator for Quantifying Uncertainty in the Prediction of Convectively-Enhanced Dissolution in CO₂ Geological storage due to Heterogeneity of the Media

D. G. Crevillen^a, R. Wilkinson^a and H. Power^b

In Carbon Dioxide (CO₂) geological storage, supercritical CO₂ is injected into an underground aquifer, dissolution in brine causes an increase in the density of the CO₂-brine mixture inducing a convective flow and the formation of density fingering. The descending mixed fluid along the fingers will induce recirculation cells of brine fluid with an associated fluid entrainment into the fingers. The entrained brine reduces the density difference and the CO₂ concentration at the interface diffusive boundary layer, resulting in enhancement of the dissolution process (Convectively-Enhanced Dissolution).

To quantify the CO₂ dissolution into the brine a finite element computer simulator of two-dimensional convection in a finite-depth porous medium was developed. Unfortunately the permeability field is usually not known in practice, and so this uncertainty about the permeability thus makes us uncertain about the expected dissolution flux. We model the permeability as a log Gaussian random field, and examine the Convectively-Enhanced Dissolution process by looking at the expected distribution of the dissolution flux given our stochastic model of the unknown permeability field, in a process known as uncertainty analysis (UA). The standard approach to UA is via Monte Carlo sampling: simulate many random permeability fields, and for each one calculate the dissolution flux and then examine the empirical distribution function of all the fluxes. However, for computationally expensive models, it is not always possible to run the simulator enough times to reduce the Monte Carlo error to acceptable levels.

In this talk, we present the use of an alternative method for UA based around the use of emulators (sometimes known as meta models). Emulators are computationally cheap statistical surrogates for the true model, which can be run many times in order to perform any analysis we may be interested in doing with the simulator (such as UA), but are unable to do so because of the computational expense. The basic idea behind Bayesian emulation methodology is that we can use a small sample of simulator runs on a carefully chosen set of permeability fields to build a statistical model that can predict the simulator output for any permeability field. In this talk we will show how to an emulator using Gaussian processes applied to the Karhunen-Loeve expansion of the permeability field covariance function. We will demonstrate that accurate UA can be carried out at considerably reduced cost compared to the Monte Carlo analysis. We will give details of how to design the ensemble of permeability fields used to train the emulator, and on the modelling choices we have found to work well for the Gaussian process emulator.

^a School of Mathematical Sciences, University of Nottingham, Nottingham, NG7 2RD, UK

^b Faculty of Engineering, University of Nottingham, Nottingham, NG7 2RD, UK

Stability of pancake vortices in stratified-rotating fluids

E.Yim^a and P.Billant^a

In geophysical fluids, vortices have a pancake shape with a small thickness relative to their horizontal extent due to the stable density stratification. A famous example is the Mediterranean eddies (Meddies) formed by salty water flowing from Mediterranean sea to Atlantic ocean. The two-dimensional and three-dimensional instabilities of columnar vortices are well-known but only few results exist on the stability of such pancake vortices. Here, we investigate the linear stability of an axisymmetric pancake vortex in the strongly stratified regime ($F_h = \Omega_0/N \ll 1$ where Ω_0 is the maximum angular velocity of the vortex and N the Brunt-Väisälä frequency) in terms of the ambient rotation ($Ro = \Omega_0/\Omega_b$, where Ω_b is the background rotation rate around the vertical axis), the aspect ratio ($\alpha = Z_0/R_0$ where Z_0 and R_0 are the thickness and radius of the pancake vortex, respectively), and the viscosity Re . The angular velocity of the base state is chosen as Gaussian both in radial and vertical directions (Figure 1a). Several types of instability are found for the azimuthal wavenumbers $m=0,1,2$ depending on the aspect ratio (α) and the Rossby number (Ro). These instabilities can be similar to two-dimensional or three-dimensional instabilities of columnar vortices but modified by the confinement due to the pancake shape (Figure 1b). Other types of instabilities specific to the pancake shape also appear for small aspect ratio as shown by Nguyen et al.(2012)¹ and Hua et al.(2013)² in the quasi-geostrophic regime and Negretti & Billant (2013)³ in the strongly stratified regime. The domain of existence and the physical mechanism of these instabilities will be discussed.

^a LadHyX (Hydrodynamics Laboratory), Ecole Polytechnique, CNRS, Palaiseau, 91128, France

¹ Nguyen et al., *Geophys. Astrophys. Fluid Dyn.* **106**, 305 (2012)

² Hua et al., *J. Fluid Mech.* **731**, 418 (2013)

³ Negretti & Billant *J. Fluid Mech.* **718**, 457 (2013)

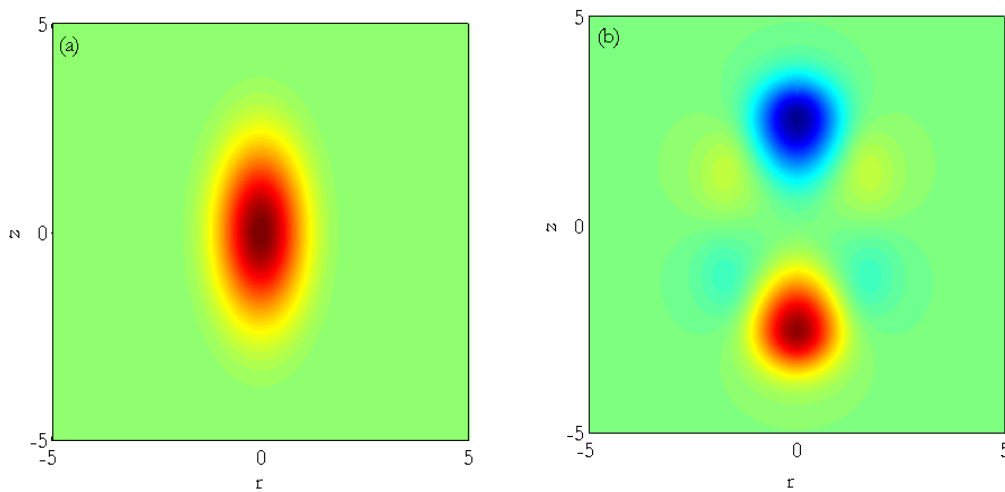


Figure 1: (a) Angular velocity of the base state for $\alpha=2$, (b) radial velocity of dominant perturbation for $m=1$ for $F_h=0.05$, $Ro=0.1$ and $Re=1000$.

Internal waves radiated by a rotating ellipsoid in a stratified rotating flow

B. Miquel¹, P. Meunier, Stéphane Le Dizès

Geophysical motivations. Geosismic observations have revealed the stacking of horizontal layers of water with different densities in the ocean, particularly above and beneath meddies¹. Meddies, sometimes referred to as “pancake-vortices”, are coherent, lens-shaped vortex structures localised around a thousand meters beneath the surface of the sea and produced as the mediterranean water flows into the ocean. Amidst other mechanisms², internal waves emitted by the radiative instability³ or by the visco-diffusive instability⁴ may account for the emergence of these vertically stacked horizontal layers. We present a simplified model and experimental setup used to reproduce and understand the mechanism responsible for layering in the vicinity of meddies in the ocean: we mimic the boundary conditions associated with a pancake vortex by considering the flow around a rotating ellipsoid in a rotating and linearly stratified fluid.

Experimental observations. In a rotating tank filled with linearly stratified salted water, an ellipsoid is smoothly set into rotation around the vertical axis. The case of the sphere is investigated as a first step of moderate complexity: indeed, we derived a purely azimuthal solution with a simple analytical expression for the base flow. PIV measurements of the velocity field around the sphere are in good agreement with this analytical solution. When the Reynolds number increases, two instabilities are visualised by means of shadowgraph and synthetic schlieren visualisation. Internal waves are radiated by the equator of the sphere: an helical mode that corresponds to an azimuthal wavenumber $m=1$ grows, which is reminiscent of the radiative instability that develops around a rotating cylinder in a stratified flow. However, at the poles of the sphere, an axisymmetric $m=0$ mode appears. This instability leads to the formation of thin layers of stratification as already observe for the visco-diffusive instability⁵. Similar observations are made when an ellipsoid is considered. The onset of the layering and radiative instability is quantified as the Reynolds number, the Froude number, the Rossby number and the aspect ratio of the ellipsoid are varied.

Numerical investigation of linear stability. A linear stability analysis of the analytically predicted and experimentally measured base flow is performed with a 2D pseudospectral code. Each azimuthal mode is decomposed on a Chebyshev-Chebyshev basis in the meridional plane. Similarly to the experimental study, the influence of the stratification, global rotation and aspect ratio of the ellipsoid on the characteristics of the most unstable mode are analysed.

¹ Aix Marseille Université, CNRS, Centrale Marseille, IRPHE UMR 7342, 13384, Marseille, France

¹ Papenberg et al., *Geophys. Res. Lett.* **37** (2010)

² Hua et al., *J. Fluid. Mech.* **731** (2013)

³ Riedinger et al. *J. Fluid Mech.* **672** (2011)

⁴ McIntyre, *Geophys. Fluid. Dyn.* **1** (1970)

⁵ Calman, *Dyn. Of Atm. And Oceans* **1** (1977)

Hydrodynamic aspects of explosive volcanic eruptions

Valeriy Kedrinskiy

Lavrentyev Institute of Hydrodynamics, SB RAS

Novosibirsk, 630090, Russia

The behavior of compressed magmatic melt at explosive volcanic eruptions is analysed within the framework of the hydrodynamics model of high-speed multi-phase processes. The state dynamics of the melt saturated by gas and microcrystallites is characterized by phase transitions, diffusive processes and bubbly cavitation development behind a decompression wave front which is formed in the result of volcanic channel depressurization. The structure dynamics of such complicated multi-phase flow in which the melt viscosity can be changed by the orders is considered on the base of the multi-phase homogeneous-heterogeneous physic-mathematical model which includes the conservation laws for mean characteristics (pressure, mass velocity and density). The model is supplemented by a system of kinetic equations, which takes into account the physical processes that occur in the compressed magma during its explosive decompression under a volcanic eruption. As it was noted in previous studies the micro-crystallites saturating the magma can serve as cavitation nuclei in decompression waves and, as a result, appreciably increase the saturation density predicted by the homogeneous nucleation model.

The paper presents one of the recent results concerning the ejections cyclicity problem at explosive eruption which is characteristic one for some closed and opened volcanic systems. Numerical investigations of the flow structure showed that an increase in the cavitation nuclei density even by one or two orders of magnitude leads to formation of zones with anomalously high values of flow parameters, which exceed the corresponding values outside these zones at least by an order of magnitude. As follows from the calculations the saturation zone with anomalous parameters is located in the vicinity of the free surface of the cavitating magma column. Its formation is explained by diffusion flows redistribution and by the change of values distribution of main flow characteristics (such, for example, as mass velocity and volumetric gas concentration) in the abnormal zone from a gradual increase of their values to the gradients jump of mentioned characteristics. In the result of the analysis the cyclic ejections mechanism model was developed. According to this model, the formation of the anomalous zone with an jump of mass velocity in the flow is finalized by instantaneous formation of a discontinuity directly in front of the velocity jump with a simultaneous "explosive" transformation of the anomalous zone to a gas-droplet system (with a subsequent ejection) and formation of a free surface on the discontinuity boundary. The calculations of the dynamics of the magma column state remaining in the channel showed that the typical structure of the flow and its anomalous zones with jumps of the main characteristics of flow is again recovered in the vicinity of the new free surface. We have the base to conclude that the cyclic mechanism is determined, controlled, and triggered by the mere evolution of the cavitation process under specific features of the magmatic melt and the cyclic ejections regime under explosive volcanic eruption can be considered as self-sustained one.

1. Gonnermann H. M. and Manga M.: The fluid mechanics inside a volcano, *Annu. Rev. Fluid Mech.* 39, 321-356, (2007)
2. Kedrinskiy V. K., Davydov M. N., Chernov A. A., and Takayama K.: The Initial Stage of Explosive Volcanic Eruption: the Dynamics of the Magma State in Decompression Waves, *Doklady Physics*, 407, (3), 190-193, (2006).

Granular

Modelling immersed granular avalanches

E. Izard^{a,b}, L. Lacaze^{a,b} and T. Bonometti^{a,b}

Immersed granular flows have been extensively studied for the past decades because of their implications in industrial processes (chemicals engineering, aeronautics, oil transport) and in natural situations (sediment transport, landslides, avalanches). Experimental measurements, modelling and predictions of such flow remain challenging since a wide range of scales is involved, namely from a fraction of a grain diameter at which lubrication and solid contact occurs up to that of the system.

In order to simulate these types of flow at the scale of $O(10^3)$ grains, we develop an immersed boundary method (IBM) which reproduce the motion of an assembly of spherical particles in an incompressible Newtonian fluid, coupled with a discrete element method (DEM) which takes into account the solid contacts between the grains in the system. Using an additional lubrication force when a pair of particles is close to contact, the present method has been shown to reproduce reasonably well experiments in the case of binary contacts¹.

In the present work, the IBM/DEM code² is first used to simulate the tridimensional collapse of a granular column of $O(10^3)$ grains immersed in a viscous fluid, for various initial aspect ratios and compacities. In particular, the method is shown to qualitatively reproduce the dependence observed in experiments³ of the final shape of the column with respect to the initial compacity, due to a pore-pressure feedback mechanism.

In a second time, the free-fall, viscous and inertial granular regimes⁴ are investigated by computing the motion of various immersed granular avalanches flowing down a rough inclined plane (figure 1) from the initiation of motion up to steady state. The characteristics of the local flow is described and analysed in the various regimes. Spatial averaging and coarse-graining are then performed, and the results are compared with larger-scale continuous two-phases approaches⁵ using the $\mu(I)$ rheological law.

^a Université de Toulouse; INPT, UPS; IMFT (Institut de Mécanique des Fluides de Toulouse); Allée Camille Soula, F-31400 Toulouse, France

^b CNRS; IMFT; F-31400 Toulouse, France

¹ Izard et al., *J. Fluid Mech.* submitted.

² Izard et al., *J. Comp. Multiphase Flows*, submitted.

³ Rondon et al., *Phys. Fluids* **23**, 073301 (2011).

⁴ Courrech du Pont et al., *Phys. Fluids* **90**, 044301 (2003).

⁵ Jackson, *The dynamics of fluidized particles*, Cambridge University Press (2000).

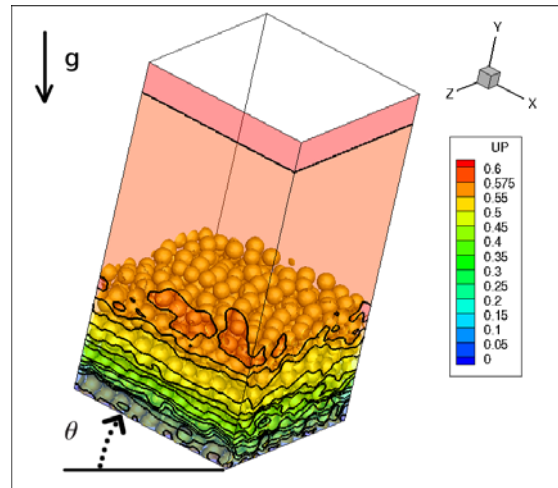


Figure 1: Granular avalanche in a viscous fluid on a rough inclined plane ($\Theta=25^\circ$) at time $t(g/D)^{1/2}=4360$ (860 grains of mean diameter D , density ratio ρ_p/ρ of 4, Archimedes number $Ar=\rho(\rho_p-\rho)gD^3/\mu^2\approx 9$, Reynolds number $Re=\rho u_g D/\mu\approx 4$, and Stokes number $St=(\rho_p+0.5\rho)u_g D/(9\mu)\approx 2$ where μ is the dynamic viscosity and u_g is the maximum velocity of grains). The stationary state is reached. Periodic boundary conditions are imposed in the x - and z -direction and no-slip (resp. slip) boundary condition is imposed at the bottom (resp. at the top). The longitudinal fluid velocity in the x -direction (UP) is plotted in colour on a x - and z -plane and iso-contours of UP from 0 m/s to 0.6 m/s with steps of 0.05 m/s.

Characterization of shear-induced granular motion on regular substrates under laminar conditions

A. Wierschem^a, J. R. Agudo^b

We experimentally study the critical conditions for incipient motion of spherical particles deposited on a regular substrate under laminar flow conditions. The substrates are triangular and quadratic arrangements of identical glass spheres of same size. For the latter, the distance between the substrate spheres is varied, resulting in different partial shielding of the deposited particle to the shear flow. For a single particle the critical Shields number is independent from particle density at particle Reynolds numbers of one and smaller but it depends significantly on the geometry of the substrate. Neighboring particles in stream-wise direction affect the onset of motion only if they are closer than about 3 particle diameters. Unlike for a single bead, pairs of identical beads may continuously move on different substrates at about the same critical Shields number. This is due to particle contact and different mechanism of motion, i.e. rolling or sliding, taking place in each of the configurations. Avoiding particle contact by a sudden jump in the Shields number, the critical Shields number for continuous particle motion can be reduced considerably.

Besides incipient motion we also study the particle motion along the substrate at supercritical Shields numbers and show how the substrate geometry also affects the mean velocity of the particle. The velocity appears to be a linear function of the supercritical Shields number for the substrates studied. The slope of the curve strongly depends again on the substrate geometry. Taking data for different viscosities, particle densities and substrate geometries and based on ideas of Bagnold and Charru *et al.*¹, we obtained a master curve between the particle velocity normalized by the Stokes settling velocity and the super critical Shields number.

^a Institute of Fluid Mechanics, University Erlangen-Nuremberg, Cauerstr. 4, D-91058 Erlangen, Germany

^b Institute of Fluid Mechanics, University Erlangen-Nuremberg, Cauerstr. 4, D-91058 Erlangen, Germany,
FAU Campus Busan, 1276 Jisa-Dong, Gangseo-Gu, Busan 618-230, Republic of Korea

¹ Charru et al., *J. Fluid Mech.* **570**, 431 (2007)

On the convective/absolute nature of dunes and antidunes

R. Vesipa^a, J.-M. Chomaz^b

River dunes and antidunes are induced by the interfacial instability of a turbulent free surface stream and a granular sediment boundary. In the present work, riverbed dynamics will be modelled following Colombini¹.

The assessment of the absolute/convective nature of morphodynamic instabilities (i.e., waves with null group velocity tends to infinity/decays asymptotically to zero) has proven to be fundamental for the interpretation of flume experiments, numerical simulations and real behaviour of rivers². For dunes and antidunes such analyses haven't been performed yet, mainly because the analysis of such bedforms requires a refined modelling of the flow field along the non-homogeneous vertical direction. This prevents the dispersion relation that describes the linear stability of the stream-sediment boundary system to be obtained analytically. The complex frequency ω is then an implicit function of the complex wave number k , and the nature of the instability is here determined using the less standard cusp map method³. We recall that the amplitude of elementary waves evolve as $\exp[i(\omega_r - i\omega_i)t + i(k_r - i k_i)x]$. Waves with null group velocity are then identified recalling that a point ω_0 that satisfies the saddle point condition, in the ω -plane has a local map $(\omega - \omega_0) \approx (k - k_0)^2$, i.e., when a curve lying in the complex k -plane and passing through k_0 is mapped into the ω -plane, it displays a cusp-like singular point at the branch point ω_0 . In order to find ω_0 , contours $k_i = k_i^*$ are mapped in the ω -plane, for k_i^* decreasing from zero. The mapping of $k_i = k_i^*$ generates in the ω -plane the curve $\Omega(k_i^*)$, (red lines in Fig. 1 *a,b*), and a branch point is obtained when $\Omega(k_i^*)$ displays (at ω_0) a cusp-like singularity (blue lines in Fig. 1 *a,b*). This occurs when $k_i = \text{Im}(k_0) = k_{0,i}$. The check for the pinch point condition is then performed by considering the position of ω_0 with respect to $\omega_F = \Omega(0)$ (black lines in Fig. 1 *a,b*). Branch points ω_0 covered an odd number of times by ω_F are pinch points. Moreover, if $\text{Im}(\omega_0) > 0$ in at least one pinch point, the instability is absolute.

In Fig. 1*c* we report a synthesis of the results. We have assessed the nature of the instability for the two most important nondimensional parameters, the relative grain diameter, $d_s = d_s^*/D_0$ (D_0 is the mean flow depth and d_s^* the dimensional grain diameter) and the Froude number F the ratio of the friction velocity time the friction coefficient by the shallow water gravity wave speed. Five zones emerge: (i) no sediment transport (gray zone); (ii) stable flat bed (black zone); (iii) convective dunes; (iv) convective antidunes; (v) absolute antidunes. Dune patterns are invariably convectively unstable, whereas antidunes can be either absolutely or convectively unstable, slightly depending on d_s , but mainly on F . The results of this analysis have been validated through the interpretation of flume experiments and numerical simulation available in the literature^{4,5}.

These findings are important for the interpretation of flume and numerical experiments as well as field data. In the parameter domain of convective instability the sediment bed behaves like a noise amplifier, and bed forms are the result of the spatial development (eventually non linear) of instabilities forced by the upstream perturbation. In the parameter domain of absolute instability, the dynamics is self sustained, i.e. the intrinsic result of the saturation of an absolute instability that prevails over the noise.

^a Dept. of Environmental, Land and Infrastructure Eng., Politecnico di Torino, C.so Duca degli Abruzzi 24, 10129 Torino (TO), Italy

^b Laboratoire d'Hydrodynamique, Ecole Polytechnique, 91128, Palaiseau, France

¹ Colombini, *J. Fluid Mech.* **502**, 1 (2004).

² Federici et al., *J. Fluid Mech.* **487**, 125 (2003).

³ Kupfer et al., *Phys. Fluids* **30**(10), 3075 (1987).

⁴ Venditti et al., *J. Geophys. Res.* **110**, F01009 (2005).

⁵ Giri et al., *Water Resour. Res.* **42**, W10422 (2006).

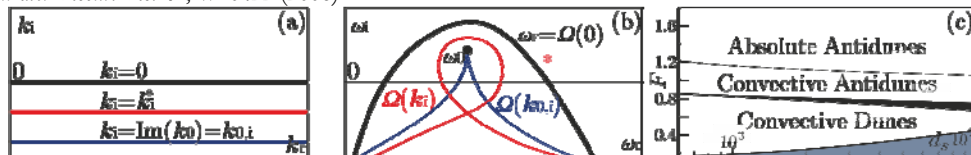


Figure 1: (*a,b*) Cusp map method. (*c*) Different types of instabilities as a function of d_s and F .

Probing the axisymmetric collapse of granular columns with the use of X-ray tomography

J. M. Warnett^a, P. J. Thomas^b, P. Denissenko^b, D. Norman^a and M. A. Williams^a

X-ray computed tomography (XCT) is a non-destructive imaging technique used to investigate the internal characteristics of a given sample which would otherwise be unobtainable. In the presented study XCT is used to evaluate the granular packing within a column of sand pre and post collapse leading to some suprising results, and is one of the first investigations using this methodology in an evolving granular flow system. The potential benefit to the field is evident, enabling experimental observations that were previously not possible.

The collapse of granular column has been studied by numerous authors over the last decade^{1,2,3}. The setup consists of a cylindrical column of radius r_0 filled with granular material to a height h_0 , giving the non-dimensional parameter of aspect ratio $a = h_0 / r_0$. The cylinder is then quickly removed vertically resulting in the formation of a pile through an avalanching mechanism akin to a dam break situation.

XCT allows a non-destructive method to virtually split the resultant pile as in Figure 1 (a), and further enables the analysis of any segregated region – applied in this case to evaluate the granular packing. By subdividing the volume occupied by the column/pile into annular regions a packing density map was extracted as in Figure 1 (b).

By comparing the packing pre and post collapse the hypothesis that the material within the failure envelope does not contribute to the collapse is tested, as assumed by previous authors². For a < 1.7 a marked increase in packing density in this region is found, demonstrating that the disturbance propagates compaction throughout the pile. For a > 1.7 the result is more complex, showing evidence of a denser central region surrounded by less compact volume in comparison to its original state. The distinction in comparative states ties with different surface flow regimes and a resultant change in power law scaling for the final runout. Further intricacies within the density mapping are presented, with links to divergent results found in some hydrodynamic approximations of the collapse.

^a Warwick Manufacturing Group, University of Warwick, Coventry, CV4 7AL, UK

^b School of Engineering, University of Warwick, Coventry, CV4 7AL, UK

¹ Lube et al., J. Fluid Mech, **508**, 175 (2004)

² Lajeunesse et al., Phys. Fluids, **16**, 2371 (2004)

³ Warnett et al., Granular Matter, **16**, 115 (2014)

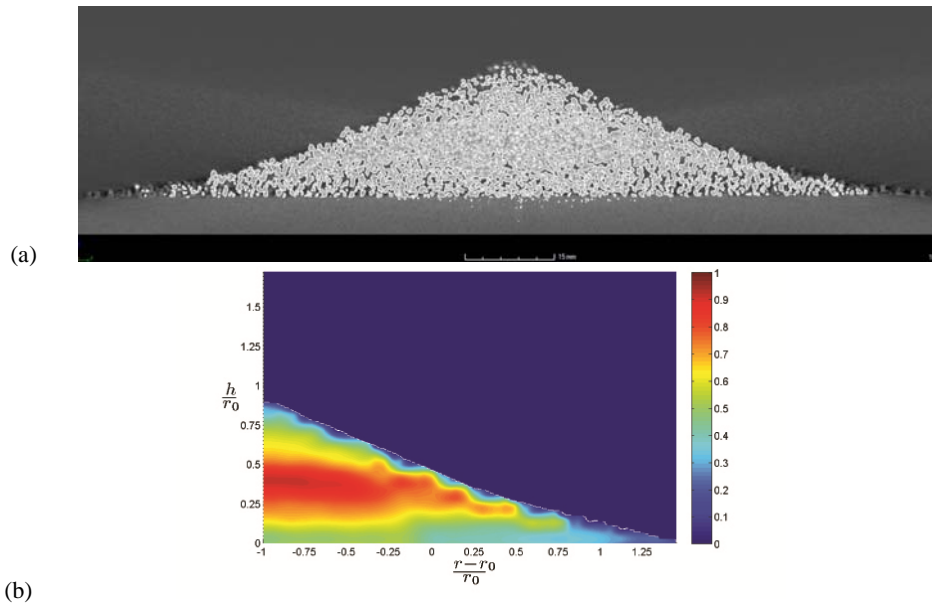


Figure 1: A column of aspect ratio $a = 1.70$ scanned using XCT post collapse. (a) 2D slice through centre of pile obtained from image reconstruction. (b) Calculated packing density map.

Drag and Lift forces when moving in a granular medium

F. Guillard^a, Y. Forterre^b and O. Pouliquen^b

The forces experienced by a cylinder moving in a granular medium are experimentally and numerically investigated. This problem, which is of practical importance in many applications (stirring, mining, problems of impact, locomotion in sand¹, design of robots...), is also of fundamental interest to probe the rheology of particulate materials. Our experiment consists in a horizontal cylinder rotating around the vertical axis in a container full of glass beads. Both the drag force and the lift force experienced by the cylinder are measured. During the first half rotation, before the cylinder crosses its own wake, we measure a strong lift force, although the object is symmetric. Whereas the drag force increases linearly with depth, the lift force is shown to saturate at large depths and to scale like the buoyancy with a large amplification factor of order 20. The origin of this strikingly high lift force is discussed based on the stress distribution measured in discrete numerical simulations. The lift force comes from the gravitational pressure gradient, which breaks the up/down symmetry and strongly modifies the flow around the obstacle compared to the case without pressure gradient. The lift is thus intrinsically related to the frictional nature of the granular rheology. After several rotations, when the cylinder goes through its own wake, the drag force suddenly drops and becomes independent of depth. This striking observation suggests that the rotation of the cylinder induces a structure in the granular packing, which screens the weight of the grains above it².

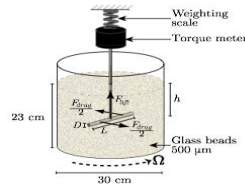


FIG. 1: Sketch of the experiment. A static cylinder is buried in a rotating tank filled with glass beads. A torque meter and a precision weighting scale record the drag and lift force on the cylinder. Note that each half of the cylinder experiences a force equal to $F_{drag}/2$, which implies eq. 1.

II. EXPERIMENTS

A. Experimental setup

The experimental setup is sketched in Fig. 1. It is composed of a tank 30 cm in diameter filled with 23 cm of glass beads $530 \pm 30 \mu\text{m}$ in diameter and density $\rho_g = 2.5 \text{ g.cm}^{-3}$. The tank is fixed on a rotating table and rotates around its vertical axis. All our experiments are performed at a rotation speed equal to 0.8 rpm, which corresponds to the quasi-static regime for which we have checked that the measured forces are independent of velocity¹⁷. The obstacle is a steel cylinder of length L and diameter D , which is buried at the centre of the tank, at depth h . The cylinder is kept static and horizontal by a 3 mm vertical rigid rod fixed at the top of the experiment to a torque meter (Meiri CS1). The measured torque \mathcal{M} experienced by the cylinder when the tank is rotating provides a measurement of the drag force using the following relation²⁸ (see caption of Fig. 1):

$$F_{drag} = \frac{4}{L} \mathcal{M}. \quad (1)$$

Figure 1: experimental setup

^a Particles and Grains Laboratory, School of Civil Engineering, The University of Sydney, Sydney, NSW 2006, Australia

^b CNRS-Aix Marseille university, IUSTI, 5 rue Enrico Fermi, 13013 Marseille

¹ Ding et al., *Phys. Rev. Lett.* **106**, 028001 (2011).

² Guillard et al., *Phys. Rev. Lett.* **110**, 138303 (2013)

Modelling of material flow in sand mould manufacturing based on Bingham plasticity - analytical and numerical approaches

E. Hovad^{a,b}, 2nd J. Thorborg^{a,c}, 3rd P. Larsen^b and 4th J. Hattel^a

This work presents preliminary work on modelling the production process of sand moulds for steel casting in the DISAMATIC process. To ensure high quality of the metal casting a sufficient density and strength of the mould is required. The sand mould is constructed in the following way, see fig. 1;

- The “sand shot” is denoting when the sand is shot into the moulding chamber with high pressure (P_{sand}) from the top of the silo into the chamber (cham).
- The sand is built up in the chamber (cham), first in a conical shape in the bottom followed by
- Filling up the corners and lastly the top of the mould.
- The mould is squeezed until a sufficient compaction of the sand is attained to ensure a dense and high quality mould. Finally the sand mould is ready for casting.

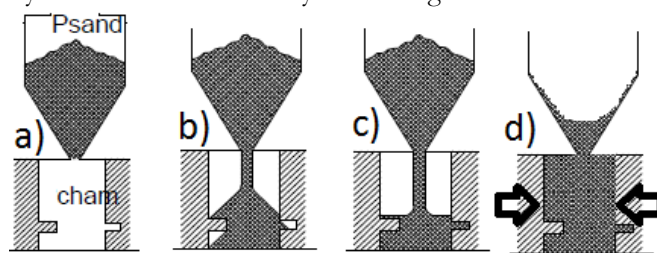


Figure 1: (a) The sand shot. (b) Conically shaped, “sand castle”. (c) Filling of the corners and the top of the mould. (d) Squeezing of the sand mould.

Simulating the formation of the conically shaped “sandcastle” and the flow of the sand towards the sides is accomplished by describing the sand as a homogeneous Bingham fluid¹.

The fluidity is a very important characteristic of the sand and in the Bingham model it is in general expressed by its yield stress and plastic viscosity. A well-known test measure for the former in Self Compacting Concrete (SCC) is the LCPC-BOX test², fig. 2(a-b) in which the spread length L and height h_0 are measured and correlated to the yield stress. A similar flow ability test has been applied for characterising moulding sand at the company Georg Fischer and that test bears many similarities to the LCPC-box test³.

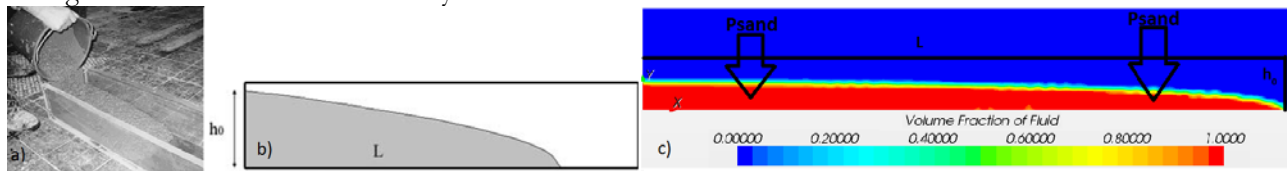


Figure 2: (a) LCPC BOX test². (b) Length L and height h_0 in the LCPC BOX test². (c) Numerical simulation of the LCPC with additional horizontal pressure (P_{shot}) with STAR-CMM+.

In the presented work an analytical solution is presented for LCPC-box test with an additive overpressure (P_{sand}). Moreover, the commercial CFD program STAR-CCM+ is used numerically to compare with the analytical solution and an example of this can be seen in figure 2(c).

^a Dep. Mechanical Engineering, DTU, Produktionstorvet., 2800 kgs. Lyngby, Denmark

^b DISA Industries A/S, Højager 8, Høje Taastrup, 2630 Taastrup, Denmark

^c MAGMA, Kackertstr. 11, 52072 Aachen, Germany

¹J. Bast, ARCHIVES OF METALLURGY AND MATERIALS. **58**, Issue 3 (2013)

²Roussel, *Materials and Structures* **40**, 889–896 (2007)

³Fließbarkeitsmessung, Georg Fischer Katalog für Formstoffprüfgeräte des Unternehmens Georg Fischer AG Schweiz.

Blowing in the wind: granular heaps

W. van de Water^a, and D. Snouck^a

Wind-blown travelling granular heaps, such as Barchan dunes, are a striking manifestation of the interaction between sand and wind. The turbulent wind shapes the dune, which, in turn, modifies the shear stress. As sand grains are not picked up readily by the wind, wind erosion is an activation process: grains travelling with the wind collide with the dune surface, and release grains upon impact. Some of these grains are again accelerated by the wind, and are able to release new grains again, but most crawl over the surface.

We measure the fluxes of flying and crawling grains on tiny dunes that sit in the turbulent boundary layer above the sand bed. We vertically oscillate the sand bed, and thus modulate effective gravity. This greatly facilitates the activation of sand by wind and dramatically reduces length scales. We image the grains flying above the heap and those crawling over its surface using a high-speed camera, and measure the granular fluxes using streak velocimetry and a variant of particle image velocimetry. The Figure shows a side view of a heap that is eroded by the wind, with the grain number flux in shades of gray.

Using this new experimental technique, we can make up the flux balance and relate it to the erosion rate, identifying the grains that carry the erosion and those that trigger it. In addition, it is possible to observe granular splashes and rebounds on a laboratory scale; single-grain processes that shape a wind-blown heap.

^a Dept. of Applied physics, Eindhoven University of Technology, Eindhoven, The Netherlands

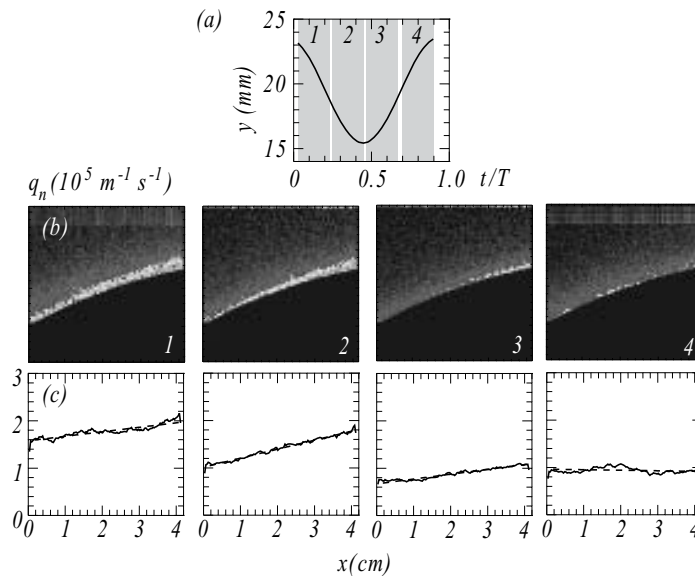


Figure: Side view of the windward side of a dune, with the (turbulent) wind coming from the left. (a) Vertical displacement of the sand bed during one oscillation period; a reduction of effective gravity occurs in episodes 1 and 2, an enhancement in episodes 3, 4. (b) Averaged grain number flux during the 4 episodes indicated in (a). (c) Vertically integrated grain number flux parallel to the dune crest. Dune erosion is proportional to the flux gradient, it is largest during episode 2 of the table oscillation.

Computational Techniques

Physical Modes for Reduced Order Flow Models

M. Morzyński^a, B. R. Noack^b, K. Kotecki^a, W. Stankiewicz^a and M. Nowak^a

Stability properties of fluid flow are of large interest in many areas of fluid mechanics^{1,3}. With the knowledge of linear stability, we gain information about flow evolution and transition.

Assessment of stability properties of the fluid generally involves one of two approaches. Unsteady flow, in sense of experimental measurements or results of CFD simulation, can be processed with signal processing tools like DMD¹. An alternative method, addressed in this paper, is investigating the governing equations for stability properties. It should be noted that most computational solutions of eigenproblems in CFD rely on investigation of the system in response to some form of perturbation.

We present here the computation of modal response of the flow to random or localised perturbation. In contrary to common DNS receptivity studies, we are interested not only in dominating mode response. With the knowledge of stability properties in wider frequency and growth rate range we gain general information about actuator placement and flow modes which can be excited and used for control.

The method is demonstrated on the linearised incompressible Navier-Stokes equations. We discretise the problem with a second-order FEM for 2D and 3D. We introduce the actuation within the computational domain or on boundaries of the flow obtaining the clear response of the flow in the whole domain. In Fig. 1 we present the example pair of modes for the wall mounted cylinder. The dominating von Kármán mode has been suppressed in this case. The presented method of modal basis design will be used for Reduced Order Modelling of the flow.

Acknowledgements. This work was supported by the Polish National Science Center (NCN) under the Grant No.: DEC-2011/01/B/ST8/07264 and by the French ANR Chair of Excellence TUCOROM.

^a Institute of Combustion Engines and Transport, Poznan University of Technology, 60-965 Poznan, Poland

^b Institut PPRIME, CNRS Universite de Poitiers ENSMA, UPR 3346, Departement Fluides, Thermique, Combustion, CEAT, 43, rue de l'Aerodrome, F-86036, Poitiers Cedex, France

¹ Theofilis, *Ann. Rev. of Fluid Mechanics*, **43** (1), 319–352, (2011)

² Schmid J. *Fluid Mechanics* **656**, (1), 5-28, (2010)

³ Noack, Morzynski & Tadmor, *Reduced-Order Modelling for Flow Control*, **528**, Springer, 2011.

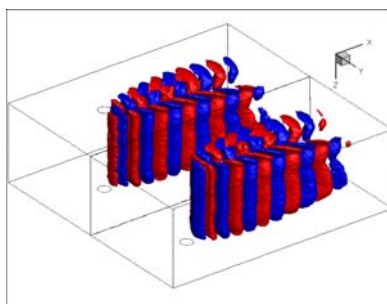


Figure 1: Real (left) and imaginary (right) part of mode, wall-mounted circular cylinder flow at $Re = 200$, transversal iso-velocity surfaces.

Numerical prediction of pipe flows with uncertain parameters

S. Schmelter^a, A. Fiebach^a, R. Model^a, and M. Bär^a

In many metrological flow applications, pipe flows are of special interest since they are a crucial element of many flow meters. In this context, the precise determination of the flow properties is of great importance in metrology. In some applications not only integral quantities, like the flow rate or pressure loss, are of interest, but also the entire flow field, described by velocity profiles at certain cross sections through the pipe. Some influencing parameters, e.g., the wall roughness or deformations of the inflow profiles caused by a bend or a diaphragm, cannot be accurately determined. The influence of such uncertain parameters on the flow field is the purpose of this investigation.

To quantify the uncertainty in the flow field, a generalized Polynomial Chaos method in conjunction with a commercial deterministic CFD code is used. The so-called “non-intrusive” spectral projection approach is based on the spectral representation of the uncertainty where the flow simulator can be used as a black box. In connection with modern sampling methods the expense is considerably smaller than for a conventional Monte Carlo analysis for cases with only a few simultaneous random parameters. It can be stated that for computationally expensive models, that are common in fluid dynamics, the use of Monte Carlo methods is impractical.

In this contribution, the influence of different parameters, like the uncertain inflow as well as the wall roughness, on the outflow profile is investigated. As an example, Fig. 1 shows the variation of velocity profiles in different cross-sections in the pipe caused by the prescription of uncertain inflow profiles. Besides the deformation of the profiles also characterizing quantities like the asymmetry, the turbulence, and the profile factor, respectively, are considered. In addition, the simulations are validated against Laser Doppler Velocimetry measurements of flow profiles in specified cross-sections of a pipe.

^a Dep. Mathematical Modeling and Data Analysis, Physikalisch-Technische Bundesanstalt (PTB), Berlin, Germany

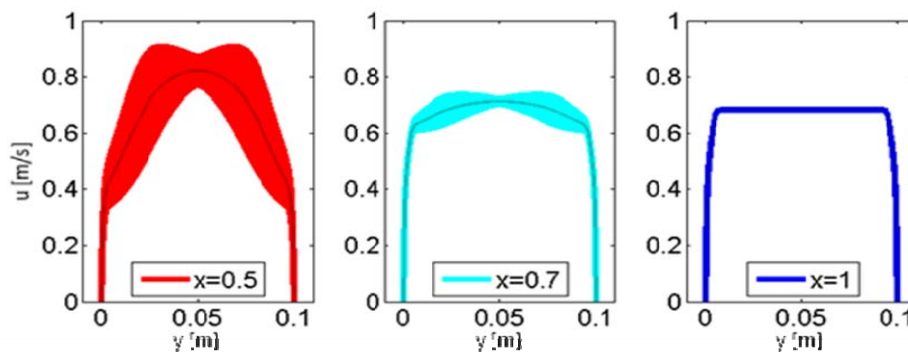


Figure 1: Mean \pm standard deviation of velocity profiles at different cross-sections downstream in the pipe resulting from uncertain inflow profiles. Left: $x = 0.5$ m, middle: $x = 0.7$ m, right: $x = 1$ m.

Fluctuating force-coupling method for simulating Brownian suspensions

Eric E Keaveny^a

Brownian motion plays an important role in the dynamics of colloidal suspensions. It affects suspension rheological properties, influences the self-assembly of structures, and regulates particle transport. While including Brownian motion in simulations is necessary to reproduce and study these effects, it is computationally intensive due to the configuration dependent statistics of the particles' random motion. In addition, particle motion occurring at unresolved inertial timescales yields a drift term proportional to the divergence of the hydrodynamic mobility matrix. Even to achieve the correct particle distribution under equilibrium conditions requires the proper treatment of this drift term, further complicating an already arduous calculation.

I will discuss recent work that speeds up this calculation for the force-coupling method (FCM), a regularized multipole approach for simulating suspensions at large-scale. I will show that by forcing the surrounding fluid with a configuration independent, white-noise stress, fluctuating FCM yields the correct, configuration dependent particle motion, even when higher-order terms, such as the stresslets, are included in the multipole expansion. Additionally, I will discuss time-integration schemes that automatically account for the drift term, rendering its direct computation unnecessary. I will present the results from several simulations demonstrating the effectiveness of this approach and also discuss the extension of fluctuating FCM to dense suspensions.

^a Department of Mathematics, Imperial College London, South Kensington Campus, LONDON, SW7 2AZ, UK

Enrichment of Reduced Order Models using Physical Modes

W. Stankiewicz^a, M. Morzyński^a, K. Kotecki^a, and R. Roszak^a

Substantial progress in the methods of computational fluid dynamics and the rapid development of computer hardware in the past decades have increased the role of computer simulations at the expense of wind tunnel experiments.

On the other hand, as shown by C. Rossow¹, the flow analysis of the new aircraft design leads to hundreds of thousands of different cases, varying in aircraft configuration, mass distribution, flow conditions (e.g., gusts, angle of attack) and so on. Such a number of variants is very challenging even with the use of simplified flow models (like URANS) and large computer cluster.

The solution of this problem might be the design of accurate Reduced Order Models of the flow. Unfortunately, the Galerkin models based on empirical modes like POD² or DMD^{3,4}, resulting from modal decomposition of the flow at limit cycle oscillations precisely reproduce the dynamics only in the close vicinity of that operating condition. Due to the truncation of mode basis^{5,6}, even small change in the value of Reynolds number, angle of attack, level of actuation, etc. leads to the deterioration of the model and wrong prediction of the phase of the flow. In the case of feedback flow control, such issue may lead to the reverse of the effect of control.

To broaden the scope of the model and to increase its accuracy, enrichment of the modal basis with the use of physical modes is required.

The article discusses the methods of obtaining the physical modes matching global stability eigenmodes. Model order reduction techniques, based on the Galerkin expansion and projection, are presented on the example of three-dimensional, low Reynolds number incompressible flows past the bluff-bodies.

^a Institute of Combustion Engines and Transport, Poznan University of Technology, 60-965 Poznan, Poland

¹ Rossow and Kroll, *46th ALAA Aerospace Sciences Meeting and Exhibit, Reno, USA* (2008)

² Lumley and Poje, *Phys. Fluids* **9**, 2023 (1997)

³ Schmid and Sesterhenn, *J. Fluid Mech.* **665**, 5 (2010)

⁴ Frederich and Luchtenburg, *7th International Symposium on Turbulence and Shear Flow Phenomena* (2011)

⁵ Noack et al., *J. Fluid Mech.* **497**, 335 (2003)

⁶ Rowley et al., *J. Fluid Mech.* **641**, 115 (2009)



Figure 1: Iso-surfaces of λ_2 criterion for real (left) and imaginary (right) parts of the physical mode for a flow past a sphere.

Criteria for particle Lagrangian stochastic models

J.-P. Minier^a, S. Chibbaro^b

In this paper, we discuss the various forms under which Lagrangian stochastic models, used for the simulation of the fluid seen by discrete particles in a turbulent flow, can be found. These models are typically applied in numerical studies of environmental and industrial applications, but should be handled with care to avoid inconsistencies and potentially-inconsistent results. The present analysis does not address the question of the relative predictive capacities of different models but concentrates on their formulations since advantages and disadvantages of these formulations are not always clear. Indeed, hidden in the changes from one structure to another are some possible pitfalls leading to flaws in the construction of practical models and in physically-unsound numerical calculations.

In the frame of the present discussion, a first purpose is to clarify issues related to the formulation of Lagrangian stochastic models and to propose guidelines, as well as safeguards, useful for experts and non-experts alike. A second purpose is to recall that a single and consistent theoretical framework exists for Lagrangian stochastic models, also called PDF (Probability Density Function)^{1,2} models and that, by choosing a relevant formulation, modelling efforts, which are still needed to improve present Langevin models, can be safely channelled and devoted to building new ideas. Apart from putting forward the importance and the physical interpretation of the different terms which appear as one goes from one formulation to another, a central issue is to come up with reliable requirements which must be met by Lagrangian stochastic models. For that purpose, the choice made here is to consider the fluid-limit, or particle-tracer limit, and to check whether models are fully consistent with Reynolds-stress type of models. This criterion allows assessing modelling proposals while ensuring that they are built on safe grounds, corresponding to state-of-the-art turbulence modelling. It will be recalled that one formulation, in terms of the instantaneous velocity, stands out as both the easiest and the safest road to follow to develop well-based Lagrangian stochastic models. Then, going to the actual two-phase flow world, the analysis is extended to include an in-depth discussion of available criteria that should be met by stochastic models developed to simulate the velocity of the fluid seen. Simple and practical considerations reveal significant errors that can be made but that can be avoided in a straightforward manner.

The present contribution addresses concerns of both non-experts and experts in the field of so-called dispersion models. In this way, we will be able also to review critically the old issue of the well-mixed condition or the so-called drift velocity in the two-phase flow case.

^a EDF R&D, Mécanique des Fluides, Energie et Environnement, 6 quai Watier, 78400 Chatou, France

^b Sorbonne Universités, UPMC Univ Paris 06, CNRS, UMR7190, Institut Jean Le Rond d'Alembert, F-75005 Paris, (France)

¹ Pope, *J. Fluid Mech.* **582**, 54 (2009).

² Minier and Peirano *Phys. reports* **18**, 034210 (2001)

A finite element solution of a generalized Newtonian Hele-Shaw flow with a level set method for free surface tracking

P. Guerrier^a and J. H. Hattel^a

The aim of this work is to solve a Hele-Shaw flow, which is a flow between two closely placed parallel plates. The main motivation for solving this type of flow, is to use it to analyze the filling of an injection molding process, as typical injection molded parts consist of thin-walled parts, and this process is typically considered as a viscous flow since the Reynolds number typically is in the order of 10^{-5} . An additional implication is that the polymers injected are sensible to the shear rate, and therefore the flow cannot be considered Newtonian, and a generalized Newtonian material model has to be implemented.

The main assumption for the Hele-Shaw approximation is that the gap between two parallel plates has to be sufficiently small¹. Analyzing the incompressible continuity equation with this assumption, will show that the z-velocity component will be small compared to the x- and y-components, and can therefore be ignored. Analyzing the momentum equations in a similar manner, ignoring the inertia term and using the continuity equation, they can be cast into a more simple form. The reduced momentum equations can then be integrated across the gap in order to compute the gap-wise average x- and y- velocity components. A characteristic of the Hele-Shaw flow is that although the velocities change in magnitude through the gap, they do not change in direction. Using the gap-wise average velocity and the continuity equation, a pressure equation can be formulated and solved, see figure 1 for a solution example. This is a clever way of reducing the full 3D problem to a 2.5D problem. The pressure equation depends on what is called the fluidity, S , which depends on the shear rate (which is a function of the pressure gradient) because the material is generalized Newtonian. Hence, an iteration process is needed. A Cross model has been used to describe the viscosity dependence of the shear rate.

A free surface tracker has to be used to track the flow front of the polymer, as it fills the mold cavity. A level set method² has been employed for this. This is a transport equation which is solved for a signed distance function. At the zero contour of the distance function is the location of the front. In each time step a reinitialization process is executed to ensure that the function remains a signed distance function.

The implementation has been tested against commercial software to verify the code. Furthermore have a real industrial application, consisting of a plate with two different thicknesses, been simulated with the code.

^a Dep. Mechanical Engineering (MEK), Technical University of Denmark (DTU), DTU Building 425, Produktionstorvet, 2800 Kgs. Lyngby, Denmark

¹ Osswald and Hernandez-Ortiz, Polymer Processing, Carl Hanser (2006).

² Sussman et al., *J. of Comp. Phys.* **114**, 146 (1994)

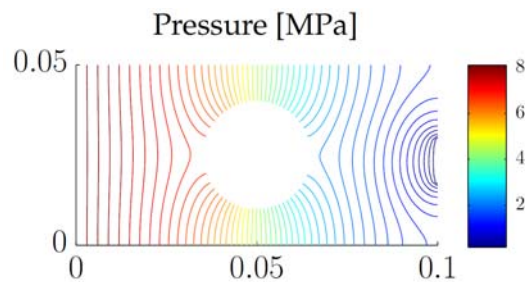


Figure 1: Pressure distribution at the end of filling of a thin plate with a hole. Solved by a Poisson type equation in the Hele-Shaw formulation.

A probabilistic cellular automaton for bypass transition in boundary layers

T. Kreilos^{ab}, T. Khapko^c, P. Schlatter^c, Y. Duguet^d, D. S. Henningson^c and B. Eckhardt^a

We present a probabilistic cellular automaton model to describe the spatio-temporal aspects of bypass transition in boundary layers. With this we extend recent results on parallel shear flows to spatially developing external flows.

The spatial behaviour of shear flows close to transition has successfully been related to probabilistic cellular automata and directed percolation^{1,2,3}. The most notable results stem from pipe flow, where at low Reynolds number turbulence exists in the form of localized puffs, which may decay or split with probabilities depending on Re . We extend the concept to turbulence transition in a flat-plate boundary layer subject to free-stream turbulence. If the amplitude of the free-stream disturbances exceeds a threshold, the traditional route via Tollmien-Schlichting waves can be bypassed and transition happens without exponential amplification of linear instabilities. In this context, turbulent spots are created, which spread while travelling downstream. The intermittency factor, measuring the fraction of turbulent sites, grows from zero at the inflow to one for full turbulence in an S-shaped.

We develop a probabilistic cellular automaton (PCA) describing the evolution of turbulent spots in the boundary layer flow. The model parameters are obtained directly from statistical analysis of data from large LES at various turbulence intensities with a setup similar to ref. 4, see figure 1. The PCA reproduces the statistics of the LES data extremely well (figure 2), showing that the spatial evolution of turbulent spots in a transitional boundary layer is described by our model.

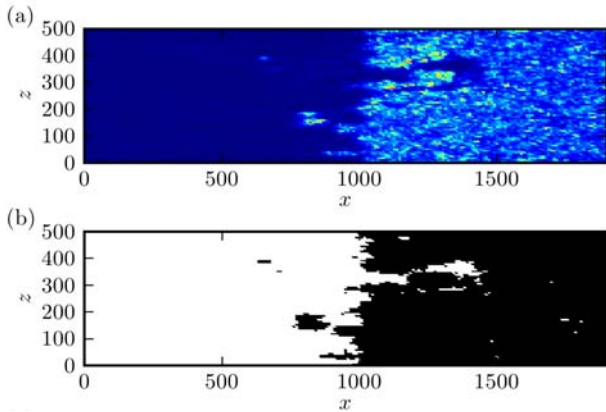


Figure 1: Visualization of turbulent spots in the LES data. (a) The untreated LES data. The colors indicate the level of turbulence by measuring the spanwise shear stress at the wall. Dark blue indicates low intensities, the bright regions higher intensities. (b) Digitized LES data where only laminar (white) and turbulent (black) regions are distinguished. These data are then used to extract the parameters for the cellular automaton model.

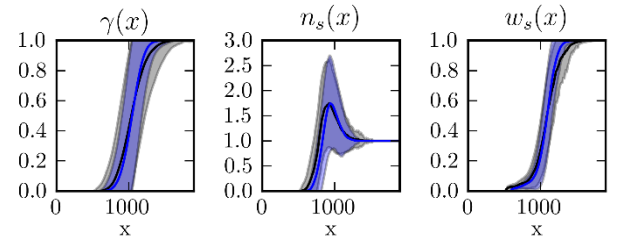


Figure 2: Comparison of statistics between the LES data (black) and the probabilistic cellular automaton (blue). (a) Intermittency factor. (b) Number of spots at every downstream position. (c) Width of independent spots in units of the domain width as a function of downstream position. The shaded areas indicate one standard deviation and show that not only the mean of the quantities agrees very well but also the second moment of the distribution.

^a Fachbereich Physik, Philipps-Universität Marburg, 35032 Marburg, Germany

^b Max Planck Institute for Dynamics and Self-Organization, 37077 Göttingen, Germany

^c Linné FLOW Center, KTH Mechanics, Royal Institute of Technology, 10044 Stockholm, Sweden

^d LIMSI-CNRS, UPR 3251, Université Paris-Sud, 91403 Orsay, France

¹ Moxey & Barkley, PNAS 107, 8091-8096 (2010)

² Barkley, Phys. Rev. E 84, 016309 (2011)

³ Avila et al., Science 333, 192-196 (2011)

⁴ Brandt et al., J. Fluid. Mech. 517, 167-198 (2004)

Numerical simulation of non-Newtonian free surface flows in moulding process using the lattice Boltzmann method

O. Bublik^a, J. Vimmr^a and A. Jonasova^a

This work is focused on numerical simulation of non-Newtonian free surface fluid flows using the lattice Boltzmann method, which gained popularity during the last decade^{1,2}. The method is based on the Boltzmann equation describing the fluid on mesoscopic level unlike the classical methods that utilise the system of incompressible Navier-Stokes equations describing the fluid on macroscopic level. The main advantage of the lattice Boltzmann method compared to classical methods is that the solution of the Poisson equation, required to meet the condition in the form of the continuity equation, is avoided. Because of this, the lattice Boltzmann method is simpler and less computationally demanding than the finite element and finite volume methods.

The lattice Boltzmann method originates from the lattice gas cellular automata (LGCA) representing a simplified molecular dynamics. However, unlike the LGCA, the lattice Boltzmann method operates with virtual particles. This approach makes it possible to solve various complex flow problems such as free surface flow and multiphase flow within a reasonable time frame.

To capture the free surface of the fluid in this study, we adopt the algorithm based on the volume of fluid (VOF) method established by Thürey³. The advantage of this algorithm is that the mass flow between grid points is calculated directly using the distribution functions, avoiding so the need to introduce a new equation for the movement of the liquid-gas interface as is the case of the classical VOF. For the simulation of non-Newtonian effects, the power-law viscosity model^{6,7} is introduced as well. The rate of deformation tensor is computed in a simple way using the finite difference method. To increase the stability of the whole calculation, the multiple relaxation times (MRT) model⁴ of collision operator is used instead of the common single relaxation time (SRT) model⁵.

The developed algorithm is applied to the simulation of moulding process with a non-Newtonian fluid (polyurethane). The results of a simple 2D test case in an idealised geometry at selected time instants are shown in Fig. 1, where the fluid motion is caused by the gravitational force and the moulding form is filled with vacuum. The developed algorithm is also applied to the numerical simulation of polyurethane moulding in a real 3D form geometry. From the obtained results, it is apparent that the free surface of the fluid could be well captured and this computational algorithm is well suited for the solution of this type of flow problems.

This work was supported by the the project TA03010990 of the Technology Agency of the Czech Republic.

^a European Centre of Excellence NTIS – New Technologies for the Information Society, Faculty of Applied Sciences, University of West Bohemia, Univerzitni 22, 306 14 Pilsen, Czech Republic

¹ Succi, *Oxford university press* (2001)

² Chen and Doolen, *Annu. Rev. Fluid Mech.* **30**, 329 (1998)

³ Thürey, *Ph.D. thesis* (2007)

⁴ d'Humières et al., *Philos. T. R. Soc. Lond.* **360**, 437 (2002).

⁵ Bhatnagar et al., *Phys. Review* **94**, 511 (1954)

⁶ Chai et al., *J. Non-Newtonian Fluid Mech.* **166**, 332 (2011)

⁷ Gabbanelli et al., *Phys. Rev. E* **72**, 046312-1 (2005)

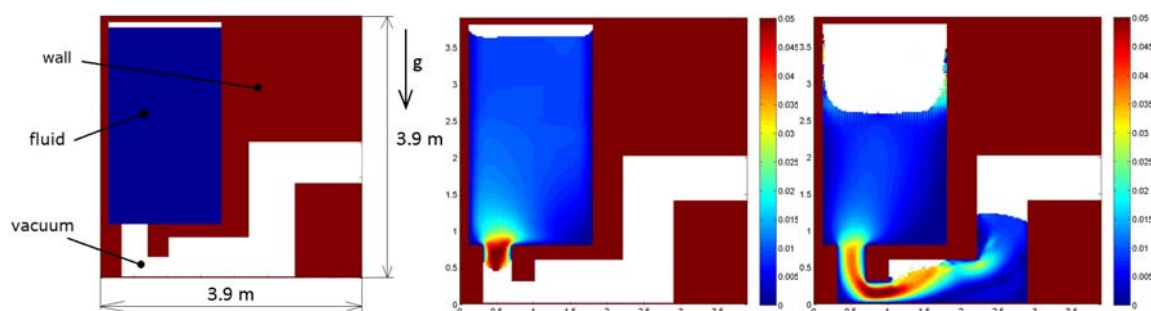


Figure 1: Gravity moulding in a simple 2D test case - velocity magnitude in lattice units at selected time instants.

Numerical modeling of cavitating flows with the NSMB solver

C.-K. Huang¹, Y. Hoarau¹ and E. Goncalves²

This study presents implementation and validation of several cavitation modeling in the NSMB solver. Cavitation is a phenomenon that occurs frequently in conventional hydraulic components such as pumps, valves, turbines and propellers. Over-speeds imposed by the local geometry, shear phenomena, acceleration or vibration may cause local pressure drops in the fluid. When the flow pressure is less than the vapor pressure of the fluid, there is a partial vaporization and vapour structures arise. The so formed structures are entrained by the flow and when they reach a higher pressure zone they condense and implode violently. Cavitation leads to significant loss of system performance, problems of instability of operation of machines and erosion of the component walls. It is thus a primary source of technical problems in the field of hydraulic turbomachinery, naval propulsion and space as well as in high pressure fuel injection.

Numerical prediction of cavitation remains a challenge for several reasons. The modeling of phase transition (thermodynamics) and the interactions with the turbulence is not fully established yet. Specific issues to numerical techniques in this type of flow also persist. From the point of view of modeling, the vast majority of computer codes dedicated to the simulation of cavitation is based on an averaged approach for both the two-phase flow and the turbulence. A hierarchy of models exist: simple model of three equations (one-fluid) model up to seven equations models (two-fluid) which remain rather suited for inviscid and simple geometries.

In this recent on-going study, the cavitation models developed at the LEGI are implemented in the NSMB solver (structured parallel multiblocs compressible solver with chimera grid) and validated on simple case. Furthermore the cavitation modelling is coupled to the Level-Set technique and will be presented. The end goal of this study is to assess the validity of various turbulence modelling approach in cavitating flows.

¹ ICube Laboratory, 2 rue Boussingault, 67000 Strasbourg, France

² LEGI, INP-Grenoble, France

Fully Lagrangian approach to mesh-free modelling of two-phase vortex flows

N.A. Lebedeva^a, A.N. Osipov^b

The main goal of the study is to develop novel models and approaches for mathematical modeling of the interaction of localized vorticity zones of different kind with an inertial dispersed admixture. The method proposed is applicable to simulation of unsteady viscous flows with a dilute admixture of non-colliding particles which do not affect the carrier phase. The approach is based on a modification and combination of the full Lagrangian method¹ for the dispersed phase and a Lagrangian mesh-free vortex method based on the diffusion velocity for Navier-Stokes equations describing the carrier phase²⁻³. In the combined numerical algorithm, both these approaches have been implemented and used at each time step. In the first stage, the vortex-blob approach is used to calculate the fields of velocity and spatial derivatives of the carrier-phase flow. In the second stage, using full Lagrangian approach, the particle velocity and number density are calculated along chosen particle pathlines. In this case, the problem of calculation of all parameters in both phases (including particle concentration) is reduced to the solution of a high-order system of ordinary differential equations, describing transient processes in both carrier and dispersed phases. Due to a very high ‘compressibility’ of dilute admixture in complex transient flows, various flow features can be manifested, e.g. discontinuities and singularities in the dispersed-phase concentration, multiple intersections of particle trajectories, formation of ‘folds’ in the particle continuum, etc. The correct simulation of these flow features involves serious difficulties when conventional Eulerian or Eulerian/Lagrangian methods, described in the literature, are used. The combined fully Lagrangian approach, proposed here, allows one to study in detail local zones of particle accumulation in transient two-phase flows with different ratios of phase material densities, including aerosol or dusty-gas flows and flows of bubbly liquids or dilute suspensions.

As an example, the method is applied to simulate the development of vortex ring-like structures in an impulse two-phase jet flows. This flow involves the formation of local zones of particle accumulation, regions of multiple intersections of particle trajectories, and multi-valued particle velocity and concentration fields. The proposed combined Lagrangian mesh-free approach enables one to reproduce with controlled accuracy all these flow features without excessive computational costs.

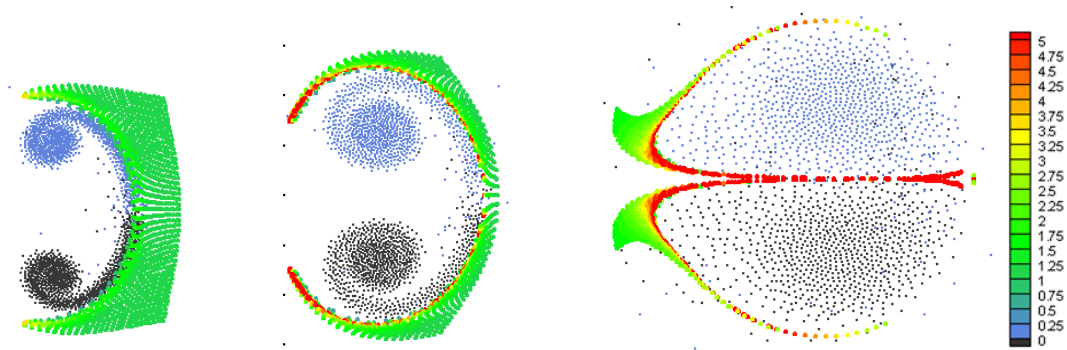


Figure 1: Time evolution of inertial particle cloud in impulse jet flow at subsequent time instants; grey and blue dots show the positions of vortex blobs, color dots show the positions of the particles and the values of the dimensionless particle number concentration.

^a Reservoir Testing Department, Schlumberger Moscow Research, 13 Pudovkina Str., Moscow, Russian Federation

^b Institute of Mechanics, Lomonosov Moscow State University, 1 Michurinsky Ave., Moscow, Russian Federation

¹ Osipov, *Astrophys. Space Sci.* **274**, 377 (2000)

² Ogami and Akamatsu, *Comp. and Fluids* **19**, 433 (1991)

³ Dynnikova, *Fluid Dyn.* **38**, 670 (2003)

Detached eddy simulation of a high Reynolds number turbulent boundary layer with uniform blowing

R. Kidogawa^a, Y. Kametani^{a,b} and K. Fukagata^a

Reduction of skin-friction drag in turbulent flows has been studied for many years in order to mitigate environmental burden or to enhance energy efficiency. However, the Reynolds number assumed in the previous studies using numerical simulation is quite low as compared to that in practical engineering applications. In order to explore the possibility of drag reduction control in practical applications, investigation of control effects at high Reynolds numbers is necessary.

In the present study, a detached eddy simulation¹ (DES) of a spatially developing turbulent boundary layer with uniform blowing (UB) is performed. The mechanism of drag reduction is investigated and the Reynolds number dependency of the drag reduction rate is discussed.

The DES is one of hybrid turbulence models, which works as a Reynolds-averaged Navier-Stokes equation (RANS) in the region near the wall and as a large eddy simulation (LES) in the region away from the wall. The governing equations are the incompressible continuity, spatially filtered Navier-Stokes equation, and transport equation for the eddy viscosity. The friction Reynolds number, Re_τ , is set to be 160 and 2000 in the present study. The magnitude of UB from the wall is 0.1% or 0.5% of the free-stream velocity.

It is found from the present DES that UB makes the velocity profiles shifted away from the wall. The mean streamwise velocity profile at $Re_\tau = 2000$ is shown in Figure 1. The vertical chained line in the figure represents the boundary between the RANS region and the LES region. The effect of UB depends on the control amplitude. This tendency coincides with the results at $Re_\tau = 160$ and DNS results at $Re_\tau = 160$ of Kametani and Fukagata².

The drag reduction rate, R , at two different Reynolds numbers is shown in Figure 2 as functions of the blowing velocity in wall units, V^+ . It is found that the drag reduction rate is increased with the blowing velocity; a drag reduction of 81.1% is obtained in the case of 0.5% UB at $Re_\tau = 2000$. It is also found that the relationship between V^+ and R is nearly insensitive to the Reynolds number.

In the final presentation, we also discuss the mechanism of drag reduction in comparison with the low Reynolds number cases.

^a Keio University, Hiyoshi 3-14-1, Kohoku-ku, Yokohama 223-8522, Japan

^b Linné FLOW Centre, KTH, 100 44 Stockholm, Sweden

¹ Spalart et al., *Advances in DNS/LES*, pp. 137-148 (1997)

² Kametani and Fukagata, *J. Fluid Mech.* **681**, 154-172 (2011)

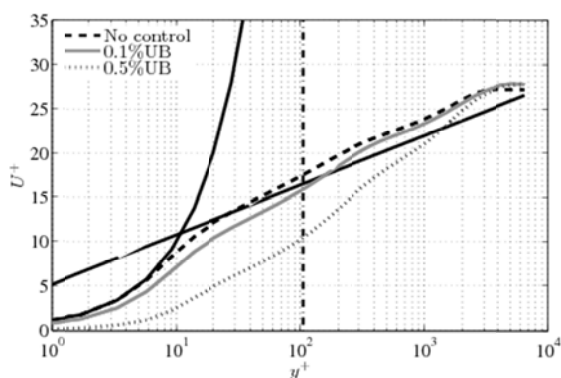


Figure 1: Mean streamwise velocity.

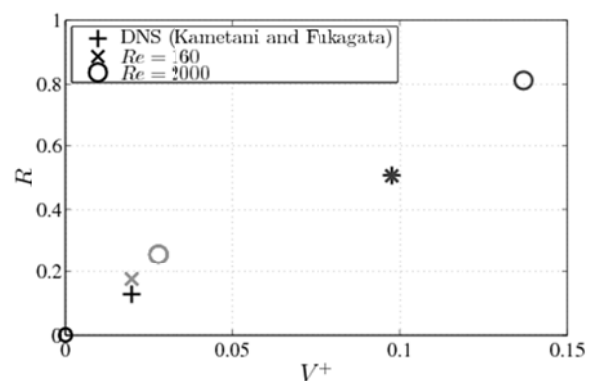


Figure 2: Drag reduction rate.

Optimal subgrid scale model for passive scalar based on artificial neural network

A. Volland^a, G. Balarac^a and C. Corre^a

Due to the large range of motion scales in turbulent flows and the associated simulation cost, the direct numerical simulation (DNS) of realistic applications remains out of reach. To overcome this limitation, the large-eddy simulation (LES) technique explicitly solves the large scales of the flow only and models the smallest scales. The separation between resolved and modeled scales is performed by a filtering operation applied to the equations governing the flow. The filtering process yields subgrid-scale (SGS) terms, which have to be modelled in LES. Various approaches have been proposed to define a SGS model, based either on a functional or structural strategy¹. A structural strategy emphasizes accuracy with respect to DNS while a functional strategy focuses on the robustness / stability of the SGS model. This work assesses the use of an artificial neural network (ANN) to define a SGS scalar flux model, in the context of the turbulent transport of a passive scalar, offering an optimal trade-off between accuracy and stability.

Following Moreau et al.², an *optimal estimator* can be defined in the LES context, which leads to the best structural performance of a SGS model based on a given set of input parameters. In other words, the optimal estimator yields the smallest quadratic error for the SGS scalar flux with respect to a DNS computation. This concept of *optimal estimator* has already been successfully used as an analysis tool to improve existing models since it gives access to the irreducible error attached to a given model template³. The present work goes one step further since a SGS model is directly derived as a surrogate model (SM) of the optimal estimator, with ANN used to build the SM. The selected input parameters are derived from the complete and irreducible dynamic non-linear tensor diffusivity model⁴. The ANN is built with a filtered DNS database of a mixing passive scalar in a forced homogeneous turbulence ($Sc = 1$ and $Re = 90$, performed on a 256^3 grid); it is based on a perceptron multi-layer fully connected with sigmoid activation function, as already used by Sarghini et al.⁵.

The SM built with the ANN is used as SGS model in a LES on a 32^3 grid and compared with filtered DNS results and with results from a LES using a classic dynamic eddy-diffusivity model (DEDM). The temporal decay of the resolved scalar variance is displayed in Fig.1: the SM prediction is in better agreement than DEDM with the filtered DNS ; DEDM predicts a stronger decay because of an over-prediction of the SGS dissipation. Due to this over-dissipation, the scalar variance spectrum (see Fig. 2) predicted by DEDM under-estimates the smallest resolved scales, whereas the results obtained with SM stay closer to the DNS results. These preliminary results will be completed with model robustness taken into account in the derivation of the SM.

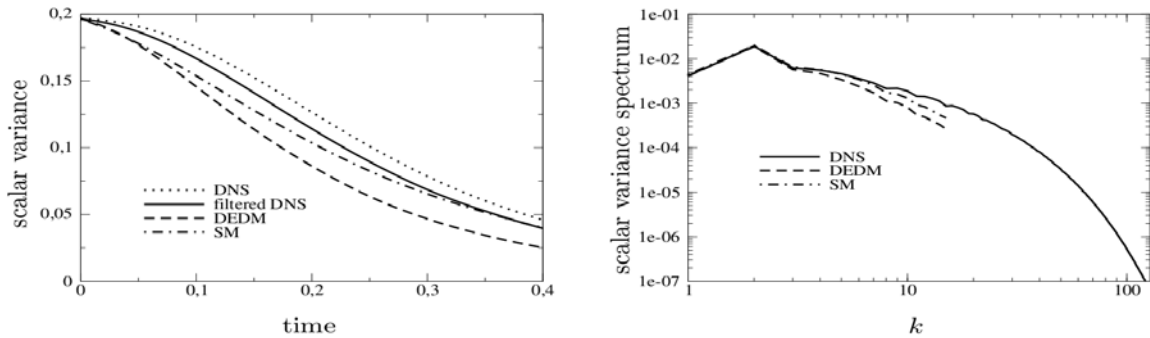


Figure 1: Evolution of the resolved scalar variance with time (left) and scalar variance spectrum at $t = 0.2$ (right).

^a Grenoble-INP/CNRS/UJF-Grenoble 1, LEGI UMR 5519, Grenoble, F-38041, France

¹ Sagaut, *Large eddy simulation for incompressible flows : an introduction*, Springer, (2006)

² Moreau et al., *Phys. Fluids* **18** (2006)

³ Balarac et al., *Phys. Fluids* **25** (2013).

⁴ Wang et al., *International Journal of Heat and Fluid Flow* **28** (2007)

⁵ Sarghini et al., *Computers and Fluids* **32** (2003)

Structure-preserving discretization of the Stokes equations in fluid dynamics

Bo Gervang^a and Marc Gerritsma^b

Mimetic methods or structure-preserving methods constitute an emerging field of scientific computing. Where in the past a differential equation was solved by *approximating* all derivatives individually using nodal approximations, the new paradigm considers the governing equations in a more global form. Enzo Tonti, [1,2], explicitly made a distinction between topological and metric-dependent relations in physical models. The topological relations consist of conservation laws, equilibrium and compatibility conditions, while the metric-dependent part consists -- according to Tonti -- of phenomenological equations provided by constitutive laws, also referred to as material equations or equations of state. The class of topological equations is further divided into inner-oriented relation and outer-oriented relations. In terms of differential forms this distinction amounts to topological relations between true forms and pseudo-forms, respectively. Tonti classifies nearly all physical theories in terms of their topological and constitutive relations in so-called Tonti-diagrams.

The advantage to distinguish between topological and metric-dependent relations, is that the former possess a discrete representation which does not involve mesh-dependent parameters, while only the constitutive equations dependent explicitly on the mesh. As a result discrete (global) topological equations are *exact*, while all the approximation takes place in the metric-dependent (local) constitutive laws.

Mimetic discretizations are available for differential forms, [3-5], but continuum models require higher order tensors for a proper description. While conservation of mass may still be expressed in terms of differential forms, conservation of momentum should be expressed in terms of covector-valued pseudo volume forms. This description of momentum can be found in [6-9] and [10], although Frankel treats momentum as a *vector*-valued form. The reason for the use of more extended tensors is because in continuum mechanics physics '*is smeared out*' over volumes, surfaces and lines. In classical mechanics we have momentum which can be described by a 1-form, but in continuum mechanics we use momentum *per unit volume*, which only yields momentum 'after integration over a volume'. Likewise, stress needs to be represented as a force density per unit area.

In this talk results will be presented of a mimetic discretization where both momentum and stress are represented as convector-valued differential forms.

- [1] E.Tonti, *On the formal structure of physical theories*, Prepr. Ital. Natl. Res. Counc.(1975).
- [2] E.Tonti, *Why starting from differential equations for computational physics?*, J. Comp. Physics, 257, pp. 1260–1290, 2014.
- [3] P. B. Bochev and J. M. Hyman, *Principles of mimetic discretizations of differential equations*, Compatible Spatial Discretizations The IMA Volumes in Mathematics and its Applications Volume 142, pp 89-119, 2006.
- [4] J. Kreeft and M. Gerritsma, *Mixed mimetic spectral element method for Stokes flow: A pointwise divergence-free solution*, J. Comput. Physics, 240, pp. 284-309, 2013.
- [5] M. Desbrun, A. N. Hirani, M. Leok and J. E. Marsden, *Discrete Exterior Calculus*, arXiv:math/0508341, 2005.
- [6] E. Kanso, M. Arroyo, Y. Tong, A. Yvari, J.E. Marsden and M. Desbrun, *On the geometric character of stress in continuum mechanics*, Zeitschrift für Angewandte Mathematik und Physik 58 (5) , pp. 843-856, 2007.
- [7] A. Yvari, *On geometric discretization of elasticity*, Journal of Mathematical Physics 49 (2) , art. no. 022901, 2008.
- [8] J. E. Marsden and T. J. R. Hughes, *Mathematical Foundations of Elasticity*, Dover Publications, New York, 1983.
- [9] R. Segev, *Notes on Metric Independent Analysis of Classical fields*, Math. Meth. Appl. Sci., 36, pp. 497 - 566, 2013.
- [10] Th. Frankel, *The geometry of Physics. An Introduction*, 2nd edition, Cambridge University Press, 2004.

^a Aarhus University School of Engineering - Fluid Mechanic, Dalgas Avenue 2, building DA2, room 309, 8000 Aarhus C, Denmark (bge@iha.dk)

^b Faculty of Aerospace Engineering, TU Delft, Kluyverweg 1, 2629 HS, Delft, The Netherlands (M.I.Gerritsma@TUDelft.nl)

Towards a stochastic closure approach for Large Eddy Simulation

Thomas von Larcher^a, Rupert Klein^a, Illia Horenko^b, Philipp Metzner^(b), Matthias Waidmann^a, Dimitri Igdaiov^b, Andrea Beck^c, Gregor Gassner^d and Claus-Dieter Munz^c

We present a stochastic sub grid scale modeling strategy currently under development for application in Finite Volume Large Eddy Simulation (LES) codes. Our concept is based on the integral conservation laws for mass, momentum and energy of a flow field that are universally valid for arbitrary control volumes. We model the space-time structure of the fluxes to create a discrete formulation. Advanced methods of time series analysis for the data-based construction of stochastic models with inherently non-stationary statistical properties and concepts of information theory based on a modified Akaike information criterion (mAIC) for the model discrimination are used to construct stochastic surrogate models for the non-resolved fluctuations^{1,2}. Vector-valued auto-regressive models with external influences (VARX-models) form the basis for the modeling approach. We realize non-stationary statistical properties of these models by allowing for time dependent switches between different fluctuation regimes which are represented by different, but fixed, sets of the stochastic model parameters.

The reconstruction capabilities of the modeling ansatz are tested against fully three dimensional turbulent channel flow data computed for an incompressible, isothermal fluid at Reynolds number $Re_\tau=590$ by direct numerical simulation (DNS). We present here the outcome of our reconstruction tests. We have identified the VX-model as the model of choice, i.e. this model does not incorporate auto-regressive terms. Furthermore, the model selection study resulted in a stationary, non-homogeneous model as the best-fit model. Thus, the channel flow data model deviates from standard models which are typically based on homogeneous statistical approaches. Secondly, considering the stochastic model approach, we found, surprisingly, that the deterministic model part alone is good enough to fit the flux correction terms well. The best-fit deterministic flux corrections agree very well despite the roughness of the coarse-grid data. This non-trivial result mentions also the role of deterministic LES closure approaches. The results encourage us for the ambitious attempt at dynamic LES.

^a Institute for Mathematics, Freie Universität Berlin, Arnimallee 6, 14195 Berlin, Germany

^b Institute of Computational Science, Università della Svizzera Italiana, Via Giuseppe Buffi 13, 6900 Lugano, Switzerland

^c Institute of Aerodynamics and Gas Dynamics, University of Stuttgart, Pfaffenwaldring 21, 70569 Stuttgart, Germany

^d Mathematical Institute, University of Cologne, Weyertal 86-90, 50931 Köln, Germany

¹ Horenko, *J. Atm. Sci.* **67**, 1559 (2010).

² Metzner et al., *CamCoS* **7**, 175 (2012)

An immersed-body method for wind energy applications

A. Viré^a, J. Xiang^b and C.C. Pain^b

Wind turbine rotors are becoming increasingly large, in order to increase the power generated per turbine and reduce the cost of energy. Concurrently innovative concepts are actively investigated, for example, floating offshore wind turbines. In this context, the mutual interactions between fluids (e.g. air, water) and wind turbine cannot be neglected. The accurate computational modelling of such interactions is however challenging, due to the complexity of the geometry, the deforming fluid-structure interfaces, and the turbulent wind flow. In this context, non-linear models for fluid- and structural- dynamics are required. This work focuses on developing high-fidelity numerical techniques that can accurately compute fluid-structure interactions.

This study uses an immersed-body approach where the Navier-Stokes equations are solved on an extended domain covering both fluid and structure. The extended domain is discretised by an unstructured finite-element mesh (fluid mesh), while a separate mesh covers solely the structure (solid mesh). A solid-concentration field is computed on the fluid mesh through conservative mapping between solid and fluid meshes. A novel algorithm was developed in the fluid/ocean dynamics model Fluidity-ICOM¹ and ensures spatial conservation of the action-reaction force when it is projected between both meshes². As opposed to other existing techniques, the method enables: (i) arbitrarily high orders of representation of the discrete fields, and (ii) different representations of the discrete fields on each mesh.

The talk will be organised as follows. First, the fluid-structure interaction algorithm will be presented. Second, the method will be validated on cases that are relevant to wind energy research. At this stage, flow past an airfoil has been successfully represented by using dynamic mesh adaptation to resolve the boundary layer (Fig. 1). Application to other test cases is ongoing and results will be presented at the conference. Recommendations for future work will also be given.

^a Fac. Aerospace Engineering, Delft University of Technology, Kluyverweg 1, 2629 HS Delft, The Netherlands

^b Dep. Earth Science and Engineering, Imperial College London, SW7 2AZ London, United Kingdom

¹ Pain et al., *Ocean Modelling* **10**, 5-33 (2005)

² Viré et al., *Ocean Dynamics* **62**, 1487-1501 (2012)

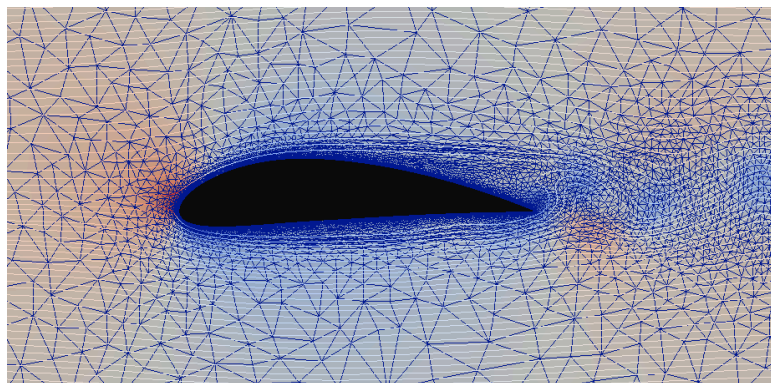


Figure 1: Snapshot of the pressure field for flow past an airfoil using the immersed-body approach.

State your age at the time of the poster submission here if you want to participate in the Young Scientist Award: 29 years old

Combustion

Stability of Subsonic Microjet Flows and Combustion

Yu.A. Litvinenko^a, G.R. Grek^a, M.M. Katasonov^a, V.V. Kozlov^a, O.P. Korobeinichev^b,
and A.G. Shmakov^b

Results of experimental studies of round and plane propane microjet combustion in a transverse acoustic field at small Reynolds numbers are presented in this paper. Features of flame evolution under the given conditions are shown. Based on the new information obtained on free micro - jet evolution, new phenomena in flame evolution in a transverse acoustic field with round and plane propane micro - jet combustion are discovered and explained (see Figures 1 and 2).

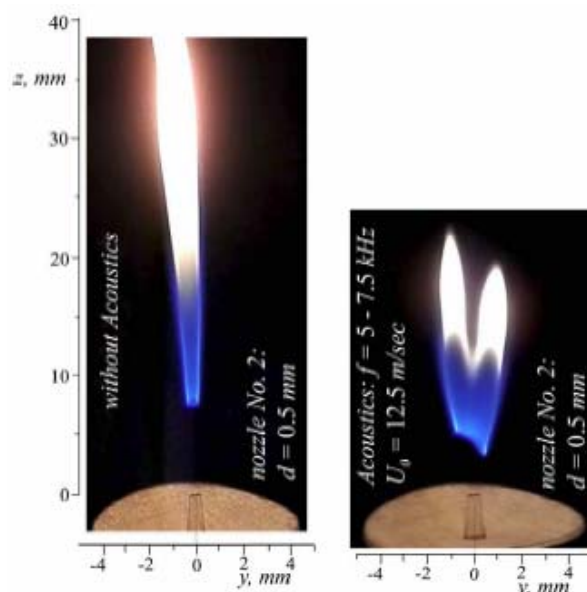


Figure 1: Round microjet (for nozzle $d = 0.5 \text{ mm}$) flame bifurcation in a transverse acoustic field.

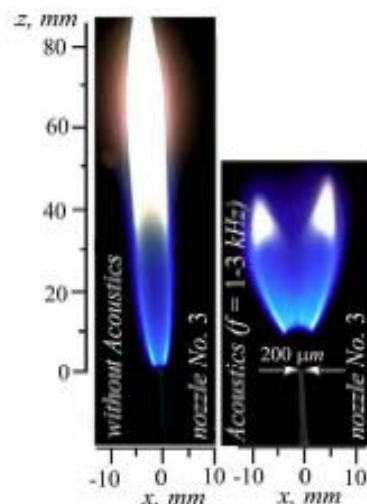


Figure 2: Plane microjet flame bifurcation in a transverse acoustic field: short nozzle ($l = 2 \text{ mm}$, $b = 200 \text{ μm}$, $l/b = 10$).

This work was supported by the Integration Project SB RAS No. 24 and by the Russian Foundation for Basic Research, project Nos. 11-01-00292, 12-08-31083, 12- 07-00548, and 13-07-00616

^a Khristianovich Institute of Theoretical and Applied Mechanics, Siberian Branch of Russian Academy of Sciences, Novosibirsk, Russia

^b Voevodsky Institute of Chemical Kinetics and Combustion, , Siberian Branch of Russian Academy of Sciences, Novosibirsk, Russia

Multicontinua description of spray diffusion flames in counterflow mixing layers

D. Martínez-Ruiz¹, J. Urzay², A. L. Sánchez^a, A. Liñán^c and F.A. Williams^d

Much of our present understanding of the local chemistry-mixing interactions occurring in turbulent reacting flows stems from analyses of simple laminar-flow problems¹. The counterflow mixing layer considered here may be thought to be representative of local flow conditions in vortex-braid regions along unstable shear layers, and also around the stagnation point that forms near the injector exit as a result of vortex breakdown of the swirling feed streams in typical combustion chambers; see Fig.1(a,b). This simple configuration has been used widely in numerical and experimental studies of spray combustion.

The solution depends fundamentally on the droplet Stokes number, St , defined as the ratio of the characteristic droplet acceleration time to the characteristic counterflow strain time. Droplets with small St act as tracers of the gaseous flow, remaining on the injection side, with their number density building up on the vicinity of the stagnation plane. By way of contrast, droplets with St above a critical value of order unity, St_c , cross the stagnation plane to undergo oscillatory motion around it. The associated droplet trajectories display multiple plane and interdroplet crossings, whose description requires, in general, particle tracking techniques.

We show in this work that a continuous formulation of the liquid phase is possible even for $St > St_c$, provided that an adequate treatment of the droplet reversing motion is implemented. The resulting Eulerian-Eulerian description provides an appropriate framework to assess different spray-combustion phenomena, including influences of droplet inertia, spray dilution, and fuel vapor diffusivity.

¹ Dep. Ingeniería Térmica y de Fluidos, Universidad Carlos III de Madrid, 28911, Leganés, Spain

² Center for Turbulence Research, Stanford University, Stanford, CA 94305-3024, USA

^c E.T.S.I. Aeronáuticos, Universidad Politécnica de Madrid, 28040, Madrid, Spain

^d Department of Mechanical and Aerospace Engineering, UCSD, La Jolla, 28040, CA 92093-0411, USA

¹ D. Martínez-Ruiz et al., *J. Fluid Mech.* **734**, 387 (2013).

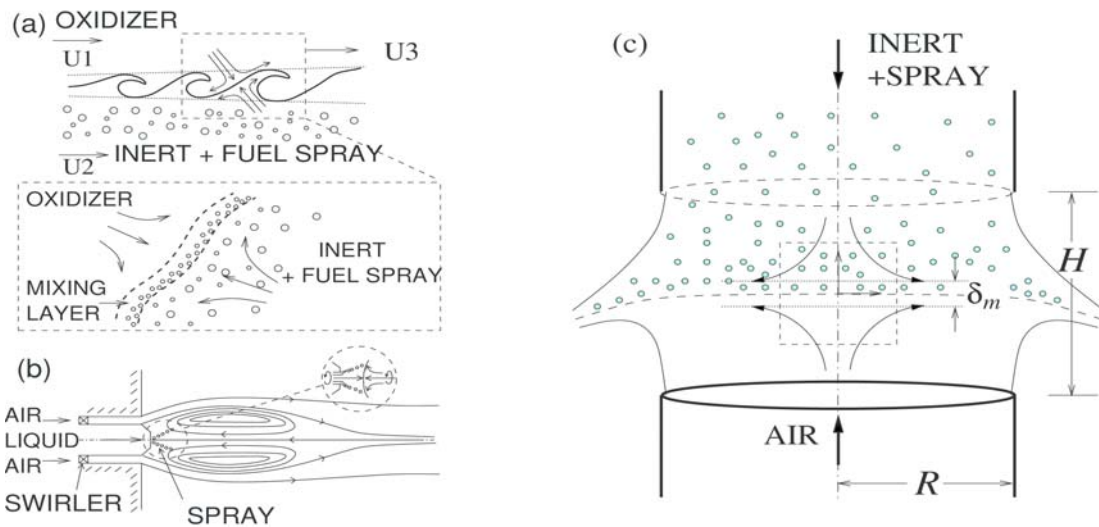


Figure 1: Counterflow regions in (a) droplet-laden shear layers, and (b) swirling injectors. (c) Typical arrangement of a spray in counterflow configuration.

Propagation of premixed flames in long narrow channels from a closed end: transition from constant speed to rapid acceleration

Vadim N. Kurdyumov^a and Moshe Matalon^b

Propagation of a premixed flame in narrow channels from the closed end is considered analytically and numerically. An asymptotic approach shows that in sufficiently narrow channels there are two distinct solutions with a constant flame velocity corresponding to slow and fast flames. The solution with the highest velocity is unstable and therefore cannot be observed in experiments. The two solutions merge when the channel width is increased to a critical value, suggesting that the slow propagation with a constant velocity changes to a rapid exponentially-like acceleration. This has been corroborated by direct numerical simulations. The results thus provide a clear criterion for the conditions and onset of exponentially-like acceleration in long channels. Influence of heat losses and differential diffusion (Lewis number) are also reported.

^a Department of Energy, CIEMAT, Avda. Complutense 40, 28040 Madrid, Spain

^b Mechanical Science and Engineering, University of Illinois at Urbana-Champaign, Urbana, IL 61801, USA

Effect of a forcing on auto-ignition time and a flame lift-off height

A. Tyliszczak^a, E. Mastorakos^b

Efficiency of combustion processes is directly related to a fuel-oxidizer mixing and interactions between a flame and a flow field. Control of these two processes may lead to considerable improvement of efficiency, safety and performance of various technological devices. Such control may be obtained applying a passive and/or an active flow control technique¹. Passive control relies on manipulation of the flow field without adding any external energy and relies on geometric shaping or adding fixed elements. Active flow control methods involve energy input whose type and level may be fixed or may be varying depending on the instantaneous flow behaviour. In the field of fundamental research the active flow control techniques became important subject of research in 70s starting from an experiment of Crow and Champagne² devoted to circular jet flows. They

showed that applying an axial excitation with properly chosen frequency the jet exhibits significantly different behaviour from the natural unexcited jet, they managed to intensify turbulence intensity and mixing. Possible applications of this type of excitation in combustion processes were demonstrated in experimental studies of non-premixed swirl-stabilised burner³ and also in premixed flame in a bluff-body configuration⁴. It was found that the excitation improves lean flammability limits and also changes the flame behaviour qualitatively. They observed that excitation may lift-off the flames or reattach already lifted flames. In the jet type flows the appli-

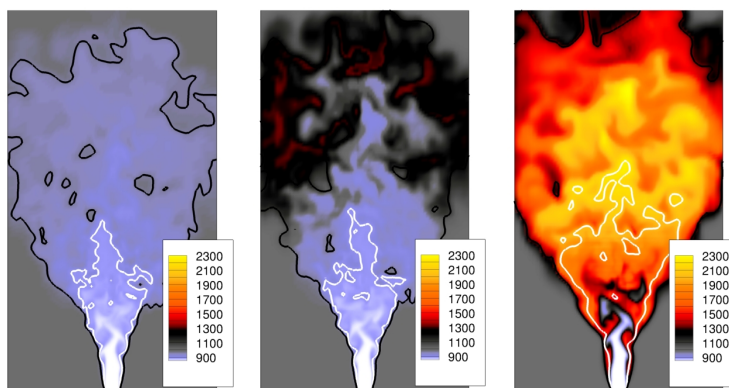


Fig.1 Contours of the temperature evolution in auto-igniting excited hydrogen jet in the central cross-section plane.

cation of excitation was studied⁵ from the point of view of interaction with absolute instability modes. It was found that in the absolute instability regimes the reacting jets are much less sensitive to the forcing than the non-reacting jets, even if they are forced with the amplitude of the order of the jet velocity.

In the present research we focus on excited lifted/attached hydrogen flame issuing from a circular nozzle into a hot ambient air. This flame (unexcited) was previously studied experimentally in Ref. [6] to which we refer to validate the numerical results. We apply the Large Eddy Simulation and Conditional Moment Closure combustion model which allows for accurate prediction of very complicated phenomena including spontaneous auto-ignition, flame propagation and flame lift-off. We study the effect of the forcing on auto-ignition time, a flame propagation speed and a flame lift-off height. We analyse two different type of the forcing (axial, axial+helical) with varying frequencies and amplitudes. The fuel jet is a mixture of hydrogen ($Y_{H_2}=0.13$) and nitrogen ($Y_{N_2}=0.87$) at the temperature 691K. We consider two temperature of the ambient air: 980K at which the resulting flame is attached to the nozzle and 930K for which the flame is lifted a few diameter from the nozzle. Simulations are performed using a high order LES code validated based on the Sandia flames and Cabra flame. Sample results showing the evolution of temperature - from the auto-ignition to a fully developed flame - are shown in Fig.1. In the presented case the forcing was prescribed as the combination of axial and helical excitation. The bold lines in Fig. 1 indicate the most reactive mixture fraction (black line) and the stoichiometric value (white line). It is seen that before the ignition the jet significantly expands radially and reminds a balloon. The auto-ignition starts far from the inlet and appears almost simultaneously in a large volume of the flow. Then the flame quickly propagates to the inlet along the most reactive lines and attaches to the nozzle.

^a Faculty of Mech. Eng. Comput. Sci., Czestochowa Univ. of Tech., Al. A. Krajowej 21, 42-200 Czestochowa, Poland

^b Hopkinson Laboratory, Dep. of Engineering, University of Cambridge, Cambridge CB2 1PZ, United Kingdom

¹ Kral, ASME Fluids Eng. Div. Technical brief (1998).

² Crow and Champagne, J. Fluid Mech., 48:547-691 (1971)

³ Hardalupas and Selbach, Prog. Energy Combust. Sci., 28:75-104 (2002)

⁴ Balachandran et al., Combust. Flame, 143:37-55 (2005)

⁵ Juniper et al. Proc., Combust. Inst., 32:1191-1198 (2008)

⁶ Markides and Mastorakos, Proc. Combust. Inst. 30:883-891 (2005)

Massively parallel simulation of soot formation in turbulent flames

Antonio Attili^a, Fabrizio Bisetti^a, Michael E Mueller^b, and Heinz Pitsch^c

Soot is an aerosol consisting of tiny carbonaceous particles clustered in aggregates of a few hundreds microns. Soot originates from large Polycyclic Aromatic Hydrocarbon (PAH) species, such as naphthalene, pyrene, and coronene. Upon formation, soot grows by further addition of PAH molecules and by chemical reactions on the particles' surface, and may lose mass due to oxidation. Collisions among particles lead to a decrease in the soot number density. Since soot poses important health and environmental hazards, there exists significant interest in improving our understanding of the details of its formation and growth with the aim of reducing harmful emissions. Recently, emphasis has been placed on the characterization of toxicity, particulate size distribution, and surface fraction of soot emissions from newly introduced combustion devices.

A set of direct numerical simulations (DNS) of turbulent combustion coupled with soot formation has been performed¹. These DNS studies constitute the state-of-the-art in terms of scope, physical models, and numerical methods for massively parallel reactive flow simulations. A detailed chemical mechanism, which includes PAH, and a high-order method of moments for soot modeling are employed for the first time in the three-dimensional simulation of turbulent flames. The DNS calculations feature 500 M grid points and consumed more than 50 M cpu-hours on 32,768 cores of an IBM Blue Gene/P system and generated in excess of 100 TB of data.

It is observed that the sensitivity of soot precursor to turbulent mixing causes large inhomogeneities in the precursor fields, which in turn generate even stronger inhomogeneities in the soot fields (Fig.1a). From the analysis of Lagrangian statistics, it is shown that soot nucleates and grows mainly in a layer close to the flame and spreads on the rich side of the flame due to the fluctuating mixing field (Fig.2a). The results show the leading order effects of turbulent mixing in controlling the dynamics of soot in turbulent flames. Given the difficulties in obtaining quantitative data in experiments of turbulent sooting flames, these simulations provide valuable data to guide the development of models for Large Eddy Simulation and Reynolds Average Navier Stokes approaches.

^a Clean Combustion Research Center, King Abdullah University of Science and Technology, Thuwal 23955, Saudi Arabia

^b Department of Mechanical and Aerospace Engineering, Princeton University, Princeton, NJ 08544, USA

^c Institut für Technische Verbrennung, RWTH Aachen University, 52056 Aachen, Germany

¹ Attili A. et al., *Comb. Flame*, in press (2014). Doi: <http://dx.doi.org/10.1016/j.combustflame.2014.01.008>

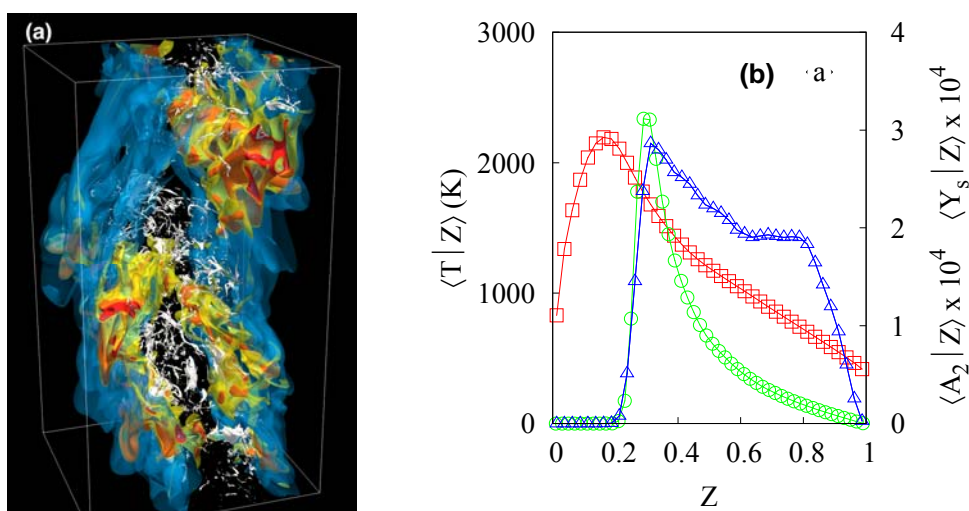


Figure 1: (a) Render of the turbulent flame: the blue isosurface of temperature marks the flame location at 1800 K; the yellow and red isosurfaces show the naphthalene concentration; the white isosurface indicates regions of high soot mass. (b) Mean of temperature (red squares), naphthalene mass fraction, A_2 (green circles), and soot mass fraction (blue triangles) conditioned on mixture fraction.

Taylor dispersion and the thick-flame asymptotic limit

J. Daou^a, P. Pearce^a and F. Al-Malki^b

We examine Taylor dispersion problem in the context of premixed combustion. The model considers a flame propagating against a two-dimensional parallel flow of small scale but large amplitude. A formula for the effective propagation speed of the travelling wave is derived in the asymptotic limit corresponding to a flame which is thick compared to the flow scale. The formula neatly describes how the flame speed is enhanced by the presence of the flow, and shows that this enhancement is in full agreement with the shear-augmented diffusion phenomenon known as Taylor dispersion. The distinguished asymptotic limit considered is argued to be of high relevance for understanding, within simple tractable analytical laminar-flow models, the so called *bending-effect of the turbulent flame speed* U_T , which is observed experimentally under high intensity turbulent flow. In fact, several additional distinguished limits are also analysed, both asymptotically and numerically, which identify various behaviours depending on the non-dimensional flow intensity A , the non-dimensional flow scale ε^{-1} and the Reynolds number Re , see figure. The findings seem to be able to explain the differing and often apparently contradictory results found in experimental and numerical studies concerned with flame propagation in more complex flows and in particular with those concerned with turbulent premixed combustion.

^a School of Mathematics, University of Manchester, Manchester M13 9PL, UK

^b Department of Mathematics, Taif University, Saudi Arabia

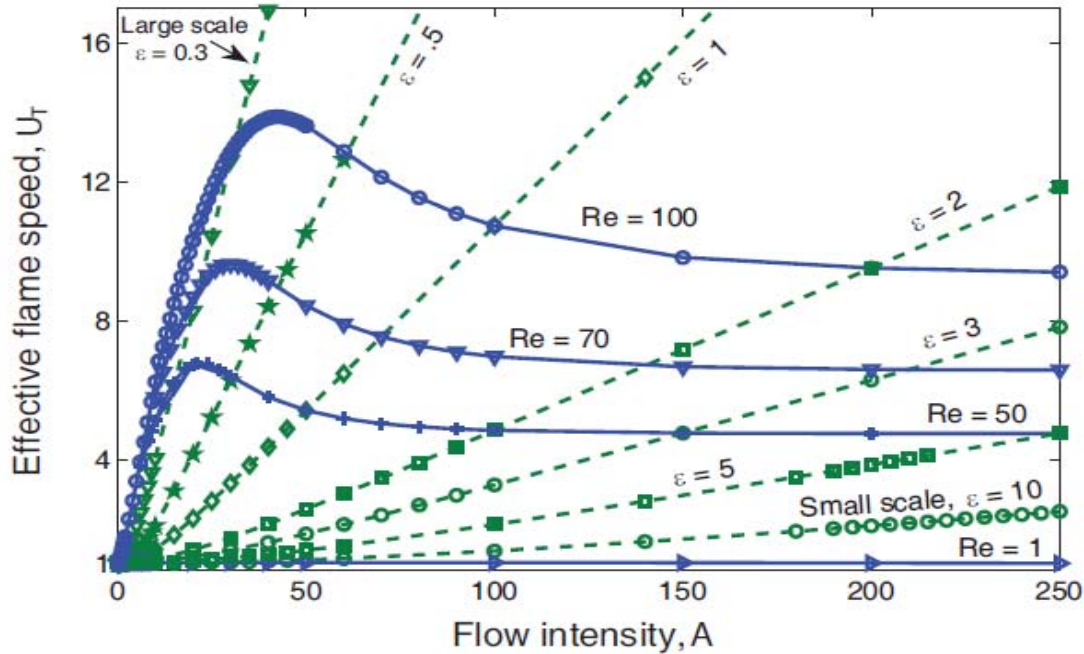


Figure: Effective flame speed U_T in the presence of a Poiseuille flow as a function of the flow intensity A for selected values of the flow scale ε^{-1} and the Reynolds number Re .

Numerical investigation of a supersonic H₂-Air combustion chamber

A. Coclite^{1,2}, L. Cutrone^{b,3}, M. Gurtner⁴, O. Haidn^d, P. De Palma^{a,b} and G. Pascazio^{a,b}

The industrial and scientific communities are devoting major research efforts to develop and assess innovative technologies for advanced propulsion system. Among such technologies, scramjet propulsion systems, based on hydro-carbon combustion is considered as a key issue to achieve better propulsive performance and lower environmental impact. In order to improve the know-how to build more efficient engines with lower emissions, it is necessary to enhance the knowledge of the combustion phenomena. In this context, the simulation of turbulent reacting flows is very useful to cut down experimental costs and to achieve a thorough comprehension of the physical mechanisms involved. The aim of the present work is to analyse both the flow field and the hydrogen supersonic combustion in the combustion chamber of the Institute for Flight Propulsion at TUM¹. The model used to study such a supersonic combustion phenomenon is an extension of the standard flamelet-progress-variable (FPV) turbulent combustion model, combined with a Reynolds Averaged Navìer-Stokes (RANS) equation solver². In the FPV model, all of the thermo-chemical quantities are evaluated by solving transport equations for the mixture fraction Z and a progress variable C . When using a turbulence model in conjunction with FPV model, a probability density function (PDF) is required to compute statistical averages (e.g., Favre average) of chemical quantities. The choice of such PDF must be a compromise between computational costs and accuracy. State-of-the-art FPV models are built presuming the functional shape of the joint PDF of Z and C . The mixture fraction is widely accepted to behave as a passive scalar with a mono-modal behaviour modelled by a β -distribution. Moreover, Z and C are assumed statistically independent so that the joint PDF coincides with the product of the two marginal PDFs. The model employed³ in this work discards these two constitutive hypotheses and evaluates the most probable joint distribution of Z and C without any assumption on their behaviour using the Statistically Most Likely Distribution approach⁴. Preliminary results have been obtained for the supersonic non reacting flow through the combustion chamber with air-jet Mach number equal to 2.1, total pressure of 950 kPa, and total temperature of 1000 K, without any H₂ injection. Figure (1) shows the Mach number contours in the near-strut injector zone. One of the major issue with the supersonic air-breathing system is the fuel injection device, since the topology of the complex shock-expansion structure is crucial for the stability and efficiency of the combustion process. In the final work, supersonic reactive-flow computations will be discussed.

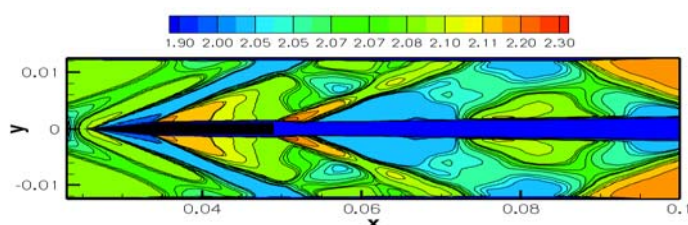


Figure 1: Mach number contours in the near-strut injector zone

¹ Dipartimento di Meccanica, Matematica e Management, Politecnico di Bari, Via Re David 200, 70125, BARI, ITALY

² Centro di Eccellenza in Meccanica Computazionale, Politecnico di Bari, Via Re David 200, 70125, BARI, ITALY

³ Centro Italiano Ricerche Aerospaziali, Via Maiorise, 81043, CAPUA, ITALY

⁴ Institute for Flight Propulsion, Technische Universitat Munchen, Boltzmannstr. 15, 85748, GARCHING, GERMANY

¹ S. Fuhrmann et al., Investigation on Multi-Stage supersonic combustion in a Model combustor, 17th AIAA International Space Planes and Hypersonic System Conference

² L. Cutrone et al., A RANS flamelet-progress-variable method for computing reacting flows of real-gas mixtures, Computers & Fluids 39 (2010), 485-498

³ A. Coclite et al, A general SMLD approach for presumed probability density function in flamelet combustion model. AIMETA 2013 proceeding

⁴ M. Ihme and H. Pitsch, Prediction of extinction and reignition in nonpremixed turbulent flames using a flamelet progress variable model, Combustion and Flames 155, (2008), 70-89

Soot evolution in a turbulent flame via Monte Carlo methods

M. Lucchesi^a, A. Abdelgadir^b, A. Attili^b, F. Bisetti^b, C.M. Casciola^a

Soot formed during the rich combustion of fossil fuels is an undesirable pollutant and health hazard. Recently, *Attili et al.* simulated soot formation and growth in a n-heptane three dimensional non premixed jet flame². using an high order method of moments¹ to model soot. During the simulation, variables relevant to soot formation have been tracked along Lagrangian trajectories.

In this work, Monte Carlo method is used to simulate the soot evolution along selected trajectories as post-processing of the DNS². The Monte Carlo solver is based on an operator splitting approach to separate deterministic processes, as soot nucleation and surface growth, from stochastic events, as soot particles coagulation.

The scope of the work is twofold. Firstly, the results obtained with the method of moments employed in the DNS are compared with those calculated with the Monte Carlo approach. This comparison allows a cross-validation of the two methods and a verification of the hypotheses made to formulate the closure in the method of moments. Secondly, the Monte Carlo approach provides a much richer description of the soot particulate with respect to the method of moments as the complete probability of soot particles size is directly calculated.

Approximately 70 trajectories are selected for this study. At the final DNS time ($t=20\text{ms}$) all these trajectories are located at $Z=0.3$ in mixture fraction space and are characterized by a soot mass fraction approximately equal to the conditional mean at $Z=0.3$. The location of these trajectories is shown as a square in fig. 1a. The distribution of particle diameter for single trajectories (coloured lines) and using the whole ensemble from all the trajectories (black line) are plotted in fig. 1b. All the curves show a strong peak at the size at which soot particles nucleate and a broad distribution at larger size due to coagulation. The differences between different trajectories are due to the different trajectory histories in composition space.

^a Dipartimento di Ingegneria Meccanica ed Aerospaziale, Universita' "La Sapienza", Rome, Italy.

^b Clean Combustion Research Center, KAUST, Thuwal, Saudi Arabia.

¹ Mueller et al., *Comb. Flame* **156**, (2009).

² Attili et al., *Comb. Flame*, in press (2014).

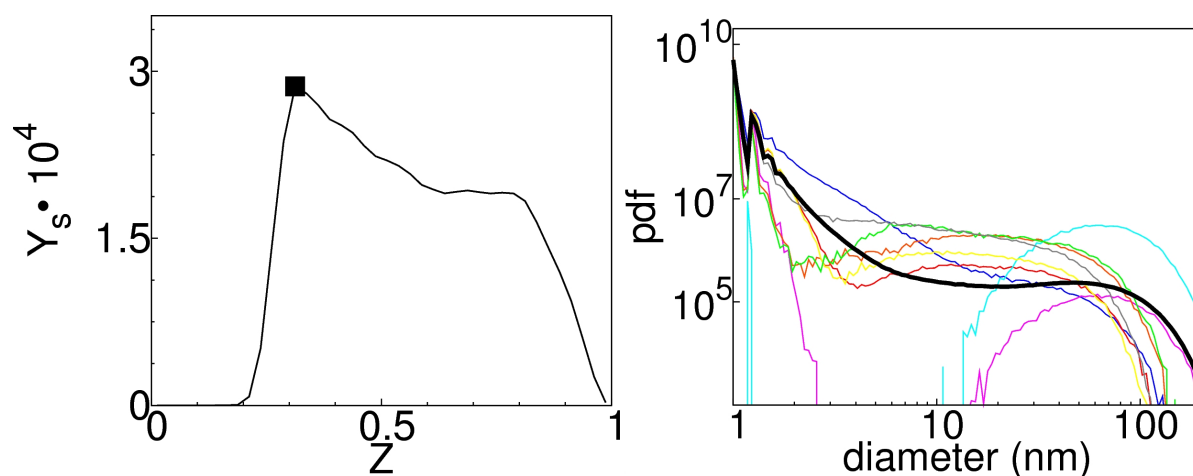


Figure 1: (a) Mean mass fraction as function of mixture fraction at final time (from *Attili et al.*²); the black square marks the location in Z -space for all processed trajectories. (b) Probability density function of particles diameter: average over all trajectories (line) and selected trajectories (colors).

3-Component LDA Measurements of Cold Flow in an Annular Combustor Model

Z. Aslan^a, E. G. Hasdal^b, F. O. Edis^c and K. B. Yuccil^c

Gas turbine combustors have quite complex aerodynamics due to the components such as diffuser, swirler and liner. Air partitioning between the components have a huge effect on combustion efficiency and temperature pattern factor at turbine inlet. Swirlers are commonly used in industrial combustor for flame holding since they create a zone of recirculation flow that traps flame inside. Primary and secondary liner holes contribute to the combustion process and dilution holes substantially affect pattern factor.

In order to have a better understanding of this phenomenon, an atmospheric test rig was designed and developed for cold flow measurements inside a combustor sector model. Measurements are conducted using a 3-component LDA system. Combustor sector model is a simplified rectangular geometry of an annular combustor and is manufactured using acrylic plates in different thicknesses for diffuser, casing and liner. One of the combustor walls is manufactured from glass in order to have good optical access for LDA measurements. A CAD model of the model is showed in Figure 1.

This study focuses on velocity and turbulence results of cold flow experiments in three dimensions in an annular combustor sector model. Figure 2 shows velocity contours and velocity vectors on a vertical plane passing through the centre of the swirler. Two different swirler designs inside the combustor are used for comparison of the swirler performance. The full paper will include detailed results and analyses of velocity and turbulence characteristics at different measurement planes within the combustion region.

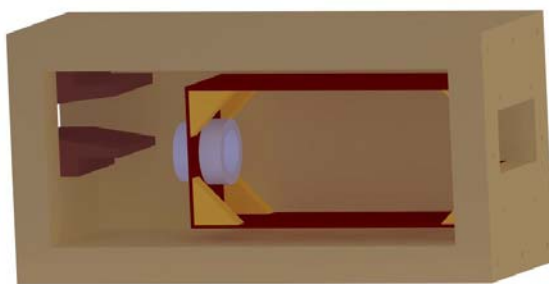


Figure 1 Combustor sector model

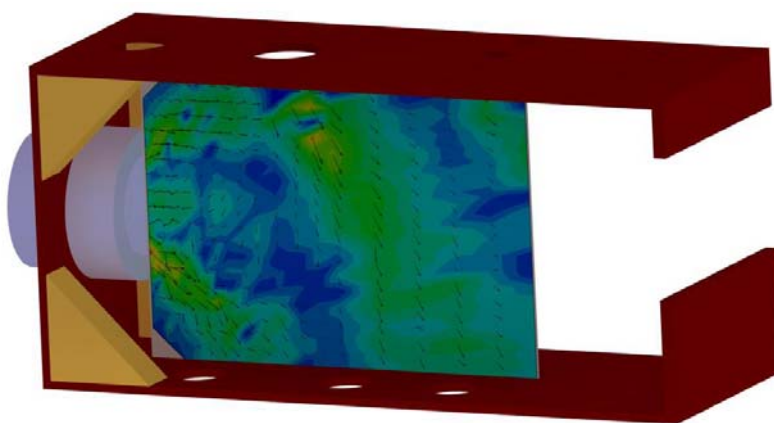


Figure 2 Velocity vectors and contours on a plane through the swirler centreline

^a Kale Aerospace, Tuzla, Istanbul, Turkey

^b EDS Aerospace Technologies, Maslak, Istanbul, Turkey

^c Astronautical Engineering Department, Istanbul Technical University, Maslak, Istanbul, Turkey

Numerical Simulation of Syngas Turbulent Premixed Bunsen Flame

F. Battista^a, F. Picano^b, G. Troiani^c, C.M. Casciola^{ad}

Increasing demand of fuel flexibility prompted the use of hydrogen-based combustible that have been considered a viable alternative to classical fossil fuels in modern engines and gas turbines. While huge attention has been devoted to address the dynamics of the hydrogen flame front evolution in laminar and in turbulent flows¹, less studies, concerning hydrogen-based fuels, e.g. syngas, are present in literature. Syngas is a mixture of hydrogen and carbon-monoxide with few parts of methane and carbon dioxide, depending on the production methodology.

The aim of the present work is to address the syngas flame dynamics affected by turbulence fluctuations with different composition (hydrogen/carbon-monoxide mole ratio, $\alpha = n_{H_2}/n_{CO}$) and different equivalent ratio ($\varphi = (n_{fuel}/n_{air})/(n_{fuel}/n_{air})_{st}$). To this purpose direct numerical simulations of a premixed turbulent Bunsen flame are performed. The simulation is characterized by a Reynolds number (based on the jet diameter and inlet conditions) of $Re = 12000$, and the inlet equivalent ratio and fuel composition of $\varphi = 0.4$ and $\alpha = 0.5$, respectively². Panel (a) of figure shows the instantaneous configuration of the hydrogen (H_2) mass concentration iso-level. The flame appears highly corrugated with sharp peaks protruding towards the products.

Data obtained from the present simulation allow us to evidence the interaction between the flame front and the turbulent fluctuations that are intense due to the high Reynolds number. Panel (b) of figure shows the temperature-based instantaneous progress variable $C_T = (T - T_u)/(T_{ad} - T_u)$ (with T the actual temperature, and T_{ad} and T_u the adiabatic and unburned gas temperature, respectively) that is expected to range from zero to one. In the present simulation we observe, as occurs in pure hydrogen flame, a local overcoming of the adiabatic temperature, induced by the joint effects of turbulent corrugation and differential diffusion of species and radicals involved in the syngas combustion. The intense combustion in the high temperature region is corroborated by the corresponding high OH radical concentration shown in panel (c), moreover, unlike the pure hydrogen flame, local quenching is not observed in flame front cusps, panel (c). This is due to the CO oxidation occurring on the cusps keeping high the local temperature, inhibiting the local quenching. We stress that the peculiar geometry is suitable to address both the basic feature of the considered phenomenon and to study the combustion/turbulence interaction in a configuration very close to the real applications, of fuel injectors. Unlike the plane flame, typically used in the fundamental study of flame/turbulence interaction³, here the cylindrical geometry enforces a mean curvature that affects the turbulence structures and could significantly influence the flame front dynamics. An extensively analysis of this aspect is expected to provide important information on the injectors behavior aimed at improving their efficient design.

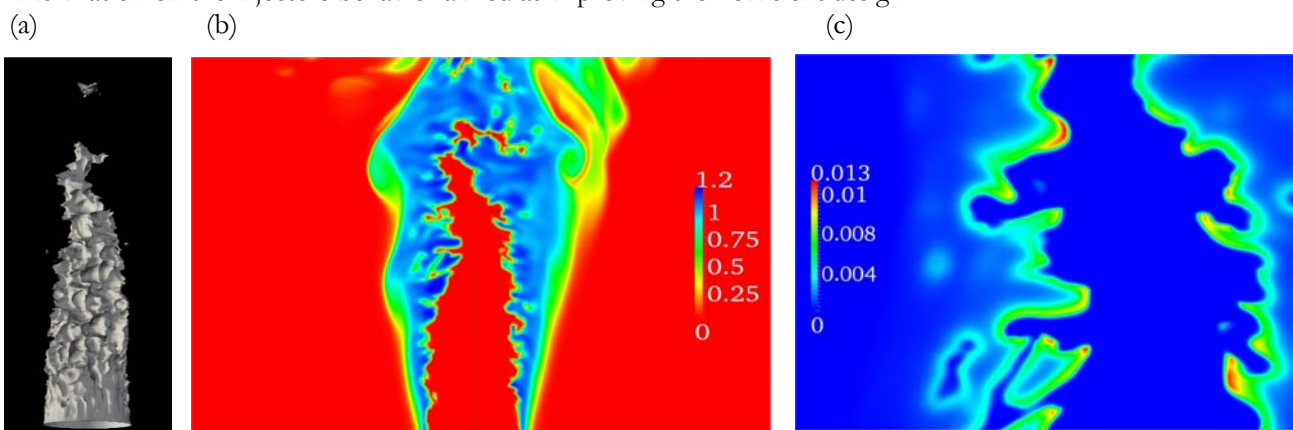


Figure 1: Panel (a): instantaneous configuration of hydrogen mass concentration iso-level. Panel (b): temperature-based instantaneous progress variable $C_T = (T - T_u)/(T_{ad} - T_u)$. Panel (c): instantaneous OH mass concentration, tip flame magnification.

^a Dep of Mechanical and Aerospace Eng, “La Sapienza” University, via Eudossiana 18, 00184 Roma, Italy

^b Dep of Industrial Eng, University of Padova, via Venezia 1, 35131 Padova, Italy

^c Sustainable Combustion Lab, ENEA CR Casaccia, via Anguillarese 301, 00123 Roma, Italy

^d Center of Life Nano Science@Sapienza, Istituto Italiano di Tecnologia, via Regina Elena 291, 00161 Roma, Italy

¹ Hong G Im, JH Chen. Combustion and Flame 131:246-258 (2002)

² F Battista, F Picano, G Troiani, CM Casciola. 14Th European Turbulence Conference, 1-4 September 2013

³ N Chakraborty, RS Cant. Combustion and Flame 158:1768-1787 (2011)

Experiments on Premixed Flame Confined in a Tube with Radial Air Injection

Nilajkumar Deshmukh, S.D. Sharma and Sudarshan Kumar

In a lean combustion with internal flow environment, coupling between pressure fluctuations and heat release fluctuations lead to acoustic instabilities which are seen to enhance combustion efficiency and reduce NO_x emission. However, these acoustic oscillations, when grow sufficiently loud, may cause serious structural damage thereby reducing the life span of gas turbine, jet engines, industrial burners etc.

The aim of the first part of study is to define acoustically stable (without sound) and acoustically unstable (with sound) regions. The second part is focus on study the effect of change in pressure field near to the premixed flame on the amplitude and frequency of the oscillations of instability. This study is carried out for three burner positions from the inlet of the tube as $x/L = 0.25, 0.2$ and 0.1 . For each burner position, stability regions are established for fixed equivalence ratio of 0.7 by varying heat supply and total mean flow rate (20 LPM - 80 LPM) through the tube. The results shows two acoustically unstable regions for 0.1 and 0.2 burner positions and only one acoustically unstable region for 0.25 burner position. The pressure field near to the premixed flame is vary using radially pointed injection and radially diffused injection over a flame using two different ring with eight circumferentially equi-distanced holes (at an angle of 45°) over the burner. The ring with inward holes is used for pointed injection and diffused injection. For diffused injection deflector ring is attached with the ring with inward holes. The other ring with outward holes is used for diffused air injection from the tube wall. This is carried out for three position of ring from the burner as $g/L = 0.033, 0.02$ and 0.006 for equivalence ratio of 0.7 . The SPL data is acquire using NI USB-6212 PC based system with Lab View 7.1. The results show for burner position of $x/L = 0.2$ and ring position from burner as $g/L = 0.033$ there is 25 dB (third mode of 783 Hz frequency) suppression is possible using pointed injection over premixed flame with higher flow rate. Whereas for burner position 0.25 and ring position 0.006 there is 13 dB (second mode of 487 Hz frequency) amplification with pointed injection at higher flow rates and low total mean flow rates is notice. The experiment of diffused injection shows sound amplification more than 12 dB is observed for burner location 0.02 and all ring position studied. The diffusion of air from wall and deflector ring has shown no significant effect on peak SPL.

Shear

Double-layered exact coherent structures in shear flows

M. Nagata^a, K. Deguchi^b

For the past two decades invariant sets of Navier-Stokes equations, often called *exact coherent structures*, have played important roles in understanding subcritical transition from laminar state to turbulence. Several exact coherent structures for various shear flows are known to date and it would be of interest to examine connections among them in terms of their symmetries and to investigate common flow structures that appear during transitional states. For this aim we first consider annular Poiseuille-Couette flow because it could serve as an intermediary between two canonical shear flows without linear instabilities, namely plane Couette flow and pipe flow. Being linearly stable for all Reynolds numbers they are bound to undergo subcritical transition. Although plane Couette flow and pipe flow are very different geometrically, annular Poiseuille-Couette flow recovers plane Couette flow by taking the narrow gap limit and also pipe flow by taking the limit of vanishing inner cylinder though some additional care must be taken of the conditions at the centre.

Recently, by using the steady three-dimensional plane Couette flow solution, which is the first-ever exact coherent structure often referred to as Nagata solution¹, as a seed, a homotopy continuation with respect to the radius ratio of the cylinders has successfully been conducted² to obtain non-axisymmetric solutions in sliding Couette flow, i.e. annular Poiseuille-Couette flow without axial pressure gradient, via transformation from plane geometry. In the course of the homotopy continuation, solutions possessing a double-layered mirror-symmetric flow structure are found to bifurcate from those non-axisymmetric solutions continued from Nagata solution. These double-layered mirror-symmetric solutions in sliding Couette flow are traced back to the previously reported mirror-symmetric solutions^{3,4} in plane Couette flow. Applying further homotopy continuations which concern the adjustment of the axial velocity to a parabolic profile and a smooth change of the basis functions from no-slip to regular conditions at the centre, we demonstrate that only the double-layered mirror-symmetric solutions in annular Poiseuille flow, as shown in Figure 1(a), successfully reach the pipe flow limit, reproducing the double-layered mirror-symmetric solution classified previously as M1 in pipe flow⁵ (see Figure 1(b)).

Also, we present a study on the symmetry connection of invariant sets between plane Couette flow and plane Poiseuille flow and demonstrate the existence of double-layered mirror-symmetric solutions in plane Poiseuille flow⁶ (see Figures 1(c) and (d)).

The double-layered mirror-symmetric exact coherent structures existing in shear flows in common may play an active role in subcritical transition to turbulence⁷.

^a School of Mechanical Engineering, Tianjin University, Nankai District, Tianjin City, CHINA

^b Dep. Mathematics, Imperial College London, South Kensington, SW7 2AZ, UK

¹ Nagata, *J Fluid Mech.* **217**, 519 (1990).

² Deguchi and Nagata, *J Fluid Mech.* **678**, 156 (2011).

³ Gibson et al., *J Fluid Mech.* **638**, 243 (2009)-

⁴ Itano and Generalis, *Phys. Rev. Lett.* **102**, 114501 (2009).

⁵ Pringle and Kerswell, *Phys. Rev. Lett.* **99**(2), 074502 (2009).

⁶ Nagata and Deguchi, *J Fluid Mech.* **735**, R4 (2013).

⁷ Nagata, *J Fluid Mech.* **727**, R1 (2013).

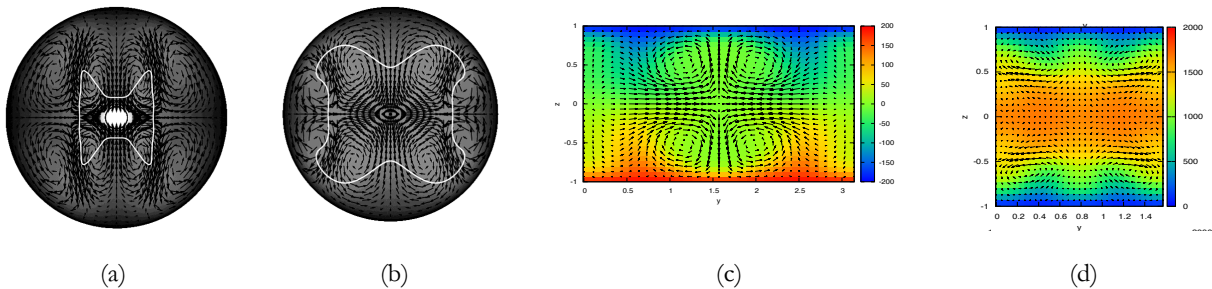


Figure 1: Cross-sectional flow field with a double-layered mirror-symmetric structure. (a) Annular Poiseuille flow. (b) Pipe flow. (c) Plane Couette flow. (d) Plane Poiseuille flow.

Effect of ambient flow inhomogeneity on shear-induced lift on a sphere at finite Reynolds numbers

Jungwoo Kim^a

In particle-laden flows involving particle transport and dispersion, the prediction capability of hydrodynamic forces on the particle in a non-uniform flow is one of the central issues. However, existing analytical expressions and empirical correlations are mainly based on uniform or other simple linear ambient flows such as uniform shear and uniform vortex. Therefore, the objective of this study is to investigate the effect of flow inhomogeneity on shear-induced lift on a sphere. In this study, two kinds of flow inhomogeneity are considered: inhomogeneous shear and inhomogeneous fluid velocity. For the case of an inhomogeneous shear, it is considered the sine profile having the form of $u(x, y)/U_\infty = 1 + K \sin(2\pi \frac{y/D}{L/D})$. Here, U_∞ is the fluid velocity at the center of the sphere, D the sphere diameter, L the period of the sine profile. Also, the Reynolds number is $\frac{U_\infty D}{\nu} = 100$. The present simulations show that the lift forces are decreased with increasing the degree of the flow inhomogeneity (that is, D/L) while the non-dimensional shear rate at the location of sphere center is fixed to be $2\pi \frac{K}{L} = 0.1$. Comparing the change in the lift force with respect to surface-averaged vorticity under uniform inlet shear, that under inhomogeneous shear has certain systematic deviations, which is mainly caused by the viscous effect. Also, it is observed that higher-order components (e.g. $\nabla^3 u$) alone do not generate the shear-induced lift. Rather, they have an indirect influence that they change the shear rate seen by the sphere, and then the lift force is modified. On the other hand, when the fluid velocity seen by the particle is inhomogeneous, the lift is increased (or decreased) with decreasing (or increasing) the surface-averaged fluid velocity. In the final presentation, more details of the shear-induced lift on a sphere in inhomogeneous flow conditions considered would be presented.

^a Department of Mechanical System Design Engineering, Seoul National University of Science and Technology, Seoul 139-743, Korea

Crisis and Chaos in Shear Flows

T. Kreilos^{ab}, B. Eckhardt^{bc} and T.M. Schneider^{ad}

In linearly stable shear flows turbulence spontaneously decays on a characteristic transient lifetime τ . The lifetime sharply increases with Reynolds number Re so that a possible divergence marking the transition to sustained turbulence at a critical point has been discussed, yet the mechanism underlying the increase has not been understood. We demonstrate a mechanism by which the lifetimes increase: a locally attracting orbit forms a *turbulent pocket* via a route-to-chaos sequence of bifurcations, followed by a boundary crisis in which the chaotic attractor turns into a chaotic saddle. The complexity of the turbulence supporting saddle hence increases and it becomes more densely filled with unstable periodic orbits, increasing the time it takes for a trajectory to leave the saddle and decay to the laminar state. We demonstrate this phenomenon in the state space of plane Couette flow and show that as a result characteristic lifetimes vary non-smoothly and non-monotonically with Reynolds number.

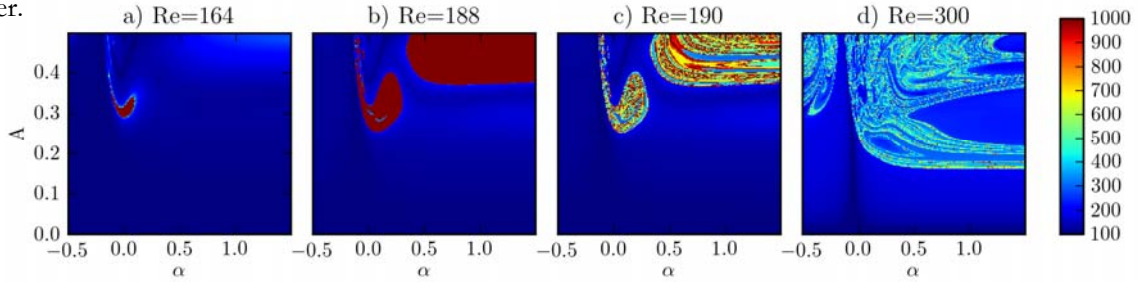


Figure 1: The turbulent saddle fills state space visualized by the lifetime of initial conditions in a 2D section. As Re is increased a new turbulent pocket emerges. [1]

In a small periodic domain, the emerging chaotic saddle is visualized for successively growing Re in Fig. 1. The first known coherent structures are created in a saddle-node bifurcation, with an attracting upper branch whose basin of attraction (small dark-red region in (a)) is separated from the attracting laminar state by the stable manifold of the lower-branch. The fixed-point undergoes a series of bifurcations that result in a chaotic attractor (b). At $Re = Re_c$ the chaotic attractor collides with the lower-branch state, leading to boundary crisis where it turns into a chaotic saddle (c). At higher Re a complex saddle has formed (d).

At higher Re , the same mechanism creates further new pockets embedded in the chaotic saddle (Fig. 2). Once the local chaotic attractor undergoes a boundary crisis it joins the surrounding saddle at a discrete Re . This sudden expansion of the chaotic saddle allows for longer transients quantified by an increased τ . Consequently, a growth of the saddle via discrete bifurcations is associated with non-smooth and non-monotonic variations of the lifetime [2]. Smooth variations are only recovered in a statistical sense.

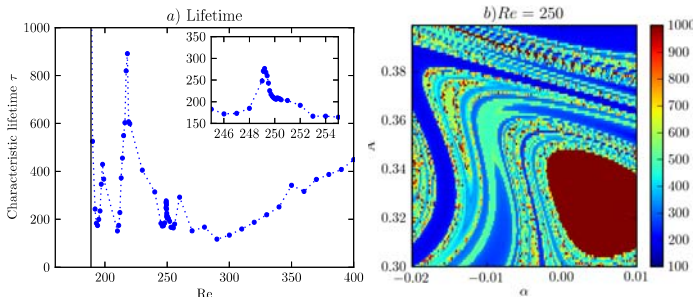


Figure 2: (a) The characteristic lifetime varies non-monotonically as a function of Reynolds number. (b) A new *turbulent pocket* associated with a saddle-node bifurcation of periodic orbits, immersed in the chaotic saddle. At slightly higher Reynolds number, the local chaotic attractor breaks open in a boundary crisis and the dynamical structures join the surrounding saddle. [2]

^a Max Planck Institute for Dynamics and Self-Organization, Am Fassberg 17, 37077 Göttingen, Germany

^b Fachbereich Physik, Philipps-Universität Marburg, 35032 Marburg, Germany

^c J.M. Burgerscentrum, Delft University of Technology, Mekelweg 2, 2628 CD Delft, The Netherlands

^d School of Engineering, École Polytechnique Fédérale de Lausanne, 1015 Lausanne, Switzerland

¹ T. Kreilos, B. Eckhardt *Chaos* **22**, 047505 (2012)

² T. Kreilos et al., *Phys. Rev. Lett.* **112**, 044503 (2014)

Stratified shear flow: experiments in an inclined duct

P. F. Linden, C.R Meyer and S. Vincent

Department of Applied Mathematics and Theoretical Physics, Centre for Mathematical Sciences,
University of Cambridge, Wilberforce Road, Cambridge, CB3 0WA, UK.

We present results of experiments on stratified shear flow in an inclined duct. The duct connects two reservoirs of fluid with different densities, and contains a counterflow with a dense layer flowing beneath a less-dense layer moving in the opposite direction. We identify four flow states in this experiment, depending on the fractional density differences, characterised by the dimensionless Atwood number, and the angle of inclination, which is defined to be positive (negative) when the along-duct component of gravity reinforces (opposes) the buoyancy-induced pressure differences across the ends of the duct. For sufficiently negative angles and small fractional density differences the flow is observed to be laminar (L state) with an undisturbed density interface separating the two layers. For positive angles and/or high fractional density differences three other states are observed. For small angles of inclination the flow is wave-dominated and exhibits Holmboe modes (H state) on the interface with characteristic cusp-like wave breaking. At the highest positive angles and density differences there is a turbulent (T state) high-dissipation interfacial region containing Kelvin-Helmholtz (KH)-like structures sheared in the direction of the mean shear and connecting both layers. For intermediate angles and density differences an intermittent state (I state) is found, which exhibits a rich range of spatio-temporal behaviour and an interfacial region that contains features of other three lower-dissipation states: thin interfaces, Holmboe-like and KH-like structures. We map the state diagram of these flows in the Atwood number – inclination-angle plane, and examine the force balances that determine each of these states. We find that the L and H states are hydraulically controlled at the ends of the duct and the flow is determined by the pressure difference associated with the density difference between the reservoirs. As the inclination increases, the along-slope component of the buoyancy force becomes more significant, and the I and T states are associated with increasing dissipation within the duct. We replot the state-space in the Grashof–angle phase plane and find the transition to the T-state is governed by a critical Grashof number. We find that the corresponding buoyancy Reynolds number of the T-state is of order 100 and that this state is also found to be hydraulically controlled at the ends of the duct, and with the dissipation in balance with the force associated with the along-slope component of buoyancy, the counterflow has a critical composite Froude number. We also present PIV and PLIF measurements of the flow in the different states and examine the relation between the observed flow structures and the mean and fluctuating velocity and density fields.

Biofluid

Wall patterning effects on swimming motion

D. Pimponi^a, M. Chinappi^b, P. Gualtieri^a and C.M. Casciola^a

In recent years, the interest on the dynamics of small particles and microswimmers moving in low Reynolds number flows has largely increased, due to their relevance in micro and nano scale devices. The surface modification is a promising strategy to control separation, sorting, selection, adhesion or clustering. We already know that superhydrophobic (SH) surfaces, when created by geometrical modifications on the surface such as grooves or pillars, induce flow patterns which give rise to completely different dynamics of transported passive particles (Fig.1), compared to those observed near standard homogeneous walls, with apparent trajectory deviations¹.

Our aim is to extend the investigation to the behavior of self-propelled bodies moving close to SH grooved surfaces. The approach based on Boundary Element Methods accounts for all hydrodynamic interactions, even in dealing with complex geometries, allowing to predict velocities and stresses on the swimmer, a simple model of *E.coli* bacteria, hence its trajectories. Such numerical tool might be employed to investigate the reasons why swimmers undergo completely different dynamics depending on the surrounding environment: being close to no slip or free slip surfaces makes them prefer clockwise² or counter-clockwise³ trajectories. The understanding of these phenomena is crucial in designing wall patterns to achieve desired behaviors.

^a Dep. Mechanical and Aerospace Engineering, Sapienza University, Via Eudossiana 18, Rome, Italy

^b Center for Life Nano Science@Sapienza, Italian Institute of Technology, Rome, Italy

¹ Pimponi et al., *Microfluidics and Nanofluidics* **15** (2013).

² Lauga et al., *Biophys. J.* **90** (2006)

³ Di Leonardo et al., *Phys. Rev. Lett.* **106** (2011)

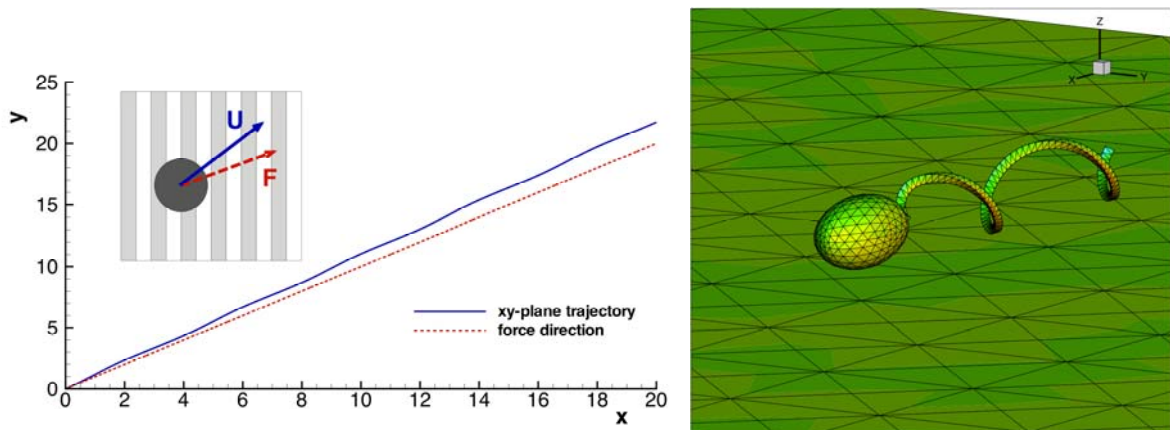


Figure 1: (a) Trajectory deflection for a sphere moving close to a grooved SH wall. (b) Stress distribution (x-component) over a swimmer moving close to a SH wall.

Hydrodynamics and energetics of jumping copepod nauplii and adults

N. Wadhwa^a, A. Andersen^a and T. Kiørboe^b

Copepods are millimetre sized crustaceans which are ubiquitous in aquatic habitats. They swim at intermediate Reynolds numbers, where both viscosity and inertia are important. Moreover, within its life cycle, a copepod goes through drastic changes in size, shape, and swimming mode from the early (nauplius) to the later (copepodid) stages. The swimming Reynolds number (Re) changes by two orders of magnitude in the process. We expect these changes to result in hydrodynamic and energetic differences, ultimately affecting the fitness. To quantify these, we have measured the swimming kinematics (figure 1) and fluid flow around jumping *Acartia tonsa*, at different stages of its life cycle. We show that the flow structures around nauplii and copepodids are topologically different, with one and two vortex rings respectively (figure 2). Our measurements suggest that copepodids are hydrodynamically more inconspicuous in terms of the spatial decay of the flow velocity, and we compare this with some models of swimming organisms. We discuss the increase in energetic efficiency from nauplii to copepodids, due to the change in hydrodynamic regime accompanied with a body form and swimming stroke well suited for it.

^a Department of Physics and Centre for Ocean Life, Technical University of Denmark, DK-2800 Kgs. Lyngby, Denmark

^b National Institute for Aquatic Resources and Centre for Ocean Life, Technical University of Denmark, DK-2920 Charlottenlund, Denmark

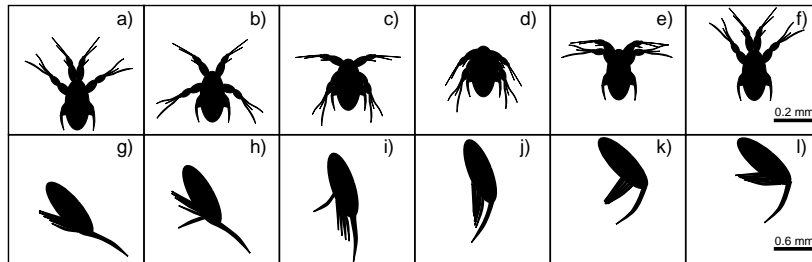


Figure 1: Time series of the jump of a nauplius (a-f) and a copepodid (g-l). In both, the first four images show the power stroke and the last two the recovery stroke, with successive images being 2 ms apart. The nauplius swims using two pairs of antennal appendages. The copepodid uses five pairs of swimming legs for propulsion and the tail (uropod) for steering.

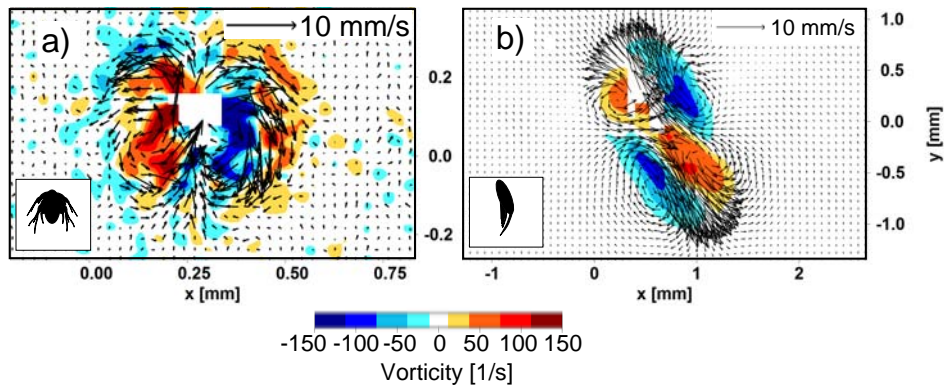


Figure 2: Flow fields around a jumping (a) nauplius and (b) copepodid at the end of their power stroke. (a) $Re = 7.7$, and (b) $Re = 44.7$. (a) and (b) correspond to (d) and (j) in figure 1, respectively. The nauplius jump results in a single vortex ring around the organism, and the copepodid jump in one ring in the front and another in the wake of the organism.

The role of helical swimming and rotational diffusivity on the turbulent 'unmixing' of microorganisms

Salvatore Lovecchio¹, Eric Climent², William M. Durham³ and Roman Stocker⁴

Aquatic microorganisms have developed a wide range of movement strategies to explore their environment and colonize the niches essential for their survival. For example, marine phytoplankton rarely swim in straight lines, but instead follow trajectories that are helical and characterized by substantial rotational noise.

Here we investigate how these departures from the most common assumption in motility models (straight runs) affect their interaction with turbulent flow, an unavoidable feature of their oceanic habitat. Specifically, we explore how the patchiness in the spatial distribution of motile cells triggered by turbulence is modified by helical swimming and rotational diffusion. We find that both the location of patches and the mechanisms of interaction between cells and turbulent structures are different from what has been reported for straight-swimming plankton.

Our findings reveal that phytoplankton may employ these simple departures from straight runs motility to actively control their spatial distribution to find mates or avoid predation.

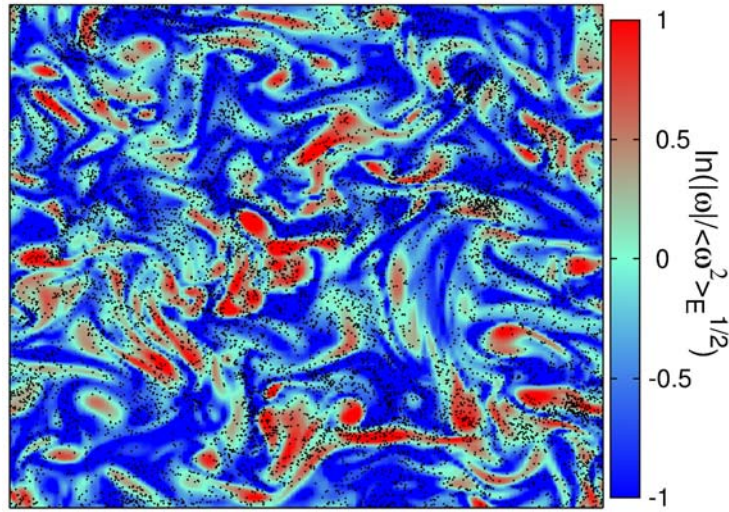


Figure: Horizontal snapshot of a 3D turbulent flow, at $Re_\lambda = 55$ showing cell clustering (black dots) in vorticity regions for elongated and gyrotactic particles. Color code shows the magnitude of fluid vorticity relative to Eulerian average.

¹ ^a Dipartimento di Ingegneria Elettrica, Gestionale e Meccanica, Università degli studi di Udine, 33100, Udine, Italy

² Institut de Mécanique des Fluides, Université de Toulouse, INPT-UPS-CNRS, Allée du Pr. Camille Soula, F-31400 Toulouse, France

³ Department of Zoology, University of Oxford, South Parks Road, Oxford, OX1 3PS, UK

⁴ Ralph M. Parsons Laboratory, Department of Civil and Environmental Engineering, Massachusetts Institute of Technology, 77 Massachusetts Avenue, Cambridge, Massachusetts 02139, USA

Stability of Downflowing Swimming Gyrotactic Microorganism Suspensions: Formation of the Blip Instability

Y. Hwang^a and T. J. Pedley^b

Hydrodynamic focusing of cells is a robust feature in downflowing suspensions of swimming gyrotactic microorganisms. In the early experiments with a downward pipe flow, Kessler (1986, *J. Fluid Mech.*, 173:191-205) observed that the focussed beam-like structure of cells in the region of most rapid downflow exhibits regular-spaced axisymmetric blips, but the mechanism by which the blips are formed has not been well understood yet. For this purpose, in this study, we perform a linear stability analysis of a downflowing suspension of randomly swimming gyrotactic cells in a two-dimensional vertical channel (left in figure). As the flow rate is increased, the basic state exhibits a focussed beam-like structure. It is shown that this focussed beam is unstable with the varicose mode (right in figure), and its spatial structure, wavelength, phase speed, and behaviour with the flow are remarkably similar to those of the blip instability in the pipe flow experiment. An analysis, which calculates the term-by-term contribution to the instability, is designed to understand the origin of the varicose mode. It is found that the leading physical mechanism in generating the varicose instability stems from the horizontal gradient in the cell-swimming-vector field formed by the non-uniform shear in the base flow. This mechanism is found to be supplemented by cooperation with the gyrotactic instability mechanism observed in uniform suspensions.

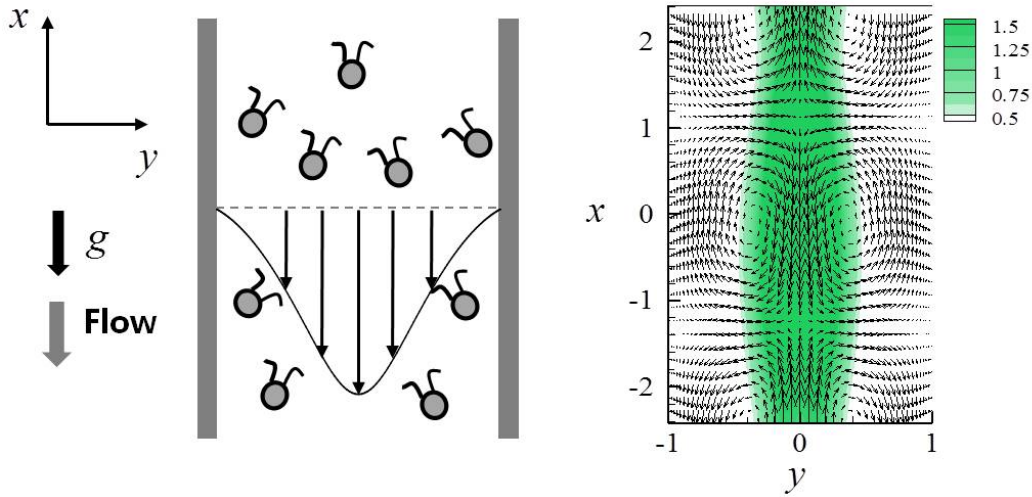


Fig. 1 Schematic flow configuration of the present study (left) and the spatial structure of the most unstable varicose mode (right). In the right, the contours indicate cell number density and the vectors represent the corresponding perturbed velocity field.

^a Dep. Civil and Environmental Engineering, Imperial College London, South Kensington, London, SW7 2AZ, UK

^b Dep. Applied Mathematics and Theoretical Physics, University of Cambridge, Wilberforce Road, Cambridge, CB3 0WA, UK

Flagellar synchronization with a periodic background flow

Greta Quaranta^a, J. Westerweel^a, M-E Aubin-Tam^b and Daniel Tam^a

Eukaryotic cilia and flagella are central to many micron scale physical processes such as locomotion, fluid transport, mixing and mechanical signal transduction. These processes rely on the unique ability of thousands of cilia to spontaneously beat and synchronize. Elucidating the physical mechanisms underlying flagellar synchronization has been at the center of several recent studies. Different mechanisms have been suggested and investigated including hydrodynamic interaction^{1,2,3} and "cell-body rocking"^{4,5}. Here we address the following question: how difficult or easy it is for flagella to synchronize?

In this study, we focus on biflagellated green algae *Chlamydomonas reinhardtii*. We investigate experimentally synchronization between the flagella and an external periodic forcing, whose amplitude and frequency can be controlled and varied. An open flow chamber containing a suspension of cells is placed on a piezoelectric stage mounted on an inverted microscope (see figure 1). A micropipette is inserted into the bulk of the fluid with no direct contact between the pipette and the walls of the chamber. A single cell is captured at the tip of the pipette by suction, allowing the motion of the flagella to be visualized. The actuation of the piezo-stage results in a periodic translation of the flow cell with respect to the micropipette, which remains fixed in the laboratory frame of reference. A relative motion between the cell (fixed element) and the surrounding fluid (periodic oscillator) is generated. This background flow is used as an external hydrodynamic forcing whose amplitude and frequency can be imposed to investigate synchronization. The deformations of the flagella are recorded with a sCMOS camera at 1000 fps. Images are processed to extract the stroke sequence and the beating frequency.

Flagella of *Chlamydomonas reinhardtii* spontaneously beat at frequency of about 50 Hz. With the external forcing applied, a shift in the beating frequency towards the frequency of the external forcing is observed. Forcing of high enough amplitude trigger the synchronization of the two flagella with the background flow. The synchronization regions are fully characterized as a function of the amplitude and the frequency of the background flow. The relevance of these results to previous studies on flagella synchronization¹⁻⁵ are discussed.

^a Laboratory for Aero- and Hydrodynamics, TU Delft, Leeghwaterstraat 21, 2628 CA, Delft, Netherlands

^b Bionanoscience Department, TU Delft, Lorentzweg 1, 2628 CJ, Netherlands

¹ Goldstein et al., *Phys. Rev. Lett.* **103**, 16 (2009)

² Goldstein et al., *Phys. Rev. Lett.* **107**, 14 (2011)

³ Golestanian et al., *Soft Matter*, **7**, 3074 (2011)

⁴ Friedrich and Jülicher, *Phys. Rev. Lett.* **109**, 13 (2012)

⁵ Bennet and Golestanian, *Phys. Rev. Lett.* **110**, 14 (2013)

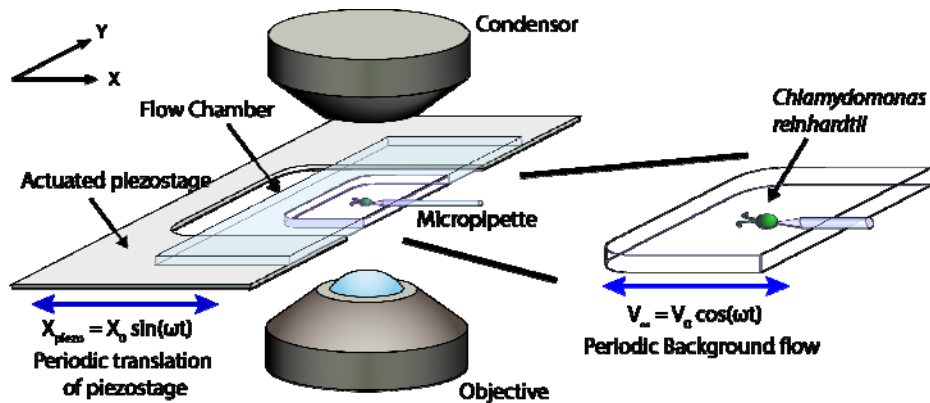


Figure 1: Schematic of the experimental setup

Hydrodynamics of Filter Feeding in Choanoflagellates

Anders Andersen^a, Lasse Tor Nielsen^b, and Thomas Kjørboe^b

Many aquatic microorganisms are filter feeders which use cilia or flagella to drive water through filter structures to capture prey such as bacteria. In this study we focus on choanoflagellates which are unicellular organisms that form a biologically important group of aquatic filter feeders¹. Far field flows created by choanoflagellates have been successfully described using point force models and have recently been measured in detail for a sessile species². However, the essential near field of the feeding flow in choanoflagellates is poorly understood and has not been resolved experimentally. Studies indicate that the pressure differences created by the beating of the single flagellum are insufficient to produce an adequate water flow through the collar filter, the mechanism which is believed to transport prey to the cell. The collar is composed of closely spaced microvilli which are arranged as a palisade, and the low porosity of the filter provides high resistance to the water flow. We present high-speed video of live material showing the particle retention and the beating of the flagellum in the choanoflagellate species *Diaphanoeca grandis*. Our experimental goals are to describe the feeding flow and the flagellum motion and to understand the effect of the filter resistance on the feeding flow. In addition we aim to describe the effect of the so-called lorica structure which surrounds the cell and directs the feeding flow toward the filter. Theoretically we model the filter resistance and the force generation by the flagellum using low Reynolds number hydrodynamics, and we suggest that the high filter resistance significantly constrains cell shape and filter morphology.

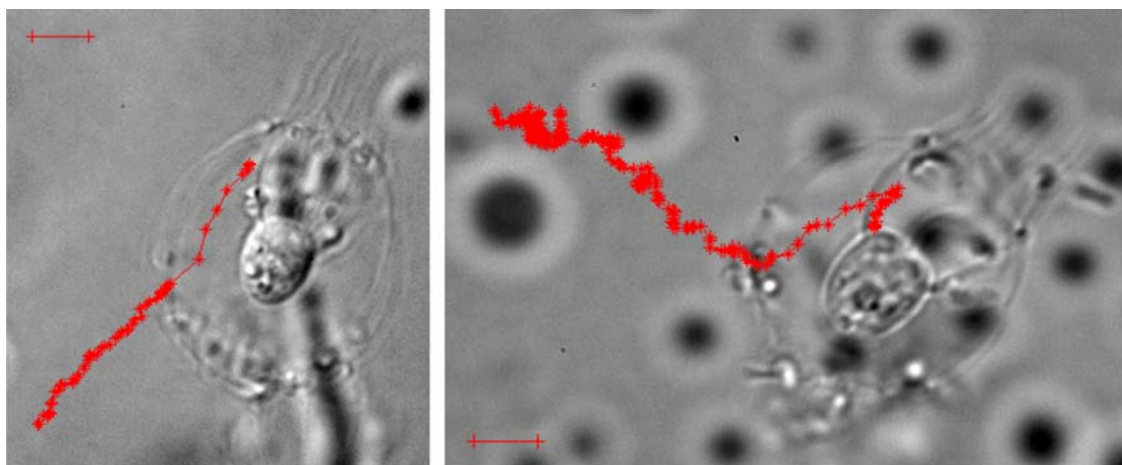


Figure 1: Typical particle trajectories in the choanoflagellate feeding flow observed with light microscopy, which shows the particle acceleration as the particle approaches and is eventually caught in the funnel shaped collar filter extending from the cell. In both images the scale bars are 5 μm in length.

^a Department of Physics, Technical University of Denmark and Centre for Ocean Life, Villum Kann Rasmussen Centre of Excellence

^b National Institute of Aquatic Resources, Technical University of Denmark and Centre for Ocean Life, Villum Kann Rasmussen Centre of Excellence

¹ Fenchel, Prog. in Protistology **1**, 65-113 (1986).

² Roper et al., Phys. Rev. Lett. **110**, 228104 (2013).

Subcritical bifurcation in asymmetric stenotic pipe flow

J.-Ch. Loiseau^{ab}, S. Acharya Neelavara^c, J.-Ch. Robinet^a and E. Leriche^b

Atherosclerosis is a widely spread cardio-vascular disease predominant in the industrialised countries. It is a condition in which an artery wall thickens as a result of the accumulation of fatty material, e.g. cholesterol, eventually leading to health conditions as serious as break-up of the blood vessels walls. Over the past decades, numerous experimental and numerical studies have modelled this geometry of sick arteries using idealised axisymmetric stenotic pipes having non-elastic walls. Sherwin & Blackburn¹ have investigated the global instability and resulting transition to unsteadiness occurring for non-pulsatile flows within such geometries. They have found that, as for two-dimensional confined jet flows, the first bifurcation taking place is a symmetry-breaking one related to a Coanda-like instability triggering a deflection of the stenotic jet from the pipe's centreline. The flow then displays self-regenerating localised turbulent puff-like structures in the vicinity of the stenosis throat before being eventually convected further downstream. Unfortunately, recent experimental results have put in the limelight large discrepancies between these numerical predictions and the actual experimental observations.

These discrepancies might be explained by small asymmetric defects inherent to any experimental setup. The aim of the present work is thus to fully characterise the influence of such small defects of the geometry on the linear stability of the flow. This problem is essentially addressed by fully three-dimensional global stability analyses and direct numerical simulations (DNS) of the non-pulsatile flow within a stenotic pipe with non-elastic walls where the throat of the stenosis has been slightly offset from the pipe's centreline. Such modelling of these geometric defects has already been used by Varghese et al.² and Griffith et al.³ who have also investigated this problem. Varghese et al.² have observed in their DNS that, as for the Coanda-like instability in the axisymmetric stenotic pipe flow, small eccentricity of the stenosis throat could potentially trigger an early wall reattachment of the stenotic jet yielding to strong asymmetry of the reversed flow region as illustrated on the figure. Griffith et al.³ and the present authors have moreover found that, for both axi- and asymmetric cases, evidences exist relating this symmetry-breaking instability to a subcritical pitchfork bifurcation of the flow. Despite the underlying physical instability mechanisms appearing to be the same in both cases, it is worthy to note that this early wall-reattachment of the stenotic jet occurs at a substantially lower Reynolds number in the eccentric case, as low as $Re=360$ for a 0.1% offset of the stenosis throat as compared to $Re=721$ in the axisymmetric case. Moreover, steady state computations performed by the present authors have highlighted that, further increasing the Reynolds number, these wall-attached solutions are experiencing a secondary bifurcation. This new bifurcation appears to be related to a centrifugal instability of the strongly asymmetric reversed flow region. Further calculations will fully characterise these new steady states and their subsequent transition to unsteadiness.

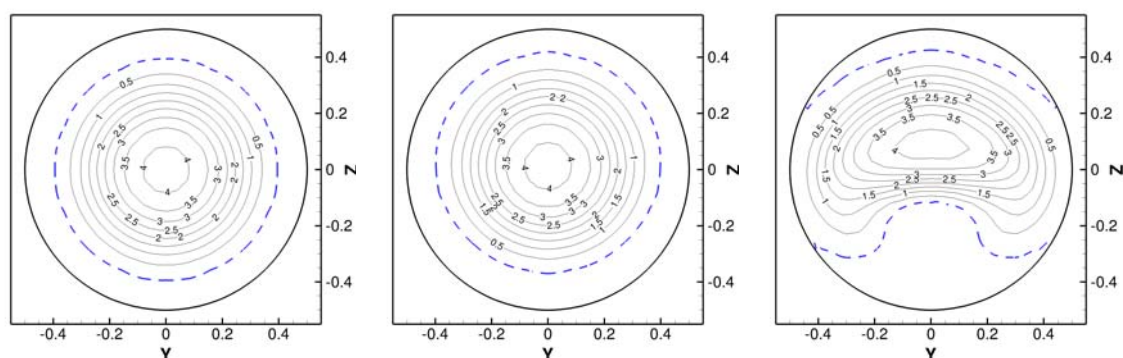


Figure: Streamwise velocity contours for stenotic pipe flows at $Re=400$ in the $x=5$ cross-sectional plane. Left: Axisymmetric. Middle: 0.1% eccentricity. Right: 1% eccentricity.

^a DynFluid, Arts et Métiers ParisTech, 151 Bd de l'hôpital, 75013 Paris, France

^b Laboratoire de Mécanique de Lille, Université Lille-1, 59650 Villeneuve d'Ascq, France

^c LIMSI-CNRS, B.P. 133, 91403 Orsay Cedex, France

¹ Sherwin & Blackburn, *J. Fluid Mech.*, **533**, 297 (2005)

² Varghese et al., *J. Fluid Mech.*, **582**, 253 (2007)

³ Griffith et al., *J. Fluid Mech.*, **721**, Rapids (2013)

Net transport mechanisms in the upper human lung

K. Bauer^a, C. Brücker^a

Especially for drug delivery and aerosol transport the knowledge about transport pathways is important. At normally ventilated lungs gas transport down to the lower airways is dominated by convective mass transport in the upper bronchial tree. However, if the tidal volume drops below the anatomic dead space of the bronchial tree, as this is the case during High Frequency Oscillatory Ventilation (HFOV), bulk flow convection is not sufficient to maintain mass exchange within the distal branches. A net cycle-to-cycle transport has to occur.

In order to investigate mass transport in the human lung a 3D model of the upper bronchial tree is generated. The geometry is based on statistical data from Weibel¹ and Horsfield² and consists of 6 bifurcating generations. Unsteady numerical flow simulations are carried out with boundary conditions employing parameters for conventional mechanical ventilation (CMV) as well as for HFOV conditions.

Qualitatively, the flow patterns are similar for CMV and HFOV. The instantaneous streamlines during inspiration (Fig. 1a)) and expiration (Fig.1b)) demonstrate typical pathways during ventilation, exemplarily shown here for CMV. The core streamlines indicate a straight flow from the top to the bottom and vice versa. The streamline location in the trachea reflects the distribution into the lower branches. This means particle location in the trachea determines its pathway into the distal branches. Near wall, low inertia flow is redirected due to Dean vortices which are generated by centrifugal forces in the branching curvature. Hence, these outer regions predominantly contribute to mixing in the lung. Further mixing occurs during the phases of flow reversal and is enhanced at HFOV by Pendelluft.

Information about net flow is gained by integrating the unsteady flow velocities in the branching tree in time over one breathing cycle. The remaining net flow is called steady streaming and is typical for oscillatory flows with asymmetric flow in opposite directions. Steady streaming patterns are further investigated. Strength and structure of resulting flow patterns are analysed for varying Womersley and Reynolds numbers according to CMV and HFOV conditions. Geometry as well as the peak Reynolds number govern the net flow phenomena. Increasing frequencies seem to be of minor importance for net streaming flow.

^a Inst. of Mechanics and Fluid Dynamics, TU Bergakademie Freiberg, Germany

¹ Weibel, Springer-Verlag (1963).

² Horsfield, J. Appl Phys. 24(3), 373 (1968)

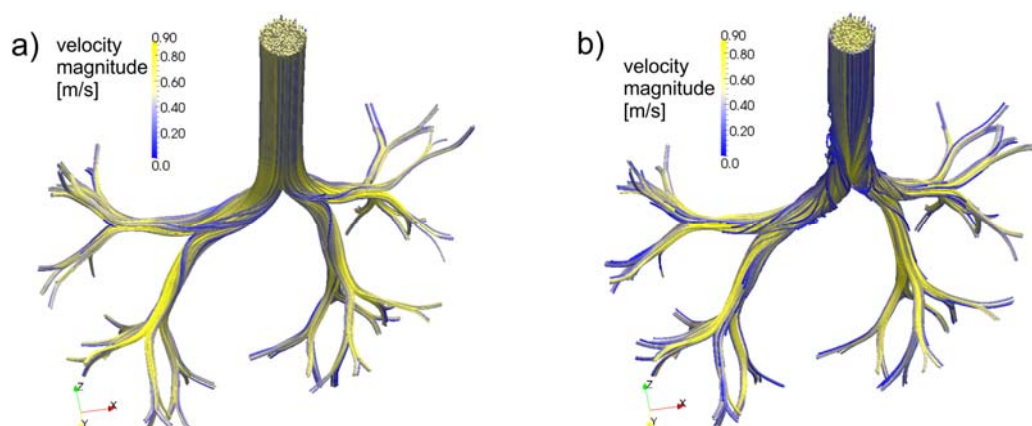


Figure 1: Streamlines colour coded with the velocity magnitude, a) deceleration phase during inspiration, b) deceleration phase during expiration.

Structural sensitivity of flow dynamics through aneurysms

Shyam Sunder Gopalakrishnan*, Benoît Pier* and Arie Biesheuvel*

Aneurysms are localized permanent arterial dilatations due to disease or other complex processes that result in the weakening of the arterial walls¹. Of these, abdominal aortic aneurysms (AAA) are commonly found in the abdominal aorta and are characterised by a bulge about the vessel centerline. Recent studies^{2,3,4} have used different idealized AAA geometries to investigate the flow dynamics. In the present work, we address more specifically the sensitivity of these results to details in the geometry and the pulsatile flow rate waveform. Figure 1(a) shows two equivalent AAA geometries of sinusoidal and gaussian shapes respectively. Though both AAA geometries are almost indistinguishable, small but significant differences in flow dynamics are observed. Flow separation is found to occur earlier in the pulse cycle in a sinusoidal AAA, with the flow field obtained in a gaussian AAA lagging in phase in comparison to a sinusoidal AAA. A linear stability analysis using these two geometries reveals similar trends. The dominant mode occurs for azimuthal mode number $m = 3$, but it is seen that the sinusoidal AAA has significantly higher growth rates than the gaussian AAA (see figure 1(b)). Also, the sensitivity to specific flow conditions is investigated by using different flow rate waveforms.

These findings reveal a surprisingly strong structural sensitivity of the flow dynamics through model aneurysms. Implications for patient-specific modeling will be discussed.

*Laboratoire de mécanique des fluides et d'acoustique (CNRS - Université de Lyon), École centrale de Lyon, 36 avenue Guy-de-Collongue, 69134 Écully, France

¹Lasheras, J. C., *Annu. Rev. Fluid Mech.* **39**, 293 (2007).

²Salsac, A. -V., Sparks, S. R., Chomaz, J. -M. & Lasheras, J. C., *J. Fluid Mech.* **560**, 19–51 (2006).

³Sheard, G. J., *J. Eng. Math.* **64**, 379–390 (2009).

⁴Gopalakrishnan, S. S., *PhD thesis, École centrale de Lyon* (to be presented on 19/02/2014).

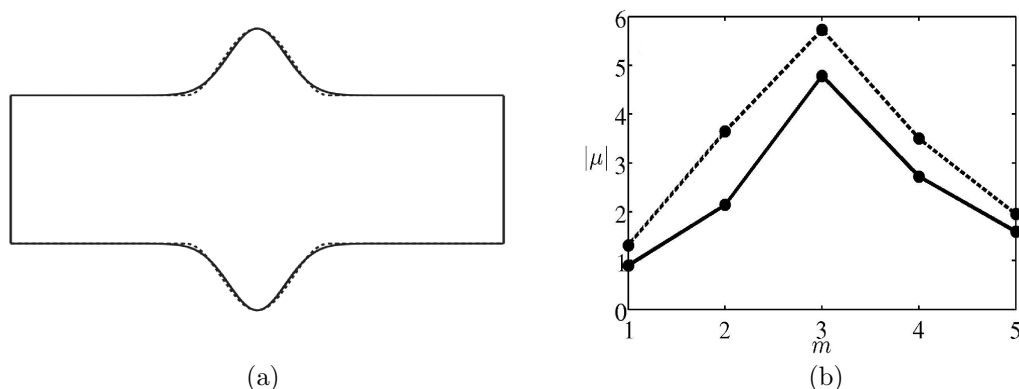


Figure 1: (a) The sinusoidal geometry is shown using dotted lines and the gaussian equivalent is shown using continuous lines. (b) The absolute value of Floquet multipliers corresponding to sinusoidal (dotted line) and gaussian (continuous line) AAA geometries.

Microfluidics of sugar loading in leaves

Hanna Rademaker^a, Julia Dölger^a, Alexander Schulz^b, Johannes Liesche^b and Tomas Bohr^a

The transport of sugars is of paramount importance for plants, since all growth is based upon carbon from the sugars generated by photosynthesis in the leaves. The long-distance translocation of sugars takes place in the phloem vascular system and is believed to be driven by pressure differences caused by osmosis due to the concentration differences of sugars between the leaves, where they are produced, and the roots or new shoots, where they are used. It is possible to model this translocation by standard hydrodynamical equations (without “active” components) and from that to infer the typical length scales for the phloem tubes¹. A question of considerable current interest is how far this hydrodynamical treatment can be taken back into the “pre”phloem: the pathway of the sugar in the leaves from the mesophyll cells, where the sugar is produced, to the sieve elements of the phloem, where it is shipped away for growth.

An interesting case is the so-called polymer trap mechanism², where sucrose molecules are enzymatically converted into heavier sugar molecules (like raffinose and stachyose) after diffusing through the interface between bundle sheath cell and intermediary cell (cp. Fig. 1). The sucrose molecules move into the intermediary cell through small channels (plasmodesmata) without “active” sugar transporters, while the heavier sugar molecules do not seem to be able to move back through these plasmodesmata. It was recently pointed out³ that the hydro-dynamic radii of the different sugars do not seem sufficiently different for the plasmodesmata to carry out this filtering process efficiently. The inner structure of the plasmodesmata is not exactly known, but if the plasmodesmata are narrow enough to avoid back-diffusion of raffinose and stachyose, they will also strongly hinder the diffusion of sucrose, making this mechanism untenable.

We argue in the present work that bulk osmotic water transport from bundle sheath cell to intermediary cell is probably an important component. In particular, we show that it is possible that the large concentration of heavier sugars built up in the intermediary cell creates an osmotic water flow through the plasmodesmata, which strongly enhances the translocation of sucrose and makes the polymer trap work.

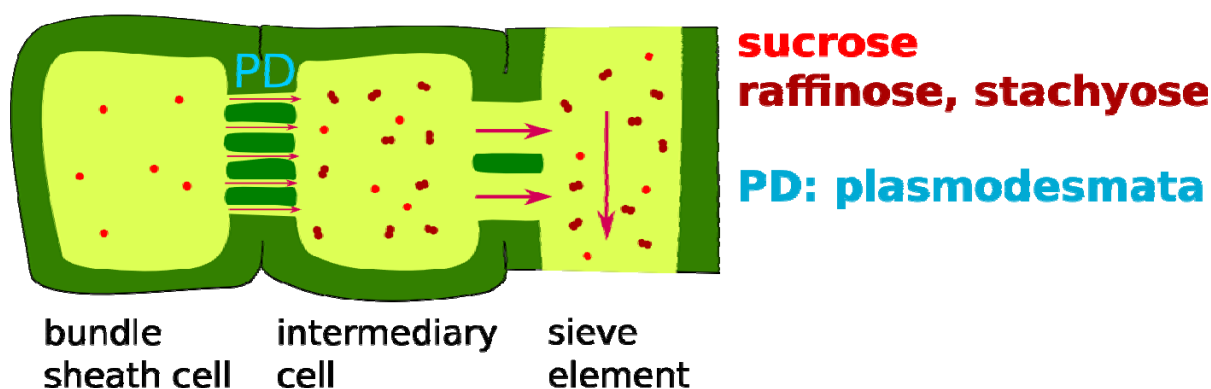


Figure 1: The mechanism of the “polymer trap” loading mechanism. Sucrose enters the bundle sheath cell (left) and moves into the intermediary cell (center), where it is transformed into raffinose and stachyose, present at a much higher concentration. From there it moves rather easily into the sieve element (right) and is translocated to the rest of the plant.

^a Department of Physics, the Technical University of Denmark

^b Department of Plant and Environmental Sciences, University of Copenhagen, Denmark

¹ K. H. Jensen, J. Liesche, T. Bohr, and A. S. Schulz *Plant, Cell & Environment* **35**, 1065 (2012)

² A. E. Rennie and R. Turgeon, *Proc. Natl. Acad. Sci. USA* **106**, 14162 (2009)

³ J. Liesche and A. Schulz, *Frontiers in Plant Science* **4**, 207 (2013)

Study of the flow in coronary bifurcations with bifurcated stent angioplasty

J. García^a, F. Manuel^a, F. Castro^b, A. Crespo^a, J. Goicolea^c and J.A. Fernández^c

This work is a result of previous investigations with conventional stents and arises after the recent emergence of several devices specifically designed for coronary bifurcations angioplasty. The aim is to compare the hemodynamic performance of these new devices compared to conventional devices and techniques in a coronary bifurcation model. Three different stenting techniques: simple stenting of the main vessel, simple stenting of the main vessel with kissing balloon in the side branch and culotte have been considered. To carry out this study an idealized geometry of a coronary bifurcation is used. Both experiments in the laboratory and numerical simulations will be used, focusing on important factors for the atherosclerosis development, like the wall shear stress, the oscillation shear index, the pressure loss and the vorticity. Micro-CT images were used to reconstruct coronary stents implanted in silicone models (Fig. 1). First, steady simulations are carried out with the commercial code ANSYS-Fluent, and then, experimental measurements with PIV (Particle Image Velocimetry) obtained in the laboratory are used to validate the numerical simulation. The steady computational simulations show a good overall agreement with the experimental data. Second, pulsatile flow is considered to take into account the transient effects. The results obtained permit to evaluate whether the new designs really result in an improvement in the hydrodynamic behaviour of the devices. Obviously the present simulations focus only on the hemodynamic aspects and other factors should be taken into account before choosing the most appropriate stenting technique. Moreover, even if only fluid dynamic criteria are considered, it should be noticed that the configurations studied are idealized coronary bifurcations. The behaviour patterns obtained in this work should be verified in more realistic geometries.

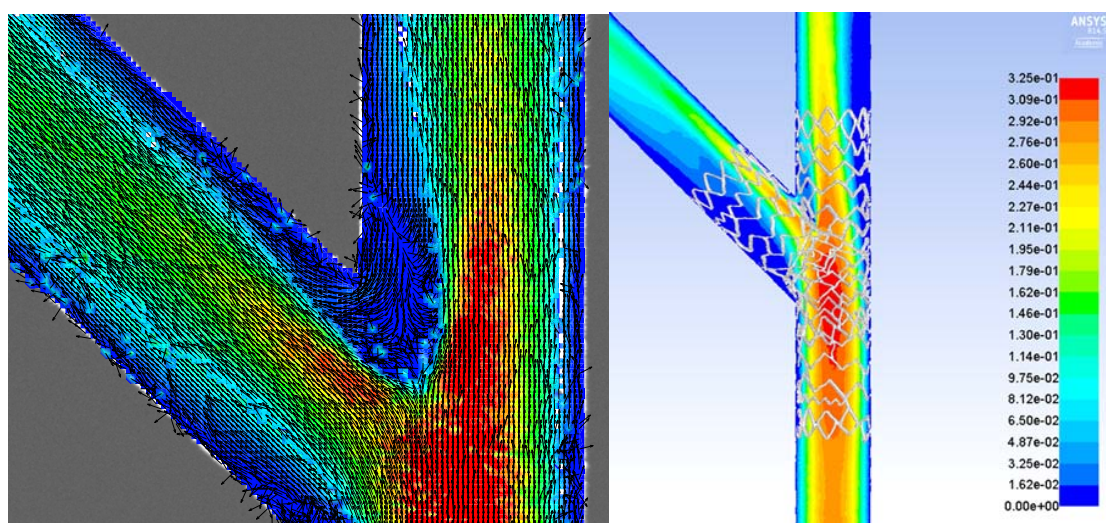


Figure 1: Contours of mean velocity obtained (a) experimentally and (b) numerically in the culotte technique.

^aDep. Ing. Energética y Fluidomecánica, ETSI Industriales. Universidad Politécnica de Madrid, Spain.

^bDep. Ing. Energética y Fluidomecánica, Escuela de Ingenierías Industriales. Universidad de Valladolid, Spain.

^cHospital Universitario Puerta de Hierro. Majadahonda, Spain.

Modelling flow through the Endothelial Glycocalyx Layer

P. Sumets^a, J. Cater^a and R. Clarke^a

Numerous vascular diseases result from abnormal blood flow. Micro-vessels walls are coated by a brush-like layer, the Endothelial Glycocalyx Layer (EGL), which acts as a buffer between blood and the wall. One of the main physiological functions of the EGL is provide biomechanical responses. In particular, it is believed to act as a mechanotransducer of fluid shear stress to endothelial cells. The behaviour of the EGL is difficult to measure in-vivo; hence a mathematical model has the potential to offer some useful insights.

We treat the EGL as a poroelastic medium, and flow within the vessel lumen as a viscous Newtonian liquid. A biphasic mixture model is used to approximate the dynamics of the EGL, employing Brinkman's Equation for the fluid phase and forced Navier's Equation for the solid phase. An efficient method for solving these linear coupled PDE's is the Boundary Element Method (BEM). However, implementation of BEM is complicated by the appearance of integrals over the entire physical domain, rather than just surface integrals, when the governing equations are written in integral form. These domain integrals arise due to the momentum transfer terms within the biphasic medium. In order to take advantage of the computational efficiency of BEM effectively, these domain integrals must be converted into surface integrals.

Therefore, we have developed an exact technique to convert these domain integrals to surface integrals. This is achieved through the construction of a carefully chosen complementary problem, which requires solving the physical equations under forcing by appropriate Green's function tensors. To this complementary solution, and the solution to the fluid phase, we have applied Lorentz Reciprocal relation to eliminate the domain integrals. As a result, we have derived a true boundary integral representation of biphasic flow, which we have then solved numerically using BEM for regimes representative of the EGL.

^a Dept. of Engineering Science, The University of Auckland, New Zealand

Simulation of the movements and deposition rates of oblate and prolate nano- and micro-particles in a virtual model of the human airways

Holmstedt, E^a, Åkerstedt, H^b, Lundström, T.^c

A model simulating the movements of oblate and prolate spheroids in the nano- and micro-scale was developed. The aim was to simulate the environment of the human lung and the deposition of fibres during inhalation, but the model is in itself general and can be applied for different flows and geometries for small fibre Stokes and Reynolds numbers. The model simulates an evenly random distribution of particles and follows them in a steady, laminar, fully developed parabolic flow in a straight airway. The effect of gravitational settling and Brownian motion was included and the particle was said to be deposited when its centre of mass moved outside the wall of the bronchi. To study the effect of the change of particle shape alone without the influence of particle mass the diameters of the particles was change in correlation with the aspect ratios so the volume of the particles remained constant.

A statistical study was done comparing the deposition rates of oblate and prolate spheroid of different size and aspect ratio as they travel down the narrowing bronchi. The model shows a clear correlation between increased depositions with increase of the particle size and yielded a higher deposition for oblate spheroids as compared to prolates with the same aspect ratio. There was also a noticeable influence on the results from changing the aspect ratios of the particles. The deposition rates was the lowest for both the oblate and prolate spheroids with the highest aspect ratio, but interesting enough the peak deposition was not for the spherical particles but for those who were slightly oblate with an aspect ratio of about 1.5.

A study of the motion and orientation of a single oblate and prolate particle has also been done. To more clearly be able to see the particles distinct motion the simulation was done for a micro-particle with a very high aspect ratio. First the motion of the particles was only influenced by the flow field with a periodically flip over 180°, Jeffery orbits. This behaviour was observed for both oblate and prolate particles although the period between flips was much shorter for oblates. When the effect of Brownian motion was introduced on the particle the overall behaviour of the prolate spheroids remained mainly the same. The periodicity of the flips, however, increased and a randomization of them was observed. The behaviour of the oblate particles on the other hand was greatly changed to a seemingly random tumbling behaviour.

^a Division of Fluid and Experimental Mechanics, LTU, Luleå, Sweden.

^b Division of Fluid and Experimental Mechanics, LTU, Luleå, Sweden.

^c Division of Fluid and Experimental Mechanics, LTU, Luleå, Sweden.

Experimental study of the effect from bio-solid particles on fully developed turbulent duct flow

Ammar Hazim Saber^{a,b}, T. Staffan Lundström^a and J. Gunnar I. Hellström^a

Turbulent flow characteristics can be changed in the presence of particles. Results from the literature yields an enhancement in turbulence with large particles caused by transfer of kinetic energy to turbulence through vortex shedding behind the particles. This mechanism is related to the particle Reynolds number. Smaller particles will instead attenuate the turbulence by acting like dampers for eddies that they follow. For spherical particles this can be related to the ratio between the particle diameter and the turbulent enargic length scale. Recently, turbulent flow with non-spherical particles has been in focus due to its wide applications in industry. In numerous cases, more dissipation in turbulence energy was reported as compared to spherical particles¹. In addition to being non-spherical most of the bio-fuel particles are irregular and have a random shape. Over that, the surface roughness of these particles is function of resources and methods of milling, as one example see the wood particles in figure 1.

Experiments were performed in a duct with nearly two-dimensional fully developed turbulent airflow. Using a high-resolution PIV system, the effect of the presence of spherical glass particles and pine wood particles on the turbulent intensity was investigated and compared with results from the literature. The results with glass particles showed good agreement with results from the literature see figure 2. On other hand, wood particles dissipated more turbulent kinetics energy see figure 2. This may be due to less density ratio compared to glass and plastic particles leading to a lower particle Reynolds number. Also more dissipation may emanate from the near surface region^{2,3} caused by the rough surface of the wood particles. The results are in agreement with most previous studies showing a reduction in turbulent intensity with non-spherical particles as compared to spherical particles.

^a Divi. of Fluid and Experimental Mechanics, Lulea University of Technology, Luleå- Sweden.

^b Mechanical Engineering Dep., University of Mosul – Iraq

¹MANDO, *International Journal of Heat and Fluid Flow*, **30**(2), 331 (2009)

² BELLANI et al. *Journal of Fluid Mechanics*, **1**(1), 1 (2012)

³ TANAKA, *Journal of Fluid Mechanics*, **643**, 177 (2010)



Figure 1: Micrograph of wood powder Microscope Image

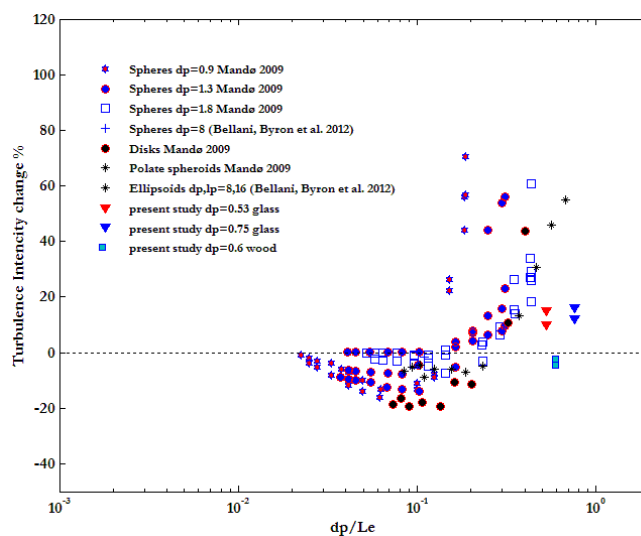


Figure 2: Turbulent intensity as a function of dimensionless length scale.

Undulatory swimming close to the wall

R. Fernandez-Prats^a, V. Raspa^b, B. Thiria^b, F. Huera-Huarte^a and R. Godoy-Diana^b

Biolocomotion in fluids is in many cases is influenced by the presence of a boundary. Flatfishes, bacteria, benthic organisms, pelicans and batoids experience significant ground effects, which are an unavoidable element of their locomotion strategy. In the case of birds, they can glide with a fixed wing configuration for long distances without loss of altitude^{1, 2}. The ground effect in fixed wing flight is well understood, but between the substrates and the undulation of fish⁶, a reliable model that is able to describe the dynamics with accuracy remains to be invented³. We study experimentally the propulsive dynamics of a flexible foil in a self-propelled swimming configuration near a wall. The swimmer has an aspect ratio of 0.9 and it is allowed to move freely in a rectilinear direction assisted by an air-bearing slider outside the free surface, while a stepper motor generates the pitch motion^{4,5}. Measurements of swimming speed were carried out using an ultrasonic distance sensor. Propulsive forces were obtained from swimming trajectories and a dynamic model, full recordings of the elastic wave kinematics and particle image velocimetry were carried out to determine the flow pattern and to find out the interaction between the foil and the wall. Experiments covered Reynolds numbers between 2200-19000. We show that the presence of the wall can enhance the cruising velocity in some cases by up to 15%. The physical mechanism responsible for this augmentation is first discussed qualitatively by studying the vorticity dynamics of the wake. We present how the usual wakes^{8, 9} are modified by ground effects (see LIF visualization in the figure below). A quantitative picture of the problem is then established using POD⁷ analysis of the velocity fields in the wake, which shows that the first POD mode is a good indicator of the kinetic energy in the propulsive jet.

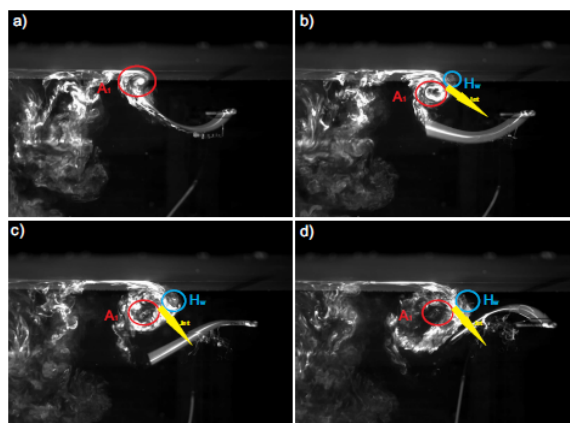


Figure : Four snapshots over half a period of oscillation of an undulating foil swimming near a boundary (from left to right). Vortices are visualized using dye and a dipolar structure highlighted schematically.

^a Dep. of Mechanical Engineering, Escola Tècnica Superior d'Enginyeria Química, Universitat Rovira i Virgili, 26 Avinyuda Paisos Catalans, 43007 Tarragona, Spain.

^b Physique et Mécanique des Milieux Hétérogènes (PMMH) CNRS UMR 7636 ; ESPCI ParisTech ; UPMC (Paris 6) ; Univ. Paris Diderot (Paris 7) 10 rue Vauquelin, 75231 Paris, Cedex 5, France.

¹ Blake, *J. of Biomechanics*. **16**, 649-654 (1983).

² Withers & Timko, *J. of Experimental Biology*. **70**, 13-26 (1977).

³ Blevins and Lauder, *Bioinspiration & Biomimetics*. **8**, 016005 (2013).

⁴ Raspa et al, *J. of Fluid Mechanics*. **729**, 377-387 (2013).

⁵ Ramananarivo et al., *J. of the Royal Society Interface*. **10**, 20130667-20130667 (2013).

⁶ Rosenberger, *J. of Experimental Biology*. **204**, 379-394 (2001).

⁷ Huera-Huarte and Vernet, *Experiments in Fluids*. **48**, 999-1013 (2009).

⁸ Godoy-Diana et al., *Physical Review E* **77**, 016308 (2008)

⁹ Williamson & Roshko., *J. of Fluids and Structures* **2**, 355-381 (1988)

Vortex-induced drag and the role of aspect ratio in undulatory swimmers

V. Raspa, S. Ramananarivo, B. Thiria and R. Godoy-Diana^a

During cruising, the thrust produced by a self-propelled swimmer is balanced by a global drag force. For a given object shape, this drag can involve skin friction or form drag, both being well-documented mechanisms. However, for swimmers whose shape is changing in time, the question of drag is not yet clearly established. We address this problem by investigating experimentally the swimming dynamics of undulating thin flexible foils. Measurements of the propulsive performance together with full recording of the elastic wave kinematics are used to discuss the general problem of drag in undulatory swimming. We show that a major part of the total drag comes from the trailing longitudinal vortices that roll-up on the lateral edges of the foils. This result gives a comparative advantage to swimming foils of larger span thus bringing new insight to the role of aspect ratio (AR) for undulatory swimmers.

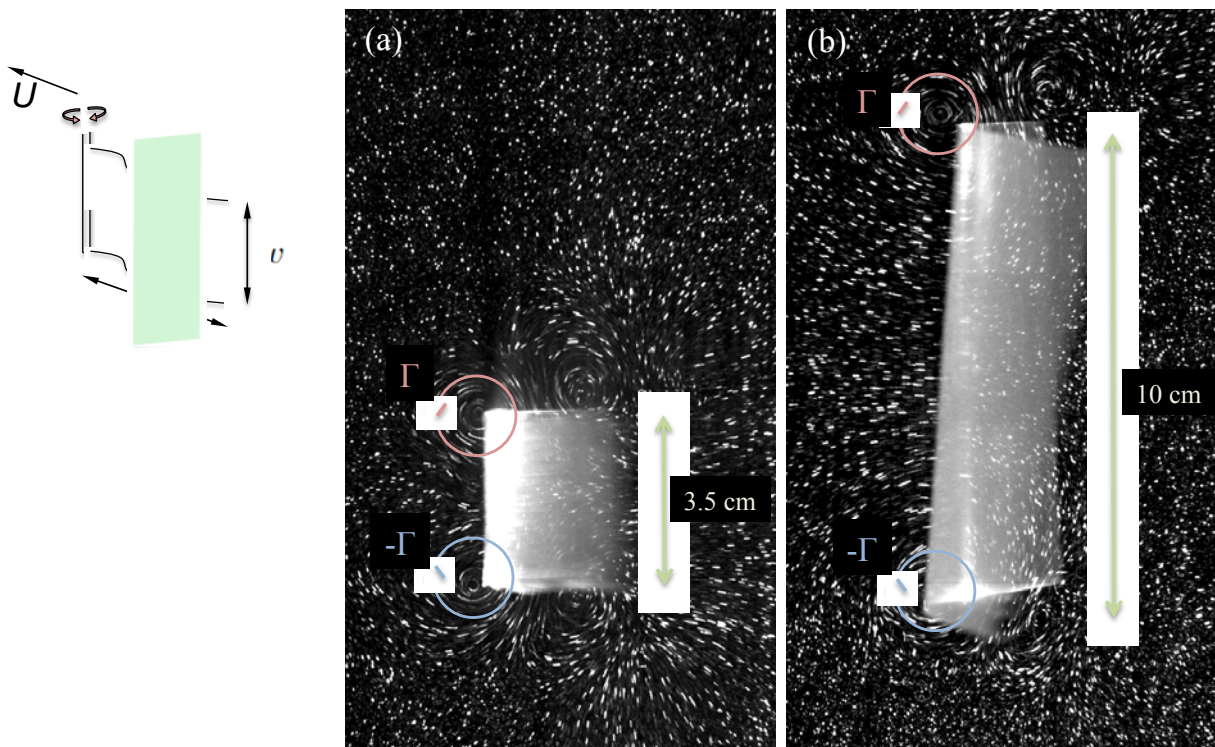


Figure 1: Visualisation of the longitudinal vortical structures on top and bottom edges of self-propelled swimming foils (the viewing plane is a cross section with the foils swimming away from the camera). The driving frequency was set to 1 Hz. (a) AR = 0.2. (b) AR = 0.7. Particle streaks are illuminated by a vertical laser sheet placed at the foils' mid length plane.

^a PMMH Laboratory, CNRS UMR 7636; ESPCI ParisTech; UPMC (Paris 6); Univ. Paris Diderot (Paris 7)
10 rue Vauquelin, 75231 Paris, Cedex 5, France

Skin friction formula for a rectangular plate in swimming-like motion

U. Ehrenstein^a, C. Eloy^a and M. Marquillie^b

To calculate the energy costs of swimming, it is crucial to evaluate the drag originating from skin friction. While many investigations focused on drag reduction mechanisms employed by swimming animals, others proposed that drag may actually be enhanced,¹ referring to the so-called ‘Bone-Lighthill boundary-layer thinning hypothesis’.² This latter assumption has recently been readdressed,³ using a theoretical boundary-layer model for a plate in uniform flow U_∞ moving perpendicular to itself at velocity U_\perp (Figure 1a), showing that the enhanced drag is proportional to $\sqrt{U_\perp}$. The boundary-layer model cannot predict the genuine three-dimensional flow dynamics and in particular the friction at the leeward side of the moving plate. In the absence of reliable skin-friction measurements along moving boundaries, a full three-dimensional numerical simulation remains necessary to confirm the theoretical prediction. Using a multi-domain compact finite-differences Navier-Stokes solution procedure, the boundary-layer structure along the moving plate is analysed for several plate velocities and plate length-to-span ratios l/s (Figure 1b shows typical streamwise vorticity structures in a wall-normal plane). Focusing on the shearing stress integrated along the span of the plate, the simulation results reinforce the formula² $D = C_{3D} \mu U_\infty \sqrt{\text{Re}_s} \sqrt{U_\perp^*}$, U_\perp^* being the wall normal velocity made dimensionless with the uniform incoming flow U_∞ and Re_s the Reynolds number based on the span. We compute a friction coefficient $C_{3D} \cong 2$ with however some variation along the plate streamwise direction. The influence of the plate length-to-span ratio is also highlighted and interpreted in the context of fish swimming energetics.

^a Aix-Marseille Univ, CNRS, Centrale Marseille, IRPHE UMR 7342, F-13384 Marseille, France

^b CRI, Université Lille Nord de France, F-59655 Villeneuve d’Ascq

¹ Anderson et al., *J. Exp. Biol.* **204**, 81 (2001).

² Lighthill, *Proc. R. Soc. Lond B.* **179**, 125 (1971).

³ Ehrenstein and Eloy, *J. Fluid Mech.* **718**, 321 (2013)

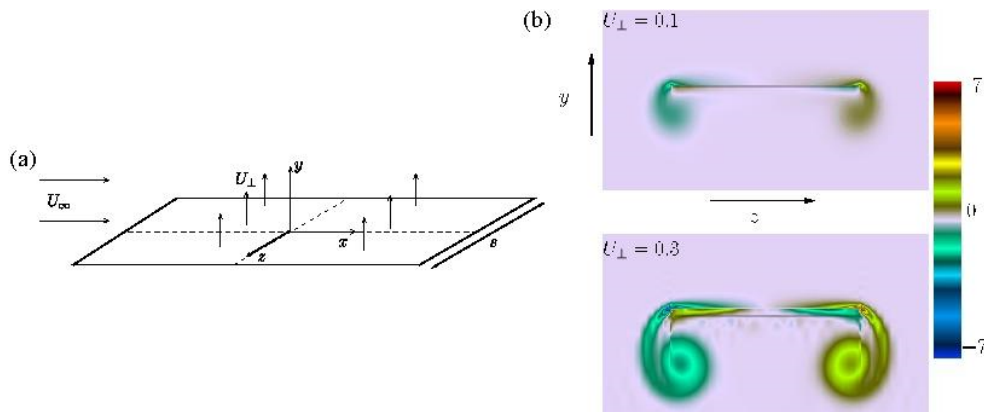


Figure 1: (a) Sketch of the plate in a uniform flow moving at a normal velocity. (b) Streamwise vorticity in the (z, y) plane at a position $x = l/3$, for a plate with $l/s = 6$, $\text{Re}_s = 1200$ and two different wall velocities.

Propulsion by a flapping flexible plate

F. Paraz¹, L. Schouveiler¹ and C. Eloy¹

Many aquatic animals, such as tunas, dolphins, or whales, propel themselves with a flapping flexible caudal fin. To gain some insight into this mode of propulsion, an experimental study has been conducted, which consists in mimicking the motion of a caudal fin.

A flexible plate of length $2c$, immersed in a uniform water flow, is actuated into a harmonic heave motion at its leading edge. The experimental setup, schematically shown in Fig. 1(a), allows the variation of the flow velocity U , the amplitude A_{LE} and angular frequency ω of the leading edge actuation, and of the bending rigidity B of the plate. The passive response of the free trailing edge is then recorded for different values of these parameters. Resonances are evidenced when the forcing frequency approaches the natural frequencies of the system plate+fluid. The experimental frequency responses of Fig. 1(b) show the first two resonance peaks observed in the range of the tested parameters. It has also been shown that the Reynolds number, defined as $Re = 2Uc/\nu$, where ν is the fluid viscosity, as well as the plate flexibility B , do not have a significant effect on the response dynamics as long as the frequency of the leading edge is normalized by the natural frequency of the plate ω_0 . In contrast, comparing in Fig. 1(b) the frequency responses obtained for two different values of the forcing amplitude A_{LE} , it can be seen that this parameter has a strong effect on the plate response, which is a signature of a non-linear effects playing an important role in the response.

To extend the study, a weakly non-linear model has been developed. The asymptotic limit of small U is considered, i.e. $U \ll c \omega$. The coupling between the surrounding fluid and the plate is modelled through a potential linear approach. The dissipations due to both the fluid the plate material are taken into account in the model. The associated dissipation coefficients have been measured independently in damped oscillation experiments. Although the amplitude is overestimated in the model, a good qualitative agreement between experiments and theoretical predictions is obtained. In particular, the variation of the ratio A_{TE} / A_{LE} with the forcing amplitude A_{LE} is recovered.

¹ Aix Marseille Université, CNRS, Centrale Marseille, IRPHE UMR 7342, 13384, Marseille, France.

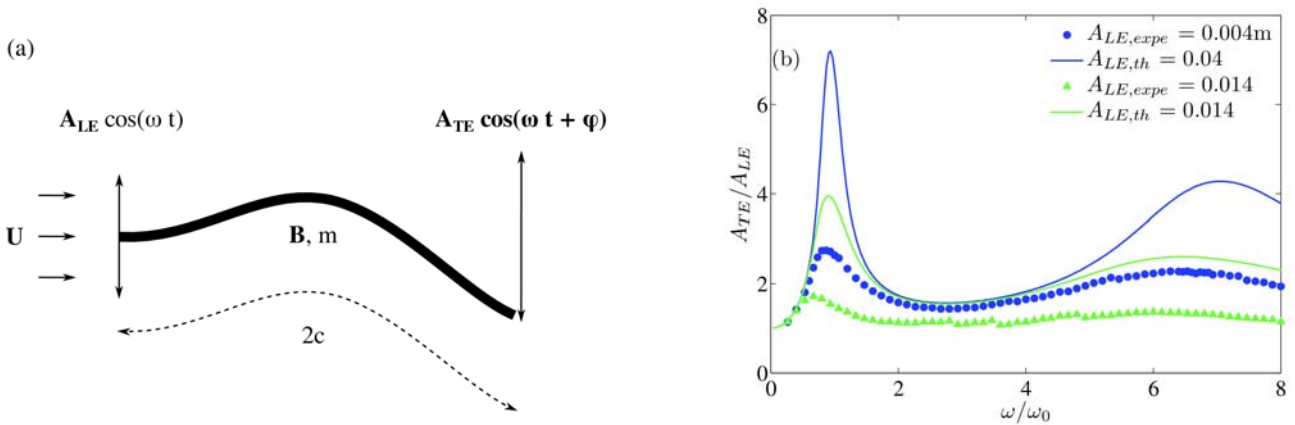


Figure 1: (a) Drawing of the experimental setup. (b) Frequency response of the trailing edge. Filled symbols represent the experimental measurements and the continuous lines the theoretical predictions for a bending rigidity sets to $B = 0.018$ Nm.

Tran- & Supersonic Flows

Mach number effects on the flowfield structure of hypersonic cavity flows

Luis T. L. C. Paolicchi^a and Wilson F. N. Santos^a

A reliable prediction of the thermal and aerodynamics load acting on the vehicle surface is of major importance for the design of a hypersonic vehicle. Contour discontinuities, such as cavities, are usually present in the surface, even though a smooth aerodynamic shape of the surface is attempted in the design. Such surface discontinuities may constitute in a potential source in a heat flux rise to the surface or even though in a premature transition from laminar to turbulent flow. For the particular case of cavities, many experimental and theoretical studies have been conducted in order to understand the physical aspects of a hypersonic flow past to this type of surface discontinuities. Usually, as the length-to-depth (L/H) ratio of the cavity is sufficiently large ($L/H > 14$), the main flow reattaches to the cavity floor and the cavity is defined as being a “closed” cavity. However, if L/H ratio decreases to a critical value ($1 < L/H < 10$), the flow presents a different behavior, and the cavity is an “open” one. In general, the major interest in the experimental and theoretical studies has gone into considering laminar or turbulent flow in the continuum flow regime. Nevertheless, there is little understanding of the physical aspects of a hypersonic flow over cavities related to the aerothermodynamic environment associated to a reentry vehicle. In this fashion, Palharini and Santos¹ have studied cavities situated in a rarefied hypersonic flow by employing the Direct Simulation Monte Carlo (DSMC) method. The work was motivated by the interest in investigating the L/H ratio effects on the flowfield structure and on the aerodynamic surface quantities. The primary emphasis was to examine the behavior of the primary properties, such as velocity, density, pressure and temperature, as well as pressure, heat transfer, and skin friction coefficients due to changes on the cavity L/H ratio. In continuation of the previous analysis¹, the current study expands on the results presented earlier by investigating the influence of the compressibility on the flowfield structure of a hypersonic flow on a family of cavities. The sensitivity of the primary properties (velocity, density, pressure and temperature) due to changes on the freestream Mach number (5, 15, and 25) and on the cavity L/H ratio (1, 2, 3, and 4) will be examined in the transition flow regime, i.e., between the continuum flow and the free collision flow regime. Due to the non-equilibrium flow conditions, the DSMC method will be employed to calculate the hypersonic two-dimensional flow on the cavities. Figure 1 displays map contours for density (normalized by freestream density) along with streamline traces inside the cavities for freestream Mach number of 25 and L/H ratio of 1, 3 and 4. According to this set of plots, the cavity flow behavior in the transition flow regime differs from that found in the continuum flow regime, for the conditions investigated. It is clearly noticed that the external stream reattaches the cavity floor for L/H ratio of 4.

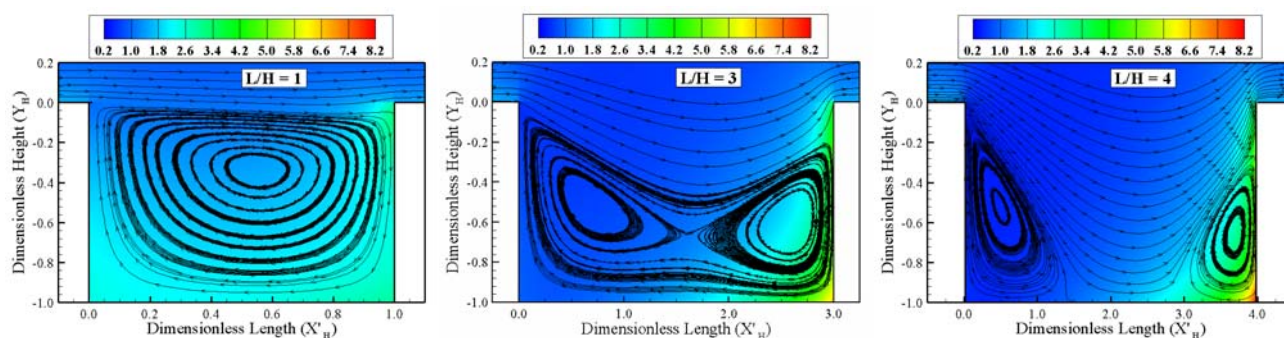


Figure 1: Density ratio (ρ/ρ_∞) contours with streamline traces inside the cavities for Mach number of 25 and L/H ratio of (a) 1, (b) 3, and (d) 4.

^a Combustion and Propulsion Laboratory (LCP), National Institute for Space Research (INPE), Cachoeira Paulista, SP, BRAZIL.

¹ Palharini and Santos, 42nd AIAA THERMOPHYSICS CONFERENCE, AIAA Paper 2011-3130, Honolulu, Hawaii, June 27-30, 2011.

Impinging of Supersonic Jet on Gas-permeable Obstacle of Periodic Structure

V. M. Fomin*, K. A. Lomanovich*, and B. V. Postnikov*

Impinging of supersonic jet against an obstacle was investigated past decades rather thoroughly. Gasdynamics and shock-wave pattern of jet-obstacle interaction are sophisticated. There are regimes when intensive self-oscillation of shock-waves observed. Two main mechanisms of the oscillations considered as acoustic feedback passing from oscillating veer jet in vicinity of the obstacle to a nozzle exit and internal one. Latter case concerns of gas accumulation between Mach disc and surface of the obstacle due to specific pressure distribution near the obstacle. It is the veer jet appearance when intensive self-oscillations occur in front a permeable obstacle. Gasdynamics aspects of shock-wave pattern of supersonic jet impacting gas-permeable obstacle are under consideration and discussion. Experiments were carried out with both underexpanded and overexpanded jets. Cylindrical obstacles were machined from aperiodic structure of porous nickel and periodic structure of cordierite blocks prepared for catalytic industry, see Fig.1 (a). Cordierite structure had a periodic set of square channels with wall thickness about 0.1 mm and density of the channels from 300 to 600 per square inch. We used shadow device with adaptive visualization transparent to register developing of intensive self-oscillations. Shock-wave pattern of the jet in front of cordierite obstacle is defined by Mach disc, bow shock and shock in front of individual channels, see Fig.1 (b). Jet Mach numbers investigated were from 2 to 4 and stagnation pressures up to 40 bars. If a rear part of the obstacle had a nonpermeable screen than temperature inside channels increased up to 200-300 K due to shock-wave interaction inside. Self-oscillations observed were accompanied by intensive acoustic noise.

* Khristianovich Institute of Theoretical and Applied Mechanics, 4/1 Institutskaya Str., Novosibirsk, Russia

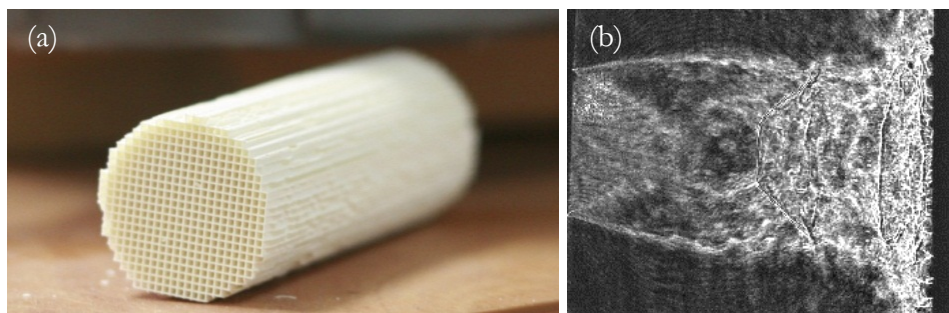


Figure 1: (a) Cordierite block. (b) Supersonic jet impinging cordierite block.

On generation and development of controlled disturbances in 3D supersonic boundary layer on surface with roughness

A. V. Panina^a, A. D. Kosinov^{a,b}, N. V. Semionov^a and Yu. G. Yermolaev^a

This paper presents investigations of the generation and development of disturbances and the receptivity to controlled disturbances in supersonic boundary layer on swept wing at Mach 2.0. A comparative experimental study of the evolution of controlled fluctuations in the boundary layer on a smooth swept wing and in the spanwise modulated boundary layer on a swept wing at a fixed electrical power of source disturbances and the same unit Reynolds number were performed. These investigations continue the series of experiments that were conducted before on flat plate¹.

The experiments were conducted in low noise T-325 supersonic wind tunnel of ITAM SB RAS at Mach 2.0 and unit Reynolds number $Re_1 = 5 \times 10^6 \text{ m}^{-1}$. The model of a swept wing with a sharp leading edge and $\chi = 45^\circ$ was used. Source of artificial disturbances was built in the model. Controlled pulsations are delivered into boundary layer through an aperture of 0.4 mm in diameter and they were excited by high frequency glow discharge in chamber. Constant temperature hot-wire anemometer (CTA) was used for mean and pulsating flow characteristic measurements. The square stickers from a scotch tape were applied to induce the spanwise modulation of mean flow in the boundary layer. The sizes of labels were $3 \text{ mm} \times 3 \text{ mm}$, and the height – 60 microns. The pulsation amplitude as time traces distributions in spanwise direction at $x = 20, 30, 40$ and 50 mm were obtained. After data processing the amplitude and phase mass flow perturbation spectra over β' (spanwise wave number) were determined. The procedure for obtaining frequency-wave spectra of controlled disturbances corresponded two-dimensional Fourier transform in time t and the coordinate Z :

$$\tilde{A}_{f\beta}(x_k, \beta, f_l) = \frac{2}{\delta_n \cdot T \cdot Q} \sum_{n=1} \sum_{j=1} A(x_k, z_j, t_n) \cdot e^{-i(\beta z_j - \omega_l t_n)} \Delta z_j \Delta t, \quad A(x_k, z_j, t_n) = \frac{e^i(x_k, z_j, t_n)}{E(x_k, z_j)},$$

where Δt - time discretization step ADC, Δz_j - discretization step in the transverse coordinate, T - the length of time for realization, $A(x_k, z_j, t_n)$ - the instantaneous value of the dimensionless pulsation signal of hot-wire, Q - sensitivity factor to mass flow pulsations, $\delta_n = 1 \text{ mm}$ - length scale for the dimensionless of wave spectra.

For the first time the results on the generation and development of the wave train in spanwise modulated supersonic boundary layer on the swept wing at Mach 2 were obtained experimentally in the same conditions of controlled experiment. Obtained that for a fixed power of disturbance source the amplitude of the fundamental wave train in the spanwise modulated boundary layer on the swept wing is less in comparison with the case of a smooth surface of the model. Similar results were obtained for subharmonic wave train. The evolution of the wave train subharmonic and the fundamental frequency proceeds differently in the boundary layer on a smooth wing and wing with roughnesses.

This work has been supported by the RFBR grant 13-01-00520.

^a Khristianovich Institute of Theoretical and Applied Mechanics SB RAS, Novosibirsk, Russia

^b Novosibirsk State University, Novosibirsk, Russia

¹ Kosinov et al., *EFMC9: book of abstracts*. (2012).

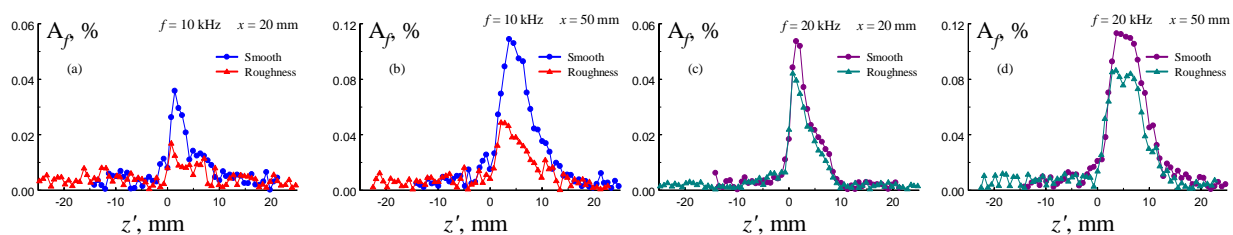


Figure 1: Comparison of the spanwise amplitude distribution for subharmonic wave train (a) in the initial section and (b) in the chosen section. Comparison of the spanwise amplitude distribution for fundamental wave train (c) in the initial section and (d) in the chosen section.

Resonant interaction of controlled disturbances in 3D supersonic boundary layer at Mach 2

G.L. Kolosov^a, A.D. Kosinov^{a,b}, N.V. Semionov^a and Yu.G. Yermolaev^a

The paper is devoted to investigation of nonlinear wave train development in three-dimensional supersonic boundary layer on swept wing with swept angle of $\chi=45^\circ$. The controlled disturbances technique was used. It is a more preferable method to study the nonlinear interaction mechanisms of unstable waves¹. By this method the subharmonic mechanism was detected. The investigations continue the series of experiments that were performed before².

The experiments were conducted in low noise T-325 supersonic wind tunnel of ITAM SB RAS at Mach 2.0 and unit Reynolds number $Re_1 = 5 \times 10^6 \text{ m}^{-1}$. Source of artificial disturbances was built in the model at $x_0 = 56 \text{ mm}$ from the leading edge. Controlled pulsations are generated in boundary layer through aperture in diameter of 0.4 mm by glow discharge in chamber at high frequency ($f = 10 \text{ kHz}$). The space structure of controlled pulsations in spanwise direction at $x = 50, 60, 70, 80 \text{ mm}$ from the source of artificial disturbances were obtained. Two waves had the largest amplitudes relative to others: the main wave train with frequency of 20 kHz and its unstable subharmonic wave train with frequency of 10 kHz. After data processing for these waves the amplitude and phase mass flow perturbation spectra over β' (spanwise wave number) were determined.

The development of amplitude β' -spectra in downstream direction is shown in Fig. 1. For wave with frequency 10 kHz the value of the transverse wave number at which the main maximum amplitude is located is 0.8 and 1.1 rad/mm for wave with frequency 20 kHz. These values are consistent with previously obtained for linearly propagating and amplifying downstream waves². For subharmonic wave the excitation of the side peak at $\beta' = 0.2 \text{ rad/mm}$ can be explained by three-wave resonant interaction (3WRI) between waves with $f = 10, 20 \text{ kHz}$. Estimations of longitudinal wave numbers $a'_1 = 0.04, -0.62, -0.54 \text{ rad/mm}$ also satisfy the synchronism condition for resonant triplet:

$$f_1 + f_2 = f_3,$$

$$a_1 + a_2 = a_3,$$

$$\beta_1 + \beta_2 = \beta_3.$$

Thus experimentally it was shown a principal possibility of parametric amplification of stable in the linear sense disturbances.

This work has been supported by the RFBR grant 12-01-00158-a.

^a Khristianovich Institute of Theoretical and Applied Mechanics SB RAS, Novosibirsk, Russia

^b Novosibirsk State University, Novosibirsk, Russia

¹ Kosinov A.D. et al., *Nonlinear Instability of Nonparallel Flows*, Springer-Verlag, 196-205 (1994).

² Kolosov G.L. et al., 14TH ETC, Lyon, France (2013).

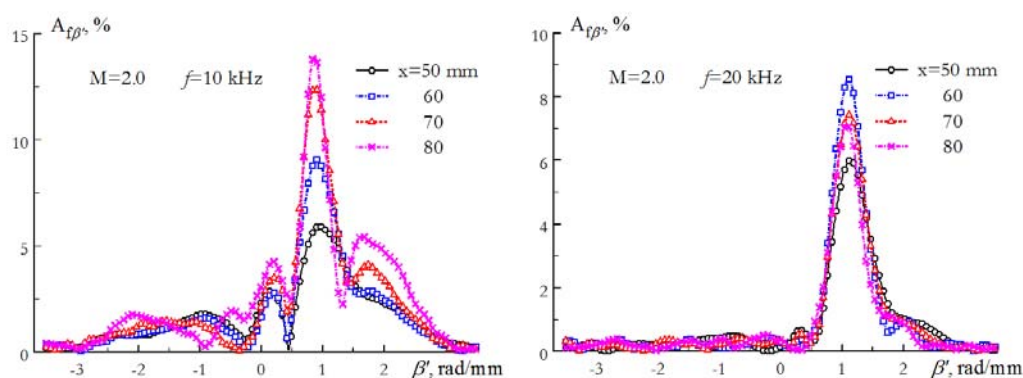


Figure 1: The amplitude spectra over β' (a) $f = 10 \text{ kHz}$ and (b) $f = 20 \text{ kHz}$.

Effect of condensation on hypersonic argon flow

E. Mogilevskiy^a, R. Ferrer^a, L. Gaffney^a, C. Granados^a, M. Huyse^a, Yu. Kudryavtsev^a,
S. Raeder^a, P. Van Duppen^a, A. Zadvornaya^a

The principle of supersonic gas expansion is used in a wide range of applications in different areas as e.g. chemical reaction studies and nanoparticles production. Recently, it has been proposed to use cold gas jets for laser spectroscopy studies of radioactive isotopes¹. In this so called IGLIS technique (In-Gas Laser Ionisation Spectroscopy) products of a nuclear reaction are stopped inside a gas cell filled with argon as a buffer gas at typically 500 mbar, carried by the gas through a sonic or a de Laval nozzle and stepwise ionised by laser radiation. In order to obtain an optimum frequency resolution it is crucial to achieve very low temperature to reduce Doppler broadening of the observed spectral lines. However, the necessary temperature and pressure near the nozzle are found in the unstable for gas phase region, thus argon is likely to condensate. The goal of this work is to investigate how this condensation affects the thermodynamic properties of gas phase and as well as estimate the minimal temperature that can be achieved after expansion into the low-pressure region.

The consideration is based on 1D diabatic steady Euler equations for the gas phase, taking the release of latent heat of condensation into account. For the condensed phase (clusters formation) mean kinetics nucleation theory² is used. This model was chosen since it allows to deal with small clusters accurately and to predict pseudospinodal decomposition. As especially the small clusters (dimers, trimers) are responsible for the majority of condensed mass this fact is important. The Becker-Döring equation is used for modelling the cluster distribution function. The model is validated against results from experiments on argon condensation in a cryogenic nozzle³ were used. Good agreement between the calculated and measured values for the onset of condensation can be observed (fig. 1). The nucleation rate for the onset is of order of $10^{20\pm1} \text{ cm}^{-3} \text{ s}^{-1}$ which is above the experimental value reported³, however it was not measured directly.

Using the parameters of the IGLIS setup, the gas conditions reach the limit for pseudospinodal decomposition, thus the minimal temperature that can be obtained for pressures above 0.1 mbar is about 28 K. These results are to be validated in the IGLIS laboratory at KU Leuven.

This work has been funded by FWO-Vlaanderen (Belgium), by GOA/2010/010 (BOF KU Leuven), by the Interuniversity Attraction Poles Programme initiated by the Belgian Science Policy Office (BriX network P7/12), by the European Commission within the Seventh Framework Programme through I3-ENSAR (contract no. RII3-CT-2010-262010) and by a grant from the European Research Council (ERC-2011-AdG-291561-HELIOS).

^a KU Leuven, Instituut voor Kern- en Stralingsfysica, Departement Natuurkunde en Sterrenkunde, Celestijnenlaan 200 D B-3001 Leuven Belgium

¹ Yu. Kudryavtsev et al. *Nucl. Instrum. Meth. B* **297**, 7 (2013)

²V.I. Kalikmanov *J. Chem. Phys.* **129**, 044510 (2008)

³S. Sinha et al. *J. Chem. Phys.* **132**, 064304 (2010)

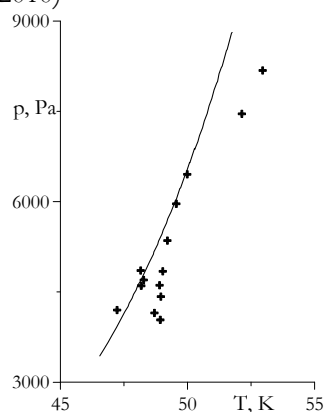


Figure 1: The condensation onset pressure as a function of temperature is shown. Solid line – calculation, crosses – experimental results of Sinha et al³

Control of a supersonic flow around using gas-permeable porous materials

I. S. Tsyryulnikov^a, S. G. Mironov^{a,b}

The report presents results of experimental and numerical investigation supersonic flow of bodies using gas-permeable porous inserts. This study is a continuation papers^{1,2}. Supersonic flow ($M = 5$) around the model of cylinder with front porous nickel foam inserts was studied. The numerical simulation of air flow in the porous material and the external flow was carried out with the package ANSYS Fluent. The dependence of drag force of the cylinder with porous inserts on the length of the porous insert streamlined supersonic flow was obtained and compared with data of measurements. The problem was solved in the frame of quadratic law of resistance in air flow in pores of the materials. The coefficients of linear and quadratic terms of the resistance law were determined experimentally by measuring the velocity of one-dimensional air flow through the gas-permeable porous samples of different size and different pressure drop across the material. The effect of temperature of the gas-permeable materials on flow rate of air through it was studied. On the basis of these data was developed and tested scheme of a supersonic flow around control using symmetric and asymmetric changes in hydraulic resistance of the porous material by heating it. Scheme of heating of gas-permeable materials by electric glow discharge was implemented, the dependence of the longitudinal and transverse aerodynamic forces on the discharge power was obtained. Schlieren photograph of flow field around the model with an asymmetric impact on the flow through the porous insert heating by electric glow discharge is presented in Figure 1.

^a Dep. Physical Problems of Flow Control, Khristianovich Institute of Theoretical and Applied Mechanics, Novosibirsk, Russia

^b Novosibirsk State University, Novosibirsk, Russia

¹ Fomin et al., Techn. Phys. Letters. **35**, (2009).

² Bedarev et al., J. Appl. Mech. Techn. Phys. **52**, 13 (2011).

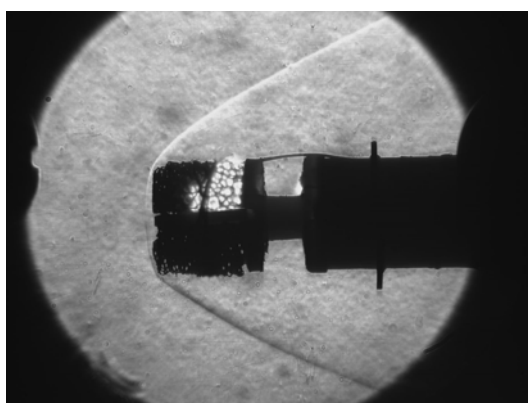


Figure 1: Flow field around the model with an asymmetric heating by glow electric discharge.

² M. Swoboda and W. Nitschef. *Journal of aircraft*. **33**, (1996)

Identifying buffet mechanisms in transonic Shock-wave/Boundary-layer interaction

J. Brouwer^a, J. Reiss^a, J. Sesterhenn^a

Unsteady shock-wave/boundary layer interaction (SBLI) is an important subject in many engineering applications. A prominent example for SBLI is the transonic flow over an airfoil. The flow is accelerated over the wing, a supersonic pocket forms which is terminated by a shock. The strong pressure gradient leads to flow separation and recirculation bubble forms. Under certain conditions the position of the shock begins to oscillate. Lee¹ gives a comprehensive overview of the conditions under which transonic SBLI occurs. In summary, two main factors are believed to be responsible for the shock movement. The first is the breathing motion of the recirculation bubble that forms behind the adverse pressure gradient at the shockfoot. The second mechanism that leads to shock-buffeting are acoustic waves that are generated downstream of the interaction zone and travel upstream to interact with the shock.

While there exist many recent numerical studies of supersonic shock-wave/boundary-layer interactions, see Clemens et al.² for an overview, the case of transonic SBLI has not received as much attention. In this study, the DNS of a transonic boundary-layer flow over a bump is investigated, using an energy-preserving skew-symmetric finite-difference code³. The flow is accelerated over the bump and a λ -shock forms. Shock-buffeting due to upstream travelling acoustics is observed. To gain insight in the underlying feedback mechanism, the acoustic sources generating the upstream travelling waves are identified.

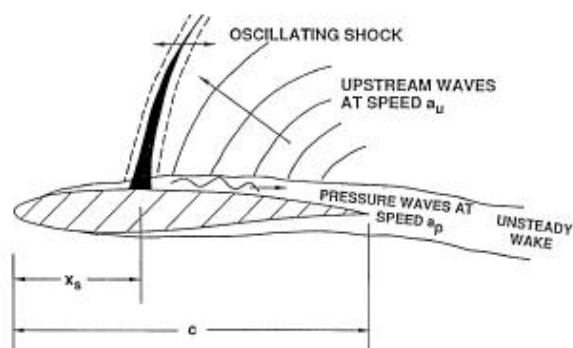


Fig. 1: Model of SBLI mechanisms taken from Ref. 1

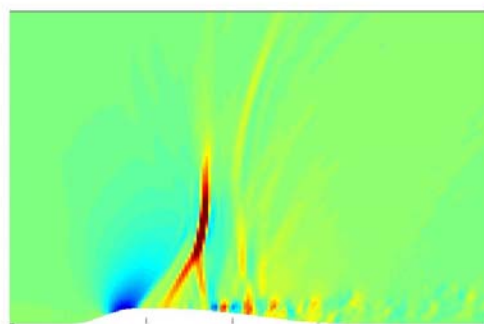


Fig. 2: Snapshot of pressure gradient with λ -shock and upstream travelling acoustics

^a Institute for Fluid Dynamics and Technical Acoustics, TU Berlin, Mueller-Breslau-Str., Berlin, Germany

¹ Lee, Self-sustained shock oscillations on airfoils at transonic speeds, Progress in Aerospace Sciences, Elsevier, 2001, 37, 147-196

² Clemens & Narayanaswamy, Low-Frequency Unsteadiness of Shock Wave/Turbulent Boundary Layer Interactions, Annu. Rev. Fluid Mech, 2014, 46, 469-92

³ Reiss & Sesterhenn, A conservative, skew-symmetric Finite Difference Scheme for the compressible Navier--Stokes Equations, submitted to Computers & Fluids

The wake behind a body in a subsonic and transonic flow of viscous gas

A.I. Aleksyuk^a, V.P. Shkadova^b and V.Ya. Shkadov^a

The report presents the numerical investigations of the Mach number effect on the flow around bluff (a circular cylinder) and streamlined (NACA0012 airfoil) bodies. The numerical simulations are based on solving two-dimensional Navier-Stokes equations for viscous perfect gas at small and moderate Reynolds numbers Re ($Re \leq 10000$) and Mach number range of $0.1 \leq M \leq 1.5$.

The previous experimental and numerical studies have shown that the change of Mach number at a fixed Reynolds number has a significant impact on the near wake flow structure. For example, the flow around airfoil NACA0012 at zero incidence at $Re=10000$ has regimes with a vortex street in the near wake ($0.3 < M < 0.95$) and without it ($M < 0.3$ and $M \geq 0.95$), and the transonic regime of $0.7 < M < 0.85$ forms an additional mode of instability¹.

The work focuses on studying the development of self-oscillations in the subsonic and transonic wakes and related phenomena like unsteady shock/boundary layer and shock/vortex interactions. Fig. 1 shows different types of vortex street formation obtained in the present work: vortex street originates on the body (b) and in the wake in subsonic and transonic flow regimes (a, c).

Detailed numerical study of the influence of Mach number on the nature of the flow and forces has been carried out. Initial-boundary value problems for the Navier-Stokes equations are numerically solved by the stabilized finite elements method². Solutions are built on unstructured meshes using the procedure of adaptation, which automatically creates a good resolution of the grid in the places of local features, such as shock wave, boundary layer and vortex wake. The reported computations have been carried out on Lomonosov supercomputer.

The work is supported by RFBR grants (12-01-00405 and 14-01-31106).

^a Faculty of Mechanics and Mathematics, Lomonosov Moscow State University, 1 Leninskiye Gory, Moscow, Russia, 119991

^b Institute of Mechanics, Lomonosov Moscow State University, 1 Michurinsky Pr., Moscow, Russia, 119192

¹ Bouhadji and Braza, *Computers and Fluids* **32**, 1233 (2003)

² Aleksyuk et al., *Mosc. Univ. Mech. Bull.* **67**, 53 (2012)

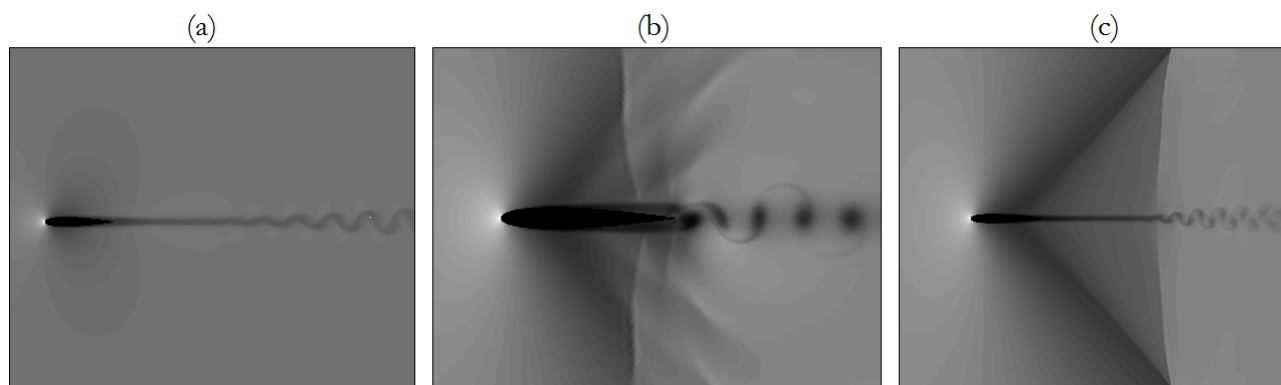


Figure 1: Subsonic and transonic flows around airfoil NACA0012: density field at (a) $M=0.5$, (b) $M=0.85$, (c) $M=0.95$.

An investigation of dense gas dynamics

F.J. Dura Galiana^a and A.P.S. Wheeler^b

Heat recovery systems generally use the Organic Rankine Cycle (ORC) due to the necessity to generate power from a low temperature source. These engines usually have single stage turbines to maximise the power density, although the high pressure ratios result in losses due to transonic flows (such as shock and trailing-edge losses). As an added complexity, high-density gases with a high molecular weight and complexity are used in ORC engines. These fluids enter the turbine at near-critical point conditions, where dense gas effects are dominant. At these conditions, the Fundamental derivative $(\Gamma)^1$ of the gas is close to unity, and this affects the development of shock waves and subsequent shock-losses which degrade the turbine performance.

In this paper we present experimental and CFD studies of dense gases. We study the flow of different gases (CO_2 , air and SF_6) over a backward-facing step geometry intended to simulate wake and shock losses of the flow over the vane trailing edge of a typical ORC turbine. Different nozzles were generated to achieve the same free-stream Mach number conditions for all fluids. This was achieved using a new code that uses an axisymmetric Method of Characteristics (MOC) that takes into account real gas effects during an isentropic expansion.

The flows were tested in a new Ludwig tube that simulates ORC turbine conditions (i.e. Mach number, Reynolds number and reduced pressure and temperature). Using fast response pressure transducers, static and stagnation pressures were measured to help us study the flow features. The data gathered from the experiments shows that the nozzle design achieved the desired Mach number within 1% of the design intent of 2. Comparison between the experimental data and CFD prediction using real-gas modelling showed generally good agreement, with some differences in total pressure, indicating modelling inaccuracies related to loss/entropy production.

Acknowledgements

This work was supported by the EPSRC (EP/J006394/1) and GE Global Research. The authors are also grateful to Prof. John Denton for use of TBLOCK research codes.

^a Faculty of Engineering and the Environment, University of Southampton, Southampton, SO17 1BJ, UK

^b Faculty of Engineering and the Environment, University of Southampton, Southampton, SO17 1BJ, UK

¹ Thompson, P.A: "Fundamental Derivative in Gas Dynamics." *Physics of Fluids* **14**, 9 (1971)

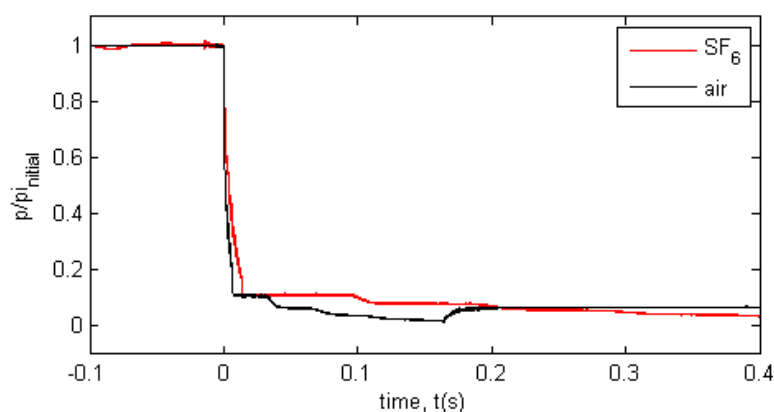


Figure 1: Nozzle exit static pressure comparison between SF_6 and air for Mach number $M=2$.

Geometric shock dynamics and the generic singularities of converging shock fronts

J. Eggers^a, M. A. Fontelos^b and N. Suramlishvili^a

We are concerned with singularities of the shock fronts of converging perturbed cylindrical shock waves. Our considerations are based on Witham's theory¹ of geometrical shock dynamics. The solution of shock dynamics is found in implicit form using the 'hodograph' transformation and then the shock front in real space is reconstructed. The geometrical singularities of shock fronts are determined by the singularities of 'hodograph' transformations. The propagation of entire shock front is studied and the local analysis is applied in order to determine generic singularities. In particular, we found that the propagation of the front is accompanied by the development of swallowtail singularities described by the germ of E_6 mapping $(\mathbf{C}, 0) \rightarrow (\mathbf{C}^2, 0)$. The space of control parameters of the singularities is analysed, the unfolding describing the deformations of the canonical germ is found and corresponding bifurcation diagram is constructed.

^a School of Mathematics, University of Bristol, University Walk, Bristol, BS8 1TW, United Kingdom

^b Instituto de Ciencias Matematicas, C/Serrano 123, 28006, Spain

¹ Witham, *Linear and Nonlinear Waves* (John Wiley & Sons, 1974)

Mach Number Dependency of Drag Reduction Effect by a Uniform Blowing in a Supersonic Turbulent Channel Flow

Ayane Kotake^a, Yukinori Kametani^{a,b} and Koji Fukagata^a

Reduction of the skin friction drag in a wall-bounded turbulent flow is important for mitigation of environmental impacts and more efficient energy utilization, especially for reducing the fuel consumption in aircrafts and trains. Various control techniques for the reduction of friction drag have extensively studied for incompressible turbulent flows. In contrast, a few studies have been reported for compressible turbulent flows, despite that flows in the real applications mentioned above are often supersonic.

A DNS of a compressible turbulent channel flow was performed by Coleman et al.¹ More recently, Lagha et al.² performed DNS of a turbulent boundary layer at various Mach number (Ma). These results demonstrated that the turbulent statistics are essentially the same as those in the incompressible flows even at a very high Mach number up to $Ma = 20$. In turn, these results suggest that the drag reduction techniques developed for the incompressible flows, such as a uniform blowing may be effective for compressible flows.

In the present study, direct numerical simulations (DNS) of supersonic turbulent channel flows with a uniform blowing (UB) on one side and a uniform suction (US) on the other side are performed. The effects of UB and US on the skin friction drag and the differences of the effects among Mach number will be explored. The governing equations are the compressible continuity, the Navier-Stokes, and the energy equations. A periodic boundary condition is imposed to x- and z- directions. The Reynolds number, Re , is set to be 3000 and the bulk Mach number, Ma , is set to be 0.3, 1.0, 1.5 and 2. The UB and US velocities are given on the lower and upper walls, respectively. These velocities are set to be 0.1 % or 0.5 % of the bulk-mean velocity.

The modifications of the mean velocities by UB and US at $Ma = 1.5$ are shown in Figure 1. Here, the velocity is made dimensionless by the wall unit of the base flow. As the amplitude of UB and US increases, the mean streamwise velocities are found to decrease on the blowing side and increase on the suction side. Although the profiles at other Mach number are omitted here for brevity, their behaviors are similar to that of $Ma = 1.5$, which suggests that the drag reduction effect (on the blowing side) is relatively insensitive to the Mach number. This tendency is similar to the results of the incompressible flow by Sumitani and Kasagi³. Figure 2 shows the dependency of the drag reduction rates on the Mach number. Unlike the initial expectation, the drag reduction rate on the blowing side is observed to be increased as the Mach number increases. Its mechanism will be investigated and presented at the final presentation.

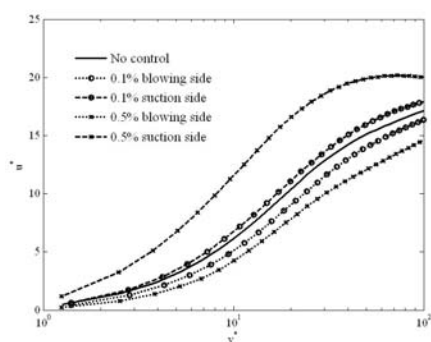


Figure 1 Mean streamwise velocity at $Ma = 1.5$

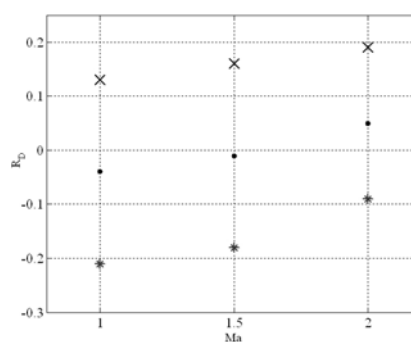


Figure 2: Dependency of drag reduction rate on the Mach number. Cross, blowing side; asterisk, suction side; circle, average of both walls.

^a Dept. Mechanical Engineering, Keio University, Hiyoshi 3-14-1, Kohoku-ku, Yokohama, 223-8522, JAPAN

^b Linne Flow Centre, KTH, 100 44 Stockholm, SWEDEN

¹ G. N. Coleman et al., *J. Fluid Mech.* **305**, 159-183 (1995).

² M. Lagha et al., *Phys. Fluids* **23**, 015106 (2011).

³ Y. Sumitani and N. Kasagi, *ALAA J.* **33**, 1220-1228 (1995).

Numerical Investigation of Nanosecond Pulsed Dielectric Barrier Discharge Actuator in Sub- and Supersonic Flow

J. G. Zheng^a, Z. J. Zhao^a, J. Li^a, Y. D. Cui^a and B. C. Khoo^{a, b}

Dielectric barrier discharge (DBD) actuator driven by a high voltage pulse with rise and decay time of nanosecond order is being investigated intensively as a potential active flow control means. The mechanism whereby the nanosecond DBD actuator achieves flow control authority is believed to be related to thermal effect of plasma discharge which causes the rapid, localized heating of near surface gas and generation of a micro shock wave. This type of actuator has been applied to a wide range of flow regimes and demonstrated flow control potential. In the current study, the nanosecond pulsed plasma actuator in sub- and supersonic flow over a flat plate and its application to airfoil leading edge flow separation control are investigated numerically. A one-dimensional, self-similar plasma model, which is well validated and verified, is employed to predict the key parameters of nanosecond plasma discharge and loosely coupled with compressible Navier-Stokes equations solver¹. The behaviors of plasma actuator in flat plate boundary layer as shown in Fig. 1, especially the characteristic of residual temperature due to repetitive pulse discharge and the discharge induced perturbation as well as its evolution in the boundary layer are studied. In addition, the efficacy of nanosecond pulse discharge for suppressing flow separation on the leading edge of an airfoil with freestream flow Mach number up to 0.2 has been reproduced numerically. The details of interaction between shock wave and external flow and of the induced vortex structures are resolved. The flow control in high subsonic regime where experimental data is lacking is also simulated. The focus is on the examination of effects of electrical parameters such as voltage amplitude, actuator repetition rate and operation mode on the generated spanwise vortices as well as on flow control authority.

^a Temasek Laboratories, National University of Singapore, Singapore 117411

^b Department of Mechanical Engineering, National University of Singapore, Singapore 119260

¹ Zheng et al., *Phys. Fluids* **26**, 036102 (2014).



Figure 1: Schlieren image showing a sequence of shock waves generated by nanosecond pulsed plasma discharge at frequency of $f=100\text{kHz}$ in a Mach 1.5 supersonic flow over a flat plate.

Control

Open-loop control for vortex breakdown in compressible, swirling nozzle-jet flows

T. Luginsland^{1,2}

The scope of the present investigation is to study the controllability of vortex breakdown in compressible, swirling nozzle-jet flows by means of Large-Eddy simulations (LES). High-order numerical schemes in space and time are utilized together with the ADM-RT subgrid scale model¹. A nozzle of length $L=5$, which rotates in the mean flow direction, is included into the numerical framework to allow for an interaction of the developing vortex breakdown with the upstream flow field². The Reynolds number is $Re=5000$, the Mach number is $Ma=0.6$ and the swirl parameter defining the rotation rate of the nozzle is $a=1$, which is above the threshold for vortex breakdown to occur.

Blowing/Suction at the nozzle lip is applied to control the vortex breakdown of the swirling jet flow. The influence of the forcing amplitude A , the forcing frequency f and the forcing wave number n on the vortex breakdown is investigated. Depending on the specific combination of forcing parameters (A, f, n) the position of the stagnation points at the centreline of the swirling jet as well as the spatial extend of the recirculation region changes. The minimum streamwise centreline velocity, a measure for the intensity of vortex breakdown, is decreased significantly leading to a recirculation, which is half as strong as for the natural, unperturbed flow. Independent of the specific forcing applied, azimuthal modes grow within the outer shear-layer of the swirling jet saturating at higher amplitudes compared to the natural flow. The single-helix type instability believed to be globally unstable and triggered by the rotation of the vortex core at the centreline of the swirling jet is not significantly suppressed by the growth of those modes. Contrarily, the single-helix mode seems to be amplified by the forcing applied throughout the present study.

Although the size, the shape and the location of the vortex breakdown is sensitive to the forcing applied in the present study, the mechanism leading to vortex breakdown is not affected. Applying a forcing at the nozzle lip does not influence the precessing vortex core at the centreline of the swirling jet and therefore the mechanism leading to vortex breakdown. This finding is in agreement to results reported in literature concerning the controllability of vortex breakdown in the incompressible regime.

¹ Institute of Fluid Dynamics, ETH Zurich, 8092 Zurich, Switzerland.

²

Aachen Institute for Advanced Study in Computational Engineering Sciences (AICES), RWTH Aachen University, Germany (current affiliation).

¹ Luginsland and Kleiser, *Proc. Appl. Math. Mech.* **10**, 727 (2010).

² Luginsland, *Diss. ETH No.* **21616**, (2014).

Figure 1: Time-averaged streamwise, w (red-blue), and azimuthal velocity, v (green-yellow), with streamlines of the natural flow field. The rotating nozzle wall is indicated in grey.

Optimal feedback control of the unsteady wake past a wall-mounted cube

Vincenzo Citro^a, Marco Carini^b, Flavio Giannetti^a and Jan Oscar Pralits^c

The flow past a cubical obstacle is an archetype of a wide variety of engineering problems dealing with the occurrence of bluff-body flows, such as the design of buildings or ships. For this considered flow configuration the primary instability leads to the development of an unsteady three-dimensional wake characterized by vortical structures called ‘Hairpin’ vortices¹. The alternate shedding of these vortices results in non-stationary forces acting on the obstacle and can cause serious structural problems associated with fluid-structure resonance phenomena. Therefore the possibility to mitigate and even suppress this flow instability by means of an active control is of general interest for several applications. In recent years linear optimal control has been established as a mathematically rigorous and almost general model-based approach to flow control². However the computation of the feedback gains for large-scale plants (such as those derived from the discretized Navier-Stokes equations) still remains intractable using standard control algorithms. One possibility is to resort to a reduced-order model of the open-loop plant^{3,4} and thereby introduce different types of approximations of the flow dynamics.

In this work the optimal control of the three-dimensional wake behind a wall-mounted cube is investigated based on a full-order flow model, providing an useful analysis tool to support and improve the design of more realistic controllers. In our linearized study a full-state feedback rule is designed by exploiting the Minimal Control Energy (MCE)^{5,6} solution of the classical Linear Quadratic Regulator (LQR) problem. Indeed for such case the feedback gains can be computed based only on the information provided by the spatial structure of the unstable direct and adjoint global modes of the linearized Navier-Stokes equations, thus bypassing the solution of an high-dimensional Riccati equation. In the considered control setup, spatially distributed blowing/suction located e.g. near the cubical element or on the obstacle itself is used for the actuation. The spatial structure of the computed feedback gain field is thoroughly described and the performance of the resulting controller is assessed on the fully nonlinear Navier-Stokes equations above the critical threshold of instability.

^a Dip. di Ingegneria Industriale (DIIN), Università degli Studi di Salerno, Via Giovanni Paolo II, 84084 Fisciano (SA), Italy

^b Dip. di Scienze e Tecnologie Aerospaziali, Politecnico di Milano, Via La Masa 34, 20156 Milano, Italy (marco.carini@polimi.it)

^c Dip. di Ingegneria Civile, Chimica e Ambientale, Università degli Studi di Genova, Via Montallegro 1, 16145 Genova, Italy

¹ J.-Y. Hwang & K.-S. Yang, Phys. Fluids, **16**, 2382-2394 (2004)

² J. Kim & T.R. Bewley, Annu. Rev. Fluid Mech., **40**, 113-119 (2007)

³ A. Barbagallo et al., J. Fluid Mech., **641**, 1-50 (2009)

⁴ Dergham et al., Phys. Fluids, **23**, 064101-20 (2011)

⁵ T.R. Bewley et al., BBVIV5, *Fifth Conference on Bluff Body Wakes and Vortex-Induced Vibrations*, Bahia, Brazil, December (2007).

⁶ M. Carini et al., J. Fluids Struct. special issue (2013).

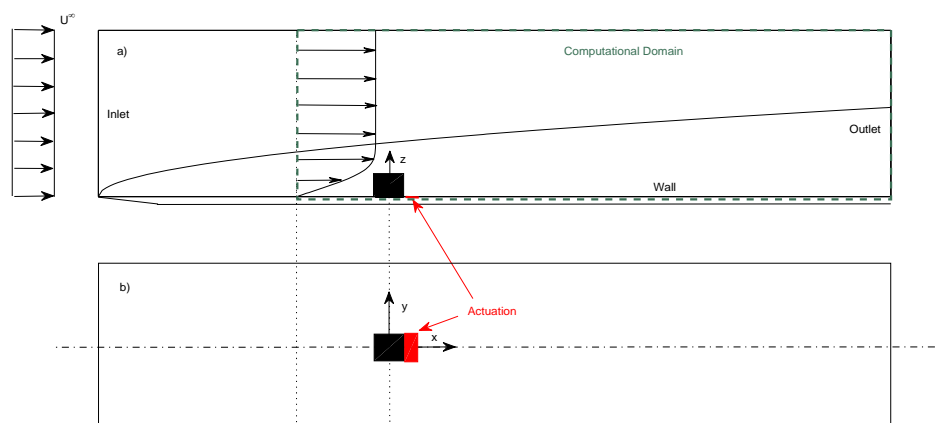


Figure 1: Flow configuration, frame of reference and computational domain (not to scale) are depicted using: a) side view and b) top view. The computational domain is enclosed by a dashed green line. The example **actuation** (blowing/suction) is located just downstream the cubical element.

A linearized approach for the control of aerodynamic forces in flow past a square cylinder

P. Meliga^a, E. Boujo^b, G. Pujals^c and F. Gallaire^b

The analysis of Strykowski & Sreenivasan¹ provides experimental evidence that a small control cylinder suitably positioned in the wake of a main cylinder can alter vortex shedding close to the instability threshold. This problem was addressed from a theoretical perspective by Hill², who used adjoint-based gradient to compute the sensitivity of the global instability mode correlated to the shedding activity, and thereby retrieved the experimental sensitivity regions without knowledge of the actual controlled states. Such an approach is an attractive alternative to bottleneck “trial and error” procedures in that it allows spanning quickly all possible positions of the control cylinder without ever calculating any controlled state. It has sparked interest as a means to gain beforehand valuable information regarding the most sensitive regions for open-loop control based on the underlying physics.

The present research aims at predicting similarly the optimal placement of the control cylinder in the attempt to modify the aerodynamic forces. The main focus is on drag of a square cylinder, intended to serve as a testbed for developing the related methodology. We compute the drag variation caused by a small control cylinder whose diameter is 1/10 that of the main cylinder, whose presence in the flow is modeled by a pointwise reacting force². Calculations are performed for two values of the Reynolds number. The first one $Re = 40$ is subcritical in the sense of bifurcation theory, as the flow settles down to a steady state. All results are presented in terms of maps of the steady asymptotic drag (i.e., the value reached after the initial transient), whose sensitivity is computed solving a steady adjoint problem from knowledge of the base solution (leftmost part of Fig.1). The second one $Re = 100$ is supercritical as the flow conversely develops to the time-periodic, vortex-shedding state. Results are rather presented in terms of maps of the time-averaged mean drag, whose sensitivity is computed integrating backwards in time an unsteady adjoint problem from knowledge of the DNS solution (rightmost part of Fig.1).

^a M2P2 UMR 7340 CNRS, Aix-Marseille University, Centrale Marseille - 13451 Marseille Cedex, France

^b LFMI Swiss Federal Institute of Technology of Lausanne, CH1015 Lausanne, Switzerland

^c PSA Peugeot Citroën Centre Technique de Velizy, 78943 Vélizy-Villacoublay Cedex, France

¹ Strykowski & Sreenivasan, *J. Fluid Mech.* **218**, 71 (1990).

² Hill, *NASA Technical Report* **103858** (1992).

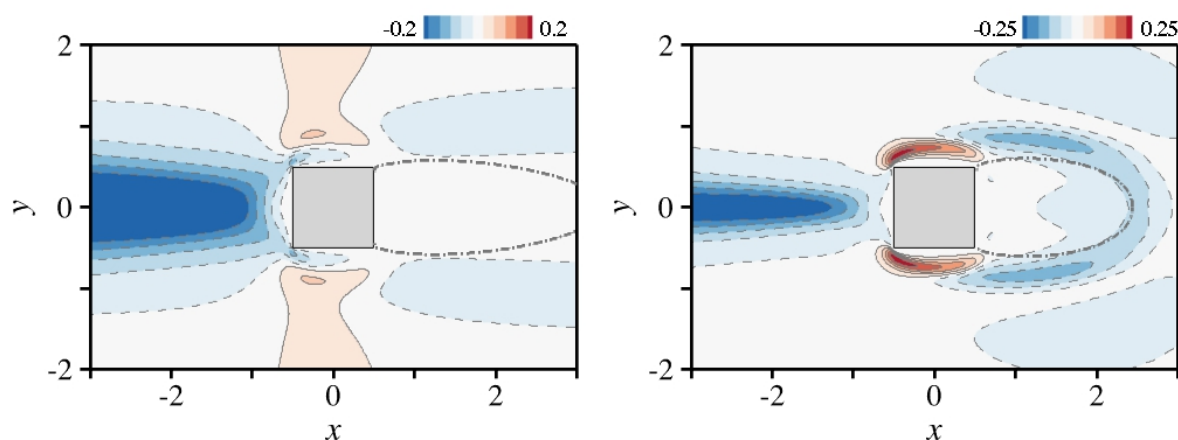


Figure 1: Map of the drag variation caused by the introduction of a small control cylinder. Left : steady asymptotic drag at $Re=40$. Right : time-averaged drag at $Re=100$.

Experimental closed-loop control of a detached boundary layer at high Reynolds number

C. Raibaud¹, A. Polyakov^{2,3}, D. Efimov^{b,c}, F. Kerhervé^{a,4}, J.P. Richard^{b,c,d} and M. Stanislas^{a,d}

A large variety of flow control strategies has been used in the last decades to avoid separation of boundary layers for, as major concern, aerodynamic benefits. The paper addresses closed-loop control of a quasi two-dimensional turbulent boundary layer with massive separation. The experiments are conducted in the LML boundary layer wind tunnel in Lille. Special attention is paid to the transient dynamics between the separation and reattachment regimes. For the control itself, 22 round air jets distributed in the spanwise direction upstream of the separation line are used as actuators. The jets generate co-rotating vortices which re-energise the near-wall region, and force the flow to reattach more or less depending on the actuation parameters.

The transition between the separated and the attached flow is first examined. Hot-film sensors placed along the separation region are used to obtain an instantaneous measurement representative of the skin-friction during reattachment regime. Both continuous and pulsed actuations are considered. The actuation parameters considered for the present study are: the velocity ratio between the jets exit and the freestream, the jets' frequency, the duty cycle, and the freestream velocity. In order to quantify the sensitivity of the flow with regards to these parameters, different sets of values are considered.

The hot-film responses are here considered as a good metric for the flow state (fully/partially attached or fully detached). The control strategy implemented therefore leans on the possibility to predict hot-film responses when the flow is subjected to various forcing/actuation. Modelling of the hot-film responses is thus effected for the range of control parameters covered. At first, characteristic time constants (rising time etc...) are determined by fitting a first-order law. Secondly, time-series models identification (ARMAX, Box-Jenkins, etc.) and dynamical systems are built in order to have a better approximation of the transient dynamics than the first-order model.

From these models, closed-loop experiments are performed. Closed-loop feedback based on P, PI & PID algorithms with the duty cycle as control input are first implemented to serve as a reference. The duty cycle is normalized and estimated from the difference between the friction wanted and the measure of the hot-film sensors. Optimal control (LQR) is also considered. The algorithm is aimed at the maximisation of the gain in friction with minimal flow rate input. The various time delays of the system "actuator+flow+sensor" are also taken into account for the control design.

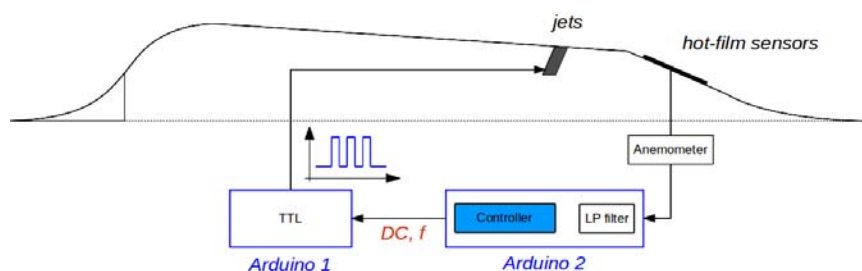


Figure 1: Closed-loop control experiment based on pulsed jets.

¹ CNRS UMR 8107, Laboratoire de Mécanique de Lille, 59650 Villeneuve d'Ascq, FRANCE

² Inria project-team Non-A, Parc Scientifique de la Haute-Borne, 40 avenue Halley, 59650 Villeneuve d'Ascq, FRANCE

³ CNRS UMR 8219, Laboratoire d'Automatique, Génie Informatique et Signal, 59650 Villeneuve d'Ascq, FRANCE

⁴ Ecole Centrale de Lille, Boulevard Paul Langevin, Cité Scientifique, 59650 Villeneuve d'Ascq, FRANCE

Suboptimal control of spatially developing turbulent boundary layers

A. Stroh^a, K. Fukagata^b, P. Schlatter^c and B. Frohnäpfel^a

The reactive flow control scheme of opposition control exhibits drag reduction of 25% in a fully turbulent channel flow¹. However, in order to realize opposition control, information about flow properties inside the flow domain is required. This problem can be solved by the introduction of suboptimal control schemes in which wall quantities are used as sensor information. Suboptimal control with the same type of control input as opposition control, i.e. suction and blowing in wall normal direction, yields about 20% drag reduction in a fully turbulent channel flow². In the present work suboptimal control schemes are transferred from the channel flow configuration to the spatially developing boundary layer.

The spanwise wall-shear stress is chosen as sensor information for the suboptimal control scheme, so the control input in form of wall-normal velocity at the wall can be estimated as a convolution between sensor input, $\partial w / \partial y(x, 0, z)$, and a weight distribution, $W(x', z')$:

$$v(x, y = 0, z) = \int_0^{x'_{\max}} \int_0^{z'_{\max}} W(x', z') \frac{\partial w}{\partial y}(x + x', y = 0, z + z') dx' dz'.$$

Two weight distributions are considered in the present work: the distribution presented by Lee et al.² and a distribution based on the derivation of Jeon and Choi³. In the latter case, the distribution is estimated as a simplified response of the flow to a local wall-normal velocity impulse. The implementation of both schemes shows good agreement with literature data^{2,4} in a fully turbulent channel flow at $Re_\tau = 180$. It is found that the frequency at which the control is updated significantly influences the performance of the control scheme.

Both suboptimal control schemes are then applied in a DNS of a spatially developing turbulent boundary layer with zero pressure gradient in a Reynolds number range of $Re_x = 1 \cdot 10^5$ to $3 \cdot 10^5$ ($Re_0 = 400$ – 700). In the boundary layer simulations the control is applied in the middle of the numerical domain only. The resulting local drag reduction is shown in Fig. 1(a) demonstrating similar streamwise development for all investigated control schemes: a transient section of $0.5 \cdot 10^5$ to $0.6 \cdot 10^5$ in terms of Re_x , followed by a saturated drag reduction state and a relaxation of the flow $0.2 \cdot 10^5$ to $0.3 \cdot 10^5$ units downstream of the control area. Both suboptimal control schemes result in an almost identical drag reduction distribution with a maximum of 17%, while opposition control yields a maximum drag reduction value of 23%. However, the spatial distribution of the control input intensity, as shown in Fig. 1(b), indicates the existence of differences between the different control schemes.

In the presentation we will report the differences between the two investigated suboptimal control schemes and the opposition control scheme in detail. The analysis will include the corresponding FIK-decomposition⁵ of the drag reduction and also evaluation of the control performance in terms of energy gain and energy saving rate.

Acknowledgements. The authors greatly acknowledge the support by Karlsruhe House of Young Scientists (KHYS) through scholarship for research abroad.

^a Institute of Fluid Mechanics, Karlsruhe Institute of Technology, Karlsruhe, Germany

^b Department of Mechanical Engineering, Keio University, Yokohama, Japan

^c Linné FLOW Centre, KTH Mechanics, Stockholm, Sweden

¹ Choi et al., *J. Fluid Mech.* **262**, 75–110 (1994)

² Lee et al., *J. Fluid Mech.* **358**, 245–258 (1998)

³ Jeon and Choi, *J. Int. J. Heat Fluid Flow* **31**, 208–216 (2010)

⁴ Iwamoto et al., *J. Int. J. Heat Fluid Flow* **23**, 678–689 (2002)

⁵ Fukagata et al., *Phys. Fluids* **14**, L73–L76 (2002)

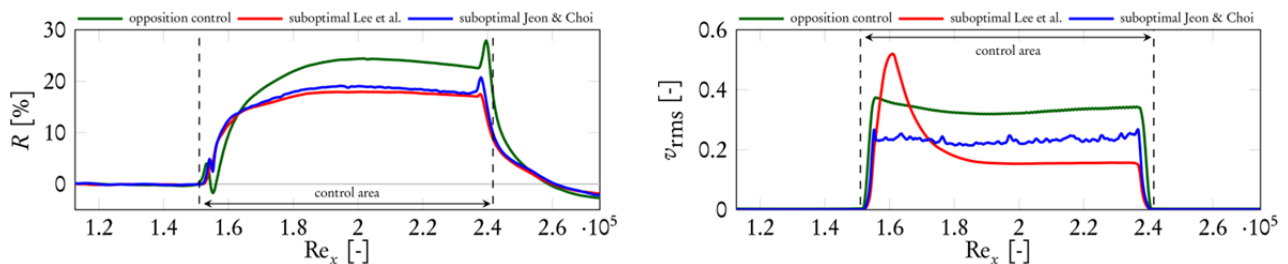


Figure 1: Streamwise development of (a) skin friction drag reduction (b) control input intensity.

Accurate pressure measurements for the determination of skin friction drag variations in internal turbulent air flows

A. Güttler^{a,b}, T. Schickel^a, T. Damaske^a and B. Frohnäpfel^b

During the last decades large research effort in the field of flow control has been devoted to the development of new strategies aimed at reducing turbulent skin-friction drag. Many of these new strategies are mostly evaluated numerically through Direct Numerical Simulation (DNS) of low Reynolds number flows in channel geometries. Though DNS enables relatively easy implementation of new control strategies and offers good accuracy in estimating changes in skin-friction, proof-of-principle laboratory verifications are required to finally assess the real potential and applicability of flow control techniques. From the practical viewpoint of handling an experimental set-up it is often advantageous to use air as a working fluid. However, the accurate detection of skin-friction drag variations is made challenging by the small values of the skin-friction drag itself, at least in the low Reynolds number range.

We describe the construction of an experimental facility in which skin-friction drag is detected by measuring the pressure loss of an internal air flow. The related cost effort is moderate while it is possible to detect changes of skin friction drag with the same or even better resolution and accuracy than with complex shear stress balances. In the present work particular care is taken to maximize the capabilities of the experimental facility in respect to the resolution of small pressure differences. As a result, it is possible to resolve changes in wall friction smaller than 0.5% at relatively low Reynolds numbers ($Re_b=5000-24000$).

The facility consists of a blower tunnel configuration with a flat channel test section (aspect ratio 12:1, length of 157 channel heights). Pressure taps are installed in regular intervals along the test section and flow rate measurements are realized with standard pressure difference based flow meters. We discuss possible error sources for the quality and repeatability in determination of the two main quantities, namely flow rate and corresponding pressure drop along the test section. In this respect, the influence of varying air density and viscosity as well as the one of manufacturing tolerances is considered. Different measurement strategies are compared from the viewpoint of resolving the smallest skin friction drag variations possible. Further, it is discussed how to ensure fully developed turbulent flow conditions, at least as far as the skin friction values are concerned.

The design of the presented experimental facility allows accurate testing of different drag reduction techniques under equivalent conditions. We present measurement results obtained for riblets^{2,4}, surface-embedded grooves¹ and spanwise wall-oscillation realized with dielectric electroactive polymers^{5,6}. The attained accuracy is finally discussed on these exemplary measurement results in comparison to available literature data.

^a Center of Smart Interfaces, Technische Universität Darmstadt, 64287 Darmstadt, Germany;

^b Institute of Fluid Mechanics, Karlsruhe Institute of Technology, 76131 Karlsruhe, Germany

¹ Frohnäpfel et al. , *J.Fluid Mech.*, **590**, 107(2007)

² Bechert et al. , *J.Fluid Mech.* , **338**, 59 (1997)

³ Walsh et al. , *ALAA Papers*, **82**, 0169 (1982)

⁴ Grüneberger and Hage, *Exp Fluids*, **50**, 363 (2011)

⁵ Jung et al. , *Phys. Fluids*, **4**, 1605 (1992)

⁶ Gouder et al. , *Exp. Fluids*, **54**, 1441 (2013)

Non-Newtonian

Stability of the boundary layer on a rotating disk for power-law fluids

P. T. Griffiths^a, S. O. Stephen^b, A. P. Bassom^c, and S. J. Garrett^d,

The stability of the flow due to a rotating disk is considered for non-Newtonian fluids, specifically shear-thinning fluids that satisfy the power-law (Ostwald-de Waele) relationship. In this case the basic flow is not an exact solution of the Navier-Stokes equations, however, in the limit of large Reynolds number the flow inside the three-dimensional boundary layer can be determined via a similarity solution. The solution methodology is purely an extension of the classical von Kármán similarity reduction that exists in the Newtonian limit. It is important to note that since the flow is not an exact solution of the Navier-Stokes equations asymptotic matching constraints need to be considered. No such considerations are necessary for Newtonian flows as the von Kármán similarity reduction provides an exact solution of the Navier-Stokes equations.

An asymptotic analysis is presented in the limit of large Reynolds number. It is shown that the stationary spiral instabilities observed experimentally in the Newtonian case can be described for shear-thinning fluids by a linear stability analysis. The additional viscous terms associated with the power-law model are dealt with via asymptotic matching between the inviscid layer and the wall layer.

Predictions for the wavenumber and wave angle of the disturbances suggest that shear-thinning fluids may have a stabilising effect on the flow. Fewer spiral vortices with a greater wave angle are predicted as the power-law index decreases from unity. The stabilising or destabilising effect of the power-law index in terms of the critical Reynolds number can only be determined via numerical solution of the full governing stability equations. This is outside of the scope of the current study, however, we expect this work will form a strong basis for such future numerical investigations.

^a School of Mathematics, University of Birmingham, Edgbaston, Birmingham B15 2TT, UK

^b School of Mathematics, University of Birmingham, Edgbaston, Birmingham B15 2TT, UK

^c School of Mathematics & Statistics, The University of Western Australia, Crawley 6009, Australia

^d Department of Mathematics & Department of Engineering, University of Leicester, University Road, Leicester LE1 7RH, UK

Linear stability of viscoelastic Poiseuille flows in cylindrical configurations

A. Petrucci Orefice^a, G. Coppola^a, A. Orazzo^a and L. de Luca^a

The linear stability of annular and pipe Poiseuille flow for a viscoelastic fluid in inertial regime is investigated by considering both linear modal and nonmodal stability properties of infinitesimal disturbances. The viscoelastic fluid is described by the Oldroyd-B model, and the analysis is conducted at moderately high values of the Reynolds number by varying the Weissenberg number and the viscosity ratio between the Newtonian solvent and the polymeric solution. The equations governing both flow and elastic variables are written in polar coordinates and are discretized by an accurate Chebyshev pseudospectral code, suitably adapted in order to mitigate the negative effects of the presence of continuous spectrum on the accuracy of the numerical discretization. The code has been validated by comparing the results against classical and recent numerical studies for pipe and channel viscoelastic Poiseuille flows^{1,2}.

In the case of annular Poiseuille flow, the effects of viscoelasticity on marginal curves of the Newtonian case is such that the critical Reynolds number is decreased at low Weissenberg numbers, while high values of polymer relaxation time have a stabilizing effect. This behaviour, which is in agreement with previous findings for channel flow, vanishes as the mean radius of the annulus reduces. The concentration of the polymer has a destabilizing effect.

Non modal analysis shows that significant transient growth of kinetic energy is present, as in the case of Newtonian fluids, in both annular and pipe configurations. Viscoelasticity is active in reducing the transient growth for high values of streamwise wavenumber. Energy analysis shows that the reduction of the viscosity ratio produces an increase of the dissipation term due to the interaction of the polymer stress with the flow, while increments of the Weissenberg number reduce the production of energy due to the Reynolds stresses.

^a Dip. Ingegneria Industriale, Università degli Studi di Napoli “Federico II”, P.le V. Tecchio 80, Napoli, ITALY

¹ Sureshkumar and Beris, *J. Non-Newtonian Fluid Mech.* **56**, 151 (1995).

² Zhang et al., *J. Fluids Mech.* **737**, 249 (2013).

Transient growth for non-Newtonian fluids in Taylor-Couette flow

Y. Agbessi^a, C. Nouar^b, C. Lemaitre^a and L. Choplin^a

The present communication deals with the transient growth of Taylor-Couette flow of shear-thinning fluids (fluids which viscosity decreases with increasing shear rate). The case of plane shear flows of such fluids has already been considered by Nouar *et al.* (2007)¹ and Liu & Liu (2011)². It was shown that for weakly shear-thinning fluids, transient growth is driven by the lift-up mechanism, while for strongly shear-thinning effect, the Orr mechanism is at work. For flows in rotation, the mechanisms described above may be modified. We consider here the flow between two rotating co-axial cylinders of purely viscous shear-thinning fluids with or without yield stress. Three rheological models were adopted: power law, Carreau and Bingham models.

Classically, a linear stability analysis was conducted, focusing as a first step on the long-time behaviour of the perturbations. The influence of the rheological parameters on the stability curves in the (Re_1, Re_2) plane (Re_1 and Re_2 : inner and outer Reynolds numbers respectively) was determined. A comprehensive analysis of the spectra was performed in the different zones of the (Re_1, Re_2) plane.

In a second step, we have studied the behaviour at short times of the perturbations by using the classical tools of transient growth theory, Schmid and Henningson (2001)³. The shear-thinning character without yield stress is found to enhance considerably the optimal energy amplification of the perturbations, while the yield stress reduces it significantly. Following Dubrulle *et al.* (2005)⁴ and Maretzke *et al.* (2013)⁵, we introduced a shear Reynolds number Re and a rotation number R_Ω , which quantify the shear and rotation effects respectively. For Newtonian fluids, the energy amplification G^{opt} is found to scale as $Re^{2/3}$ everywhere in the (Re_1, Re_2) stable domain, except on the Rayleigh line. On this line, the angular momentum is uniform in the gap, the epicyclic frequency is zero and G^{opt} scales as Re^2 . For non-Newtonian fluids, the amplification scales as $Re^{2/3}$ everywhere. The mechanisms associated to these scalings are proposed. For Re^2 scaling the anti-lift-up mechanism prevails: in that case the optimal perturbation is initially in the form of azimuthal velocity streaks and evolves towards azimuthal rolls. For $Re^{2/3}$ scaling, a three-dimensional Orr mechanism is at work. Initially, the perturbation is oriented against the base shear and it tilts to align practically with the base shear. Unlike the 2D situation, the optimal amplification is reached when the perturbation almost aligns with the base shear. These results have been verified for a wide range of rheological parameters.

^a LRGP UMR 7274 CNRS Université de Lorraine, 1 rue Grandville, BP 20451, 54001 Nancy, France

^b LEMTA UMR 7563 CNRS Université de Lorraine, 2 avenue de la Forêt de Haye, BP 160, 54504, Vandoeuvre Les Nancy, France

¹ Nouar *et al.*, *J. Fluid Mech.* **577**, 211 (2007)

² Liu and Liu, *J. Fluid Mech.* **676**, 145 (2011)

³ Schmid and Henningson, *Applied Math. Sciences* **142**, (2001)

⁴ Dubrulle *et al.*, *Phys. Fluids* **17**, 9 (2005)

⁵ Maretzke *et al.*, *J. Fluid Mech.* (*ArXiv e-prints* Nov. 2013)

Linear and weakly nonlinear instability of streaks in pipe flow of shear-thinning fluids

M. Jenny^a, S.N. Lopez Carranza^b and C. Nouar^a

The present communication is motivated by experimental results^{1,2,3} dealing with the transition to turbulence in a pipe flow of shear-thinning fluids, i.e. fluids for which the viscosity decreases with increasing the shear rate. A streaky flow with an azimuthal wavenumber $n = 1$ (Fig.1c) is obtained in the transitional regime. A linear instability analysis of pipe flow of shear-thinning fluids modulated azimuthally by finite amplitude streaks was investigated recently by the authors⁴. The shear-thinning behaviour is described by the Carreau model. The streaky base flow is computed as the nonlinear temporal evolution of one pair of counter-rotating longitudinal rolls superimposed to a laminar Poiseuille flow and by extracting the velocity field at time t_{max} where the amplitude of the streaks is maximum. The linear instability of the streaky base flow is treated using a normal mode analysis. When the streaks amplitude reaches a threshold value A_c , an instability occurs. This instability originates from inflection points in the streamwise velocity profiles and can be triggered by two different modes depending on the value of A_c . If the threshold amplitude exceeds 41.5% of the Poiseuille centreline velocity, with streaky base flow generated by longitudinal rolls, the instability mode is located near the pipe axis, it is a “center-mode”. For lower values of A_c , the instability mode is located near the pipe wall, in the region of highest normal wall shear, it is a “wall mode”. The numerical results show that for a given kinetic energy of the longitudinal rolls, the threshold amplitude A_c decreases with increasing shear thinning effects. The emergence and the dominance of a wall mode, when shear-thinning effects increase, is clearly highlighted. The analysis of the kinetic energy equation shows that for both instability modes the exchange of energy between the base flow and the perturbation is dominated by the work of the Reynolds stress against the normal wall shear. This is in contrast with the situation of plane Poiseuille flow and plane Couette flow of Newtonian fluid, considered in⁵, where the streak instability is mainly induced by the work of the Reynolds stress against the spanwise shear.

In order to determine how the nonlinear viscous terms sustain the streaky flow observed experimentally, and to elucidate the role of the nonlinear viscous terms, i.e. those arising from the viscosity perturbation, a weakly nonlinear stability of the bifurcation to critical modes is used as a first approach to take into account nonlinear effects. The amplitude expansion method is used. The results show that the bifurcation to a center mode is supercritical and it is subcritical for a wall mode, i.e. for sufficiently strong shear-thinning effects. This encouraging result enables to consider the possibility of using a continuation method for determining nonlinear solutions having an azimuthal wave number $n = 1$.

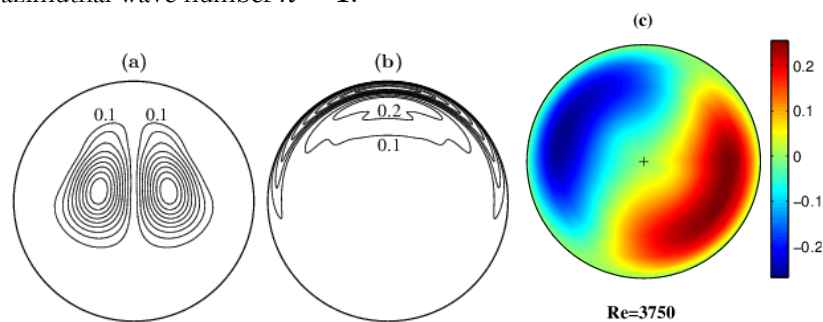


Figure 1. Contours of the amplitude of the streamwise component of the eigenfunction. (a) Center mode for a Newtonian fluid. (b) wall mode for strong shear-thinning fluid. (c) high and low velocity streaks obtained experimentally.

^a LEMTA, UMR 7563 CNRS UNiversit  de Lorraine, 2 avenue de la For t de Haye, TSA 60604, Vandoeuvre-l s-Nancy. France

^b Schlumberger Information Solutions, Oxford United Kingdom

¹ Escudier et al., *J. Non-Newtonian Fluid Mech.* **127**, 143 (2005).

² Esm el and Nouar, *Phys. Rev. E*, **77**, 057302 (2008)

³ Esm el et al., *Phys. Fluids*, **22**, 101701 (2010)

⁴ Lopez Carranza, *Phys. Rev. E*, **88**, 023005 (2013)

⁵ Reddy et al., *J. Fluid Mech.*, **88**, 365, 269 (1998)

Non-Newtonian effects on Droplet-deformation and breakup in confined geometries

A. Gupta^a, M. Sbragaglia^a, A. Scagliarini^a, E. Foard^a and F. Bonaccorso^b

The deformation and breakup of a confined Newtonian/viscoelastic droplet suspended in a Newtonian/viscoelastic matrix under a steady shear between parallel plates is investigated numerically using a diffuse interface lattice Boltzmann method. The viscoelasticity is modelled using the FENE-P constitutive equation, which is solved by means of finite difference schemes. The deformation and breakup of the droplet is investigated as a function of the confinement ratio, viscosity ratio, the polymer relaxation time (Deborah number), and for different polymeric concentrations. Our code is first benchmarked against analytical solutions for droplet deformation at small Capillary numbers. At higher Capillary numbers, the critical velocity at the onset of droplet breakup is found to strongly increase from its Newtonian value with increasing droplet viscoelasticity and confinement ratio, whereas matrix viscoelasticity promotes droplet destabilization. Our results are important for the control of viscoelastic droplets in confined microfluidic geometries.

^a Department of Physics and INFN, University of Tor Vergata, Via della Ricerca Scientifica 1, 00133 Rome, Italy

^b Department of Physics, University of Tor Vergata, Via della Ricerca Scientifica 1, 00133 Rome, Italy

Displacement of Bingham Suspensions in a Slot

S.A. Boronin^a, A.A. Osipov^a, J. Desroches^b

With the development of hydraulic fracturing for stimulation of oil and gas production, modeling of non-Newtonian fluid flows in fractures is becoming increasingly important. Only a few studies in the open literature are devoted to two-dimensional flows of Bingham fluids^{1,2}. Comprehensive analysis of interactions of Bingham particle-laden fluids in a narrow slot has not been carried out yet. The aim of the present study is to analyze various physical phenomena accompanying multiphase flow in a Hele-Shaw cell, such as combined effect of gravitational slumping and viscous fingering, particle settling and granular packing.

We consider a flow of a mixture of non-Newtonian particle-laden fluids in a Hele-Shaw cell. The suspension flow is described within the framework of the two-fluid approach³, where the two interpenetrating continua are assumed to be a carrier medium (composed of several immiscible fluids), and a dispersed continuum (large non-Brownian particles with the diameter much smaller than the fracture width). In the lubrication approximation, 3D governing equations are reduced to a system of 2D width-averaged equations, including hyperbolic equations for transport of fluids and particles coupled with a quasi-linear elliptic equation for the pressure. Governing parameters involve the Bingham number (Bn), which is the ratio of the typical yield stress to the shear stress, the Buoyancy number, the Stokes-to-Froude number ratio determining the particle settling velocity, as well as density and viscosity ratios of the fluids. Governing equations are solved numerically using flux-limiting scheme for hyperbolic equations and the BiCGStab method with ILU(2) preconditioner for the pressure equation. The model and its numerical implementation are validated against available lab data on Newtonian viscous fingering in a slot⁴ and also against some unpublished lab data on channelling of Bingham suspensions in a slot.

Parametric study of different injection sequences is carried out. It is found that in the absence of fingering no unyielded zones are created, and Bingham fluids behave similarly to Newtonian ones. In the presence of fingers, Bingham fluid becomes essentially unyielded due to decrease in local pressure gradient. Yield stress mitigates gravitational slumping, therefore the slumping rate of a Bingham fluid is always lower than that of a Newtonian fluid with the same viscosity and density. Increase in the Bingham number leads to the increase in finger shielding effect: smaller fingers of the displacing fluid left behind tend to stop completely (Fig. 1). Simulations of fluid injection under the conditions when both viscous fingering and gravitational slumping occurs showed that slumping damps fingering.

^a Schlumberger Moscow Research, Pudovkina Street 13, 109147 Moscow, Russian Federation

^b Services Pétroliers Schlumberger, 76 route de la Demi-Lune, 92057 Paris La Defense Cedex, France

¹ Bittleston et al., *J. Eng. Math.* **43**, 229 (2002).

² Pelipenko and Frigaard, *J. Eng. Math.* **48**, 1 (2004).

³ Boronin and Osipov, *Doklady Physics* **55**, 199 (2010).

⁴ Smirnov et al., *Phys. Fluids* **17**, 084102 (2005).

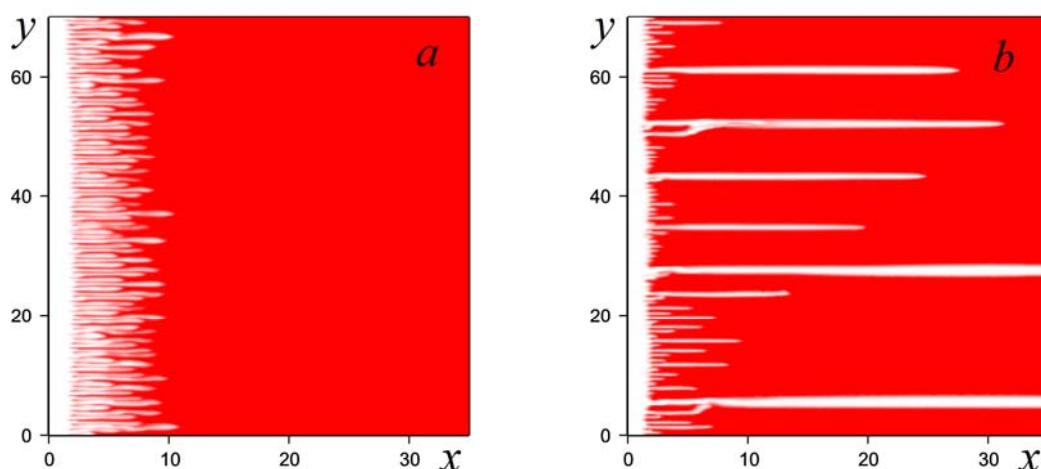


Figure 1: Fluid tracer distributions for iso-density displacement of Bingham fluid (red) by a Newtonian fluid (white) in a slot at $Bn = 0.36$ (a) and $Bn = 5.72$ (b). Mesh is 300×300 , dimensionless time is 0.082.

Non-linear dynamics of the electro-hydrodynamic patterning of viscoelastic materials

G. Karapetsas^a and V. Bontozoglou^b

Recent experimental¹ and theoretical^{2,3} work has shown that interfacial electro-hydrodynamic instabilities can be used in the manufacturing process of micro/nano-structures. The scope of this work is to investigate the non-linear dynamics of the electro-hydrodynamic instability of a viscoelastic polymeric film under a patterned mask. The polymer film is in general considered to be separated from the mask by another viscous fluid. We develop a computational model and carry out 2D numerical simulations fully accounting for the flow and electric field in both phases. For the numerical solution of the governing equations we employ the mixed finite element method combined with a quasi-elliptic mesh generation scheme which is capable of following the large deformations of the liquid-liquid interface. We model the viscoelastic behavior using the Phan-Thien and Tanner (PTT) constitutive equation⁴ taking fully into account the non-linear elastic effects as well as a varying shear and extensional viscosity. We perform a thorough parametric study and investigate the influence of the various rheological parameters, the applied voltage and geometrical characteristics of the mask in order to define the fabrication limits of this process in the case of periodic structures.

ACKNOWLEDGMENTS

The authors would like to acknowledge the financial support by the General Secretariat of Research and Technology of Greece under the Action Supporting Postdoctoral Researchers (grant number: PE8/906), co-funded by the European Social Fund and National Resources.

^a Dep. Mechanical Engineering, University of Thessaly, 38334 Volos, Greece

^b Dep. Mechanical Engineering, University of Thessaly, 38334 Volos, Greece

¹ E. Schaffer, T. Thurn-Albrecht, T. P. Russel, U. Steiner, *Nature (London)* **403**, 874 (2000).

² L. F. Pease and W. B. Russel, *J. Non-Newtonian Fluid Mech.* **102**, 233 (2002).

³ H. Li, W. Yu, L. Zhang, Z. Liu, K. E. Brown, E. Abraham, S. Cargill, C. Tonry, M. K. Patel, C. Bailey and M. P. Y. Desmulliez, *RSC Advances* **3**, 11839 (2013).

⁴ N. Phan-Thien, *J. Rheol.* **22**, 259 (1978).

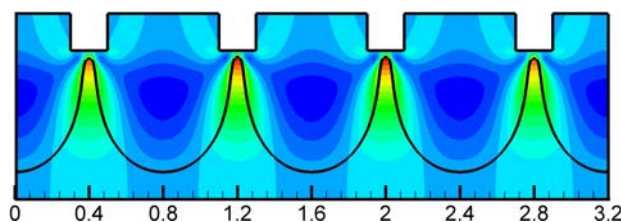


Figure 1: Contour plots of the vertical velocity component. The black line shows the polymer-air interface as predicted by the non-linear numerical model.

Mathematical modelling of coupled Newtonian and non-Newtonian flows at different space and time scales

N. Kizilova^a

Detailed modeling of the cardiovascular system allows *in silico* medical diagnostics on the patient-specific multiscale models, planning the therapy and surgery, estimation of the results of treatment and rehabilitation procedures. Biological fluids are the most complex in nature exhibiting viscoelasticity, anisotropic viscosity, reversible aggregation, and shear thinning. The space scale determines necessity of coupling the Newtonian and non-Newtonian flows, while the time scale defines the influence of the local flow characteristics on the long time behaviour, like aggregation and conglomeration, sediment accumulation, calcification, phase transitions and the related phenomena. In the biofluids the latter are blood clot and atherosclerotic plaque formation which lasts from several months to years, while the direct negative influence of the chemical components and hydrodynamic factors (blood pressure, local pressure oscillations and wall shear stress) are at the heart beat scale ($t \sim 1s$).

Complete 3D modeling of the circulatory system is still impossible due to incredible computer power needed and the number of the model parameters to be specified. The reasonable simplifications are based on incorporation of the realistic 3D models of some regions into the synthetic 1D+0D or 2D+0D model of the systemic and intraorgan blood circulation. The 3D models of the aortic arch, carotid and cardiac vessels combined with 0D model of the heart, larger and smaller vessels have been developed¹. The boundary condition problem at the interfaces of the 3D and 0D models has been discussed for the Newtonian flows only². A new coupling schema for the blood flow in the regions of interest as suspension of aggregating particles in the complex multiscale system is presented in Fig.1.

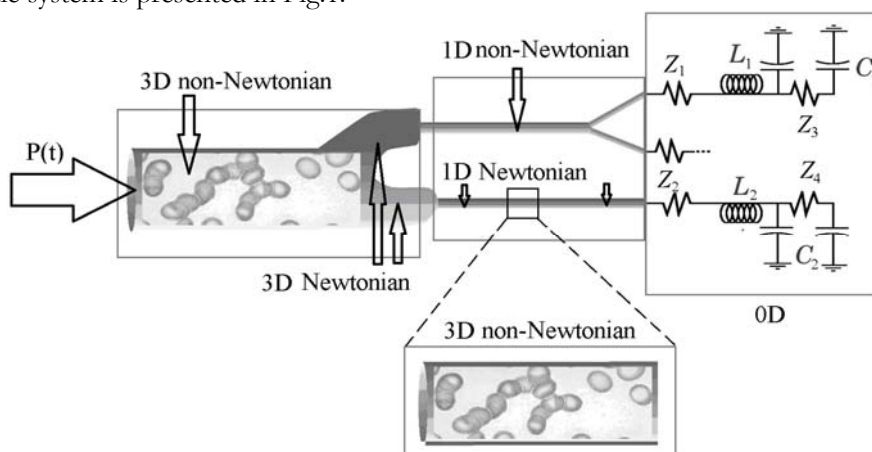


Fig.1. Circulatory system as combination of coupled 3D, 1D and 0D models.

In the paper the boundary condition problem for the non-Newtonian fluid flows coupled with Navier-Stokes equations for Newtonian fluids and viscoelastic solid equations for the distensible vessel walls is solved by application of the mass, particle concentration, momentum and energy balance equations at the interfaces of the regions. The corresponding relations for 3D+1D+0D (I) and 3D+2D+0D (II) models are obtained. The parameter-dependent changes in types of the systems are studied and the conditions preserving hyperbolicity of the coupled system and correct description of the pulse wave propagation are found. Solutions as compositions of 'slow' and 'fast' terms are obtained and analyzed for I and II models.

¹ Quarteroni, *Mathematics Unlimited and Beyond*, Springer, Berlin, 961 (2000).

² Formaggia, et al, *Comp. Meth. Appl. Mech. Eng.*, **191**, 561 (2001).

^a Interdisciplinary Centre for Mathematical and Computer Modeling, Warsaw University, 69 ul. Prosta, Warsaw, Poland

Turbulence Simulations I

Sensitivity analysis of optimal transient growth for turbulent boundary layers

F. ALIZARD¹

T

Structural approaches based on modal decomposition of the turbulence flow dynamics have gain acceptance for a wide variety of turbulent shear flows. In this context, an optimal modes decomposition (i.e. based on optimal transient growth analysis), aiming to model the linear amplification of coherent structures in turbulent flows, is used by Cossu *etal*¹ to reproduce some fundamental motions in a turbulent boundary layer. In particular, the latter authors show that the most amplified optimal modes correspond to elongated streaky structures scaled in inner and outer units (see Figure 1 (a)). The sensitivity of these optimal modes to mean flow modification is here analysed. By assuming that the optimal transient growth linear model is relevant for describing the coherent structures for both the inner and the outer layer, we show that the linear amplification of very large scales which populate the outer motion is not affected when the most temporally amplified optimal mode associated with the inner layer is damped (see Figure 1 (b)). Moreover, we illustrate that the resulting optimal mean flow deviation is consistent with findings of Xu *etal*² who investigate the active control of a turbulent boundary layer by carrying out direct numerical simulation.

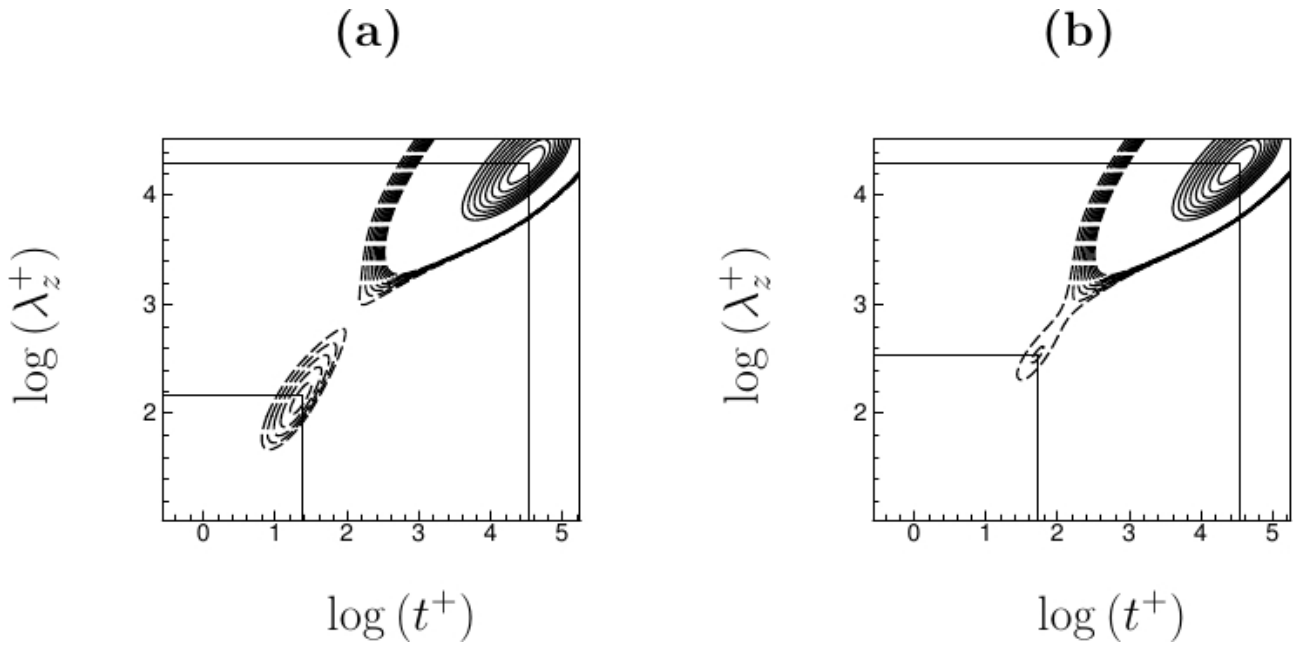


Figure 1: (a) Spanwise size and time scale in inner units for optimal modes associated with infinitely elongated structures in the streamwise direction for a turbulent boundary layer mean flow at $Re\tau=2200$. The dashed and full lines correspond to iso-contours of the energy gain. (b) Influence of the optimal mean flow deviation of a given magnitude equal to $r=0.015$ on the optimal modes properties when the damping of the inner mode is targetted. The same iso-contours for the energy gain are considered.

¹ DynFluid laboratory CNAM. 151 Boulevard de l'Hôpital 75013 Paris (FRANCE)

¹ C. Cossu, G. Pujals and S. Depardon. *J. Fluid Mech.* **619**, 79 (2009).

² J. Xu, S. Dong, M.R. Maxey and G.E. Karniadakis. *J. Fluid Mech.* **582**, 79 (2007).

A marker for studying the turbulent energy cascade in real space

J.I. Cardesa^a, J. Jiménez^a

We introduce a real-space marker for instantaneous fluxes of energy across scales in a 3D turbulent flow. Whereas the widely known subgrid-scale (SGS) dissipation¹⁻³ arises from the evolution equation for the kinetic energy of the large (filtered) scales, our marker originates from the evolution equation of the kinetic energy in the small (residual) scales. We analysed the statistics of both markers by filtering direct numerical simulation (DNS) data in the centreline of turbulent channels. The DNS data span the range $Re_\tau = 1000-4000$, i.e. Re_λ values in the channel centreline of 57-162. Our marker exhibits the expected behaviour of an energy source for the scales below filter-width size: it is positive on average. It is also positively skewed, hinting at intense events occurring preferentially in the direction of a forward cascade. This is consistent with the SGS dissipation being on average an energy sink for the large scales, and negatively skewed. Backscatter is studied from the point of view of both the filtered and residual scales. The probability density functions (PDFs) of these instantaneous energy fluxes show a milder dependence to the filter width for our marker than for the SGS dissipation. The kurtosis shows a higher level of intermittency in the PDF of our marker than in the SGS dissipation. Results will be compared with other DNS flows providing a larger scale separation. It is interesting that the new measure, which only involves small scales, and is therefore more independent of the large-scale forcing than the classical one, is also much more symmetric. This suggests an even more vigorous bi-directional inertial cascade than that observed using older backscatter measures.

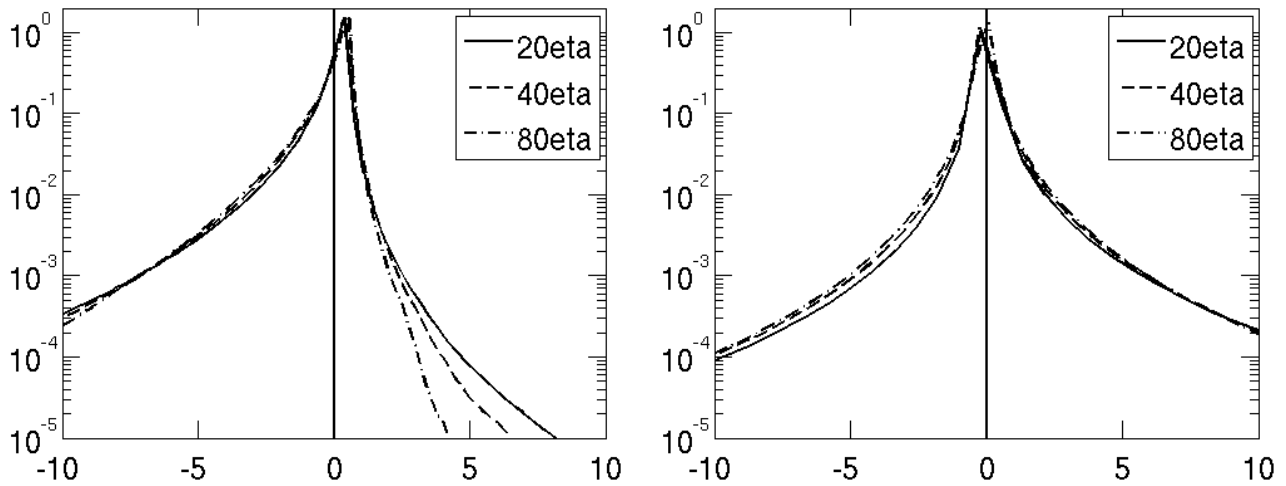


Figure 1: PDFs of energy transfer measured with a Gaussian filter of varying width in the centreline of a turbulent channel at $Re_\tau = 2000$. (left) PDF of SGS dissipation. (right) our marker.

^a School of Aeronautics, Universidad Politécnica de Madrid, 28040, Spain

¹ Piomelli et al., *Phys. Fluids* **3**, 1766 (1991)

² Cerutti and Meneveau, *Phys. Fluids* **10**, 928 (1998)

³ Aoyama et al., *J. Phys. Soc. Japan* **74**, 3202 (2005)

Statistical structure of buoyancy-induced turbulence in a long tilted pipe

J. Magnaudet^{a,b} and Y. Hallel^{c,d}

Based on direct numerical simulation, we investigate the statistical structure of a low-Reynolds-number turbulent flow generated by destabilizing buoyancy forces in a long circular pipe closed at both ends and tilted at an angle of 15° from vertical¹. The flow, which combines features of Rayleigh-Taylor turbulence and homogeneous sheared turbulence, is found to involve a rich phenomenology with striking differences compared with pressure-driven flows. Owing to the transverse stabilizing stratification and axial density gradient, the turbulent shear stress and transverse density flux vary in a quadratic manner across the pipe cross section, decreasing from a maximum on the axis to near-zero values at the outer edge of the near-wall region. Turbulence is essentially produced near the axis, both by negative buoyancy and shear, and diffuses toward the periphery. Most of its dissipation takes place within a thin near-wall region, so that production significantly exceeds dissipation over most of the pipe section. The wall is observed to significantly affect the energy redistribution among the three fluctuating velocity components. Owing to this influence, the closely related density and axial velocity fluctuations reach their maxima at the core periphery, while the spanwise and crosswise velocity fluctuations decrease monotonically from the axis to the wall. The two-point statistics reveal that the large-scale structure, especially that of the density field, keeps track of the long plumes that travel up and down along the pipe. The small-scale structure is found to be deeply influenced by shear and negative buoyancy almost down to the smallest scales, with marked anisotropy and unusually large velocity-derivative skewness coefficients. To get some insight into the connection between turbulent fluxes and density gradients, we introduce a two-time algebraic model of the former in which we inject numerical data to determine all components of the diffusivity tensor. This tensor is found to be strongly non-diagonal and its components to be significantly modified by axial and transverse buoyancy effects. We determine an eddy viscosity and an eddy diffusivity for the turbulent shear stress and transverse mass flux, respectively, the ratio of which reveals that the Reynolds analogy holds within the central part of the flow, whereas nonlocal effects dominate over a large peripheral region.

^a Institut de Mécanique des Fluides de Toulouse (IMFT), Université de Toulouse – INPT, Allée du Professeur Camille Soula, 31400, Toulouse, France.

^b CNRS, IMFT, 31400, Toulouse, France.

^c Laboratoire de Génie Chimique (LGC), Université de Toulouse – UPS, 118 Route de Narbonne, 31062, Toulouse, France .

^d CNRS, LGC, 31030, Toulouse, France.

¹ Hallel & Magnaudet, *J. Fluid Mech.* submitted (2014).

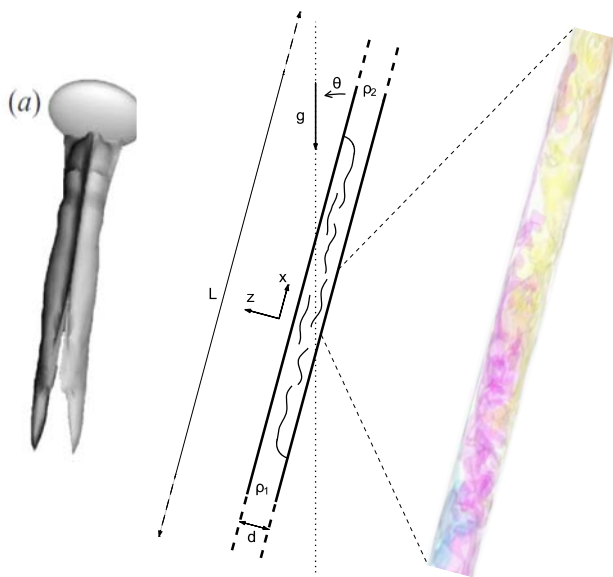


Figure 1: Sketch of the geometry and instantaneous view of the density field in a short central section of the pipe.

Wave energy cascade in forced-dissipative one-layer shallow-water flows

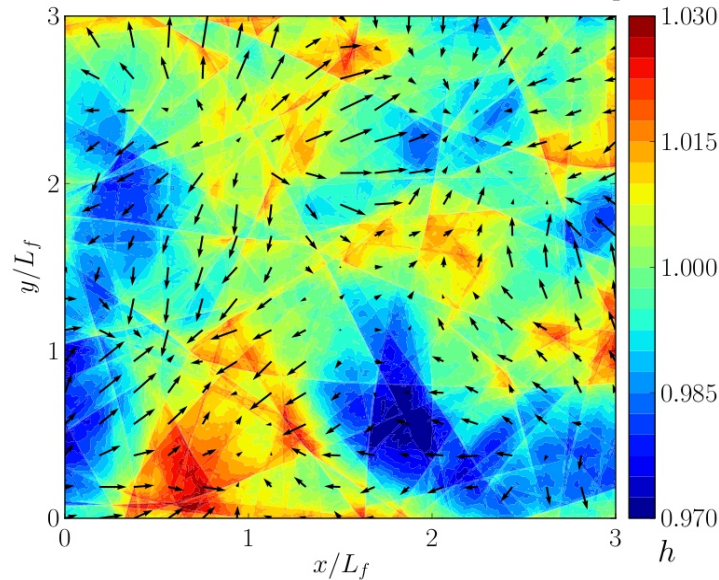
Pierre Augier¹ and Erik Lindborg²

The dynamics of one-layer shallow-water flows forced in medium-scale wave modes and dissipation acting at small scales is investigated by means of theoretical analysis and numerical simulations with resolutions up to 7680^2 .

We first focus on the non-rotating case for which a statistically stationary regime is obtained for all resolutions and Froude numbers $F_f = P/(k_f c)$, where P is the energy dissipation rate, k_f the forcing wave number and c the wave speed.

All the injected energy goes into a downscale energy cascade. Consequently, the spectral energy flux is constant and positive between the forcing wave number and the wave numbers where dissipation is active. The spectral energy flux is exactly equipartitioned between kinetic and potential energy. An exact third order structure function law of Kolmogorov type is derived and numerically verified. However, the downscale cascade is less efficient than in three-dimensional Navier-Stokes turbulence, since the mean energy of the statistically stationary flow scales as $\sqrt{P c / k_f}$ and varies with the dissipative scale. Moreover, the spectra scale as k^{-2} and the structure functions of order larger than two scale approximately as the separation scale r . This intermittent scaling is explained by a simple model based on the assumption that the statistics is totally determined by discontinuities due to hydraulic jumps. These structures are common in these flows as can be seen in the figure showing a snapshot for $F_f = 0.005$ (the arrows represent the velocity and the colours the layer thickness).

It is verified that the dynamics is not drastically modified by system rotation as long as the forcing wave number is larger than the deformation wave number $k_d = f/c$, where f is the Coriolis parameter.



¹ Department of Applied Mathematics and Theoretical Physics, University of Cambridge, Cambridge CB3 0WA, United Kingdom

² Linné Flow Centre, KTH Mechanics, SE-100 44 Stockholm, Sweden

Two-point statistics in variable-viscosity temporal mixing layer

N. Taguelmimt^a, L. Danaila^a and A. Hadjadj^a

Predicting turbulence statistics is a difficult task because of the presence of a very large number of scales within any turbulent flow, and the complex way the energy travels between different scales, thus making any theoretical analysis challenging. The theory of Kolmogorov (1941) premises that small-scale turbulence at infinitely large Reynolds numbers is statistically independent of the large scales, and is stationary, homogeneous and isotropic. The statistical properties of the small scales should be determined universally by ν and $\langle \epsilon \rangle$ (the kinematic viscosity and the mean energy dissipation rate). Inertial range statistics (if the Reynolds number allows one to exist) should be determined by $\langle \epsilon \rangle$ only.

However, in flows involving two fluids with different viscosities, the basic theory of turbulence clearly fails and many physical concepts should be carefully reconsidered. Little attention has been paid to the variable viscosity turbulent flows, which is the most relevant for practical applications (e.g. combustion). The objective of the present investigation is to assess the effects of viscosity variations in low-speed temporally evolving turbulent mixing layers characterized by a velocity difference of ΔU across the vertical direction Y (the two other directions X and Z are considered as homogeneous).

Direct Numerical Simulations (DNS) are performed for several viscosity ratios, $R_\nu = \nu_1/\nu_2$, varying between 1 and 9, whereas the density ratio $R_\rho = \rho_1/\rho_2 = 1$ is kept constant. The space-time evolution of Variable-Viscosity Flow (VVF) is compared with the Constant-Viscosity Flow (CVF for which $R_\nu = 1$). The initial Reynolds number, based on the initial momentum thickness, $\delta_{\theta,0}$, is $Re_{\delta_{\theta,0}} = (\Delta U \delta_{\theta,0})/\nu_{ref} = 160$ for the considered cases. The viscosity reference is the mean viscosity between the two streams $2\nu_{ref} = (\nu_1 + \nu_2)$. The simulations are conducted up to the dimensionless time $\tau = t \Delta U / \delta_{\theta,0} = 400$. It is shown that in VVF (with respect to CVF):

- i) Large-scale quantities (e.g., mean velocity profile) are affected by the viscosity variations, thus dispelling the myth that viscosity is a ‘small-scale quantity’.
- ii) Turbulent fluctuations are created earlier in VVF. Therefore, they are more developed at the same time. This is illustrated by both an enhancement of the total kinetic energy of the VVF velocity field (Fig. 1 (a) where turbulent structures are illustrated through the Q criterion), as well as a promotion of small-scale energy distribution. Fig. 1 (b) represents the second-order structure functions of the vertical velocity component v , $S_{2v}(r)$ normalised by the variance of v , as a function of the scale r (normalized by the Kolmogorov scale). VVF exhibits larger values of $S_{2v}(r)$ than the CVF, thus suggesting a more important amount of energy at smaller scales. The issue of the scaling ranges will be addressed in the full paper. Lastly, the energy transfer at a scale r (quantified through the third-order structure functions, not illustrated here) is enhanced for VVF, thus suggesting an accelerated cascade, most likely due to the presence of the coherent structures, but also to the viscosity variations. These effects will be clearly assessed in the full paper.

^aCORIA UMR 6614, Université and INSA de Rouen, BP 12 76801 Saint Etienne du Rouvray, France.

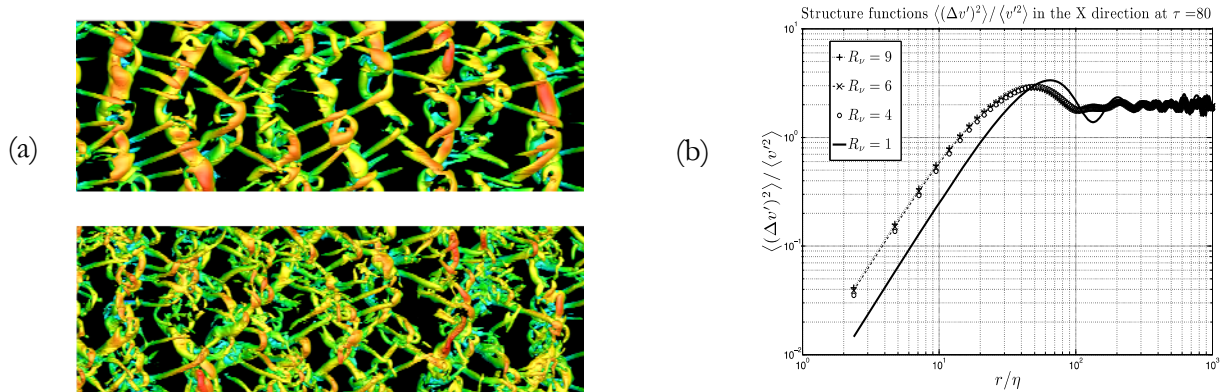


Figure 1: (a) Q criterion for CVF (top) and VVF (bottom) at $\tau = 150$. (b) Second-order structure function for the vertical velocity fluctuation, v , normalized by its variance at $\tau = 80$.

Velocity statistics in turbulent Couette flow up to $Re_\tau=1000$

M. Bernardini¹, S. Pirozzoli^a, P. Orlandi^a

Couette flow is probably the most canonical prototype of wall-bounded flow, featuring zero pressure gradient, and hence constant total stress. As a matter of fact, Couette flow has served as a basis for several early investigations of the mechanisms of self-sustainment of the near-wall turbulence. Despite its utmost theoretical importance, it appears that Couette flow has received much less attention from both experiments and DNS investigations than Poiseuille flow, mainly because of severe technical difficulties in the experimental set-up, and the need to use very large computational boxes in numerical simulations. Hence, the currently explored range of friction Reynolds number in DNS extends to $Re_\tau=170$, approximately. Experiments achieve higher Reynolds number, but typically exhibit wide scatter in the flow statistics.

It is the purpose of this contribution to extend the range of available Reynolds numbers to values close to those reached in Poiseuille flow. For that purpose, a series of DNS have been performed in a relatively wide computational box extending for $12\pi h \times 4\pi h$, where h is the channel half-height. Flow statistics have been collected over a very long time interval, to make sure that the effect of the long coherent structures which form in the channel core are properly averaged out. The mean velocity profiles are shown in figure 1a. A wide region with nearly logarithmic behaviour is observed, with log-law constants $k=0.41$, $C=5.0$, as in the classical theory. It is worth noticing that recent DNS of turbulent Poiseuille flow at Re_τ up to 4000 indicate, on the other hand, that $k=0.386$, $C=4.30$. The streamwise velocity variance is shown in figure 1b for various Reynolds number. The same increasing (near logarithmic) trend also noticed in Poiseuille flow is observed, and associated with the influence of Townsend's inactive motions. Most interesting, an outer energetic peak seems to emerge in the outer part of the wall layer at $Re_\tau = 1000$, whose existence has been speculated for Poiseuille flow, and associated with the increased activity of h -scaled outer eddies.

A full account of the results, including wall friction, mean core velocity profile, and additional velocity statistics, will be presented.

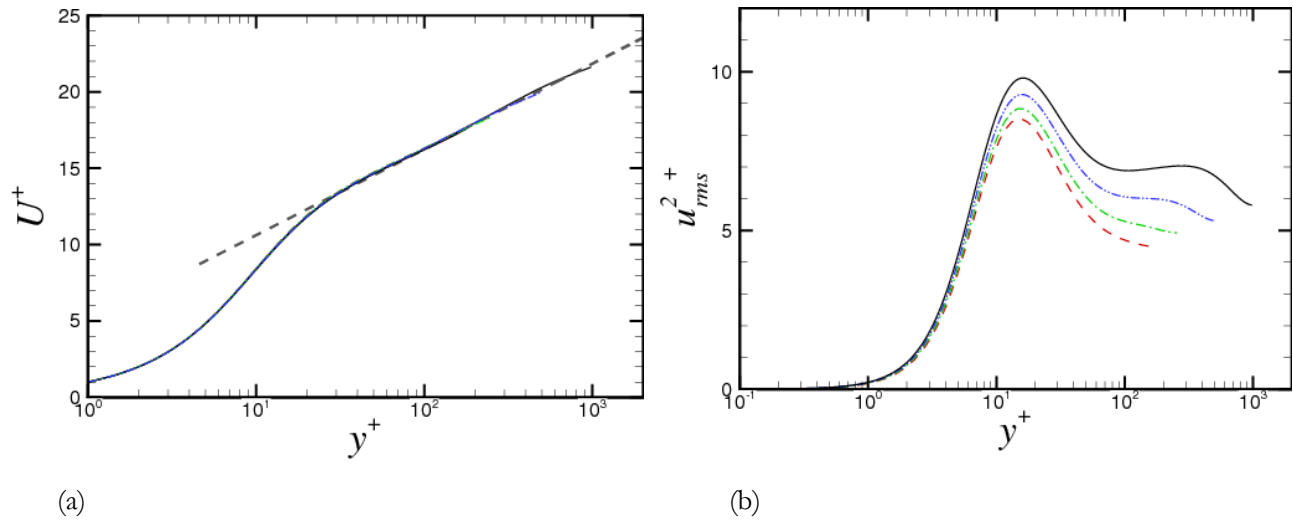


Figure 1: eDistributions of mean velocity (a) and streamwise velocity variance (b) in wall units for $Re_\tau = 180$ (dashed), $Re_\tau = 250$ (dash-dot), $Re_\tau = 500$ (dash-dot-dot), $Re_\tau = 1000$ (solid).

¹ Dep. Mechanical and Aerospace Engineering, University of Rome "La Sapienza", 00184 Via Eudossiana, Rome.

Analytical

UNFOLDING OF NON-SIMPLE DEGENERATE STREAMLINE PATTERNS NEAR A NO-SLIP WALL WITH APPLICATION TO BOUNDARY LAYER ERUPTION

A. Balci^a, M. Brøns^a

In incompressible two-dimensional flows one can find the streamline patterns using a Taylor expansion of the stream function ψ . The stream function close to a no-slip wall can be expanded as

$$\psi = y^2 \sum_{n,m=0}^{\infty} a_{n,m+2} x^n y^m \quad (1)$$

where the wall is located at $y = 0$. The coefficients $a_{n,m}$ are functions of the physical parameters of the flow and time if the flow is unsteady. The streamlines are found from the differential equations

$$\dot{x} = u = \frac{\partial \psi}{\partial y}, \quad \dot{y} = v = -\frac{\partial \psi}{\partial x}. \quad (2)$$

The topology of streamlines of (1) has been considered by many authors, e.g. [1, 2, 3]. Important object in a topological analysis is the critical points of the stream function. A critical point occurs on the wall if $a_{0,2} = 0$. The Jacobian matrix is written as

$$J = \begin{pmatrix} u_x & u_y \\ v_x & v_y \end{pmatrix} = \begin{pmatrix} 2a_{1,2} & 3a_{0,3} \\ 0 & -a_{1,2} \end{pmatrix}. \quad (3)$$

When the Jacobian matrix is regular, the origin is a point of separation or attachment. If the Jacobian is not regular, the critical point is structurally unstable: arbitrarily small variations of the parameters may give rise to a change of the topology of streamlines. One is interested in obtaining an unfolding of the degeneracy, that is, a bifurcation diagram showing all possible streamline patterns that can occur when the parameters are close to degeneracy.

The critical point has a simple degeneracy if $a_{1,2} = 0, a_{0,3} \neq 0$. The unfolding of this case is studied in detail in [1, 2]. If $a_{1,2} = 0, a_{0,3} = 0$, the origin is a non-simple degenerate point. The bifurcations occurring in this case under the non-degeneracy conditions $a_{2,2} \neq 0, \tilde{a}_{0,4} = \frac{a_{0,4}}{a_{2,2}} - \frac{a_{1,3}^2}{4a_{2,2}^2} \neq 0$ are studied by Hartnack [2]. We study the case where the condition $\tilde{a}_{0,4} \neq 0$ is broken, i.e. $a_{0,2} = a_{1,2} = a_{0,3} = \tilde{a}_{0,4} = 0, a_{1,2} \neq 0$. Using these conditions, the stream function is expanded to higher order. By a normal form approach we obtain the complete unfolding and show it depends on three parameters. We sketch the bifurcation diagram which includes both local and global bifurcations.

We apply our theory to give a systematic description of the topological changes of the streamline pattern that occur during a boundary layer eruption or separation. Kudela and Malecha [4] investigated numerically the boundary-layer eruption caused by a two dimensional patch of vorticity above a wall. We show that all the streamline bifurcations that are observed at moderate Reynolds numbers can be explained by the bifurcation diagrams we have found.

^a Department of Applied Mathematics and Computer Science, Technical University of Denmark, Building 303B, DK-2800, Kgs. Lyngby, DENMARK

¹ Bakker, Bifurcation in Streamline Patterns. *Kluwer Academic Publishers*, (1991).

² Hartnack, *Acta Mechanica* **136**, 55-75 (1999)

³ Brøns, *Advances in Applied Mechanics* **41**, 1-42 (2007)

⁴ Kudela and Malecha, *Fluid Dynamics Research* **41**, 055502 (2009)

Influence of compressibility on the vortex force

R. Tognaccini^a and B. Mele^a

A new exact expression of the aerodynamic force acting on a body in steady high Reynolds number (laminar and turbulent) compressible flow is proposed. The aerodynamic force is obtained by integration of the Lamb vector field, given by the cross product of vorticity times velocity. The theory links the force generation to local flow properties, in particular to the Lamb vector field and to the kinetic energy.

In incompressible flows, the idea to compute the aerodynamic force in terms of vorticity integrals is not new. Noca et al.¹, for instance, proposed a method limited to unsteady conditions. The analysis of steady flow could be obtained by replacing vorticity with the Lamb vector². The price to be paid is, however, the need to perform a volume integration of the Lamb vector (the vortex force), less suitable for post processing experimental data. Marongiu and Tognaccini³ extended the latter to the analysis of high Reynolds number turbulent flows. These expressions highlighted the key role played by the Lamb vector field on the generation of the aerodynamic force.

Another interesting feature of these formulae is the possibility to express the aerodynamic force in terms of volume integrals of a limited part of the flow domain (*mid field* method): the body boundary layer and wake, an alternative to the straight forward formulae obtained by the momentum integral equation with surface integrals of momentum flux far from the body (*far field* method) or by body surface integration of stresses (*near field* method).

It is here proposed the extension to compressible flow of the method proposed by Marongiu and Tognaccini. In case of steady, two-dimensional, uniform laminar flow around a body the new obtained *exact* formula for the aerodynamic force is

$$\underline{F} = - \int_{\Omega} (\rho \underline{l} + \underline{m}_{\rho}) d\Omega - \int_S \underline{r} \times (\underline{n} \times \rho \underline{l}) dS,$$

where ρ is the fluid density, \underline{l} is the Lamb vector, \underline{r} is the position vector, Ω is a portion of the fluid domain surrounding the body and containing the boundary layer and wake, S is its external surface with outward unit normal vector \underline{n} . $\underline{m}_{\rho} = -\underline{r} \times [\underline{\nabla} \times (\underline{V}^2 / 2 \underline{\nabla} \rho)]$ is the explicit compressibility correction term. It can be easily verified that also in this case the integration can be limited to the rotational region. In presence of curved shock waves we only have to add the shock wave wakes. An equivalent formula has been obtained for turbulent flows considering Favre averaging of the fluid properties. The proposed equation provides a straightforward breakdown of the aerodynamic force in lift (given by the volume integral on Ω) and drag (given by the surface integral on S).

The theoretical results are confirmed analyzing numerical solutions obtained by a standard RANS solver. Results are discussed for the case of a two-dimensional airfoil in subsonic, transonic and supersonic free stream conditions. The results evidence interesting features of the compressible regime. For low Mach numbers the aerodynamic force only depends on the Lamb vector field. As the Mach number increases the Lamb vector contribution to lift (vortex force) diminishes and is compensated by the compressibility correction term. An interesting relation between vortex force and Kutta-Jukovskij force (proportional to the circulation around the body) is also evidenced by the theoretical and numerical analysis.

^a Dipartimento di Ingegneria Industriale, Università di Napoli *Federico II*, Naples, Italy

¹ Noca et al., *J. Fluids and Struct.*, **13**, 5, 1999.

² Wu et al., *J. Fluid Mech.*, **576**, 2007.

³ Marongiu and Tognaccini, *ALAA J.*, **48**, 11, 2010.

On some analytical solutions for Navier-Stokes equations

Francisco J. Sánchez-Bernabe^a

In this work we review several particular analytical solutions for Navier-Stokes equations¹. The first one is for primitive variables (velocity and pressure) and then, some analytical solutions for Vorticity-stream function formulation are considered. The most common benchmark problem to test a code that solves Navier-Stokes equations is the driven cavity, Erturk et al², due to the simplicity of geometry and also the fact that the Dirichlet boundary conditions are constant.

However, the discontinuity of velocity at the upper corners have motivated several authors to propose alternative problems. One of them is the backward step channel, Hossain et al³, which involves a more complicated geometry. Shih et al⁴, have considered a similar problem to lid cavity problem, but the boundary conditions are continuous. Another possibility is concerned with jet injection in rectangular⁵ and square⁶ cavities.

With respect the Vorticity-stream function formulation⁷, Chadna et al⁸, have proposed three types of analytical solutions by studying generalized Beltrami flow when the vorticity function present a special form. Also, Polyanin and Zaitsev⁹ present some solutions. Kumar and Kumar¹⁰ obtained three new analytical solutions by using the Similarity Transformation Method. Muriel and Dresden¹¹ have presented a 3D analytical solution.

^a Dep Matemáticas, Universidad Autónoma Metropolitana Iztapalapa, 09340 México, D F, Mexico

1 Temam R, Navier-Stokes equations: theory and numerical analysis, North-Holland (1984)

2 Erturk et al., Int. J. Num. Meth. Fluids **60**, 275 (2009).

3 Hossain et al, Int J Eng Research & Tech 2, 3700 (2013).

4 Shih et al, Int. J. Num. Meth. Fluids **9**, 193 (1989).

5 Breggren, SIAM J. Sci. Comput. **19** No 3, 829 (1998).

6 Glowinski, Num meth for fluids, Part 3 (Handbook of Num Analysis IX) Elsevier (2003).

7 Majda, Vorticity and incompressible flow, Cambridge University Press (2002).

8 Chadna et al, Internat. J. Math. & Sci. **17**, No 1, 155 (1994)

9 Polyanin and Zaitsev, Handbook of Nonlinear Partial Diff Eq, Chapman & Hall (2004)

10 Kumar M and Kumar R, Meccanica, **49**, 335 (2013)

11 Muiriel and Dresden, Physica D **101**, 297 (1997)

Variational Formulations for Viscous Flow

M. Scholle^a and F. Marner^a

For physical systems, the dynamics of which is formulated within the framework of Lagrange formalism the dynamics is completely defined by only one function, namely the Lagrangian. As well-known the whole conservative Newtonian mechanics has been successfully embedded into this methodical concept. Different from this, in continuum theories many open questions remain up to date, especially when considering dissipative processes. The viscous flow of a fluid, given by the Navier-Stokes equations is a typical example for this.

Two different approaches are used for finding a Lagrangian for viscous flow: in case of steady flow a first integral of the Navier-Stokes equations has been found recently². By a slight modification a set of self-adjoint equations is obtained leading to a respective Lagrangian. Different from this, for unsteady flows universal symmetries and associated Noether balances are considered¹. The equations of motion resulting from the suggested Lagrangian are compared to the Navier-Stokes equations. Differences become manifest in a different form of the viscous terms, including their order (third order instead second order terms), but also in an additional field, the thermasy, appearing explicitly.

For some simple flow geometries solutions are calculated and compared to those of the Navier-Stokes equations. By means of three flow examples of prototypic character, the flow over a suddenly moving plate, the plane Couette flow and the decay of a vortex (see Fig. 1), it has been demonstrated that the phenomenon of viscosity is taken into account, as required. In case of the steady example, the Couette flow, the wellknown solution of Navier-Stokes equations has been exactly reproduced, whereas the two unsteady examples revealed some quantitative differences in the profile compared to the solution of the original Navier-Stokes equations.

Perspectives toward a further improvement of the method are discussed.

References:

1. M. Scholle, *Proc. R. Soc. Lond. A* **460** (2004) 3241–3260
2. M. Scholle, A. Haas and P. H. Gaskell, *Proc. Roy. Soc. Lond. A* **467** (2011) 127–143

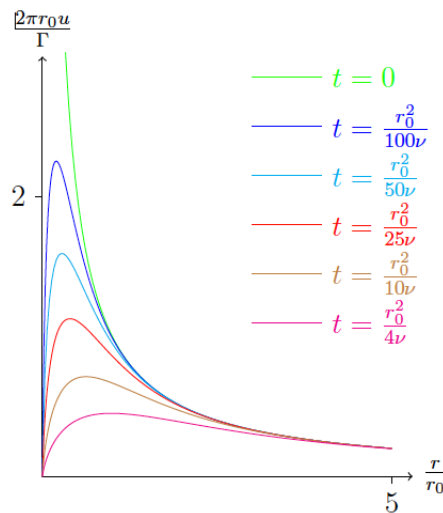


Fig1: Decay of a vortex.

^a Institute for Automotive Technology and Mechatronics, Heilbronn University, D-74081 Heilbronn, Germany

On a potential-velocity formulation of Navier-Stokes equations

F. Marner^a, P. H. Gaskell^b and M. Scholle^a

Computational methods in continuum mechanics, especially those encompassing fluid dynamics, have emerged as an essential investigative tool in nearly every field of technology. Despite being underpinned by a well-developed mathematical theory and the existence of readily available commercial software codes, computing solutions to the governing equations of fluid motion remains challenging, especially if nonlinearities and free surface problems are involved. Therefore, there is a continuous demand for developing new efficient methods in continuum mechanics.

Recently, by introduction of an auxiliary potential field, a first integral of the two-dimensional incompressible Navier-Stokes equations has been constructed leading to a set of equations, the differential order of which is lower than that of the original equations^{1,2}. In this talk the new formulation is shown to be naturally extendible to full three dimensional problems, including to free surfaces along which a dynamic boundary condition has to be considered. In principle the method is not restricted to Newtonian fluids but can also be applied to fluids implicating more complex material laws, for instance to fluids with viscoelastic character.

The potential-velocity formulation of incompressible Navier-Stokes equations requires the development of new but potentially advantageous numerical solution methods. Numerical methods and their application to selected flow problems are presented in the talk and results are shown in order to demonstrate the capabilities of the first integral formulation. In the case of free surface flow the dynamic boundary condition can be reduced to a standard Dirichlet-Neumann form, which allows for an elegant numerical treatment. See below for two-dimensional results of thin gravity-driven film flow, generated by an implementation of the new approach.

^a Dep. Autom. Technology and Mechatronics, Heilbronn University, D-74081 Heilbronn, Germany

^b School of Engineering and Computing Sciences, Durham University, Durham, DH1 3LE, UK

¹ Scholle et al., *Proc. R. Soc. Lond. A* **467** (2011).

² Ranger, *Quart. J. App. Math.* **52** (1994)

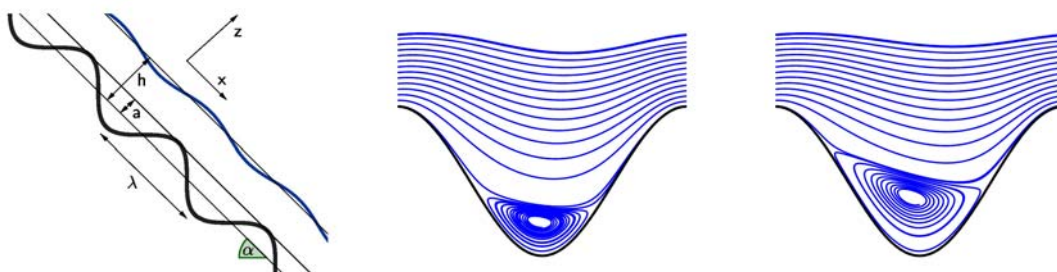


Figure 1: Thin gravity-driven film flow over corrugated substrate with inclination angle α : Increasing Reynolds number from left ($Re = 30$) to right ($Re = 50$).

Parity violation in two-dimensional fluids

A. Lucas¹, P. Surówka²

Recent progress in physics has demonstrated that isotropic fluids in two spatial dimensions generically have parity-violating terms in the equations of motion [1]. Such parity-violating terms are known to be present in fractional quantum Hall fluids and topological insulators [2], and are expected to be present in fluids consisting of chiral molecules as well [3]. In 2+1 dimensions, one such possible term involves the dissipationless Hall viscosity, which is a first order correction on the same footing as the standard shear and bulk viscosities. The effects of parity-violation and Hall viscosity on an external probe sitting in an incompressible fluid have been studied, where there are new stresses normal to the surface. However, the effects of parity-violation on the hydrodynamic flows themselves are poorly understood, as the Hall viscosity is effectively a “topological” surface term in the incompressible Navier-Stokes equation [4], and so more terms must be added to see new physics away from boundaries. In this talk we will provide examples of the effects of parity-violation in a variety of flows, including both incompressible and compressible flows, isothermal flows and flows with temperature gradients. We focus on the possible experimental signatures of parity-violating fluids that are observable in the absence of external probes or boundaries. As examples, we will study the consequences of the parity-violating terms in the Poiseuille and Couette flows, and in the normal modes of waveguides, when the Hall viscosity depends on the position, and demonstrate chiral corrections to the standard results. We also demonstrate the presence of modified sound propagation with “helicon” waves in a dissipationless limit, and present new phenomena for compressible flows in magnetic fields (See Fig. 1). Moreover, we will study the corrections due to parity-violation in the Rayleigh-Benard convective instability in the Bousinesq approximation, and explain the role of new parity-violating terms in thermal transport, where the effects are most pronounced.

¹ Dep. Physics, Harvard University, Cambridge, MA, USA

² Center for the fundamental Laws of Nature, Harvard University, Cambridge, MA, USA

¹ Jensen et al., JHEP. **05**, 102 (2012).

² Hughes et al, Phys. B

³ Andreev et al, P

⁴ Avron, J. Stat. Phys.

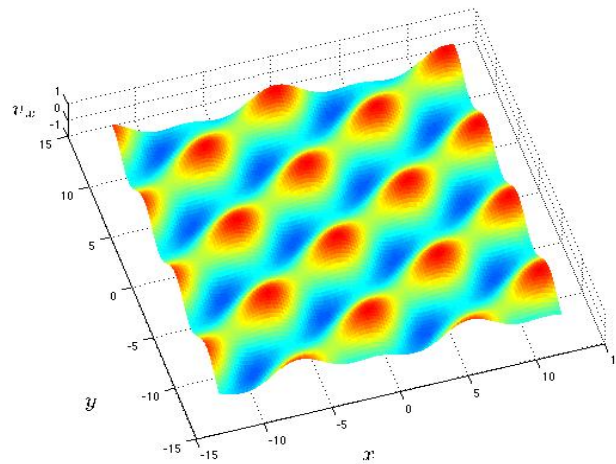


Figure 1: Example of robust hexagonal pattern of fluid (x-velocity pictured). This flow is stabilized by a magnetic field and a small speed of sound. Flows such as this are unstable without Hall viscosity.

T U E S D A Y

16th September 2014

Free Surface Flows

Liquid Films

EXPANDED COANDA EFFECT

Ioan Rusu

Electrica Serv Romania

ioandanrusu@yahoo.com

The fluid flow, liquids and gases, on solids, pursue the solids surface. This phenomenon was discovered by Henry Coanda and was named the Coanda effect (Figure 1).



Figure 1

By simply researches, the author Ioan Rusu discover that the Coanda effect could be expanded also for fluid flow on discontinuous solids. Practically, was demonstrate that on a solid surface with many orifices and at a special angle and for minimum speed of a fluid, on the surface of solid, the fluid follows the apparent surface of solid as a continuous sheet (Figure 2, 3 and 4).



Figura 2



Figura 3



Figura 4

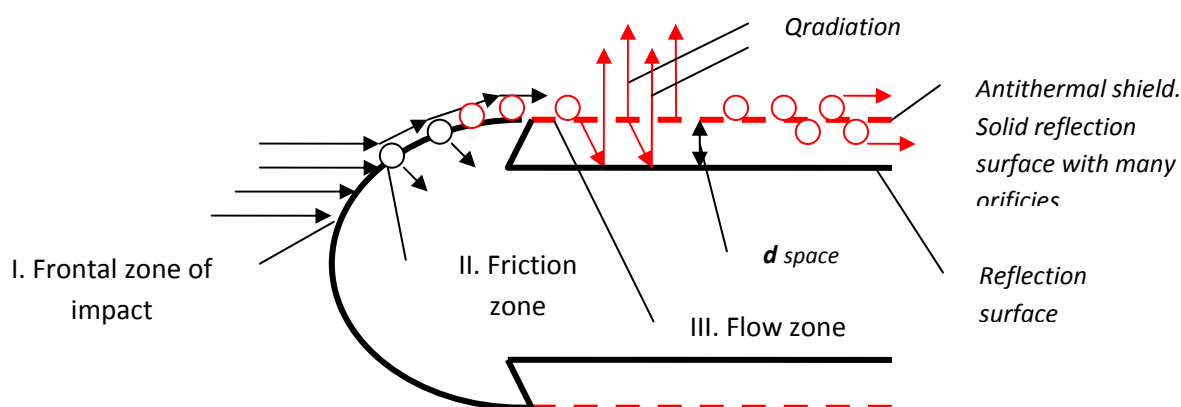


Figure 4

APPLICATION for EXPANDED COANDA EFFECT:

ANTITHERMAL SHIELD FOR ROCKETS WITH HEAT EVACUATION BY INFRARED RADIATION REFLECTION

At high speed, the friction of air mass with the rocket surface produce local heating more than 1000°C . For heat protection of rocket, on their outside surface are install antithermal shields.

Studing Coanda effect, respectively, the fluid flow on solids surface, the author Ioan Rusu discover by simply researches that the Coanda effect could be expanded also for the fluid flow on discontinuous solids, respectively, on solids with orifices. This phenomenon was named by the author, the expanded Coanda effect.

Start with this discovery, the author Ioan Rusu invent an antithermal shield, registered at Romanian Patent Office, OSIM, deposit F 2010 0153

This antithermal shield:

- is built as a covering rocket sheet with many orifices install with a minimum space from the rocket body
- take over the heat fluid generate by the frontal part of rocket and avoid the direct contact of heat fluid with the body of the rocket

- *assure the evacuation of infrared radiation, generate by the heat fluid who flow on shield by expanded Coanda effect by reflection from rocket body surface*

NOTE: for participation of this conference, I need financial support (sponsorship) to paid registration and hotel.

Thank you,

Ioan Rusu

The effect of soluble surfactants on the linear stability of liquid film flow

G. Karapetsas¹ and V. Bontozoglou²

The formation of instability waves in gravity-driven liquid films flowing down inclined surfaces is of importance in a broad range of engineering, geophysical and biomedical applications. It is known that these instabilities can be significantly affected by the presence of surfactants, and the role of insoluble surfactants (i.e. species that are assumed to reside only on the interface) has been repeatedly addressed¹. Soluble surfactants have been investigated to a lesser extent, and a mechanistic understanding of their role appears to be missing. These species are expected to exhibit more complex behaviour, because interfacial dynamics is intricately coupled with mass exchange with the bulk.

In the present work, we investigate analytically and computationally the linear stability of liquid film flow in the presence of a surfactant of arbitrary solubility. The Navier–Stokes equations are supplemented by mass balances for the concentrations at the interface and in the bulk and by a Langmuir model for adsorption-desorption kinetics at the interface. The resulting linear eigenvalue problem is solved analytically in the limit of long-wave disturbances and numerically (by a finite-element method) for disturbances of arbitrary wavelength.

The instability is shown to be a long-wave one, and to depend only on surfactant solubility and interfacial concentration. Insoluble surfactants stabilize the flow most effectively at maximum concentration (closest interfacial packing), whereas strongest stabilization moves to lower concentrations with increasing solubility. Disturbances of finite wavelength are found to be significantly more stable than long-wave ones, because interfacial gradients are intensified by the shorter length scale. Also, sorption kinetics begins to play a key role, with very slow kinetics leading to a virtually frozen interface and an insoluble-like behaviour².

The analysis permits an extension of the physical mechanism of the long-wave instability in order to take into account the presence of the surfactant. The longitudinal flow perturbation, known to result from the perturbation shear stress which develops along the deformed interface³, is shown to contribute a convective flux that triggers an interfacial concentration gradient. This gradient is, at leading order, in phase with the interfacial deformation, and as a result produces Marangoni stresses that stabilize the flow. The strength of the interfacial concentration gradient is shown to be maximum for an insoluble surfactant and to decrease with increasing surfactant solubility. The decrease is explained in terms of the spatial phase of mass transfer between interface and bulk, which mitigates the interfacial flux by the flow perturbation and leads to the attenuation of Marangoni stresses.

¹ Dept. Mechanical Engineering, University of Thessaly, 38334 Volos, Greece

² Dept. Mechanical Engineering, University of Thessaly, 38334 Volos, Greece

¹ Pereira & Kalliadasis, *Phys. Rev. E* **78** (3), 036312 (2008).

² Karapetsas & Bontozoglou *J. Fluid Mech.* **729**, 123 (2013).

³ Smith, *J. Fluid Mech.* **217**, 469 (1990).

Creating localized drop train in a liquid film by traveling thermal waves

A. Oron ^a, V. Frumkin ^b, Wenbin Mao ^c and A. Alexeev ^c

Using long-wave theory and direct numerical simulations (DNS) of the Navier-Stokes and energy equations, we investigate the nonlinear dynamics of a bilayer system consisting of a thin liquid film and an overlying gas layer driven by the Marangoni instability. The bottom solid substrate is heated in the form of periodical thermal waves propagating along the substrate with a constant frequency ω . In the case of a stationary thermal wave, $\omega=0$, the liquid film rupture takes place with a flattish wide trough when both Marangoni number and the amplitude of the thermal wave are sufficiently large. Regimes in which the film forms a train of localized drops traveling along the substrate arise for sufficiently small, but non-zero ω . In this case, localized traveling drops are interconnected by thin liquid bridges with negligible small flow velocities, see curve 1 in Fig.1a. With an increase of ω , the interfacial profiles represent traveling waves with less localized shapes. We show that the liquid is trapped inside the drops during the drop train motion, see curve 1 in Fig. 1b, and the total flow rate q is linearly proportional to ω . When the minimal thickness of the bridges between consecutive drops is increased, a faster flow rate q can be achieved than in the localized drop-train configuration. In this case, however, fluid in the bridges has the negative (backward) velocity and can migrate from one drop to another, see curve 2 in Fig. 1b, thereby leading to a gradual exchange of the content of drops in the train. Thus, the localized drop-train mechanism can be tuned to allow for the delivery of the entire drop content in the direction of the thermal wave propagation.

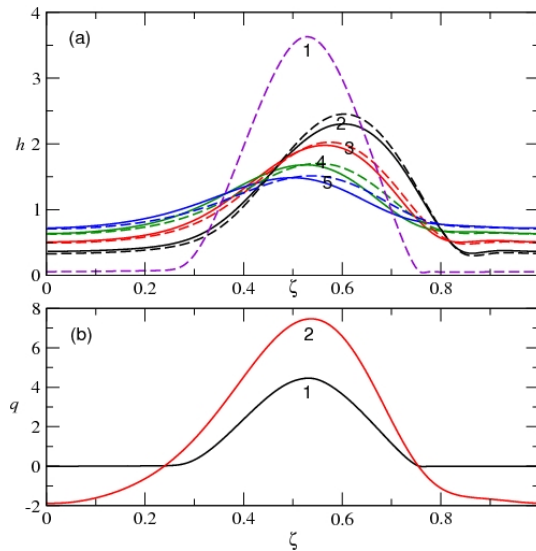


Figure 1: Evolution of the liquid film in a bilayer gas-liquid system for a certain set of parameters. (a) Curves 1-5 show interfacial shapes $h(\zeta)$ of the film in the saturated state as a function of the longitudinal coordinate ζ scaled with the period size for increasing values of ω . The solid and dashed curves correspond to the DNS and the long-wave theory, respectively. Note that DNS computation fails for the smallest value of ω . (b) Variation of the flow rate q within a periodic domain. Curves 1 and 2 correspond to the cases displayed by curves 1 and 5 in (a).

^a Dep. Mechanical Engineering, Technion- Israel Institute of Technology, Haifa, 32000 Israel

^b Dep. Mathematics, Technion- Israel Institute of Technology, Haifa, 32000 Israel

^c Woodruff School of Mechanical Engineering, Georgia Institute of Technology, Atlanta, GA 30332, USA

Experiments on the evolution of traveling waves over an undulated incline

Daniel Reck^a, Nuri Aksel^a

We present experimental results on the evolution of traveling waves over a strongly undulated incline. In order to investigate the difference between waves in the linearly stable and unstable region, we set the Reynolds number near the neutral curve. That way, we were able to cross the neutral curve by increasing the frequency of excitation, without changing the velocity field of the basic flow. The amplitude of excitation was also varied, to analyze the evolution of both linear and nonlinear waves. We were able to increase the resolution of our measurements significantly by dividing the traveling waves into fragments. In order to receive the wave over the whole length of our channel, we reassembled the fragments by using the periodic nature of the traveling waves.

We report on a rich variety of phenomena, including:

- a) energy transfer from the excitation frequency to its higher harmonics
- b) the growth rate of the traveling waves
- c) the stability of traveling waves depending on its amplitude
- d) the amplitude of saturation depending on the excitation frequency
- e) the phase velocity of the traveling waves being equal to the phase velocity of a corresponding Nusselt flow.

To our knowledge, this is the first experimental work on the development of traveling waves over strongly undulated substrate geometries. For further information, we refer to our publication in *Physics of Fluids*¹

^a Dep. Applied Mechanics and Fluid Dynamics, University of Bayreuth, Germany

¹ Reck and Aksel, *Phys. Fluids*, **25**, 102101 (2013)

Experiments beyond the limits of Nusselt theory: The linear stability of gravity-driven films over undulated inclines

M. Schörner^a, D. Reck^a and N. Aksel^a

We present experimental results on the linear stability of gravity-driven films over strongly undulated inclines. Within our parameter study we vary the Reynolds number, the liquid's viscosity and the inclination angle of the substrate. Furthermore, we change the frequency of the linear disturbances which we impose to the basic flow. That way, we obtain stability charts which show a rich variety of phenomena induced by the undulation of the incline: We found a slight destabilization as well as a very significant stabilization of the flow compared to the corresponding Nusselt flow. Moreover, we report on transmutations from long-wave to short-wave type instabilities. Even a fragmentation of the stability chart, which leads to stable and unstable isles, is observed.

Our study extends former approaches^{1,2} and explores the above-mentioned complex stability behavior of gravity-driven films over strongly undulated inclines in-depth. We are now able to classify the stabilizing and the destabilizing effects. Concerning the stabilizing effects, we identified a significantly increased mean film thickness of the flow due to the undulation compared to the corresponding Nusselt flow. Consequently, this leads to a decreased average flow velocity and hence the flow is stabilized. Beyond this, we proved the destabilizing effect of hydraulic jumps and a strongly curved free surface of the liquid. This enabled us to explain the fragmentation of the stability charts and thus the existence of stable and unstable isles – phenomena which clearly exceed the limits of Nusselt's theory.

^a Dept. Applied Mechanics and Fluid Dynamics, University of Bayreuth, Germany

¹ Pollak et al., *Phys. Fluids* **25**, 024103 (2013)

² Cao et al., *J. Fluid Mech.* **718**, 304-320 (2013)

Liquid Film Coating over Patterned Substrates with Air Inclusion inside the Trench

P. K. Nguyen¹, M. Pavlidis^a, Y. Dimakopoulos^a and J. Tsamopoulos^a

Although film flow over topography has been studied extensively when the substrate is in full contact with either Newtonian^{1,2,3} or nonNewtonian⁴ liquids, the very interesting case of partial contact has not yet been addressed. Particularly, the liquid film forms inside the trench an air inclusion where the inner interface is bounded between three-phase contact points. The latter are either fixed at the top sharp-edges of the trench or may translate along its side or bottom boundaries. These types of arrangements have important effects both on microelectronic applications and on microfluidics (super-hydrophobic surfaces). One such configuration is numerically studied and depicted in Fig. 1. We want to predict shapes of air inclusions for Newtonian liquid by solving the 2D steady Navier-Stokes equations using the mixed Galerkin finite element method and the quasi-elliptic mesh generation methodology⁵.

While keeping the same liquid, trench geometry and contact angles, the inertial effect on the air-inclusion is not so trivial. For example, in the range $0 < \text{Re} < 6$, the air inclusion shrinks to its minimum size at an intermediate value of flow rate, $\text{Re} = 3$. This is due to the complicated coupling between capillary and inertia effects resulting in a large deformation of the outer free surface. The capillary ridge^{3,4} is closer to the trench entrance and forces the liquid more effectively into it. At lower inertia, $\text{Re} = 0.3$, the capillary ridge stays further upstream. That weaker capillarity around the step in cannot force liquid into the concave corner and leaves an empty space therein. Whereas at higher $\text{Re} = 6$, inertia flattens both interfaces up to the capillary depression^{3,4}. The higher inertia on the one hand helps the liquid circumvent the trench and on the other hand requires a larger capillary depression to push the liquid out of the trench. Overall, air inclusion growth is observed to couple with the contraction of the cross section of liquid film around the step-in.

Using pseudo arc-length continuation, we have computed the parametric evolution of both free surfaces and generated several solution families. This method was required to capture turning points, and multiplicity of solutions for the same parameter values⁵. Finally, in the examined parameter space, the free surfaces, the contact lines and the flow field vary in a complex way in terms of the flow rate and liquid properties.

¹ Dep. Chem. Eng., University of Patras, 26504, Patras, Greece

¹ Mazouchi and Homsy, *Phys. Fluids*, **13**: 2751 (2001)

² Nguyen and Bontozoglou, *Phys. Fluids*, **23**, 052103 (2011)

³ Kalliadasis, Bielarz, Homsy, *Phys. Fluids*, **12**, 1889 (2000).

⁴ Pavlidis, Dimakopoulos and Tsamopoulos *J. Non Newt. Fluid Mech.*, **165**, 576 (2010)

⁵ Dimakopoulos and Tsamopoulos, *J. Comp. Phys.*, **192**, 494 (2003).

⁶ Kistler and Scriven, *J. Fluid Mech.*, **263**, 19-62 (1994).

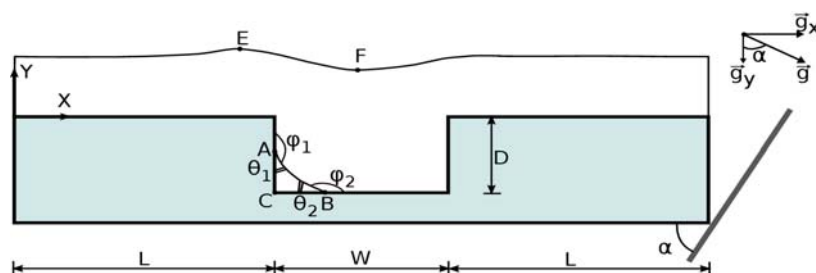


Figure 1: Sketch of the coating flow along a patterned substrate with air inclusion inside the trench.

Eddy genesis within and the stability of heated films flowing under gravity on an inclined wavy substrate

S. Veremieiev^a, M. Scholle^b and P.H. Gaskell^c

The problem of interest [1, 2, 3] consists of the two-dimensional, gravity-driven, free-surface laminar, film flow of a Newtonian liquid over a uniformly heated wavy substrate, which is inclined at an angle α to the vertical, see Figure 1. There is no evaporation from the surface of the film and heating is provided via a source inside the substrate which generates heat in such a way as to maintain the temperature, Θ , at a constant substrate value Θ_w . The air above the film is taken to be stationary with constant temperature Θ_a and pressure P_a ; the heat transfer at the liquid-air interface is assumed to follow Newton's law of cooling. The specific heat, c_p , and the thermal conductivity, λ , of the liquid are assumed constant, while the density, $\rho(\Theta)$, dynamic viscosity, $\mu(\Theta)$, and surface tension, $\sigma(\Theta)$, obey the following temperature dependencies: $\rho = \rho_0[1 - \beta'\Theta_r]$; $\mu = \mu_0[1 - \mu'\Theta_r]$; $\sigma = \sigma_0[1 - \gamma'\Theta_r]$; $\Theta_r = (\Theta - \Theta_a)/(\Theta_w - \Theta_a)$; where ρ_0 , μ_0 and σ_0 are their values at the reference temperature Θ_a , while β' , μ' , γ' denote the associated thermal expansion, thermo-viscosity, thermo-capillary coefficients, respectively.

First, for the range of parameters of interest a linear stability analysis of the flow is performed to identify the critical Marangoni number, Ma_{crit} , for the onset of thermocapillary instability. This is done in the form of the linearised integral-boundary layer approximation equations and Floquet-Bloch theory [2]. The influence and importance of substrate waviness, capillary number, Ca , Biot number, Bi , substrate inclination angle, α , and especially thermo-viscosity and thermal-expansion on Ma_{crit} is investigated and corresponding neutral stability curves constructed.

Next, in regions where the flow is stable the underpinning steady-state flow structure, temperature field and the global heat transfer across the film are obtained via solution of the full Navier-Stokes, continuity and associated temperature equation. This is achieved using a finite element discretisation of the governing equation set, based on Bubnov-Galerkin mixed interpolation with the free-surface parameterised via an Arbitrary Lagrangian-Eulerian (ALE) method of spines. It is shown that thermo-viscosity, thermal-expansion and Marangoni number all affect the internal flow structure (and heat transfer), in that when they are non-zero a skewed eddy is observed to be present. Comparisons are drawn with eddy genesis resulting from the subtle interplay between inertia and varying surface geometry in the case of isothermal film flow [4, 5, 6].

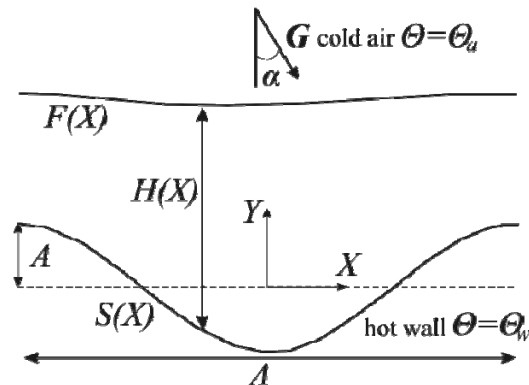


Fig. 1. Schematic diagram of gravity-driven flow over a heated wavy substrate, showing the coordinate system adopted and surface geometry.

^a School of Engineering, Technology and Maritime Operations, Liverpool John Moores University, Liverpool, L3 3AF, UK

^b Institute for Automotive Technology and Mechatronics, Heilbronn University, 74081 Heilbronn, Germany

^c School of Engineering and Computing Sciences, Durham University, Durham, DH1 3LE, UK

¹ Haas, PhD Thesis, University of Bayreuth (2010).

² D'Alessio et al., K.A., *J. Fluid Mech.* **665**, 418 (2010).

³ Blyth and Bassom, *Proc. Roy. Soc. A*, **468**, 4067 (2012).

⁴ Wierschem et al., *Acta Mech.* **179**(1-2), 41 (2005).

⁵ Scholle et al., *Phys. Fluids* **20**(12), 123101 (2008).

⁶ Veremieiev et al., *Computers & Fluids*, **39**, 431 (2010).

Meandering instability of a liquid rivulet on an inclined plane

A. Daerr^a, S. Couvreur^a, J. Eggers^b and L. Limat^a

We have investigated the stability of a rivulet of water flowing down on a vertical glass pane. This system exhibits different flow regimes for increasing flow rate^{1,2,3}: at very low flow rate no stream can form and water runs down in distinct drops. As the flow rate is increased, one observes first stationary, pinned rivulets (straight or meandering), then non-stationary streams meandering and breaking up, and at even higher flow rates again straight streams. Our aim was to determine why water does not always run down along a straight path, namely how straight rivulets become unstable and start meandering.

In total wetting conditions, where there are no pinning forces, both an experiment in a Hele-Shaw cell and a theoretical model demonstrate that anisotropic friction due to the dissipation in the contact lines leads to an inertial instability⁴. In partial wetting the pinning of the contact lines suppresses the linear instability mechanism. The instability still exists however, because a flow rate increase will eventually increase the contact angle beyond its maximum static value, at which point the contact line recovers its mobility.

We have recently shown experimentally⁵ that the critical flow rate at which this happens can be predicted by analysing the initial rivulet shape, specifically its width and roughness. This dependence of the instability threshold on the shape is due to the hysteretic nature of contact line pinning. Just as the rupture threshold of solids depends on pre-existing stresses, rivulets prepared at different widths, contact angles or contact line roughness will become unstable at different flow rates.

^a MSC UMR CNRS 7057, Physics dep., Univ. Paris Diderot, F-75205 Paris cedex 13

^b School of Mathematics, University of Bristol, Bristol BS8 1TW, United Kingdom

¹ Nakagawa & Scott, *J. Fluid Mech.* **149**, 89 (1984).

² Culkin & Davis *AIChE J.* **30**, 263 (1984).

³ Kern, *Verfahrenstechnik* **3**, 425 (1969)

⁴ Daerr *et al.*, *Phys. Rev. Lett.* **106**, 184501 (2011).

⁵ Couvreur & Daerr, *Europhys. Lett.* **29**, 24004 (2012).

⁶ Le Grand-Piteira *et al.*, *Phys. Rev. Lett.* **96**, 254503 (2006).

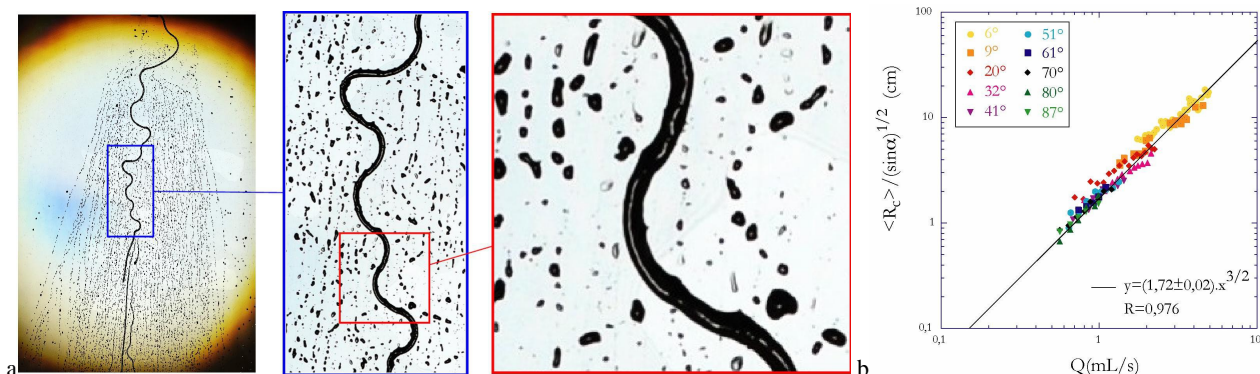


Figure 1: (a) Fluid rivulet meander on a glass pane. The white line visible at the highest magnification (middle) marks the locus of maximum height, and indicates that the rivulet profile is asymmetric in the bends. (b) The characteristic bending radius of stationary meanders is given by an equilibrium of inertial and pinning forces.⁶

Mini Symposia: Wind Energy

The important role of aerodynamic measurements for the reliable and cost effective design of wind turbines

J.G. Schepers, Energy Research Center of the Netherlands, ECN

EFMC10 conference, Mini-Symposium on Wind Energy Aerodynamics

The presentation addresses results from several projects in which detailed aerodynamic measurements have been (or will be) used for the validation and improvement of wind turbine design codes.

Important examples are the IEA Tasks 14 and 18 projects which were carried out in the 1990's and in which experiments were performed in atmospheric conditions on several wind turbines with diameters ranging from 10 to 27 meters. The unique feature of these projects lied in the measurements of pressure distributions at different positions along the rotor blade. The IEA Tasks 14 and 18 projects were followed by IEA Task 20 in which measurements were analyzed as taken by NREL in the USA on a wind turbine with a diameter of 10 meter placed in the large NASA-Ames wind tunnel.

Most of the attention in the presentation will be paid to the Mexico measurements which were carried out on a rotor with a diameter of 4.5 meter placed in the large Low Speed Facility (LLF) of the German Dutch Wind Tunnel (DNW). The unique feature of these measurements lied in the addition of PIV flow field measurements next to pressure measurements along the blade. The Mexico measurements were taken in 2006 after which they were analyzed in a large international consortium within the IEA Task 29 Mexnext project. The analysis led to unique insights on the flow field in and around a wind turbine and the subsequent impact on the aerodynamic loads. It also led to recommendations for a future experiment, which is scheduled to be carried out in summer 2014 on the same 4.5 meter turbine model in the same LLF of DNW.

Other plans on aerodynamic measurements will also be touched upon. In this respect it is important to note that the aerodynamics community, i.e. the subgroup aerodynamics of EERA, clearly stated that the time is ripe for a new public field aerodynamic measurement program on a scale which is as large as possible (5MW+). The definition of such experiment will be worked out in the recently started EU FP7 AVATAR project. Other interesting experiments which are expected from AVATAR are high Reynolds number airfoil measurements in the pressurized DNW-HDG wind tunnel in Gottingen. These measurements are tentatively scheduled for August 2014.

Navier-Stokes Computations of the MEXICO Turbine in Yawed Flow

I. Herráez^a, B. Stoevesandt^b and J. Peinke^a

In spite of yawed flow being a common issue in wind turbines, the prediction of its associated loads remains a major challenge for wind turbine designers.

Under yawed flow conditions, the angle of attack becomes a function of (among other quantities) the azimuth position. Thus, the cyclic variation in angle of attack during a rotor revolution might lead to dynamic stall, especially at inboard regions of the blade, where the flow usually presents a higher tendency to separate. Furthermore, at high angles of attack this region of the blade is also commonly affected by 3D rotational effects, which make the stall angle to be delayed and the maximum lift to be enhanced. The combination of dynamic stall and rotational augmentation under yawed conditions makes the flow in the root region of wind turbines extremely complex and unsteady.

In this work, we present our efforts for predicting such complex flows by means of transient Reynolds Averaged Navier-Stokes simulations performed with the open source numerical tool-box OpenFOAM. The numerical results are validated against the MEXICO turbine, which offers a unique experimental data set including surface pressure data and Particle Image Velocimetry (PIV) flow measurements. The comparison is performed for the turbine operating at 15 m/s and two different yaw angles, namely 30° and -30 degrees. The wake of the wind turbine is analyzed by comparing numerical results with axial and radial traverses extracted from the PIV data. The loads are also validated after integration of the surface pressure data.

First results show that for the wake, the agreement between experiments and simulations is very satisfactory. However, greater discrepancies arise when the blade loads are compared. The correct prediction of the hysteresis loops associated with the dynamic stall effect is the main challenge we are working on.

These results highlight the great potential of RANS computations, as well as their main limitations, for the prediction of complex flows in wind turbines.

^a Institute of Physics, University of Oldenburg, D-26111, Oldenburg, Germany

^b Fraunhofer IWES, Ammerländer Heerstr. 136, Oldenburg, Germany

Experiment test and CFD simulation of 5kW horizontal-axis wind turbine flows

Z.W. Li^a, L. Chen^a, S.M. Li^a and D.X. He^b

Although the China wind energy industry has achieved a great progress in the past ten years, the fundamental research activities are still weak for the wind turbine flow. We are lack of comprehensive knowledges about the unsteady aerodynamic forces acting on the wind turbine blades. The design tool is mainly based on BEM that needs more modification in the condition of blade movement such as yaw and pitching. Recently, the China ministry of science and technology approved several fundings concerning the researches on the aerodynamic property of wind turbine. It will help to override the gap between the design and the manufactory of large wind turbines in China.

Computational Fluid Dynamics (CFD) has long been applied successfully to solve the Aeronautic and Astronautic engineering problems. However, it doesn't play the same role in the wind turbine design, due to the complexity of the wind turbine flow. The rotating blades generate strongly nonlinear, unsteady, separated, shear, unstable and turbulent flows that are considered to be the most difficult problems to model and predict. Despite its large uncertainty, CFD could provide more knowledges about the flow, helping the engineering model improvement.

In the paper, we introduce some CFD validation results in China Aerodynamic Research and Development Center (CARD C). A 5 kW horizontal axis wind turbine has been designed and the experiments have been conducted in the 12m by 16m test section in the Low Speed Wind Tunnel in CARD C. The pressure and force measurements are used to validate the CFD codes, which one is developed with the pressure-based SIMPLE method and the other with density-based MUSCL method. Both solve the RANS equations. Grid sequence process from coarse to fine is used to obtain the grid-independent solution (Verification). Different turbulent models ($k-\omega$ and $k-\epsilon$, etc) have been compared. Their effects on the flow structure have been analyzed. The other experiment models, such as from NREL UAE and MaxNext, are also been simulated. Finally, the uncertainty of the CFD code has been identified.

^aChina Research and Development Center(CARD C),Mianyang, Sichuan, PRC.

^bChina Wind Energy Association(CWEA), Yiheng buildings, East north section of the 3rd ring road, Chaoyang district, Beijing, PRC.

Main results on wind turbine aerodynamics and aeroacoustics from the DANAERO full scale experiments

H.Aa. Madsen^a, C. Bak^a and N. Trolborg^a

A considerable amount of detailed experimental data on wind turbine aerodynamics and aeroacoustics, such as e.g. pressure distributions at different radial stations, have been acquired in the past from dedicated wind tunnel experiments like the NASA Ames experiment conducted in year 2000 on a 10m rotor and the MEXICO experiment in 2006 using on a 10m rotor. However, one major limitation of the wind tunnel experiments on model rotors is the lack of the effects of the real atmospheric inflow characteristics (shear and turbulence) on the aerodynamic and aeroacoustic response. This was the main motivation to conduct the DANAERO experiments from 2007-2009¹ where the main focus has been to explore and characterize the influence of turbulence and shear in the inflow to full scale rotors.

The DANAERO experiments comprised three different major coordinated parts: 1) inflow measurements on a 3MW, 107m diameter rotor with a five hole pitot tube mounted on one of the blades; 2) inflow and surface pressure measurements plus high frequency surface pressure fluctuation measurements with flush mounted microphones on the blade of an 2MW, 80m diameter rotor and 3) wind tunnel measurements of 2D airfoil section data in different wind tunnels to provide reference data without influence of atmospheric turbulence.

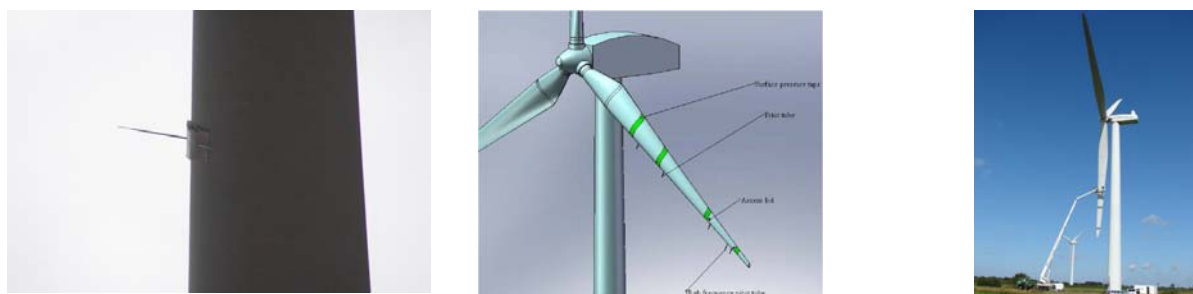


Figure 1: (a) Five hole pitot tube mounted at radius 36m on the 107m diameter Siemens 3W turbine. (b) Overview of instrumentation on the 40m test blade build for installation on the NM80 2MW 80m diameter rotor. (c) The test blade installed on the rotor.

In the DANAERO II project² conducted from 2011 to 2013 the experimental data from the experiments have been calibrated and stored into a suitable data base enabling an efficient use of the data. Examples of studies are shown in Figure 2 and will be further elaborated in the final paper.

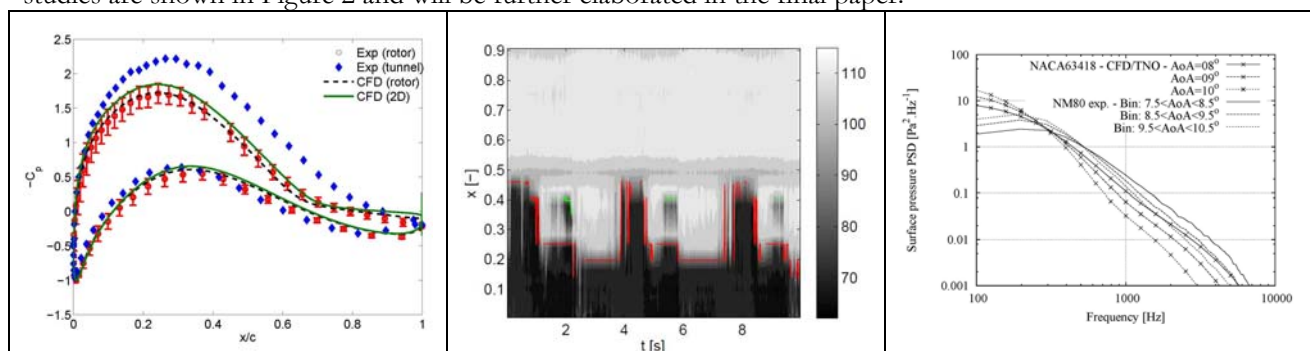


Figure 2: (a) Inboard surface pressure coefficients computed and measured. (b) Measured position of transition (read line) on the rotor over 10 seconds. (c) Surface pressure spectra for characterization of trailing edge noise from a microphone close to the trailing edge in comparison with the TNO model.

^a DTU Wind Energy, Campus Risoe, Frederiksborgvej 399, DK 4000 Roskilde

¹ Madsen et al., AIAA 2010-645, 48th AIAA Aerospace Sciences Meeting, Orlando, Florida 4 - 7 January 2010

² Trolborg, Bak and Madsen, DTU Wind Energy E-0027, April 2013

Three-dimensional instability analysis for an optimized Glauert rotor

D. M. Smith^a, F. Gómez^a, H. M. Blackburn^a, and J. Sheridan^a

Recent advances in renewable energy include the optimization of offshore arrays of Horizontal Axis Wind Turbines (HAWT). In this clustered configuration, individual turbine inlet conditions can be significantly influenced by the wake of upstream turbines. Hence, the understanding of the stability of the HAWT wake, composed of a system of blade root and tip counter-rotating vortices, is of utmost importance, since large fluctuations in pressure and velocities exacerbate fatigue loading on individual turbines, besides reducing the performance. It is desirable to facilitate early breakdown of a turbine wake into small scale flow structures, particularly when ambient free-stream turbulence is low. Thomsen et al.¹ and Dahlberg et al.² identified wake effects playing a significant role in fatigue loading of turbines for low turbulence intensity free-stream conditions.

Outcomes of the three-dimensional stability analysis outlined by Gómez et al.³ will be presented for a Glauert optimum rotor wake computed from an Actuator Line computation. The investigation considers variations to Reynolds number, tip speed ratio and blade geometry. We vary blade geometry such that the root vortex is generated closer to the tip vortex to investigate the root vortex mutual inductance mode observed by Sherry et al.⁴ in a computational setting. We also examine interactions between root and tip vortices. Comparisons of leading eigenmodes with varying tip speed operation will elucidate differences associated with close and loosely spaced vortex systems.

Preliminary results for the three-dimensional analysis applied with Reynolds number of 2000 with base-flow and eigenmode shown by Figure 1 have identified the mutual inductance mode in the tip and root vortices, as well as instabilities in the farfield turbine wake consistent with leading modes arising from the linear stability analysis of an actuator disc turbine wake under similar conditions.

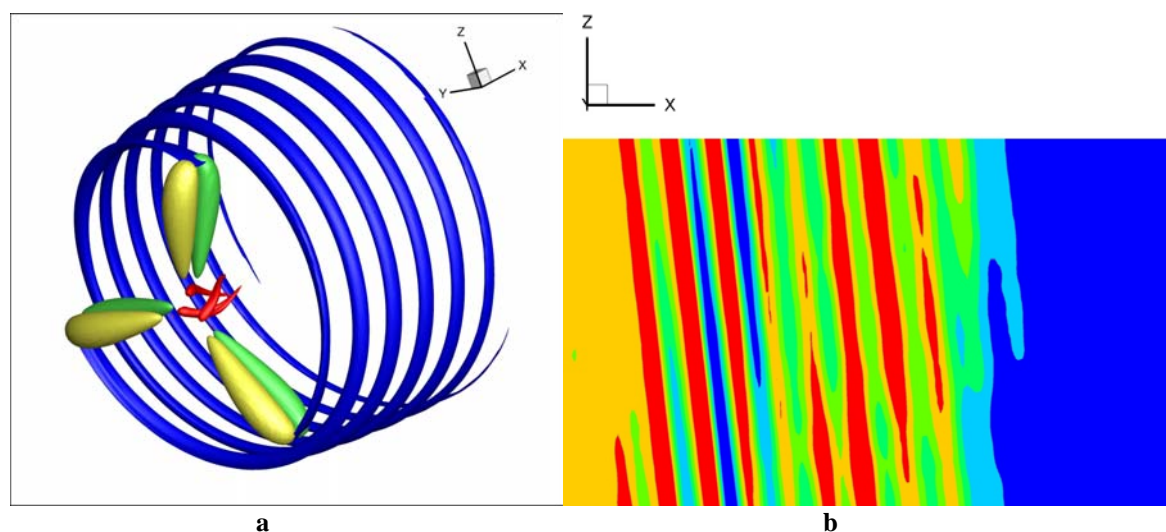


Figure 1: a: Turbine base flow, with red/blue iso surfaces showing helical vortex arrangement and green/gold pressure contours showing blade region. b: Leading eigenmode shown for radial velocity a radial plane at radius 1.15.

^a Dep. Mechanical and Aerospace Engineering, Monash University, Victoria 3800, Australia.

¹ K. Thomsen, et al. *Riso National Laboratory* **743** (1994)

² Å Dahlberg et al. *EWEA Special Topic Conf. 92: The potential of Wind farms*, Herning, Denmark (1992)

³ F. Gómez et al., *Aerospace Science and Technology*, **32**, 223-234 (2013)

⁴ M. Sherry et al. *Physics of Fluids* **25** (2013)

Experimental analysis of turbulent mixing in wind turbine and actuator disc wakes

L. E. M. Lignarolo^a, D. Ragni^a, C. J. Simão Ferreira^a and G. J. W. van Bussel^a

A common approach to the numerical simulation of wind farms is to model the rotors as actuator discs; this approach misestimates the effects of flow turbulence and disregards the effects of the tip vortex helix instability. Consequently the mixing process across the wake interface and ultimately the rate at which the wake recovers momentum is incorrectly modelled. ² explains how the strong velocity gradients introduced at the wake edges in the actuator disc model cause unrealistic turbulence peaks enhancing the near wake dissipation. ³ show how results from experiments on a wind turbine and numerical simulations of an actuator disc have discrepancies till the far wake. The present investigation focuses on the experimental analysis of the different physics governing the mixing processes in the shear layer of a wind turbine wake and of an actuator disc wake. The experiments are conducted with high-resolution stereoscopic particle image velocimetry in the OJF wind tunnel of at TUDelft. The wind turbine model is a 60-centimeter diameter two bladed rotor (see ¹) and the actuator disc is reproduced with a porous disc matching the diameter and drag coefficient of the wind turbine. A double decomposition of the flow is applied and the different terms of the transport equation of the kinetic energy are estimated. The mean flow kinetic energy fluxes at two wake locations (before and after the onset of the turbine's wake instability) are compared with the ones obtained in the wake of the actuator disc. The study will show how the high kinetic energy of the free stream is entrained in the inner regions of the two wakes: the discrepancies between the two models will be investigated in their physical origins.

^a Dep. Aerodynamics Wind Energy Flight Performance and Propulsion, TUDelft, 1 Kluyverweg, Delft, The Netherlands

¹ Lignarolo et al., *Renew. Energ.*, (under review) (2014).

² Schepers, J.G. TUDelft. PhD. Thesis (2012).

³ Wu and Porté-Agel, *Bound-Lay Meteorol* **138(3)**, 345-366 (2011).

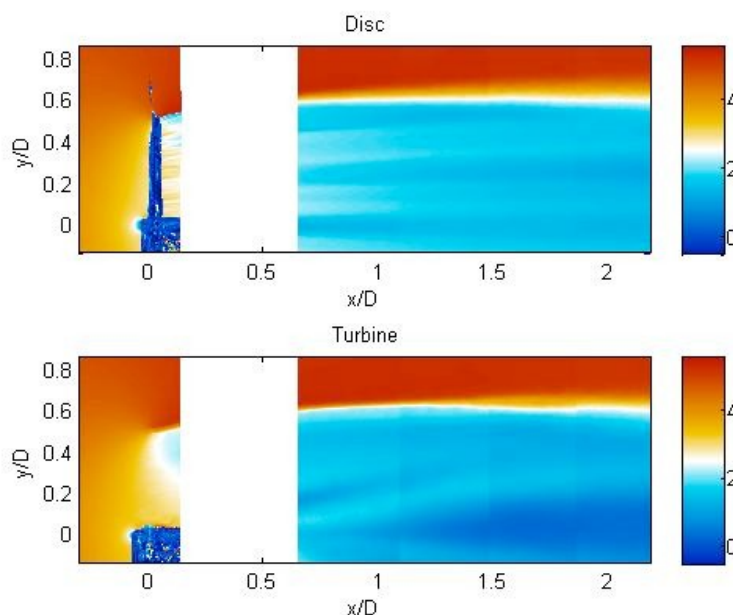


Figure 1: (a) Velocity distribution in the porous disc wake. (b) Velocity distribution in the wind turbine wake.

Prediction of the hub vortex instability in a wind turbine wake: stability analysis with eddy-viscosity models calibrated on wind tunnel data

G. V. Iungo^a, F. Viola^b, S. Camarri^c, F. Porté-Agel^a, and F. Gallaire^b

The evolution and downwind recovery of wind turbine wakes are crucial factors for the evaluation of wake-to-wake interactions within a wind farm and, in turn, for the prediction of wind power harvesting. Wind turbine wakes are affected by the design of wind turbine blades and the produced aerodynamic loads, by the characteristics of the incoming wind, such as turbulence, shear, thermal stability, and by the topography of the site. Moreover, it is observed that dynamics and instabilities of vorticity structures present in a wind turbine wake can affect remarkably the downstream evolution of the whole wake. Indeed, the flow past a wind turbine is characterized by the presence of two main large-scale vorticity structures: the helicoidal tip vortices, which detach from the tip of each turbine blade, and the hub vortex, which is a streamwise-oriented vorticity structure located approximately at the wake center. The dynamics of these vortices and their mutual interactions determine their downstream extent. Consequently, these wake vorticity structures can modify significantly the flow entrainment from the external flow field into the wake, thus the recovery of the wind turbine wake. Instability modes of the helicoidal tip vortices have been deeply characterized by several authors in the past; however, dynamics of the hub vortex are not clearly identified yet.

With this spirit, wind tunnel experiments were performed for the wake produced by a three-bladed wind turbine immersed in uniform flow. It was observed that the hub vortex is characterized by oscillations with frequencies lower than that connected to the rotational velocity of the rotor, which previous works have ascribed to wake meandering. This phenomenon consists in transversal oscillations of the wind turbine wake, which might be excited by the vortex shedding from the rotor disc acting as a bluff body. In this work, temporal and spatial linear stability analyses of a wind turbine wake are performed on a base flow obtained with time-averaged wind tunnel velocity measurements. This study shows that the low-frequency spectral component detected experimentally matches the most amplified frequency of the counter-winding single-helix mode, and the hub vortex instability has been spatially reconstructed, as shown in figure 1. Then, simultaneous hot-wire measurements confirm the presence of a helicoidal unstable mode of the hub vortex, with a streamwise wavenumber roughly equal to that predicted from the linear stability analysis¹.

More recently, stability analysis has been performed taking into account the Reynolds stresses, which are modeled via eddy-viscosity models calibrated on the wind tunnel data. This new formulation leads to a univocal detection of the hub vortex instability and the prediction of the related instability frequency.

^a Wind Engineering and Renewable Energy Lab (WIRE), EPFL, Lausanne, CH-1015, Switzerland

^b Laboratory of Fluid Mechanics and Instabilities (LFMI), EPFL, Lausanne, CH-1015, Switzerland

^c Department of Civil and Industrial Engineering, University of Pisa, Pisa, 56122, Italy

¹ Iungo *et al.*, *J. Fluid Mech.* **737**, (2013).

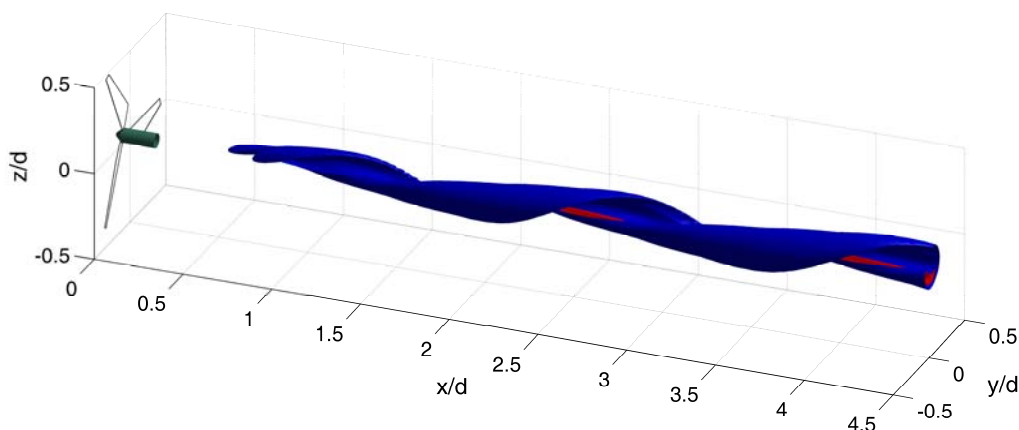


Figure 1: Spatial reconstruction of the hub vortex instability. Iso-surface of the axial vorticity.

On the tip vortex moving inboard before wake expansion drives it outboard

G.A.M van Kuik^a, D. Micallef^b, I. Herraiz^c, D. Ragnia^a

Several SPIV experiments on model wind turbine rotors^{1,2,3} focussing on the flow around the tip have shown that after being released the tip vortex first moves to a lower radius. This is in contrast to what is generally assumed, namely that the wake expansion starts immediately. A detailed analysis of one of these experiments, the 2m Ø TUDelft-B rotor tested in the TUD 3m Ø Open Jet Facility, is combined with CFD calculations and a vortex panel code using the full blade geometry. Figure 1 shows the tip of the rotor, the coordinate system and the contour of the flow analysis. For 6 chordwise positions of this contour the spanwise and chordwise vorticity, the associated circulation and the Kutta-Joukowski loads acting on the chordwise vorticity have been determined. Figure 2 shows the results as a function of the chordwise position. The squares show the CFD data, the diamond marker indicates the experimental data and the triangles present the results of a momentum balance applied to the experimental data.

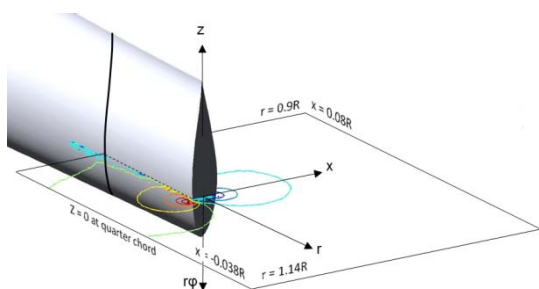


Figure 1: the tip of the TUD Rotor B

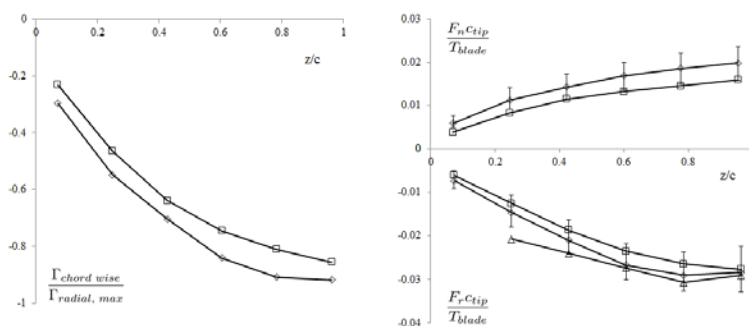


Figure 2: $\Gamma_{chordwise}$, F_{normal} and F_{radial} as function of chordwise position

The ratio of the integrated normal force \mathcal{N} and radial force \mathcal{R} to the thrust of the blade is 1 to 2%, so the contribution of the tip loads on chordwise vorticity to the overall rotor load is very small. However, when \mathcal{N} and \mathcal{R} are normalized by the thrust at the blade for $r > 0.9R$, the order of magnitude changes to 10%. \mathcal{N} and \mathcal{R} are the components of the conservative load on chordwise vorticity. It is conservative as it does not convert power and does not generate vorticity, in contrast to the non-conservative load on radial vorticity. Analyses methods based on the true blade surface, like full CFD or vortex panel codes, automatically take account of the conservative tip load as part of the pressure distribution. However, analyses methods in which chordwise information is discarded, like lifting line and actuator line methods, cannot include the conservative load as part of the solution. The impact of this is shown in figure 3, showing the tip vortex evolution as experimentally observed, as a result from a full (blade) CFD as well as vortex panel code and as an actuator line CFD (AL) result. Indeed the blade CFD predicts the inboard motion reasonably well, whereas the AL misses it. If this higher order tip effect has to be modelled, the conservative force tip load should be included.

An extensive treatment of this topic is to be published⁴. This contains a part on conservative loads on actuator discs, reported in a previous Euromech seminar⁵.

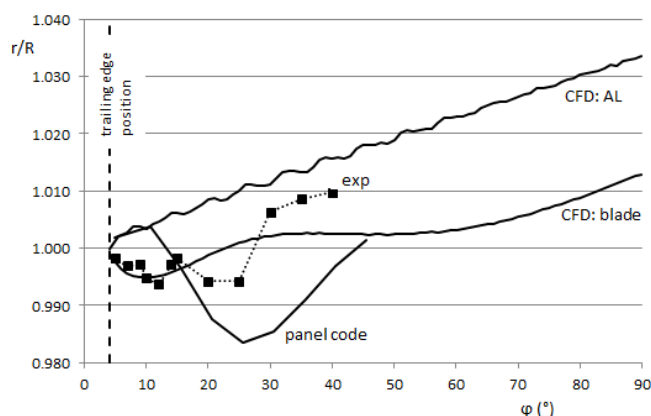


Figure 3: the trajectory of the tip vortex as function of the azimuthal angle after the c/4 position.

¹ Schepers *et al.*, conf. proc. Science Making Torque from Wind 2012

² Micallef *et al.*, conf. proc. Science Making Torque from Wind 2012

³ Xiao *et al.*, *Appl. Math. Mech. -Engl.*, **32**, (6) 729-738

⁴ van Kuik *et al.* submitted to JFM

⁵ van Kuik & van Zuylen. 2009 Euromech Symp.**508** 26-28

^aTU-Delft Wind Energy Research Institute DUWIND, Aerospace Engineering, Delft, the Netherlands

^bFaculty of Engineering, Depart. Mechanical Engineering, Univ. of Malta, Malta

^cForWind, Carl von Ossietzky University Oldenburg, Germany

Aerodynamic Performance of a Wind Turbine: BEM versus CFD

S.Y. Lin^a, K. Mulleners^a and J. Seume^a

Accurate prediction of a wind turbine performance is of crucial importance for the effective blade design and optimization of the power output. In present, wind turbine blade design relies mainly on the performance prediction by means of blade element momentum (BEM) methods, which are based on two-dimensional (2D) airfoil characteristics¹. Some three-dimensional (3D) effects can be taken into account by applying correction models, e.g. Prandtl tip/root loss correction model and empirical 3D stall delay models. Other 3D effects such as local solidity and pitch angle variations for pitch-controlled wind turbines are generally ignored in current design procedures. Recently, computational fluid dynamic (CFD) investigations on inboard flow separation, tip and wake flow have shown the influence of 3D flow on the performance of wind turbines²⁻⁵. Although CFD can provide more accurate predictions of the wind turbines performance than BEM, CFD is currently not suited for wind turbine design because it is more time-consuming. However, the more detailed flow information provided by CFD, including 3D effects as well as rotational effects, can be used to study wind turbine performance prediction differences between CFD and BEM methods. Based on an increased understanding of the limitations of both methods, improvements to the BEM methods can be formulated.

In this study, a full-scale wind turbine based on the NREL offshore 5 MW baseline wind turbine was modelled under different operating conditions using CFD and BEM methods. The model was simplified by assuming that the rotor blade is rigid and undeformable. By comparing the results from both methods, an increasing deviation of power output with increasing wind speed can be observed, whereas the thrust shows only a slight difference. The local power, thrust and torque coefficients were generally over-predicted by BEM in the inboard region for $0.2 \leq r/R \leq 0.4$, and under-predicted by BEM for $r/R < 0.2$ where the blade geometry undergoes a smooth transition from a cylinder to DU airfoil profiles. In addition, local angle of attack and aerodynamic coefficients of the CFD results were evaluated and compared with BEM predictions. A remarkable deviation is revealed in the inboard airfoil sections where there is flow separation (Fig. 1). For the other airfoil sections, the aerodynamic coefficients of the CFD results agree well with the airfoil input data in BEM methods. The circulation gradient in function of radius indicates that the strength of the tip vortex decreases with increasing wind velocity, whereas the strength of the trailing edge vortex sheet increases with increasing wind velocity. Based on the results of the circulation gradient and the distribution of vorticity and helicity, the complex wake structure of a wind turbine can be better understood.

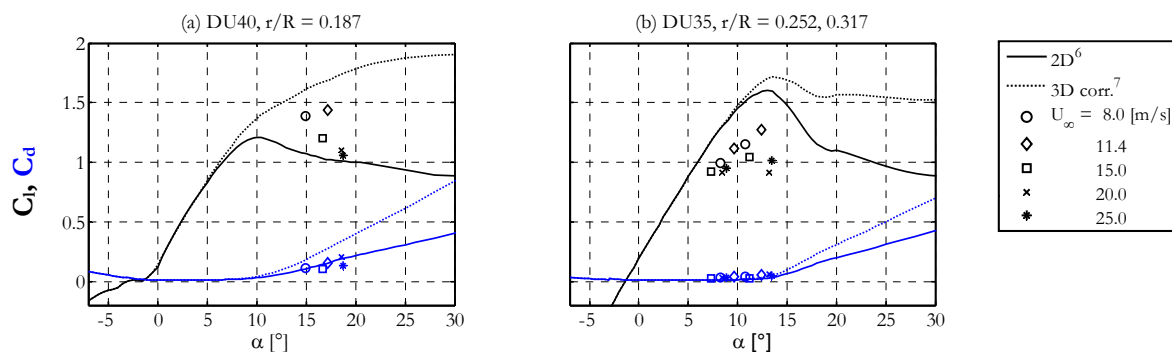


Figure 1: Lift and drag coefficients in function of angle of attack of the (a) DU40 and (b) DU35 airfoil sections from the CFD results.

^a Institute of Turbomachinery and Fluid Dynamics, Leibniz Universität Hannover, Appelstrasse 9, Hannover, Germany

¹ Burton et al., *Wind Energy Handbook* (2011)

² Johansen et al., *Wind Energy* **12**, 261 (2009)

³ Chow and van Dam, *Wind Energy*, DOI: 10.1002/we.1505 (2012)

⁴ Hansen and Johansen, *Wind Energy* **7**, 343 (2004)

⁵ Johansen and Sørensen, *Wind Energy* **7**, 283 (2004)

⁶ Kooijman et al., DOWEC-F1W2-HJK-01-046/9 (2003)

⁷ Jonkman et al., NREL/TP-500-38060 (2009)

3D steady simulation of a 7.5 MW wind turbine with OpenFOAM

E. Daniele^a, B. Stoevesandt^a

In this work a steady simulation of a 7.5 MW wind turbine with OpenFOAM library is presented. The wind turbine blade has been designed within the Germany national research project “Smart Blades”¹ (funded by the Ministry of Environment, Nature Protection and Nuclear Plant Security) with the aim of developing a new concept of blade that can “smartly” react to wind inflow and operating condition in a such way to keep the load at an acceptable level in order to enhance the fatigue life.

Comparison with Blade Element Momentum (BEM) Theory based code ONEWIND² are presented for a rigid blade case, with pitch control mechanism setup describing the normal operating condition range, from design point speed to cut-out inflow speed. Both power and thrust outputs are provided for both CFD and BEM simulations. The 3D CFD simulation is referred to a single blade, taking advantage of periodic condition for such an axial inflow configuration, and the pitch angle setup is obtained by rotating the inner cylindrical portion of the numerical grid which envelopes the blade. Special attention is paid to the blade root region where the flat back airfoils are located, and thus a more difficult agreement between BEM and CFD is expected, because of the complicated separation phenomenon that occurs even at low angles of attack.

For a limited number of cases, defined by a combination of inflow speed and pitch angle, a comparison between CFD and BEM simulations for an elastic blade are presented: under these circumstances for each case a new numerical grid should be generated because of different blade deformation derived by BEM calculation. In this situation the comparison of power and thrust outputs could provide information on the reliability of the aero-elastic coupling assumed within the BEM model.

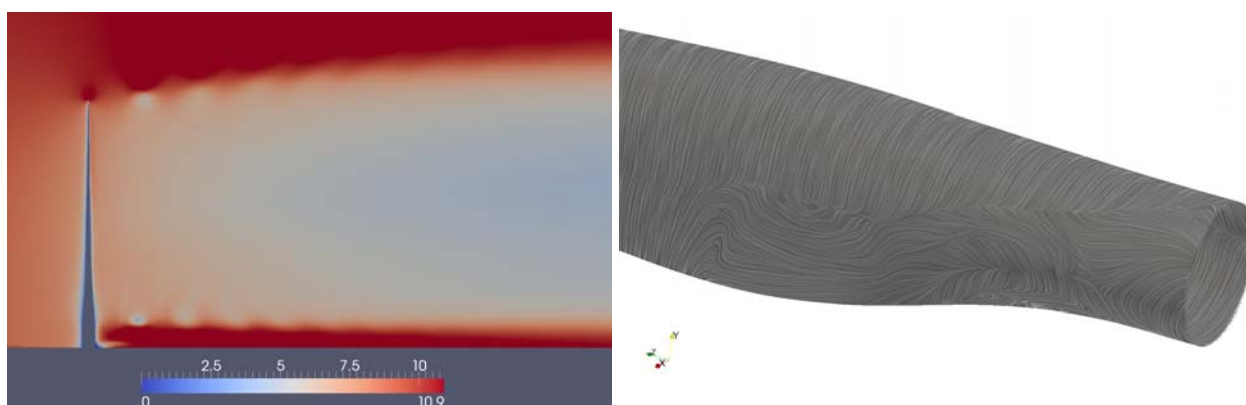


Figure 1: On the left side: Velocity component along rotor axis for the design condition. A detail of the wake is shown by limiting the scale between 0 and inflow speed value equal to 10.9 m/s. On the right side: line integral convolution patterns for the wall shear stress vector field on the root region of the blade.

^a Fraunhofer IWES, Ammerländer Heerstr. 136, D-26129, Oldenburg.

¹ <http://www.bmub.bund.de/newsletter/de/newsletter-zur-forschung-im-bereich-erneuerbarer-energien/bmu-newsletter-zur-forschung-im-bereich-erneuerbarer-energien-ausgabe-022013/smart-blades-intelligente-rotorblaetter-fuer-hohe-und-zuverlaessige-anlagenleistung/>

² <http://www.onewind.de/>

Smart Airfoil Gust Response

T. Gillebaart^a, A.H. van Zuijlen^a, H. Bijl^a

Reducing the Cost of Energy (CoE) drives the increase in wind turbine size. In a response to the increasing wind turbine size, there is a trend towards designing smart wind turbines with active control to reduce fatigue loading, decrease the tip deflection and increase power production. Feasibility studies on active trailing edge flaps (TEF) have shown that a significant reduction of the root bending moment can be obtained when appropriate controllers are used. Active control can also alleviate peak loads during operation in extreme conditions, especially during local gusts. A key aspect in these new wind turbines is Fluid-Structure-Interaction (FSI), due to lighter and more flexible blades: combined with the increase in turbine diameter, prediction of aeroelastic response of such an active wind turbine becomes increasingly more important in the turbine design. Especially in the harsh (turbulent) conditions experienced in the atmospheric boundary layer a detailed understanding on the aero-servo-elastic response of new generation smart wind turbines is needed.

Traditionally, the load alleviation simulations are carried out using a blade element momentum formulation with engineering models for sectional aerodynamics. However, the flapping action of a trailing edge flap is a complex Fluid-Structure-Control-Interaction (FSCI) problem and needs to be analyzed in more detail. Especially the regime with high reduced frequency response and near separation flow conditions result in the need for a high fidelity model of such a smart rotor system. In this study the interaction between the aero-elastic response of a wind turbine airfoil to gusts and the trailing edge flap controller is analyzed using two models: Reynolds Averaged Navier- Stokes (RANS) and an unsteady aerodynamic engineering model (ATEFlap). Different angles of attack (attached flow, near separation and separated flow) are used to assess the different flow regimes. Earlier studies showed the model differences increase at higher angles of attack and reduced frequencies for fixed airfoils¹. Additionally the gust frequency is varied from quasi-steady regime to unsteady regime. The aim is to understand the details of a smart airfoil and to assess the applicability of state-of-the-art engineering models in this aero-servo-elastic framework. Therefore, the aero-servo-elastic response of a typical wind turbine airfoil with spatially varying gust inflow conditions is assessed at different angles of attack and gust frequencies.

A fluid-structure-interaction solver is developed in OpenFOAM using Unsteady Reynolds Averaged Navier-Stokes (URANS), (efficient) radial basis function mesh deformation algorithm, Aitken's under-relaxation FSI coupling scheme and a 3DoF rigid body structural model. Prescribing a temporally and spatially varying gust is done using the mesh velocity technique². This study results in detailed insight of the smart rotor system on itself, while assessing the widely used engineering models in a range of conditions. The main focus will be on understanding the effects in the non-linear regions: high angle of attack, high reduced frequencies.

^a Dep. Aerospace Engineering, Delft University of Technology, P.O. Box 5058, 2600GB Delft, The Netherlands

¹ Bergami et al., *Wind Energy*, pre-print (2014)

² Singh et al., *Journal of Aircraft* **34**, p. 465-471 (1997)

Effect of roughness on the power production of a wind turbine: Large Eddy Simulation

C. Santoni^a, K. Carrasquillo^a, and S. Leonardi^a

With the shortage of fossil fuel and increasing environmental awareness, wind turbines have become the most promising source of renewable energy. Despite the progresses made in the last decade, the flow physics is far to be completely understood. In fact, it is still unclear how to maximize the power extraction in a large wind farm, how to minimize the power fluctuations, the effect on the large-scale coherent structures of the atmospheric boundary layer and which is the effect of the topography. In the present paper we focus on the latter aspect. A finite difference scheme with a fractional step and a Runge Kutta, which couple the actuator line model (ALM)¹ and the Immersed Boundary Method (IBM)² has been used to study the effect of the topography on the power production of a wind turbine, the topography made of wavy walls, the tower and nacelle have been modeled using the IBM, while the turbine blades are represented with the ALM. A detailed preliminary study on circular cylinders and steady blades has been performed to validate the ALM with respect to a full IB. By comparing the two numerical methods we were able to improve the accuracy of the ALM in the near wake.

^a Dep. Mechanical Engineering, The University of Texas at Dallas, 800 W. Campbell Road, Richardson, Texas, USA

¹ Orlandi & Leonardi, *Journal of Turbulence* vol.7, pp. 1 (2006).

² Martinez-Tossas et al., *J. Wind Energy* (2014)

Support from NSF PIRE grant # OISE 1243482 is acknowledged.

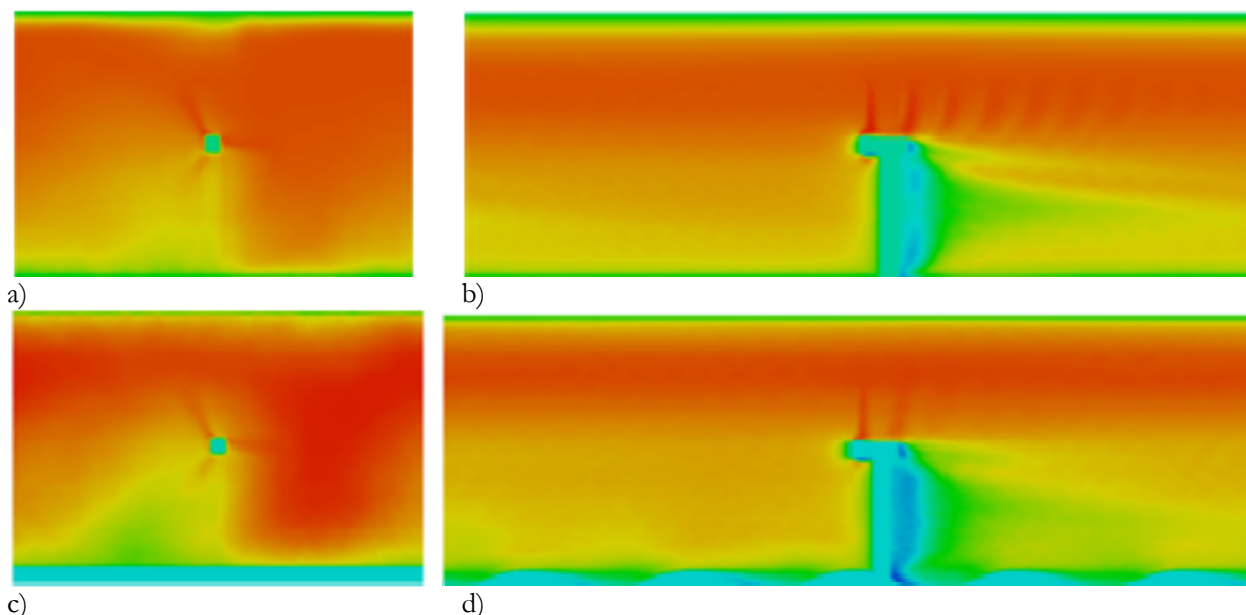


Fig.1 Colour contours of streamwise velocity past a wind turbine in a smooth channel (a,b) and in a channel with the lower undulated wall (c,d)

Colour contours of streamwise velocity of the turbulent flow in a channel with and without undulations on the lower wall are shown in Fig.1. The undulations are 10% the half width of the channel. The waviness on the wall causes a pressure gradient, which induces the ejection of low momentum fluid from the wall to the centre of the nacelle. This affects the power production because lower momentum fluid impinges the blade. Turbulent intensities, two points correlations and power production fluctuations will be shown at the conference as function of the undulation on the wall.

LES of the Lillgrund wind farm using a torque based power controller.

K. Nilsson^a, 2nd S-P. Breton^a, 3rd S. Ivanell^{ab} and 4th D. Henningson^b

The aim with the study is to quantify the effects of using an active power controller when performing large-eddy simulations (LES) combined with an actuator disc (ACD) method.

Large-eddy simulations are performed using the EllipSys3D Navier-Stokes solver developed at DTU/Risø by Michelsen [1][2] and Sørensen [3] to compute the power production and the wake effects of the wind turbines in the Lillgrund offshore wind farm. Lillgrund is ideal for wake studies thanks to its layout which is characterized by a small internal turbine spacing. The turbines in the farm are modeled using an actuator disc (ACD) method, Mikkelsen [4]. The ACD method models the rotor with body forces determined from drag and lift coefficients which are tabulated as functions of the angle of attack. As the boundary layer over the blades is not resolved, this approach greatly reduces the computational costs compared to simulations involving the modeling of the full blade geometry. The atmospheric conditions are modeled using pre-generated synthetic turbulence, Mann [5], and a prescribed boundary layer in order to save computational costs. The simulations are performed both with a recently implemented power controller, see Nilsson [6], which forces the turbines to adapt their rotational speed to the conditions they are operating in, and without any controller, where all turbines are given a fixed rotational speed. The relative power predicted from the different simulations are compared with measurement data as depicted in Figure 1. In this figure it can be seen that both the simulations with and without the power controller are predicting the measured production very well. There is however a tendency that the controlled simulations are performing slightly better than the uncontrolled ones in comparison with the measurements.

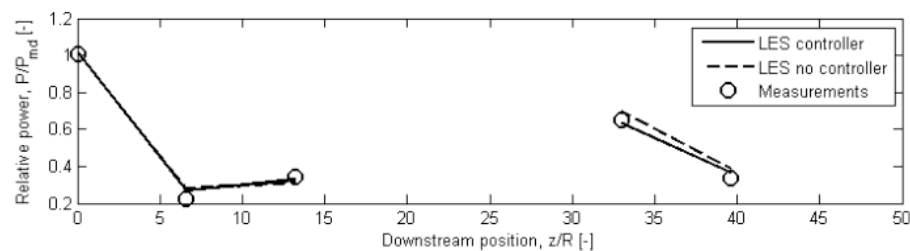


Figure 1: Relative production for a row of turbines in the farm

^a Uppsala University, Campus Gotland, Dep. of Earth Sciences, Section of Wind Energy, Visby, Sweden.

^b KTH, Department of Mechanics, Stockholm, Sweden.

¹ Michelsen, *Tech. Rep. AFM 92-05 DTU* (1992).

² Michelsen, *Tech. rep. AFM 94-06 DTU* (1994).

³ Sørensen, *PhD th. Risø-R-827-EN* (1995).

⁴ Mikkelsen, *PhD th. MEK-FM-PHD 2003-02* (2003).

⁵ Mann, *Probabilistic Engineering Mechanics* **13**; 269-282 (1998);

⁶ Nilsson, *Lic.th. TRITA-MEK 2012:18 KTH* (2012).

Optimal control of infinite and finite wind-farm boundary layers

Johan Meyers^a, Jay Goit^a and Dries Allaerts^a

In large wind farms, the effect of turbine wakes, and their interaction leads to a reduction in farm efficiency, with power generated by turbines in a farm being lower than that of a lone-standing turbine by up to 50%. In very large wind farms, this efficiency loss is related to interaction of the wind farms with the planetary boundary layer, leading to lower wind speeds at turbine level. In the current study, we investigate the use of optimal control techniques combined with Large-Eddy Simulations (LES) of wind-farm boundary layer interaction for the increase of total energy extraction in very large 'infinite' wind farms and in finite farms with and without temperature effects. We consider the individual wind turbines as flow actuators, whose energy extraction can be dynamically regulated in time so as to optimally influence the turbulent flow field, maximizing the wind farm power.

For the simulation of wind-farm boundary layers we use large-eddy simulations in combination with actuator-disk and actuator-line representations of wind turbines. Simulations are performed in our in-house pseudo-spectral code SP-Wind. For the optimal control study, we consider the dynamic control of turbine-thrust coefficients in an actuator-disk model. They represent the effect of turbine blades that can actively pitch in time, changing the lift- and drag coefficients of the turbine blades. First optimal model-predictive control (or optimal receding horizon control) of an infinite wind farm is studied, where the model simply consists of the full LES equations, and the time horizon is approximately 280 seconds. The optimization is performed using a nonlinear conjugate gradient method, and the gradients are calculated by solving the adjoint LES equations. We find that the extracted farm power increases by approximately 20%. However, the increased power output is also responsible for an increase in turbulent dissipation, and a deceleration of the boundary layer. Further investigating the energy balances in the boundary layer, it is observed that this deceleration is mainly occurring in the outer layer as a result of higher turbulent energy fluxes towards the turbines. In a second optimization case, we penalize boundary-layer deceleration, and find an increase of energy extraction of approximately 10%. In this case, increased energy extraction is balanced by a reduction in dissipation by turbulence. Further results of optimal control in finite wind farms and optimal control in boundary layers that include temperature effects and a capping inversion are also presented.

J.M. acknowledges support from the European Research Council (FP7-Ideas, grant no. 306471). Simulations were performed on the computing infrastructure of the VSC Flemish Supercomputer Center, funded by the Hercules Foundation and the Flemish Government.

^a Dep. Mechanical Engineering, KU Leuven, Celestijnenlaan 300A, B3001 Leuven, Belgium

Mini Symposia: Thermo Acoustics

Progress in combustion dynamics of annular systems

J-F Bourgouin^{ab}, D. Durox^{ab}, T. Schuller^{ab}, J. Moeck^{abc}, Y. Méry^d and S. Candel^{ab}

New results on the dynamics of annular combustors equipped with multiple injectors will be reviewed. Studies are carried out on a novel set up (MICCA) which comprises a plenum fed with a mixture of air and propane, a backplane with 16 injectors and a combustor formed by two concentric cylindrical walls¹. These lateral walls made of quartz allow a full view of the flames established in the neighborhood of the multiple injectors. High-speed imaging is used to examine flame dynamics in combination with pressure measurements delivered by a set of waveguide microphones plugged on the chamber backplane and another set of microphones flush mounted on the plenum walls. Studies are carried out with two types of injectors, the first is swirled and imposes a rotation to the flow with a measured swirl number of 0.8, the second type is formed by a matrix of small orifices. Experiments are mainly focused on combustion instabilities coupled by azimuthal modes. These types of oscillations have received considerable attention in recent years because the underlying coupling is often observed in the advanced premixed combustion systems used in modern gas turbines but there are few well controlled laboratory scale experiments. Recent studies have allowed a detailed examination of the dynamics of annular geometries comprising multiple swirling injectors providing insight on the coupling process between acoustics and unsteady combustion. In the case of swirling injectors, it is found that the coupling continuously evolves between standing and spinning modes and that this can be characterized by determining a spin ratio. In the configuration comprising matrix injectors combustion takes place through a set of conical flames stabilized on perforated plates allowing an interesting simplification of the combustion process. This gives rise to various couplings including purely spinning modes, purely standing modes and situations where two different modes sustain oscillations. These various situations will be considered and their analysis will be carried out with dynamical models making use of the flame describing function of individual injectors²⁻³.



Figure 1: Annular combustor with multiple injectors. Left : view of the MICCA set-up, Center : flame configuration with swirling injectors, Right : flame configurations corresponding to matrix injectors.

^a CNRS, UPR288, EM2C, Grande Voie des Vignes, 92295 Chatenay-Malabry, France

^b Ecole Centrale Paris, Grande Voie des Vignes, 92295 Chatenay-Malabry, France

^c also with TU Berlin, Berlin 10623, Germany

^d Safran, Snecma, 77550 Villaroche, France

¹ J-F Bourgouin et al. *Combust. Flame* **160**, 1398-1413 (2013)

² N. Noiray et al. *J. Fluid Mech.* **615**, 139-167 (2008)

³ P. Palies et al. *Combust. Flame* **157**, 1698-1717 (2010)

Thermoacoustic coupling in Annular Combustors

N. Noiray^a, M. Bothien^a and B. Schuermans^a

Modern gas turbine combustors operating in lean-premixed mode are prone to combustion instabilities induced by thermoacoustic coupling. In annular combustion chambers, usually azimuthal acoustic modes are the critical ones interacting with the flame. In case of constructive interference, high amplitude oscillations might result. In this study, the azimuthal acoustic field of a full-scale engine is investigated in detail. The analyses are based on measurements in a full-scale gas turbine, analytical models to derive the system dynamics, as well as simulations performed with an in-house 3d nonlinear network model. It is shown that the network model is able to reproduce the behaviour observed in the engine. Spectra, linear growth rates, as well as the system's dynamics statistics can be predicted. A thorough investigation of the azimuthal modes stochastic properties is performed. Additionally, the network model is used to show that particular azimuthal flame temperature distributions with amplitude of merely 1% of the mean flame temperature can change the azimuthal mode from dominantly rotating to dominantly standing.

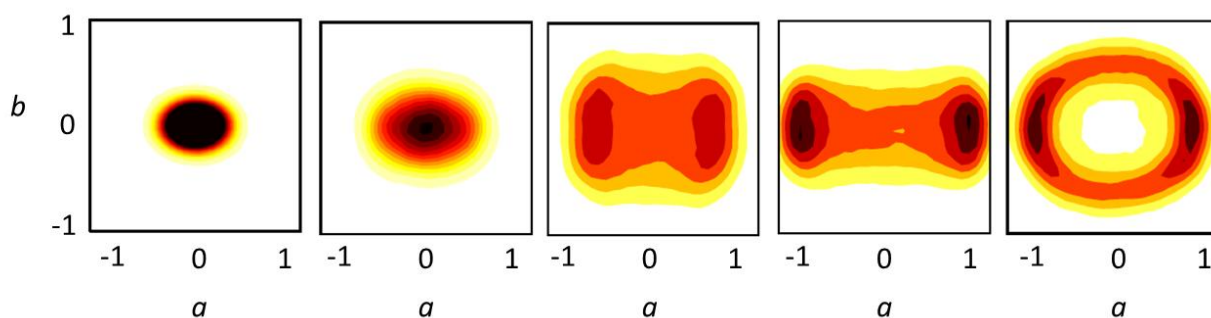


Figure 1. Joint probability densities of the amplitudes of the n^{th} order azimuthal eigenmodes obtained from simulations at various azimuthal temperature distribution. The flame temperature distribution is $T = T_0 + \Delta T \cos(2n\theta)$ where θ is the azimuthal coordinate and ΔT is incrementally varied from 0 to 4% of T_0 . The acoustic pressure in the annular combustion chamber is approximated by $p(\theta, t) \approx a(t) \cos(n\theta) + b(t) \sin(n\theta)$. Single maximum distribution corresponds to a stochastically forced linearly stable point, bimodal distribution is typical for dominantly standing mode in limit cycling state while ring shaped distribution represents dominantly rotating mode.

Age (N. Noiray) at the time of submission for participation in the Young Scientist Award: 32 years old

^a Alstom Power, Baden, Switzerland

Subcritical thermoacoustic instabilities in axisymmetric annular chambers

G. Ghirardo^a, M.P. Juniper^a and J.P. Moeck^b

Subcritical instabilities arise when the stationary solution of a system is stable but at the same time a periodic solution is sustained at finite oscillation amplitudes. This gives rise to triggering and hysteresis, which have been observed in various thermoacoustic systems. In an essentially one-dimensional setting, in which only longitudinal acoustic waves propagate, the occurrence of subcritical instabilities is reasonably well understood¹. Based on an energy argument, linear damping and nonlinear driving curves can be used to identify stable and unstable solutions, as presented in Figure 1a and 1b.

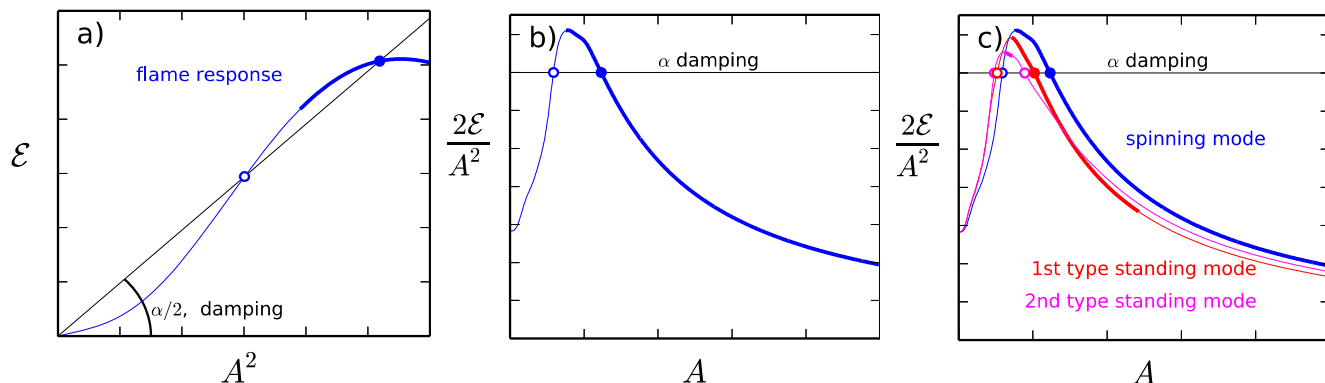


Figure 1: Energy balance in 1 limit cycle, as a function of the amplitude of oscillation A . (a): blue line: energy added to the system by the flame; black line: energy dissipated by the damping. The empty/filled circles are respectively unstable/stable limit-cycle. By varying the slope of the damping, the position of the circles changes on the blue line. The line is thick where these intersections are stable limit-cycles, and thin where they are unstable limit cycles. (b): Different representation of the same energy balance, with different scaling on the axis. (c): Results of this study for axisymmetric annular configurations.

However, in annular thermoacoustic systems with multiple sources of heat release distributed around the circumference, the effect of a nonlinear flame response supporting subcritical instabilities has not been studied. This type of system is of practical importance because it generically resembles combustion chambers in gas turbines and aeroengines, in which thermoacoustically driven oscillations are a major concern.

We will present the effect of a subcritical flame response on an axisymmetric annular combustor with compact flames equispaced along the annulus. We will show that there exist 3 types of non-trivial solutions: 1) spinning waves, travelling either clockwise or counter-clockwise in the chamber, stable for adequately low values of the damping; 2) standing waves with one pressure antinode positioned at one burner's position; 3) standing waves with one pressure antinode positioned exactly in-between two adjacent burners. The two types of standing waves can be stable or unstable, depending on the value of the damping, on the flame response and on the number of injectors.

This study shows that a subcritical flame response can explain the occurrence of standing waves in axisymmetric annular combustors. The analysis is based on the numerical integration of a low-order thermoacoustic model in time domain and on the application of the method of averaging, as first discussed in reference [2]. We will also present a new series expansion capable of: 1) describing the nonlinear behaviour of the flame response more accurately than a polynomial expansion; 2) surviving the process of analytical averaging.

^a Dep. Engineering, University of Cambridge, Trumpington Street, Cambridge CB2 1PZ, United Kingdom

^b Institut für Strömungsmechanik und Technische Akustik, Technische Universität Berlin, Müller-Breslau-Str 8, 10623 Berlin, Germany

¹ Moeck et al., *ALAA/CEAS Aeroacoustics Conference*, paper no. 2008-2946 (2008)

² Noiray et al., *Comb.Theor.Model*, **15**, 5 (2010)

Bloch-type thermoacoustic modes in annular domains

Jonas P. Moeck^a, Georg A. Mensah^a

Thermoacoustic instabilities appear in the form of high-amplitude pressure oscillations in combustion chambers of stationary gas turbines and aero-engines. The combustion chambers in these applications have an annular shape, with multiple flames arranged around the circumference. The configuration is usually such that one angular segment, including one flame, is copied a certain number of times. This formally results in a discrete rotational symmetry of order equal to the total number of flames in the combustion chamber. Modeling thermoacoustic instabilities for this type of configuration can be based on the Helmholtz equation taking into account the unsteady heat release rate through a frequency dependent flame response function.^{1,2} To obtain all relevant modes, the Helmholtz equation is solved in the entire domain. Because the order of rotational symmetry of the azimuthal modes can be lower than that of the configuration, it is not possible to use only one burner/flame segment with symmetry boundary conditions for the calculation. However, since the full configuration can be generated from copying one representative segment (“a unit cell”), it is evident that the information about all thermoacoustic modes is contained in one such segment. Using a Bloch-type representation, which is well known in studies of periodic media in solid-state physics, allows splitting the azimuthal dependence of the pressure eigenfunction into a circumferential Fourier mode and a local variation that is periodic with the extent of the unit cell. This greatly reduces the computational effort for the determination of thermoacoustic modes in annular configurations that exhibit discrete rotational symmetry. A further advantage is that prescribing the Bloch wave number allows to target a specific azimuthal mode order, and this facilitates the iterative solution of the nonlinear eigenvalue problem associated with the thermoacoustic Helmholtz equation. We will also discuss how deviations from asymmetry can be taken into account in this framework. This permits to study, in addition to linear stability, limit cycle oscillations that emerge from the amplitude saturation of the flame response and the effect of asymmetries introduced as a means to mitigate unstable modes.

^a Institut für Strömungsmechanik und Technische Akustik, Technische Universität Berlin, Müller-Breslau-Straße 8, 10623 Berlin, Germany

¹ Nicoud et al., *ALAA J.* **45**, 426 (2007).

² Camporeale et al., *J. Eng. Gas Turbines Power* **133**, 011506 (2010).

Flame describing function calculation of turbulent premixed flame using large eddy simulation

Xingsi Han, Aimee S. Morgans^a

Lean premixed combustion in gas turbines renders the combustor prone to combustion instabilities. These arise from the coupling of unsteady heat release and acoustics within the combustor. Simulation of combustion instabilities via full CFD remains extremely expensive, and so low order network models, which combine analytical models for the acoustic waves with more complex models for the response of the flame to excitation have become an increasingly popular tool for simulating combustion instabilities.

It is well known that the non-linearity contribution to combustion instabilities, which causes saturation into limit cycle (or other complex behaviour), typically arises from the flame response to excitation. Obtaining an accurate model for this non-linear response, via well-resolved CFD simulations is thus essential for accurately predicting limit cycle amplitude under unstable conditions.

In this work, we present CFD simulations of a Flame Describing Function (FDF), and compare to experimental test data. The FDF approach assumes that the unsteady heat release of the flame responds in a weakly non-linear manner to flow disturbances. That is, the dominant contribution of the flame response to harmonic forcing will occur at the excitation frequency, but the gain and phase shift will depend on the forcing amplitude.

We consider a bluff body stabilized turbulent premixed flame for which experimental data exists¹. We use incompressible Large Eddy Simulation (LES) employing a Flame Surface Density (FSD) with wrinkling combustion model. We use the open source CFD code, Code_Saturne, for our simulations.

Our simulations capture the cold (no flame) flowfield, the unforced flame dynamics and the response of the flame to harmonic excitation with good accuracy. By extracting the gain and phase shift of the heat release rate response to harmonic forcing in velocity, we then obtain the full FDF, as could be included in a low order network model. This is found to have better agreement with experimental data than any other CFD results in the present literature.

^a Department of Aeronautics, Imperial College London, South Kensington, London SW7 2AZ, UK.

¹ R. Balachandran et al., *Combust. Flame* **143**, 37 (2005).

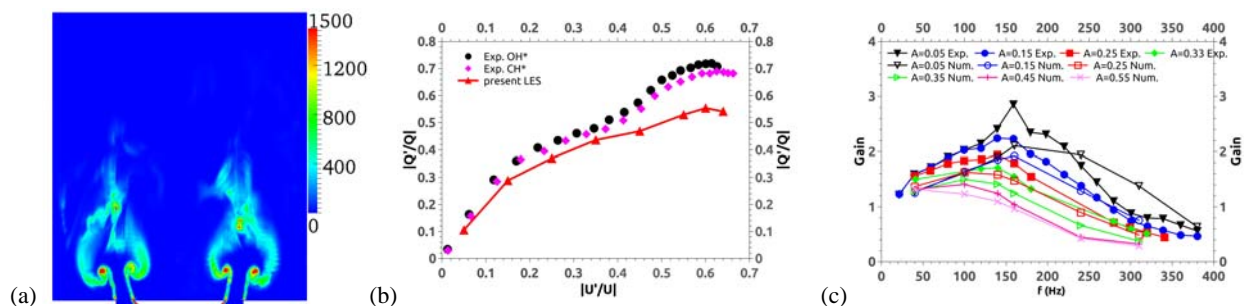


Figure 1: (a) Instantaneous FSD by present LES at forcing frequency $f=160\text{Hz}$ and amplitude $A=0.55$. (b) Amplitude response at $f=160\text{Hz}$. (c) FDF by present LES and experiment.

Nonlinear combustion dynamics in a turbulent flow-field

Vineeth Nair^a and R. I. Sujith^a

We attempt to describe the emergence of large amplitude pressure oscillations in a reacting, confined, turbulent flow-field termed combustion instability using simple models from the perspective of dynamical systems theory. It has been observed recently that the transition to combustion instability in combustion systems display states characterized by intermittent bursts of periodic oscillations that emerge from a background of chaotic unsteady fluctuations. Traditionally, combustion instability is treated as an acoustic instability problem wherein the contributions from the hydrodynamics to the dynamics are often neglected or treated as a stochastic background, as a result of which such intermittent states are not reproduced by the dynamics. We write equations from first principles for the acoustics as well as the hydrodynamic flow fields with mutual coupling to understand and characterize the intermittency observed in combustors. Finally, the generality of the model in describing oscillatory instabilities in systems without combustion are discussed.

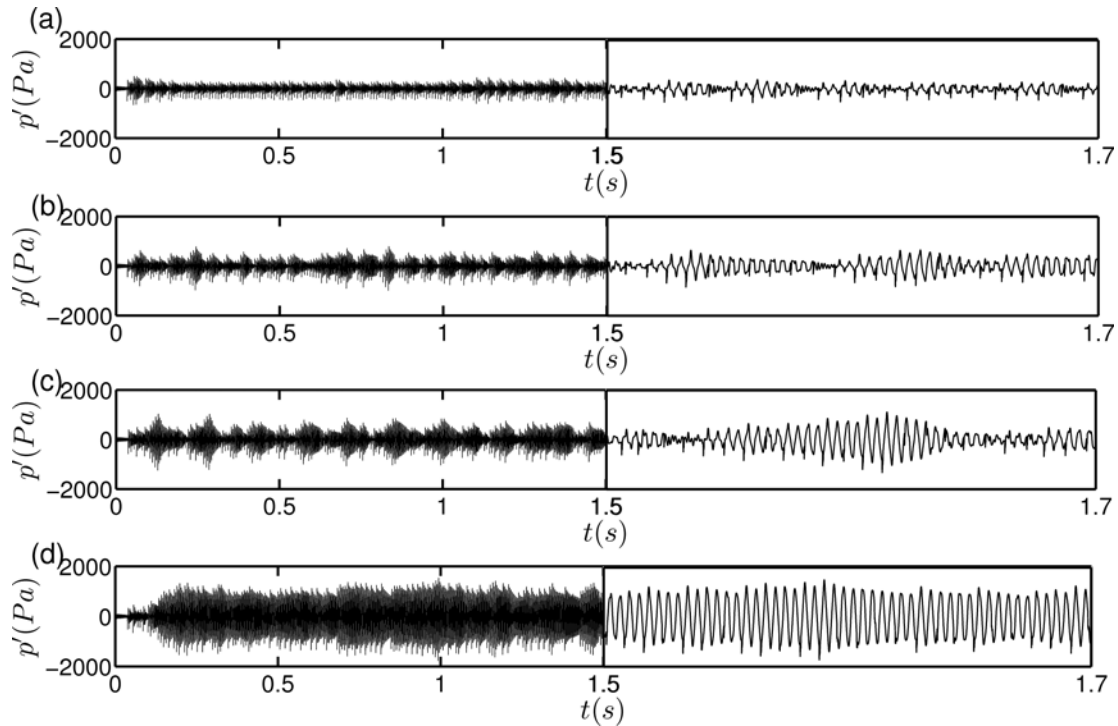


Figure 1: The transition from a chaotic stable state to an unstable oscillatory state in the model as the mean flow velocity is increased. The transition results in states characterized by intermittent burst oscillations that emerge from the chaotic background. The model mimics the intermittency seen in experiments

^a Dep. Aerospace Engineering, IIT Madras, Chennai, 600036, TN, India

Investigating recurrence patterns in turbulent combustion noise signals

Lipika Kabiraj^a, Holger Nawroth^a, Aditya Saurabh^a and Christian Oliver Paschereit^a

The subject of focus here is to understand the characteristics of acoustic noise emission from a premixed turbulent flame. As turbulent combustion involves multiple physical mechanisms acting simultaneously, unravelling the details present within combustion noise data is a difficult process. Through extensive research, certain aspects of acoustic noise emission from turbulent flames, such as the broadband nature of the acoustic spectra, have been well-established. At the same time, several studies, for instance Ref. 1, also indicate that complex interactions inherent to turbulent combustion can lead to diverse features in turbulent combustion measurements.

In the present study, we have attempted to gain additional insight into noise emission from turbulent combustion through the implementation of recurrence analysis techniques. Essentially, recurrence analysis techniques deal with the representation and subsequent analysis of the multidimensional phase space representation of a dynamical system on a two dimensional plot². This plot contains information on the recurrence features of phase space trajectories of an output from the dynamical system under study. In our case, the dynamical system is turbulent combustion, while the output that is analyzed is the acoustic emission captured by pressure microphones. The technique allows the simultaneous assessment of deterministic (such as periodic) and non-deterministic (such as uncorrelated noise) components in the phase space representation of the system. These characteristics can be visually analyzed in the recurrence plot, as well as quantified through various measures calculated from the recurrence plot³. As such, conventional techniques can be complemented by recurrence analysis in order to analyze combustion noise signals.

For our investigation, we employed a bluff-body stabilized premixed open turbulent flame. Acoustic measurements were carried out in an anechoic chamber to ensure that captured acoustic signals originate only from the turbulent flame. The recurrence features in the combustion noise signals are studied for a range of equivalence ratios of the fuel-air mixture and Reynolds number of the base turbulent flow. Results of recurrence analysis are compared to conventional time series analysis techniques.

^a Chair of Fluid Dynamics, Technische Universitaet Berlin, Germany.

¹ Strahle, W. C., *ALAA Journal* **29**, 409 (1991).

² Eckmann et al., *Europhysics Letters* **5**, 973 (1987).

³ Marwan et al., *Physics Reports* **438**, 237 (2007).

Time-series analysis and modal decomposition of heat release rate images from forcing and self-excitation of a thermoacoustic system

S. Balusamy^a, L. K. B. Li^a, P. Schmid^b, and S. Hochgreb^a

In this experimental study, we examine the spatial and temporal characteristics of the heat release rate (HRR) from a flame in a self-excited thermoacoustic system subjected to open-loop forcing. This system consists of a swirl-stabilized turbulent premixed flame (equivalence ratio of 0.8 and thermal power of 13.6 kW) enclosed in a quartz tube with an open-ended exit. We acoustically force this system at different amplitudes and frequencies, and measure its HRR response with high-speed OH* chemiluminescence imaging. We analyse these images in three different ways: (i) with a Fourier transform to determine the spatial distribution of HRR fluctuations as a function of frequency; (ii) with proper orthogonal decomposition (POD) to extract the most energetic flame structures and to examine flame-vortex interactions; and (iii) with dynamic mode decomposition (DMD) to spatially isolate the flame regions that are oscillating at the self-excited frequency from those that are oscillating at the forcing frequency.

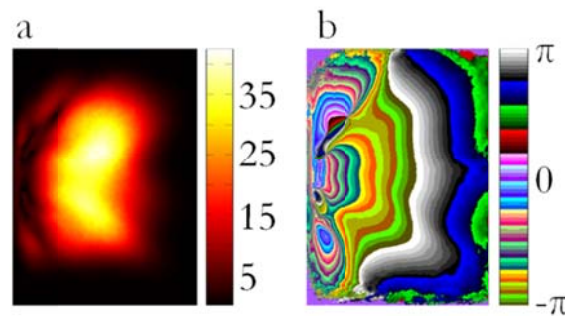


Figure 1: Fourier transform of OH* chemiluminescence images for limit-cycle oscillations. (a) Peak amplitudes at 196 Hz, (b) the corresponding phase showing coherent structures.

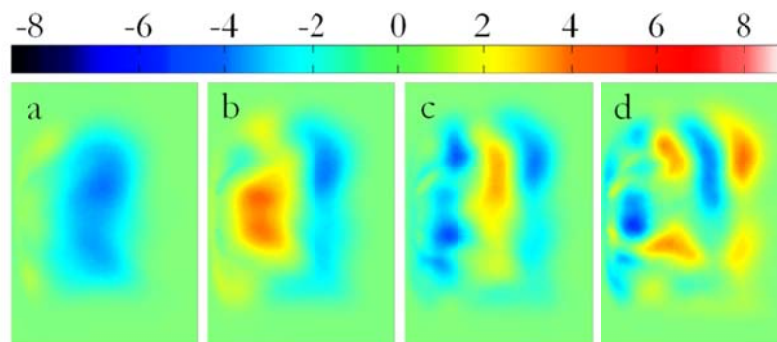


Figure 2: First four POD modes for limit-cycle oscillations. (a) First mode (64.7% of total fluctuating energy), (b) second mode (13%), (c) third mode (3.5%) and (d) fourth mode (1.3%).

^a Department of Engineering, University of Cambridge, Trumpington Street, Cambridge, CB2 1PZ, UK

^b Department of Mathematics, Imperial College London, South Kensington Campus, London, SW7 2AZ, UK

Time-domain analysis of thermo-acoustic instabilities in a ducted flame

T. Sayadi^a, V. Le Chenadec^b and P. J. Schmid^c

The modelling of thermo-acoustic instability in reactive flows represents a challenging task. In this study, the acoustic response of a duct, which includes relevant features such as a compact acoustic source, an empirical modelling of the heat source, and nonlinearities, is analysed using a time-domain approach. This thermo-acoustic system features a complex dynamical behavior, which renders the characterization of the different encountered flow regimes difficult. In order to synthesize accurate time series, we tackle this problem from a numerical point-of-view. The numerical framework is designed for dealing with the underlying stiffness, in particular, the retarded time and the discontinuity at the location of the heat source.

In addition, we introduce strategies for extracting linear and non-linear behaviour of this dynamical system. Stability analysis is performed on the limit of the low amplitude perturbations by means of the projection method proposed by Jarlebring¹, which alleviates the linearization of the retarded term and allows the extraction of parametric stability diagrams. Finally, time-series in the fully nonlinear regime, where a limit cycle is established, are analysed and dominant modes are extracted. The time-domain approach shows dependence of the limit cycle on the heat release rate and captures multiple frequency response, which demonstrates the advantage of this method to the alternative frequency-based approaches.

^a Laboratoire d'Hydrodynamique, CNRS - UMR 7646, Ecole Polytechnique, 91128 Palaiseau, France

^b Laboratoire EM2C, CNRS - UPR 288, Ecole Centrale Paris, 92295 Châtenay-Malabry, France

^c Dep. Mathematics, Imperial College London, London SW7 2AZ, United Kingdom

¹ Jarlebring, *PhD Thesis Technische Universitaet Carolo-Wilhelmina Braunschweig*. (2008)

Nonlinear low order thermoacoustic network

A. Orchini^a and M. P. Juniper^a

Thermoacoustic oscillations may occur in afterburners and gas turbines because of the interaction of unsteady heat release and acoustic waves. These oscillations may lead to structural damage or deteriorate system efficiency.

We present a low order thermoacoustic model for premixed flames that exploits the fact that the main nonlinearity of this instability is due to the unsteady heat release. We describe the flame dynamics using the G-equation model, and some of the features of a Low Order ThermoAcoustic Network (LOTAN) to describe in an efficient way the system's acoustics. The advantage of the latter approach, compared with the more diffused Galerkin decomposition of the acoustic equations, is that mean flow effects are naturally taken into account, and temperature distributions, as well as cross sectional area changes of the combustion chamber, can be easily included.

Combining flame and acoustic dynamics, we obtain a low order nonlinear tool able to predict the frequency and amplitude of thermoacoustic oscillations. With this network, we have analysed a dump combustor, accounting for fluid-walls interaction in the combustion model. The predicted frequency of oscillation compares favourably with experimental results.

We have then considered a simpler configuration, a conical Bunsen flame in a duct, to investigate two different approaches: continuation and analysis of limit cycles¹, and brute force time integration. The advantage of the limit cycle approach is its efficiency, since a fairly small number of cycles has to be integrated to understand the dynamical nature of the thermoacoustic system in a specific configuration. However, thermoacoustic systems may exhibit more complex dynamical behaviours than limit cycles, such as quasiperiodic or chaotic oscillations². In these situations, the limit cycle approach fails in predicting the amplitude of the final oscillations, which is shown by the brute force integration method. A detailed comparison between the results obtained with the two methods will be presented (Figure 1).

Finally, the linearised version of the equations is under consideration. Their analysis may help to locate the position of the first Hopf bifurcation in the parameter space. Furthermore, making use concepts of sensitivity analysis and adjoint equations, linear analysis may give useful insights into what acoustic or flame parameters should be modified to delay the onset of the instability.

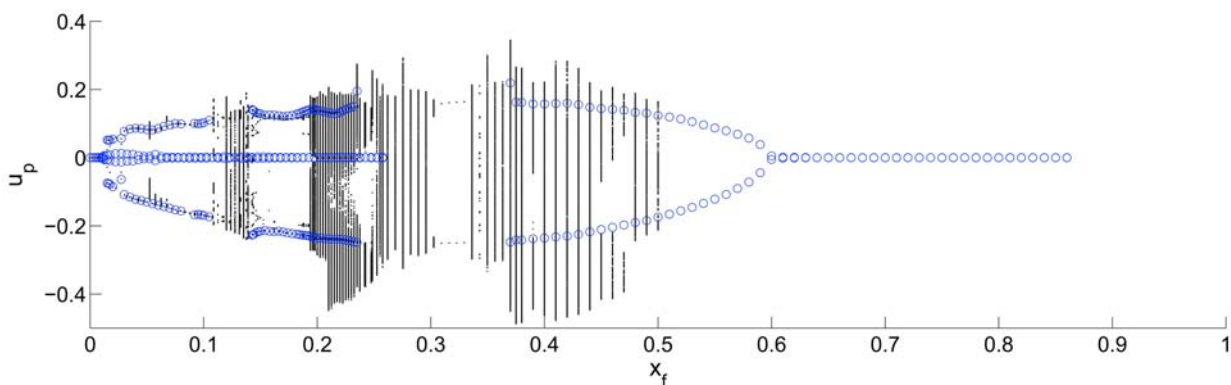


Figure 1: Thermoacoustic bifurcation diagram, amplitude of acoustic velocity fluctuations is controlled by varying flame's position along the duct. Blue circles: stable and unstable limit cycles and fixed points found by the continuation algorithm. Black dots: peaks and troughs of stable time integrated time series.

^a Dep. Engineering, Div. A, Cambridge University, Trumpington Street, Cambridge, CB2 1PZ, UK

¹ Waugh et al., *J. Comput. Phys.* **240**, 225 (2013).

² Kabiraj and Sujith., *J. Fluid Mech.* **713**, 376 (2012)

Estimating of limit cycle characteristics of a ducted premixed flame using the level-set method

Santosh Hemchandra^a

Recent experimental investigations have revealed that lean premixed combustors can potentially feature a wide range of dynamical behaviour such as limit cycles, quasiperiodic and intermittent oscillations as well as chaotic behaviour. Of these, limit cycles present a potentially problematic scenario from the standpoint of system health and operability as they are characterized largely by coherent periodic acoustic pressure oscillations that can result in fatigue failure of combustor hardware and/or structural vibrations elsewhere in the system by exciting resonances. Thus, it is of interest to the combustor designer to be able to predict operating conditions at which limit cycles can arise using physically realistic, low-order models of the combustor that have modest computation and execution time requirements.

Waugh¹ has developed techniques to find limit cycles of thermoacoustic systems with both premixed and non-premixed flames. This technique involves finding a time period (T) and initial conditions ($\eta_k(0)$) that yields periodic solutions for a system of coupled inhomogeneous ODEs for the amplitudes $\eta_k(t)$, in a representation of the acoustic pressure field in terms of natural acoustic eigenmodes of the combustor using a shooting technique. However, advancing the guesses for ($\eta_k(0)$, T) between successive iterations of the shooting procedure requires computing the sensitivity of the residual to perturbations in the shape of the flame. This so called shape derivative is challenging to compute when the flame shape is represented implicitly using a level-set function for reasons discussed in Waugh¹. This is achieved by parametrizing the flame surface shapes at $t=0$ and $t=T$ in a discrete manner and computing the shape sensitivity of the residual as the sensitivity to changes in these parameters.

The present work will use a parametrization based on Non-Uniform Rational B-Splines (NURBS) curves in order to compute shape sensitivities – given the versatility of these curves in representing complex shapes – within the framework of a technique to compute limit cycle solutions for the case of a premixed two-dimensional slot flame in a duct. A level-set based method based technique will be introduced to advance the flame shape itself from one shooting iteration to the next, as governed by the sensitivity of the residual to the shape parameters. The limit cycle amplitudes and frequencies will be compared with predictions from prior work².

^a Dep. Aerospace Engineering, IISc, Bangalore, India.

¹ Iain Waugh, Ph.d. thesis, Cambridge University, (2013).

² Kashinath et al., *ASME J. of eng. for gas turb. and power*, **135**, 061502-1 (2013).

Characterization of complexity in combustion instability in a lean premixed gas-turbine model combustor using nonlinear time series analysis

H. Gotoda^a, Y. Okuno^a and S. Tachibana^b

A better understanding of the physical process underlying combustion instability is of current interest in modern combustion physics and related branches of nonlinear science. The characterization of complexity in combustion instability in a lean premixed gas-turbine model combustor, which is of fundamental and practical importance for combustion systems, has been done by Gotoda et al [1], [2] based on the concept of dynamical system theory. They have mainly reported that the dynamical behavior of combustion instability undergoes a significant transition from stochastic motion in close proximity to lean blowout to periodic oscillations caused by thermoacoustic combustion oscillations through low-dimensional chaos with increasing equivalence ratio. The nonlinear time series analysis involving permutation entropy in combination with surrogate data method [2], colored version of recurrence plots [3] and the extended version of nonlinear forecasting method [4] proposed by Gotoda et al [3], [5], is considered in this work to capture the signature of chaotic oscillations and stochastic fluctuations in combustion instability.

References

- [1] H. Gotoda, H. Nikimoto, T. Miyano and S. Tachibana, *Chaos* 21, 013124 (2011).
- [2] H. Gotoda, M. Amano, T. Miyano, T. Ikawa, K. Maki and S. Tachibana, *Chaos* 22, 043128 (2012).
- [3] H. Gotoda, Y. Shinoda, M. Kobayashi, Y. Okuno and S. Tachibana, *Physical Review E* 89, 022910 (2014).
- [4] G. Sugihara and R. May, *Nature* 344, 734 (1991).
- [5] H. Gotoda, M. Pradas and S. Kalliadasis, *Physical Review E* (2014) (under review).

^a Department of Mechanical Engineering, Ritsumeikan University, 1-1-1 Nojihigashi, Kusatsu, 525-8577, JAPAN

^b Aerospace Research and Development Directorate, Japan Aerospace Exploration Agency, 7-44-1 Jindaiji-Higashi Chofu, Tokyo 182-8522, JAPAN

Noise induced transition in a horizontal Rijke tube

Gopalakrishnan E. A.^a & Sujith R. I.^b

The presence of a heat source which releases heat in an unsteady manner in a confinement often results in high amplitude pressure oscillations. Pressure oscillations are amplified when the inherent acoustic oscillations of the confinement are in phase with the heat release rate fluctuations and results in thermoacoustic instability. A horizontal Rijke tube, a horizontal duct with a concentrated heat source, is often chosen as a prototypical system to study the physics of thermoacoustic instabilities in the past. Through experimental and numerical investigations conducted in the past, it is confirmed that Rijke oscillations are nonlinear and capable of depicting rich dynamical phenomena such as limit cycle oscillations, period-2 oscillations, quasi-periodic oscillations and chaotic vibrations.

Experimental and numerical studies on Rijke tube show that the transition to instability happens through a subcritical Hopf bifurcation. A system which becomes unstable through a subcritical Hopf bifurcation can be *triggered* to instability even when the system is linearly stable. Zinn & Lieuwen^c reported that perturbations of the order of background noise levels are sufficient enough to trigger a thermoacoustic system. Since triggering is possible in the case of thermoacoustic system, which will happen in the parameter range where the system is bistable, the influence of noise on the hysteresis characteristics is worth investigating. Waugh *et al.*^d analyzed the behavior of the Rijke tube model of Balasubramanian & Sujith^e with stochastic forcing and found that triggering is dependent on noise strength as well as heat release rate. Waugh & Juniper^f conducted numerical studies on a hot wire Rijke tube model and obtained stochastic stability maps. Jegadeesan & Sujith^g showed that for a ducted non-premixed flame, noise-induced transitions to instability are possible. They also obtained the deterministic and stochastic stability boundaries. However, experimental results on the effect of external noise on the hysteresis behavior of thermoacoustic systems are not available to the best of authors' knowledge.

In the present work, the influence of external noise on the hysteresis characteristics of a thermoacoustic system, namely a horizontal Rijke tube, is experimentally investigated. The width of the hysteresis zone is found to decrease with increase in the amplitude of external noise. Once the noise intensity is above a threshold, hysteresis zone completely vanishes and the transition resembles a supercritical bifurcation. During the onset of instability, a drop in acoustic pressure amplitude is observed as the external noise levels increase.

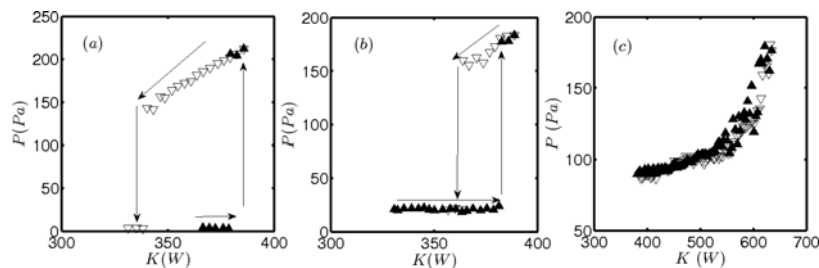


Figure: 1 Variation of acoustic pressure P with heater power K in the presence of external noise of different intensities β . (a) $\beta = 0$ Pa. (b) $\beta = 11$ Pa. (c) $\beta = 100$ Pa. The heater is located at $L/4$ and the mass flow rate is $\dot{m} = 2.34$ g/s. The cold decay rate $a = 18.5$ s⁻¹.

^a Dep. Aerospace Engineering, IIT Madras, Chennai-600036, India

^b Dep. Aerospace Engineering, IIT Madras, Chennai-600036, India

^c Zinn & Lieuwen, *Progress in Astronautics and Aeronautics* **210** (2005)

^d Waugh *et al.*, *Proceedings of the Combustion Institute* **33**, 2945–2952 (2011)

^e Balasubramanian & Sujith, *Phys. Fluids* **20**, 044103 (2008)

^f Waugh & Juniper, *IJSCD* **3**, 225–242 (2011)

^g Jegadeesan & Sujith, *Proceedings of the Combustion Institute* **34**, 3175–3183 (2013)

Determination of equivalence ratio fluctuations through optical measurement in radially stratified flames

Z. Han^a, M. M. Kamal^a, S. Lowe^a and S. Hochgreb^a

Equivalence ratio fluctuations are known as one of the key factors in controlling thermoacoustic instabilities in lean premixed gas turbine engines. The local equivalence ratio distribution in a flame affects its shape and response under velocity perturbations. However, it is difficult to account for the mixing and spatial-temporal distribution of these perturbations in the flame. In the present paper we adopt a previously introduced methodology based on the intensity of the chemiluminescence of the excited CH^* over CO_2^* as indicators of equivalence ratio, and apply it to the present case of radially stratified flames. Calibration of the chemiluminescence emission is provided by a series of premixed and stratified turbulent CH_4/air swirl flames, from which emission intensity is collected by a single intensified camera with split filtered images. The flames are subject to well-defined radial equivalence ratio distributions created via a split annular fuel delivery system with a swirling stabilizer. A siren excites the flow from the upstream side of the system, producing flames stabilized in a quartz combustor. Simultaneous measurements of the oscillations of inlet velocity and chemiluminescence images are carried out, leading to a map of the spatial equivalence ratio fluctuations during the cycle. The modification of the flame structure by stratification changes the nonlinear response of flames and distribution of local equivalence ratio to acoustic forcing. This information is used to generate mixing transfer function via spectral analysis, which relates the acoustic velocity fluctuation to the corresponding fluctuations of local equivalence ratio in a flame.

The results show the equivalence ratio distribution is the key factor governing the response of heat release rate. Increasing stratification towards the inner zone increases the gain and susceptibility to instabilities via affecting the distribution and fluctuation of equivalence ratio of stratified flames.

^a Department of Engineering, University of Cambridge, Trumpington St., Cambridge, UK

CH*/CO₂* Imaging for Equivalence Ratio Fluctuations in Turbulent Stratified Flames

M. M. Kamal^a, S. Lowe^a, Z. Han^a and S. Hochgreb^a

Equivalence ratio fluctuations play an important role in reliably evaluating the heat release or exploring thermoacoustic instabilities associated with lean pre-mixed gas turbine combustors. Measuring local equivalence ratio is difficult, and we often rely on ratios of chemiluminescent emissions estimates. A typical flame spectrum is composed of distinct peaks associated with radicals CH*, OH* and C₂*, with broadband distributed background attributed to CO₂* emittance. Recent experiments have indicated that the equivalence ratio scales with the ratio of CH* and CO₂* chemiluminescence measured in the visible range (431 and 410 nm, respectively). In contrast with the previously used CH*/OH* method, this allows a single visible camera to be used rather than multiple cameras and filters. This procedure has been previously calibrated by taking emissions measurements from fully premixed flames, under the assumption that the local emission ratio will be proportional to the chemiluminescence ratio.

The present work evaluates the accuracy of the methodology in determining local equivalence ratios, by comparing the equivalence ratio obtained by the ratio of simultaneous chemiluminescence measurements of CH* and CO₂* with previously obtained Raman-Rayleigh line measurements of all species to obtain the local equivalence ratio. The line of sight measurements obtained from the calibrated images of CH*/CO₂* are filtered and Abel de-convoluted in order to appropriate comparisons with the line scans obtained from Raman measurements. The comparison is discussed in the light of the required accuracy for estimating fluctuations of equivalence ratio in dynamic measurements.

^a Department of Engineering, University of Cambridge, Trumpington St., Cambridge, UK

Experimental observations of hydrodynamic and acoustic interactions during thermoacoustic instabilities in dump and swirl combustors

S. R. Chakravarthy^a

Systematic experiments have been performed in combustors of identical dimensions containing a backward-facing step, a V-gutter bluff-body, or an annular swirler, to examine their combustion instability characteristics. The length of the combustor, the axial location of the step/bluff-body/swirler, fuel injection location or upstream of the flame holder, etc. have been varied. The air and (gaseous) fuel flow rates are widely varied to obtain acoustically induced blowout conditions as well as onset of transition from low amplitude broadband noise to high-amplitude discrete tones exhibited by combustion instability. Under most conditions, the onset of combustion instability is accompanied by shifts in dominant frequency from a constant Helmholtz number to constant Strouhal number representing a flow-acoustic lock-on. In some cases, particularly in the swirl combustor, this shift occurs between “mixed modes” of the combustor, i.e., neither purely acoustic nor purely hydrodynamic modes. Certain conditions indicate constructive and destructive interferences of this mechanism with equivalence ratio fluctuations due to fuel injection upstream of the flame stabilization zone. Upstream fuel injection at an intermediate location between non-premixed and premixed extremes in the swirl combustor clearly shows huge rise in amplitudes, suggesting flame structure fluctuations as a hitherto unacknowledged mechanism of heat release fluctuations driving combustion instability. High-speed particle image velocimetry of the flow field of the premixed flame dynamics in the dump combustor has been performed under conditions that exhibit intermittent burst oscillations as the system shifts back and forth between dominant hydrodynamic and acoustic modes. The burst oscillations are characterized by alternating instances of loud sound and relative silence. The dominance of hydrodynamic mode is characterized by large-scale vortex roll-up downstream of the step, whose periodic shedding causes excitation of high amplitude acoustic oscillations. However, the dominant acoustic mode, being of a shorter time scale than the hydrodynamic mode, induces small scale vortices to be shed at the step corner, when the acoustic amplitude is high. The small scale vortices undermine the existence of the large scale vortex, leading to attenuation of the source of high amplitude acoustic excitation and corresponding instance of relative silence.

^a National Centre for Combustion Research & Development, and Department of Aerospace Engineering, Indian Institute of Technology Madras, Chennai 600036 India.

Acoustic Response of Helmholtz Dampers in the Presence of Hot Grazing Flow

D. Wassmer^a, B. Cosic^a, S. Terhaar^a and C.O. Paschereit^a

Due to lean premixed combustion, which allows for the reduction of NOx emissions in gas turbine engines, combustion chambers are more susceptible to thermoacoustic instabilities. Cooled passive dampers, such as liners or Helmholtz dampers, are eligible means to attenuate or suppress these instabilities in the combustion chamber. This study comprehensively investigates the influence of hot grazing flow on the acoustic response of Helmholtz dampers in the linear regime as well as in the nonlinear regime. The flow field inside the resonator, in its neck and in the vicinity of the neck in the combustion chamber is measured with high-speed particle image velocimetry for various amplitudes and at different mass-flux ratios of grazing and purging flow. Seeding is used as a tracer to qualitatively assess the mixing of the grazing flow, which consists of the hot combustion gas, and the cold purging flow, which cools the Helmholtz damper and emanates through the damper neck into the combustion chamber, as well as the ingestion into the neck of the resonator. The acoustic response for various temperature differences between the grazing flow and the purging flow is experimentally investigated via the multi microphone method. Together with two microphones flush-mounted in the resonator volume and two microphones in the plane of the resonator entrance, it is used to determine the impedance, the ratio between the acoustic pressure and the acoustic velocity, of the Helmholtz damper in the linear and nonlinear amplitude regime for various temperatures and different mass-flux ratios. Additionally, a thermocouple was used to measure the temperature in the neck. A well-known analytic acoustic network model, which is validated for isothermal conditions, is employed to calculate the admittance of the Helmholtz damper. This model is extended by an analytical approach to incorporate the measured acoustic energy dissipation caused by the density gradients at the neck vicinity. Therefore, a pressure loss-coefficient was determined for the isothermal case and based on this value and the measured admittance, the temperature dependent pressure loss-coefficient is evaluated. The damping efficiency, which corresponds to the losses in the system, is depicted in Fig.1 on the left hand side for different excitation amplitudes. A distinct decay of damping efficiency is denoted for increasing temperature differences. Additionally, the impact of the temperature differences on the virtual neck length of the resonator, which triggers the resonance frequency, is investigated. The evolution of the measured resonance frequency is shown in Fig.1 on the right hand side. By means of the model, a correlation between the temperature differences and the change of the virtual neck length is derived.

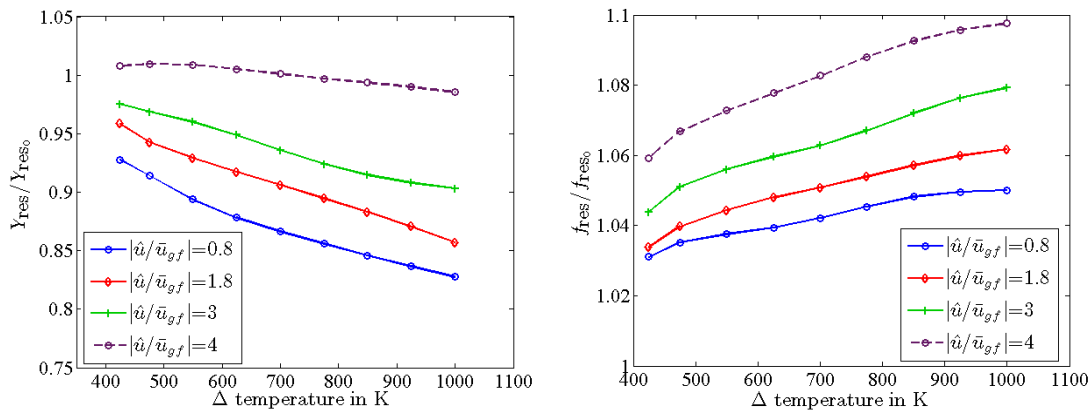


Figure 1: Damping efficiency over temperature difference for 4 different amplitudes (left). Normalized resonance frequency of the damper over temperature difference for 4 different amplitudes (right).

These results allow for a better understanding of the physical flow phenomena arising in the vicinity and inside the resonator neck and allow for a more precise prediction of the acoustic behavior of Helmholtz dampers under non-isothermal conditions.

^a Institut für Strömungsmechanik und Technische Akustik, Chair of Fluid Dynamics, -Hermann-Föttinger-Institut- Technische Universität Berlin, 10623 Berlin, Germany

Flame-Intrinsic and Acoustic Modes of a Premix Combustor

T. Emmert¹, S. Bomberg^a, W. Polifke^a

Thermoacoustic instabilities of combustors are frequently conceptualized as acoustic eigenmodes that grow in amplitude due to resonant interaction with unsteady heat release. However, *flame-intrinsic modes* of velocity-sensitive premix flames have been identified by an analysis of acoustic-flow-flame-acoustic interactions, which properly reflects the underlying causality of wave propagation, convective transport, and flame dynamics^{1,2}. The sequence of events may be described as follows: unsteady heat release by the flame generates acoustic waves that travel in the upstream direction, where they contribute to the fluctuations of velocity, which in turn triggers a perturbation in heat release, as described by a flame transfer function. Thus a flame-intrinsic feedback loop is formed, which may go unstable under certain conditions. The physical mechanisms involved in the velocity sensitive heat release modulation may be, e.g., flame front kinematics, a convective transport of fuel inhomogeneities or swirl modulation. Flame intrinsic eigenvalues, i.e. frequencies and growth rates of corresponding eigenmodes, may be determined easily if the flame transfer function is known.

The flame-intrinsic modes are clearly distinguishable from the acoustic modes and result in a number of interesting phenomena. For example, intrinsic modes have been identified as the cause of strong acoustic response to incident perturbations², and significant instability potentiality¹. Furthermore, intrinsic modes can result in thermo-acoustic instability of a flame that is placed in an anechoic environment³.

The present study explores consequences of flame-intrinsic modes for a flame that is placed in a combustor with non-zero reflection coefficients of plenum inlet and combustor outlet (an acoustic resonator). Such a thermoacoustic system may exhibit two types of eigenmodes: those that should be attributed to the flame intrinsic dynamics, as well as those that may be identified as acoustic eigenmodes. With increasing coupling between the acoustic and flame intrinsic sub-systems, these eigenvalues will be shifted.

By way of example, the analysis is applied to a turbulent premix swirl combustor (BRS burner). It is found that an experimentally observed unstable mode of this combustion system can be identified as resonances of the intrinsic thermoacoustic eigenmodes. The frequency of this mode does not coincide with any of the acoustic modes (Helmholtz mode, quarter wave mode), or a maximum of the gain of the flame transfer function, but does coincide with a maximum of the closed loop intrinsic thermoacoustic feedback.

¹ Dep. Mechanical Engineering, TUM, Boltzmannstr. 15, D-85747 Garching, Germany

¹ T. Emmert, S. Bomberg, and W. Polifke, "Intrinsic Thermoacoustic Instability of Premixed Flames," *Submitted for Publication in Combustion and Flame* (2014).

² S. Bomberg, T. Emmert, and W. Polifke, "Thermal versus acoustic response of velocity sensitive premixed flames," *submitted for presentation at Combustion Symposium* (2014)

³ Maarten Hoeijmakers, "Flame-Acoustic Coupling in Combustion Instabilities" (Technische Universiteit Eindhoven, 2014).

Heat Transfer

Turbulent heat transfer in pipes with variable circumferential heat flux

A. Antoranz^a, A. Gonzalo^a, O. Flores^a and M. García-Villalba^a

We report on turbulent heat transfer in a pipe calculated using Direct Numerical Simulations (DNS) of incompressible, fully-developed turbulent flow. We consider constant fluid properties, a Reynolds number in the range 5300-10000 and a Prandtl number 0.7. We study the different heat transfer characteristics obtained when varying the heat flux at the pipe wall. Three cases are considered. The first one which is used for validation purposes consist of homogeneous heat flux on the wall. This case has been previously studied by Piller¹. The heating condition imposed on the wall corresponds to the addition of a given amount of heat Q to the flow. This implies a linear increase of the bulk temperature in streamwise direction. In the second case, the heat flux is sinusoidal. The same amount of heat Q is added to the flow in the upper part of the flow, however it is removed from the lower half. Therefore, no net heat is added. The third case aims to reproduce the heat transfer conditions that occur in the pipes of the heat receiver of a concentrated solar power. Typically the sun radiation only affects half of the circumference with a sinusoidal distribution, while the other half can be considered adiabatic. The heating condition is imposed such that the same amount of heat Q is added to the flow as in the first case.

The Navier-Stokes equations are solved using the massively parallel spectral-element method solver NEK5000 developed by Fischer et al.². El Khoury et al.³ studied turbulent pipe flow without heat transfer using also NEK5000. We have selected the computational domain and grid resolution following their study. For illustration, a snapshot of the temperature fluctuations is shown in figure 1. The data corresponds to the third case, i.e. sinusoidal heat flux in half of the perimeter only. The main objective of the study is to generate a numerical database for RANS turbulence models benchmarking. The database will allow to assess the accuracy of the prediction of non-homogeneous temperature distributions in the circumferential direction from mean velocity fields and Reynolds stresses that only depend on the radial coordinate, a typical assumption employed in industrial applications.

^a Dep. Bioingeniería e Ingeniería Aeroespacial, Universidad Carlos III de Madrid, Leganés 28911, Spain

¹ Piller. Int. J. Num. Meth. Fluids **49**, 583 (2005)

² Fischer et al. NEK5000 Web page: <http://nek5000.mcs.anl.gov/> (2008)

³ El Khoury et al. Flow, Turbul. Combust. **91**, 475 (2013)

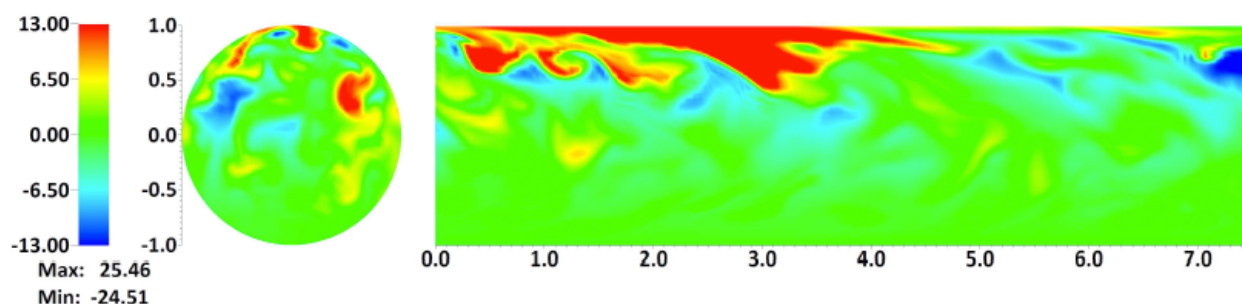


Figure 1: Instantaneous temperature fluctuations. Left, transverse plane. Right, vertical mid-plane showing about 1/3 of the computational domain in streamwise direction.

Effects of Local Flow Parameters of Cooling Water on Heat Transfer of Pool-Type Heat Exchanger

Byung Soo Shin^a, Ae Ju Cheong^b and Bok Ki Min^a

To assessment the performance of heat transfer on the condensation heat exchanger with tube bundle in storage tank, the mechanisms of heat transfer inside and outside each tube should be investigated clearly. For the condensation heat exchanger, the condensation heat transfer phenomena inside the tube mainly depend on local quality and flow pattern. Whereas the boiling heat transfer outside a tube is determined by thermal hydraulic conditions of cooling water, on which numerical analysis should be conducted in detail if the effects of those are considerable. The objective of this study is to estimate the effects of thermal hydraulic condition of cooling water on the overall heat transfer capacity.

The considerable geometry is water storage tank including single horizontal U-type tube. The high pressure steam entered into the tube inlet is flowing through with phase change by condensation. On the other hand, subcooled nucleate boiling occurs at the outside surface of a tube when static head by level of cooling water is given to the outside of a tube and the surface of cooling water is exposed to atmospheric pressure. In the circumstance, it is assumed that the total mass flow rate is constant along a steam flowing direction and water/steam properties inside the tube are the same as saturated condition at the inlet of a tube. Tandon map was used to predict two-phase horizontal flow pattern. Basically, Chato correlation and Shah correlation was used for laminar flow and for turbulent flow respectively on the condensation heat transfer coefficient and well-known Chen correlation was also used for boiling heat transfer relation. In addition, some different kinds of heat transfer correlation were also compared with each other.

From the results, it was verified that the variation of properties which is a function of saturated pressure, local temperature, local quality and local velocity at the outside of a tube affected the overall heat transfer capacity. Especially, the boiling heat transfer coefficient was sensitive to local quality as shown in Figure 1(a). It means that, if the cooling water level and local pressure in the storage tank becomes lower, the overall heat transfer capacity could be changed significantly due to active boiling phenomena. In spite of relatively weak sensitivity of local velocity from Figure 1(b), local velocity could be also considerable parameter according to circumstance. It is because local velocity could affect the distribution of local quality and pressure. Finally, with realizable conditions of cooling water, the results of this study were compared with the results of computational analysis code and experimental data. This calculation predicted the heat transfer coefficients slightly less than experimental data but similarly to the experimental results as shown in Figure 1(c).

^a System Evaluation Department, KINS, Daejeon 305-338, Republic of Korea

^b Safety Issue Research Department, KINS, Daejeon 305-338, Republic of Korea

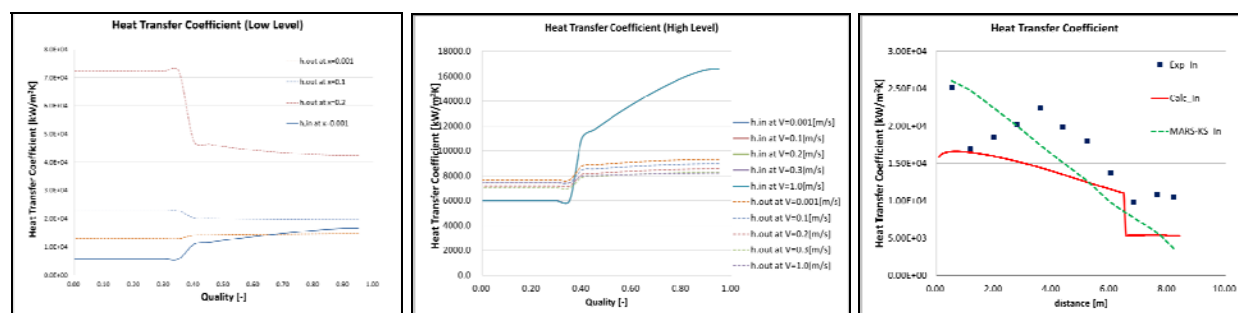


Figure 1: (a) Comparison of heat transfer coefficient. (b) Effect of local quality. (c) Effect of local velocity

NUMERICAL INVESTIGATION OF NATURAL CONVECTIVE HEAT TRANSFER CHARACTERISTICS OF Al_2O_3 -WATER NANO FLUID THROUGH POROUS MEDIA EMBEDDED IN A SQUARE CAVITY

Siva Sai Vadri^a, Arul Prakash. K^a, Arvind Pattamatta^b

Nano fluids are the colloidal suspensions of nano meter sized particles present in the base fluids such as water, ethylene glycol etc. Fluid flow and heat transfer in porous media are becoming extensive due to their wide applications in the field of heat transfer enhancement. Many researchers have studied the heat transfer characteristics of either nano fluids or porous media. But very few studies [1] have been done so far in the combination of both. So, the main aim of the present work is to study the combined heat transfer characteristics of nano fluids and porous media.

In this study, the natural convective heat transfer characteristics of Al_2O_3 -water nano fluid through porous media embedded in a square cavity with several pairs of heat sources and sinks will be investigated numerically. The two dimensional governing equations for fluid flow and heat transfer are solved by using in-house code based on Stream line Upwind Petrov-Galerkin finite element method, proposed by Brooks and Hughes [2]. The Darcy-Forchheimer-Brinkman's generalized porous media model is used in this analysis. The walls of the cavity are proposed to be insulated and heaters and coolers are maintained at temperatures t_h and t_c ($t_h > t_c$) respectively. The main objective of this study is to investigate the effect of Rayleigh number ($10^4 - 10^6$), Darcy number ($10^{-2} - 10^{-4}$), nano particle volume fraction (1% - 4%) and porosity (0.4, 0.6 & 0.9) on the performance of heat transfer.

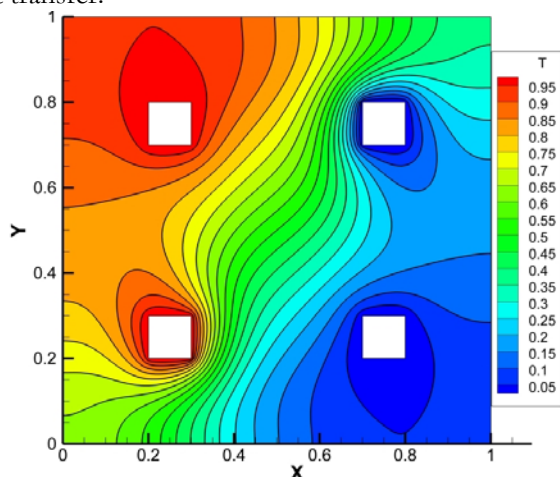


Fig 1:(a)

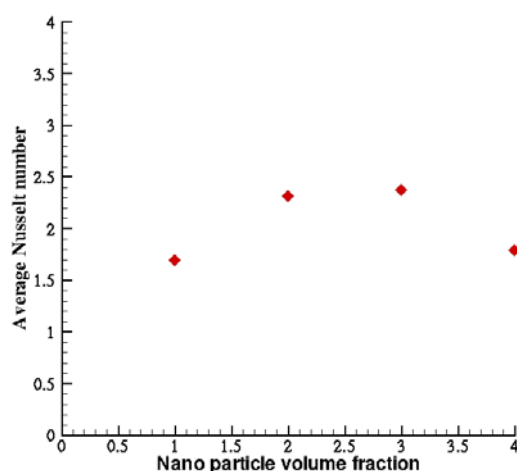


Fig 1:(b)

Fig 1: (a) Isotherms for nano particle volume fraction=0.01. (b) Average Nusselt number vs nano particle volume fraction for $Ra=10^4$, $Da=10^{-2}$ and Porosity=0.4.

For a pair of heaters and coolers model, it is observed that the isotherms are almost parallel to the vertical walls as shown in Fig 1 (a). This is because the conduction heat transfer is more dominant when compared to convective heat transfer at Rayleigh number 10^4 . Fig 1 (b) shows the effect of nano particle volume fraction on the performance of average Nusselt number. It is observed that as the volume fraction increases, the average Nusselt number increases up to 3% and then decreases. In addition to these, design parameters such as number and position of heaters and coolers and their effect on Nusselt number will be investigated for various cases.

^aDep. Applied Mechanics, Indian Institute of Technology Madras, India.

^bDep. Mechanical Engineering, Indian Institute of Technology Madras, India.

1. G.C. Bourantas et al., *European Journal of Mechanics B/Fluids* **43** (2014).

2. A.N. Brooks et al., *Computer Methods in Applied Mechanics and Engineering* **32** (1982).

Direct numerical simulation of heat transfer augmentation using traveling wave-like wall deformation

Keisuke Uchino^a and Koji Fukagata^a

Simultaneous achievement of heat transfer augmentation and drag reduction in turbulent flow is desired for more efficient use of energy. Nakanishi et al.¹⁾ investigated the drag reduction effect of traveling wave-like deforming wall in a turbulent channel flow. A traveling wave-like wall deformation decreases the drag when the wave travels in the downstream direction; the flow is stabilized and eventually relaminarized under several sets of parameters. The effect of the traveling wave-like wall deformation on the heat transfer is still to be investigated for achievement of dissimilar control. Therefore, in this paper, we investigate the heat transfer effect of traveling wave-like wall deformation in a turbulent channel flow using direct numerical simulation. (DNS)

A schematic of the traveling wave-like wall deformation is shown in Figure 1. The DNS results under different values of parameters a (deformation amplitude), k (wavenumber) and c (phase-speed), are tabulated in Table 1. It is found that the heat transfer is augmented in the cases with upstream traveling wave-like wall deformation. Heat transfer increases as the deformation period becomes shorter and the amplitude becomes larger. The maximum heat transfer augmentation rate, R_H , is achieved in the present study is 213% (Case 5).

In order to quantify the cause of heat transfer modification, we extend the decomposition of heat transfer coefficient based on Kasagi et al.²⁾ and Tomiyama and Fukagata.³⁾ Figure 2 shows the different contributions to the Nusselt number. It is found that the random components are significantly increased by the traveling wave-like wall deformation. Although the periodic components have negative values and contribute to the reduction of heat transfer, their amplitudes are much smaller than the increments in the random component. Namely, the increase of the random component of the turbulent heat flux is the main contributor to the heat transfer augmentation.

^a Department of Mechanical Engineering, Keio University, Kohoku-ku, Yokohama 223-8522, Japan

¹ Nakanishi et al., *Int. J. Heat Fluid Flow* **21**, 152-159 (2012).

² Kasagi et al., *J. Heat Transfer* **134**, 031009 (2012).

³ Tomiyama and Fukagata, *Phys. Fluids* **25**, 105115 (2013).

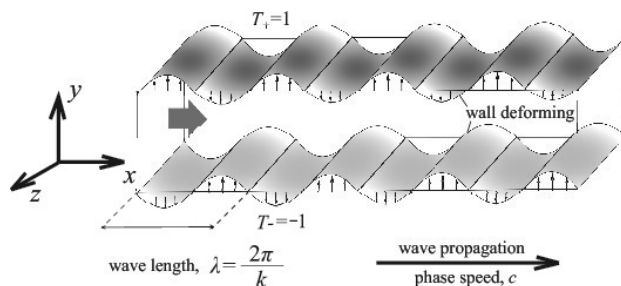


Figure 1: Schematics of a flow in a channel with traveling wave-like wall deformation.

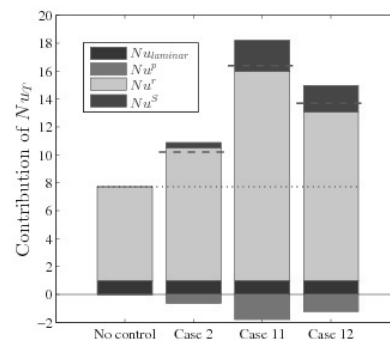


Figure 2: Dynamical contributions to the heat transfer. The dashed line represents the total value.

Table 1: Set of wave parameters and heat transfer rate.

Case	a	k	c	R_H	Case	a	k	c	R_H
1	0.05	2	-1	1.10	7	0.2	1	-3	1.72
2	0.1	1	-1	1.32	8	0.2	2	-2	1.60
3	0.1	1	-3	1.09	9	0.2	2	-3	1.35
4	0.1	2	-3	1.09	10	0.25	2	-3	1.52
5	0.15	2	-2	1.31	11	0.3	2	-2	2.13
6	0.2	2	-1	1.96	12	0.3	2	-3	1.77

A conjugate-heat-transfer immersed-boundary method for turbine cooling.

D. De Marinis^a, M. D. de Tullio^a, G. Pascazio^a and M. Napolitano^a

The first high pressure stage of modern gas turbines operates at very high temperatures that require very complex blade cooling systems. In order to design a cooling system that guarantees high performance and efficiency of the gas turbine, while maintaining a very low level of energy losses though using compressed air for cooling, it is crucial to predict the internal-air and external-gas flow and temperature fields, as well as the blade temperature, by solving a conjugate heat transfer (CHT) problem, numerically. The fluid flow and temperature fields are predicted by the Navier-Stokes and energy equations, whereas the heat conduction within the blades is described by a parabolic partial differential equation.

The CHT approach uses the same numerical method to solve the above differential equations coupled by the boundary conditions at the fluid-solid interface. Due to the very high geometrical complexity of the cooling channels within the blades, generating a body fitted mesh that captures all high gradient regions is extremely difficult and time consuming. Nevertheless, many turbine blade cooling simulations, using body fitted meshes and the Reynolds Averaged Navier-Stokes (RANS) equations, have been performed with success, though at large computational cost, see, e. g., Luo and Razinsky¹. A promising alternative approach is provided by the Immersed Boundary (IB) Method, which discretizes both the solid and fluid fields by means of a single Cartesian grid, thus reducing the grid generation process to a relatively simple and very quick task—an interesting review of the IB method and its application is provided by Mittal and Iaccarino².

And in fact, the computational fluid dynamics group at the Department of Mechanics, Mathematics and Management of the Polytechnic of Bari has developed and improved an IB Method for the compressible Navier-Stokes equations^{3,4}, by also extending it to solve CHT problems⁵. However, these works are limited to two-dimensional serial calculations so that they are not suitable for computing complex three-dimensional flows. On the other hand, thanks to the simplicity and efficiency of the IB Method, Kang et al.⁶ have been able to develop even a three-dimensional large eddy simulation (LES) IB solver based on the original approach of Fadlun et al.⁷.

The aim of this work is to extend the very efficient LES IB solver developed by Kang for the incompressible Navier-Stokes equations to the compressible RANS equations. More in detail, the authors propose a CHT method, using appropriate interface conditions at the interface grid-points, which allow to satisfy the Dirichlet and Neumann conditions (equal temperature and heat fluxes) exactly along the fluid-solid boundary. In spite of using an IB approach and the RANS equations, the computational effort is still formidable and a parallel solver is employed so as to obtain accurate results within reasonable computer time.

^a Dipartimento di Meccanica, Matematica e Management, Politecnico di Bari, via Re David 200, 70125, Bari, Italy.

¹ Luo G., Razinsky E.H., *Journal of Turbomachinery*, 129,773 (2007)

² Mittal R. and Iaccarino G., *Annual Review of Fluid Mechanics*, **37**, 239 (2005);

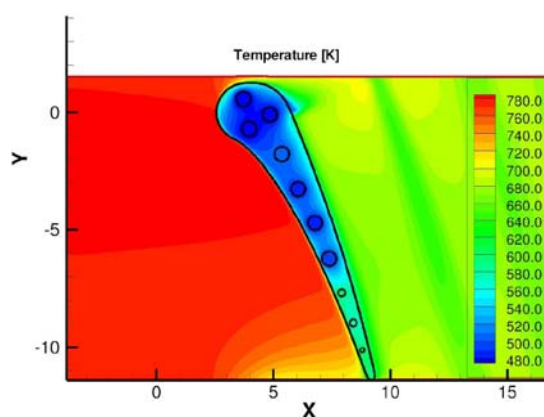
³ De Palma P., de Tullio M.D., Pascazio G., Napolitano M., *Computers & fluids*, **35**, 693 (2006);

⁴ de Tullio M. D., De Palma P., Iaccarino G., Pascazio G., Napolitano M., *Journal of Computational Physics*, **225**, 2098 (2007);

⁵ de Tullio M.D., Latorre S.S., De Palma P., Napolitano M., Pascazio G., *V European Conference on Computational Fluid Dynamics ECCOMAS CFD*, (2010);

⁶ Kang S. Iaccarino G., Ham F., Moin P., *Journal of Computational Physics*, **228**, 6753, (2009);

⁷ Fadlun E.A., Verzicco R., Orlandi P. and Mohd-Yusof J., *Journal of Computational Physics*, **161**, 35 (2000);



Effects of natural convection on thermal explosions in spherical vessels

I. Iglesias^a, A. L. Sánchez^a, A. Liñán^b and F.A. Williams^c

The problem of thermal explosion in a spherical container is analysed in this work. The formulation used follows the classical Frank-Kamenetskii time-independent problem but includes the effects of the buoyant motion associated with the density differences induced by the chemical reaction. The chemistry is described with a one-step irreversible reaction, whose Arrhenius rate includes an activation temperature T_a that is much greater than the wall temperature T_o , so that their ratio $\beta = T_a/T_o$ can be used as an asymptotically large quantity in describing the thermal explosion. Since the resulting thermal runaway is associated with a small temperature increase $(T - T_o)/T_o \sim \beta^{-1}$, the associated density decrement with respect to the chemically frozen value $(\rho_o - \rho)/\rho_o$ is also of order β^{-1} , with the consequence that the Boussinesq approximation can be used to investigate the resulting motion. The characteristic flow velocity $u_c = \beta^{-1}ga^2/\nu$ follows from a balance between viscous forces and buoyancy forces, with g and ν representing the gravity acceleration and the unperturbed value of the kinematic viscosity, and a being the radius of the spherical vessel. Besides the Prandtl number of the gas $Pr = \nu/D_T$ (the ratio of the kinematic viscosity to the thermal diffusivity D_T of the gaseous mixture), two dimensionless parameters appear in the problem, namely, the Grashof number and the Damköhler number

$$Gr = \frac{ga^3}{\beta\nu^2} \quad \mathcal{D} = \frac{\beta[q/(c_p T_o)]BY_o e^{T_a/T_o}}{D_T/a^2}$$

where q , c_p , Y_o , and B represent the amount of heat released per unit mass of reactant consumed, the specific heat at constant pressure, the initial reactant mass fraction, and the reaction-rate frequency factor. The governing equations are formulated in spherical coordinates in terms of the stream function and the vorticity variables and are solved numerically and asymptotically. An example of the simulated temperature and flow field is shown in Figure 1.

Previous efforts to address effects of buoyancy on thermal explosions in closed vessels have employed numerical integrations of the conservation equations; see¹⁻² for some recent publications. The present work focuses instead on the use of asymptotic methods, based on expansions in different limits that provide explicit formulae for critical explosion conditions, giving predictions that are in excellent agreement with numerical integrations of the conservation equations. The analytic results accounting for buoyancy perturbations display exceedingly small multiplicative factors in the corrections to the critical Damköhler number for explosion, thereby clarifying why the classical buoyancy-free theory developed by Frank-Kamenetskii remains accurate even for very large values of the Grashof number, a surprising outcome that has remained largely unexplained.

^a Dep. Ingeniería Térmica y de Fluidos, Universidad Carlos III de Madrid, Leganés 28911, Spain.

^b ETSIA Aeronáuticos, Pl. Cardenal Cisneros 3, Madrid 28040, Spain.

^c Dep. Mechanical and Aerospace Engineering, University of California San Diego, La Jolla, CA 92093-0411, USA

¹ Liu et al., *Physical Chemistry Chemical Physics* **10**, 5521 (2008).

² Liu et al., *Combustion and Flame* **157**, 230 (2010).

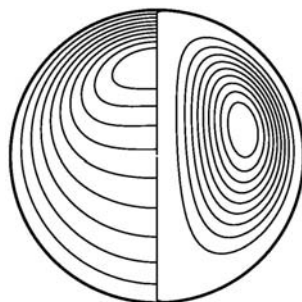


Figure 1: Isotherms (left) and streamlines (right) obtained from numerical simulation of the flow field for $Pr = 1$, $Gr = 1000$ and $\mathcal{D} = 4.5$.

Non Oberbeck-Boussinesq effects in Rayleigh Bénard convection

P. Urban^a, V. Musilová^a, T. Králík^a, M. La Mantia^b and L. Skrbek^b

We present experimental results on heat transfer efficiency of Rayleigh-Bénard convection (RBC) confined in a cylindrical cell 0.3 m in size¹. The working fluid is cryogenic helium gas with in situ tuneable properties, allowing very high turbulent intensities to be reached in a clean cryogenic environment². The heat transfer efficiency described by the Nusselt number $Nu(Ra, Pr)$ is investigated for the region of Rayleigh number $Ra > 10^{12}$, with the Prandtl number Pr varying as $0.7 \leq Pr < 15$. Below $Ra \approx 10^{12}$, our data can be treated as Oberbeck-Boussinesq (OB), in the sense that the value of the absolute temperature at which the fluid properties are evaluated can be taken anywhere between the temperatures of the plates of the cell.

Upon increasing Ra , our data are gradually affected by non-OB effects. The directly measured bulk temperature T_c (in the turbulent core of the cell) becomes different from the arithmetic mean of the plate temperatures T_m , confirming a thermal boundary layer asymmetry of the top and bottom plates. As the bulk of the RBC cell has the temperature T_c , it is natural to define Ra , Nu and Pr based on this temperature rather than on T_m . Using T_c instead of T_m leads to relatively small changes in Nu , but significantly larger changes in Ra . Replacing T_m by T_c can be thought of as a first order correction to take into account non-OB effects. When applied to our data, the observed $Nu(Ra)$ dependence closely displays a $1/3$ power law behaviour up to $Ra \approx 10^{14}$. The following step is to ignore the non-OB effects in the top half of the RBC cell and replace the latter by the inverted (nearly OB) bottom half in order to eliminate the boundary layer asymmetry. This leads to an effective temperature difference ΔT_{eff} between the plates and to effective Nu_{eff} and Ra_{eff} . The corresponding heat transfer efficiency $Nu_{eff}(Ra_{eff})$, up to $Ra_{eff} \approx 2 \times 10^{15}$, does not show any tendency of crossover to the so-called ultimate regime of RBC³.

Additionally, we have obtained scaling laws for the Reynolds number Re , based on plumes frequency. The corresponding $Re(Ra, Pr)$ dependence, calculated by using T_c instead of T_m , similarly to $Nu(Ra, Pr)$, is compared with relevant theoretical models. Preliminary results on the statistical analysis of temperature fluctuations, which includes the calculation of temperature structure functions, are also discussed.

We acknowledge the support of GAČR 14-02005S.

^a Institute of Scientific Instruments ASCR v.v.i., Královopolská 147, 612 64 Brno, Czech Republic

^b Faculty of Mathematics and Physics, Charles University, Ke Karlovu 3, 121 16 Prague, Czech Republic

¹ Urban et al., *Rev. Sci. Instrum.* 81, 085103 (2010).

² Urban et al., *Phys. Rev. Lett.* 109 154301 (2012).

³ Kraichnan, *Phys. Fluids* 5, 1374–1389 (1962)

Spatio-temporal Patterns in Inclined Layer Convection

P. Subramanian^a, W. Pesch^b and T. M. Schneider^{c,a}

Convection driven by temperature gradient across a layer of fluid has been investigated extensively in terms of the Rayleigh-Bénard system. A related system that mimics meteorological and geophysical flows is that of Inclined Layer Convection (ILC), where the fluid layer is inclined to the horizontal plane and subject to a temperature gradient. In the ILC system, both convection and shear induced pattern forming instabilities come into play to generate a wide variety of interesting patterns. Buoyancy driven instabilities such as longitudinal rolls, sub-harmonic oscillations, Busse oscillations, crawling rolls and undulation chaos occur at small angles of incline. At high angles of incline, shear driven instabilities such as transverse rolls, bimodal oscillations, localised bursts and switching diamond patterns dominate.

We obtain the evolution of the full nonlinear ILC system by our numerical simulation (Oberbeck-Boussinesq equations). Our simulations allow us to quantitatively compare different measures between our numerical simulations and experimental results [1] including the patterns observed in the temperature field along with their frequency content, wavelength of patterns, the velocities of localised structures, etc.

The system parameters of interest in the comparison are the non-dimensional thermal gradient ϵ which is indicative of the thermal driving in the system, the angle of incline γ and the Prandtl number Pr . As observed in Figures 1(a)-(b), we see that the simulations of the ILC system closely match the experimental results at the same system parameters. So far the case of medium $Pr \sim 1$ has been predominantly considered. These explorations of the Pr number range close to $Pr \sim 1$ have already yielded a variety of novel instabilities and even discovered that longitudinal rolls are unstable to spatio-temporal chaos rather than the stationary undulations [2]. In addition to comparing our simulations with experiments, we concentrate on the regime of small Pr , where shear flow driven instabilities dominate and produce spots and stripe patterns observed in shear flows which are not well understood.

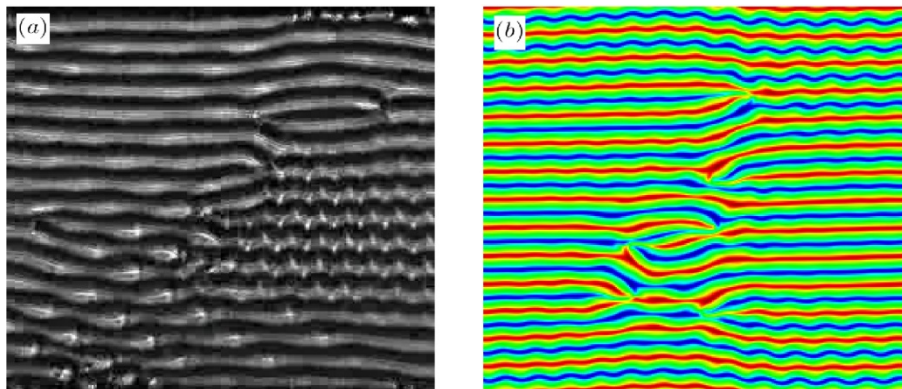


Figure 1: Co-existence of sub-harmonic oscillations with Busse oscillations at small angles of incline $\gamma=11$ degrees and strong thermal driving $\epsilon=5.3$ for a fluid with $Pr=1.07$. (a) mid-plane temperature fluctuations from experiments [1] (b) mid-plane temperature fluctuations from simulation.

^a MPRG-ECPS, Max-Planck Institute for Dynamics and Self-Organisation, Göttingen, 37077 Germany

^b Physikalisches Institut der Universität Bayreuth, Bayreuth 95440, Germany

^c School of Engineering, Ecole polytechnique fédérale de Lausanne, CH-1015 Switzerland

¹ Daniels, PhD thesis, Cornell University (2002).

² Daniels et. al, Bull. Am. Phy. Soc. CENT99:QC28.01 (1999).

Accurate interface tracking for phase-change problems with natural convection

I. Danaila^a, R. Moglan^a, F. Hecht^b, S. Le Masson^c

We present a new single domain numerical approach for phase-change systems with natural convection. The key ingredients of the method are the use of an adaptive finite element method with a new regularization of the functions representing the variation of thermodynamic properties at the solid-liquid interface, and a fully linearized Newton algorithm for the time integration of the system of equations. The advantage of our adaptivity method is to allow accurate and simultaneous tracking of different interfaces in the system (the solid-liquid interface, but also the density inversion interface for water flows, as shown in the figure). Compared to classical finite difference or finite volume methods on fixed meshes, which require high resolutions for an accurate interface tracking, our finite element method offers the possibility to dynamically refine the mesh only in the regions of the domain where sharp phenomena take place and thus reduce the computational time.

The numerical method is validated against classical benchmarks that progressively add strong non-linearities in the system of equations: (i) natural convection of air (described by the Navier-Stokes equations with a linear buoyancy term), (ii) natural convection of water (introducing a nonlinear buoyancy term), (iii) melting of a phase-change material (introducing variable viscosity and nonlinear enthalpy source term), (iv) water freezing (displaying together all previous non-linearities).

Very good agreement with experimental data is obtained for each test case, proving the capability of the method to deal with both melting and solidification problems with convection. An example is provided in the figure below, for the difficult case of water freezing; our results for the interface tracking are closer to experimental data than any other previously published numerical results¹.

Since the method is implemented using the free software FreeFem++², it could be easily used or tested by anyone interested in simulating difficult configurations of phase-change systems with natural convection.

^a Université de Rouen, Laboratoire de Mathématiques Raphaël Salem, F-76801 Saint-Étienne-du-Rouvray, France.

^b Université Paris 06, Laboratoire Jacques-Louis Lions, F-75005 Paris, France.

^c France Telecom, 2 Avenue Pierre Marzin, BP 40, 22307 Lannion Cedex, France.

¹ Kowalewski and Rebow, *Int. J. of Computational Fluid Dynamics* **11**, 193 (1999).

² www.freefem.org

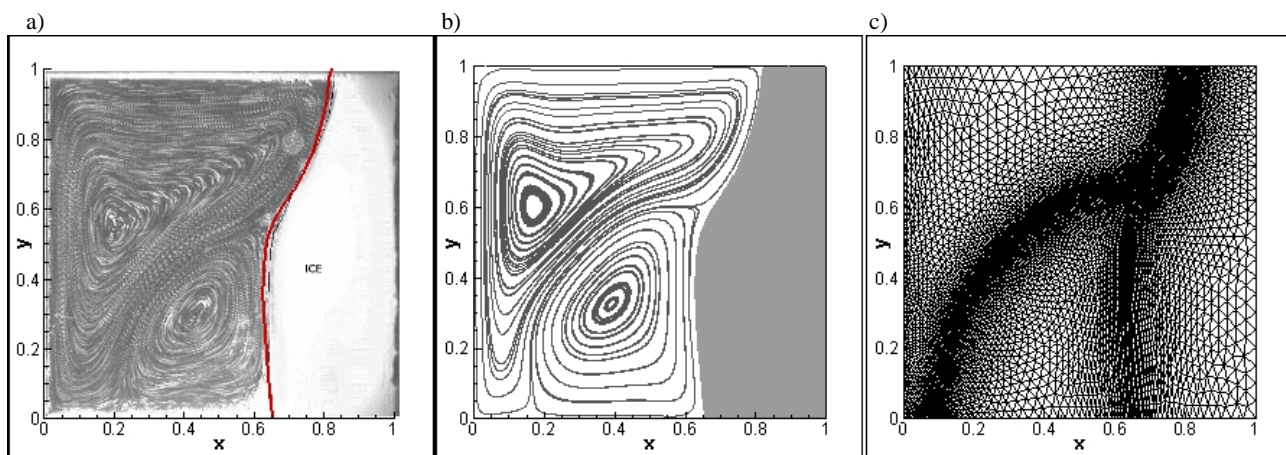


Figure 1: Freezing of pure water. Configuration at physical time $t=2340$ seconds (a) experimental image from Ref. 1; the thick red line represents the solid-liquid interface computed with the present method (b) computed streamlines showing the two recirculating zones in the fluid phase, generated by the nonlinear variation of water density with temperature (density inversion at 4°C) (c) computational mesh showing the accurate capture of two interfaces (solid-liquid and water density inversion interface).

Thermal boundary layer properties near roughnesses in turbulent Rayleigh-Bénard convection

J. Salort^a, O. Liota, E. Rusaouena, F. Seychelles^{a,b}, J.-C. Tisserand^a, M. Creyssels^{a,c}, B. Castaing^a and F. Chillà^a

We present global heat-transfer and local temperature measurements, in an asymmetric parallelepiped Rayleigh-Bénard cell, in which controlled square-studs roughnesses have been added. A global heat transfer enhancement arises when the thickness of the boundary layer matches the height of the roughnesses. The enhanced regime exhibits an increase of the heat transfer scaling.

Systematic characterizations of the temperature statistics near the boundaries have been carried out in the enhanced regime. They indicate, in the range of parameters explored, that the fluid inside the notches (between the obstacles) is essentially at rest and that the boundary layer on the top of the obstacles is very thin: this seems to explain most of the enhancement of the heat transfer. The boundary layer on top of the obstacles is destabilised by the mean flow.

We also report intermittent transitions to a more agitated state associated with a higher Nusselt number. This additional increase is much smaller (of order 1 %), in the range of parameters that we can investigate in this cell. Our interpretation is that this is caused by another mechanism, maybe close to the Du and Tong scenario¹: the enhancement of plume emissions by the roughnesses. Indeed, we have observed intermittent burst of coherent plumes in this more agitated state.

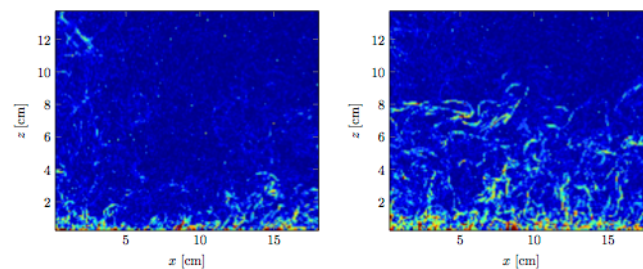


Figure 1: Instantaneous

module of dot displacement (proportional to the time difference of the temperature gradients), with the same color code. Left: Typical field in the lower Nusselt state. Right: Example of plume bursts in the higher Nusselt state.

^a Laboratoire de Physique, ENS Lyon, France

^b CORIA, Rouen, France

^c Laboratoire de Mécanique des Fluides et d'acoustique, EC Lyon, France

¹ Y.-B. Du and P. Tong, "Enhanced heat transport in turbulent convection over a rough surface", PRL **81**, 987-990 (1998)

Numerical and experimental study of turbulent convection in thin vertical layers

A. Teimurazov^a, A. Vasiliev^a and P. Frick^a

Turbulent Rayleigh-Benard convection in a bounded vertical layer of size $L \times d \times L$ demonstrates a variety of dynamical regimes governing by the aspect ratio, Rayleigh and the Prandtl numbers. For thin layers the structure of large-scale motion is quasi-two-dimensional, and different Q2D models could be used to take into consideration effects provided by the lateral walls which affect the velocity and temperature profiles. In this work we compare the numerical simulations executed by pure 2D and Q2D approximation of Boussinesq equations for convective flow in a square $L \times L$ box (2D) or squared vertical layer of finite depth $d \ll L$ (Q2D model). Q2D model uses modified 2D equations, which derived from Navier-Stokes equations in assumption of laminar transverse velocity profile. Our work was performed using «Uran» supercomputer of IMM UB RAS, Yekaterinburg. The aspect ratio $\Gamma = d/L$ of depth per height is varied between 0.03 and 0.2.

We compare our numerical results with experimental data from a water flow in a rectangular box heated from below. The experimental setup is a cubic cell with the side $L = 250$ mm whose horizontal walls are massive copper heat exchangers and vertical walls are made of 25 mm thick plexiglass. Two opposite walls of the cell are equipped with a system of vertical slots in which plexiglass partitions are mounted, which separate a rectangular region with the thickness d in the central part of the cube. The experiments were performed with $d = 15, 25$, and 50 mm (which corresponds to $\Gamma = 0.06, 0.1$ and 0.2). The cube was completely filled by distilled water and the motion of water in the central cross section of the inner cell was investigated using particle image velocimetry (PIV).

Direct numerical simulations mainly performed for Rayleigh number $Ra = 2.2 \cdot 10^9$ and Prandtl number $Pr = 7$ (it corresponds to average water temperature 25 C and temperature difference between heat exchangers $\Delta T = 10$ C. We show that the linear friction (Q2D model) essentially improves not only the modelling of the large-scale dynamics of the turbulent flow, but also reproduces much better the spectral properties of smaller scales for the turbulent flow with the aspect ratio $\Gamma \leq 0.1$. Furthermore influence of aspect ratio Γ on heat transport in the cell was studied using both 2D and Q2D models.

Financial support from the International Research Group Program supported by Perm region Government and RFBR project 14-01-31262 is gratefully acknowledged.

^a Institute of Continuous Media Mechanics, Academ. Korolyov, 1, Perm, 614013, Russia

Thermal convection in a rotating inclined plane layer

A.A.Ivanova^a, K.Y.Rysin^a, V.G.Kozlov^a

Thermal convection in a tilted plane layer rotating about an axis oriented perpendicular to its plane is experimentally investigated. The threshold of convection excitation and the structure of supercritical flows depending on the angle of inclination, the temperature difference and the rotational speed are studied.

The layer of thickness h with cylindrical lateral boundary is located on a table rotating at a definite speed around an inclined axis. Hydraulic distributor provides the circulation of liquid from the thermostats in the heat exchangers. Experiments are carried out with water and glycerol-water solutions. The layer thickness, speed of rotation and temperature difference at the boundaries of the layer vary.

In the experiments there are two limiting cases of the layer orientation: the horizontal ($\alpha = 90^\circ$) and vertical ($\alpha = 0^\circ$). For the horizontal orientation (the classical case of gravitational convection) the results obtained are in good agreement with theory¹ and experiment². The increase of the dimensionless rotation velocity (Taylor number) leads to growth of stability threshold. In case of vertical layer orientation the average convection is excited in a threshold way by the action of thermovibrational mechanism³.

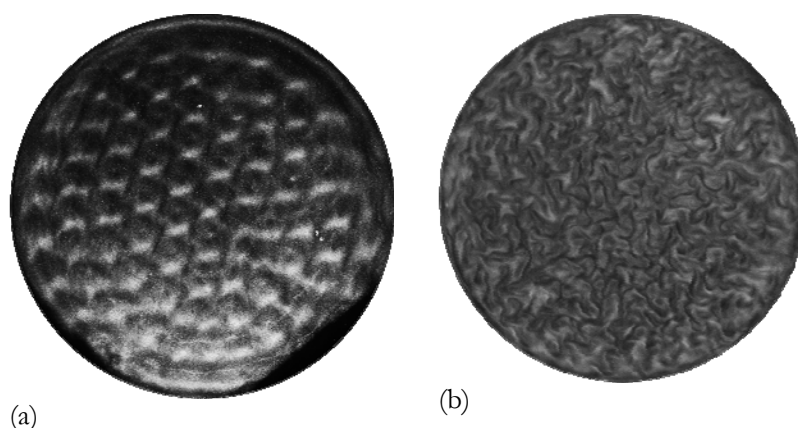


Figure 1: Convective structures: $\alpha = 0^\circ$ (a), $\alpha = 90^\circ$ (b).

The influence of the inclination angle on the occurrence of thermal convection and structure of supercritical flows are studied. It is found that the deviation of layer orientation from the horizon leads to stabilization of quasi-equilibrium. The heat transfer versus the angle of layer inclination is studied for different values of temperature difference at the layer boundaries. It is found that the change of convective mechanisms is accompanied by change of convective structure and heat transfer and takes place at $\alpha \approx 30^\circ$. At lower angles of the layer inclination the thermovibrational mechanism⁴ comes to replace the Rayleigh convective mechanism. In this case the gravity causes fluctuations of nonisothermal fluid in the cavity frame and generates the average vibroconvective flows. The results of investigation of the quasi-equilibrium stability and heat transfer in the supercritical region are plotted against the dimensionless parameters: gravitational Rayleigh number, vibrational parameter and dimensionless rotation velocity. It is found that the excitation of the average thermovibrational convection is possible at $\alpha < 0^\circ$ (heating of inclined layer from the upper plane).

The work is done in the frame of Strategic development program of PSHPU (project 029-F), with partial support from RFBR (grant 13-01-00675a) and Minobrnauki RF (task 2014/372).

^a Lab. of vibrational hydromechanics, PSHPU, 24 Sibirskaya Ave., Perm, Russia

¹ Chandrasekhar S. Hydrodynamic and hydromagnetic stability. Oxford University Press, 1961.

² Rossby, J. *Fluid Mech.* 36, 309 (1969).

³ Ivanova et al., *J. Fluid Dynamics* 38, 9 (2003).

⁴ Kozlov, J. *Fluid Dynamics*. 39, 3 (2004).

Regular convective patterns in a reactive miscible fluids system

A. Mizev^a, K. Kostarev and E. Mosheva

Bringing into a contact of two miscible liquids leads to appearance of intensive mass fluxes resulting under a certain conditions to development of spontaneous hydrodynamic structures. A series of spectacular convective patterns can be observed depending on initial density difference (Rayleigh-Taylor instability) and diffusion coefficients ratio (double-diffusive fingering or diffusive-layer convection) of the contacting liquids. The situation becomes more complex in the case of reacting fluids. A possible heat release and formation of a reaction product with different density and diffusion rate can trigger additional buoyancy-driven instabilities. The convective structures in the form of plumes or fingers observed in both nonreactive and reactive case are irregular and of global type, i.e. once develop the patterns grow until they reach the upper or the lower boundary of the reactor. Here we present the results of experimental observation of a new type of instability resulting in formation of a regular and spatially localized convective patterns observed for the initially stably stratified system of two miscible reactive liquids.

The experimental setup consists of vertically oriented Hele-Shaw cell made of two glass plates 2.5 cm width and 9.0 cm high separated by the gap thickness of 1.2 or 2.4 mm. Initially the cell is filled with two-layer system consisting of aqueous solution of nitric acid which is put on top of a denser miscible equimolar (from 0.5M to 2.0M) aqueous solution of sodium hydroxide. Fizeau interferometry and standard trace particles technique were used to visualize the concentration and velocity fields correspondingly. Our observations show that, soon after solutions contact, a buoyancy-driven convection, caused by formation of a depleted zone of acid solution, develops above the reaction front in the whole upper layer (Figure 1), while the zone below the front remains free of convection widening diffusively downwards. After some time (order of a few minutes depending on the reactants concentration) an accumulation of the reaction product, namely sodium nitrate, which is denser than both reactants, forms inside the zone below the front the local “pocket” with unstably stratified density. In the case of low reactants concentration (below 0.5M) the fluid in this “pocket” remains stable. Increase of the concentration results in the appearance of buoyancy-driven convection in the form of periodic array of convective cells existing within the unstable zone (Figure 1). It is interesting to note that the cells exist between two stable regions situated above and below it and they at first glance don't interact with the convection structure existing above the reaction front. The lower convective structure can exist for a long time (some hours) only widening with time that gives rise to an increase of the wavelength of the convective pattern.

The study was supported by the RFBR project No. 13-01-00508 and grant of the research program of the Ural Branch of RAS No. 12-T-1-1008.

^a Institute of Continuous Media Mechanics, Acad. Korolev st. 1, Perm, 614013, Russia

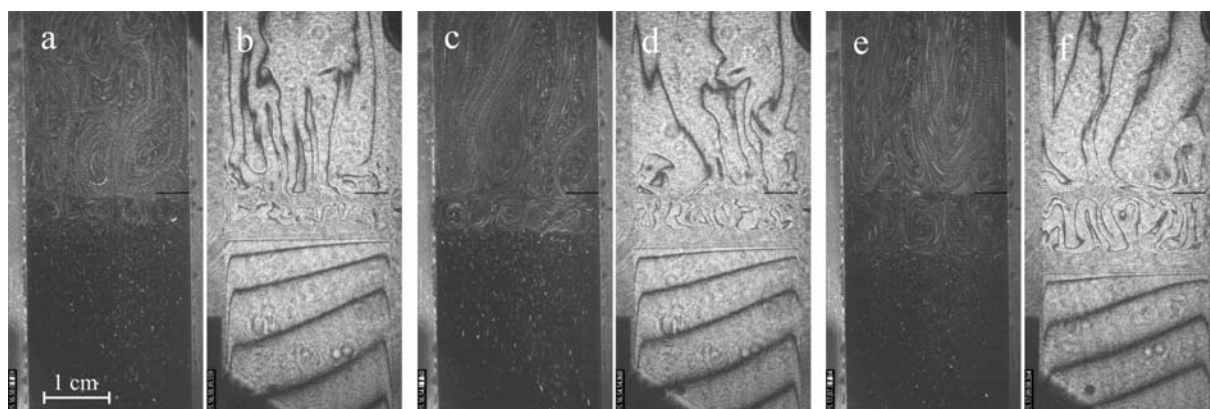


Figure 1: Time series of tracer images and interferograms demonstrating velocity and density distribution in the cell observed a certain time after the beginning of the neutralization reaction: (a) and (b) – 720 s, (c) and (d) – 960 s, (e) and (f) – 1800 s. The black stripe in the middle of the cell indicates the initial position of the reaction front.

Classical and quantum two-phase convective heat transfer

D. Schmoranzer^a, P. Urban^b, P. Hanzelka^b and L. Skrbek^a

A study of anomalous heat transfer via the two-phase liquid-vapour system of cryogenic helium is presented. This phenomenon was experimentally observed in our earlier work¹. It was found that in a convection cell, under certain circumstances, heat flowed against the temperature drop through normal liquid and gaseous layers of cryogenic helium from constantly heated but cooler bottom plate of the cell to its hotter, constantly cooled top plate. The bottom plate was heated uniformly by a resistive heater and the top plate was cooled by heat exchange with liquid helium maintained at 4.2 K. Additionally, for certain experimental conditions, a rain of helium droplets was detected by small sensors placed in the cell interior.

Because there was no other external source of heating around the cell except the bottom plate heater, the situation might at first sight appear to contradict the second law of thermodynamics, particularly Clausius' formulation²: „*No process is possible whose sole result is the absorption of heat from a body of lower temperature to a body of higher temperature.*“ Nevertheless, without any conflict with this fundamental law, the observed behaviour was confirmed and explained by means of a developed phenomenological model¹ that describes this process quantitatively based on open system thermodynamics, proving that nucleate boiling was the key mechanism.

The presented study extends our previous findings, attempting to answer both theoretically and experimentally an interesting question: what happens when the liquid phase adjacent to the bottom plate is not the normal liquid He I but a quantum fluid, namely the superfluid phase He II? Nucleate boiling that proved to be essential for the above observation, would hardly take place at the bottom plate and the heat transfer might be significantly affected. We would like to point out that cryogenic conditions allow these experiments to be performed using extremely clean working fluids with all possible impurities frozen out and effectively excluding any parasitic heat fluxes³.

We acknowledge the support of GAČR 14-02005S.

^a Faculty of Mathematics and Physics, Charles University, Ke Karlovu 3, 12116 Prague, Czech Republic

^b Institute of Scientific Instruments ASCR v.v.i., Královopolská 147, 61264 Brno, Czech Republic

¹ Urban et al., Proc. Natl. Acad. Sci. USA, 110 (20) 8036-8039 (2013).

² Clausius, Annalen der Physik 79:368–397, 500–524 (1851).

³ Niemela, Proc. Natl. Acad. Sci. USA, 110 (20), 7969-70, (2013).

Transition of heat transfer by turbulent Rayleigh-Bénard convection at high Ra

Xiaozhou He^a, Dennis P. M. van Gils^a, Eberhard Bodenschatz^a and Guenter Ahlers^{a,b}

We report measurements of dimensionless heat transfer, the Nusselt number Nu , in turbulent Rayleigh-Bénard convection of two cylindrical samples with the aspect ratio (diameter/height) $\Gamma = 0.50$ and 0.33 . Both samples have the same diameter of 1.1 m but different heights. Compressed sulfur hexafluoride gas (SF_6) at pressures up to 19 bars was used as the fluid. The measurements were conducted over the Rayleigh-number range $10^{12} \leq Ra \leq 4 \times 10^{15}$ and for Prandtl numbers Pr near 0.8 . As shown in figure 1, the reduced Nu data for the $\Gamma = 0.50$ sample clearly reveal a transition from the classical scaling $Nu \sim Ra^{0.312}$ to the ultimate scaling $Nu \sim Ra^{0.38}$ [1], which was consistent with the predictions by Grossmann and Lohse [2]. The transition region is $Ra^*_{11} \leq Ra \leq Ra^*_{22}$ with $Ra^*_{11} \approx 1.3 \times 10^{13}$ and $Ra^*_{22} \approx 5.0 \times 10^{14}$. For $Ra < 1.2 \times 10^{14}$ preliminary $\Gamma = 0.33$ data are in good agreement with the $\Gamma = 0.50$ data, which indicates that the onset of the transition Ra^*_{11} remains unchanged for the two Γ values. For $Ra > 1 \times 10^{15}$ the $\Gamma = 0.33$ data suggest that the range of the transition to the ultimate state becomes larger, which yields a higher Ra^*_{22} . With the ultimate scaling as shown by the dashed line, we estimate $Ra^*_{22} \approx 2.5 \times 10^{15}$ for $\Gamma = 0.33$.

^a Max Planck Institute for Dynamics and Self Organization, D-37073 Göttingen, Germany

^b Dep. of Physics, University of California, Santa Barbara, CA 93106, USA

¹ He, Funfschilling, Nobach, Bodenschatz and Ahlers, *Phys. Rev. Lett.* **108**, 024502 (2012).

² Grossmann and Lohse, *Phys. Fluids* **23**, 045108 (2011).

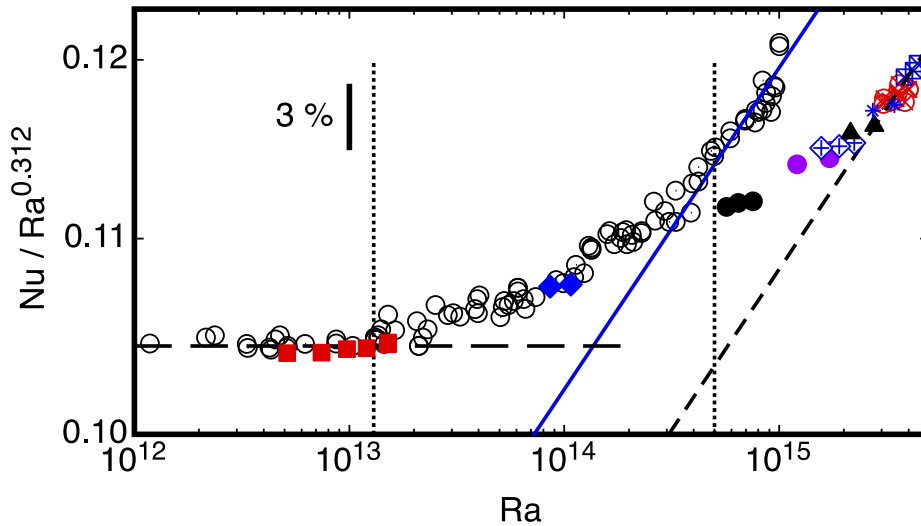


Figure 1: Reduced Nusselt number $Nu/Ra^{0.312}$ as a function of Ra measured in the sample with $\Gamma = 0.50$ (black open circles) and $\Gamma = 0.33$ (color symbols). Different symbols correspond to different pressure and thus to different Ra ranges. Solid squares (red): 2.0 bars; Solid diamonds (blue): 5.0 bars; Solid circles (black): 11 bars; Solid circles (purple): 14.0 bars; Diamond with cross (blue): 15.0 bars; Black triangles: 16 bars; Blue stars: 17 bars; Circles with crosses (red): 17.6 bars; Squares with crosses (blue): 18.6 bars; Black vertical dotted line: $Ra^*_{11} = 1.3 \times 10^{13}$ (left) and $Ra^*_{22} = 5.0 \times 10^{14}$ (right). Solid line (blue) represents $Nu = 0.01142 Ra^{0.38}$. Dashed line (black) is the power-law $Nu = 0.01035 Ra^{0.38}$.

Large Eddy Simulation of Transition of Free Convection Flow over an Inclined Heated Surface

M. C. Paul^a, A. S. Alzwayi^a and S. Navarro-Martinez^b

Research on the transition of thermal boundary layer flow over an inclined heated plate has received significant attention over the years due to its wide range of applications, which are closely linked to various engineering systems: such as transistors, mainframe computers, heat exchangers, solar energy collectors, and nuclear reactor cooling elements. Recently, Alzwayi and Paul¹ have numerically investigated the transition of thermal boundary layer in a vertical parallel plate channel with an effect of its width and temperature. In the context of a heated surface facing downward, Alzwayi and Paul² have also studied the transition of free convection flow inside an inclined parallel walled channel considering variations including inclination angle and width of the channel. However, very little is known about the transition of flow developing on a heated surface facing downward and how it is affected by its inclination angle.

The aim of this paper is therefore to carry out an in-depth investigation on the transition characteristics of free convection flow of air over an inclined heated surface by using a Large Eddy Simulation (LES) method. In particular, we focus on how the flow transition is affected by the inclination angle of the heated plate facing upward. Special attention is paid to the development of thermal boundary layer of flow and its process of transition from the laminar to turbulent stage. Results show that the transition occurs early when the plate is moved from its vertical position due to the rapid growth of both the velocity and thermal boundary layers. As a consequence, the critical Grashof number drops. Effects of the inclination of plate on the turbulent velocity fluctuations are also investigated, and the predicted results have very good agreement with various experimental data available in the literature.

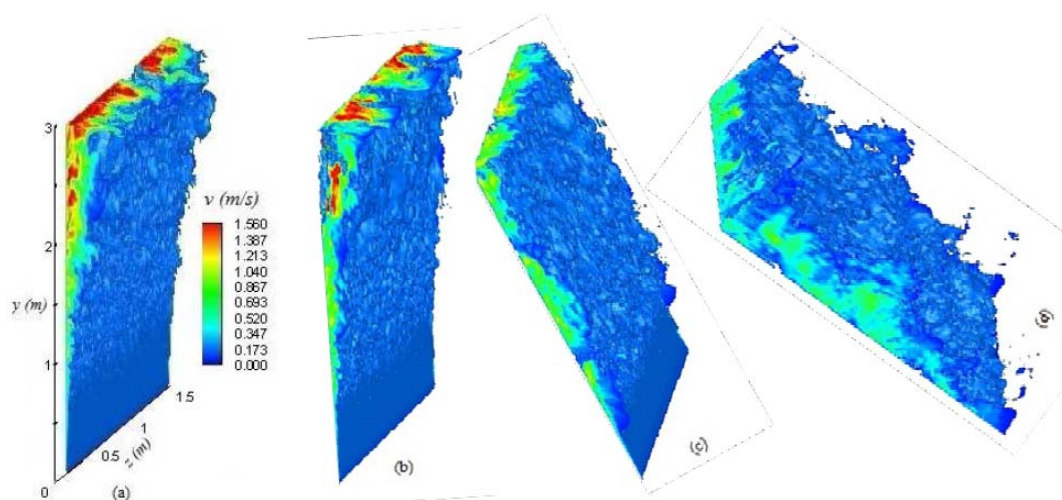


Figure 1: Velocity iso-surface contour plots showing the development of convection flow at various angular orientations of heated surface: (a) $\theta = 0^\circ$, (b) $\theta = 20^\circ$, (c) $\theta = 45^\circ$ and (d) $\theta = 70^\circ$.

^a Systems, Power & Energy Research Division, School of Engineering, University of Glasgow, Glasgow G12 8QQ, UK

^b Department of Mechanical Engineering, Imperial College London, London SW7 2AZ, UK

¹ Alzwayi and Paul, *Int. J. Heat and Mass Transf.* **63**, 20 (2013)

² Alzwayi and Paul, *Int. J. Heat and Mass Transf.* **68**, 194 (2014)

Magnetic field effects on three dimensional stability of natural convection flows in differentially heated cavities

D. Dimopoulos^a and N. Pelekasis^a

In the Helium Cooled Lithium Lead blanket concept¹ lead lithium is used for breeding tritium in separate rectangular boxes. Liquid metal is pumped through each one of these boxes at a very low speed and flow mainly takes place in the form of free convection as a result of the large neutronic heat load. In the present study, linear stability of a liquid metal layer of rectangular cross section is investigated² numerically, in the presence of a strong magnetic field that is aligned with the horizontal direction and a heat flux from the bottom wall. The critical Grashof was seen by asymptotic analysis to scale like Ha^2 thus signifying the balance between buoyancy and Lorentz forces, fig 1a. For well conducting side walls, the nature of the emerging flow pattern is determined by the combined conductivity of Hartmann walls and Hartmann layers, $c_H + Ha^{-1}$. When poor electrically conducting Hartmann walls are considered, $c_H \ll 1$, the critical eigensolution is characterized by well defined Hartmann and side layers, fig 1b. The side layers are characterized by fast fluid motion in the magnetic field direction as a result of the electromagnetic pumping in the vicinity of the Hartmann walls. Increasing the electrical conductivity of the Hartmann walls was seen to delay the onset of thermal convection, while retaining the above scaling at criticality. Furthermore, for both conducting and insulating Hartmann walls and the entire range of Ha numbers that was examined, there was no tendency for a well defined quasi two dimensional structure to develop. The role of the above flow pattern in the onset of secondary time dependent instabilities, also observed in experiments³, is pointed out. Furthermore, the importance of convective effects in the heat that is being transferred in the direction perpendicular to the side walls is stressed, as well as the significance that this bears on the design of HCLL blanket breeder units. Numerical analysis allowing for nonlinear mode interaction to take place in three dimensions is underway, in order to examine the possibility for quasi 2d structures to arise and to assess their importance in heat transfer and transition to turbulence.

^a Dep. Mechanical Engineering, UTH, Leoforos Athinon, Volos, GREECE

¹ Buhler and Mistrangelo, *IEEE Tran. Pl. Sci.* **38**, 254 (2010).

² Dimopoulos and Pelekasis, *accepted to Fluid Dyn. Res.*, (2014).

³ Burr and Muller, *J. Fluid Mech.* **453**, 345 (2002).

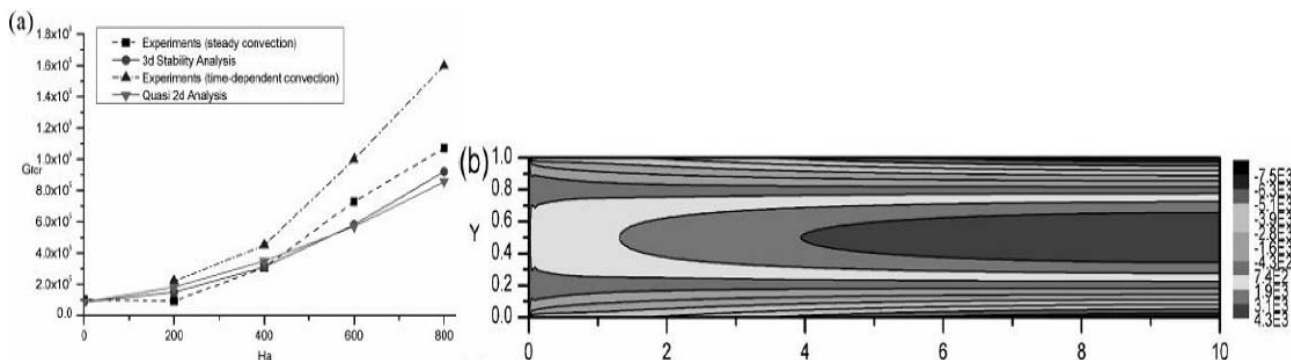


Figure 1: (a) Neutral stability diagram and (b) contour of x-component of vorticity by using the symmetry in the mid-plane of the duct cross-section at $x=10$ for $Ha=100$, in case of poor electrically conducting Hartmann walls ($c_H=4.15 \times 10^{-3}$).

Multiple convective flows in tilted parallelepiped cavities

D. Henry^a, J. F. Torres^{ab}, A. Komiya^c, and S. Maruyama^c

Hydrodynamic instability of natural convection in cavities subject to temperature gradients is an important problem in fluid mechanics, for both its industrial importance and scientific value. Some quite recent studies have conducted thorough three-dimensional instability studies inside a cubical cavity heated from below [1,2]. However, in real applications, it is common that the cavity is inclined at certain degrees and, even when the cavity is intended to be placed horizontally, small angles of inclination exist. Therefore, addressing the problem of natural convection inside a tilted cavity is of great importance. Some studies have focused on tilted cavities [3,4]. Nevertheless, unlike the three-dimensional calculations of Puigjaner *et al.* [1,2], these studies have been limited to a two-dimensional domain, ignoring the three-dimensional effects [3] or focusing on an infinite cavity [4]. In our study, three-dimensional numerical calculations are conducted to analyze in details the instability of the flow inside inclined cavities. We use a spectral element code with a continuation algorithm [5], which allows the precise calculation of bifurcation and stability diagrams.

Steady natural convection is studied first for a tilted truncated square duct with its length two times longer than the side of its square cross-section [5] and then for a tilted cubical cavity [6]. In both cases, precise bifurcation diagrams are first obtained for the horizontal case (Rayleigh-Bénard situation) featuring all the different branches. The calculations are then extended to the case where a tilt is imposed, and bifurcation diagrams as well as stability diagrams following the main bifurcation points as a function of the inclination angle are calculated. Beside the convective solution induced by the tilt, different other stable solutions are obtained for small tilt angles. The domains of existence of these stable solutions have been determined as a function of the Rayleigh number, Ra , and inclination angle, θ (see the diagrams in figures 1 and 2). Three different stable solutions are thus obtained in the square duct whereas numerous stable solutions are obtained in the cubical cavity, a configuration involving more symmetries. All these results are a motivation to conduct further experiments in this field.

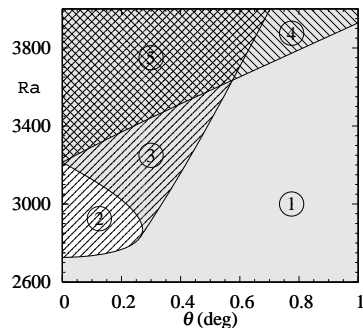


Figure 1: Bifurcation lines delimiting the domains of existence of the three different stable solutions for the tilted square duct.

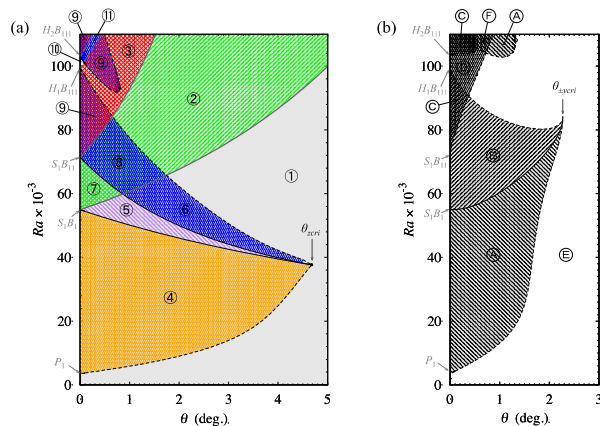


Figure 2: Bifurcation lines delimiting the domains of existence of the numerous different stable solutions for the tilted cubical cavity. (a) rolls favored by the tilt or opposite to the tilt; (b) rolls perpendicular to the tilt.

References:

- [1] D. Puigjaner *et al.*, *Phys. Fluids* **16**, 3639 (2004).
- [2] D. Puigjaner *et al.*, *J. Fluid Mech.* **598**, 393 (2008).
- [3] K.A. Cliffe *et al.*, *J. Comput. Phys.* **54**, 531 (1984).
- [4] T. Adachi, *Int. J. Heat Mass Transfer* **49**, 2372 (2006).
- [5] J. F. Torres *et al.*, *Phys. Rev. E* **88**, 043015 (2013).
- [6] J. F. Torres *et al.*, submitted to *J. Fluid Mech.* (2014).

^a Lab. Mécanique des Fluides et Acoustique, CNRS, Ecole Centrale de Lyon, 36 av. Guy de Collongue, 69134 Ecully Cedex, France

^b Dept of Mech. Syst. and Des., Grad. School of Eng., Tohoku University, Sendai 980-8579, Japan

^c Institute of Fluid Science, Tohoku University, Sendai 980-8577, Japan

Lagrangian Pair Dispersion and Transport in Near-Onset Thermal Convection

S. Schütz^{a,b}, E. Bodenschatz^b

The transport of heat and mass by convective fluid motion lies at the heart of many applications in science and engineering. Here, we present results for the transport of diffusive tracer particles in the laminar flow field of near-onset thermal Rayleigh-Bénard Convection¹, and a quantitative model that explains these numerical findings.

To investigate the transport and mixing properties of the convective flow field, we consider large aspect ratio systems ($\Gamma \sim 100$), where the lateral extent of the system is two orders of magnitude larger than the cell height. In this setting, pair dispersion² $R^2(t) = \langle (\delta r)^2 \rangle$ can be observed over a large range of time scales, on which different physical processes dominate. After an initial range of normal diffusion ($R^2 \sim t$), we observe a t^3 -scaling that persists up to a plateau in R^2 . For long times, dispersion is normal diffusive again.

To obtain the convective flow field in the large system, we have developed an efficient numerical scheme to find weak solutions of the Boussinesq equations. This pseudospectral scheme uses the parallel processing capabilities of GPUs to advance the nonstationary flow field in time, and to find the trajectories of more than 10^4 tracer particles at any time step, where the characteristic time scale of particle motion is much faster than the change of the flow field.

We compare our results to experimental findings³ and present an analytical model capable of explaining the behaviors that we observe. These behaviors differ vastly over different time scales, and depend mostly on the particle diffusivity and strength of thermal forcing. By a proper rescaling, we show that universal principles underly our observations.

^a Institute of Mechanical Engineering, École Polytechnique Fédérale de Lausanne (EPFL), Station 9, CH-1015 Lausanne, Switzerland

^b Max Planck Institute for Dynamics and Self-Organization (MPIDS), Am Faßberg 17, 37077 Göttingen, Germany

¹ Bodenschatz et al., *Annu. Rev. Fluid Mech.* **32**,709–778 (2000).

² Salazar and Collins, *Annu. Rev. Fluid Mech.* **41**,405–432 (2009).

³ Solomon and Gollub, *Phys. Fluids* **31**,1372 (1988).

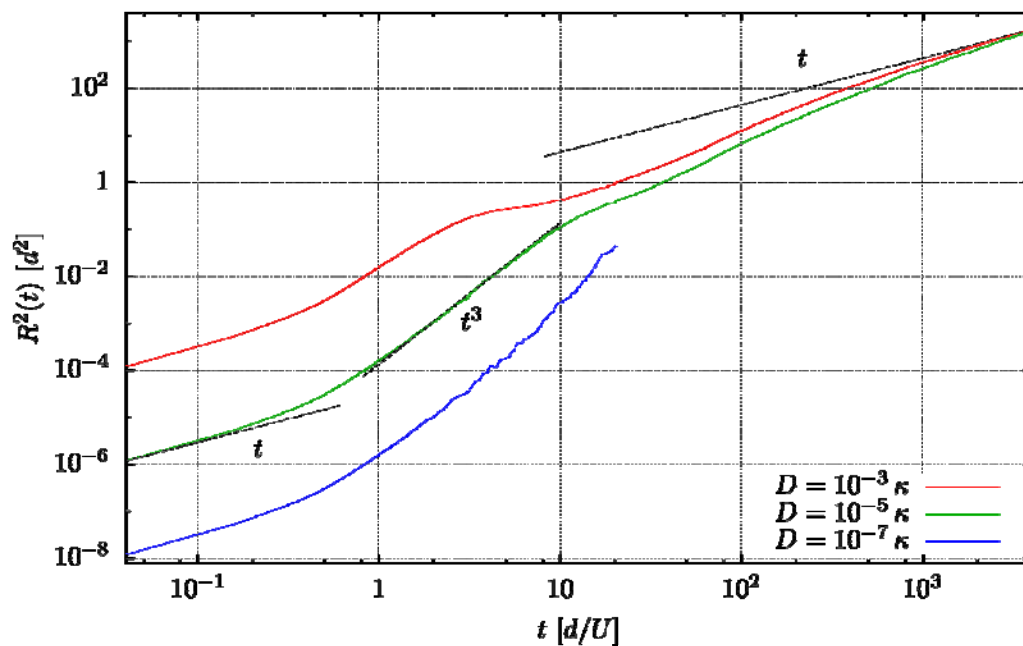


Figure 1: Lagrangian pair dispersion for diffusive tracer particles in convective flow, for different particle diffusivities D . d is the system height, U the characteristic fluid velocity. Particle diffusivity is given in units of thermal diffusivity κ .

Shape optimization of a cell to trigger natural convection

C. Hennekinne^a, M. P. Juniper^a

Transitions (e.g. the emergence of the Kármán vortex street for a flow behind a cylinder) play an important role in many hydrodynamic systems and the control of these transitions is the focus of many research projects. In most hydrodynamic applications, the transition from laminar to turbulent flow is not desired as it is often accompanied by an increase in the rate of dissipation of mechanical energy. In other applications such as mixing or heat convection, an unsteady flow is usually desired. Numerous active and passive control strategies have been considered to delay or trigger the transition from the initial steady solution but one of the simplest passive control strategies, boundary modification, has received less attention.

Shape optimization algorithms have flourished in recent years and are now well used within the fluid mechanics community. They made possible a systematic search for a locally optimal shape with respect to a given cost function. However, as it stands, the cost function cannot include information related to the stability of the flow. We present some advances to introduce this information for systems that are globally unstable.

In the case of modal stability, this first instability can be accurately predicted by performing a linear stability analysis. The growth rate of the leading mode provides then a scalar measure of the instability, a measure that can be included in an optimization routine. The shape gradient of the growth rate, required in a descent method based algorithm, can be computed using a double-decker extension of the traditional shape optimization algorithm. It consists of solving both the main steady equation, the stability eigenproblem and their adjoint counterparts before obtaining the desired shape gradient.

This routine was implemented using a low order finite element method and applied to the Rayleigh-Bénard instability in a rectangular convection cell. More precisely, we looked for triggering the transition from a steady stratified state to a steady rolling state at lower Rayleigh numbers, by changing the shape of the hot plate. To get both an interesting and well-posed problem, we only allow the hot plate to evolve toward the inside of the convection cell. We manage to decrease the critical Rayleigh number in both two and three-dimensional cells.

^a Engineering Department, Trumpington Street, CB2 1PZ Cambridge, UK

The onset of thermal instabilities in an evolving temperature gradient

Oliver S. Kerr^a and Zoë Gumm^a

When a large body of fluid is heated from below at a horizontal surface the heat diffuses into the fluid, giving rise to a gravitationally unstable layer adjacent to the boundary. However, this layer of heated fluid is initially stable, and only becomes unstable after a finite time. This transition from an initially stable regime to an unstable regime can be observed in other geometries, such as heating a large body of fluid from the side, where an upward flow develops near the boundary which subsequently becomes unstable.

When the evolving thermal boundary layer first becomes unstable the growth rate of the instabilities may be comparable to the time-scale of the evolution of the background temperature profile, and so analytical approximations such as the quasi-static approximation (assuming the time-evolution of the background state can be ignored) are not strictly appropriate. Looking at the evolution of instabilities by adding noise to the background state and looking for when instabilities appear can lead to significant scatter in the apparent time for the onset of instability.

Perturbations to the flow that are tracked from the time of the start of the heating of the boundary can show an initial decay, which may be significant depending on the exact problem under consideration. We will look at the growing phase of the instabilities as an initial value problem where the initial time for the instabilities is a parameter to be determined. Following Foster¹, who looked at the heating from below of a semi-infinite fluid, we will consider the flow to have become unstable when the disturbances have grown by a predetermined amount. Along with the time for the start of the growth of the instabilities we will determine numerically the optimal initial conditions to ensure the growth occurs at the earliest time.

We will focus on heating from horizontal and vertical boundaries, and compare and contrast the results obtained with those obtained by other methods.

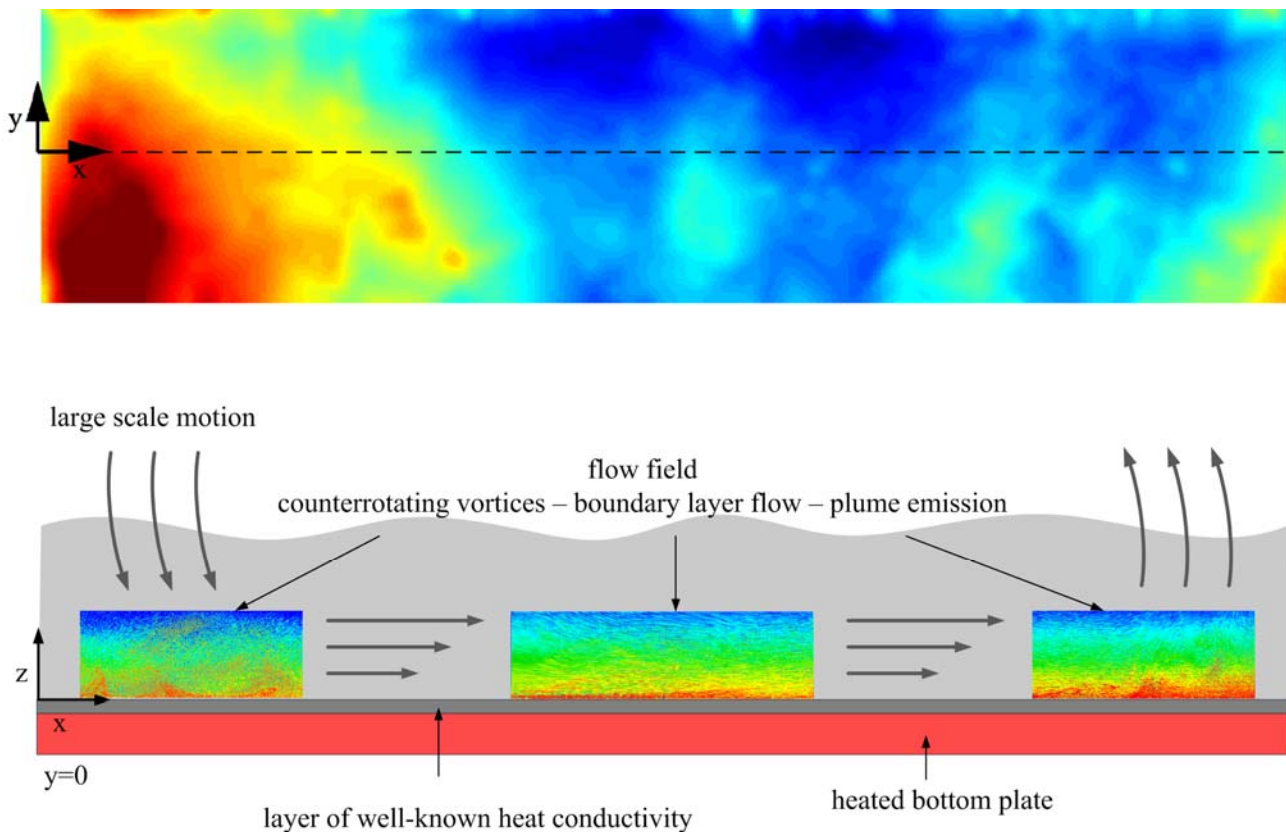
¹ Foster, *Phys. Fluids* **11**, 1257 (1968).

^a Department of Mathematics, City University London, Northampton Square, London EC1V 0HB, UK.

High resolved heat flux map in turbulent Rayleigh-Bénard convection

Robert Kaiser¹ and Ronald du Puits^a

Thermal convection is an omnipresent mechanism in nature and technique. One of the simplest model is the Rayleigh-Bénard set-up to study thermally driven flow phenomena. In this set-up, a fluid layer is heated from below and cooled from above which generates a temperature drop ΔT against the gravitation. This system is fully described by three dimensionless parameter: the Rayleigh number $Ra = g\beta\Delta TH^3/(\nu\alpha)$, the Prandtl number $Pr = \nu/\alpha$ and the aspect ratio $\Gamma = D/H$, whereas the g is the gravitation acceleration, β the thermal expansion coefficient, H the height of the fluid layer, ν the kinematic viscosity, α the thermal diffusivity and D the lateral extension of the fluid layer. The main objective is the convective heat flux compared the case of pure heat conduction which is expressed as the Nusselt number. In the past, a lot of efforts have been taken to investigate the global heat flux. But it is still unclear how the local wall heat flux varies across the horizontal plates. Therefore, we have assembled a thin layer of well-known heat conductivity on the bottom plate. While the temperature of the bottom plate is kept constant, the free surface of the layer is observed with an infrared camera. Based on Fourier's law of heat conduction, a map of the local wall heat flux is computed¹. Inside our large convection facility, called the Barrel of Ilmenau, we measured the map of the local wall heat flux for different aspect ratios at a fixed Rayleigh number. The measurements reveal a strong variation of the local heat flux up to 100% which can be linked to different local flow phenomena, like the emission of plumes or the impact of the large scale flow on the heating plate.



¹ Dep. Mechanical Engineering, Technische Universität Ilmenau, Thuringia, Germany

^a Kaiser, du Puits. *IJHMT*. Under revision.

Turbulent thermal convection: velocity inside the boundary layer near roughnesses

O. Liot^a, J. Salort^a, R. Kaiser^b, R. du Puits^b, B. Castaing^a and F. Chillà^a

Turbulent thermal convection is a very efficient thermal transfer process. Temperature gradients are confined into thermal boundary layer near top and bottom plates. Thermal transfer efficiency is directly linked to boundary layers size and structure, which are quite well documented for the classical Rayleigh-Bénard case¹.

We study turbulent thermal convection in the particular case of controlled roughness on the bottom plate. In a parallelepipedic cell (length: 40cm, height: 40cm, width: 10cm) filled with water with parallelepipedic roughnesses (length: 5mm, width: 5mm, height: 2mm), we observed enhancement of the global thermal transfer beyond a transitional Rayleigh number (determined by the condition $Nu=H/2h_0$ where h_0 is the roughness height, Nu the Nusselt number and H the cell height) and local changes of the thermal boundary layer structure near roughnesses².

To go beyond, we performed velocity measurements inside the Barrel of Ilmenau (with the support of EuHIT). A cell 6 times larger, with similar proportional roughnesses was built. We used air as the working fluid. In this configuration, the range in Nusselt number is similar to our water experiment. The boundary layer thickness is therefore 6 times larger at the transition, giving very good conditions for flow visualisations.

We used PIV technique to measure the velocity field just close to roughnesses, at different positions defined both by the roughnesses shape and the direction of the wind (see figure 1). We worked at different Rayleigh numbers between 4.10^9 and 5.10^{10} . We computed velocity profiles to determine the structure and the size of the viscous boundary layer. We brought out very different flow structures: into the notch, a recirculation has been observed. Furthermore, the boundary layer structure is quite different in the groove compared to the situation above the obstacle. This recirculation has a different shape depending on the Rayleigh number (see figure 2). For the lowest Rayleigh number, the bulk does not get into the notch which remains very quiet. On the contrary, for a higher one, we can observe that flow goes inside the notch.

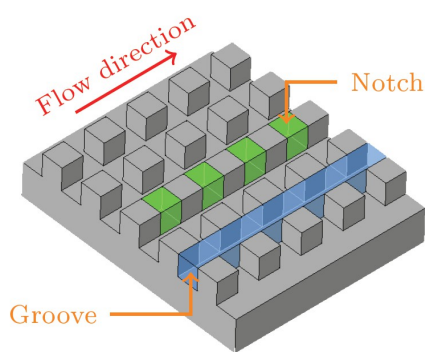


Figure 1: Bottom plate roughnesses

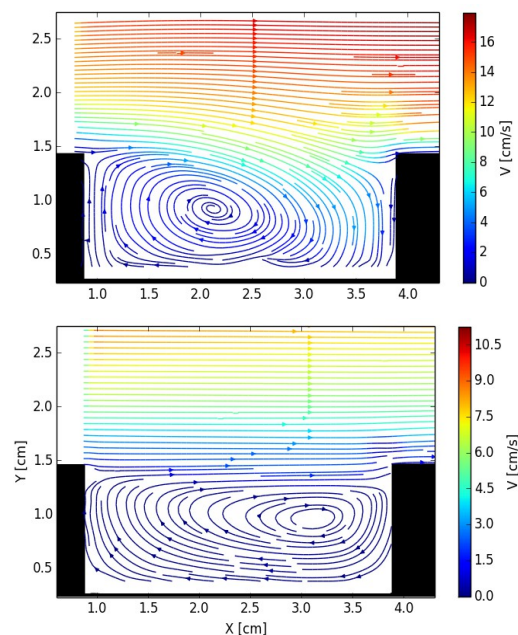


Figure 2: Recirculation into the notch at $Ra=4 \cdot 10^9$ (down) and $Ra=2.8 \cdot 10^{10}$ (up)

^a Physics Laboratory, ENS de Lyon, 46, allée d'Italie, 69007 Lyon, France

^b Technische Universität Ilmenau, Postfach 100 565, 98684 Ilmenau, Germany

¹ Chillà and Schumacher., *Eur. Phys. J. E* **35**, 58 (2012)

² Salort et al., *Phys. Fluids* **26**, 015112 (2014)

Lagrangian chaos in confined two-dimensional oscillatory convection

L. Oteski¹, Y. Duguet^a, L. Pastur^a and P. Le Quéré²

The chaotic advection of passive tracers in a two-dimensional confined convection flow is addressed numerically near the onset of the oscillatory regime. We investigate here a differentially heated cavity flow with aspect ratio two and Prandtl number 0.71 for Rayleigh numbers around the first Hopf bifurcation.

A scattering approach¹ reveals different zones (see figure 1) depending on whether the statistics of the return times exhibit exponential or algebraic decay. Melnikov functions are computed and predict the appearance of the main mixing regions via the break-up of the homoclinic and heteroclinic orbits². The non-hyperbolic regions are structured around Kolmogorov-Arnold-Moser tori³.

Based on the numerical extraction of many unstable periodic orbits and their stable/unstable manifolds, we suggest a coarse-graining procedure to estimate numerically the spatial fraction of chaos inside the cavity as a function of the Rayleigh number.

We show that mixing is almost complete before the first transition to quasi-periodicity takes place. The algebraic mixing rate is estimated for tracers released from a localised source near the hot wall.

This work is funded by the EADS foundation.

¹ LIMSI-CNRS, Université Paris Sud, UPR 3251, 91403 Orsay Cedex, France

² Ecole Polytechnique, 91128 Palaiseau Cedex, France

¹ Ott and Tél, *Chaos* **3**, 417 (1990)

² Rom-Kedar et al., *J. Fluid Mech.* **24**, 347 (1990)

³ Ottino, *Cambridge University Press* (1990)

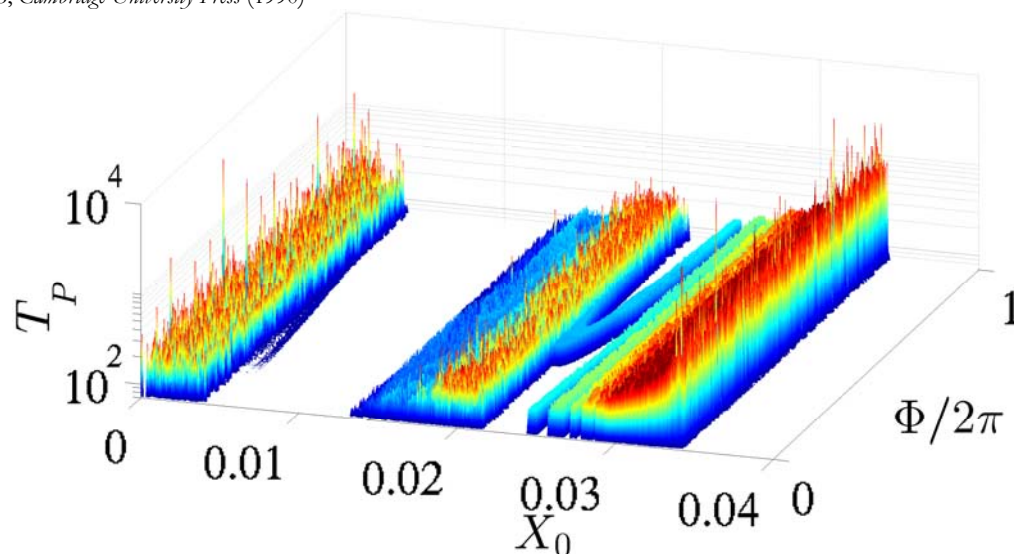


Figure 1: Release of $O(10^5)$ tracers initially distributed on a segment near the hot boundary layer of the cavity. Return times T_P are measured as a function of the initial condition X_0 and the phase of the velocity field Φ .

Turbulent Natural Convection Boundary Layer along a Heated Vertical Cylinder

A. Shiri^a and W. K. George^b

The symmetrical natural convection boundary layer flow over a vertical heated cylinder was experimentally investigated. Instantaneous velocity and temperature were measured at heights of 1.5m, 3m and 4m, which corresponds to the Rayleigh number $Ra = g\beta\Delta T L^4/\alpha\nu \approx 1.7 \times 10^{11}$ at the highest measuring point with a fully developed turbulent natural convection boundary layer flow. The turbulence quantities and average values of velocity and temperature are presented and the conservation of momentum and energy balance are investigated to properly determine the true behaviour of the naturally created flow in the experimental facility.

The boundary layer equations in cylindrical coordinate also have been revisited to establish the scaling laws for inner and outer parts of the boundary layer. It appears that the outer confinement of the rig had some effect on the changing the boundary condition into the thermally driven flow between two differentially heated walls. The temperature measurement also revealed the difficulties in placing the probe in a boundary layer with a high temperature gradient. It was possible to correct the data for the conduction along the prongs of the thermocouple and the cold-wire probes. Unsteady temperature measurements, however, had to be abandoned; but temperature-velocity moments could be evaluated from the energy balance equations.

The proper form of the thermal energy equation for incompressible numerical simulations is also discussed. In particular, while C_p is appropriate for describing experiments in gases, C_v should be used for simulations. The difference explains historical difficulties in handling thermally varying flows numerically.

^a SSPA Sweden AB, Chalmers Tvärgata 10, Gothenburg, Sweden

^b Department of Mechanical and Aerospace Engineering, Princeton University, NJ 08544

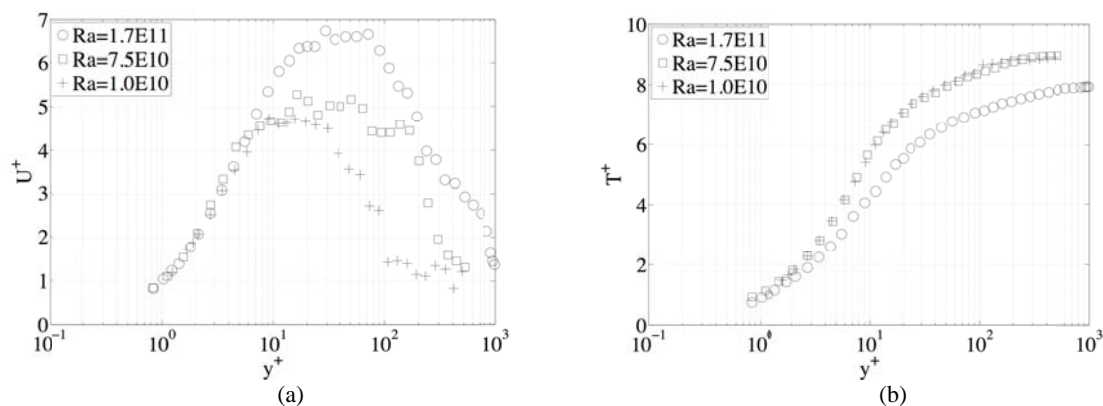


Figure 1: (a) Velocity and (b) Temperature profiles in different Rayleigh numbers.

Fluid Structure Interaction

Simulation of Fluid-Structure Interaction in Automotive Filtration Applications

A. Traut^a, M. J. Lehmann^b and M. Piesche^c

Filtration systems in automotive applications protect the engine from abrasion and damage caused by dirt particles under miscellaneous operating conditions. Meeting the increasing requirements for filtration tasks today's filter element performance is continuously enhanced, e.g. by deploying new filter materials. However, a highly efficient filter media and good mechanical load capacity of the material are not necessarily associated with each other. In case of lower mechanical stability, fluid forces may lead to deformations of the filter structure which affect the flow field, e.g. increasing the system's pressure drop. This coupling mechanism is generally known as Fluid-Structure Interaction (FSI). Therefore, new optimization measures regarding the flow and structural behavior are required. Hereby, today's computational capabilities enable to address this task by numerical simulation; furthermore they deliver insight into problems which could not be easily investigated by experiments to date.

Flow simulations of pleated filter elements have been presented in literature in different ways. A common approach¹ is to assume the porous pleat structure as a rigid body that does not interact with the fluid phase. Beyond this, a mathematical model² for filter element simulation was developed, taking the medium compression into account. In case of FSI with porous flat filter media, fundamental work³ was recently presented.

Facing the complex FSI problem for pleated filter media, we are focusing on a partitioned approach with non-matching grid interfaces using the commercial software ANSYS Workbench. Thereby, the fluid system is solved by a Finite-Volume-Method, the structural system by a Finite-Element Method. By connecting the two physical systems it is important to determine if the coupling in between the systems is loose or strong and it is necessary to decide if the solution is time-dependent relating to the problem. In this context, we present the current progress of our research work on FSI with pleated filter media, contributing to the knowledge based development for automotive filter elements.

^a Graduate School of Excellence advanced Manufacturing Engineering, Univ. of Stuttgart, Nobelstr. 12, 70569 Stuttgart, Germany

^b MANN+HUMMEL GMBH, Hindenburgstr. 45, 71638 Ludwigsburg, Germany

^c Institute for Mechanical Process Engineering, University of Stuttgart, Boeblingen Str. 72, 70199 Stuttgart, Germany

¹ Wiegmann et al., *Filtech Conf. Proc.* **1**, 79 (2007)

² Wakeman et al., *Chem. Eng. Res. Des.* **83**, 1246 (2005)

³ Dederling et al., *Filtech Conf. Proc.* G16-03-138 (2013)

Wrinkly fingers – fluid-structure interaction in elastic-walled Hele-Shaw cells

Matthias Heil^a, Draga Pihler-Puzović^a, and Anne Juel^a

Viscous fingering in Hele-Shaw cells is a classical and widely studied fluid-mechanical instability: When air is injected into the narrow, liquid-filled gap between parallel rigid plates, the axisymmetrically expanding air-liquid interface tends to be unstable to non-axisymmetric perturbations when the capillary number - the ratio of (destabilising) viscous to (stabilising) capillary forces acting at the air-liquid interface - becomes sufficiently large. The introduction of wall elasticity (via the replacement of one of the bounding plates by an elastic membrane) can weaken or even suppress the fingering instability^{1,2}, but it also makes the system susceptible to additional solid-mechanical instabilities. We show that in elastic-walled Hele-Shaw cells that are bounded by sufficiently thin elastic sheets, the (fluid-based) viscous fingering instability can arise concurrently with a (solid-based) wrinkling instability. We study the interaction between these distinct instabilities, using a theoretical model that couples the depth-averaged lubrication equations for the fluid flow to the Föppl-von Kármán equations, which describe the deformation of the thin elastic sheet. We employ a linear stability analysis to determine the growth rate of non-axisymmetric perturbations to the axisymmetrically expanding bubble, and perform direct numerical simulations to study the nonlinear interactions between the instabilities. We show that the system's behaviour may be characterised by a non-dimensional parameter that indicates the strength of the fluid-structure interaction. For small [large] values of this parameter the system's behaviour is dominated by viscous fingering [wrinkling], with strong interactions between the two instabilities arising in an intermediate regime.

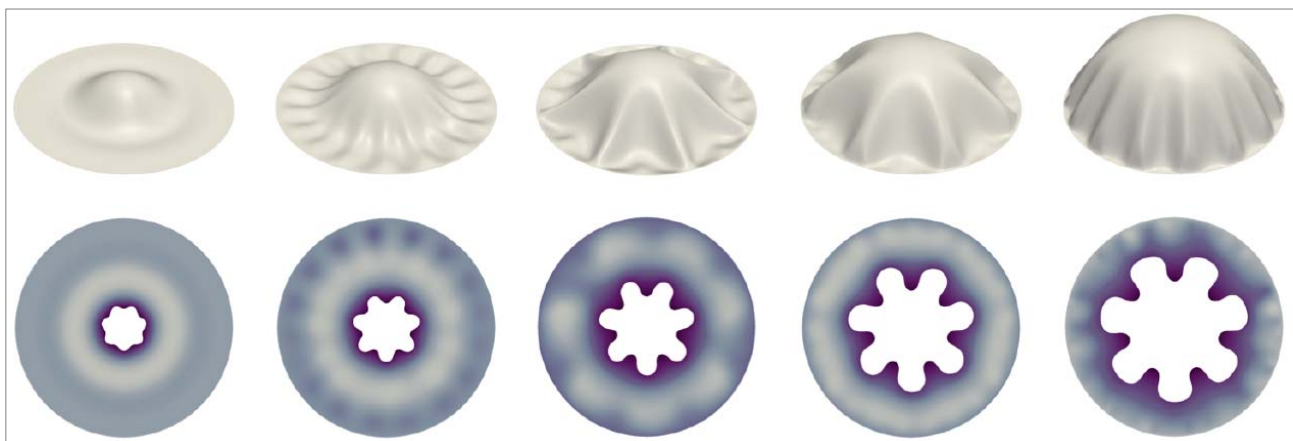


Figure 1: Simultaneous viscous fingering and wrinkling in an elastic-walled Hele-Shaw cell. The bottom row shows the evolution of fluid domain (with colour contours representing the fluid pressure); the top row shows the corresponding evolution of the elastic membrane that bounds the Hele-Shaw cell (transverse deflection increased ten-fold).

^a School of Mathematics and Manchester Centre for Nonlinear Dynamics, University of Manchester, Manchester M13 9PL, UK.

¹ Puzović et al., *Phys. Rev. Lett.* **108**, 074502 (2012)

² Puzović et al., *J. Fluid Mech.* **731**, 162 (2013)

Model order reduction of fluid-structure interaction in high pressure centrifugal compressors

Jithin Jith^a and Sunetra Sarkar^b

Centrifugal compressors used for enhanced oil recovery through gas injection or for CO₂ sequestration deal with very high pressures going up to 20 MPa. Non-ideal behaviour of gases, especially CO₂, at such high pressures coupled with the visco-thermal effects in the side cavities of the centrifugal impeller demand a detailed study of the fluid-structure interactions in order to determine the coupled natural frequencies of the system.

Thermodynamics of CO₂ at very high pressures is modelled using Span-Wagner¹ equation of state and later approximated with a modified ideal gas equation of state. Linearised compressible Navier-Stokes equations are invoked to model the behaviour of the gas in the side cavities of the impeller. The linearised Navier-Stokes equations are symmetrised using an energy inner product² and solved using the finite element method. Dynamics of the impeller, represented by an equivalent circular disc, are coupled with the Linearised Navier-Stokes equations to obtain a monolithic frequency-domain fluid-structure interaction solver. Frequency response of this system to periodic excitations of the impeller are studied and compared against acousto-elastic frequency response.

Model order reduction(MOR) is performed on the fully coupled system using Proper Orthogonal Decomposition(POD)³ in the frequency domain as well as Arnoldi iteration in the Krylov subspace⁴. The eigenspectrums and frequency responses of the reduced systems are compared with the full system at a range of temperature and pressure inside the side cavities to ascertain their validity and accuracy.

^a Dep. Applied Mechanics, Indian Institute of Technology Madras, Chennai 36, India

^b Dep. Aerospace Engineering, Indian Institute of Technology Madras, Chennai 36, India

¹ Span and Wagner, *J. Phys. Chem.* **25**, 6 (1996).

² Gustafsson and Sunstrom, *SIAM J. Appl. Math.* **35**, 2 (1978).

³ Kalashnikova et al., *Int. J. Numer. Meth. Engng.* **95**, 121-144 (2013)

⁴Puri and Morrey, *Struct. Multidisc. Optim.* **43**, 495-517 (2011)

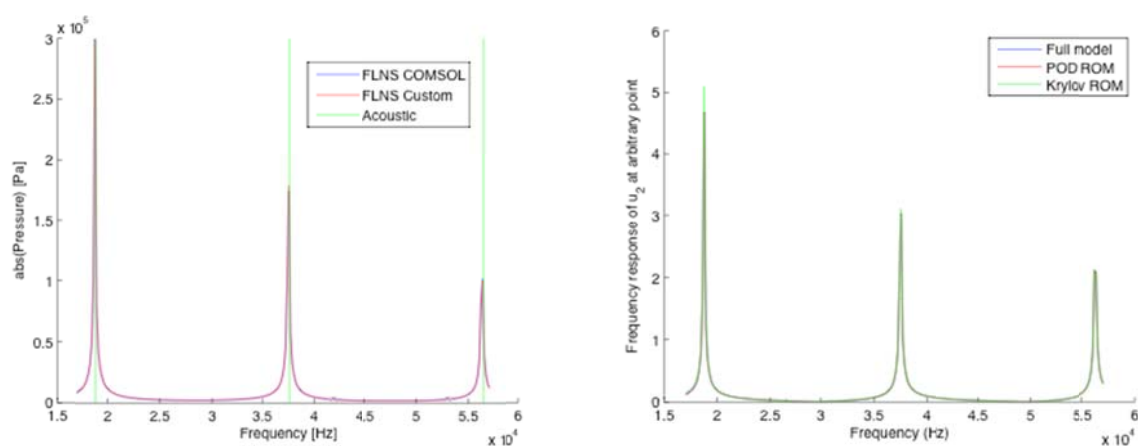


Figure 1: (a) Frequency response of pressure, obtained from Linearised Compressible Navier-Stokes equations, at an arbitrary point in a square cavity. Comparison between Linearised Navier-Stokes (FLNS) and acoustic resonant frequencies (green lines). (b) Frequency response of velocity for the same case. Comparison between full model (~ 29000 dofs), POD MOR (20 dofs) and Krylov subspace MOR (300 dofs).

Fluid-solid-electric lock-in of energy-harvesting piezoelectric flags

Y. Xia^a, S. Michelin^a and O. Doaré^b

Placed in a fluid flow, a flexible plate flaps spontaneously above a critical flow velocity. The resulting self-sustained vibrations of such a flag may be used to produce electrical energy and power an output circuit using piezoelectric patches covering the flag that are deformed by its flapping motion (Fig. 1a). Previous work^{1,2} showed only moderate harvesting efficiency with a resistive output circuit, but proposed numerous directions for improvement.

In this work, we propose a numerical investigation of the coupled dynamics of such a fluid-solid-electric system, and analyze the influence of the output circuit on the dynamics and harvesting efficiency. In particular, inductive-resistive circuits are considered (Fig. 1b). We show that such resonant circuits lead to a destabilization of the system and a spontaneous flapping at lower fluid velocities. Also they significantly enhance the energy harvesting efficiency of the piezoelectric flag as a result of a frequency lock-in between the flag and the electrical circuit. These results suggest promising efficiency enhancements of such flow energy harvesters through the optimization of the output circuit.

^a LadHyX – Département de Mécanique, Ecole Polytechnique, Route de Saclay, 91128 Palaiseau, France

^b ENSTA Paristech, Unité de Mécanique (UME), Chemin de la Hunière, 91761 Palaiseau, France

¹ Doaré and Michelin, *J. Fluids. Struct.* **27**, 1357 (2011).

² Michelin and Doaré, *J. Fluid. Mech.* **714**, 489 (2013)

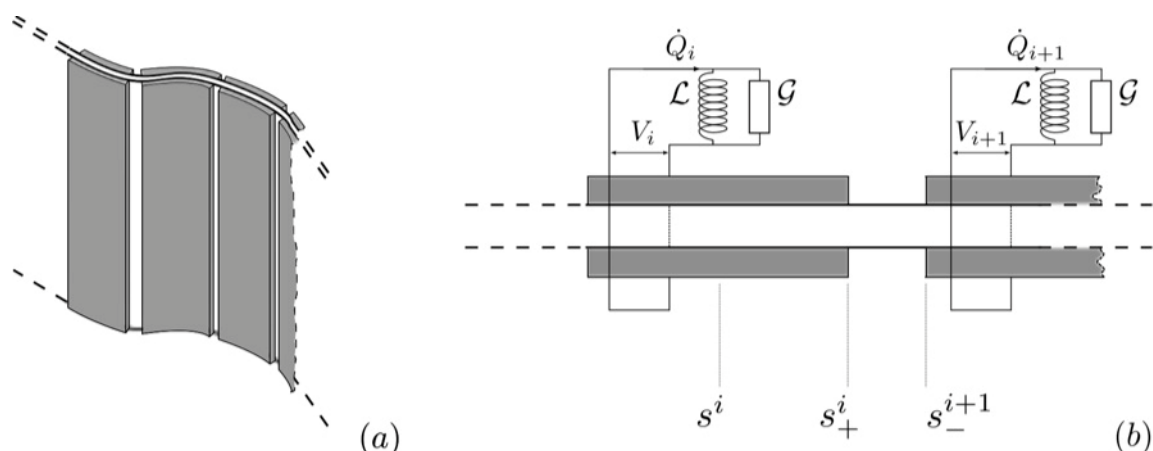


Figure 1: (a) 3-dimensional view of a piezoelectric flag. (b) Inductive-resistive circuit connected to piezoelectric patches.

Stability of a stratified fluid over a periodically oscillating flat surface

K. Isakova¹, J. O. Pralits¹, and R. Repetto¹

Retinal detachment (RD) in the eye occurs when the sensory layer of the retina detaches from the retinal pigment epithelium. This is a serious condition, which might occur due to aging, by trauma, diabetes or eye diseases, and might lead to permanent loss of sight and needs immediate treatment. A commonly adopted surgical technique to treat RD is vitrectomy: the vitreous humor is removed from the eye and replaced by a so-called tamponade fluid, typically silicone oil. The role of the tamponade fluid, which is immiscible with water, is to push back the retina in contact with the pigment epithelium. Due to its hydrophobic properties a thin layer of aqueous humour usually separates the tamponade fluid from the vitreous chamber wall. It is known that silicone oils cannot be left in the vitreous chamber for too long since emulsion of oil droplets in the aqueous humour is often formed. The mechanisms leading to emulsion are still unclear. Many authors, however, believe that generation of emulsion might be caused due to the shear stress at the oil-aqueous interface^{2,3}. From a fluid mechanics point of view it is well known that the wall-shear stress changes dramatically when the flow transitions from laminar to turbulent flow. However, no clear indications are given in the literature regarding the flow characteristics within the vitreous in the presence of silicone oils and possible relations to the formation of emulsion.

In order to, first of all, understand the threshold values regarding the flow characteristics we investigate the stability of the interface between the layer of aqueous and the silicone oil. The mathematical model represents an idealised situation given by two superposed fluids over an oscillating flat surface in a semi-infinite domain, we thus neglect the wall curvature (see figure 1a). The lower fluid represents the thin layer (d^*) of aqueous humour and the upper fluid represents the silicone oil. The stability characteristics are investigated numerically assuming wave-like solutions using both a quasi-steady approach (for cases in which the perturbation time scale is much smaller than that of the basic flow) and a more general Floquet analysis. The governing parameters are the Reynolds number (Re), viscosity ratio (m), surface tension (S), oscillation frequency (ω), and the streamwise wavenumber (α). The results from the quasi-steady approach show that for values of the parameters that are suitable for the real eye movements the interface can be unstable, see figure 1b). The short waves are stabilized when surface tension is increased, while lowering the viscosity brings the system towards instability. We conclude that shear-instability of the oil-aqueous interface might be a mechanism leading to emulsification with a high probability especially if the presence of surfactants has lowered the surface tension between two fluids.

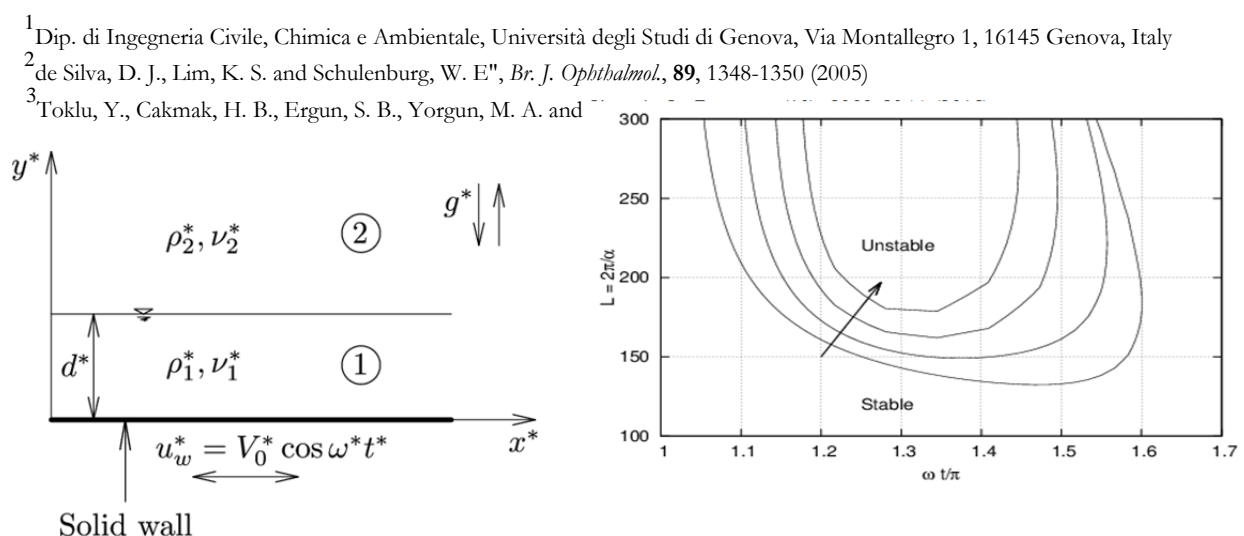


Figure 1: (left) sketch of the problem, (right) neutral curves as a function of the wave length (L), time ($\omega t/\pi$) and viscosity ratio (m); the arrow indicates increasing value of m .

Influence of the air-layer flow on drag reduction by superhydrophobic surfaces

A. Busse^a, G. McHale^b, M.I. Newton^c and N.D. Sandham^d

Superhydrophobic surfaces are hydrophobic surfaces which are structured on micro- or nanoscales. When they are submerged in water, pockets of air or an air layer can be trapped on these surfaces. Due to a lower shear stress at a water-air interface compared to a water-solid interface superhydrophobic surfaces can be applied for hydrodynamic drag reduction. In the laminar regime analytic solutions can be found for flow past superhydrophobic surfaces if the considered geometry is sufficiently simple. We present analytic results for the change of drag, the apparent slip length and the optimum gas layer thickness for an idealised superhydrophobic surface, consisting of a gas layer of constant thickness retained on a wall. The general case of two immiscible fluids is considered, where the trapped fluid, called gas, has a lower viscosity, μ_{gas} , than the liquid which flows past the surface, giving rise to a viscosity contrast, $c_\mu = \mu_{\text{liquid}} / \mu_{\text{gas}}$, between the two fluids. Thus the results are also applicable in the context of oleophobic and omniphobic surfaces.

In the Couette flow case the drag is always reduced provided that the viscosity contrast is high enough. In the case of pressure-driven pipe and channel flows, the gas layer causes blockage and thus an optimum gas layer thickness can be found. The assumptions made for the flow in the gas layer have a strong influence on the change in drag and the apparent slip length. The standard assumptions made in previous studies are constant shear rate¹ in the gas layer (in the case of Couette flow) or equal streamwise pressure gradient in the liquid and the gas layer² (in the case of pressure-driven flows). However, these standard assumptions are not valid if we consider that the gas on a superhydrophobic surface is trapped. In this case, a zero mass flow rate should be assumed for the flow in the gas layer since otherwise the gas layer would be depleted³. We show that a minimum viscosity contrast of $c_\mu = 4$ needs to be exceeded to achieve drag reduction if a zero mass flow rate is assumed for the flow in the gas layer. Under standard assumptions the minimum viscosity contrast is $c_\mu = 1$. The predicted values for the drag reduction and apparent slip length are lower under the zero mass flow rate assumption (see figure 1). Hence, traditional formulae from lubrication theory overestimate the potential drag-reduction for superhydrophobic surfaces, but significant drag reduction is nonetheless possible.

^a School of Engineering, University of Glasgow, Glasgow G12 8QQ, United Kingdom

^b Faculty of Engineering & Environment, Northumbria University, Newcastle upon Tyne NE1 8ST, United Kingdom

^c School of Science and Technology, Nottingham Trent University, Nottingham NG11 8NS, United Kingdom

^d Faculty of Engineering and the Environment, University of Southampton, Southampton SO17 1BJ, United Kingdom

¹ Vinogradova, *Intl J. Miner. Process.* **56**, 31-60 (1999)

² Joseph et al., *Annu. Rev. Fluid Mech.* **29**, 65-90 (1997)

³ Busse et al., *J. Fluid Mech.* **727**, 488 (2013).

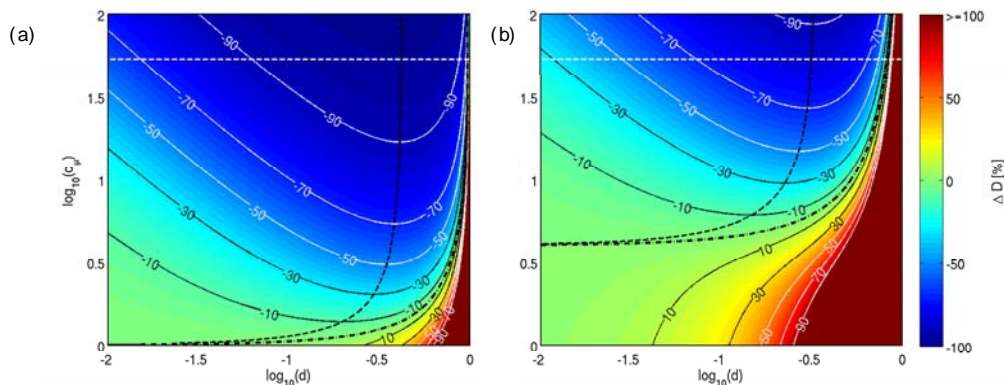


Figure 1: Change in drag in pressure driven channel flow as a function of relative gas layer thickness and viscosity contrast. (a) Standard assumption. (b) Zero mass flow rate assumption. The black dashed line shows the optimum gas layer thickness.

A generalized slip boundary condition for fluid flows

J. J. Thalakkottor^a, K. Mohseni^{a,b}

The no-slip boundary condition has been contested for several decades. Although it has been successful in reproducing most continuum and macroscopic results, the condition breaks down in situations such as contact line motion, corner flow and in many micro- and/or nano-scale applications. Recently, Thalakkottor and Mohseni had extended the Maxwell slip model to encapsulate unsteady flows¹. It was shown that slip velocity at the wall depends on the gradient of shear rate in addition to shear rate. Using the concept of Maxwell's theory for slip in a single phase flow, a modified slip model is established for two phase and corner flows that demonstrates the dependence of slip velocity on the velocity gradient tensor at the wall. Slip velocity tangential to the wall is given as,

$$U_s = \frac{(2-\sigma_d)}{\sigma_d} \hat{i}_{\parallel} \cdot [\lambda_j \nabla_j U_i^f]$$

The model shows that in addition to shear strain rate, slip velocity is also dependent on the linear strain rate and vorticity of the fluid flow. In the case of a single phase, fully developed, steady, incompressible flow the model reduces back to the Navier/Maxwell's expression. In the vicinity of the triple contact point the magnitude of linear strain rate is of the same order as that of vorticity and shear strain rate, hence it cannot be neglected. Non-Newtonian behaviour of the fluid near the triple contact point is observed as viscosity varies from the bulk value in the vicinity of the triple contact point. We also aim to develop a universal condition to calculate slip length for contact line motion and corner flows.

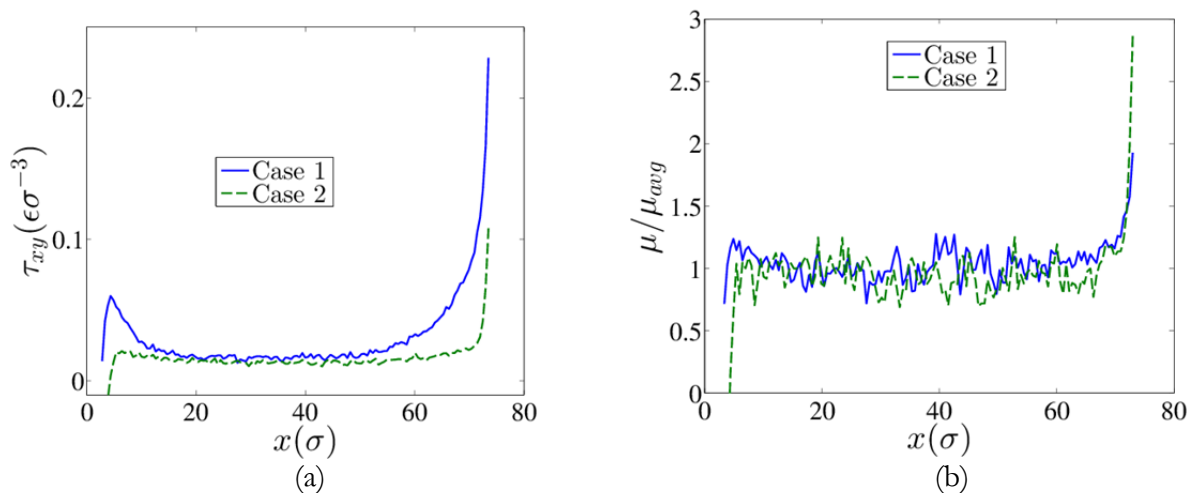


Figure 1: Behaviour of, (a) shear stress and (b) viscosity, along the wall for different cases of wall-fluid properties are studied. From Case 1 to Case 2 there is an increase in the degree of slip at the wall. In Fig. (a) sharp increase in shear stress is seen at the trailing edge of the droplet in comparison to the leading edge. In Fig. (b), similarly the viscosity increases sharply at the trailing edge.

^a Dep. of Mechanical and Aerospace Engineering, University of Florida, Gainesville, FL, USA

^b Dep. of Electrical and Computer Science Engineering, University of Florida, Gainesville, FL, USA

¹ Thalakkottor and Mohseni, *Phys. Rev. E*, **87**,033018 (2013)

Momentum and mass transport over a superhydrophobic bubble mattress

P. A. Tsai ^a, A. S. Haase ^a, E. Karatay ^a, and R. G.H. Lammertink ^a

We investigate the influence of interface geometry on momentum and mass transport on a partially slippery bubble mattress. The bubble mattress, forming a superhydrophobic substrate, consists of an array of alternating slippery (shear-free) gas bubbles and (no-slip) solids walls. We consider pressure-driven laminar flow over the bubble mattress, with a solute being supplied from the gas bubbles. The results show that solute transport can be enhanced significantly due to effective slippage, compared to a fully saturated no-slip wall. The enhancement depends on the interface geometry of the bubble mattress, i.e. on the bubble size, protrusion angle, and surface porosity. In addition, we demonstrate that the mass transfer enhancement disappears below a critical bubble size. The effective slip vanishes for very small bubbles, whereby interfacial transport becomes diffusion dominated. For large bubbles, solute transport near the interface is greatly enhanced by convection.

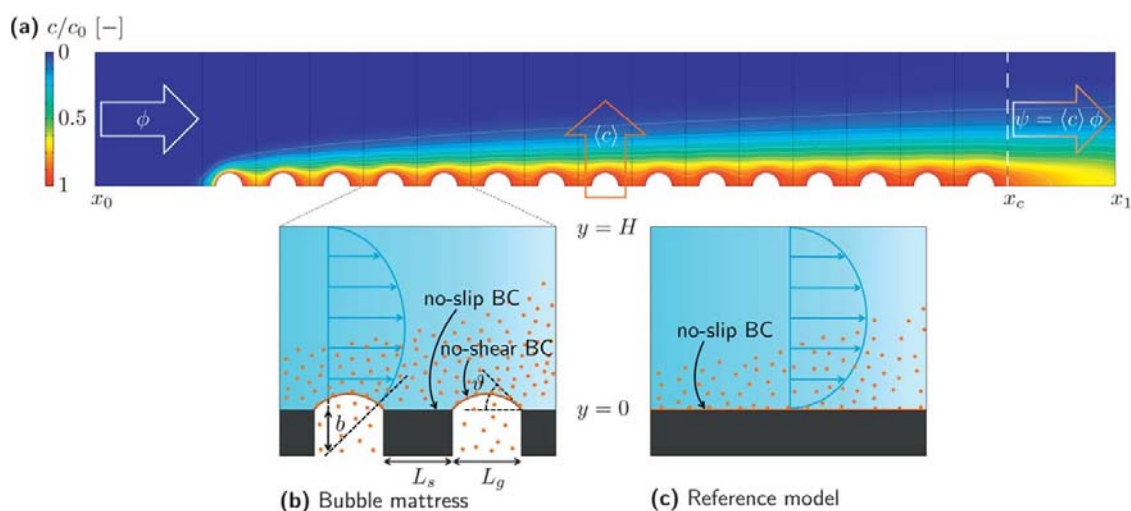


Figure 1 (a) Concentration of solute over a bubble mattress, while the solute being supplied from the gas bubbles; (b) Schematic of the computational model for a pressure-driven laminar flow, where the dots represent the dissolving solute. (c) The reference model used for calculation of the mass transfer enhancement with non-slippery bottom wall.

Soft-matter, Fluidics and Interfaces Group, MESA+ Institute for Nanotechnology, University of Twente, The Netherlands

¹E. Karatay et al., Proc. Natl. Acad. Sci. USA 110, 8422 (2013).

²A. S. Haase et al., Soft Matter, 9, 8949 (2013).

^a Dep. Mechanical Engineering, MIT, 77 Massachusetts Ave., Cambridge, MA, USA

Coupling between sloshing and wave-induced vibrations of a monotower

O. M. Faltinsen and A. N. Timokha^a

Sloshing inside the shaft of the Draugen platform (see figure 1) can play an important role in the coupled dynamics influencing both the coupled eigenfrequencies and the forced motions, which are, normally, excited by external water waves. Being challenged by an illustrative example from the authors' book¹ where a particular case was considered, we employ the *linear multimodal method* (replacing the original free-surface “sloshing” problem with a system of ordinary differential equation) to derive an *analytical model* of the mechanical system and use it for an extensive parameter study. As it has been in the aforementioned book example¹, (i) the water level inside the shaft is assumed coinciding with the outer mean level with a negligible in/out flow, (ii) the concrete tower column is represented as a beam with varying stiffness and mass per unit length, (iii) structural damping is neglected, (iv) the ocean wavelengths are of the order of the tower diameter at the waterplane, and (v) the ratio between the submerged tower height and the maximum cross-sectional diameter is large so that the non-wave part of the flow can be handled by slender body theory without free-surface effects. Novelty consists of (a) accounting for effect of internal pipes on the coupled natural sloshing modes and damping, (b) the top platform is modelled as a rigid body (not a mass point) and (c) various mathematical models of the fundement-soil interaction are tested. Emphasis is on the lowest natural frequency of the entire mechanical system as well as on the wave-induced oscillations when the incoming wave frequency is close to this natural frequency.

^a Centre of Excellence AMOS & Dep. Marine Technology, NTNU, NO-7491, Norway

¹ Faltinsen and Timokha, *Sloshing*. Cambridge University Press (2009)

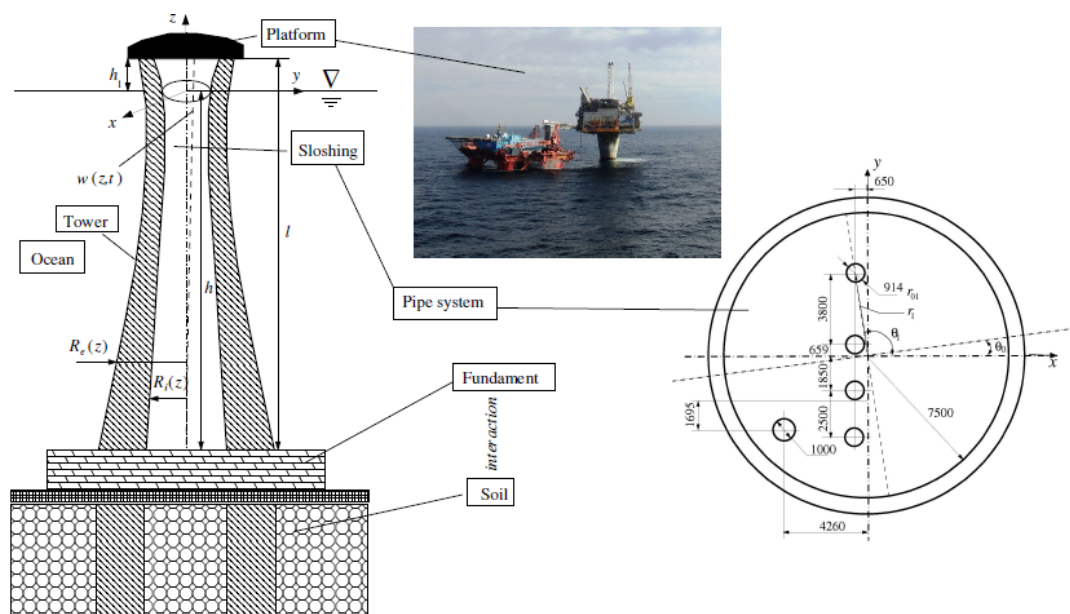


Figure 1: A schematic view of the Draugen platform consisting of (a) a hollow concrete axisymmetric tower, (b) external sea (ocean) water, (c) water inside the tower (there is a complex piping system inside), (d) a rigid heavy body on the top (platform), (e) fundement, and (f) soil. Photo from free Wikipedia.

Experimental study of the interaction between a flexible plate and the vortex street

Erika Sandoval Hernández^a, Anne Cros^a

Alben¹ studied theoretically a flexible plate placed inside the von Kármán street. Its deformation depends upon the plate length, its rigidity, the vorticity of the street among other parameters. In this experimental study, a passive sheet is placed behind a cylinder in a water channel. The Reynolds number is varied from 50 to 200. The vortex street is visualized via dye injection and the sheet fluctuates. The system is recorded via a CCD camera. We find thanks to the analysis of the spatio-temporal diagrams that: (1) the frequency of oscillation of the sheet is the same as the vortex one and (2) the pressure difference between both sides of the sheet is of the same order of magnitude as the elastic force generated by the deformation of the flexible plate.

^a Departamento de Física, Universidad de Guadalajara, México.

¹ Alben S., *J. Fluid Mech.*, **642**, 95, (2010).

Trajectories of freely falling/ascending oblate spheroids of variable aspect ratio

W. Zhou^a, M. Chrust^b and J. Dušek^a

Recent numerical results brought significant progress in understanding the intriguing variety of trajectographies of disks and flat cylinders freely falling or ascending under the action of gravity and buoyancy in a quiescent Newtonian fluid. The topic, brought to the spotlight by the Nature paper by Field et al.¹, was taken up recently by numerical means^{2,3}. In this communication we focus on oblate spheroids of variable aspect ratio $\chi=d/(2b)$ where d is the diameter and b the small half axis of the spheroid. The purpose is to establish a link between very flat bodies corresponding to an infinite aspect ratio and almost spherical ones for χ close to one. The problem involves two other parameters, the non-dimensionalized mass $m^*=m/\rho d^3$ characterizing the inertia of the solid body and the Galileo number $G=(m^* g_{\text{eff}} d^3)^{1/2}/\nu$ representing a ratio between the effect of the driving force and the viscosity. (In the formulas, ρ stands for the fluid density, m for the mass of the spheroid assumed to be homogenous, g_{eff} for the effective acceleration resulting from gravity and buoyancy and ν for the kinematic viscosity.) The resulting three parameter space is swept in planes of constant χ going from infinity to 1.5 in which G is varied from the critical value at which the vertical trajectory loses its stability (30 – 100) to 300 and m^* varies from zero to 5. The results are represented in the form of similar state diagrams as in the paper¹. They provide comprehensive information on the transitional regimes of trajectories of homogenous oblate spheroids of any aspect ratio, solid/fluid density ratio and diameter in any Newtonian fluid. The figures below represent two sample trajectories and the state diagram at $\chi=6$.

^a Institute Icube (Fluid Mechanics), University of Strasbourg/CNRS, France

^b Dep. Mechanical Engineering, Polytechnique Montréal, Canada

¹ Field, Klaus, Moore, *Nature*, **388**, 252 (1997)

² Chrust, Bouchet, Dušek, *Physics of Fluids*, **25**, 044102 (2013)

³ Auguste, Magnaudet, Fabre, *Journal of Fluid Mechanics*, **719**, 388 (2013)

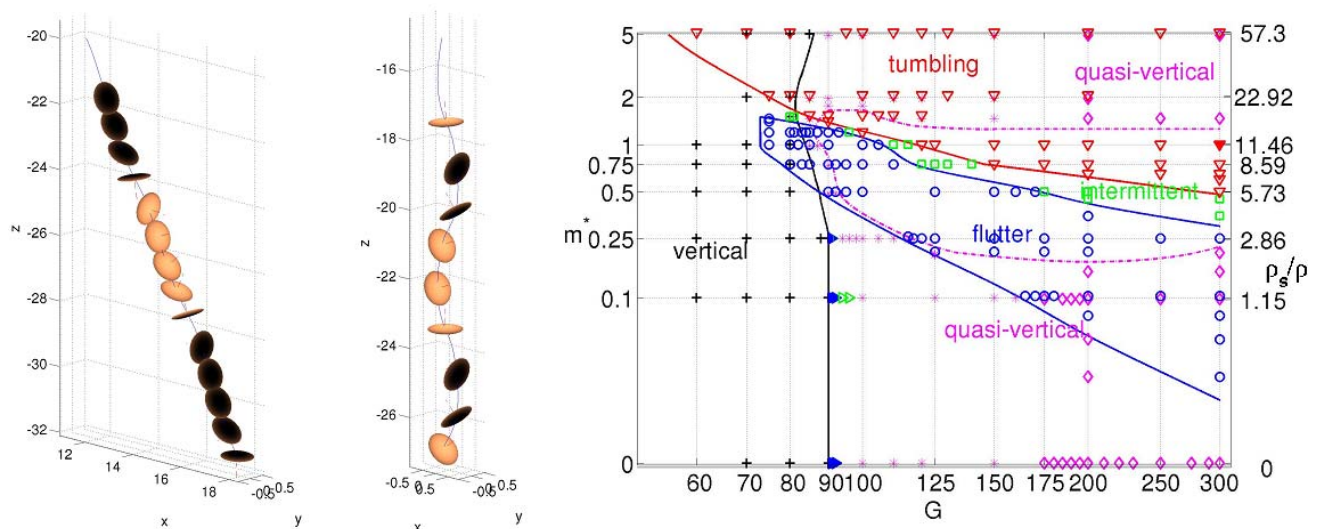


Figure 1: $\chi=6$: (a) Fluttering spheroid ($m^*=1$, $G=125$). (b) Tumbling spheroid ($m^*=0.5$, $G=150$). (c) State diagram.

Flow-induced vibrations of a rectangular cylinder at low mass ratios

T. Massai^a, D. Lo Jacono^b, J. Sheridan^c

This study examines the features concerning the cross-flow response of a rectangular cylinder with an aspect ratio $L/W = 1.5$. The interest in this particular section stem from the fact that it has been observed¹ to be particularly prone to the interaction between vortex-induced vibration and galloping instability². It was shown that the interaction can occur in a range of aspect ratio varying from 0.6 to 3.5 approximately, and for system damping levels such that the quasi-steady galloping onset velocity, U_0 , approach the resonance one, U_r (or even lower than this value). Given the higher density of the fluid a low mass ratio is readily available³.

The interaction was investigated during the past decades almost entirely referring to square cylinders, with some exceptions⁴⁻⁵ concerning comprehensive studies for several different section types, aimed in defining the quasi-steady galloping dynamical characteristics. However none for the studies on the square section with low values of mass ratios were investigated⁶⁻⁷⁻⁸. Recently the interaction was approached with a square section in water at several angles of attack⁹ (α).

In the water channel facility (FLAIR - Monash university), a rectangular cross-section rigid cylinder model made from anodized aluminium tubing with a final side depth of $W = 24.75$ mm and a side width of $L = 37.45$ mm has been tested: the lowest mass ratio has been $m^* = 2.24$ with a system damping ratio $\zeta = 2.47\%$. The model is set free to oscillate in the transverse direction being it connected to an air bearing system through a force balance which measure the forces exerted by the flow via 4 strain gauges. In the vibration direction the model is connected to the system with a variable number of springs allowing different natural frequencies.

The study shed a deeper insight on the responses describing precisely the evolution of the different mechanisms at play. A wide range of parameters were carefully varied making it possible to investigate amplitude response with varying both the mass ratio of the cylinder and the angle of attack. When the interaction occurred the amplitude response branch had the characteristics of galloping instability, developing at $U^* = U_r$: it has been observed, in particular for the lowest mass ratios, the violation of this usual “empirical rule”, with galloping response starting from a reduced velocity much higher than U_r and showing a sub-harmonic resonance bell which got wider as the mass ratio got lower.

^a Centro di Ricerca Interuniversitario di Aerodinamica delle Costruzioni e Ingegneria del Vento (CRIACIV), Civil and Environmental Engineering Department, Florence University, 50139 Florence, Italy

^b Institut de Mécanique des Fluides de Toulouse (IMFT), CNRS, UPS, Université de Toulouse, Allée Camille Soula, F-31400 Toulouse, France

^c Fluids Laboratory for Aeronautical and Industrial Research (FLAIR), Department of Mechanical and Aerospace Engineering, Monash University, , VIC 3800, Melbourne, Australia

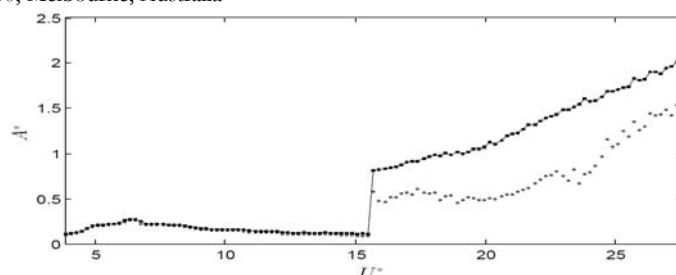


Figure 1: hydro-elastic response of the model for $m^* = 2.24$ and $\alpha = 0$. filled squares: mean of the top 10% of the peaks; empty circles: mean of the peaks.

¹ Mannini et al., VIV and galloping interaction for a 3:2 rectangular cylinder. *Proceedings of EACWE2013* (2013)

² Smith, *MSc Thesis*. University of British Columbia (1962)

³ Parkinson, *Prog. Aerosp. Science*. **26**, 2 (1989)

⁴ Novak & Tanaka, *J. Wind Eng. Ind. Aerodyn.* **100**, EM1 (2009).

⁵ Bokaian & Geoola, *ICE Proceedings*. **75**, 2 (2009).

⁶ Parkinson & Smith, *Quart. J. of Mech. and App. Math.* **17**, 2 (1964).

⁷ Bouclin, *MSc Thesis*. University of British Columbia (1977)

⁸ Bearman et al., *J. Fluids Str.* **1**, 1 (1987).

⁹ Nemes et al., *J. Fluids Mech.* **710** (2012).

Oscillations of free cylinders at low Reynolds numbers inside a Hele-Shaw cell

V. D'Angelo^a, L. Gianorio^a, M. Cachile^a, H. Auradou^b, J.P. Hulin^b, B. Semin^c

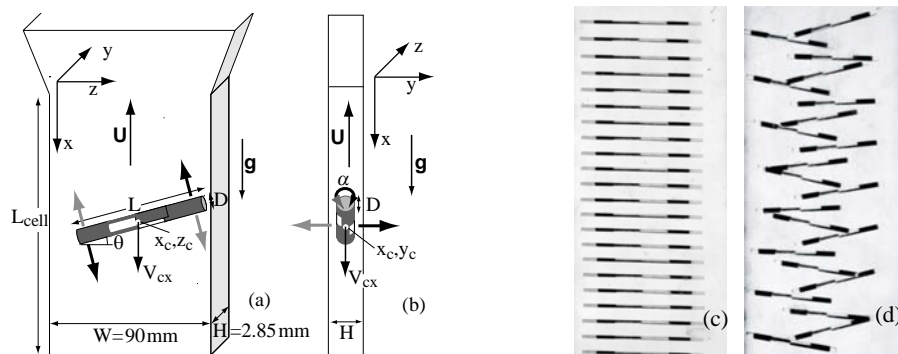


Fig. 1: (a)-(b) Front and side view of the experimental set-up. Thick arrows correspond to the motion of the cylinder in the transverse oscillation (b) and fluttering (a) regimes. (c), (d) Sequences of views of the cylinder in these two latter regimes.

We studied experimentally two oscillatory instabilities of a free horizontal cylinder moving in a vertical flow inside a vertical Hele-Shaw cell¹ (Figs. 1a-b) as a function of the ratios D/H and L/W of the diameter (resp. the length) of the cylinder to the gap (resp. the width) of the cell. The occurrence and type of the instabilities depends mostly on D/H . For $0.4 \leq D/H \leq 0.6$, one observes transverse horizontal oscillations (Fig. 1b) of the cylinder perpendicular to the walls without a variation of their angle with respect to the horizontal (Fig. 1c) but with a synchronous oscillation of the roll angle α around the axis.

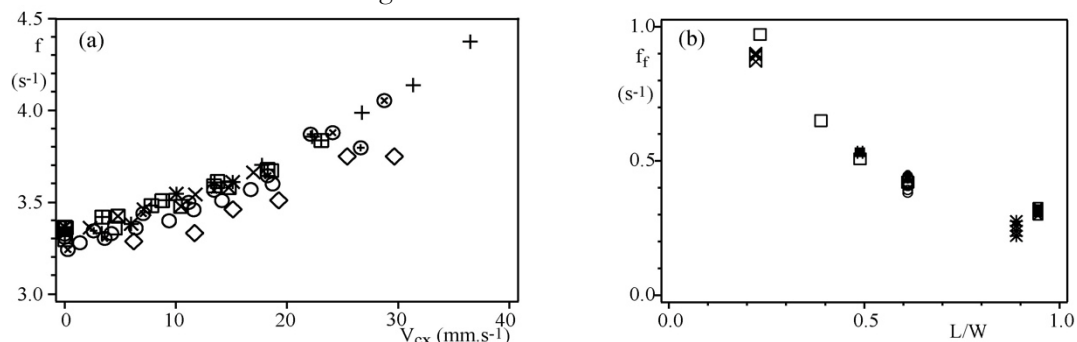


Fig. 2: (a) variation of the transverse oscillation frequency f with the cylinder velocity V_{∞} for different ratios L/W (symbols). (b) variation of the fluttering frequency f_f with the normalized length L/W for different diameters D (symbols).

For a given cylinder velocity V_{∞} , the frequency f of these oscillations is constant with L/W (Fig. 2a) over a broad range of values ($0.1 < L/W < 0.95$) and with D/H . This instability is shown to be locally two-dimensional and controlled by the relative velocity V_r^{loc} between the cylinder and the local flow upon it. The corresponding Reynolds number $Re = V_r^{loc} H / \nu$ is independent of L/W and V_{∞} but can be varied by changing the fluid viscosity: the instability is still observed for $Re = 15$, far below the vortex shedding threshold. The corresponding variation of the Strouhal number with Re is close to previous results for tethered cylinders with $L/W \approx 1$; 2D numerical simulations have analyzed the relative influence of the additional degrees of freedom for free cylinders.

For $D/H \geq 0.55$, free cylinders with $L/W < 1$ display a new instability inducing a fluttering motion of the cylinder with periodic oscillations of its tilt angle from the horizontal and its horizontal position. In contrast to f , the frequency f_f decreases strongly between $L/W = 0.22$ and 0.95 while it is constant with D/H and V_{∞} (Fig. 2b): this shows that this fluttering instability is three-dimensional and controlled by the fluid flow between the ends of the cylinder and the sides.

^a Grupo de Medios Porosos, Facultad de Ingeniería, Paseo Colon 850, 1063, Buenos Aires (Argentina), CONICET (Argentina).

^b Univ Paris-Sud, CNRS, F-91405. Lab FAST, Bât 502, Campus Univ, Orsay, F-91405 (France).

^c LPS Laboratory, Département de Physique de l'ENS, 24 rue Lhomond, 75231 Paris Cedex 05.

¹ M.V. D'Angelo, J.P. Hulin and H. Auradou, Phys. Fluids 25, 014102 (2013).

² B. Semin, A. Decoene, J.P. Hulin, M.L.M. Francois and H. Auradou, J. Fluid Mech. 690, 345–365 (2012).

Linear analysis of 2D pendulum subjected to an incoming flow

A.Fani^a, F. Gallaire^a

Flow induced oscillations of slender bodies facing an incoming flow are relevant in a large number of engineering applications, such as the design of tubular structures of offshore platforms, heat exchangers and energy harvesting¹. Numerical simulations and experiments available in the literature often consider a circular cylinder in an uniform flow which can move only transversally with respect to the flow direction. In a recent work Semin et al.² studied a tethered 2D cylinder placed between two parallel plane walls. It is shown that confinement alters significantly the flow dynamics, with a new instability, denoted confinement induced vibration (CIV), which occurs at a Reynolds number much lower than the vortex induced vibration (VIV) critical one. Different behaviors have been observed, depending on the density ratio between the body and the surrounding fluid. In the present work, we characterize the instability scenario of a confined tethered cylinder by means of a global stability analysis of the fluid-structure problem, as shown in Fig. 1. In strongly confined channels, a periodic unstable mode, related to CIV vibrations, is observed, while for moderated confinement a new steady static instability is founded.

In addition, in order to investigate the physical mechanisms involved in the cylinder motion, we propose a quasi-static model which has been able to recover the different dynamic behavior.

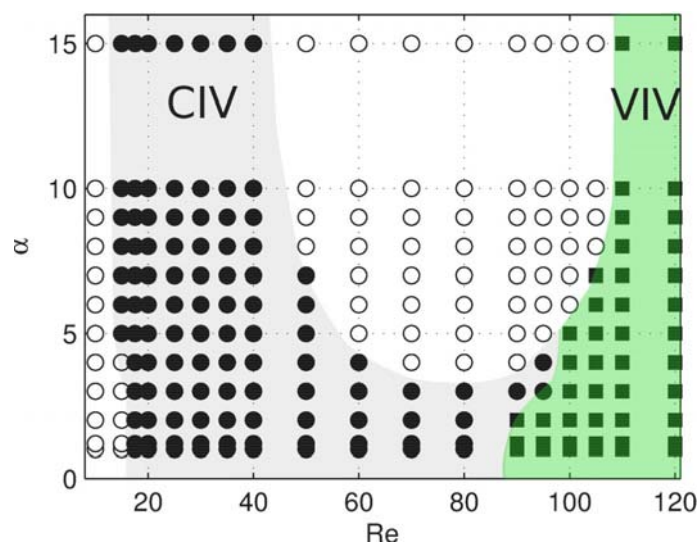


Fig. 1: Stability map for the strongly confined case in the Re - α plane. Two different instability branches have been observed: CIV (grey) and VIV (green)

^a LFMI, EPFL, 1015 Lausanne, Switzerland

¹ Williamson CHK and R. Govardhan, Ann. Review of Fluid Mech. **36**, 1 (2004).

² Semin et al., J. Fluid Mech. **690**, 345 (2011).

Particles settling in a cellular flow field at low Stokes number

D. Lopez^a, L. Bergougnoux^a, G. Bouchet^a and E. Guazzelli^a

The transport of particles in a turbulent environment is relevant to many industrial and natural processes. Very often, the sedimentation of particles is a dominant phenomenon, which is important to understand in a fundamental way. Examples include fluidized-bed reactors, the treatment of waste materials in clarifiers, the transport of sediment in rivers and estuaries, pyroclastic flows from volcanic eruptions, and bioconvection of planktons. Based on the model proposed by Gatignol¹ and Maxey & Riley², multiple numerical studies have been performed on the sedimentation of particles in vortical flows, generally modelled by Taylor-Green vortices. In the model, particle motion is driven by different contributions whose intensity depends on various parameters, in particular the Stokes number, scaling the particle response time with respect to the timescale of the background flow. Yet, the competition between these different terms has never been addressed experimentally.

We present a jointed experimental and numerical study examining the influence of vortical structures on the settling of solid particles under the action of gravity at low Stokes numbers. The two-dimensional model experiment uses electro-convection to generate a two-dimensional array of controlled vortices, which mimics a simplified vortical flow³. At very low Reynolds number, the generated flow is accurately modelled by Taylor-Green vortices. As the Reynolds number increases, the vortices deform but remain stationary in the range of interest. Using Particle Image Velocimetry and Particle Tracking, we determine the motion of settling particles within this vortical flow.

We investigate the role of inertia on the settling rate as well as trajectories, for small spherical particles and slender rods. In the latter, drag anisotropy yields chaotic motion even at negligible inertia. The experimental results (see Figure 1) will then be compared to the theoretical model, testing the influence of the different forces acting on the particle motion.

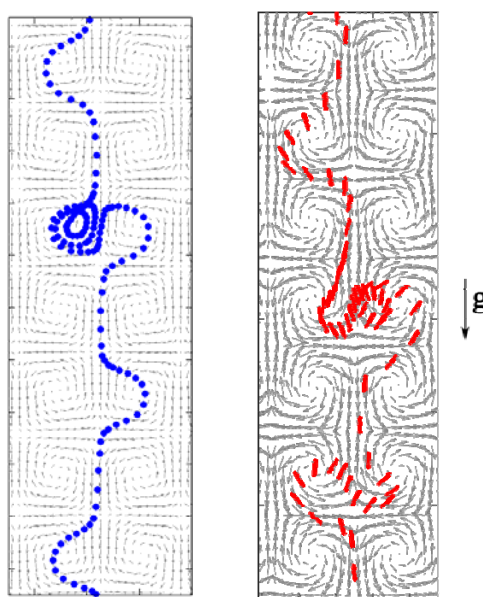


Figure 1: (a) Rigid sphere and (b) rigid fibre settling in a vortical flow.

^a Aix Marseille Université, CNRS, IUSTI UMR 7343, 13013 Marseille, France

¹ R. Gatignol, "The Faxen formulae for a rigid particle in an unsteady non-uniform Stokes flow," *J. Méca. Théo. Appli.* 2, 143 (1983).

² M. R. Maxey and J. J. Riley, "Equation of Motion for a Small Rigid Sphere in a Nonuniform Flow," *Phys. Fluids* 26, 883 (1983).

³ L. Rossi, J. C. Vassilicos and Y. Hardalupas, "Electromagnetically controlled multi-scale flows," *J. Fluid Mech.* 558, 207-242 (2006).

Flow-induced response of a cantilevered cylinder in the wake of different diameter cylinders

Md. Mahbub Alam^a, Zong Bin^a and Y. Zhou^a

Flow-induced vibrations of two inline cylinders subjected to a cross flow have been the subject of intensive research because of relevance to the engineering structural design and acoustic emission problems. A detailed survey of the literature relating to flow-induced response of two cylinders suggests that previous investigations mostly were performed for two cylinders of an identical diameter^{1,2}.

Presently a wind tunnel test is conducted on flow-induced vibration response of a cantilever-supported circular cylinder (diameter D) placed in the wake of both-end fixed cylinder varied in diameter (d) from $0.24D$ to $1.0D$. The cylinder spacing ratio, L/d , examined is $1.0 \sim 5.5$, where L is defined in Fig. 1(a). While the vibration amplitude is measured using a laser vibrometer, vortex shedding frequency is estimated from a power spectral density function of hotwire-measured streamwise velocity behind the cylinders. A violent vibration of the cylinder is observed for $d/D = 0.24 - 0.8$, $0.24 - 0.6$, $0.24 - 0.4$ and 0.24 at $L/d = 1.0$, 1.5 , $2 - 2.5$ and $3 - 5.5$, respectively. Figure 1(b) explicates dependence of violent vibration generation on d/D and L/d . It is clear that a decreasing d/D is prone to generate violent vibration, perhaps causing a higher instability in the flow and/or increasing of negative damping on the cylinder. It is noted that the flow behind the vibrating cylinder is characterized by two predominant frequencies, corresponding to the cylinder vibration frequency and the natural frequency of vortex shedding from the downstream cylinder, respectively. While the former persists downstream, the latter vanishes rapidly.

^aInstitute for Turbulence-Noise-Vibration Interaction and Control, Shenzhen Graduate School, Harbin Institute of Technology, Shenzhen, China

¹Bokaian A, Geoola F, *J. Fluid Mech.* 146, 383 (1984).

²Alam MM, Meyer JP, *J. Fluids Struct.* 41, 135 (2013).

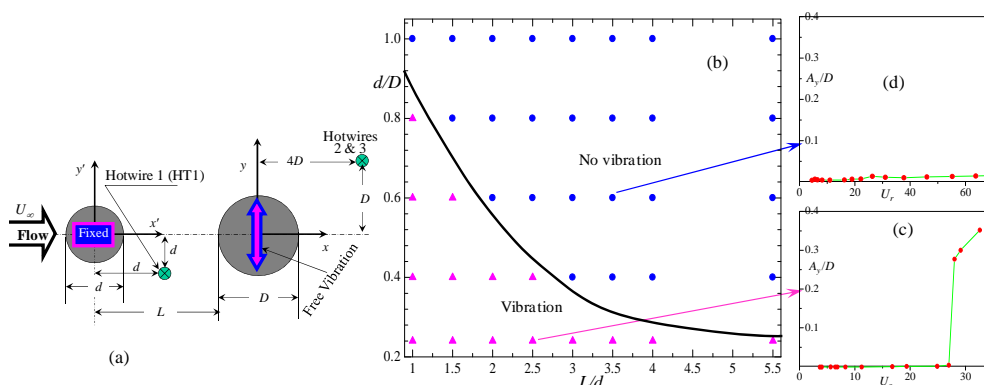


Figure 1: (a) Experimental arrangement. (b) Flow-induced response map on $d/D - L/d$ plane showing the region of violent vibration generation. \blacktriangle , violent vibration generated; \bullet , no vibration. (c, d) Dependence of vibration amplitude A_v/D on reduced velocity U_r .

Circular cylinder drag reduction using cross-section geometry variation from circular to elliptic shape

H. Oualli^a, M. Mekadem^a, A. Boutemdjet^a, H. Chetitah^a, C. Boulahbal^a and A. Bouabdallah^b

This work is devoted to study the wake structure of a flow around a circular cylinder executing periodic variation of the cross-section shape from circular to elliptic shape. Results are examined for a Reynolds number $Re \approx 3900$, vibrating amplitude ranging from 0 to 50% of the cylinder initial diameter and a non-dimensional vibrating frequency ranging from 0.2 to 10. In these conditions, it is shown that the von Karman eddy street can be inhibited leading to a drastic drag reduction (up to 65%).

Drag reduction is one of the crucial aerodynamic problems which continues instilling great interest from both scientists and industrials. One reason of this central importance resides in the huge amounts of economic and financial savings resulting from drag reduction and the subsequent positive impacting on the environment. In fact, it is commonly reported in literature that for a drag reduction of 20% in aeronautics, maritime navigation and automobile USA and EEC can yearly save about 2 billion dollars and 2.4 billion Euros respectively. Regarding these motivations, a numerical and experimental study is developed to make investigation of an active controlling technique applied to a circular cylinder executing cross-section geometry variation from circular to elliptic shape according to a pre-defined sinusoidal law. In these conditions, the cylinder extends and retracts streamwisely to the outer flow direction. This modulating movement is characterized by its amplitude, considered in the range of 5 to 50% of the cylinder initial diameter, and its frequency extending from 0.2 to 10 when reported to the cylinder natural shedding frequency.

The obtained results show that for the considered Reynolds number $Re=3740$, the near wake and the von Karman eddy street are substantially altered both topologically and physically. The flow exhibits a cascade of bifurcations identified by the shedding mode shifting. A central result for this study consists in the eddy shedding mechanism quasi-inhibition resulting in a drag reduction rate of more than 65%.

^a LMF Laboratory, Ecole Militaire Polytechnique, BP 17 Bordj El Bahri, Algiers, Algeria.

^b LTSE Laboratory, USTHB, BP 32, Bab Ezzouar, Algiers, Algeria.

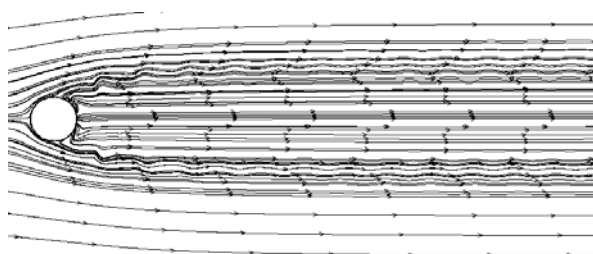


Figure 1: Inhibited von Karman eddy street.

Vortex structures in the node to anti-node transition of an oscillating flexible cylinder

Zafar A. Bangash^a and Francisco J Huera-Huarte^a

The amplitude distribution along a flexible cylinder undergoing vortex-induced vibrations yields very complex flow dynamics in its wake, as there are regions along the length characterised by high cross flow oscillations (anti-nodes) and others with very low amplitudes (nodes). Previous research has shown the appearance of singular structures in the wake of flexible cylinders undergoing flow-induced oscillations^{1,2,3} as compared to the structures that appear in stationary or flexibly mounted rigid cylinders. It has also been suggested that both mean transverse forces, as well as instantaneous transverse forces at nodes are zero⁴.

We have studied the wake of a flexible cylinder that is oscillating in its second structural mode when excited by vortex shedding. The experimental set-up consisted of a flexible cylinder with an aspect ratio (L/D) of 150, made of a long spring wrapped in an elastic tube, able to vibrate at high structural modes. The model was towed in a motorized tow-tank and Digital Particle Image Velocimetry (DPIV) was used to quantify the flow. Long-exposure photography was also used for qualitative analysis of the wake. Reynolds numbers were in the range from 500 to 2000. The work is focused in the identification of the structures that appear in the region where the amplitudes change from maximum at the anti-nodes to near zero at the nodes. We have found that at the node region the wake is symmetric instead of the classical Karman Street.

^a Dept. Of Mechanical Engineering, Universitat Rovira i Virgili, Tarragona, Spain.

¹ Gilbert, Sigurdson, *Exp. Fluids* **48**, 461-471 (2010).

² Hammache and Gharib, *J. Fluid Mech.* **232**, 567-590 (1991)

³ Bourguet et.al *J. Fluid Struct.* **32**, 52-64 (2012)

⁴ Huera Huarte et.al. *J. Fluid Struct.* **22**, 897-903 (2006)

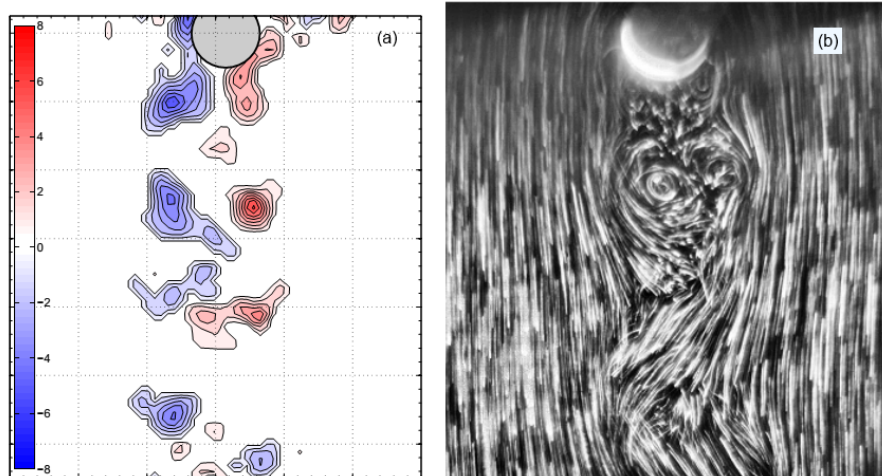


Figure 1: (a) Instantaneous vorticity fields obtained from DPIV, at the node of a flexible oscillating cylinder, and (b) Flow visualization image using long-exposure photography at the same conditions.

On the spanwise pressure coherence of a turbulent boundary layer over a flat plate

W.C.P. van der Velden^a, A.H. van Zuijlen^a, A.T. de Jong^a and H. Bijl^a

Far field noise pollution is one of the main design drivers for on-shore wind energy. The turbulent trailing edge noise of a wind turbine blade is currently one of the most dominant noise sources on a wind turbine and therefore understanding the physics associated with the generation and propagation is of main importance for the design of more silent wind turbines. The airfoil self-noise originates from unsteady flow over the airfoil. Brooks et al.¹ defined some fundamental airfoil self-noise mechanisms associated with the trailing edge, such as laminar and turbulent boundary layer noise and bluntness noise. Regarding aero acoustics on a wind turbine blade, where turbulent trailing edge noise is the primary noise source, pressure and velocity fluctuations are the main quantities of interest for determining the acoustical sources. Especially the spanwise coherence of the wall pressure is of importance for the estimation of the far field trailing edge noise and other vibro-structural problems. Several authors, such as Amiet² and Howe³ have discussed diffraction theory regarding trailing edge noise. Here, the power spectral density and spanwise coherence length of hydrodynamic pressure fluctuations were used to estimate the acoustic far field spectrum. Amiet² and Howe³ assumed that the incident pressure fluctuations on the wall below the turbulent boundary convect over the trailing edge, which acts as an impedance discontinuity, where the fluctuations are scattered in the form of acoustical waves. This theory forms the basis of multiple experimental and numerical studies, such as the Large Eddy Simulation (LES) study of Christophe⁴ or the surface pressure measurements of Brooks and Hodgson⁵.

The current study focuses on the analysis of the turbulent boundary layer generated by various forms of tripping. Both zig-zag strips and structured blocks are tested together with different grid sizes, as a effective method to generate a fully turbulent boundary layer. The commercial Computational Fluid Dynamics (CFD) package, Exa PowerFLOW, is used. This is a fully transient, explicit, compressible code based on the Lattice Boltzmann Method (LBM). A Large Eddy Simulation (LES) methodology with a k-epsilon RNG model coupled with wall-law is used as closure turbulence model. Flow with Reynolds numbers of 2.68E5 and 5.36E5 are considered. Boundary layer characteristics are analyzed and compared with literature⁶, as well as the development of the turbulent boundary layer (see Fig. 1).

Further, a streamwise and spanwise correlation and coherence study is performed analyzing the capabilities of PowerFLOW regarding capturing aero-acoustic noise. Streamwise and wall normal velocity coherence are considered at a small distance from the wall, while pressure fluctuations on the wall below the turbulent boundary layer are analyzed for their coherence.

^a Department of Aerodynamics, Faculty of Aerospace Engineering, Delft University of Technology, Kluyverweg 2, 2629 HT Delft, the Netherlands

¹ Brooks T., Pope D., Marcolini M., *NASA Reference Publication*, **1218**, (1989)

² Amiet R., *Journal of Sound and Vibration*, **47**, 387-393, (1976)

³ Howe M.S., *Journal of Sound and Vibration*, **225**, 2, 211-238, (1999)

⁴ Christophe J., *Université Libre de Bruxelles*, PhD Thesis, (2011)

⁵ Brooks T., Hodgson T., *Journal of Sound and Vibration*, **78**, 69-117, (1981)

⁶ Pröbsting S. et al. *Experimental Fluids*, **54**, 1567-1582, (2013)

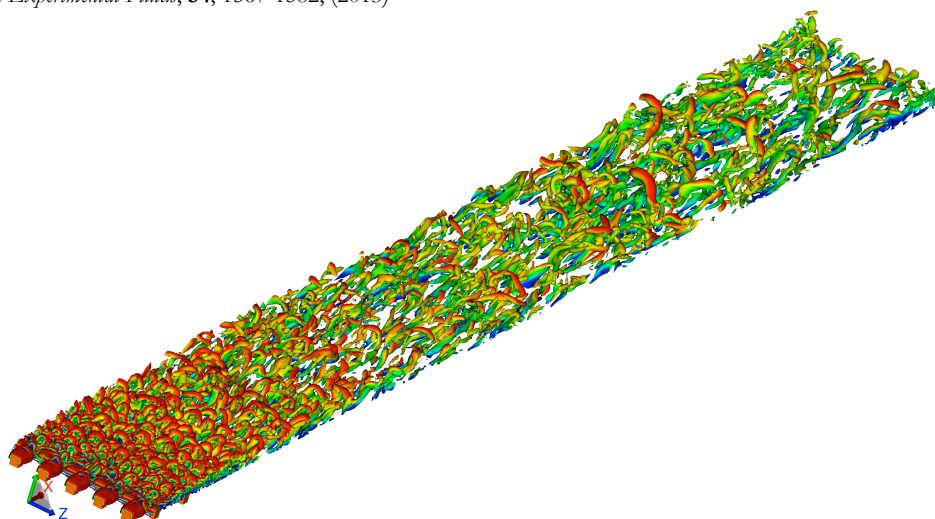


Figure 1: λ_2 isosurfaces indicating the streamwise development of the turbulent boundary layer, colored by the velocity magnitude

Wake interference effects on the heat transfer enhancement around a row of circular cylinders

F. Fornarelli¹, P. Oresta², A. Lippolis^b

The numerical simulations of the heat transfer around an array of isothermal circular cylinders immersed in a stream has been carried out solving the two-dimensional Navier-Stokes equations. The cylinders have been placed in a single row configuration aligned with the free stream velocity at Reynolds number 100 and Prandtl number 0.7.

In Fig.1 it is shown the instantaneous temperature distribution for the case of six in-line circular cylinders at spacing ratio (s/d) equal to 4 and 3.6, where s is the center-to-center cylinder spacing and d is the cylinder diameter.

In the latter case, a transition in the flow patterns occurs with the flow organized in a vortex shedding responsible for the entrainment of cold fluid in the gaps. This phenomenon makes stronger the thermal gradient close to the cylinders leading the heat transfer enhancement with the Nusselt number 25 % higher respect to the case at $s/d=4$.

Furthermore a frequency analysis of the time dependent Nusselt number, Nu_i , at the i -th cylinder, shows that the main frequency is the same for all the cylinders.

We found evidences that the signature of the heat transfer enhancement could be related to the phase shift between two successive cylinders ($\phi_{i+1} - \phi_i$), where the phase shift (ϕ_i) is defined as the difference between the phase of each main harmonic component of the Nu_i respect to the phase of the signal at the first cylinder.

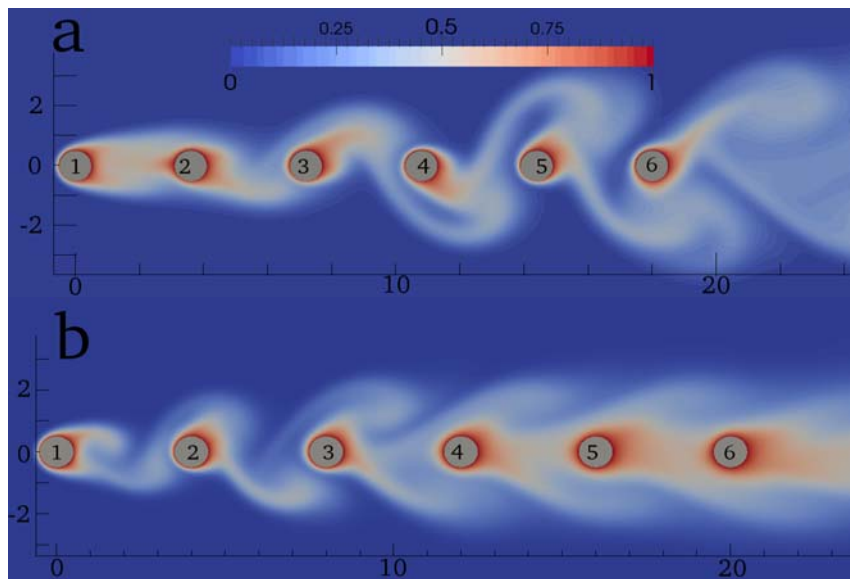


Figure 1: Instantaneous dimensionless temperature around the cylinders for a spacing ratio of 3.6 (a) and 4.0 (b).

¹ Dipartimento di Ingegneria dell'Innovazione, Università del Salento, 73100 Lecce, Italy.

² Dipartimento di Meccanica, Matematica e Management, Politecnico di Bari, 70126 Bari, Italy.

Adaptive Finite Element Approximation of Monolithic Fluid-Structure Interaction (FSI) Problem

B.S.M. Ebna Hai^a and Markus Bause^b

Will an aircraft wing or wind turbine blade have the structural integrity to withstand the forces or fail when it's racing at a full speed? Fluid-structure interaction (FSI) analysis can help you to answer this question without the need to create costly prototypes. However, combining fluid dynamics with structural analysis traditionally poses a formidable challenge for even the most advanced numerical techniques due to the disconnected, domain-specific nature of analysis tools. In a monolithic nonlinear fluid-structure interaction (FSI), the fluid and structure models are formulate in different coordinate systems. This makes the FSI setup of a common variational description difficult and challenging. This article present the state-of-the-art of recent developments in the finite element approximation of FSI problem based on monolithic variational formulation in the well-established arbitrary Lagrangian Eulerian (ALE) framework. In such a setting, the fluid equations are transformed to a fixed reference configuration via the ALE mapping. We present the state-of-the-art in computational FSI methods and techniques that go beyond the fundamentals of computational fluid dynamics and solid mechanics. In fact, the fundamental rule require transferring results from the computational fluid dynamics (CFD) analysis as input into the structural analysis and thus can be time-consuming, tedious and error-prone. The principal aim of this research is to explore and understand the behaviour of the fluid-structure interaction during the impact of a deformable material (e.g. an aircraft wing) on fluid. This work consists of the investigation of different time stepping scheme formulations for a nonlinear fluid-structure interaction problem coupling the incompressible Navier–Stokes equations with a hyperelastic solid. Temporal discretization is based on finite differences and a formulation as one step- θ scheme, from which we can extract the implicit Euler, Crank-Nicolson, shifted Crank-Nicolson and the Fractional-Step- θ schemes. The time discretization is based on finite difference schemes whereas the spatial discretization is done with a Galerkin finite element scheme. The nonlinear problem is solved with Newton's method. To control computational costs, we apply a simplified version of a posteriori error estimation using the dual weighted residual (DWR) method. This method is used for the mesh adaption during the computation. The implementation using the software library package DOpElib¹ and deal.II² serves for the computation of different fluid-structure configurations. DOpElib is a modularized high-level algorithms toolbox based on the deal.II finite element library.

^{a, b} Department Mechanical Engineering, Helmut Schmidt University-University of the Federal Armed Forces Hamburg, Holstenhofweg 85, 22043 Hamburg, Germany.

¹ C. Goll, T. Wick and W. Wollner, DOpE lib: The deal.II based optimization library, web: www.dopelib.uni-hamburg.de.

² W. Bangerth, T. Heister and G. Kanschat. deal.II Di_ifferential Equations Analysis Library, web: www.dealii.org.

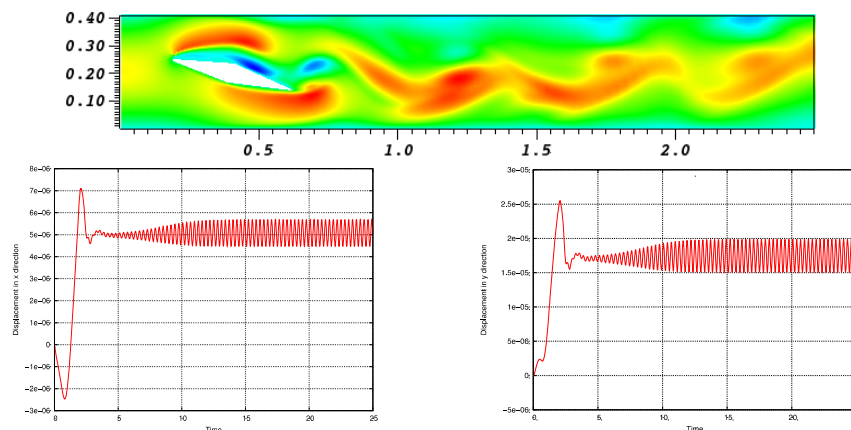


Figure 1: FSI effect on a double wage airfoil (2D): (a) Velocity field (b) Displacement in x & y direction with time

DNS of turbulent channel flow with a flexible finite-length square cylinder

K. Tsujimoto^a, Y. Hada^a, T. Shakouchi^a and T. Ando^a

Fluid-Structure Interaction (FSI) problem is concerned with in various research fields such as mechanical, aerospace, civil and medical engineering. Their accurate prediction and control are desired. In particular, since the wake of wall-mounted cylinder is a common flow regime in above-mentioned research, the detail of the flow has been aggressively investigated so far¹. In this study, we pay attention to the flow control using flexible structures in the above mentioned flows. To investigate the potentiality of the control in advance, both high accurate and stable computational scheme is needed so that the actual phenomena including turbulence is well predicted. Therefore, in order to analyze the fluid-structure interaction, we propose a weak-coupling method in which for flexible structures, the rigorous equations of motion are discretized with finite volume method (FVM²); for a flow computation, the finite difference method (FDM) is used and the flexible structures is reproduced via immersed boundary method³. Figure 1 shows the computational conditions. The wall condition is enforced on the both upper and lower boundary. The cantilever is placed on the lower boundary. The inflow being generated by the upstream channel, is imposed on the left side boundary and a convective outflow boundary is used on the right side boundary. Periodicity is enforced in spanwise direction. The Reynolds number define with friction velocity is $Re=150$. We perform the computation of both rigid and elastic square-cylinder. Figures 2 show the instantaneous vortical structure. The coherent vortices (white color) are visualized using the Iso-surfaces of the second invariance of velocity gradient tensor Q . Since a high threshold value is set, strong vortex structures are captured and distribute in the wake of the cylinder. In general, it is well known that quasi-streamwise vortices govern near-wall turbulence, however not show here, we have confirmed that the quasi-streamwise vortices near the wall are observed when the threshold of Q value is set as low. Also it can be seen that the effect of cylinder on the instantaneous flow structures is limited around the wake region. In the case of both rigid and elastic square cylinder, the periodicity of vortex shedding in the wake of the cylinder are observed from the animations. In particular, in the case of the elastic square cylinder, the vortex shedding occurs according to the spanwise motion of cylinder. In the calculation of the rigid square cylinder, it demonstrated that the computational result in which two pairs of the large vortices are formed in the wake of cylinder is qualitatively agreement with the experimental finding reported in the previous literatures. It reveals that the elastic deformation induces the different flow pattern from that of rigid case.

^a Division of Mechanical Engineering Graduate School of Eng., Mie University, Tsu, Japan

¹ Wang et al., *J. Fluid Mech* **638**, 453(2009).

² Wilkins, Springer Verlag GmbH (2006).

³ Fadlun et al., *J. Comp. Physics*, **161**, 35(2000).

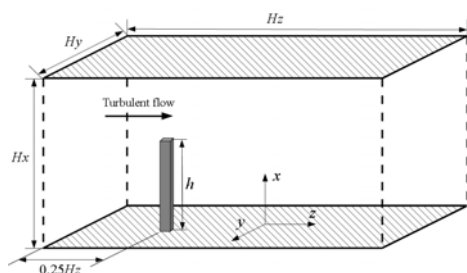
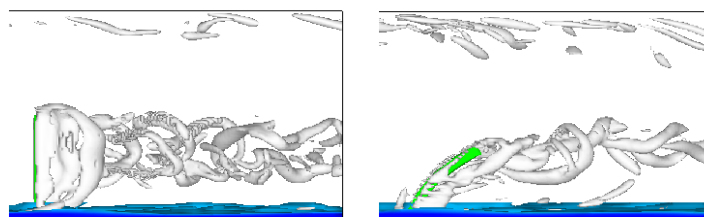


Figure 1: Computational conditions



(a) rigid cylinder

(b) elastic cylinder

Figure 2: Coherent vortices visualized with Q

Jets

Optimal linear transient growth in axisymmetric coaxial jets

J. Canton^a, F. Auteri^b, and M. Carini^b

A large number of applications and industrial processes, such as the mixing of two fluid streams in jet-engine combustors to cite just an example, involves the flow described by two axisymmetric coaxial jets.

Until now, the stability properties of this class of flows have been investigated either using experimental techniques^{1,2} or by means of an inviscid analysis under the common assumption of a locally-parallel flow³. While a global stability analysis could be performed, it is well known that for linearly stable convection-dominated flows like jets and boundary layers, the modal approach provides us with a limited description of the linear stability properties of the flow⁴. As a consequence of the strong non-normality of the linearised Navier-Stokes operator, relevant transient growth of the perturbation energy can occur, as in the case of a single axisymmetric jet⁵.

In the present work, a transient growth analysis of the flow generated by two incompressible, axisymmetric coaxial jets is carried out for several Reynolds numbers and for a unitary ratio between the maximum axial velocities in the two jets. The spatial structure of the computed optimal axisymmetric perturbations is thoroughly described. It turns out that these perturbations are highly localised in a region close to the end of the inlet pipes, Figure 1(a), and their energy can reach an amplification of several orders of magnitude, as shown in Figure 1(b). Quite interestingly, and rather surprisingly, the amplification in this case is orders of magnitude larger than the one reported for a single jet at the same Reynolds number⁵.

In addition to the linear transient-growth analysis, the evolution of optimal perturbations in the nonlinear regime has also been investigated. In this case, as expected, the maximum growth of the perturbations is significantly lower than in the linear case. Nevertheless, an amplification up to five orders of magnitude has been observed even in the nonlinear regime.

^a Linné FLOW Centre, KTH Mechanics, Royal Institute of Technology, SE-100 44 Stockholm, Sweden

^b Dipartimento di Scienze e Tecnologie Aerospaziali, Politecnico di Milano, via La Masa 34, 20156 Milano, Italia

¹ Segalini and Talamelli, *Phys. Fluids* **23**, 024103 (2011)

² Rehab et al., *J. Fluid Mech.* **345**, 357 (1997)

³ Talamelli and Gavarini, *Flow Turbulence Combust.* **76**, 221 (2006)

⁴ Schmid, *Annu. Rev. Fluid Mech.* **39**, 129 (2007)

⁵ Garnaud et al., *Phys. Fluids* **25**, 044103 (2013).

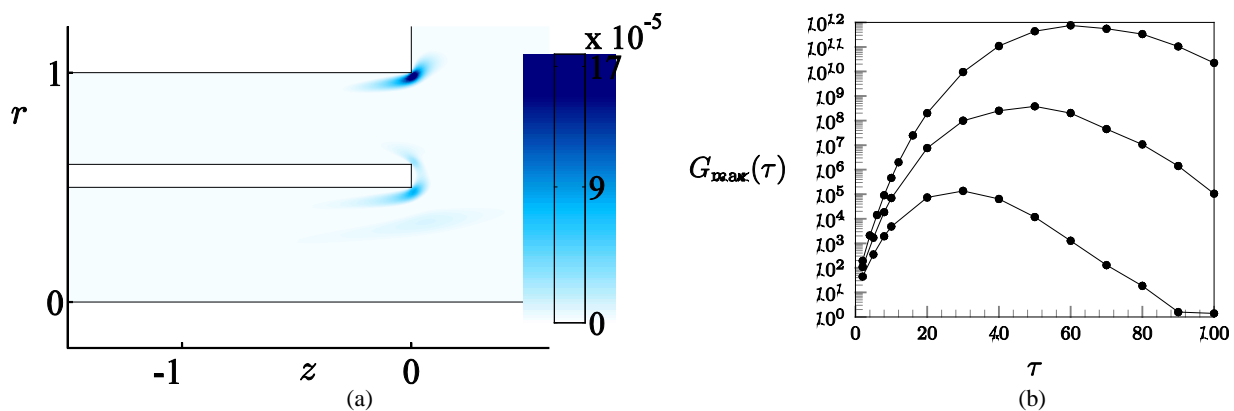


Figure 1: (a) Kinetic energy of the optimal initial perturbation for $Re=500$ and $\tau=30$. (b) Behaviour of the maximum amplification as a function of time horizon for three Reynolds numbers (500, lower curve, 750, intermediate curve, 1000, upper curve) based on the internal jet diameter and on its maximum velocity.

Experimental investigation of a variable area ratio on steam-jet ejector efficiency

Banipal N. Yaqob^a

In the present paper, experimental investigation on variable primary nozzle geometry on steam ejector were presented and compared. The variable geometry was achieved by applying a movable spindle at the primary nozzle inlet. Operating conditions were considered in a range that would be suitable for an air-conditioning application. Through enlarging the designed area ratios by connecting the replaceable nozzles with a main body, optimum area ratios under air-conditioning working conditions were studied experimentally. Three parameters, namely, the entrainment ratio, cooling capacity as feed water heater under variable temperatures and pressures, and efficiency as pump are evaluated. With a fixed area ratio, experiments also show that the influence of the ejector area ratio on the ejector performance largely depends on the operating conditions. Consequently, the effects of operating conditions such as primary flow pressures on the ejector system performance are evaluated.

^a Ref. & Air Conditioning Engineering Techniques Department, Erbil Technical Engineering College, Erbil Polytechnic University, Erbil, Kurdistan Region, Iraq.

The initial development of a jet caused by fluid, body, and free surface interaction

Meurig Gallagher^a, David Needham^b

We consider the problem of a rigid plate, inclined at an angle $\alpha \in (0, \pi/2)$ to the horizontal, accelerating uniformly from rest away from a semi-infinite expanse of inviscid incompressible fluid, as shown in Figure 1. This work generalises that of Needham, Chamberlain and Billingham¹, who showed that, in the case of a plate accelerating *into* such a fluid, a weak jet rises up the plate when $t = 0^+$.

The sudden change in the uniform motion of a fluid and/or a surface piercing rigid body leads to the localised formation of a jet-like behaviour in the neighbourhood of the contact point between the free surface and the rigid body as the non-uniform transition takes place. This jet-like behaviour has significant consequences in practical applications; it can affect the stability of a floating and manoeuvring vessel and can cause damage to a rigid body structure, as in the case of flood defences being attacked by waves.

In modelling such jet-like behaviour, there are two approaches that are widely used. Namely, investigation of scale-model experiments and the construction of a full numerical solution to the set of governing hydrodynamic equations with corresponding initial and boundary conditions. We use the method of matched asymptotic expansions to investigate the asymptotic structure of the solution to our problem as $t \rightarrow 0^+$.

In this talk I will present the previous work in this field, including the models for the case of an inclined accelerating plate. Particular attention will be devoted to the inner and inner-inner asymptotic regions in the vicinity of the intersection point of the rigid plate and the fluid free-surface, as it is in these regions that the initial interaction between the plate and the fluid takes place.

^a School of Mathematics, University of Birmingham, Birmingham B15 2TT

^b School of Mathematics, University of Birmingham, Birmingham B15 2TT

¹ Needham et al. *The Quarterly Journal of Mechanics and Applied Mathematics*, **61**(4) 581 (2008.)

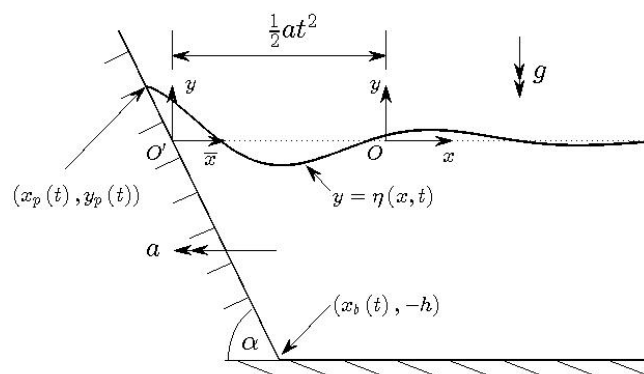


Figure 1: Definition sketch showing the displacement of the plate and the free surface at a time

Optimal forcing of subsonic jets

O. Semeraro^a and L. Lesshafft^a

We investigate the instability and the noise generation of turbulent, subsonic jets for three experimentally obtained datasets characterised by high Reynolds number and ranging from moderate to higher Mach number ($Ma=0.4, 0.6$ and 0.9).

Jet flows are known to amplify ambient noise due to their strong convective nature (amplifier-type flows); the main aim is to address the presence of linear wavepackets that recent experimental investigations have identified as the responsible flow structures for acoustic radiation¹. To this end, stability analysis is carried out in a fully non-parallel framework by analysing the optimal frequency response of the flow to external, harmonic excitations. The formalism relies on the singular mode analysis of the linear global resolvent operator². The strategy is particularly advantageous due to its robustness³; moreover, compared to temporal stability analysis (“global modes”), it provides a more insightful modal representation for the noise-amplifier flows.

Fully compressible Navier-Stokes equations are introduced for the modal analysis, based on higher-order finite-difference schemes for the numerical discretization. The effects of turbulence are taken into account through the use of a turbulent viscosity, based on the mixing length. The numerical setup enables us to investigate the exact acoustic far field within the linear approximation. Two different objectives are used for the optimization: the maximum energy of the near-field wavepacket and the maximum radiated acoustic power. A comparison will be proposed with recent results carried out using parabolised stability equations (PSE)⁴, and linearized Euler equations (LEE)⁵

In Fig. 1a the turbulent mean flow is shown ($Ma=0.4$), while in Fig. 1b the resulting axisymmetric dilatation field is depicted.

^a LadHyx, Ecole Polytechnique – CNRS, 91128 Palaiseau, France

¹ Jordan & Colonius, *Annu. Rev. Fluid Mech.* **45** (2013).

² Monokrousos et al., *J. Fluid Mech.* **650** (2010).

³ Garnaud et al., *Phys. Fluids* **25**, 044103 (2013)

⁴ Cavalieri et al., *ALAA*, 2011-2743 (2012)

⁵ Baqui et al., *ALAA*, 2013-2087 (2012)

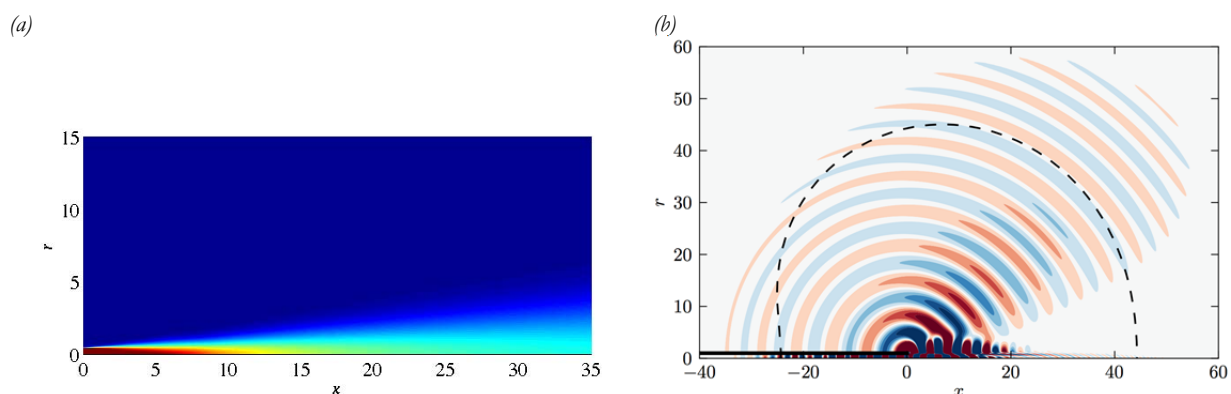


Figure 1: (a) Mean axial velocity distribution ($Ma=0.4$). (b) Dilatation field for the optima axisymmetric response

Dynamics of a flashing liquid jet

Avick Sinha^a, Sridhar Balasubramanian^a, Shivasubramanian Gopalakrishnan^a

The study of liquid flashing phenomena that occurs at high temperature and pressure is important in avionics, nuclear and automotive industries. The flashing phenomenon occurs when both aerodynamic fragmentation and violent boiling controls the flow dynamics of a multi-phase fluid jet. The enthalpy of the fluid needs to be above the local or saturation enthalpy at the downstream location for the flash-boiling of the fluid to take place. The mass flow rate may drastically get reduced due to the phase change process and the time scale over which it occurs is comparable to the time required for the liquid to flow through the nozzle. In order to model such finite rate process, Homogenous Relaxation Model (HRM) ¹ will be employed. There are many factors governing the atomization of a liquid jet inside a chamber but most importantly, the inlet pressure, temperature and the flow characteristics of the fluid inside the injector nozzle plays a significant role. Understanding the physics and mechanism of superheated jets is still a fairly open problem. Spray characteristics in terms of droplet size distributions, spread angle, penetration length will be obtained in this study. Both internal and external flow of the jet will be studied to understand the physics behind jet disintegration. Numerical modelling will be carried out to study the droplet characteristics and velocity profiles of flashing jets. To validate the numerical results, experimental studies will also be conducted to measure the bulk parameters such as, spread angle, penetration and breakup length. In real situations, the flashing flow in aero combustion chamber is compressible and superheated however as a first step, incompressible, cold flow assumption is made to benchmark the model. As shown in Figure 1, lighter fluid (red colour in phase diagram) from the nozzle comes out as two dimensional, axisymmetric jet into a chamber containing heavier fluid (blue colour in phase diagram) which is at atmospheric condition. The volume of fluid model ² is chosen to simulate the multiphase problem. Standard $k-\epsilon$ turbulence model ³ is used to model the turbulence and dissipative phenomenon. The axial distance has been non-dimensionalized using the total length of the chamber, $y^*=0$ and $y^*=1$ represents the bottom plate and nozzle exit respectively. It is observed that because of sharp gradient, the heavier fluid get entrapped into the lighter fluid. The effect of viscosity changes the profile from top-hat to Gaussian. The effect of temperature is currently being incorporated into the HRM model.

i

^a Dep, Mechanical Engineering, IIT Bombay, Powai 400076, Maharashtra, India.

¹ Lee et al., *Proceedings of the combustion institute*, **32**, 3215 (2009).

² Hirt et al., *J.Computational Physics*, **39**, 201 (1981).

³ Jones et al., *Int. Journal of heat and mass transfer*, **15**, 301 (1972).

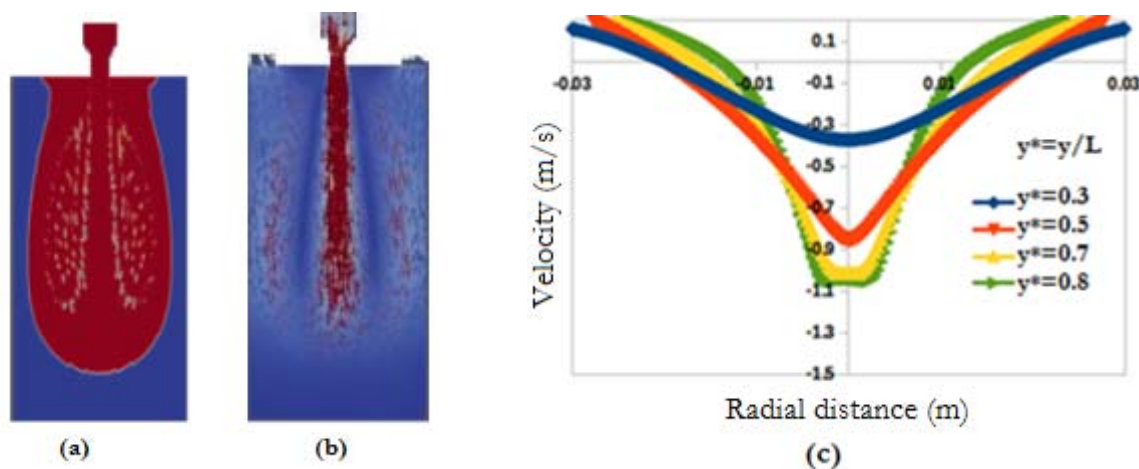


Figure 1: (a) Phase diagram (b) Vector diagram (c) Velocity profiles at different axial location for $Re=12,600$.

LIF measurements of the jet behind a sphere moving vertically in a stratified fluid

S. Okino^a, S. Akiyama^a and H. Hanazaki^a

It is well known that the fluid in the ocean and the atmosphere has a density gradient in the vertical direction. Smaller scale phenomena such as the motion of the buoys for the ocean observation and the zooplanktons are dominated by the vertical fluid motion, and the buoyancy force plays a crucial role. In this study, we have experimentally observed the flow behind a sphere moving vertically downward at constant speeds in a salt-stratified fluid. In previous experiments using shadowgraph methods and dye visualizations by Hanazaki et al.¹, it has been found that a strong vertical “jet” is generated upward of the descending sphere. The wake patterns behind the sphere are determined by the Froude number Fr and the Reynolds number Re .

Planer-distributions of the density around the jet are measured using a laser-induced fluorescence (LIF) method as shown in figure 1. The buoyancy force makes the lighter fluid dragged down by the sphere return near its original height, generating the vertical jet. It is found that the thickness of the density boundary layer and the width of the jet become thinner under stronger stratification. This is because the return occurs sooner by the stronger buoyancy and the volume of the fluid dragged by the sphere becomes smaller. Thinner boundary layer explains also the thinner jet, since the latter is a continuation of the boundary layer across the upper stagnation point of the sphere. The Froude number dependence of the jet width obtained by the experiments and the numerical simulations² is presented in figure 2. Both results agree well, showing the linearity to the square root of the Froude number. The linearity is explained by the dimensional analysis assuming the length scale of density is determined by the diffusion coefficient and the Brunt-Väisälä frequency.

^a Dep. Mechanical Engineering and Science, Kyoto University, Kyoto-daigaku Katsura, Nishikyo-ku, Kyoto, Japan

¹ Hanazaki et al., *J. Fluid Mech.* **638**, 173 (2009).

² Hanazaki et al., submitted to *J. Fluid Mech.* (2014).

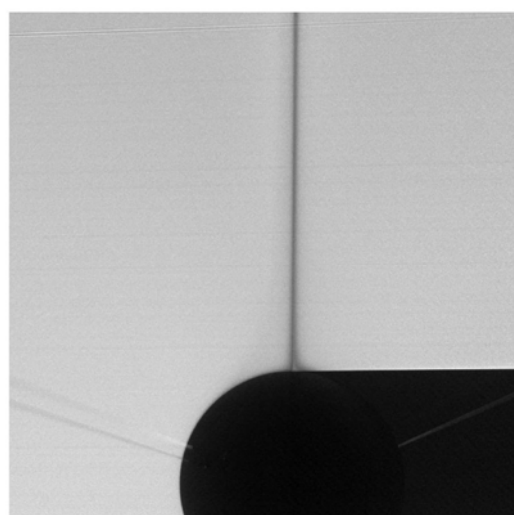


Figure 1: Non-dimensional density distribution around the sphere for $Fr=0.8$, $Re=180$. The density is non-dimensionalised by the diameter of the sphere and the vertical gradient of the basic density field. The laser sheet emitted from the left makes a shadow at the right side of the sphere.

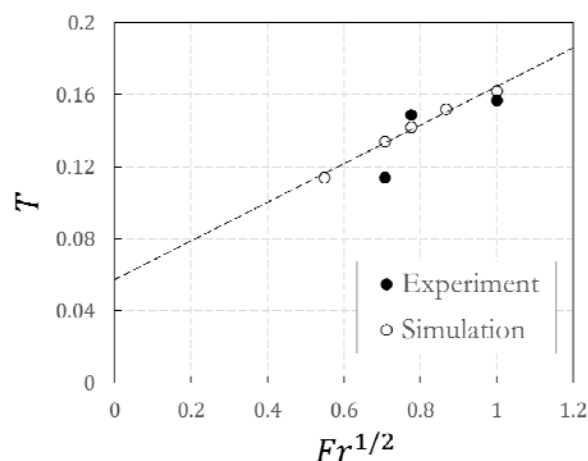


Figure 2: Froude number dependence of the jet width T .

A focused liquid jet with cavitation bubbles

A. Kiyama^a, Y. Noguchi^a, Y. Tagawa^a

A focused liquid jet is of great importance in many industrial applications such as medical devices. The jet can be induced by pressure impulse and a concaved liquid-air interface¹⁻³. In order to understand its mechanism, we describe a theory using a pressure impulse approach¹ and considering kinematic flow focusing^{2,3}. We also conduct systematic experiments using a high-speed camera for verifying the theory. A test tube filled, freely falls and impacts a rigid floor, leading to the generation of the jet. The experimental parameters are the depth of a liquid l , the initial velocity given to the liquid U_0 and the diameter of the test tube d .

We find that the jet velocity V_{jet} linearly increases with the initial velocity U_0 within certain experimental conditions as predicted by the theory (Fig. 1(A)). In another conditions, however, the jet can be faster than the theoretical value as shown in highlighted area of Fig. 1(B). It shows that the jet velocity increment can be larger for larger depth of a liquid l . In this case, cavitation bubbles emerge inside a liquid. Here we further examine a relation between the velocity increment of a jet and cavitation. Fig. 1(C) shows that the jet velocity monotonically increases with the maximum volume of cavitation bubbles. Thus it indicates that the cavitation bubbles play a significant role in the velocity increment. For describing the condition of the cavitation occurrence, we introduce the cavitation number Ca as a criterion. The applicability of the criterion is confirmed by additional experiments. The fact found in this presentation may shed light on positive effects of cavitation for fluid devices.

^a Dep. Mech. Sys. Eng., Tokyo University of Agriculture and Technology, 2-24-16 Nakacho, Koganei, Tokyo, Japan

¹ Antkowiak et al., *J. Fluid Mech.* **577**, 241 (2007)

² Tagawa et al., *Phys. Rev. X* **2**, 031002 (2012)

³ Peters et al., *J. Fluid Mech.* **719**, 587 (2013)

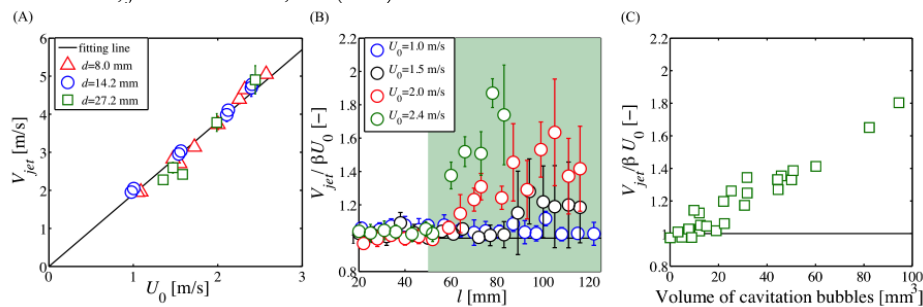


Figure 1: (A) Jet velocity V_{jet} vs. initial velocity U_0 for $20.0 \text{ mm} < l < 50.0 \text{ mm}$. The V_{jet} linearly increases with U_0 . (B) Dimensionless jet velocity $V_{jet} / \beta U_0$ vs. depth of liquids l , where β is 1.90. The jet can be faster than the theoretical value for larger l . (C) Dimensionless jet velocity $V_{jet} / \beta U_0$ vs. volume of cavitation bubbles. The jet velocity monotonically increases with the volume of cavitation bubbles.

Acoustic streaming jets in water

B. Moudjed^a, V. Botton^a, D. Henry^a, S. Millet^a, H. Ben-Hadid^a, J.P. Garandet^b,

We present our work on acoustic streaming free jets. These jets are steady flows generated far from any wall by progressive acoustic waves. The approach combines an experimental characterization of both the acoustic field (hydrophone) and the obtained acoustic streaming velocity field (PIV visualization) on one hand, with CFD using an incompressible Navier-Stokes solver on the other hand.

It is shown that good comparisons between experimental and numerical results can be obtained with a theoretical model based on a linear acoustic propagation model accounting for diffraction coupled to a hydrodynamic model including inertia effects. The coupling is obtained by the introduction of a momentum source term, the acoustic streaming force f_{ac} , in the hydrodynamic model such as $f_{ac} = 2\alpha I_{ac}/c$, where α is the sound absorbing coefficient, I_{ac} , the acoustic intensity and c , the sound celerity in the fluid. Both experimentally and numerically, the shape of the flow is thus found to be directly affected by both the overall shape of the acoustic beam and the local variations in acoustic intensity. This is in particular the case in the acoustic near field as depicted in figure 1. Otherwise, an oscillatory feature of the hydrodynamics jet was observed in the far field of the present experimental configuration.

Finally, an order of magnitude analysis leads to two scaling laws for the streaming velocity level with the acoustic power. A dimensional analysis is also performed and shows that small acoustic powers can yield relatively high Reynolds numbers and velocity levels in liquid metals like sodium or silicon; this could be a benefit for heat and mass transfer applications but a drawback for ultrasonic velocimetry as Acoustic Doppler Velocimetry (ADV) which is frequently used in opaque MHD.

^a LMFA, UMR CNRS 5509, Université de Lyon, ECL/INSA Lyon/Univ. Lyon 1, 36 avenue Guy de Collongue, 69134 Ecully Cedex, France.

^b LIEF, CEA-Saclay, 91191 Gif-sur-Yvette cedex, France

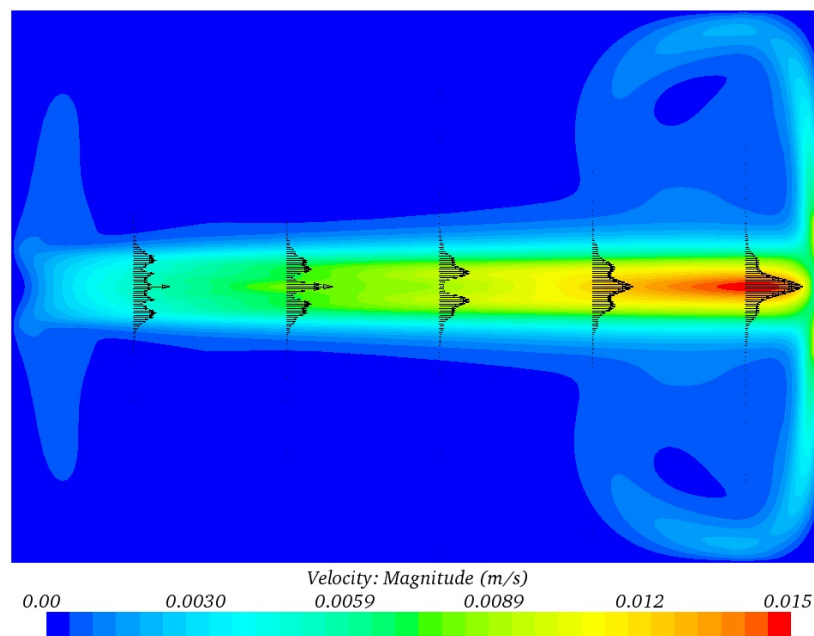


Figure 1: Numerical velocity field in the horizontal plane including the beam axis of a 29mm diameter circular plane transducer which emitted ultrasound at 2MHz. Acoustic force profiles are also plotted with arrows.

Turbulent breakup and dispersion of droplets of a phosphorescent jet

D.D. van der Voort^a, W. van de Water^a, N.J. Dam^b, H.J.H. Clercx^a and G.J.F. van Heijst^a

The breakup of a high speed turbulent liquid jet is of high importance in the field of combustion¹. The breakup mechanism determines the size of the produced droplets and has an impact on the generation of pollutants. In this study the dispersion of fluid particles in a water jet is investigated using a phosphorescent Europium-TTA-TOPO solution with a relatively long half-life². By exciting a small volume of the dye using a Nd:YAG laser at 355 nm, the jet will emit light around 613 nm for up to a millisecond, that can be imaged using an intensified high speed camera capable of recording at a speed of 40 kHz.

The nozzle used to create the jet consists of a capillary with a length of 2mm and a diameter of 200 μ m. A novel mount is developed which allows for both external and internal excitation of the phosphorescent dye. Using internal excitation the fluid can be analysed from a Lagrangian point of view, showing the breakup mechanism from the moment it exits the nozzle. An example of a relatively slow jet is shown in figure 1, where the emergence of the tagged fluid from the nozzle is developing over time.

Using external (sheet) excitation, the dispersion of the jet can be quantified. The experiment is repeated with a frequency of 10Hz, and ensemble averaged over ~ 300 sequences. An example is shown in figure 2. By averaging the data over a dimension, as shown for the radial direction in figure 3, a measure of the dispersion in the jet can be achieved. First qualitative and quantitative results are reported together with a complete overview of the possibilities and challenges of using phosphorescence in the measurements of breakup and dispersion.

^a Dep. Applied Physics, Eindhoven University of Technology, Eindhoven, The Netherlands

^b Dep. Mechanical Engineering, Eindhoven University of Technology, Eindhoven, The Netherlands

¹ Dec, *SAE Technical Paper* 970873 (1997)

² Arnaud., *Spectrochimica Acta part A*, **59**, 1829 (2003)

³ Reitz, PhD. Dissertation, Princeton, (1978)

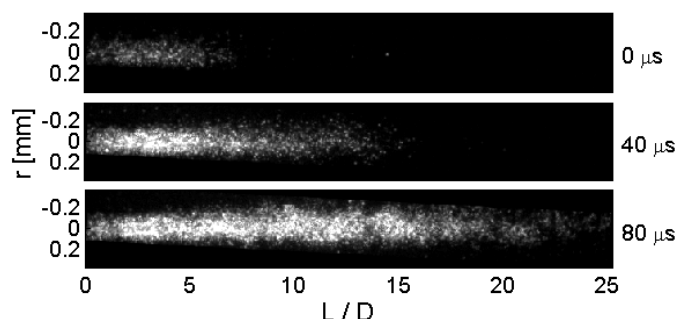


Figure 1: A sequence of consequent images of a 46 m/s jet internally excited jet taken at 0, 40, and 80 μ s after emergence of phosphorescent fluid from the nozzle.

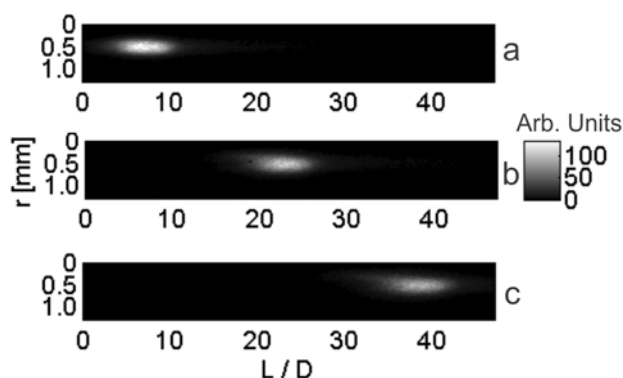


Figure 2: Ensemble average of a tagged 125 m/s jet (a) visualized 25 μ s (b) and 50 μ s (c) after excitation.

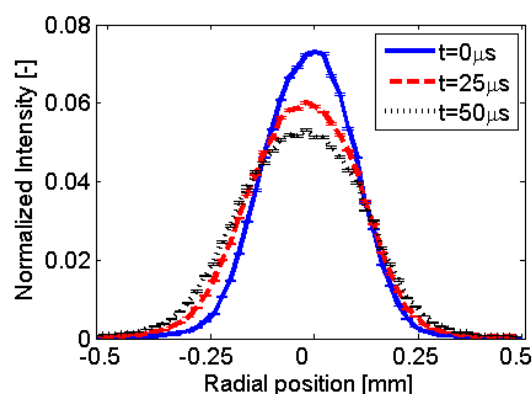


Figure 3: Normalized intensity of figure 2, averaged over the axial direction, showing std. dev. Over 300 sequences.

Experimental Study of Dispersed Buoyant Jet in a Linearly Stratified Medium

Harish N^a, Shubham Yadav^b, Sridhar Balasubramanian^c

Stratification, i.e. density or temperature variation with height is ubiquitous in many geophysical and engineering flows in nature¹. The study of flows with density variations has applications to ocean and atmospheric mixing, open channel hydraulics, gravity currents, ocean overflows, volcanic eruption etc. The presence of stratification alters the turbulent mixing behaviour, thus posing a challenging fluid dynamics problem having important consequences in physical modelling of such flows. In this communication, the entrainment dynamics of a positively buoyant vertical jet into a linearly stratified medium is discussed based on the evolution of large-scale and small-scale flow structure. The experimental facility for this study mainly consists of two square acrylic tanks. One of them is the main

tank, which is linearly stably-stratified ($\frac{d\rho}{dz} < 0$) with the help of water and commercial salt (NaCl). The

density profile in the main tank was measured using a conductivity probe (Delta Ohm: model HD 2106). Water from the secondary tank was pumped into the main tank using a jet nozzle. High resolution camera and commercial dye are used to measure the mixing characteristics of the ensuing buoyant jet. The experiments were carried out for different values of gradient Richardson number (Ri_{go}) to understand the effects of momentum and buoyancy fluxes on the entrainment and mixing mechanisms. Experiments were carried out without the dispersed phase (i.e. no particles) and with dispersed phase, i.e. with dilute particle concentrations (glass beads with diameter of 100-150 μm , $\Theta < 1\%$). Bulk flow parameters were obtained by performing image analysis using MATLAB. The trap height, defined as the height at which the plume traps in the linearly stratified medium and starts moving horizontally, was measured and compared with theoretical results². Secondly, radial intrusion of the plume in the neutral buoyant layer, shown in figure 1(a), was measured as function of time, t , for the single phase and dispersed phase. As seen from the figure, the radial propagation of the dispersed plume is lower compared to the single phase plume. This could be attributed to the particles drag that slows down the plume propagation. The thickness of plume intrusion, $h(r,t)$, was also compared and is shown in figure 1(b). For the case of dispersion phase, we observed the plume had higher thickness and slower intrusion propagation (radially) compared to the single phase plume. This could be due to the presence of particles in the neutral buoyant layer that pulls the plume vertically down, thus increasing the thickness.

^{a, b, c} Dept of Mechanical Engineering, IIT Bombay, Maharashtra, India

¹Turner, J. *Fluid Mech.*, **173**, 431(1986)

²Morton et al, *Proc. R. Soc. London*, **234**, 1196 (1956)

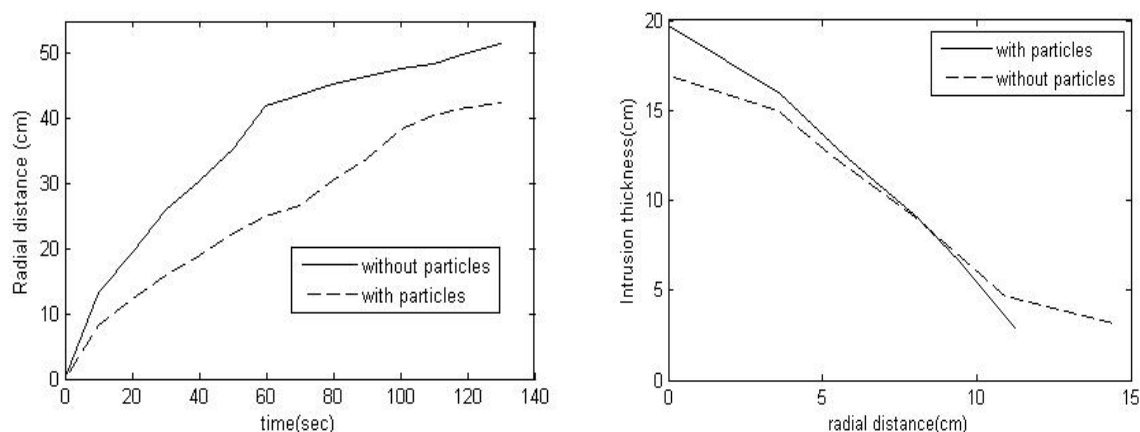


Figure1: (a) Radial intrusion as function of time for stratification strength with Brunt-Väisälä frequency $N=0.28\text{s}^{-1}$. (b) Plume thickness as function of radial distance for $t=40\text{sec}$.

Dispersion in steady and unsteady turbulent jets. Theory and direct numerical simulation.

J. Craske^a and M. van Reeuwijk^a

In this presentation we study the physics of statistically unsteady turbulent jets. Specifically, we present results from the direct numerical simulation of a steady jet and a jet subjected to an instantaneous step-change (both up and down) in the source momentum flux. For the steady case our focus is on the value of several dimensionless flux and turbulence production parameters. These parameters have an influential role in the unsteady case, where we pay particular attention to the propagation speed and rate of spread of the resulting fronts. We show that accurate prediction of the propagation speed requires information about the rate at which energy is transported. In addition, we demonstrate that the evolution of the fronts is a self-similar process that accords to the classical dispersive scaling $z \sim t^{1/2}$. In the analysis of the problem we demonstrate that the use of a momentum-energy framework of the kind used by Priestley and Ball (1955) has several advantages over the classical mass-momentum formulation. In this regard we extend and generalise the work of Kaminski et al. (2005) to unsteady problems, neglecting only viscous effects in the governing equations.

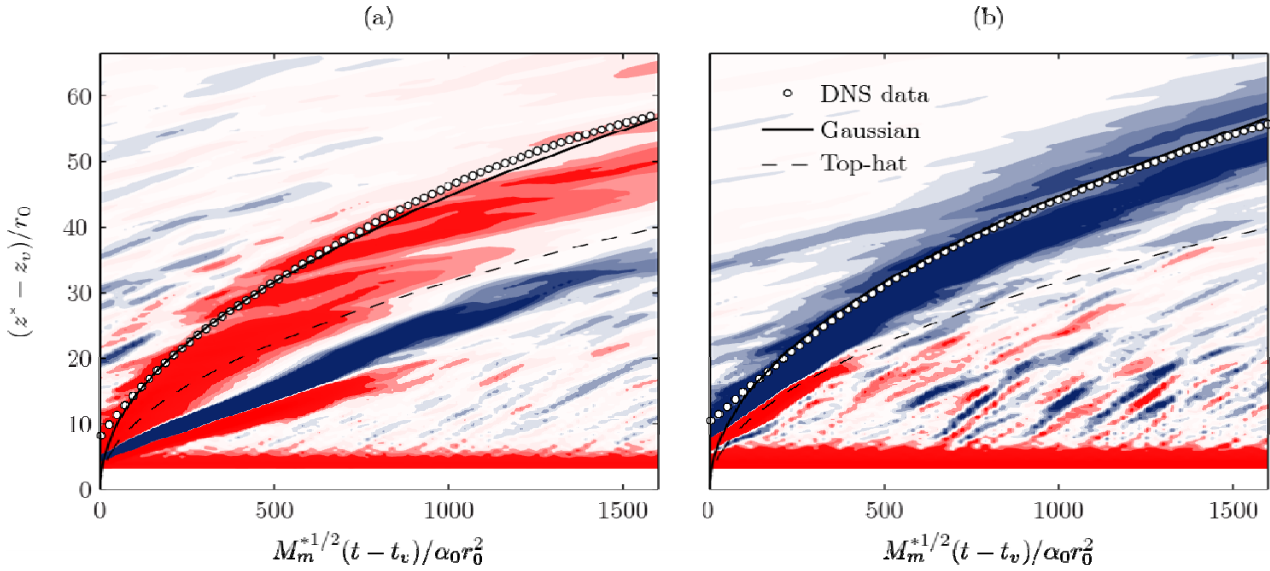


Figure 1: Position of an unsteady front in a jet subjected to a sudden decrease (a) and increase (b) in the source momentum flux. The position obtained from DNS data is compared to theory, assuming a Gaussian or uniform ('top-hat') distribution of vertical velocity. The data is plotted over iso-regions of the vertical gradient of the momentum flux.

Using the energy-momentum framework, we show that dispersion originating from non-uniform velocity profiles plays a fundamental role in longitudinal transport. Indeed, one is able to find dispersion in the steady state, although it has received little attention because its effects can then be absorbed into the entrainment coefficient. Specifically, we identify two types of dispersion. Type I dispersion exists in a steady state and accounts for the fact that energy is transported through the system faster than momentum due to the shape of the vertical velocity profile. In unsteady jets type I dispersion is responsible for the separation of characteristic curves and for the hyperbolic, rather than parabolic, nature of the governing equations. Type II dispersion is equivalent to Taylor dispersion and results in the longitudinal mixing of fronts. This mixing is achieved by local deviation from the self-similar profiles that one finds in steady jets.

Our work addresses the recent observation that several unsteady plume models are ill-posed³. We develop a simple but robust model for unsteady jets, which incorporates dispersion of type I and II. In contrast to existing models for unsteady plumes, our model is in good agreement with the simulation data.

^a Dept. Civil and Environmental Engineering, Imperial College London, SW7 2AZ, UK

¹ Priestley and Ball, *Quarterly Journal of the Royal Meteorological Society* **81**, 348 (1955)

² Kaminski et al., *J. Fluid Mech.* **526** (2005)

³ Scase and Hewitt, *J. Fluid Mech.* **697** (2012)

Non-Boussinesq forced turbulent fountains

R. Mehaddi^a, O. Vauquelin^a and F. Candelier^a

The behaviour of a non-Boussinesq turbulent fountain (air-helium mixture injected downward into ambient air) is studied experimentally. Such a flow covers various applications in industry (pollutant dispersion, ventilation of buildings) and in nature (replenishment of magma chamber, lava fountains). The majority of the past studies^{1,2} have focused on Boussinesq fountains only, and it was well established that, in this case, the fountain height H can be written as :

$$H = 2.46 b_i Fr \quad \text{with} \quad Fr = w_i / (g \eta b_i)^{1/2}$$

where Fr is the Froude number, b_i is the radius of the fountain at the source, $\eta = (\rho_0 - \rho_i)/\rho_0$ is the density deficit at the source, ρ_0 and ρ_i are, respectively, the ambient density and the density of the fountain at the source and w_i is the fountain bulk velocity at the source.

The purpose of the current study is to investigate the non-Boussinesq effects (large density differences) on the fountain height by means of laboratory experiments (see figure 1) covering a wide range of Froude conditions ($3 < Fr < 45$) under turbulent conditions.

These experiments show that the previous (Boussinesq) relation is no longer valid for large density contrasts. A modified relation is then sought in the form $H = 2.46 b_i Fr f(\rho_i/\rho_0)$. As shown in figure 2, experimental results lead to a function f given as the square root of the density ratio.



Figure 1 – Photo taken from experiments ($Fr = 13.2$ and $\rho_i/\rho_0 = 0.6$)

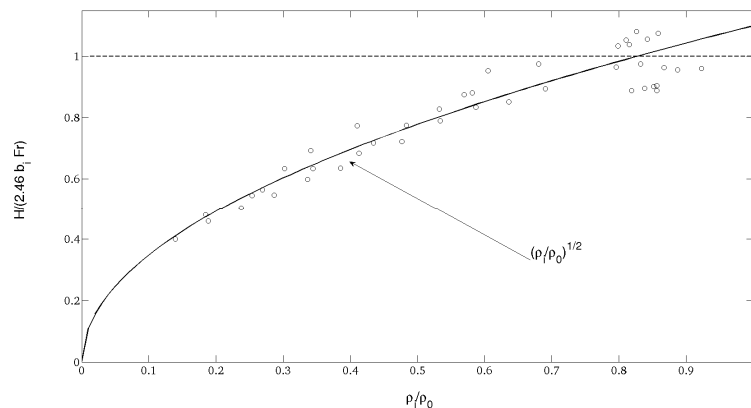


Figure 2 – Non-dimensional fountain height as a function of the density ratio ρ_i/ρ_0 .

As a consequence, for a non-Boussinesq turbulent fountain, the height can be given as $H = 2.7 b_i Fr_{NB}$ where Fr_{NB} is the so-called non-Boussinesq Froude number defined from the density difference $\eta^* = (\rho_0 - \rho_i)/\rho_i$.

From these experiments, fountain height fluctuations have also been investigated. We are led to a standart deviation $H_{rms} = 0.18 b_i Fr_{NB}$.

^a IUSTI CNRS 7343, Aix-Marseille University, 5 rue Enrico Fermi, 13 453 Marseille, France.

¹ Turner, J. S., *J. Fluid Mech.*, **26**, 779 (1966).

² Bloomfield L. J. and Kerr R. C., *J. Fluid Mech.*, **424**, 197 (2000).

Numerical simulations of a liquid sheet surrounded by a fast stream: interaction between phase interface dynamics and coherent vortices

N. Odier^a, G. Balarac^a and C. Corre^a

Air-assisted liquid jets have been studied for many years because of their key use in several aircraft propulsion systems. For liquid jets surrounded by a high-speed stream of gas, a large-scale dynamic of the liquid is observed both on plane¹ and axisymmetric² configurations. The occurrence conditions and frequency of this so-called flapping phenomenon remain poorly understood due to the large number of parameters involved in the analysis. Besides, the near field in such flow configurations is characterized by intense shear layers, which can lead to various coherent vortices. The main goal of this work is to better understand the interaction between these coherent vortices and the flapping phenomenon.

Plane liquid jets surrounded by a fast stream are numerically studied using the massively parallel finite-volume code YALES2³. The interface between phases is accurately tracked with a conservative level-set method and coupled with the momentum equation thanks to a ghost-fluid method⁴. The simulations are performed at moderate Reynolds and Weber numbers, $Re = 4000$ and $We = 500$, based on the liquid jet thickness, the velocity and the molecular properties of the rapid stream. The velocity ratio and the density ratio between the fast stream and the liquid jet are 6 and 0.1, respectively.

The first configuration analyzed in this work is such that the stream surrounding the liquid jet is a uniform high-speed co-flow. The only shear layers present in the flow are created at the liquid/gas interface where the liquid and surrounding fast stream boundary layers merge. As shown in Figure 1, a large-amplitude flapping occurs close to the jet inlet, with intense spanwise vortices generated downstream the flapping oscillations. The flapping dynamics has been parametrically studied and a linear variation of its frequency with the inlet boundary layer thickness of the surrounding stream has been evidenced.

In the second flow configuration, the surrounding stream is two-layered: a high-speed stream of given width is surrounded by a low-speed co-flow. In addition to the shear layers developing at the liquid / gas interface, monophasic shear layers also develop between the high and low-speed stream. As illustrated in Figure 2, these additional shear layers display the usual scenario of free shear flow development, which begins with the generation of Kelvin-Helmholtz vortices. Next, and depending on the width of the high-speed stream, the interaction of coherent vortices between both shear layers can limit the flapping amplitude. Our current research effort is focused on a refined understanding of the relationship between the flapping occurrence and inlet condition flow features.

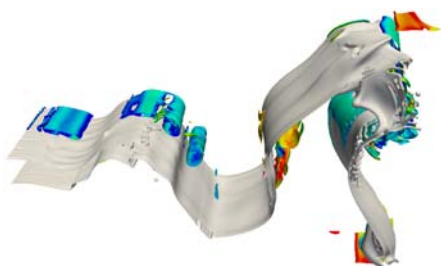


Figure 1: Phases interface (grey) and coherent vortices (isosurface of Q criterion, colored by the spanwise vorticity) for the first flow configuration

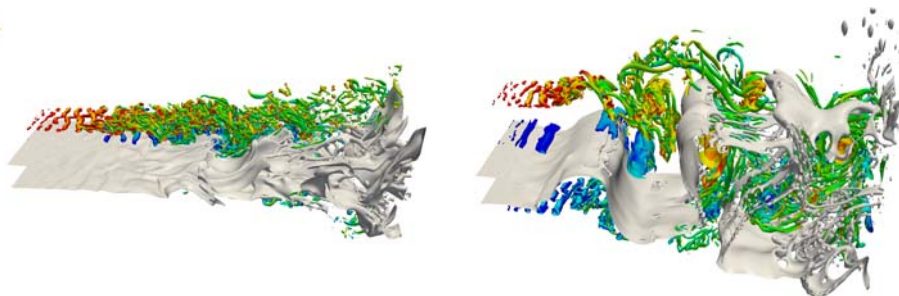


Figure 2: Phases interface (grey) and coherent vortices (isosurface of Q criterion, colored by the spanwise vorticity) for the second flow configuration, with two different widths (width on left smaller than width on right) for the high-speed stream.

^a Grenoble-NP/CNRS/UJF-Grenoble 1, LEGI UMR 5519, Grenoble, F-30841, France

¹ Lozano et al., *J. Fluid Mech.* **437**, 143 (2001).

² Matas et al., *CR Mécanique*, **341**, 35 (2013).

³ Moureau, et al., *CR Mécanique*, **339**, 23 (2011).

⁴ Desjardins et al., *J. Comp Phys.* **227**, 8395 (2008).

Modal instability analysis of low-density jets

W. Coenen^a, L. Lesshafft^b, X. Garnaud^b and A. Sevilla^a

Low-density jets support global self-sustained oscillations when the jet-to-ambient density ratio is sufficiently small. This phenomenon has been linked to the presence of a region of local absolute instability in the underlying parallel base flow. However, the use of local stability analysis requires introducing ad-hoc criteria¹ to match the experimental observations². In the present work we therefore use a global approach, where the wavepacket structures are temporal eigenmodes of the linearized equations of motion in a 2D domain. As a base state we employ a numerical solution of the low-Mach number Navier-Stokes equations for a He/N₂ jet emerging into an ambient of N₂. The jet is characterized through the jet-to-ambient density ratio S , the Reynolds number Re , and the inverse of the dimensionless momentum thickness of the velocity profile at the jet exit plane, D/θ_0 .

The linear global mode analysis shows that for certain combinations of the control parameters S , Re , D/θ_0 , an isolated eigenmode dominates the eigenvalue spectrum, and its associated growth rate varies with the values of these control parameters. Figure 1(a) shows a case where an isolated eigenmode is located at $St = 0.29$ and $\omega_i \approx 0$. This is thus a marginally stable setting, and a small destabilizing departure in one of the control parameters should trigger the onset of a global self-sustained oscillation of the jet. Figure 2(c) shows how the neutral curve that can be constructed in this manner (dots) in the $Re - D/\theta_0$ plane for the case of a pure He jet ($S=0.143$), agrees encouragingly well with the experimentally measured² transition points (squares with error bars). However, for higher values of the Reynolds number, the construction of a neutral curve based on the spectrum becomes less robust, since for these cases the spectrum is dominated by a continuous branch of eigenvalues, sensitive to changes in domain length and grid refinement, as reported before for the case of a constant-density jet³. An example is shown in figure 1(b).

Finally, the flow response to external forcing in a globally stable setting is also investigated, through the computation of the pseudospectrum. At real frequencies, the response is found to be dominated by a resonance of the stable eigenmodes, and no clear effect of non-normality is found.

^a Área de Mecánica de Fluidos, Universidad Carlos III de Madrid, Av. Universidad 30, 28911 Leganés (Madrid), Spain

^b LadHyX, CNRS - École Polytechnique, 91128 Palaiseau, France

¹ Coenen W., Sevilla A., *J. Fluid Mech.* **713** (2012).

² Hallberg M.P., Strykowski P.J., *J. Fluid Mech.* **569**, 493-507 (2006).

³ Garnaud X. et al., *Phys. Fluids* **25**, 0044103 (2013).

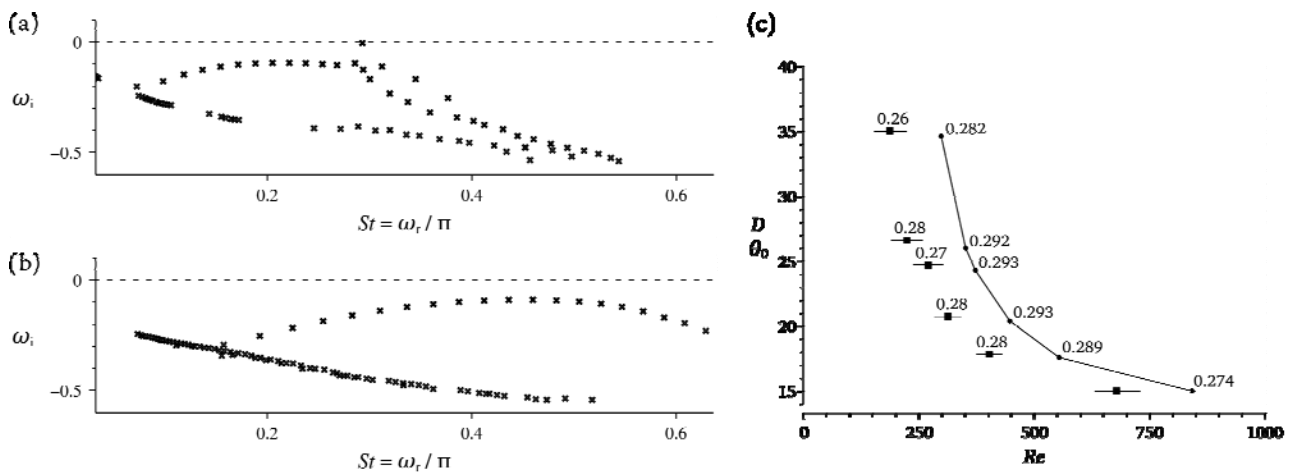


Figure 1: (a) Eigenvalue spectrum for a light jet with a jet-to-ambient density ratio $S = 0.143$, a Reynolds number $Re = 360$ and an initial momentum thickness $D/\theta_0 = 24$: an isolated eigenmode at $St = 0.29$ dominates the spectrum. The growth rate $\omega_i \approx 0$ indicates a marginally stable setting. (b) Spectrum for the case $S = 0.5$, $Re = 1000$, $D/\theta_0 = 24$: a continuous branch dominates the spectrum. (c) Onset of global instability for pure He jets ($S = 0.143$), from experiments² (squares with error bars), and from the linear global mode analysis (dots), together with the Strouhal numbers of the oscillating jet mode.

Real geometry effects and scaling of strain rate in a counterflow configuration

G. Scribano^a, A. Alsharawi^a, A. Attili^a, F. Bisetti^a

In a counterflow configuration, two opposed jets impinge and a Hiemenz-type stagnation flow is generated. In the region between the two nozzles, a laminar, steady mixing layer is established. Under appropriate simplifications, these flows are characterized by a single time scale or global strain rate. Counterflow configurations are adopted when the control of stream composition and mixing is needed. For this reason, it is a fundamental flow configuration in the study of combustion¹, chemical reactions, and nucleation of aerosols.

In Chapman², the analytical solution for the counterflow is presented for two nozzles separated by a distance $2L$ and assuming infinite nozzle diameter and zero inlet velocity gradient. The Reynolds number is defined as $Re = UL/2\nu$, where U is the bulk velocity at the nozzle outlet. The velocity along the centerline obeys a similarity solution of the form $u_c/U = f(x/L; Re)$. The Reynolds number is the governing parameter in the family of similarity solutions. As shown in Chapman², the solution becomes nearly independent of Re for $Re > 200$. In the limit of large Re , the gradient of the centerline velocity at the stagnation plane is $a = -2U/L$, indicating that the strain rate or flow time scales may be varied by changing the global strain U/L .

In real counterflows, the assumptions of infinite nozzle diameter and zero velocity gradient at the nozzle outlet may not be adequate. The real geometry effects on the dimensionless velocity gradient are the focus of this work.

Two different diameters D equal to 10 and 25 mm are considered. In the experiments, values of L/D equal to 0.25, 0.5, 1, and 2 are studied, and the Reynolds number is varied in the range 200 to 1200. PIV (Particle Image Velocimetry) is used to measure the velocity field between the two nozzles.

Two-dimensional numerical simulations are also performed. The full geometry of the nozzles is considered in the simulations for both the diameters used in the experiment. The solution is highly resolved and converged and the simulation the Reynolds number is varied in the range 10 to 4000 and L/D in the range 0.1 to 4.

The simulation results show a remarkable agreement with the PIV data, while there are differences between the experiments and the quasi one-dimensional analytical solution of Chapman². From the experiments, it is shown that θ'_0 depends on L/D , while the analytical solution implies a constant value. These findings are confirmed also by the numerical simulation for the same geometry and flow parameters.

The velocity field in the domain depends on the boundary layer development inside the nozzle just upstream of the exit plane and the effect of the stagnation plane on the incoming axial velocity. The boundary layer development depends on the nozzle geometry, while the separation distance controls the effects related to the stagnation plane.

^a Clean Combustion Research Center, KAUST, Saudi Arabia

¹ Tsuji, *Progress in energy combustion science* **8**, 93 (1982)

² Chapman and Bauer, *Applied Scientific Research* **31**, 3 (1975)

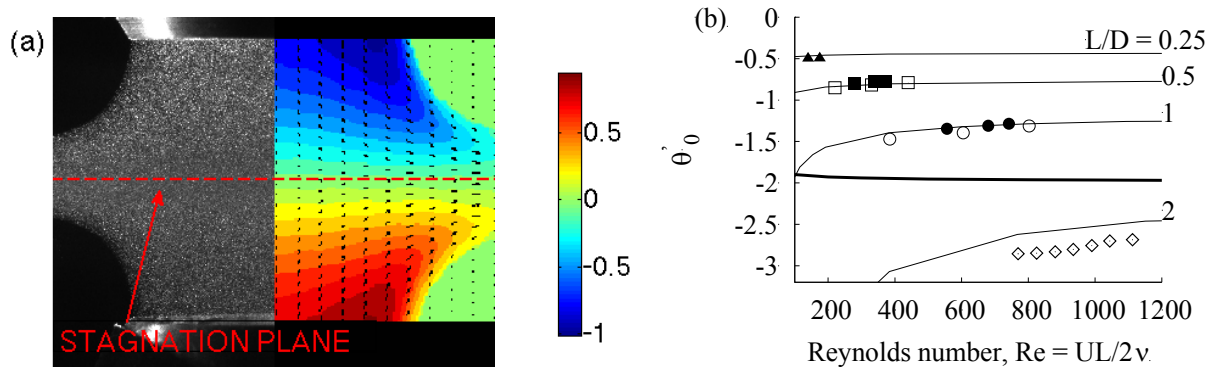


Figure 1: (a) PIV image and post processed velocity and vector field. (b) θ'_0 at the stagnation plane. Open symbols for $D = 10$ mm, closed symbols for $D = 25$ mm. Lines for two-dimensional simulation (solid lines) and analytical solution (bold solid line)

Transition to jetting in a dripping faucet at high Bond numbers

M. Rubio-Rubio^a, P. Taconet^a, I. Chakraborty^a and A. Sevilla^a

When liquid is injected from a nozzle or tube at small flow rates into a stagnant gas under the presence of gravity, drops grow at the outlet until their weight overcomes the confining surface tension force, and droplet detachment takes place. In this *dripping regime*, the drop formation frequency increases with the liquid flow rate, until a critical value is reached at which an abrupt *transition to jetting* takes place¹⁻³. Three dimensionless parameters govern this process, which can be conveniently expressed through the Bond, Bo , Weber, We , and Kapitza, Γ , numbers, as natural measures of the injector radius, the flow rate and the liquid viscosity, respectively⁴.

Both the dripping regime and the transition leading to the jetting regime have been widely studied due to their importance in many applications¹⁻³. Specifically, a detailed description of the rich dynamics of a dripping faucet as a function of the flow rate and the liquid viscosity was reported in^{2,3}, where only two different values of Bo were considered. Since recent work⁴ has highlighted the interest of capillary jets at large Bo , the present study aims at extending previous works on the characterization of both the dripping-jetting transition, as well as the main features of the dripping regime, by using larger injector diameters that allow us to reach values of Bo considerably larger than those explored up to date. In particular, we report the results of new experiments on the dynamics of a dripping faucet for wide ranges of both Γ and Bo , being the latter up to one order-of-magnitude larger than the values considered in previous studies. In addition, we present numerical simulations of the dripping regime performed with a combined level-set-volume-of-fluid method, showing good agreement with our experiments. As an example, figure 1 shows the influence of the Weber number on two of the main characteristics of a dripping faucet, namely: (a) the limiting length of a drop at pinch-off and (b) the ratio between the volume of the detached drop and that of the liquid ligament that remains attached to the injector right after pinch-off, for a given liquid and a given injector diameter. The insets in figure 1(a) show the experimental shapes of the pendant drop at pinch-off, for two different values of the flow rate. This work has been supported by project number DPI2011-28356-C02.

^a Departamento de Ingeniería Térmica y de Fluidos, Universidad Carlos III de Madrid, 28911 Leganés, Spain

¹ Clanet and Lasheras, *J. Fluid Mech.* **383**, 307 (1999)

² Ambravaneswaran et al., *Phys. Rev. Lett.* **93**, 034501 (2004)

³ Subramani et al., *Phys. Fluids* **18**, 032106 (2006)

⁴ Rubio-Rubio et al., *J. Fluid Mech.* **729**, 471 (2013)

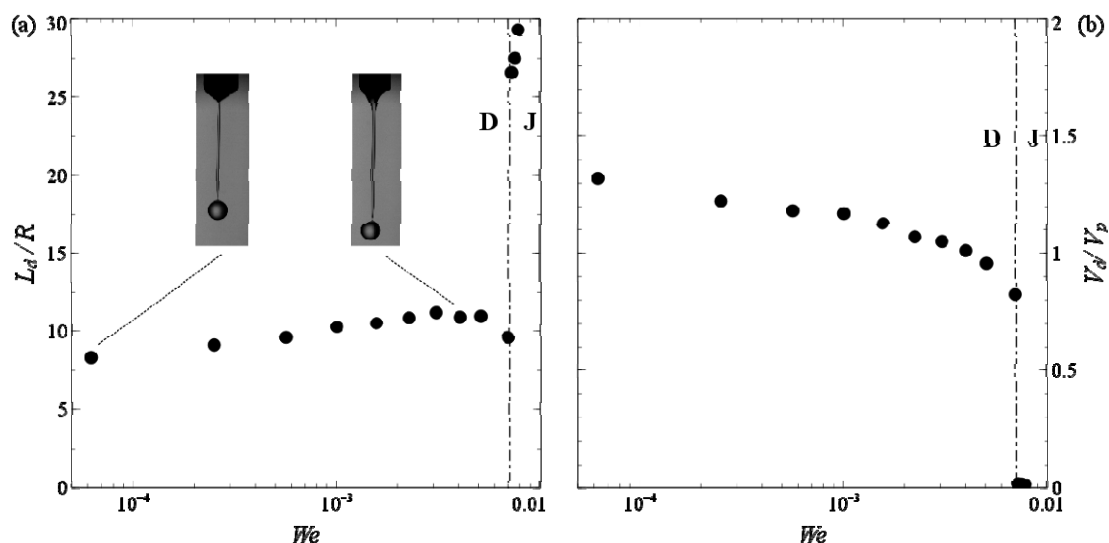


Figure 1: (a) Dimensionless limiting length of the pendant drop and (b) detached-to-pendant drop volume ratio, as functions of the Weber number, for $Bo = 3.42$ and $\Gamma = 0.84$.

Comparison of Eulerian and Lagrangean power auto-spectra in a turbulent jet

C. M. Velte^a, W. K. George^b, P. Buchhave^c and M. Wänström^d

Taylor's frozen field hypothesis can sometimes be a useful assumption when studying turbulent flow fields with measuring techniques such as hot-wire or laser Doppler anemometry. Taylor's assumption is especially valuable in the process of computing temporal power spectra from the same, but it is often applied without concern for whether the assumption is valid in the specific flow of concern. Different arguments have been presented in the past^{1,2} challenging this idea, at least for parts of the turbulence spectrum, and some factors affecting the successful application of Taylor's hypothesis have been identified³:

1. **Spatially non-uniform convection:** Various wavenumber components convected at different velocities.
2. **Unsteady convection:** The convection velocity is fluctuating, i.e., the smaller eddies are carried within the energy containing eddies. Further, temporal disturbances may be important.
3. **Aliasing:** Changes in convection velocity while travelling past the probe can cause spectral broadening.
4. **Anisotropy:** Produced by the mean shear stress.

Our study is therefore conducted in a high intensity and high shear flow constituted by a turbulent far axisymmetric jet at an exit Reynolds number of 20,000, comparing temporal and spatial power spectra across several transverse positions. Hot-wires are unsuitable for these types of flows due to their inability to distinguish the velocity components in the flow. Temporal and spatial power spectra from LDA and PIV, respectively, have therefore been used in the comparison.

The spatial spectra naturally require statistical homogeneity of the flow, which is predicted by the Equilibrium Similarity theory⁴ applied to the two-point Reynolds stresses and has been confirmed experimentally using planar PIV in a 0.4 m by 0.7 m field of view⁵, see Figure 1 (left). The PIV data are extracted in the streamwise direction from the logarithmically transformed and scaled velocity field, so called similarity coordinates. The 'random', but velocity dependent, sampling of the LDA requires special processing of the signal⁶ and the effects of the finite measuring volume can be crucial to the resulting spectra⁷, so this will also be discussed.

We have used Taylor's hypothesis to convert the spatial PIV spectra to time spectra using the measured mean velocity at each respective location. The time and space spectra comparison shows that the Taylor's hypothesis is not valid across the entire jet width, only approximately near the jet centre.

^a Dep. Mechanical Engineering, DTU, Nils Koppels Allé b. 403, 2800 Kgs. Lyngby, Denmark

^b Dep. Mechanical and Aerospace Engineering, Princeton University, Princeton, NJ 08544, USA

^c Intarsia Optics, Sønderkovvej 3, 3460 Birkerød, Denmark

^d Energimyndigheten, Eskilstuna, Sweden

¹ Fisher and Davies, *J. Fluid Mech.* **18**, 97 (1964).

² Lumley, *Phys. Fluids* **8**, 1056 (1965)

³ George, Hussein, Woodward, *10th Australasian Fluid Mech. Conf., U. Melbourne* **11 A - 2** (1989)

⁴ Ewing et al., *J. Fluid Mech.* **557** (2007)

⁵ Wänström, *PhD dissertation, Chalmers U. Tech.* (2009)

⁶ Velte, George, Buchhave, *Accepted for publ. Exp. Fluids* (2014)

⁷ Buchhave, Velte, George, *Exp. Fluids* **55**, 2 (2014)

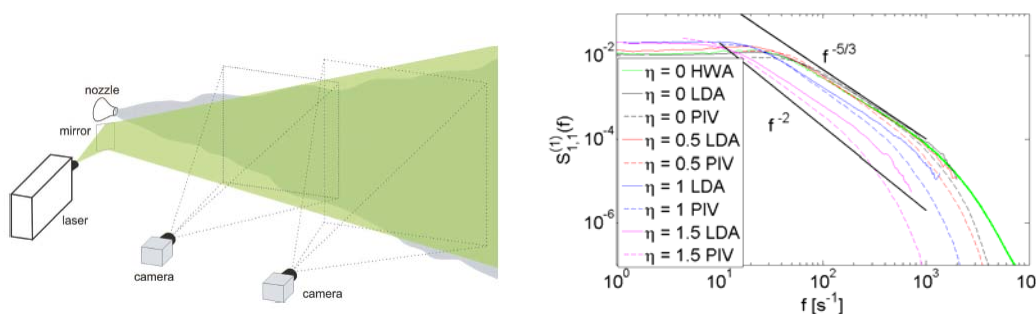


Figure 1: Left: Experimental setup. Right: Comparison of temporal and spatial power spectra from LDA and PIV.

Velocity statistics in Negatively Buoyant Jets

M. G. Badas^a, L. A. Besalduch, S. Ferrari and G. Querzoli

We have studied in the laboratory the velocity fields and their statistics, up to the fourth order, in two Negatively Buoyant Jets (NBJs) with different densimetric Froude numbers (Fr), and we have compared them with the relative ones in Simple Jet (SJ), with $Fr = \infty$.

A NBJ is a complex phenomenon that comprehends the features of both a SJ and a plume in a relatively small space, so not any asymptotic behaviour is reached and the physics of NBJ is nowadays not completely understood. For this reason and for their many practical applications NBJs (see Ferrari and Querzoli¹), there are many recent studies focusing on this topic (e.g., Oliver et al.², Lai and Lee³).

The experimental set-up simulates the sea discharge of brine, by-product of the desalination process, from a sharp-edged orifice in the lateral wall of a pipe laid on the sea bottom; see Ferrari and Querzoli¹ for more details. The velocity fields are obtained via FTV (Feature Tracking Velocimetry), a novel non intrusive image analysis method, described in Besalduch et al.⁴, which is less sensitive to the appearance and disappearance of particles, and to high velocity gradients, than classical Particle Image Velocimetry (PIV).

The accurate FTV measures allow us to present here an in-depth analysis of the velocity fields and of their statistics, from the first order ones (mean velocity fields, axial velocity decay), to the second order (Reynolds stresses, Turbulent Kinetic Energy), third order (skewness) and fourth order (flatness) ones. These statistics have been studied on profiles orthogonal to the NBJ axis and along the axis, and decomposing the velocity vectors in axial and radial components.

The results highlight the influence of Fr on the behaviour of NBJs and, in particular, the complexity of the physics in the region close to the maximum NBJ height, where the uprising branch interacts with the descending one. This complex behaviour is apparent also at values of Fr and release angles at which the concentration statistics, analyzed in previous studies, were not able to show.

^a DICAAR (Dipartimento di Ingegneria Civile, Ambientale e Architettura, University of Cagliari, via Marengo 2, Cagliari (Italy))

¹ Ferrari and Querzoli, *J. Hydr. Res.*, **48**, 5, 2010

² Oliver et al., *J. Hydr. Eng.*, **139**, 2013

³ Lai and Lee, *J. Hydro-Environ. Res.*, **6**, 2012

⁴ Besalduch et al., *EPJ WOC*, **45**, 2013

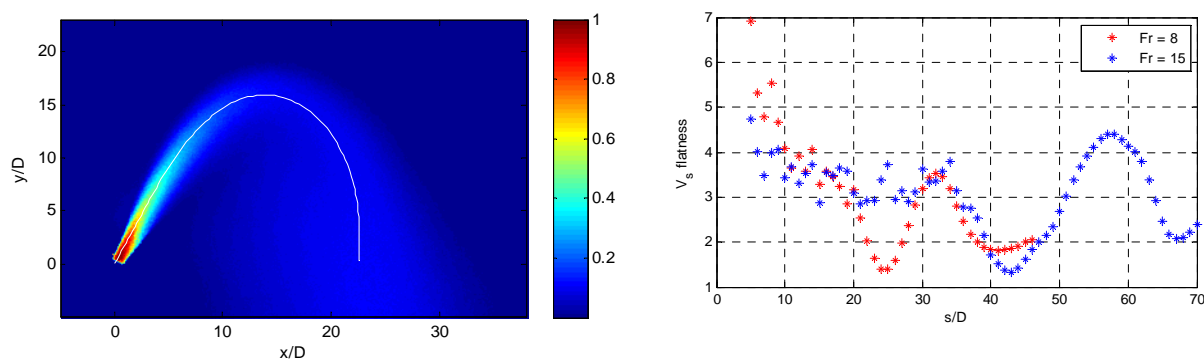


Figure 1: on the left, a map of the non-dimensional mean velocity U/U_0 (U_0 is the mean velocity at the jet origin) for a NBJ with $Fr = 8$, $Re = 1000$ and a release angle to the horizontal $\theta = 65^\circ$, the white line is the jet axis (defined as the locus of maximum intensity velocity); on the right, the flatness of the axial component of the velocity along the axis for the same NBJ on the left (red) and for a NBJ with the same Re and $Fr = 15$ (blue).

Internal Cavity Pressure and Work Analysis of a Pulsed Jet Underwater Thruster

M. Krieg^a and K. Mohseni^{a,b}

This study examines the fluid dynamics internal to the cavity of a pulsed-jet underwater thruster, during both jetting and refilling cycles. These dynamics are correlated to the total energy required to operate this type of thruster, and how this affects the propulsive efficiency of vehicles which use this technology. A theoretical model for the pressure distribution inside the cavity is derived in terms of total circulation generated within the cavity, taking advantage of the axial symmetry of the problem. A prototype thruster was fabricated specifically for this study to be completely transparent allowing DPIV measurements to be performed on the fluid inside the thruster cavity. Experimental testing was performed for both sinusoidal and impulsive refilling velocity programs, and different cavity geometries. The circulation based pressure modelling is validated using a load cell to measure the forces acting on the cavity plunger. It is observed that the total work required to refill the cavity is lower at all plunger starting heights is lower for the impulsive velocity program. Also the total work is generally reduced by lowering the starting height, except after a critical height where the work drops again. The work results are summarized in Figure 1.

^a Dep. Mechanical Engineering, University of Florida, Gainesville, FL, USA
Institute for Networked Autonomous Systems

^b Dep. Computer Science and Electrical Engineering, University of Florida, Gainesville, FL, USA

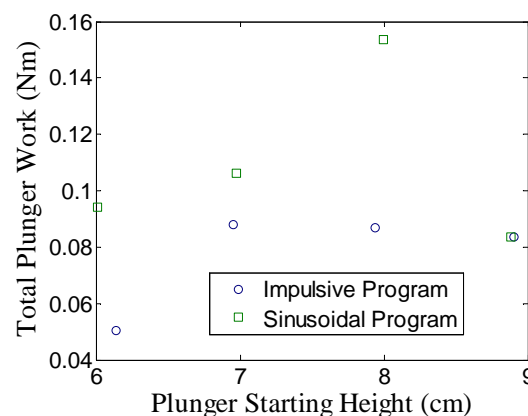


Figure 1: Total work required to fill the cavity for two different plunger velocity programs, and a range of plunger starting heights.

DNS of vector-controlled jet under a rotational mod

K. Tsujimoto^a, N. Shibata^a, T. Shakouchi^a, and T. Ando^a

Jets are the most basic flow used in industrial field and are widely used for heating, cooling, mixing. Recently, the improvement of mixing efficiency is required in order to downsize many industrial equipments and upgrade their performance. In the case of jets, their characteristic, such as the diffusion, depends on the inlet condition. Therefore, by controlling jet to give appropriate inlet conditions, the mixing efficiency can be improved. Thus far previous studies have mainly investigated excitation control associated with the instability of jets. However, in our previous study¹, as a new method we proposed vector control to enhance mixing or diffusion of free jets and have found its characteristics. In this study, we focus on the vector control in which an inflow direction is rotating around the streamwise direction.

In order to investigate the performance of the proposed method, the DNS of axisymmetric jet under the vector control are conducted. Figures 1 show the instantaneous vertical structures visualized with iso-surfaces of the second invariance of velocity gradient tensor Q ($=0.05$). According to the increasing rotating frequency, the flow pattern largely changes: for fairly low St number ($St=0.002$), because of a low-speed rotation, the effect of the dynamic control does not appear. The vortex structures are directed toward the nozzle axis; for low St number ($St=0.005-0.02$), the structures distribute in a helical manner and expand radial direction depending on the rotating frequency; for moderate St number ($St=0.04-0.1$), vortical structures downstream are entangled, helical structure disappear. , it is found that the flow pattern changes due to vector control.

In order to make clear the reason for the mixing enhancement, the SPOD (snapshot proper orthogonal decomposition)² and the DMD (dynamic mode decomposition) method³ are applied. Figures 2 show the mode structures extracted with both SPOD and DMD method. Thus it confirms that the DMD method extracts the same spatial mode of SPOD, and that the frequency of the dominant dynamic mode quite agree well with the control frequency. The mode is the same as the distribution of the 3rd mode of SPOD(not shown here), and as similar to the above-mentioned result, both the DMD method and the POD method deeply correlate with each other. In addition from the frequency characteristics, we find that, in developing region of the jet, the mode having a fairly slow time scale than both the control frequency and an unstable frequency such as Column instability, may contribute to the mixing.

^a Division of Mechanical Engineering Graduate School of Eng., Mie University, Tsu, Japan

¹ Tsujimoto et al., *J. Fluid Science and Technology*, **6**, 401(2011).

² Sirovich, *Q. Appl. Math.*, **45**, 561(1987).

³ Schmid, *J. Fluid Mech.*, **656**, 5(2010).

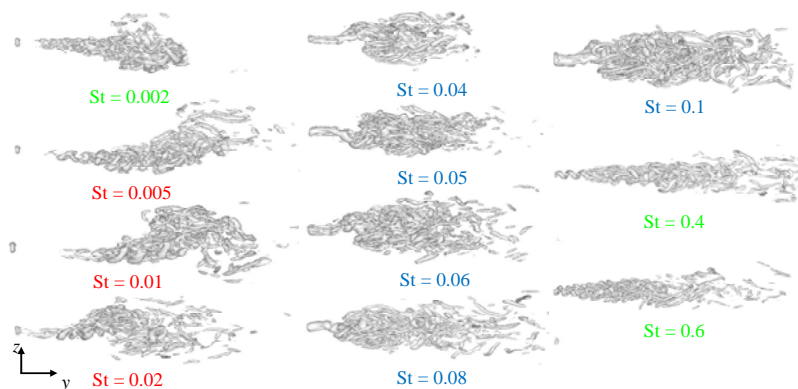


Figure 1: Coherent vortices visualized with Q

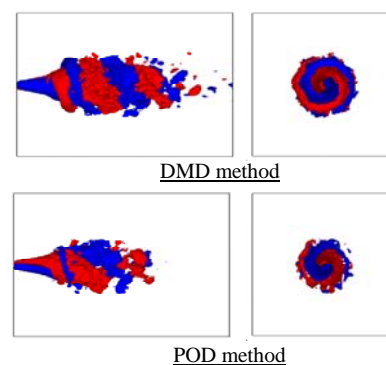


Figure 2: Extracted mode with DMD and SPOD

Numerical Investigation of High Speed Jets - Generated Edge-tones

Mohammed Khalil Ibrahim^{1,2}, Mohamed Yunus Mohamed Ismail¹, and
Ahmed Zafar Al-Garni¹

¹ Aerospace Engineering Department, Collage of Engineering Sciences, King Fahd University of Petroleum and Minerals, Dhahran 31261, KSA.

² Aerospace Engineering Department, Faculty of Engineering, Cairo University, Giza 12613, Egypt.

Corresponding author: khalilibrahim@kfupm.edu.sa

Abstract: Edge tone is a tone of discrete sound produced when a jet of gas issuing from a slit impinges wedge-shaped edge placed at a short distance from the slit exit. Numerical investigations of edge tone generation have been conducted in the present study. Two-dimensional computations of high speed jet-edge system are conducted and the resulting flow and acoustic fields are carefully examined. The effect of Mach number, jet shear layer thickness, edge angle and nozzle lip on the characteristics of edge-tone is reported. The study also proposed passive technique to suppress the edge-tone noise. The compressible Navier-Stokes equations are considered with a second order implicit scheme for spatial discretization. The commercial CFD code, FLUENT, is employed to simulate flow field. The low speed edge-tone case was used to validate the numerical model with experimental data from Andreas Bamberger [1]. The results were found to be in good agreement with the experimental data. For high speed case, the computations were validated with the experimental data from Krothapalli et al. [2]. The high speed edge-tone results also were found to be in good agreement with the experimental data, as shown in Fig. 1. The computed cases reveals that two stages of edge-tone exits which in agreement with the experimental observations regarding frequency jump due to change in the edge-slit separation distance or jet Mach number. The results reveal that as the Mach number increases the edge-tone increases. This is attributed to the decrease in downstream propagation time of disturbances. The phase lag, p , computed using the Powell's feedback formula is -0.28 for low speed edge-tone and -0.35 for high-speed edge tone which is in agreement with values proposed by Kwon [3] and Nomomura [4].

Keywords: Computational Fluid Dynamics, High Speed Jet, Edge-tone, Aeroacoustics.

References

- [1] Andreas Bamberger, Eberhard Bansch, and Kunibert G. Siebert. Experimental and numerical investigation of edgetones. *ZAMM Z. Angew. Math. Mech.*, 84(9):632–646, 2004.
- [2] A. Krothapalli, K. Karamcheti, Y. Hsia, and D. Baganoff. Edge tones in high speed flows and thier application to multiple jet mixing. *AIAA Journal*, 21(7):937–938, 1983.
- [3] Young-Pil Kwon. Feedback mechanism of low-speed edgetones. *KSME International Journal*, 12(4):701–708, 1998.
- [4] Taku Nonomura, Hiroko Muranaka, and Kozo Fuji. Computational analysis of Mach number effects on edgetone phenomenon. *AIAA Journal*, 48(6):1248–1251, June 2010.

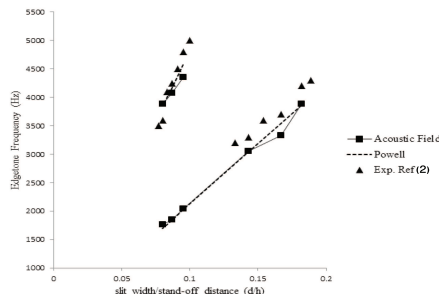


Figure 1: Validation of High Speed Jet Edge Tones

Aerodynamics

Numerical and experimental study of the wake behind a NACA0012 airfoil and comparison with theoretical models at moderate Reynolds numbers

A. Domínguez-Vázquez^a, J.J. Serrano-Aguilera^b, L. Parras^a and C. del Pino^a

Axial wing tip vortex characterization is a relevant issue not only from a theoretical point of view, but also due to its interest in control engineering applications. An experimental study has been performed displacing a NACA0012 wing model at moderate Reynolds numbers in a towing tank. We have measured the velocity field at every cross section in the axial direction using Particle Image Velocimetry (PIV). In addition, numerical simulations were carried out under the same conditions by means of OpenFOAM. These numerical and experimental results show, among other features, the vorticity evolution of the core center in the wing tip vortex, describing the vortex intensity decay when the small scale wing model moves downstream.

Both, experimental and numerical results were compared with the theoretical models proposed by Batchelor¹ and Moore and Saffman² in order to compute their parameters for the trailing vortex along the axial coordinate. These theoretical models have been modified by introducing a new parameter which represents a virtual origin in the axial coordinate, according to C. del Pino *et al.*³ It has been observed a precise agreement between numerical and experimental results, as shown in figure 1. It has been also studied the evolution of the theoretical parameters as function of Reynolds numbers, aiming to obtain a fit model, that allow us to analyze the vortex stability in a future research.

^a ETSII Industriales, C/ Doctor Ortiz Ramos S/N, 29071 Málaga, Spain.

^b CIEMAT-Plataforma Solar de Almería, Crta. de Senés, km. 4.5, E04200 Tabernas, Almería, Spain

¹ G. K. Batchelor. *Axial Flow in trailing line vortices*. J. Fluid Mech. 20,645 (1964).

² D. W. Moore and P. G. Saffman. *Axial flow in laminar trailing vortices*. Proc. R. Soc. London, Ser. A 333, 491 (1973).

³ C. del Pino, L. Parras, M. Felli y R. Fernández-Ferá. *Structure of trailing vortices: Comparison between particle image velocimetry measurements and theoretical models*. Physics of Fluids. 23, 013602 (2011).

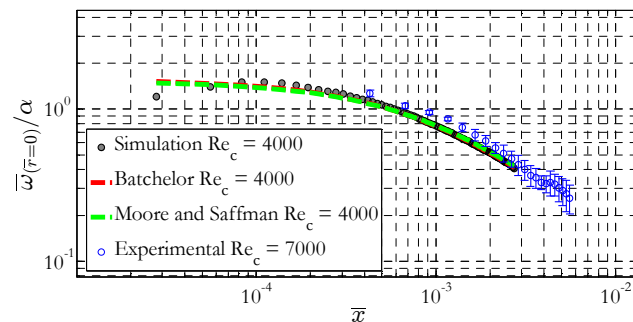


Figure 1: Axial evolution of the axial component of the vorticity at the vortex core.

Reshaping of separation bubble in wavy wing boundary layer at different value of swept angle

I.D. Zverkov^a, A.V. Kryukov^a, V.V. Kozlov^a.

Nowadays the interest of researchers turned again to the wing aerodynamics at low Reynolds numbers. Here the term “low Reynolds numbers” means $Re < 0.5 \cdot 10^5$ based on the wing chord. Such an interest is closely related to rapid development of unmanned air vehicles and wind turbines. A wide range of unmanned aircraft (UA) with the take-off weight less than 10 kg has a small wing chord and speeds of their flight which are comparable with atmospheric wind speeds. Such conditions mean that UA wings are exploited at the Reynolds numbers of the order of 10^5 , moreover, due to aircraft construction peculiarities or side gusts, UAs can be used at a significant sweep angle. Similar conditions are also observed on blades of wind turbines with power up to 100 kilowatt. A significant change in Reynolds number from the blade root to its tip can be referred to as a peculiarity of the wind turbine blade. Consequently, the situation when a part of the blade operates at $Re < 10^5$ and another one operates at $Re > 10^5$ is very frequent. Also, we note that the structure of the boundary layer in the range $Re = 10^5 - 10^6$ changes significantly. At $Re = 10^5$ the laminar-turbulent transition takes place through formation of a separation bubble, while at $Re = 10^6$ the separation bubble can be completely eliminated. Such difference in the boundary layer structure determines different approaches to control of the leading-edge stall. In this paper the research results on aerodynamics of a wing and boundary layers structure at Re about 10^5 are reported. Improvement of wing aerodynamic performance was achieved by wavy surface [1]. The physical principal of the such improvement is supposed.

In a first part of work the boundary layer structure on Z-15-25 airfoil by PIV method was investigated.. To reduce the reflection, the models were made of transparent acrylic plastic.

To obtain an impression of the laminar-turbulent transition in the wavy wing boundary layer a set of representative isosurfaces of rms disturbance amplitudes of the streamwise velocity for the top and bottom sides of the wing are shown in Fig. 1(a).

In a second part of the work the separation bubble transformation at different swept angle was investigated. The wing model has the same airfoil but chord length was 195 mm and aspect ratio 3.5 (Fig 1(b,c)). At near critical angle of attack separation bubble form has changed but turbulent boundary layer keeps the attached flow regime. So the advance in critical angle of attack which has been given by wavy surface at no sweep regime (Fig. 1(b)) remains at the 30° swept angle (Fig.1(c)).

^a Khristianovich Institute of Theoretical and Applied Mechanics SB RAS, Novosibirsk, Institutskaya 4/1, Russia.

The investigation was supported by following grants: RFFI 14-08-00369 A; RFFI 13-07-00616 A; RFFI 13-08-00395 A.

¹ Zverkov I.D., Kozlov V.V., Kryukov A.V. 2012 Experimental research of the boundary layer structure at near-critical angles of attack for the classical and wavy wings // EUCASS Book Series on Advances in Aerospace Sciences, Vol. 5, p. 252-265

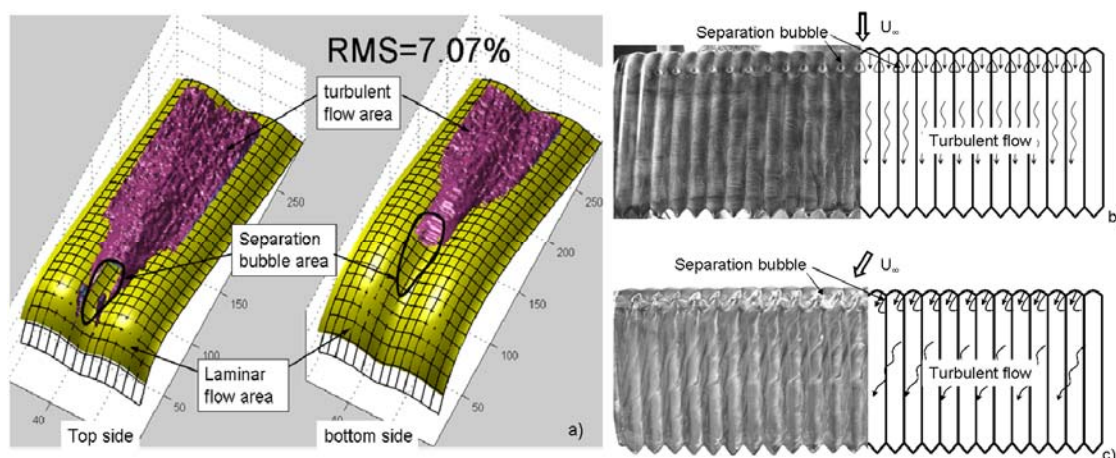


Figure 1: Isosurfaces of rms disturbance amplitudes in the boundary layer of the wavy wing at angle of attack $\alpha = 0^\circ$ (a); attached flow regime at no swept angle and $\alpha = 13^\circ$ (b); attached flow regime at swept angle $\gamma = 30^\circ$ and $\alpha = 16^\circ$ (c);

Angle of Attack Effects in Flapping Foil Power Generation

J. Young^a and J.C.S. Lai^a

Flapping foils are under active consideration as an alternative to traditional rotary turbines, for power generation in wind, tidal and oceanic currents, and rivers, following an approach pioneered by¹. In the power generation application, flapping foils depend for their effectiveness on the creation and evolution of leading edge vortices (LEVs) and their interaction with the foil. In this respect they mimic the action of fish, shark and cetacean tails, as well as insect wings, for all of which LEVs can play a significant role in fluid dynamic forces developed². Young et al.³ provide a comprehensive review of progress and challenges in the flapping foil power generation literature. Emerging from all these studies is the finding that flapping kinematics is a primary determinant of performance (that is, greatest extraction of power from the available fluid stream).

This work explores the effect of the angle of attack trajectory (i.e. time history) for the power generation problem, particularly noting that this application has been shown to be highly unsteady and dependent on the formation, evolution and interaction of LEVs³, which are in turn sensitive to angle of attack. The aim of the work is to investigate the effect of changes in the trajectory on the flow physics, to understand the sensitivity of the power output to these changes and provide guidance for control system developmental strategy.

A NACA0012 foil section was simulated in 2D using a viscous Navier Stokes solver, at Reynolds number $Re = 1100$ (laminar) and 1.1×10^6 (turbulent).

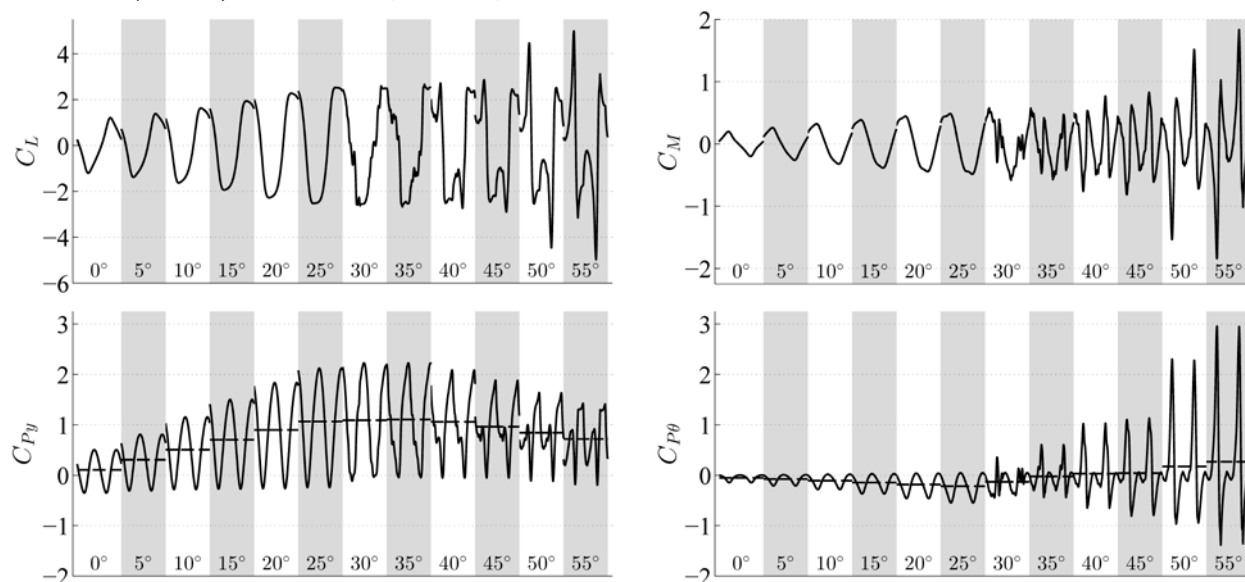


Fig. 1. Time histories of lift and moment coefficient (top row) and power output coefficient for plunging and pitching motion components (bottom row). One motion cycle shown for each angle of attack amplitude (indicated along the bottom of each frame). Time-average power coefficients indicated by dashed lines.

Fig. 1 shows an example of the results, for turbulent flow at a fixed frequency and foil pivot point, for a range of different amplitudes of angle of attack. The trajectory here is sinusoidal, leading the plunge motion by 90° phase. The plunge motion is also sinusoidal, with amplitude of one chord. The pitch angle is controlled to achieve the required angle of attack. The onset of leading edge vortex shedding is apparent in the lift and moment coefficients at 30° angle of attack amplitude, becoming dominant at the higher amplitudes. For this parameter combination the optimum angle of attack amplitude, based on the sum of the plunging and pitching power outputs, is $35\text{--}40^\circ$.

^a School of Engineering and Information Technology, University of New South Wales Canberra, Northcott Drive, Campbell, Australian Capital Territory, 2600, AUSTRALIA

¹ McKinney and DeLaurier, *J. Energy* **5**, 109 (1981).

² Shyy et al., *Prog. Aero. Sci.* **46**, 284 (2010).

³ Young et al., *Prog. Aero. Sci.* in press (2014), DOI: 10.1016/j.paerosci.2013.11.001.

Flapping Airfoil Simulations at Very Low Reynolds

M.Moriche¹, Ó.Flores^a, M.García-Villalba^a

Unsteady aerodynamics has been the focus of attention for many researchers for the last decades. In aeronautics, the models of Wagner and Theodorsen have been widely used for unsteady flows with high Reynolds number (Re) and motions with relatively small amplitudes. Recently, there has been an increased interest in the development of Micro Air Vehicles (MAV) able to fly at low or very low Re . In this flow regime, some MAVs make use of a flapping-wing design, mimicking bird or insect flight. The hope is to achieve the high maneuverability and flight efficiency of natural flyers. Working towards this goal, it is necessary to improve the understanding of flapping-wing aerodynamics.

We present fully resolved DNS simulations of flow over moving airfoils. The in-house code solves the Navier-Stokes equations for incompressible flow. The presence of the airfoil is modelled using the immersed boundary method of Uhlmann¹ and the motion of the airfoil is prescribed. We have carried out a parametric study, changing the pitching and plunging amplitude, the flapping frequency and the phase shift. An example of a heaving NACA airfoil at $Re=500$ and Strouhal number (St) 0.25 is shown in figure 1. The analysis of the results will be focused on unsteady aerodynamics mechanisms like the leading edge vortex and the rotational lift phenomenon².

¹ Dep. Bioengineering and Aerospace Engineering, UC3M, Avda. De la Universidad 30, Leganés, Madrid, España

¹ M. Uhlmann, *J. Comput. Phys.* **209**, 448 (2005).

² W. Shyy et al, *An Introduction to Flapping Wings Aerodynamics*. Cambridge Univ. Press (2013).

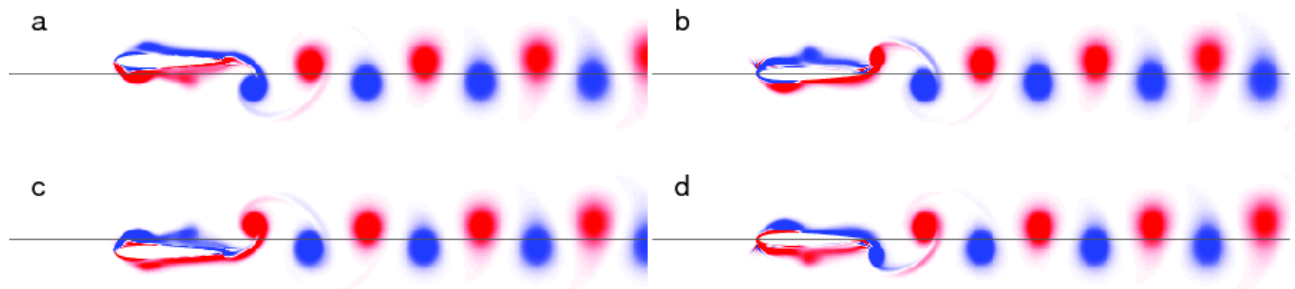


Figure **Fejl! Kun hoveddokument.**: Contours of the spanwise vorticity around a heaving NACA-0012 airfoil. Data is from a 2D-DNS at $Re=500$ and $St=0.25$. a) upstroke to downstroke transition, b) mid-downstroke, c) downstroke to upstroke transition, d) mid-upstroke.

Aeroelastic analysis for high-lift devices at large angle of attack using chimera technique

R. Roszak^a, W. Stankiewicz^a, M. Morzynski^a, M. Nowak^a

This paper presents the fluid structure interaction (FSI) tools used to analyse high-lift device configuration using chimera technique. In the case of CFD calculation of high-lift devices, definitions of individual fluid domains are required, as the aeroelastic calculations are associated with the moving fluid grid.

In the case the high-lift devices the simulation is even more complicated due to the continuously changing gap distance between the wing and flap. In the case of the classical approach, based on the mesh deformation, the change of the gap's size causes degeneration of the elements inside the gap, that makes aeroelastic calculations for the high-lift devices impossible. It is therefore necessary is to use the chimera method in these cases.

The paper presents a complete aeroelastic analysis for the wing and Fowler's flap configuration based on the real aircraft geometry. Proper discrete models for structure (solid – CSM) and fluid (CFD) domains for URANS calculation are successfully established [Fig. 1]. The most challenging part of the calculation in this case is the process of the deformation of the meshes representing the main fluid domain and the fluid in the vicinity of the flap. This step also involves the displacement and rotation of the flap's domain using chimera technique.

The authors present as well a solution to the problem of direct interpolation between the CFD domain and Fowler's flap construction elements such as ribs and beams.

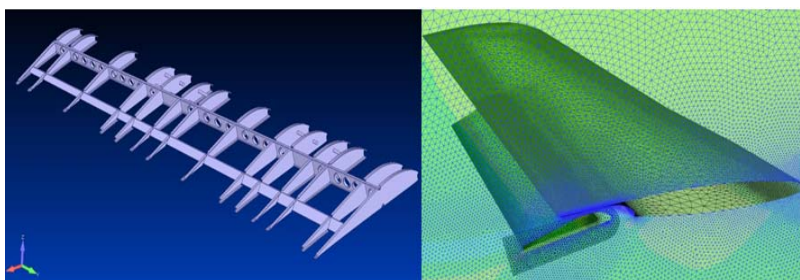


Figure 1: Discrete models for aeroelastic analysis: model CSM on left, CFD chimera mesh on right.

Finally the authors presents a dynamic response resulting from aeroelastic analysis for high-lift devices based on real configuration of the aircraft.

This work was supported by the Polish National Science Centre under the grant - decision no. DEC-2011/01/B/ST8/06925

^a Poznan University of Technology, Department of Virtual Engineering, Pl. M. Skłodowskiej-Curie 5, 60-965 Poznan, Poland

¹ Farhat C. and Degand C. and Koobus B. and Lesoinne M. Torsional springs for two-dimensional dynamic unstructured fluid mesh. *Comput. Methods Appl. Mech. Eng.*, **163**, 231–245 (2000).

² Roszak R., Posadzy P., Stankiewicz W., Morzyński M., Fluid structure interaction for large scale complex geometry and non-linear properties of structure), *Archives of Mechanics*, vol. **61**, pp. 1-24, (2009).

³T. Schwarz, F. Spiering, N. Kroll, Grid coupling by means of Chimera interpolation techniques, DLR, 2010

⁴Fung Y.C., An Introduction to the theory of aeroelasticity, Dover Publications, New York, 2002

Investigation of Flow Structure on Low and Moderate Swept Delta Wings

M. Zharfa^a, I. Ozturk^b, M. M. Yavuz^c

Aerodynamic investigations of flow structure over generic and complex delta wing configurations have been performed for many years. Turbulent flow fields and unsteady surface pressures caused by leading-edge vortices or three-dimensional surface separation may result in severe dynamic loading problems including buffeting. In addition, recent investigations have revealed the appearance of a distinctive type of leading edge vortex, dual vortex structure, over simple delta wing planforms having low and moderate sweep angles for certain ranges of Reynolds number and attack angle. In the present study, experimental investigations on low and moderate swept delta wings have been performed using laser based flow visualization, surface pressure measurements, and Laser Doppler Anemometry (LDA) techniques in low-speed wind tunnel. Delta wings of sweep angles, 35 and 45 degrees, are tested, which are considered as low and moderate swept wings, respectively. The Reynolds number is varied from 10^4 to 10^5 and the attack angle is varied from 3 to 13. Smoke visualizations are performed at planes of cross flow and vortex axis. The footprint of flow regimes on the surface of the planform is captured by the surface pressure measurements, which are performed from pressure tabs located at three different stations along the wing cord in spanwise direction. For the corresponding Reynolds Numbers and attack angles, dual vortex structure, vortex breakdown, prestall and poststall regimes are identified. Using statistics and spectral analysis, the unsteadiness of flow is studied in detail. The amplitude and the frequency of the pressure and velocity fluctuations at different locations are compared. The results of the study indicate that vortex breakdown and three-dimensional surface separation cause significant loss in suction pressure of the vortex core and reattachment pressure at the wing surface. The surface pressure measurements are quite inline with the smoke visualization results where the vortex cores correspond to the largest suction pressures at the surface of the planform. Considering FFT studies, distinctive pressure and velocity fluctuation peaks can be evident for the regions upstream of vortex breakdown, however appearance of vortex breakdown or three-dimensional surface separation causes broader spectrum in velocity and pressure signals. It is also evident that the maximum surface pressure fluctuations happen at regions between vortex core and reattachment zone, which is quite inline with some of the recent investigations.

^{a, b, c} Dep. Mechanical Engineering, Middle East Technical University, Dumlupinar Blvd., 06800, Ankara, Turkey

Dynamic Mode Decomposition of the transitional separated wing flow

A. Ducoin^a, J.-C. Robinet^b and J.-C. Loiseau^b

The objective of this talk is to study numerically the different physical mechanisms developing in the transition to turbulence of a separated boundary layer flow around an airfoil with a low incidence. This transition typically occurs for a moderate Reynolds number and is controlled by a laminar separation bubble on the upper surface of the wing. Kelvin-Helmholtz instabilities are responsible of the first phase of destabilization of the bubble and quickly lead to 3-D vortex structures. Although the laminar separation bubble localization is well known, its dynamics and particularly the mechanisms of transition to turbulence are poorly understood. In this study, a SD7003 wing profile has been chosen, it has been extensively studied for a wide range of transitional Reynolds number ($20,000 < Re < 66,000$). The angle of incidence is chosen relatively small ($\alpha=4$), which indicates a recirculation zone and a turbulent reattachment near the trailing edge. Numerical 3-D simulations were conducted with the Nek5000 code, solving the incompressible Navier-Stokes equations with a spectral element method. Several laminar cases are studied ($2000 < Re < 10000$) to validate this method on this type of airfoil. A comparison with 3-D computations shows that the flow remains two-dimensional. A gradual increase of the Reynolds number is then used to study a transitional case at $Re = 20,000$. The computations are compared with the experimental results where the mechanisms of instabilities in the separated zone and near wake zone are analyzed. A "bursting" phenomenon is identified and analyzed by the DMD (Dynamic Mode Decomposition) method for connecting instability modes to the characteristic frequencies associated with fluctuations in the separated boundary layer.

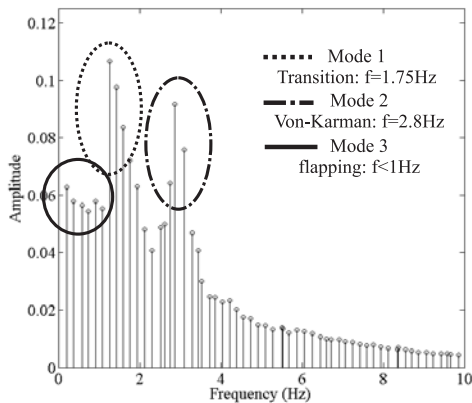


Figure 1: Dynamic Mode Decomposition, Koopman spectrum, $Re=20,000$.

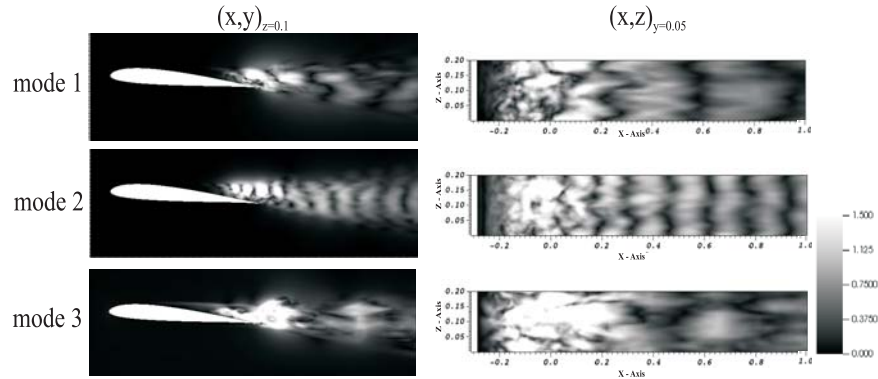


Figure 2: Velocity field $|V|$ for the 3 first modes. (X,Y) planes are taken at mid span ($Z=0.1$); (X,Z) planes are taken at the LSB level ($Y=0.05$). $Re=20,000$.

^a LHEEA laboratory, Ecole Centrale de Nantes, 44300 Nantes, France

^b DynFluid laboratory, Arts et Métiers ParisTech, 75013 Paris, France

Open Loop Separation Flow Control Using an Active Slat

B. Elhadidi^a

An active slate is used to improve the aerodynamic performance of separated flow over a DU96-W180 airfoil at $Re=50,000$ and $\alpha=15^\circ$. This airfoil section is used in wind turbine blades and active flow control can be used to improve the energy capture efficiency of wind turbines. The “active slat” is simply an airfoil with a fixed stationary leading edge slat that has a rotating plug within the flow passage (figure 1a). The plug can be rotated such that the slat is closed, fully open or rotating at a prescribed rotational speed. The rotational speed of the plug permits the passage of flow within the slat at different excitation frequencies with adds momentum to the separating boundary layer on the upper surface improving the ability to overcome separation caused by the adverse pressure gradient. The use of the “active slat” is beneficial compared to current control techniques using plasma actuators and zero-net-mass-flow actuators. First the actuation is based on simple rotational motion of a plug, second it does not require high energy or heavy transformer equipment, third the flow passage is wide enough and fear of blockage is limited.

Two dimensional numerical simulations were performed for an airfoil with no slat, a slatted airfoil, and three actuated cases. The different excitation frequencies were tested to examine effectiveness to control separation by enhancement of mixing corresponding to frequencies of the shear layer, wake shedding and separation bubble instability. Figure 1b compares the mean unsteady lift coefficient for all test cases. The standard deviation (RMS) lift is represented by the errorbars. The results show that it is possible to increase the unsteady lift by up to 20%. Figure 1c and d compare the contours for the instantaneous and mean velocity magnitude for a plug rotating at $\omega=0.36$ radians/second. The instantaneous contours show the complex vortex interaction caused by the slat flow and the Helmholtz instability caused by the shear layer on the upper surface. Here the actuation frequency is low corresponding to the separation bubble instability and is the most efficient in active flow separation control in this case.

A full study comparing the effectiveness of this control technique will be examined for different flow angles of attack and Reynolds numbers will be investigated in the full paper.

^a Department of Aerospace, Faculty of Engineering, Cairo University, Giza, Egypt

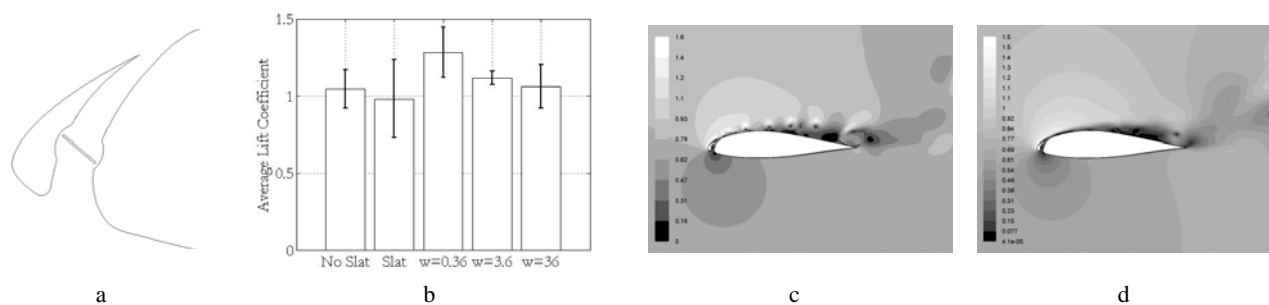


Figure 1: (a) Schematic of active slat (b) Unsteady lift for different test conditions, (c) Instantaneous velocity magnitude contours for actuation of $\omega = 0.36$ radians/second and (d) mean velocity magnitude contours for $\omega = 0.36$ radians/second.

Wide Range of Low Reynolds Number Effect on Two-dimensional Airfoil Characteristics Measured in High Viscosity Fluid Tank

Gaku Sasaki^a, Itaru Tamai^a, Hidemasa Saito^a, Takaaki Matsumoto^a and Koichi Yonemoto^a

MELOS (Mars Exploration with Lander-Orbiter Synergy) is proposed for the near future multi-objective planet exploration mission in Japan. Mars exploration aircraft, one of the mission systems of MELOS, is now being researched by a working group of JAXA/ISAS and university researchers. Our laboratory is in charge of the aerodynamic design such as the airfoil of propeller.

The order of Mars flight Reynolds number around propeller is about the range from 10^2 to 10^4 due to ultra-low Martian atmospheric density, which is an about one-hundredth of that of the earth. The order of Reynolds number is called ultra-low Reynolds number flow. It is said that the wing characteristics in the Reynolds number flow further changes compared with that in high Reynolds number flow such as the order of 10^6 . However, previous study on wing characteristics in ultra-low Reynolds number flow is only a few. It is partly because the difficulties of ultra-low Reynolds number flow generation and measurement of small fluid force using wind tunnel.

In this research, force balance test using towing fluid tank filled with highly viscous fluid was conducted to clarify the two-dimensional wing characteristics in ultra-low Reynolds number flow ($Re < 10^4$). Test airfoils are NACA0012, triangle, and Ishii¹ (Figure 1). Ishii which is developed for hand launch glider has good aerodynamic performance in the range of Reynolds number from 10^4 to 10^5 . Test Reynolds number ranges from 5.0×10^2 to 1.0×10^4 . The angle of attack is changed from -10 to 20 [°] with the increment of 1 [°].

Figure 2 shows the experimental results. The results are roughly in accordance with the previous research by wind tunnel. Note that $Re = 1.0 \times 10^4$ is the lower measurement limits of a normal wind tunnel. And result of comparison the $Re = 1.0 \times 10^4$ and 5.0×10^3 , drag coefficient is larger in the lower Reynolds number. The additional data includes ultra-low Reynolds number experiment will be presented on EFMC10.

^a Kyusyu Institute of Technology, 1-1 Sensui-cho, Tobata-ku, Kitakyusyu-city, Fukuoka, Japan

¹ M. Anyoji, et al., *8th Int. Conf. on Flow Dynamics*, **344**, 2011.

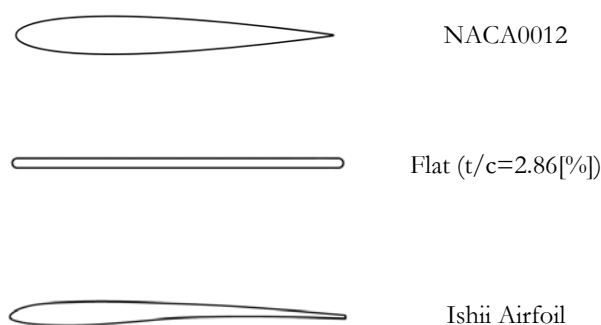


Figure1: Test Airfoils

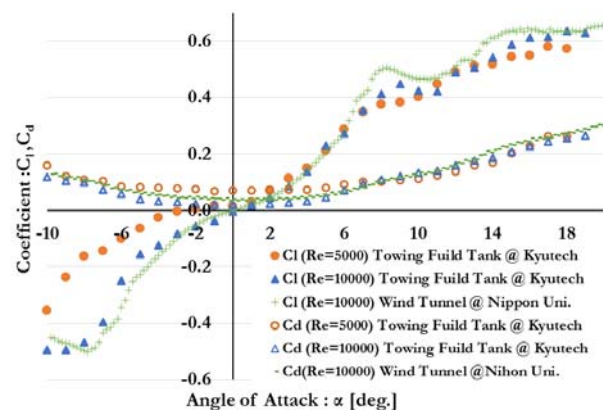


Figure2 : Results of Force Balance Test

Experimental characterization of three-dimensional stall behaviour over a model wind turbine blade

M. S. Melius^{a,b}, L. K. Neuhaus^a, R. B. Cal^b, and K. Mulleners^a

As the wind energy industry continues to grow, the need for detailed information about the power output is more important than ever. The power generation of a wind turbine is influenced by many factors including the unsteady incoming flow characteristics, pitch regulation, and the geometry of the various turbine components. Within the framework of maximizing energy extraction, it is important to understand, optimize and tailor the aerodynamics of a wind turbine.

In addition to the unsteady operating conditions of a wind turbine blade, the three dimensional flow fields are strongly influenced by rotation. Separated flow over a rotating airfoil experiences a centrifugal force as well as a coriolis force, driving the volumes of separated air to larger radial positions, commonly known as centrifugal pumping. This phenomenon is understood to influence the lift characteristics of the airfoil by delaying stall and raising the dynamic suction peak.

In the interest of seeking further understanding into the complex unsteady flow behavior, a three-dimensional scaled wind turbine blade model has been designed and manufactured to be dynamically similar to a rotating full-scale NREL 5MW wind turbine blade. A wind tunnel experiment has been conducted in the 2.2m x 1.8m cross-section closed loop wind tunnel at the DLR in Göttingen by means of time-resolved stereoscopic PIV. An extensive coherent structure analysis of the three-dimensional time-resolved velocity field over the suction side of the blade was conducted to study the unsteady flow development following a sudden change in flow configuration. This change was obtained by swiftly changing the blade pitch angle to simulate a sudden change in wind speed or pitch angle regulation. The resulting time scales of rise time and settling time pertaining to stall propagation were determined as a function of radial position. By analyzing the adjacent three dimensional flow fields under these testing conditions, the influence of rotation and three-dimensionality on a scaled wind turbine blade and the resulting aerodynamics effects have been quantified.

a. Department of Mechanical Engineering, Leibniz Universität, Hannover, Germany

b. Department of Mechanical and Materials Engineering, Portland State University, Portland OR, USA

On the Efficiency of Fluidic Oscillators for Flow Control

A. Seifert^a, D. Dlgopyat and D. Sarkorov

The paper will describe two recent experiments in which the Suction and Oscillatory blowing (SaOB) actuator was used to control the flow on aerofoils.

The first experiment dealt with performance recovery of a thick aerofoil in laminar and turbulent flow conditions. Performance was significantly degraded due to premature boundary layer separation. An array of 12 SaOB actuators was used to effectively restore lift and reduce drag. Overall system efficiency was increased in both turbulent and laminar flow conditions.

The second experiment used two arrays of SaOB actuators to either keep attached or separate the flow near the trailing edge of a high-lift low Reynolds number airfoil, with the purpose of creating forced and moment alternations without moving control surfaces. Significant changes can be imposed. Experiments on a bench-top setup were supplemented by CFD to create an effective design tool for AFC fluidic effectors. Unsteady Fluidic “Gurney flap” effects were documented for the first time, to our knowledge.

^a School of Mechanical Engineering, Tel Aviv University, Levanon St., Tel Aviv, Israel (all authors)

Low Reynolds number roll stability regimes

K. Mohseni^a and M. Shields^b

Micro Aerial Vehicle (MAV) design still relies on iterative build-and-fly design techniques due to the poorly understood aerodynamic regime; these aircraft are highly sensitive to lateral instabilities, particularly those resulting from gust perturbations, which has anecdotally been attributed to the near-unity aspect ratios of their wings. Recently published results by the authors have discussed a potential mechanism for this behaviour; for low aspect ratio (LAR) wings ($AR < 3$) at increasing sideslip angles (β), a significant roll moment was measured which increased linearly with angle of attack (α) and then stalled in a manner reminiscent of a lift curve¹. This behaviour, referred to as ‘roll stall’, was not expected for canonical flat plate wings with no vertical geometric features (ie, tail surfaces). Smokewire visualization of rectangular and tapered wings indicated that as the sideslip angle increased, the core of the trailing vortices remained nominally aligned with the freestream velocity. This caused the upstream tip vortex to propagate over the surface of the wing while the downstream vortex was convected downstream, as seen in Fig. 1.a. As the core of the tip vortex is known to create a local increase in lift², the roll moment is attributed to the resulting asymmetry. At higher angles of attack ($\alpha > 30^\circ$), the core of the vortex becomes more disrupted by the adverse pressure gradient and dissipates, resulting in the stall event seen in Fig. 1.b. Recent results from the authors have shown that roll stall is responsible for creating an unstable oscillatory mode in LAR wings for small perturbations from equilibrium³.

A model is developed for roll stall which determines the effect of tip vortices on the surface pressure distribution of the wing. By representing the trailing vortices as semi-infinite line vortices with a circulation equal to that of the starting vortex, their radial pressure gradient may be computed; this in turn is used to calculate the relative pressure on the surface of the wing. A comparison of the pressure distributions at zero and nonzero sideslip angles is integrated along the surface of the wing and is found to match nicely with experimental data for the roll moment coefficient (Fig. 1b). Using this model to obtain the roll stability derivative ($C_{l,b}$) and estimating the roll damping derivative ($C_{l,p}$) from the variation in sectional lift induced on a rolling wing, the stability parameters of high and low aspect ratio wings are compared. At aspect ratios below 4.5, the complex eigenvalue shifts from stable (negative) value to unstable (Fig. 1.c); this indicates that the stability regime of MAVs is inherently different than that of conventional aircraft.

^a W.P. Bushnell Endowed Professor, Deps. of Mechanical & Aerospace Engineering and Electrical & Computer Engineering, University of Florida, Gainesville, FL, USA

^b Dep. of Mechanical & Aerospace Engineering, University of Florida, Gainesville, FL, USA

¹ Shields and Mohseni, *J. Aircraft* **50**, 4 (2013).

² Viieru, et al, *J. Aircraft* **42**, 6 (2005).

³ Shields and Mohseni, *J. Aircraft*, accepted for publication (2014).

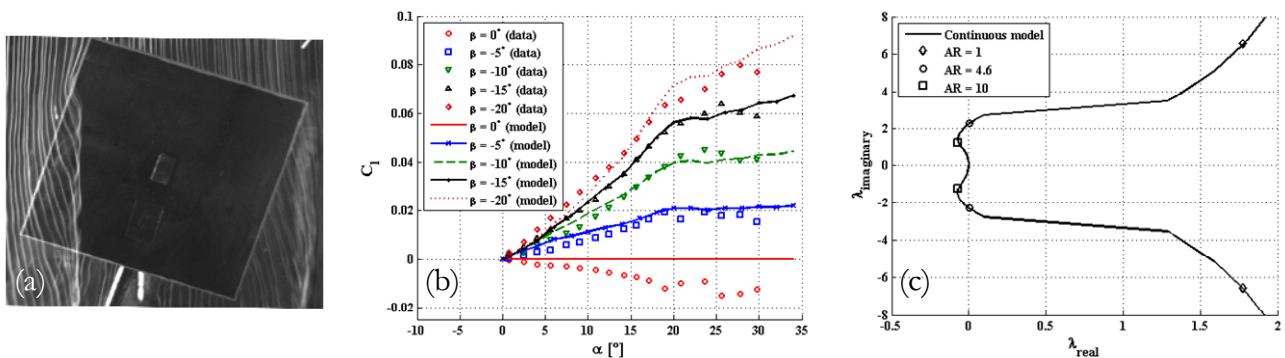


Figure 1: Flat plate results at $Re=7.5 \times 10^4$ and $\alpha=10^\circ$: (a) Smokewire visualization¹. (b) Experimental¹ and modelled roll moment for $AR=1$. (c) Complex eigenvalues for increasing aspect ratios.

Wave impact and slamming on an Oscillating Wave Energy Converter

T. Abadie¹, Y. Wei^a, A. Rafiee^b, F. Dias^a

Oscillating Wave Surge Converters (OWSCs) are efficient devices to absorb energy contained in the horizontal motion of water in ocean waves. OWSCs consist in buoyant flaps, hinged at the bottom of the ocean that oscillate back and forth under the action of incoming incident waves. This study aims at understanding the effects of the wave impact on the oscillations of a wave energy converter and the pressure loads applied on the device.

The mechanisms of the flap motion have been identified in a previous study¹ based on both high-speed camera experiments and numerical simulations. As the flap oscillates forth, *i.e.* towards the ocean, it has been shown that slamming phenomenon can occur when the flap hits the wave, leading to an impulsive load on the device. Up to now, the slamming impact has been extensively studied through two main situations: the wave impact on walls or fixed bodies² and the entry of a rigid body in water at rest³. However, the slamming phenomenon in such complex situation still needs some fundamental understanding. Indeed, in the case of wave impact on a fixed structure², or the water entry problem, the relative motion between the solid and the fluids are known whereas it is not the case with OWSCs devices and there is a strong interaction between incident waves and flap motion. In addition, the effects of scaling, water depth, wave and flap characteristics on the pressure load during this slamming process have not been identified.

To study the slamming phenomenon, 2D numerical simulations are performed with both a Smoothed Particle Hydrodynamics code and a Finite Volume code in which the water-air two-phase flow is modelled with a Volume of Fluid method. First, the waves generated are compared with 2D experiments performed at ECM (Ecole Centrale Marseille). The motion of the flap as well as the pressure loads are then investigated under various operating conditions (*e.g.* different water depths, wave amplitudes, flap lengths and densities) to study their effects on the slamming phenomenon.

¹ School of Mathematical Sciences, University College Dublin, Belfield, Dublin, Ireland

^a Carnegie Wave Energy Ltd, Perth, WA, Australia

¹ Henry et al., *Proceedings of the 23rd International Offshore and Polar Engineering Conference* (2013)

² Peregrine, *Annual Review of Fluid Mechanics* (2003)

³ Zhao and Faltinsen, *Journal of Fluid Mechanics* (1993)

10th European Fluid Mechanics Conference, DTU - Copenhagen, 14-18 September 2014

IMPACT OF BLADE SURFACE SOILING AND DEGRADATION ON BLADE SECTION AND WIND TURBINE PERFORMANCE

C.P. van Dam, Christopher Langel, Henry Shiu, Raymond Chow
Department of Mechanical and Aerospace Engineering
University of California – Davis
Davis, CA 95616
USA

Wind plant performance is ostensibly characterized by a power curve – a simple relationship between instantaneous wind speed and power production. In reality, performance is dependent on a large number of factors and accurately predicting energy capture of a wind plant is fraught with uncertainty. With 1,084 MW of new wind capacity in the U.S. in 2013 and a total installed capacity in the U.S. of more than 61 GW, error in the prediction of wind energy production has significant economic, operational, and reliability ramifications for grid operators as well as financial impacts on wind plant developers, owners, and operators. In 2009, this issue came to the fore as the wind industry acknowledged a 10% average fleet-wide underperformance of wind plants from pre-construction estimates. Study since then have identified sources of this error and quantified the energy production losses they incur: wake losses (2%-10%), turbine availability (3%-5%), balance of plant availability (0.5%-1.0%), electrical losses in the collection system (2%-3%), curtailment (0%-3%), shortfalls in turbine performance (1%-4%), and environmental losses (including icing, blade soiling, blade degradation; 1%-20%).

Significant attention has been devoted to some of these loss contributors, but others – in particular, aerodynamic losses due to blade surface soiling and degradation – have seen less scrutiny. Blade soiling/degradation losses have been previously investigated on earlier stall-regulated turbines. On these machines, the aerodynamic effect of surface soiling/degradation were recognized because blade pitching was generally unavailable to counter changes in aerodynamic behavior and early onset of stall lowered the maximum power output. When the industry standardized on pitch-regulation, surface soiling/degradation became a lesser concern. It has re-emerged as an issue in recent years as wind plant owners have struggled to maximize the performance of their existing fleet and rotor aerodynamic design has pushed more aggressively to higher lift coefficients and lift-to-drag ratios. On a modern, moderately thick outboard airfoil designed specifically for wind turbine application, wind tunnel testing has shown that a relatively small amount of leading edge erosion can result in approximately 5% loss in energy production and a moderate to heavy amount can result in energy production loss as high as 25%.

This presentation will focus on the impact of soiling on the aerodynamic performance of typical section shapes used for state-of-the-art wind turbine blades, particularly the thicker sections shapes that are now more common. These thicker shapes (maximum thickness-to-chord ratios greater than approximately 24%) are especially vulnerable to premature flow separation and loss of lift as a result of surface soiling. We will present a detailed look at the underlying aerodynamic effects of surface contamination and at the experimental and computational research being conducted to more accurately predict its impact on wind turbine rotor performance.

Aerodynamic characteristics of a single aerofoil for wind turbine blade applications

S. T. Mitchell^a, K. N. Volkov^a, O. Al-Khudairi^a and H. Hadavinia^a

The implementation of an innovative aerodynamic control technique in wind turbines is a point of extensive investigation since the conventional wind turbine blade technology is reaching its limits. The main effort of the wind turbine industry in the field of aerodynamics is related to the development of blades which offer better performance, increased reliability and faster control of larger wind turbines.

The aerofoils of horizontal axis wind turbines (HAWT) and vertical axis wind turbines (VAWT) normally experience conditions that are different from aerospace applications due to smaller chord length and lower wind speed, resulting in significantly lower Reynolds numbers. They also operate with an unusually wide range of angle of attacks (from 0 to 90 degrees for HAWTs and from 0 to 360 degrees for VAWTs), including both unstalled and stalled conditions. Calculation of the aerodynamic forces on the wind turbine blade at different AOAs is fundamental task in the design of the wind turbine blades. Accurate and efficient calculation of aerodynamic forces (lift and drag) and prediction of stall of an aerofoil at realistic operating conditions is still challenging task. Computational fluid dynamics (CFD) offers a way to model the complex flow features that occur during the operation of a wind turbine blades.

CFD simulations are carried out to determine the aerodynamic characteristics of a single aerofoil in a wide range of conditions. Reynolds-averaged Navier-Stokes (RANS) and large-eddy simulation (LES) results of flow over a single NACA0012 aerofoil are presented in a wide range of AOAs from low lift through stall. A hybrid mesh is used. The mesh contains a structured layer emanating from the surface of the aerofoil that contains sufficient points to model the flow as it interacts with the no slip wall of the aerofoil, and a tetrahedral unstructured mesh filling the rest of the domain. Sizing controls used include inflation emanating from the aerofoil surface, edge sizing along the aerofoil surface in the flow-wise direction, edge sizing in the span-wise direction, global growth rate, maximum face size, body of influence radius and body of influence sizing.

The results obtained are verified and validated against experimental and computational data from previous works. Validation with experimental data for the aerodynamic characteristics of the single NACA0012 aerofoil has shown reasonable agreement, although some notable difference were observed. The comparisons demonstrated that the RANS model considerably overpredicts the lift and drag of the aerofoil at post-stall AOAs due to the inaccurate vorticity diffusion behavior described by the 2D Navier-Stokes equations. LES provides a much better agreement with the experimental results and a more realistic description of the aerodynamic details. The process of breakdown to turbulence is captured in the LES. Starting from the leading edge, the shear layer is detached from the aerofoil surface with laminar 2D behaviour. Transition to turbulence becomes visible as a small distortion of the shear layer and the 3D of the flow starts to grow. Large-scale structures form and then break down into small structures followed by fully 3D turbulent flow. There are spanwise variations of the flow structures, and these structures could not be captured by the LES in narrow domain.

^a Faculty of Science, Engineering and Computing, Kingston University, SW15 3DW, London, United Kingdom

Non conventional flat back thick airfoils for very large offshore wind turbines

F. Grasso^a, Ö. Ceyhan^a

In developing new rotor blades, the selection of the proper airfoils play an important role. This is because the rotor performance are strongly dependent on the airfoil characteristics. While at the tip the aerodynamic efficiency is probably the most important parameter to be considered, the driven parameter at the root is the structural resistance of the sections. This leads to sacrifice the aerodynamic performance of the root to ensure good structural properties. Especially for very large modern rotor blades, thick airfoils with flat back trailing edge are adopted. In this way, beside the structural performance, the lift performance of the sections can be also ensured so the root of the blade is contributing to the power production of the blade too. In addition, saving blade surface helps to reduce transportation problems and loads in parking conditions.

However, the flat back shape of the airfoils has also negative effects, mainly due to the unstable and unsteady flow generated by such geometries. The consequences can be abrupt stall and wake disturbance due to this.

The present work is focused on investigating a new solution to keep the positive effects of flat back airfoils and limiting the above mentioned problems. Firstly, the general idea behind the proposed solution is presented, with the expected beneficial effects. Then the results of a numerical study are illustrated and discussed. In this study, preliminary results have been obtained by using the ECN panel code RFOIL. However, due to the complexity of the flow around the airfoil for the problem that is being examined, the need of a higher accuracy approach is required. Ansys CFX version 14 has been used to investigate the problem in more details. Structured high resolution meshes have been generated by using ICEM CFD mesh generator. Both steady and transient simulations are performed by using Menter's k-omega turbulence model with Langtry's correlation based transition model. Analysis results obtained so far have showed that the new solution can lead to a reduction in the effect of the unsteady wake and immediate drag reduction due to that (figure 1). These promising results are indicating that this new idea has a lot of potential to be applied both to the existing large wind turbine blades and to the future very large offshore wind turbine blades.

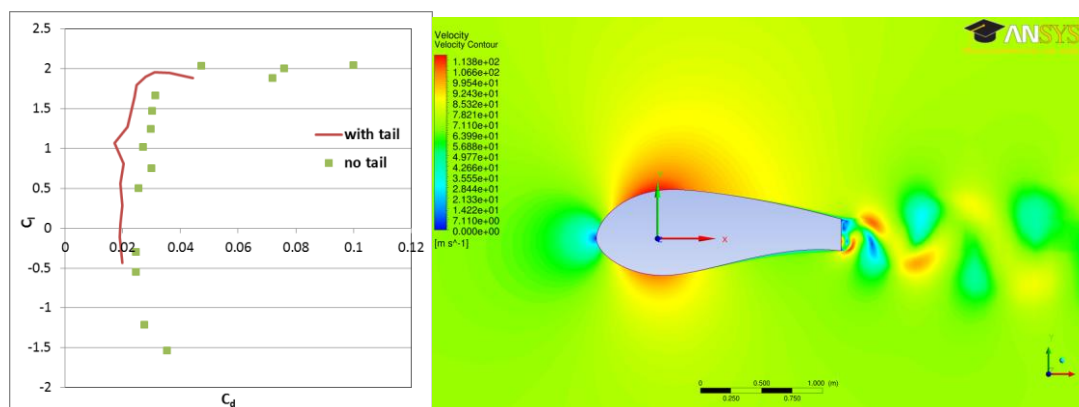


Figure 1: (a) Drag polar, comparison between conventional flatback thick airfoil and new solution. (b) Velocity contour (at $t=0.1$ sec) around a conventional flatback thick airfoil, CFX results.

^a Wind Energy Technology Group, ECN, Westerduinweg 3, 1755LE Petten, NL

Challenges in high Reynolds number flows for large offshore wind turbines

Ö. Ceyhan^a and H. Snel^a

Wind turbine rotor sizes are growing continuously. Today, a wind turbine prototype with rotor diameter larger than 170m is being tested and it is expected to be in the market this year. With these sizes, wind turbine rotors are one of the largest aerodynamic machines that are operating at Mach number regimes of 0.2-0.4. Relevant parameter of scaling in aerodynamics is the local Reynolds number that a blade section experiences. Local Reynolds numbers of these rotors are varying between 1million to 12 million already and they will reach 18 to 20 millions with the introduction of 10MW+ wind turbines in the near future. Below

Figure 1 (a) illustrates the change in local Re numbers of a reference rotor blade for a 10MW wind turbine used in Innwind.EU project in different wind speeds. Wind tunnel testing of such large rotating devices in their actual scales are quite challenging due to the fact that high Reynolds numbers are achieved by increasing the length scale, not by increasing the velocity. Moreover, the airfoils that are used in wind turbine blades have never been tested for such large Reynolds numbers at low speeds. Large wind turbines designed for offshore conditions have higher tip speeds and they are designed for higher tip speed ratios which increases the loss due to the drag component on the overall power production. This means especially for operating in higher Reynolds numbers, laminar-turbulent transition prediction is becoming more important in order to predict the right drag values for the right estimations of the power generated by a large offshore wind turbine. Unfortunately, current knowledge in high Reynolds number aerodynamics in aerospace sciences is not sufficient to deal the flow regime that large wind turbines will experience in the near future¹. This has been partially illustrated in

Figure 1 (b) by comparing the operating regimes of large scale commercial aircrafts and wind turbines. This figure shows clearly there is a lack of interest in the area that wind turbines are operating.

To investigate the challenges in operating in high Reynolds numbers with future 10MW+ wind turbines, wind tunnel tests are planned in AVATAR.EU project to test one of the wind turbine airfoils in its actual conditions. These wind tunnel tests will be performed in the pressurized wind tunnel of DNW (DNW-HDG) in order to cover the high Reynolds number flows for low Mach number. The tests will be performed in August 2014. Preliminary results will be presented in this symposium together with the challenges in aerodynamic modelling in high Reynolds numbers.

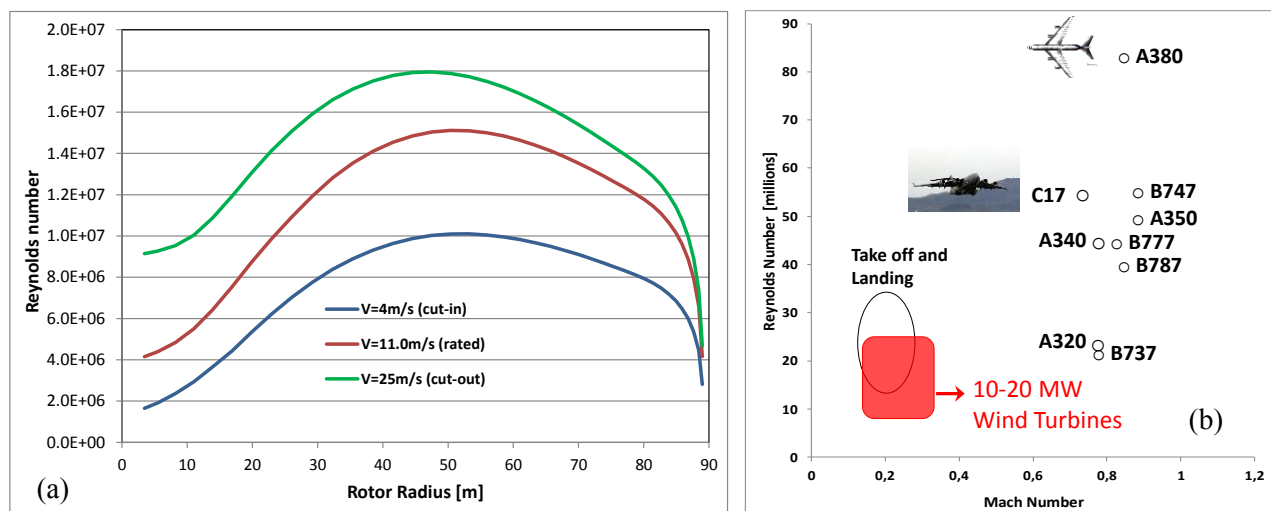


Figure 1: (a) Reynolds number change along Innwind.EU reference wind turbine blade at different operating wind speeds. (b) Reynolds number vs. Mach number comparisons between the wind turbines and aircrafts².

^a Energy research Center of the Netherlands, ECN, Westerduinweg 3, 1755LE, Petten, the Netherlands

¹ Ceyhan, AIAA-1157 (2012).

² Source: <https://www.etw.de/>, reproduced.

Airfoil prediction at high Reynolds numbers using CFD

Niels N. Sørensen^a, Frederik Zahle^a

In connection with the newest generation of wind turbines with sizes above 10 MW and the future turbines that are already now being designed, several new challenges must be faced. From an aerodynamic perspective the two most obvious issues are the increase of the Reynolds numbers (Re) with increasing size and the possibility of increased Mach numbers in the tip region. While the Mach numbers can be controlled and kept sufficiently low by specific design choices, the increase of the Re with size is difficult to avoid. For the combination of high Re and low Mach numbers, the available measurements are very sparse and one will need to address and extrapolate the aerodynamic effects of high Re by modelling, as the experimental approach become prohibitive expensive in this range. In connection with the ongoing EU projects INNWIND and AVATAR, these activities are already addressed on a European level with a moderate effort on the experimental side and the main focus on the computational perspective.

In the present paper we investigate the capability of state of the art CFD models to handle airfoil aerodynamics at high Re , with specific focus on correct predictions of the transition process for incompressible flow. The investigations are based on the multi-block incompressible flow solver EllipSys2D, developed at DTU Wind Energy^{1,2}, based on the pressure correction method using Rhie-Chow³ approach on a non-staggered grid. The turbulence is modelled using the k- ω SST model by Menter⁴ while the transition process is model with either the correlation based model of Menter et al.⁵ or the E^n model as suggested by Drela and Giles⁶ and originally implemented in EllipSys by Michelsen⁷.

In the present work it will be demonstrated how the correlation based transition model, that has previously been shown to work well for a series of wind turbine aerodynamic cases at moderate Re ⁸ over-predicts the viscous drag due to premature transition at high Re caused by the limitations of the empirical correlation functions inherent to the model. In contrast it is demonstrated how the more fundamental E^n model is capable of predicting transition in better agreement with available measurements for the full range of Re , and additionally is capable of predicting the correct drag trend with increasing Re .

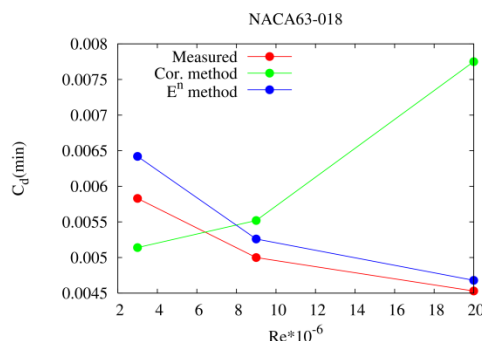


Figure 1. Variation of the minimum drag with increasing Reynolds number for the NACA 63-018 airfoil.

Acknowledgements: The original implementation of the E^n model in the EllipSys2D/3D framework were accomplished by Jess A. Michelsen shortly before his untimely death in 2005, his contribution to our computational tools is highly appreciated. The advice of F.R. Menter and R.B. Langtry concerning the correlation based transition model is highly appreciated.

^a DTU Wind Energy, Aeroelastic Design Section, Frederiksborgvej 399, DK-4000 Roskilde, DK

¹ Michelsen. Technical Report, AFM 92-05, Technical University of Denmark, 1992.

² Sørensen. PhD thesis, Riso-R-827-(EN), Riso National Laboratory, Denmark, 1995.

³ Rhie. PhD thesis, Univ. of Illinois, Urbana-Champaign, 1981.

⁴ Menter. AIAA Paper 932906, AIAA, 1993.

⁵ Langtry and Menter. AIAA Journal, Vol 47, No 12, Dec. 2009.

⁶ Drela and Giles. AIAA Journal, Vol 25, No 10, 1987.

⁷ Michelsen. Riso-R-1349(DA).

⁸ Sørensen et al., Wind Energy, 14, 1, 2011, p 77-90.

⁹ Loftin and Bursnall, NACA-964, 1950.

Wind tunnel measurements on the influence of turbulence on polars and flow separation of an airfoil

T. Homeyer^a, G. Kampers^a, A. Manso Jaume^b, J. Wild^b, J. Peinke^a, G. Gülker^a, M. Hölling^a

The influences of turbulence on the performance of the airfoil and on the appearing forces are of great interest in wind energy since fluctuations and gusts are common in the atmospheric boundary layer¹. To analyse and understand the effects, measurements in laminar and turbulent inflow conditions on a DU91-W2-250 airfoil are performed in a Göttingen type wind tunnel. An adjustable and reproducible turbulent flow is generated with an active grid². Different experimental methods are used and compared with each other. With this knowledge active and passive control strategies to alleviate loads can be envisaged.

Polar lines are measured with 3 different methods. Two force sensors and a pitch moment sensor are attached to the airfoil that is arranged in a closed test section with rotatable end plates and allow an analysis of the force dynamics under turbulent conditions. First results of the force balance under laminar conditions are in good agreement with the coefficients gained with wall pressure measurements in the wind tunnel (Figure 1a) and with comparative CFD simulations applying the DLR structured flow solver FLOWer³. The local pressure distribution on the airfoil (Figure 1b) is obtained by pressure tabs, which are sampled with a 32-channel pressure scanner. This allows a direct measurement of the local flow separation and the stall effect on the suction side. The integrated pressure distribution yields lift and drag curves that are also in good agreement with the results of the other methods (Figure 1a). The side walls of the wind tunnel out of Plexiglas allow optical access to the turbulent flow around the airfoil. Measurements with a high speed stereo PIV system are possible to investigate the local flow separation with a high temporal resolution. The presentation will summarize first measurements with the mentioned experimental methods for laminar and the planned turbulent inflow conditions.

^a ForWind - Center for Wind Energy Research, Institute of Physics, University Oldenburg Carl-von-Ossietzky-Str. 9-11, 26129 Oldenburg, GER, Email of corresponding author: tim.homeyer@uni-oldenburg.de

^b German Aerospace Center (DLR), Institute of Aerodynamics and Flow Technology, Lilienthalplatz 7, 38108 Braunschweig, GER

¹ Mücke et al., *Wind Energ.* **14**, 301 (2011)

² Wächter et al., *JTurb* **13**, 26 (2012)

³ Raddatz and Fassbender, *Notes on Numerical Fluid Dynamics and Multidisciplinary Design* **89**, 27, ISBN 3-540-24383-6 (2005)

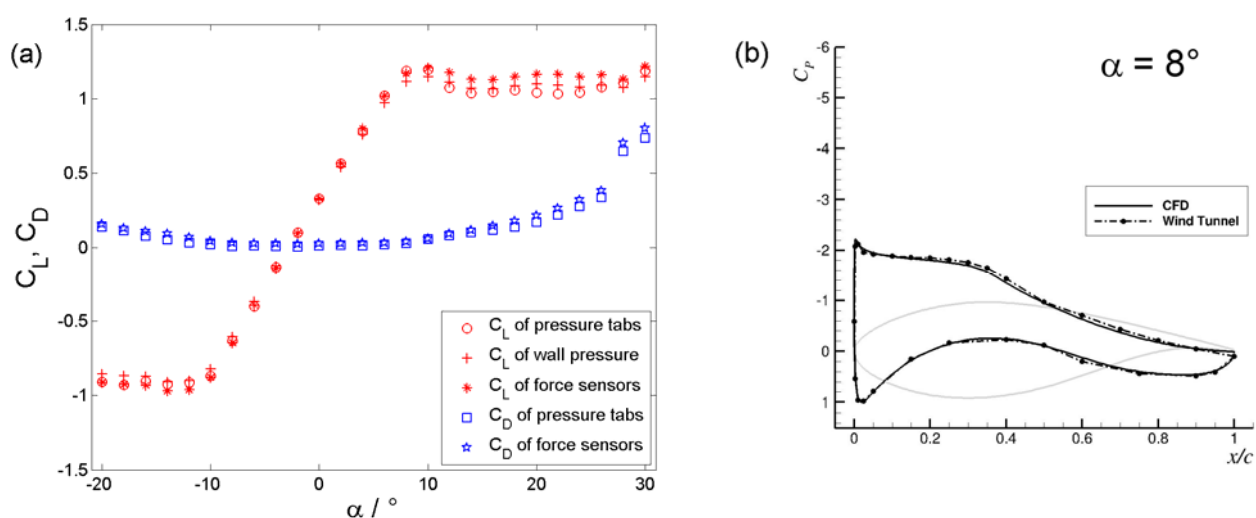


Figure 1: (a) Lift and drag coefficients for the DU91-W2-250 airfoil measured with different methods for a Reynolds number of approximately 643,000 and boundary layer tripping. (b) Comparison of pressure distributions on the airfoil for an angle of attack close to stall obtained by CFD and wind tunnel, respectively.

On the dynamics of turbulent wedges generated by different single surface roughness elements

D. Traphan^a, P. Meinlschmidt^b, O. Lutz^c, J. Peinke^a and G. Gülker^a

It is known that small surface defects on rotor blades of wind turbines can cause significant power loss and unfavourable loads. In order to better understand the governing physical effects, in this experimental study, the formation of a turbulent wedge over a flat plate and an airfoil induced by single surface roughness elements is under investigation.

The experiments are performed at different Reynolds numbers and inflow conditions, thus allowing conclusions about the formation of a turbulent wedge in vivo. With respect to typical initial faults on operating rotor blades, the roughness elements are modified in both size and shape (raised or recessed). None intrusive experimental methods, such as high-speed stereoscopic PIV and LDA, and HWA enable investigations based on temporally and spatially highly resolved velocity measurements. In this way, a spectral analysis of the turbulent boundary layer is performed and differences in coherent structures within the wedge are identified (see figure 1). These findings are correlated with global measurements of the wedge carried out by infrared thermography. This correlation aims to enable distinguishing the cause and main properties of a turbulent wedge by the easy applicable method of infrared thermography, which is of practical relevance in the field of condition monitoring of wind turbines (see figure 2). Finally, the impact of a fault on the performance of an airfoil is quantified by lift and drag measurements in the wind tunnel. By means of HSPIV and a temporally highly resolving multi-component scale, these measurements show a change in the stall behaviour and the dynamical loads of the airfoil.

The obtained findings are in good agreement with other experimental studies on similar topics.¹

^a ForWind - Center for Wind Energy Research, Inst. of Physics, University of Oldenburg, Germany

^b Fraunhofer Wilhelm-Klauditz-Institute for Wood Research (WKI), Braunschweig, Germany

^c Authorized Expert on Fibre Composite Materials, Bundorf, Germany

¹ Zhong et al., J. Fluids Engineering, 125(2): 267-274 (2003)

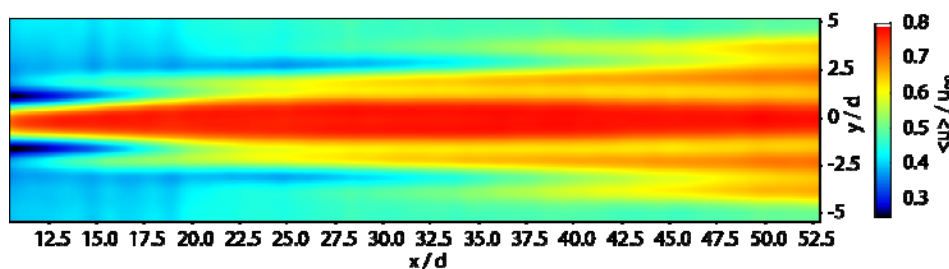


Figure 1: Averaged HSPIV measurement of a turbulent wedge over a flat plate downstream of roughness element (roughness element at $(x/d; y/d) = (0; 0)$, $Re_d=1200$, normalized to height of roughness element d and free stream velocity u_∞ , light sheet parallel to surface).

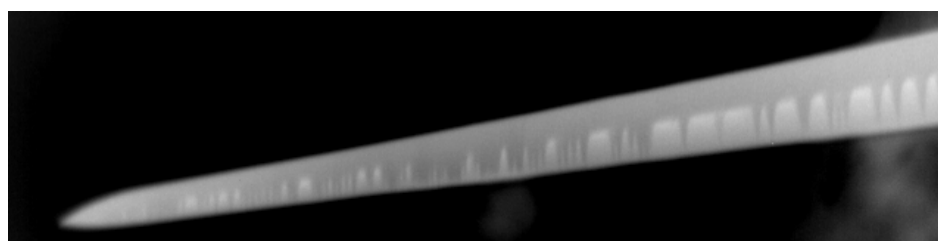


Figure 2: Thermogram of a blade's suction face on an operating wind turbine (movement is downwards): the turbulent wedges generated by surface defects appear colder (dark).

Particles

On the Hybrid-Type Method of Brownian Dynamics and Lattice Boltzmann for a Magnetic Colloidal Suspension

Akira Satoh^a

From the viewpoint of applying the lattice Boltzmann method to a flow problem of magnetic suspensions, we have investigated the feasibility of the hybrid-type method of lattice Boltzmann and Brownian dynamics combined with the viscosity-modifying technique. The viscosity-modifying technique is employed for sophisticating the activating level of the translational and rotational Brownian motion of magnetic particles. In the present study we have treated aggregation phenomena in thermodynamic equilibrium for verifying the feasibility of the present hybrid-type simulation method and for clarifying the characteristics of the scaling coefficients of viscosity. From the results regarding the snapshots and pair correlation functions of magnetic particles, the present hybrid-type simulation method combined with the viscosity-modifying technique is seen to show good agreement with the results of Monte Carlo method in both quantitative and qualitative points. For example, physically reasonable aggregate structures can be obtained such as linear chain-like and network-like clusters in the cases of strong magnetic particle-field and particle-particle interactions, respectively. Moreover, the characteristics of the magnetization as a function of the magnetic field strength are also in good agreement with Monte Carlo results, which implies that the rotational Brownian motion is activated at a physically reasonable level. The characteristics of the translational and rotational scaling coefficients are summarized as follows. These scaling coefficients are seen to be almost constant and independent of the strengths of magnetic particle-field and particle-particle interactions. Moreover, they are also almost constant for the change in the volumetric fraction and also for the change in the number of particles unless a significantly coarse lattice system is used. We may conclude from these results that the present hybrid-type method combined with the viscosity-modifying technique is quite a possible technique for simulating a flow problem of magnetic particles in the situation of a gradient (non-uniform) applied magnetic field.

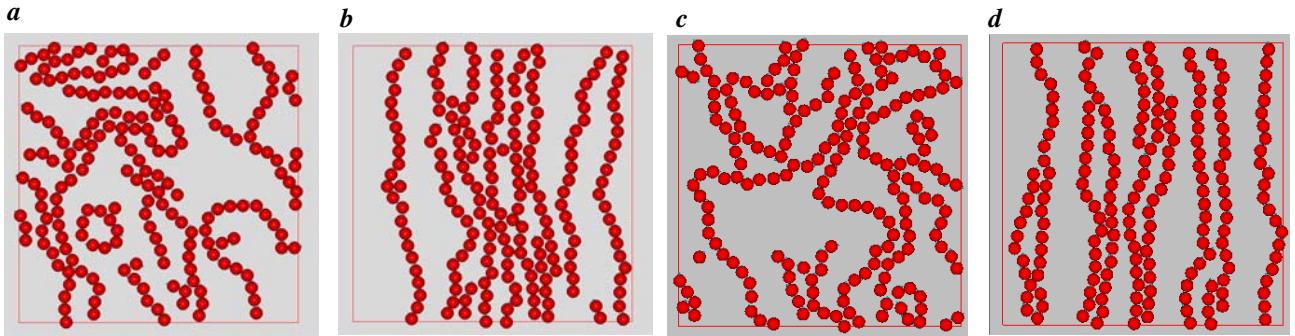


Fig.1. Aggregate structures: (a) for the magnetic particle-particle interaction strength $\lambda=10$ and the magnetic field strength $\xi=1$, hybrid LB; (b) for $\lambda=10$ and $\xi=10$, hybrid LB; (c) for $\lambda=10$ and $\xi=1$, MC; (d) for $\lambda=10$ and $\xi=10$, MC; a magnetic field is applied in the upward direction.

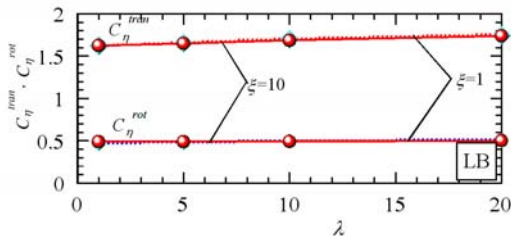


Fig.2 Dependence of the scaling factors of the viscosity on the magnetic particle-particle interaction strength for $\xi=1$ and 10.

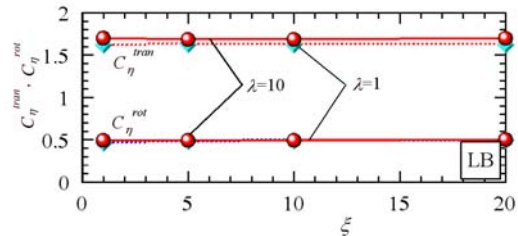


Fig.3. Dependence of the scaling factors of the viscosity on the magnetic field strength for $\lambda=1$ and 10.

^a Faculty of Systems Science and Technology, Akita Prefectural University, 84-4, Ebinokuchi, Tsuchiya-aza, Yuri-honjyo 015-0055, Japan

Breakup of small particle aggregates in wall-bounded turbulent flows

M. U. Babler^a, L. Biferale^b, L. Brandt^c, U. Feudel^d, K. Guseva^d, A. S. Lanotte^e, C. Marchiolif, F. Picano^c, G. Sardina^c, A. Soldati^f, and F. Toschi^g

Turbulence affects suspended particles in many ways,¹ i.e. preferential concentration, dispersion, and collisions. In many particulate systems, e.g. colloids and micrometer sized particles, the particles upon collision stick together and form aggregates. The formation and evolution of these aggregates is affected by turbulence in multiple ways: On one hand, turbulence enhances the growth of aggregates due to particle collisions; while on the other hand, it also can cause their breakup due to hydrodynamic stress. Breakup is an important process in many engineering applications and natural processes. In particular, it is one of the two main mechanisms that can stop aggregate growth in a suspension of infinite extension² and it crucially affects the particle dispersion in engineering applications.

In the past the role of turbulence on aggregate breakup was mainly addressed experimentally, e.g. by measuring the evolution of the aggregate size, or by means of population balance modelling. Recently, we used direct numerical simulations of particle laden flows to explore the dynamics of breakup of small aggregates in homogeneous turbulence.³ In these simulations, the aggregates had negligible inertia and were assumed small with respect to the Kolmogorov length scale. Furthermore, breakup was assumed to occur whenever the local hydrodynamic stress, taken proportional to local energy dissipation, exceeds a predefined threshold which is a characteristic of a given type of aggregates.⁴ From measuring the evolution of dissipation along an aggregate trajectory we then obtained the breakup rate, i.e. the number of breakup events per unit time as function of the threshold dissipation, which presents an elementary quantity for describing dynamics of aggregating particles.

In this work, we extend the analysis to wall-bounded turbulent flows, namely a boundary layer flow and a channel flow. Aggregates are released close to the wall and away from it and their trajectories are followed until the first occurrence of a local dissipation exceeding a predefined threshold representing the aggregate strength. From the timespan in between release of an aggregate to the point of breakup, the breakup rate is obtained.

Despite the strong non-homogeneity and the presence of a mean shear in wall-bounded flows, the measured breakup rate shows some remarkable similarities to the breakup rate in homogeneous turbulence. In particular, for weak aggregates the breakup rate as a function of the critical threshold dissipation describes a power law that, within error bars, is consistent in both scaling and magnitude among the different flows. To corroborate and better understand this behavior we additionally considered a synthetic turbulent flow obtained by stochastically evolving the Fourier modes of a random velocity field. Measuring the breakup rate in this flow leads to a similar power law behaviour, suggesting that the latter is caused by weak turbulent fluctuations, well represented by Gaussian statistics.

Strong aggregates, on the other hand, survive for a longer time during which they move further away from the point of release until suffering breakup due to the mean shear close to the wall. The breakup rate of strong aggregates therefore is substantially larger in wall-bounded flows when compared with homogeneous turbulence where only rare intermittent burst can break strong aggregates.

Support from EU-COST action MP0806 “Particles in Turbulence” is kindly acknowledged.

^a Dept. Chemical Engineering and Technology, KTH Royal Institute of Technology, Stockholm, Sweden.

^b Dept. Physics and INFN, University of Rome Tor Vergata, Rome, Italy.

^c Linné FLOW Center, KTH Mechanics, Stockholm, Sweden.

^d Theoretical Physics/Complex Systems, ICBM, Carl von Ossietzky University, Oldenburg, Germany.

^e ISAC-CNR and INFN, Sez. Lecce, Lecce, Italy.

^f Dept. of Electrical, Managerial & Mechanical Eng., University of Udine, Udine, Italy, and Dept. Fluid Mechanics, CISM, Udine, Italy.

^g Dept. Applied Physics, Eindhoven University of Technology, Eindhoven, the Netherlands.

¹ Toschi and Bodenschatz, *Ann. Rev. Fluid Mech.* **41**, 375-404 (2009)

² Soos et al., *J. Colloid Interface Sci.* **319**, 577-589 (2008)

³ Babler et al., *Phys. Rev. E* **85** 025301 (2012)

⁴ Babler et al., *J. Fluid Mech.* **612**, 261-289 (2008)

Positron Emission Particle Tracking in Particle-Laden Rimming Flow

P. J. Thomas^a, P. Denissenko^a, E. Guyez^b, D.J. Parker^c and J.P.K. Seville^d

Positron Emission Particle Tracking (*PEPT*) is an experimental measurement technique, developed at the University of Birmingham, that enables tracking the motion of single, small tracer particles among large (opaque) granular samples of similar particles in motion. The *PEPT* technique relies on the tracer particle being tagged with a radioactive isotope and upon the detection of positrons emitted from the tracer particle during beta decays of unstable nuclei [1]. We describe results from the first experimental study that employed *PEPT* to study the motion of a single tracer particle within a particle-laden rimming flow.

Rimming flow is the flow established when a partially liquid-filled rotating cylinder rotates with rotational velocity ω around a horizontal axis as schematically illustrated in a cross-sectional representation in Fig. 1. For rimming flows of particle-laden liquids we first reported a pattern-formation phenomenon [2] where particle samples initially distributed uniformly throughout the carrier liquid were observed to segregate and accumulate to form the type of banding pattern shown in Fig. 2. The figure displays a head-on view of the cylinder and shows a structure of regularly-spaced circumferential particle-rich regions separated by regions of liquid almost entirely free of granules. Subsequently we observed that these particle bands can drift along the length of the cylinder to develop highly complex but often very regular space-time dynamics of the entire pattern on timescales of up to several weeks (see Ref. [3] and our publications cited therein).

It was hitherto unknown what drives the space-time dynamics of the granular bands, how the particles enter and exit from the bands, how the motion of a single particle relates to the overall macroscopic pattern dynamics and what the effects of the cylinder end walls on the band dynamics are. In order to begin answering these questions we have performed our *PEPT* study and here we will briefly summarize the first results obtained from the analysis of the data obtained [4].

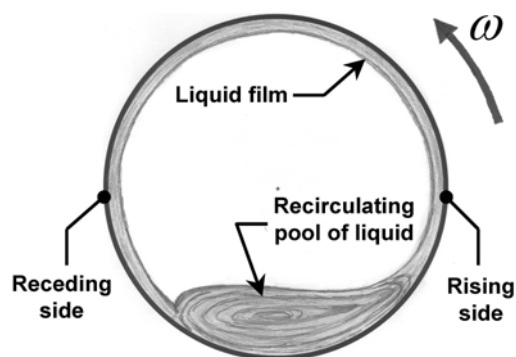


Fig 1: Rimming flow in cross-sectional representation of the horizontally rotating cylinder.

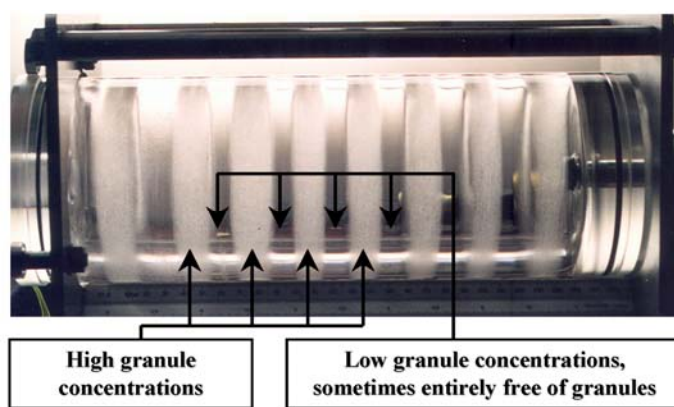


Fig. 2: Segregation-band pattern.

^a Fluid Dynamics Research Centre, School of Engineering, University of Warwick, Coventry CV4 7AL, United Kingdom

^b CEA DEN, 17 rue des Martyrs, 380 Grenoble, France

^c School of Physics and Astronomy, University of Birmingham, Birmingham B15 2TT, United Kingdom

^d Department of Chemical and Process Engineering, University of Surrey, Guildford GU2 7XH, United Kingdom

¹ Parkert *et al.*, *Nuclear Instr. & Methods in Phys. Res. A*, **477**, 540, (2002)

² Boote & Thomas, *Phys. Fluids* **11**, 2020, (1999)

³ Seiden & Thomas, *Rev. Mod. Phys.* **83**, 1323, (2011)

⁴ Denissenko *et al.*, *Phys. Fluids*, under review, (2014)

Modeling particle accumulation in large-Prandtl-number thermocapillary liquid bridges using high-resolution numerical simulations

T. Leme^a and H.C. Kuhlmann^b

We consider the particle-laden flow in a liquid bridge which is formed in the gap between two solid concentric cylinders. A thermocapillary flow is driven along the liquid-gas interface when the ends of cylinders are kept at different temperatures. The setup represents an elementary model of the floating-zone crystal-growth technique¹.

Schwabe et al.² observed that, under certain flow conditions, tracer particles de-mix and form peculiar closed rotating patterns. These line-like particle accumulation structures (PAS) have been investigated numerically and experimentally (Fig. 1). One of the objectives of the JEREMI experiment, which is expected to be launched to the ISS in 2016, is to study the formation of PAS under microgravity. In the space experiment high-Prandtl-number liquids will be employed. To prepare the experiments reliable numerical predictions for high-Prandtl-number fluids are mandatory to preselect the parameters which are required to observe PAS. Furthermore, numerical simulations are key to understanding this complex non-linear phenomenon. To date, accurate numerical simulations³ have been performed for flows with a relatively small Prandtl number ($Pr=4$).

Our work focuses on the modeling of the flow structure and the particle accumulation in thermocapillary liquid bridges with Prandtl number $Pr=28$ using high-resolution three-dimensional numerical simulations using OpenFOAM. For a precise modeling the material properties of the liquid and the particles, buoyancy forces (for comparison with ground experiments) and the hydrostatic shape of the liquid bridge are taken into account.

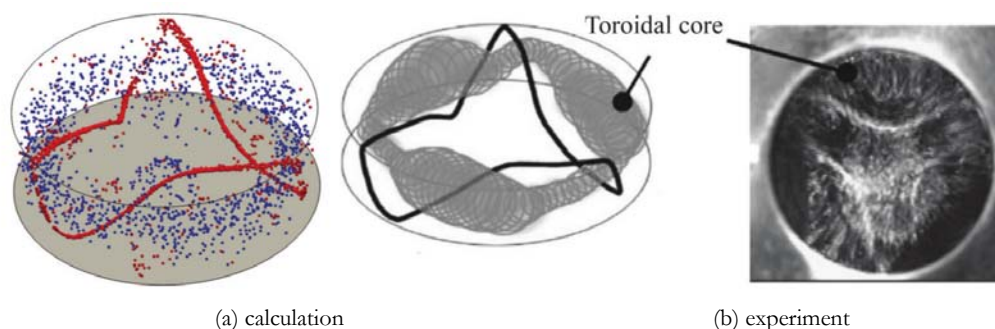


Fig 1 Visual comparison of PAS (a) computed³ for $Pr=4$ and $Re=1800$ and (b) experimental observation⁴ for $Pr=28$

^a Institute of Fluid Mechanics and Heat Transfer, TU Wien, Resselgasse 3, 1040 Vienna, Austria,

^b Institute of Fluid Mechanics and Heat Transfer, TU Wien, Resselgasse 3, 1040 Vienna, Austria,

¹ H. C. Kuhlmann, Springer Tracts in Modern Physics, vol. 152, Springer, Berlin, Heidelberg (1999).

² D. Schwabe et al., *Microgravity Sci. Technol.* **9**, 163-168 (1996).

³ R. V. Mukin and H. C. Kuhlmann. *Phys. Rev. E* **88**, 053016-1-053016-20 (2013).

⁴ S. Tanaka et al., *Phys. Fluids* **18**, 067103 (2006).

Experimental study of sedimentation dynamics of concentrated fluid-solid mixtures in tilted conducts

S. Palma ^a, C. Ihle ^b, A. Tamburrino ^c and S. Dalziel ^d

Long distance slurry pipelines in complex topographies often exhibit inclined sections throughout their routes. It is known that such sloping sections affect both pressure losses and particle organization after system shutdown. This process may have important implications on subsequent restarting operations. In this research, an experimental and numerical work have been done to study the particle migration details after stopping a quasi-homogeneous, turbulent transport pumping of a high concentration suspension of spheres in a Newtonian fluid. The purpose of the present experimental work is to obtain a more complete understanding of the conditions leading to wave formation and growth during sedimentation in tilted conducts by extending the analysis over a wider range of parameter space than was covered up to now. Problems parameters considered in present experiments are particle concentration of different species, physical properties of the particles and conduct slope. Experiments have been done using a perspex, square-shaped section conduct for different inclinations, filled with highly concentrated water-resin slurries. Sedimentation process and particle trajectories have been analyzed using particle tracking velocimetry (PTV) and light-extinction algorithm.

Figure 1 shows some results of the sedimentation dynamics of concentrated fluid-solid mixtures in tilted conducts. Left panel shows the final deposition of particles within a conduct of 27° relative to the horizontal plane for volume concentrations of 10% (Figure 1a), 20% (Figure 1c), and 30% (Figure 1e). On the other hand, right panel shows sedimentation process after system shutdown for volume concentrations of 10% (Figure 1b), 20% (Figure 1d), and 30% (Figure 1f). Wave formation and growth during the sedimentation process may be observed in certain experimental conditions.

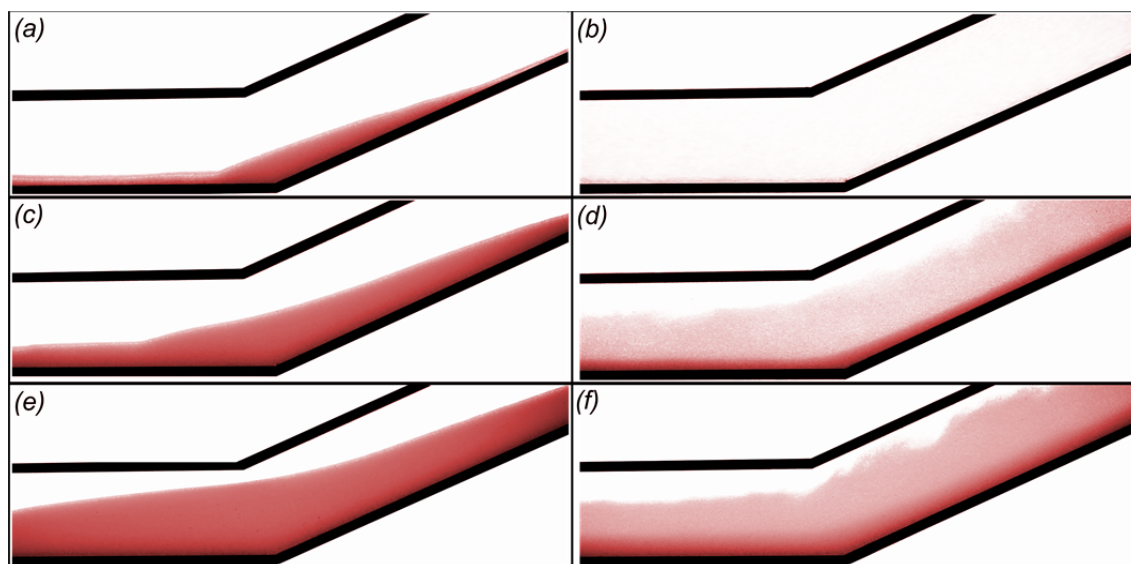


Figure 1: Left panel: final deposition of particles. Right panel: sedimentation process after system shutdown for volume concentrations of 10% (a-b), 20% (c-d) and 30% (e-f).

^a Advanced Mining Technology Center, University of Chile, Chile.

^b Department of Mining Engineering, University of Chile, Chile.

^c Department of Civil Engineering, University of Chile, Chile.

^d Department of Applied Mathematics and Theoretical Physics, University of Cambridge, UK.

DNS of the initiation of subaqueous sedimentary patterns in a horizontal channel flow

A. G. Kidanemariam^a and M. Uhlmann^a

Direct numerical simulations (DNS) of the formation of subaqueous sedimentary patterns in a statistically uni-directional channel flow configuration have been performed both in the laminar and turbulent regimes. A very large number of freely moving spherical particles (of the order of 10^5) are considered which make up an initially flat, mobile sediment bed. All the relevant length and time scales of the (turbulent) flow, even in the vicinity of the particles, have been accurately represented by employing an immersed boundary method¹ to resolve the fluid-solid interface. A soft-sphere model has been incorporated into the flow solver to treat inter-particle contacts. The Reynolds number of the flow, based on the bulk velocity u_b and the channel half-height δ , was set at a value $Re_b \approx 350$ for the laminar case and at a value $Re_b \approx 3000$ for the turbulent case. The spherical particles are monodispersed with a diameter $D \approx \delta/25$ and a density $\rho_p = 2.5\rho_f$, where ρ_f is the density of the fluid. The value of the Galileo number, defined as $Ga^2 = (\rho_p/\rho_f - 1)gD^3/\nu^2$ where ν is the kinematic viscosity of the fluid and g is the acceleration due to gravity, is chosen such that the value of the Shields number, which is the ratio of the bottom shear stress to the apparent weight of the particle, is above the critical value for incipient particle motion. These sets of parameter values lie in the regimes of ‘small-dune’ and ‘vortex-dune’ formation, when compared to the phase diagram proposed in the experimental study² where the formation of different dune patterns was investigated.

As a result of the net effect of the driving hydrodynamic force, gravity force as well as forces arising from inter-particle contacts, particle erosion and transport is observed to take place. The continued process of erosion from certain preferred regions and deposition at other downstream regions, introduces small perturbations to the initially flat sediment bed which ultimately leads to the organization and formation of the patterns as is shown in figure 1. In this contribution, we characterize the time evolution of the sediment bed and address the aspects related to the initial bed instability.

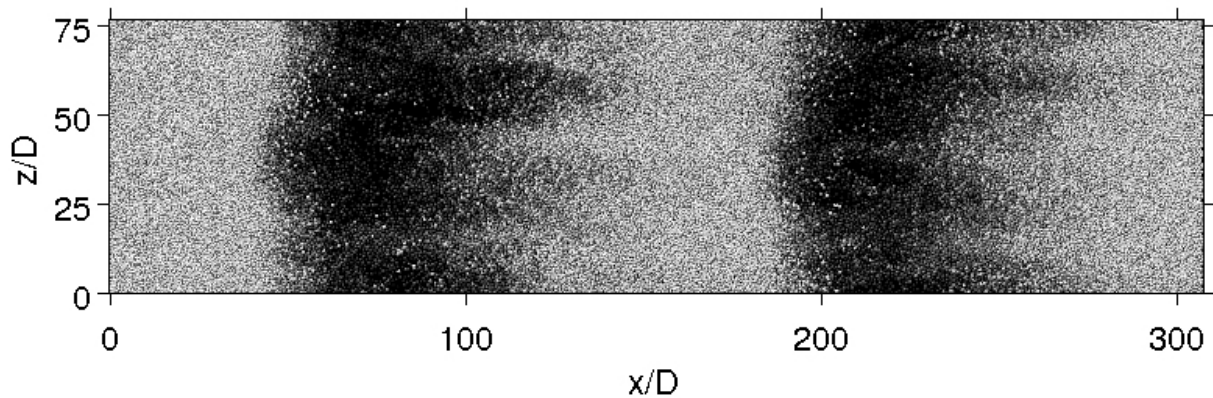


Figure 1: An instantaneous snapshot of particle positions corresponding to the turbulent regime. The particles are coloured based on the wall-normal location of their centre, bright colour showing particles located at higher wall-normal location and vice-versa.

^a Institute for Hydromechanics, Karlsruhe Institute of Technology (KIT), Kaiserstr.12, 76131, Karlsruhe, Germany

¹ Uhlmann M., *J. Comput. Phys.* **209**, 448-476 (2005).

² Ouriemi M., Aussillous, P., and Guazzelli E., *J. Fluid Mech.* **636**, 295-319 (2009).

Reynolds number effects in particle-laden turbulent channel flow

Helge I. Andersson^a, Lihao Zhao^a, Christopher Nilsen^a and Niranjana Reddy Challabotla^a

Direct numerical simulation (DNS) studies of turbulent flow are restricted to fairly low Reynolds numbers, especially for particle laden flows. Almost all simulations of particle-laden turbulent channel flows are performed at low friction Reynolds numbers, typically $Re = 150$ or $Re = 180$, and although some exceptions exist¹⁻³, there are, to the best of our knowledge, no systematic investigations of the effect of Reynolds number on basic particle statistics.

The present work aims to investigate the statistics of particle-laden flow and the dependence on flow Reynolds number, by using DNS of turbulent channel flow with suspended Lagrangian point-particles. Three different Reynolds numbers $Re_1=100$, $Re_2=180$ and $Re_3=395$, and four different Stokes numbers between 1 and 100, are used to evaluate Reynolds number effects for particle flow with varying degree of particle inertia. To better interpret the results, we defined ratios $R1=(\Phi(Re_2)-\Phi(Re_1))/\Phi(Re_1)$ and $R2=(\Phi(Re_3)-\Phi(Re_2))/\Phi(Re_2)$ where Φ can be either a fluid (f) or particle (p) velocity. If $R2$ is smaller than $R1$, this indicates that the Reynolds number dependence of fluid or particle velocities is reduced when the Reynolds number increases. The Reynolds number effects on the mean and RMS velocities are examined with this method. Only the results of fluid and particle mean streamwise velocities with Stokes number 1 and 30 are shown in Figure 1 and further results will be shown in the conference presentation. The reduction from $Rf1$ to $Rf2$ indicates that the mean fluid velocity statistics are converging at higher Reynolds number. While the particle statistics for Stokes number 1 shows a similar converging trend as the fluid for $y^+ > 10$ the Reynolds number dependence becomes stronger close to the wall ($y^+ < 10$). At Stokes number 30, the results reveal increasing Reynolds number dependence at higher Re for $y^+ < 20$. Additional fluid and particle statistics will be analyzed at all four Stokes numbers before final conclusions are drawn about the Reynolds number dependence of particles.

^a Department of Energy and Process Engineering, Norwegian University of Science and Technology, Trondheim, Norway

¹ Marchioli and Soldati, *Advances in Turbulence XI*, **117**, 298-300 (2007), Springer Proceedings Physics.

² Zhao and Andersson, *Commun. Comput. Phys.* **11**, 4 (2012).

³ Nilsen, Andersson and Zhao, *Phys. Fluids* **25**, 115108 (2013).

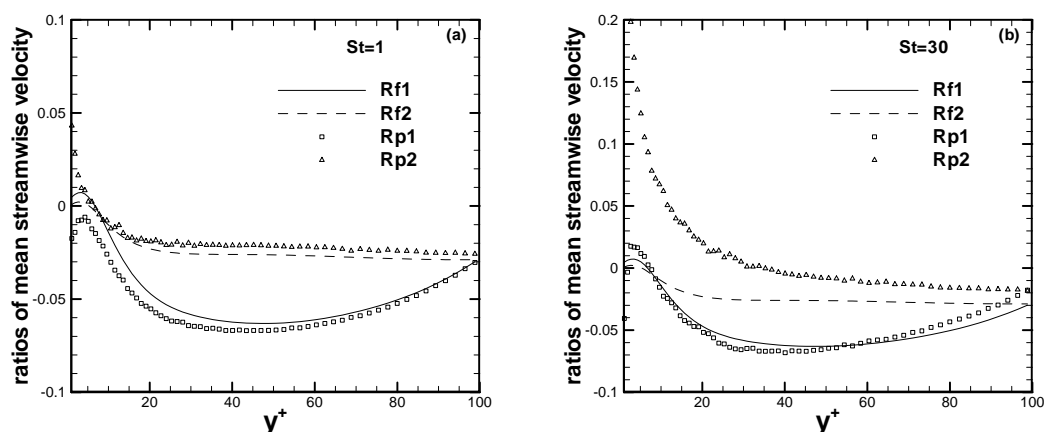


Figure 1: Ratio of mean fluid (lines) and particle (symbols) velocity in streamwise direction. (a) $St=1$, (b) $St=30$.

Turbulent Mixing of diffusiophoretic particles in a density stratified flow

Lukas Schmidt^a, D. Krug^b and M. Holzner^a

Turbulent mixing is ubiquitous in everyday life, nature as well as industrial applications. The ability of turbulent flows to promote mixing of particles and passive tracer is incontestable. Particle transport may additionally be affected by “active” particles which move relative to the flow due to chemical or biological activity. This activity originates at small scales but leads to macroscopic effects, e.g. particle aggregation or swarming of organisms. The coupling between small and large scale effects is not yet fully clarified, nevertheless it is important to advance the understanding of biological (e.g. collective behaviour) and technological (e.g. gels, polymer drag reduction) applications. The focus of this study is the behaviour of diffusiophoretic particles, i.e. particles that move towards regions of higher concentrations of a solute, in a turbulent flow. The aim is to improve the understanding of the possible role of diffusiophoresis on particle clustering and aggregation in density stratified environments. In addition, the setup serves as a model system for the dynamics of chemotactic organisms.

At ETH Zurich a facility has been designed to analyse particle distribution in density stratified flows across a turbulent/non-turbulent interface with simultaneous particle tracking velocimetry (PTV) and laser induced fluorescence (LIF) measurements¹ (see Fig. 1a). A density stratified flow is created by letting a water/ethanol mixture flow ($\rho=996.7\text{ kg/m}^3$, $Re_{Inlet}=4000$) along a sloping wall ($\alpha=10^\circ$) on top of a water/salt mixture ($\rho=1000.7\text{ kg/m}^3$) which is gently resupplied through perforated pipes located at the ground of the tank to compensate for the fluid drained through the outflow (Fig. 1). Both fluids are matched in terms of refractive index in order to avoid any undesired distortion of light used to visualize particles as well as fluorescent dye¹. A planar investigation domain of $9.5 \times 9.5\text{ cm}^2$ illuminated by a laser is used to observe the flow, particularly the interfacial region. Two high-speed cameras record simultaneous PTV and LIF measurements. Thus, it is possible to obtain information on particle position, velocity and simultaneously the density field (see Fig. 1b).

In a first step, particle distribution conditioned on distance from the upper wall, as well as density are being compared for polystyrene particles ($d=45\mu\text{m}$) and diffusiophoretic particles ($d_{mean}=54\mu\text{m}$). Since particles have only been seeded into the upper, lighter fluid it is possible to specifically analyse how the density stratification affects particle movement. Further analysis will address a more detailed investigation of the diffusiophoretic effect using a three dimensional analysis of particle trajectories.

^a Inst. Environmental Eng. – Environmental Fluid Mechanics, ETH Zürich, Stefano-Franscini-Platz 5, 8093 Zürich, CH

^b Inst. Environmental Eng. – Groundwater and Hydromechanics, ETH Zürich, Stefano-Franscini-Platz 5, 8093 Zürich, CH

¹ Krug et al., *Experiments in Fluids* **54**, 1530 (2013)

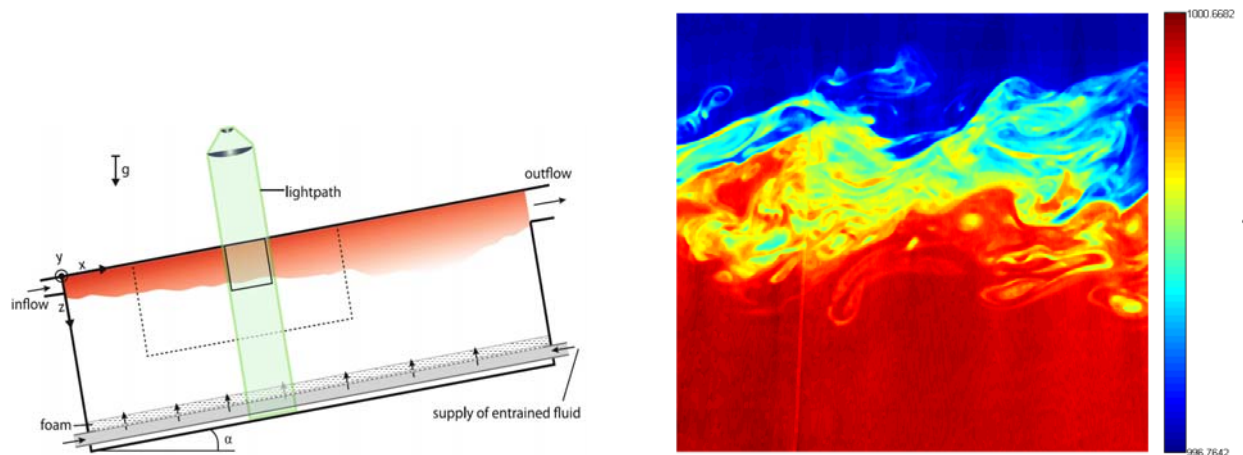


Figure 1: (a) Experimental setup with lighter (red) fluid on top¹ (b) Density field in the investigation domain (LIF)

Diffusiophoresis at the macro-scale

C. Mauger^{a,e}, N. Machicoane^{b,e}, R. Volk^{b,e}, M. Bourgoïn^{c,e}, C. Cottin-Bizonne^{d,e},
C. Ybert^{d,e} and F. Raynal^{a,e}

Diffusiophoresis is a spontaneous motion of particles induced by a salt gradient. Recently, Abecassis *et al.*¹ have shown in a *micro-channel* that this osmotic surface effect, the roots of which are fundamentally at the *nano-scale*, could provide a mechanism for tuning the rate and direction of particles transport with orders of magnitude in efficiency compared to the usual Brownian diffusivity. The aim of this work is to show that the effects of diffusiophoresis are still visible at the *macro-scale*, in mixing laboratory experiments.

To this aim, we have performed two experimental setups: the first one involves chaotic mixing in a square Hele-Shaw cell of side 5 cm, while the second one, at even larger scale, is a turbulent jet, in which turbulent mixing naturally takes place. In both cases, we consider mixing of colloidal particles in the presence of a tiny amount of salt; the salt can be initially introduced with the colloids (salt-in), or on the contrary being already mixed with the bulk (salt-out). This problem involving multi-scales phenomena, from scales naturally involved in (chaotic or turbulent) mixing down to those involved in diffusiophoresis, we chose to study spatial concentration spectra instead of the scalar variance decay; finally, we compare with the reference case, colloids without salt.

Figure 1a shows a snapshot of spatial concentration in the Hele-Shaw cell, while 1b is an instantaneous image of the jet. In figure 2 we show the spectral scalar energy dissipation: the effect of salt, in or out, is clearly visible.

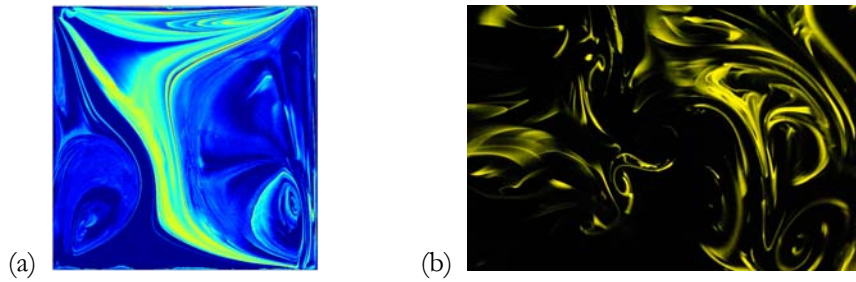


Figure 1 : instantaneous concentration field in (a) the chaotic flow and (b) in the turbulent jet.

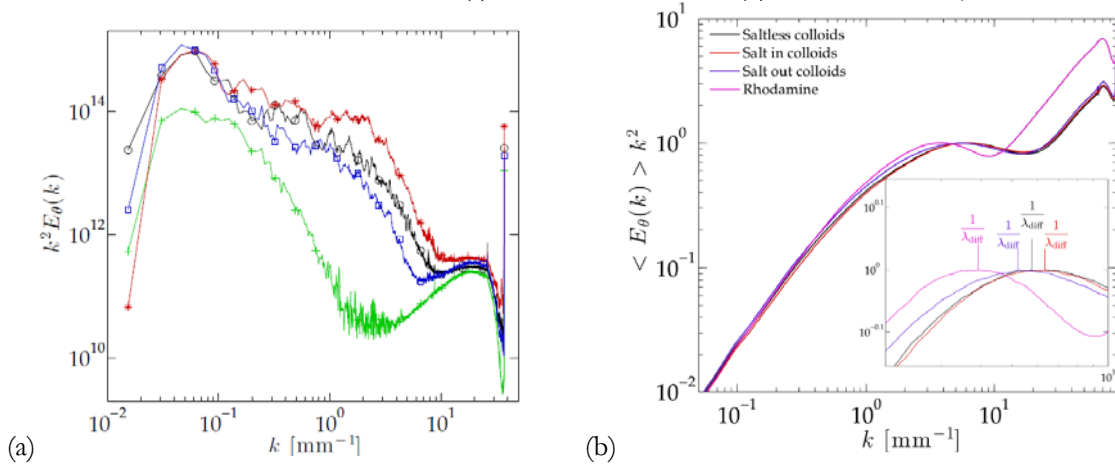


Figure 2 : Spectral scalar dissipation (a) instantaneous for the chaotic flow ; (b) averaged for the turbulent flow. Red: salt-in; black: reference (without salt); blue: salt-out. Green (a): fluorescein ; purple (b): rhodamine

^a LMFA, CNRS UMR 5509 - École Centrale Lyon - INSA de Lyon, Ecully, France

^b Laboratoire de physique de l'ENS Lyon, CNRS UMR 5672 - École Normale Supérieure de Lyon, France.

^c LEGI, CNRS UMR 5519 - Université Joseph Fourier - Grenoble INP, Grenoble, France.

^d Institut Lumière Matière, CNRS UMR 5306 - Université Lyon 1, Villeurbanne, France.

^e Labex IMUST - Université de Lyon.

¹ Abécassis et al., *New Journal of Physics*, **11**, 075022 (2009).

Fully resolved, finite-size particles in statistically stationary, homogeneous turbulence

A. Chouippe^a and M. Uhlmann^a

The migration of many particles under the influence of both turbulence and gravity is a complex problem with different interaction mechanisms that are competing with each other. In this study we employ a numerical approach, and consider a dispersed phase composed of monodisperse finite-size heavy rigid particles, and homogeneous isotropic turbulence as a background flow. The aim of our study is to focus on configurations where particles are larger than the smallest scales of the flow, which has been rarely explored in numerical experiments, in order to shed more light on interaction mechanisms involved in such configurations.

The numerical method is based on direct numerical simulation of the Navier-Stokes equations using a finite-difference technique in association with an immersed boundary method (Uhlmann¹). In order to generate homogeneous isotropic turbulence, and maintain it at a statistically stationary state, we use an external random forcing relying on large scale energy input.

First part of this study proposes to focus on the generation of the background turbulence and compare forcing methods proposed by Alvelius² and Eswaran and Pope³. Both of them consist in adding a random forcing term in momentum equation. This forcing term has to be formulated in spectral space, and acts on the smallest wavenumbers of the system. The main difference between these two methods is that Alvelius forcing is fully uncorrelated in time, while Eswaran and Pope forcing not. The methods are compared here, and then one forcing scheme is selected.

Second part of this study proposes to focus on flow laden with particles of diameter $D/\lambda \sim 1$ with a density ratio $\rho_p/\rho_f = 1.5$ in the dilute regime (volume fraction $\phi_v = 0.005$). In order to explore the influence of gravity we consider three different Galileo numbers, which are defined as $Ga = u_g D / \nu$ with $u_g = ((\rho_p/\rho_f - 1)gD)^{1/2}$. Simulations will be analysed under different aspects, focusing on the influence of the background flow on particle migration: first the influence of turbulent structures on particle trajectories and dispersed phase organization. Modification of particle settling velocity as well as wake structure will then be explored. Results will be finally compared with the numerical experiment of Doychev and Uhlmann⁴ involving the same particles but settling in an ambient fluid and highlighting clustering effects.

^a Institute for Hydromechanics, Karlsruhe Institute of Technology, 76128 Karlsruhe, Germany

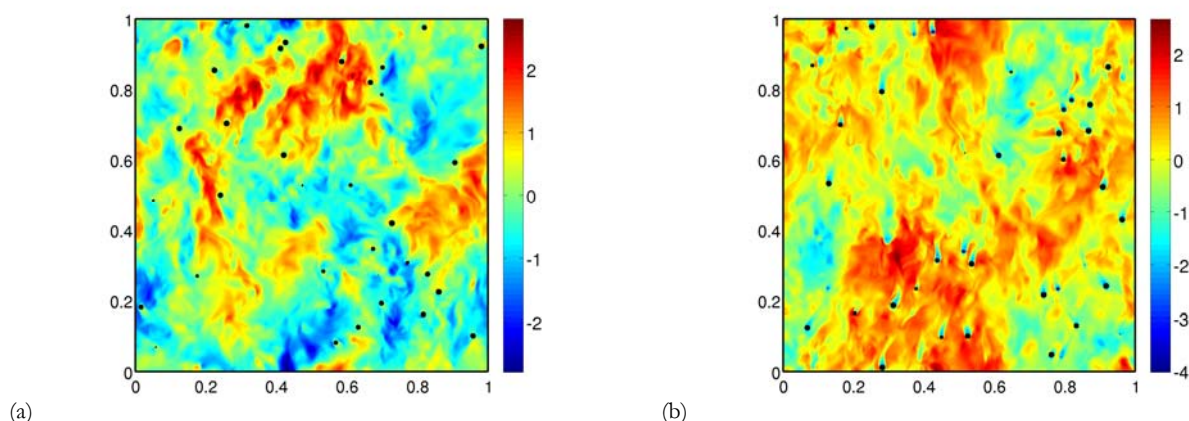


Figure 1: Vertical velocity of a flow laden with particles without gravity effects (a), and with (b)

¹ Uhlmann, J. *Comput. Phys*, **209**, 448 (2005)

² Alvelius, *Phys. Fluids*, **11**, 1880 (1999)

³ Eswaran and Pope, *Comp. Fluids*, **16**, 257 (1998)

⁴ Doychev and Uhlmann, *6-th International Conference on Multiphase Flow* (2013)

Spatially Developing Particle Laden Turbulence Subject to Radiative Heating

Hadi Pouransari^a, Ari Frankel^a, Ali Mani^a

We present results from our analysis of the three-way coupled interactions between fluid turbulence, particle transport, and radiative heating in a spatially developing turbulent flow in an inflow/outflow configuration. Such interactions are found in oil-burning furnaces, explosive solid detonation, and particle-based solar energy receivers. While the preferential concentration of inertial particles in turbulence has been investigated in numerous previous studies, little is known about the coupling between such systems and radiation. The critical focus in our study is radiative heating, which is primarily absorbed by the dispersed phase and then conductively transferred to the carrier fluid. We show that the three-way coupling between transport modes associated with momentum, particles and radiation can impact the particle field and the inhomogeneities associated with the heat transfer and temperature fluctuations. To this end, we have performed direct numerical simulations of the compressible Navier-Stokes equations under a low-Mach approximation coupled with a Lagrangian method for particle tracking. Radiative transport is solved either with an optically thin approximation or with the method of spherical harmonics to account for the effects of the optical thickness. The impact of fluid heating on local gas expansion is accounted for by solving the energy equation for the mixture. We present results for an inflow-outflow configuration with inflow initiated with homogeneous isotropic turbulence and compare three scenarios: 1) non-radiated mixture 2) radiated mixture in the optically thin limit and 3) radiated mixture in the optically thick limit. We will discuss the impact of radiative heating on the particle field over a wide range of Stokes numbers and show that radiation can lead to high-wavenumber activity in the fluid kinetic energy spectrum.

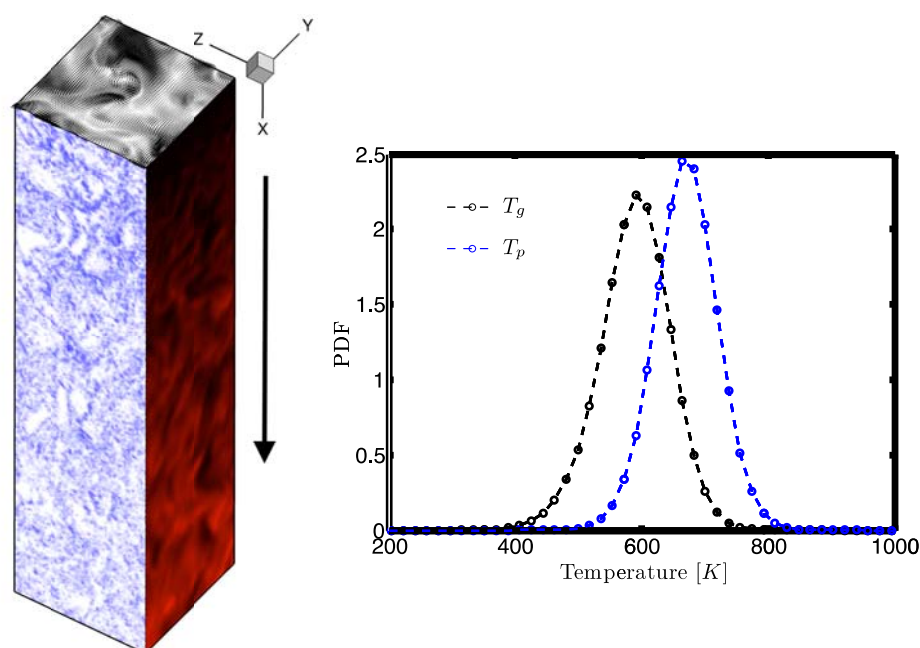


Figure 1 Left: contours of particle concentration (left side), gas temperature (right side), and projected gas velocity field (top side). Inflow gas temperature is 300K, while the average outflow gas temperature is about 600K. Right: probability distribution function of gas and particle temperature at the domain outlet.

^a Department of Mechanical Engineering, Stanford University, Stanford, CA, 94305, USA

Interface-resolved direct numerical simulations of turbulent channel transport of finite-sized particles

P. Costa^a, B. J. Boersma^b, J. Westerweel^a and W.-P. Breugem^a

Flows laden with solid particles are present in a wide range of applications. Examples are the sediment transport in a riverbed, the enhanced mixing due to the presence of particles in a fluidized bed reactor, or the flocculation/sedimentation processes in the treatment of drinking water. In all these examples and many others the flow is turbulent, the particle size is larger than the smallest length-scale of the turbulent fluid motion (i.e., the particles are finite-sized) and the volume fraction of particles can be considerably high. Studying turbulent flows laden with finite-sized particles by means of interface-resolved numerical simulations became possible with the recent developments of computationally efficient numerical methods for 2-way coupling, such as immersed boundary methods (IBM), together with the continuous increase in computing power. When the flow is dense, it is important to combine the detailed 2-way coupling solver with a realistic model for short-range particle-particle/-wall interactions (4-way coupling). Otherwise, the physical realism of the solution is lost whenever a collision occurs.

We simulated turbulent transport of finite-sized, spherical particles in a plane channel. The governing equations for the fluid phase are solved with a standard second-order pressure-correction/finite-volume method. This set of equations is coupled with the governing equations of the particle motion (Newton-Euler) through the imposition of no-slip/no-penetration boundary conditions at the particle surface. To achieve this we used a second-order accurate IBM¹.

The numerical algorithm was extended with a lubrication model and a variant of a soft-sphere collision model for oblique particle-particle/-wall collisions. The effect of this model on the computational efficiency of the overall numerical algorithm is negligible. We validated the model against several benchmark experiments of particle-particle/-wall interactions in viscous liquids. As an example, Figure 1 shows a comparison between our simulations and experiments of Gondret et al.² of the bouncing motion of a 3mm steel sphere colliding onto a planar surface in a viscous liquid.

We present the validation of our model for short-range particle-particle/-wall interactions and some preliminary results of interface-resolved direct numerical simulations (DNS) of turbulent channel transport of finite-sized particles, to illustrate the potential of our method for describing with detail this complex flow.

^a TU Delft, Laboratory for Aero and Hydrodynamics, Leeghwaterstraat 21, 2628 CA Delft, The Netherlands

^b TU Delft, Dep. Process and Energy – Energy Technology, Leeghwaterstraat 39, 2628 CA Delft, The Netherlands

¹ Breugem, *J. Comp. Phys.* **231**, 4469 (2012)

² Gondret et al., *Phys. Fluids* **14**, 643 (2002)

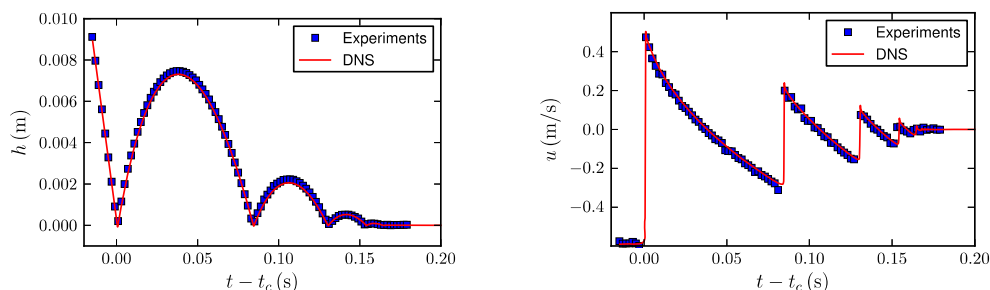


Figure 1: Trajectory (left) and temporal evolution of the particle velocity (right) of the bouncing motion of a steel sphere colliding onto a planar surface in silicon oil RV10. At the first impact, the particle Stokes number is $St = (1/9)\rho_p U_p D_p / \mu_f = 152$. The experimental data was kindly provided by Gondret et al.²

Fully resolved simulations of polydisperse particle suspensions

W.-P. Breugem^a and L. Brandt^b

Examples of particle-laden flows are the transport of water/sediment mixtures through pipe lines in land reclamation projects, sediment transport in rivers and fluidized-bed chemical reactors. In these examples the sediment is typically polydisperse, i.e. it exhibits a broad particle size distribution. Furthermore, in land reclamation projects the suspended particle volume fraction may be very high, well beyond 0.1. It is intuitively clear that particle-particle/wall interactions can not be neglected in this case.

Over the past years we have developed an efficient and second-order accurate Immersed Boundary Method (IBM) for fully resolved simulations of flows laden with finite-size particles¹. The IBM is embedded in a standard finite-volume/pressure-correction scheme. Furthermore, it has been extended with a soft-sphere collision model for accomodating particle collisions².

Recently, we have extended our model to accomodate polydisperse suspensions of spheres. To validate the implementation we have performed simulations of the slow approach of two spheres with different diameters (1) towards each other and (2) in sliding motion, for which results for the force on the spheres are available from lubrication theory. It was found that the IBM can accurately capture case 1 down to a gap width between the spheres of about 2.5% of the radius of the biggest sphere. For smaller gap widths asymptotic analytic force expressions have been implemented to correct the simulation results (see Fig. 1). Interestingly, for case 2 the simulations are in good agreement with lubrication theory for all gap widths, even for very small gap width; this is presumably related to the fact that in case 2 the forces on the freely rotating spheres remain finite in the limit of zero gap width. More results will be presented at the conference.

^a TU Delft, Laboratory for Aero and Hydrodynamics, Leeghwaterstraat 21, 2628 CA Delft, The Netherlands

^b KTH, Dep. of Mechanics, SE-100 44 Stockholm, Sweden

¹ Breugem, *J. Comput. Phys.* **231**, 4469 (2012)

² Breugem, *Proc. ASME FEDSM2010 conference*, Montreal, Canada (2010), paper number FEDSM-ICNMM2010-30634

³ Jeffrey, *Mathematika* **29**, 58 (1982)

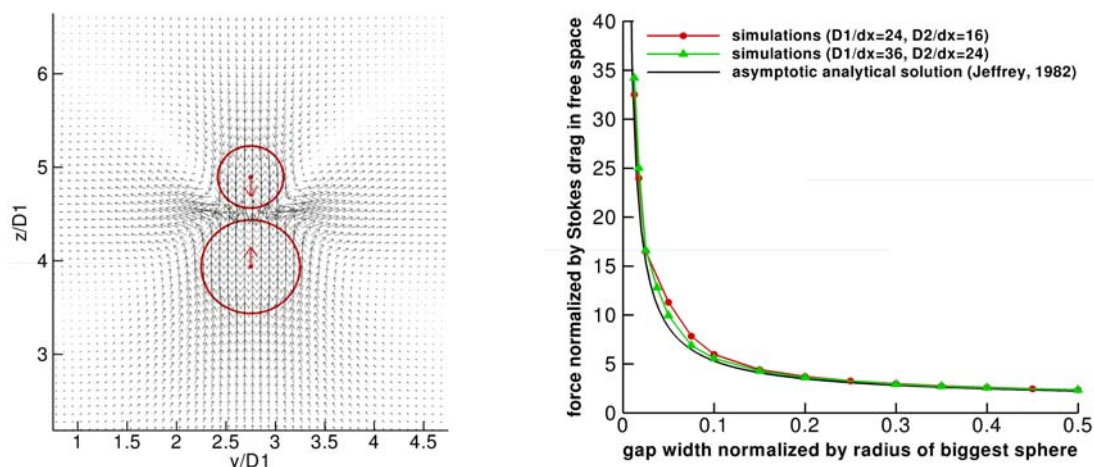


Figure 1: Normal approach of 2 unequal spheres at equal but opposite velocity. The Reynolds number is 0.1, based on the sphere velocity and the diameter of the biggest sphere. The ratio of the sphere diameters is 2/3. Left: cross-section of flow field, ratio of (gap width)/(biggest sphere radius) = 0.25. The grid is uniform in space; the biggest sphere diameter corresponds to 24 grid cells. Right: Force on biggest sphere normalized by Stokes drag force in free space, shown as function of the normalized gap width. The black line without symbols is the asymptotic analytic solution of Jeffrey³. The lines with symbols represent the simulation results for two different grid resolutions (red/dots: 24 grid cells over biggest sphere diameter; green/triangles: 36 grid cells over biggest sphere diameter).

On the relative motion between rigid fibers and fluid in turbulent channel flow

C. Marchiolli^a, L. Zhao, H.I. Andersson^b

Elongated fibers are commonly encountered in a wide variety of environmental processes and industrial applications: examples include pulp and paper making, polymer processing and molding of fiber-reinforced composites, to name a few. In all these applications, spatial and orientational distribution of fibers plays a crucial role: Hence the need for a thorough understanding of how fibers are dispersed and oriented by turbulence. In addition to specific industrial applications, fiber dynamics is of fundamental interest since statistical characterization of fiber translation and rotation is crucial for model validation.

In this work, our main objective is to examine how fibers with different elongation and inertia translate and rotate with respect to the surrounding carrier fluid in presence of non-linear mean shear and flow anisotropy. To this aim, two main observables will be investigated: the relative fiber-to-fluid translational velocity (slip velocity) and the relative angular velocity (slip spin). The slip velocity is directly related to the drag force exerted on the particles and plays an essential role in the transfer of mechanical energy between the phases. The slip spin is directly related to rotational dispersion coefficients and its statistical characterization is crucial to provide accurate closure relations for rheological models (e.g. for the probability density function of fiber orientation).

Slip velocity and spin are investigated for the reference case of turbulent channel flow, modeling fibers as prolate spheroids with Stokes number $1 < St < 100$ and aspect ratio $3 < \lambda < 50$. Statistics are compared with those obtained for spherical particles ($\lambda = 1$) to highlight effects due to fiber elongation. Comparison is also made at different Reynolds numbers ($Re_\tau = 150, 180$ and 300 based on the fluid shear velocity) to discuss effects due to an increase of turbulent fluctuations.

Results^{1,2} show that elongation has a quantitative effect on the statistics of both slip velocity and slip spin, particularly evident for fibers with small St . As St increases, differences due to the aspect ratio tend to vanish and the relative translational motion between individual fibers and surrounding fluid is controlled by fiber inertia through preferential concentration. A clear manifestation of inertial effects is the different distribution of slip velocities for fibers trapped in sweep/ejection events and for fibers segregated in near-wall fluid streaks. The corresponding conditional probability distribution functions are found to be non-Gaussian, thus suggesting that fiber motion relative to the fluid cannot be modeled as a standard diffusion process.

For the range of simulation parameters investigated, no significant Reynolds number effects are observed, indicating that fiber dynamics exhibit a scaling behavior with respect to the shear velocity up to $Re_\tau = 300$.

^a Dep. Electrical, Management and Mechanical Engineering, University of Udine, 33100 Udine, Italy

^b Department of Energy and Process Engineering, Norwegian University of Science and Technology, 7491 Trondheim, Norway

¹ Zhao et al., “Slip velocity of fiber suspensions in wall-bounded flows,” *Phys. Fluids* (2013) Submitted.

² Zhao et al., *Phys. Fluids* **24**, 021705 (2012)

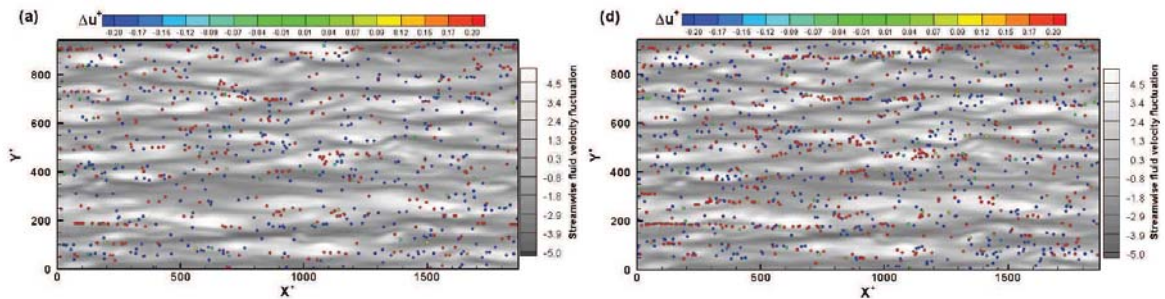


Figure 1: Instantaneous streamwise slip velocity, Δu^+ , and $St = 30$ fiber distribution in the wall-parallel plane at $z^+ \approx 8$ in the $Re_\tau = 150$ simulation. Fibers are colored according to the value of Δu^+ at their location: red/blue indicate fibers with large positive/negative slip velocity. The near-wall fluid velocity streaks (represented as gray-scale contours of the streamwise fluid velocity fluctuation) are also shown. Panels: (left) $\lambda = 1$, (right) $\lambda = 50$.

Helium Flows Superfluids

Superfluid turbulence in $^3\text{He-B}$: theory and numerical analysis of Andreev reflection by vortices and turbulent structures

Y. A. Sergeev¹, C. F. Barenghi², N. Suramlishvili^c, S. N. Fisher^d and V. Tsepelin^d

In the zero-temperature limit, a pure superfluid has no viscosity. The superfluid ^4He is formed by atoms which have condensed into the quantum ground state. In liquid ^3He , the condensate is formed by Cooper pairs of atoms. The superflow is irrotational; however, superfluids can support topological defects: these are quantized vortices, each carrying a single quantum of circulation. Interaction of quantized vortices via their self-induced flow leads to a formation of the vortex tangle displaying a complex dynamics and supporting flow structures with a large range of length scales.

New experimental techniques were developed to measure quantum turbulence at low temperatures in both ^4He and $^3\text{He-B}$. One such technique being developed for superfluid $^3\text{He-B}$ utilizes the Andreev reflection of thermal quasiparticle excitations from superfluid flow^{1,2}.

This work is concerned with theoretical and numerical analysis of Andreev reflection from quantized vortices, turbulent vortex structures, and saturated vortex tangles. We address the problem of Andreev scattering of incident beam of thermal excitations from the quantized vortex, calculate exactly the fraction of incident beam Andreev reflected by the flow field of the vortex, and define and calculate the effective scattering length (Andreev cross-section per unit length of the vortex line). Our earlier results^{3,4} showed that interpretation of Andreev scattering measurements in turbulent $^3\text{He-B}$ should necessarily account for screening phenomena resulting from collective flow effects. Based on our calculations of the effective scattering length, we estimate the range of vortex line densities (length of vortex lines per unit volume) and spatial extensions of turbulence for which the screening effects may play a dominant rôle in the Andreev scattering process. We calculate numerically, as functions of the vortex line density, the scattering cross-sections of fully saturated tangles, and analyse the relation between spectral characteristics of quantum turbulence and those of the Andreev-reflected signal.

¹ Joint Quantum Centre and School of Mechanical & Systems Eng., Newcastle University, Newcastle upon Tyne, NE1 7RU, UK

² Joint Quantum Centre and School of Mathematics & Statistics, Newcastle University, Newcastle upon Tyne, NE1 7RU, UK

^c School of Mathematics, University of Bristol, Bristol, BS8 1TW, UK

^d Dep. Physics, Lancaster University, Lancaster, LA1 4YB, UK

¹ Fisher et al., *Phys. Rev. Lett.* **86**, 244 (2001).

² Fisher et al., *PNAS* (2014, in print).

³ Barenghi et al., *Phys. Rev. B* **79**, 024508 (2009).

⁴ Sergeev et al., *Europhys. Lett.* **90**, 56003 (2010).

Inverse energy transfer induced by vortex reconnections

C. F. Barenghi¹, A.W. Baggaley², Y.A. Sergeev^c

In low-temperature superfluid helium, viscosity is zero, and vorticity takes the form of discrete, vortex filaments of fixed circulation and atomic thickness. Turbulence takes the form of a tangle of such filaments (see Figure 1) which move under their mutual influence, and reconnect when they become sufficiently close to each other.

Recent experimental, numerical and theoretical studies¹ have revealed that, at length scales larger than the average distance between individual filaments, homogeneous isotropic quantum turbulence has properties similar to ordinary turbulence, notably the Kolmogorov energy spectrum arising from an energy cascade from large length scales to small length scales.

This work is concerned with the inverse effect². We present numerical evidence³ of three-dimensional inverse energy transfer from small length scales to large length scales in superfluid turbulence generated by a flow of vortex rings. We argue that the inverse energy transfer arises from the anisotropy of the flow, which favours vortex reconnections of vortex loops of the same polarity, and that it has been indirectly observed in the laboratory⁴. The effect open questions about further analogies between quantum turbulence and related processes in ordinary turbulence.

¹ Joint Quantum Centre and School of Mathematics and Statistics, Newcastle University, Newcastle upon Tyne, NE1 7RU, UK

^b School of Mathematics and Statistics, University of Glasgow, Glasgow, G12 8QW, UK

² ^c Joint Quantum Centre Durham-Newcastle and School of Mechanical and Systems Engineering, Newcastle University, Newcastle upon Tyne, NE1 7RU, UK

¹ Barenghi et al., arXiv:1306.6248 (2013), submitted to PNAS.

² Biferale et al., *Phys. Rev. Lett.* **108**, 164501 (2012).

³ Baggaley et al., *Phys. Rev. E* **89**, 013002 (2014).

⁴ Walmsley et al., *Phys. Rev. Lett.* **100**, 245301 (2008), and arXiv:1308.6171 (2013)

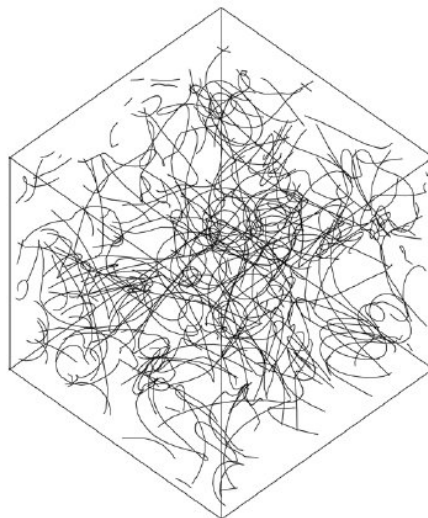


Figure 1: Snapshot of a tangle of vortex filaments computed in a periodic domain.

Turbulent flow of superfluid helium in channels and effective viscosity in quantum turbulence: experiments and simulations

S. Babuin^a, E. Varga^b, L. Skrbek^b, E. L  v  que^c and P.-E. Roche^d

Quantum turbulence is the turbulent state of a quantum fluid¹, a fluid with quantum mechanical effects appearing on the macroscopic scale. We study the superfluid state of ⁴He, occurring below the transition temperature $T \approx 2.18$ K. In this state helium behaves as a mixture of two interpenetrating fluids: a normal component which is viscous and entropic, and a superfluid component which is viscosity- and entropy- free. The former supports a vorticity field as in classical viscous fluids, whilst the latter, originating from a quantum-mechanical macroscopic coherent state, requires that vorticity must be concentrated along very thin vortex lines, around which the superfluid velocity circulation is quantised. At finite temperatures, both normal and superfluid components coexist, and such landscape of discrete vortices interacts with the viscous normal component. It has been clearly understood¹ that this interaction leads to an effective macroscopic classical-like behaviour of the two-fluid system, despite the superfluid component being governed by quantum mechanics.

We are interested in the effective viscosity of the two-fluid system in the turbulent state. Traditionally the effective viscosity has been deduced by measuring the decay of quantum turbulence², but here we address it by studying the steady turbulent flow of superfluid helium in a channel (Figure 1), in the near and far wake of a grid. The main observable is the density of quantum vortices, L , deduced from the attenuation of second-sound (Figure 1), a peculiar temperature wave propagating in superfluid helium. The mean inter-vortex separation, $\delta = L^{-1/2}$, scales with the (superfluid) Reynolds number, as $\delta \sim Re_\kappa^{-3/4}$ (Figure 2), as does the Kolmogorov dissipation length scale in classical turbulence. We have derived a proportionality factor between δ and $Re_\kappa^{-3/4}$ which allows us to deduce the effective viscosity of the fluid over the temperature range $1.17 \text{ K} \leq T \leq 2.16 \text{ K}$. This value is in agreement with other experimental determinations, and also with values that we obtain from the numerical solution of the two-fluid equations of motion. This study allowed us to point out the severe uncertainties which currently are limiting the experimental determination of the effective viscosity. The numerical modelling on the other hand has highlighted the physical mechanisms which lead to energy dissipation in this complex two-fluid system where the superfluid component would otherwise be dissipationless in the potential state.

^a Institute of Physics ASCR, Na Slovance 2, 18221 Prague, Czech Republic

^b Faculty of Mathematics and Physics, Charles University in Prague, Ke Karlovu 3, 12116 Prague, Czech Republic

^c ENS Lyon & CNRS, Univ. de Lyon, F-69364 Lyon, France & EC Lyon & CNRS, Univ. de Lyon, F 69134, Ecully, France

^d Univ. Grenoble Alpes, Inst NEEL, F-38042 Grenoble, France & CNRS, Inst NEEL, F-38042 Grenoble, France

¹ Skrbek and Sreenivasan, *Phys. Fluids* **24**, 011301, (2012)

² Skrbek and Sreenivasan, Chapter 10 in *Ten chapters of turbulence*, Cambridge University Press, (2013)

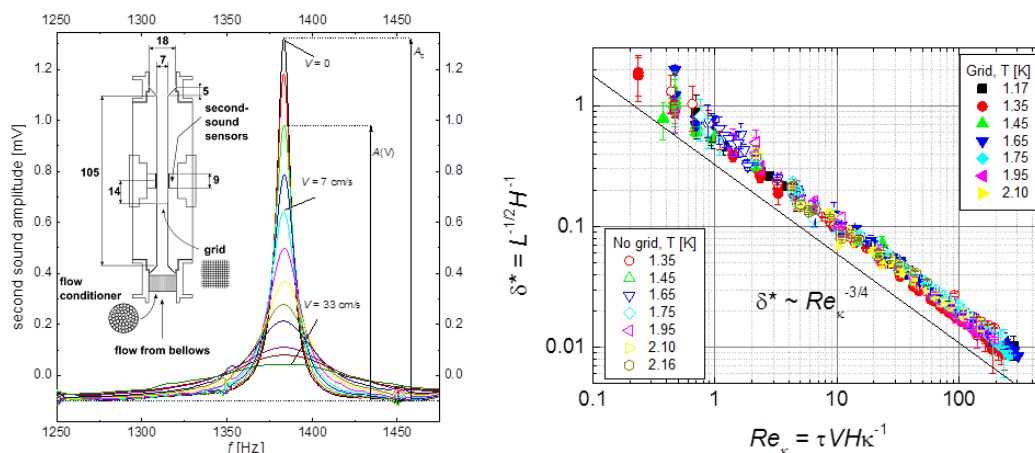


Figure 1: (left) Attenuation of second-sound resonance with increasing flow velocity, with a diagram of the flow channel.

Figure 2: (right) Scaling of non-dimensional inter-vortex spacing with superfluid Reynolds number revealing analogy with scaling of Kolmogorov dissipation length in classical turbulence.

Visualisation of quantum flows

M. La Mantia^a, D. Duda^a, M. Rotter^a and L. Skrbek^a

Quantum turbulence¹, which occurs in flowing quantum fluids displaying superfluidity, such as superfluid ⁴He, combines quantum physics with classical fluid dynamics. Superfluid ⁴He, also known as He II, exists at temperatures below about 2.2 K and its motion does not generally obey the Navier-Stokes equation. It is viewed as consisting of two interpenetrating fluids, whose density ratio depends on temperature. The normal component of He II can be considered as a viscous fluid, carrying the entire entropy content of the liquid, while its superfluid component is assumed inviscid. It follows that the circulation of the superfluid velocity is quantized and that quantized vortices exist in He II, usually arranged in a tangle, whose dynamical behaviour is an essential ingredient of quantum turbulence.

Well-known visualisation techniques, such as Particle Tracking Velocimetry, have been recently fine-tuned to gain, e.g., deeper understanding of the similarities and differences between quantum and classical turbulent flows². To this end, an experimental apparatus³ has been devised by us. The Lagrangian dynamics of micron-sized solid particles is specifically being studied and it was already shown that the obtained experimental data are consistent with the present physical understanding of quantum flows³, when probed at relevant length scales.

In fact, both quantum and classical features can be observed in the same quantum flow, depending on the scale at which we probe it. At large enough scales, larger than the average distance l between quantized vortices, quantum turbulence displays classical features, while its quantum nature become obvious at smaller scales. We show, e.g., that in the case of a well-known quantum flow of He II, thermal counterflow¹, the statistical distribution of the particle velocity changes from the power-law shape, typical of quantum turbulence, at scales smaller than l , to the nearly Gaussian form, typical of classical turbulent flows, at scales larger than l .

Additionally, we are investigating the occurrence of macroscopic vortical structures in quantum flows, as their nature is still not entirely understood², by probing thermal counterflow past circular cylinders⁴, and recent results, obtained by us in the proximity of an oscillating rectangular cylinder, suggest that macroscopic vortices may also be observed in superfluid ⁴He.

We acknowledge the support of GAČR P203/11/0442.

^a Faculty of Mathematics and Physics, Charles University, Ke Karlovu 3, 121 16 Prague, Czech Republic

¹ Vinen and Niemela, *J. Low Temp. Phys.* **128**, 167 (2002); Skrbek and Sreenivasan, *Phys. Fluids* **24**, 011301 (2012).

² Sergeev and Barenghi, *J. Low Temp. Phys.* **157**, 429 (2009); Guo et al., *Visualization of two-fluid flows of superfluid helium-4*, to be published in *Proc. Natl Acad. Sci. USA*.

³ La Mantia et al., *Rev. Sci. Instrum.* **83**, 055109 (2012); La Mantia et al., *J. Fluid Mech.* **717**, R9 (2013); La Mantia and Skrbek, *Quantum, or classical turbulence?*, to be published in *Europhys. Lett.*

⁴ Duda et al., *On the visualization of thermal counterflow of He II past a circular cylinder*, to be published in *J. Low Temp. Phys.* DOI 10.1007/s10909-013-0961-z.

Transition to Turbulence in Oscillatory Flows of Cryogenic Helium

M.J. Jackson^a, D. Schmoranzera, T. Skokánková^a and L. Skrbek^a

Employing cryogenic helium (specifically, the isotope ^4He) to experimental studies of various fluid dynamics problems offers a wide range of working fluids with unique and easily tunable properties. Its normal liquid phase has one of the lowest kinematic viscosities of all known substances reaching as low as $2 \cdot 10^{-8} \text{ m}^2\text{s}^{-1}$ near 2.2 K at the saturated vapour pressure of $\sim 50 \text{ mbar}$. When cooled below 2.17 K, helium enters the superfluid¹ phase (also called He II) which behaves as a quantum liquid. Its dynamics differ from classical fluids and is well described by the phenomenological two-fluid model, which states that He II consists of two inter-penetrating fluids: (i) the normal component which behaves as a classical fluid, and (ii) the superfluid component with zero viscosity and zero entropy. With decreasing temperature, the fraction of the normal component decreases, becoming negligible below $\sim 0.7 \text{ K}$.

In this work, we discuss the measured in-line forces acting on oscillating objects such as quartz tuning forks² (resonating at frequencies between 4 kHz and 32 kHz) immersed in normal or superfluid helium. These resonators are driven over a range of velocities around the onset of the first non-linearities. The magnitude and scaling of the drag and inertial coefficients with velocity is compared to the predictions given by the Morison equation and other models developed in the literature³ for superfluids.

Our aim is to resolve the onset of turbulence triggered by classical-like instabilities in the normal component and as well as the first instabilities occurring in the superfluid component leading to the generation of quantized vortices⁴ (vortices with quantized values of circulation). This is achieved by extracting the critical values of flow parameters such as the Stokes and Keulegan-Carpenter numbers and their temperature dependence. Emphasizing both the similarities and the differences between classical and predominantly quantum flows, we hope to gain a better understanding of the nature of both types of fluids and their dynamics near the transition to turbulence.

^a Faculty of Mathematics and Physics, Charles University in Prague, Ke Karlovu 3, 121 16, Prague 2, Czech Republic

¹ D.R. Tilley and J. Tilley, *Superfluidity and Superconductivity* 3rd Edition, Institute of Physics Publishing, Bristol and Philadelphia, 2003.

² R. Blaauwgeers, M. Blažková et al., J. Low Temp. Phys. **146**, 537 (2007).

³ D. Schmoranzera, M.J. Jackson et al., J. Low Temp. Phys., in print, DOI:10.1007/s10909-0130920-8.

⁴ R. Donnelly, *Quantized Vortices in Helium II*, No. v. 2 in *Cambridge Studies in Low Temperature Physics* 3, Cambridge University Press, Cambridge, 1991.

Comparison of drag crisis on a free falling sphere in HeI and HeII

N. F. Sy^a, M. Bourgoïn^b, P. Charvin^a, P. Diribarne^a, M. Gibert^{cd} and B. Rousset^a

Liquid helium exists in two different phases, HeI and HeII. While the former behaves as a classical fluid, the latter can be considered as the superposition of a normal and a quantum media with a relative density ratio depending upon the temperature.

Previous studies¹⁻³ suggest that high Reynolds number turbulence in HeII exhibit classical large scale behaviors with an effective Reynolds number (defined with the kinematic viscosity of the normal component and the total bulk density of the fluid). This is related to the mutual friction that couples the two fluid components at large scale and sufficiently high Re. However, a complete understanding of the underlying coupling mechanism is still lacking. In particular, this coupling is expected to affect the development of boundary layers differently in HeII and HeI flows. Previous attempts to investigate the drag coefficient of a sphere⁴⁻⁶ at high Re in HeII did not give satisfactory conclusions, despite the wide variety of approaches (static sphere in a wind tunnel, integration of the pressure distribution over the body surface, terminal velocity of falling spheres, etc.). Choi and co-workers⁵ found that using the total density for the Reynolds number, a temperature dependent drag crisis threshold could be observed in He II. They suggested using the normal helium density to collapse the Reynolds thresholds.

Concerning free falling balls experiments, uncertainties were the major issues and concern both the apparatus and the instrumentation. Indeed, the critical Re number for the drag crisis strongly depends on the surface roughness of the sphere and on the presence of residual turbulence in the fluid. These factors cause the transition to occur at lower Re than expected for smooth surfaces in a quiescent fluid. Furthermore, the necessary height to actually reach a terminal velocity with Re above 10^5 when the sphere is released with no initial velocity require a quite large cryostat. Finally, velocity measurements are often too localized in space to determine unambiguously a trustable value of the terminal velocity.

We will present a new cryogenic facility that overcomes these drawbacks. A dedicated homemade “cryogenic launcher” allows launching the sphere with an adjustable vertical velocity, chosen at will to be close to the terminal velocity. Spheres with identical diameter (6 mm) but different densities permit to explore a range of Re between 10^5 and 10^6 . Continuous velocity measurements are performed using homemade Doppler ultrasonic anemometers. We also perform optical endoscopic tracking, with a high speed camera at room temperature recording the sphere trajectory at a few thousands frames per second, with an instantaneous word-pixel calibration based on the sphere diameter. First results in HeI and HeII will be presented.

^a Service des Basses Températures, UMR-E 9004 CEA/UJF-Grenoble 1 CEA/INAC/SBT 17, rue des Martyrs 38054 Grenoble Cedex 9 France

^b Dep. Laboratoire des Ecoulements Géophysiques et Industriels, CNRS/UJF/G-INP, UMR5519, Université de Grenoble, BP53, 38041, Grenoble Cedex 09, France

^c Université Grenoble Alpes, Institut NÉEL, F-38042 Grenoble, France, CNRS, Institut NÉEL, F-38042 Grenoble, France

¹ Walstrom et al., *Cryogenics* **28**, 101 (1988).

² Maurer and Tabeling, *Europhysics Lett* **43**, 29 (1998)

³ Salort et al., *Physics of Fluids* **22** 125102 (2010)

⁴ Hemmati et al., *PhysicJ. Low Temp. Phys.* **156** 71 (2009)

⁵ Choi et al., *Lecture Notes in Physics* **571** 66 (2001)

⁶ Laing Ronald A., *PhD* (1960)

Instability

Non-swirls

Numerical experiments and visualization of a slightly supercritical flow inside a cubic diagonally lid-driven cavity

Yu. Feldman^a

Lid-driven cavity flow has been the subject of intense theoretical and experimental research for many decades because of the overwhelming importance of this kind of flow to the basic study of fluid dynamics¹. Begun by the early theoretical works^{2,3} that were followed by the numerical studies^{4,5} state-of-the art lid-driven flow research represents the entire range of fluid transport phenomena, including longitudinal vortices, corner eddies, non-uniqueness, transition to unsteadiness and turbulence¹.

Although it constitutes a popular benchmark for the verification of numerical methods and the validation of experimental methodologies, “classical” lid-driven cavity flow has certain limitations. Chief among these is that, although it was realized for 3-D geometry, this flow still has 2-D similarities. In fact, symmetry breaking observed for the slightly supercritical flow regime is associated with small distortions of the base flow while the leading eigenfunctions of all velocity components retain their midplane reflectional symmetry⁶. Therefore, the unsteady flow generally preserves its 2-D character (i.e., magnitude of spanwise, z velocity component remains small relative to the magnitudes of both x and y velocity components).

The limitations discussed above were remedied by formulating an alternative benchmark problem that simulates flow inside a cubic diagonally lid-driven cavity⁷⁻⁹. In contrast to its “classical” analogue, the proposed configuration essentially hosts fully 3-D, highly separated vortical flow whose steady state is characterized by a diagonal plane of reflection symmetry. The transition to unsteadiness of a flow inside a cubic diagonally lid-driven cavity with no-slip boundaries is numerically investigated by a series of direct numerical simulations (DNS) performed on 100^3 and 200^3 stretched grids. The observed oscillatory instability is found to set in via a subcritical symmetry-breaking Hopf bifurcation. Critical values of the Reynolds number $Re_{cr} = 2320$ and the non-dimensional angular oscillating frequency $\omega_{cr} = 0.249$ for transition from steady to oscillatory flow are accurately estimated. A slightly supercritical oscillatory flow regime is thoroughly investigated by Fourier analysis. A symmetry breaking mechanism of the slightly supercritical flow is visualized by tracking the mixing of passive particle tracers initially seeded from both sides of the diagonal plane of symmetry.

^a Dep. Mechanical Engineering, Ben Gurion University of the Negev P.O.B. 653., Beer Sheva, 8410501, Israel

¹ Shankar and Deshpande, *Annual Review of Fluid Dynamics* **32**, 93 (2000).

² Batchelor, J. *Fluid Mech.* **1**, 177 (1956).

³ Moffatt, J. *Fluid Mech.* **18**, 1 (1963).

⁴ Kawaguti, J. *Phys. Soc. Japan* **16**, 2307 (1961).

⁵ Simuni, J. *Appl. Mech. Tech. Phys.* **6**, 106 (1965).

⁶ Feldman and Gelfgat, *Physics of Fluids* **22**, 093602 (2010).

⁷ Povitsky, *Tech. Rep.* **211232** (NASA/CR, 2001).

⁸ Povitsky, *ALAA Paper* **2847**, 2001 (2001).

⁹ Povitsky, *Nonlinear Analysis* **63**, e1573 (2005).

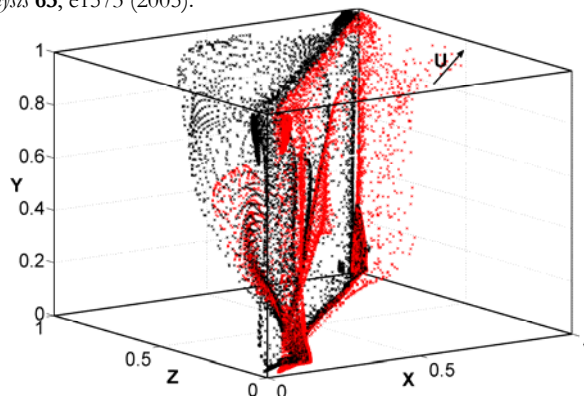


Figure 1: Visualization of a spontaneous symmetry breaking mechanism inherent to slightly supercritical flow.

Instability of pulsatile channel and pipe flows

Benoît PIER*

Pulsatile flows occur in a variety of practical applications and most notably in the human body. While many studies have addressed the dynamics of steady flow through channels or pipes with spatially varying diameters, surprisingly few investigations have considered time-dependent flows with uniform diameter. Hence, the purpose of the present work is to systematically establish the linear instability characteristics of pulsatile channel and pipe flows.

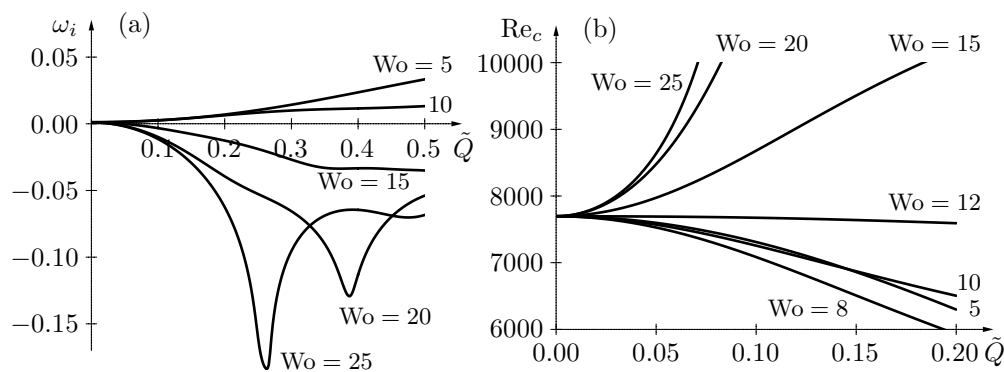
Such a flow configuration is completely determined by the Reynolds number Re (here based on diameter, mean velocity and viscosity), the Womersley number Wo (a dimensionless expression of the frequency) and the flow-rate waveform $Q(t) = \sum_n Q_n \exp(i\Omega t)$, specified by its Fourier coefficients

Small-amplitude perturbations are governed by the incompressible Navier–Stokes equations linearized around the basic flow and solutions may be sought as Floquet normal modes. The numerical implementation of this Floquet eigenproblem has been validated by comparison with some existing results¹ as well as by direct numerical simulation of the linearized equations.

For steady plane Poiseuille flow, the critical Reynolds number for onset of instability is known to be $Re_c = 7696$ (Reynolds number based on channel diameter and mean velocity) and is associated with a marginal streamwise wavenumber $\alpha_c = 2.041$.

For a flow-rate of the form $Q(t) = 1 + \tilde{Q} \cos \Omega t$, figure (a) shows how the temporal growth rate at $Re = 8000$ and $\alpha = 2$ varies with \tilde{Q} and Wo , while figure (b) plots the evolution of the critical Reynolds number. As can be seen, the unsteady flow component can have a stabilizing or a destabilizing effect, and the change in behaviour occurs within the physiologically relevant frequency range ($Wo = 10$ – 15).

Currently, the stability of three-dimensional perturbations is being investigated by considering non-zero spanwise wavenumbers or azimuthal modenumbers. In the future, more complex flow-rate waveforms will be used, corresponding to physiological conditions.



*Laboratoire de mécanique des fluides et d'acoustique (CNRS—Université de Lyon), École centrale de Lyon, 36 avenue Guy-de-Collongue, F-69134 Écully, France.

¹von Kerczek, *J. Fluid Mech.* **110**, 91–114 (1982); Rozhdestvenskii *et al.*, *USSR Comput. Maths. Math. Phys.* **29**, 65–73 (1989); Straatman *et al.*, *Phys. Fluids* **14**, 1938–1944 (2002); Fedele *et al.*, *Eur. J. Mech. B/Fluids* **24**, 237–254 (2005); Thomas *et al.*, *Proc. R. Soc. A* **467**, 2643–2662 (2011).

Scaling laws for instabilities in Czochralski crystal growth configuration at large Prandtl numbers

E. Miroshnichenko^a, V. Haslavsky^b, E. Kit^a, A.Yu.Gelfgat^a

The aim of the present research is to perform systematic study of three-dimensional steady-oscillatory Czochralski melt flow. Measurements are focused on the steady-oscillatory flow transition, which is defined by appearance of temperature oscillations measured mainly by optical methods. The performed research aimed to extend our understanding of destabilization of convection at various Prandtl and Grashof numbers in order to validate experimentally a series of numerical predictions indicating on a strong destabilization of CZ flow (Figure 1). The results show that that critical temperature differences (critical Grashof number) scale with the power of -0.815 of the Prandtl number. To achieve the goal we modified the existing so called small experimental facility. This facility now enables to vary in a wide range the diameters of dummy as well as the height of working liquid while taking care of the meniscus between the working fluid and the dummy. In a real crystal growth facility the ratio of these values lead to variety of aspect ratio due to transition of crystal from liquid to solid phase during actual growth of a crystal. This process affects the conditions of instability. The different silicon oils are used as experimental liquids for examination of influence of different aspect ratio values on instability onset at different Prandtl numbers. In Figure 2 the results are presented for silicon oil with viscosity 5 cSt showing that critical temperature difference dependence according to power of about -4.5 of the dummy diameter for all aspect ratios.

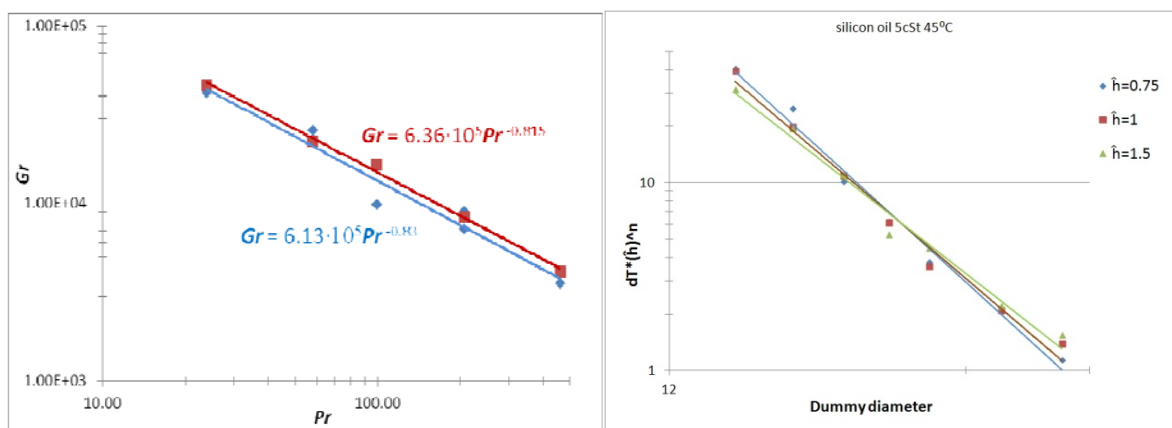


Figure 1. Critical Grashof number Gr depending on Prandtl number Pr and comparison of correlations obtained by experimental observations (blue and diamonds) and computational results (red and squares).

Figure 2. Normalized critical dT vs. dummy diameter for silicon oil of 5 cSt at varying heights \hat{h} . Parameter \hat{h} is normalized height of oil: $\hat{h}=h/r_c$, where r_c – radius of crucible.

^a School of Mechanical Engineering, Faculty of Engineering, Tel-Aviv University, 69978, Israel

^b Mechanical Engineering Department, Azrieli, Academic College of Engineering, Jerusalem 9103501, Israel

Local and global instability of free and confined plumes

L. Lesshafft^a, R.V.K. Chakravarthy^a and P. Huerre^a

The instability dynamics of plumes are driven by buoyancy- and shear-related mechanisms. A local temporal analysis of self-similar laminar plumes without confinement is carried out over large ranges of Prandtl and Grashof numbers, characterizing the destabilizing effect of buoyancy and shear in various regimes¹. Helical ($m=1$) modes are consistently found to be the most unstable in this type of flow, both in the buoyancy- and in the shear-dominated regimes. The physical mechanism behind buoyancy-induced plume instability is explained. Spatio-temporal instability characteristics of parallel base flows are obtained from direct numerical simulations of the impulse response.

Confinement of the plume drastically changes the behaviour. A recent numerical study by Lopez & Marques² demonstrates that several symmetry-breaking bifurcations occur in a thermal plume that is confined inside a short cylinder, starting with axisymmetric perturbations. We find that these bifurcations are not justified by the onset of absolute instability in a corresponding unconfined case. A linear global analysis is performed for the configurations studied by Lopez & Marques². The global eigenfunctions do contain, in many cases, local instability modes. However, global feedback and the impingement of the base flow on the lid of the cylinder appear to be essential for the global destabilization.

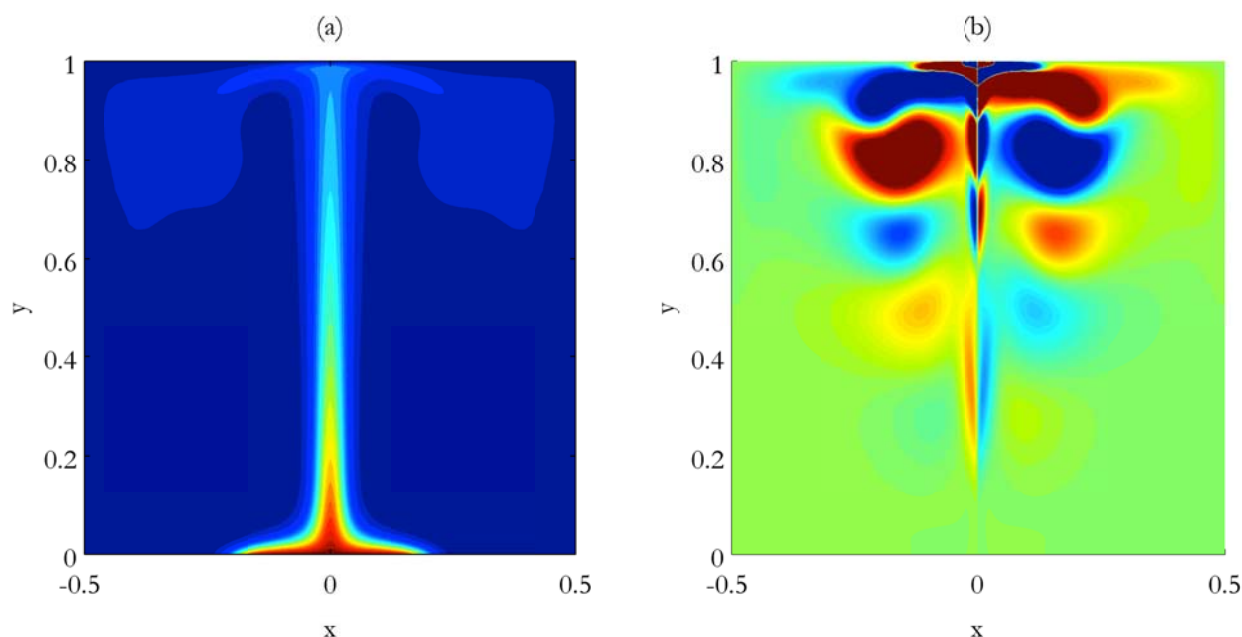


Figure 1: Temperature distribution in a plume, enclosed inside a cylinder with isothermal walls. a) Base flow temperature (axisymmetric) at Rayleigh number $Ra = 10^7$, as defined in reference 2; b) perturbation temperature of the most unstable helical instability mode (linear).

^a Laboratoire d'Hydrodynamique, CNRS / École polytechnique, Palaiseau, France

¹ Chakravarthy *et al.*, submitted to *Phys. Fluids* (2014).

² Lopez and Marques, *J. Fluid Mech.* **736**, 616 (2013)

Stability of the wavy film falling down an inclined corrugated plate: The DNS computations and Floquet theory

Y. Y. Trifonov^a

The paper is devoted to a theoretical analysis of the viscous liquid film falling down an inclined corrugated plate (inclination angle, amplitude and period of the sinusoidal corrugations are β , A and L , respectively). Based on the Navier-Stokes equations (DNS) in their full statement, we carried out the linear stability analysis of the steady-state viscous solutions. The Floquet theory gives us a general form of the disturbances as $\Psi(x, y) \exp[-\gamma t + 2\pi i Q x]$, $\Psi(x+1, y) = \Psi(x, y)$. Here $Q \in [0, 0.5]$ is the Floquet parameter and finally we have the generalized eigenvalue problem for the complex matrixes (see paper by Trifonov¹ for the case of vertical plate $\beta=90^\circ$). There are five independent parameters in the problem¹ - β , A/L , $L/\sqrt{\sigma/\rho g}$, $Fi \equiv (\sigma/\rho)^3/gv^4$, Re . As a first step we carried out the stability computations for three different geometries of the recent experiments²⁻⁴ using the same physical properties of the liquid and the same values of the inclination angles and Reynolds number. As a second step we did the stability analysis for two values of both the Kapitza number $Fi^{1/11} = 10, 2$ and the inclination angle $\beta = 10^\circ, 40^\circ$ varying in wide range period and amplitude of corrugations $A/L \in [0, 0.1667]$, $L/\sqrt{\sigma/\rho g} \in [1, 100]$ and the liquid Reynolds number Re . Figure 1 gives an example of the computations. The period of corrugations, inclination angle and the liquid physical properties correspond to the experiment by Pollak and Aksel². For different values of A/L and Re we computed if the disturbances with different values of the Floquet parameter Q are stable or unstable. In the case of the flat plate, the viscous flow is stable at $Re \leq Re_{flat} = 5ctg(\beta)/6$. In the case of the finite values of A/L , the critical value of the Reynolds number when the different two-dimensional disturbances are unstable depends on the value of the Floquet parameter Q (see fig.1a). The most dangerous disturbances ("the nose" of the curves 1-4 in fig.1a) have small values of Q for the case of the small values of A/L and Q_{nose} increases with the increasing of A/L (fig.1b). The dependence Re_{nose}/Re_{flat} vs. A/L has very clear maximum and the corrugations have destabilizing effect at large values of A/L in fig.1.

The stability analysis demonstrates essential influence of all parameters in the problem on the conclusions regarding the behaviour of disturbances with different values of Q . Some of these conclusions become opposite at variation of the Kapitza number value or the corrugations parameters

^a Inst. of Thermophysics, Sib. Branch of Russian Academy of Sciences, Ac. Lavrentyev St., 1, Novosibirsk, 630090, Russia

¹ Trifonov, *Int. J. of Multiphase Flow* **33**, (2007).

² Pollak, Aksel, *Phys. Fluids* **18**, 024103 (2013)

³ Cao et al., *J. Fluid Mech.* **718**, 54 (2013)

⁴ Wierschem et al., *Acta Mechanica* **179**, (2005)

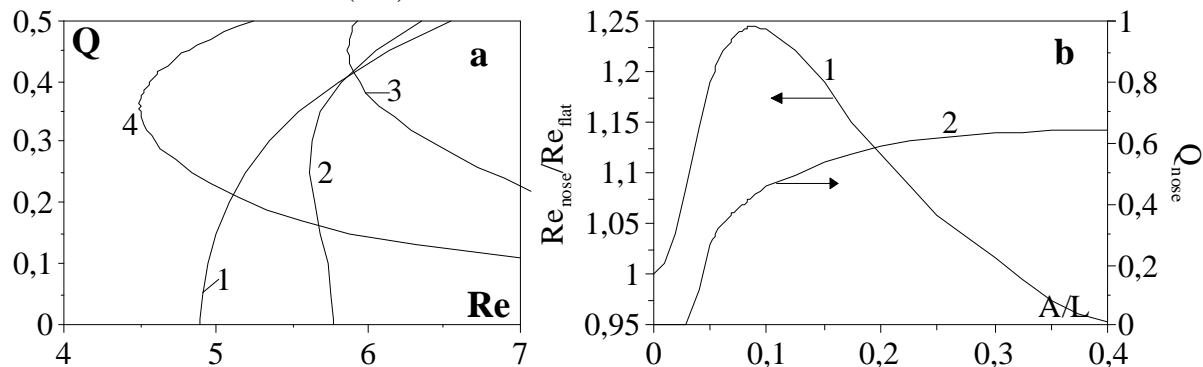


Figure 1: (a) Lines 1-4 bound the unstable disturbances at different values of A/L (1 – 0.02, 2 – 0.05, 3 – 0.1, 4 – 0.4). (b) Values of the critical Reynolds number and the Floquet parameter corresponding to the "beginning" of the region of the unstable disturbances. $Fi^{1/11} = 1.434$, $\beta = 10^\circ$, $L/\sqrt{\sigma/\rho g} = 13.746$.

Perfectly matched layer absorbing boundaries for global stability analysis of compressible flow

M. Merle^{ab}, U. Ehrenstein^b and J.C. Robinet^a

Laminar separated flow occurs in many engineering applications such as turbomachinery flow and in low-Reynolds-number aerodynamics. The resulting recirculation bubbles in compressible flows represent sources of hydrodynamic instabilities such as the well-known Kelvin-Helmholtz instability but also acoustics instabilities. When formulating the stability problem as an eigenvalue problem, acoustic waves are ill-treated and for instance non-reflecting boundary conditions or sponge zones have to be introduced which however may affect the whole eigenspectrum. Here we consider an alternative approach known as “perfectly matched layer” (PML), initially used for electromagnetics problems¹, in the aim of damping the acoustic waves while letting the hydrodynamic modes unaffected. This method relies on a complex coordinate transformation $y \rightarrow y + i \int_{y_0}^y \sigma(\eta) d\eta$, which attenuates perturbations, such as acoustic waves, in the far-field region $y \geq y_0$. We apply this approach to the example of a separated compressible boundary layer along a bump geometry, which has previously been considered for incompressible flow.² Equilibrium states, solution of the compressible Navier-Stokes equations, are obtained by applying a quasi-Newton approach, the system being discretized using Chebyshev-collocation. The governing equations are linearized around the base flow and two-dimensional temporal instability modes $(u, v, \rho, T)(x, y)e^{-i\omega t}$ are computed by solving the eigenvalue problem, the modes being unstable for positive imaginary parts of ω . An example of the stability results is shown in figure 1, for a Mach number $M = 0.5$ and a Reynolds number $Re = 600$ (based on the displacement thickness of the incoming flow), introducing in the flow domain a perfectly matched layer of width 10 starting at a distance $y_0 = 50$ from the wall. The spectrum in the absence of the perfectly matched layer is seen to exhibit neutral or unstable far-field acoustic modes which become stable when the complex coordinate transformation is applied, as seen in figure 1(b). The hydrodynamic modes, which are zero far from the wall, are not affected by the perfectly matched layer, an example being shown in figure 1(c). The influence of compressibility on the hydrodynamic modes as well as their interaction is assessed, focusing in particular on the low-frequency phenomenon due to non-normal mode interactions.

^aDYNFLUID Laboratory Arts et Métiers ParisTech, 151 Bd. de l'Hôpital, 75013 Paris, France

^bAix-Marseille Univ, CNRS, Centrale Marseille, IRPHE UMR 7342, F-13384 Marseille, France

¹J.-P. Béranger, *J. Fluid Mech.* **114**, 185 (1994)

²Ehrenstein and Gallaire, *J. Fluid Mech.* **614**, 315 (2008)

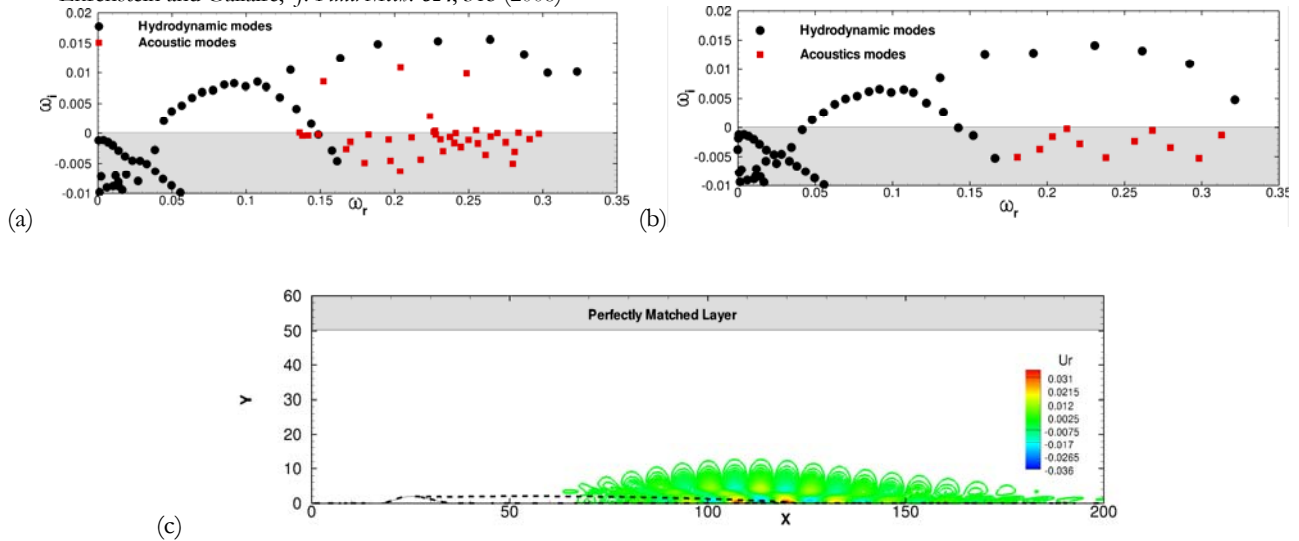


Figure 1: (a) Global stability spectrum without perfectly matched layer. (b) Global stability spectrum with perfectly matched layer. (c) Streamwise velocity component of the most unstable eigenmode.

Partially cavitating symmetric bodies: high-speed imaging and PIV measurements

A. Yu. Kravtsova^{a,b}, D. M. Markovich^{a,b}, K. S. Pervunin^{a,b}, M. V. Timoshevskiy^{a,b} and K. Hanjalić^{a,c}

Cavitation encountered in various machineries and devices operating with liquids are by far the major cause of damages that seriously impair the equipment availability, reliability and durability. The problem is in particular challenging in large-scale hydropower plants where the efficiency and longevity are the key requirements for successful and safe operation.

Cavitating flows around a flat plate with semi-circular leading edge and a NACA0015 hydrofoil at attack angles ranging from 0° to 9° and with varying cavitation number were investigated using high-speed-imaging visualization and particle imaging velocimetry. The cavitation patterns are different in case of attack angles less than 6° for plate and foil. Cavitation on the plate begins in the form of a streak array (bubble-band) whereas on the hydrofoil as travelling bubbles. Once the incidence angle increased to 9°, the cavitation on the hydrofoil changes to a streaky pattern like that on the plate at zero attack angle, whereas the regime on the plate shows no significant changes. The integral cavitation parameters were analyzed and the following dependences were obtained: $L_c/C = A\sigma^{-3} + B$ for flow over the plate and by $L_c/C = A\sigma^{-1} + B$ for the NACA0015 hydrofoil, where L_c/C is cavity length, σ is cavitation parameter, A and B are constants different for each angle of attack. Application of a new suggested procedure – Cluster validation – allowed us to improve significantly the quality of instantaneous velocity fields as well as the accuracy of the mean and turbulence characteristics calculation. In addition, we could also measure flow velocity within the gas–vapor phase, albeit with reduced accuracy that was evaluated and accounted for on the basis of the effective (validation-surviving) number of imaging samples.

We demonstrated that, for the plate at each attack angle considered and the NACA0015 foil at relatively high angles of incidence, the cavities are totally controlled by the re-entrant jet instability. In these cases the cavities are relatively short (less than half of the plate length) and thick. However, the cavities on the NACA0015 hydrofoil at small and moderate angles of attack (no more than 6°) are subjected generally to system instabilities for short cavities and surge-type instabilities for long cavities due to their small width and relatively large length. The time-averaged velocity and turbulence moments show that the incipience of cavitation is governed by the development of the carrier-fluid flow around the foil leading edges, but the subsequent flow pattern depends strongly on the cavitation regime displaying markedly different distributions compared to the noncavitating case.

^a Novosibirsk State University, Novosibirsk, Russian Federation

^b Kutateladze Institute of Thermophysics, Siberian Branch of the Russian Academy of Sciences, Novosibirsk, Russian Federation

^c Department of Chemical Engineering, Delft University of Technology, the Netherlands

Non-modal stability of a dusty-gas boundary layer flow

S.A. Boronin^a, A.N. Osipov^b

We consider the stability of a dusty-gas flow in the boundary layer on a flat plate. The flow is described in the framework of the two-fluid model^{1,2} with an incompressible Newtonian carrier fluid and non-Brownian particles. The particle volume fraction is negligibly small but their mass loading is finite and therefore the two-way coupling model is used. In the interphase momentum exchange, the Stokes drag and the Saffman lift force³ arising due to a large fluid velocity gradient on the particle scale are taken into account. The flow is considered in the region remote from the leading edge of the plate, where the velocities of both phases coincide and correspond to the Blasius profile. The particle number density $N(y)$ is assumed to be nonuniform and have a Gaussian distribution with given thickness (ξ) and the coordinate of the maximum (ζ). The set of governing parameters includes also the Reynolds number (Re), the particle inertia parameter or inverse Stokes number (β), the parameter determining the lift force scale (K), and the particle mass loading α .

A parametric study of the first normal mode (modal stability) is performed and the transient growth is investigated, based on the analysis of 'optimal disturbances' (non-modal stability). The increment of the most unstable 2D mode is calculated using an orthonormalization method, while the parameters of 3D optimal perturbations are calculated using a finite-difference method and the QR -algorithm. The most pronounced effect of particles on the first mode is indicated in the case when the particles are concentrated in the vicinity of the so-called 'critical layer', located at a point where the main-flow velocity is equal to the phase velocity of the mode. In contrast to the pure-fluid flow, in a certain range of governing parameters corresponding to sufficiently small ξ and ζ (Fig. 1a), there exist two unstable normal modes. In the case of a sufficiently thick particle layer located close to the plate, the critical Reynolds number increases by two orders of magnitude as compared to the pure-fluid flow.

It is found from the calculations that the optimal disturbances are streaky structures. The transient growth is most pronounced when the distance of the particle concentration maximum to the plate is of the order of the displacement thickness (Fig. 1b). For a fixed particle mass concentration averaged over the boundary layer thickness, the maximum energy of optimal disturbances corresponds to the flow with a narrow particle distribution. The work was supported by RFBR (Nos. 14-01-0014 and 12-708-31420).

^a Schlumberger Moscow Research, Pudovkina Street 13, 109147 Moscow, Russian Federation

^b Institute of Mechanics, Lomonosov Moscow State University, Michurinskii Prospekt, 1, 119192 Moscow, Russian Federation

¹ Saffman, J. *Fluid Mech.* **13**, 120 (1962).

² Marble, *Annu. Rev. Fluid Mech.* **2**, 397 (1970).

³ Saffman, J. *Fluid Mech.* **22**, 385 (1965); Corrigendum: *J. Fluid Mech.* **31**, 624 (1968).

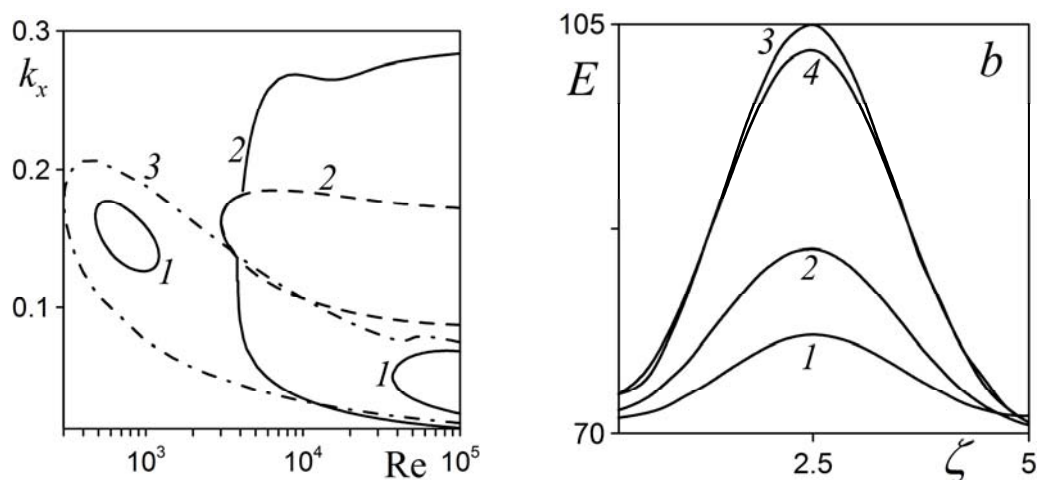


Figure 1: (a) – Neutral curves for boundary-layer flow at $\beta = 0.04$ and $K = 4.6 \cdot 10^{-3}$. 1 – $\zeta = 0.25$, $\xi = 0.35$; 2 – $\zeta = 0.5$, $\xi = 2$; 3 – pure gas flow. (b) – Maximum energy of optimal perturbations E against distance of the particle layer to the wall ζ at $\beta = 1$ and $K = 2.3 \cdot 10^{-2}$, $Re = 125$, $k_x = 0$, $k_z = 0.4$. (1, 2) – $\xi = 0.25, 0.5$ at $\max N(y) = 5.62$; (3, 4) – $\xi = 0.25, 0.5$ at $\alpha = 0.05$.

Steady and unsteady three-dimensional bifurcations in separated flow

O. Marquet^a and L. Lesshafft^b

The stability of the separated flow over a rounded backward-facing step is characterized by means of a temporal global analysis, in order to investigate its laminar/turbulent transition process. Several recent global instability studies of various separated flow configurations^{1,2,3} have found the first unstable mode to be steady and three-dimensional in nature; this finding indeed appears to be a rather common feature in separated flows. It suggests that the first bifurcation in such flows leads to a three-dimensional steady state, from whereon secondary three-dimensional instabilities determine the unsteady dynamics.

To further investigate the first steady bifurcation, a weakly nonlinear analysis has been performed for the rounded backward-facing step. It is found that this bifurcation, at Reynolds number $Re=505$, is in fact subcritical. The global mode amplitude in the vicinity of this threshold is governed by a fifth-order Stuart-Landau equation. The coefficients of this equation have been determined, thus allowing to trace the bifurcation diagram, and to obtain, in approximate form, the shape of the new three-dimensional steady flow states. These results will be presented and discussed.

Successive unsteady bifurcations could now be predicted by computing three-dimensional temporal eigenmodes of these new base states. While this procedure is numerically feasible, it is conceptually interesting to instead base the prediction on a *local* analysis of the convective or absolute nature of instability modes in the three-dimensional separation bubble. These local modes have two-dimensional eigenfunctions in the cross-stream plane, and they vary exponentially in the main flow direction⁴. Results from this local analysis will be presented.

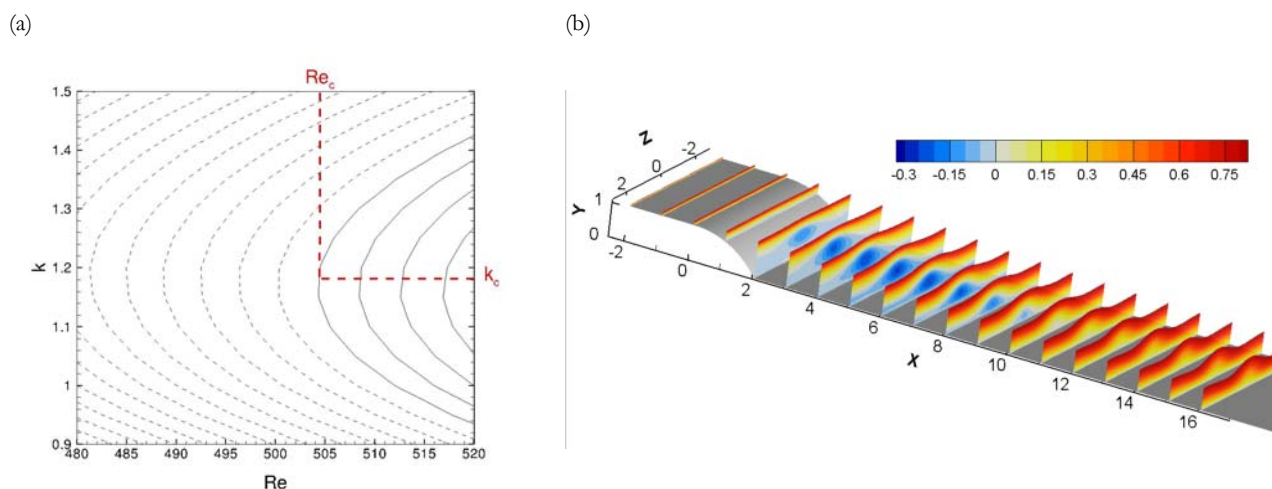


Figure 1: (a) Isocontours of the growth rate of the leading three-dimensional steady global mode, as functions of Reynolds number and transverse wavenumber. (b) Weakly non-linear solution: streamwise velocity in several cross-stream planes.

^a Dep. of Fundamental and Experimental Aerodynamics, ONERA, 8 rue des Vertugadins, 92190 Meudon, France

^b Laboratoire d'Hydrodynamique, CNRS / École polytechnique, 91128 Palaiseau, France

¹ Barkley et al., *J. Fluid Mech.* **473**, 167 (2002).

² Gallaire et al., *J. Fluid Mech.* **571**, 221 (2007).

³ Marquet et al., *J. Fluid Mech.* **622**, R4 (2009).

⁴ Pier, *J. Fluid Mech.* **603**, 39 (2008).

Convective instabilities in a porous medium: the role of chemical dissolution

T. Ward^a, K.A. Cliffe^{a†}, O.E. Jensen^b and H. Power^a

During carbon sequestration in an underground saline aquifer, CO₂ is dissolved in brine occupying a porous rock formation. This raises the brine density and drives convective mixing, an important factor in determining the overall carbon uptake rate. Once dissolved, the CO₂ undergoes a sequence of chemical reactions leading to brine acidification and interaction with the host medium^{1 2}. Here we investigate the influences of chemical reaction on the physical solution structure and the mathematical properties of this dynamical system.

We model flow of the solute in the porous medium using Darcy's law for an incompressible liquid, and solute transport using a convection-diffusion-reaction equation, assuming first-order reaction kinetics. We consider a rectangular domain in which a solute concentration is imposed from above; no-flux or periodic boundary conditions are imposed on the lateral walls and no-flux conditions are imposed at the base of the domain. This defines a system dependent on the Rayleigh number, Ra , the Damköhler number, Da , and the aspect ratio, L , of the domain.

Linear stability analysis is used to identify parameter values at which the system loses stability to convective overturning. We track steady solution branches emerging from bifurcation points using a high-accuracy spectral method and numerical continuation. For fixed L and Da , successive modes become unstable as the Rayleigh number increases. Many of these branches lose stability via secondary bifurcations to mixed states with increasingly broken symmetry. A projection of a trajectory, illustrated in figure 1, reveals the complexity of the steady solution structure at moderately low Ra . Spectral methods are also used to find time-dependent states, predicting the net rate of solute uptake as a function of time and the system parameters. Examination of such solutions reveals how steady states organise the structure of the high-dimensional phase space.

For $RaDa \gg 1$, the system is approximated by flow in a deep domain that is parameterized by Ra/Da and the width of the domain. Using linear stability analysis we derive asymptotic approximations of the short-wave and long-wave cut-off eigenmodes; nonlinear simulations reveal how an active boundary layer structure forms near the upper surface that feeds a pattern of larger plumes beneath.

^a School of Mathematical Sciences, University of Nottingham, University Park, Nottingham, NG7 2RD, UK

^b School of Mathematics, University of Manchester Oxford Road, Manchester, M13 9PL, UK

[†] This work is dedicated to the memory of Prof. Andrew Cliffe, who died on 5 January 2014.

¹ M.J. Mitchell et al, *Proc. Roy. Soc.* **466**, 1265 (2010).

² K. Ghesmat et al., *Phys. Fluids* **673**, 480 (2011)

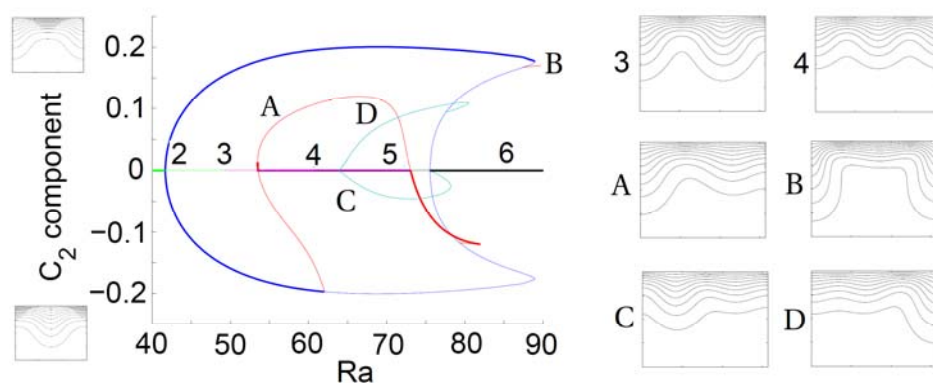


Figure 1: A bifurcation diagram of steady state solutions at low Ra , showing the projection onto a low-order eigenmode (insets, left) versus Ra . Insets (right) show an example of steady solutions arising from secondary bifurcations.

Linear stability of the flow around a spinning bullet-shaped body: global modes and sensitivity to base bleed

J.I. Jiménez-González^a, A. Sevilla^b, E. Sanmiguel-Rojas^c, W. Coenen^b and C. Martínez-Bazán^a

Flows around spinning axisymmetric slender bodies are encountered in important engineering applications as, for instance, projectile flight, jet engines or turbomachinery. The development of control strategies for such flows can be improved by studying the behaviour of unstable modes at low Reynolds numbers. For laminar flows, the application of spin substantially modifies the stability properties of the wake¹, as reported for a rotating bullet-shaped body with moderate angular velocities in ², acting as a stabilizing mechanism for certain values of the dimensionless rotation velocity, $\Omega = \omega D / 2u_\infty$, and the Reynolds number, Re . In the present work³, we investigate the stability properties of the laminar wake behind a spinning bullet-shaped body of length-to-diameter ratio $L/D = 2$, by performing a stability analysis for $0 \leq \Omega \leq 1$ and $140 < Re < 420$, seeking global eigenmodes of the form $\mathbf{q} = \hat{\mathbf{q}}(r, z)e^{\sigma t + im\theta}$. The spectra of complex eigenvalues $\sigma(Re, \Omega)$ shed results that are in good agreement with direct numerical simulations (see Fig. 1). Thus, for $\Omega \leq 0.232$ an eigenmode with azimuthal number $m = -1$ becomes unstable at a critical value of $Re = Re_{c1}$ that increases with Ω , leading to a low-frequency frozen state where axially-elongated structures co-rotate with the body with a different angular velocity. In the range $0.232 \leq \Omega < 0.52$ a different eigenmode with $m = -1$ becomes unstable at $Re = Re_{c3}$, explaining the high-frequency frozen spiral wake found in ². However, for $\Omega \geq 0.52$ and low values of Re , the wake is destabilized by a third $m = -1$ oscillatory mode of intermediate frequency, characterized again by a frozen spiral state that becomes dominant at higher values of Ω . Additionally, the suitability of base bleed as a control method for the wake of the spinning bullet-shaped body has been investigated, finding that it effectively stabilizes the leading eigenmodes at moderate rotation parameters, although its effect is less efficient when Ω is high (see grey lines in Figure 1). To understand this behaviour, adjoint global eigenmodes are computed to identify the wavemaker region and evaluate the combined sensitivity of the near wake to base bleed and spin.

^a Departamento de Ingeniería Mecánica y Minera, Universidad de Jaén, Campus Las Lagunillas, 23071, Jaén, Spain

^b Departamento de Ingeniería Térmica y de Fluidos. Universidad Carlos III de Madrid, 28911 Leganés, Spain

^c Área de Ingeniería Mecánica, Departamento de Mecánica. Universidad de Córdoba. Campus de Rabanales, 14071 Córdoba, Spain

¹ Pier, *J. Fluids & Struct.* **41**, 43-50 (2013).

² Jiménez-González et al., *J. Fluids & Struct.* **43**, 200-219 (2013).

³ Jiménez-González et al., *Submitted to J. Fluid Mech.* (2014).

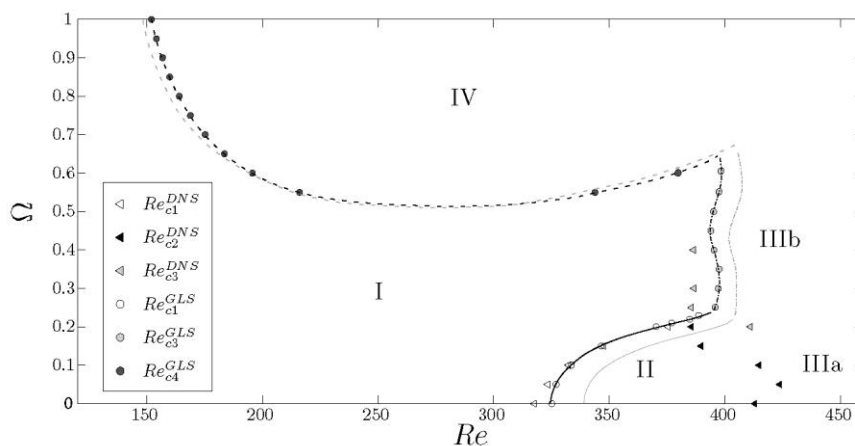


Figure 1: Bifurcation diagram in the (Ω, Re) parameter plane, according to the results of numerical simulations (DNS) and global stability analysis (GLS). The different wake states correspond to the following regions: I-axisymmetric, II-frozen, IIIa-spiral unsteady, IIIb-high frequency spiral frozen and IV-medium frequency spiral frozen. Grey lines correspond to the transitions for a bleed coefficient $C_b = u_b/u_\infty = 0.01$ obtained from linear stability analysis.

An overview of the centrifugal instabilities experimentally observed in an incompressible open cavity flow

C. Douay^{a,b}, L.R. Pastur^{b,c}, F. Lusseyran^b, J. Basley^{b,c} and Th.M. Faure^{b,d}

Open cavity flows are most usually considered with respect to the self-sustaining oscillations experienced by the impinging shear layer. Yet, as in the case of lid-driven cavity flows, open cavity flows exhibit the development of centrifugal instabilities in the inner flow, due to the curvature of the main recirculating flow.

A systematic experimental study of the inner flow organisation was initiated by Faure and co-authors^{1,2}, Basley *et al* (2013)³ and Douay (2014)⁴. Meanwhile, numerical linear stability analyses of the two-dimensional steady base-flow shed light on the mechanisms at play at the onset of the centrifugal instabilities. One may notably refer to Brès & Colonius (2008)⁵ and other recent studies^{6,7}, which brought more insight about the three-dimensional waves reported experimentally.

In this contribution, we propose an overview of the patterns observed in the cavity inner flow when both the Reynolds number and the cavity aspect ratio are varied. We describe the primary and secondary regimes encountered in the experiment, and discuss them with regards to the numerical expectations from linear stability analysis.

^a Sorbone University, UPMC, 4 place Jussieu, F-75005 Paris, France

^b LIMSI-CNRS, rue von Neumann, F-91403 Orsay Cedex, France

^c University Paris Sud, Bât 508, F-91405 Orsay Cedex, France

^d Ecoles d'Officiers de l'Armée de l'Air, Centre de Recherche de l'Armée de l'air (CRéA), BA 701, F-13661 Salon Air

¹ Faure et al, *Exp. In Fluids* **42**, 169-184 (2007).

² Faure et al., *Exp. In Fluids* **42**, 395-410 (2009).

³ Basley et al., *Phys. Fluids* **25**, 064105 (2013).

⁴ Douay, *PhD Thesis* **18**, 034210 (2014).

⁵ Brès ans Colonius., *J. Fluid Mech.* **599**, 309-339 (2008).

⁶ Meseguer-Garrido et al., *ALAA Paper* **3605**, 1-17 (2011).

⁷ Alizard et al., *Computers and Fluids* **66**, 63-84 (2012).

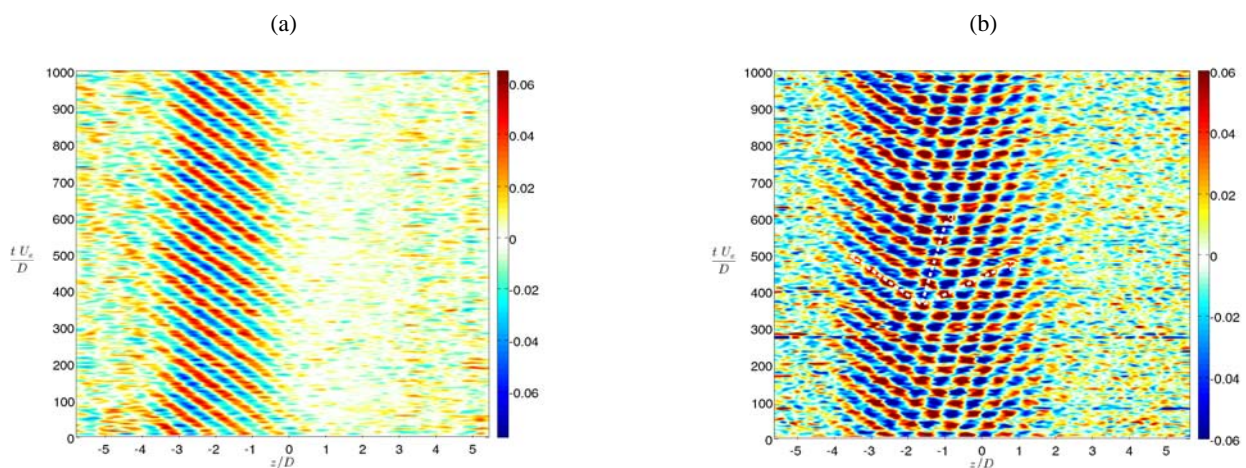


Figure 1: Space-time diagrams exhibiting travelling waves in the cavity inner flow: (a) in the primary regime, (b) in the secondary regime. The plane of observation is a horizontal cut of the inner flow at a depth $D/3$ below the cavity top plane (D is the cavity depth). The spatial line z is span long.

Sensitivity of stochastic perturbations in a noise amplifier flow

E. Boujo^a and F. Gallaire^a

It is a well-known fact that small-amplitude perturbations can be amplified in globally stable flows due to non-normal mechanisms. This leads in the time domain to the transient growth of some initial disturbances, and in the frequency domain to the amplification of some harmonic disturbances. It is of interest to look for the most amplified of these disturbances: the optimal perturbations. We consider here random perturbations which are being continuously advected in the laminar flow past a backward-facing step. The response of the flow to this sustained stochastic input can be analysed in the frequency domain in terms of amplification at each individual frequency¹, and the problem therefore boils down to combining appropriately harmonic optimal and sub-optimal perturbations at all frequencies.

In this work we use a variational technique to compute the sensitivity of noise amplification to steady control, either passive (e.g. a small cylinder inserted in the flow) or active (e.g. wall blowing or suction). Sensitivity maps allow identifying regions where control is most effective in reducing amplification. Our work extends existing sensitivity methods² in two ways: (i) from time-harmonic to time-stochastic, (ii) from perturbations distributed in space in the whole flow to perturbations localized at the inlet. We therefore deal with a more realistic representation of incoming noise. We also simplify the process of control design by integrating all harmonic sensitivity maps for each individual frequency³ into one single stochastic sensitivity map.

In the backward-facing step flow, harmonic disturbances are strongly amplified around one preferred frequency⁴. The amplification of stochastic noise can be reduced by inserting a small control cylinder in regions of large streamwise velocity, particularly at streamwise locations between the step corner and the upper reattachment point. Alternatively, boundary control is most effective when using wall suction upstream of the step corner, or wall blowing on the vertical wall; this results in a shorter separation bubble on the lower (resp. upper) wall when using boundary actuation at the lower (resp. upper) wall, as confirmed by applying sensitivity analysis to recirculation length in this flow⁵.

We find that sensitivity maps for stochastic noise are largely similar to those for the optimal harmonic perturbation at the most amplified frequency. This suggests that the design of steady control in strong noise amplifiers (globally stable but convectively unstable flows) can be conducted restricting one's attention to the most dangerous perturbation at the most dangerous frequency.

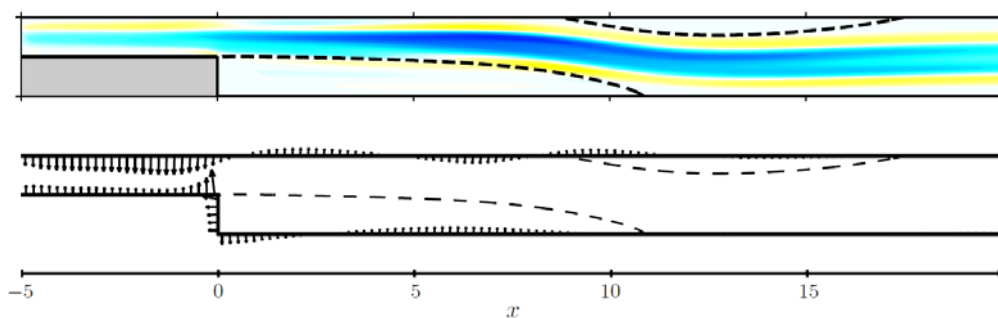


Figure 1: Sensitivity maps of the amplification of stochastic perturbations entering the flow at the inlet: (a) effect of a small cylinder of diameter $d=0.05$ (amplification is increased in yellow regions and decreased in blue regions), (b) sensitivity to wall forcing (amplification is increased if using blowing/suction in the same direction as arrows).

^a Lab. of Fluid Mechanics and Instabilities, EPFL, Lausanne, Switzerland

¹ Farrell and Ioannou, *J. Atmos. Sci.* **53**, 2025 (1996)

² Brandt, Sipp, Pralits and Marquet, *J. Fluid Mech.* **687**, 503 (2011)

³ Boujo, Ehrenstein and Gallaire, *Phys. Fluids* **25**, 124106 (2013)

⁴ Marquet and Sipp, *7th IUTAM Symposium on Laminar-Turbulent Transition* **18**, 525 (2010)

⁵ Boujo and Gallaire, *J. Fluid Mech.* **742**, 618 (2014)

Behaviours of Tollmien-Schlichting waves undergoing small-scale distortion

Hui Xu^{a, b}, Spencer J. Sherwin^b and Philip Hall^a

Transmitted behaviour of Tollmien-Schlichting (T-S) waves undergo short local wall imperfection distortion is investigated in laminar boundary layer, which is one of the fundamental problems on addressing laminar-turbulent transition. In terms of triple-deck theoretical scheme and asymptotic analysis, it has been shown as instability waves undergo rapid distortion and height (+ h)/depth ($-h$) of local wall roughness elements is far less than $\mathcal{O}(LRe^{-5/8})$, transmission behaviours of T-S waves are depicted by an analytical expression which is dominated by the first order of h . Theoretically, for hump and indentation distortion, T-S waves show different transmitted features. It has been predicted that positive h can stabilize T-S waves and vice versa. With high Reynolds number Re , accessing extreme small h is not a trivial problem by numerical validation. With the aid of high precision numerical investigations, it is discovered that generally, for $h \lesssim \mathcal{O}(LRe^{-5/8})$, both of hump and indentation have only destabilizing effect. By observing T-S wave transmission coefficient distribution around short ($\mathcal{O}(LRe^{-3/8})$) rapid distortion, recovering Blasius boundary layer profile needs a long distance ($\gg \mathcal{O}(LRe^{-3/8})$) from rapid distortion position and shear stress distribution has profound influence on T-S waves before recovering Blasius shear stress. It is indicated directly that estimating T-S wave transmission coefficient on scale $\mathcal{O}(LRe^{-3/8})$ for current $h \sim \mathcal{O}(LRe^{-5/8})$ configuration (even for smaller h) is inapplicable. Frankly, the classical triple-deck theory cannot be employed to formulate a universal analytical expression of transmission coefficient. Moreover, the perturbed frequency response to local wall distortion is also investigated by numerical strategy. For practical interests, the investigations on humps/indentations with width scale comparable with T-S wavelength are also performed and the corresponding transmission coefficient is formulated. Further, the influences of small height scale of forward/backward-facing steps on T-S waves' behaviours are investigated.

^a Dep. Mathematics, Imperial College London, 180 Queen's Gate, London SW7 2AZ, UK

^b Dep. Aeronautics, Imperial College London, 180 Queen's Gate, London SW7 2AZ, UK

[†] Wu and Hogg, *J. Fluid Mech.* **550**, 307 (2006).

Too big to grow: the mean flow saturation mechanism of the backward-facing step response to harmonic forcing captured by a self-consistent model.

V. Mantic-Lugo^a, F. Gallaire^a

Certain flows denominated as amplifiers are characterized by their global stability while showing large amplifications to sustained linear perturbations. For instance, the well known 2D backward-facing step flow presents a maximum sustained energy linear growth of order 10^7 at the frequency 0.075 and $Re = 500$, which is related to convective instabilities growing in the shear layer of the separated flow¹.

However, a simple physical picture describing the saturation of the response to higher amplitudes of the sustained forcing is still missing. We present a simple self-consistent model that captures the saturation mechanism of the response to harmonic forcing in a simple manner. The amplifier is forced at one frequency with an optimal body forcing structure calculated from the receptivity analysis around the base flow. As the forcing amplitude increases, a strong saturation of the response appears when compared to the linear prediction.

The model consists of a decomposition of the full nonlinear Navier-Stokes (NS) equations in a mean flow equation plus a linear perturbation equation around the mean flow. This linear response equation feeds back onto the mean flow through the Reynolds stress. The full fluctuating response and its corresponding Reynolds stress are approximated by only the first harmonic calculated from the linear response of the forcing around the aforementioned mean flow. This set of coupled equations is closed and solved in an iterative way as partial nonlinearity is still preserved in the mean flow equation despite the assumed simplifications.

The results show an accurate prediction of the response energy when compared to DNS, thus capturing the saturation process, as seen in Figure 1. It seems that the aforementioned coupling is enough to retain the main nonlinear effects of the saturation process. Hence, a simple physical picture is revealed, wherein the response modifies the mean flow through the Reynolds stress in such a way that the correct response energy is attained. Moreover, the saturated mean flow and fluctuating velocity fields and the Reynolds stress spatial structure are thereby well approximated in a self-consistent manner, without resorting to DNS.

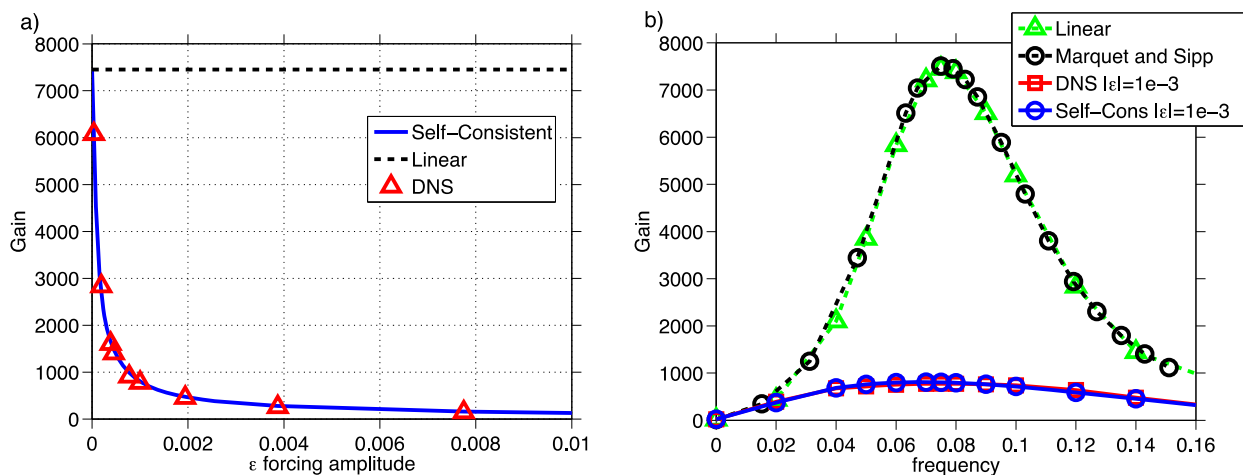


Figure 1: (a) Gain saturation with forcing amplitude increase at frequency 0.075. Forcing shape fixed as linear optimal of the base flow, $Re=500$. (b) Gain variation for different forcing frequency and Gain saturation of the model compared to DNS for a forcing amplitude of $\varepsilon=10^{-3}$, $Re=500$. Forcing shape optimal around base flow at each frequency.

^a Laboratory of Fluid Mechanics and Instabilities, École Polytechnique Fédérale de Lausanne. EPFL-STI-IGM-LFMI, Switzerland

¹ Marquet and Sipp, Seventh IUTAM Symposium on Laminar-Turbulent Transition, 525-528, 18 (2010).

On the origin of the viscous instability mechanism

J. J. Healey¹

Tollmien's discovery that viscosity can destabilize boundary layers and channel flow is one of the most surprising and famous results in hydrodynamic stability theory. However, although we have detailed asymptotic and numerical descriptions of viscous instability, it is not easy to explain why the inclusion of dissipative terms should destabilize a shear flow. On the other hand, if viscosity is destabilizing, why does viscosity not destabilize plane Couette flow, or circular pipe flow?

In contrast, the inviscid Kelvin-Helmholtz instability mechanism is easily understood in terms of a resonant interaction between a pair of waves on the interface between two uniform flows in relative motion. We suggest that viscous instability is also the result of a resonant interaction. The difference with KH instability is that an inviscid noninflectional boundary layer, or channel flow, only has a single lightly damped (due to critical layer effects) inviscid mode. A flow with only a single mode cannot exhibit resonance, and so is stable. The introduction of viscosity creates a new family of damped viscous modes. We show that the lightly damped inviscid mode can resonate with one of the viscous modes and this creates instability.

In summary: mixing layers support two inviscid waves which can resonate to produce inviscid instability; noninflectional boundary layers have a single lightly damped inviscid mode which can resonate with viscous modes to produce viscous instability; and plane Couette flow and pipe flow have no lightly damped inviscid mode, and so remain stable when viscosity is included.

Curiously, pipe flow supports a lightly damped inviscid mode with fractional (therefore unphysical) azimuthal wavenumbers, which becomes unstable when viscosity is included. Such modes could be introduced approximately as an initial condition and might produce transient exponential growth.

¹ Department of Mathematics, Keele University, Keele, Staffs, ST5 5BG, UK

Mixing

Buoyancy induced turbulent mixing in a long narrow tilted tank

Tiras Y. Lin^{a,b}, C. P. Caulfield^{b,c} and Andrew W. Woods^b

We consider the turbulent mixing that occurs due to the injection of a small constant volume flux of dyed fluid of density ρ_s at the top of a long narrow tank tilted at an angle θ from the vertical. The tank is initially filled with fluid of density $\rho_0 < \rho_s$ and has a square cross section ($d \times d \times 40d$). Using dye and a light attenuation technique, the evolution of the reduced gravity $g' = g(\rho - \rho_0)/\rho_0$, where g is the acceleration due to gravity and ρ is the local fluid density, can be extracted throughout the tank. The injected fluid mixes vigorously with the fluid that initially occupies the tank, and a mixed region of turbulent fluid slowly propagates through the tank due to the unstable density gradient that is set up along the length of the tank. At a large tilt angle θ , a stable density gradient across the width of the tank is formed throughout the mixed region of dense fluid, although the flow continues to be turbulent both across and along the tank. However, for sufficiently small tilt angles, the evolution of the mixing region can be described as a diffusive process using Prandtl's mixing length theory, analogously to an approach described previously¹, which considered purely vertical tanks with $\theta = 0$. Turbulent eddies that are of the order of the tank width dominate the turbulent flow, and the cross-tank component of the gravitational acceleration has only a weak effect on the orientation of the wall-normal density gradient across the width of the tank, with statically unstable density gradients frequently occurring. At intermediate tilt angles, however, the behaviour of the propagation of the turbulent fluid is a combination of the features observed in these two end-member cases, and we delineate the contributions from each of these effects.

^a Department of Earth Sciences, University of Cambridge, Cambridge CB2 3EQ, UK

^b BP Institute, University of Cambridge, Cambridge CB3 0EZ, UK

^c Department of Applied Mathematics and Theoretical Physics, University of Cambridge, Cambridge CB3 0WA, UK

¹ van Sommeren et al., *J. Fluid Mech.* **701**, 278 (2012).

Direct Numerical Simulation of a turbulent mixing layer with variable density

A. E. Almagro^a, O. Flores^a and M. García-Villalba^a

We present preliminary results of direct numerical simulations of a turbulent mixing layer with variable density. These simulations are a first step in the development of a numerical solver able to simulate spray diffusion flames in the limit of infinitely fast chemical reaction, using the coupling-function formulation¹. The set-up of the simulations consists of a three-dimensional temporally evolving, plane, variable-density mixing layer. The in-house code solves the Navier-Stokes equations in the Low-Mach number approximation, with the pressure split into a thermodynamic component and a mechanical component. In order to remove the mechanical pressure from the momentum equations, an extended version of the velocity-vorticity formulation for incompressible flows² is used. In this formulation, the momentum equations are rewritten as evolution equations for the vertical components of the laplacian and curl of the momentum vector. A key advantage of this formulation is the elimination of the mechanical pressure from the momentum equations and, as a consequence, the errors and complications associated with pressure boundary conditions and pressure-splitting algorithms. The new algorithm is implemented into a highly parallel solver that uses a pseudospectral numerical method, expanding all variables in Fourier series in the two homogeneous directions. Compact finite differences are used in the vertical direction. The temporal discretization is an explicit Runge-Kutta with three sub-steps.

^a Biongeniería e Ingeniería Aeroespacial, Universidad Carlos III de Madrid, Leganés 28911, Spain.

¹ Arrieta-Sanagustín et al., *Fuel Processing Tech.*, **107**, 81 (2013)

² Kim et al., *J. Fluid Mech.*, **177**, 133 (1987).

Experimental Investigation of Spatially-periodic Scalar Patterns in an Inline Mixer

O. Baskan^a, M.F.M. Speetjens^b and H.J.H. Clercx^a

Spatially persisting patterns that form during the downstream evolution of passive scalars in three-dimensional (3D) spatially periodic flow fields is a fundamental aspect of industrial mixing processes that rely on the static mixing principle: a continuous stirring of a throughflow by the systematic reorientation of the transverse flow via static elements. Despite many numerical/experimental studies on 3D spatially periodic flow fields, experimental research on the scalar field is still scarce. This research aims to fill the gap by performing the state-of-the-art measurements on realistic geometries.

The study focuses on a comparative analysis between laboratory experiments and numerical simulations on the evolution of scalar fields (temperature, concentration) and concerns the correlation between the coherent structures of the flow field and the scalar field in a representative inline mixer.

The representative configuration is the Quatro static mixer, which is composed of a cylindrical tube, chevron-shaped central plates and perpendicular elliptical segments extending to the inner wall of the tube. Systematic successive placement of the static elements in the axial flow direction results in a spatially periodic flow field. The experimental setup consists of an optically accessible test section with transparent internal elements, accommodating a pressure-driven pipe flow seeded with tracer particles. The 3D streamlines (and the flow field) and the scalar fields are measured by 3D Particle-Tracking Velocimetry and 3D Laser-Induced Fluorescence, respectively. The preliminary numerical studies have proven the existence of spatially periodic patterns with exponentially decaying intensities and their evolution from non-homogeneous initial state towards homogeneous final state (Figure 1), which agrees well with the eigenmode analysis of scalar transport in periodic flow fields in literature.

^a Dep. Applied Physics, TUE, P.O. Box 513 5600 MB, Eindhoven, The Netherlands

^b Dep. Mechanical Engineering, TUE, P.O. Box 513 5600 MB, Eindhoven, The Netherlands

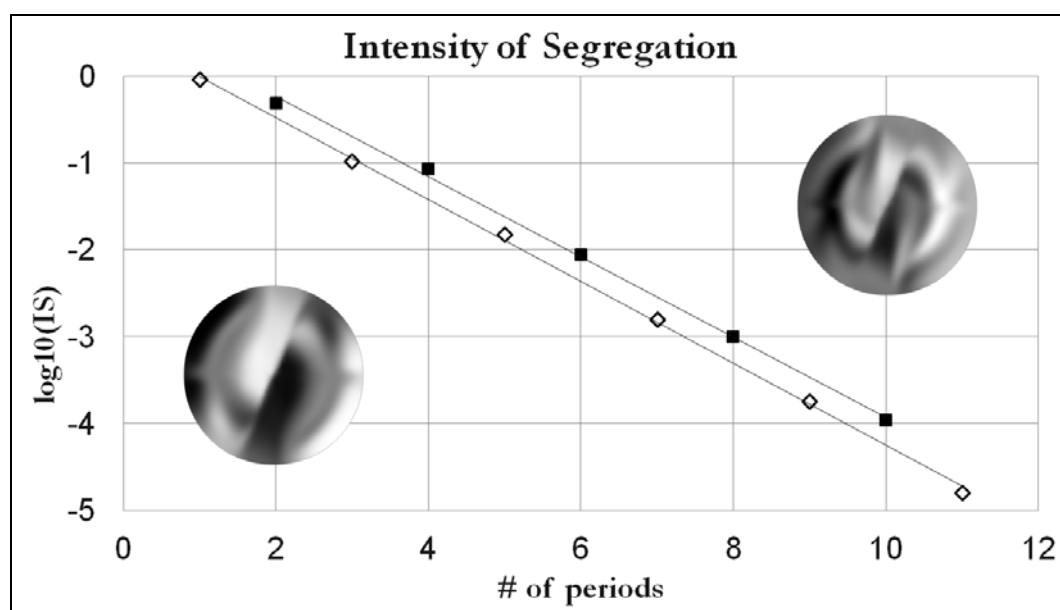
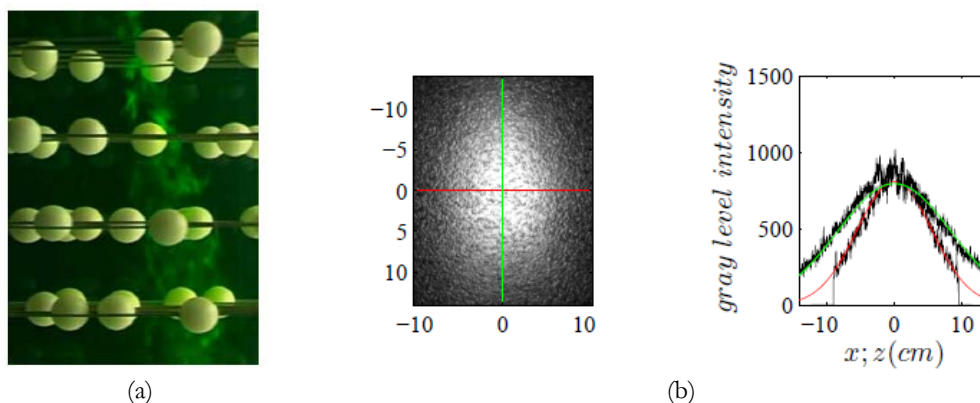


Figure 1: The spatially-periodic persistent patterns and the exponential decay of the variance in Quatro mixer at $Pe=10^3$. Left pattern: for odd number of periods. Right pattern: for even number of periods.

Mixing induced by bubble agitation

E. Almeras^a, C. Besnaci^a, C. Plais^b, F. Augier^b, V. Roig^a, F. Risso^a

The purpose of this work is to understand the mechanisms responsible for mixing of a low-diffusive solute in a 3D bubble column. The agitation in a homogeneous bubble swarm was previously demonstrated to be similar to that produced in a flow through a random array of obstacles^{c,d}. We then first investigated the mixing of a passive scalar in a flow crossing a random array of spheres with a volume fraction of 2%. A fluorescent dye is injected through a point source (Fig. a) and its concentration is measured by PLIF. We observed two different mixing mechanisms. For a Reynolds number Re less than 400, the main mixing mechanism is the deformation of the flow in the vicinity of the spheres. At higher Re , turbulence is responsible for the mixing. An effective diffusivity was shown to be able to describe the mixing. Next, we investigated the mixing of a passive scalar in a stable homogeneous column for gas volume fractions α ranging from 1 to 10% with a bubble diameter $d \sim 2$ mm, which corresponds to a Reynolds number Re around 600. A finite volume of a fluorescent dye is injected and its expansion measured by video processing (Fig. b). The mixing rates are different in vertical and horizontal directions, but tend to become isotropic as α is increased. Finally, the bubble column has been destabilized by imposing a slight inhomogeneity of α at the bottom of the tank, which generates large flow recirculations. The transport of the dye by the buoyancy-driven advection is observed to be much faster than the mixing by the bubble-induced turbulence. The mixing of a low-diffusive solute thus combines three mechanisms: (1) at large scales corresponding to gradients of α , the transport is dominated by buoyancy-driven flow cells; (2) at intermediate scales of order d , bubble-induced agitation dominates; (3) at very small scales, micro-mixing is achieved by molecular diffusion.



Figures: (a) Mixing in a random array, (b) Mixing in the homogeneous swarm of bubbles.

^a Institut de Mécanique des Fluides de Toulouse, Université de Toulouse and CNRS, Allée du Prof. C. Soula, 31400 Toulouse, France

^b IFP Energies nouvelles, Lyon, Rond-point de l'échangeur de Solaize, BP 3, 69360 Solaize, France

^c Amoura, INPT PhD, Toulouse, France (2008)

^d Riboux et al., *J. Fluid Mech* **719**, (2013)

Experimental and numerical investigations of heat transfer in a static and chaotic mixer

M. Creyssels^a, S. Prigent^a, Y. Zhou^a, X. Jianjin^a, C. Nicot^a and P. Carrière^a

Microfluidic exchangers/reactors are often used for carrying out complex chemical reactions with samples of small sizes and allow a rapid analysis of the resulting products. The monitoring of the chemical reaction needs a good mixing of the chemicals that is often difficult to achieve in microfluidic devices since flows are generally laminar and turbulence is absent. Mixing can then be achieved by chaotic advection-based processes. Our team has developed a static and chaotic mixer named « MLLM » for Multi-Level Laminating Mixer which perfectly mimics the baker's transformation, thus enabling a good mixing^{1,2} (see figure 1). An exothermic chemical reaction also requires the reactor to be efficiently cooled. The goal of the present study is to characterize the ability of the MLLM to transfer the thermal energy produced by a chemical reaction to the outside environment. An experimental set-up has been developed in order to measure the heat transfer performance of the MLLM and then to compare it with the efficiency of conventional heat exchangers like straight tubes (Graetz configuration). A three-dimensional numerical simulation of the flow inside the MLLM has also been performed using the finite-volume code « Saturne », which enabled a direct comparison with the thermal efficiency of the MLLM measured experimentally. Besides, the numerical simulation gives the structure of the flow and the temperature gradients within the chaotic mixer. The numerical predictions are in good agreement with the experimental results showing a net increase of the heat transfer for the MLLM compared to a straight tube with the same area of surfaces in contact between the inner and external flows. Two different kinds of chaotic mixing can explain this observed heat transfer improvement. The first one is closely related to the unique structure of the MLLM which is composed of repetitive sequences of appropriate flow splitting and stacking. The second mechanism that generates chaotic mixing comes from the large number of bends that compose the MLLM. Indeed, each bend induces some Dean vortices that stir the flow and thus enhance heat transfer.

^a Laboratoire de Mécanique des Fluides et d'Acoustique, CNRS, Ecole Centrale de Lyon - Université

Lyon 1 - INSA Lyon, 69134 Ecully cedex, France

¹ Carrière, *Phys.. Fluids* **19**, 118110 (2007).

² Liao et al., *Lab on Chip* **12**(4), 746 (2012).

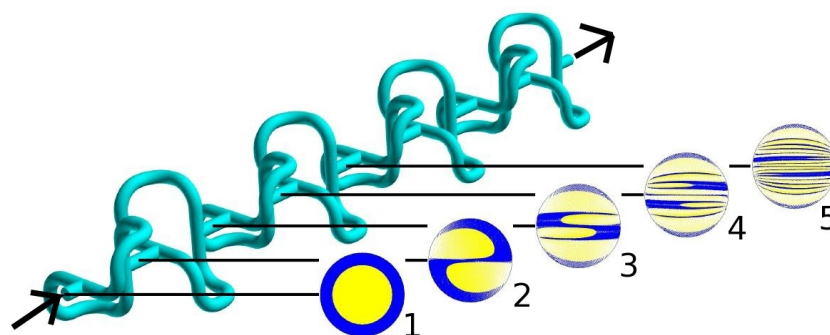


Figure 1: Design of the MLLM and plots of coloured fluid particles distribution in cross-section planes at the inlet of the first five elements.

Distribution of miscible admixture in the compound vortex

E. V. Stepanova^a and A. Yu. Vasiliev^a

Waves and vortices have strong influence on the transport of a substance in the flow. The results of the experimental study of the transport of marking admixture in a vortex under specified conditions of its introduction are only presented in a few works. Impressive flow images¹ entered many famous albums and monographs, but the process of admixture transport from the compact source in the vortex flow has not been systematically studied.

This paper presents the results of laboratory studies of the fixed volume vortex flow with free surface. The experiments were carried out on the setup “Vortex currents with torsion” (VTK), included in USU “GFK IPMech RAS”². The observed flow pattern can be schematically reduced to a combination of two vortices, one of which is a vertical cylindrical vortex and the other – toroidal with a circular axis, comprising the central vertical axis. As a result of their combined action the complex flow is formed within the cylindrical container.

From the dye spot introduced on the rotating free surface the spiral arms grow in two opposite directions. When the initial dye spot is placed not in the centre of the rotating water surface the outer spiral arm grows towards the sidewall of the cylindrical container and in the same time the other spiral arm elongates towards the center of the free surface. Regardless of the displacement along the free surface the dye penetrates into the water body along thin helical lines, which eventually form cylindrical surfaces.

The details of the substance transfer in the lower part of the considered vortex flow near the activator are revealed by injecting the dye near the disk. Dye spreads, following the main flow, in a thin layer, and then abruptly changes direction and begin to rise along the sidewall of the container. The border line of painted and unpainted liquid is non-monotonic, the formation of dye vortices can be observed on this line.

During the carried out experiments the three significantly different modes of admixture distribution are found: a dual behaviour of the dye on the free surface and drawing the dye along the flow, when the small volume of dye is injected on the edge of a rotating disc.

Acknowledgments. The work is supported in part by RFBR project № 14-05-00714-a.

¹ Taylor G.I., *Roy. Soc. Proc. A*. **100**. Pl. 2. (1921)

² Stepanova E. V., Chashechkin Yu. D., *Fluid Dynamics* **45** (6). (2010)

^a Lab. Fluid Mechanics, A. Ishlinsky Institute for Problems in Mechanics, 101-1 Vernadskogo ave., Moscow, 119526, Russia

Turbulence

Model/Theory

Turbulence intermittency in stably stratified boundary layers and eddy mixing in free atmosphere

A. F. Kurbatskiy^a, L. I. Kurbatskaya^b

Introduction. The possibility of the RANS description of intermittent turbulence both near the surface and over it, and above the surface in vicinity of the low-level jet flow (LLJ) formed above the stably stratified boundary layer is analyzed. Applicability of three turbulence models ($k-\varepsilon$ model modified for stratified flows, algebraic stress model and the three-parameter RANS turbulence scheme) – were examined for the upper troposphere and the lower stratosphere, using radar observation values of the TKE and turbulent energy dissipation rate.

Low-Level Jet and Elevated Turbulence. Figure 1(a) shows time evolution of the intermittent TKE calculated by the three-parameter RANS scheme of turbulence for a quasi-steady state of a strong stable stratified boundary layer with a specified constant negative heat flux on the surface. Though the shear increases both under and above the jet, turbulence overshoots are more probably expected to occur under the jet (diagrams 2-4 in Fig. 1(a)).

Eddy diffusivities for momentum and heat in the upper troposphere and lower stratosphere. Eddy diffusivity for momentum was calculated by the $k-\varepsilon$ model, algebraic stress model, the three-parameter RANS turbulence model and compared with the observed one in Fig. 1(b). The comparison of the eddy diffusivity profiles from all three turbulence models with the directly observed ones by Doppler radar indicates that the RANS turbulence scheme gives the best prediction.

^a ITAM SB RAS, 630090 Novosibirsk, Russia

^b ICMG SB RAS, 630090 Novosibirsk, Russia

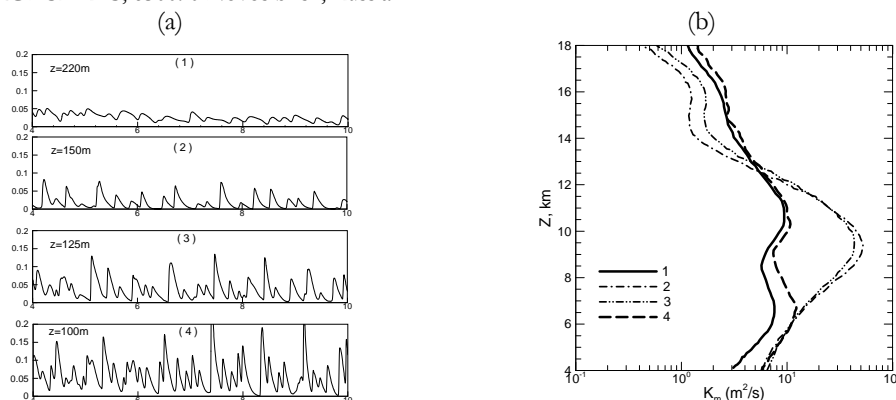


Figure 1: (a) Time evolution of the turbulent kinetic energy above the upper side of the LLJ (1) and on the lower part of LLJ (2-4) in a strong stable boundary layer predicted by the RANS-scheme of turbulence at different distances from the surface, (b) Eddy diffusivity for momentum measured directly by Doppler radar (solid thick line-1) and its comparison with values simulated using turbulence models: $k-\varepsilon$ model (thin line-2), the algebraic turbulence model (thin line-3) and the three-parameter RANS turbulence model (thick line-4).

Jet noise as a signature of turbulent pulsation physics

V. F. Kopiev^a, S. A. Chernyshev^b

Description of the dynamics of turbulent disturbances in the jet is still an unsolved problem. Study of this phenomenon is usually focused on the analysis of fluctuations in the immediate region of the turbulent flow. However, analysis of indirect turbulence manifestation also can be fruitful in this effort. One of such manifestation is the noise generated by the turbulent flow. Along with the practical importance of this phenomenon, it can be used as a diagnostic tool of the processes occurring in turbulent flow. A specific feature of the turbulence acoustic manifestations is that perturbations passively transferred by main flow do not give a significant contribution to the noise generation. That is, in the acoustic manifestations the dynamic part of the turbulence is observed, while passive perturbations are filtered out.

The aim of the current work is an analysis of the turbulent jet noise with the object of better understanding of the turbulence dynamics. The jet noise sources are described with the correlation model developed by the authors^{1,2}. This model allows to associate specific features of acoustic radiation with possible dynamics of turbulent fluctuations.

Used experimental data are obtained at Central Aerohydrodynamic Institute (TsAGI) based on advanced methods for measuring noise (Azimuthal Decomposition Techniques). These data allow to expand the sound field on the independent azimuthal components and obtain detailed information about the directivity and spectra of these components³. Data used in this work are obtained for the cold jet, $V = 120$ m/s. The inverse problem is solved that recovering the sound sources from the measured acoustic field. A good agreement of simulation results and measurement data is achieved in a wide range of parameters. Figure 1 shows a comparison for one of the azimuthal components of the noise.

The obtained results allow to draw some conclusions about the features of turbulent disturbances in the jet. From the aeroacoustics point of view, the directivity of the noise azimuthal components confirms the assumption of quadrupole nature of the noise sources. From the turbulence dynamic point of view, the shape of the noise spectra is consistent with the representation of turbulence as a random disturbance bursts followed by convection of these disturbances in main flow and their slow evolution, or as perturbations developing on a large vortex structure suddenly born followed by its convection. This means that the idea of turbulence as a stochastic sum of linear disturbances (spatial instability waves) on the background of the mean flow for the turbulent jet with considered parameters is not valid.

^a Acoustic Dep., TsAGI, 17 Radio str. Moscow, RF;

^b Acoustic Dep., TsAGI, 17 Radio str. Moscow, RF.

¹ Kopiev and Chernyshev, *ALAA*, 2250 (2012)

² Kopiev and Chernyshev, *Acoustical Physics*, 58, 4, 442–456 (2012)

³ Kopiev et al, *International J. of Aeroacoustic*, 6, 4, 375–405 (2007).

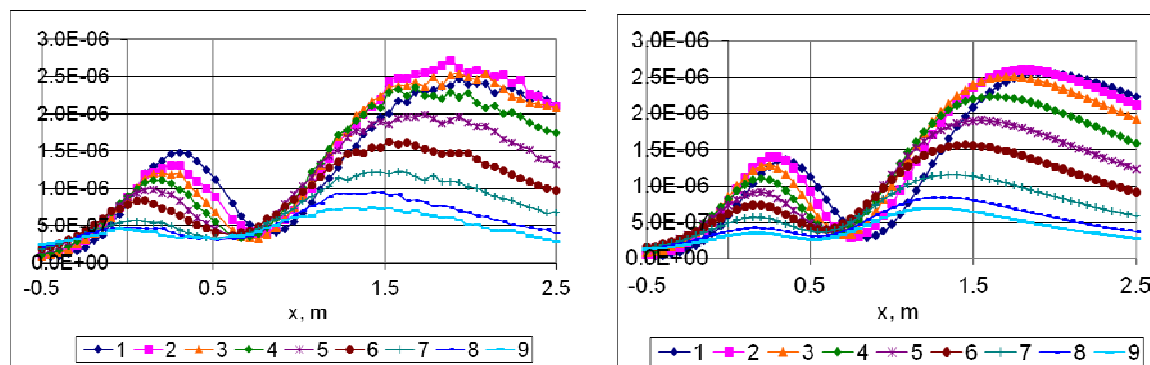


Figure.1. Directivities of radiated noise at distance 0.85m from the jet axis for the 0-th azimuthal harmonics, (a), measured, (b) calculated, x - distance along the jet axis from the nozzle.

Several curves correspond to different frequencies in the range of Strouhal number $0.15 < St < 1$.

On the multifractal structure of fully developed hydrodynamic turbulence

K. P. Zybin¹, V. A. Sirota^a

Understanding of statistical properties of a turbulent flow is one of the classical problems of hydrodynamics. In particular, experiments and numerical simulations demonstrate scaling behaviour of velocity structure functions with intermittent scaling exponents [1-2]. The most successful, and conventional nowadays, way to interpret this intermittency is the Multifractal approach introduced in [3]. It allows, in particular, to express all observed intermittent characteristics by means of velocity scaling exponents [4].

However, the Multifractal method is a phenomenological theory: it does not derive the scaling properties from the Navier-Stokes (or Euler) equation, and it does not specify the structures, or configurations, that are responsible for the intermittency. The attempts to derive the Multifractal formalism directly from the first principles (Navier-Stokes equation) have not been successful yet.

On the other hand, the numerical simulations [5] reveal the importance of high-vorticity regions called vortex filaments for power-law structure functions.

In this work we investigate the stochastic Navier-Stokes (Euler) equation to describe the formation of these filaments.

To derive statistical properties, one has to introduce randomness into the Navier-Stokes equation. This is usually done by adding a large-scale random external force into the right-hand side of the Navier-Stokes equation. We propose another way: large-scale fluctuations of velocity are themselves treated as independent random quantities. The stochastic properties of small-scale fluctuations can then be derived based on the properties of the large-scale fluctuations.

We analyse the stochastic equation for small-scale velocity fluctuations that is a stochastic analog to the Navier-Stokes equation [6]. It appears that, for a large class of solutions, high-vorticity regions undergo exponential stretching, despite the stochastic symmetry of the large-scale velocity. This stretching produces exponential growth of vorticity and formation of vortex filaments. It also provides the scaling behaviour of structure functions. This stretching, and not decay, of vortices appears to be the main mechanism of turbulence development. We note that in our model there is no finite-time singularity, even in the non-viscous case. Scaling of velocity structure functions is achieved by stationary scaling profiles of velocity and vorticity in the vortex filaments, while in the middle of a filament there is always a constantly narrowing non-stationary inner part.

The dispersion of the stochastic large-scale parameters results in nonlinear dependence of scaling exponents of their orders, i.e., in intermittency. This gives an explanation of multifractal formalism: different scalings are produced by different vortex filaments. We derive a simple approximation to the dimension function $D(h)$ expressed in terms of the properties of large-scale velocity distribution.

References

1. F. Toschi and E. Bodenschatz, *Annu. Rev. Fluid Mech.* 41, 375, 2009.
2. R. Benzi, L. Biferale, R. Fisher et al., *J. Fluid. Mech.* 653, 221, 2010.
3. G. Parisi, U. Frisch, in: *Turbulence and Predictability in Geophysical Fluid Dynamics*, *Proceed. Intern. School of Physics 'E. Fermi'*, 1983, Varenna, Italy; North-Holland, Amsterdam edited by. M. Ghil, R. Benzi, and G. Parisi, 84-87, 1985.
4. G. Boffetta, A. Mazzino and A. Vulpiani, *Journal of Physics A* 41, 363001, (2008).
5. N. Okamoto, K. Yoshimatsu, K. Schneider et al., *Phys. Fluids* 19, 115109, (2007)
6. K.P. Zybin, V.A. Sirota, *Phys. Rev. E* 88, 043017 (2013)

¹ P.N. Lebedev Physical Institute of RAS, Leninskii pr. 53, Moscow, Russia

A friction law for self-similar turbulent boundary layers with imposed pressure gradient

I. I. Vigdorovich^a

The self-similar flow of incompressible fluid in a turbulent boundary layer, when the free-stream velocity u_e is specified as a power function of the longitudinal coordinate, $u_e = Bx^m$, is considered. The self-similar formulation not only simplifies solving the problem by reducing the equations of motion to ordinary differential equations but also provides a mean for formulating the closure conditions for these equations. It is shown that for the class of flows under consideration that depend on the three governing parameters B , m and the kinematic viscosity ν , the dimensionless mixing length is a function of the normalized distance from the wall and the exponent m in the outer region and a universal function of the local Reynolds number in the wall region, the latter corollary being true even when the skin friction vanishes^{1,2}. Such a general formulation enables us to obtain an asymptotic solution to the problem. It is shown that there exist four different characteristic flow regimes each of which is characterized by its own similarity parameter¹⁻⁵. A friction law, which covers all the four regimes, is established. It can be written in the form

$$\text{Re}_{\delta^*} = \frac{\Omega^3 D(\Omega) [2 - \Omega D(\Omega)]}{4(\frac{1}{2}c_f)^{3/2}} \exp \left[\frac{\kappa[1 - \Omega D(\Omega)]}{\sqrt{\frac{1}{2}c_f}} + \Phi \left(\frac{1}{1 + \beta} \right) - K(\tau) + 2 - C \right]. \quad (1)$$

Here Re_{δ^*} is the Reynolds number based on the displacement thickness, c_f is the skin friction coefficient, $\kappa=0.41$ is the von Karman constant, $C=2.05$ is the second constant in the logarithmic law for the velocity profile in the wall region. The formulation of the law contains three universal functions. The function $\Phi(1/(1+\beta))$ depends on the known Clauser equilibrium parameter $\beta = -2\delta^* u'_e / (u_e c_f)$, where u'_e is the derivative of the free-stream velocity with respect to the longitudinal coordinate. It corresponds to the flow regime with favourable and moderate adverse pressure gradients^{1,2}. The function $\Omega D(\Omega)$ depends on a new similarity parameter $\Omega = \sqrt{\delta^*} u'_e / u_e$. It is obtained from the solution for a near-separation flow regime⁴. And the function $K(\tau)$, where $\tau = \frac{1}{2}c_f \text{Re}_p^{-2/3}$ and $\text{Re}_p = u_e^2 / (u'_e \nu)$ is the Reynolds number based on the longitudinal pressure gradient, is essential only when the skin friction is very close to zero⁵. Experimental and calculated values of the functions Φ and ΩD are shown in Fig. 1. Formula (1) gives the skin-friction values differing from experimental ones by at most ten percents.

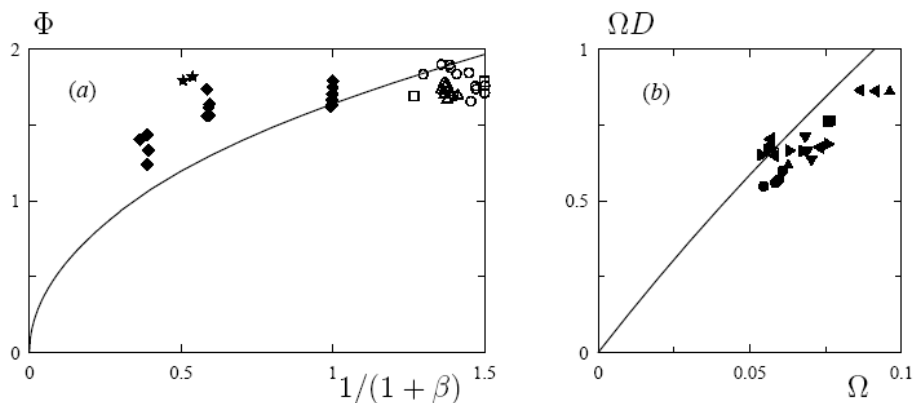


Figure 1: Universal functions (a) Φ and (b) ΩD according to calculated and experimental data

^a Institute of Mechanics, Lomonosov Moscow State University, 1 Michurinski Ave., Moscow, Russia

¹ Vigdorovich, *Doklady Phys.* **56**(4), 249 (2011).

² Vigdorovich, *J. Exp. Theor. Phys.* **117**, 356 (2013).

³ Vigdorovich, *Doklady Phys.* **57**(5), 197 (2012).

⁴ Vigdorovich, *Doklady Phys.* **57**(8), 312 (2012).

⁵ Vigdorovich, *Doklady Phys.* in press. (2014).

Spectral modelling of Unstably Stratified Homogeneous Turbulence (USHT)

Alan Burlot¹, Benoît-Joseph Gréa^a, Fabien Godeferd^b and Claude Cambon^b

Unstably Stratified Homogeneous Turbulence (USHT) is an idealized approach for buoyancy driven flows under Boussinesq approximation. This concept is aimed at analysing the properties of turbulent fluctuating quantities developing in Rayleigh-Taylor mixing zones or in turbulent convection. In particular, it is dedicated to investigate the unsteadiness and anisotropy of the flow, while getting rid of inhomogeneity effects. USHT has been explored extensively through numerical simulations¹ and theoretical studies² which focus particularly on the self-similar aspects of this flow. These works have shown the fundamental importance of large scales in the time evolution of turbulent quantities. They also have proved the limitations of simulations, due to confinement effects induced by the growth of energetics scales fed by constant injection of potential energy.

In order to overcome this difficulty, we develop a spectral model based on an Eddy-Damped Quasi-Normal Markovian³ method which takes into account energy production by buoyancy terms. This two-point statistical model describes axisymmetric turbulence through a set of velocity-density correlation spectra.

In our talk, we will introduce the equations for the model and we will confront its results with high resolution DNS of USHT. Afterwards, we will present two applications of our EDQNM model: (a) the time evolution of turbulent quantities at very large Reynolds number; (b) the study of large-scale dynamics controlling the evolution of self-similar regime.

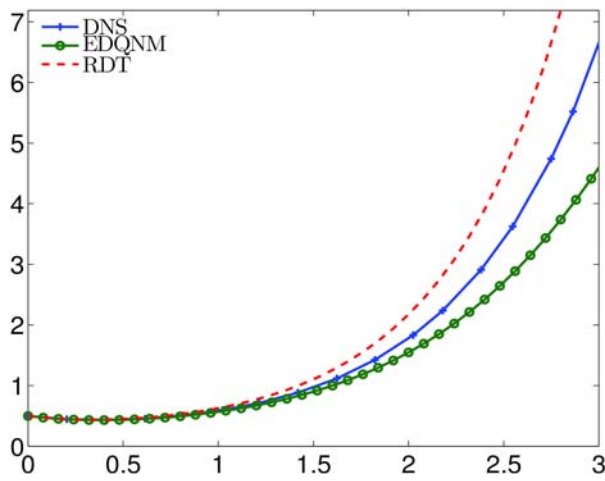


Figure 1: Kinetic energy evolution (ordinate) vs. non-dimensional

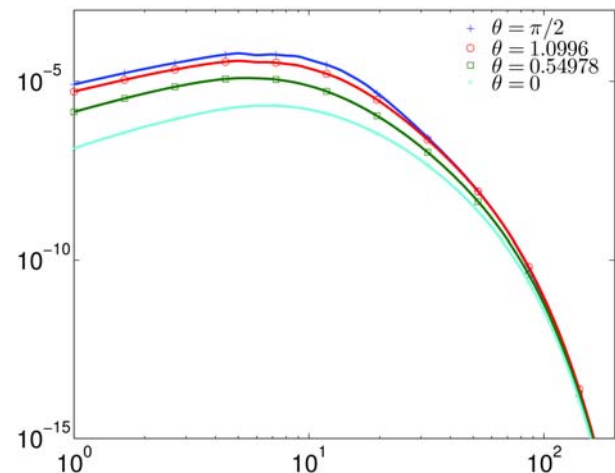


Figure 2: Kinetic energy spectrum (ordinate) vs. wavenumber (abscissa) for 4 angles at $T^*=3$

¹ CEA, DAM, DIF, F-91297 Arpajon, France

^b LMFA, École centrale de Lyon, CNRS, INSA, UCB, F-69134 Écully cedex, France

¹ Griffond et al, *Journal of Fluid Engineering*, Accepted (2013)

² Soulard et al, *Physics of Fluids* **26**, 1 (2014)

³ Orszag, *Journal of Fluid Mechanics* **41**, 363 (1969)

The wavelet p -model for turbulent flow and its applications of CFD

L.Zhou^a, C. Rauh^a, A. Delgado^a

The energy cascade p -model¹ was firstly proposed in the 1980s. It has been shown that the p -model is capable to describe the one-dimensional (1-D) turbulence signal concerning high order statistics². However, the theory is based on kinematic assumption without dynamic description. The extension to higher dimensions will generally lose turbulent intermittency. In this work, the p -model is extended to 2-D and 3-D under the wavelet framework³. Intermittent velocities are constructed on each scales. The constructed velocities are then treated as inviscid particles to create dynamic motions. Due to the inviscid assumption, the N-S equations are reduced to the Euler equations which have analytical solutions under Lagrangian framework. As a result, the comparison between modeled turbulence and DNS shows good agreement both in statistical properties and in flow field where filament shapes and coherent vortices can be observed.

As an application, the initial conditions used for LES or DNS are constructed by proposed model. Because the model is derived from inertial range of fully developed turbulence, the computational time for flow development is significantly reduced, from $1/4$ to $1/10$ times shorter for different test cases when comparing with traditional initial techniques such as spectrum method.

The proposed model can also generate the instantaneous flow for RANS or LES, which can be used as a sub-grid model for LES or a fluctuation generator for RANS simulation. The example discussed here is an incompressible jet flow calculated by RANS simulation. The wavelet p -model strongly improves the intermittency of velocity fields as well as the prediction of aeroacoustic intensity.

^a Institute of Fluid Mechanics (LSTM), Friedrich-Alexander University of Erlangen-Nürnberg, Germany

¹ Meneveau and Sreenivasan, *Phys. Rev. Lett.* **59**(13):1424-1427 (1987).

² Juneja et al., *Phys. Rev. E* **49**(6):5179 (1994)

³ Arneodo et al., *J. de Physique II* **7**(2):363-370 (1997)

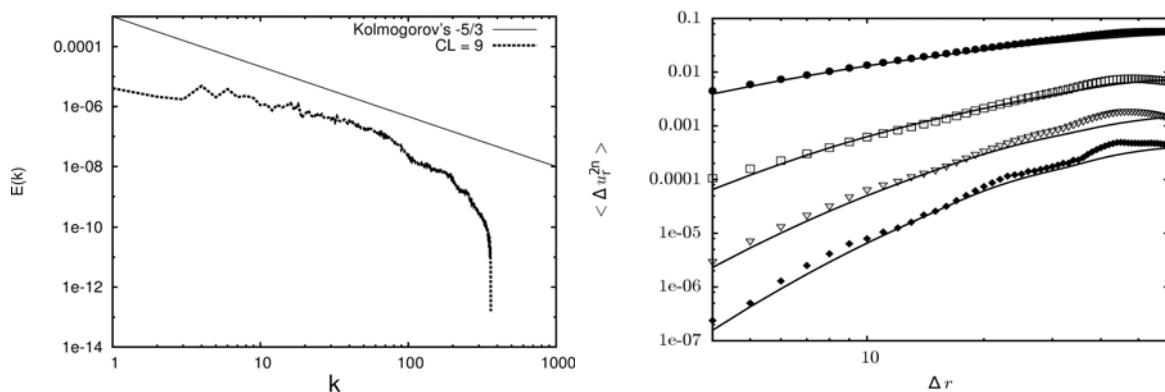


Figure 1: Left: The energy spectrum for isotropic turbulence using wavelet p -model (dotted line) and Kolmogorov's 5/3 law (solid line). Right: Comparison between the second order to eighth order structure functions (even orders, from top to bottom) from p -model (dotted line) and a DNS test case (solid line).

Anisotropic synthetic turbulence using constrained MTLM

Y. Li^a and C. Rosales^b

Synthetic turbulence has been found useful for turbulence modelling and as a surrogate to understand the dynamics of Navier-Stokes turbulence. In a recently proposed Multi-scale Turnover Lagrangian Map (MTLM) method¹, a random field is transformed into a synthetic field by advecting Lagrangian fluid particles iteratively while maintaining incompressibility and a given energy spectrum. It is shown that the resulted fields reproduce highly realistic statistics on many aspects of isotropic hydrodynamic turbulence, including small-scale intermittency, geometric statistics, and pressure statistics. Thus, it is of great interests to generalize the method to flow fields with additional features, such as large scale inhomogeneity. In this paper, we formulate this problem as an optimization problem, where the initial random field is taken as the control variable, and the additional features we desire is taken as a target function to be matched by the synthetic fields. The aim is to find the optimal control variable so that the difference between the target function and the synthetic field is minimized. Using the adjoint formulation of the optimization problem, we derive the adjoint mapping of the MTLM as well as the optimization condition for the system. The formulation, which is called the Constrained MTLM (CMTLM), is applied to synthesize two types of Kolmogorov flows where persistent large scale structures produce non-trivial mean flow statistics and local anisotropy in small scales. We compare the synthetic fields with direct numerical simulation data, and show that the former reproduces closely the mean flow statistics such as Reynolds stress distribution and mean turbulent kinetic energy balance. They also reproduce the effects of large scale structures, as is manifested in the distributions of mean subgrid scale energy dissipation, and the alignment between the sub-grid scale stress tensor and the filtered strain rate tensor, among others. We conclude that the method is a useful tool to further extend the applicability of synthetic turbulence.

^a School of Mathematics and Statistics, University of Sheffield, Sheffield, UK, S3 7RH

^b Dep. Mechanical Engineering, Universidad Tecnica Federico Santa Maria, Valparaiso, Chile

¹ Rosales and Meneveau, *Phys. Rev. E*, **79**, 016313 (2008).

Comparison of three turbulence models in the modeling of kiln aerodynamics

I. A. Sofia Larsson^a, T. Staffan Lundström^a and B. Daniel Marjavaara^b

Rotary kilns are large, cylindrical, rotating ovens with a burner in one end that are used in various industrial processes to heat up materials to high temperatures. The kiln burners are characterized by long diffusion flames where the combustion process is largely controlled by the turbulent diffusion mixing between the burner fuel jet and the surrounding combustion air. The combustion air flow patterns can have a significant effect on the mixing and hence the combustion efficiency, motivating a systematic study of the kiln aerodynamics.

The objective of this work is to compare turbulence models when modeling the aerodynamics of an iron ore pelletizing rotary kiln. Simulations of the non-reacting isothermal flow, without the burner jet, using three different ω -based turbulence models are performed on a simplified, down-scaled model of the kiln. Some of the results are validated against PIV-experiments on a similar model. The turbulence models used are the two-equation model SST, the Reynolds stress model BSL and the Detached eddy simulation turbulence model based on the SST formulation. It is found that the turbulence models produce quite different results yielding different predictions of the flow field.

The geometry gives rise to vortex shedding resulting in large-scale oscillations of the flow field. This process characterizes the flow and represents the most energy containing movements of the flow, hence the turbulence model must be able to capture this. The recirculation zone that develops behind the dividing wall between the jets is important from a combustion perspective as the reversed flow stabilizes the flame. The appearance and size of this zone is affected by the vortex shedding process. The SST model is not able to capture the large-scale oscillations of the flow, leading to an over prediction of the length of the recirculation zone. The DES model resolves a wide range of scales of the flow, but is sensitive to grid resolution and numerical settings and quite computational heavy. Therefore the extra information regarding the resolved scales provided by the DES model has to be weighted against the more demanding mesh requirements and computational effort.

The Reynolds stress model agrees best with the experimental results and provides a good trade-off between details captured and computational effort. Figure 1 shows a qualitative and quantitative comparison of simulation results obtained with the Reynolds stress model BSL and PIV experiments. The quantitative results are presented with error bars corresponding to the estimation of the discretization uncertainty for the simulation and the average experimental uncertainty.

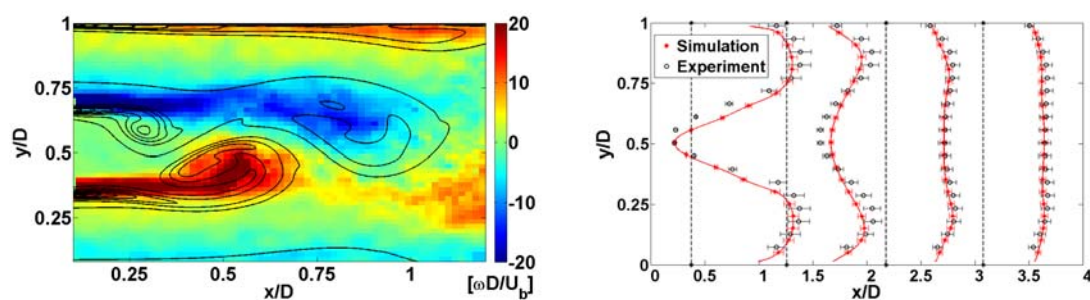


Figure 1: (a) Snapshot from the shedding cycle showing vorticity for simulation (black contours on top) and experiment (colored contours below). (b) Time-averaged streamwise velocity profiles, red dots show simulation and black dots experiment.

^a Division of Fluid and Experimental Mechanics, Luleå University of Technology, SE-97187, Luleå, Sweden

^b LKAB, Kiruna, Sweden

Dependence of turbulence decay on initial conditions

J. Schönke¹, F. Sprung^a, G. Bewley² and T.M. Schneider^a

We consider freely decaying turbulence and ask how the decay rate of turbulence energy depends on initial conditions. It is clear that if the flow is neither homogeneous nor isotropic, many outcomes are possible (e.g., [1]). But even for homogeneous and isotropic turbulence, it may not be that the energy decay can be modeled by a power law with a universal exponent (e.g., [2]).

Our approach, then, is to look for answers to questions like: What properties of the initial conditions control the decay rate? Which initial conditions decay fastest, if the initial turbulent energy and Reynolds number are fixed? What is the maximum decay rate of homogeneous isotropic turbulence? In [3] the minimum decay rate is considered, but the other limit has so far not received comparable attention. The classical theory for homogeneous and isotropic turbulence relates long-range correlations to the energy decay rate. Therefore we focus on the variation of these long-range correlations as a way of generating different initial conditions.

Connected to this problem are questions about the transient phase from an initial condition to the build-up of the cascade. Which flow features from the initial condition are still prominent in the cascade? Especially the redistribution of energy and helicity in this transient phase and the detailed structure of the flow are of great interest.

We are currently performing direct numerical simulations of freely decaying isotropic turbulence with a pseudo-spectral code [4] on our clusters of the MPIDS in Göttingen. Having access to 1024 nodes (InfiniBand interconnected), we are able to simulate several different initial conditions simultaneously, with a resolution of up to 1024^3 over the whole range of relevant timescales.

¹ ECPS – MPRG, Max-Planck-Institute for Dynamics and Self-Organization, Göttingen 37077 Germany

² LFPB, Max-Planck-Institute for Dynamics and Self-Organization, Göttingen 37077 Germany

¹ Kerr, R.M., PoF 25, 065101 (2013)

² Ishida, T. et. al, JFM vol. 564, pp. 455–475 (2006)

³ Davidson, P.A., PoF 23, 085108 (2011)

⁴ Brucker, K.A. et. al, JCP 225 20–32 (2007)

Introduction of Longitudinal and Transverse Lagrangian Velocity Increments in Homogeneous and Isotropic Turbulence

A. Naso¹ and E. L  v  que¹

Based on geometric considerations, a new decomposition of the Lagrangian velocity increments in homogeneous and isotropic turbulence is introduced. It is argued that the resulting ‘‘longitudinal’’ ($\delta u_{\parallel}(\tau)$) and ‘‘transverse’’ ($\delta u_{\perp}(\tau)$) Lagrangian velocity increments probe preferentially the stretching and spinning of material fluid elements at time scale τ , respectively.

The statistics of the low-order moments (up to order six) of these quantities are examined by direct numerical simulation for different values of R_{λ} . Interestingly, the distributions of $\delta u_{\parallel}(\tau)$ are found negatively skewed at all scales τ (see Fig. 1 (a)), thus evidencing the time-irreversibility of turbulence in this Lagrangian framework. Also, the flatness of the transverse increment is shown to be larger than that of the longitudinal one (see Fig. 1(b)), a feature that may reveal that the spinning mechanisms are more intermittent than the stretching ones in the turbulence dynamics.

During this conference, we would like to introduce physically longitudinal and transverse Lagrangian velocity increments, and to show that these new statistical objects allow to better characterize the dynamics of turbulence in a Lagrangian framework by disentangling stretching and spinning effects.

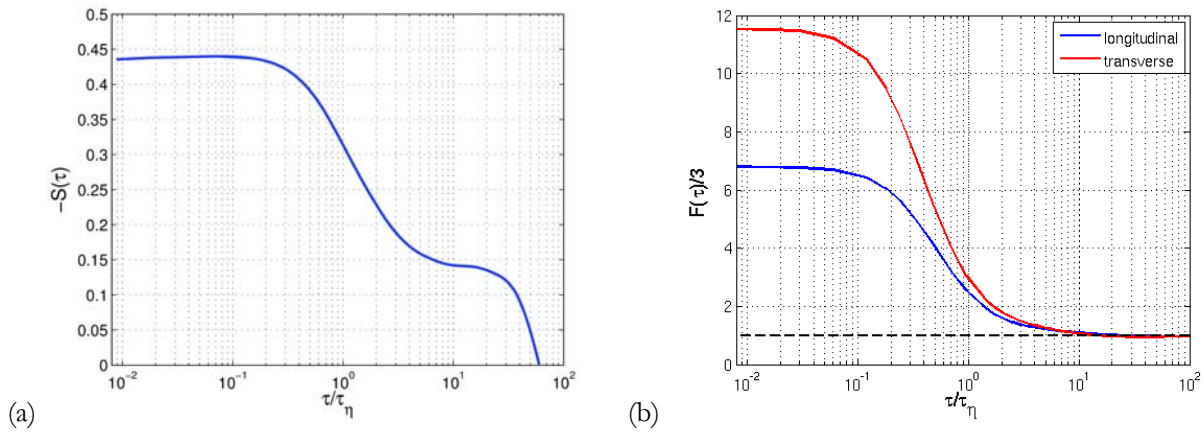


Fig. 1: Normalized moments of the longitudinal and transverse Lagrangian velocity increments vs. time increment τ normalized by the Kolmogorov time scale ($R_{\lambda}=275$). (a) Opposite of the skewness of the longitudinal increment. (b) Flatnesses of the longitudinal and transverse increments. The dashed line indicates the Gaussian expectation.

¹ Laboratoire de M  canique des Fluides et d'Acoustique, CNRS, Ecole Centrale de Lyon, Universit   Lyon 1 and INSA Lyon, Ecully, France

Using symmetry reduction to capture relative periodic orbits in turbulent pipe flow

A. P. Willis¹, K. Y. Short² and P. Cvitanović^b

Over the last decade a new theoretical framework has emerged for the study of turbulence, where chaotic turbulent flow is viewed as a trajectory embedded in a high-dimensional space, with transitory visits to the neighbourhoods of invariant solutions. The visited solutions are weakly unstable relative equilibria, known as travelling waves (TWs), and relative periodic orbits (RPOs), patterns that repeat in time, but after one period are translated in space.

TWs have been shown to play a key role in the transition to turbulence, where they often lie in the laminar-turbulent boundary¹. To capture the dynamics of persistent turbulence, we turn to RPOs, which are expected to form the skeleton underpinning the natural measure of turbulent flow.

Continuous symmetries (translations and rotations), however, obscure the relationships between the invariant solutions, apparently knotting trajectories, as seen in projected visualizations of the flow. *Symmetry reduction* is thus a crucial step in untangling trajectories in state space, and for revealing the true relationship between influential solutions.

Recently in Willis et al.², we described the 'method of slices', which systematically removes shifts along symmetry directions, closing RPOs into POs, and providing a means for untangling state space trajectories. We recap the method, which is global and reduces symmetry, and comment on the coordinate transformation to the local 'comoving frame', which is a geometrically natural way of separating symmetry drifts from the 'shape-changing' dynamics, but is not a symmetry reduction scheme.

Our latest refinements of the 'method of slices', applied to two different computational domains with conceptually and physically distinct slices, have enabled us to determine a set of new RPOs. Implementation of the method does, however, require care. We discuss the origin of difficulties in reducing continuous symmetries, and approaches that alleviate them.

¹ School of Mathematics and Statistics, University of Sheffield, S3 7RH, U.K.

² School of Physics, Georgia Institute of Technology, Atlanta, GA 30332, USA

¹ Duguet et al., *J. Fluid Mech.* **613**, 255 (2008).

² Willis et al., *J. Fluid Mech.* **721**, 514 (2013).

Figure 1: (left) A relative periodic orbit projected relative to an arbitrary starting point on the orbit, using a local comoving frame. (right) The same orbit with symmetry reduction, method of slices. As every orbit shifts at a different rate, automated symmetry reduction is essential for unknotting dynamical connections.

The onset of fully turbulent flow

D. Barkley^a, B. Song^b, M. Vasudevan^b, M. Avila^c and B. Hof^b

In many shear flows turbulence first arises in the form of localised spots surrounded by laminar fluid. Fully turbulent flow is only observed at somewhat larger Reynolds numbers. Although the first observation of localised turbulence and the later transition to fully turbulent flow already dates back to Reynolds experiments in pipe flow, this transition has remained unexplained. We present detailed experimental and numerical (DNS) measurements of this transition. In particular we focus on laminar turbulent interface speeds at the onset of expanding turbulence. We demonstrate that the scaling of interface speeds as well as the different turbulent structures (puffs, slugs) are explained by an excitable media model. The onset of fully turbulent flow is characterized as a transition from excitability to bistability.

^a University of Warwick, Coventry CV4 7AL, UK

^b IST Austria, Am Campus 1, 3400 Klosterneuburg, Austria

^c University of Erlangen, 91058 Erlangen, Germany

¹ Reynolds, *Philos. Trans. R. Soc.* **174**, 935 (1883).

Scaling of spectra in grid turbulence with mean cross-stream temperature gradient

Carla Bahri^a, Gilad Arwatz^a, William George^a and Marcus Hultmark^a

Scaling of grid turbulence with a constant mean cross-stream temperature gradient is investigated using a combination of theoretical predictions and experimental data, acquired with novel nano-scale temperature probes (T-NSTAP). Conditions for self-similarity of the governing equations and the scalar spectrum are investigated, which reveals necessary conditions for self-similarity to exist. These conditions provide a theoretical framework for scaling of the temperature spectrum as well as the temperature flux spectrum, which offers new insight into the interaction of the turbulent velocity field with the scalar field. One necessary condition, predicted by the theory, is that the characteristic length scale describing the scalar spectrum must vary as $\propto \sqrt{t}$ for a self-similar solution to exist. In order to investigate this, T-NSTAP sensors were deployed in a heated passive grid turbulence setup together with conventional hot-wires. The T-NSTAPs are sub-miniature, free-standing, platinum wires suspended between silicon supports, especially designed for temperature measurements at high frequencies, operated in constant current mode. These sensors have previously been shown to have a bandwidth far superior that of conventional sensors, which minimizes the effect of temporal filtering on the data and allows for a unique investigation of the full scalar spectrum, including the dissipation range. The experimental data is used to compare the behaviour of different length scales and how they compare to the theoretical predictions.

^a Dep. Mechanical and Aerospace Engineering, Princeton University, E-Quad, Princeton, NJ, USA

A study of a model for an intermittency region evolution in turbulence-interface interaction

T. Waławczyk^a, M. Waławczyk^b

The reliable modelling of the turbulence-interface interaction in two-fluid multiphase flows is crucial for robust simulations of the momentum, the heat and the mass transfer in engineering applications, e.g. numerical simulations of physical and chemical processes in heat exchangers or chemical reactors. In this work, we present and discuss the first results obtained using the new model for intermittency region evolution^{1,2}. The new model is derived for the ensemble or Favre averaged governing equations in the one-fluid formulation. The intermittency region $0 < \alpha < 1$, where $\alpha = \langle \chi(x-s, t) \rangle$ is the averaged instantaneous position of the interface, can be interpreted as a region where the probability of the interface location is non-zero. As a result of the ensemble averaging^{2,3}, unclosed terms arise in the governing equations. Our modelling approach for the α function transport equation results in two additional terms: diffusion responsible for the local spreading of the intermittency region and the contraction term with the opposite action². The first term is associated with the disturbing action of turbulent eddies beneath the interface, the second term is associated with the stabilizing effects of surface tension and gravity^{1,2}. In a priori study of the vortex interacting with the flat interface³ we have shown that such interpretation of these two terms is justified, see Fig. 1.

In this work, we first present the 1D one-way coupling studies. We demonstrate that the new model can also reconstruct the temporal evolution of the intermittency region. To achieve this we use the model coefficient $D_t = C_D q(t) L(t)$ in the diffusion term and $C_t \approx C_D q(t = t_{\max})$ in the contraction term where $q(t)$ is the turbulent intensity in the intermittency region and $L(t)$ is the turbulent length scale. This test case allows us to find the value of a C_D constant that determines the balance between the diffusion and contraction terms in the intermittency region. Next, the intermittency region evolution model is implemented into the finite volume flow solver FASTEST with the interface capturing conservative Level-Set method and is coupled with the RANS flow solver. Since the selection of the ensemble or Favre averaging influences the final form of the model equations, we discuss differences and difficulties that arise during numerical implementation of both aforementioned approaches. In particular, the solution of the modified α function transport equation and continuity equation in the Favre formulation are addressed. In the first case, presence of the compressive term on the right hand side requires splitting of the solution to the advection and reinitialization step, where appropriate flux limiting procedure is required. In the latter case non-zero source term in the Poisson equation appears in the intermittency region what additionally affects the pressure-velocity coupling procedure. The model for intermittency region evolution is tested in the case of submerged jet interaction with the flat interface⁴. The obtained results are compared with experiment and previous numerical studies.

^a Inst. Numerical Methods in Mechanical Engineering, TUD, 15 Dolivostrasse, Darmstadt 64293, DE

^b Inst. Fluid Dynamic, TUD, 30 Petersenstrasse, 64293, DE

¹ Brocchini and Peregrine, *J. Fluid Mech.* **449**, 255-299 (2001).

² Waławczyk and Oberlack, *Int. J. Multiphase Flow* **37**, 967-976 (2011)

³ Waławczyk and Waławczyk, *Int. Conf. Multiphase Flow* **48**, 325-345 (2013)

⁴ Hong and Walker, *J. Fluid Mech.*, **417**, 183-209 (2000)

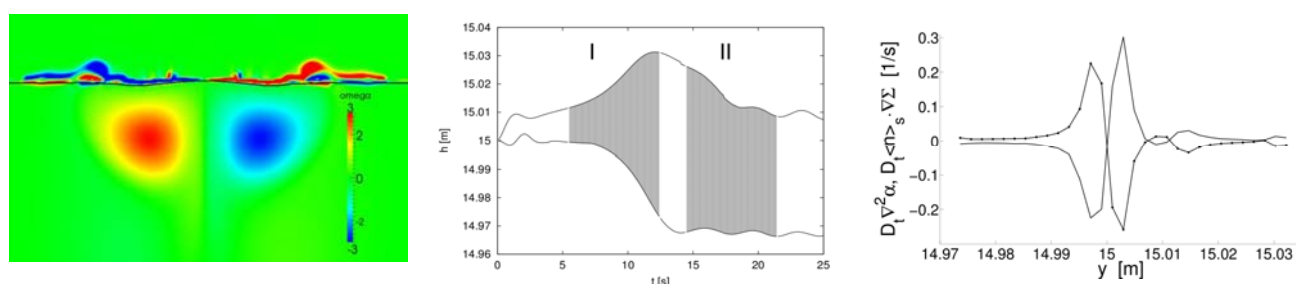


Figure 1: (a) Vortex-interface interaction, vorticity distribution. (b) Evolution of the intermittency region: I diffusion stage, II contraction stage. (c) The diffusion and compression terms in the intermittency region during contraction stage II.

Porous Media

Instability in open-channel flow overlying a porous medium

A. C. de Lima^a and N. Izumi^a

Instability mechanisms in open-channel flows overlying a sediment layer have been widely studied. In particular, a number of linear stability theories on the mechanism of formation of dunes and anti-dunes in erodible channels has been developed. In these theories, the flow domain into the sediment layer, if considered, was assumed to be restricted to a thin layer. In parallel, the modelling of combined free and porous flows has been successfully attempted in a wide range of industrial and geophysical applications. Because the fluid mobility in each application is dependent on many factors, amongst them the inherent structural properties of the porous substance, different interfacial and boundary conditions, and the flow potentials across the domain, models representing specific cases are developed¹.

In this paper, we perform a linear stability analysis of an open-channel flow which overlies a porous medium with constant porosity saturated with the same fluid. Darcy flow takes place at the porous layer. A Brinkman equation is employed at the boundary layer between the Navier-Stokes fluid layer and the Darcy layer. The system of perturbation equations is solved by means of a spectral method with the Chebyshev polynomials. We evaluate the effect of various parameters, i.e., the fluid layer Reynolds number (Re), channel slope, ratio of the fluid layer depth to the sediment layer depth (δ), porosity and boundary condition parameters, on the growth of instabilities. Results depicted in Figure 1 show that the instabilities can be dominated by either the fluid layer or the porous layer, the latter visualised in Figure 1(a) at $500 \leq Re \leq 2000$. At $\delta \geq 0.2$ the most unstable mode for any Re switches from the porous layer to the fluid layer. Similar changes in the dominance of bi-modal instabilities with δ have been found in other problems of flow over porous media^{2,3}.

Because the flow in the porous medium affects instability characteristics up to the open flow, as corroborated by the present results, the Darcy flow is expected to affect erosion processes which take place at the channel bed, i.e., the upper surface of the porous layer. Therefore, the present study provides a basis for further developments in stability theories of bed forms in superficial flows over saturated porous media.

^a Dep. of Civil Engineering, Hokkaido University, Sapporo, 060-8628, Japan

¹ Das et al., *Adv. Environ. Res.* **7**, 35 (2002).

² Chen and Chen, *Trans. ASME* **110**, 403 (1988).

³ Hill and Straughan, *J. Fluid Mech.* **603**, 137 (2008).

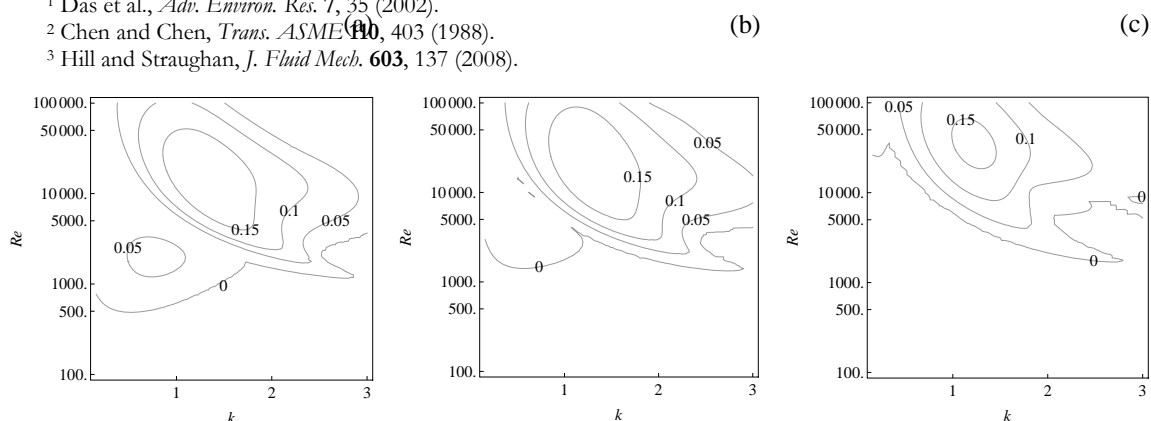


Figure 1: The contours of the growth rate of perturbations for various Re and wavenumber k for (a) $\delta=0.1$, (b) $\delta=0.2$, (c) $\delta=0.5$. Laminar flow case.

Flow of foams in two-dimensional porous media

B. Géraud^a, B. Dollet^a, S. A. Jones^a, S. J. Cox^b, Y. Méheust^c and I. Cantat^a

Liquid foams, dispersions of gas bubbles in a continuous liquid phase, are a yield stress fluid with elastic properties. When a foam flow is confined by solid walls, viscous dissipation mostly arises from the contact zones between the soap films and the walls, which gives very peculiar friction laws. In particular, foams potentially invade narrow pores much more efficiently than Newtonian fluids, which is of great importance for enhanced oil recovery.

To quantify this effect, we study experimentally flows of foam in a model two-dimensional porous medium, consisting of an assembly of circular obstacles placed randomly in a Hele-Shaw cell (Fig. 1), and use image analysis to quantify foam flow in detail at the local scale.

We show that bubbles split as they flow through the porous medium, by a mechanism of film pinching during contact with an obstacle. We identify experimentally the conditions (especially the bubble size/pore size ratio) under which splitting occurs, and we quantify the evolution of the bubble size distribution as a function of the distance along the porous medium. We propose an evolution equation to model this splitting phenomenon and compare it to the experiments, showing how at long distance, the porous medium itself dictates the size distribution of the foam.

We analyse the flux distributions in the porous medium, and show that they are intermittent, with zones with narrow pores and small bubbles that can be temporarily blocked. We rationalise this finding in terms of a yield capillary pressure to overcome for flow to proceed through a pore.

Finally, we study the influence of various foam parameters: bubble size, liquid fraction and total flux, on its flow in the porous medium.

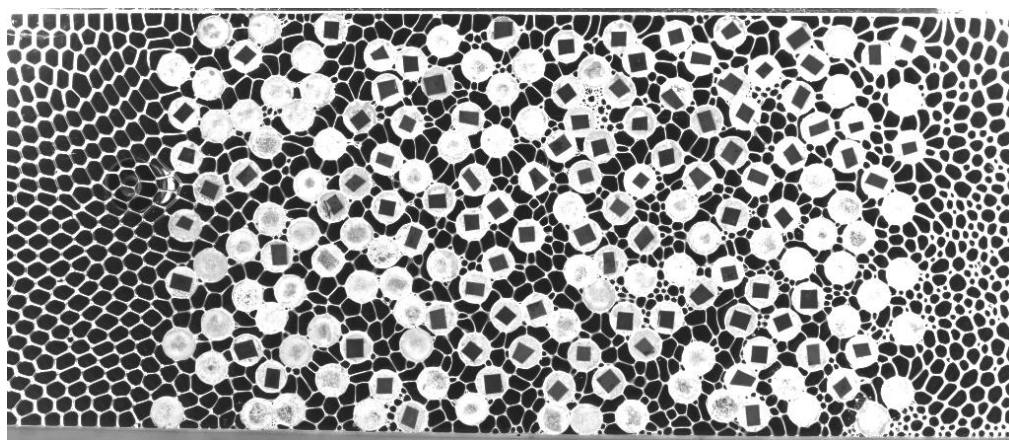


Figure 1: Snapshot of a foam flowing through a two-dimensional porous medium.

^a Institut de Physique de Rennes, UMR 6251 CNRS/Université Rennes 1, 35042 Rennes Cedex, France

^b Department of Mathematics and Physics, Aberystwyth University, UK

^c Géosciences, UMR 6118 CNRS/Université Rennes 1, 35024 Rennes Cedex, France

Representative volume size when modelling flow through porous structures

J. G. I. Hellström^a, F. Forsberg^{a,b}, T. S. Lundström^a and M. Sjödahla^a

Porous media flow is significant in a large number of industrial applications such as internal erosion in embankment dams, drying of iron ore pellets, composites manufacturing and paper-making, to mention a few. When modelling and simulating the flow in these contexts the choice of computational domain is often dependent on the field of application. Still there might be some common issues between the different industrial fields. To exemplify, when performing measurements or simulations of porous media flow it is usually difficult to determine a representative volume of the material. This is also true when mapping the porous media with X-ray Microtomography.

Here, a cylindrical bed of compacted granular sugar was scanned using X-ray Microtomography. From the resulting 3D microstructure, shown in Fig.1a, a number of volume subsets, Fig.1b, of increasing size were acquired. The porous network within each volume was isolated, meshed, and imported into a commercial CFD code Ansys CFX.

When performing CFD-simulations on any volume of a porous media it is of highest importance that the discretization of the pore space geometry is fine enough both from a geometrical point of view as from a grid resolution point of view. Hence, we here discretise the volumes obtained with X-ray Microtomography with increasing number of computational cells in order to capture the main flow features of interest; such as the velocity distribution, the pressure drop over the geometry and also, of course, from a porous media viewport the permeability of the material. But also comparing how the flow parameters change with the choice of the representative volume size, if possible, find a unit cell of the porous structure.

Preliminary results indicate that this method finds the velocity “hot spots”, see Fig.1c below, and also that the other main flow features show potential to be resolved in an qualitative way.

^a Div. Fluid and Experimental Mechanics, Luleå University of Technology, Sweden

^b LKAB R&D, Sweden

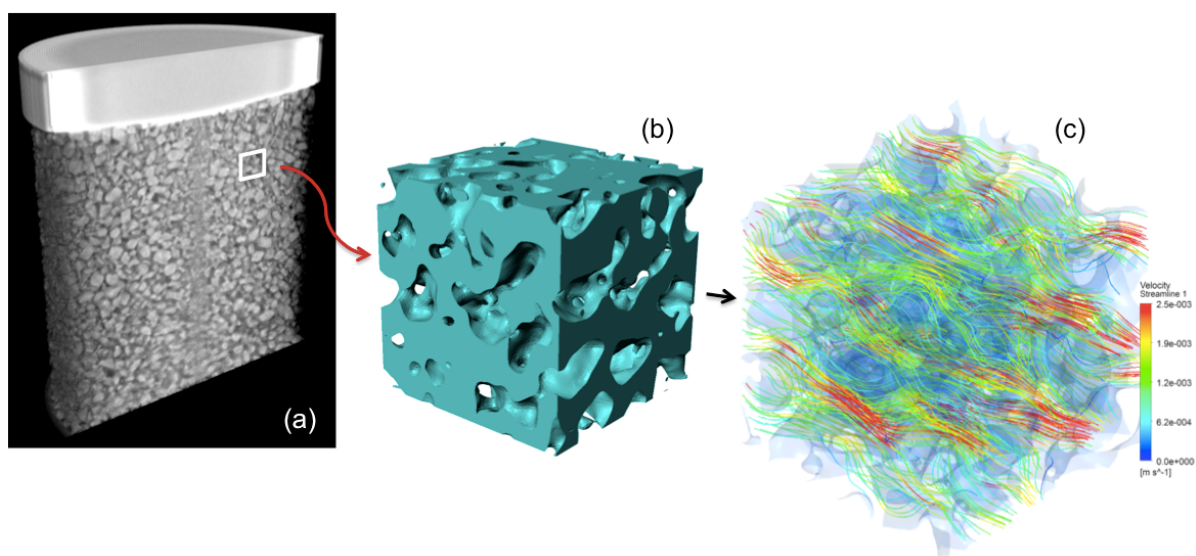


Figure 1: The 3D microstructure of granular sugar is acquired using X-ray Microtomography (a). Volume subset in which the analysis is carried out (b). Preliminary CFD results (c) shows coloured streamlines that describes the velocity through the corresponding geometry.

Rotating Flows

Float height and quasi-steady spin-down of a rotating air hockey disk

P. D. Weidman^a

A similarity reduction of the Navier-Stokes equations for the motion of an infinite rotating disk above an air bearing table yields a coupled pair of ordinary differential equations governed by a Reynolds number $R = Wh/\nu$ and a rotation parameter $S = \sqrt{2}h\Omega/W$, where h is the float height, W is the air levitation velocity, Ω is the disk rotation rate, and ν is the kinematic viscosity of air. After deriving the small- and large-Reynolds number behavior of solutions, the equations are numerically integrated over a wide range of R – S parameter space. The theory is applied to model the steady float height of a finite air hockey disk under the assumption that the float height to diameter ratio is small. Zero lift boundaries are computed as well as the boundaries separating pure outward flow from counterflow in the gap. At large values of R for which variations in float height are small, a model for quasi-steady spin-down to rest of an air hockey disk is presented.

^a Department of Mechanical Engineering, University of Colorado, Boulder, CO 80309-0427, USA

The flow external to a rotating torus

S.A.W. Calabretto^a, J.P. Denier^a and T.W. Mattner^b

We consider the flow behaviour exterior to a solid toroidal body that is impulsively rotated from rest to a constant angular velocity. We demonstrate that this flow is similar in many ways to that which arises on the exterior of a sphere impulsively rotated from rest in that the flow develops boundary layers that collide at the eastern equator with a subsequent boundary-layer eruption (see figure 1a). This behaviour is associated with the development of a finite-time singularity within the boundary layer equations at the equator (a phenomena also observed within the flow inside an impulsively started/stopped fluid filled torus^{1,2}). We show that the subsequent post-boundary-layer eruption results in a radial jet³ (see figure 1b). This radial jet subsequently breaks down, resulting in the generation of an isolated toroidal vortex far from the solid torus (see figure 1c). The remainder of the jet, which remains attached to the torus surface and is driven by its rotation, develops an absolute instability (see figure 1d) that propagates backwards towards the torus surface. The complex dynamics of the flow will be explored using a combination of asymptotic and computational methods⁴.

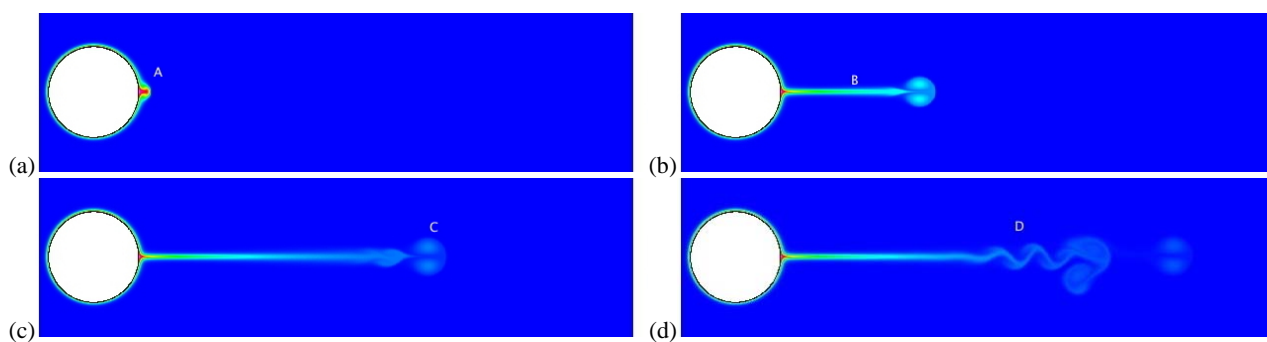


Figure 1: Plots of contours of azimuthal velocity. The torus is rotating around an axis (not shown at this scale) with major radius $L=7.2$ and minor radius $a=2.0$. Here we observe (a) the initiation of the boundary-layer eruption (label A) (b) the development of the radial jet (label B) (c) the detachment of the toroidal vortex (label C) and (d) the development of the absolute instability within the radial jet (label D). All results are for a Reynolds number $Re=500$, where the Reynolds number Re is defined via $Re=\Omega a/\nu$, where Ω is the final angular velocity of the torus, a is the minor radius of the torus cross-section and ν is the fluid's kinematic viscosity.

^a Department of Engineering Science, The University of Auckland, New Zealand

^b School of Mathematical Sciences, The University of Adelaide, Australia

¹ R.E. Hewitt et al. *J. Fluid Mech.* **688**, 88-119 (2011)

² del Pino et al. *Physics of Fluids* **20**, 124104 (2008)

³ N. Riley, *QJMA*, **15**, 435-458 (1962).

⁴S.A.W. Calabretto, et al. (in preparation)

Experimental Study on the Internal Rotating Flow Driven by a pair of Rotating Disks in a Non-Axisymmetric Enclosure

K. Shirai^a, R. Tada^a, T. Kawanami^a and S. Hirasawa^a

We studied complex behaviour of the internal rotating flow driven by the rotation of a pair of disks confined in a non-axisymmetric enclosure. This study aims at clarifying the mechanism of flow induced vibrations, which lead to fatal crashes in hard disk drives (HDDs). In the present study, we performed a series of flow visualization experiments using a simplified experimental model with a refractive-index matching technique.

HDDs used for information storage device contain stack of rotating disks, on which data is stored via read-and-write magnetic head. The air flow induced by the disk rotation is used for flying a magnetic head slightly above the disk surface and the fly height is maintained to a few nanometres by servo control. As the air goes through the complex geometry, resulting flow exhibits highly three-dimensional turbulence. This complex flow seems to be a major source of fatal crashes. The disk vibration is known to decrease its amplitude as the reduction of the tip clearance between the disk and shroud. There have been many studies in which flow inside an axisymmetric enclosure was investigated without obstacles. Such studies derived some fundamental features on the flow. In the planes parallel to the disks, vortex structures appear as polygonal patterns of the solid-body rotation in the inner area of the disks, while counter-rotating large-scale vortices appear in the outer area. Secondary flow has also been identified in the axial planes. However, real drives are non-axisymmetric – they have a shroud opening and arms inserted to read/write the data. So the findings obtained from axisymmetric configuration without arms may not represent the phenomena occurring in real drives. Numerical simulations are performed based on real design data as well. Despite their efforts, the flow remains difficult to be simulated due to a wide range of the relevant scales from centimetres to tens of micrometres. The number of computational grids required for covering such a wide dynamic range is beyond the reach of current computer.

An experimental model was built. It is simplified but still represents major HDDs' features including a large shroud opening and a simulating arm (Fig. 1 (a, b)). Flow visualization was carried out by observing the flow illuminated with laser sheet. Flow behaviour was investigated based on eye inspection and visualization images acquired by camera. The model was made of PMMA (poly-methyl methacrylate), completely transparent including the rotating shaft. Ternary aqueous solution of ammonium thiocyanate and glycerine was used as refractive index-matched working fluid in order to avoid reflections and scatterings occurring at the interfaces.

We focused on the three issues: 1) the formation of the polygonal structures under different Reynolds numbers and arm insertion angles, 2) the flow behaviours in the disk and shroud areas, and 3) the secondary flow structure in the plane containing the rotating shaft. The visualization images show the existence of the polygonal structures under a certain Reynolds number range and at several angles of the arm insertion. The flow exhibits various behaviours on the different planes parallel to the disks (Fig. 1 (c)). The flow is largely deflected by the arm inserted into the disk area. The rotating flow in the disk area and the stagnation flow interact at their boundary. The secondary flow seems to be asymmetric with respect to the middle plane of the disks. The resulting flow in the inter-disk area is highly distorted due to the shears in disk-parallel and vertical planes (the bold arrows in Fig. 1 (d, e)). Stronger shears are induced by the deep insertion of the arms into the interdisk area, which seems to lead a highly turbulent complex flow hitting against the head after each disk revolution.

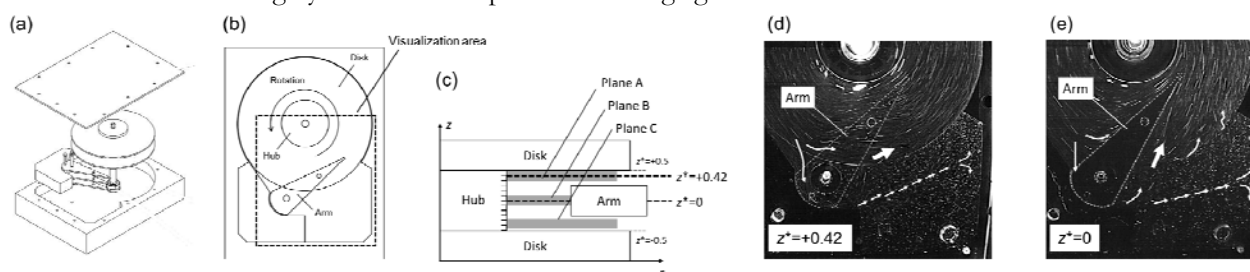


Figure 1: (a) 3D view of the experimental model (b) upper view of the model (c) side view of the observation planes (d) visualization image in $z^*=+0.42$ (arm-disk middle plane) (e) image in $z^*=0$ (arm middle plane).

^a Dep. Mechanical Engineering, Kobe University, 1-1 Rokkodai, Nada, Kobe, 657-8501, JAPAN

New type of flow instability in rotating spherical shell

V. G. Kozlov^a, N. V. Kozlov^a, S. V. Subbotin^a

The flow excited by the differential rotation of a free spherical body in a rotating about horizontal axis cavity filled with liquid is experimentally investigated. The body is lighter than the liquid and is located near the rotation axis under the action of centrifugal force. The gravity force field leads to the circular oscillations of the body relative to the cavity. As a result of the pulsating motion in the Stokes boundary layer the averaged mass force arises, spinning the body¹. The cavity rotation velocity Ω_{rot} is always larger than the body rotation velocity Ω_s .

The body differential rotation leads to the formation of the flow in the Taylor column form. At slow differential rotation the column has the circular cylinder shape (Figure 1(a)). With increase of the differential rotation $\Delta\Omega = |\Omega_s - \Omega_{rot}|$ the column boundary becomes unstable and an azimuthal wave develops on it surface (Figure 1(b)). The wave phase velocity in the laboratory frame is less than the body rotation velocity. Inside the column the presence of a two dimensional vortex system is found². The stability of the structures of different type is determined by Reynolds number $Re = \Delta\Omega r^2/\nu$ ($Re = 52 \pm 5$ for the appearance of the vortex system and $Re = 105 \pm 7$ for the wave instability of the column boundary).

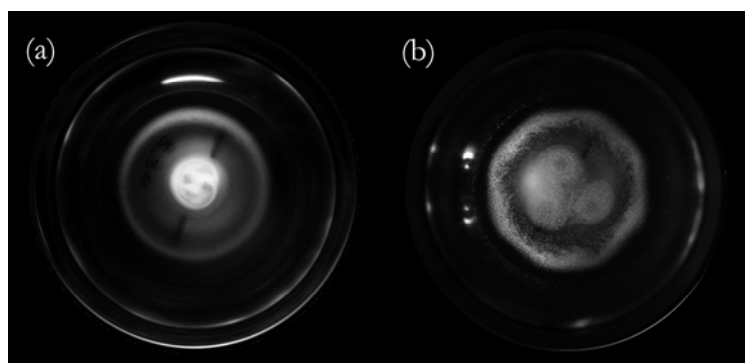


Figure 1: Photos of the flows.

Earlier, the stability of the Taylor column was studied in the case when the body was fixed on the cavity rotation axis, and its differential rotation was set independently by an additional drive³. In this work the wave-type instability of the column boundary was also found but it was one order higher while the vortex system inside the column was absent.

Thus, there are different mechanisms of the Taylor column instability. If the body rotation axis is fixed, then we have the classical shear layer instability. In the case of the free body the differential rotation has a vibrational nature that determines the qualitatively different flow structure and, consequently, the reduction of the instability threshold.

The work is done in the frame of the Strategic development program of PSHPU (project 029-F), with partial support from RFBR (grant 13-01-00675a) and Minobrnauki of RF (task 2014/372).

^a Laboratory of Vibrational Hydromechanics, PSHPU, 24 Sibirskaya Ave., Perm, Russia

¹ Kozlov and Kozlov. *Doklady Physics* **52**, 458 (2007)

² Kozlov et al. *Doklady Physics* **59**, 40 (2014)

³ Schaeffer and Cardin. *Phys. Fluids* **17**, 104111 (2005)

Inertial wave pattern generated by a librating disk in a rotating fluid

Stéphane LE DIZÈS^a, Michaël LE BARS^a

As stratified fluids, rotating fluids have the properties to support (inertial) waves and propagate singularities. In a fluid rotating at the angular frequency Ω , any localized disturbance oscillating at a frequency ω in the inertial range $0 < \omega < 2\Omega$ propagates along a characteristic cone that makes an angle $\theta = \arcsin(\omega/(2\Omega))$ with respect to the rotation axis. Boundary discontinuities propagate similarly and are generally the cause of the presence of thin shear layers within the fluid. In a close geometry, these thin layers are reflected on boundaries and sometimes form an attractor, which make the problem very intricate. Even in the simplest geometry, the asymptotical structure of the solution is unknown when internal shear layers are present. In order to make progress, in this work, we consider an open domain (to avoid reflections), and a simple oscillating object for which an approximate solution with internal shear layers can be calculated.

We consider the flow field generated by a librating disk of radius a in a fluid rotating with respect to the vertical axis Oz . The disk has a radius a , is horizontal and centred on the origin. It oscillates around the vertical axis with a rotation rate $\varepsilon \sin(\omega t)$. We are interested in characterising the inertial wave pattern when the oscillation amplitude ε/Ω and the Ekman number $E = \nu/(\Omega a^2)$ are both small, and the libration frequency ω is within the inertial range.

The problem is analysed using asymptotical methods and axisymmetrical numerical simulations. We assume that the main source of inertial waves is the weak oscillating Ekman pumping generated by the small azimuthal oscillations of the disk. An exact integral expression of the velocity field generated by this weak axial oscillating flow is obtained in the presence of viscosity. At leading order, this expression is found to reduce to simple non-viscous expressions in the different regions limited by the characteristics issued from the border of the disk. These expressions exhibit discontinuities or logarithmic singularities across the characteristics. We show that these singularities are smoothed in a universal way by viscous effects.

Comparisons with the numerical simulations performed at $E=10^{-5}$ and $\varepsilon=0.016$ demonstrate a good qualitative agreement for all the velocity components (see figure for the axial velocity). Extension of the results to a librating sphere is discussed in the context of planetary applications.

This work is supported by the French *Agence Nationale de la Recherche* through the A*MIDEX grant ANR-11-IDEX-0001-02, the LABEX MEC project ANR-11-LABX-0092 and the ANR LIPSTICK project ANR-13-JS05-0004-01.

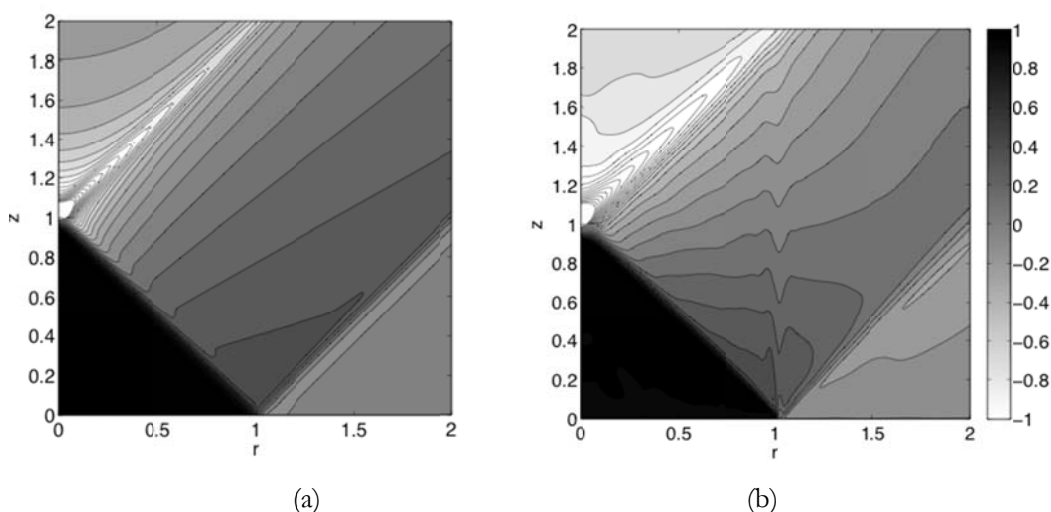


Figure : Normalized axial velocity contours in the (r, z) plane for a disk of radius 1 librating at the frequency $\omega=2^{1/2}\Omega$ for $E=10^{-5}$ (at the instant where the axial pumping is maximum) (a) Asymptotical solution. (b) Numerical solution for $\varepsilon=0.016$.

¹ Aix-Marseille Université, CNRS, Centrale Marseille, IRPHE UMR7342, 49 rue F. Joliot Curie, 13013 Marseille, France

Effects of anisotropic surface roughness on the boundary-layer transition over rotating disks

M. Özkan^a, J. M. Harris^a, S. J. Garrett^b, A. J. Cooper^c and P. J. Thomas^a

The rotating-disk boundary-layer is the paradigm to study fully three dimensional boundary-layer flows with a cross-flow component such as occurring, for instance, over highly swept wings. Hitherto the investigation of the flow and its laminar-turbulent transition has almost exclusively focussed on smooth disks or disk with a small number of isolated roughness elements. We have started investigating the effects of distributed roughness on the transition process. We will present first theoretical and experimental results for the effects of anisotropic surface roughness represented by concentric circular grooves with sinusoidal cross-sectional profiles along the radial direction of the disk.

Two alternative theoretical approaches were adopted to obtain steady-flow profiles that were then subjected to a linear stability analysis similar to that in Garrett *et al.*¹. We discuss that this revealed stabilizing (i.e. energetically beneficial) and destabilizing (i.e. energetically detrimental) effects. Figure 1 shows neutral curves obtained for various values of the wavelength, γ and the amplitude, δ of the sinusoidal roughness pattern. The figure reveals that increasing roughness has a stabilizing effect on the Type I (cross-flow) instability mode represented by the upper lobe in the figure while it concurrently destabilizes the Type II (streamline curvature) mode (lower lobe). We present preliminary experimental hot-film data² supporting our theoretical results.

In order to extract possible underlying physical mechanisms behind the effects of roughness, and in order to reconfirm the results of the linear stability analysis, we derived an integral-energy equation following the methods of Cooper & Carpenter³. The results obtained from this analysis suggest potential strategies to exploit surface roughness for new drag-reduction techniques for boundary layers with a cross-flow component.

^a School of Engineering, University of Warwick, Coventry, CV4 7AL, UK

^b Department of Mathematics, University of Leicester, Leicester, LE1 7RH, UK

^c Mathematics Institute, University of Warwick, Coventry, CV4 7AL, UK

¹ Garrett *et al.*, *J. Fluid Mech.*, **622**, 209 (2009)

² Harris *et al.*, PhD thesis, School of Engineering, University of Warwick (2013)

³ Cooper & Carpenter, *J. Fluid Mech.*, **350**, 231 (1997)

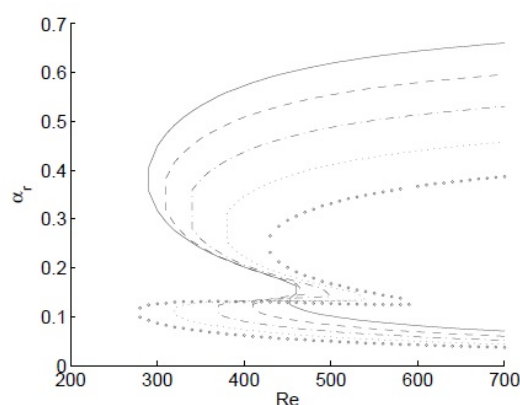


Figure 1: Neutral curves from the stability analysis; von Karman (-); $\delta/r = 0.08$ (- -); $\delta/r = 0.12$ (- .); $\delta/r = 0.16$ (..); $\delta/r = 0.2$ (o).

The dynamics of a draining vortex in a rotating fluid tank

G.J.F. van Heijst^a & L.P.J. Kamp^a

A remarkable feature of the vortex driven by a sink in the bottom of a rotating fluid container is the pronounced upward motion around the fast-rotating cyclonic vortex core with downward motion into the sink. This phenomenon is clearly observed by dye visualisation of the flow near the sink: the flow towards the sink is confined to the Ekman layer at the tank bottom, in which it spirals inwards. Before reaching the sink the fluid first rises to a substantial height, and subsequently flows downwards to the sink in the core of the vortex.

Although this phenomenon has been observed before^{1,2}, a full explanation was still lacking. We have performed a theoretical analysis of the flow near and in the draining vortex, by distinguishing different dynamical balances at different distances from the sink: a geostrophic potential flow at large distance, and a gradient flow and a cyclostrophic flow balance, respectively, when moving closer to the sink. The theoretical prediction of the flow behaviour in the sink vortex agrees well with the experimental observations.

Additional numerical simulations show very good agreement with the theoretical model.

^a Fluid Dynamics Laboratory, Dept. of Physics, Eindhoven University of Technology, The Netherlands

references

¹ H.A. Einstein & H. Li – Steady vortex flow in a real fluid. *Proc. Heat Transfer and Fluid Mech. Inst.*, Stanford, pp. 33-42 (1951).

² A. Andersen et al. – The bathtub vortex in a rotating container. *J. Fluid Mech.* **556**, 121-146 (2006).

Large azimuthal wavenumber instabilities in a small height/radius ratio rotating disk – cylinder configuration (rotor-stator cavity)

A. Yu. Gelfgat^a

This research continues our previous studies of three-dimensional instabilities of axisymmetric flow in a rotating disk – cylinder configuration. Early computational stability studies¹ considered the cylinder aspect ratio (height/radius) in the range of 1 to 3.5. Those results were completely validated experimentally² and verified numerically in several independent studies. Later, these results were extended both experimentally and computationally to tall cylinders³ with the aspect ratio varying from 3.5 to 6. In the present work we continue our numerical stability studies for small aspect ratios varying from 1 to 0.1. At small aspect ratios we arrive to so-called rotor-stator configuration that was rather extensively studied both experimentally and numerically⁴, however, a numerically converged stability results were never reported. The convergence studies performed for numerical stability analysis of different axisymmetric flows⁵ showed that convergence can be reached with the use of at least 100 points in the shortest spatial direction. The rotor-stator configuration at small aspect ratios appears to be even more computationally demanding, so that to reach a converged result we use up to 2000×200 grid points, followed by the Richardson extrapolation. This allows us to obtain a good comparison with experimental results⁶ that report the instability onset at $Re=2.5\times 10^4$ for aspect ratio 0.1. The current result is $Re_{cr}=22,350$ with the dimensionless circular frequency of oscillations 2.43. The latter value agrees well with the experimental results⁷ performed for the aspect ratio 0.114, where the oscillation frequency was measured to be 2.1. Considering different azimuthal wavenumbers k (3D perturbation $\sim \exp(ik\theta)$), we found that the primary instability sets in for $k=19$.

In the course of the present studies we report stability diagrams showing dependence of the marginal Reynolds numbers and critical oscillation frequencies on the aspect ratio varying from 0.1 to 1, for the azimuthal wavenumbers k in the range from 0 to 25 (Fig. 1). We report also patterns of the most unstable perturbations and discuss possible sources of instability.

^a School of Mechanical Engineering, Faculty of Engineering, Tel-Aviv University, Tel Aviv 69978, Israel

¹ Gelfgat A. Yu. et al., *J. Fluid Mech.* **311**, 1-36 (1996).

² Sorensen J.N. et al., *Exp. Fluids* **41**, 425-440 (2006).

³ Sorensen J.N. et al., *Phys. Fluids* **21**, 054102 (2009).

⁴ Launder B. et al., *Ann. Rev. Fluid. Mech.*, **42**, 229-248 (2010).

⁵ Gelfgat A. Yu. *Int. J. Numer. Meths. Fluids* **54**, 269-294 (2007).

⁶ Schouvilleier L. et al., *J. Fluid Mech.*, **443**, 329-350 (2001).

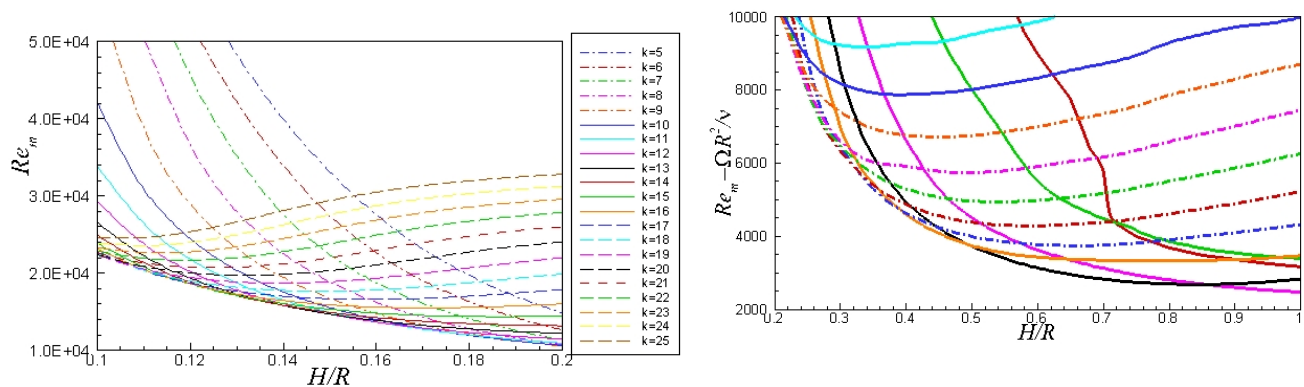


Figure 1. Marginal Reynolds number at different azimuthal wavenumbers k versus aspect ratio.

Rotation number dependence of the torque in small-gap Taylor-Couette flow

Hannes J. Brauckmann^a and Bruno Eckhardt^a

Taylor-Couette flow, the fluid motion between two independently rotating concentric cylinders, serves as a fundamental system to study, how wall curvature and mean system rotation affect turbulent characteristics, such as the radial transport of momentum that results in the torque exerted on the cylinders. Both, curvature and rotation, can be selected independently in terms of the ratio between inner and outer radius $\eta = r_i/r_o$ and the rotation number R_Ω , that measures the ratio between system rotation and shear¹. Recent experimental and numerical torque determinations for $\eta = 0.71$ and 0.5 revealed that the torque features a maximum as a function of the system rotation, R_Ω , when keeping the shear between the cylinders constant²⁻⁷. The occurrence of this maximum has been linked to the emergence of an intermittent turbulence near the outer cylinder that decreases the momentum transport efficiency^{4,8}.

Since this phenomenon is an effect of the curvature, it has to disappear when the curvature vanishes, i.e. for $\eta \rightarrow 1$. Then, also a change in the rotation influence on the turbulence and on the torque is expected. We here present a study of this small-gap limit in direct numerical simulations for various radius ratios $\eta \geq 0.9$. As a measure of the differences between the outer and inner cylinder fluctuations, we study the ratio $\xi = \sigma(\text{outer})/\sigma(\text{inner})$, where σ denotes the standard deviation of the torque fluctuations. We find that ξ decreases monotonically with η towards a value of 1. Parallel to this, the torque maximum disappears. Subsequently, the influence of the rotation (R_Ω) on the turbulence is nearly independent of the radius ratio, as evidenced by a collapse of the torque data and velocity profiles for different η . In qualitative contrast to the results for medium radius ratios, the torque features two maxima as a function of the rotation number for radius ratios $\eta \geq 0.9$.

To rationalize this new rotation dependence of the turbulence, we present a model of the flow that is based on the boundary-layer behavior. The results of this model agree with many features found in our direct numerical simulations of the small-gap Taylor-Couette flow.

^a Fachbereich Physik, Philipps-Universität Marburg, Renthof 6, D-35032 Marburg, Germany

¹ Dubrulle et al., *Phys. Fluids* **17**, 095103 (2005)

² Paoletti and Lathrop, *Phys. Rev. Lett.* **106**, 024501 (2011)

³ van Gils et al., *Phys. Rev. Lett.* **106**, 024502 (2011)

⁴ van Gils et al., *J. Fluid Mech.* **706**, 118 (2012)

⁵ Brauckmann and Eckhardt, *J. Fluid Mech.* **718**, 398 (2013)

⁶ Ostilla et al., *J. Fluid Mech.* **719**, 14 (2013)

⁷ Merbold et al., *Phys. Rev. E* **87**, 023014 (2013)

⁸ Brauckmann and Eckhardt, *Phys. Rev. E* **87**, 033004 (2013)

Decay regimes in the shallow viscous rotated fluid.

S. V. Kostrykin^{ab}, A.A. Khapaev^a, I.G. Yakushkin^a

The problem of evolution of large-scale vortical structures in the rotated fluid are of significant interest due to the numerous applications, arising in the hydrodynamics, astrophysics and especially in geophysics. Such vortices are well reproduced in many laboratory experiments. In our case quasi-turbulent vortical flows are obtained on the laboratory using MHD-method¹². These experiments are devoted to the study of influence of the non-linear bottom friction on the evolution of the intensive (cyclonic and anticyclonic) vortices in the shallow layers of the rotated viscous fluid in a wide range of Rossby numbers. For the interpretation of the cyclone – anticyclone asymmetry observed in the laboratory experiments we use a modified von Karman flow model¹². This model describes the axisymmetric flow in the layer of unstratified fluid with finite depth and free surface. The model equations are solved numerically. Its solution are studied in dependence from flow parameters – initial Rossby and Ekman numbers.

On the basis of numerical simulations with the model we show, that two different stationary regimes of the flow exist. The first one corresponds to the solid-body rotation of the flow and the second one to the two-layered flow with boundary layer near the bottom and small value of absolute vorticity at the surface. The last regime is realized for the initial anticyclonic flows with small Ekman and large Rossby numbers. Also we found that the flow decay happens differently in dependence of flow parameters and we distinguish three different decay regimes: a rapid nearly exponential decay to the solid-body stationary flow, a fast non-linear decay to the two-layered stationary flow and the mixed decay regime, when the flow firstly quasi-stabilizes to the state, which is close to the stationary two-layered flow, for some time and then finally it evolves to the rapid decay to the solid-body stationary flow. The obtained numerical results are compared with laboratory data and it is found a good agreement between them.

This investigation is supported by the RFBR grant 13-05-00949-a and 19th Program of Presidium of RAS.

^a A.M. Obukhov Institute of Atmospheric Physics RAS, Moscow, Russian Federation

^b Institute of Numerical Mathematics RAS, Moscow, Russian Federation

¹ Kostrykin et al., Journal of Exp. Theor. Phys., 112: 510–515, 2011.

² Kostrykin et al., JETP Letters, 95: 583–588, 2012.

Free surface Herschel-Bulkley flow on a rotating disc with application to lubricating greases

L. G. Westerberg^a, J. Li^b

The free surface motion of non-Newtonian fluids is central in many applications such as spin coating and grease lubrication in bearings. This study is motivated by the need of a better understanding of free surface grease flow in order to obtain a better understanding of the lubrication mechanism. Lubricating greases are well described by the Herschel-Bulkley rheology model containing the yield stress- and shear thinning behaviour which are typical properties for greases. Grease is a complex two-phase material and equally a semi-fluid consisting of a (Newtonian) base oil and a thickener matrix. Traditionally, lubricating greases are used in a great variety of mechanical systems such as rolling bearings, seals, and gears where it has been shown more advantageous than oil, mainly due to its consistency allowing the grease to stay inside the system and not leak out. Knowledge in the flow dynamics of grease is highly important for the understanding and predictions of grease distribution for optimum lubrication and for the migration of wear- and contaminant particles. Free surface effects play an important role in rolling bearings and open gears as the configuration normally is filled with about 30% grease to avoid heavy churning. In this study an analytical model of the stationary uniform flow on a rotating disc is developed and validated with experiments. The model results in the velocity profile for the flow in the thin fully yielded viscous layer in connection to the surface as well as an expression for the plug flow region on top of the viscous layer. Furthermore, the depth-averaged velocity is derived as is the shear stress value on the plate; the latter resulting in a condition for the grease to start moving and in turn yielding an expression for the viscous layer thickness as a function of the grease yield stress value, grease density, angular velocity and radial position. In addition, an expression of the layer thickness containing the ratio between the flow rate and the layer width which in turn can account for effects not included in the model such as wall slip and surface adhesion and thus add another degree of freedom into the model. Experiments with two different greases having NLGI grade 1 and 2 respectively shows it is possible to obtain a good fit with the analytically obtained thickness using the rheological parameters for actual greases.

^a Division of Fluid and Experimental Mechanics, Luleå University of Technology, SE-971 87 Luleå, Sweden.

^b Division of Machine Elements, Luleå University of Technology, SE-971 87 Luleå, Sweden.

A new regime for the strato-rotational instability of Taylor-Couette flow

Junho Park^a and Paul Billant^b

We show that the stably stratified Taylor-Couette flow is unstable when the angular velocity $\Omega(r)$ increases along the radial direction, a regime never explored before¹. The instability is different from the centrifugal instability: it is highly non-axisymmetric and involves the resonance of two families of inertia-gravity waves like for the strato-rotational instability². The growth rate is maximum when only the outer cylinder is rotating and goes to zero when the angular velocity $\Omega(r)$ is constant. The sufficient condition for linear, inviscid instability derived previously²: $d\Omega^2/dr < 0$ is therefore extended to $d\Omega^2/dr \neq 0$, meaning that only the regime of solid-body rotation is stable in stratified fluids. A WKB analysis in the inviscid limit, confirmed by the numerical results, shows that the instability occurs only when the Froude number is below a critical value and only for a particular band of azimuthal wavenumbers. The physical mechanism of the instability will be explained in terms of wave resonance and over-reflection.

^a LadHyX (Hydrodynamics Laboratory), Ecole Polytechnique, CNRS, 91128 Palaiseau, France

^b LadHyX (Hydrodynamics Laboratory), Ecole Polytechnique, CNRS, 91128 Palaiseau, France

¹ Park and Billant, *J. Fluid Mech.* **725**, 262 (2013).

² Yavneh et al., *J. Fluid Mech.* **448**, 1 (2001).

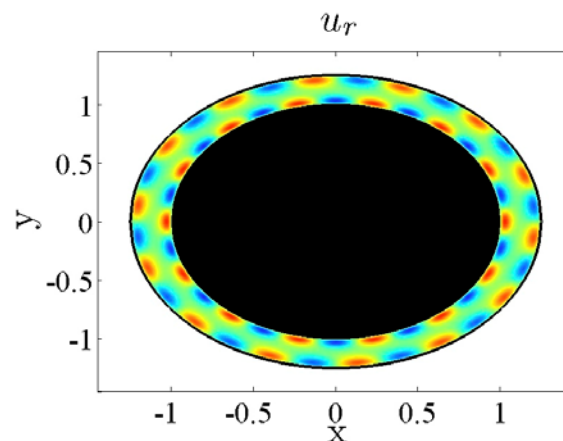


Figure 1: Example of an unstable eigenmode of the Taylor-Couette flow in a strongly stratified inviscid fluid. The inner cylinder is fixed and only the outer cylinder rotates.

Characterising localised intermittent bursts in a narrow gap Taylor-Couette setup

S. V. Jalikop¹, K. Avila², P. Steffen^b and B. Hof^a

We experimentally study the flow regimes in the counter-rotating Taylor-Couette configuration¹ with a radius ratio of $\eta = 0.98$. It has been previously observed that spatially localised flow states appear as the inner cylinder speed is increased beyond the onset of linear instability, keeping the outer cylinder speed fixed. The localised structures come in intermittent bursts at random locations, and can appear on top of either interpenetrating spirals (IPS) or wavy-vortex flow (WVF) depending on the speed of the outer cylinder (ω_o). A large value of η and the ability to vary the speeds of both cylinders allow us to follow this bursting phenomenon at varying degrees of counter rotation and to characterise them.

At lower values of outer ω_o , these structures at onset are wavy laminar bursts, similar to the ‘short-wavelength bursts’ observed by Carey et al.² They gradually undergo a qualitative change to turbulent bursts at higher outer cylinder rotation rates. This transition from wavy to turbulent patches, we believe, has not been reported before in Taylor-Couette system, and has been only observed in rotating plane Couette experiments³. We have mapped the onset curve of these wavy patches in the Reynolds number phase space, and find that it connects to the curve for the onset of sustained turbulence in the sub-critical regime. We also find that the lifetimes of these patches are exponentially distributed and that the mean lifetime increases with increasing degree of counter rotation.

¹ IST Austria, Am Campus 1, 3400 Klosterneuburg, Austria

² Max Planck Institute for Dynamics & Self-organization, Bunsenstrasse 10, 37073 Göttingen, Germany

¹ Avila, K. and Hof, B. *Rev. Sci. Instrum.* **84**, 065106 (2013)

² Carey, C. S. and Schlender A. B. and Andereck C. D. *Phy. Rev. E* **75**, 016303 (2007)

³ Tsukahara, T. and Tillmark, N. and Alfredsson, P. H. *J Fluid Mech.* **648**, pgs 5-33 (2010)

WIND TUNNEL AND EXPERIMENTEL TECHNIQUES

Customized turbulent flow fields generated by means of an active grid

N. Reinke^a, M. Hölling^a and J. Peinke^a

Wind tunnel experiments, which should clarify the interaction of wind energy converters and the ambient turbulent field, should be performed under realistic flow conditions. For the generation of realistic turbulent flow conditions we use an active grid, inspired by Makita¹. This grid allows for the generation of flows with high turbulence intensity and even to repeat those turbulent fields to a certain degree. Moreover, flow features are to a certain extent tuneable, e.g. velocity profiles or energy density spectrum, realized by individually controllable horizontal and vertical rotating axes, which are equipped with flaps. The rotation patterns of the axes over time are defined in an excitation protocol. Early works, e.g. Mydlarski and Warhaft², show that turbulent features depend on the kind of excitation. The challenge is designing an excitation protocol, which generates a flow field for a specific application. A general approach is still missing. Our approach allows estimating the flow features to given excitation protocols. The approach is based on the assumption that the flow field behind an active grid consists basically of different turbulent pulses, which belong to the excitation setting. Our approach gives a sequence of those pulses, which we call synthetic velocity time series, which is made on a computer. The synthetic time series serves as an estimation of the expecting flow field. Figure 1 compares stochastic properties of a synthetic time series and a time series recorded in wind tunnel, both generated under the same excitation conditions.

We will present how the approach works and what kind of assumptions we put in. Furthermore we will show how we are able to find a suitable excitation protocol to a reference dataset.

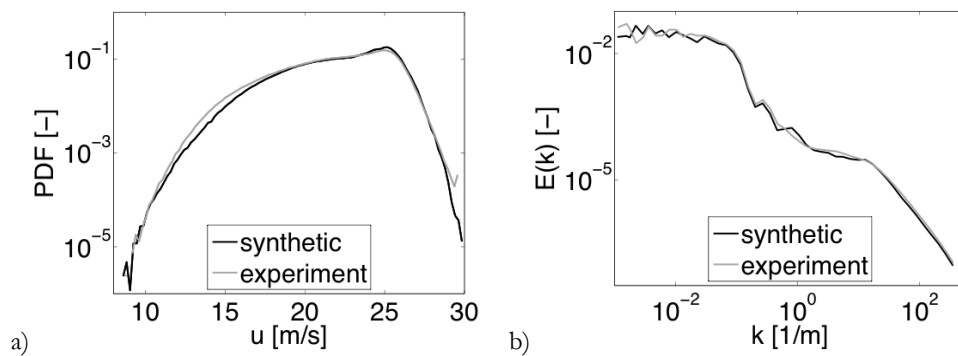


Figure 1: (a) Velocity distribution as probability density function (PDF). (b) Energy density spectrum vs. the wave number

^a Dep. of Physics, ForWind, Center for Wind Energy Research, University of Oldenburg, 26111 Oldenburg, Germany

¹ Makita, *Fluid Dyn. Res.* **8**, 53 (1991)

² Mydlarski and Warhaft, *J. Fluid Mech.* **320**, 331 (1996)

Experimental study of turbulent diamagnetism in liquid sodium flow

P.Frick^a, S.Denisov^a, V.Noskov^a, R.Stepanov^a, A.Pavlinov^a

The intensive small-scale turbulence in electroconducting fluids provides a variety of induction effects, described by about 20 terms in the general form of mean electromotive force¹. Very few among them have been isolated and studied in detail. For laboratory study it is a hard problem to provide a MHD configuration which permits to separate the contribution of different effects.

In our talk we present results of laboratory study of the magnetic field suppression in the domain of strong turbulent fluctuations. We perform series of experiments with a nonstationary turbulent flow of liquid sodium, generated in a fast rotating toroidal channel after its abrupt braking. The peak level of the Reynolds number reached about 10^6 , which corresponds to the magnetic Reynolds number about 30. We applied the stationary curl-free magnetic field which is collinear to the streamline of the large-scale mean flow. This excludes an induction effects by the mean flow and the contribution of effective diffusion (so-called beta-effect). The magnetic field is produced by a DC current in the toroidal coil, wound around the toroidal channel filled by sodium.

Our measurements show that during the highly turbulent stage of flow evolution the mean magnetic field is reduced by a factor of 0.6. The observed effect can be explained as the result of turbulent diamagnetism described by the term $(\mathbf{g} \times \mathbf{B})$ in the mean-field induction equation (here \mathbf{g} is the gradient of the energy of turbulent fluctuations and \mathbf{B} is the mean magnetic field).

^a Institute of Continuous Media Mechanics, Perm, 614013, Russia

¹ Raedler et al., *Phys. Rev. E*, V.73, 056311 (2006)

Angular momentum flux in turbulent Taylor-Couette flow

S. Merbold^a, C. Egbers^a

The flow in a gap between two rotating cylinders is of fundamental interest for a large number of technical applications. Also for geophysical and astrophysical processes turbulence in rotation drives the formation of structures such as accretion disks. In this work, turbulent structures in concentric rotating Taylor-Couette flow (TC) and its dependency on different parameters is investigated. Depending on the rotation rate of the cylinders, one is able to create huge amount of different flow cases and coherent structures inside the annulus. Eckhardt et al.¹ defined a transverse velocity flux for pipe flow, a heat flux for Rayleigh-Bénard and angular momentum flux for Taylor-Couette flow. They all have a similar analytical form. It is of great interest to quantify the angular momentum flux as a global answer of the flow and its dependence on the flow states observed. At the cylinder wall the angular momentum flux becomes proportional to the torque the fluid works on the cylinders. Thus the dimensionless torque can be used to calculate the angular momentum flux globally. Measuring the torque and therefore the angular momentum flux and the identification of different flow behaviours is the purpose of this work.

In our investigation we use two experimental systems. One is able to measure the torque precisely using strain gauges at a radius ratio of $R_1/R_2=0.5$. The inner cylinder as well as outer one rotates in co-rotating and counter-rotating direction. The inner cylinder measures the torque. In Merbold et al.² the behaviour of the angular momentum flux with the rotation for Reynolds numbers in the range of 10^3 to 10^6 has been discussed for this experiment. The behaviour for another geometry is also known by van Gils et al.³. Our second apparatus works with different geometries, while the both known are included. Flow visualisation and Laser Doppler Velocimetry are performed to identify the different phenomena observed in the previous work.

^a Dep. of Aerodynamics and Fluid Mechanics, BTU Cottbus-Senftenberg, Germany

¹ Eckhardt et al., *Europhys. Lett.*, **78**, 24001 (2007)

² Merbold et al., *Phys. Rev. E*, **87**, 023014 (2013)

³ van Gils et al., *J. Fluid Mech.*, **706**, 118 (2012)

Dielectric Electroactive Polymers for drag-reducing wall oscillations in low-Reynolds number internal turbulent flows

D. Gatti^a, A. Güttler^{a,b}, M. Quadrio^c, H. F. Schlaak^d, C. Tropea^a and B. Frohnäpfel^b

Spanwise wall oscillations have been widely investigated since the seminal work of Jung et al.¹ in 1994 as an active means to reduce turbulent skin-friction drag. In spite of its relative simplicity, the spanwise oscillations concept has been tested almost solely numerically, and only few experimental implementations have been attempted²⁻⁷. Moreover, most of them are proof-of-principle laboratory experiments in which the spanwise wall velocity is achieved by moving the wall through bulky crank-driven mechanisms. Though effective in reaching their aim, such solutions are generally energetically inefficient, require significant modifications of the wind tunnel test section and, most importantly, do not lend themselves to developing a system-integrated, compact solution. Moreover, it has been recently demonstrated⁸ that achieving a high Reynolds number, is important to understand the true capabilities of the drag reduction technique.

Gouder et al.⁹ realised the spanwise wall oscillation through a novel actuator concept: the dielectric electroactive polymers (DEAP). However they found this technology to be unattractive due to the fragility of the actuators, having a lifetime of only a few minutes¹⁰, and electromagnetic linear motors have been preferred instead.

In the present work, we describe the design, fabrication and wind-tunnel testing of long-lasting spanwise-oscillating active surfaces based on DEAP actuators. We point out some advantages and drawbacks of this particular actuator and verify whether some potential advantages, such as low power consumption, low cost, low weight and simplicity can in fact be realised. Two soft surfaces with integrated dielectric elastomer actuators have been fabricated, capable of producing spanwise oscillations at their resonant frequency of 65 Hz with 4 mm peak-to-peak amplitude. The actuators have a moving surface of 25 cm x 25 cm area. Each actuator has been flush mounted on a Plexiglas plate, located 2m downstream of the inlet of an air channel flow and 1m before its outlet. The rectangular cross-section of the channel has a width-to-height ratio of 12:1 and a height of 25 mm. The two DEAP active surfaces have been mounted on the two opposite walls of the channel at the same spanwise position. Changes in wall skin-friction drag have been measured with highly accurate pressure measurements over a 20 cm long portion of the actuators, while the channel flow has been operated at velocities between 2.7 m/s and 9 m/s, corresponding to $Re_t=150$ and $Re_t=450$.

The streamwise length of the actuated section, when expressed in wall units, is 4500, therefore shorter than the streamwise onset length of drag reduction, leading to a space-averaged drag reduction of about 3%. On the other hand, their short length combined with the choice of a channel flow geometry make the setup suitable for a Direct Numerical Simulation, in which finite-size actuators are considered. We can thus verify whether the well-known differences between numerical and laboratory experiments reduce to a reasonable margin when the effect of the onset transient is taken into account. The final aim of this research is to evaluate the suitability of DEAP for laboratory implementations of spanwise oscillations through fabrication of an array of actuators to control larger sections of the wind tunnel.

^a Center of Smart Interfaces, Technische Universität Darmstadt, 64287 Darmstadt, Germany

^b Institute of Fluid Mechanics, Karlsruher Institut für Technologie, 76131 Karlsruhe, Germany

^c Department of Aerospace Sciences and Technologies, Politecnico di Milano, 20156 Milano, Italy

^d Institute of Electromechanical Design, Technische Universität Darmstadt, 64283 Darmstadt, Germany

¹ Jung, Mangiavacchi and Akhavan, *Phys. Fluids A*, **4**, 1605 (1992)

² Laadhari, Skandaji and Morel, *Phys. Fluids*, **6**, 3218 (1994)

³ Trujillo, Bogard and Ball, *ALAA Papers*, **97**, 1870 (1997)

⁴ Choi, Roach, DeBisschop and Clayton, *ALAA Papers*, **97**, 1795 (1998)

⁵ Choi and Clayton, *Int. J. Heat Fluid Fl.*, **22**, 1 (2001)

⁶ Ricco, *J. Turbulence*, **5**, N24 (2004)

⁷ Auteri, Baron, Belan, Campanardi and Quadrio, *Phys. Fluids*, **22**, 115103 (2010)

⁸ Gatti and Quadrio, *Phys. Fluids*, **25**, 125109 (2013)

⁹ Gouder, Potter and Morrison, *Exp. Fluids*, **54**, 1441 (2013)

¹⁰ Gouder, *PhD Thesis*, Imperial College London, 171 (2013)

WEDNESDAY

17th September 2014

Mini Symposia: Cardiovascular

Asymptotic Model of Fluid-Tissue Interaction for Cardiac Valve Dynamics

F. Domenichini^a and G. Pedrizzetti^b

Blood motion in the left ventricle is characterized by the development of vortices from the mitral orifice that smoothly drive the redirection of the incoming jet towards the outlet track¹. The vortex formation process is intrinsically connected to the dynamics of the mitral leaflets while they interact with the flow crossing the valve during the diastolic filling phase. Modelling the dynamics of a natural mitral valve still represents a challenging issue, both for the mathematical and numerical difficulties and because the material properties of the tissue, inhomogeneous and anisotropic, are not available. Medical imaging can provide some indications about the geometry of the valve during a few phases of its motion, but it is not able to give informations on the mechanical properties of the tissue.

A parametric model of the mitral valve geometry is here introduced. Its motion is described in the asymptotic limit, under the assumption that the valve having infinitesimal thickness moves with the flow, without any resistance other than that given by its shape, and without the need to specify its material properties. The valvular time - varying shape is completely described by a single degree of freedom, represented by a properly defined opening angle. The valvular model is coupled with a simple description of the left ventricle geometry²; they are integrated with a pseudo-spectral numerical code for the solution of the fluid equations, based on an efficient Immersed Boundary elements Method (IBM)³.

The intra-ventricular fluid evolution and the vortex formation are analysed in their relationship with the resulting valvular motion. Differences are evaluated with respect to the geometric parameters, such as the valve eccentricity and leaflets' asymmetry, and quantified in terms of integral quantities. It will be shown that vortex formation immediately reflects small differences in the mitral valve geometry and dynamics.

Notwithstanding the simplifying assumptions, the model represents a starting reference for more complete ones. It may also permit a functional description of a real valve in term of parameterization of its geometry and dynamics that can be recorded by medical imaging. More realistic geometries and additional degrees of freedom, like the presence of two independent leaflets, represent the further developments of this work.

^a Dipartimento di Ingegneria Civile e Ambientale, University of Firenze, Via S. Marta 3, 50139, Firenze, Italy

^b Dipartimento di Ingegneria e Architettura, University of Trieste, P.le Europa 1, 34127 Trieste, Italy

¹ Kilner et al., *Nature* **404**, 759 (2000)

² Domenichini et al., *J. Fluid Mech.* **539**, 179 (2005)

³ Mangual et al., *Ann. Biomed. Eng.* **40**, 1790 (2012)

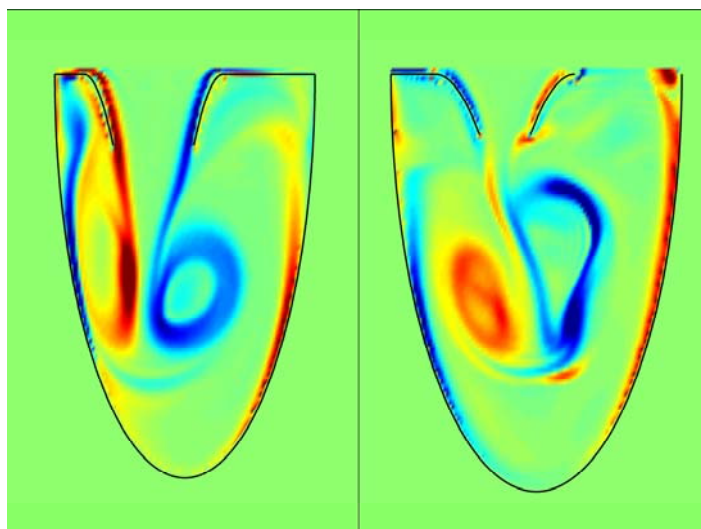


Figure 1: Normal vorticity distribution on a vertical plane cutting the mitral and aortic orifices. (left) mid-diastole. (right) early systole.

Axisymmetry Index: A Measure for Asymmetry of Vortex Rings

A. Falahatpisheh^a and A. Kheradvar^a

There are many conditions in which vortex rings deviate from axisymmetry. Shape of the vortex rings represent the symmetry of propulsion, which has applications in animal locomotion (e.g., free-swimming of a jellyfish), rocket and marine propulsion devices as well as the flow downstream the heart valves. However, no fluid dynamics' measure is yet defined to quantify the asymmetry of a vortex ring. In this work, we introduce an index, ξ , that measures the deviation of a vortex ring from axisymmetry. The index ξ is defined as the ratio of the impulse of a naturally-formed vortex ring to that of its equivalent axisymmetric vortex ring. To validate, we test the performance of the index in the analytical cases of axisymmetric Gaussian vortex rings and Hill's spherical vortex. The axisymmetry index shows full agreement with the axisymmetric nature of both Gaussian vortex rings and Hill's spherical vortex (i.e., $\xi=1.000$). In addition, ξ is examined in CFD-obtained flow fields downstream two different nozzle shapes with circular and oval cross sections to measure the asymmetry of the formed vortex rings downstream the nozzle.

^a Department of Biomedical Engineering, University of California, Irvine

Role of blood viscosity on the development of arterial disease arteriosclerosis

Professor G. C. Layek

Department of Mathematics, The University of Burdwan, Burdwan-713104, India

Email:goralayek@yahoo.com, gclayek@math.buruniv.ac.in

Abstract

The flowing blood is a special type of fluid containing plasma, protein, erythrocytes and different kinds of nutrients. Naturally, flowing blood is non-homogeneous and the viscosity of blood is not uniform as in classical fluid dynamical equations. The haematocrit (the percentage volume of red cells: 41.8-49% approximately for males and 38.6-45.6% for females) plays important roles in arterial blood flow in particular, the development and progression of the disease arteriosclerosis are very significant in course of time. High haematocrit level can deadly affect in cardiovascular flows. It has the dominant contribution to the viscosity of flowing blood. Blood becomes thicken significantly for greater haematocrit levels. As a result, the arterial flow-rate becomes slow. This can increase the risk of tissue infarction. It is clinically known that the blood hematocrit level increases due to several diseases, so the blood viscosity also increases rapidly. The blood viscosity also depends on velocity shear. The mathematical model for variable blood viscosity has been developed. Suitable numerical code has been employed for finding the approximate solution of incompressible Navier-Stokes equations taking into account of arterial wall deformability and pulsatile flow conditions. The estimation of flow quantities, relevant clinically, are obtained and discussed in the context of arterial disease. In particular, the arterial wall stress decreases with increasing values of haematocrit concentration.

Pathophysiological secondary flow structures in the human cardio-vasculature

K. V. Bulusu^a, L. Prah Wittberg^b, S. van Wyk^b, L. Fuchs^b and M. W. Plesniak^a

The arterial network consists of branches and curvatures that are present ubiquitously in the human vasculature. Several cardiovascular-related pathophysiological phenomena have been linked to “spiral blood flow structures”, clinical parlance for secondary flow (vortical) structures. In the aortic arch, for example, the presence of such vortical flow structures tends to have beneficial effects on aortic endothelial layer [1]. The loss of spiral blood motion in the abdominal aorta has been linked to renal artery stenosis and rapid deterioration of renal functions [2]. The motivation for this study began from our experimental observation of the multiplicity of secondary flow structures in a 180° test section model for curved arteries, possessing a variety of scales, strengths and morphologies under physiological (pulsatile) inflow conditions.

A rigorous *in plastico* experimental investigation of secondary flow structures with this model of a curved artery was performed using phase-averaged PIV technique under physiological inflow conditions. Complicated morphological changes such as asymmetry and multi-scale, spatio-temporal distributions could not be predicted from simple theories. Accordingly, continuous wavelet transform, vorticity (ω) fields, were employed to characterize secondary flow structures quantitatively. Computational models treated the blood mixture as a function of RBC and plasma densities. The RBC phase is represented as an active scalar, coupled to the blood viscosity represented by the Quemada [4,5](non - Newtonian viscosity) model. Bulk flow behavior is assessed by Navier-Stokes equations for an incompressible fluid, modeling the distribution of RBCs using a transport equation.

The temporal evolution of large-scale coherent structures viz., deformed Dean-, Lyne- and Wall-type (D-L-W) vortices was characterized using regime maps based on two dimensionless parameters; dimensionless pumping power (E_p) and secondary flow Reynolds number (R_s) [3] (see Figure 1). Experimental results suggest that D-L-W vortices evolved during the systolic acceleration phase, followed by the predominant loss of D-L-W coherence during systolic deceleration phase. Computational modeling revealed shear layer instabilities as the rheological (non-Newtonian) effect of blood flow. These instabilities further altered the formation of vortical structures during the systolic deceleration and diastole (see Figures 2a, b).

The paper will summarize our experiments and complementary flow simulations, and pathophysiological blood flow scenarios that are linked to concomitant secondary flow hydrodynamics.

^a Biofluid Dynamics Laboratory, Dep. Mechanical and Aerospace Engineering, GWU, 801 22nd Street NW, Washington DC, USA

^b Linné FLOW Centre, KTH Mechanics, Osquars backe 18 SE-100 44 Stockholm, Sweden

¹ Sengupta et al., *Heart Failure Clin* **4**, 325 (2008)

² Houston et al., *Nephrol Dial Transplant* **19**, 1786 (2004)

³ Siggers and Walters, *J. Fluid Mech.* **600**, 133 (2008).

⁴ Quemada, *Rheologica Acta* **16**, 82 (1977).

⁵ Quemada, *Rheologica Acta* **17**, 632 (1978).

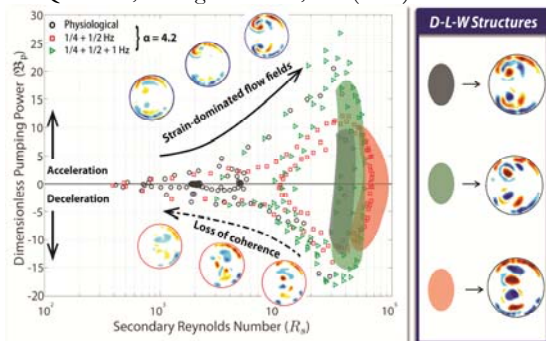


Figure 1: Morphological groups in the secondary flow regime map for Womersley number, 4.2.

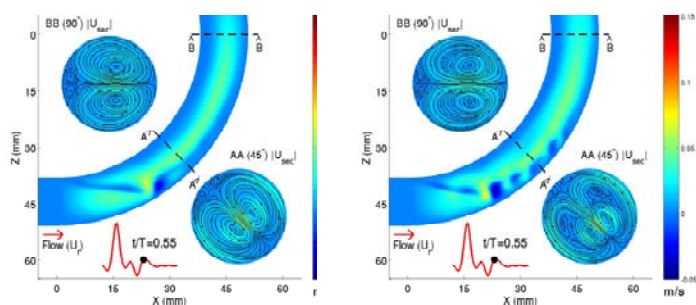


Figure 2: Contours and streamlines of secondary flow and streamwise velocity fields (a) with Newtonian blood analog fluid and (b) non-Newtonian blood analog fluid of uniform RBC distribution

A new imaging method for *in vivo* assessment of intra-ventricular flow in athletes

G. Galanti^a, S. Pedri^b, D. Mazzeranghi^b, A. Frusciante^b, L. Toncelli^a and L. Stefani^a

We present a study for the pre-competitive development of advanced imaging tools to assess intra-ventricular flow patterns, which may provide new and incremental prognostic information in the management of patient at risk of cardiac modifications. Blood flow is closely linked to the morphology and function of the cardiovascular system and there is an increasing consensus that cardiac fluid dynamics may play a central role in several clinical endpoints¹. Following this new concept, maladaptive fluid mechanics can potentially highlight early signs of cardiac inefficiency and, out of that, provide predictive information in favour of possible future ventricular remodelling. However current imaging technology has very limited tools for the assessment of cardiovascular fluid mechanics. As far as echocardiography is concerned, one solution currently available is the so called Echographic Particle Image Velocimetry (Echo-PIV)². However this method requires intravenous infusion of contrast agent, as fluid marker for PIV, which limits its routinely application.

This study is an activity of Project ASSO, financially supported by the Tuscany Region through its Regional Operational Programme "POR CREO 2007-2013", co-financed by the ERDF under the "Regional competitiveness and employment" objective for 2007-2013. Under the Project ASSO the study is to verify the feasibility to use a method to manipulate the Doppler velocity information obtained by Color Flow Mapping (CFM) and reconstruct the two-dimensional velocity vector field. From this, fluid dynamics concepts are employed to evaluate quantitative indicators of blood motion. The new algorithm processes CFM dataset into a velocity field using a weak version of the incompressibility constraint to reconstruct the missing velocity component. The underlying concept is similar to previous solutions^{3,4} (see also Hitachi's Vector Flow Mapping) and introduces technical solutions that improve the continuity with physical and numerical consistency. It was altogether fundamental to develop a new CFM imaging acquisition settings to acquire dataset having high temporal resolution, high sensitivity to low velocities and reduced aliasing.

This novel technique is applied to study the intra-ventricular flow pattern in athletes in baseline conditions and during intense exercise stress. It is hypothesized that the development of modified, sub-optimal, flow transformation at peak exercise may provide further indication on the individual cardiac tolerance to prolonged exercise stress.

^a Sport Medicine Center, University of Florence, Italy

^b Esaote S.p.A., Via di Caciolle 15, Florence, Italy

¹ Sengupta et al., *JACC Cardiovasc. Imaging* 5, 305 (2012)

² Kim et al., *Experiments in Fluids* 36, 455 (2004)

³ Uejima et al., *Ultrasound in Med. & Biol.* 36, 772 (2010).

⁴ Garcia et al., *IEEE Trans Med Imag* 29, 1701 (2010)

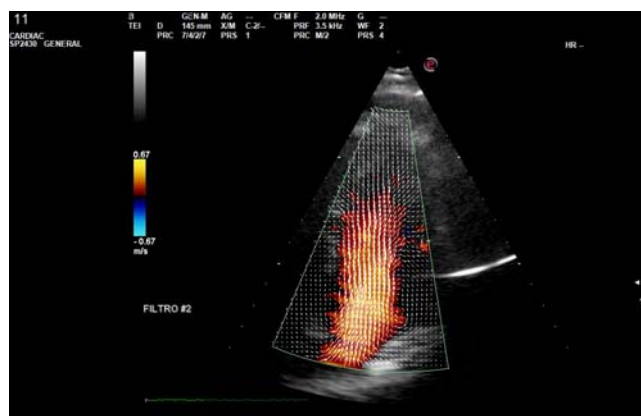


Figure 1: Example of a reconstructed velocity distribution during ventricular filling.*

Flow Dynamics of Thrombogenesis in Infarcted Left Ventricles

J.H. Seo^a, R. George^b, and R. Mittal^a

The formation of blood clots (thrombogenesis) in the left ventricle (LV) leads to clinically significant complication such as thromboembolism. Blood hypercoagulability, endocardial injury, and blood stasis are three major factors that are implicated in left ventricle thrombus (LVT) formation¹. Among these factors, abnormal blood flow patterns associated with ventricular dysfunction is the main trigger of LVT formation in ventricles affected by the myocardial injury. Global assessment of ventricular function and image-based assessment of ventricular wall motion to identify LV regional wall abnormality that result in blood stasis are currently used for the stratification of patients at risk for LVT formation. These approaches are however limited since the actual correlation between blood flow patterns and coagulation is not known, especially for the complex intraventricular flows. The general notion is that flow stasis will allow sufficient time for the coagulation cascade and thus result in thrombus formation. However, the biochemical species in the coagulation cascade are primarily transported by the blood flow and thus their deposition also depends on the flow dynamics. The study of the interaction between the blood flow dynamics and biochemical reactions in the coagulation process will provide insights on flow mediated thrombus formation and improve the prediction and stratification of the LVT risk in the heart failure patients. In the present study, we apply a multi-physics computational model to study the flow mediated thrombogenesis in infarcted left ventricles. Blood flow in the left ventricle is simulated by solving the incompressible Navier-Stokes equations using the immersed boundary method² and this is coupled to a convection-diffusion-reaction equations based model of the coagulation cascade³ and platelet activation⁴. Thrombus formation patterns are then correlated with the hemodynamic metrics such as wall shear stress and residence time to investigate the correlation between LVT risk and hemodynamics. The effects of LV ejection fraction and stroke volume on the flow pattern and resulting thrombus formation are also investigated.

^a Dep. Mechanical Engineering, Johns Hopkins University, Baltimore, MD, USA

^b School of Medicine, Johns Hopkins University, Baltimore, MD, USA

¹ Delewi et al., *Heart* **98**, 1743 (2012).

² Seo and Mittal, *Physics of Fluids* **25**(11), 110801 (2013).

³ Biasetti et al., *Frontiers in Physiology* **3**, 266 (2012)

⁴ Leiderman and Fogelson, *Math. Med. Biol.* **28**, 47 (2011)

The Impact of Numerical Simulation Strategies on the Prediction of Hemodynamic Changes in an Artery Stenosis

A. Slotosch^a, B. Frohnapfel^a

The severity of an arterial stenosis may significantly influence the downstream hemodynamic characteristics and lead to critical flow conditions that result in hemolysis or activation of platelets¹. In order to study the detailed flow characteristics downstream of a stenosis, computational fluid dynamics (CFD) is nowadays widely used. In the present work, we investigate the impact of the employed simulation strategy on the resulting flow field prediction.

In the numerical simulation of internal flows, i.e. flows through ducts, most CFD studies enforce a prescribed flow rate. As a result, the corresponding pressure gradient, required to drive the flow against viscous losses, is obtained. Another approach, which is not so commonly used, prescribes the pressure gradient and yields the flow rate as result. For a given duct geometry both simulation strategies lead to identical results for flow rate and pressure gradient. However, once geometry changes are introduced and the flow field with and without this change is to be compared, e.g. one artery with and one without stenosis, the simulation strategy is reflected in the obtained results. This difference is visualized in figure 1 where the recirculation zone behind an obstacle in a pipe is shown. These predictions of the recirculation zones are obtained by first extracting the flow rate and the corresponding pressure gradient from a pipe flow without obstacle. Consecutive simulations are then run in which either this flow rate or this pressure gradient is prescribed. As a result the pressure gradient increases in case of the fixed flow rate and the flow rate decreases in case of the fixed pressure gradient. A difference that is clearly visible in the size of the recirculation zone which is mainly a function of the flow rate in the typical Reynolds number range of arterial flows.

Naturally, the question arises which of the simulation strategies best represents hemodynamic conditions. In reality, it is neither realistic that the heart will be able to maintain a constant flow rate through an almost closed artery nor will the heart realize a constant pressure gradient independent of the frictional losses within an artery. A third, recently presented², alternative simulation strategy is one in which the power input into the system is fixed. In this case the product of flow rate and pressure gradient is prescribed. For the pipe flow with an inserted obstacle this strategy yields a decrease of the flow rate and an increase of the pressure gradient. The corresponding recirculation zone is located between the two other strategies and is also shown in figure 1.

We study the differences between these simulation strategies for steady and periodically varying blood flow; patient specific stenosis geometries will also be included in future. With the corresponding results we intend to highlight that the choice of the simulation strategy is one important issue in hemodynamic CFD (amongst many) that deserves careful consideration.

^a Institute of Fluid Mechanics, Karlsruhe Institute of Technology, Karlsruhe, 76131, Germany

¹ Ghalichi et al., *Biorheology*, **35**, 281 (1998)

² Hasegawa et al., *European Turbulence Conference*, **14**, (2013)

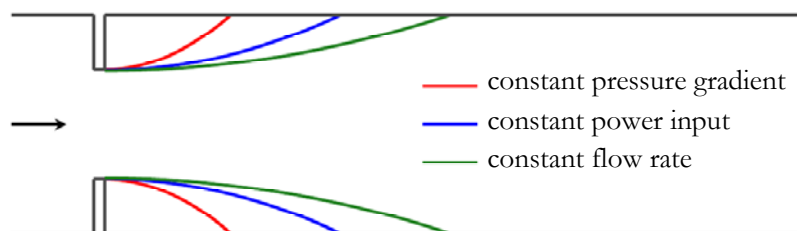


Figure 1: Depending on the simulation strategy, the recirculation zone downstream of an obstacle in a pipe changes its length. The recirculation zone is enclosed by corresponding streamlines, which also mark the varying reattachment point.

Lagrangian coherent structures downstream of biological and mechanical aortic valves

M.D. de Tullio^a

With the aim of accurately investigate the flowfield through prosthetic heart valves, a numerical approach is presented, that couples a finite-difference direct numerical simulation flow solver with a simple structural solver describing the dynamics of deformable bodies, using an iterative approach. In order to account for the presence of the bodies in the fluid domain, the method is based on a suitable version of the immersed boundary technique, which is able to handle rigid and deformable geometries with zero-thickness. The structures are modelled by means of a discrete spring network integrated with the continuum model on the base of the minimum energy concept [1].

The solution of the fluid-structure-interaction (FSI) problem produces detailed information of the flow patterns through realistic geometries for the valves and the initial tract of ascending aorta. Two different valve models are considered: a mechanical bi-leaflet, made of two semi lunar rigid disks attached to a rigid valve ring by small hinges, and a tissue one, composed of three deformable leaflets that open closely resembling the native tri-leaflet aortic valve.

In order to reveal fluid flow structures and to better understand the transport mechanics, Lagrangian coherent structures (LCS) are used. LCS are distinguished material surfaces that can be identified as boundaries to regions with dynamically distinct behaviour, and are revealed as hypersurfaces that locally maximize the finite-time Lyapunov exponent (FTLE) fields [2]. Post-processing the flow simulation data, first FTLE fields are calculated integrating dense meshes of Lagrangian particles backward in time, and then attracting LCS are extracted.

A three-jet configuration is distinctive of bi-leaflet mechanical valves, with high turbulent shear stresses immediately distal to the valve leaflets, while a jet-like flow emerges from the central orifice of bio-prosthetic valves, with high turbulent shear stresses occurring at the edge of the jet (Figure 1). Details of the numerical methodology along with a thorough analysis of the different flow structures developing during the cardiac cycle for the two configurations will be provided.

^a Dep. Mechanics, Mathematics and Management, Politecnico di Bari, Via Re David 200, 70125 Bari, Italy

¹ Tanaka et al., *Computational Biomechanics*, Springer (2012).

² Shadden et al., *Chaos* **20**, 017512 (2010).

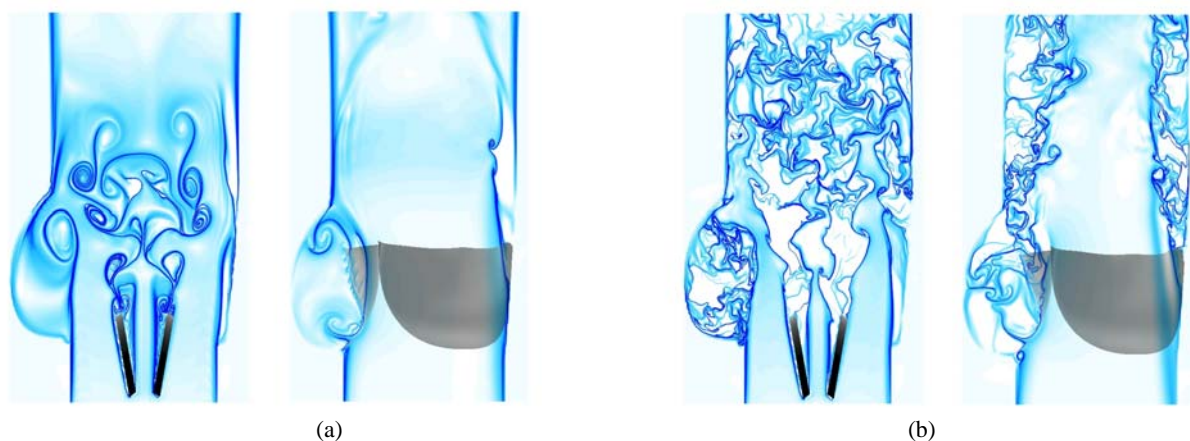


Figure 1: Cross section of backward time FTLE during the acceleration (a) and deceleration (b) phases, revealing attracting LCS (blue). The left frames of each sub-figure refer to the mechanical valve, while right ones to the biological valve.

Hemodynamic simulation in real vessel geometry at physiological hematocrit

R.Messina^a, F.Battista^a, S. Melchionna^b and C. M. Casciola^{ac}

Hemodynamics of physiological vessels is of paramount interest for medical implications (e.g. cardiovascular diseases) and presents fundamental issues related to blood rheology, which is still poorly understood. Blood is a complex suspension of particulate, mostly red blood cells (RBCs) with a minor component of erythrocytes, leukocytes and platelets, in plasma, which is a solution of proteins, glucose and dissolved gases in water (92%). At physiological hematocrit (volume fraction of RBCs) the suspended phase makes blood a non-Newtonian fluid, with the apparent viscosity (ratio actual and pure plasma viscosity) dependent on hematocrit¹, shear stress and vessel dimension². The realistic simulation of such flows is indeed a challenging task, due to both fluid and morphological complexity of the system. Here a Lattice Boltzmann formulation coupled with a Lagrangian scheme for the RBCs is used to describe the particle-fluid and particle-particle interactions³. Our purpose is to perform a numerical simulation of the hemodynamic flow, explicitly accounting for the presence of the RBCs at different concentrations up to physiological hematocrit (40%). Panel b) in the figure shows the typical geometry of a bifurcation extracted from Computational Axial Tomography (CAT), while panel a) provides a snapshot of the instantaneous configuration of RBCs. The two other panels report the mass flux through the two branches at different hematocrit (0%, 10%, 20%, 30%, 40%). Companion data from circular ducts allow extracting the apparent viscosity and comparing with the results in the actual vessel. Based on this kind of data, the role of the actual vessel configuration, vessel dimension and wall shear stress will be discussed, analyzing segregation effects and the correlation between RBCs configuration and local shear stress. In the final results the dependence of viscosity on the hematocrit, shear stress and vessel dimension will be presented.

^a Dipartimento di Ingegneria Meccanica e Aerospaziale, Università di Roma "La Sapienza," via Eudossiana 18, 00184 Roma, Italy

^b CNR-IPCF, Consiglio nazionale delle Ricerche, P.le A. Moro 2, 00185, Rome Italy

^c Center for Life Nano Science@Sapienza, Istituto Italiano di Tecnologia, Via Regina Elena 291, 00161, Roma, Italy

¹ Roe e. Wells and Edward W. Merrill. Influence of flow properties of blood upon viscosity haematocrit relationships. Journal of clinical investigation Vol. 41, No. 8, 1962

² A.R.Pries, D. Neuhaus and Gaetgens. Blood viscosity in tube flow: dependence on diameter and hematocrit. The American Physiological Society, 1992

³ S. Melchionna. A model for red blood cells in simulations of large-scale blood flows. Macromolecular Theory and Simulations. 2011, 20, 548-561

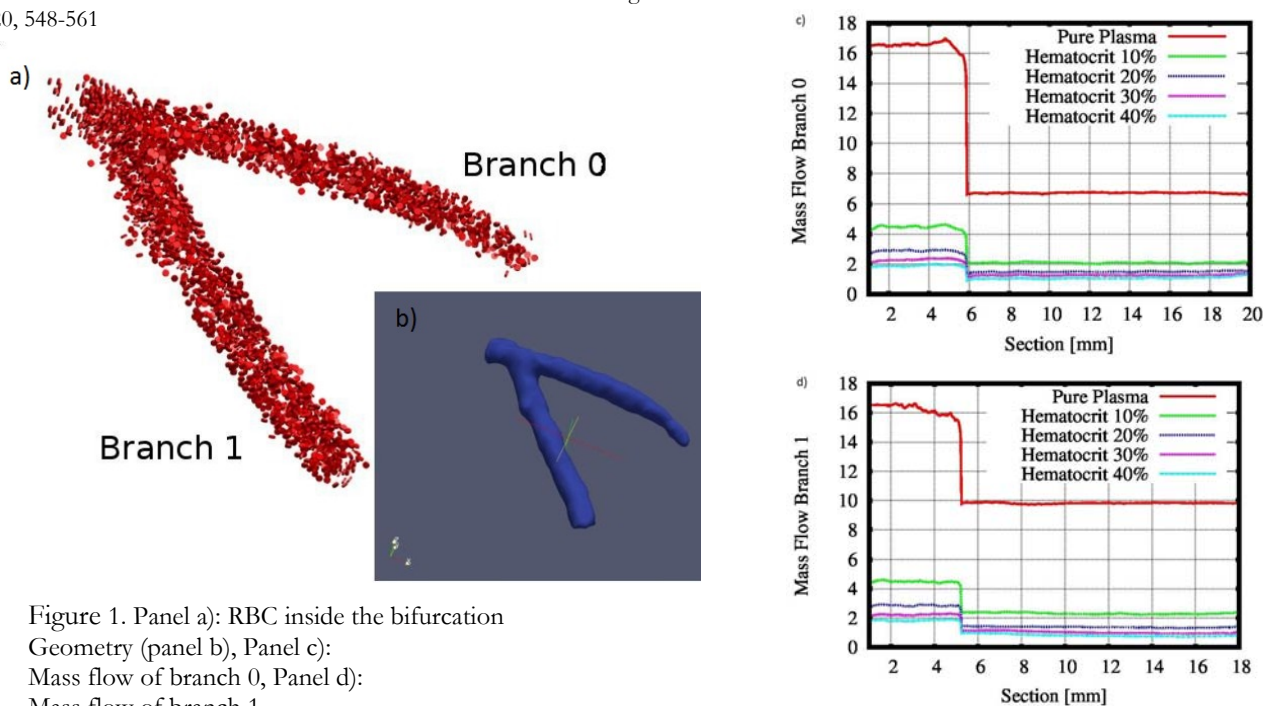


Figure 1. Panel a): RBC inside the bifurcation
Geometry (panel b), Panel c):
Mass flow of branch 0, Panel d):
Mass flow of branch 1.

Numerical simulation of hemolysis in a mechanical aortic valve with a non-Newtonian fluid model

Francesco De Vita^a, Marco D. de Tullio^b, and Roberto Verzicco^c

The blood is a concentrated suspension of cells (mainly red blood cells) in a Newtonian matrix (plasma) and consequently its dynamics as single-phase continuum is that of a non-Newtonian fluid. The dependence of the viscosity on the shear-rate is that of a shear-thinning fluid which is given in figure 1. It can be noticed that the viscosity approaches a constant asymptotic limit if the shear-rate is high enough and this condition is usually achieved for large values of the Reynolds number. Accordingly the common practice accepts the assumption that blood in large vessels behaves as a Newtonian and the aortic root should be the safest context for the application of this hypothesis fluid the artery diameter ($\sim 25\text{mm}$) and the flow rate (on the average $\sim 5\text{ l/min}$) are the largest.

In this paper we show that this is not always true owing to the pulsatile and transitional nature of the flow. Using a Newtonian and a non-Newtonian fluid model, numerical simulations of the blood flow through the functional unit aortic root/aortic valve are performed showing a different dynamics of the large- and small-scales which have several consequences on the overall dynamics. Our results show that the aortic valve dynamics (computed from a fluid/structure interaction procedure) is negligibly affected by the non-Newtonian fluid model and equally insensitive is the transvalvular pressure drop. In contrast, the shear thinning constitutive relation adversely impacts the red blood cells haemolysis and platelet activation by increasing the mean value of the viscous stresses by 20% and the blood damage index (BDI) by the same amount.

^a Dep. Ing. Engineering, Università di Roma Tor Vergata, Roma Italy

^b Department of Mechanics, Mathematics and Management, Politecnico di Bari, Italy

^c Dep. Ind. Engineering, Università di Roma Tor Vergata, Roma Italy & PoF MESA+ University of Twente, Enschede, The Netherlands

¹ Maffettone, P.L. & Minale, M. *J. Non-Newton. Fluid Mech.* **78**, 227–241, (1998).

² de Tullio, M., Cristallo, A., Balaras, E. and Verzicco, R., *J. of Fluid Mech.*, **622**, 259290, (2009).

³ L.Goubergrits&K.Affeld, *Artif. Organs*, **28**, 499507, (2004).

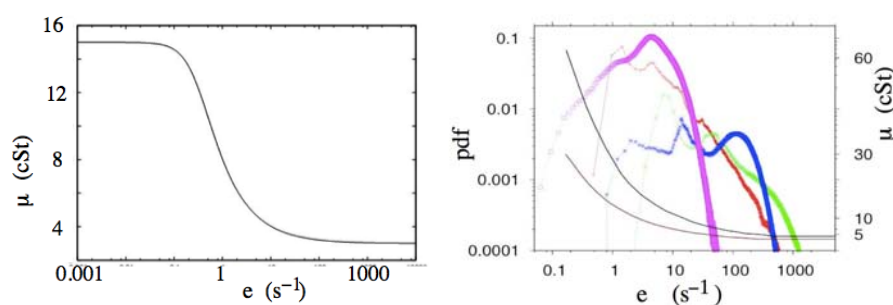


Figure 1: (a) Variation of the dynamic viscosity μ (related to the kinematic viscosity by $\nu = \mu/\rho$) as function of the shear rate norm e for an hematocrit of 40%. (b) Probability density functions of the shear rate for 4 representative instants in the cycle for the non-Newtonian fluid model. The pdfs are overlaid onto two curves for the shear rate dependence of the blood viscosity (hematocrit 45% and 60%). Colour coding: valve fully open (red), peak flow (green), valve closed (blue) and flow settling (purple).

A hemodynamic study on diseased carotid bifurcations

J. Vimmr^a, A. Jonasova^a and O. Bublik^a

In recent years, the modelling of blood flow has received a new impulse in the form of patient-specific models, which compared to idealised models offer a closer co-operation with vascular surgeons and radiologists. In this regard, it is a fact that any knowledge about the local hemodynamics gained from numerical simulations can bring numerous potential benefits to the treatment of patients with cardiovascular diseases and help in pre-operative planning. One of the fields, where the non-invasive CFD modelling can aid vascular surgeons in their decision making, is the indication of surgery for diseased arteries¹, especially those with threshold stenoses between 50 % and 60% angiographic stenosis severity.

The main objective of the present numerical study is to investigate pulsatile non-Newtonian flow characteristics in several models of clinically significant carotid bifurcations reconstructed² from CT scans and to provide a preliminary assessment of their hemodynamic significance and necessity for surgical intervention. For all numerical simulations of blood flow, we adopt the assumption that the blood is an incompressible fluid with shear-dependent dynamic viscosity. The governing equations coupled with the well-known Carreau-Yasuda model³ is solved by means of an in-house software, computational algorithm of which is based on the stabilised variant of the projection method and the cell-centred finite volume method formulated for hybrid unstructured tetrahedral grids⁴. Because of the difficulties associated with clinical determination of physiological pressure in human vessels, each carotid outlet is coupled with one three-element Windkessel model that is able to approximate the flow resistance of the downstream vascular bed and to provide a physiological value of pressure at this outlet.

This investigation was supported by ERDF, project “NTIS – New Technologies for the Information Society”, European Centre of Excellence, CZ.1.05/1.1.00/02.0090.

^a European Centre of Excellence NTIS – New Technologies for the Information Society, Faculty of Applied Sciences, University of West Bohemia, Univerzitni 22, Pilsen, CZ

¹ Nakazato et al., *Circ. Cardiovasc. Imaging* **6**, 881 (2013).

² Jirik and Lukes, DICOM2FEM software, University of West Bohemia (2014).

³ Cho and Kensey, *Biorheology* **28**, 241 (1991).

⁴ Vimmr et al., *Int. J. Numer. Meth. Bio.* **29**, 1057 (2013).

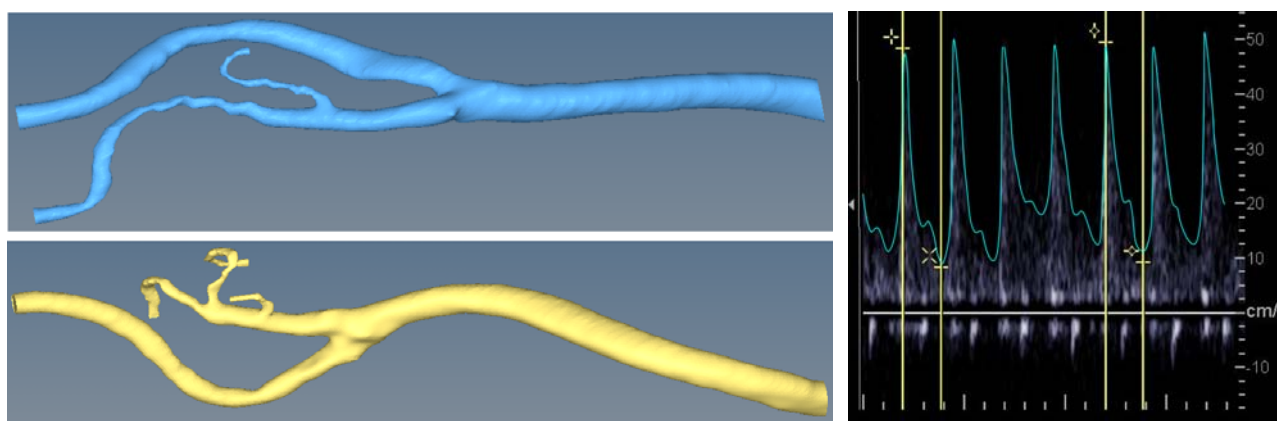


Figure 1: Patient-specific models of carotid bifurcation (left) and common carotid artery velocity waveform acquired by Doppler ultrasound (right).

Clinical Assessment of Intraventricular Vortices in Healthy and Diseased Hearts

Javier Bermejo^a, Pablo Martínez-Legazpi^b, Sahar Hendababi^c, Yolanda Benito^a, Marta Alhama^d, Raquel Yotti^a, Candelas Pérez del Villar^a, Esther Pérez-David^a, Ana González-Mansilla^a, Cristina Santa-Marta^e, Alicia Barrio^a, Francisco Fernandez-Avilés^a, Shawn Shadden^f, Juan C. del Álamo^b

Vortices may have a role in optimizing mechanical efficiency and blood mixing of the human left ventricle (LV). To assess this potential role, novel processing of Doppler-echocardiography data¹ was used to study intraventricular flow, vortex properties (i.e. trajectory, circulation) and blood transport in the LV of relatively large ($N > 60$) populations of healthy volunteers and patients with non-ischemic dilated cardiomyopathy (NIDCM)². In a significant subset ($N > 20$) of the patients, the Doppler measurements were validated studied head-to-head with phase-contrast magnetic resonance imaging (Figure 1). Blood transport was quantified by trajectory-based computation of Lagrangian coherent structures (LCS)³. These LCS were shown to reveal the boundaries of blood injected and ejected from the heart over multiple beats.

Vortex features showed a characteristic biphasic temporal course during diastole. Because late filling contributed significantly to flow entrainment, vortex strength reached its maximum at the time of peak-A wave. Thus, the biphasic nature of filling determines normal vortex physiology. Vortex formation was exaggerated in patients with NIDCM due to chamber remodeling, and enlarged vortices are helpful for ameliorating convective pressure losses, connecting the E-wave and A-wave inflows, and facilitating transport. However, strong stable vortices often led to high blood stagnicity in their central cores. These findings can be accurately studied using ultrasound.

^a Department of Cardiology, Hospital General Universitario Gregorio Marañón, and the Instituto de Investigación Sanitaria Gregorio Marañón, Madrid, Spain

^b Mechanical and Aerospace Engineering Department. University of California San Diego, La Jolla, CA

^c Illinois Institute of Technology, Chicago, IL

^d Current address Scripps Green Hospital, La Jolla, CA.

^e Department of Mathematical Physics and Fluids, Facultad de Ciencias, Universidad Nacional de Educación a Distancia, Spain

^f Mechanical Engineering Department, University of California Berkeley, Berkeley, CA

¹ García et al. *IEEE Trans Med Imaging* **29**: 1701-1713 (2010).

² Bermejo et al., *Am. J. Physiol - Heart and Circ. Physiol.* doi: 10.1152/ajpheart.00697.2013 (2014).

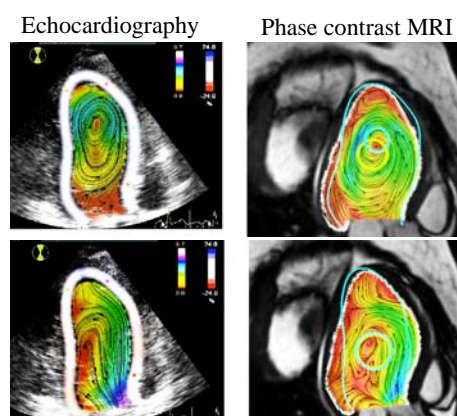


Figure 1: Head by head comparison of LV flow obtained by color-Doppler echocardiography analysis (left) and phase-contrast magnetic resonance imaging (right) in the same human patient, for late diastole (top) and systole (bottom).

³ Hendababi et al. *Ann Biomed Eng* **41**, 2603-2616 (2013).

Exploring the potential of blood flow network data

C. Poelma^a

To gain a better understanding of the role of hemodynamic forces during the development of the cardiovascular system, a series of studies have been reported recently that describe flow fields in the vasculature of model systems. An example is the extensive study documenting the extra-embryonic blood vessels in the chicken model system by Kloosterman et al.¹ Such data sets, in particular those reporting networks at multiple stages, mark a transition in the focus from single blood vessels to large parts of vascular networks. This opens up many exciting ways to study the role of hemodynamics during development. It becomes possible to investigate the behaviour of a blood vessel in the context of its surroundings, rather than as an isolated entity. For instance, is the change in diameter of a blood vessel solely due to local parameters (e.g. wall shear stress) or is there also a dependence on the overall structure (e.g. scalar concentration)? In this study, we present a framework to address such questions and report preliminary results.

A second example of the potential of the data is the ability to study hemorheology in vivo. Human blood is a well-known example of shear-thinning fluids. Furthermore, the effective viscosity is a function of the diameter of the blood vessels, due to the Fåhræus–Lindqvist effect² (i.e. the formation of a cell-free layer near the vessel wall). Due to a lack of available data, the rheology for most model systems - such as the embryonic chicken - is assumed to be similar to the well-documented human case, despite major biological differences (hematocrit, erythrocyte shape). With the data now available, it is possible to check this assumption. Figure 1 explains how this can be achieved: microscopic particle image velocimetry provides velocity measurements of vascular networks. This data is subsequently reduced to a simplified hydraulic circuit representation, which models the network as a series of interconnected resistors. For each of these resistors (i.e. blood vessel segments), the flow rate, length and diameter are known. We assume that Poiseuille's law holds for each vessel, which is a safe assumption in this application¹. Analogous to Kirchhoff's laws, we know that (1) mass is conserved at nodes and (2) the pressure drop from one node to another is independent of the path taken between these nodes. While the absolute pressure at each node is unknown, it is still possible to find the expression for the effective viscosity from the pressure drop along two different paths that connect the same two nodes. In particular, we are interested to see if the established models for $\mu/\mu_0 = f(D)$ are also valid for avian blood.

¹ Kloosterman, Hierck et al. (2014) *submitted*; see also [doi:10.4233/uuid:7352d753-b9f8-489a-ab0f-eb0f0bc9b632](https://doi.org/10.4233/uuid:7352d753-b9f8-489a-ab0f-eb0f0bc9b632)

² Secomb and Pries (2013) *Comptes Rendus Physique* 14 (6) pp.470–478

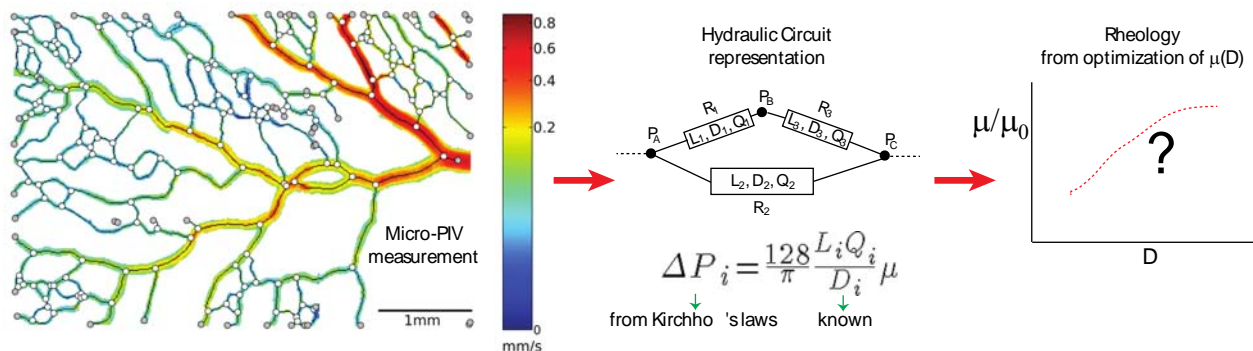


Figure 1: Extracting rheology from flow network data (a) A micro-PIV result (b) The network is converted to a graph (or hydraulic circuit) representation, with each vessel segment modelled as a resistance with known flow rate Q , diameter D and length L . (c) Conservation of mass at bifurcations and consistency of pressure (independence of path) make it possible to estimate the effective viscosity $\mu/\mu_0 = f(D)$ using optimization.

^a Dep. Mechanical, Maritime and Materials Engineering, Delft University of Technology; Mekelweg 2 2628 CA Delft, The Netherlands; e-mail: c.poelma@tudelft.nl

Influence of the coronary arteries on the flow in the aortic root

S. Fortini^a, G. Querzoli^b, S. Espa^a and S. Melchionna^c

The blood flow from the left ventricle of the heart enters the aorta artery and distributes nutrients (i.e. oxygen) to the whole body through the primary cardiovascular network. The initial tract of the aorta, called the aortic root, is characterized by three sinuses (sinuses of Valsalva) where, from two of them, the coronary arteries originate. These small arteries and their branches supply all parts of the heart muscle, the myocardium.

The *in vitro* analysis of the fluid dynamics inside the aortic root has widely studied; worldwide several Pulse Duplicators (PD) have been designed to simulate the heart/circulatory system behavior. The objective of this study is to analyze the influence of the coronary arteries on the flow inside an elastic and transparent aortic arch laboratory model, designed with the sinuses shape and the two small arteries and placed in an experimental set-up already used in previous investigations of the intraventricular flow [1].

The 2D instantaneous velocity fields were measured by means an image analysis technique [2] in order to investigate the evolution of the inlet jets during the aortic arch model filling. In the performed experiments a series of 100 cardiac cycles have been acquired and phase averaged have been computed; as a result two-dimensional two-components velocity field (2D2C) were obtained.

In this work, we focused only on the very early vasculature of the coronary system, namely the two vessels connected to the Valsalva sinuses. First results presented here are related to the left main coronary and the preliminary description of the phenomenon time evolution is outlined in Figure 1. On the left, the Lagrangian particles trajectories are shown whereas the instantaneous 2D velocity and vorticity fields are on the right; the plots correspond to the middle plane at one salient instant of the diastole. The experimental parameters are: stroke volume $SV = 64$ ml, and period $T = 2.4$ s. The coronary flow occurs mainly during the diastole when the ventricle dilates and is smaller during systole (although not negligible), increases abruptly after the valve closure, and then it remains constant up to the end of the cardiac cycle when it becomes zero again.

This study proves that our experimental apparatus is suitable to analyze the influence of the coronary arteries on the flow inside the aortic arch laboratory model, highlighting how these affect the aortic root filling during the systolic phase.

^a Dipartimento di Ingegneria Civile, Edile e Ambientale, Sapienza University of Rome, Via Eudossiana 18, 00184 Rome, Italy.

^b Dipartimento di Ingegneria Civile Ambientale e Architettura, University of Cagliari, Via Marengo 3, 09123 Cagliari, Italy.

^c IPCF - CNR, Consiglio Nazionale delle Ricerche, P.le A. Moro 2, 00185 Rome, Italy.

¹ Fortini et al., *Exp. Fluids* **54** 1609 (2013)

² Cenedese et al., *Exp Fluids* **39**, 322 (2005).

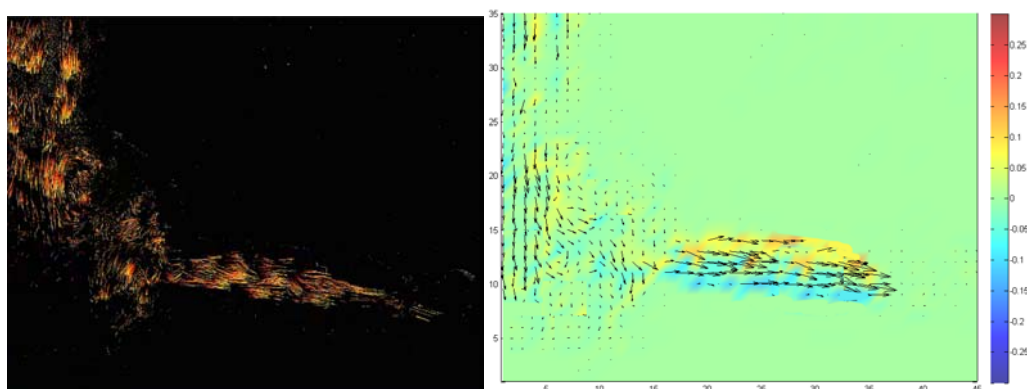


Figure 1: Lagrangian trajectories (on the left) and Eulerian instantaneous velocity field (black vectors) and vorticity (colour scale) during the systolic wave (on the right).

Blood flow and wave propagation in the coronary vasculature : a reasonable approach for truncated tree models

N. Kizilova^a, O. Zenin^b

Modeling of the coronary vasculature is important for understanding the coronary fluid dynamics, blood flow heterogeneity, pressure distribution, and diagnostics of stenosis severity especially for the multivessel coronary artery disease¹. Detailed structure of the coronary vasculatures can be examined on their plastic casts, and many general features and regularities in geometry² and hemodynamics³ of human and porcine coronary arteries have been studied. Coronary vasculatures contain >1000 small vessels, and the problem of reasonable truncation of the coronary tree for direct real-time numerical computations of the pressure and flow distributions, pressure oscillations and wall shear stress is very important. Development of virtual patient-specific models of human heart and coronary vasculature for medical diagnostics purposes is also based on reasonably simplified models of the coronary microcirculation⁴. Most of the numerical computations are done on the steady 3D blood flow in rigid tubes or 1D and 2D pulsatile flow models with fluid-structure interaction. Negative wave reflection in the coronary vasculature and the corresponding ‘suction’ phenomenon is very important for the blood supply of the heart, but neither steady flow models nor truncated models can describe wave reflections in the coronary tree.

In this paper the results of the measurements on 10 plastic casts of human hearts containing from 980 to 1350 arterial segments (Fig.1a) and numerical computations on the 2D linearized model of axisymmetric wave propagation in the viscoelastic tube are presented. The smallest arteries in the initial models have $d=0.1\text{mm}$. Gradual truncation has been carried out by progressive replacing the smallest tubes by the computed Windkessel models. The final truncated models only include the larger epicardial arteries terminated by complex computed Windkessels (Fig.1b). The 2D model allows real-time ($t=20\text{-}60\text{ s}$) numerical computations even on complete trees. It was shown, the proposed approach for computations of the wave conductivity for the terminal tubes (circles in Fig.1b) in the truncated model allows keeping the negative wave reflection effect. Basing on geometrical regularities of the coronary vasculatures, the algorithm of generation of the patient-specific coronary model basing on angiographic or CT images of the epicardial arteries has been developed. *In vivo* pressure and flow curves measured on five healthy volunteers have been used for validation of the developed coronary model.

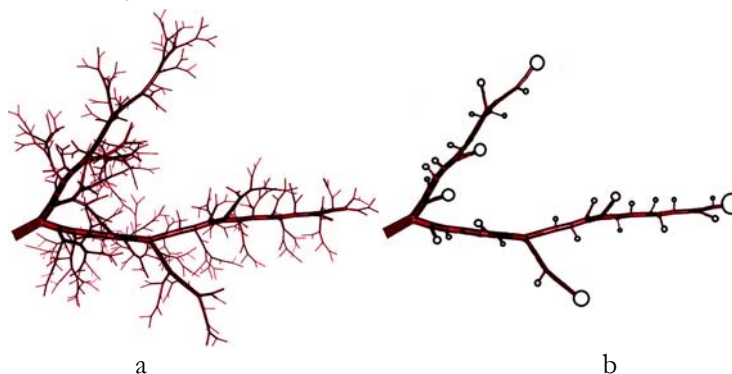


Fig.1. Complete (a) and truncated (b) models of the coronary tree.

¹Kizilova, *Computer Methods in Mechanics*, Poznan Univ. Press, 621 (2013). - P.621-22.

²Kassab, *Am. J. Physiol.*, 289, H2559 (2005).

³Zenin et al., *Biophysics*, **52**, 499 (2007).

⁴Vignon-Clementel, *Comput. Methods Appl. Mech. Engrg.*, 195, 3776 (2006).

^a Interdisciplinary Centre for Mathematical and Computer Modeling, Warsaw University, 69 ul. Prosta, Warsaw, Poland

^b Donetsk National Medical University, 60 Universitetska st., Donetsk, Ukraine

Tornado-like Flow Compatible Mechanical Aortic Valve Prosthesis – Concept Description and Experimental Testing

A. Gorodkov¹, G. Kiknadze², A. Agafonov^a, and L. Bockeria^a

50-year-old history of mechanical heart valve prostheses includes many original technical solutions, none of which up to this day does not fully restore the function of the valve and get rid of aggressive anticoagulation therapy, significantly affecting the quality of patient's life.

Studies of the hydrodynamic structure of the flow of blood in the chambers of the heart and aorta are performed in the Bakulev Center for Cardiovascular surgery since 1992. These studies have shown that blood flow, generated in the left ventricle of the heart corresponds to the structure of self-organizing tornado-like flows described by the exact solution of non-stationary hydrodynamic equations for this class of flows which was published in the 1986¹. The previous attempts to adapt the geometry of the flow channel of prosthetic heart valve to swirling blood flow were not successive since there were no any quantitative criteria of the flow swirling which were derived from the exact solution.

A new model of a mechanical aortic valve – Tornado-compatible valve (TCV) was developed (patent RU 2434604 C1), the lumen of which is circular in cross-section throughout the streamlined part of the prosthesis and is completely free from any kind of obstacles that can disrupt the flow pattern. The valve consists of a body and three cusps attached to the outer hull lines with rotary joints (Fig. 1). Cusps profile is arranged so that the part of the flow cross section in the open state of the lumen was circular and the cusps reverse side surface follows the curvature of the sinuses, which allows to keep the hydrodynamic interface of the flow in the aorta with the flow in the coronary arteries when the valve is closed.

The standard hydrodynamic testing of this valve has shown its significant advantage compared with other valve types currently used in cardiac surgery.

A special testing was developed using original bench which generates the Tornado-like jet. For this a converging channel was worked out, which profile corresponds to the streamlines of Tornado-like jet, derived from the exact solution. The resulted jet manifested all principal properties of Tornado: laminarized “glass-transparent” jet without any visible perturbations in the flow core which flows out from the supply vessel with higher velocity compared to the turbulent flow. Several valve types were testing at this bench, including TCV which did not affected the jet structure and time of water flowing out.

The valve was implanted in the pig without anticoagulant administration. According to echocardiography and coagulation control the valve function is satisfactory up to five months of observation. The experiment continues.

¹ Bakulev Research Center for Cardiovascular surgery (Moscow, Russia)

² Inventors network GmbH (Humburg, Germany)

¹ G. Kiknadze, et al. *J. Of Material Sciences : Materials in Medicine*, 7, p. 153-160(1996).



Figure 1: Tornado-compatible aortic valve prosthesis

Free Surface Flows

Other

Experimental study of splashing mechanisms by an immersed rotating body

D. H. Rodríguez^{a,b}, R. Berger^b, J.-P. Matas^a, M. Bourgoïn^a

Splashing of water by an immersed rotating wheel is a common situation, which may have important impacts in particular in automotive applications. The water projections during the rotation of car wheels can indeed result in undesired effects such as the obstruction of the field of view, the presence of water in air intake, electronic failures, etc.. Several mechanisms are responsible for the splashing phenomenon.

We present an experimental study of the model situation where a smooth rotating wheel partially immersed in a water tank is considered (see figure 1). We first discuss some overall qualitative observations of this configuration, which is almost undocumented in the literature. For a given diameter and immersion depth, when the rotation rate of the wheel is increased, we observe the formation of a dynamical meniscus (whose dimensions increase with the rotation) at the rear of the wheel. Most of the water extracted in the meniscus falls back into the tank except a thin liquid layer which remains attached to the wheel surface. Above a critical rotation rate, this film is destabilized by a Rayleigh-Taylor instability, creating elongated fingers in the front of the wheel which eventually break into small droplets via a Rayleigh-Plateau mechanism. The complete splashing phenomena therefore involves several physical processes: water extraction by the meniscus, water entrainment in the film, fingers creation by Rayleigh-Taylor instability and fingers fragmentation by Rayleigh-Plateau instability (see figure 1). For the largest wheels investigated, the meniscus has also been found to become unstable above a rotation threshold.

As a first step towards a quantitative description of these mechanisms, we will present here a systematic study of the influence of the rotation rate, of the wheel diameter and of the immersion depth, on the geometry and the dynamics of the meniscus. We show that the meniscus is mainly dominated by inertial effects which can be partially described by a simple “parabolic model” where fluid particles are assumed to be ejected ballistically at the periphery of the wheel. However, we will show that subtler mechanisms must be taken into account for an accurate description of the water entrainment in the meniscus.

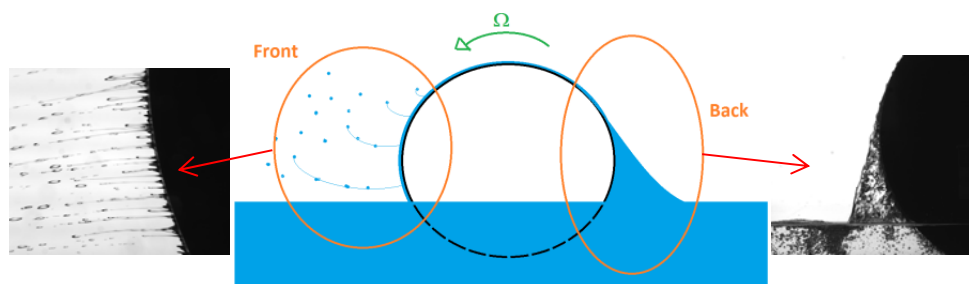


Figure 1: Overall qualitative observation on a rotating wheel partially immersed in a water tank

^a Laboratoire des écoulements Géophysiques et Industriels, CNRS/UJF/G-INP UMR 5519, BP53, 38041 Grenoble, France

^b PSA Peugeot Citroën, Centre technique de Vélizy, 78943, Vélizy Villacoublay, France

Convective structures in a cooled water layer in the presence of a surfactant and an imposed shear flow

V.P. Reutov^a and G.V. Rybushkina^a

The convective structures arising in a thin horizontal water layer cooled from above are studied. The layer contains a shear flow produced by tangential stresses on the top and an insoluble absorption-type surfactant film on the free surface. The analysis is based on numerical solution of a standard three-dimensional equation for the Boussinesq gravity-capillary convection supplemented with the equation governing the surfactant concentration. The approximation of nondeformable surface and the condition of thermal insulation at the bottom are used. Besides, the linear dependence of surface tension on temperature and surfactant concentration is adopted.

A numerical procedure based on the pseudospectral method together with appropriate reformulation of the basic equations is employed¹. The dimensionless parameters of the flow are the Grashof (Gr), Prandtl (Pr), Marangoni (Ma), Reynolds (Re), and Biot (Bi) numbers as well as normalized elasticity (E') and diffusivity (D') of the surfactant film. The computations showed that the small-scale thermocapillary patterns were suppressed with increasing E' , while the large-scale patterns (the size of which was several layer thicknesses) demonstrated the transition from cells to longitudinal rolls (Figure 1). For moderately large E' , a similar transition was revealed with increasing Re. Note that the mentioned effects agree with the results of earlier experiments^{2,3}. It was found also that the values of mean kinetic energy of the pulsations obtained at large enough E' are reached in purely buoyancy-driven convection without surfactant with essential (two-fold) effective decrease of Gr.

The work was carried out with financial support from the Russian Foundation for Basic Research (project No. 13-05-97056-r_povolzhye_a).

^a Dep. Nonlinear Dynamics, Institute of Applied Physics RAS, 46 Ulyanov Str. Nizhny Novgorod, 603950, Russia.

¹ Reutov and Rybushkina, *Phys. Fluids* **25**, 074101 (2013).

² Phongikaroon and Judd, *J. Fluids Eng.* **128**, 913 (2006).

³ Bower and Saylor, *Int. J. Heat and Mass Transfer* **54** 5348 (2011).

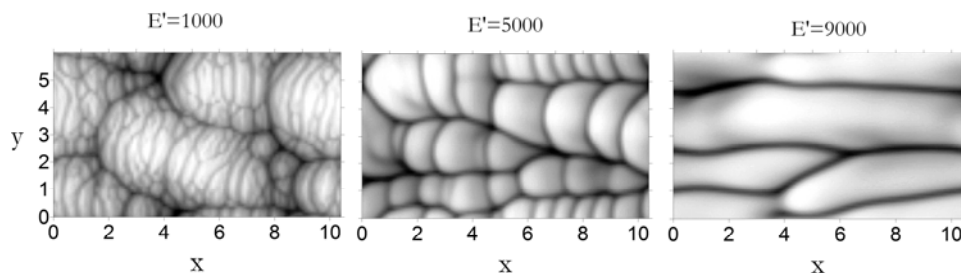


Figure 1: Surface temperature images with increasing E' at fixed $Pr=7$, $Gr=4000$, $Ma=20000$, $Re=10$, $Bi=0.4$, and $D'=3$ (the black and white colors correspond to minimal and maximal values, respectively); x -axis is oriented in the downstream direction.

Numerical Simulation of Free-Surface Reattachment inside an Air Cavity Ship

A. Shiria^a, R. E. Bensow^b, M. Leer-Andersen^a, Jacob Norrby^c

Air lubrication is used to reduce the viscous resistance in different type of marine vessels. For a displacement ship with a large flat of bottom area, the use of confined pressurized air cavity under the hull is preferable since this method requires minimum of air supply (Fig. 1). At the front edge of the cavity water separates from the wall and forms a free surface flow inside the cavity. Due to sudden disruption in wall presence, the boundary layer flow on to the hull continues as a free shear flow with air-water interface. The disturbance is controlled by air pressure and surface gravity waves form inside the cavity. The wavy free surface flow reattaches to the aft part of the ship at the rear end of the cavity.

Experimental study has been carried out ¹ to determine the role of different parameters, i.e. flow velocity, air pressure and geometry of the cavity, on its performance. The goal was to maximize the drag reduction with the minimum of air loss. This study showed the importance of the reattachment process in total resistance force exerted to the hull.

A series of numerical simulations have been performed using unsteady RANS, to estimate the viscous and pressure forces acting on the beach section of the cavity. The Volume of Fluid method (VoF) is used to capture the air-water interface. To simulate the air release process in detail, a very fine mesh is required at the beach region with a very short time step of the simulation (see Fig. 2). To estimate the average forces acting on the beach in a lower mesh resolution, a Fluent routine is used to extract the excessive air from the air-water mixture at every few time steps. The result provided a more realistic simulation of the boundary layer flow and reattachment and a better estimation of the viscous resistance force at this section of the hull.

^a SSPA Sweden AB, Chalmers Tvärgata 10, Gothenburg, Sweden

^b Dep. Shipping and Marine Tech., Chalmers University, Gothenburg, Sweden

^c Stena Rederi AB, Gothenburg, Sweden

¹ Shiria et al., 29th Symposium on Naval Hydrodynamics, Gothenburg, Sweden (2012).

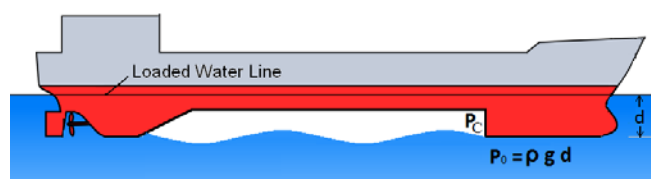


Figure 1: Schematic of the air cavity ship.

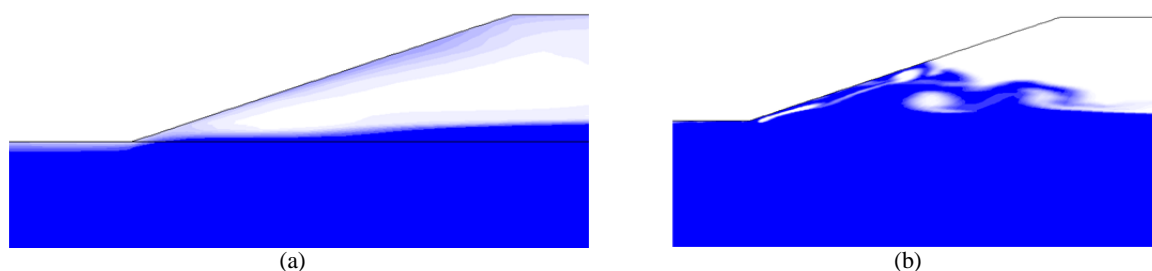


Figure 2: Free surface reattachment at the beach in (a) Low mesh resolution, with unphysical air release. (b) High mesh resolution with more detail of reattachment process.

Settling of a sphere through a horizontal fluid-fluid interface

J. Pierson^a, J. Magnaudet^{a,b}

The passage of a sphere through a horizontal interface separating two immiscible fluids is encountered in many applications such as coating, encapsulation or liquid-liquid extraction but also meteorology and oceanography. This situation is known to exhibit two different behaviours. The regime where viscous and capillary effects dominate frequently gives rise to a film drainage configuration where the sphere is maintained nearby the interface until the film located between the two of them is entirely drained. In contrast, when capillary effects are small enough and/or inertia effects dominate, the sphere is able to fall/rise through the interface and tows a tail of one fluid while settling into the other. This is the so-called tailing mode.

While the first configuration has been extensively studied because of its relevance to coalescence, much less is known about the tailing mode, except in the Stokes limit which was investigated experimentally by Maru *et al.*¹ and Pitois *et al.*² and computationally by Geller *et al.*³ using a boundary integral technique.

We investigate this problem both experimentally and numerically, mostly in inertia-dominated regimes. Experiments make use of two high-speed video cameras to follow the motion of spheres of various diameters and densities falling through an oil-aqueous solution interface whose deformation is tracked as well. Computations are performed by solving the full Navier-Stokes equations using a combination of the Volume of Fluid (VOF) technique without explicit interface reconstruction⁴ with the Immersed Boundary Method (IBM) to enforce the no-slip condition at the sphere surface.

We investigate a broad range of flow conditions, with settling Reynolds numbers varying from $O(10^{-1})$ to $O(10^2)$, viscosity and fluid density ratios varying from $O(10^{-1})$ to $O(10^2)$ and $O(1)$ respectively, sphere-to-heavy fluid density ratios from 1.5 to 8 and interfacial Bond numbers from $O(10^{-1})$ to $O(10)$. This allows us to observe and analyse contrasting tail evolutions, with or without the formation of a skirt at the back of the sphere, and various pinch-off dynamics.

^a Institut de Mécanique des Fluides de Toulouse (IMFT), Université de Toulouse-INPT-UPS, Allée du Professeur Camille Soula, 31400, Toulouse, France

^b CNRS, IMFT, F-31400, Toulouse, France

¹ Maru *et al.*, *Chem. Eng. Sci.*, **26**, 1615 (1971).

² Pitois *et al.*, *C.R. Acad. Sci. Paris, Série IIB-Mechanics-Physics-Astronomy*, **327**, 605 (1999).

³ Geller *et al.*, *J. Fluid Mech.*, **169**, 27 (1986).

⁴ Bonometti & Magnaudet, *Int. J. Multiphase Flow* **33**, 109 (2007).

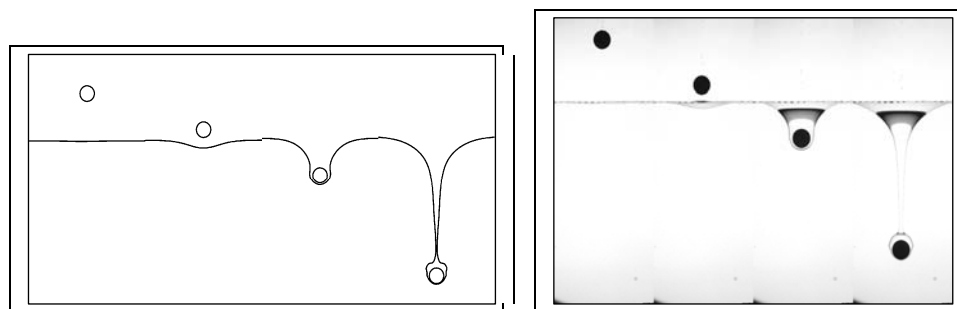


Figure 1: Passage of a 10 mm PTFE sphere through a silicon oil (H47V500) - water interface. Computational results (left) vs. experimental evolution (right). The time step between two frame is $dt=0.25s$.

The thin-film flow beneath a vesicle during adhesion processes

M. J. Blount^a, M. J. Miksis^b and S. H. Davis^b

We analyse the motion of a two-dimensional vesicle as it adheres to a rigid substrate, in the regime where the adhesive interaction is not strong enough to significantly dilate the vesicle's membrane wall. We use a long-range attractive, short-range repulsive potential to model the adhesive interaction so that a very thin precursor-type film is formed beneath the vesicle as it adheres, and focus on the flow within this film as the vesicle adheres.

We first consider the behaviour of an adhered vesicle that is close to equilibrium. The underside of the vesicle is almost flat, with narrow 'contact regions' at the edges that are governed by adhesive and bending stresses, and which match away from the substrate towards an 'outer region' where adhesive stresses are negligible. We use a lubrication approximation to analyse the evolution of these regions, and obtain travelling-wave solutions that represent the vesicle either spreading or retracting along the substrate. These solutions yield an estimate for the rate of spreading (or retraction) of the vesicle, which depends on the curvature of the membrane in the outer region as it approaches the substrate. By matching the travelling-wave solution towards a quasi-static outer solution, we derive an estimate for the spreading rate of the vesicle throughout the adhesion process. We compare this estimate against boundary-integral simulations, but find that it is accurate only if the vesicle's initial shape is close enough to equilibrium that its underside is already flat. In general, there is typically a transient behaviour in which the underside of the vesicle does not simply form a flat adhered region, but instead deforms and traps a 'dimple' of fluid, in a similar way as has been observed in the context of sedimenting viscous droplets.

We develop a modified lubrication model that describes the formation and subsequent behaviour of the dimple of fluid beneath the vesicle. This model is similar to an earlier modified lubrication analysis developed for viscous droplets in that it allows the membrane's inclination to have a finite amplitude. A novel aspect of the present model is that the interface is not a fluid-fluid interface for which the tension is known, but is instead a membrane whose tension varies spatially and must be solved for as part of the problem. The results of this model are compared with boundary-integral simulations, and the implications towards vesicle-vesicle interactions are discussed.

^a School of Mathematics, Cardiff University, Cardiff CF24 4AG, UK

^b Engineering Sciences and Applied Mathematics, Northwestern University, Evanston IL 60208, USA

Free Surface Flows Waves

Surface waves generated with an underwater movable bottom

L. Gordillo^a, T. Jamin^a, M. Berhanu^a and E. Falcon^a

We report several laboratory experiments on surface waves generated in a fluid layer whose bottom undergoes vertical motion. The layer is confined in a long channel whose bottom central region is deformable. The region is composed of sixteen independent pistons that can be moved upward or downward with an arbitrary displacement function. The outcome of the system is characterized in terms of the velocity field and the free-surface deformation via Particle Image Velocimetry and Fourier-Transform Profilometry.

Depending on the choice of the displacement function, we are able to reproduce different one-dimensional tsunami scenarios as: varying bathymetry, simultaneous bed downthrust and upthrust, fault propagation, submarine landslides and other more complex spatiotemporal scenarios. The system also allows high amplitude deformations that yield nonlinear responses of the systems.

Besides some theoretical analysis, many of these scenarios have never been studied through experiments. Our results can be used to identify potential threats in tsunami areas. They also provide useful information for tsunami generation in current numerical simulations.[†]

^a Laboratoire Matière et Systèmes Complexes (MSC), UMR 7057 CNRS, Université Paris 7 Diderot, 75205 Paris Cedex 13, France

[†] This work is financed by the AXA Research Fund.

Shear flow and free surface effects generated by a surface-piercing plate

L. G. Westerberg^a, S. Lindqvist^a, J. Sheridan^b and T. S. Lundström^a

The two-dimensional vortical flow induced by a vertical flat plate submerged in the normal direction to the flow direction in a water channel is experimentally investigated using flow visualisations, particle image velocimetry, and proper orthogonal decomposition. The main objectives with this study are: i) The generation of vorticity and the Froude- and Reynolds number dependency of the flow pattern in terms of the shear layer angle, separation point upstream of the plate and point of reattachment with the free surface downstream, and ii) The vortical flow effect on the free surface with respect to surface level and surface structure. The Froude- and Reynolds number which both are based on the free stream velocity and insertion depth of the plate ranges from 0.07 to 2.25 and $1.8 \cdot 10^2$ to $1.24 \cdot 10^4$ respectively. It is shown that the flow in connection to the free surface undergoes a series of transformations as the Froude- and Reynolds number increases, with growth and decay of the recirculation region downstream of the plate, and waves occurring upstream of the plate and on the surface depression downstream. Furthermore, a relation between the Reynolds number and the shear layer angle is suggested, where the angle is proportional to the Reynolds number to the power 0.1. A relation between the difference in surface level up- and downstream of the plate is also obtained, showing the level difference to be proportional to the square of the Froude number.

^a Division of Fluid and Experimental Mechanics, Luleå University of Technology, SE-971 87 Luleå, Sweden.

^b Fluids Laboratory for Aeronautical and Industrial Research (FLAIR), Department of Mechanical and Aerospace Engineering, Monash University, VIC 3800, Australia.

Capillary-gravity wakes

M. Rabaud¹ and F. Moisy¹

Contrary to what is usually thought, ship wakes narrower than the Kelvin prediction are observed for boats moving at large hull Froude number. This result has been recently explained^{2,3} by taking into account the finite range of wave numbers excited by a disturbance of finite size. We investigate here the wake behind small objects, for which capillary effects cannot be neglected. In the case of a small cylinder towed at constant velocity U at the air/water interface, we show experimentally that, in the far field and above a critical velocity, the waves of maximum amplitude are again located on a V-shape, and that the half-angle α of the wake decreases as c/U . However, whereas the relevant velocity c is the group velocity of wavelength given by the disturbance size in the pure gravity case, we show here that c is now the minimum value of the group velocity of capillary-gravity waves⁴. This new behaviour, confirmed by numerical simulations, can be understood from the presence of a capillary cusp angle in the wake pattern, distinct from the usual Kelvin cusp angle at 19.47° .

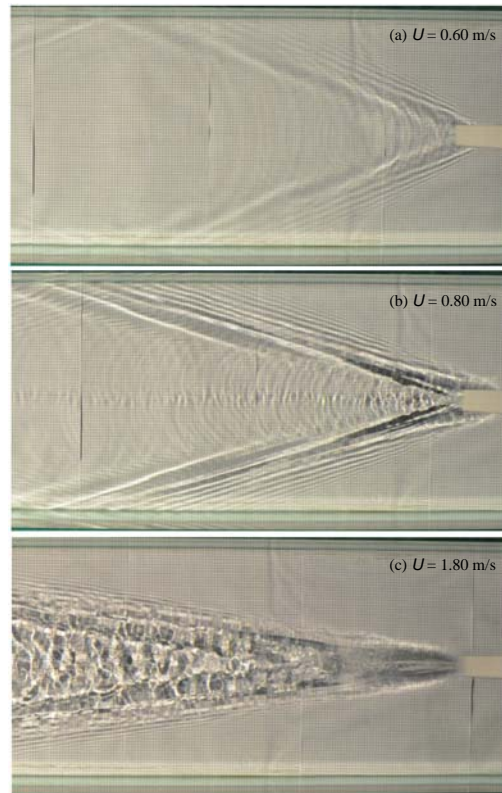


Figure 1: Wave pattern for a cylinder of diameter 1.5 mm moving at 0.60 (a), 0.80 (b) and 1.8 m/s (c).

¹ Univ. Paris-Sud, CNRS, Laboratory FAST, bât. 502, 91405 Orsay Cedex, France

² Rabaud and Moisy. *Phys. Rev. Lett.*, **110**, 214503 (2013).

³ Darmon et al., *J. Fluid Mech.* 738, R3 (2014).

⁴ Moisy and Rabaud. Mach-like capillary-gravity wakes, preprint (2014).

On the destabilizing influence of the surface tension in planar wakes

L. Biancofiore^a, F. Gallaire^b and E. Heifetz^c

A counterintuitive destabilizing effect of the surface tension in planar wakes was observed by Tammisola et al.¹ and Biancofiore et al. (2014)² by means of a linear global analysis and DNS, respectively. This destabilization can be interpreted by the presence of two different temporal unstable modes found when analyzing the local stability of an extracted velocity profile from the base flow¹.

In the present study, we approximate the velocity profile of a wake flow through a piecewise broken-line profile. We then explain the presence of these two temporal unstable modes using the counterpropagating Rossby wave (CRW) perspective, which associates to each vorticity discontinuity an individual Rossby wave³. The introduction of a finite amount of surface tension at the interface creates two capillary waves (CW) which move with the same velocity but in opposite directions. The interaction of these four waves originates in two temporal unstable modes for both sinuous and varicose symmetries.

Furthermore, we have captured the spatio temporal evolution of the interacting four-waves system by means of an impulse response analysis. The spreading of the wavepacket is enhanced by the surface tension as illustrated in figure 1 causing the destabilization.

^a Department of Mechanical Engineering, Imperial College London, London SW7 2AZ, United Kingdom

^b LFMI EPFL, Route Cantonale, CH-1015, Lausanne, Switzerland

^c Department of Geophysics and Planetary Sciences, Tel-Aviv University, Tel-Aviv 69978, Israel

¹ Tammisola et al., *Phys. Fluids*, **23**, 014108 (2011).

² Biancofiore et al., *Fluid Dyn. Res.*, accepted, (2014)

³ Heifetz et al., *Q. J. R. Meteorol. Soc.*, **125**, 2835 (1999).

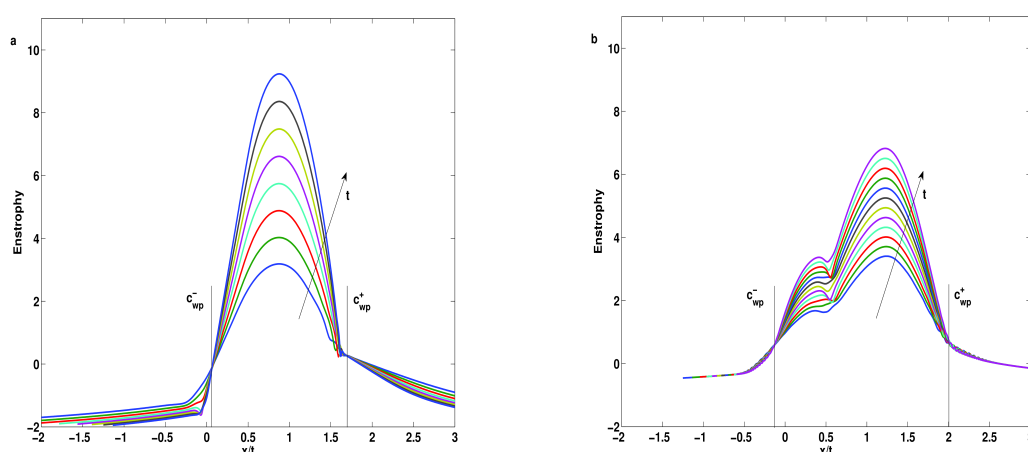


Figure 1: Enstrophy wave packet (a) without surface tension (b) with surface tension.

Constant Froude number in a circular hydraulic jump and its implication on the jump radius selection

A. Duchesne^a, L. Lebon^a and Laurent Limat^a

In the literature, it is known that the properties of a standard hydraulic jump depend critically on a Froude number Fr defined by the ratio between the flow speed and the gravity waves speed: Fr is larger than 1 upstream of the shock, and smaller than 1 downstream, an accumulation of gravity waves occurring at the shock with formation of a sharp liquid wall. Surprisingly, to our knowledge, the question of the Froude number value has never been explored in detail for the circular hydraulic jump formed by an impinging jet on a horizontal surface (see figure 1) although the circular hydraulic jump has inspired a rich literature^{1,2,3,4,5,6}.

We have investigated carefully this question, varying the flow rate, the liquid viscosity, the surface tension and geometrical parameters (nozzle diameters, disk diameters, nozzle-plate distance...). We have found that, in the specific case of a circular jump with no confinement walls, the Froude number defined at the jump exit is independent of the physical parameters (flow rate, viscosity, surface tension) and weakly dependent on the geometrical parameters.

We examine the implications of a constant Froude number on the selection of the jump radius R_j , after combining it with the large-scale flow structure⁵ around the jump, calculated in the lubrication limit. In agreement with our data, R_j is very close to follow the scaling proposed by Bohr⁴, but this scaling has to be modified by introducing non negligible logarithmic corrections (see Figure 2):

$$R_j \ln\left(\frac{R_\infty}{R_j}\right)^{3/8} \propto Q^{5/8} \nu^{-3/8} g^{-1/8} \quad (1), \text{ where } Q \text{ is the flow rate, } \nu \text{ the kinematic}$$

viscosity and g the acceleration due to gravity. We also discuss the influence of the geometrical parameters on the Froude number value and the implications of our results in terms of Watson description of the shock².

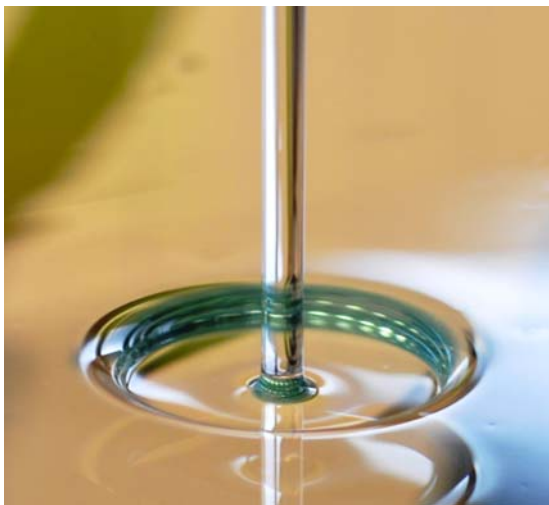


Figure 1: A jet of liquid impacts vertically a horizontal surface. A circular hydraulic jump is observed

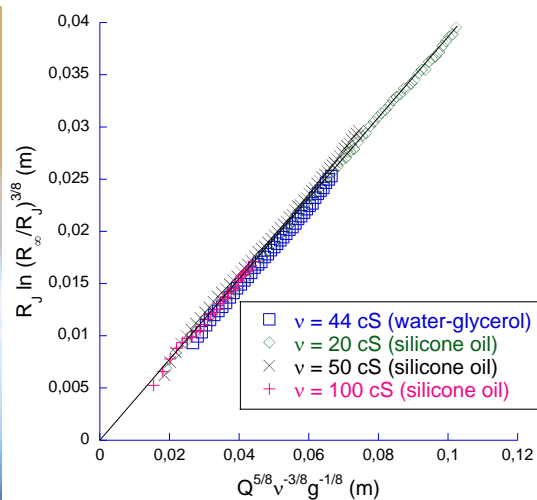


Figure 2: Experimental test of eq. (1) for three silicone oils of different viscosities and for a water-glycerol-mixture.

^a Matière et Systèmes Complexes, CNRS and Université Paris Diderot, UMR 7057, Bâtiment Condorcet, 10 rue Alice Domon et Léonie Duquet, 75013 Paris, France

¹ Tani, *J. Phys. Soc. Japan* **4**, 212 (1949)

² Watson, *J. Fluid Mech.* **20**, 481 (1964)

³ Craik et al., *J. Fluid Mech.* **112**, 347 (1981)

⁴ Bohr et al., *J. Fluid Mech.* **254**, 635 (1993)

⁵ Watanabe et al., *J. Fluid Mech.* **480**, 233 (2003)

⁶ Bush and J. M. Aristoff, *J. Fluid Mech.* **489**, 229 (2003)

Normal impact of a jet on an inclined plate, varying the wetting properties

A. Duchesne^a, R. Herbaut, L. Lebon^a and L. Limat^a

We have experimentally investigated the structure of the flow on an inclined plate, when this one is impacted by a continuous jet of liquid under normal incidence, varying the fluid properties, the plate inclination and the wetting conditions. Under partial wetting, a hydraulic jump is formed on the plate, strongly interacting with the contact line surrounding the wetted domain, the hydraulic jump remaining closed at low plate slope but becoming opened at high slope (horseshoe structure). A similar structure is observed under total wetting conditions, the "true" contact line being replaced with an effective contact line, static but under dynamical equilibrium, and surrounded by a very thin layer of liquid. Focussing on the hydraulic jump structure, we found that its typical scales follow closely the scaling laws upon flow rate and fluid properties proposed by Bohr et al¹ in the total wetting case, but not in the partial wetting case at low flow rate, where a cross-over to a linear flow rate dependance is observed². In the case of a superhydrophobic plate, the jump and the contact line are coalesced in a single atomisation front, whose typical radius is governed by a balance between the radial momentum carried by the liquid in a Watson approximation of the flow³, and the surface tension effects. We present the results obtained in the three cases, propose approximate solutions for each of these ones, and compare with other available approaches of this kind of flow^{4,5}.

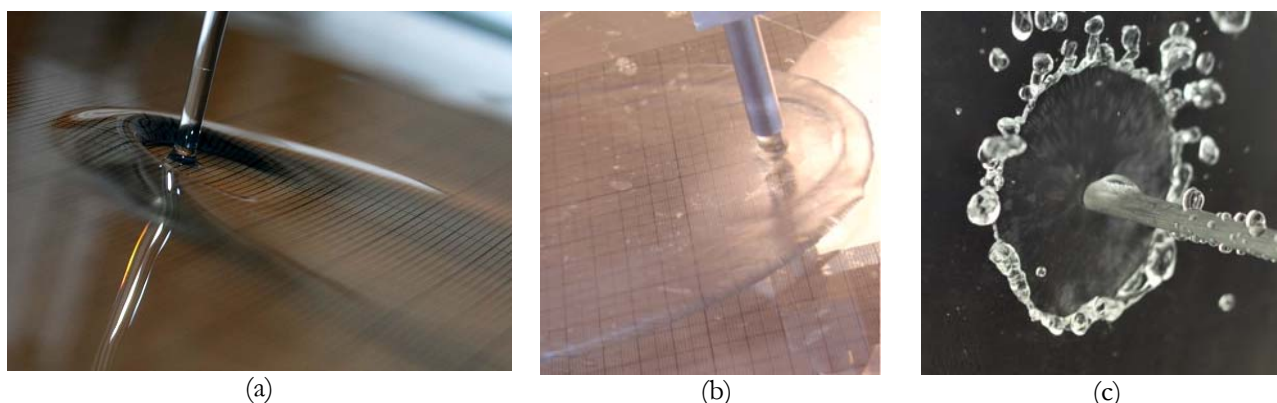


Figure: From left to right: (a) impact under total wetting conditions, (b) under partial wetting conditions, and (c) on a superhydrophobic plate.

^a MPatière et Systèmes Complexes, CNRS and Université Paris Diderot, UMR 7057, Bâtiment Condorcet, 10 rue Alice Domon et Léonie Duquet, 75013 Paris, France

¹ T. Bohr, P. Dimon and V. Putkaradze, "Asymptotic Properties of the Circular Hydraulic Jump", *J. Fluid Mech.* **254**, 635 (1993)

² A. Duchesne, L. Lebon and L. Limat, "Impact on an inclined plate: contact line versus hydraulic jump", ECS2013, European Coating Symposium, Mons, Belgium, September 11-13 (2013), Book of extended abstracts, p. 48.□□□□□□□□

³ E. J. Watson, "The radial spread of a liquid jet over a horizontal plane", *J. Fluid. Mech.* **20**, 481-499 (1964)

⁴ J.-L. Thiffeault, A. Belmonte, "Hydraulic jumps on an incline", *arXiv:1009.0083*, (2010)

⁵ T. Wang, D. Faria, L.J. Stevens, J.S.C. Tan, J.F. Davidson, D.I. Wilson, "Flow patterns and draining films created by horizontal and inclined coherent water jets impinging on vertical walls", *Chemical Engineering Science*, **102**, 585-601 (2013).

Global dynamics of *transonic* gravitational liquid sheet flows

Michele Girfoglio^a, Fortunato De Rosa^a, Gennaro Coppola^a, and Luigi de Luca^a

It is known that the basic nature of the global dynamics of gravitational (and, therefore, spatially developing) liquid sheet flows, in the presence of surface tension effects, depends crucially^{1,2} on the inlet Weber number, $We = \rho U_o^2 h_o / \sigma$, where ρ is the liquid density, U_o is the inlet liquid velocity, h_o is the initial half thickness of the sheet, σ is the surface tension at the air-liquid interface. When $We > 1$, the local Weber number too is greater than unity at each streamwise (i.e., vertical) location, so that the flow can be defined *supersonic* everywhere, in the sense that the local flow velocity exceeds the capillary waves velocity $\sqrt{\sigma / \rho h}$, where h is the local sheet thickness. On the other hand, when $We < 1$, there exists an initial region where the sheet flow is *subsonic*, up to the *transonic* location, downstream of which the flow becomes *supersonic*. Since the experimental evidence is that the sheet breaks-up in flow conditions of $We < 1$ only, the analysis of the flow field initially *subsonic*, and hence including the *transonic* line, is mandatory to predict the rupture conditions.

From the theoretical viewpoint the problem is not straightforward, because the equation governing the evolution of global linear disturbances exhibits a singularity just at the *transonic* station, as documented also by previous contributions of literature^{3,4}, although the solution to the problem is not yet yielded. Thus, the present work is aimed at developing a theoretical/numerical procedure to fill up this lack of information.

Within this framework, the flow is assumed inviscid and the problem is arranged in 1D formulation along the streamwise direction by expressing all the physical quantities through a coordinate-type expansion in terms of powers of the local lateral distance from the centerline position. The interaction with the external environment refers to an air enclosure located on one side of the curtain. The linearized perturbation equations are determined in a standard fashion by superimposing infinitesimal disturbances to the steady solution and the modal global stability is studied by addressing the relevant singular eigenvalues problem.

The dimensionless governing equation of sinuous disturbances can be written as:

$$U \left(U - \frac{1}{We} \right) \frac{\partial^2 f}{\partial x^2} + 2U \frac{\partial^2 f}{\partial x \partial t} + \frac{\partial^2 f}{\partial t^2} + \frac{\partial f}{\partial x} = -kU \int_0^L f dx$$

where $U = \sqrt{1+2x}$ is the classic free-fall Torricelli's solution, f is the centerline deflection of the sheet, k is a proper compressibility coefficient of the air enclosure and L is the curtain length.

It is shown that the *transonic* location can be classified as a regular singular point and a solution in terms of Frobenius series⁵ is introduced in order to provide the local solution around the singularity. The non-linear eigenvalues problem obtained accordingly is faced as a nonlinear two-point boundary problem (in which the searched eigenvalue is considered as an unknown function) that is solved by means of a shooting technique⁶. The boundary conditions are of null sheet displacement at inlet and boundedness at the singularity location^{3,4}.

The numerical results show the spectra pattern obtained when the inlet We number is varied from *subsonic* to *transonic* values, with particular attention to their evolution with respect to cases of entirely *supersonic* flow analyzed with standard spectral methods. The physical relevance of the present findings is discussed as well.

^a University of Naples Federico II, Dept. Industrial Eng., Aerospace Sector, Piazzale Tecchio 80, Naples, ITALY, deluca@unina.it

¹ de Luca, J. *Fluid Mech.* **399**, 355 (1999).

² Le Grand-Piteira et al., *Phys. Rev. E* **74**, 026305 (2006)

³ Finnium et al., J. *Fluid Mech.* **255**, 647 (1993).

⁴ Weinstein et al., *Phys. Fluids* **9**, 1815 (1997).

⁵ Bender and Orszag, *Springer* (1999).

⁶ Press et al., *Cambridge University Press* (1992).

Vortical

Experimental observations of trailing vortices at high Reynolds numbers

A. Gallardo-Claros^a, J.J. Serano-Aguilera^b, L. Parras^a and C. del Pino^a

Experimental techniques applied to the study of wingtip vortices are of great interest for the Fluid Mechanics Community. The available experimental techniques to obtain new insights into trailing vortices, focus on quantitative methods, e.g. Particle Image Velocimetry (PIV)^{1,2}. In fact, this technique requires high costs associated not only to equipments but also to image processing that is a complex, and time consuming task. A novel, easier, faster and cheaper experimental procedure is presented in this research work to compute experimentally the vortex structure in comparison to a theoretical model.

Different theoretical models have described the velocity field for every cross section along the axial coordinate, once the vortex was created at the wing tip. These models depend on several parameters and provide the axial evolution of the velocity field. We used in this study a q-vortex or Batchelor's³ model, based only on two free parameters: swirl value, q , and the virtual origin in the axial coordinate, z_0 . These parameters have been processed with the experimental trailing vortex formed by a NACA0012 aerofoil over a Reynolds number range of 10^5 .

The experimental setup consists of one smoke wire device together with a laser beam, and a digital camera installed in a subsonic wind tunnel. A smoke segment was generated upstream the model, but near the wing edge. This line followed the main stream passing through the wing tip. Lift forces produced the characteristic vortex pattern, highlighted by the swirling smoke segment, and whose topological structure was recorded by a digital camera. Several sections at different axial distances from the wing edge have been analyzed. The integration of the velocity field in the theoretical model allowed us to know two theoretical parameters in order to obtain similar experimental streaklines at a given axial position, as shown in figure 1. The experimental results using this procedure were in agreement with those found in the literature¹.

This work has been supported by the Grant Proyecto de Excelencia nº TEP-7776.

^a ETSI Industriales, C/ Doctor Ortiz Ramos S/N, 29071 Málaga, Spain.

^b CIEMAT-Plataforma Solar de Almería, Crta. de Senés, km. 4.5, E04200 Tabernas, Almería, Spain

¹ C. del Pino, L. Parras, M. Felli y R. Fernández-Feria. *Structure of trailing vortices: Comparison between particle image velocimetry measurements and theoretical models*. Physics of Fluids. 23, 013602 (2011).

² Myong Hwan Sohn, Jo Won Chang. *Visualization and PIV study of wing-tip vortices for three different tip configurations*. Aerospace Science and Technology. 16(1), 40 (2012).

³ G. K. Batchelor. *Axial Flow in trailing line vortices*. J. Fluid Mech. 20,645 (1964).

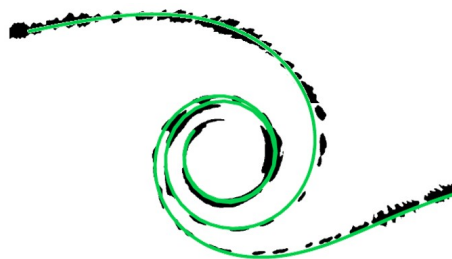


Figure 1: Processed image: Smoke (black) and theoretical streakline (green) for a trailing vortex.

Buoyancy-Induced Columnar Vortices Formed by Solar-Heated Air

Mark Simpson^a, and Ari Glezer^a

Naturally-occurring, buoyancy-driven columnar vortices (“dust devils”) that are driven by an instability of the thermally stratified, ground-heated air layer and are sustained by entrainment of the ground-heated air, occur spontaneously in the natural environment with core diameters of 1-50 m and heights up to one km. These vortices convert low-grade waste heat in the air layer overlying the warm surface into a flow with significant kinetic energy that may be exploited for power generation by coupling the vortex to a vertical-axis turbine. Unlike “dust devil” vortices which are typically free to wander laterally, an anchored column vortex can be deliberately triggered within a cylindrical domain bounded by an azimuthal array of stationary ground-mounted vertical vanes sustained by continuous entrainment of the heated air through these vanes. The considerable kinetic energy of the vortex column cannot be explained by buoyancy alone, and the fundamental mechanisms associated with the formation, evolution, and dynamics of an anchored, buoyancy-driven columnar vortex are investigated in a laboratory facility using a heated ground plane and an azimuthal array of flow vanes. The present investigation focuses on the vortex formation, structure, and the dependence of its scaling and strength on the thermal resources and the characteristic scales of the anchoring flow vanes. Specific emphasis will be placed on the production, advection, and tilting of vorticity within the entrained boundary layer and, in particular, the manipulation of these mechanisms for increasing the available kinetic energy and therefore the generated power. Outdoor tests of a meter-scale prototype coupled with a simple vertical axis turbine and placed on a surface that is directly heated by solar radiation have demonstrated continuous rotation of the turbine with significant extraction of kinetic energy from the columnar vortex in the absence and presence of cross wind.

^a Mech. Eng., Georgia Institute of Technology, 771 Ferst Drive., Atlanta, GA, USA

Curvature instability of a helical vortex tube with axial flow

Francisco J. Blanco-Rodriguez^a, Stéphane Le Dizès^a

The linear stability of a helical vortex tube with axial flow is studied in the regime of large Reynolds numbers using a combination of asymptotical and numerical methods. The base flow mimics the flow generated by a wind turbine or helicopter rotor.

The base flow is described using asymptotical methods by assuming that the ratio ε of vortex core radius to the curvature radius is small. At leading order, the base flow is then a columnar vortex aligned along with the helix centreline. We assume that the axial velocity and the vorticity of the vortex are both Gaussian (Batchelor vortex). Curvature corrections are obtained as first order corrections, while torsion and strain field corrections appears at second order¹.

As for the elliptical instability², curvature instability can be interpreted as a resonant coupling of two quasi-neutral Kelvin modes³ of the vortex with the correction terms. The azimuthal structure of the curvature terms in $e^{i\varphi}$ is however different from that of the strain field responsible for the elliptical instability. The condition of resonance is therefore different. For the curvature instability, it amounts in finding two neutral modes of azimuthal wavenumbers m and $m+1$ of same frequency ω and same axial wavenumber k_c . By using a *WKB* description⁴ of the Kelvin modes, we first show that this condition of resonance can only be fulfilled in a small parameter range and that it necessarily involves a Kelvin mode with a critical layer. The resonant modes are obtained numerically using a Chebyshev collocation method and an adequate contour deformation rule⁵ to avoid the critical layer singularity. For each resonant configuration, the growth rate σ is obtained by considering the interaction between the curvature terms and the Kelvin modes, and as for the elliptical instability⁶, it reduces to an explicit expression

$$\left(\sigma + (k - k_c) Q_m - \frac{1}{\text{Re}} P_m \right) \left(\sigma + (k - k_c) Q_{m+1} - \frac{1}{\text{Re}} P_{m+1} \right) - \varepsilon^2 R_m R_{m+1} = 0, \quad (1)$$

in terms of the wavenumber k , the Reynolds number Re and ε , with numerically computed complex coefficients Q_j , P_j and R_j .

The growth rate of each resonant configuration has been systematically calculated for the Batchelor vortex for swirl numbers ranging from 2 to ∞ . Typically, we observe that the maximum normalized growth rate remains small (typically 0.01ε the maximum vorticity) contrarily to what has been recently obtained for the Rankine vortex⁷. We explain this difference by the more complicated structure of the resonant modes for the Batchelor vortex.

Due to the small value of the growth rate, the curvature instability may be dominated by the elliptical instability generated at the order ε^2 if ε is not small enough. We provide the critical value of ε for this occurrence.

This work is supported by the French *Agence Nationale de la Recherche* through the A*MIDEX grant ANR-11-IDEX-0001-02, the LABEX MEC project ANR-11-LABX-0092 and the ANR HELIX project ANR-12-BS09-0023-01.

^a IRPHE, UMR7342, Aix-Marseille University, CNRS, Centrale Marseille, 49 rue Frédéric Joliot Curie, 13384 Marseille, FRANCE

¹ Fukumoto and Okulov, *Phys. Fluids* **17**, 107101 (2005).

² Moore and Saffman, *Phil. Trans. R. Soc. Lond. A* **346**, 413 (1975).

³ Hattori and Fukumoto, *Theor. Comp. Fluid Dyn.* **24**, 363 (2010).

⁴ Le Dizès and Lacaze, *J. Fluid Mech.* **542**, 69 (2005).

⁵ Lin, *The Theory of Hydrodynamics Stability*, Cambridge (1955).

⁶ Eloy and Le Dizès, *J. Fluid Mech.* **378**, 145 (1999).

⁷ Hattori and Fukumoto, *J. Fluid Mech.* **738**, 22 (2014).

Optimal non-linear perturbation of a vortex column

H. Johnson^a, V. Brion^a and L. Jacquin^a

Vortices are present in all complex fluid flows and can have either desirable or undesirable effects on the flow properties depending on the application. For example, for security and economic reasons, it is advantageous to accelerate destruction of trailing vortices in aircraft wakes in order to increase airport take-off and landing recurrences¹. On the contrary, mixing is improved by the presence of turbulent vortices, which is therefore encouraged in combustion chambers. For all of these applications, vortex stability control is key.

It has been established in relevant literature^{2,3} that the optimal long-term linear initial condition corresponds to the adjoint of the most unstable direct mode. However, including the non-linearity of the flow changes its dynamics and may greatly modify the appearance of the optimal long-term initial condition. Similar non-linear studies have been undertaken for other flows such as shear flow turbulence^{4,5} which provide validation cases for the optimization method.

In the present study, a non-linear optimization technique is applied to a simple columnar vortex by direct numerical simulation. Using a lagrangian method, we optimize perturbation energy growth by successive integrations of the direct and adjoint incompressible Navier-Stokes equations until convergence. Comparisons are made between the results of the non-linear optimization and the adjoint of the most unstable direct mode which is also computed. Physical insight into the non-linear mechanisms at play is given.

^a Fundamental and Experimental Aerodynamics Department (DAFE), Onera, Meudon, France

¹ Crow, *ALAA Journal* **8**, 2172 (1970)

² Farrell, *Phys. Fluids* **31**, 2093 (1988)

³ Schmid and Henningson, *Applied Mathematical Sciences* **142** (2002)

⁴ Pringle et al., *J. Fluid Mech.* **702**, 415 (2012)

⁵ Cherubini and De Palma, *J. Fluid Mech.* **716**, 251 (2013)

Simulations of vortical flow using an unbounded, regularized particle-mesh based vortex method

M. M. Hejlesen¹ and J. H. Walther^{a,2}

In the present work we use an unbounded vortex method to perform direct numerical simulations of vortical flow. The method uses a recently developed unbounded Poisson solver¹, which is based on regularized Greens functions to obtain high order convergence. By simulating vortical flows with unbounded conditions we are able to: minimize the size of the computational domain, avoiding the effect of periodicity and thus performing simulations at high Reynolds number. The high order Poisson solver has been implemented in an unbounded particle-mesh based vortex method which uses a re-meshing of the vortex particles to ensure the convergence of the method. Furthermore, a re-projection of the vorticity field is performed at each time step to ensure a divergence free vorticity field.

The primary focus of the presentation is a detailed analysis of the vorticity topology obtained from numerical simulations of vortical flows. The deformation and alignment of vorticity (see Fig. 1) has been identified as an essential process in the characteristic energy cascade of turbulence. As the vorticity is stretched into sheet- and tube-like structures, the conservation of angular momentum constitutes an energy transfer between different length scales of the flow. The alignment of vorticity is also directly related to other phenomena in fluid dynamics such as sound generation. Thus an in depth knowledge of vortex deformation and alignment is essential for multiple disciplines in fluid dynamics.



Figure 1: Simulation of a single vortex ring at a circulation based Reynolds number of 10.000. The vortex ring motion is from left to right. The pictures show the evolution of a single isosurface of the vorticity colored by the mis-alignment of the vorticity and the second eigenvector of the strain rate tensor.

¹ Dep. Mechanical Engineering, Technical University of Denmark, DK-2800 Kgs. Lyngby, Denmark.

² Computational Science and Engineering Laboratory, ETH Zürich, CH-8092 Zürich, Switzerland

¹ Hejlesen et al., *J. Comp. Phys.* **252**, (2013).

Vortex breakdown in the near-wake of 25° Ahmed body

C. Jermann^{ab}, P. Meliga^a, G. Pujals^b, E. Serre^a and F. Gallaire^c

The Ahmed body is an academic test-case meant to reproduce a wide range of the flow features encountered in automotive aerodynamics. In the present study, we focus on the 25 deg. slanted rear end, which is known to produce a fully three-dimensional, unsteady state consisting of a separation bubble over the slanted surface with highly energetic streamwise vortices issuing from the slant side edges, as observed experimentally by Lienhart et al². The present work relies on high resolution Automated Stereo-PIV to clarify the structure and dynamics of the longitudinal vortices at high Reynolds number ($Re = 2.8 \times 10^6$ based on the length of the geometry). A collection of 40 planes along the rear slant and 40 additional planes in the wake with a spatial resolution of $dx = 5$ mm, $dy = 1.5$ mm and $dz = 1.5$ mm was used to reconstruct the fully three-dimensional (3D) time averaged mean flow. In addition, static pressure was acquired in the vortex core along the streamwise direction by the use of a pitot tube inclined following the vortex path deduced from 3D velocity field. The vortex core undergoes a sharp decay of streamwise velocity in the near wake ($1 < x < 2$, see Figure 1(a)) which suggests possible occurrence of vortex breakdown. Confirmation comes from the sign switch of the azimuthal vorticity in the longitudinal plane intersecting the vortex core. An abrupt change occurs 0.4 times the projected length of slanted window downstream of the square back, as marked by the vertical dashed line in Figure 1(b), and can be seen as the result of the divergence of axial vortex lines brought by an adverse pressure gradient, according to the work of Brown and Lopez¹. The location of the sign switch seems strongly correlated to the modification of streamwise velocity as seen from Figure 1(c): initially in a uniform state, a low speed region appears followed by a conical shape of similar aspect than the experimental data obtained by Sarpakaya³ in slightly diverging cylindrical tube at high Reynolds number.

^a M2P2, UMR 7340 CNRS, Aix-Marseille Université, Centrale Marseille, 13451 Marseille, France

^b PSA Peugeot-Citroën, 78943 Vélizy Villacoublay, France

^c LFMI, Ecole Polytechnique Fédérale de Lausanne, CH1015 Lausanne, Suisse

¹ Brown and Lopez, *J. Fluid Mech.* **221**(1), 553-576 (2009)

² Lienhart et al., *New Results in Numerical and Experimental Fluid Mechanics III*, 323-330 (2002)

³ Sarpkaya, *Phys. Fluids* **7**(10), 2301-2303 (1995)

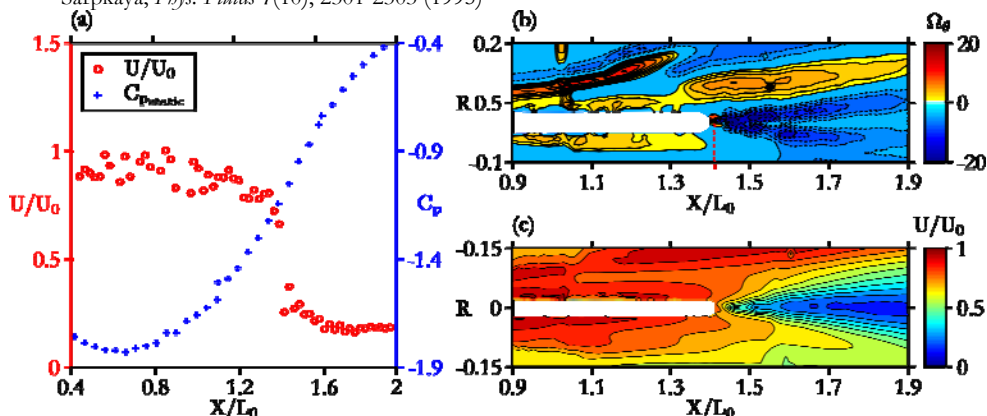


Figure 1: (a) Evolution of streamwise velocity and static pressure in the vortex core along the streamwise direction. (b) Contours of time-averaged azimuthal vorticity in the longitudinal plane intersecting the vortex core axis. (c) Contours of time-averaged streamwise velocity in the longitudinal plane intersecting the vortex core axis.

Experimental evidence of a complex topology in confined vortex flows

I.V. Naumov^a, R.F. Mikkelsen^b, I.K. Kabardin^a, V.L. Okulov^{a,b} and J.N. Sørensen^b

A fundamental fluid mechanics subject concerns the problem of how to mix fluid most efficiently. In most cases mixing in confined flows is accomplished by introducing rotation in closed devices filled by different fluid components. The simplest prototype of such a device is a closed cylinder with rotating top or bottom endwalls in which the flow undergoes a vortex breakdown. Vortex breakdown appears in strongly swirling flow and is characterized by an abrupt structural change of the flow topology, resulting in the appearance of helical vortices and/or axisymmetric zones with recirculating flows, which strongly enhances the mixing properties of the flow. In order to control mixing it is important to understand and to model correctly confined flows associated with vortex breakdown.

In the cylindrical cavity at a high height to radius ratio ($H/R > 3.5$) we have experimentally resolved a number of new topologies of swirling flows with different regions of counter flows (modes of vortex breakdown with many bubbles). In our experimental series we have generated the swirling flow by one or both rotating endwalls at co- and counter directions. Until now, the possibility of bubble modes from one, two and three breakdowns has been experimentally analysed in cavities at moderate aspect ratio ($H/R < 3.5$), while flows in cylinders of high aspect ratio are associated with regimes of self organized helical vortex multiplets¹. For cases with co- and counter-rotating top and bottom of a cylindrical cavity at small aspect ratio $H/R \leq 2.5$ the flow regimes with recirculation bubbles has up to now been investigated numerically^{2, 3} by solution of the steady equations for motion of the viscous flow. In the present work we continue the numerically investigations by detailed experimental analysis using PIV and LDA measurements. Examples of the flow patterns with unstable bubble modes of vortex breakdown is shown in the figure 1. This regimes were observed in the cavity with $H/R = 4$ for case with one and two rotating lids.

^a Dep. of Physical Hydrodynamics, Institute of Thermophysics SB RAS, Lavrentyeva Ave.1, Novosibirsk, 630090, Russian Federation

^b Dep. of Wind energy, Technical University of Denmark, 403 Nils Koppels Alle, Lyngby, 2800, Denmark.

¹ Sørensen et al., *J. Fluid Mech.* **682**, 430 (2011)

² Nore et al., *J. Fluid Mech.* **477**, 51 (2003)

³ Okulov et al., *European J. Mechanics B*, **24**, 137 (2005)

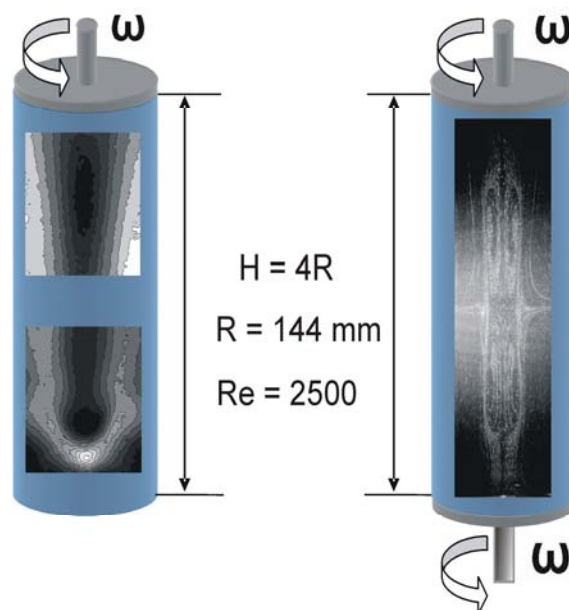


Figure 1: Axial velocity components from PIV measurements in configuration with up lid rotation (a) and two lids co rotation by particles visualization (b) in the same flow parameters

Long-wave instability of a helical vortex

H. U. Quaranta^a, T. Leweke^a

The near wake behind single- or multi-bladed rotors consists of one or several interlaced helical vortices, generated at the tips of the rotor blades. Various instabilities can exist in this system, involving perturbations at different wavelengths: long-wave displacement modes or short-wave vortex core deformations. The former, whose general dynamics can be described by a filament approach involving the Biot-Savart law for self- and mutually induced motion, can be interpreted as a global or local pairing of neighbouring helix loops.

Motivated by recent experimental results concerning this phenomenon, we here revisit and extend the theoretical analyses of long-wave instabilities in an infinite single helical vortex of Rankine type made by Widnall¹ and Gupta & Loewy². In these studies, two different approaches were used to deal with the singular behaviour of the Biot-Savart integrals for the self-induced motion of vortex filaments, introducing a finite core size: Widnall used a cut-off length, proportional to the core radius, to exclude the singularity from the integration, and Gupta & Loewy employed a method initially proposed by Rosenhead³, adding a constant finite length to the denominator of the Biot-Savart integral to avoid its divergence, but using an incorrect proportionality with the core size.

Both analyses predict instability of the helical vortex, involving deformations leading to local pairing at various locations along the filament, depending on the perturbation wave number. We illustrate the structure of the unstable modes (e.g. in figure 1a), and compare the two predictions for the growth rate, as function of the geometrical parameters (radius R , pitch, core radius) and the circulation Γ of the initial helix. The domain of validity of these results, with respect to the long-wave approximation used in these studies, is also determined.

We then extend the analysis to include more realistic vortex velocity profiles (Gaussian vorticity, axial flow), using the concept of equivalent core size⁴, as well as the effect of a central “hub” vortex. Finally, this theory is compared to experimental measurements made in the wake of a small-scale single-bladed rotor placed in a water channel, where controlled perturbations could be introduced by modulating the speed of the stepper motor driving the blade rotation. Despite the spatial evolution of the rotor wake (as opposed to the uniform helix considered in the analysis), the measured growth rates agree very well with the theoretical predictions (figure 1b).

This work is supported by the French *Agence Nationale de la Recherche* through the A*MIDEX grant (ANR-11-IDEX-0001-02), project LABEX MEC (ANR-11-LABX-0092) and project HELIX (ANR-12-BS09-0023-01).

^a IRPHE, UMR 7342 CNRS, Aix-Marseille Université, Centrale Marseille, 13382 Marseille, France

¹ Widnall, *J. Fluid Mech.* **54**, 641 (1972).

² Gupta and Loewy, *AIJA Journal* **12**, 1381 (1974).

³ Rosenhead, *Proc R. Soc. London A* **127**, 590 (1930).

⁴ Saffman, *Vortex Dynamics*, Cambridge (1992).

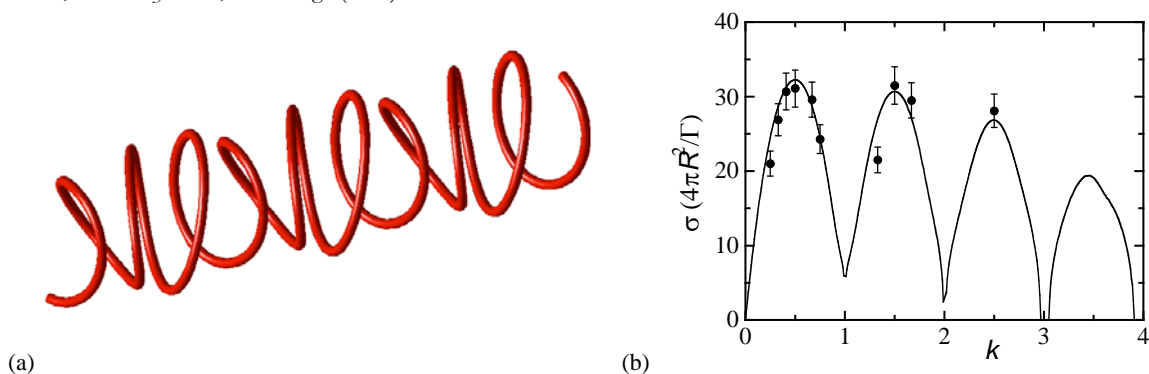


Figure 1: (a) Long-wave deformation of a helical vortex: mode with wavenumber $k = 4/3$, i.e., 4 locations of local pairing in 3 helix turns. (b) Comparison between theoretical prediction² and experimental measurements of the growth rate σ

Linear stability analysis of helical vortices

C. Selçuk¹, I. Delbende², M. Rossi^c

Understanding the dynamical properties of helical vortices is of great importance both from a fundamental point of view, and with respect to the numerous applications as they dominate the near wake of wind turbines, helicopter rotors, ship propellers. Theoretical approaches¹ are able to predict the inviscid dynamics however with a strong hypothesis concerning the vortex core structure. By contrast, some experiments reveal that a significant axial flow may be present inside the core. The goal of the present study is to investigate how viscous helical vortex states and their instabilities are affected by the presence of such an axial flow component.

Locally these wake flows display a helical symmetry: fields are invariant through combined axial translation of distance Δz and rotation of angle $\theta = \Delta z/L$ around the same z -axis, where $2\pi L$ denotes the helix pitch. A DNS code² with built-in helical symmetry is used to compute viscous quasi-steady basic states with one or multiple vortices. These states will be characterised (core structure, ellipticity, ...) as a function of the pitch, without or with an axial flow component.

The instability modes growing in the above base flows and their growth rates are investigated by three different tools: (1) a model of helical thin-cored vortex filaments within the “cut-off” theory; (2) a linearised version of the helical DNS code coupled to an Arnoldi procedure; (3) a linearised version of a fully three-dimensional flow solver. Helically symmetrical modes obtained through (1) and (2) will be compared, and modes breaking the helical symmetry obtained through (3) will be presented.

¹ LIMSI-CNRS B.P. 133 91403 Orsay Cedex, France Can.Selcuk@limsi.fr

² UPMC, Université de Pierre et Marie Curie-Paris 6 LIMSI-CNRS B.P. 133 91403 Orsay Cedex, France, Ivan.Delbende@limsi.fr

^c UPMC, Université de Pierre et Marie Curie-Paris 6, d'Alembert-UPMC, 75232 Paris Cedex 05, France, Maurice.Rossi@upmc.fr

¹ Okulov and Sorensen, *J. Fluid Mech.* **576**, 1-25 (2007).

² Delbende, Rossi and Daube, *Theor. Comput Fluid Dyn.* **26**, 141-160 (2012).

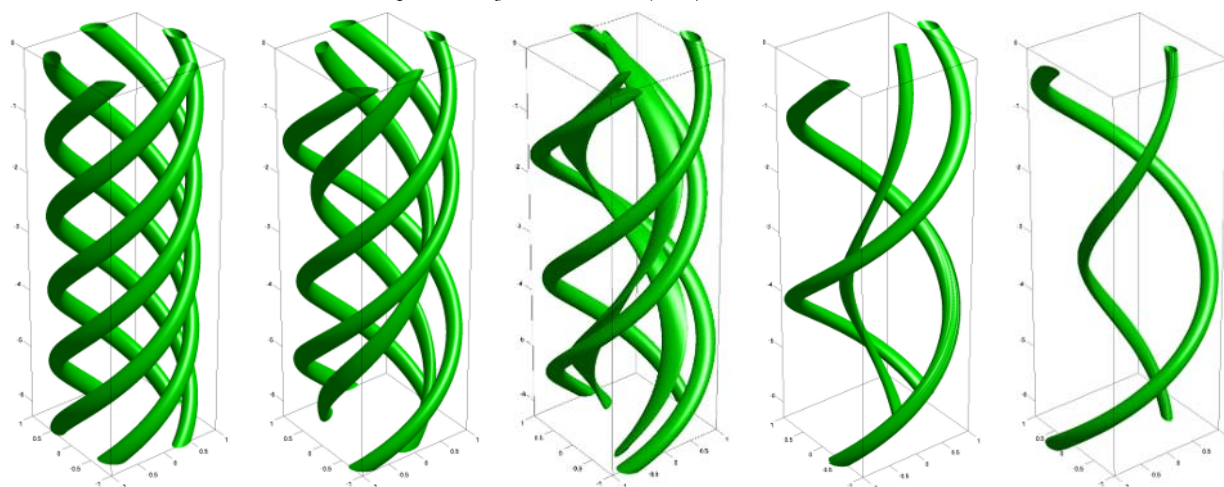


Figure 1: Temporal evolution of an unstable array of 5 helical vortices. $Re=10000$. $L=1$.

The interaction of monopolar and dipolar vortices with a shear flow

L.P.J. Kamp^a, V.H. Marques Rosas Fernandes^a, G.J.F. van Heijst^a and H.J.H. Clercx^a

The interaction of monopolar and dipolar vortices with a shear flow plays an important role both in fluids, e.g. geophysical (zonal) flows, and in magnetically confined plasmas. Although these interactions have been studied since the early nineties of the last century¹, the topic has recently gained renewed interest because of its relevance for improved confinement of a tokamak fusion plasma². In such a plasma zonal flows are held responsible for turbulence self-regulation. One of the mechanisms at work in this self-regulation is the shear decorrelation mechanism resulting from turbulent eddies that are torn apart by the shear flow in which they are embedded.

The present work aims to study this mechanism using numerical simulation of two-dimensional parallel shear flows of two types (a Couette flow and a Poiseuille flow) interacting with coherent vortical structures as well as a turbulent vorticity field. In case of a monopolar vortex we observe a deformation of the vorticity patch if its strength and the flow's shear have opposite signs. If the signs are the same, after a transitional phase, the vortex attains a quasi-steady elliptical shape. For a dipolar vortex the evolution is quite different. Contrary to the monopolar case (having oppositely signed vorticity as compared to the shear flow) a dipole turns out to be a much more robust coherent structure when interacting with the shear flow and being less susceptible to the straining action of the background flow. Using the rotational part of the velocity-gradient tensor, we are able to describe theoretically the trajectory of the dipole as it is being advected by the shear flow. In order to study the interaction of multiple monopolar and dipolar vortices with a shear flow, we also numerically simulated two-dimensional driven turbulence interacting with a background flow. Using turbulent kinetic energy and enstrophy we are able to quantify the suppression of turbulence as a function the ratio of the shear rate of the turbulent eddies and of the background flow. Contrary to previous studies on vortex-shear flow interactions the present work also takes into account the influence of the no-slip walls bounding the background (channel) flow. The vorticity generated in the boundary layers at these walls is shown to have a decisive influence on the temporal evolution of the bulk vorticity. Preliminary experiments in shallow two-fluid layers validate the numerically simulated behaviour of dipolar structures interacting with an electromagnetically driven Poiseuille-like channel flow.

^a Fluid Dynamics Laboratory, Dept. of Physics, Eindhoven University of Technology, The Netherlands

references

¹ Philip S. Marcus – Vortex dynamics in a shearing zonal flow. *J. Fluid Mech.* **215**, 393-430 (1990).

² P.H. Diamond et al. – Zonal flows in plasma-a review. *Plasma Phys. Controlled Fusion* **47**, R35 (2005).

Linear response to harmonic forcing of the non-parallel Batchelor vortex

F. Viola^a, C. Arratia^a and F. Gallaire^a

The Batchelor vortex¹ is a slowly developing asymptotic solution of the flow of a trailing line vortex. This flow has been comprehensively studied in its parallel approximation. In particular, the convective/absolute nature of the instability has been investigated². In the non-parallel case, the Batchelor vortex can be whether stable or unstable, depending on the inlet conditions. For the globally unstable flow, linear stability analysis has been carried out through modal analysis³. In contrast, when the flow is stable, all global modes are damped and the most suitable technique to investigate the dynamics of coherent structures is to compute the response to an external forcing⁴.

In the present work, we investigate the linear response to harmonic forcing of the non-parallel Batchelor vortex through global resolvent calculations, considering both boundary and volume forcing. The base-flow is directly calculated by axisymmetric DNS in cylindrical coordinates. At the inlet, a Batchelor vortex profile is imposed, with swirl and wake defect parameters chosen in order to obtain a globally stable flow and enhance mode competition. The Reynolds number is set to 1000.

Figure 1 a) reports the energy gain as a function of the frequency for all amplified helical modes, for prescribed inlet forcing. Single and double helical modes are the most amplified in the low frequency range, although at higher forcing frequency, higher wavenumber modes become more amplified. Figure 1 b) and c) depict the shape of harmonic responses at the frequencies corresponding to the maximum gain for single and double helical mode, respectively. This problem has been also assessed through WKB analysis in the framework of weakly-non-parallel flows. Remarkably, local and global analyses predict practically the same amplification factors and mode selection (figure 1).

The validity of this predicted linear mode selection is confirmed through the computation of the nonlinear evolution of the response, via 3D-DNS simulations, harmonically forced in time at the inlet. The nonlinear response is seen to be dominated by different helical numbers depending on the forcing frequency, in accordance with the linear analysis.

^a Laboratory of Fluid Mechanics and Instabilities, École Polytechnique Fédérale de Lausanne, Lausanne, CH-1015, Switzerland.

¹ Batchelor *J. Fluid Mech.* **20**, 645 (1964).

² Delbende et al. *J. Fluid Mech.* **355**, 229 (1998).

³ Heaton et al., *J. Fluid Mech.* **629**, 139 (2009).

⁴ Garnaud et al., *J. Fluid Mech.* **716**, 189 (2013).

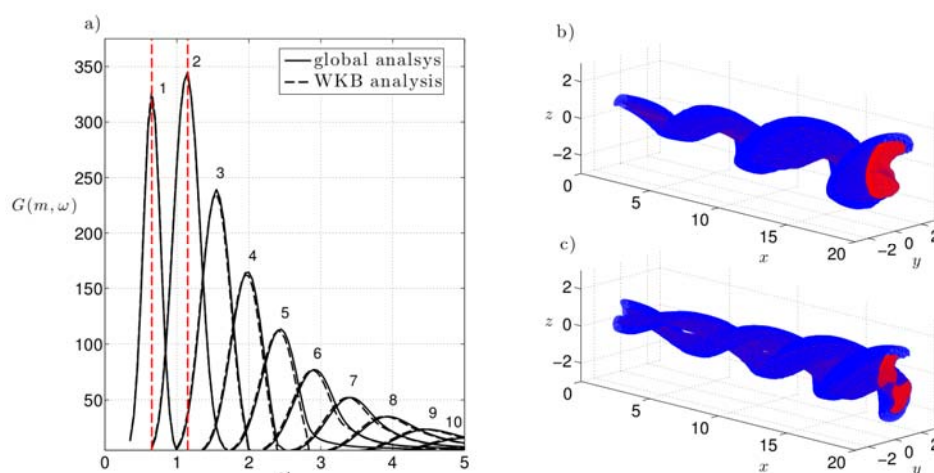


Figure 1: (a) Energy gain as a function of the frequency and the helical number. Isosurfaces of axial vorticity of the most amplified (b) single and (c) double helical modes.

Tomographic PIV measurements behind vortex generators

K. E. Meyer^a, C. M. Velte^a, V. Jaunet^b, N. Bøtkjær^b and D. Hess^b

Vortex generators are small passive devices placed in a boundary layer with the purpose of delaying or avoiding flow separation. They are commonly assumed to generate longitudinal vortices that enhance transport of momentum towards the wall and are applied on e.g. aircrafts, wind turbines and diffusers. Relatively recent studies have shown that they also increase turbulent mixing which can often be very efficient indeed¹. There have been numerous studies of vortex generators¹, but flow dynamics and interaction with boundary layer turbulence is still not understood in detail. The present study looks at vortex generators on a plate with a turbulent boundary layer and almost negligible streamwise pressure gradient. No separation is expected and the focus is the dynamical flow structures behind the vortex generators. A relatively new measurement technique, Tomographic Particle Image Velocimetry (PIV), provides all velocity components in a three-dimensional grid. Another purpose of the study is to test this technique on a relatively complex (3D), but still fairly well understood flow^{2,3}.

A plate mounted in a wind tunnel is fitted with vortex generators with a height $h=5$ mm, a rectangular shape, a counter-rotating configuration and an angle with respect to the main flow direction of 18° . The wind tunnel speed is 10 m/s and the boundary layer thickness just before the vortex generators is $1.5h$. A region from the wall to a distance $2h$ above the wall is illuminated downstream of the vortex generators with a pulsed Nd:YAG laser. Glycerol droplets with a diameter of about $2\text{ }\mu\text{m}$ are imaged into four different 4 Megapixel cameras looking at the same region from different angles. The images are processed into instantaneous velocity fields using Dantec DynamicStudio with Least Square Matching (LSM) instead of cross correlation. An example of a part of a measured instantaneous flow field is shown in figure 1.

The results confirm the expected existence of clearly identifiable longitudinal counter rotating vortices^{1,2,3}. These result in streaks of high and low velocity at quite fixed positions. However, the magnitude of these high and low velocities varies a great deal in time. Analysis with Proper Orthogonal Decomposition (POD) suggests that this is the most important dynamic variation of the flow.

^a Dep. Mechanical Engineering, Technical University of Denmark, Lyngby, Denmark

^b Dantec Dynamics, Skovlunde, Denmark

¹ JC Lin, *Progress in Aerospace Science*, **38**, 389-420 (2002).

² CM Velte, MOL Hansen, VL Okulov, *Journal of Fluid Mechanics*, **619**, (2008).

³ CM Velte, *ALAA Journal*, **51**, 2, 526-529 (2013).

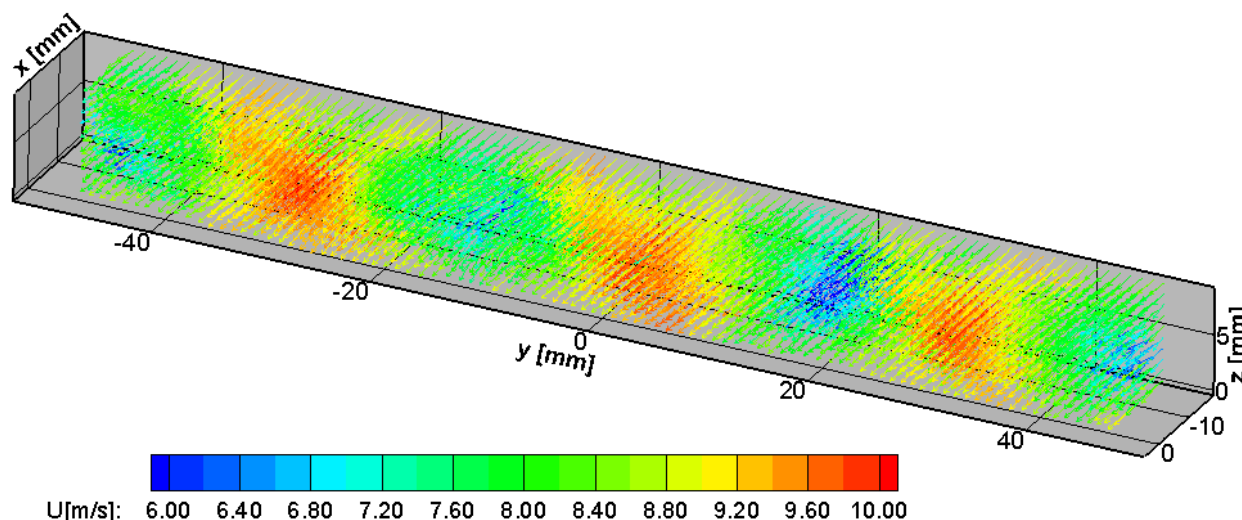


Figure 1: Velocity vectors in a selected block of the full three-dimensional measurement space located about $10h$ downstream of the VGs. Colour indicates the streamwise velocity component U in the main flow direction x .

Numerical simulation of vortex structures in turbulent pipe flow

Amir Shahirpour^a, Sebastian Merbold^a and Christoph Egbers^a

Wall bounded turbulent shear flow is an extremely significant field of study which has long attracted experimental and numerical researchers. Increasing interest in the physics of turbulent pipe flow at high Reynolds numbers has motivated construction of experimental facilities, able to run at such turbulent regimes. The same motivation has triggered countless numerical studies in terms of Direct Numerical Simulation (DNS) and Large Eddy Simulation (LES) as a consequence of recent advances in high performance computing.

During the past decades, considerable attention has been given to the study of coherent structures in various geometries and at different Reynolds numbers. This has resulted in new findings and has given rise to new questions concerning their identification and scaling methods. According to Marusic¹, these organized structures are classified to three basic eddy motions. While near-wall streaks obey a near wall cycle and have a spanwise scale of about 100 viscous length scales, large-scale motions (LSMs) are described as packets of individual eddies (Adrian²) and have a scale of pipe radius. On the other hand very large-scale motions (VLSMs) are interpreted differently by various scientists as joint series of vorticity packets (Adrian²) or as meandering superstructures (Marusic¹) and have a scale of 10 pipe radii. At this stage many key questions concerning LSMs and VLSMs are still unanswered including a uniform scaling law for their identification. Differing views on the origin and definition of low wave number VLSMs exist which questions their dependence on geometry and outer layer variables.

In the present study LES has been performed for turbulent incompressible viscous flow in a pipe at friction Reynolds number of $Re_\tau = 181$ and 361 ($Re_b = 5300$ and $11,700$). Streamwise periodic length of $25R$ is selected for a pipe of radius R . To validate the results in lower ranges of Reynolds number, DNS results by El Khory et al.³ have been used as a benchmark to compare the flow statistics. For higher ranges of Reynolds number, DNS and LES of pipe flow are being performed and the results are to be compared against experimental data from Cottbus Large Pipe (CoLa-Pipe) test facility. Additionally, kinetic energy budget of the mean flow and turbulent flow is investigated. Effect of interactions between coherent structures in pipe flow, their effects on the mean flow and streamwise turbulent intensity are compared with experimental data from CoLa pipe.

^a Dep. Aerodynamics and Fluid Mechanics, Brandenburg University of Technology Cottbus-Senftenberg

¹ Marusic et al., *Phys. Fluids*, **22**, 065103 (2010).

² Adrian, *Phys. Fluids*, **19**, 041301 (2007).

³ El Khory et al., *Flow, Turbulence and Combustion*, **91**, 475 (2013).

The Dynamics of Micro-vortices Induced by Ion Concentration Polarization

J. C. De Valena^{a, b}, R. M. Wagterveld^b, R. G.H. Lammertink^a and P. Amy Tsai^a

We experimentally investigate the coupled dynamics of global ion-flux and local hydrodynamics of an electrolyte solution close to a charge selective membrane under an electric forcing. At small voltages, cations transport diffusively across a cation exchange membrane (CEM), whereas the transport of oppositely charged anions is blocked, causing the main resistance of the system. At higher voltages this resistance suddenly increases and in addition to diffusive transport, hydrodynamic convection sets in within a boundary layer of $O(100\text{ }\mu\text{m})$, resulting in the so-called over-limiting current. In this regime we measured the fluid flow with particle image velocimetry (PIV) combined with chronopotentiometric resistance measurements for the first time. Our results reveal that the micro-vortices are caused by gravitational unstable gradients and by electro osmotic-coupling between the membrane surface and the solution. Moreover, under a constant applied electric current, the electroconvective micro-vortices start with a voltage jump and grow linearly both in size and speed. After this initial linear growth, the resultant voltage levels off around a fixed value. The average vortex size stabilizes as well, however the individual vortices are unsteady and dynamical. Our experimental setup and results offer a complete picture of the coupled dynamics of the hydrodynamics and electrical responses of an electrolyte, beneficial for characterizing a variety of charge selective membranes in order to improve electrodialysis desalination processes.

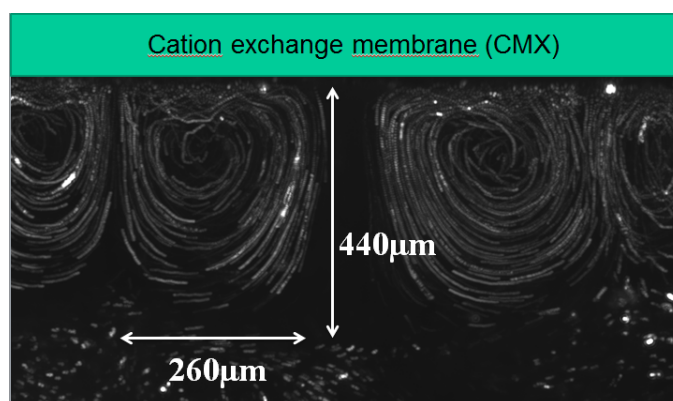


Figure 1. Micro-vortices induced by ion concentration polarization adjacent to a cation exchange membrane under an applied electric field.

^a Soft Matter, Fluidics and Interfaces, MESA⁺ Institute of Nanotechnology, University of Twente, P.O. Box 217, 7500 AE Enschede, The Netherlands. ^b Wetsus, centre of excellence for sustainable water technology, Agora 1, 8934 CJ Leeuwarden, The Netherlands.

Aeroacoustics of Cyclone Separators

T. A. Grimble^a, A. Agarwal^a and M. Juniper^a

A cyclone separator is a commonly employed system for separating solid particles from fluid flow. The device operates by generating swirling flow within a conical or cylindrical chamber. The centrifugal forces on the particles cause them to separate out and fall into a hopper. Cyclones have been commercially employed in vacuum cleaners as a replacement for conventional filter based systems.

The aim of this work is to develop an understanding of the noise generation mechanisms within the fluid flow. Cyclone separators generate a tonal whistle whose frequency varies with the flow rate through the device. By determining the mechanisms by which such sounds are generated it is hoped that novel methods of controlling or eliminating such sound can be developed while maintaining the same performance.

The axis of the vortex within the cyclone is known to precess and it is this oscillation that is thought to lead to tonal noise. This has led to the approach of examining the stability of a cyclone flow to disturbances, to see how such motions can be generated. Using steady, two-dimensional, axisymmetric RANS simulations of a conical cyclone, the effect of small amplitude harmonic perturbations to the flow has been modelled using Instaflo¹. Instaflo solves the equations of motion for the fluid as an eigenvalue problem with small, linear perturbations on top of a base flow from the RANS simulation. The flow is assumed to be locally parallel, that is slowly varying along the axis of the cyclone. Using this tool, temporal, spatial and temporo-spatial stability analyses can be carried out at each local axial position along the flow field for different perturbing waveforms. Radial slices have been taken and possible solutions of axial wavenumber, frequency and radial variation of the perturbing waveform are evaluated. Each section of a modelled cyclone separator was found to be absolutely unstable² to a helical waveform with a non-zero azimuthal wavenumber. This unstable waveform was consistent along the length of the cyclone and remained approximately constant in frequency. The estimated frequency was found to also vary with flow rate. This result was confirmed across a range of cyclone sizes with different operating characteristics.

Flow visualisation experiments were carried out in water to validate the modelled waveform solutions from local analysis. Acoustic tests were carried out using external and internal microphones to characterise the acoustic tones generated by the cyclone. The measured sound frequencies were found to closely match the linear solutions, lending credence to the analysis. A further aim of these acoustic measurements is to characterise the frequency, based on the operating conditions of the cyclone.

^a Cambridge University Engineering Department, Trumpington Street, Cambridge, UK

¹ Juniper, *ASME Turbo Expo*, (2012)

² Huerre and Monkewitz, *Annual Review of Fluid Mechanics*, **22**, 473, (1990)

Multiphase

SOURCE-II Sounding Rocket Experiment – Multiphase Flow with Phase Change in a Microgravity Environment

Sebastian Schmitt^a and Michael Dreyer^a

Future cryogenic upper stages demand a save storage of the propellant for several hours. So far, there is not enough information about the characteristics of cryogenic liquids in a two phase system in microgravity. Superheated tank walls drive phase change and have a severe influence on the fluid's behaviour. During the Apollo program Knoll et al.¹, McArdle et al.², Nunamaker et al.³ and Regetz, Jr. et al.⁴ conducted suborbital tests with liquid Hydrogen to evaluate the pressure progression inside a propellant tank during the coasting phase. Drop tower experiments by Kulev et al.⁵ were carried out to investigate the reorientation of liquid Argon upon gravity step reduction. The behaviour of a two species system containing of a storable liquid and a non-condensable gas was evaluated by Fuhrmann et al.⁶ within the SOURCE sounding rocket experiment.

The SOURCE-II sounding rocket experiment is a two phase, one species system. It consists of a cylindrical test chamber with a temperature gradient along the side wall. The temperature of the wall in the vicinity of the free surface is of great importance since it steers evaporation of the test liquid. The cylinder was partly filled with liquid HFE7000 after the rocket's propelled ascend. Pressurisation with superheated HFE7000 is used to modify the saturation temperature. Due to the temperature gradient along the wall the liquid experiences a higher temperature the further it moves upwards. Several temperature and pressure sensors inside the test cell and in the wall are used to record pressure and temperature progression at desired locations. A camera is installed to record the free surface during the experiment. The partly filled test cell is shown in Figure 1.

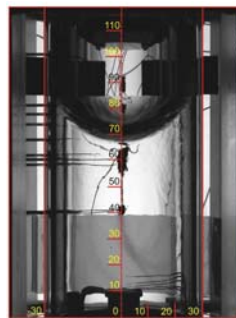


Figure 1: Experiment during the flight, partly filled with HFE7000

The focus of this Experiment lies on the behaviour of the system and especially the free surface in a microgravity environment with non-isothermal boundary conditions. An important part of the experiment is the pressure progression inside the test cell throughout the experiment. The behaviour of the contact line and the apparent contact angle is of interest as well. Furthermore, the experiment was used to create a benchmark for CFD- codes. Phase change and conjugated heat transfer is included in this benchmark. The commercial flow solver Flow3D was used to model the experiment. The results were compared with experimental data to gain more information about the system's behaviour.

^a Center of Applied Space Technology and Microgravity, University of Bremen, Am Fallturm, Bremen, Germany

¹ Knoll, Richard H.; Smolak, George R.; Nunamaker, Robert R., *NASA Technical Memorandum X-484* (1962).

² McArdle, Jack G.; Dillon, Richard C.; Altmos, Donald A., *NASA Technical Memorandum X-718* (1962).

³ Nunamaker, Robert R.; Corpas, Elias L.; McArdle, Jack G., *NASA Technical Memorandum X-872* (1963).

⁴ Regetz, Jr., John D.; Conroy, Martin J.; Jackson, Robert G., *NASA Technical Memorandum X-873* (1964).

⁵ Kulev, N., Dreyer, M., *Microgravity Science and Technology* **22**, 87 (2009).

⁶ Fuhrmann, E., Dreyer, M., *Microgravity Science and Technology* **21**, 243 (2009).

Numerical modelling of a two-phase vortex ring flow using the FLA method for the dispersed phase

O. Rybdylova^a, S.S. Sazhin^a, S. Begg^a and M. Heikal^a

The mixture preparation phase in gasoline engines is a key process central to automotive engineering. The air-fuel mixture quality directly affects the fuel consumption, exhaust gas emissions and engine life-cycle. One of the most promising concepts in engine design involves injecting the fuel directly into the combustion chamber; gasoline direct injection, (G-DI). In a G-DI engine, the liquid fuel exits the injector nozzle and accelerates the surrounding gas forming mushroom-like patterns of various sizes. These vortex ring-like structures in gasoline fuel sprays have been observed experimentally¹ and the results were compared with the analytical model for a classical vortex ring flow² (single phase flow). The current study is focused on the investigation of the droplet distribution in a two-phase vortex-ring flow.

The axi-symmetric, non-stationary problem of a gas-droplet flow is investigated theoretically. The problem is studied in the framework of the one-way coupled two-fluid approach³. The carrier phase is a viscous incompressible fluid (air). The dispersed phase is a cloud of identical, non-deformable, spherical particles. The parameters of the carrier phase are calculated using the analytical solution for a vortex ring flow². The dispersed phase modelling is based on the Fully Lagrangian Approach⁴ (FLA). According to the FLA, all particle parameters, including concentration, are calculated by solving systems of ordinary differential equations along chosen particle trajectories.

Two types of initial conditions corresponding to different ways of introducing particles into the flow are considered: (i) a two-phase jet injected into air; (ii) a cloud of quiescent particles ahead of the vortex ring. Fig. 1b, 1c present the dispersed phase number density distribution in a bisecting plane of symmetry at different times both for the first (Fig. 1b) and the second (Fig. 1c) cases ($\beta = 3$, where β is the particle inertia parameter; the inverse to the Stokes number). Low-inertia particles are easily entrained into the vortex-ring flow. The original particle cloud is deformed into a mushroom-type structure. In the case (i), a region with high concentration is formed at the leading edge of the jet. This is in qualitative agreement with the experimental data for the spray generated by G-DI fuel injector (Fig. 1a).

The authors are grateful to the EPSRC (grant EP/K005758/1) (UK) and Russian Foundation for Basic Research (RFBR) (project 14-01-00147) for the financial support of this project.

^a Sir Harry Ricardo Laboratories, Centre for Automotive Engineering, School of Computing, Engineering and Mathematics, Faculty of Science and Engineering, University of Brighton, Brighton, BN2 4GJ, UK

¹ Begg et al., *Int. J. Engine Res.* **10**, 195 (2009).

² Kaplanski and Rudi, *Phys. Fluids*, **17**, 087101 (2005).

³ Marble, *Annu. Rev. Fluid Mech.* **2**, 397 (1971).

⁴ Osipov, *Astrophysics and Space Science*, **274**, 377 (2000).

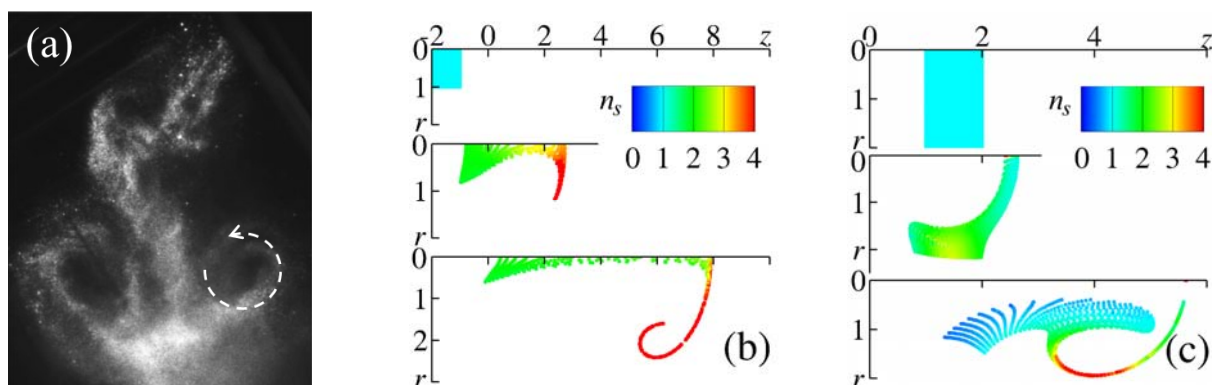
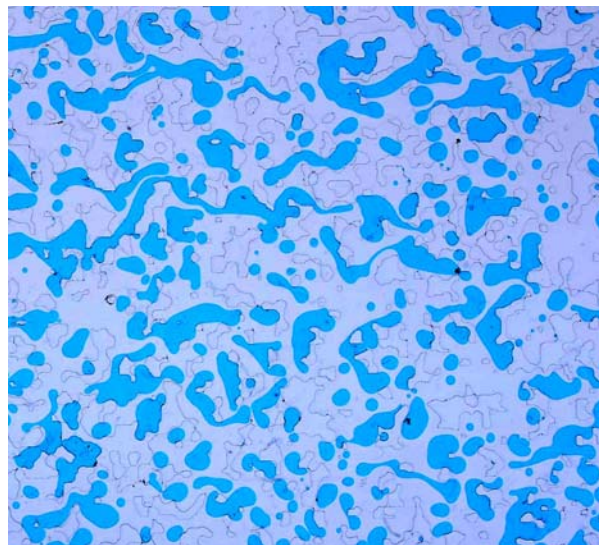
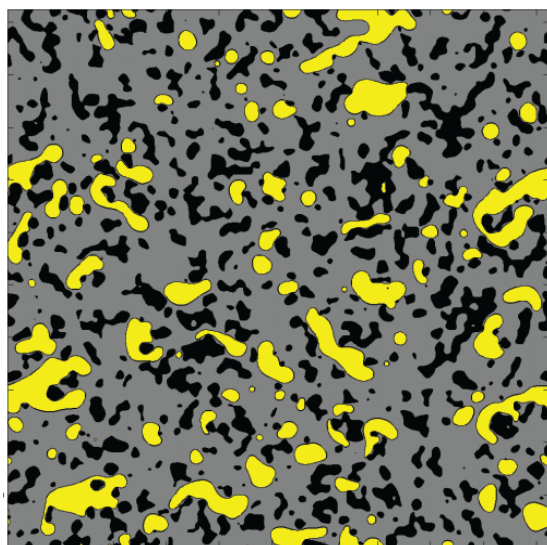


Figure 1: (a) A typical high-speed photograph of a spray generated by a high-pressure atomiser that injects fuel directly into an engine combustion chamber (G-DI); (b) Number density distribution in a two-phase jet at $t_0 = 0.2$, $t_1 = 10$, $t_2 = 180$; (c) A cloud of particles ahead of the vortex ring; number density distribution at $t_0 = 0.01$, $t_1 = 7.5$, $t_2 = 50$.

Two-phase flows blob dynamics in reconstructed porous media : Experiments versus Numerical Simulations

A.G. Yiotis^{a,c}, M. Freytes^{a,d}, L. Talon^a and D. Salin^{a,b}

We study, both numerically and experimentally, the dynamics of non-wetting liquid blobs during immiscible two-phase flows in stochastically reconstructed porous medium¹. The porous medium is represented by 2D porous domains in the form of discrete permeability fields. Each domain consists of solid (impermeable) and void (permeable) sites, where the spatial distribution of the solid sites is stochastically reconstructed that recover the statistical properties of natural porous media, like sandstone, such as the porosity and the two-point auto-correlation function¹; the solid is represented in black in the left figure (porosity 20%). The flow problem is solved using a Lattice-Boltzmann model that captures both the bulk phase and interfacial effects¹: the continuous wetting phase is grey whereas the blob non wetting phase is yellow. The experiment is achieved in a thin (300 μm) Hele-Shaw cell where the solid obstacles are milled following the same statistic as the numerical one: the contours of the solid obstacles are barely visible on the right pictures; the transparent continuous wetting phase is an oil (heptane or dodecane) and the blobs non-wetting phase is blue dyed water; Flow rates are controlled with two pumps and the pressure drop is measured.



Left: Numerical simulations. Black: solid; Grey: continuous wetting phase; Yellow: blobs of non-wetting fluid.
Right: Picture of the experiment. Contour of the solid obstacles; Transparent wetting phase; Blue: non-wetting phase.

We observe both experimentally and numerically that the non-wetting blobs undergo a continuous life-cycle of dynamic breaking-up and coalescence producing two populations of blobs, a mobile and a stranded one, that exchange continuously mass between them. The process reaches a 'steady-state' when the rates of coalescence and breaking-up become equal, and the macroscopic flow variables remain practically constant with time. At steady state, when the rates of blob breaking up and coalescing become equal, both populations follow a log-normal size distribution with an average size and cumulative volume that depends strongly on the applied flow rate. Three flow regimes are identified; a single phase Darcy-type regime at low flow rates, a non-Darcy 2-phase flow regime at intermediate flow rates and again a Darcy type 2-phase regime at higher flow rates.

^a Laboratoire FAST, CNRS & Univ. Paris-Sud , Bâtiment 502 Orsay 91405, France

^b University Pierre & Marie Curie, 4 place Jussieu 75252 Paris Cedex 05, France

^c Environmental Research Laboratory National Center for Scientific Research 'Demokritos' 15310 Agia Paraskevi Greece

^d Grupo Medios Porosos, University of Buenos Aires (FIUBA, Conicet), Av Paseo Colon 850 Argentina

¹ Yiotis et al, *Phys. Rev E* **87**, 033001 (2013)

Modelling and numerical analysis of a confined two-phase flow

G. Laval^a, J. P. Vila^b, C. Laurent^a and F. Charru^c

Confined two-phase flows are recurrent in many industrial devices, such as heat exchangers and distillation columns. The analysis of such a flow has thus been the subject of several studies in the past. The interaction between the two phases takes place at the interface, and is governed by pressure gradient and shear stress provided by the gas. These can feed the liquid film instability, and, as a consequence, travelling waves can grow at the interface, modifying in turn the gas behavior¹.

The dynamics of a confined two-phase horizontal flow driven by pressure gradient is hereby investigated. A liquid film occupies the bottom of the domain, and a laminar gas flows on the top of it. Such a two-phase flow is studied with a reduced model. By integrating the boundary-layer equations over the respective thicknesses and by assuming that the two layers are thin compared to the wavelength of the travelling waves, a system of consistent shallow water equations for both phases is found. This system is closed by providing an asymptotic development of the boundary-layer equations up to the first order, which also leads to the expressions of interfacial shear stress and pressure gradient. To validate this reduced model, the wave celerity given by the linear stability analysis has been compared with Yih's².

The computational approach used in the analysis of this confined two-phase flow represents a compromise between the Direct Numerical Simulation (DNS)^{3,4} and the full reduced model⁵. In fact, the liquid film is analyzed by means of shallow water equations, whereas the gas phase is solved with Navier-Stokes equations. This choice is justified by considering that in the typical applications investigated in the aerospace domain, the gas layer is usually not thin compared with the wavelength. The computational coupling between the two phases is assured by the continuity of velocities and stresses at the interface. In addition, an Arbitrary-Lagrangian Eulerian (ALE) method ensures the transfer of the interface movement from the liquid to the gas.

The performed computational analysis has been validated by comparing interfacial shear stress and pressure gradient evolutions with those provided by the asymptotic development. Indeed, the tendencies are in good agreement. Unlike the others, this numerical approach can also be easily extended to the case of a laminar boundary layer over a wavy liquid film, which will be the natural extension of the present work.

^a Aerodynamics and Energetic Modelling Department, ONERA, Toulouse, France

^b Institut National des Sciences Appliquées, Toulouse, France

^c Institut de Mécanique des Fluides de Toulouse, Toulouse, France

¹ Hanratty, *Waves on Fluid Interfaces*, 221 (1983).

² Yih, *J. Fluid Mech.* **27**, 337 (1967).

³ Franck, *Phys. Fluids* **20**, 122102 (2008).

⁴ Valluri et al., *J. Fluid Mech.* **656**, 458 (2010).

⁵ Dietze and Ruyer-Quil, *J. Fluid Mech.* **722**, 348 (2013).

Formation of disturbance wave in annular gas-liquid flow with entrainment

S.V. Alekseenko^a, A.V. Cherdantsev^a, M.V. Cherdantsev^a, S.V. Isaenkov^a, D.M. Markovich^a

Annular gas-liquid flow in pipes is simultaneous flow of liquid film on the pipe wall and high-velocity gas stream in the pipe core. At high gas and liquid flow rates, entrainment of liquid droplets from film surface occurs. In this case, the wave pattern is represented by two types of waves: disturbance waves and ripples. Disturbance waves are fast large-scale long-living waves; they are considered to be necessary for entrainment to occur. Ripples are small-scale waves, covering the disturbance waves and base film between them.

Generation of ripples occurs on the back slopes of the disturbance waves¹. After inception, part of ripples propagates with lower velocity than that of disturbance wave («slow ripples»); the other part propagates with higher velocity («fast ripples») over the tops of disturbance waves. This part is finally entrained into the gas core as droplets. At present, formation of disturbance waves is not fully understood. In the most recent and relevant work² devoted to disturbance waves' development, conductance probes were used to study the film thickness records at different distances below the inlet. A wave was considered to be a disturbance wave if its amplitude was 1.6 times larger than the mean film thickness. Authors conclude that the disturbance waves appear at the distances of 5-10 pipe diameters below the inlet.

The goal of the present paper is to investigate the process of disturbance waves' formation. For this, high-speed laser-induced fluorescence (LIF) technique was used. This technique enables one to perform the field measurements of film thickness with high spatial (0.2 mm/pixel) and temporal (10 kHz) resolution. Thus, space-time evolution of each perturbation of film surface can be studied.

Experiments were performed in cylindrical pipe with inner diameter 15 mm. The working area is represented by a single longitudinal section of the pipe with length 10 cm, beginning from the inlet. Water is used as the working liquid. The measurements were performed at high gas velocities ($V_g = 18 - 57$ m/s) and Reynolds numbers ($Re = 140 - 400$).

Figure 1 shows spatial and temporal evolution of film thickness. Results obtained in such manner make it possible to use different definition of disturbance waves. Namely, a wave is considered to be a disturbance wave if its top is covered by the fast ripples (see above). At the highest gas velocities, disturbance waves are formed at the distances of 40-60 mm below the inlet. They are formed due to multiple acts of coalescence of initial high-frequency low-amplitude perturbations generated at the inlet. For quantitative study of the formation process, an automatic algorithm of data processing based on Canny method of edge detection was developed.

^a Institute of Thermophysics of SB RAS (IT SB RAS), 1, Lavrentiev Ave., 630090, Novosibirsk, Russia

¹ Alekseenko et al., *Phys Fluids* **21**, 061701 (2009).

² Zhao et al., *Int J Multiphase Flow*, **55**, 111-129 (2013).

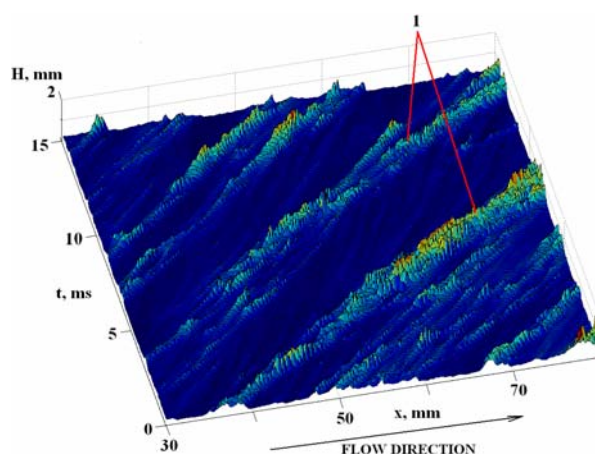


Figure 1: Spatial and temporal evolution of film thickness. $Re=400$, $V_g=57$ m/s. 1 – disturbance waves

Behavior of Jet Flow Issued Vertically into Two-Layer Density-Stratified Fluid

Shogo Shakouchi^a, Shota Fukue^a, Tomomi Uchiyama^b

1. Introduction

Density stratified fluid may occur in liquefied natural gas (LNG) storage tank. The stratification could lead to a violent mixing or a rollover, vaporizing a large amount of the gases. As the gases damage the tank, the prevention of the stratification is very important to operate the LNG tank. Jet flows are utilized to mix the LNG in the tank so as to prevent the stratification. This study is concerned with an experimental investigation on the behavior of a jet issued vertically into two-layer density-stratified fluid.

2. Experimental set-up

The experiment is conducted in a rectangular tank, which is made of transparent acrylic resin. The width and depth of the tank are 600 mm and 200 mm respectively. The upper and lower layers are composed of water and sodium chloride aqueous solution (NaCl water) respectively. The NaCl water in the lower layer is vertically issued from a nozzle mounted on the tank bottom. The nozzle diameter d is 10 mm. The jet behavior is visualized by adding fluorescent dye (Rhodamine) to the jet. The origin of the vertical z axis is set at the center of the nozzle outlet. The Reynolds number Re based on the jet velocity and the nozzle diameter ranges from 95 to 2378, and the concentration of the NaCl water C_0 varies from 0.01 to 0.04.

3. Results

Figure 1 shows the jet flows visualized at $C_0=0.02$. When $Re=95$, the jet just reaches the density interface ($z/d=5$). But it does not penetrate the interface, spreading in the horizontal direction. When $Re=476$ and 1427, the jet penetrates the density interface and becomes non axisymmetric. As the jet density is larger than the upper (water) layer, the top of the jet falls. The jet does not reach the water surface ($z/d=9$). When $Re=2378$, the jet penetrating the density interface reaches the water surface and spreads along the surface. The downward flow from the water surface toward the density interface is also observed. Active mixings between the jet and the surrounding fluid are observed. When the height of the jet measured from the nozzle exit, z_m , is expressed in the nondimensional form $H_m=z_m/(z_1+z_2)$, it changes as the function of the Froude number Fr as shown in Fig. 2, where z_1 and z_2 are the thicknesses of the upper and lower layers respectively. The Froude number Fr is defined as $U_0/[dg(\rho_1-\rho_2)/\rho_2]^{1/2}$, where U_0 is the jet velocity at the nozzle exit, ρ_1 and ρ_2 are the densities of the upper and lower layers respectively. One can find that the jet height is expressed as the function of the Froude number irrespective of the concentration of the NaCl water C_0 .

^a Graduate School of Information Science, Nagoya University, Furo-cho, Chikusa-ku, Nagoya 464-8603, Japan

^b EcoTopia Science Institute, Nagoya University, Furo-cho, Chikusa-ku, Nagoya 464-8603, Japan

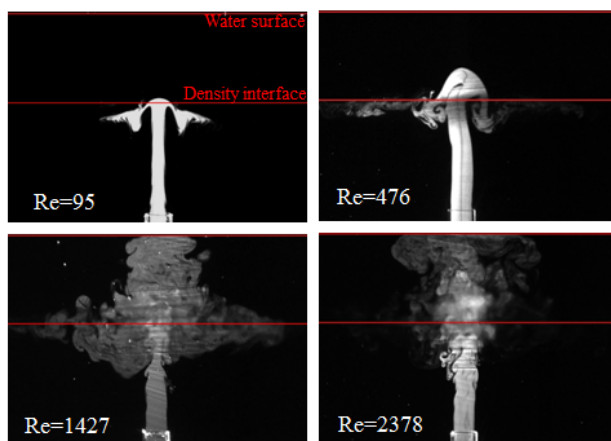


Figure 1: Jet behaviour in case of $C_0=0.02$.

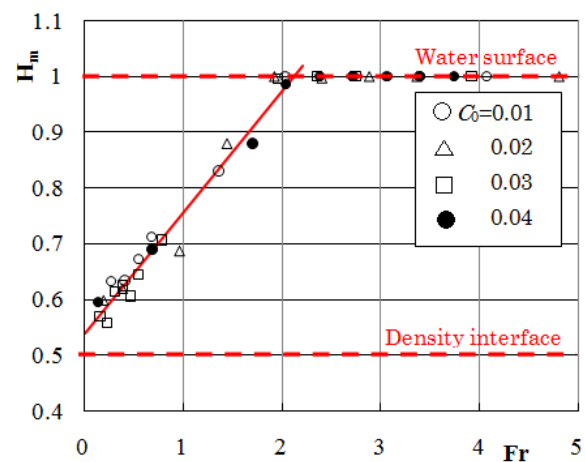


Figure 2: Height of jet in case of $Re=476$

Heat transfer enhancement in multiphase Rayleigh-Bénard convection

P. Oresta¹, F. Fornarelli², A. Prosperetti^{3,4}

In Rayleigh-Bénard convection flow is driven by the density difference between heavier and lighter fluid regions superposed in a gravitational field. In the present work we study by means of direct numerical simulation the effect of the presence of a second phase - vapor in a liquid or particles in a gas - on this phenomenon. The fluid is enclosed in a cylindrical cell with a height equal to twice the diameter and, in the single-phase situation that we take as reference, the flow is organized in a mildly turbulent annular roll with a horizontal axis; the Rayleigh number is 2×10^6 and the Prandtl number 0.7 for the particle-gas case and 1.75 for the bubbly liquid case.

Vapor bubbles are nucleated and grow in the hotter liquid near the lower heated plate of the cell. Their increasing volume reinforces the buoyancy of the liquid-vapor mixture making the annular roll stronger. Some smaller bubbles survive their encounter with the colder liquid near the upper plate, return to the lower plate and are swept up with the bigger ones in the ascending stream¹. This process causes a marked non-uniformity of the bubble distribution, which is significantly larger in the ascending than in the descending portions of the roll.

Particles are introduced at the top, cold plate with the same temperature as the plate. Unless they are very small (less than about $1 \mu\text{m}$ in diameter), due to their large density they remain essentially uniformly distributed over the cross section of the cell. In this case heat transfer in the cell is also increased, but due to different mechanisms. In the first place, by dragging cold fluid away from the upper plate toward the hot one, they favor heat extraction from the latter. Secondly, the enhanced descending stream that they cause constrains the ascending hot stream to a smaller and smaller fraction of the cross section, thus increasing the axial flow velocity by continuity². Thus, both particles and bubbles enhance the circulation and eventually the heat transfer even though by different mechanisms³.

The heat transfer in the cell is strongly dependent on the degree of thermal coupling of the disperse and continuous phases as expressed by the Jakob number in the case of bubbles and by a similar quantity involving the particle specific heat in the case of particles. As the Jakob number increases, bubbles grow larger and convection is enhanced. If the specific heat of the particles is large so that they retain their cold temperature as they fall, they cool the gas near the hot plate thus increasing the heat extracted from it.

¹ Dep. of Engineering for Innovation, University of Salento, 73100 Lecce, Italy.

² Dep. Of Mathematics, Mechanics and Management, Polytechnic of Bari, 70126 Bari, Italy.

³ Dep of Mechanical Engineering, Johns Hopkins University, Baltimore MD 21218, USA

⁴ Physics of Fluids Group, Department of Science and Technology, J. M. Burgers Centre for Fluid Dynamics, University of Twente, 7500 AE Enschede, The Netherlands

¹ Oresta et al., *Phys. Rev. E* **80**, 026304 (2009).

² Oresta and Prosperetti, *Phys. Rev. E* **87**, 063014 (2013)

³ Oresta et al., *Mech. Eng. Rev.* **1**, FE0003 (2014)

Transitions from core-annular flow to bubbling, pulsing or spray flow in a periodically constricted circular tube

D. Fraggedakis^a, Y. Dimakopoulos^a and J. Tsamopoulos^a

Two-phase flows arise in many engineering processes such as the enhanced oil-recovery and the reforming process in packed bed reactors. The two-phases can be either liquid-liquid or gas-liquid. In all cases, the configuration of the interface plays a significant role in the transfer mechanisms of heat and mass and also controls the flow^{1,2} type that may occur, depending on the physical properties of the system.

Several experimental³ and theoretical^{4,5} studies have been conducted in order to predict the flow regimes, but none of them was able to predict the whole map of flows that arise due to different interfacial mechanisms. In the current work we predict the transition of a perfectly core-annular flow (fig. 1a) to bubbling, pulsing or spray flow by solving the transient NS equations with the Volume-of-Fluid technique, which enables to capture very accurately the complicated topological changes of the interface. We simulate the axisymmetric flow of two immiscible fluids in a periodically constricted tube, driven by an externally imposed constant pressure gradient.

First we perform a parametric analysis in terms of the Reynolds and Weber numbers, the viscosity and volume ratio of the two fluids, the aspect ratio and the ratio maximum to the minimum radius of the tube. For example, we find that when the more viscous fluid occupies the outer area in the range $10 < Re < 400$ for $We = 1$, the interface moves near the wall area forming a thin film. When Re exceeds 500, wetting of the wall from the initially inner phase is observed, forming drops of the annular fluid in the core. This comes from the large oscillations of the interface due to the high pressure-gradient along with the tube constriction. When the volume ratio is smaller combined with large surface tension, large droplet formation is favoured (fig. 1b) and pulsing flow develops.

Finally, we construct global flow maps to describe the transitions to different flow regimes with a good resolution. These maps are constructed on a system with axis the Reynolds and Weber numbers. It should be noticed that all the previously reported flow maps were expressed in terms of dimensional quantities for particular fluid phases, and thus cannot be generalized in other systems.

^a Laboratory of Fluid Mechanics and Rheology, Department Chemical Engineering, University of Patras, 26500 GR, Patras, Greece

¹ De Santos, Melli and Scriven, *Ann. Rev. Fluid Mech.*, **23**: 233-260 (1991).

² Melli, De Santos, Kolb and Scriven, *Ind. Engng Chem. Res.* **29**, 2367-2379 (1990).

³ Aul and Olbricht., *J. Fluid Mech.* **215**: 585-99 (1990b).

⁴ Kouris and Tsamopoulos *Phys. Fluids*, **13**, 841-858 (2001).

⁵ Kouris and Tsamopoulos, *J. Fluid Mech*, **470**, 181-222 (2002).

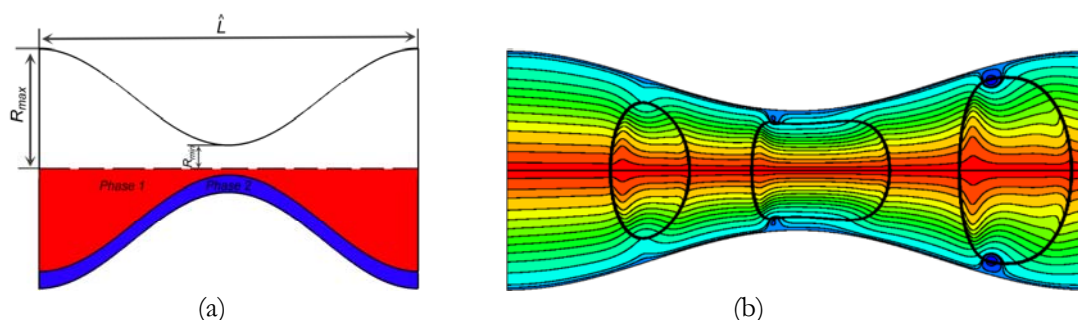


Figure 1: (a) Illustration of the initial configuration of the two-phase flow system, (b) Case where the more viscous fluid (initially on the core region) has transformed into multiple slug form droplets.

A NUMERICAL SOLUTION OF DIFFERENTIAL EQUATIONS OF THE FLOW OF SUSPENSION BETWEEN TWO COAXIAL CYLINDERS

D. Salemović ^a, A. Dedić ^b, B. Jovanović ^c

Abstract: The paper describes the flow of suspension which is a mixture of two phases: liquid and solid granules. The continuum model with microstructure is introduced which involved two independent kinematic quantities: the velocity vector and the micro rotation vector. The physical analogy is based on the movement of suspension between two coaxial cylinders. The inner cylinder is stationary and the outer one rotates with constant angular velocity (Fig. 1).

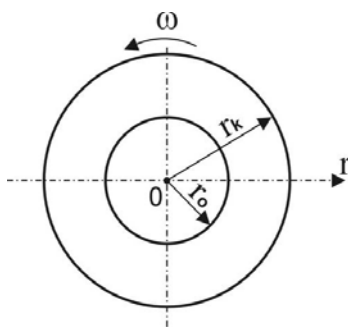


Figure 1: A simplified functional diagram of the movement of suspension between two coaxial cylinders

This physical analogy enabled mathematical model in a form of two coupled differential equations with variable coefficients. The aim of the paper was to present the numerical aspect of the solution of this complex mathematical model. It is assumed that the solid granules are identically oriented and that under the influence of the fluid they move translationally or rotate around symmetry axis but the direction of their symmetry axes does not change. The solution was obtained by the improvement finite difference method, and then the corresponding sets of points (nodes) were routed by interpolation graphics. Some results are given on Fig.2, and the results in references [1, 2, 3] shows good agreement with the obtained model.

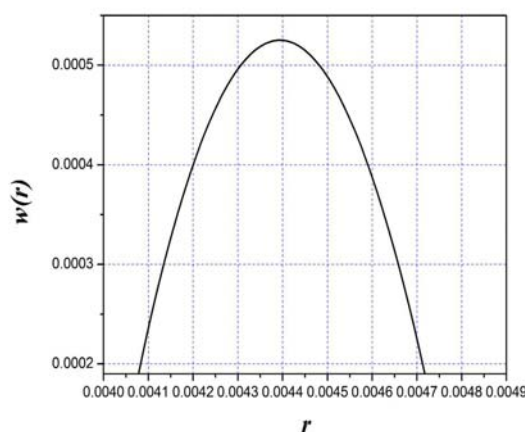


Figure 2: Graph size $w(r)$ depending on radial coordinate (r)

^a Dep. Mechanical Engineering, High Technical School, Zrenjanin, Serbia

^b Prof., PhD, Dep. TMD, Faculty of Forestry, University of Belgrade, Serbia, e-mail: aleksandar.dedic@sfb.bg.ac.rs; adedic@eunet.rs

^c Prof., PhD, Mathematical Faculty, University of Belgrade, Serbia

¹ Jovanović et al., *Engineering* **63/5**, 1, (2008).

² Srinivasacharya and Shiferaw, *Int. J. of Appl. Math and Mech.* **4(2)**, 77, (2008).

³ Tomantschger, *Journal of Computational and Applied Mathematics* **140**, 773, (2002)

Bubbles

Surface Nanobubbles: Their stability and their spatical distribution and what we learn from that on their formation process

Henri Lhuissier, Joost Weijs, Xuehua Zhang, Detlef Lohse

Physics of Fluids Group, University of Twente, 7500 AE Enschede, The Netherlands

Nano- or micro-gas bubbles [1] often form on hydrophobic solid surfaces which are in contact with an aqueous environment. Their presence has been supported by many experiments of all kinds, but their long lifetime remains mysterious. Here we present a theoretical model for the exceptionally long lifetime of surface nanobubbles [2]. We can explain why, under normal experimental conditions, surface nanobubbles are stable for many hours or even up to days rather than the expected microseconds. The limited gas diffusion through the water in the far field, the cooperative effect of nanobubble clusters, and the pinned contact line of the nanobubbles lead to the slow dissolution rate. The key idea is that it is not the local length scale of the bubble itself, but the length scale of the pool in which the bubbles are sitting which is responsible for the lifetime. Due to the pinning of the contact line, the Laplace pressure decreases with decreasing bubble volume, and does not increase as for a free bulk microbubble, see figure 1. This leads to a close to zero concentration gradient at the bubble-liquid interface and thus to a tremendous delay in the bubble depletion.

We also study [3] the size and spatial distribution of surface nanobubbles formed by the solvent exchange method to gain insight into the mechanism of their formation. The analysis of Atomic Force Microscopy (AFM) images of nanobubbles formed on a hydrophobic surface reveals that the nanobubbles are not randomly located, which we attribute to the role of the history of nucleation during the formation. Moreover, the size of each nanobubble is found to be strongly correlated with the area of the bubble-depleted zone around it. The precise correlation suggests that the nanobubbles grow by diffusion of the gas from the bulk rather than by diffusion of the gas adsorbed on the surface.

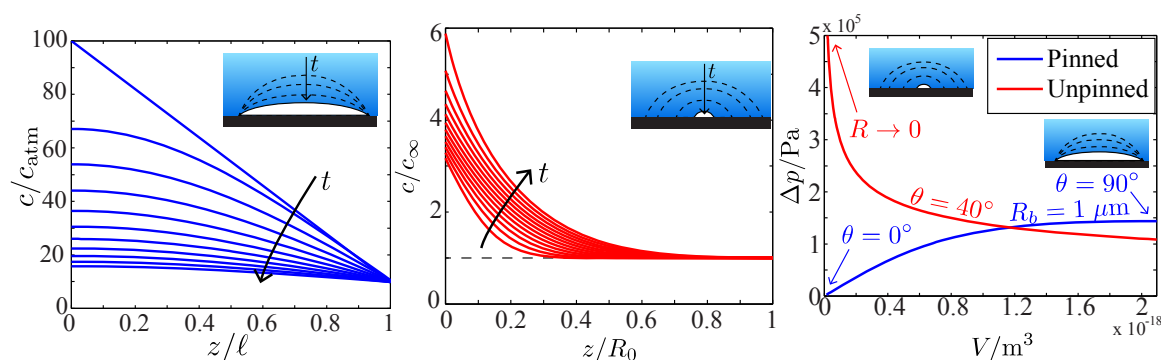


Fig. 1: Concentration profiles shown at various times following from the traffic jam theory [1] (a), which assumes pinning of the contact line. The gradient at the bubble wall $z = 0$ quickly becomes flat. In (b), no pinning is assumed, leading to a steep concentration gradient at the bubble wall and thus to much faster shrinkage, as for a spherical bubble in the bulk. In (c) the Laplace pressures $P_{\text{Laplace}} = 2\sigma/R$ with and without pinning are compared.

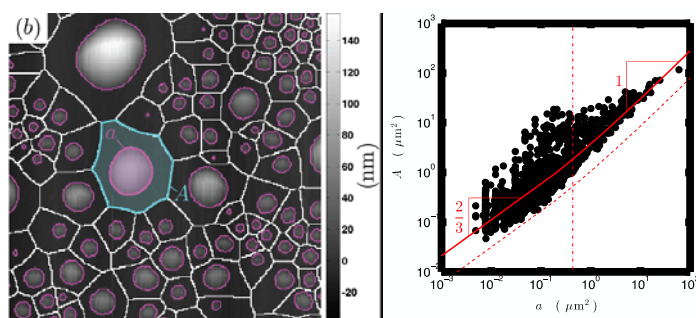


Fig.2: Voronoi tessellation of the surface nanobubbles: The (modified) Voronoi are A and the bubble footprint area a are correlated. Assuming that the surface nanobubble nucleate from the bulk gives a crossover of the slope from $2/3$ to 1 at the vertical dashed line, in agreement with the observations.

[1] Seddon and Lohse, J. Phys.: Condens. Matter 23, 133001 (2011).

[2] Weijs and Lohse, Phys. Rev. Lett. 110, 054501 (2013).

[3] Lhuissier, Lohse, and Zhang, Soft Matter 10, 942 (2014); see also the Cover of that issue.

Electrohydrodynamic deformation of fluid globules at large Reynolds numbers

O. Schnitzer^a, I. Frankel^b and E. Yariv^a

The leaky-dielectric model was put forward by Taylor¹ in the mid 1960's as an explanation to puzzling observations of drops deforming into an oblate spheroidal-type shape when subjected to a steady electric field (as opposed to the prevailing electrostatic models which predicted a prolate shape). The model was further advanced by Melcher who employed it to study numerous practical scenarios, laying the foundations of the now wide field of electrohydrodynamics.² A key assumption in Taylor's theory, appropriate in many applications involving high-viscosity liquids, is that inertia may be neglected, resulting in fluid velocities that scale as the square of the applied-field magnitude.

In this talk we will describe our recent analysis of electrohydrodynamic deformation in the limit of large Reynolds numbers³; this limit is approached with increasing field strength in low-viscosity liquids and large (i.e. millimetric) drops. Balancing viscous stresses and electrical shear forces in this limit reveals a novel electrohydrodynamic velocity scaling, with the 4/3-power of the applied-field magnitude: see fig. 1a.

For simplicity, we focus upon the flow about a gas bubble. It is essentially confined to two boundary layers propagating from the poles to the equator, where they collide to form a radial jet. The transition occurs over a small deflection region about the equator where the flow is effectively inviscid, see fig. 1b. (This asymptotic structure is reminiscent of the problem of a rigid sphere rotating at high Reynolds numbers.) The deviation of the bubble shape from the original sphericity is quantified by the capillary number given by the ratio of a characteristic Maxwell stress to Laplace's pressure. At leading order the bubble deforms owing to: (i) the surface distribution of the Maxwell stress, associated with the familiar electric-field profile; (ii) the hydrodynamic boundary-layer pressure, engendered here by centrifugal forces; and (iii) the intense pressure distribution acting over the narrow equatorial deflection zone, appearing on the bubble scale as a concentrated load.

Remarkably, the unique flow topology and associated scalings allow the obtaining of a closed-form expression for the deformation through the mere application of integral mass and momentum balances. On the bubble scale, the concentrated pressure load is manifested in the appearance of a non-smooth equatorial dimple.

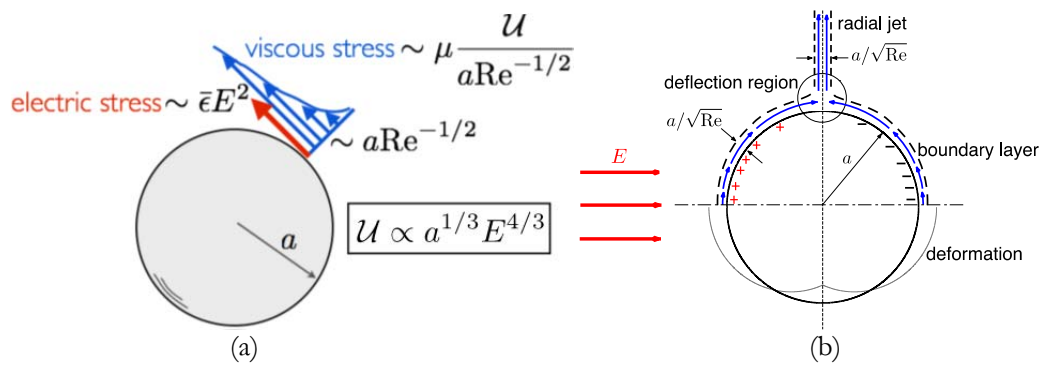


Figure 1: (a) The characteristic electrohydrodynamic velocity scaling and its corresponding Reynolds number are not externally imposed; rather, the flow is driven at the fluid-fluid interface via a balance between viscous and electrical shear stresses. At low Reynolds numbers, this balance provides Taylor's familiar field-squared scaling. At high Reynolds numbers, however, a boundary layer forms, whereby balancing the stresses we find a new velocity scaling, with the 4/3-power of the applied-field magnitude. (b) Schematic view in the meridian plane of the asymptotic regions in the limit of large Reynolds numbers. The thin line depicts the deformed bubble boundary.

^a Department of Mathematics, Technion – Israel Institute of Technology, Haifa 3200, Israel

^b Department of Aerospace Engineering, Technion – Israel Institute of Technology, Haifa 3200, Israel

¹ Taylor, *Proc. Roy. Soc. London A* **291**, 159 (1966).

² Melcher and Taylor, *Ann. Rev. Fluid Mech.*, **1** 111 (1969).

³ Schnitzer et al., *J. Fluid Mech.* **743**, R3 (2013).

A diffuse interface approach to study the pressure-induced collapse of a vapor bubble

F. Magaletti^a, L. Marino^a and C.M. Casciola^a

The vapor bubble dynamic plays a crucial role in a wide range of phenomena and technological applications such as the cavitation, naval propulsion, turbomachinery and more recently biomedical technologies. Since Lord Rayleigh, researchers developed mathematical models in order to predict the bubble behavior and response to hydrodynamic, thermal or acoustic forcing¹. In complex situations such as near wall phenomena, cloud bubble dynamics or extremely intense forcing, it is however necessary to analyze the entire hydrodynamic fields and it is not possible to use reduced models. Also the simple, but not trivial problem, of the pressure-induced collapse of a single vapor bubble requires a complete mathematical model in order to analyze the detailed thermo-mechanic fields during the shock formation and soon after its propagation into the liquid.

The tiny spatial scale and the highly rapid dynamic of the process make non-invasive and accurate experimental analyses very difficult to carry on. Hence, numerical investigation can be very useful to understand the complex mechanism during the bubble collapse. We here propose to adopt a diffuse interface approach to easily describe the two-phase fluid and to overcome all those difficulties of front-tracking methods (i.e. phase transition, topology changes, etc.). In particular, it will be used the Van der Waals extension of the free energy as a functional of temperature, density and density gradient ("second gradient fluids"). This model allows the description of the capillary stresses as a function of the density distribution inside the interfacial layer between liquid and vapor. Furthermore, owing to the Van der Waals equation of state, below the critical temperature it allows to describe liquid-vapor coexistence and transition².

In particular, the present proposal is focused on a numerical investigation of the effects of phase transition (that can change drastically the temperature and pressure involved with respect to the gas-bubble case³) and the so-called non-equilibrium condensation, extremely important in the final stage of the collapse when the interface velocity is high.

^a Dip. Ingegneria Meccanica e Aeronautica, Sapienza Università di Roma, Italia

¹ Plesset M.S., Prosperetti A., *Ann. Rev. Fluid Mech.*, **9**, 145 (1977)

² Jamet D., Lebaigue O., et al., *Nucl. Eng. And Design*, **204**, 155 (2001)

³ Johnsen E. and Colonius T., *J. Fluid Mech*, **629**, 231(2009)

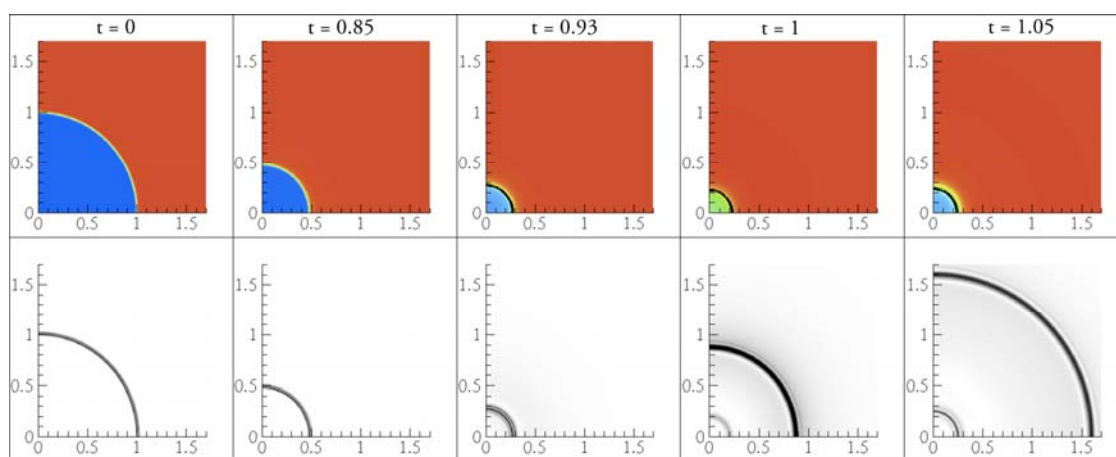


Figure 1: Figure shows successive configurations of the system during the collapse. The first colored row represents the density field (in blue the vapor, in red its liquid). The black solid line in the third-fifth pictures divide the fluid in supercritical conditions (inside pressure and temperature are greater than the critical values) from the liquid phase. The second row represents the intensity of the pressure gradient that helps to identify the interface and the shock (clearly visible in the forth and fifth pictures) positions.

Numerical simulations of bubble-bubble interactions using Smoothed Particle Hydrodynamics

K. Szewc^a

Bubble rising through viscous liquids is one of the most common gas-liquid flow phenomena and, as such, is encountered in various industrial processes. In the most practical problems, bubbles do not move as a single, but rather large groups of moving bubbles. Therefore, the present work is devoted to the problem of modelling bubble-bubble interactions. This is a continuation of the previous research, presented in EFMC9, on the application of the Smoothed Particle Hydrodynamics (SPH) method for simulation of single bubbles rising in water, cf. Szewc et al.¹. The SPH method is a fully Lagrangian, particle-based approach for fluid-flow simulations. In the work, the first, fully 3D, SPH studies on the bubble-bubble interactions are presented. For that purpose, a multi-phase SPH formulation that can address large density differences is retained, while surface tension effects are explicitly accounted for through the Continuum Surface Force (CSF) model. One of the main advantages over Eulerian techniques is no necessity to handle the shape of the interface as in Volume-of-Fluid, Level-Set or Front-Tracking methods. Therefore, this method appears as suitable for multi-phase flows with interfaces or free-surface flows. Numerical simulations of bubble-bubble interactions were performed for different regimes, corresponding to different relative importance of surface tension, viscosity and buoyancy effects. The SPH results of bubble coalescence simulations are compared with the experimental data of Duineveld², as well as, other numerical results obtained with the Moving Particle Semi-implicit method by Chen et al.³, the Lattice Boltzmann Method (LBM) by Cheng et al.⁴ and Front-Tracking by Hua et al.⁵. All the presented SPH calculations were accelerated using Graphical Processing Units (GPU). Some issues related to SPH programming on GPU are also discussed.

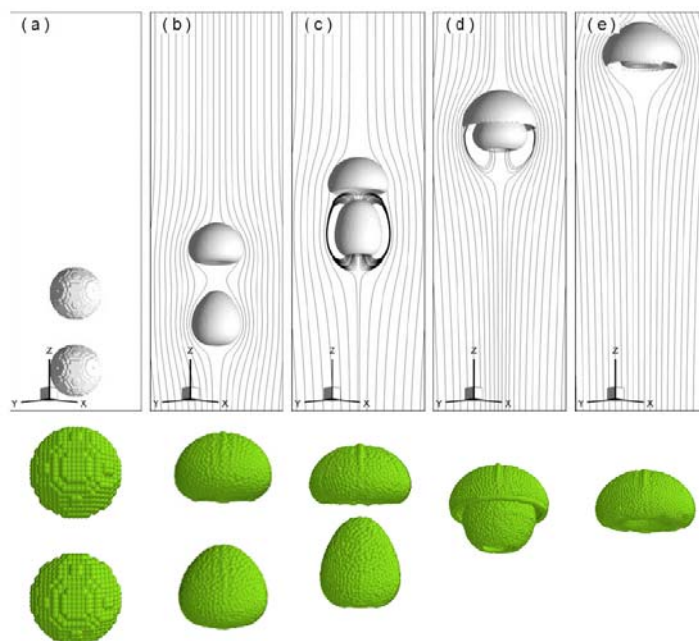


Figure 1. LBM (upper) and SPH (lower) simulations of bubble shapes evolution for coalescence of two bubbles at different times; LBM results obtained by Cheng et al.⁴.

^a Institute of Fluid-Flow Machinery, Polish Academy of Sciences, ul. Fiszerza 14, 80-231 Gdańsk, Poland

¹ Szewc et al., *Int. J. Multiphase Flow* **50**, 98-105 (2013)

² Duineveld, *Appl. Sci. Res.* **58**, 409-439 (1998)

³ Chen et al., *Chem. Eng. Sci.* **66**, 5055-5063 (2011)

⁴ Cheng et al., *Comput. Fluids* **39**, 260-270 (2010)

⁵ Hua et al., *J. Comp. Phys.* **227**, 3358-3382 (2008)

Pipe wall thinning by flow accelerated corrosion of single-phase and gas-liquid two-phase bubbly flows

Toshihiko Shakouchi^a, Koichi Kinoshita^a, Koichi Tsujimoto^a and Toshitake Ando^a

The pipe wall thinning by flow accelerated corrosion, FAC, is a serious problem because it leads to the destruction of piping system of power plant, chemical plant, and others. Figure 1 shows the wall thinning rate in the downstream of orifice flow meter of the Lines A and B at the Unit 3 of Mihama Nuclear Power Plant, Japan.

Bignold, et al. and Yoneda, et al. showed a pipe wall thinning rate TR [mm/year] in the downstream of orifice for a single phase water flow can be expressed as a function of square of the pipe mean velocity u_m , $TR=F(u_m^2)$, and we have shown TR can be expressed as a linear function of the pressure fluctuation p' , $TR=F(p')$, on the pipe wall. Then, it was known that TR can be estimated by the measurements of p' , and in other word this means a decrease of p' leads to the decrease of a wall thinning rate.

In this study, the wall thinning in the downstream of the orifice for a single-phase and gas-liquid two-phase bubbly flow in a vertical pipe of diameter $D=40.0$ mm were examined. The flow pattern was observed, recorded by a high speed video camera and examined, and the pressure fluctuation p' was measured by a semi-conductor type small pressure transducer. Figure 2 shows an example of visualized flow pattern of gas-liquid bubbly flow of $\alpha=2.5\%$ passing through the orifice plate of contraction area ratio $CR=0.36$. Where, α is the volumetric flow rate ratio of air to air-water mixture flow. White coloured parts are bubbles and the mean size in the up- and downstream of orifice were about 2.4 and 2.2 mm, respectively. Figure 3 shows an example of p' distribution in the downstream of the orifice for a gas-liquid bubbly flow. p' for bubbly flow takes a larger value than that for single phase water flow and it increases with increasing α . As mentioned above, the increase of p' results in the increase of TR . By the way, reducing the pipe diameter $D_p (< D)$ of the downstream of orifice p' decreases with a same pressure loss Δp of Std. Figure 4 shows the maximum pressure fluctuation p'_{max} for $\alpha=2.5\sim 10\%$. Std- $D_p=38.8$ mm took a minimum of p'_{max} with a same pressure loss Δp of Std for all α . This means Std- $D_p=38.8$ mm can reduce the wall thinning rate TR for bubbly flow with a same pressure loss Δp of Std.

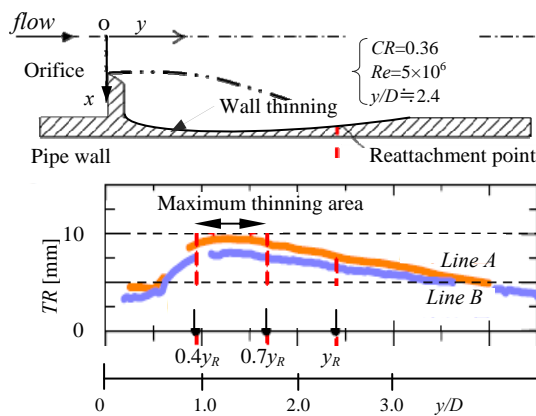


Fig.1 Wall thinning rate by FAC (by Yoneda, et al.)

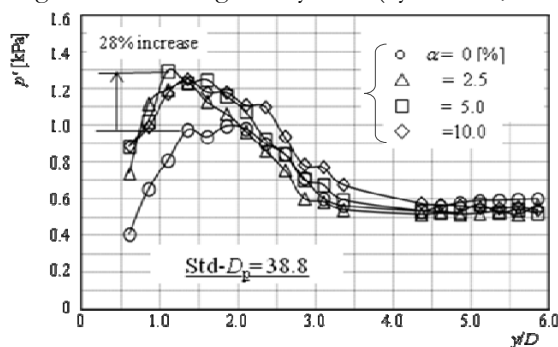


Fig.3 Pressure fluctuation p' on the pipe wall

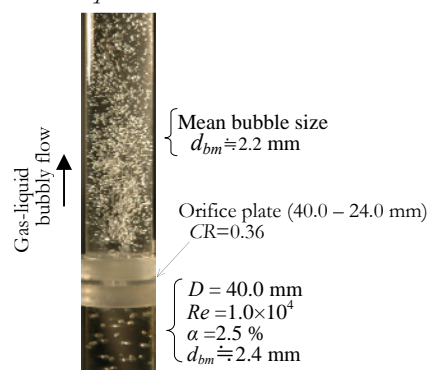


Fig.2 Visualized flow pattern

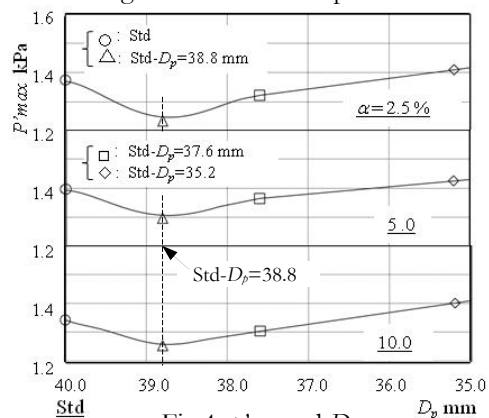


Fig.4 p'_{max} and D_p

^a Graduate School of Engineering, Mie University, Kurimamachiya-cho 1577, Tsu-shi, Mie 514-8507, Japan

On path instability of a rising bubble in dilute surfactant solution

Y. Tagawa^a, S. Takagi^b and Y. Matsumoto^b

We experimentally investigate the effect of surfactant on three-dimensional motion of a single bubble rising in quiescent liquid. Fig. 1(a) shows our experimental setup, consisting of two high-speed cameras and vertical traverse systems for measuring three-dimensional trajectories, velocities, and aspect ratios of the bubble. The control parameters are the diameter of the bubble in the range of 1–4 mm and the surfactant concentration of 1-Pentanol or Triton X-100. Owing to so-called Marangoni effect, the addition of surfactant changes the surface slip condition from a free-slip to a no-slip. We quantify the slip condition using the normalized drag coefficient C_D^* which is the measured drag coefficient scaled with the drag coefficients of a free-slip and a no-slip condition. We demonstrate that the three-dimensional motion has been changed drastically with varying surfactant concentration. We examine the relationship between the slip condition and the forces acting on the bubble. Remarkably, the lift force shows a non-monotonic dependence on the slip condition, although the direction of the lift is almost constant in the reference frame that rotates with the bubble along its trajectory. It implies that the double-threaded wake has the fixed alignment of the vortices. We also observe the transient trajectory starting from helical to zigzag (see Fig. 1(b)), which has never been reported before. Its instantaneous frequency of the bubble horizontal velocity agrees with that of quasi-steady motions, indicating that the wake can follow the time evolution of the slip condition in a very short time in our case. In addition, we investigate the parameter range for obtaining straight/helical/zigzag motion in the Re - C_D^* space as shown in Fig. 1(c). In the case of a free-slip and a no-slip condition, types of bubble motions are strongly dependent on Re while those in intermediate slip conditions of $0.4 < C_D^* < 0.6$ are helical for the broad Re range of $300 < Re < 900$.

^a Dep. Mech. Sys. Eng., Tokyo University of Agriculture and Technology, Nakacho, Koganei, Tokyo, Japan

^b Dep. Mech. Eng., The University of Tokyo, 7-3-1 Hongo, Bunkyo-ku, Tokyo, Japan

¹ Tagawa et al., *J. Fluid Mech.* **738**, 124 (2014).

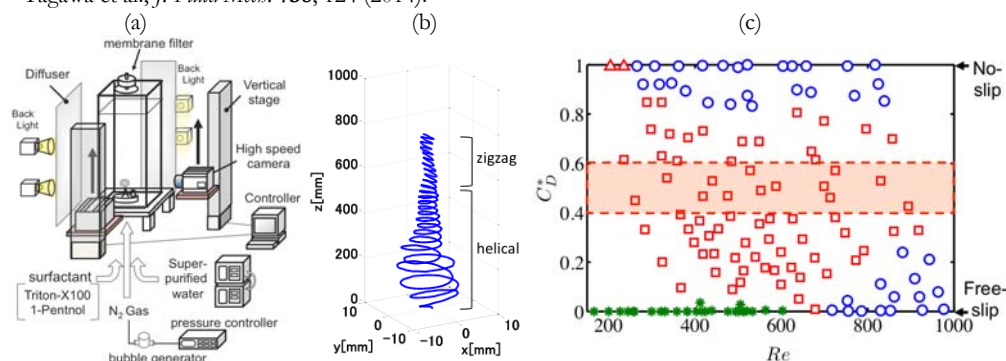


Figure 1: (a) Experimental setup (b) A trajectory of a bubble in surfactant solution (c) Phase diagram of bubble motions; straight (green star), zigzag (blue circle), and helical (red square).

Effect of the injector geometry and the operation conditions on the bubble formation in a planar air-water coflow configuration

R. Bolaños-Jiménez^a, C. Gutiérrez-Montes^a, A. Sevilla^b and C. Martínez-Bazán^a

In this work, an exhaustive numerical study, employing the open source CFD code OpenFOAM, has been conducted to analyse the effects of the nozzle geometry and operating conditions on the dynamics of a planar water-air-water jet. In particular, we quantify both the jetting-to-bubbling transition threshold and the main features of the periodic bubbling regime, as functions of the water-to-air thickness ratio, $h=H_w/H_o$, the inner-to-outer thickness ratio of the air injector, $\beta=H_i/H_o$, the shape of the splitter plate edge (sharp or rounded), the water velocity profile at the exit slit, and the air feeding conditions. Regarding the jetting-to-bubbling transition, our results have revealed that the air sheet becomes more stable as the wall thickness grows (decreasing β , Fig. 1a), the water sheets are thicker (increasing h , Fig. 2a), the injector shape is more sharpened, and the boundary layer in the water stream grows. In addition, the jetting-to-bubbling transition found numerically is in good agreement with the predictions given by a model based on local stability analysis, proposed in Bolaños-Jiménez et. al.¹, indicating that the model properly captures the effects of h and β . Concerning the bubbling regime, it has been found that, for a given air velocity, the bubble formation frequency increases with β (Figs. 1 b,c), in the range of values herein explored, with a particularly strong dependence on the wall thickness for $\beta < 0.54$, in agreement with the scaling law developed by Gutiérrez-Montes et. al.². Moreover, the bubbling frequency is shown to increase when the water sheets are thinner (smaller h , Fig. 2 b,c), a rounded air injector lip is used, and an increasing water boundary layer is established. Finally, we demonstrate the important effect of the air feeding conditions, revealing that bubbles produced under constant pressure conditions are bigger than those produced under constant gas flow rate conditions. To summarize, our results clearly highlight the importance of the geometrical parameters and the operating conditions, usually disregarded in the analysis of bubble formation processes.

^a Área de Mecánica de Fluidos, Departamento de Ingeniería Mecánica y Minera, Universidad de Jaén, 23071 Jaén, Spain

^b Área de Mecánica de Fluidos, Departamento de Térmica y de Fluidos, Universidad Carlos III de Madrid, 28911 Leganés, Spain

¹ Bolaños-Jiménez et al., *J. Fluid Mech.* **682**, 519–542 (2011).

² Gutiérrez-Montes et. al., *Int. J. Multiphase Flow* **50**, 106–119 (2013).

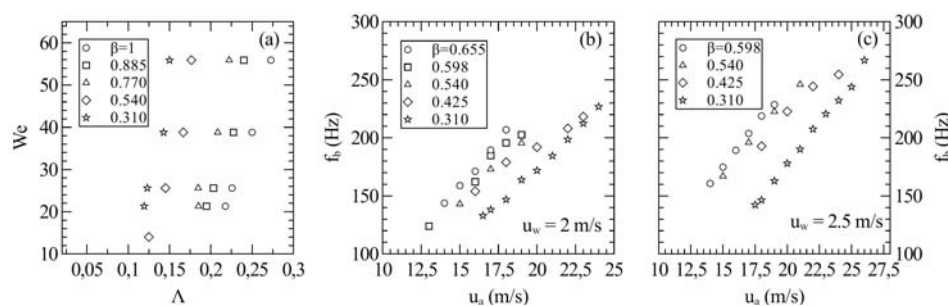


Figure 1: Influence of β on the (a) jetting to bubble transition in the $We = \rho_w u_w^2 H_o / \sigma - \Lambda = u_w / u_a$ plane, (b) bubbling frequency, f_b , as a function of the air velocity, u_a , for water velocity $u_w = 2$ m/s (c) bubbling frequency $u_w = 2.5$ m/s.

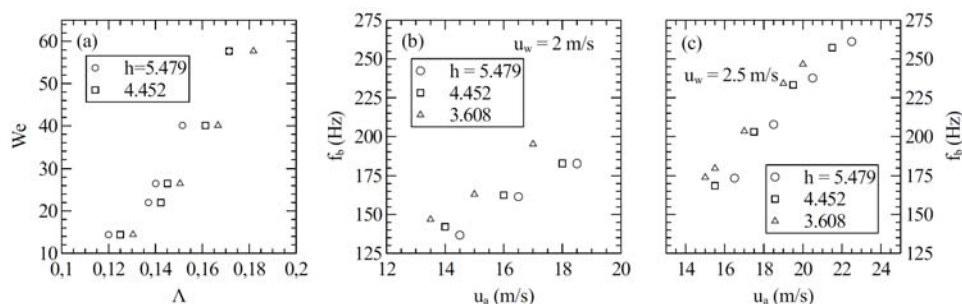


Figure 2: Influence of h on the (a) jetting to bubble transition, (b) bubbling frequency f_b , as a function of the air velocity, u_a , for water velocity $u_w = 2$ m/s (c) bubbling frequency for water velocity $u_w = 2.5$ m/s.

A global stability approach to the path instability of a freely rising spheroidal bubble

J. Tchoufag¹, J. Magnaudet², D. Fabre¹

A great amount of work has been devoted to understand the mechanisms at the root of path instabilities of isolated rising bubbles. Indeed, this problem can be tracked back to Leonardo's drawings of the spiralling motion of such bubbles¹.

In this work we investigate the path instability of rising oblate spheroidal bubbles in a viscous fluid otherwise at rest. This is done in the framework of global stability, with the aim of understanding the fundamental (linear) processes that break the stability of the initially vertical path. To this end, we make use of a novel stability approach² which considers the fully coupled fluid+bubble system. In line with previous studies³ which proved relevant, we consider oblate ellipsoidal bubbles with a prescribed fore-aft symmetric shape characterized by their aspect ratio χ , rising at a velocity which defines the second control parameter Re . The results to be presented at the conference are two-fold.

First, we confirm the prominent role of the wake on the path instability by comparing the stability phase diagram of the freely rising bubble in the (χ, Re) plane to that obtained with a fixed bubble. Secondly, contrary to disks and spheres which always shed short vortices (with length about two to three equivalent diameters), oscillating bubbles can be followed by elongated counter-rotating vortices (with length about eight to ten equivalent diameters) as if the wake had rather undergone a steady bifurcation. On the basis of our global stability study and of previous investigations^{4,5} (see figure 1), we provide a heuristic explanation to the origin of this peculiar unsteady double-threaded wake.

¹ Université de Toulouse, IMFT, Allée Camille Soula, 31400 Toulouse, France.

² CNRS, IMFT, 31400, Toulouse, France.

¹ Prosperetti, *Phys. Fluids* **18**, 1852 (2004)

² Tchoufag et al., *J. Fluid Mech.* **740**, 278 (2014)

³ Magnaudet and Mougin, *J. Fluid Mech.* **572**, 311 (2007)

⁴ Mougin and Magnaudet, *Phys. Rev. Lett.* **82**, 014502 (2002)

⁵ Zenit and Magnaudet, *Int. J. Multiphase Flow* **35**, 195 (2009)

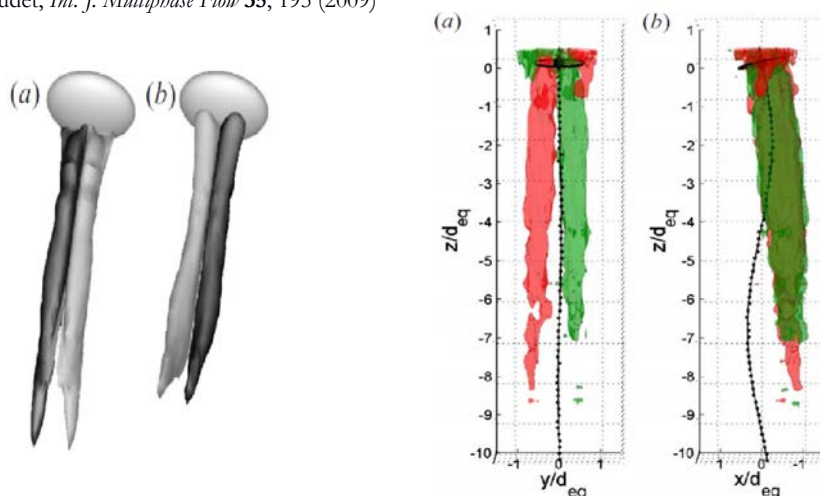


Figure 1: Iso-surfaces of axial velocity of a rising spheroidal bubble from DNS (left) and experiment (right). On the left are two snapshots separated by a period of oscillation for a bubble with $\chi=2.5$ and $Re=835$. On the right are two orthogonal views of the motion of a bubble with $\chi=2.1$ at $Re \approx 113$.

Evolution of the wake of an oscillating bubble rising in a thin-gap cell

A. Filella¹, P. Ern^a, V. Roig^a

As a first step to improve our understanding of the hydrodynamical interaction between two bubbles rising in a thin-gap cell, we investigate the dynamics of the wake of an isolated bubble. A single bubble rising in a liquid at rest at high Reynolds number is a complex dynamical system where shape and path oscillations are coupled to the instability of the wake. When a bubble of diameter d is confined in a thin-gap cell of width w , with $w < d$ and $w \leq l_c$ (l_c being the capillary length), various contrasted regimes of oscillations appear depending on the Archimedes number Ar^2 , and their dynamics are strongly modified with respect to the unconfined case due to the shear stress exerted at the walls.

In the present experimental contribution, we focus on the analysis of the unsteady wake of a bubble rising in water for $Ar = 1535$ and $w/d = 0.5$. The bubble is flattened in the gap and has a constant ellipsoidal shape in the plane of the cell. Far enough from the interface, the perturbation induced by the bubble in the liquid is mainly an in-plane motion. We investigate the relation between the bubble motion and the bubble wake using simultaneous measurements of the bubble kinematics and of the liquid velocity averaged over the gap $\mathbf{u}(x, y, t) = u_x \mathbf{e}_x + u_y \mathbf{e}_y$ (where x and y are in-plane coordinates). High-speed shadowgraphy and high-frequency PIV with volume enlightening were implemented to explore the dynamics in a fixed window crossed by the bubble during its rise.

When the bubble moves, an intense ascending flux of liquid is generated in its wake and significant vortices are observed in the plane of the cell. Their location, intensity and size have been determined. Three different stages can be identified for the wake evolution:

- (i) an *initial stage* where vortices coupled to the oscillations of the bubble path are released periodically and translate while decaying in intensity. After the bubble passage this initial stage lasts for a short duration of the order of T , the period of oscillation of the bubble. The time evolutions of the intensity of the vortices and of the velocity in the ascending region show clear exponential decay during this initial stage.
- (ii) an *intermediate stage* where complex non-linear interactions are observed between vortices, the wavelength of the array relaxing to a value equal to twice the initial wavelength.
- (iii) and finally a *long-term stage* where the spatial organization of the vortices persists for long times, while the global intensity of the motion is damped by the shear stress at the walls. The exponential decay in this stage is controlled by the viscous time scale $\tau_v = w^2/(4\nu)$.

¹ Institut de Mécanique des Fluides de Toulouse, Université de Toulouse and CNRS, Allée du Prof. C. Soula, 31400 Toulouse, France.

² Roig et al., *Journal of Fluid Mechanics*, **707**, 444, (2012).

Passive scalar transport in bubbly flows

A. Loisy^a, A. Naso^a and P.D.M. Spelt^a

Bubbly flows are encountered in a wide range of applications (oil/gas transport, nuclear reactors, CO₂ capture). In such flows the rate of heat and mass transport is strongly coupled to the dynamics of bubbles and to the disturbances they create in the surrounding fluid. As a first step toward the formulation of a macroscale model of bubbly flows with scalar transport, we focus on the characterization of the finite size and finite volume fraction effects of bubbles on scalar transport in suspensions.

Three-dimensional direct numerical simulations of passive scalar transport involving laminar flow of a suspension (modeled as a periodic array) of deformable bubbles have been conducted at the microscale (bubble scale). This remains still largely unknown territory ; prior work is either on scalar transport in systems with a single bubble¹ or on rising periodic arrays of bubbles in the absence of scalar transport^{2,3}. Our present approach does allow us to simulate strongly deformable bubbles in an array (Figure 1a).

The influence of volume fraction on bubble dynamics have been assessed for various combinations of Morton and Eötvös numbers leading to various bubble shapes (spherical, ellipsoidal, dimpled ellipsoidal-cap). We show that commonly used empirical correlations for the bubble drift velocity do not capture properly finite volume fractions effects and propose an alternative description for this system.

The main problem is though to characterize scalar transport in bubbly liquids in terms of macroscale transport properties. We use a macroscale model where the closure is performed by means of an effective diffusivity tensor and investigate its dependency on the bubble volume fraction, Péclet number and flow regime, allowing for substantial bubble deformation and inertial effects. Existing theory⁴ for the effective diffusivity in the context of fixed point-particles is extended to finite-size bubbles and compared to our numerical simulations for Péclet numbers ranging from 0 to 10⁴ (Figure 1b). Preliminary results will also be presented for turbulent bubbly flows in otherwise the same configuration, which would result in isotropic turbulence in the absence of bubbles.

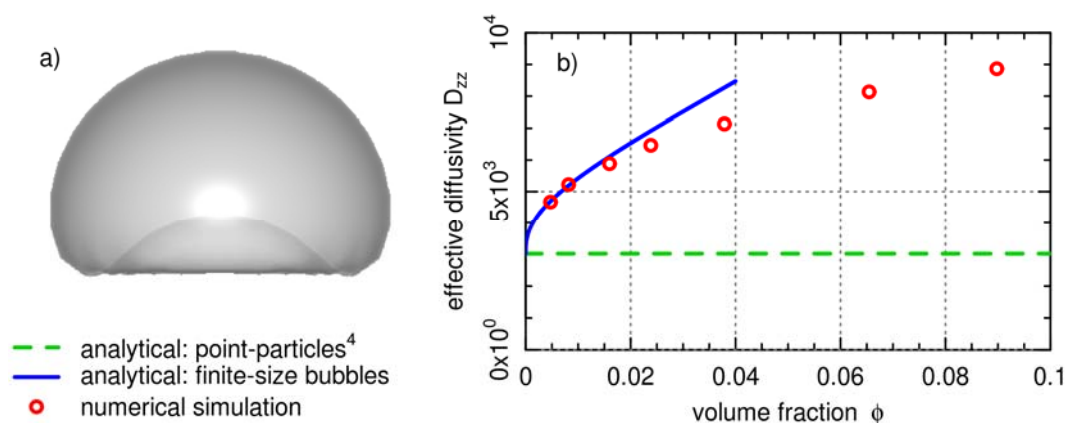


Figure 1: a) Example of strongly deformed bubble; b) Streamwise component of the effective diffusivity as a function of bubble volume fraction in a Stokes flow at Péclet = 1000.

^a Laboratoire de Mécanique des Fluides et d'Acoustique (LMFA), CNRS, Ecole Centrale de Lyon, Université Claude Bernard Lyon 1, INSA Lyon, Ecully, France.

¹ Figueroa-Espinoza and Legendre, *Chem. Eng. Sci.* **65**, 6296 (2010).

² Esmaeeli and Tryggvason, *J. Fluid Mech.* **385**, 325 (1999).

³ Sankaranarayanan et al., *J. Fluid Mech.* **452**, 61 (2002).

⁴ Koch et al., *J. Fluid Mech.* **200**, 173 (1989).

The wetting of a bubble

S. T. Thoroddsen^a, E. Q. Li^a and I. U. Vakarelski^a

The partial coalescence of drops^{1,2,3} and bubbles⁴ at a liquid interface has been studied extensively, owing to its relevance to the coarsening of emulsions. For a liquid drop the resulting satellite is about 50% of the original drop size, which can lead to a cascade of coalescences¹. The pinch-off of a satellite also occurs when two bubbles coalesce, but the satellite is much smaller in this case, at only about 10% of the mother bubble⁴. Here we study a related configuration where a bubble passes through an interface between two immiscible liquids. For the bubble to pass fully through the interface, the liquid-air surface tension must be lower in the receiving liquid, for net energy release, but the hydrodynamics at the triple line also influence the surface dynamics of this process. For sufficiently low viscosity we also observe satellite pinch-off from the bubble during this transition, as is shown in Fig. 1.

The controlling parameter for partial coalescence for drops and bubbles is the Ohnesorge number². However, for our configuration there are three separate surface tensions at play, i.e. between the air and each of the liquids as well as between the two liquids. We use numerous different liquid combinations to determine the most appropriate Oh , which is based on the net surface tension acting at the triple line⁵. We also study the growth rate of the neck connecting the bubble to the receiving liquid, finding power-laws with exponents slightly smaller than $1/2$.

We also focus on the role of the triple line friction, when the viscosity of the receiving liquid is increased, using a range of silicone oils. The initial motions of the neck are greatly slowed down when the receiving liquid viscosity is increased. This is qualitatively different from the coalescence of two miscible drops of different viscosities, where the lower viscosity controls the neck motion. This highlights the importance of the triple-line dynamics, which is absent in the miscible case. This configuration may be ideal to study these dynamics over a range of liquid properties.

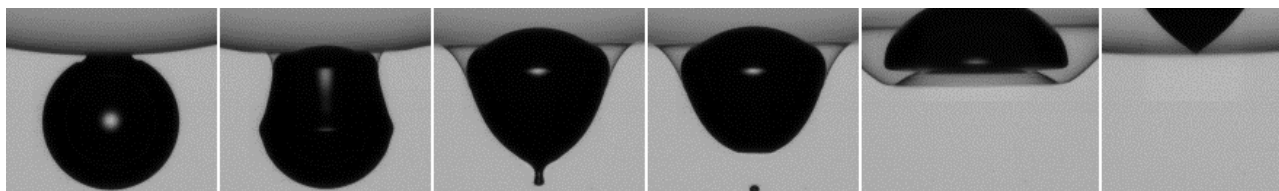


Figure 1: Bubble passing through an interface between two immiscible liquids, showing the pinch-off of a bubble satellite. The initial bubble is 446 microns in diameter and the total sequence takes 1.7 ms.

^a Division of Physical Sciences and Engineering, King Abdullah University of Science and Technology (KAUST), Thuwal 23955-6900, Saudi Arabia.

¹ Thoroddsen and Takehara, *Phys. Fluids*, **12**, 1265 (2000).

² Blanchette and Bigioni, *Nat. Phys.*, **2**, 254 (2006).

³ Gilet et al. *Phys. Rev. E*, **75**, 036303 (2007).

⁴ Zhang and Thoroddsen, *Phys. Fluids*, **20**, 022104 (2008).

⁵ Li, Al-Otaibi, Vakarelski and Thoroddsen, "Satellite formation during bubble transition through an interface between immiscible liquids", *J. Fluid Mech.* (in press).

⁶ Thoroddsen et al., *Phys. Fluids*, **19**, 072110 (2007).

Geometry as Catalyst: Flow Induced Cavitation at Surface Defects

C.M. Casciola, A. Giacomello, S. Meloni, M. Chinappi

Liquid motion is known to induce cavitation when the local pressure falls below a certain threshold. The onset of cavitation is strongly enhanced by the presence of rough surfaces or impurities in the liquid. Despite decades of research, the way these defects promote the nucleation of bubbles remain however largely unclear. As a consequence the modeling of cavitation inception still largely relies on purely empirical models. We present here a comprehensive explanation of the catalytic action that roughness elements exert on the nucleation process [1] and discuss, along the lines of [2], a thermodynamic continuum theory of the cavitation process. The approach allows determining the nucleation rate at the surface defects, as a function of the local thermodynamic conditions set by the flow. Knowledge of the nucleation rate, in its turn, can be exploited to develop stochastic models for the activation of cavitation nuclei, both at the solid walls bounding the flow and at solid impurities transported by the flow. Overall, the approach we illustrate highlights a sharp decrease of the free energy barriers connected with cavitation and demonstrates the existence of intermediate metastable states that break the nucleation process in multiple steps, see the figure reported below. The devised continuum theory can be coupled to standard fluid dynamic models in view of the rational simulation of flow-induced cavitation.

[1] A. Giacomello, M. Chinappi, S. Meloni, C.M. Casciola, *Langmuir* 2013.

[2] A. Giacomello, M. Chinappi, S. Meloni, C.M. Casciola, *Phys. Rev. Lett.* 2012.

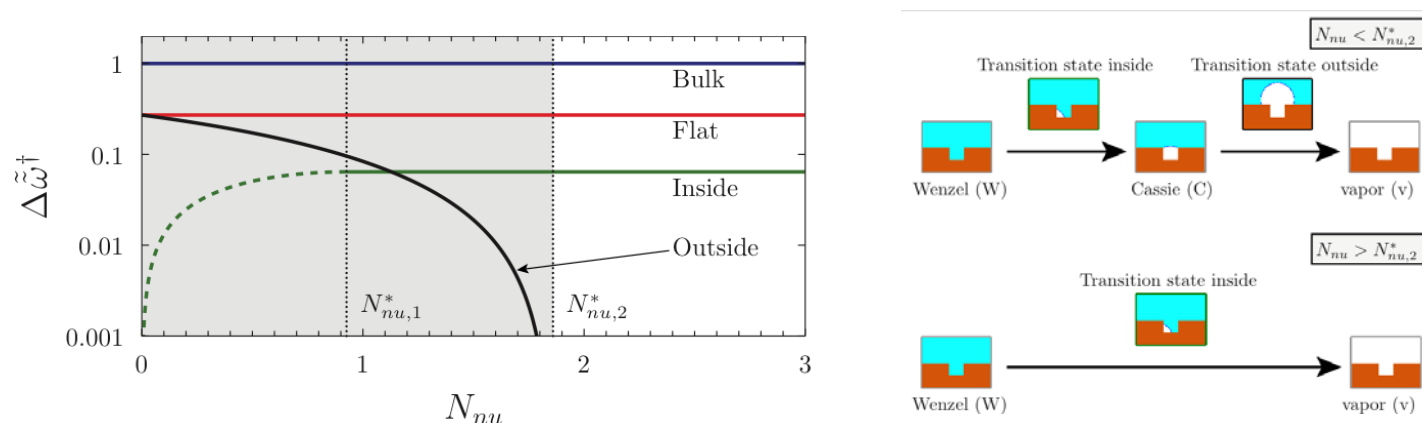


Figure - Left: Free-energy barriers for the nucleation of a vapor bubble. Different nucleation modes are possible, with the process occurring in one or two steps. Right: Sketch of metastable states and transition states.

Deformation statistics of sub-Kolmogorov-scale ellipsoidal drops in isotropic turbulence

Luca Biferale^a, Charles Meneveau^b, and Roberto Verzicco^c

Small droplets in turbulent flows can undergo highly variable deformations and orientational dynamics. For neutrally buoyant droplets smaller than the Kolmogorov scale, the dominant effects from the surrounding turbulent flow arise through Lagrangian time histories of the velocity gradient tensor. Here we study the evolution of representative droplets using a model that includes rotation and stretching effects from the surrounding fluid, and restoration effects from surface tension including a constant droplet volume constraint, while assuming that the droplets maintain an ellipsoidal shape [1]. The model is combined with Lagrangian time histories of the velocity gradient tensor extracted from Direct Numerical Simulations of turbulence [2] to obtain simulated droplet evolutions. These are used to characterize the size, shape and orientation statistics of small droplets in turbulence. A critical capillary number is identified associated with unbounded droplet growth. Exploiting analogies with dynamics of polymers in turbulence, the critical capillary number can be predicted based on the large deviation theory for the largest Finite Time Lyapunov exponent quantifying the chaotic separation of particle trajectories. Also, for sub-critical capillary numbers near the critical value, the theory enables predictions of the slope of the power-law tails of droplet size distributions in turbulence. For cases when the viscosities of droplet and outer fluid differ in a way that enables vorticity to decorrelate the shape from the straining directions, the large deviation formalism based on the stretching properties of the velocity gradient tensor loses validity and its predictions fail. Even considering the limitations of the assumed ellipsoidal droplet shape, the results highlight the complex coupling between droplet deformation, orientation and the local fluid velocity gradient tensor to be expected when small viscous drops interact with turbulent flows. The results also underscore the usefulness of large deviation theory to model these highly complex couplings and fluctuations in turbulence that result from time integrated effects of fluid deformations.

The results are compared with the orientation dynamics and statistics of rigid triaxial ellipsoidal particles in isotropic turbulence of [3].

^a Dep. Physics, Università di Roma Tor Vergata, Roma Italy

^b Dep. Mechanical Engineering, The Johns Hopkins University, Baltimore, MD 21218, USA

^c Dep. Ind. Engineering Università di Roma Tor Vergata, Roma Italy & PoF MESA+ University of Twente, Enschede, The Netherlands

¹ Maffettone, P.L. & Minale, M. *J. Non-Newt. Fluid Mech.* 78, 227–241, (1998).

² Cencini, M., Bec, J., Biferale, L., Boffetta, G., Celani, A., Lanotte, A.S., Musacchio, S. & Toschi, F. *J. of Turbulence* 7, 1–16., (2006)

³ Chevillard, L. & Meneveau, C., *J. Fluid Mech.* 337, 187–193, (2013)

Experimental Technique

Impact of the mesh/twine ratio on the flow through a porous hollow cylinder

B. Levy^a, H. Friedrich^b, J. Cater^a, R. Clarke^a and J.P. Denier^a

With the expansion of affordable, accurate and small-scale machineries, it has become possible to precisely investigate the flow through and around objects with a regular, well defined, regular porosity. The flow around a cylinder is robust and well documented¹⁻², and is important in many flow control applications. Recent research has showed that a porous cylinder surrounding a solid cylinder could have significant impacts on the two-dimensional flow topology³. We extend this work by considering the three-dimensional flow and the resulting forces associated with a solitary porous cylinder.

We have investigated the impact of the mesh/twine ratio on the flow through a porous hollow cylinder named “pen” at moderate Reynolds numbers (800 to 20 000). For this purpose, 30 circular “pens”, with a surface porosity varying from 0.56 to 0.90, were manufactured. The geometry of our small-scale laboratory approach mimics the structures that are employed in aquaculture net cages⁴. Our results show that the porosity factor ε is not the key parameter on the flow topology and the load applied by the currents on the structure.

Experimental data acquired with Time-Resolved Particle Image Velocimetry (TR-PIV) show the impact of the geometry on the diffusivity of the flow as it passes through the pen. At a constant porosity, but differing mesh/twine ratio, the flow can significantly vary. Firstly, a time averaged wake, with multiple vorticity strips inside and outside the pen generated by the twines, is observed (Fig. 1a). Our experiments show a recirculation zone, with only two bulbs of vorticity detectable inside the pen (Fig. 1b). We identify a parameter, α , based on the pen geometry that collapses the averaged flow velocity in the wake of the pens thereby providing a criterion for the velocity magnitude in the wake of similar structures. Plotting the drag coefficient C_d versus α , collapses our data and displays an asymptotic behaviour, suggesting the existence of an optimized mesh/twine ratio. Finally, we present experimental load cell measurement, which are used to predict the load acting on the pen as a function of the pen geometry. For this purpose a second parameter, β , is introduced.

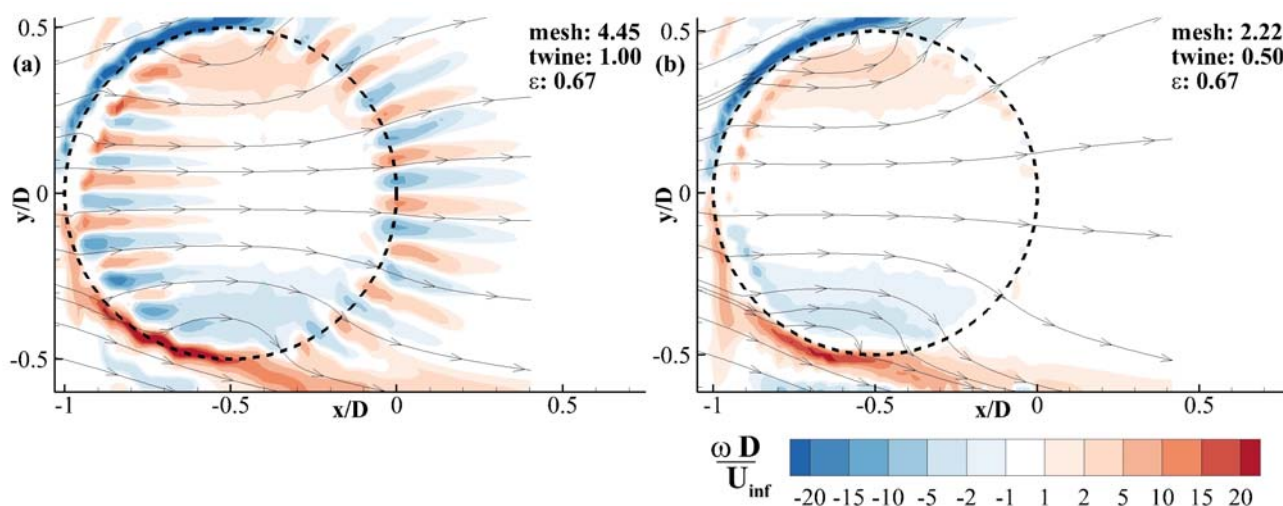


Figure 1: Time averaged vorticity distribution and stream lines around two pens of same porosity ($\varepsilon = 0.67$) but varying mesh and twine size (a) mesh = 4.45 mm and twine = 1.00 mm (b) mesh = 2.22 mm and twine = 0.50; $Re = 900$.

^a Dept. Engineering Science, The University of Auckland, Auckland, New Zealand

^b Dept. Civil and Environmental Engineering, The University of Auckland, Auckland, New Zealand

¹ Williamson, *Annu. Rev. Fluid. Mech.* **28**: 477-539 (1996)

² Berman, *J. Fluids and Structures* **27**, 648-658 (2011)

³ Ozkan et al., *Exp. Fluids* **53**: 1751-1763 (2012)

⁴ Kristiansen and Faltinsen, *J. Fluids and Structures* **34**, 218-235 (2012)

An experimental investigation of influence of initial conditions on generation of vortex structures in a round jet by visualisation

M.V. Litvinenko^a, Yu.A. Litvinenko^a

The vortex structures, formed in jets, are an instrument of heat transfer intensification, increasing combustion efficiency, reducing aerodynamic noise. There are a lot of kinds of vortices, which can be generated in jets and they have different reasons of origin.

The results of experimental studies of influence of initial conditions (mean and fluctuation velocity distributions, a nozzle configuration, the presence of periodic roughnesses on the nozzle outlet) on the flow structure and generation of vortex structures in the round jets at low Reynolds numbers are presented. A round jet with a “top-hat” velocity profile at the nozzle exit is exposed to Kelvin–Helmholtz instability, associated with the formation of ring vortices. Visualisations of the jet cross-sections demonstrate the presence of the azimuthal “beams” spaced regularly on the jet periphery. Such beams indicate the streaky structures are generated directly from the outlet of the nozzle. Interaction of the ring vortices and streaky structures results in the generation of azimuthal Λ or Ω – like vortices. To fix azimuthal position and to exclude radial oscillations of the streaks these were forced artificially by roughnesses pasted onto the internal surface of the nozzle near the outlet. Evolution of longitudinal vortices downstream leads to the intensification of the mixing process of the jet with the surrounding gas and, then, its turbulization. It was found that acoustic field leads to intensification of interaction between Kelvin–Helmholtz vortices and streaky structures.

Changing the initial conditions at the nozzle exit, i.e. the streamwise mean velocity distribution, leads to a radical change of the flow characteristics. In the case of a laminar round jet with a parabolic velocity profile at the nozzle exit the flow is laminar for ten calibers, no the Kelvin–Helmholtz vortex rings and streaky structures. Influence of acoustic forcing on the laminar round jet with a parabolic velocity profile is not detected.

The round jet, formed at the exit of the curved channel with Dean vortices, has the features of development. It is known that secondary flow in curved channel creates conditions of formation of two counter-rotating Dean vortices. Fig. 1,a shows a smoke visualization of the round jet cross-section directly on the curved channel outlet and at various distances downstream (Fig. 1,b,c). Fig. 1,a shows two counter-rotating Dean vortices, which were generated in the curved channel. Downstream, deformation of the vortex structures can be observed, however, the vortex pair is clearly visible (Fig. 1,b). More complex vortex motion inside the jet flow can be observed in Fig. 1,c.

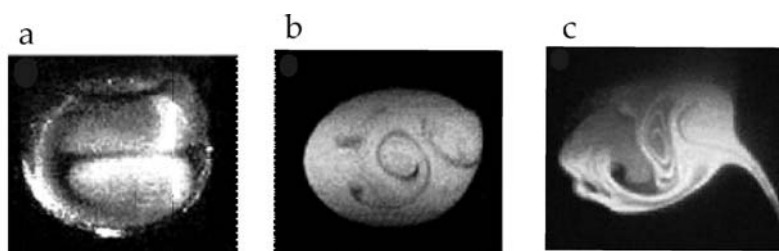


Figure 1: (a) The round jet cross-section directly on the channel outlet. (b, c) The round jet downstream cross-sections.

This study was supported by the Russian Foundation for Basic Research (Grant № 14-08-00201 a).

^a Khristianovich Institute of Theoretical and Applied Mechanics, Siberian Branch of Russian Academy of Sciences, Novosibirsk, Russia

Receptivity, stability and transition of supersonic boundary layer on swept wing

N. V. Seminov^a, A.D. Dryasov^{a,b}, A. D. Kosinov^{a,b}, and Yu. G. Yermolaev^a

The paper is devoted to an experimental study of excitation and evolution of instability disturbances and laminar-turbulent transition in a three-dimensional supersonic boundary layer. This problem is very interesting for the practical applications (similar boundary layers are observed in the flow around a swept wing of an airplane), and, on the other hand is very complicated^{1,2}. Excitation and evolution of all instability disturbances and their relative role in transition strongly depend on the environmental conditions. Note that up to now no experimental studies of receptivity of supersonic boundary layer on a swept wing.

The experiments were made in a low noise supersonic wind tunnel T-325 of the ITAM with test section dimension 200×200×600 mm at Mach numbers $M=2$ and 2.5, and unit Reynolds number $Re_1 = 5 \times 10^6 \text{ m}^{-1}$. Model was a symmetrical wing with a 45° sweep angle, a 3-percent-thick circular-arc airfoil. The model length was 0.4 m, its width was 0.2 m, and the maximum thickness was 12 mm. Edges of the model were with different bluntness. The disturbances were measured by constant temperature hot-wire anemometer. The frequency spectra of disturbances were determined by the discrete Fourier transformation. For receptivity experiments the source of vortex disturbances was designed and tested. Vortex perturbations were generated by a wire of various diameters, stretched in front of nozzle inserts.

Was designed and tested source of external disturbances (such sources are used at subsonic speeds). Vortex perturbations produced by a wire of various diameters, stretched in front of nozzle inserts. The experiments used a wire with a diameter $d = 0.63 \text{ mm}$, 0.95 mm , 1.9 mm and 3 mm . The research of structure of the disturbances created by the source of external disturbances was made. It was well known method, proposed by Kovasznay, that was applied for the interpretation of the hot-wire measurements in the supersonic flows. It was found that the level of mass flux pulsation and stagnation temperature increases with the growth of wire diameter.

The positions of the laminar-turbulent transition for all sources of external perturbations were determined. The effect of the wire diameter on the intensity of generated in the boundary layer disturbances and the transition location was obtained. Streamwise disturbances evolutions at different sources of external disturbances for the cases of sharp leading edge (left) and blunted leading edge (right) are shown in fig. 1. Maxima in these dependences correspond to laminar-turbulent transition. The curves of disturbances growth, profiles of mass flux pulsations and mean voltage were measured, amplitude-frequency spectra were obtained and statistical analysis was conducted. Profiles of pulsation have two maxima, first corresponds to critical layer, second – subsonic layer. It was found that the source of disturbances with wire diameter $d = 0.6 \text{ mm}$ does not affect the intensity of the perturbation generated in the boundary layer model and on the location of the laminar-turbulent transition. Increasing the diameter of the wire leads to the growth of the intensity of the excited disturbances and early appearance of non-linear processes, which in turn leads to the destabilization of the boundary layer. Factors of the receptivity were determined.

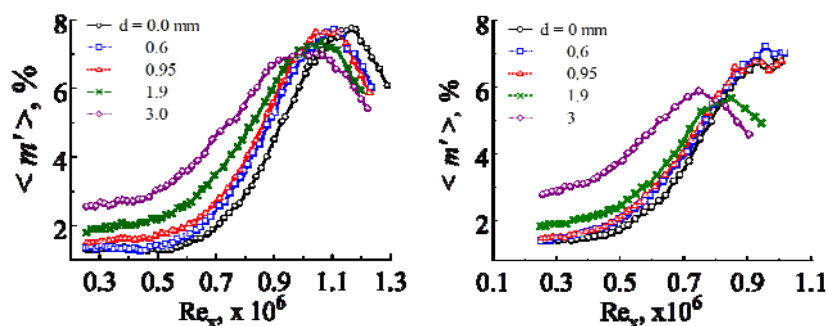


Figure 1: Dependences of mass flux pulsation $\langle m' \rangle$ versus Reynolds number Re for different wire diameters.

^a Khristianovich Institute of Theoretical and Applied Mechanics SB RAS, Novosibirsk, Russia

^b Novosibirsk State University, Novosibirsk, Russia

¹ Ermolaev et al., *TsAGI Science Journal*, XLII (1), 1 (2011)

² Semionov et al., *Progress in flight physics*, V.5, 73 (2013)

Size and density effect on the flow felt by a particle

N. Machicoane^a, Jean-François Pinton^a, Mickael Bourgoïn^b, and Romain Volk^a

The understanding of material particles dynamics in turbulence is a challenge with many impacts in industrial or natural applications. We call material particles objects whose size D is greater than the smaller length scale of the flow (Kolmogorov scale, noted η) and whose density can be different from the one of the carrying flow. Those particles, because of additional forces acting on them, behave very differently from fluid particles. Most studies conducted focus on how Lagrangian statistics, such as velocity or acceleration variances, are affected by the particle characteristics. However, very few studies refer to material particles dynamics in a large flow volume, as it leads to deal with an inhomogeneous and/or anisotropic turbulence. How the flow felt by particles changes with their characteristics is a question that has only been briefly addressed. It has been shown that large neutrally buoyant particles present the same mean velocity flow in a counter-rotating von Kármán setup in the range of diameters $D/\eta=40-270$ ¹.

We use a 3D Shadow Particle Tracking Velocimetry with 2 high-speed cameras to track particles in the volume of a counter-rotating von Kármán flow, of square section for better optical access. We create two parallel light beams that go through the tank in two perpendicular directions and are each collected by a camera (figure 1). We can then obtain the 3D trajectories of micrometric particles in a 7 cm side cube (the disks are spaced by 15 cm), where the two beams intersect, for times of the order of several large-eddy turnover times. This large region in the center of the tank corresponds to a good part of this von Kármán mean flow (composed of two counter-rotating toroidal cells and poloidal recirculations). We use different particles (of size 250-750 μm) and change the Kolmogorov length scale using different rotating frequencies or fluid viscosities to cover a range of size ratio $D/\eta=1-35$ and density ratio $\rho_{\text{particle}}/\rho_{\text{fluid}}=1-2.5$ with Taylor micro-scale based Reynolds number $R_\lambda=150-500$. With this technique, we investigate the Lagrangian statistics of the particles but we also reconstruct the fields felt by the particles in 3D through an Eulerian-Lagrangian conditioning. Doing so, we quantify the effect of the particles characteristics on the mean or fluctuating fields of velocity or acceleration and the impact of the flow structure on the Lagrangian statistics (such as velocity auto-correlation functions).

^a Laboratoire de Physique de l'École Normale Supérieure de Lyon, CNRS UMR 5672, 46 Allée d'Italie, F-69007 Lyon, France.

^b Laboratoire des Écoulements Géophysiques et Industriels, CNRS/UJF/G-INP UMR 5519, BP53, F-38041 Grenoble, France.

¹ Machicoane et al., *New J. Physics* **16**, 013053 (2014).

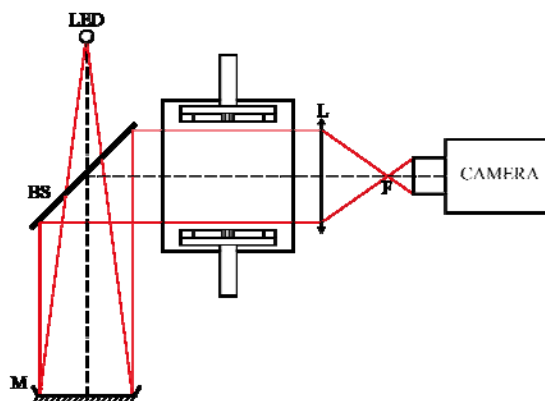


Figure 1: Shadow Particle Tracking Velocimetry setup (shown only in one direction for clarity). The light source is a light-Emitting Diode, made point-like with a converging lens of short focal length and a pinhole, placed in the focal length of a converging mirror M . The light from the source goes through a beam splitter BS and reflects itself on the mirror into a large parallel ray of light that goes through the apparatus. The shadows of the particles advected in the apparatus are collected with the objective of a high-speed camera, using a large converging lens F as a magnifying glass.

Visualization of Very Low Reynolds Number Flow around Two-dimensional Airfoils in Highly Viscous Fluid Using Hydrogen Bubble Method

Itaru Tamai^a, Hidemasa Saito^{Fejl! Bogmærke er ikke defineret.}, Gaku Sasaki^a, Takaaki Matsumoto^a and Koichi Yonemoto^a

Mars exploration aircraft is being researched and developed by a working group of JAXA/ISAS (Japan Aerospace Exploration Agency/Institute of Space and Astronautical Science) and several universities for the purpose of observation of the magnetic field and surface exploration. The aircraft-type explorer has the advantage in conducting wider range of planet surface survey area to rover, and more precise ground surface survey than orbiting satellite. Mars atmosphere density is about 1/100 of the Earth. Therefore, flight Reynolds number of the aircraft becomes low ($Re=10^4 \sim 10^5$). Many researchers have reported that the aerodynamic characteristics of Mars flight differ considerably from that of commercial aircrafts on the Earth owing to the flow phenomenon, that is, it is easy to generate laminar separations on the upper surface and more difficult to predict vortex behaviors around the airfoil.¹ The flow around the propeller of the Mars exploration aircraft is ultra low Reynolds number ($Re < 10^4$). It is said that the wing characteristics of ultra low Reynolds number flow further changes compared with that of low Reynolds number flow. However, previous study on wing characteristics and flow field in the flow is few.

In this study, a towing tank is developed to research ultra low Reynolds number flow because the aerodynamic force and moment of ultra low Reynolds number flow in conventional wind tunnel are too small to measure. Flow visualization experiments using hydrogen bubble method were conducted to research the correlation between the two-dimensional wing characteristics and flow field in ultra low Reynolds number flow. The airfoil is NACA0012 and Reynolds number is set to 1.0×10^4 and 5.0×10^3 .

The result shows that trailing separation was observed in the low angle of attack. It is also confirmed the transition of the separation point from the trailing edge to the leading edge with increasing angle of attack. When the angles is from 7 to 9 [°] (Fig. 1), the airfoil has separation bubbles. In force balance test (Fig. 2), lift coefficient is nonlinearly increasing at between 7 and 9 [°]. However, in $Re=5.0 \times 10^3$, lift slope is relatively linear than that of $Re=1.0 \times 10^4$. There are no separation bubbles and the flow field changes from trailing separation to leading separation with increasing the angle of attack. The correlation of both results indicates that separation bubble generates negative pressure area at the upper surface. In addition to, no separation bubbles are observed in any airfoil when Reynolds number becomes lower than 5.0×10^3 .

^a Dep. Mechanical Engineering, Kyusyu Institute of Technology, 1-1 Sensui-cho, Tobata-ku, Kitakyusyu-city, Fukuoka, Japan

¹ S. Shigeoka et al., *Proc. of the 8th Int. Conf. on Flow Dynamics*, **332**, (2011).

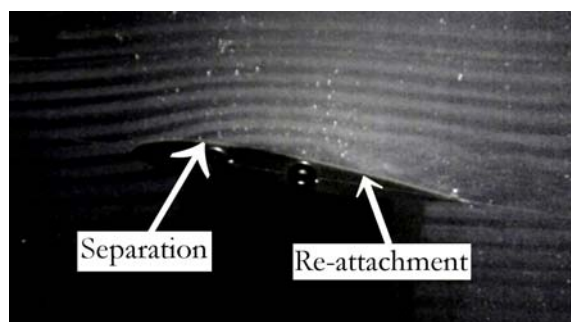


Figure 1: Flow Visualization (NACA0012, $Re=1.0 \times 10^4$, 9[deg.]

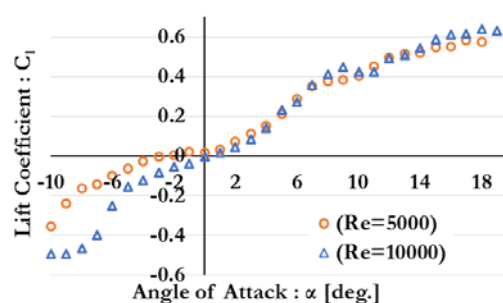


Figure 2: Two-Dimensional Wing Characteristics

On dynamic masking of time resolved PIV data

F. G. Ergin^a

Objects and surfaces often appear in PIV images. Unless masked, these contribute to the cross correlation function and may introduce an uncertainty in the PIV calculation in the flow field. It is quite common and straightforward to use static masks to remove stationary objects, as these can be defined manually. However, it is not as trivial to mask moving objects or surfaces and literature on dynamic masking is quite limited. In practice, it is possible to create dynamic masks of moving objects using the original image ensemble using a number of image processing functions. Subsequently these can be applied to mask either the raw images and/or the PIV results. In this work we present the PIV results and a dynamic masking technique developed for a microorganism (*Euglena Gracilis*) swimming in water (Figure 1). MicroPIV experiments are performed in a microchannel to capture both the detailed time history of the organism's location and to compute time-resolved vector maps. In biological flows, pulsed laser illumination is often not preferred as this can simply kill and disable the organism. For this reason, LED-based pulsed illumination was used in transmission mode. The shadow displacements of $1\mu\text{m}$ seeding particles were analysed using an Adaptive PIV algorithm with refinement steps, vector validation and deforming windows. *Euglena Gracilis* uses a thin whip-like structure (flagellum) to move through water, in combination with stretching and contracting its flexible body. Nevertheless, the exact mechanism of locomotion is not well understood. Although it was not possible to image the flagellum, the flow field around the organism suggests that the flagellum is at the leading edge, pulling strokes backwards.

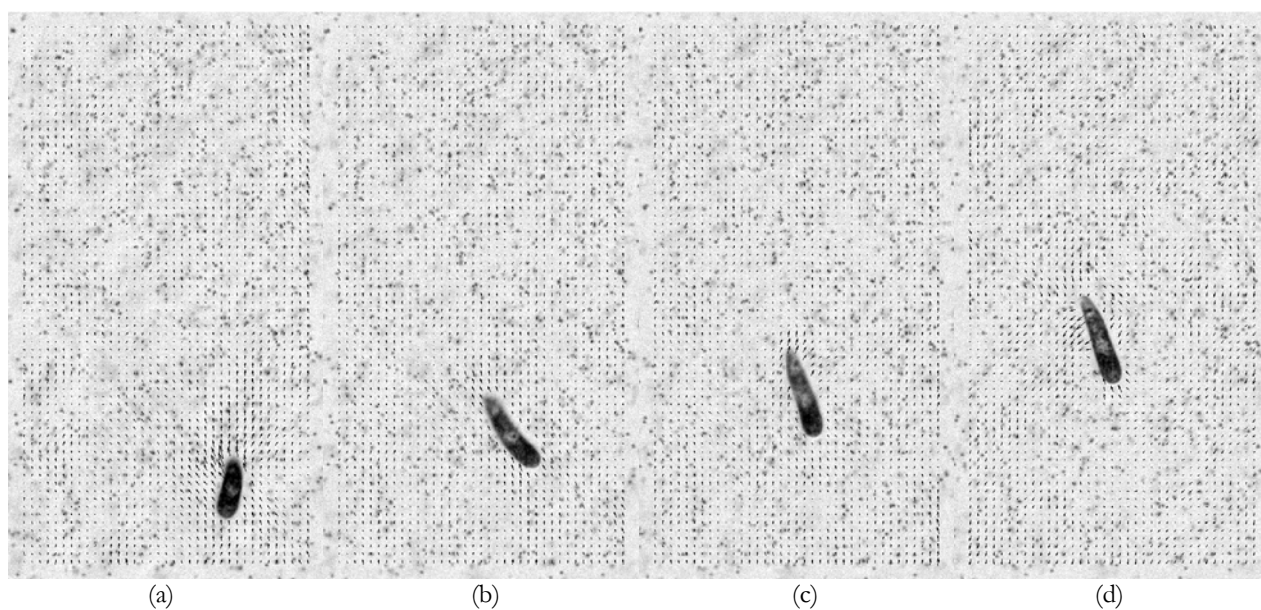


Figure 1: Raw PIV images and and MicroPIV measurement results of *Euglena Gracilis* swimming in water
(a) $t=0\text{s}$, (b) $t=0.8\text{s}$, (c) $t=1.6\text{s}$, (d) $t=2.4\text{s}$

^a Dantec Dynamics A/S, Tonsbakken 16-18, Skovlunde, DK

Cross-correlation analysis of laser Doppler flowmetry and precise temperature records

I. Mizeva^a, P. Frick^b, S. Podtaev^c

Non-invasive methods of physiological systems functional state analysis very often are based on measurement of values which characterises the system indirectly. The typical example of such indirect measurements is investigation of the blood microcirculation system. Considering the reaction of microcirculation system on some physiological tests it becomes possible to estimate its properties. In this case the influence of measurement system should be minimal. The blood microcirculation system is characterized by complex of parameters, but it is difficult to choose one - which directly reflects the functional status.

The laser Doppler flowmetry¹ is used to estimate blood circulation in the micro vessels. The characteristic value, which is measured by LDF perfusion, is proportional to the product of mean velocity and the concentration of red blood particles. The significant attention of researches is attracted to the pulsation of perfusion in a wide frequency band, which are provoked by different physiological mechanisms. The subitaneous idea of using precise thermometry (PT) for blood flow pulsations investigation was stated in the paper². This opportunity is not obvious, but the method has a lot of advantages in comparison with LDF, and it is very attractive idea to have such simple technique for analysis the very complicated system. The main argument for this was the correlation of low frequency pulsation in precise temperature and LDF records. Cross-correlation wavelet analysis was used to prove correlation of pulsation in different frequency bands.

We present a detail comparison of Fourier and wavelet cross-correlation analysis for the first time. For this purpose we measured 10 simultaneous records of LDF and PT signals on the healthy subjects under the rest conditions. Both probes are situated on the same finger in the distance 4 mm, the duration of one record is 20 minutes. We consider 5 frequency bands (E: 0.01-0.02, N: 0.02-0.05, M: 0.07-0.15, B: 0.15-0.4, H: 0.8-1.6 Hz) which characterise different physiological mechanisms³, and established that low frequency pulsation (<0.1) of LDF and PT are correlated, and the correlation differs from surrogate noise signals of the same length significantly (Fig.1).

We have shown that PT and LDF pulsations are correlated, and conclude that temperature pulsation analysis can be used for blood flow oscillation analysis in microcirculation system.

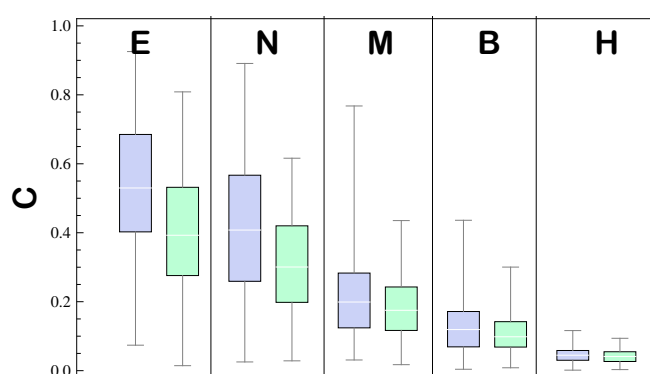


Fig.1 Averaged cross-correlation coefficients in different frequency bands (blue rectangles) in comparison with noise surrogate data.

^a Institute of continuous media mechanics UB RAS, 1 ak. Koroleva 1, Perm, Russia

¹ Stern M., Appl. Opt., 1985, N 13 1968-1986

² Podtaev S. et al. Cardiovasc Eng., 2008, N 8, P. 185-189.

³ Kvernmo H.D. et al. Mic. Res., 1998. N 56, P. 173-182.

A local scattering theory for the effect of isolated roughness on boundary-layer instability and transition: transmission coefficient as an eigenvalue

Xuesong Wu^a, Ming Dong^b

This paper is motivated by the need for better understanding of how isolated surface roughness affects boundary-layer transition. A roughness element induces a local distortion to the flow, thereby modifying the stability property. This effect was in the past accounted for by local stability analysis of the distorted flow. That approach is, however, invalid when the streamwise length scale of the roughness is relatively short in the sense that it is comparable with the characteristic wavelength of the inherent instability. In this paper, we investigate the impact of roughness on transition from an entirely new perspective, namely, scattering of an existing instability wave by the roughness-induced local mean-flow distortion. The problem is sketched in Fig. 1: an incident Tollmien-Schlichting (T-S) wave, with an amplitude of $A_I(x) = e^{i\alpha x}$ upstream, approaches a roughness element (a hump or an indentation), which is at a distance L to the leading edge. As the T-S wave propagates through the non-uniform flow in the vicinity of the roughness, it is scattered and as a result acquires a different amplitude of $A_T(x) = \tau e^{i\alpha x}$ downstream, where τ is the ratio of the T-S wave amplitude after the scattering to that before the scattering, and is referred to as the transmission coefficient, which offers a natural characterisation of the impact of the roughness on instability and transition. The roughness plays a stabilising/destabilising role according to $|\tau| < 1$ or $|\tau| > 1$ respectively.

To fix the idea, we formulate a local scattering theory using triple-deck formalism, in which the roughness height is assumed to be $h^*/L = \text{Re}^{-5/8} h$, with Re being the Reynolds number based on L . This gives rise to a boundary-value problem, which is discretised appropriately, leading to a generalised eigenvalue problem. This numerical approach is found to be robust and efficient. For nonlinear roughness cases, i.e. $|h| = O(1)$, both humps and indentations would enhance the T-S wave, i.e. $|\tau| > 1$, but the transmission coefficient is larger for a hump than for an indentation. The transmission coefficient is found to increase with the frequency ω and the roughness height h . For a fixed h and ω , the transmission coefficient attains its maximum when the width of the roughness is about half the wavelength of the T-S wave. Specifically, for $h = 1$ and $\omega = 6$, the transmission coefficient $|\tau| \approx 2$, which amounts to a significant effect; for $h = 2$ and $\omega = 6$, the transmission coefficient can be as large as 7, suggesting that immediate transition may be caused at the roughness site.

The conventional linear stability analysis of the distorted flow is performed in order to assess its range of validity. The result is found to be different from the local scattering theory when the length scale of the roughness is comparable with the wavelength of the T-S wave. Interestingly, when the length scale of the roughness is about twice the wavelength of the T-S wave, the local instability theory starts to give a reasonable approximation. We have also studied the effect of the distance separating two adjacent roughness elements, and found that each element can be treated as being isolated once the distance is greater than four times the wavelength. The result of this study allows us to extend the traditional e-N transition prediction criterion for smooth boundary layers to those with isolated roughness elements.

^a Department of Mathematics, Imperial College London, London SW7 2AZ, UK

^b Department of Mechanics, Tianjin University, Tianjin 300072, China

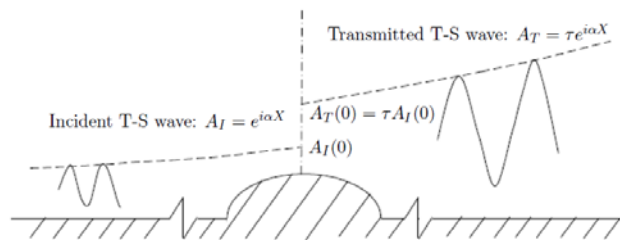


Figure 1: Sketch of the problem: a T-S wave scattered by a local roughness and the associated transmission coefficient τ .

PIV and LDA measurements of the swirling flow in a low-speed two-stroke diesel engine

K. M. Ingvorsen^a, K. E. Meyer^a, J. H. Walther^{a,b} and S. Mayer^c

Low-Speed two-stroke (LSTS) marine diesel engines are used to power oil tankers and container ships. To replace the old combustion gas in the cylinder with a fresh air charge for the next engine cycle, the uniflow-scavenging method is used. At the end of the power stroke, the piston uncovers a series of angled scavenge ports located circumferentially around the bottom of the liner. Fresh air is blown into the cylinder through the ports thereby creating a swirling flow that forces the combustion gas out through the exhaust valve in the cylinder cover. Detailed knowledge of the turbulent swirling in-cylinder flow is needed in order to reduce the emissions levels and optimize the overall engine performance.

Recently, Ingvorsen et al.¹ developed an experimental scale model of an engine cylinder and characterized the turbulent swirling flow under steady-flow conditions using stereoscopic particle image velocimetry (PIV) and laser Doppler anemometry (LDA). The present work extends this work, by considering a dynamic case, where the scavenge ports are opened and closed by the moving piston. The purpose of the work is to obtain an increased understanding of the dynamic behavior of the complex swirling flow, including the coherent structures such as the vortex breakdown. Furthermore, the experimental results serve as a database for validation of computational fluid dynamics (CFD) models.

The model has a transparent cylinder with a diameter of $D = 190$ mm and a movable piston driven by a programmable linear motor. The swirl is generated using 30 equally spaced ports, and cases with port angles of 0° , 10° , 20° , and 30° are investigated. The swirling flow is characterized using phase-locked PIV and LDA for a Reynolds number of $Re = 50,000$. The results include radial profiles of phase-averaged mean and rms-velocity, proper orthogonal decomposition analysis (POD), probability density functions of the instantaneous velocity, and visualizations of the mixing process between the combustion gas and the scavenge air.

Among other things, it is shown that for the 20° case, a central recirculation zone is formed shortly after the piston has passed the bottom position (see Figure 1), indicating that a vortex breakdown has occurred. The POD analysis indicates that a double helical structure exist near the breakdown region. Time resolved LDA measurements of the axial velocity component indicates that large unsteady flow structures exist in the cylinder after the piston has closed the ports. The rate of swirl decay is investigated by computing the angular momentum from the radial velocity profiles. It is found that the decay rate can be accurately predicted using simple friction formulas based on the flow over a flat plate.

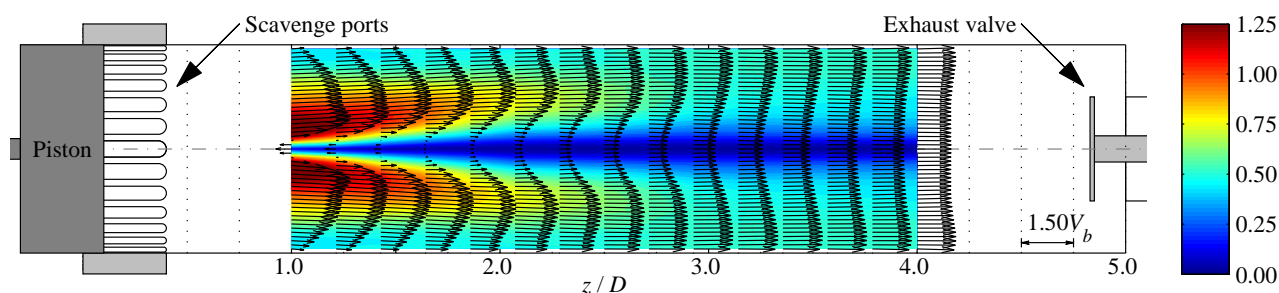


Figure 1: Visualization of the measured phase-averaged velocity field shortly after the piston has passed bottom dead center. The radial and axial velocity is shown by vectors and the tangential/swirl velocity (V_θ/V_b) is shown by the color contours. Note the reverse flow near the centerline at $z/D = 1.0$ indicating that a vortex breakdown is formed.

^a Dep. of Mechanical Engineering, Technical University of Denmark, Nils Koppels Allé Building 404, 2800 Kgs. Lyngby, Denmark

^b Chair of Computational Science, ETH Zurich, Clausiusstrasse 33, 8092, Switzerland

^c MAN Diesel & Turbo SE, Tegholmsgade 41, 2450 Kbh. SV, Denmark

¹ Ingvorsen et al, Exp. Fluids. **54**, 1494 (2013)

Grade of geometric resolution of a rough surface required for accurate prediction of pressure and velocities in water tunnels

L. R. Andersson^{*}, A. G. Andersson^{*}, P. Andreasson[†], J.G.I. Hellström^{*} and T. S. Lundström^{*}

Computational modelling of flow over rough surfaces is a very important question for hydropower tunnels, channels and other applications where wall boundaries are far from smooth. When performing simulations of flow over rough surfaces it is of essence to know to what extent the roughness should be geometrically resolved. Full resolution of the roughness (as a part of the geometry) is usually too costly in CPU-time, in most practical application. However, within the resolution needed to resolve the large scale geometry (i.e. tunnel) still usually allows for a partial resolution of the large scale roughness elements. With such an approach the effect of the sub-grid scale roughness need to be assessed. This task is the focus of this work. From an excavated tunnel, a geometrical computer model was created via detailed laser scanning. Also a 1:10 physical scale model of the same geometry (including roughness) was created; the physical model was a side wall from the tunnel with the dimensions 10x0.25 m, which was tested in an otherwise smooth tunnel of cross section 0.25x0.20 m. On the physical model, measurements were carried out via Particle image velocity¹ (PIV). On the computer model, mathematical simulations were carried out via Computational fluid dynamics (CFD) with unsteady RAANS model, k- ϵ turbulence model. In Figure 1 the results from the CFD simulation is visible¹. As seen the pressure variation over the surface is very pronounced. A similar strong influence is also shown on the velocity variation over the surface. This is a good illustration of the need to include at least a part of the geometrical roughness in the simulations, to just consider roughness as wall functions influencing the overall momentum and turbulent quantities will not reproduce these variations. So one question that needs to be addressed is how well the roughness of the wall needs to be represented in the computer model, in order to give a solution that corresponds well with the experiments conducted on the physical model. Simulations with similar numerical grids but altering resolutions showed that the geometric resolution was important to accurately predict the resulting flow field.

^{*} Div. Fluid and Experimental Mechanics, Luleå University of Technology, SE-971 87, Luleå, Sweden

[†] Vattenfall Research and Development, SE-814 70 Älvkarleby, Sweden

¹ Andersson et al, *9th Euromech Fluid Mechanics Conference (EFMC9)*, Rome, Italy (2012)

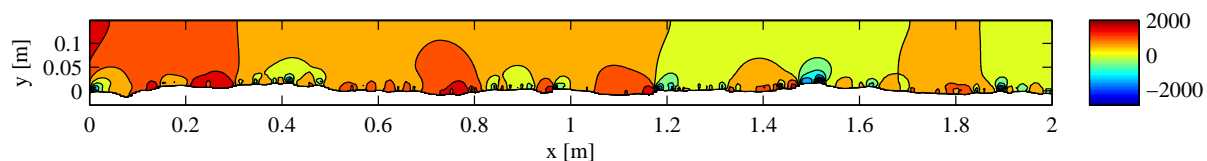


Figure 1: The static pressure [Pa] in the central plane of the geometry

The effect of dead time on power spectra from randomly sampled data

C. M. Velte^a, P. Buchhave^b, W. K. George^c

Power spectral estimation of a random process such as a turbulent velocity is always a challenging endeavor. Further problems arise when data is sampled by a random process, especially when the sampling rate is correlated with the process to be measured, such as the velocity bias that occurs in burst-type laser Doppler anemometry (LDA)^{1,2}. Further, the random sampling can sometimes give rise to signal processing effects that are not observed for equispaced data. This talk will focus on the practical limitation that *no instrument can acquire true point measurements*, but must always measure across some finite volume/time. As it turns out, the fact that a burst – type LDA data point is obtained from a finite length digitized velocity trace sampled within the measurement volume, and that a subsequent data point cannot be obtained until the current measurement is concluded, has a profound influence on the measured power spectrum which will exhibit a redistribution of the energy across frequency and oscillations in the high frequency range³. In some cases the effects may distort the spectrum across all frequencies beyond recognition, see Fig 1 left. The power spectrum is distorted accordingly:

$$S_0(f) = \frac{\overline{u_{\Delta t_p, \Delta t_d}^2}}{v_0} + \left[\left(S_u(f) \cdot \text{sinc}^2(\pi f \Delta t_p) \right) \otimes \left[\delta(f) - 2\Delta t_d \text{sinc}(2\pi f \Delta t_d) \right] \right] \quad (1)$$

The measured signal is averaged across the processing/sampling time Δt_p , but the main focus will be on the effect of the dead time, Δt_d . In addition, at least some processors require an additional fixed time for data transfer/processing before new data can be acquired. We also illustrate the effects of finite sampling and dead time on a power spectrum computed from data obtained with a burst – type LDA which is compared to computer generated data from a fitted von Karman spectrum with dead time and the analytical solution of eqn (1), see Fig 1 right. The dead time model will be shown to be applicable also in the complex case of the LDA⁴.

^a Dep. Mechanical Engineering, DTU, Nils Koppels Allé Building 403, 2800 Kgs. Lyngby, Denmark

^b Intarsia Optics, Sønderkovvej 3, 3460 Birkerød, Denmark

^c Dep. Mechanical and Aerospace Engineering, Princeton University, Princeton, NJ 08544, USA

¹ Buchhave, George, Lumley, *Ann. Rev. Fluid Mech.* **11**, 443-504 (1979).

² Velte, Buchhave, George, *Submitted for publ. in Exp. Fluids* (2014)

³ Buchhave, Velte, George, *Exp. Fluids* **55**, 2 (2014)

⁴ Velte, George, Buchhave, *Accepted for publ. in Exp. Fluids* (2014)

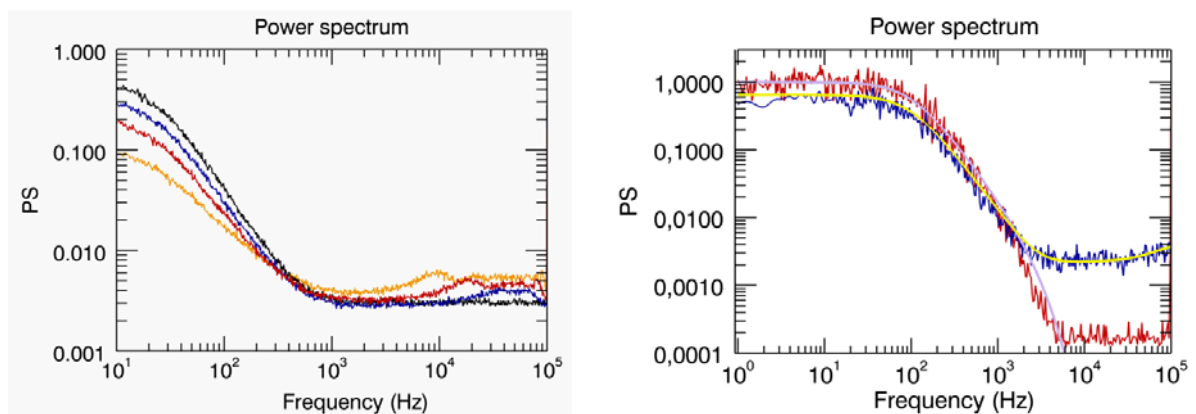


Figure 1: Effect of dead time on the processing of a simulated von Karman spectrum. LHS: Black: $\Delta t_d = 0$. Blue: $\Delta t_d = 2 \cdot 10^{-6}$ s. Red: $\Delta t_d = 4 \cdot 10^{-6}$ s. Orange: $\Delta t_d = 8 \cdot 10^{-6}$ s. RHS: Light blue: Von Karman filter. Yellow: Analytical solution. Blue: CG with dead time, randomly sampled $\nu = 40$ kHz Red: CG with dead time, regular sampling at 100 kHz.

Experimental study of the dynamics of a light sphere on a Stokes flow

Tania Sauma Pérez¹, Outtabar Boubakar, Yang Li and Tom Mulin¹

A light sphere placed inside of a cylinder completely filled with glycerol which rotates around it's symmetry axis, perpendicular to gravity, presents a rich dynamical behaviour. We defined the Reynolds number in this system as:

$$Re = \frac{a^2 \omega}{\nu}$$

Where a is the radius of the sphere, ω is the angular velocity of the cylinder and ν is the viscosity of the glycerol. In our experiment, for high rotation rates, therefore for high Reynolds numbers the sphere settled in an equilibrium position in the centre of the cylinder, the work of Ladd et al, predicts this is the only equilibrium in the system, and that for smaller Reynolds numbers, the sphere should spiral outwards, colliding with the wall of the cylinder. By the other hand the work of Coimbra et al. predicts the existence of another fixed point out of the centre of the cylinder for all Reynolds numbers, which should be stable.

Our experiment showed that, when decreasing the Reynolds number, the sphere migrated outwards the centre of the cylinder and described circular orbits, and the centre these orbits corresponded to the theoretical prediction of Coimbra's fixed point, Suggesting that the fixed point exists, but is not stable.

In figure 1 is showed the average position of the sphere, for spheres of different radii, the solid line corresponds to Coimbra's prediction of fixed points, the big error bars are due to the oscillation described. In figure 2 is showed the radius of the orbit in function the Reynolds number for spheres of different radii, the onset of the oscillations occurs at a finite Reynolds number, the growth of this oscillations is proportional to the inverse square of the Reynolds number.

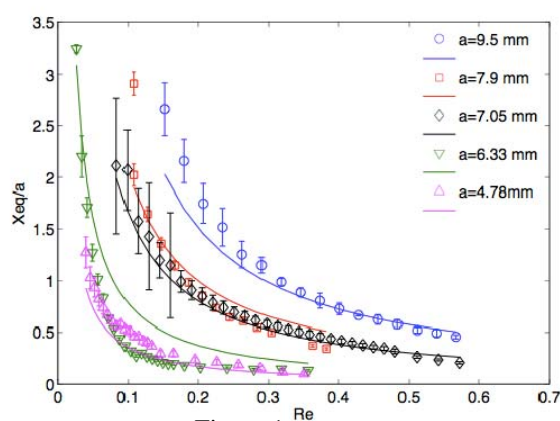


Figure 1

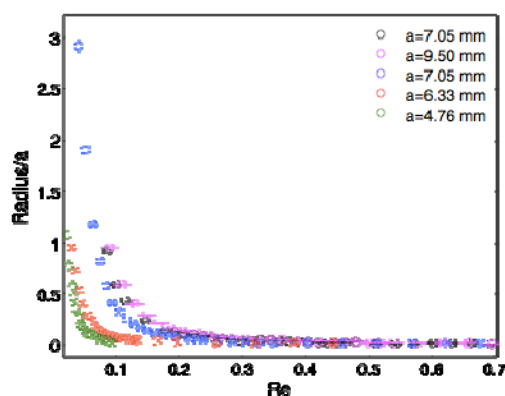


Figure 2

¹ Manchester Centre for Nonlinear Dynamics, University of Manchester, Oxford Road, Manchester M13 9PL, United Kingdom

¹ Lee et al. J. Fluid Mech. (2007), vol. 577, pp. 183–209

² Coimbra et al. J. Fluid Mech. (2002), vol. 469, pp. 257–286.

Application of 3D acoustic Lagrangian velocimetry to a turbulent ferrofluid flow

T. Grünberg^a and T. Rösgen^a

Ultrasound is suitable for Lagrangian particle tracking in turbulent flows. In contrast to optical particle tracking velocimetry, the velocity of a tracer particle is measured directly by evaluating the Doppler shift of the reflected echoes. Information about large scale quantities such as RMS velocity and integral time scale can be obtained as well as the acceleration time scale.

We track tracer particles in a measurement volume of 10mm diameter in the centre of a cylindrical flow cell. Our measurement setup includes one ultrasound transducer to continuously insonify the particles and three receiving transducers which measure all three velocity components of the particles simultaneously. A particle crossing the sound beam scatters the sound, producing a frequency-shifted echo with a frequency-shift proportional to its projected velocity. The Doppler shift is small compared to the original frequency, hence we use undersampling to significantly reduce the data rate. We sample the bandpass filtered signals with separate 24bit Sigma-Delta analog-to-digital converters. A parametric method enables us to analyse the Doppler shift with high resolution in time and frequency.

A validation measurement was performed using water as fluid at $Re \approx 300$. A turbulent flow is created between two counter-rotating disks at the ends of the flow cell. Measurement results will be presented for a turbulent ferrofluid flow in an external magnetic field. The ferrofluid used is a colloidal suspension of nano-sized magnetite aggregates in water, whose micro-structure can be changed by a magnetic field. The reported measurement technique is well suited for ferrofluids since they are opaque and not accessible by optical methods.

^a Institute of Fluid Dynamics, ETH Zürich, Sonneggstr. 3, 8092 Zürich, Switzerland

Transitional Flows

A new mode of instability in compressible boundary-layer theory

A. Tunney^a, J. Denier^a, T. Mattner^b and J. Cater^a

The development of new technologies in defence and transport demands advanced understanding of the laminar-turbulent transition process in compressible flows. In low disturbance environments such as aerodynamic flight, the initial growth of disturbances that cause the transition process in a boundary layer can be investigated with linear stability theory, and is currently used in transition prediction calculations¹.

A large collection of results using linear stability theory are available in the literature, however, excluded are the class of boundary-layer flows with region of velocity overshoot, where the fluid velocity is higher than that of the external, free-stream velocity. This velocity overshoot is present in compressible, flat-plate boundary layers with a heated wall and a favourable pressure gradient² and occurs due to a large decrease in the density near the heated wall that promotes a rapid acceleration of the flow³.

Using this family of boundary layers as a prototype, the viscous and inviscid linear stability of this class of boundary layers is investigated numerically. The results uncover a new family of eigenvalues that are most unstable in the inviscid regime and have the potential to be the dominant instability. The maximum inviscid growth rate tends to increase with the maximum velocity ratio in the boundary layer.

There are two inviscid neutral modes associated with this new family of eigenvalues. The first neutral mode has a zero wavenumber and a critical layer located at the point of maximum velocity. This neutral mode is formally analysed by posing a singular perturbation problem in the small wavenumber limit. The second neutral mode has a non-zero wavenumber and has two critical layers; neither of which correspond to the classical⁴ generalised point of inflection criterion.

^a Department of Engineering Science, University of Auckland, Auckland 1142, New Zealand

^b School of Mathematical Sciences, North Terrace Campus, University of Adelaide, SA 5005, Australia

¹ Fedorov, *Annu. Rev. Fluid Mech.* **43**, 79 (2011)

² McLeod and Serrin, *J. Fluid Mech.* **34**, 337 (1968)

³ Cohen and Reshotko, *NACA Technical Report* **1293** (1955)

⁴ Lees and Lin, *NACA Technical Note* **1115** (1946)

Investigation of cross-flow vortices and its secondary instability after the roughness element on the leading edge of swept wing

V.V. Kozlov^a, S.N. Tolkachev^a, V.N. Gorev^a

The problem of the aircraft drag reduction makes urgent the task of near-wall flow laminarization of the lifting surface. Of greatest interest is the process of laminar-turbulent transition on a swept wing, because of its widely using.

The laminar-turbulent transition process on the swept wing has a feature in comparison with straight wing, it occurs in favourable pressure gradient area because of three-dimensional structure of the boundary layer, which is result of non-parallelism of the free stream velocity vector to the pressure gradient and the viscosity effects. The laminar-turbulent scenario consists of several stages. The leading edge boundary layer becomes unstable to longitudinal vortices. Surface roughness makes the stationary mode primary, which modifies the mean flow. The boundary layer destabilizes to secondary high-frequency disturbances further, development of which leads to the laminar-turbulent transition.

In this work studied the process of laminar-turbulent transition after the roughness element and influence of turbulator on the flow near the attachment line.

Experiment was carried out in a low-turbulent wind tunnel T-324 of the Institute of Theoretical and Applied Mechanics with a cross section of the working section 1000×1000 mm and a length of 4000 mm. Free-stream velocity was monitored by the Prandtl-Pitot tube. The free-stream turbulence level didn't exceed 0.03%. The air temperature was 293°K. For investigations were chosen hot-wire measurements and liquid crystal thermography.

The first part of investigation used one of three spherical roughness elements near the attachment line or 140 mm width turbulator made of abrasive paper with 1.3 mm typical diameter of grains for excitation disturbances. Diameter of spherical roughness elements was 1 mm, 2 mm and 3 mm. Velocity range was $U_{\infty} = 2.8 - 24$ m/s. Angle of attack was -0.2° .

In the second part of investigation cylindrical roughness element was used with 0.8 mm height and radius. Free-stream velocity was in interval $U_{\infty} = 8.1 - 10.9$ m/s. The model angle of attack was set up -7.2° . For excitation of secondary disturbances we used the loudspeaker inside the diffuser of the wind tunnel.

It is shown, that roughness element creates a pair of counter-rotating vortices on the leading edge. Then one of them, which has the direction of rotation opposite to the crossflow, decays quite fast. Amplitude of stationary vortex increases with the increase of velocity, roughness size and with bringing to the position of maximal receptivity, which differs from the attachment line. If the amplitude of stationary disturbance is quite large the high-frequency secondary disturbances appears in the position between the defect and exceeding of velocity. These disturbances are sensitive to the acoustic field and could change the distribution of mean velocity in the boundary layer. On visualization pictures we saw the appearance of additional longitudinal structures.

There was no turbulence along the leading edge observed, even with a help of turbulator.

^a Khristianovich Institute of Theoretical and Applied Mechanics SB RAS, Institutskaya str. 4/1, Novosibirsk 630090, Russian Federation

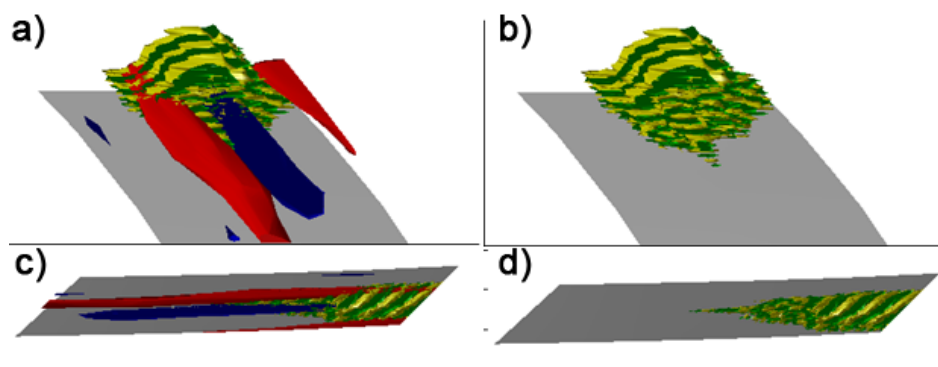


Figure 1: Exceeding (red $0.06*U_0$) and defect (blue $-0.06*U_0$) of velocity isosurfaces and also velocity disturbance isosurfaces of secondary disturbances ($3*10^{-4}*U_0$ – green; $-3*10^{-4}*U_0$ – yellow) in different views.

Minimal transition thresholds in plane Couette flow

Y. Duguet^a, A. Monokrousos^b, L. Brandt^b and D.S. Henningson^b

Subcritical transition to turbulence requires finite-amplitude perturbations. Using a nonlinear optimisation technique in a periodic computational domain¹, we identify the perturbations of plane Couette flow transitioning with least initial kinetic energy for $Re \leq 3000$. We suggest a new scaling law $Ec = O(Re^{-2.7})$ for the energy threshold vs. the Reynolds number², in quantitative agreement with experimental estimates for pipe flow. The route to turbulence associated with such spatially localised perturbations is analysed in detail for $Re = 1500$. Several known mechanisms are found to occur one after the other: Orr mechanism, oblique wave interaction, lift-up, streak bending, streak breakdown, and spanwise spreading. The phenomenon of streak breakdown is analysed in terms of leading finite-time Lyapunov exponents of the associated edge trajectory.

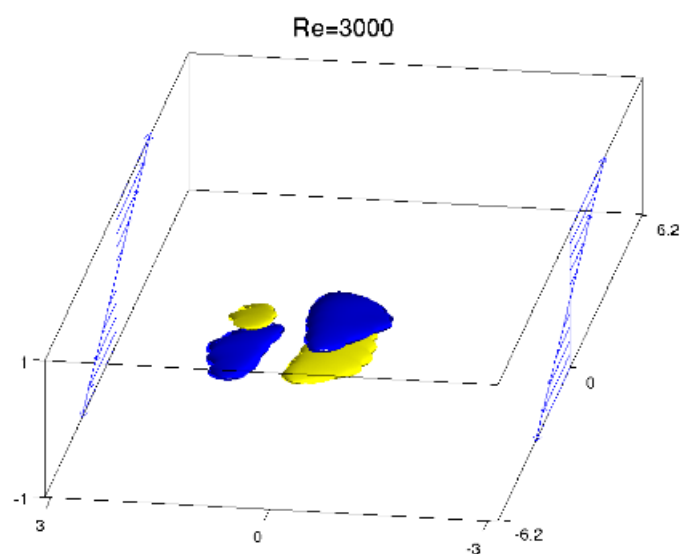


Figure 1: Isocontours of the streamwise velocity perturbation for the minimal disturbance found at $Re=3000$. The base flow is indicated using blue arrows.

^a LIMSI-CNRS, F-91403 Orsay Cedex, France

^b Linné Flow Centre, KTH Mechanics, SE-10044 Stockholm, Sweden

¹ Monokrousos et al., *Phys. Rev. Lett.* **106**, 134502 (2011)

² Duguet et al., *Phys. Fluids* **25**, 084103 (2013)

Assessment of the asymptotic theory of receptivity using numerical simulations of the compressible Navier-Stokes equations

N. De Tullio^a, A. Ruban^b

Receptivity is the process by which external perturbations interact with the boundary layer to cause the appearance of instability modes and is the initial stage of the laminar-turbulent transition process. The receptivity of boundary layers may be studied theoretically by the asymptotic analysis of the Navier-Stokes equations for large values of the Reynolds number. This approach was first used by Terent'ev¹ to study the receptivity caused by a vibrating ribbon placed on a flat plate wall and has been used for the past few decades to study the boundary layer response to different external perturbations, providing insight into the underlying mechanism responsible for the generation of TS waves. However, despite the numerous advances, theoretical predictions have very seldom been compared with experimental or numerical results and a detailed evaluation of the capabilities of the theory is missing.

In this contribution we provide an in depth comparison of the predictions of the asymptotic theory of receptivity with numerical simulations of the full compressible Navier-Stokes equations. The investigation focuses on the generation of TS waves by the interaction of acoustic waves with a small discrete roughness element on a flat-plate wall. This receptivity mechanism was first studied theoretically by Ruban² and Goldstein³ and is believed to be one of the most important causes of laminar-turbulent transition in boundary layers during flight.

The numerical results show that, as indicated by the theory, the acoustic wave/roughness element coupling provides the frequency and wavenumber resonance conditions required for the excitation of TS waves in the boundary layer (see figure 1a). The theoretical predictions for the initial TS wave amplitude are in excellent agreement with the numerical results. This is shown in figure 1(b), where the initial amplitude of the wall pressure perturbation induced by the TS wave (normalised by the acoustic wave amplitude a and the roughness height b) is plotted as a function of roughness width (Δ) to TS wavelength (λ_x) ratio.

The results of a parametric study looking at how the receptivity is modified by variations of Reynolds number, Mach number (within the subsonic regime) and roughness height will be presented at the conference, along with details of the theoretical and numerical studies.

^{a,b} Dep. Mathematics, Imperial College London, South Kensington Campus, London SW7 2AZ, UK

¹ Terent'ev., *Prikl. Mat. Mekh.* **45**, 1049 (1981).

² Ruban, *Izv. Akad. Nauk SSSR Mech. Zhidk. Gaza* **5**, 44 (1984).

³ Goldstein, *J. Fluid Mech.* **154**, 509 (1985).

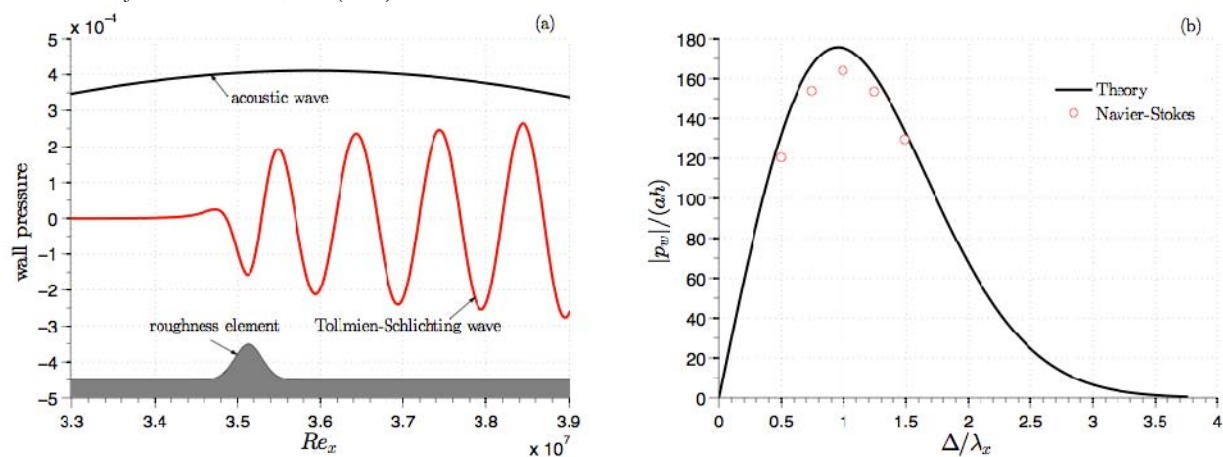


Figure 1: (a) The wavelength conversion mechanism (numerical result). The acoustic wave amplitude and the roughness height were scaled for clarity of presentation. (b) Amplitude of the excited TS wave for different roughness width to TS wavelength ratios.

Acoustic receptivity analysis of a boundary-layer flow using biorthogonal decomposition

N. Shahriari^a, A. Hanifi^{a,b} and D.S. Henningson^a

Understanding the receptivity process is crucial for reliable laminar-turbulent transition prediction. One of the main receptivity mechanisms in two-dimensional flows is generation of boundary layer perturbations due to acoustic forcing. Acoustic disturbances interact with strong streamwise gradients at the leading edge or surface non-homogeneities and create Tollmien-Schlichting (TS) waves inside the boundary layer. A number of previous studies have addressed this issue. However, there are still unexplained disagreements between the experimental and numerical findings in terms of the receptivity coefficient ^{1,2}.

Measuring amplitude of TS waves created by sound waves is challenging due to presence of Stokes wave in boundary layer with the same frequency as the TS wave. This problem has been tackled by different approaches in both experimental and numerical studies. In previous numerical work² the amplitude of TS waves has been obtained through subtraction of separately computed Stokes wave from the total velocity field resulted from direct numerical simulations (DNS). Recently, Monschke et al.¹ have used biorthogonal decomposition method³ to separate Stokes and TS waves in an experimental study to measure acoustic receptivity of a boundary layer over a flat plate with modified super ellipse leading edge. This method is shown to be more accurate and efficient than previous experimental methods⁴.

Monschke et al.¹ report a discrepancy between their measured receptivity coefficients and those computed by Wanderley and Corke². Present numerical studies are performed to address this issue. We perform DNS for the same geometry and flow configurations as in the experiment¹. We also extract the amplitude of generated TS waves using the similar technics (biorthogonal decomposition based on the modified Orr-Sommerfeld equations). DNS has been performed using spectral element code NEK5000 by which linearized Navier-Stokes equations are solved. Acoustic wave has been modelled by superposing a time periodic fluctuation on the streamwise velocity of the inflow.

^a KTH Royal Institute of Technology, Dep. Of Mechanics, Linné Flow Centre, SeRC, SE-100 44, Stockholm, Sweden

^b Swedish Defence Research Agency, FOI, SE-164 90, Stockholm, Sweden

¹ Monschke et al., *ALAA paper* **2013-0669**, (2013).

² Wanderley and Corke, *J. Fluid Mech.* **429**, 1 (2001)

³ Tumin, *Phys. Of Fluids* **15**, 2525 (2003)

⁴ Saric and White, *ALAA paper* **98-2645**, (1998)

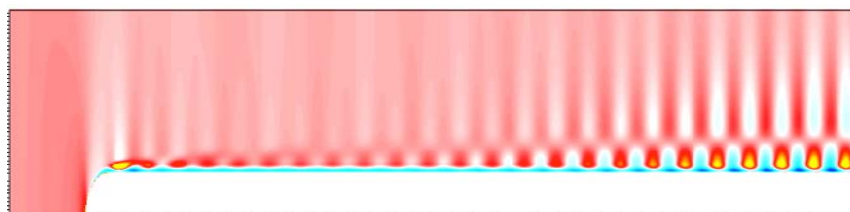


Figure 1: Streamwise perturbation velocity field demonstrating TS waves.

Transition scenarios and exact solutions in plane Poiseuille flow

Stefan Zammert^a, Bruno Eckhardt^a

In plane Poiseuille flow different paths to turbulence exists. One path is connected with a linear instability to Tollmien-Schlichting (TS) waves at Reynolds numbers above 5772, and a second one with a bypass transition at much lower Reynolds numbers. We explore the conditions for the two transition scenarios and their connections in the state space of the system by tracking the time evolution of different perturbations. In addition, we use the edge tracking algorithm for the identification of edge states. We identify two travelling waves, TW_E and TW_O , that govern the two transition processes and study their subsequent bifurcations. The bypass transition is related to TW_E (figure 1b) which appears in a saddle-node bifurcation at $Re \approx 460$. The generally slower TS-transition is connected with TW_O (figure 1a) which bifurcates from the laminar profile at $Re = 5772$. Both transition paths converge to the same turbulent state but differ strongly in the mechanism, the speed, the flow fields, and the number of initial conditions that follow the respective path. We find that the bypass transition is realized for a large set of initial conditions as soon as it appears, whereas the TS-transition process first appears in a very thin slice in the state space that grows with Reynolds number but becomes noticeable only shortly before the linear instability sets in (figure 1c). During the final stage of the transition, packets of hairpin vortices appear in the TS scenario, but not in the bypass transition. In wide and long domains, both transition scenarios can be related to streamwise localized periodic orbits that bifurcate from the spatially extended travelling waves.

^a Fachbereich Physik, Philipps-Universität Marburg, 35032 Marburg, Germany

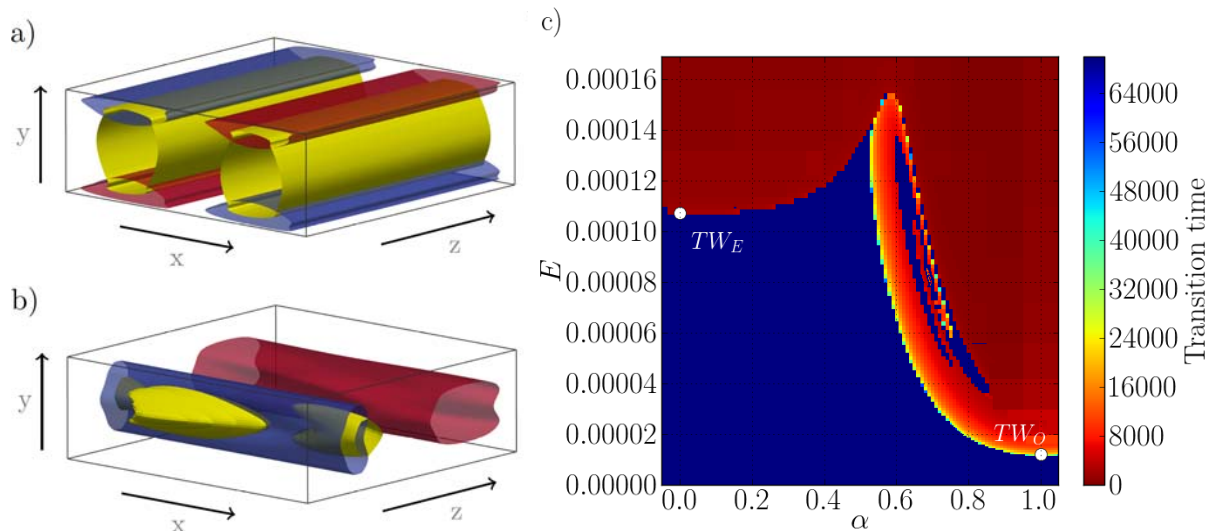


Figure 1: Isosurfaces of positive (red) and negative (blue) streamwise velocities for the travelling waves TW_O (a) and TW_E (b). (c) 2D-slice of the statespace at $Re = 5760$. The locations of the states within the cross section are marked. Initial conditions in the blue region do not become turbulent, the red ones with transition times below about 4000 follow the bypass route, and only the thin orange and yellow sliver follows the TS route.

Useful roughness-induced disturbances

R. S. Downs^a

The potential for increased energy efficiency of aircraft has spurred efforts to develop laminar flow control technologies, with passive methods appearing especially seductive. One promising method of drag reduction employs deliberately chosen surface features (broadly classified as roughness) to delay the onset of laminar-to-turbulent transition. Computations¹ reveal that spanwise shear in the mean flow working against Reynolds stresses acts to stabilise disturbances extracting their energy from viscous mechanisms. Experiments are performed building on the successes of recent research efforts^{2,3} exploring the use of streamwise streaks to attenuate or even suppress growth of forced disturbances.

The prototypical flow of these experiments develops over a flat plate aligned to avoid a streamwise pressure gradient. Regular patterns of millimetre-scale surface features, extended in the flow direction and periodic across the span of the plate, produce the requisite spanwise mean-flow modulation to exploit this stabilisation mechanism. While effective in this regard, the critical Reynolds numbers of patterned roughness are also larger than those of isolated roughness elements. This greater resistance to transition via bypass mechanisms admits the possibility of applying this flow control method at the higher Reynolds numbers encountered in flight.

To incite transition in a controlled manner, unsteady disturbances are introduced to the freestream or injected into the boundary layer through a slot near the plate's leading edge. When Tollmien–Schlichting waves are excited, the modulated mean flow disrupts the spanwise invariance of these disturbances, as shown in figure 1(a). Substantial reductions in TS-wave amplitude and increases in transition Reynolds numbers are achieved with some surface patterns compared with smooth plate reference cases; this is shown in figure 1(b). Experiments on TS-wave growth over riblets⁴ showed that riblets inhibit development of turbulent spots. Similarly, the surface patterns of the present experiments most effectively delay transition when moderate-amplitude TS waves are forced, possibly indicating a stabilising interaction of roughness-induced disturbances and secondary instability of TS waves.

This work is part of the AFRODITE research programme. The principal investigator J. H. M. Fransson acknowledges financing by the European Research Council through a starting independent researcher grant.

^a KTH – Royal Institute of Technology, Dept. Mechanics, SE-100 44 Stockholm, Sweden

¹ Cossu and Brandt, *Eur. J. Mech. B/Fluids* **23**, 6 (2004)

² Shahinfar, Sattarzadeh, Fransson and Talamelli, *Phys. Rev. Lett.* **109**, 074501 (2012)

³ Shahinfar, Fransson, Sattarzadeh and Talamelli, *J. Fluid Mech.* **733** (2013)

⁴ Grek, Rozlov and Titarenko, *J. Fluid Mech.* **315** (1996) (b)

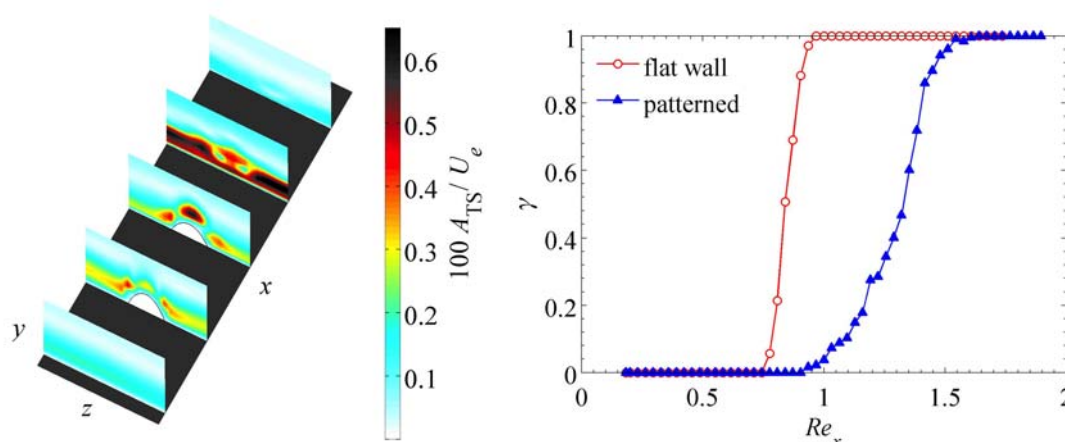


Figure 1: (a) Contours of TS-wave amplitude at several streamwise stations. (b) Intermittency measurements demonstrating delay of TS-wave-induced transition for flow over patterned surface features.

Bypass transition at the entrance of a plane channel

M. Buffat^a, A. Cadiou^a, L. Le Penven^a

Developing entrance flows are of interest in a large number of application areas. However, many aspects of these flows are not yet fully understood, for example, the stability characteristics of the flow evolving downstream from the channel entry at subcritical Reynolds number. Without any perturbations, the flow remains laminar and, in the entrance region, the velocity distribution evolves slowly from a quasi-uniform profile to a parabolic Poiseuille shape. For the plane Poiseuille flow, stability theory gives a critical Reynolds number of $Re_c=5772$ [1] whereas, in experiments, a plane channel flow can become turbulent at $Re=1000$ [2]. This has been explained by the non-normal property of the linearized Navier-Stokes operator that allows transient growth of initial perturbations [3]. Entrance flows however significantly differ from the asymptotic Poiseuille flow. For uniform inlet flow conditions and at high enough Reynolds numbers, the turbulent transition actually takes place inside the boundary layers [4] and well before the fully developed Poiseuille profile. When the boundary layers are thin and well separated, the nature of their transition and of their initial development is expected to have some similarity to the free-stream Blasius boundary layer case [5]. For Blasius flow, the linear stability theory gives a critical Reynolds number at $Re = 92000$ [3], but for entrance flows, the boundary layers are modified, in particular because of the small favorable pressure gradient existing inside the plane channel. This is known to have a stabilizing effect on the boundary layers [6]. Another aspect of the entrance flows that differs from the Blasius case is linked to the fact that two boundary layers are actually co-existing in the velocity profiles. This raises the question of their mutual interaction in the transition scenario of the flow.

In order to address these questions, we have performed DNS of bypass transition of a subcritical channel entrance flow. The computational domain starts at a small distance downstream from the origin of the boundary layers ($Re_x=40000$), where the laminar base flow is perturbed with the optimal perturbation according to the local linear stability analysis. This perturbation consists in streamwise rolls inside the boundary layers and generates steady elongated streaks whose interaction with the laminar base flow result in nonlinear mushroom-shaped structures. Confinement effect on the primary instabilities has been exhibited, that selects an optimal mode in opposition of phase between both walls. Transition is triggered by secondary instability of the non-linear streaks. Two kinds of secondary instabilities have been observed : a sub-harmonic sinuous instability for small amplitude of the streaks and a varicose instability whose frequency is related to the channel height for large amplitude of the primary instability. They are linked to the modification of the velocity profile by the non-linear streaks, as indicated by a bilocal stability analysis. Moreover, the varicose instability is dominant when walls are narrowed (corresponding to moderate Reynolds number Re_h , based on the channel height), whereas the sinuous instability occurs at large Re_h as in the free-stream boundary layer flow.



Fig. 1: visualization of the varicose streaks instability. Isocontours of the longitudinal component of the instantaneous velocity in streamwise planes at $x/h = 22:0$ (left); $32:0$ (right). Black color : low speed streaks. White color : high speed velocity. ($Re_h=2500$).

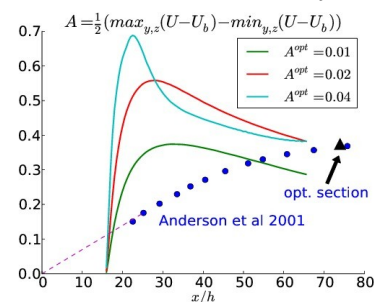


Fig. 2: Streamwise evolution of the resulting nonlinear streaks.

[1] S.A. Orszag. Accurate solution of the Orr-Sommerfeld stability equation. J. Fluid Mech., 50:689–703, 1971.

[2] M. Nishioka and M. Asai. Some observations of the subcritical transition in plane Poiseuille flow. J. Flu. Mech., 150:441–450, 1985.

[3] P. J. Schmid and D. S. Henningson. Stability and Transition in Shear Flows. Springer, 2001.

[4] M. Asai and J.M. Floryan. Certain aspects of channel entrance flow. Phys. Fluids, 16 (4):1160–1163, 2003.

[5] M. Buffat, L. Le Penven, A. Cadiou, J. Montagnier, DNS of bypass transition in entrance channel flow induced by boundary layer interaction, Eur. J. Mech. B-Fluids, 43, 1-13, 2014.

[6] P. Corbett and A. Bottaro. Optimal perturbations for boundary layers subject to stream-wise pressure gradient. PoF, 12:120–130, 2000.

^a Laboratoire de Mécanique des Fluides, Université de Lyon 1/École centrale de Lyon/CNRS/INSA de Lyon, 43, bd du 11 nov. 1918, 69622 Villeurbanne, France

Characterizing the transition to sustained turbulence in pipe flow

V. Mukund^a, B. Hof^{a,b}

Turbulence in pipe flow first arises at Reynolds numbers a little below 2000, in the form of localized structures called puffs. These puffs can decay, or proliferate through splitting. It has been shown that these processes are memoryless and the measured mean life-time before a puff decays (dotted curve) or splits (solid curve) is shown in the figure below. The two curves intersect at a Reynolds number of around 2040. At Reynolds numbers lower than this, puffs decay faster than they split, so that the pipe eventually returns to a fully laminar state. Above this value, the opposite is true and turbulence is maintained indefinitely. Hence $Re = 2040$ may be identified as the critical point at which turbulence can first be sustained in a pipe, thus resolving a long standing issue, though the exact nature of the transition remains unclear. The purpose of this contribution is to characterize in detail, the transition to sustained turbulence in pipe flow.

The chief difficulty in realizing this lies in the fact that the time scales in the vicinity of the critical point are of the order of 10^8 advective time units. We exploit the memoryless nature of the splitting and decay processes to construct a pipe with quasi-periodic boundary conditions. The Reynolds number in this pipe can be maintained with a long-term accuracy of better than 0.1%. It then becomes possible to monitor the spatio-temporal dynamics for arbitrarily long times and extract, for example, the equilibrium turbulent fraction for Reynolds number greater than critical.

We show that the transition exhibits many of the properties of a second order (continuous) transition. We present an estimate of the critical exponents characterizing the transition to sustained turbulence in pipe flow.

^a Institute of Science and Technology Austria, Klosterneuburg, Austria

^b Max Planck Institute for Dynamics and Self-Organization, Göttingen, Germany

² Avila et al., *Science* **333**,192 (2011)

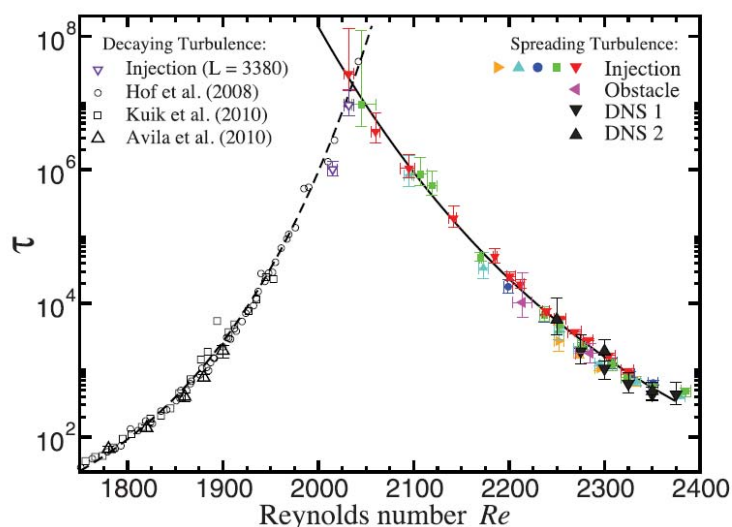


Figure: Mean lifetime of a puff before it decays (dotted curve) or splits (solid curve). The curves intersect at $Re \sim 2040$, marking the transition to sustained turbulence.

Relative-Periodic-Orbits revealing the way to turbulence

S. Altmeyer¹, A. P. Willis², B. Hof^a

Coherent structures like travelling waves (TWs) are believed to provide the skeleton of the chaotic saddles that can explain the intermittent transition to turbulence in wall bounded shear flows. The essential idea is that turbulence evolves around such solutions and that a finite number of unstable states dominate the dynamics^{1,2}. Thus such invariant sets like TWs can give a description of turbulent flows in terms of key exact solutions. More recent are so-called relative periodic orbits (RPOs) that so far are only found in pipe flow with higher, at least 2-fold symmetry⁴. We discovered new RPOs consider a minimal set of symmetry, 1-fold, only (shift-)reflect symmetry to be closest to the natural full state space. We find various RPOs in particular one with a 'long-time' period embedded in a region that seems to be a very strong attractor. In contrast to previous findings⁴ we detected such RPOs that lie in regimes of high energy nearby the solutions of upper branch TW. Various turbulent runs were detected that hang around this long-time RPO for arbitrary times. Meanwhile one of the typical similarity law of turbulence – the Prandtl wall law – is very well able to be presented by the invariant solution of RPOs. Comparison of vortex structures of this RPO with that of turbulent flow in its neighborhood reveals its similarity. This manifests the significance of it to understand the route to turbulence. Together with the finding of long time-period of the RPO suggests it to be embedded in the turbulent region and one can expect it to play a significant role.

¹ Institute of Science and Technology Austria, 3400 Klosterneuburg, Austria

² School of Mathematics and Statistics, University of Sheffield, Sheffield S3 7RH, UK

¹ H. Faisst and B. Eckhardt, *Phys. Rev. Lett.* **91**, 224502 (2003).

² Hof et al., *Science* **305**, 1595-1598 (2004).

³ Y. Duguet, C. C. T. Pringle, and R. R. Kerswell, *Phys. Fluids* **20**, 114102 (2008).

⁴ A. P. Willis, P. Cvitanovic, and M. Avila, *J. Fluid Mech.* **721**, 514 (2013).

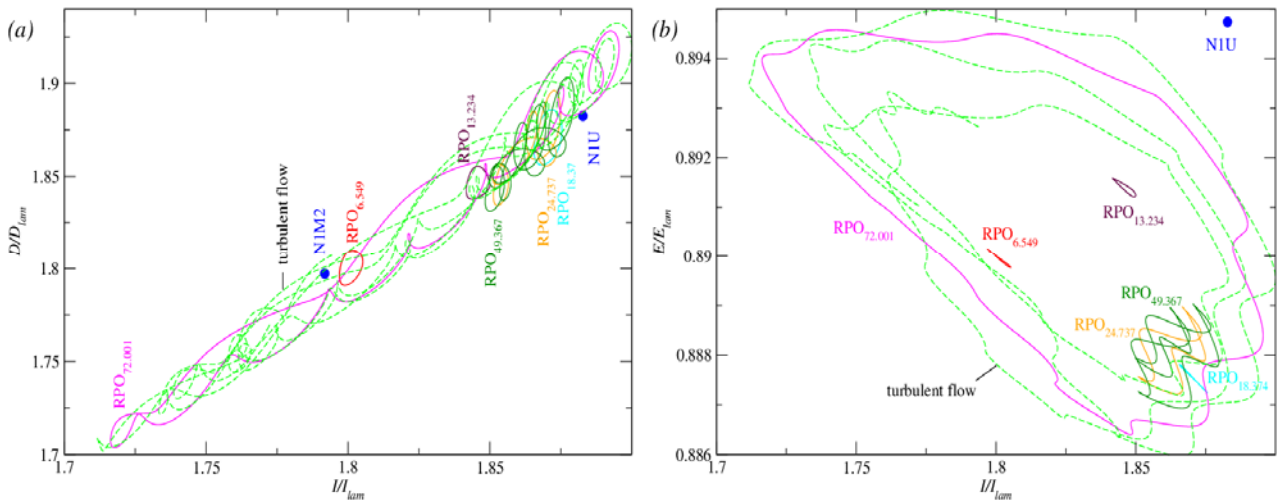


Figure 1: Rate of the energy input from the background pressure gradient I versus (a) the dissipation rate D and (b) the energy E . Plotted are TWs (points in phase space) and various RPOs (index indicates period time) together with one nearby turbulent orbit.

Industrial

CFD investigation of a transonic pulse-jet in a Fabric Filter application

B. O. Andersen^a, 2nd J. H. Walther^a, 3rd N. F. Nielsen^b

In this study a Computational Fluid Dynamics (CFD) model has been developed in order to simulate the unsteady, compressible, transonic pulse-jet used in e.g. the cleaning process of a Fabric Filter system.

In a Fabric Filter the dust transported by flue gas is arrested on the bag's external surface and by that forming a so-called "dust cake". The dust cake must be removed in order to prevent too high increase in pressure loss. The dust removal process requires frequently cleaning and this is typically done by a short pulse-jet (50 to 150 ms) of compressed air being applied from a nozzle directed at the throat of the filter bag, i.e. in a counter-current direction to the flow of flue gas during normal operation.

The pulse-jet cleaning system involves complex fluid mechanics including: transonic air speed at the outlet section of the nozzle (primary air), a near field region around the pulse-jet where air entrainment (secondary air) is an important parameter, a mixing zone of primary and secondary air in the top of the bag and a travelling and reflecting shock wave inside the full length of the bag.

In the present study the details of the jet pulse cleaning process has been studied intensively. A CFD model has been developed in order to simulate the pulse-jet, air entrainment and the shock wave travelling along the bag. The computational model setup consists of the air pressure tank, the blow tube, the nozzle(s), the venturi(s) and the fabric bag(s) (Figure 1). The CFD model has been validated against experimental results obtained on a pilot filter setup. Good agreement has been obtained between computed and experimental results (Figure 2). Based on this result the computational model has been used to investigate and improve the performance of the pulse-jet cleaning system e.g. nozzle design etcetera.

^a Dep. Mechanical Engineering, Technical University of Denmark, Build. 403, 2800 Kgs. Lyngby, Denmark

^b Airtech, Technology Development, FLSmidth A/S, Ramsingsvej 30, 2500 Valby, Denmark

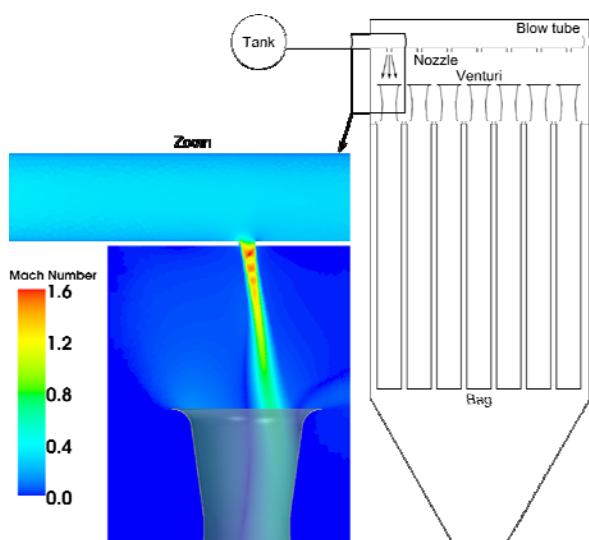


Figure 1: Geometrical set-up of the pulse-jet cleaning process. Zoom box showing CFD result.

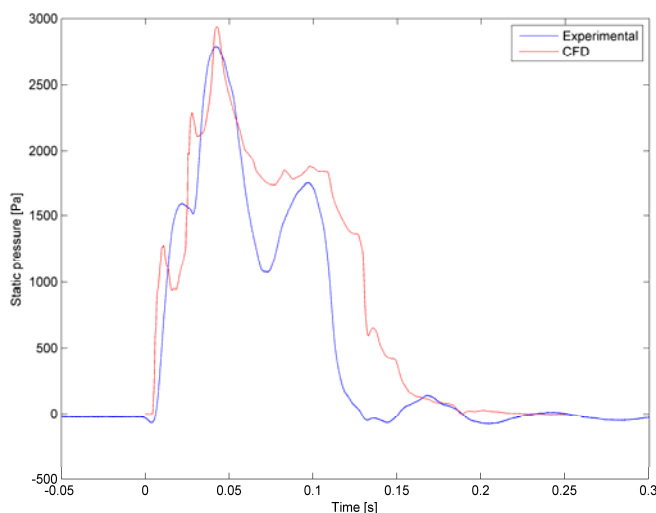


Figure 2: Computed and measured pressure in top of the filter bag as a function of time.

Fluid flow modelling in tape casting of ceramics: analytical and numerical approaches

M. Jabbari^a, J. H. Hattel^b

Since its onset, tape casting has been used to produce thin layers of ceramics that can be used as single layers or can be stacked and laminated into multilayered structures. Today, tape casting is the basic fabrication process that provides multilayered capacitors and multilayered ceramic packages. In addition, many startup products such as multilayered inductors, multilayered varistors, piezoelectrics, ceramic fuel cells and lithium ion battery components are dependent upon tape casting technology. One of the growing sciences in the processing of ceramics by tape casting is the use of fluid flow analysis to control and enhance the final tapes. The fluid dynamics analysis of the ceramic slurries during tape casting is an efficient mean to elucidate the physical parameters crucial to the process.

In this study fluid flow analysis is used to control the most important parameter in the process, i.e. the tape thickness, both numerically¹ and analytically^{2,3}. The developed numerical model is then used to track the interface between two fluids which are tape cast adjacently⁴. Moreover, the migration of a secondary phase inside the ceramic slurry is modelled⁵.

^a Process Modelling Group, Dep. Mechanical Engineering, Technical university of Denmark, Nils Koppels Allé, 2800 Kgs. Lyngby, Denmark

^b Process Modelling Group, Dep. Mechanical Engineering, Technical university of Denmark, Nils Koppels Allé, 2800 Kgs. Lyngby, Denmark

¹ Jabbari and Hattel, *J. Am. Ceram. Soc.* **96**, 1414-1420 (2013).

² Jabbari et al., *Mater. Sci. Tech.* **29**, 1080-1087 (2013)

³ Jabbari and Hattel, *Mater. Sci. Tech.* **30**, 283-288 (2014)

⁴ Jabbari et al., *Int. J. Refrigeration* **36**, 2403-2409 (2013)

⁵ Jabbari et al., *App. Math. Modell.* (under review)

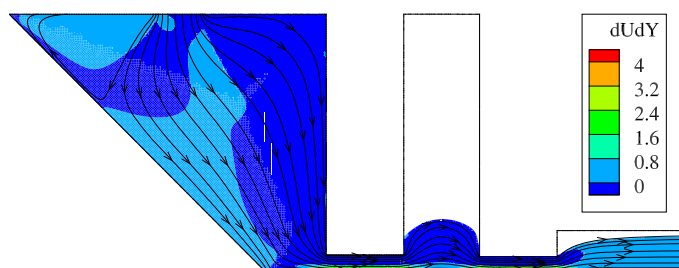


Figure 1: Contour of du/dy in tape casting of a non-Newtonian ceramic slurry using two doctor blade

Preliminary Evaluation of 1D and 3D CFD Codes for Water Hammer in Pipeline

N. S. Kim^a, A. J. Cheong^a and B. K. Min^a

The water hammer is the unexpected release and associated shock wave of high-pressure steam/condensate or the shock waves created by colliding water. Water hammers can cause extensive property damage and severe injury in pipeline. In the nuclear power plant, various systems such as an auxiliary feedwater system, residual heat removal system, emergency core cooling system, etc. have the possibility to experience water hammer because of their operational characteristics, which are rapid valve motion, pump start-up with partially empty lines, etc. Thus, it is important to correctly represent and predict the water hammer in these systems to prevent actual occurrence of these phenomenon during power operation.

The present study focuses on evaluating capabilities of 1D and 3D CFD codes, FLOWMASTER, MARS-KS and ANSYS CFX, to correctly represent this phenomenon with various operating conditions. The overpressure peak during rapid closure of a valve on a simple circuit with different boundary conditions which are different values of initial flow velocity and inlet pressure was modelled using each code with different numeric scheme, and compared with experimental results. Figure 1 shows one of comparison results between measurements and calculations. The test in figure 1 was performed without cavitation, for which all pressures were apparently greater than the vapour pressure. For figure 1 and the pressure traces the ordinates are in meters of water pressure absolute, and the abscissas in milliseconds. It is shown that the simulation results of each code are good agreement with measurements in the aspect of the pressure trends and the first pressure peaks. On the other hand, the wave propagation period is slightly different.

^a Reactor System Evaluation, Korea Institute of Nuclear Safety, 62 Gwahak-ro, Yuseong-gu, Daejeon, Republic of Korea

¹ NRC, NUREG-0933 (1984).

² Martin et al., *Proc. 4th Int. Conf. on Pressure Surges*, 77 (1983).

³ NEA, NEA/CN/IR(2007)5, 41 (2007).

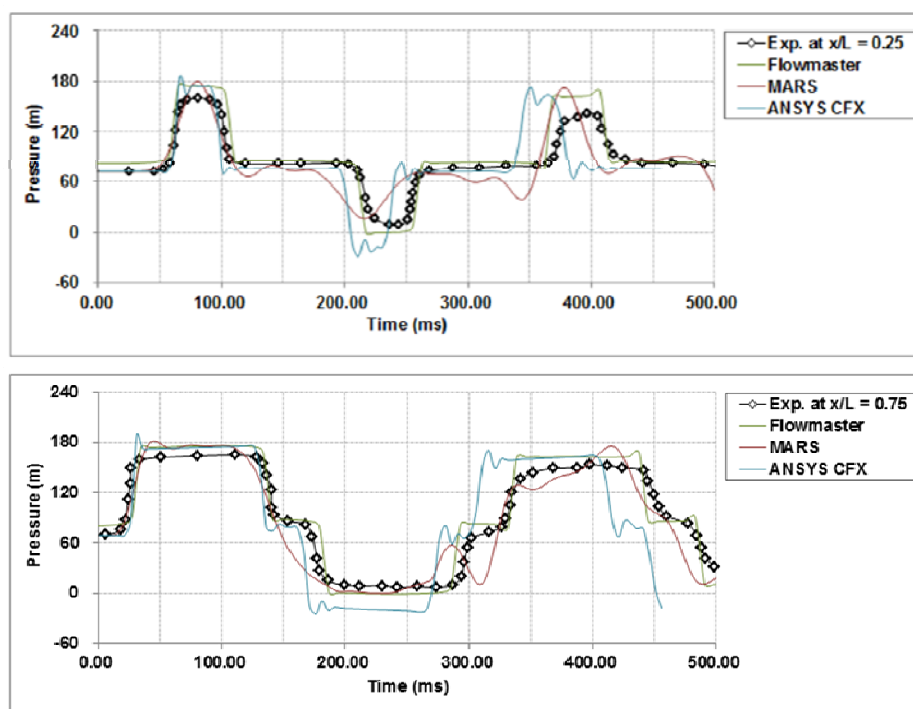


Figure 1: Measured and calculated pressure waves

Flow visualization in a vortex furnace

I. S. Anufriev^a, D. V. Krasinsky^a, E. Yu. Shadrin^b and O. V. Sharypov^{a, b}

The technology of pulverized-coal combustion in vortex flow is one of prospective ways to improve efficiency and ecological performance of boiler units for thermal power plants. The vortex transfer appears to be the aerodynamic basis of the entire combustion process in the so-called vortex furnace, the design of which usually comprises the vortex combustion chamber in the lower part of the furnace, the diffuser, and the cooling chamber exited with discharge flue. With this the tangential-injection nozzle is located in the upper part of combustion chamber (before the diffuser neck). A novel modification of this design, characterized by additional tangential-injection nozzle located horizontally at the bottom of vortex chamber, has been proposed earlier¹. In this dual-nozzle vortex furnace design, the stable swirl flow inside the vortex chamber is formed by two tangential jets released from the upper and the bottom nozzles. The results on the study of 3-D turbulent flow and coal combustion processes in the dual-nozzle vortex furnace have been reported by authors^{2,3}.

In the presented work the visualization of large-scale vortical structures in the isothermal laboratory model of dual-nozzle vortex furnace has been performed. With this, λ_2 - and Q- criteria^{4,6} were applied for the eduction of vortical structures from 3-D mean velocity fields obtained in experimental and numerical study. The three-component Laser Doppler Velocimeter "LAD-056" has been used for non-contact measurements of velocity field. The experimental flowfield data processing software has been tested on the Burgers' vortex analytical solution for the λ_2 - and Q- criteria⁶. The numerical simulation of the steady-state 3-D isothermal turbulent flow in the dual-nozzle vortex furnace model has been performed using the differential Reynolds stress turbulence model with linear pressure-strain correlation⁷. The numerical solution on unstructured computational grid consisting of 351784 hexahedral cells was obtained according to PISO⁸ algorithm for pressure-velocity decoupling. Computations have been performed with the use of CFD package FLUENT at the supercomputer cluster NKS-30T (SSCC SB RAS, Novosibirsk, Russia). To educe the vortical structures from computational results, both the Q-criterion and the "pressure minimum" criterion⁵ have been applied. The V-type vortex core structure inside the vortex combustion chamber of the furnace model has been revealed – see Figure 1 demonstrating essentially 3-D structure of swirl flow inside the furnace combustion chamber.

This study was supported in part by the Presidential Program of Support for Young Scientists (project no. SP-987.2012.1) and the RF President Grant for State Support of Leading Scientific Schools (№ NSh-5762.2014.8).

^a Institute of Thermophysics SB RAS, 1 Lavrentyev Ave., Novosibirsk, Russia

^b Novosibirsk State University, 2 Pirogova Str., Novosibirsk, Russia

¹ Golovanov et al., Russian Federation patent No.2042084 (1995)

² Anufriev et al., *Energy and Power Eng.* **5**, 306 (2013)

³ Anufriev et al., *Tech. Phys. Lett.* **39**, 466 (2013)

⁴ Jeong, Hussain, *J. Fluid Mech.* **285**, 69 (1995)

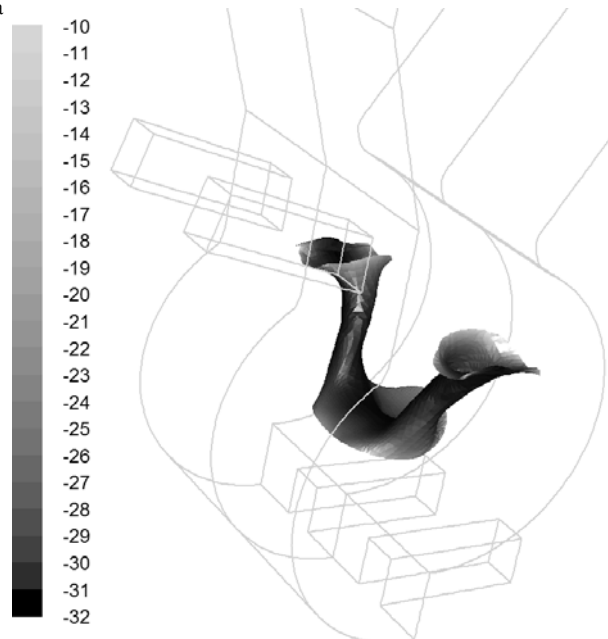
⁵ Dubief, Delcayre, *J. of Turbulence*, **011** (2000)

⁶ Chakraborty et al., *J. Fluid Mech.* **535**, 189 (2005)

⁷ Launder et al., *J. Fluid Mech.* **68**(3), 537 (1975)

⁸ Issa, *J. Comput. Phys.* **62**, 40 (1986)

Figure 1: Distribution of total pressure $P_0 = p - p_{\text{atm}} + \rho \mathbf{u}^2/2$ (Pa) over the isosurface $Q=7000 \text{ s}^{-2}$ inside the vortex chamber of the dual-nozzle vortex furnace model.



A review of the theory of Coriolis flowmeter measurement errors due to entrained particles

Nils T. Basse^a

In a Coriolis flowmeter, the driver vibrates a pipe and pickup sensors detect the twist of the pipe due to the Coriolis effect. The twist is proportional to the mass flow rate of the fluid and the driver frequency is proportional to the density of the fluid. For normal operation of Coriolis flowmeters, the mass flow rate and density of the fluid is measured under the assumption that the center-of-mass (CM) is fixed on the axis of the vibrating pipe. This assumption of a fixed CM is violated if either compressibility or phase decoupling occurs¹.

Phase decoupling is a phenomenon which takes place in two-phase flow. Errors due to phase decoupling occur because the acceleration of the two phases is different. “Bubble theory” is a theoretical treatment of errors due to phase decoupling^{2,3}. For this error type, measurement errors are negative, i.e. measurements are below the true mixture value.

To date, the published bubble theory has dealt with inviscid entrained particles having zero density combined with either viscous or inviscid fluids. In this paper, we review the complete bubble theory, which includes effects associated with finite particle density and viscosity⁴. Those particle properties enable the modelling of mixtures where the particles have non-negligible density and viscosity.

Predicted measurement errors for different two-phase mixtures as a function of the volumetric particle fraction α are shown in Figure 1.

^a Siemens A/S, Flow Instruments, Nordborgvej 81, 6430 Nordborg, Denmark

¹ Weinstein, *Ph.D. Thesis, University of Colorado* (2008)

² Hemp and Sultan, *Proc. Int. Conf. Mass Flow Measurement, IBC Technical Services*, 1 (1989)

³ Hemp et al., *IEE One-day Seminar*, 1 (2003)

⁴ Basse, *Flow Meas. Instrum.* **37**, 107 (2014)

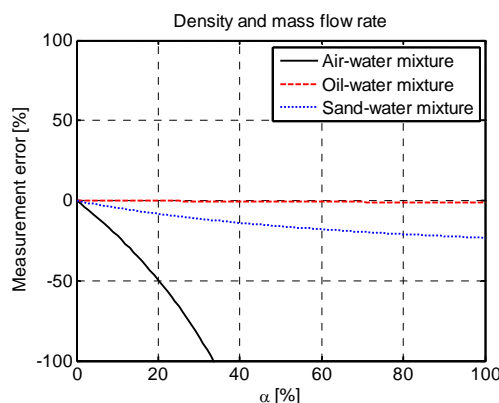


Figure 1: Density and mass flow rate error for mixtures: Air-water (solid black line), oil-water (dashed red line) and sand-water (dotted blue line).

Theoretical and experimental investigation of cavitation in main bearings for large two-stroke marine diesel engines

C. K. Christiansen^a, Peder Klit^a, J. H. Walther^{a,b} and A. Vølund^c

The journal bearing is widely used in a broad range of equipment, especially combustion engines due to their high (radial) load carrying capacity and simplicity leading to a low unit cost. However, due to the diverging-converging geometry, the bearing is prone to suffer from cavitation. While the absence of an anti-symmetric pressure profile, contrary to the predictions of Reynolds equations, is caused by a fluid's poor resistance to tensional forces and hence obtaining negative pressure, cavitation also occurs.

Cavitation is a source to wear as known from e.g. propellers with the collapsing bubbles eroding the exposed surface, but will also affect the load carrying capacity of the bearing. The latter is crucial to avoid shaft-bush contact resulting in a fatal engine failure.

To investigate the formation and behaviour of cavitation a two-sided approach is used. The commercial code STAR-CCM+ enables solution to be obtained for a complete bearing with grooves and inlets of complex geometry. Comparison with a test rig yielding visible bubble formation will be used for basic evaluation of the cavitation formation. As the thin film (order of μm) compared to circumferential and axial dimensions (order of mm) poses difficulties in effective meshing leading to increased solution time, a 2D finite element code is in development for fast predictions under possibly dynamic loading.

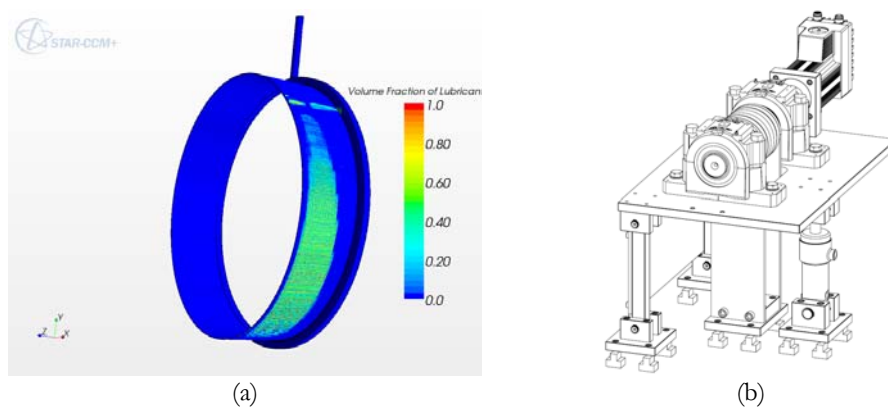


Figure 1: (a) Preliminary cavitation prediction from STAR-CCM+. (b) Illustration of cavitation test rig.

^a Dep. of Mechanical Engineering, Technical University of Denmark, Kgs. Lyngby, DK-2800, Denmark

^b Computational Science & Engineering Laboratory, ETH, Zürich, CH-8092, Switzerland

^c MAN Diesel & Turbo SE, Copenhagen, DK-2450, Denmark

CFD based analysis of heat transfer problem to improve metal erosion in high-voltage circuit breaker

X. Ye^a, M. Dhotre^a, S. Kotilainen^a

A high-voltage circuit breaker is used to interrupt short circuit current in order to protect electrical networks and apparatuses in transmission and distribution of electricity. Gas with good dielectric and thermodynamic properties such as SF₆ or another alternative gas is used to extinguish the electric arc which occurs as the electric contacts are separated¹.

In a circuit breaker, hot gas generated through burning arc is exploited to build up pressure in heating volume. The pressure build-up is used to extinguish arc at current zero and to clear hot gas to avoid dielectric problem². But the hot gas with high velocity has usually contact with metal parts, hence, it leads to erosion of metal surface and causes problem in electrical endurance test. Therefore, the control of hot gas flow pattern and the ensuring of a lower radiation and convective heat transfer to the metal surface, in order to improve the metal erosion, plays an important role in the breaker development. For this purpose, CFD simulation is used for the analysis of heat transfer problem for solving metal erosion issue.

In this paper, CFD strategy and numerical methods used to predict of heat transfer in high voltage circuit breakers are introduced³. Simulations of radiation and convective heat transfer from hot gas to metal surface are carried out. Simulation results and their comparison with measurements are shown and discussed. Based on the simulation results, an improved design of metal surface is analysed.

^a ABB Ltd., Interrupter Development, CH-5401 Baden, Switzerland

¹ Ye et al, *IEEE International Symposium on Electrical Insulation* (2008).

² Bini et al., *Phys. D: Appl. Phys.* **44**, 9 (2011)

³ Schwinne et al., *XVI International Conference on Gas Discharges and their Applications, Xi'an (China), 2006*, pp. 13-16 (2006)

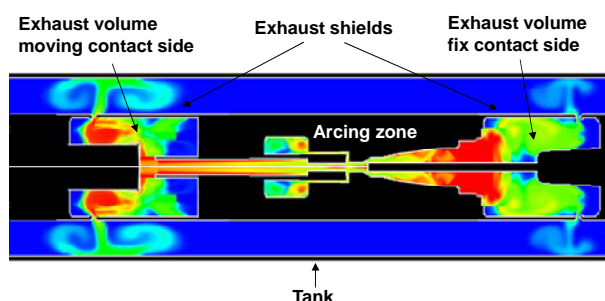


Figure 1: Contact of hot gas to metal surface: Hot gas distribution in a high-voltage circuit breaker.

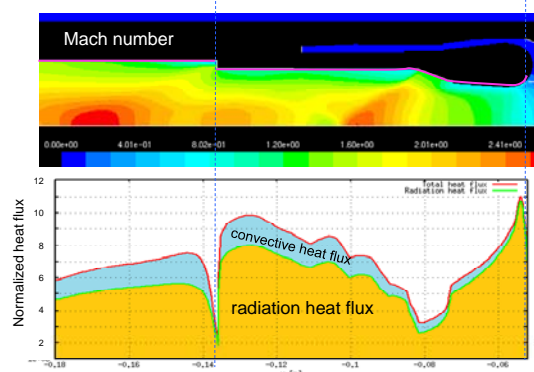


Figure 2: Influence of flow pattern on heat transfer: Correlation of Mach number distribution to the heat flux on metal surface

A numerical and experimental study of the scavenging process in a two-stroke marine diesel engine

C. S. Hemmingsen^a, K. M. Ingvorsen^a, J. H. Walther^{a,b} and K. E. Meyer^a

This study is concerned with the scavenging process in a uniflow-scavenged large two-stroke marine diesel engine. The engine cylinder is scavenged when the piston approaches the bottom dead center (BDC) and uncovers the scavenging ports. A fresh charge is flushing the burned gases out of the engine cylinder before a new combustion. The most efficient way to remove the burned gases is to introduce a swirling flow inside the engine cylinder. The strength of the swirling flow is controlled by the angle and the shape of the scavenge ports.

In the present study the scavenging process is investigated both numerically and experimentally. This is done on a static and dynamic geometrical simplified model¹ of a two-stroke engine with a diameter $D=190$ mm. Numerical simulations are carried out with the commercial Computational Fluid Dynamics (CFD) code STAR-CCM+ version 8.02.008. Experimental measurements are performed using laser Doppler anemometry (LDA).

Experimental measurements inside the scavenging ports are carried out on a static set-up, with piston at BDC, and compared with numerical simulations². Experimental measurements revealed a high axial velocity (V_z) present in the near-wall region inside of the scavenge ports. Large-Eddy Simulations (LES) confirmed the strong secondary flow cf. Fig. 1a, with a high axial velocity located at the center of the separation located inside the port. In the top of the scavenge port axial velocities exceed $V_z/V_{sc}=0.75$ where V_{sc} is the scavenge velocity.

A numerical simulation with a moving piston is studied. The moving piston is simulated by expanding and compressing cells in the axial direction but neglecting compression and combustion. Both Reynolds-Averaged Navier-Stokes (RANS) turbulence models and LES are investigated. The numerical simulations are compared with an experimental database³ using the axial and tangential velocity components. An qualitative good agreement is found with RANS models and an quantitative good agreement is found for the LES. LES simulate the gradients of the velocities near the cylinder axis more accurately whereas RANS models predict solid-body rotation. Fig. 1b shows the turbulent structures visualized with the λ_2 -criterion of the internal flow coloured with the radial position. In the core region of the swirling flow double helical structures are formed. As the ports open or close vortex rings are shed in the axial direction.

^a Department of Mechanical Engineering, Technical University of Denmark, DK-2800, Denmark

^b Computational Science and Engineering Laboratory, ETH Zürich, Switzerland

¹ Ingvorsen et al., Exp. Fluids, 1494 (2013).

² Al-Mousawi, Master's Thesis (2012).

³ Ingvorsen et al., Exp. Fluids, *under review* (2014).

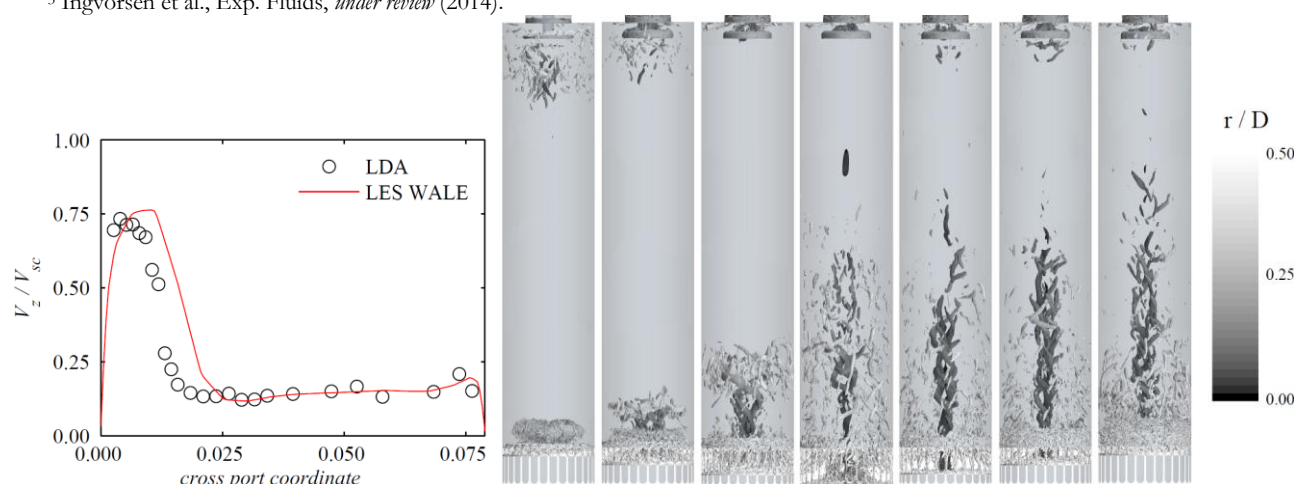


Figure 1: (a) Axial velocities across the scavenge ports. (b) λ_2 -criterion of the engine cylinder flow coloured with the radial position.

Grate aerodynamic -Model strategies for gas flow through a 2D iron ore pellet bed

Per E. C. Burström^a, A-L. Ljung^a, V. Frishfelds^b, T. S. Lundström^a and B. Daniel Marjavaara^c

^a*Division of Fluid and Experimental Mechanics, Luleå University of Technology, SE-971 87*

^b*Liēpāja University, Liēla iela 14, LV-3401*

^c*LKAB, SE-981 86 Kiruna*

Key words: pellets, grate-kiln, heat transfer, iron-ore, CFD, simulation

Abstract

Iron ore pellets are a highly refined product supplied to the steel making industry to be used in blast furnaces or direct reduction processes. The use of pellets offers many advantages such as customer adopted products, transportability and mechanical strength yet the production is time and energy consuming. Being such, there is a natural driving force to enhance the pelletization in order to optimize production and improve quality. The aim with this work is to study fluid dynamic phenomena in the traveling grate zone of a grate-kiln plant [1]. Of special interest is how the incoming process gas, leakage, and pellet bed influence the heat transfer through the bed. To be able to study this, numerical models are developed with which the heat transfer can be examined and optimized. Heat transfer to a bed of iron ore pellets is therefore examined numerically on several scales. Two different modeling strategies to handle the porous bed are compared. The first is a macro model approach that uses Computational Fluid Dynamics with a continuum based porous media model to handle the bed of iron-ore pellets. In the second strategy a discrete micro-level model is applied where the pore space between the pellets is divided into cells with modified Voronoi diagrams. The convective heat transfer of hot fluid flow through the system including dispersion due to random configuration of the pellets is then modeled [2-4]. This model is partly based on results from simulations of the drying of single pellets[5-6]. The two different strategies are compared and conclusions about the advantages and draw-backs of respective model are presented.

References

- [1] Burström, P. E. C. , Lundström, T. S., Marjavaara, D., Töyrä, S., CFD-modelling of selective non-catalytic reduction of NO_x in grate-kiln plants, *Progress in Computational Fluid Dynamics*, 10(5/6), 284-291 (2010)
- [2] Ljung, A. L., Frishfelds, V., Lundström, T.S., Marjavaara, D., Modelling heat and mass transport in drying of a porous bed of iron ore pellets, *Drying Technologies*, 30(7), 760-773 (2012)
- [3] Hellström, J.G.I., Frishfelds, V., Lundström, T.S., Mechanisms of flow-induced deformation of porous media, *Journal of Fluid Mechanics*, 664, 220-237 (2010)
- [4] Jourak, A., Frishfelds, V., Hellström, J. G. I., Lundström, T.S., Derivation of Dispersion Coefficients Inside Three-dimensional Randomly Packed Beds of Spherical Particles, *AIChE journal*, in review (2013)
- [5] Ljung, A-L. , Lundström, T. S. , Marjavaara, D., Tano, K., Convective drying of an individual iron ore pellet: Analysis with CFD, *International Journal of Heat and Mass Transfer*, 54(17-18), 3882-3890 (2011)
- [6] Ljung, A-L. , Lundström, T. S. , Marjavaara, D., Tano, K., Influence of air humidity on drying of individual iron ore pellets, *Drying Technology*, 29(9) , 1101-1111 (2011)

Mini Symposia: Wind Energy

Development and retrospect of classical rotor theories (historical review)

V. L. Okulov^a, J.N.Sørensen^a, G.A.M. van Kuik^b and D. Wood^c

The development of research in rotor aerodynamics (screw propeller, propeller, wind turbine, helicopter, etc.) has always been associated with an intensive development of the appropriate branch of industry. The first attempts to solve problems of the steamship navigation using screw propellers should be considered as the starting point for the elementary rotor theory. This resulted in the simple Rankine-Froude one-dimensional momentum theory of the screw propeller, called also the one-dimensional slim-stream or actuator disc theory.

In the early XX century, the development of rotor aerodynamics was motivated by creation and intensive evolution of aviation. At that time, all famous aerodynamic research schools in England, Russia and Germany studied this subject, but the Joukowsky's school from Russia and Prandtl's from Germany dominated in the creation of new concepts in aerodynamics and for an optimum rotor theory (Fig. 1). Their work as well as efforts of their contemporaries resulted in a development of the blade element momentum (BEM) theory to design rotor blades; in a creation of the general momentum theory of the actuator disc and in a formulation of a new vortex concept of rotor, originally designed for screw propellers with a finite number of blades. After the intensive and fruitful period in the evolution of the rotor aerodynamics for aviation needs, research activity has somewhat weakened due to change of aircraft propulsion from rotor to jet.

Current development of the rotor aerodynamics are undoubtedly associated with the rapid progress of wind energy whose status has been transformed from a minor performance capabilities of an alternative energy with small and individual wind turbines to the main branch of power economy as the most important renewable source of the global energy. In accordance with industry needs, interest of researchers to the rotor aerodynamics has significantly enlarged. Today a new stage of intensive scientific development is underway, similar to the fruitful aviation era by the scientific schools of Joukowsky and Prandtl. State-of-the-art of the investigation advances by a creation of the numerical simulation tools for the rotor optimizations, modeling of wind turbine wakes and establishing of numerical aerodynamics of the wind farms. Though most development of aerodynamic methods in wind energy concerned numerical methods, the wind-turbine era has brought a development of analytical approaches too. An explanation for the anomalous behavior of Joukowsky's infinite-bladed rotor¹ and new theories for optimum performance of finite-bladed rotors² have been developed. These give some simple guidelines for how to design optimum rotors.

^a Wind Energy Department, Technical University of Denmark, Lyngby, Denmark

^b Delft University Wind Energy Research Institute, Faculty of Aerospace Engineering, Kluyverweg 1 2629HS Delft, the Netherlands

^c Schulich School of Engineering, University of Calgary, Canada

¹ Sørensen J.N., van Kuik G.A.M. *Wind Energy*. **14**(7); 821 (2011).

² Okulov V.L., Sørensen J.N. *J. Fluid Mech.* **649**; 497 (2010).

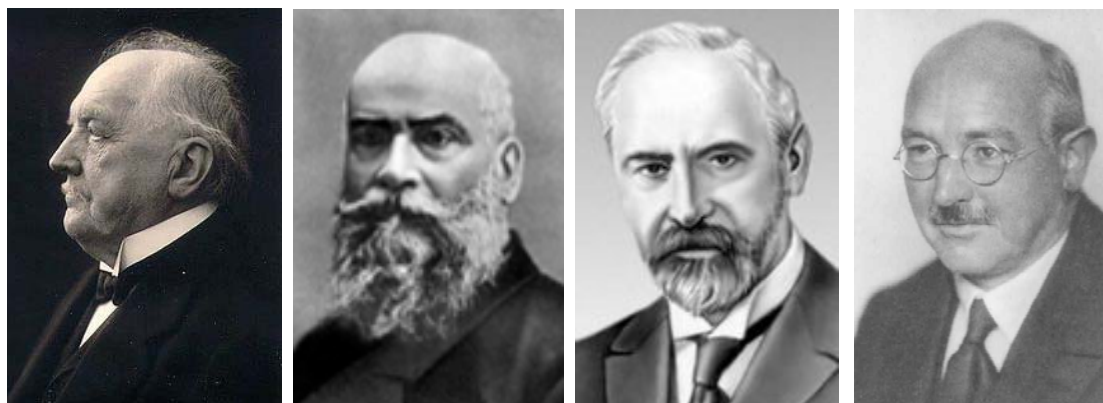


Figure 1: M. Kutta; N.E. Joukowsky; L. Prandtl and A. Betz (from left to right)

Optimal turbine spacing in fully developed and finite size wind-farms

Richard J.A.M. Stevens^{a,b}, Ben Hobbbs^c, Charles Meneveau^a

In order to achieve European and US goals of significant electricity production from wind-energy by the next decade,^{1,2} the scale of wind-farm installations must increase. For large wind farms, interactions with the atmospheric boundary layer (ABL) become crucial. These can be conveniently described by considering the wind farms as surface roughness affecting the surface layer of the ABL.

The Frandsen model³ gives a prediction for the effective roughness height $z_{0,bi}$ of a wind-farm as function of turbine diameter, hub height, inter-turbine spacing, underlying roughness and other relevant parameters. Recent large eddy simulation studies⁴ have led to improved parameterizations of this effective roughness height of wind-farms as function of the main design parameters of large wind-farms. Starting at the entrance of the wind-farm, recent work^{5,6} has used the roughness parameterizations and the notion of a growing internal boundary layer to model the downstream flow development in wind-farms. The results obtained from this modeling approach for the downstream development of power in wind farms are in agreement with trends observed in large eddy simulations and field measurement data. Since this framework allows prediction of power output of large wind-farms as function of wind turbine spacing, the framework can also be used to determine optimal inter-turbine spacings in wind farms.

Meyers and Meneveau⁷ used the power predictions resulting from the roughness parameterizations to explore optimal wind-turbine spacing in infinitely large wind-farms as function of the ratio of the cost of turbine installations and land. For representative cost ratios they found significantly larger spacings than typically used in existing wind farms. Stevens⁶ generalized these results to the case of finite-length wind farms by including the dynamics of developing internal boundary layers and found that for small wind farms, currently common spacings were optimal. However, these works only considered land costs that scale with the area and turbine costs that scale with the number of turbines. Here we extend the above approach by incorporating the effect of the finite size of the wind-farms in the model predictions for the turbine power output and by including the cabling costs that scale with length. We also incorporate the effect of turbine capital and maintenance cost, cable cost, and energy price. Instead of optimizing for maximum power output for a given cost, we also consider optimizing profit, which depends upon the price of energy. The model gives insight regarding which terms determine the best spacings in different regimes.

Acknowledgements

We thank Dennice Gayme for discussions and Andrés Ramos for providing us data on cable costs. This work is funded in part by the research program “Fellowships for Young Energy Scientists” (YES!) of the Foundation for Fundamental Research on Matter (FOM) supported by the Netherlands Organization for Scientific Research (NWO), and in part by the US National Science Foundation, grants numbers CBET 1133800 and OISE 1243482.

References

- 1 Commission of the European Communities. A European strategic energy technology plan - technology map, 2007.
- 2 U.S. Department of Energy. 20% wind energy by 2030: increasing wind energy's contribution to U.S. electricity supply, U.S. Department of Energy, 2008.
- 3 Frandsen et al, *Wind Energy* **9**, 39 (2006).
- 4 Calaf et al., *Phys. Fluids* **22**, 015110 (2010).
- 5 Meneveau, J. *Turbulence* **13**, 1 (2012).
- 6 Stevens, *Wind Energy*, submitted (2013).
- 7 Meyers and Meneveau, *Wind Energy* **15**, 305317 (2011).

^aDepartment of Mechanical Engineering and and E²SHI, Johns Hopkins University, Baltimore, Maryland 21218, USA.

^bDepartment of Science and Technology and J.M. Burgers Center for Fluid Dynamics, University of Twente, P.O Box 217, 7500 AE Enschede, The Netherlands.

^cDepartment of Geography and Environmental Engineering and E²SHI, Johns Hopkins University, Baltimore, Maryland 21218, USA.

Turbulence and wind turbine/farm interaction: The response of wind turbines

Nicolas Tobin^a, Hyun J Kim^a and Leonardo P. Chamorro^a

Power fluctuations experienced by wind turbines within wind farms are strongly modulated by the structure of the atmospheric boundary layer turbulence and the topology of the turbine array. Understanding the complex relation between wind turbines and flow unsteadiness is key for the development of advanced controls aimed at extending the life of turbines. In this study, we investigate the response of kW-range (Fig. 1 left) and miniature (Fig. 1 right) wind turbines in the field and wind tunnel under a variety of flow conditions. The research is performed at the RE-TE-G Lab, University of Illinois at Urbana-Champaign. Synchronous measurements of the three velocity components of the incoming flow, turbine power, rotational speed and deformation of turbine components are acquired at a temporal resolution that includes the majority of the scales relevant for the problem. An array of sonic anemometers (Fig. 1 left) is used in the field to characterize the incoming flow turbulence facing the turbine rotors while hot-wires are used in the wind tunnel at same relative locations. Results reveal a non-linear, scale-to-scale modulation of the flow turbulence on the dynamic response of the turbine structures and power outputs, which suggests representing wind turbines as a non-linear low pass filter. A spectral model for estimating the response of wind turbines in the spectral domain is proposed. It shows to be robust across geometrical scales and particularly useful in real space (Fig. 2). Acknowledgments: Department of Mechanical Science and Engineering, UIUC.

^a Dep. Mechanical Science and Engineering, University of Illinois at Urbana-Champaign, IL 61801, USA



Figure 1: (Left) Small field turbine and sonic, (right) Miniature wind turbines in wind tunnel.

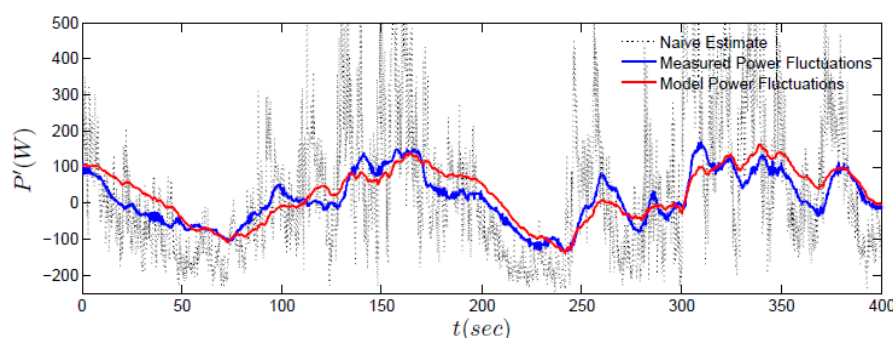


Figure 2: Real-time fluctuating power for the small field turbine.

Large Eddy Simulation of Wind Farms with Energy-Conserving Schemes

D. Mehta^{a,b}, A. van Zuijlen^b and H. Bijl^b

Recent developments in computers have enabled the use of Large Eddy Simulation (LES) for wind farm aerodynamics. As an improvement over the more popular engineering models (EM), LES has helped gain insight into the fundamental physics of wake evolution, wake-atmospheric boundary layer (ABL) interaction, wake meandering etc. However, LES is still conducted on relatively coarse grids for computational efficiency, enabled through suitable modelling of turbines and the ABL. This necessitates numerical schemes that retain their accuracy and stability even on coarse grids.

Pseudo-spectral schemes are dominant in LES due to their accuracy. However, they are computationally demanding, tough to implement and work best with periodic boundaries. The latter in the context of wind farms entails a large computational domain to prevent outflow-inflow interference due to periodicity. Thus, as an alternative to pseudo-spectral schemes, the authors intend to explore and develop Energy-Conserving (EC) schemes for the LES of wind farms.

EC schemes enforce the conservation of Kinetic Energy (KE) in a discrete setting, which is an invariant property of incompressible flows. They guarantee zero numerical dissipation and unconditional stability, even on coarse grids¹. Additionally, they permit the use of inflow-outflow boundary conditions, which helps avert large computational domains with periodic boundaries. These properties are conducive to the proper transport of wakes over the distance between consecutive turbines, unaided by spurious dissipation, while carrying the correct amount of energy, which makes these schemes suitable for the LES of wind farms. Despite their benefits, results indicate, *en passant*, a possible trade-off between using EC schemes and numerical accuracy, which is influenced by the Subgrid Scale (SGS) model used for the LES. However, with careful SGS modelling, one can achieve the desired accuracy. The authors wish to elucidate the above through the LES of a model wind farm, using the Actuator Disk approach to model the turbines, which has been deemed appropriate and apt for this purpose².

Numerical experiments will employ the Energy-Conserving Navier-Stokes (ECNS) developed by the Energy Research Centre of the Netherlands, to solve the incompressible Navier-Stokes equations on a Cartesian staggered grid³. Further, the ECNS uses EC *Runge-Kutta* methods to ensure the conservation of KE with temporal integration.

^a Wind Energy Technology, Energy Research Centre of the Netherlands, Westerduinweg 3, 1755 ZG Petten, The Netherlands.

^b Faculty of Aerospace Engineering, Delft University of Technology, Kluyverweg 1, 2629 HS Delft, The Netherlands.

¹ Verstappen and Veldman, *J. Comput. Phys.* **187**, 343 (2003).

² Wu and Porté-Agel, *Boundary-Layer Meteorol.* **138**, 345(2011).

³ Sanderse, *ECN*, **E-11-042** (2011).

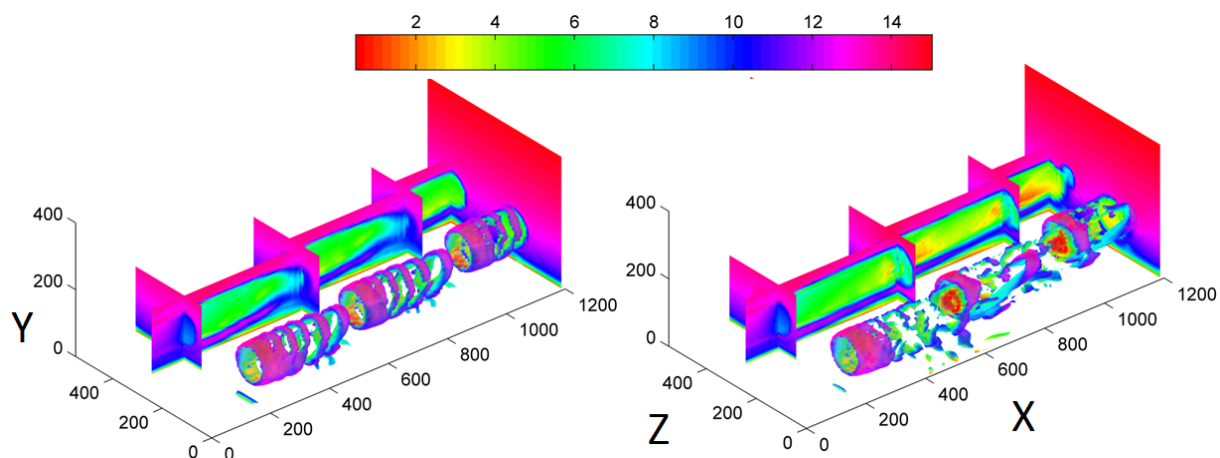


Figure 1: Isosurfaces of Q-criterion coloured by velocity and contours of velocity before and after wake-turbine interaction on a wind farm at a Reynolds number of 10^7 , obtained with the ECNS

Large Eddy Simulations of large wind farms using a body force technique to estimate power production, fatigue loads and farm wakes.

S. Ivanell^{ab}, 2nd K. Nilsson^a, 3rd S-P. Breton^a, 4th J.N. Sørensen^c, 5th Ola Eriksson^a and 6th Silke Martinen^a

Large-eddy simulations are performed using the EllipSys3D Navier-Stokes solver developed at DTU/Risø by Michelsen [1][2] and Sørensen [3] to compute the power production, fatigue loads and wake effects of wind turbines and wind farms. The turbines in the farm are modelled using an actuator disc (ACD) method, Mikkelsen [4]. The ACD method models the rotor with body forces determined from drag and lift coefficients that are tabulated as functions of the angle of attack. The atmospheric conditions are modelled using pre-generated synthetic turbulence, Mann [5], and a prescribed boundary layer in order to save computational costs.

When turbines operate in the wakes of other turbines there are two main disadvantages. First, the turbines are exposed to higher turbulence induced dynamic loads and second, these turbines produce less energy than freestanding turbines. Power curtailment of a turbine moderates the wake generated by this turbine, which results in reduced dynamic loading and increased production for any turbine placed downstream. However, these benefits have to be put in relation to the decreased production of the curtailed turbine. A certain loss in a farm's total production could indeed be justified by a reduction of fatigue damage, especially in offshore conditions where wake effects are strong and maintenance expensive.

Large offshore wind farms are also known to produce long distance wakes. As many offshore wind farms are built, there will be more occasions when the wake from one wind farm will interact with other neighbouring wind farms. Simulation results show very good agreement for power production inside wind farms. [6] Load evaluations also show that the curtailment of individual turbines can reduce the turbine loading while maintaining the power production loss at a reasonable level. The study further shows that the internal power outtake distribution inside the wind farm affect the farm wake.

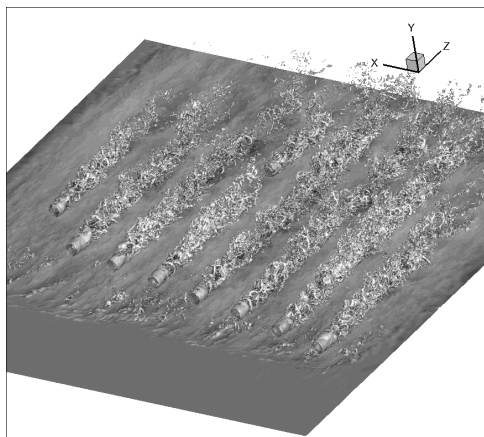


Figure 1: The figure shows simulation results of the Lillgrund wind farm using LES with a body force approach.

^a Uppsala University, Campus Gotland, Dep. of Earth Sciences, Section of Wind Energy, Visby, Sweden.

^b KTH, Department of Mechanics, Stockholm, Sweden.

^c DTU, Wind Energy, Lyngby, Denmark.

¹ Michelsen, *Tech. Rep. AFM 92-05 DTU* (1992).

² Michelsen, *Tech. rep. AFM 94-06 DTU* (1994).

³ Sørensen, *PhD th. Risø-R-827-EN* (1995).

⁴ Mikkelsen, *PhD th. MEK-FM-PHD 2003-02* (2003).

⁵ Mann, *Probabilistic Engineering Mechanics* **13**; 269-282 (1998).

⁶ Nilsson, *Wind Energy*, DOI: 10.1002/we. **1707** (2014);

Rotor Concepts for Offshore Wind Farms

Ö. Ceyhan^a and F. Grasso^b

The present work is focused on investigating the effects of low power density rotors in terms of turbine and wind farm performance. In the INNWIND.EU project a 10MW reference wind turbine (RWT) has been created. Starting from this geometry, several alternative rotors are designed and compared, as shown in Figure 1 (a), aiming to reduce the loads of the turbine while keeping high performance in terms of annual energy production. The focus is given mainly to the rotors with reduced wind-power density from 400W/m² to 300W/m², including low solidity blades since they offer very good potentialities for lightweight rotors. In addition, the effects of new airfoils are considered to improve the performance of the turbine and decrease the loads. As a result of the reduction in wind power density, all the concepts adopt a 15.5% increased radius. For each of them then, the influence of a specific operating parameter is investigated.

In order to assess the performances of the rotor concepts in wind farm level, Horns Rev offshore wind farm is used as reference. Initially, the rotors in Horns Rev are replaced with the RWT rotor. Overall power output of the farm in terms of farm efficiency in different wind speeds and in different wind directions are compared with the original wind farm by using Farmflow software. After that, the same farm layout is used with the new rotor concepts and the results are compared among each other in terms of overall power production and farm efficiency. At last, the farm layout is modified to keep the same relative distance between the turbines as in the original Horns Rev wind farm. The results that will be presented in this work clearly show the advantages of low power density and low solidity rotors in achieving high turbine performance with significantly lower loads. These benefits, already visible with standard airfoils, are emphasized by adopting new ECN airfoils where the high lift characteristics help to reduce the chord and control the loads. At wind farm level, the increased radius result in increased power output up to 12%, while the reductions in axial loading of the rotors will reduce the wake losses and this leads to further improvements in the overall wind farm power output up to 11% as shown in Figure 1 (b). Although the amount of improvements depend on the farm layout and the wind speed and direction, the lower power density rotors with ECN airfoils show potential for the future offshore wind farm applications.

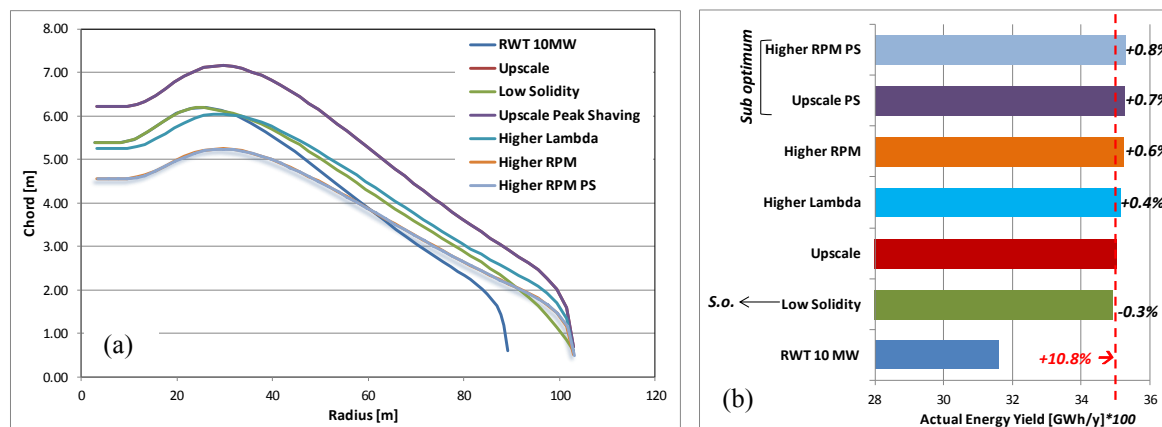


Figure 1: (a) Chord distributions for different rotor concepts. (b) Wind farm energy output of Horns Rev compared for different concepts.

^{a,b} Energy research Center of the Netherlands, ECN, Westerduinweg 3, 1755LE, Petten, the Netherlands.

Design of a scaled non-rotating model wind turbine blade

L. K. Neuhaus^a, M. S. Melius^{a,b}, R. B. Cal^b and K. Mulleners^a

Recently, numerical investigations have revealed a considerable potential for power optimisation in wind farms by varying thrust coefficients of individual turbines over time. In practice, a change in thrust coefficient is obtained by varying the pitch angle of the rotor. To fully exploit the power optimisation potential, detailed knowledge about the influence of a dynamic pitch variation on the flow past the rotor blades is desirable. To answer this and other questions related to the unsteady rotor blade aerodynamics, a scaled non-rotating three-dimensional model wind turbine blade has been designed for wind tunnel testing. To guarantee dynamic similarity between non-rotating model and the original rotating blade, the twist distribution along the blade was redesigned to compensate for the effect of rotation. The most prominent effect of rotation is the generation of a flow in the radial direction, known as centrifugal pumping, which influences the unsteady flow development over the blade and leads to stall delay. The centrifugal pumping is recognised by a span-wise pressure gradient. Matching the pressure gradient will allow for dynamic similarity between the non-rotating model and the rotating reference. Based on blade element momentum (BEM) theory, the span-wise suction peak-pressure distribution of a rotating blade can be characterised. The twist distribution for the model blade was obtained by means of a genetic optimisation algorithm with the objective to match the span-wise suction peak-pressure gradient of the reference rotating blade. The generality of the employed scaling approach was further investigated by a sensitivity analysis of the suction peak-pressure distribution of a rotating blade on wind speed and tip speed ratio.

a. Department of Mechanical Engineering, Leibniz Universität, Hannover, Germany

b. Department of Mechanical and Materials Engineering, Portland State University, Portland OR, USA

1. Meyers and Goit, Bull. Am. Phys. Soc. (2013)

3D CFD-Based Shape Optimization of a 10MW Wind Turbine Rotor

F. Zahle¹, N. N. Sørensen¹

Blade planform optimization using either gradient-based or global algorithms coupled to a Blade Element Momentum (BEM) code is a well-established discipline in the field of wind energy and widely used in industry. In this approach the chord, twist and relative thickness are typically considered as design variables, while the cross-sectional shape of the blade is pre-defined and based on an “aerofoil-family” of different thicknesses with corresponding pre-tabulated aerodynamic performance. However, to enable concurrent planform and cross-sectional shape optimization of a blade, the optimization needs to include a flow solver of some sort. This can be achieved by replacing the BEM solver with a 3D CFD solver thus resolving the full surface of the blade.

This work presents a Python-based framework developed for high fidelity shape optimization of wind turbine blades based on 3D CFD aimed for gradient-based optimization. The optimization framework uses OpenMDAO² as the underlying framework for handling the data- and workflow, declaring design variables, constraints and objectives.

While 2D-based shape optimization of aerofoils is to a large extent sufficient for the mid/outer part of the blade where the flow is mostly two-dimensional, towards the tip and more importantly towards the root, 2D based flow solutions do not fully capture the flow characteristics governing on a rotating blade.

A key requirement of a 3D CFD based approach to shape optimization is robustness of the parameterization of the shape, mesh generation and flow solver, while retaining enough degrees of freedom to arrive at an optimal shape that is not limited by the parameterization. In this work, the 3D blade shape is parameterized using a combination of Bezier curves and bi-cubic Coons patches (Figure 1). The surface meshing is an integral part of the parameterization and is thus very efficient. The volume mesh is generated using the in-house mesh generator HypGrid3D³. Two approaches are used to updating the volume mesh within the optimization: when computing gradients the mesh deformation is propagated into the volume with a mix of solid body deformation and linear blending with the original mesh, while the entire mesh is regenerated at the beginning of each outer iteration.

The flow solution is computed using the incompressible flow solver EllipSys3D^{4, 5} assuming steady flow on a mesh with 1.77 million cells, which gives rise to an error of approximately 2-4 % compared to a mesh independent solution, which is acceptable in an optimization context. Since EllipSys3D is not capable of computing analytic gradients, finite differencing is used. In the present work the blade is parameterized using 10 design variables for the chord and twist, respectively, and four cross sections with each 12 design variables, totalling 68 shape design variables. The optimization uses the DTU 10MW RWT⁶ as the starting point.

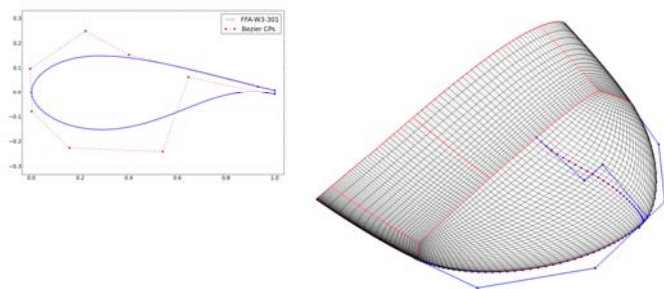


Figure 1: Example of cross-sectional Bezier spline used to deform the surface and detail of the blade tip showing the CFD-ready surface and in blue Bezier control points for detailed control of the tip shape.

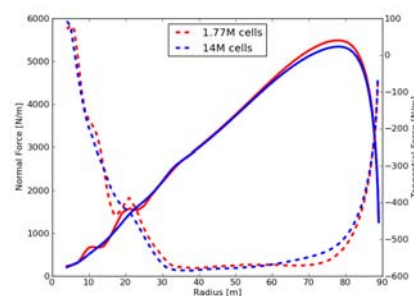


Figure 2: Normal force (fully drawn) and tangential force (dotted) for the DTU 10MW RWT operating at 8 m/s for a coarse and fine mesh solution.

¹ DTU Wind Energy, Aeroelastic Design Section, Frederiksborgvej 399, DK-4000 Roskilde, DK.

² <http://openmdao.org>

³ Sørensen, Technical report, R-1035(EN), Risø National Laboratory, Denmark, 1998.

⁴ Michelsen. Technical Report, AFM 92-05, Technical University of Denmark, 1992.

⁵ Sørensen. PhD thesis, Risø-R-827-(EN), Risø National Laboratory, Denmark, 1995

⁶ <http://dtu-10mw-rwt.vindenergi.dtu.dk>

A Free Wake Vortex Lattice Method Combined with the Øye Dynamic Stall Model for Vertical Axis Wind Turbines

T. J. Berdowski^{a,b}, F. Meng^b

The Vertical Axis Wind Turbine (VAWT) design has regained a general interest over the last few years. A VAWT offers great advantages over the classical horizontal axis wind turbine, such as an absence of a yawing system and a low centre of gravity, which are beneficial for aspects such as complexity, maintenance, and construction cost. Hence, the VAWT is a potentially interesting alternative for the offshore turbines above the 10MW range. The research on VAWTs has been limited, and the aerodynamics involved is complex due to unsteady phenomena and blade-wake interactions. A growing call from industry requires to come up with reliable and accurate, yet fast engineering design tools. Full CFD calculations are therefore to be avoided, although the complex aerodynamics requires more advanced modelling techniques than used for HAWT design.

A project has been initiated to explore the existing knowledge in VAWT aerodynamic modelling, and to implement an aerodynamic code based on the free wake vortex lattice method. This vortex lattice code has already been developed and validated¹. The current project focusses on the dynamic stall phenomenon caused by the rapid cyclic pitching behaviour of the blades with large amplitudes, which is typical during the VAWT operation. It is chosen to implement the dynamic stall model developed by Øye² in the vortex code, due its simple empirical representation and therefore the reduced amount of airfoil dependent parameters which have to be deduced from experiments. The result is compared to both the steady vortex lattice code and a water towing experiment³. This experiment consists of a 1, 2, and 3 NACA-0012 bladed small-scale VAWT for a Reynolds number of 40,000 at a tip speed ratio of 5.

Figure 1 shows the normal and tangential blade force results from the experiment, original simulation, and the simulation including the dynamic stall model for both 1 and 3 blades. It seems that Øye's model results in a modelling improvement for the normal force of a rotor with 1 blade, but that this improvement vanishes for a rotor with multiple blades. Probably the effect of blade-wake interactions is predominant for a multiple-blade turbine. Also the model fails to capture the tangential force behaviour for 1 blade, which was still captured by the simulation without the dynamic stall model implemented. This gives rise to the presumption that research has to focus on the viscous blade-wake interaction phenomena to be able to more accurately model the VAWT performance.

^a Dep. Wind Energy, DTU, Anker Engelds Vej 1, Kgs. Lyngby, Denmark

^b Fraunhofer IWES, Am Seedeich 45, Bremerhaven, Germany

¹ Meng et al., *Proc. of the Science of Making Torque from Wind* (2012).

² Øye, *Proc. of the 4th IEA Symposium on the Aerodynamics of Wind Turbines* (1991).

³ Strickland et al., *J. of Fluids Eng.* **101**, 500 (1979).

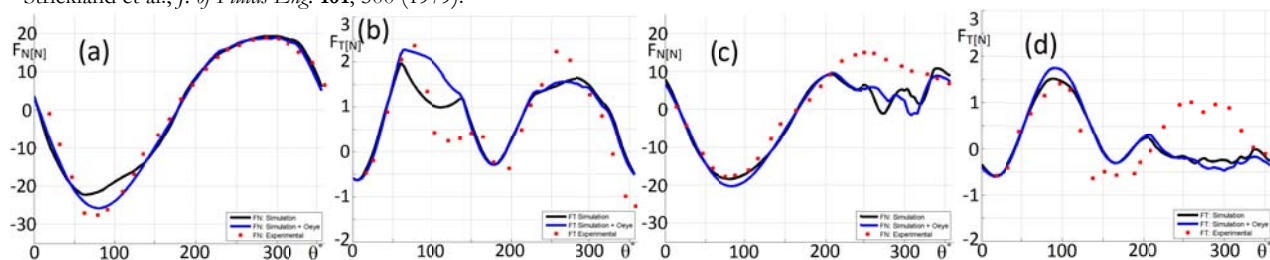


Figure 1: the blade force over the azimuthal position. (a) 1 blade, normal force; (b) 1 blade, tangential force; (c) 3 blades, normal force; (d) 3 blades, tangential force. All figures: red dots: experiment, black line: simulation, blue line: simulation + dynamic stall model.

State-of-the-art and challenges of Vertical Axis Wind Turbine aerodynamics

Carlos Simão Ferreira^a

The pursuit of an economically-feasible offshore wind turbine is driving a renewed interest in Vertical Axis Wind Turbines (VAWTs). The decrease of research on VAWTs between 1995 and 2003, and the limited research since 2003, means that the aerodynamics of VAWTs have not yet enjoyed the process of review and maturation that Horizontal Axis Wind Turbine (HAWT) aerodynamics have experienced during the last two decades. This work aims to review the state-of-the-art and the main challenges on the research and design of VAWT aerodynamics. These challenges are first of all defined by the 3D, unsteady, asymmetric nature of the VAWT. At rotor scale, the VAWT is defined by a 3D actuator surface (in opposition of the simpler actuator disk of HAWT), where streamlines cross the actuator twice; this geometry not only implies blade-vortex interaction, but also an unsteady flow field, asymmetric between leeward and windward regions. In literature, these phenomena are presented as a source of complexity and lower performance. However, that assumption is incorrect. The 3D surface actually allows for a wider design space, where thicker airfoils can be used without loss of power performance and stall regulation can be designed effectively. Additionally, active flow control allows for further power performance not only at airfoil level, but also at wind farm level, by allowing rotors to realign wakes. The 3D asymmetric aerodynamics cause an immediate instability of the near wake, which can be explored for a faster wake recovery. These opportunities appear in parallel with modelling challenges: conventional streamtube momentum models are incorrect for VAWT, while more complex models still lack a full validation. This work reviews the requirements for models for the different scales of VAWT aerodynamics: airfoil, rotor and wake/wind farm; additionally, some of the key research question of VAWT aerodynamics are presented, supported by experimental and numerical data.

^a Delft University of Technology, DUWind, Delft, The Netherlands

Review of the State-of-Art in Wind Turbine Aerodynamics

Jens N. Sørensen^a

The modern development of wind power is a remarkable story of the combined effort of enthusiastic entrepreneurs and skilled engineers and scientists. Today, wind power forms the most rapid advancing renewable energy resource with an annual growth rate of about 30%. Within the last 20 years the size of wind turbines have increased from a rotor diameter of about 30 m to 150 m, corresponding to an increase in power by a factor of more than 25. In the same period of time, the knowledge and scientific level of the aerodynamic research tools to develop optimally loaded rotor blades have increased dramatically. Today, wind turbine aerodynamics forms one of the research frontiers in modern aerodynamics.

The aerodynamics of wind turbines concerns modelling and prediction of the aerodynamic forces on the solid structures of a wind turbine, and in particular on the rotor blades of the turbine. Aerodynamics is the most central discipline for predicting performance and loadings on wind turbines, and it is a prerequisite for design, development and optimization of wind turbines. From an outsider's point of view, aerodynamics of wind turbines may seem simple as compared to aerodynamics of e.g. fixed-wing aircraft or helicopters. However, there are several added complexities. Most prominently, aerodynamic stall is always avoided for aircraft, whereas it is an intrinsic part of the wind turbines operational envelope. Furthermore, wind turbines are subjected to atmospheric turbulence, wind shear from the atmospheric boundary layer, wind directions that change both in time and in space, and effects from the wake of neighbouring wind turbines.

In the past year the development in numerical and experimental techniques dealing with rotor and wake aerodynamics of wind turbines has developed dramatically, and with appropriate simplifications it is possible to perform advanced simulations of single wakes of wind turbines as well as simulations and performance predictions of full wind farms. An example of a simulation using the so-called actuator line technique to predict the dynamics of the wake behind a wind turbine is shown in Figure 1.

In the presentation I will give a review of the state-of-the-art of fluid mechanical aspects of wind energy, focusing mainly on wake aerodynamics and the fluid mechanics of wind farms.

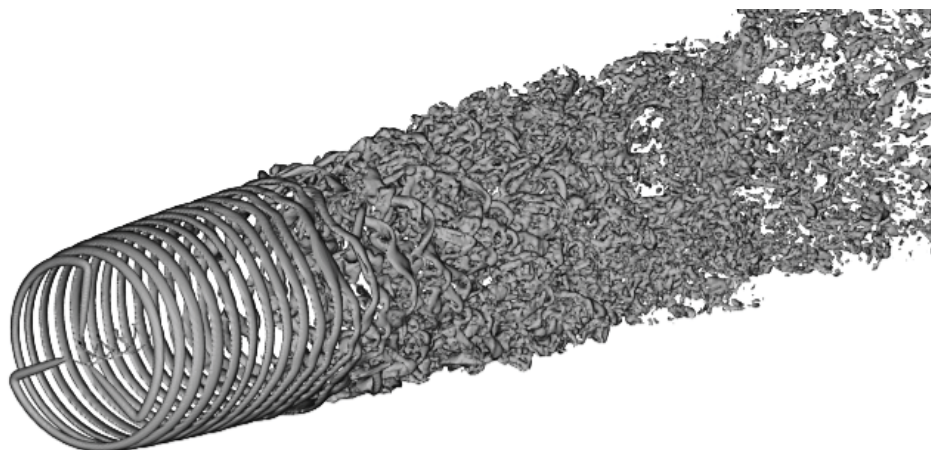


Figure 1. Isolines of vorticity based on Large-Eddy-Simulation of wind turbine wake using actuator line technique.

^a Dep. of Wind Energy, DTU, Nils Koppels Allé, Building 403, 2800 Lyngby, Denmark

Mini Symposia: Thermo Acoustics

Global modes, receptivity, and sensitivity of ducted non-premixed flames via adjoint-based analysis

Luca Magri^a and M. P. Juniper^a

In this theoretical and numerical work, we derive the adjoint equations for a thermo-acoustic system consisting of an infinite-rate chemistry non-premixed flame coupled with duct acoustics. We then calculate the thermo-acoustic system's linear global modes (i.e. the frequency/growth rate of oscillations, together with their mode shapes), and the global modes' receptivity to species injection, sensitivity to base-state perturbations, and structural sensitivity to advective-velocity perturbations. Some of these could be found by finite difference calculations but the adjoint analysis is computationally much cheaper^{1,2}.

The receptivity analysis shows the regions of the flame where open-loop injection of fuel or oxidizer will have most influence on the amplitude of the thermo-acoustic oscillation. We find that the flame is most receptive at its tip. The base-state sensitivity analysis shows the influence of each parameter on the growth rate/frequency (figure 1). We find that perturbations to the stoichiometric mixture fraction, the fuel slot width, and the heat release parameter have most influence, while perturbations to the Péclet number have least influence. These sensitivities oscillate: e.g. positive perturbations to the fuel slot width either stabilizes or destabilizes the system, depending on the operating point. This analysis reveals that the phase delay between velocity and heat release fluctuations is the key parameter in determining the sensitivities and scales with the steady flame length. The structural-sensitivity analysis shows the influence of perturbations to the advective flame velocity. The regions of highest sensitivity are around the stoichiometric line close to the inlet, showing where velocity models need to be most accurate. This analysis can be extended to more accurate models and is a promising new tool for the analysis and control of thermo-acoustic oscillations.

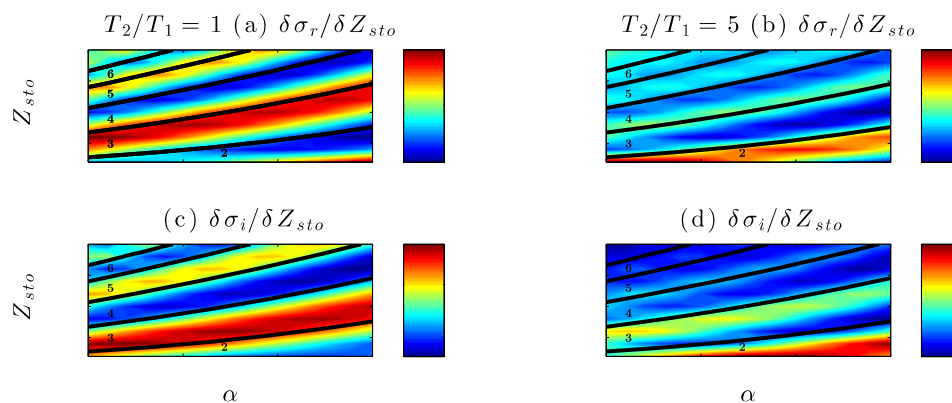


Figure 1: These charts show the sensitivity of the thermo-acoustic system's growth rate, σ_r (a,b), and angular frequency, σ_i (c,d), to perturbation to the stoichiometric mixture fraction, δZ_{sto} , as a function of different operating points (Z_{sto} , α), where α is the fuel-slot-to-duct width ratio. Solutions are calculated by two different duct acoustics models: in the left panels (a,c) the mean-flow temperature jump across the compact heat source has not been modelled ($T_2/T_1=1$), in the right panels (b,d) a realistic temperature jump has been modelled ($T_2/T_1=5$). The solid black lines represent the steady flame length contours.

^a Department of Engineering, University of Cambridge, Trumpington Street, Cambridge, CB2 1PZ, UK

¹ Magri and Juniper, *J. Fluid. Mech.*, **719**, p. 183 (2013)

² Magri and Juniper, *J. Eng. Gas Turbines Power*, **135**(9), 091604 (2013)

Modeling and analysis of combustion dynamics and flame bifurcation in a gas-turbine model combustor

Matthias Ihme^a

Gas-turbine combustors typically utilize swirling fuel-preparation strategies for flow stabilization and flame anchoring. Under such conditions, the flow inside the combustion chamber is highly unsteady and usually accompanied by dynamic flow structures such as precessing vortex cores and flow separation. Due to this unsteadiness, steady-state flow solvers are not capable of accurately predicting the flow-field. In this study, simulations of a gas-turbine model combustor are performed using large eddy simulations (LES). Simulation results are compared with experimental data to assess the capability of these modeling techniques in predicting swirling flows under gas-turbine relevant flow-field environments. Effects of combustion models and subgrid closures on the flame dynamics will be examined and modeling challenges for the prediction of the unsteady combustion behavior will be discussed.

^a Department of Mechanical Engineering, Center for Turbulence Research, Stanford University, Stanford, CA 94305

A dynamical model for instability analysis of generic combustion systems

J-F Bourgouin^{ab}, D. Durox^{ab}, T. Schuller^{ab}, J. Moeck^{abc}, Y. Méry^d and S. Candel^{ab}

The low order modeling of combustion dynamics is investigated by making use of a unified framework in which the state variables are projected on the system modes^{1,2}. A modified representation is here considered to deal with typical configurations encountered in practice, which comprise interconnected cavities. The generic case of an upstream plenum and a chamber linked by injectors is specifically considered in the present analysis. The state variables are projected on the modes of the different cavities. Dynamical models are derived for the injectors and serve to link the upstream plenum and downstream combustor cavities. The formulation obtained in this way is quite flexible. It is here validated by deriving a frequency domain version (FDV) of the time domain model and comparing this with a reference frequency domain (RFD) model used in a previous study³. The two models are then applied to the stability analysis of a set-up comprising an upstream cylindrical manifold, a single swirling injector and a cylindrical chamber open to the ambient atmosphere. It is shown that the two frequency domain descriptions provide similar results but that differences arise when one examines higher order modes of the chamber. The source of these differences is explained underlining the necessity to obtain a suitable estimation of the pressure gradient in the flame region. The final part of this study is concerned with the time domain representation of the flame response. It is shown that an impulse response can be deduced from the flame transfer function and that this can be included in the model. It is however necessary to assure that unstable fluctuations saturate at a certain level by accounting for nonlinearities of the system.

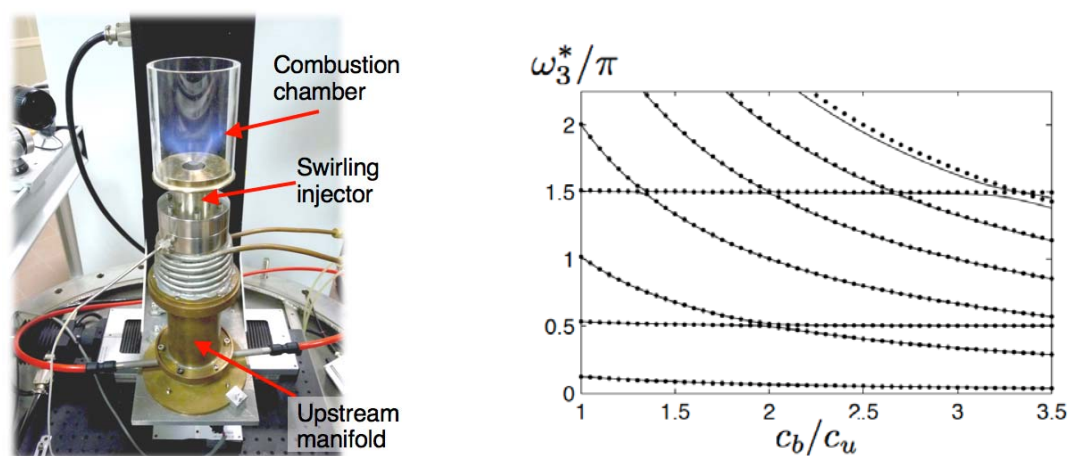


Figure 1: Left: Generic combustor comprising an upstream manifold, a swirling injector and a transparent cylindrical chamber. Right: reduced eigenfrequencies plotted as a function of the ratio of sound velocities in the chamber and in the upstream manifold. The reference frequency domain results are shown as solid lines, the dot symbols correspond to the frequency domain version of the present model.

^a CNRS, UPR288, EM2C, Grande Voie des Vignes, 92295 Chatenay-Malabry, France

^b Ecole Centrale Paris, Grande Voie des Vignes, 92295 Chatenay-Malabry, France

^c Also with TU Berlin, Berlin 10623, Germany

^d Safran, Snecma, 77550 Villaroche, France

¹ E.M. Lores and B.T. Zinn *Combust. Sci. Technol.* **7**, 245-256 (1973)

² F.E.C. Culick, Unsteady motions in combustion chambers for propulsion systems. RTO AGARDograph AG-AVT-039 (2006)

³ P. Palies et al. *Combust. Flame* **158**, 1980-1991 (2011)

Identification of Flame Transfer Functions in the Presence of Intrinsic Feedback and Noise

S. Jaensch^a, T. Emmert^a, C. Sovardi^a and W. Polifke^a

The flame transfer function (FTF) in combination with a thermo acoustic network model has been proven to be a useful tool for the prediction of thermo acoustic instabilities. It relates a velocity fluctuation upstream of the flame to the resulting fluctuation of the heat release rate. The FTF can be derived from a large eddy simulation (LES) of the particular flame. Here, the most efficient method is the so called LES/SI approach. Thereby, the LES is excited with a broadband velocity fluctuation and the resulting fluctuation of the heat release rate is measured. The generated time series are then post processed with system identification (SI) techniques in order to determine the FTF.

The system identification method that is commonly used within the LES/SI approach is the Wiener-Hopf inversion. It is based on correlation analysis and works well in configurations without feedback. This requires that the LES have boundary conditions with low acoustic reflection factor, which can be achieved by plane wave masking. However, non-reflecting boundary conditions are not sufficient to avoid feedback in an identification experiment: Recent research has shown that in compressible flow, velocity sensitive flames are unavoidably part of an intrinsic feedback loop^b. This feedback loop, shown in the figure below, can be explained as follows. A

fluctuation of the velocity u' results in a fluctuation of the heat release rate \dot{q}' . The latter creates an acoustic waves p' at the flame position, which is traveling upstream. This wave induces again a fluctuation of the velocity at the reference position and hence, the FTF is, in a compressible simulation, always under feedback.

We investigate the consequences of this effect on the LES/SI approach. Our study is based on data generated by simulating a low-order thermo acoustic network model in the time domain. We can show that the Wiener-Hopf inversion works well under feedback as long as no turbulent combustion noise is considered. If turbulent disturbances are considered the Wiener-Hopf inversions converges to wrong values. The resulting bias depends on the signal to noise ratio, which means that for high amplitudes of the input signal the influence of the combustion noise can be neglected and the Wiener-Hopf inversion properly estimates the FTF. However, in real configurations high amplitudes of the input signals result in a nonlinear response of the system. Therefore, we propose to use an advanced system identification approach based on the prediction error method (PEM). With this method it is possible to determine the FTF under closed loop conditions and a low signal to noise ratio. Furthermore, the method identifies a model for the combustion noise.

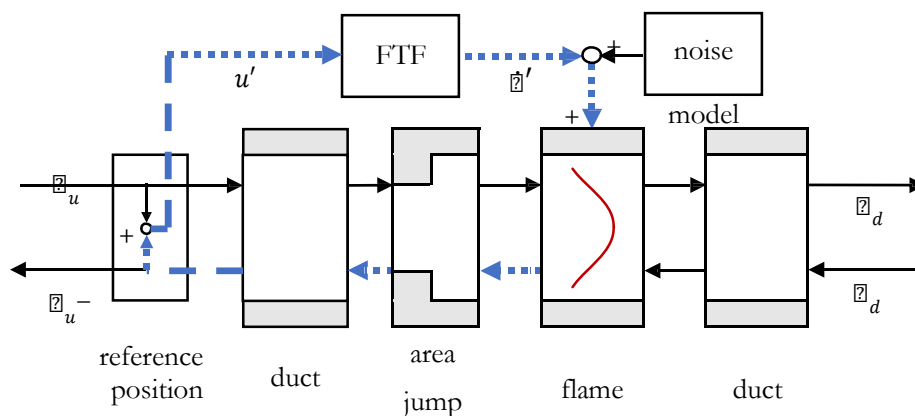


Figure: Network model of a flame burning in a duct. The intrinsic feedback loop is marked with the dotted blue line.

^a Lehrstuhl für Thermodynamik, TU München, D-85747, Garching, Germany, Email: polifke@td.mw.tum.de

^b Emmert et al., submitted to *combustion and flame*

Time-lag characteristics of thermo-acoustic instabilities in a gas-turbine model combustor with a low-swirl injector

S. Tachibana^a, K. Kanai^b, H. Yamamoto^b, S. Yoshida^a, K. Suzuki^a and T. Sato^c

In this experimental study, time-lag characteristics between pressure and heat-release variations have been investigated on thermo-acoustic instabilities in a lab-scale gas-turbine combustor. Time series measurements of dynamic pressure and global OH* chemiluminescence intensity were performed over a wide range of inlet velocity and equivalence ratio conditions. The combustion chamber was an open-ended cylindrical quartz glass tube whose length and diameter were 495 and 146 mm, respectively. A low-swirl injector which is useful for investigating the fundamental processes of lean premixed combustion was mounted in the burner plenum. The diameter of the injector was 50mm and the effective swirl number was approximately 0.55. Methane gas was used as fuel and mixed with air flow by a static mixer before entering the burner plenum. Bulk air flow rate conditions were from 5 to 15 m/s with a 2.5 m/s step. Equivalence ratio was increased from 0.60 to 0.85 with a 0.01 step at each velocity condition. Strong self-excited combustion instabilities were observed for different ranges of equivalence ratio depending on the velocity condition. The peak frequencies of the strong instabilities were consistently around 330 Hz, regardless of the velocity conditions. Looking at the dependency of the pressure oscillation amplitude on the phase lag, it turned out that there was a favorable range of phase lag to excite strong combustion instabilities. In order to clarify the mechanism of the selectivity, a simple linear mode analysis using a n - τ model was carried out. The mode analysis concluded that the unstable mode was a longitudinal three-quarters-wave mode of the test rig system which was composed of the combustion chamber and burner plenum. The mode shape agreed well with the dynamic pressure data measured at 9 axial positions of the test rig. Also, a high-speed OH* chemiluminescence image measurement was conducted. The local Rayleigh index (RI) map was computed by using the phase-averaged Abel-inverted OH* intensity distribution and band-pass-filtered pressure signal. A flame stand-off distance was defined by the intensity-weighted central position of the positive RI zone near the flame-to-wall impingement region. The stand-off distances in the strong oscillation cases showed a linear dependency against the inlet velocity condition. This indicated that there was a unique vortex residence time to excite the unstable acoustic mode of the system, and that the unstable equivalence ratios at each velocity condition were determined so that the flame structure (i.e. the RI map) satisfies the residence time requirement.

^a Institute of Aeronautical Technology, Japan Aerospace Exploration Agency, 7-44-1 Jindaiji-Higashi, Chofu, Tokyo 182-8522, Japan

^b Graduate School of Fundamental Science and Engineering, Waseda University, 3-4-1, Okubo, Shinjuku, Tokyo 169-8555, Japan

^c School of Fundamental Science and Engineering, Waseda University, 3-4-1, Okubo, Shinjuku, Tokyo 169-8555, Japan

Thermoacoustic instabilities in combustors: modelling and feedback control of nonlinear oscillations

J. Li^a and A. S. Morgans^a

Lean premixed combustion chambers are susceptible to combustion instabilities arising from the coupling between the heat release rate perturbations and the acoustic disturbances. These instabilities are not desirable and knowledge of this complex mechanism is necessary in the development of control strategies. Active feedback control can be used to interrupt the coupling between the acoustic waves and unsteady heat release and prevent or suppress instability. The design of most types of controller requires prior knowledge of how the combustor responds to actuation - the "open loop transfer function" (OLTF). This includes the flame response to oncoming flow disturbances, which becomes non-linear at larger amplitudes. This may cause the dominant unstable frequency to change, which in turn alters the OLTF and makes the design of controller more complicated. A new analytical form of a flame describing function model is proposed for modelling the dynamic response of conical-shaped flames. It assumes weak non-linearity – the flame response is primarily at the forcing frequency. This model accounts for the non-linearities of the heat release rate amplitude gain and phase lag change relative to the acoustic pressure. It is combined with the analytical acoustic network model within the combustor to analyse the thermoacoustic stabilities in the frequency domain. This reduced order model is then converted into the time domain to reproduce an important range of features of non-linear behaviour such as single tone instability, "triggering", "mode switching" and frequency shift during the limit cycle.

The v-gap metric is used to quantify the deviation of the set of OLTFs for different disturbance levels from the selected transfer function for the controller design. This provides us a bound on the minimum required "robustness stability margin" for an H_∞ loop shaping controller. Such a controller is synthesized, and it is confirmed that as long as the v-gap is smaller than the stability margin, the robust controller is guaranteed to stabilize the combustor for all possible flame responses.

^a Department of Aeronautics, Imperial College London, London, UK

¹ Candel, S., *Proc. Combust. Inst.* **29**, 1 (2002).

² Dowling, A. P. and Morgans, A. S., *Annu. Rev. Fluid Mech.* **37**, 151 (2005).

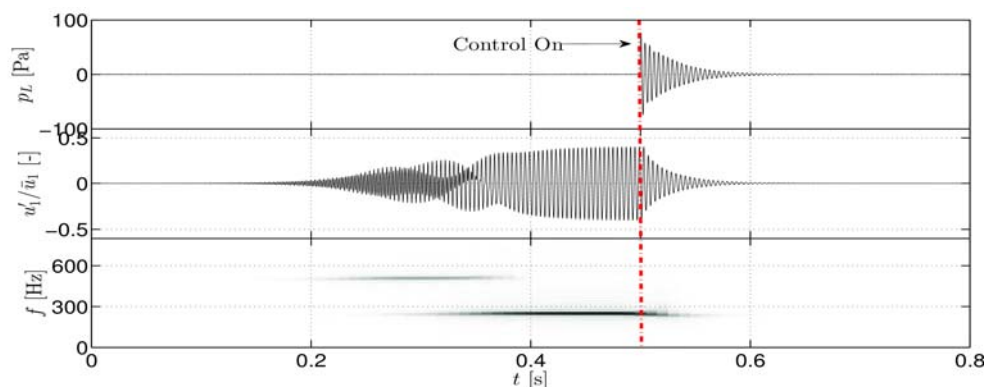


Figure 1: Evolution of the signals with time for one control test. (1). The external acoustic feedback control signal; (2). Velocity perturbations ratio before the flame; (3). Time-frequency analysis of velocity perturbations ratio. The resolution: [0.01 s, 10 Hz]. With the growth of velocity perturbation amplitude, the dominant oscillations are switched from the higher frequency of approx. 490 Hz to the lower frequency of approx. 240 Hz. When the controller is switched on, the velocity perturbations decrease rapidly to weak white noise in 0.1 seconds.

Suppression of self-excited oscillations in a coupled thermoacoustic system

T. Biwa^a, S. Tozuka^b

Thermoacoustic oscillations, unstable acoustic oscillations of a gas column maintained by heat, are also referred to as thermo-acoustic oscillations, seemingly depending on whether one wants to create intense oscillations as high as possible, or one wants to suppress them. The former aims at producing a new kind of heat engines by using sound waves in place of mechanical pistons, and the latter tries to achieve safety operation of combustion systems and cryogenics systems. Although their goals are different, these research groups have a common ancestor, Lord Rayleigh. He gave a detailed explanation on thermoacoustic oscillations of Sondhauss tube, Rijke tube, and singing flame together with various topics on acoustics and vibrations. The phenomenon of *oscillation death* is one of them. He introduced as “*when two organ-pipes of the same pitch stand side by side, ... the pipes may almost reduce one another to silence.*” In this study, we experimentally demonstrate oscillation death caused by coupling of two thermoacoustic oscillators and propose to use it as a new suppression method.

The test thermoacoustic oscillator was built by using an air-filled cylindrical tube of 720 mm in length and 24 mm in internal diameter. A differentially heated stack was inserted into the tube in order to introduce thermoacoustic instability. Acoustic oscillations of the fundamental mode were observed to start in the test oscillator when the temperature difference along the stack exceeded 270 K. We prepared two thermoacoustic oscillators and connected them by a needle valve placed one end of each oscillator. The experimental parameters were coupling strength represented by valve opening, and a frequency detuning controlled by resonator length. Acoustic pressures at the antinode were measured in two oscillators by using small pressure transducers and a spectrum analyzer. When the valve was closed, steady oscillation states were achieved. But by opening the valve, three different states were observed in the coupled thermoacoustic system; phase drift, synchronization, and oscillation death. We present the bifurcation diagram on the plane of valve opening and frequency detuning, to locate oscillation death region.

^a Dep. Mechanical Engineering, Tohoku university, 6-6-1 Aramaki, Aoba-ku, Sendai, 980-8579, JAPAN

^b Dep. Mechanical Engineering, Tohoku university, 6-6-1 Aramaki, Aoba-ku, Sendai, 980-8579, JAPAN

Coupled incompressible and acoustic solution approach to predict thermoacoustic instability in turbulent combustion systems

A. Kannan,^a C. Balaji,^b R. Sampath,^a and S. R. Chakravarthy^a

Combustion instability is a problem that plagues gas turbine combustors, afterburners, ramjet combustors, liquid rocket combustion chambers, and solid rocket motors as well. The feedback loop between the combustion and acoustic processes leads to growth of oscillations in these combustors. As opposed to aeroacoustic or combustion noise, wherein the usually turbulent flow or combustion generates sound over a broad range of frequencies without appreciable feedback from the acoustics to the flow/combustion process, the crucial aspect of combustion instability is the nature of acoustic feedback on the flame.

In the present work, the compressible Navier-Stokes equations are subjected to the simultaneous multi-time and length scales and the classic low Mach number expansion. The resultant decomposition is that the flow/combustion is governed to lowest order by the incompressible Navier-Stokes equations, subject to a first order compressibility correction by the acoustic equations. The two sets of equations talk to each other through source terms, the flow/combustion dilatation being the source of acoustic energy, and the acoustic Reynolds stress (ARS) being the source of the flow momentum.

The ARS is how the acoustic feeds back to the flame. It is well known that coherent structures exist in the flow past typical flame holding devices such as a sudden expansion or bluff-body under cold conditions such as large-scale vortex roll-up, Karman vortex street, etc. However, in the presence of a flame without acoustic feedback, these flow structures generally vanish due to dilatation due to thermal expansion at the flame, and are replaced by small-scale Kelvin-Helmholtz instability in stretched shear layers. The baroclinic torque due to density gradient from thermal expansion usually counteracts the naturally occurring coherent vortex roll-up. However, when the acoustic feedback is present, the ARS leads to an additional torque that regenerates the coherent structures. Modulation of the heat release by these coherent structures at the acoustic time scale leads to a coupling of the flow/combustion and acoustic processes and instability.

Results are shown by means of large eddy simulation (LES) of turbulent flow in a backward-facing step combustor coupled with acoustics in the duct. The role of the ARS as a source of coherent structures in the combustion zone is highlighted. Good comparison of the numerical results with experimental data is observed.

Further extensions of the above methodology include implementation in the URANS framework for the flow simulations, which involves identification and modelling of turbulence-acoustics interaction terms of scales smaller than the acoustic time scale, and linear perturbation analysis in the time domain to examine the transient growth of the coupled thermo-acoustic system due to its non-normality.

^a National Centre for Combustion Research & Development, and Department of Aerospace Engineering, Indian Institute of Technology Madras, Chennai 600036 India.

^b Metacomp Technologies, Chennai 600020 India.

Large-scale coherent motions and their control in a fuel injector

O. Tammisola and M. P. Juniper^a

Large-scale hydrodynamic oscillations in gas turbine fuel injectors help to mix the fuel and air but can also contribute to thermoacoustic instability. Small changes to some parts of a fuel injector greatly affect the frequency and amplitude of these hydrodynamic oscillations, and parametric studies at high Reynolds numbers are very time-consuming.

In this work, we first characterize the large-scale oscillations in a gas turbine's single stream radial swirler, which has been extensively studied experimentally ([1] with references). This is done by extracting nonlinear Koopman modes from DNS (fig.1d), and by computing the linear global modes (fig.1a&b). Then we identify the most influential regions for control by adjoint-based sensitivity analysis, which are found to be inside the nozzle, underlying the importance of nozzle design. We compare the dynamics, coherent structures, and control effects to observations from previous numerical and experimental studies[1,2] and we also compare the global modes around the DNS mean flow and the steady solutions to Navier-Stokes equations.

All the analyses - previous experiments, LES (fig. 1c), uRANS, local stability, and the DNS and global stability in this work show that a spiralling motion develops around the central recirculation zone. This develops into a precessing vortex core.

The adjoint-based sensitivity analysis reveals that the frequency and growth rate of the oscillation is dictated by conditions at the upstream end of the central recirculation zone (the wavemaker region). It reveals that the centre of the injector is very influential and explains why the oscillation disappears when a jet is injected through the centre of the injector, as reported in previous experiments and computations. Furthermore, the dynamics and the wavemaker of the spiralling motion are seen to be qualitatively unchanged from low Reynolds numbers (fig. 1a&b) to high Reynolds numbers (fig.1c&d).

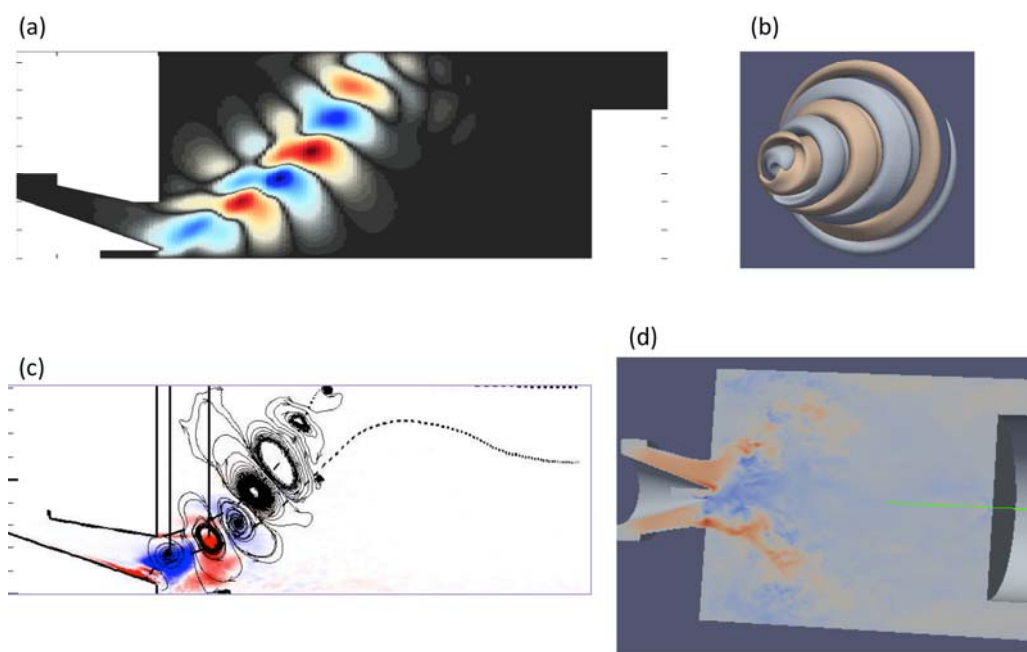


Figure 1: (a) Spiralling global mode, $Re=68$, streamwise velocity, azimuthal cross-section. (b) Same as (a), 3D view. (c) Coherent structure from LES, $Re=1250$ (Dunham et al. 2008), (d) DNS of the turbulent flow, snapshot, at $Re=1250$.

^a Dept. of Engineering, University of Cambridge, CB21PZ, Cambridge, UK

¹ Dunham, *Doctoral thesis, Loughborough U.*, (2011).

² Dunham et al., *Proceedings of ASME Turbo Expo*, (2008)

Passive Control of Thermoacoustic Instability in a Rijke Tube: Experiments vs. Adjoint-based Predictions

N. H. E. Paul^a, L. K. B. Li^a, L. Magri^a and M. P. Juniper^a

We experimentally determine how the stability of a thermoacoustic system changes in response to a control device. The setup consists of a vertical Rijke tube, with the primary heater positioned at quarter length from the inlet (bottom). The primary heater is an electrically heated wire mesh. The control device is an identical electrical (secondary) heater which and, when not supplied with power, acts as a passive drag-exerting element. First, we study the influence that drag has on the thermoacoustic stability. To do so, we change the control device position along the tube and measure, for each location, the critical power supplied to the primary heater to make the thermoacoustic system unstable (forward Hopf bifurcation point). The more the system is stabilized by drag, the higher the critical power needed to reach the Hopf bifurcation. The critical powers are shown in Figure 1 (a), normalised by the critical power at the tube mid-length. Secondly, we determine how the transient growth/decay rates and frequency shift are related to the secondary heater power and its position along the tube. This experimental data can be directly compared with linear-analysis predictions¹ (Figure 1 (b)). We find that the experimental results compare favourably with the theoretical predictions of Magri and Juniper¹, which were obtained with the aid of adjoint equations. This work provides the first experimental validation of thermoacoustic adjoint-based linear analysis. Potential discrepancies between experimental evidence and linear theory are discussed by a physics-based analysis of the modelling assumptions.

^a Dept. of Engineering, University of Cambridge, Trumpington Street, Cambridge, CB2 1PZ, UK

¹ Magri and Juniper, *J. Fluid Mech.* **719**, 183 (2013)

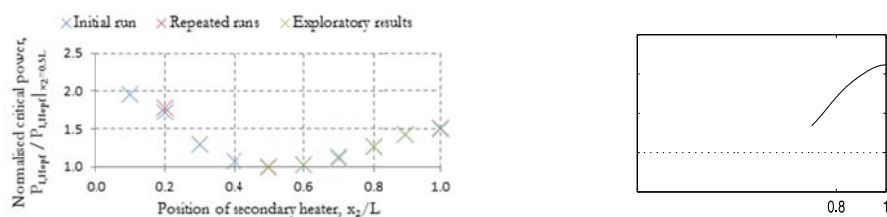


Figure 1: (a) Normalised critical powers obtained experimentally. These points indicate that positioning the secondary heater towards the ends has the most controlling effect.

(b) Sensitivity of the linear growth rate to a drag-exerting feedback mechanism, theoretically predicted by adjoint analysis.

THURSDAY

18th September 2014

Magneto

A dynamic interpretation of MHD shear instabilities in terms of interacting waves

E. Heifetz^a, J. Mak^a

The wave interaction interpretation for shear instabilities is extended here to the magnetohydrodynamic setting, to provide a dynamical rationalisation for the stabilising and destabilising of shear flow instabilities by the presence of a background magnetic field. The interpretation relies on local vorticity anomalies inducing a non-local velocity field, i.e., an action-at-a-distance mechanism, with the Counter-propagating Rossby Waves mechanism, well-known in the geophysical fluid dynamics community, being a particular case under this framework. It is shown here that wave displacement leads to a change in the magnetic field configuration that in turn generates vorticity anomalies, leading to individual wave propagation. Further, when multiple waves are present and can phase-lock in a configuration that allows for mutual amplification, this leads to instability; the stabilisation and destabilisation of the background magnetic field profile then rests upon whether the waves can phase-lock and interact. Via a Green's function approach, the eigenstructure and dispersion relations of the wave modes supported in this system are calculated, and we give two examples for which wave interaction leads to (i) the destabilisation of a hydrodynamically stable flow, and (ii) the stabilisation of a hydrodynamically unstable flow.

^a Dep. Geophysics and Planetary Sciences, Tel-Aviv University, Israel

Self-sustaining magneto-hydrodynamic structures in acoustically unstable media with heat release

N. E. Molevich^{ab}, D. I. Zavershinski^{a,b}, I. P. Zavershinski^b, and D. Ryashikov^{ab}

The evolution of magneto-hydrodynamic waves of small but finite amplitude in magnetohydrodynamic (MHD) medium with thermal instability is investigated. The MHD medium is assumed to be initially homogeneous in thermal equilibrium and with magnetic field frozen in. Thermal instability in medium is defined by heating and cooling rate density and temperature dependences. The dispersion equations for magnetoacoustic waves and Alfvén waves are obtained analytically. The amplification of magnetoacoustical waves and damping condition is defined by solving the dispersion relation. An evolutionary nonlinear equation for fast and slow magnetoacoustic waves taking into account the nonlinear saturation of the magnetoacoustical instability is derived. There is a correlation between this nonlinear magnetoacoustic equation, the nonlinear acoustical equation of nonequilibrium medium with exponential relaxation law [1] and the non-linear acoustical equation of medium with thermal instability without frozen-in magnetic field[2,3]. The coefficients of the magnetoacoustic equation have somewhat different form and nature.

The shape and parameters of the magnetoacoustic pulse that is an automodel solution of this equation under conditions of magnetoacoustic instability is determined (Fig.1). The numerical simulation of the nonlinear magnetoacoustic equation and of the full system of magnetohydrodynamic equations in one dimensional form shows the disintegration of any initial weak perturbation of compression into a sequence of these self-sustained magnetoacoustic pulses in the magneto-acoustically unstable media (Fig.2).

This work was financially supported by The Ministry of education and science of Russia, under project 608 and by RFBR under grants 13-01-97001, 14-02-97030

^a P.N. Lebedev Physical Institute of RAS, Samara Branch, 221 Novo-Sadovaya Str., Samara, Russia

^b Samara State Aerospace University, 34 Moskovskoe sh., Samara, Russia

¹ Makaryan and Molevich, *Plasma Sources Sci. Technol.* **16**, 124 (2007).

² Molevich et al., *Astrophysics and Space Science* **334**, 35 (2011)

³ Molevich et al, Book of Abstracts of 9th European Fluid Mechanics Conference, Rome, September 9-13, 2012. 0133_GD1

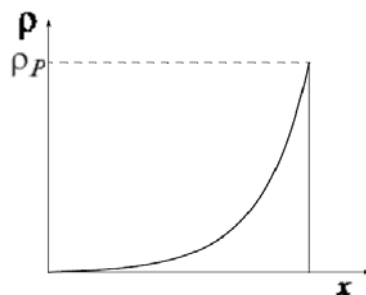


Figure1: Magnetoacoustic self-sustaining pulse.

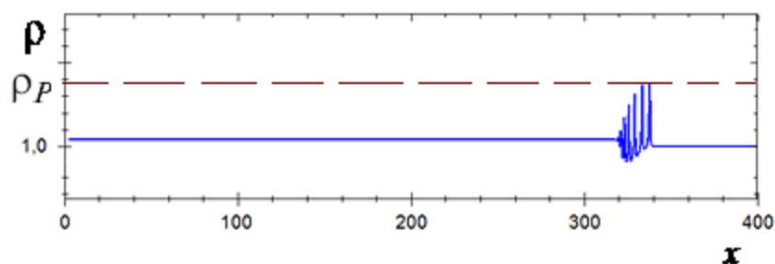


Figure 2: Perturbation of density. Disintegration of the initial step-wise perturbation into sequence of pulses with amplitude predicted analytically.

Viscous and joule dissipation ratio in isotropic MHD turbulence

R. Stepanov and F. Plunian

Institute of Continuous Media Mechanics, Perm, Russia
 Laboratoire de Géophysique Interne et Tectonophysique, CNRS/INSU, Université Joseph
 Fourier, Grenoble, France

The magnetohydrodynamics turbulence is often object for fundamental and applied studies in the electroconductive fluid mechanics. In spite of intensive researches in this field, the small-scale dynamo process at large Reynolds numbers is still difficult to investigate experimentally or numerically. Wide range magnetic Prandtl number Pm values implies strong differences between possible generation mechanisms. The kinetic energy spectrum available for generating magnetic energy depends on value of Pm . If $Pm \geq 1$ then the resistive scale is smaller than the viscous scale and all velocity scales are available for generating some magnetic field. On the other hand, for $Pm < 1$, only the velocity scales larger than the resistive scale are available for the magnetic field generation. In that case, the velocity scales smaller than the resistive stay passive in the generation process. We focus on statistical property of energy dissipation rates (its scaling and ratio) as a proper diagnostic of the kinetic and magnetic field nonlinear interaction in wide range of scales. MHD shell model has been used for numerical simulations of the isotropic MHD turbulence at extremely large Reynolds numbers. We explain the difference in dissipation ratio dependences on Pm that were suggested in [1] and [2]. The effect of nonlocal interactions in scale space is discussed.

[1] Brandenburg, A.: 2009, Large-scale dynamos at low magnetic Prandtl numbers, *Astrophys. J.* **697**, 1206-1213

[2] Plunian F., Stepanov R. 2010, Cascades and dissipation ratio in rotating magnetohydrodynamic turbulence at low magnetic Prandtl number, *Physical Review E*, **82**, P.046311

Emergence of electrically active Shercliff and Hartmann layers due to surface rheology.

J. Delacroix^a and L. Davoust^b

As a first step towards two-phase magnetohydrodynamics (MHD), this work addresses the original coupling between surface rheology (the one of an oxidizing liquid metal surface, for instance), ruled by the shear and dilatational Boussinesq numbers, Bo_{η_s} and Bo_{κ_s} , and a supporting annular end-driven MHD flow in the general layout of the very classical annular deep-channel viscometer [1,2]. In this configuration, an axisymmetric annular flow is supplied from a rotating end wall, with no-slip conditions along stationary vertical sidewalls and a generalized boundary condition along the upper liquid surface opposite the rotating floor.

First, an analytical modelling is proposed, based on the assumptions that $N \gg 1$, $Ha \gg 1$, where N is the interaction parameter and Ha is the Hartmann number. This allows us to neglect inertia and to disregard the swirling component of the flow, hence, the surface dilatational viscosity, κ_s . By using a matched asymptotic expansion based on a small ratio, $1/Ha$, the surface velocity is shown to behave as a coupling variable between supporting MHD core flow and the jump momentum balance (JMB) along the liquid surface. The Boussinesq-Scriven constitutive law is used to model the dependence of the surface stress on the surface strain in the JMB. Doing this, the shear surface viscosity, η_s , is introduced. By solving the JMB from a dedicated Green function, the whole flow is analytically calculated. A modified shear Boussinesq number is introduced as a new non-dimensional number which balances the viscous surface shear with the Lorentz force. It is shown to drive the electrical activation of the Hartmann layers, hence modifying the MHD flow topology. When it is much smaller than unity, classical electromagnetic blocking and MHD tendency towards two-dimensionality are recovered: a rigid body motion is observed, and current densities are confined within Shercliff layers along sidewalls. Conversely, when it is larger than unity, an unexpected “motionless” core is found, and both parallel and Hartmann layers are found electrically active.

When the angular velocity grows up or when the applied magnetic field decreases, the previous balance between viscous and electromagnetic forces does no longer hold, and a swirling flow arises. This affects the bulk and the surface dynamics as well since the radial component of JMB is solicited, bringing into play the dilatational surface viscosity. Consequently, a numerical approach is developed to describe the flow topology when inertial, electromagnetic and viscous effects are all together in competition. The previously mentioned analytical work is then used as asymptotic benchmark of the numerical simulation at high Ha number.

Finally, the evolution laws given in this study are hoped to guide future development of an original experimental protocol, which would make it possible to accurately determine the shear and dilatational surface viscosities of a liquid metal with respect to the quality of the ambient atmosphere.

^a University of Grenoble, SIMAP, 38402 Saint Martin d'Hères, France

^b Grenoble-INP, SIMAP, 38402 Saint Martin d'Hères, France

[1] Mannheimer, R.S., Schetcher J. (1970) An improved apparatus and analysis for surface rheological measurements, *J. Colloid Interface Sci.*, 32:195–211

[2] Davoust, L. *et al.* (2008) Flow-induced melting of condensed domains within a dispersed Langmuir film. *Phys. Fluids*, 20, 082105–82110

The 2D/3D dynamics of wall-bounded low-Rm magnetohydrodynamic (MHD) turbulence

Nathaniel Baker^{1,2}, Laurent Davoust^c, Alban Potherat^a

One of the main features of low-Rm MHD flows is the action of the Lorentz force, which tends to damp physical quantities along the magnetic field. This process can be interpreted as a diffusion of momentum along the magnetic field¹, eventually bringing the flow towards a two-dimensional state. The purpose of this study is to understand the effects of walls on the dynamics of electrically-driven low-Rm MHD turbulence, and their impact on the structure of the flow. The work presented here focuses on the analysis of the statistical quantities of turbulence such as two-point velocity correlations and higher order moments.

This study is based on an experimental rig² consisting of a (10 cm)³ box filled with Galinstan (conductivity $\sigma = 3.4 \times 10^6$ S/m, density $\rho = 6400$ kg/m³, viscosity $\nu = 4 \times 10^{-7}$ m²/s) placed inside the 45 cm bore of a superconducting magnet. The flow is driven by injecting electric current through the bottom wall via an array of 10 x 10 injection electrodes, alternately connected to the positive and negative poles of a DC current generator. The features of the resulting flow are diagnosed using two complimentary measuring techniques, whose probes are embedded flush within the cube's walls: electro-potential velocimetry, and pulsed ultrasound Doppler velocimetry.

First, we focus on the two-point longitudinal correlations perpendicular to the magnetic field, which were evaluated at five different positions across the box. The experimental parameters were set such that the Hartmann number and the Reynolds number were of order $Ha \sim 7300$ and $Re \sim 25000$, respectively. The signals show that the longitudinal velocity fluctuations perpendicular to the magnetic field become more and more correlated as they are measured further away from where the forcing takes place. This behavior could be evidence of two-dimensional dynamics far away from the forcing.

Second, we investigate the longitudinal two point correlations along the magnetic field in order to quantify the anisotropic effect of the Lorentz force on the flow structure. Furthermore, higher order moments such as the skewness and flatness on the one hand, and probability density functions for the velocity increments on the other hand, give us a better understanding of the different flow regimes encountered in the experiment.

¹ AMRC, Faculty of Engineering and Computing, Coventry University, Coventry CV1 5FB, UK

² CNRS CRETA/LNCMI, 38042 Grenoble, France

^c Grenoble-INP SIMAP, 38402 Saint Martin d'Heres, France

¹ J. Sommeria and R. Moreau. *Journal of Fluid Mechanics*, **118**:507-518 (1982).

² R. Klein and A. Potherat. *Physical review letters*, **104**(3) (2010).

Shape Oscillation of a Sessile Drop Under the Effect of Amplitude-Modulated High Frequency Magnetic Field

Zuosheng Lei^a, Jiahong Guo^b, Lijie Zhang^a, Zhongming Ren^a, Yves Fautrelle^c & Jacqueline Etay^c

The shape oscillation behavior of a sessile mercury drop under the effect of high frequency amplitude-modulated magnetic field (AMMF) is investigated experimentally. It is a new method to excite shape oscillation of a liquid metal sessile drop.

Generated by a solenoid inductor fed by a specially designed alternating electric current, the high frequency AMMF in the inductor is as follows:

$$B(t) = B_0[1 + \eta \sin(2\pi f_m t)] \sin(2\pi f_c) \quad (1)$$

where B_0 is the peak value of the magnetic flux density and η is the modulation index which changes along with the peak value of B_0 . f_m and f_c are the frequency of the modulation wave and the carrier wave respectively. In this experiment f_m ranges from 1 to 10 Hz and f_c equals to 20 kHz.

Due to high frequency of the carrier wave, the magnetic force acts on the sessile drop like a kind of surface force on the periphery which varies periodically in a frequency the same as that of the modulation wave. It is this kind of varying surface force that triggers the shape oscillation of the droplet. It is a different mechanism from the case in the presence of a low-frequency magnetic field which could be seen in literatures before.

The surface contour of the sessile drop is observed by a digital camera. The axisymmetric shape oscillation (mode $n=1$) of the droplet can be observed before the edge deformations with azimuthal wave numbers (modes $n=2, 3, 4, 5, 6$, $n=3, 5$ in Fig.1) are excited. At a given modulation frequency f_m , as B_0 increases the axisymmetric shape oscillation of the droplet appears with the same frequency as f_m . Further increases B_0 and reaches a given threshold, the edge deformations with azimuthal wave numbers will be excited. It turns out that the shape oscillation frequency of the drop equals to that of the modulation wave of the high frequency AMMF.

A stability diagram of the shape oscillation of the drop is obtained by analysis of the experimental data shown in Fig.2. From the analysis results we can find that it is similar with the stability diagram of the Mathieu-type equation the so-called parametric instability. An interesting phenomenon emerges while comparing the corresponding frequency range of different oscillation modes (mode 3, 4, 5, 6). It is found that the same oscillation mode is excited in different frequency range, and the corresponding frequencies have a ratio of 2. This is a typical character of Mathieu-type parametric instability of a liquid drop.

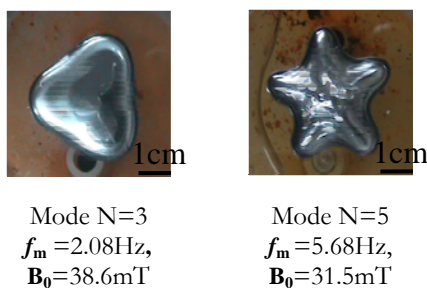


Fig.1 Free-surface patterns for various high frequency AMMF

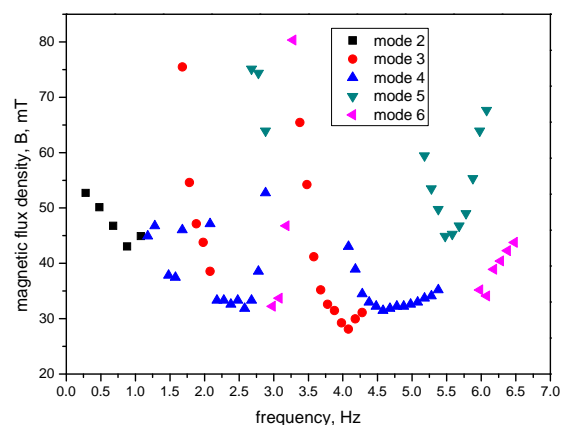


Fig.2 Stability boundary of a mercury sessile drop with 18 mm radius for various modulation frequencies of the high frequency AMMF

^a Shanghai Key Laboratory of Modern Metallurgy & Material Processing, Shanghai University, 200072, Shanghai, China

^b Shanghai Institute of Applied Mathematics and Mechanics, Shanghai University, 20072, Shanghai, China

^c SIMAP-EPM-Madylam/CNRS, ENSHMG, BP 95, 38402 St. Martin d'Heres Cedex, France

Subcritical turbulence in 2D MHD plane shear flows - self-sustenance via interplay of linear transient growth and nonlinear transverse cascade

G. R. Mamatsashvili^a, G. Z. Gogichaishvili^b,
G. D. Chagelishvili^c and W. Horton^b

We found and investigated via numerical simulations¹ self-sustained two-dimensional turbulence in a magnetohydrodynamic flow with maximally simple configuration: plane, noninflectional (with constant shear of velocity) and threaded by a parallel uniform background magnetic field. This flow is spectrally stable, so the turbulence is subcritical by nature and hence it can be energetically supported just by transient growth mechanism due to shear flow nonnormality. This mechanism appears to be essentially anisotropic in spectral (wavenumber) plane and operates mainly for spatial Fourier harmonics with streamwise wavenumbers less than a ratio of flow shear to the Alfvén speed, (i.e., the Alfvén frequency is smaller than the shear rate). To understand the sustaining mechanism of the turbulence, we Fourier transformed basic MHD equations and derived evolution equations for the perturbed kinetic and magnetic spectral energies in wavenumber plane. In these spectral equations, using the simulation results, we calculated individual terms, which are divided into two types -- terms of linear and nonlinear origin. The terms of linear origin -- the Maxwell and Reynolds stresses -- are responsible for energy exchange between the turbulence and the mean flow through transient amplification of perturbation harmonics due to shear. However, only the positive Maxwell stress appears to be a dominant (magnetic) energy injector for the turbulence; it is much larger than the negative Reynolds stress, which does not contribute to turbulent energy gain. The nonlinear terms, which do not directly draw the mean flow energy, act to redistribute this energy in spectral plane, continually repopulating perturbation harmonics that can undergo transient growth.

Thus, we demonstrated that in spectrally stable shear flows, the subcritical MHD turbulent state is sustained by the interplay of linear and nonlinear processes -- the first supplies energy for turbulence via shear-induced transient growth mechanism of magnetic field perturbations and the second plays an important role of providing a positive feedback that makes this transient growth process recur over long times and compensate viscous and resistive dissipation due to viscosity. This picture is consistent with the well-known bypass scenario of subcritical turbulence in spectrally stable shear flows. Our study, being concerned with a new type of the energy-injecting process for turbulence -- the transient growth, represents an alternative to the main trends of MHD turbulence research. The essence of the analyzed nonlinear MHD processes appears a transverse redistribution of kinetic and magnetic spectral energies in wavenumber plane and differs fundamentally from the existing concepts of (anisotropic direct and inverse) cascade processes in MHD shear flows.

^a Dep. of Physics, Faculty of Exact and Natural Sciences, Tbilisi State University, Tbilisi 0179, Georgia, E-mail: george.mamatsashvili@tsu.ge

^b Department of Physics, the University of Texas at Austin, Austin, Texas 78712, USA

^c Abastumani Astrophysical Observatory, Ilia State University, Tbilisi 0160, Georgia

¹ Mamatsashvili et al., *Phys. Rev. E* (2014), *in press*

Spectral Direct Numerical Simulations of low Rm MHD channel flows based on the least dissipative modes

Kacper Kornet¹ and Alban Potherat^a

We put forward a new type of spectral method for the direct numerical simulation of flows where anisotropy or very fine boundary layers are present. The main idea is to take advantage of the fact that such structures are dissipative and that their presence should reduce the number of degrees of freedom of the flow, when paradoxically, their fine resolution incurs extra computational cost in current methods. We overcome this problem by describing the flow using a basis of eigenvectors of the linear part of Navier Stokes equation. As the computational cost of the resulting method does not depend on the intensity of the magnetic field, it allows us to significantly reduce the computational cost incurred by traditional methods in the regime of high magnetic fields.

We applied the new method to calculate the evolution of freely decaying MHD turbulence between walls. First we validate our code by calculating the cases characterised by low magnetic field and comparing the results against ones obtained with finite volume code. The results showed very good agreement between the two codes both in terms of global quantities like energy dissipation rates and in terms of the resulting energy spectra. We also demonstrated the potential of the new scheme to efficiently resolve flows in the presence of high magnetic fields with a limited number of modes, as predicted by the theoretical considerations.

Next we use the potential of the new method to study the behaviour of MHD turbulence in a set of calculations with higher values of the magnetic field. We investigate the properties of the flow in this regime. We analyse the evolution of kinetic energies and integral lengthscales in directions perpendicular and parallel to the magnetic field and provide the interpretation of their behaviour. Comparing our results with the cases calculated in a 3D periodic domain enables us to quantify the influence of the channel walls on the character of a freely decaying MHD turbulence for the first time.

¹ AMRC, Coventry University, Priory Street, Coventry CV1 5FB, UK

A simple model for turbulent velocity profiles at side walls of MHD tube flows

T. Boeck^a, D. Krasnov^a

We propose a simple extension of Prandtl's classical mixing-length model for conducting channel flow in order to describe the damping effect of a uniform spanwise magnetic field.¹ The mixing length is assumed to be constrained by an additional length scale called the Joule damping length. It is based on the friction velocity and the Joule damping time. The limitation of mixing length is implemented by using the harmonic mean of the wall distance and the Joule damping length. Near the wall, the model captures the combined linear-logarithmic dependence of velocity on the wall distance observed in direct numerical simulations. It also provides a satisfactory prediction for the overall velocity distribution for different Reynolds and Hartmann numbers. The velocity profile of turbulent side layers in magnetohydrodynamic duct flows in a strong field can also be computed with the help of the model provided that the Hartmann layers are already laminar.

With a simple additional assumption, the model can also be applied for the prediction of relaminarization thresholds in magnetohydrodynamic channel and duct flows. Using velocity profiles from simulations with a streamwise magnetic field, we also speculate how one might describe their modification by the magnetic damping in a simple manner.

^a Insitute of Thermodynamics and Fluid Mechanics, TU Ilmenau, PO Box 100565, 98684 Ilmenau, Germany

¹ Boeck and Krasnov, *Phys. Fluids* **26**, 025106 (2014)

Turbulence Simulations

II & III

Turbulence dynamics in the separation bubble on a lower curved wall channel

J.-P. Mollicone^a, F. Battista^a and C.M. Casciola^{ab}

Boundary layer separation consists of fluid flow around bodies becoming detached, which causes the fluid closest to the object's surface to flow in reverse or different directions, most often giving rise to turbulent flow. This affects, for example, the performance of transport vehicles, by increasing the drag force, the mixing of air and fuel in engines and vibrations in structures due to vortex shedding. Interestingly, flow separation may be significant also for hemodynamics, where the bump at the wall is induced by the local degeneration of the arterial wall (atherosclerosis). Despite its importance, this classic subject is still incompletely explored in turbulent conditions, and is especially challenging for numerical simulations, given the complexity of the involved geometries.

The aim here is to study boundary layer separation using the relatively simple geometry of a channel with a lower curved wall, to address through DNS (Direct Numerical Simulation) basic issues concerning turbulence production and self-sustainment in the separation bubble. Indeed, the basic issue of turbulence sustainment, although well understood for canonical wall bounded flows, is still not exhaustively investigated for even mildly complex geometries able to induce separation. To this purpose the data obtained from a direct numerical simulation are used to evaluate the relevant terms of the turbulent kinetic energy (TKE) budget,

$$\frac{Dk}{Dt} = -\frac{1}{\rho_0} \frac{\partial \langle u'_i p' \rangle}{\partial x_i} - \frac{\partial \langle k u'_i \rangle}{\partial x_i} + \nu \frac{\partial^2 k}{\partial x_j^2} - \langle u'_i u'_j \rangle \frac{\partial \langle u_i \rangle}{\partial x_j} - \nu \left\langle \left(\frac{\partial u'_i}{\partial x_j} \right)^2 \right\rangle$$

where $k = \langle u'^2 \rangle / 2$ is the Turbulent Kinetic Energy density (TKE), u' is the velocity fluctuation with respect to the mean velocity, t is time, ρ is the density of the fluid, x is the position and ν is the kinematic viscosity, to understand where turbulence in the separation bubble is generated and how it diffuses to the outer flow.

The simulations are carried out using Nek5000¹, which is based on the spectral element method (SEM), see e.g. A. T. Patera² where SEM is quoted as a "...method that combines the generality of the finite element method with the accuracy of spectral techniques...". Figure 1 shows a contour plot of vorticity magnitude of our preliminary simulation of a channel with dimensions $(L_x \times L_y \times L_z) = (13 \times 2 \times \pi) \times h$ where L_i is the length in the i^{th} direction and h is half the channel height³. Flow is from left (inlet) to right (outflow) with wall boundary conditions at the top and bottom wall and periodic boundary conditions in the span-wise direction. The ongoing simulations to be discussed are conceived to investigate the correlation between separation phenomena and localization of TKE production, transport and dissipation at higher Reynolds numbers, thus providing more insight on the detailed dynamics of this interesting flow configuration.

^a Dipartimento di Ingegneria Meccanica e Aerospaziale, Università di Roma "La Sapienza". Via Eudossiana 18, 00184 Roma, Italy.

^b Center for Life Nano Science@Sapienza, Istituto Italiano di Tecnologia, Via Regina Elena 291, 00161, Roma, Italy.

¹ Fischer, P., et al. "NEK5000—open source spectral element CFD solver." Argonne National Laboratory, Mathematics and Computer Science Division, Argonne, IL, see <https://nek5000.mcs.anl.gov/index.php/MainPage> (2008).

² A. T. Patera. A spectral element method for fluid dynamics. Journal of Computational Physics (1984): 54:468—488

³ Marquillie et al. Direct numerical simulation of a separated channel flow with a smooth profile, Journal of Turbulence (2008), 9, N1

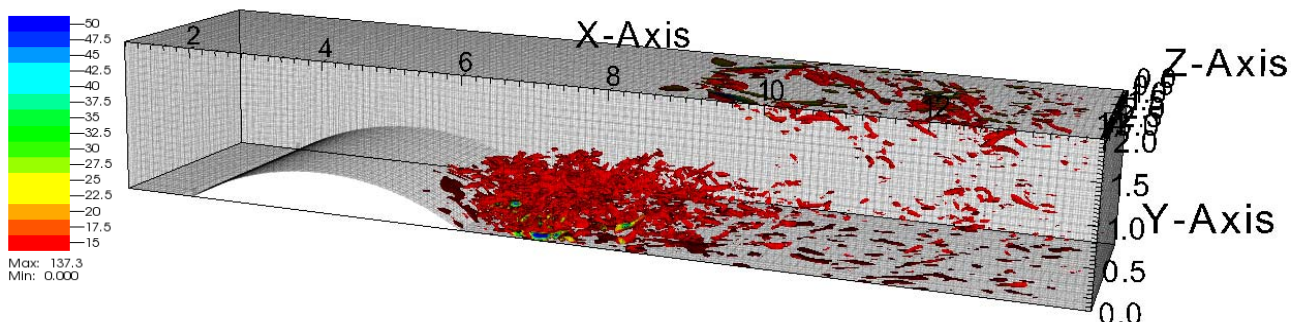


Figure 1 - Contour plot of vorticity magnitude in a 3D channel with lower curved wall (Preliminary simulation)

LES and log-law for high-order moments in turbulent boundary layers

Richard J.A.M. Stevens^{a,b}, Michael Wilczek^a, Charles Meneveau^a

The logarithmic law for the mean velocity in turbulent boundary layers has long provided a valuable and robust reference for comparison with theories, models, and large-eddy simulations (LES) of wall-bounded turbulence.¹ Recent analysis of high-Reynolds number experimental boundary layer data² has revealed logarithmic laws for the higher-order moments of the streamwise velocity fluctuations u' . Such experimental observations can be used as good reference point to validate LES models and see whether they can also accurately reproduce the logarithmic dependence for the higher-order moments. In this study we perform LES (see figure 1 left) of very high Reynolds number wall-modeled channel flow and focus on profiles of variance and higher-order moments of streamwise velocity fluctuations. In agreement with the experimental data we observe an approximately logarithmic law for the variance in the LES, with a “Townsend-Perry” constant of $A_1 \approx 1.25$, see figure 1 right. The LES also yields approximate logarithmic laws for the higher-order moments of the streamwise velocity. Good agreement is found between A_p , the generalized “Townsend-Perry” constants for moments of order $2p$, from experiments and simulations. The near-wall behavior of the variance, the ranges of validity of the logarithmic law and in particular possible dependencies on characteristic length-scales such as the domain size, the roughness scale z_0 and the LES grid scale Δ are examined. We also present LES results on moments of spanwise and wall-normal fluctuations of velocity.

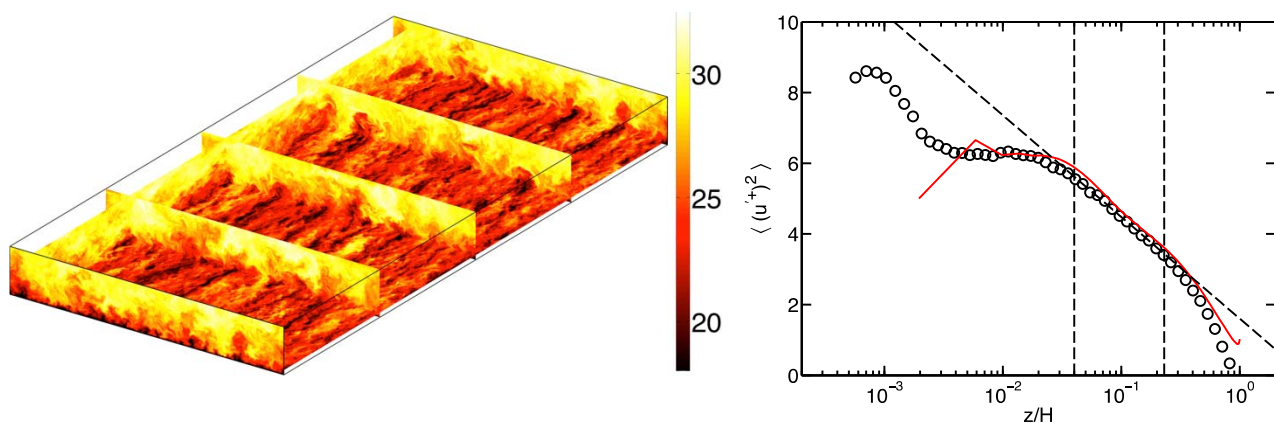


Figure 1: Left: Snapshot of the streamwise velocity from the LES performed on a $1024 \times 512 \times 256$ grid with $z_0/H = 10^{-5}$. The color indicates the streamwise velocity in non-dimensional units of u^* . Right: Comparison between Melbourne experiments³ (open circles) and LES with $z_0/H = 10^{-5}$ (line).

Acknowledgements

C.M. is grateful to I. Marusic for collaborations on wall-bounded turbulence. R.J.A.M.S. was supported by the ‘Fellowships for Young Energy Scientists’ (YES!) of FOM, M.W. by DFG funding WI 3544/2-1, and C.M. by US National Science Foundation grants numbers CBET 1133800 and OISE 1243482. Computations were performed with Surfsara resources and XSEDE (Extreme Science and Engineering Discovery Environment), which is supported by National Science Foundation grant number OCI-1053575, computational resources.

References

- 1 Smits et al., Annu. Rev. Fluid Mech. 43, 353–375 (2011)
- 2 Meneveau and Marusic, J. Fluid Mech. 719, R1 (2013)
- 3 Hutchins et al, J. Fluid Mech. 635, 103–136 (2009)

^aDepartment of Mechanical Engineering and and E2SHI, Johns Hopkins University, Baltimore, Maryland 21218, USA.

^bDepartment of Science and Technology and J.M. Burgers Center for Fluid Dynamics, University of Twente, P.O Box 217, 7500 AE Enschede, The Netherlands.

Wave decay in air/water sheared turbulence

F. Zonta^a, A. Soldati^a and M. Onorato^b

Nonstationary wave turbulence, is frequently observed in geophysical (during sudden changes of wind forcing) and industrial flows (during changes of mass flowrate in gas/liquid systems).

A detailed analysis of such phenomenon can provide informations to understand i) the process of energy conversion during transients and ii) the route to reach a new stationary state for wave turbulence.

In the present study, we use Direct Numerical Simulations (DNS) to explore the nonstationary wave-decay process of a countercurrent (horizontal) air/water flow. The motion of the air/water interface is computed by solving a pure advection equation for the interface vertical elevation (boundary fitted method). At each time step, the physical domain is mapped into a rectangular domain using a nonorthogonal transformation. Continuity and Navier-Stokes equations are first solved separately in each domain, then coupled at the interface through the continuity of velocity and stress. The physical problem is described in terms of three dimensionless numbers: the Reynolds number (Re , which measures the importance of inertia compared to viscosity), the Weber number (We , which measures the importance of inertia compared to surface tension) and the Froude number (Fr , which measures the importance of inertia compared to gravity). Regardless of the physical parameters, the transient evolution of the interface waves is characterized by an initial exponential decay followed by a new asymptotic steady state condition (characterized by a dynamical balance between gravity and capillarity). At the new steady state condition, the air/water interface is characterized by the superposition of longer gravity waves with shorter capillary waves: most of the interface energy is associated to gravity, whereas the surface tension affects mainly the smoothness of the interface. The different regimes of wave turbulence are detected upon comparison of theoretical/computational values of the wavenumber spectra. The interface deformation modifies also the turbulence activity/transfer mechanisms across the interface. In particular, the non-zero value of the Turbulent Kinetic Energy (TKE) at the interface implies that turbulence persists near the interface and enhances momentum transfer across the interface itself. All these considerations may also have important implications on the statistical description of the interface (probability density functions) and on intermittency phenomena in wave turbulence.

^a Dep. Electrical Management and Mechanical Engineering, Univ. of Udine, via delle Scienze 208, Udine, ITALY

^b Dep. Physics, Univ. of Torino, via Pietro Giuria 1, Torino, ITALY

DNS of a turbulent plume in a two-layer stratified filling box

Maarten van Reeuwijk^a, Gary R. Hunt^b, and Harm J.J. Jonker^c

We study stages of development of the flow in an initially two-layer stratified filling box, which is driven by a turbulent plume in the centre of the box base that adds buoyancy at a constant rate. The stratification is sufficiently strong to ensure that the plume impinges onto the stratification but does not fully penetrate it. The data is acquired by direct numerical simulation. The dimensions of the filling box are $72r_0 \times 72r_0 \times 36r_0$, where r_0 is the plume source radius and the density interface is initially at $z=24r_0$. The resolution of $1536^2 \times 1024$ permits a source plume Reynolds number $Re=1000$ and we present simulations at various Richardson numbers. The main simulation challenge is that the timescales associated with turbulence in the plume are far smaller than the timescales over which the large-scale dynamics take place, therefore requiring computationally intensive simulations of $O(10^6)$ CPU-hrs which were made possible by a Partnership for Advanced Computing in Europe (PRACE) project.

Various stages can be discerned in the flow development: 1) a starting plume develops which propagates unhindered through the lower layer; 2) plume impingement with the density interface and dome formation; 3) the outflow from the plume forms an intrusion; 4) a layer of intermediate density thereby develops and the classical filling-box behaviour as outlined in Baines (1974)¹ follows. The focus of this work is on stages 3-4.

One of the points of interest in this problem is the turbulent entrainment that results from the impingement of the plume with the density interface. We estimate the location of the density interface at every time step and calculate the entrainment flux by differentiating the average interface position with time. We find that the resulting entrainment flux strongly depends on whether the flow is in stage 3 (propagating intrusion) or stage 4 (regular filling-box behaviour), with the former producing higher entrainment rates than the latter. We comment on the likely reasons for this behaviour.

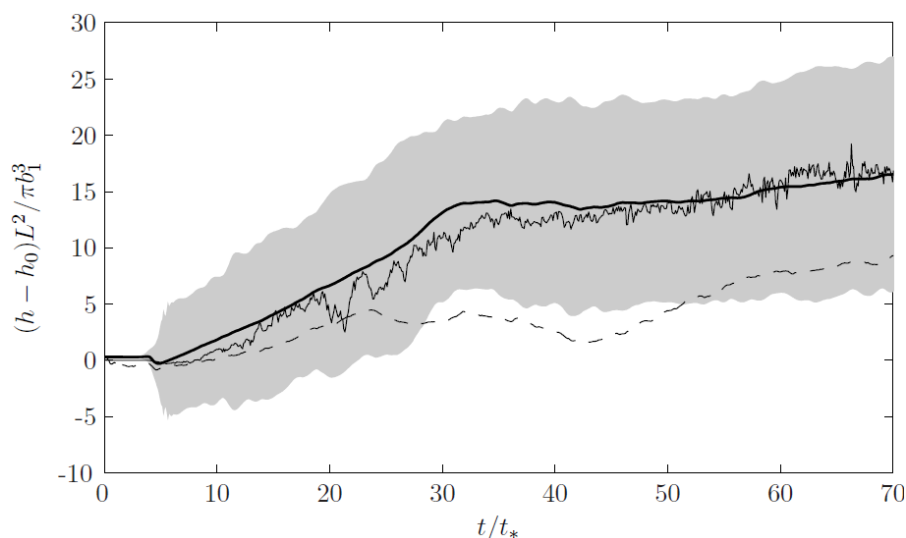


Figure 1. Evolution of the density interface position h as a function of time (thick black line). The grey band shows the spatial standard deviation of the interface.

^a Dept. of Civil and Environmental Engineering, Imperial College London, London SW7 2AZ, UK

^b Dept. of Engineering, Cambridge University, Cambridge CB2 1PZ, UK

^c Dept. of Geoscience and Remote Sensing, Delft University of Technology, 2600 GA Delft, The Netherlands

¹ Baines, J. *Fluid Mech.* **68**, 309 (1974).

On the role of helicity in 3D turbulent flows.

L. Biferale^a, S. Musacchio^b, E.S. Titi^c, F. Toschi^d

In this talk I will present recent advancements regarding the role of helicity in fully 3d homogeneous and isotropic flows at high Reynolds numbers. The main goal is to understand the correlation between energy and helicity transfer as a function of the helical degrees of freedoms carried out by the three-mode interactions in the non-linear terms of the Navier-Stokes equations. The methodology is based on a decimation of degrees of freedom in Fourier space. Results of direct numerical simulations at changing the ratio of positive/negative helicity modes will be presented. The role played by helicity to trigger inverse energy cascade events in 3d configuration will also be addressed^{1,2} as well as possible connections with regularity of solutions for Navier-Stokes equations³. The work of L.B. is supported by the ERC AdG 2013 Grant num. 339032 'NewTURB: New eddy-simulations concepts and methodologies for frontier problems in Turbulence'.

^a Dep. Physics, University of Rome "Tor Vergata"

^b CNRS, Laboratoire J.A. Dieudonné, UMR 7351, Parc Valrose, 06108 Nice, France

^c Department of Computer Science and Applied Mathematics, Weizmann Institute of Science, Rehovot 76100, Israel. Also Departments of Mathematics and of Mechanical and Aerospace Engineering, University of California, Irvine, CA 92697, USA

^d Department of Physics and Department of Mathematics and Computer Science, Eindhoven University of Technology, 5600 MB Eindhoven, The Netherlands & CNR-IAC, Via dei Taurini 19, 00185 Rome, Italy

¹ Inverse energy cascade in 3D isotropic turbulence. L. Biferale, S. Musacchio and F. Toschi. Phys. Rev. Lett. 108 164501, 2012

² Split Energy-Helicity cascades in three dimensional Homogeneous and Isotropic Turbulence. L. Biferale, S. Musacchio and F. Toschi. J. Fluid Mech. 730, 309 (2013)

³ On the global regularity of a helical-decimated version of the 3D Navier-Stokes equation. L. Biferale, E.S. Titi Journ. Stat. Phys. 151, 1089 (2013)

Large to small scale restoration of isotropy in rotating turbulence

A. Delache¹, F. Godeferd² and C. Cambon^b

Rotating homogeneous turbulence is known to exhibit structures strongly elongated along the axis of rotation as large-scale columnar structures (figure 1b). These structures can be attributed to a subtle interplay of linear² and nonlinear¹ effects depending on the context (forced or unforced turbulence, short or long times). It seems, however, that, unlike the anisotropic large scales, isotropy can be restored in the small scales. This was observed in direct numerical simulations and experiments^{4,5}. The simple relevant parameter is the wavenumber $k_\Omega = (\Omega^3/\Sigma)^{1/2}$ introduced by Zeman³ that compares the nonlinear effect associated with a turbulent structure of a given size to the Coriolis force. At large scales $k \ll k_\Omega$, anisotropy is present, whereas at small scales $k \gg k_\Omega$ a “universal” 3D isotropic characteristic of turbulence is restored. If k_Ω is sufficiently large (very large rotation) all scales may be anisotropic.

Our recent direct numerical simulations⁴ confirm the role played by Zeman's wavenumber in the separation between anisotropic and isotropic ranges: at high rotation rate, small scales (figure 1b) are axially oriented in contrast to lower rotation rate simulations where small scales appear as in classical turbulence (figure 1a). In order to clarify the small-scale isotropisation phenomenon, we present results from DNS at six different rotation rates, for freely decaying rotating turbulence. We analyse anisotropy scale-by-scale by considering the angle-dependent energy spectrum and nonlinear transfer. Moreover we separate poloidal and toroidal parts of the energy spectrum and we show that vertical velocity is increased at small scales near Zeman's wavenumber when the rotation rate is high.

¹ LMFA, site de Saint-Etienne, Université Jean Monnet de Saint-Etienne, France

² LMFA UMR 5509 CNRS, Ecole Centrale de Lyon, Université de Lyon, France

¹ C. Cambon, N. N. Mansour, and F. S. Godeferd, J. Fluid Mech. 337, 303–332 (1997).

² P. A. Davidson, P. J. Staplehurst, and S. B. Dalziel, J. Fluid Mech. 557, 135–144 (2006).

³ O. Zeman, Phys. Fluids 6, 3221 (1994)

⁴ A. Delache, C. Cambon and F. Godeferd, Phys. Fluids 26, 025104 (2014)

⁵ P-P. Cortet and F. Moisy, J. Fluid Mech. (submitted)

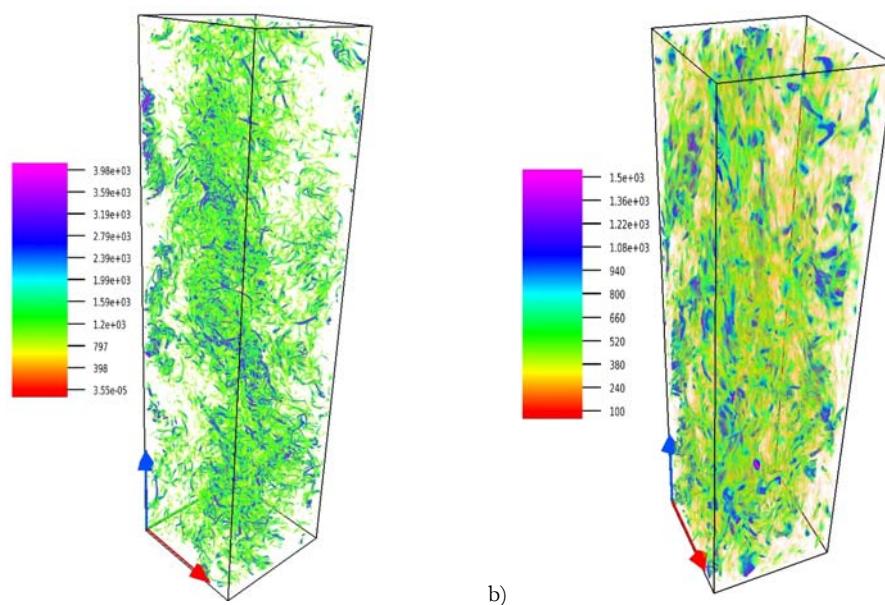


Figure 1: visualisation of the enstrophy distribution of the computational box (total vertical extent with 2048 points but only a 512^2 horizontal points are shown): (a) low rotation rate (b) high rotation rate.

A subgrid scale model for Large Eddy Simulation based on the Heterogeneous Multiscale Method

S. Hossbach^a and J. Sesterhenn^a

The importance of large eddy simulation (LES) is increasing with increasing computational resources. For most problems a direct numerical simulation (DNS) is not feasible and a statistical simulation with RANS (Reynolds averaged Navier Stokes) is too vague. LES seems to be the ideal solution to fill this gap but also for LES a universal model for complex problems is still missing. The reason is predominantly to be found in the missing scale invariance for those flow situations.

A new multiscale model for LES is proposed to help on this point. A global LES is supported by local DNS data providing the subgrid scale closure. The idea is based on the Heterogeneous Multiscale Method (HMM)^{1,2}. The HMM provides a general framework to develop multiscale methods. The aim is to develop a subgrid scale model that can be used in situations where similarity arguments fail. The basic idea is sketched with a nonlinear transport equation

$$\frac{\partial u}{\partial t} + \frac{\partial(f(u))}{\partial x} = 0$$

Filtering this equation with $\frac{\partial G}{\partial t} = 0$ and $\bar{u} = G * u$ and adding the term $\frac{\partial f(\bar{u})}{\partial x}$ on both sides leads to

$$\frac{\partial \bar{u}}{\partial t} + \frac{\partial f(\bar{u})}{\partial x} = \frac{\partial f(\bar{u})}{\partial x} - G * \frac{\partial f(u)}{\partial x} \quad (1)$$

The left-hand side can be seen as a transport equation for the variable \bar{u} . If \bar{u} on the right-hand side is expressed as $\bar{u} = G * u$ this side only depends on u . Hence we have a clear separation between the LES and the data u of the DNS that serves as subgrid scale model. For the first simulations we use existing DNS data in the whole field to test the feasibility of the concept. To generate this DNS data in future locally on affordable costs is the topic of ongoing research. It is planned to run several small DNS simulations on subregions with a characteristic flow situation and to scale this data onto topologically similar regions.

With the beforehand described model a LES of a jet is simulated and compared to DNS results. The important terms of this model are going to be shown. We look at the filtering terms in equation (1) and match the variables of the LES with a filtered DNS. Moreover we compare the new closure terms with their equivalences from conventional filtering models.

The compressible Navier-Stokes equations are solved with an inhouse code on a cartesian grid with grid refinement in stream-wise and transverse direction³. A low-storage Runge-Kutta 4th order for time integration and a 6th order compact finite-difference scheme with spectral like resolution of wavenumber for space are used⁴. As testcase a jet with Mach number $M=0.8$ and a Reynolds number of $Re=5000$ is considered.

^a Numerical Fluidynamics, TU Berlin, Mueller-Breslau-Str. 12., 10623 Berlin, Germany

¹ E and Engquist, *Communications in Computational Physics* **1**, 87 (2003)

² Abdulle et al. *Acta Numerica* **21**, 1 (2012)

³ Sesterhenn, *Computers & Fluids* **30**, 37 (2001)

⁴ Lele, *Journal of Computational Physics* **103**, 16 (1992)

Evaluation of turbulence models for Large Eddy Simulations of MHD turbulence

M. Kessar^{a,b}, G. Balarac^a and F. Plunian^b

Magnetohydrodynamic (MHD) turbulence is present in many astrophysical and geophysical objects. With today's computers, performing direct numerical simulations (DNS) with realistic values of Reynolds numbers is still out of reach. One option is to use Large Eddy Simulations (LES), the main idea being to explicitly resolve the large scales (grid-scales, GS) and to model their interactions with the smaller scales (subgrid-scales, SGS) that are not resolved.

Our goal is to perform an evaluation of several LES models found in literature of isotropic turbulence. We give below some results obtained with the cross-helicity model¹ (M1), and a Smagorinsky-like model² (M2), and we show that whereas M2 allows the achievement of LES, M1 may lead to numerical instability.

To evaluate each model performances, the global balances are studied for the resolved kinetic energy E_K , and the resolved magnetic energy E_M . These balances write formally as

$$\begin{aligned}\partial_t \langle E_K \rangle &= T_{K \rightarrow M} + T_{K_{GS} \rightarrow S_{GS}} + D^K + F^K \\ \partial_t \langle E_M \rangle &= -T_{K \rightarrow M} + T_{M_{GS} \rightarrow S_{GS}} + D^M\end{aligned}$$

where the brackets mean spatial averaging. In these balances $T_{K \rightarrow M}$ is the transfer from the resolved kinetic energy to the resolved magnetic energy (leading to dynamo effect), $T_{K_{GS} \rightarrow S_{GS}}$ (resp. $T_{M_{GS} \rightarrow S_{GS}}$) is the kinetic (resp. magnetic) energy flux from GS to SGS, D^K (resp. D^M) is the dissipation of the GS kinetic (resp. magnetic) energy, and F^K is forcing term. The terms $T_{K_{GS} \rightarrow S_{GS}}$ and $T_{M_{GS} \rightarrow S_{GS}}$ are the ones corresponding to a LES model. Thus, in this work, the modifications of these balances due to LES models are studied in comparison with the balances obtained by DNS. Then, we first perform a DNS with a resolution of 512^3 grid points, a Reynolds number (based on Taylor's microscale) equal to 60, and a magnetic Prandtl number equal to unity. The forcing leads to generation of a small-scale magnetic field through dynamo action. This DNS database then can be filtered with a given filter size. As a first test, we compute the exact transfers $T_{K_{GS} \rightarrow S_{GS}}$ and $T_{M_{GS} \rightarrow S_{GS}}$ and compare them to the fluxes given by the models computed from the filtered DNS (*a priori* test). Second, we perform LES on a 64^3 grid points using M1 and M2 models (*a posteriori* tests).

The results computed through *a priori* tests show that both models lead to an over-dissipation of total (magnetic plus kinetic) energy for a broad range of filter size (Fig.1, left). In details, M2 is over-dissipating both energies (E_K and E_M), while M1 presents a strong over-dissipation of kinetic energy, but no dissipation of magnetic energy. When LES is performed, this behaviour of M1 leads to strong accumulation of magnetic energy at the smallest resolved scales (Fig.1, middle). The LES with M1 became then quickly unstable (Fig.1, right), while the other one, using M2 is stable, thanks to a better repartition of energy dissipation. During the conference we will present results obtained with other models^{2,3} and forcings⁴.

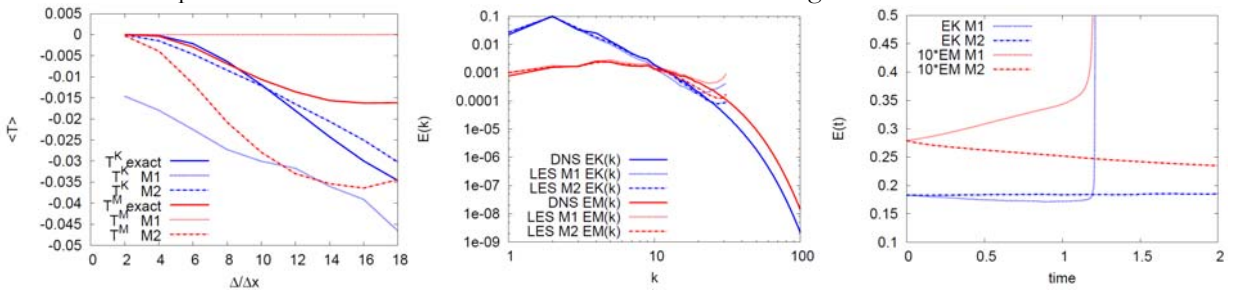


Figure 1: Exact and modelled flux of energy as function of filter size (left). LES kinetic and magnetic energy spectra using M1 and M2 models. Comparison with DNS (middle). Time evolution of resolved energies for LES performed by using M1 and M2 models (right).

^a Grenoble-INP/CNRS/UJF-Grenoble 1, LEGI UMR 5519, Grenoble, F-30841, France

^b CNRS/UJF-Grenoble 1, ISTerre UMR 5275, Grenoble, F-30841, France

¹ Muller, and Carati, *Physics of Plasmas* **9** (3), 824–834 (2002).

² Agullo, *et al* *Physics of Plasmas* **8** (7), 3502–3505 (2001).

³ Hamba, and Tsuchiya, *Physics of Plasmas* **17** (1), 012301 (2010).

⁴ Brandenburg, *The Astrophysical Journal* **550** (2), 824 (2001).

Instability Vortices

Macro- and Microjets Stability at Low Reynolds Numbers

Yu.A. Litvinenko^a, G.R. Grek^a and V.V. Kozlov^a

An overview of recent experimental results on instability and dynamics of jets at low Reynolds numbers is given. Round and plane, macro and micro jets are under the consideration. Basic features of their evolution affected by initial conditions at the nozzle outlet and environmental perturbations are demonstrated (see Figures 1 and 2).

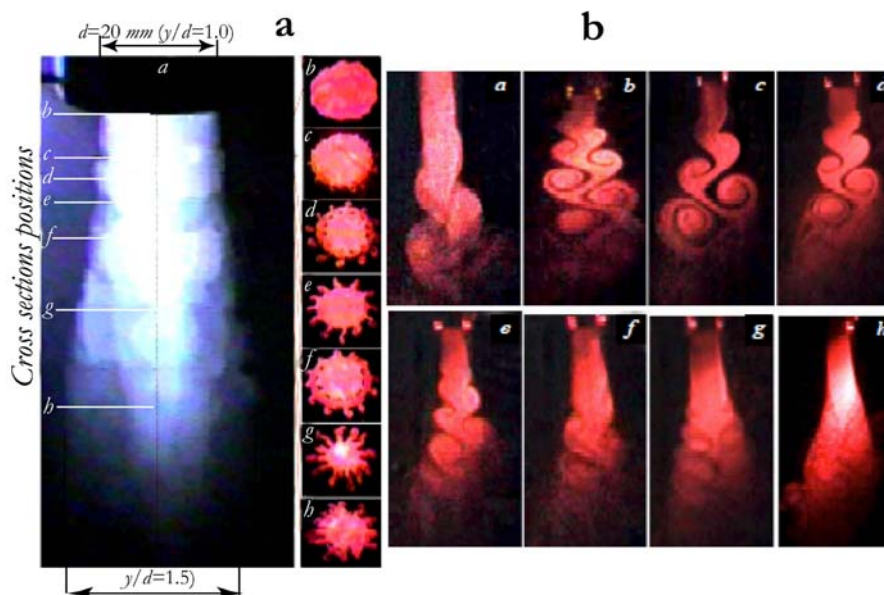


Figure 1: (a) General view of the round macrojet and its cross sections at different distance from the nozzle exit (b)-(h). (b) Visualization of the laminar plane macrojet with a parabolic mean velocity distribution in natural conditions and under external acoustic forcing at frequencies $f = 30$ (b), 40 (c), 50 (d), 60 (e), 70 (f), 90 (g), and 150 Hz (h); $Re_b = 3300$.

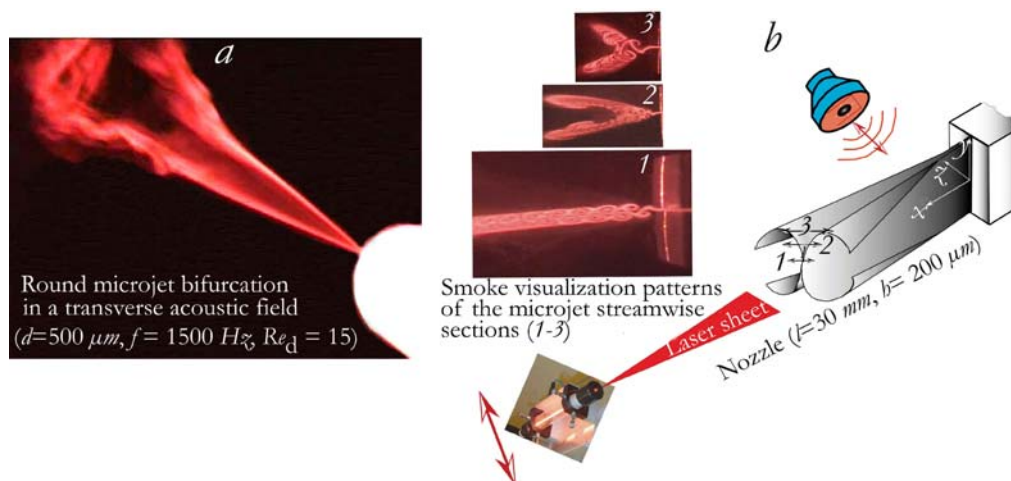


Figure 2: (a) Round and (b) Plane microjet bifurcation under action of transverse acoustic field

This work was supported by the Integration Project SB RAS No. 24 and by the Russian Foundation for Basic Research, project Nos. 11-01-00292, 12-08-31083, 12-07-00548, and 13-07-00616

^aKhristianovich Institute of Theoretical and Applied Mechanics, Siberian Branch of Russian Academy of Sciences, Novosibirsk, Russia

Exponential growth of disturbances in a boundary layer over a rotating cylinder

S. Derebail Muralidhar*, B. Pier*, J. Scott*, R. Govindarajan†

When a cylinder is placed in an axial flow, a three dimensional boundary layer develops which exhibits instability waves, when subjected to infinitesimal perturbations. The effect of curvature causes the boundary layer thickness to deviate from the classical Blasius solution. Addition of rotation results in a tangential velocity profile that modifies the stability characteristics. Rotating curved surfaces can be seen in wind turbine nose tips, airfoils, travelling arrows, etc. Hence it is important to study the instability mechanisms for such a configuration.

The boundary layer developing along a rotating circular cylinder has been studied previously and the velocity profiles were computed by Jaffe and Okamura¹. The non-rotating thin cylinder configuration has been studied by Tutty et al.² and N. Vinod³, and they have found that the flow is globally stable for Reynolds numbers below 1060. The present stability analysis takes into account the effect of both cylinder rotation and boundary layer development, in order to gain a better understanding of the physical phenomena.

Our results indicate that a small amount of rotation s , which is the ratio of tangential velocity on cylinder surface to free stream axial velocity, reduces the critical Reynolds number by an order of magnitude. The effect of curvature and rotation on the stability properties will be discussed in detail and compared with some existing results.

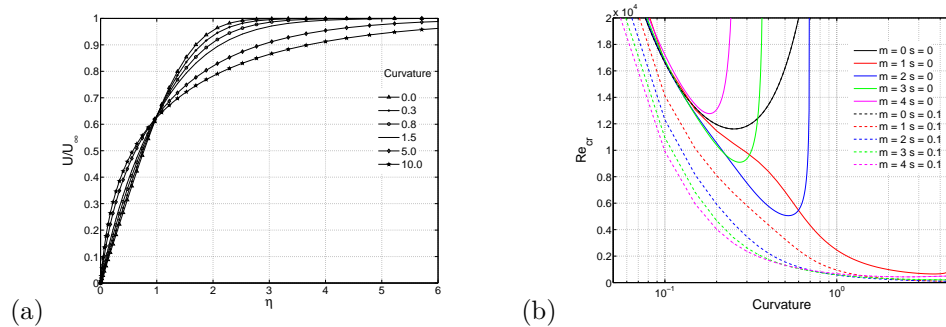


Figure 1: (a) Variation of axial velocity profile with curvature (η is a rescaled radial coordinate). (b) Variation of critical Reynolds number at different azimuthal modes m for rotating ($s = 0.1$) and non-rotating ($s = 0$) case.

*Laboratoire de mécanique des fluides et d'acoustique (CNRS—Université de Lyon), École centrale de Lyon, 36 avenue Guy-de-Collongue, F-69134 Écully, France.

†TIFR Centre for Interdisciplinary Sciences, Hyderabad, India

¹N. A. Jaffe and T. T. Okamura, *Zeitschrift für angewandte Mathematik und Physik ZAMP* **19**, 564–574 (1968).

²O. R. Tutty, W. G. Price and A. T. Parsons, *Phys. Fluids* **14**, 628–637 (2002).

³N. Vinod and R. Govindarajan, *J. Fluids Engineering* **134**, 024503 (2012).

Centrifugal instability of Stokes layers in crossflow: the case of a forced cylinder wake

Juan D'Adamo^a, Ramiro Godoy-Diana^b and José Eduardo Wesfreid^b

A circular cylinder oscillating in a viscous fluid produces an axisymmetric Stokes layer, a fundamental flow susceptible to centrifugal instabilities¹. In the present work we study such problem in the wake flow around a circular cylinder at $Re = 100$ performing rotary oscillations. For a forcing frequency f_f and amplitude U_t , the non-dimensional control parameters $f^+ = f_f / f_n$ and $\mathcal{A} = U_t / U_\infty$ are related to the flow properties, the inflow velocity U_∞ and the natural vortex shedding frequency f_n . In a previous work², we identified experimentally a zone in the parameter space with forcing at frequencies lower than the natural vortex shedding frequency, where the flow exhibited some turbulence features such as a continuous spectrum for the velocity components, and multiple vortex splitting interactions in the wake. We show here using numerical simulations that these observations result from a 3D centrifugal instability.

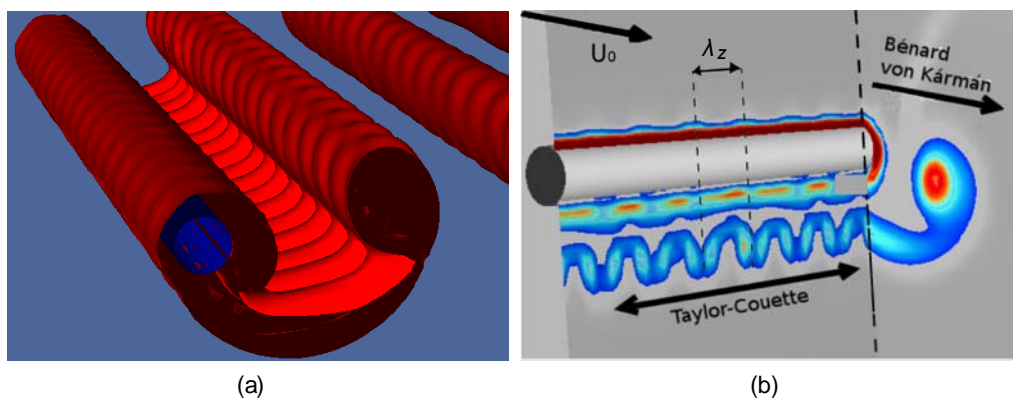


Figure 1: a) Isosurface for total vorticity modulus for $f^+ = 0.75$, $\mathcal{A} = 4.00$. b) Vorticity modulus contours for two cutting planes revealing the main flow structures ($f^+ = 0.75$, $\mathcal{A} = 4.00$).

^a Facultad de Ingeniería Universidad de Buenos Aires (CONICET), Argentina

^b PMMH, CNRS UMR 7636; ESPCI ParisTech; UPMC (Paris 6); Univ. Paris Diderot (Paris 7), Paris, France

¹ Seminara & Hall, *Proc. Roy. Soc. London A* **350**, 299 (1976).

² D'adamo et al., *Phys. Rev. E* **84**, 056308 (2011).

Zoology of unstable modes in a stratified cylinder wake

M.Bosco¹ & P.Meunier²

In this presentation, the effect of the stratification and the tilt on the 3D instabilities of a cylinder wake will be delineated. This configuration is particularly interesting for geophysical applications where stratified wakes have been usually restricted to 2D horizontal bluff bodies such as wakes of mountains, islands, submarine or off-shore platforms in oceans and in the atmosphere. As it will be shown, the dynamics becomes very complex in the presence of the stratification as it depends on the Reynolds number but also on the Froude number and on the tilt angle α between the cylinder and the vertical.

For a vertical cylinder, the 2D wake is destabilized when the Reynolds number increases above 190. Fig. 1(a) shows the periodic structures with a well-defined wavelength created about 5 diameters downstream of the cylinder. These structures are characteristic of the classical mode A, well-known in a homogeneous fluid. This mode is more unstable for moderate stratifications. This is in contradiction to the local theory of the elliptic instability which is at the origin of the mode A. The mode is more stable for strong stratifications.

When the cylinder is tilted a new unstable mode is observed at moderate Froude numbers, characterized by undulated layers of strong density gradients and axial flow. (see Fig. 1b) corresponding to Kelvin-Helmholtz billows created by the strong shear present in the critical layer of each tilted von Karman vortex. Eventually, for a strongly tilted cylinder, two other modes can be seen. For a weak stratification, an instability appears due to the overturning of the isopycnals by the von Karman vortices. For a strong stratification, a short wavelength unstable mode is observed, even in the absence of von Karman vortices. A map of the four unstable modes is established and the relevance to the dynamics of geophysical wakes is discussed.

^{1,2} IRPHE, CNRS – Aix-Marseille Universite, Marseille, 13013, France



Figure 1:(a) Visualisation of the mode A ($Re=190$, $F=4$, $\alpha=0^\circ$). (b) Visualisation of the mode S ($Re=170$, $F=2.5$, $\alpha=45^\circ$)

Numerical Simulation of the Oscillating Kelvin-Helmholtz Instability

A. Ebo Adou^{b,c}, L. S. Tuckerman^b, J. E. Wesfreid^b, J. Chergui^c, D. Juric^c & S. Shin^a

We perform numerical simulations of two superposed immiscible liquids, differing in viscosity and density, and subject to horizontal periodic oscillations. Beyond a certain threshold for the oscillation amplitude or frequency, the motion of the interface can lead to the formation of what are sometimes called frozen waves.

Our numerical investigation, using the code BLUE³, concerns the case of highly viscous silicone oil and water. The numerical domain is set to be periodic in the oscillation direction and in the spanwise direction.

We report here the height of the waves for ranges of frequencies and amplitudes of forcing. A Fourier transform shows that the wave height oscillates at a multiple of the imposed frequency. For a given amplitude, we identify two different states for the wave heights depending on the frequency. The temporal average of the streamlines in these two states shows a difference in the number of recirculation cells below the interface for high viscosity contrast; see Fig.1.

^a Department of Mechanical and System Design Engineering, Hongik University, Seoul, 121-791 Korea

^b PMMH (UMR 7636 CNRS-ESPCI-UPMC Paris 6-UPD Paris7), 10 rue Vauquelin, 75005 Paris, France

^c LIMSI (UPR 3251 CNRS Univ. Paris Sud Paris XI) BP133, Rue J. von Neumann, 91403 Orsay, France

¹ H. Yoshikawa & J.E. Wesfreid, *J. Fluid Mech.* **675**, 223-248 (2011); and 249-267 (2011).

² S. Jalikop & A. Juel, *J. Fluid Mech.* **640**, 131-150 (2009).

³ S. Shin, J. Chergui, D. Juric, A. Farhaoui, L. Kahouadji, L.S. Tuckerman, N. Périnet, in *8th Int. Conf. on Multiphase Flow*, Jeju, Korea (2013).

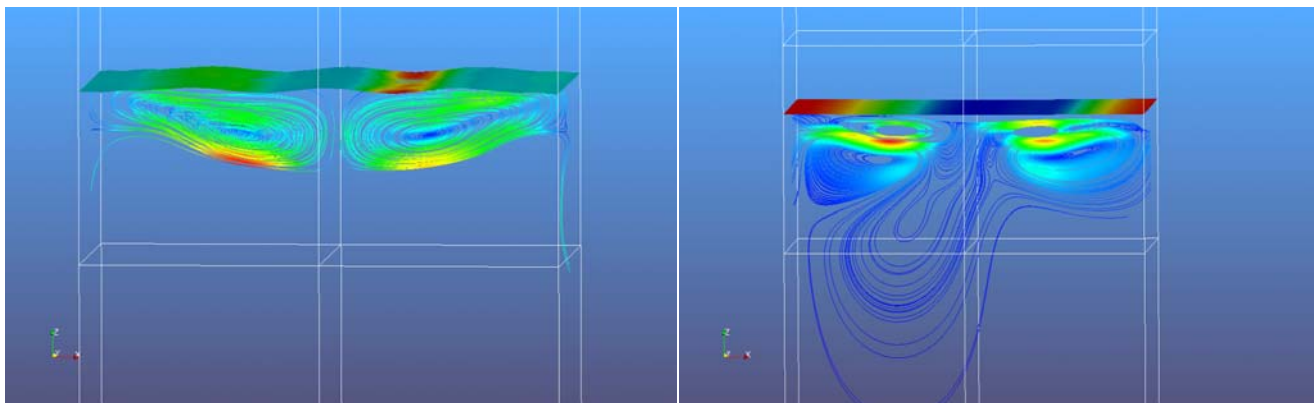


Figure 1: Temporal average of streamlines average of the two states. Low height state (right) with four recirculation cells and high height state (left) with two recirculation cells.

Oscillatory flow past a fixed cylinder versus an oscillating cylinder in still fluid

J. P. Gallardo^a, H.I. Andersson^b and B. Pettersen^a

The oscillatory flow around a straight circular cylinder gives rise to a variety of flow patterns which vary according to the Keulegan-Carpenter and Reynolds number, Re and KC respectively. Two different approaches exist for both, numerical and experimental studies: a fixed cylinder immersed in oscillating fluid (case A), and a cylinder oscillating in an otherwise still fluid (case B). In the present investigation these two approaches have been compared at different KC numbers between 1 and 4 to study the effect on the three-dimensional instabilities that arise in this type of flow. To this end, the solution of the incompressible Navier-Stokes equations has been computed numerically in the frame of reference of the body using a second-order finite volume-code. This involves the introduction of a forcing term and suitable modifications of the boundary conditions for case B, in which the cylinder oscillates. The effect of the spanwise length is also considered in the present investigation.

At $KC=2$ and $Re=400$, a spanwise length of $4D$ leads to a regular arrangement of Honji vortices with a wavelength of $0.67D$ (see figure 1), similar to the flow pattern obtained by An et al. (2011). A spanwise length of $8D$, however, resulted in spanwise rearrangements of the Honji vortices in both cases, with a larger number of rearrangements in case A. Varying the parameters (KC, Re), we intend to further investigate the differences between these two cases.

^a Department of Marine Technology, Norwegian University of Science and Technology, NO-7491 Trondheim, Norway

^b Department of Energy and Process Engineering, Norwegian University of Science and Technology, NO-7491 Trondheim, Norway

¹ An, Cheng and Zhao., *J. Fluid Mech.* **666**, 77 (2011).

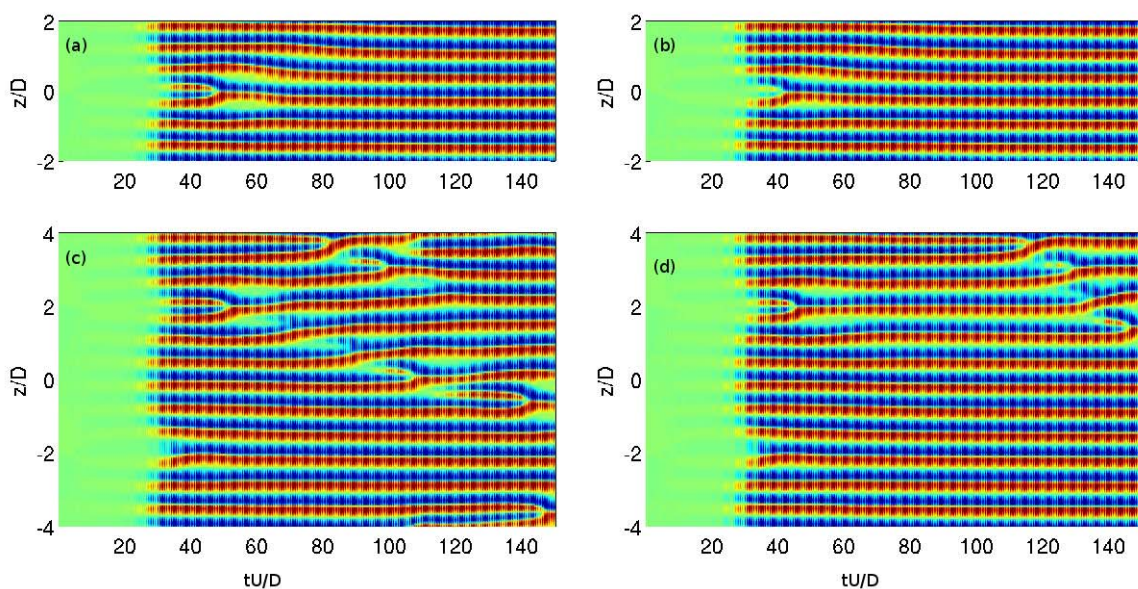


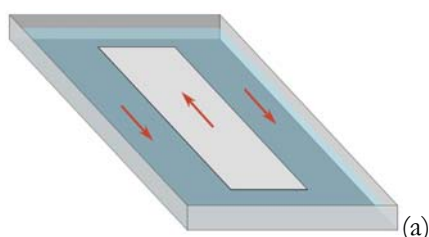
Figure 1: Case with $(KC, Re)=(2, 400)$. Temporal evolution of the vertical velocity w along a line parallel to the spanwise direction z , centered in the streamwise direction x , and with an offset of $0.06D$ in the cross-flow direction y . (a) Case A, $4D$; (b) case B, $4D$; (c) case A, $8D$; and (d) case B, $8D$.

Kelvin-Helmholtz instability and Bénard-Von Karman vortex street in a confined geometry

P. Boniface^a, M. Receveur^a, L. Lebon^a and L. Limat^a

We have experimentally investigated the appearance of Kelvin-Helmholtz vortices in a confined geometry^{1,2} : in a closed rectangular tank a tape is pulled at high speed on the water surface. This induces a flow in the same direction as the tape, and by conservation a backward flow in the opposite direction. (see figure a). With an appropriate choice of the experiment parameters (water height, tape speed) the backward flow takes place on the sides of the tank : this creates a strong shear that can induce a Kelvin-Helmholtz instability on each side of the tank.

As long as the tape width stays small enough compared to the tank width, we can observe the appearance of well organized vortex rows on each sides of the tank as illustrated on figure b where the tape is very narrow (of order a few millimeters). In this case, the vortex rows are coupled like a Bénard-Von Karman vortex street, but without the classical forcing of a wake behind an obstacle. All our experiments are in agreement with a theoretical prediction by Rosenhead³ which extended the Bénard-Von Karman vortex street stability calculation to a confined geometry. Our work seems to be one of the first experimental verification of this 80 years old model. A subtlety of our experiment is here that the double row of vortices is issued from two coupled Kelvin-Helmholtz instabilities, in a framework where the growth is absolute and not convective as in most experimental realizations with wakes.



(a)

QuickTime™ et un
décompresseur
sont requis pour visionner cette image.

(b)

Figure : **(a)** geometry of the flow induced by a tape running at high speed at the free surface of a closed pool. **(b)** a typical flow pattern observed when the tape lateral extent vanishes (running rope), with formation of a regular Bénard Von Karman streets of vortices, despite the strongly turbulent nature of the flow (view on an horizontal plane, just under the surface).

^a Matière et Systèmes Complexes, CNRS and Université Paris Diderot, UMR 7057, Bâtiment Condorcet, 10 rue Alice Domon et Léonie Duquet, 75013 Paris, France

¹ P. Boniface *et al.*, *Bull. Am. Phys. Soc.*, 65th Annual Meeting of the APS Division of Fluid Dynamics, **57**, November 18–20, 2012; San Diego, California (2012);

² P. Boniface, *Thesis*, Univ. Paris Diderot (2014).

³ L. Rosenhead, *Phil. Trans. R. Soc. Lond. A*, **228**, 275–329 (1929).

Absolute instability of variable density swirling flows

N. E. Molevich^{a,b}, D. P. Porfiriev^{a,b}, S.S. Sugak^a and I. P. Zavershinskii^a

Swirling flows are well known to be very important for devices with heat release such as swirl combustion systems, aero-engines, plasma dynamic systems, hydrogen plasma generators etc. At sufficient swirl numbers, central recirculation zone is generated. Precessing vortex core (PVC) arises at the boundary of direct and counter flows. It can play an important role in practical applications – from desired to catastrophic. PVC has helical structure and is formed by unstable bending flow modes $m = \pm 1$. The formation of either the positive (left-handed) bending mode, which winds in a direction opposite to the base flow rotation, or the negative (right-handed) bending mode, which winds in direction of the base flow rotation, depends on a number of factors including swirl ratio and expansion ratio. We show that some obtained features of PVC¹⁻³ can be qualitatively explained using the results of linear stability analysis. Taking into account the density difference between the center and wall regions for swirling flows with heat release we use the simplest analytical model of a swirling flow in a form of the Rankine vortex with the piecewise axial flow and density. The flow is assumed to be inviscid, incompressible and governed by the Euler equations. The linear dispersion relation is derived analytically as a function of azimuthal wave number m , swirl ratio S , the velocity ratio a , the confinement ratio K and the density ratio Q . For every azimuthal number m , there exists a single unstable Kelvin–Helmholtz mode and an infinite number of neutral inertial modes. The left-handed perturbations ($m > 0$) of wake-like flows displays a larger growth rate than their right-handed counterparts on the entire axial wave number range (Fig. 1). Such result is quite typical for swirling wakes and yields the qualitative explanation why PVC forming in wakes has the left-handed helical structure. In the supercritical spectral range $k > k_C$, Kelvin–Helmholtz mode frequency increases and the growth rate of the Kelvin–Helmholtz mode decreases with decrease of density parameter Q . These dependences are also in a good coincidence with known experimental and numerical results of swirl flow investigations¹⁻³. In the subcritical region $k < k_C$, we obtain conditions of parametrical instability.

This work was financially supported by The Ministry of education and science of Russia, under project 608 and by RFBR under grants 13-01-97001, 14-02-97030.

^a Samara State Aerospace University, 34 Moskovskoe sh., Samara, Russia

^b P.N. Lebedev Physical Institute of RAS, Samara Branch, 221 Novo-Sadovaya Str., Samara, Russia

¹ Alekseenko, Kuibin and Okulov, Theory of concentrated vortices, Springer Berlin Heidelberg, (2007).

² Zavershinskii *et al.*, *Tech. Phys. Letters* **39**, 333 (2013).

³ Zavershinsky *et al.*, *Book of Abstracts of 9th EFMC* (2012).

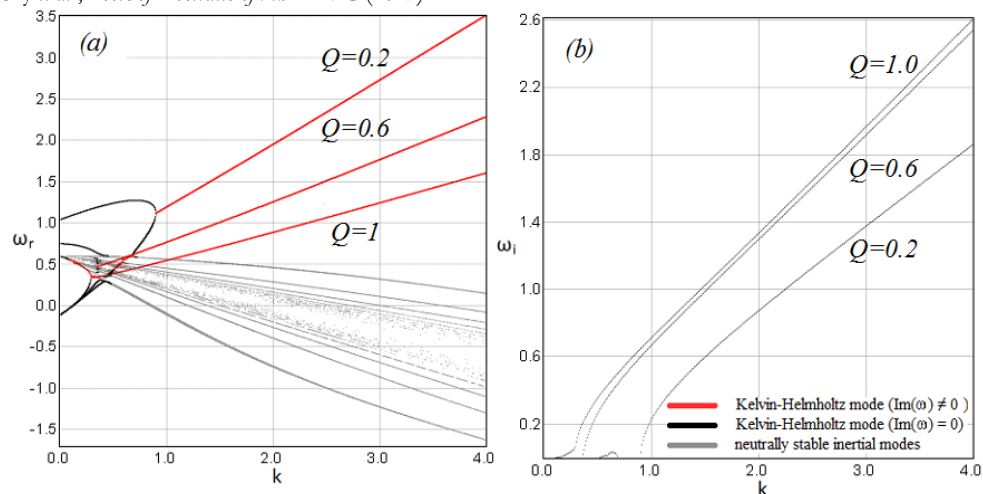


Figure 1: Real (a) and imaginary (b) parts of frequency as a function of k at different density ratio Q . Here $m = +1$, $a = -0.3$, $K = 2.5$, $S = 0.6$.

Drops

Effects of the moving interface on the heating of evaporated droplets and diffusion of liquid species

S.S. Sazhin^a

The conventional approach to the heating of evaporating droplets has been based on the assumption that during each time step the radius of droplets remains the same, although it changes from one time step to another to take into account the evaporation and thermal swelling processes. In a series of our papers¹⁻³, this assumption was relaxed and the radius of droplets was allowed to change during each time step. An analytical solution to the heat conduction equation inside a droplet was obtained, assuming that the droplet radius is a linear function of time¹. An alternative solution to this equation, assuming that the time evolution of droplet radius is known was suggested². In this case the iteration process was required to obtain the final solution. Finally, the same problem was solved numerically, assuming that the droplet radius is a linear function of time³. In all cases the results were incorporated into a zero-dimensional Computational Fluid Dynamics (CFD) in-house code and applied to the modelling of heating and evaporation of fuel droplets in conditions typical for Diesel engines. The predictions of the time evolution of droplet surface temperatures and radii by all three approaches were shown to coincide within the accuracy of plotting^{2,3}. The new solutions led to the prediction of lower droplet temperatures and slower evaporation when the effects of the reduction of droplet radii during each time step due to evaporation were taken into account. The predicted difference in evaporation times increased from about 2% for gas temperature 800 K to 7% for gas temperature 1200 K.

Two new solutions to the equation, describing the diffusion of species during multi-component droplet evaporation, taking into account the effect of the reduction of the droplet radius due to evaporation and assuming that this radius is a linear function of time, were suggested⁴. The first solution was the explicit analytical solution to this equation, while the second one reduces the solution of the differential transient species equation to the solution of the Volterra integral equation of the second kind. The analytical solution was incorporated into a zero dimensional CFD code and applied to the analysis of bi-component droplet evaporation. The case of an initial 50% ethanol – 50% acetone mixture and droplets with initial diameter equal to 142.7 μm moving in air at atmospheric pressure was considered. To separate the effect of the moving interface on the species diffusion equation from a similar effect on the heat conduction equation inside droplets, described earlier, a rather artificial assumption that the droplet temperature is homogeneous and fixed was made. It was pointed out that the effect of the moving interface due to evaporation slows down the increase in the mass fraction of ethanol (the less volatile substance in the mixture) and leads to the acceleration of droplet evaporation.

The effects of the moving interface due to evaporation on both heat transfer and species diffusion processes simultaneously were investigated in⁵. The effect of the moving interface was shown to be much stronger for the solution to the species diffusion equations than for the solution to the heat conduction equation. It was recommended that the coupling of hydrodynamic and heat/species transfer effects should be taken into account when modelling realistic mono- and multi-component droplet heating and evaporation.

The presentation will be focused on the main findings of the above-mentioned papers, which are not expected to be well known to the Euromech community. These results illustrate the importance of the linking of fluid dynamics and heat/species transfer processes.

Part of this work was supported by the EPSRC under grant EP/J006793/1.

^a School of Computing, Engineering and Mathematics, The University of Brighton, Brighton, BN2 4GJ, United Kingdom

¹ Sazhin et al., *Int. J Heat and Mass Transfer* **53**, 2826 (2010).

² Sazhin et al., *Int. J Heat and Mass Transfer* **54**, 1278 (2011).

³ Mitchell et al., *Applied Mathematics and Computation* **217**, 9219 (2011).

⁴ Gusev et al., *Int. J Heat and Mass Transfer* **55**, 2014 (2012).

⁵ Elwardany et al., *Atomization and Sprays* **21**, 907 (2011).

Oscillating drops levitated by an airflow

W. Bouwhuis^a, K.G. Winkels^a, I.R. Peters^{a,b}, P. Brunet^c, D. van der Meer^a, and J.H. Snoeijer^a

We investigate the spontaneous oscillations of drops levitated above an air cushion, eventually inducing a breaking of axisymmetry and the appearance of “star drops”^{1,2} (Fig. 1a). This is strongly reminiscent of the Leidenfrost stars that are observed for evaporating drops floating above a hot substrate. The key advantage of this work is that we inject the airflow at a constant rate below the drop, thus eliminating thermal effects and allowing for a better control of the flow rate. We perform experiments with drops of different viscosities and observe stable states, oscillations, and chimney instabilities; For the latter scenario, an air bubble develops below the drop and pierces through the center of the drop³. We find that for a given drop size the instability appears above a critical flow rate, where the latter is largest for small drops. All these observations are reproduced by numerical simulations, where we treat the drop using potential flow and the gas as a viscous lubrication layer (Fig. 1b).

Our results demonstrate that thermal effects are not important for the formation of star drops and strongly suggest a purely hydrodynamic mechanism for the formation of Leidenfrost stars, contrarily to previous suggestions⁴. Non-axisymmetric modes and chaotic oscillations could be observed near the threshold of the instability for oscillating water drops, while in the high viscosity case, only the ‘breathing’ mode (axisymmetric mode) is observed. Thus, faceted star shapes are the result of a parametric excitation that can only appear at sufficiently small damping (i.e. liquid viscosity).

^a Physics of Fluids Group, Faculty of Science and Technology, University of Twente, 7500 AE Enschede, The Netherlands

^b James Franck Institute, University of Chicago, Chicago, Illinois 60637, USA

^c Laboratoire Matière et Systèmes Complexes UMR CNRS 7057, 10 rue Alice Domon et Léonie Duquet 75205 Paris Cedex 13, France

¹ Brunet and Snoeijer, *Eur. Phys. J. Spec. Top* **192**, 207-226 (2011)

² Bouwhuis *et al.*, *Phys. Rev. E* **88**, 023017 (2013)

³ Biance *et al.*, *Phys. Fluids* **15**, 1632-1637 (2003)

⁴ Tokugawa and Takaki, *J. Phys. Soc. Jap.* **63**, 1758-1768 (1994)

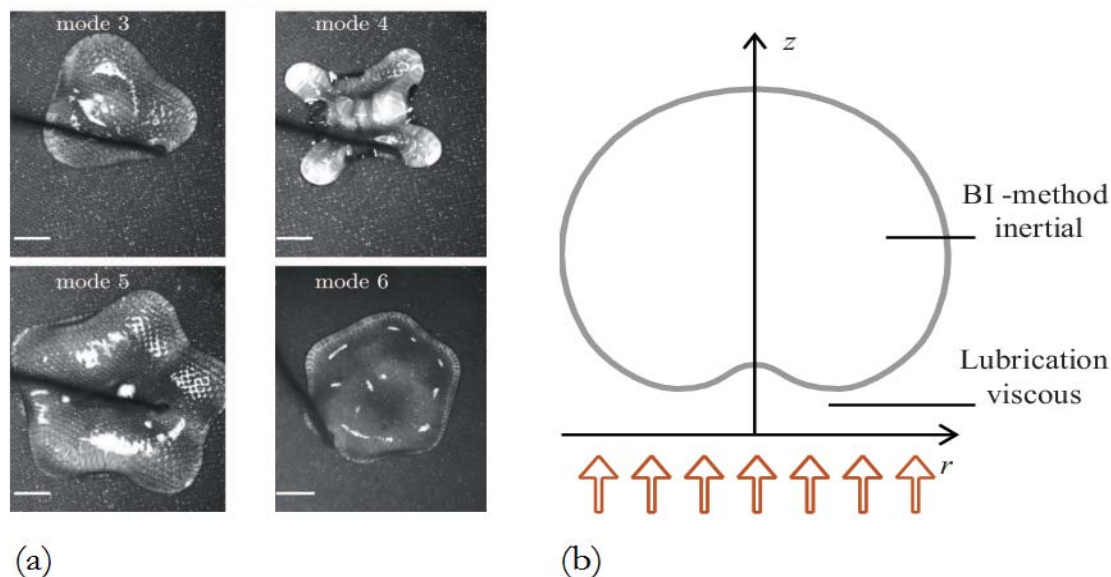


Figure 1: (a) Water drops levitated by a steady (i.e. non-pulsating) airflow performing several oscillation (“star”) modes. Figure from Ref. ². Scale bar: 3 mm. (b) Numerical implementation of the drop levitated by a uniform airflow at room temperature.

Influence of internal natural convection on water droplets freezing on cold surfaces

L. Karlsson^a, A-L. Ljung^a, T.S. Lundström^a

The freezing of water droplets is a relevant and topical subject since the areas of application are many. Ice accretion on the rotor blades of wind turbines, on the wings and propellers of aircrafts, and on cold roads exposed to freezing rain are but a few examples. The freezing of liquid water has been studied both experimentally and using different CFD-models, but for a single water droplet there are still only a few studies made using CFD. An interesting view is therefore to compare CFD-simulations to already existing results. This study aims to examine the freezing process of a water droplet using ANSYS CFX. A simple geometrical model of a droplet is created and a mesh analysis is performed to find the most suitable mesh for the set-up. By the use of a source term the velocity in the solid zone is set to zero and buoyancy is added to the model to account for the internal natural convection. Simulations to study the impact of surface tension are furthermore performed and compared to the case where there are no surface forces. The droplet is assumed not to change form during the simulations and the model do not account for a subcooled liquid. Results show that the water droplet freezes from bottom to top and the freezing front evolution depends on the internal temperature and velocity field, which is in agreement with existing experiments. A comparison between the two cases where buoyancy is present and where it is not is performed. The velocity distribution for the two cases at $t = 1$ s can be seen in Figure 1. The result shows that there is a great difference in average velocity as well as velocity and pressure distribution between the two cases. Three bottom surface temperatures are investigated, and results show that both that both the volume of the remaining liquid part as well as the overall temperature in the droplet increases as the bottom surface temperature increases. The average velocity in the liquid part instead decreases as the bottom surface temperature increases.

^a Div. of Fluid Mechanics, Luleå University of Technology, SE-971 87 Luleå, Sweden

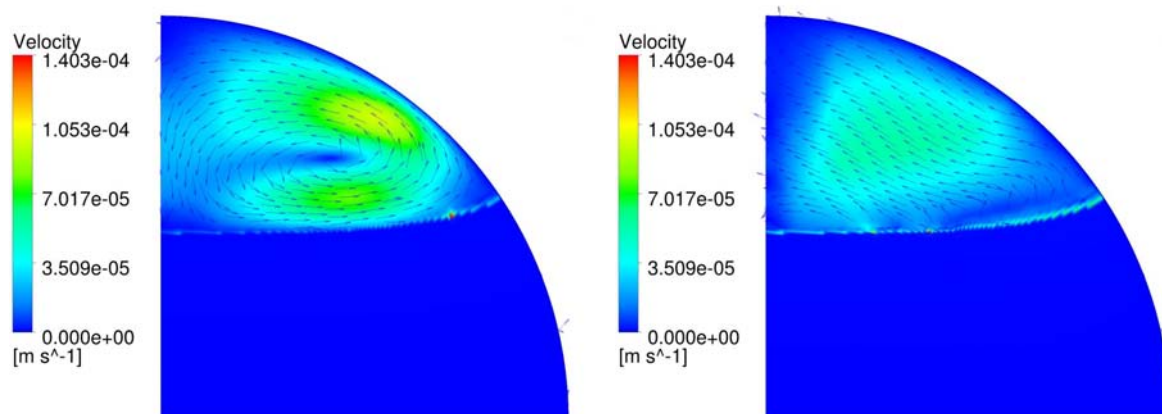


Figure 1: Velocity distribution and velocity vectors at $t = 1$ s, bottom surface temperature $T = -20^\circ\text{C}$. (a) Buoyancy is considered. (b) Buoyancy is not considered.

The critical impact speed for the splash of a drop

Guillaume Riboux^a & José Manuel Gordillo^a

Making use of experimental and theoretical considerations, in this work we present a criterion to determine the critical velocity for which a drop impacting a smooth dry surface either spreads over the substrate or disintegrates into smaller droplets. The derived equation, which expresses the splash threshold velocity as a function of the material properties of the two fluids involved, the drop radius and the mean free path of the molecules composing the surrounding gaseous atmosphere, has been thoroughly validated experimentally at normal atmospheric conditions using eight different liquids, with viscosities ranging from 0.3 to 10 cP and interfacial tension coefficients which vary between 17 and 72 mN/m. The predicted threshold velocity is also in agreement with the experimental data by Xu *et al*¹, where the critical speed for droplet splashing is investigated using gases with different densities at reduced atmospheric pressures.

^aArea de Mecánica de Fluidos, Departamento de Ingeniería Aeroespacial y Mecánica de Fluidos, Universidad de Sevilla, Avenida de los Descubrimientos s/n 41092, Sevilla, Spain.

¹Xu, L, Zhang, W & Nagel, S. R. Phys. Rev. Lett. 94, 184505 (2005).

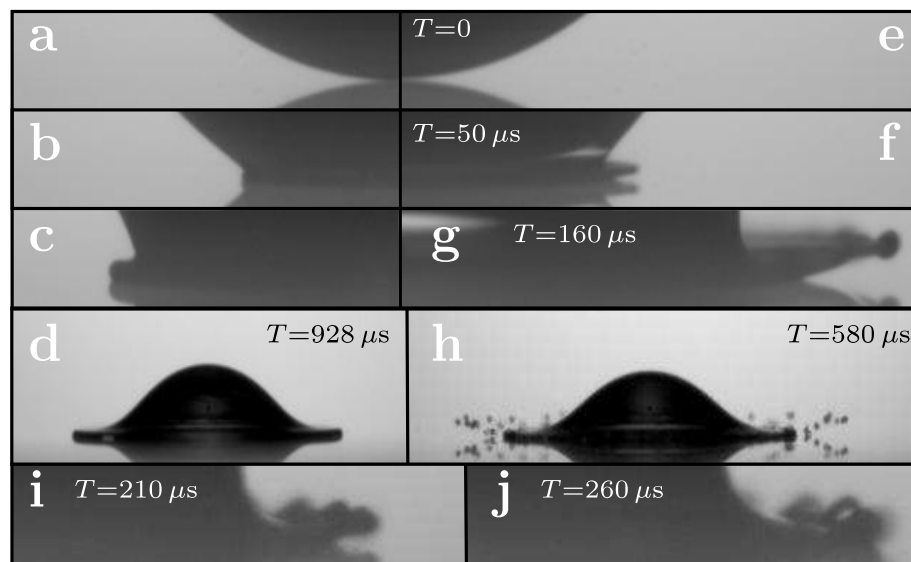


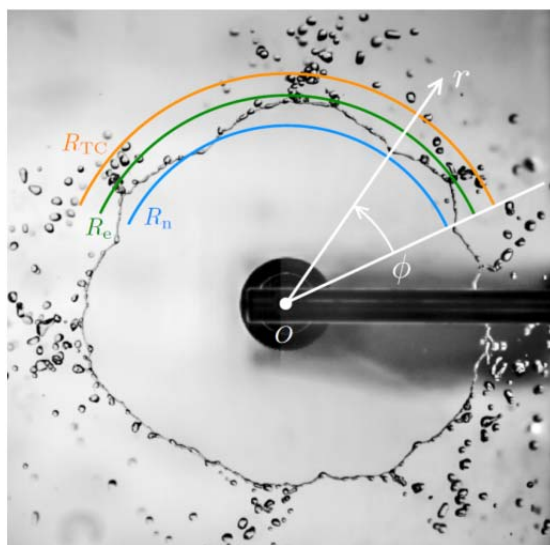
Figure 1: (a)–(h): Sequence of events after the impact of an ethanol droplet of radius $R=1.04$ mm for two different impact velocities, $V=1.29$ m/s (1(a)–(d), left) and $V=2.28$ m/s (1(e)–(h), right). The drop simply spreads over the substrate for the smaller value of V but breaks into tiny drops, violently ejected outwards, for the larger impact velocity. Note from images 1(f)–(g) that the lamella dewets the substrate before creating the splash depicted in Fig. 1(h). The sequence of events represented in Figs. 1(i)–(j), for which $V=2.01$ m/s, illustrates the existence of an intermediate range of impact velocities for which the lamella firstly dewets the solid to contact it again as a consequence of the radial growth of the edge of the lamella. The splash threshold velocity corresponding to these experiments is $V=2.19$ m/s. The times in 1(a)–(c) are identical to those corresponding to images 1(e)–(g).

On the cusps bordering liquid sheets

José Manuel Gordillo^a, H. Lhuissier^b & E. Villermaux^c

The edge of stationary, radially expanding liquid sheets or receding rims bordering plane sheets is naturally indented. It presents a collection of cusps at the extremity of which the liquid constitutive of the sheet concentrates, and is expelled. We give an experimental description of these cups for a stationary, flat, non viscous Savart sheet. We demonstrate how these cusps are the structures which accommodate for both mass and momentum conservation at the sheet edge, we compute their shape, their number around the sheet, and the remnant momentum carried by the ejected liquid.

Indeed, in a seminar paper, Taylor¹, proposed that the maximum radial extension of the expanding sheet created after the normal impact of a jet of diameter d and velocity u against a solid substrate, is given by $R_{TC} = \frac{\rho u^2 d^2}{16\sigma} = \frac{We}{16} d$ with σ the interfacial tension coefficient and ρ the liquid density. If this simple picture offers a good representation of the typical size of the sheet and of its dependence on We , it disregards the following facts: i) that the sheet is not circular since it possesses natural indentations bordering the sheet as it is illustrated in figure 1, ii) that the liquid is expelled with a non vanishing remnant radial momentum from the sheet edge and iii) that the actual radial extension of the sheet is smaller than R_{TC} . Here we provide with a model which faithfully reproduces all experimental observations and, thus, corrects the classical interpretation of Savart's experiments firstly given by Taylor.



^a Área de Mecánica de Fluidos, Departamento de Ingeniería Aeroespacial y Mecánica de Fluidos, Universidad de Sevilla, Avenida de los Descubrimientos s/n 41092, Sevilla, Spain. ^b Université Paris Diderot, CNRS, Matière et Systèmes Complexes UMR 7057, 75205 Paris, France. ^c Aix Marseille Université, CNRS, Centrale Marseille, IRPHE UMR 7342, 13384 Marseille, France.

¹ Taylor, G.I., (1959) Proc. R. Soc. A 253 (1274), 296-312.

Figure 1: Snapshot illustrating that the actual shape of a Savart sheet presents indentations at its edge and that the radial extension is smaller than that predicted using Taylor's description

Walking droplets: Limitations of the quantum analogy

Sonja Rosenlund Ahl^a, Anders Andersen^a, Jacob Madsen^a, Christian Reichelt^a,
Clive Ellegaard^b, Benny Lautrup^b, Mogens T. Levinsen^b and Tomas Bohr^a

In a series of recent papers Yves Couder and collaborators have explored the dynamics of walking droplets on the surface of a vibrated bath of silicon oil and have demonstrated a close analogy to quantum phenomena such as orbital quantization¹. Indeed the walking droplet together with the surface wave that it excites seems to be very similar to the pilot wave interpretation of quantum mechanics envisaged by de Broglie². Furthermore, Couder and Fort³ have created a double-slit experiment with walking droplets, where an interference pattern similar to the quantum version is found even though it is possible to follow the path of each droplet and unambiguously determine which slit it goes through, something which in quantum mechanics would be ruled out. However, we have repeated the experiment (shown in Figure 1) and we are not able to reproduce this interference pattern.

To explore theoretically the possibilities and limitations of this experimental quantum analogue we set up a simple model by introducing a source term in the time-dependent Schrödinger equation. This source term represents a localised particle which generates a wave-field while simultaneously being guided by the wave. We show that this model reproduces confined quantum phenomena such as orbital quantization. However, we point out that such a model in general is unable to reproduce the precise phase relations that are essential to quantum phenomena. In particular, we introduce a double-slit thought-experiment with an additional splitter plate that separates the paths leading to each of the two slits, and we argue that the appearance of an interference pattern in our model depends sensitively on the length of the splitter plate, while only the amplitude of the pattern changes with the length in standard quantum mechanics. Therefore we conclude that while the walking droplets serve as a quantum analogy for several experiments, it is not possible to reproduce the full range of quantum phenomena in this way.

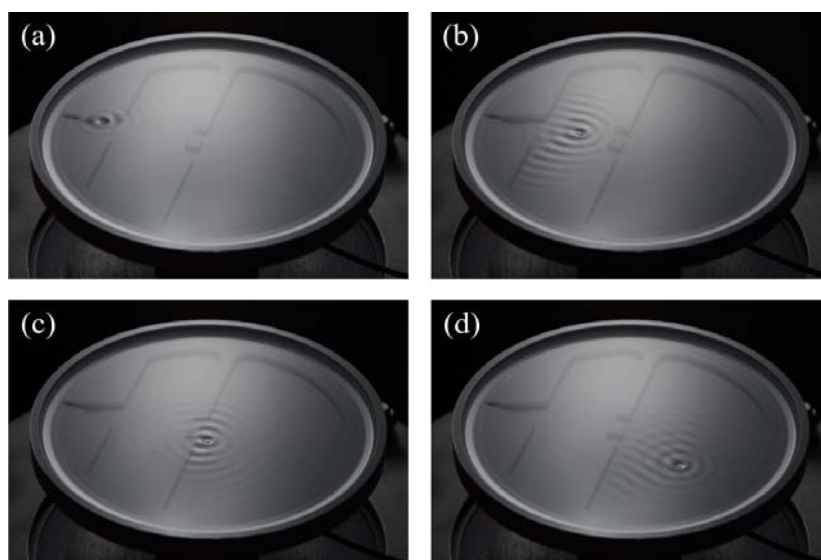


Figure 1: Snapshots at subsequent times of our double-slit experiment with walking droplets.

(a)-(b) The droplet is propelled by its own wave-field towards a barrier with two slits. (c) The droplet follows a well-defined path through one of the slits whereas part of the wave-field simultaneously goes through the other slit. (d) After passage the droplet moves along a deflected path.

^a Department of Physics, the Technical University of Denmark

^b The Niels Bohr Institute, University of Copenhagen, Denmark

¹ Fort et al., *PNAS* **107**, 17515 (2010); Harris et al., *Phys. Rev. E* **88**, 011001 (2013); Perrard et al., *Nature Comm.* **5**, 3219 (2014)

² de Broglie, *Ann. Fond. Louis de Broglie* **12** 4 (1987)

³ Couder and Fort, *Phys. Rev. Lett.* **97**, 154101 (2006)

Drop impact of a dispersion: Splashing suppressed at higher impact velocities

M.-J. Thoraval^a, F. Boyer^a, E. Sandoval Nava^a, F. Dijkstra^a, D. Lohse^a and J. Snoeijer^a

Previous studies have shown that splashing is always expected above an impact velocity threshold for a liquid drop impacting on a solid surface^{1,2}. We show here a surprising example where this behaviour can be modified by adding nanoparticles in the droplet. At low impact velocities, the droplet spreads on a smooth glass surface. By increasing the impact velocity, a first transition is observed towards splashing. However, this splashing occurs only for a limited range of impact velocities. When the impact velocity is further increased, a second transition is observed, above which no splashing is observed (Fig. 1).

By using high-speed imaging, we systematically explore the effect of the nanoparticles concentration on the splashing transitions. The geometry of the splashing changes completely between the pure solvent and the dispersion. A corona splash is observed for the pure solvent, similar to the splash of an ethanol droplet. On the other hand, the Silver dispersion splashes horizontally (Fig. 1). This difference is interpreted by a change of viscosity of the solution by the addition of nanoparticles¹. This is verified by comparing to Newtonian liquids with similar properties.

However, the second transition to non-splashing cannot be explained by the Newtonian properties of the liquid. We give some possible interpretation of this striking phenomenon.



Figure 1: Drop impact of a Silver nanoparticles dispersion on a smooth glass plate. The impact velocity increases from left to right: 1.57 m/s, 2.45 m/s, 2.68 m/s.

^a Physics of Fluids Group, University of Twente, P. O. Box 217, 7500 AE Enschede, The Netherlands

¹ Driscoll, Stevens and Nagel, *Phys. Rev. E* **82**, 036302 (2010).

² Thoroddsen, Takehara and Etoh, *J. Fluid Mech.* **706**, 560-570 (2012)

Modeling evaporation of droplets on a heated plate

A.-L. Ljung^a, T.S. Lundström^a

Droplets evaporating on a hot surface have a wide area of application including drying of dishes, cooling of electronics and drying of paint. Questions are addressed both towards increasing the drying rate as well as on how to control the deposition of particles suspended in the fluid. Uneven distribution of particles in the droplet could for example lead to unwanted marks and patterns. It is therefore important to investigate how the drying rate and deposition mechanisms can be controlled.

This work aims to investigate how the external flow around a droplet influences the internal flow pattern and evaporation rate. Natural convection in the external flow arising from the heated plate is considered and with aid of numerical simulations, the influence of the heat and mass transfer boundary condition at the droplet surface is examined. Average and local heat transfer coefficients at the surface are studied with aim to determine its effects on the internal flow. The separated influence of Marangoni effects, natural convection and conduction inside the droplet is considered. The validity of the heat and mass transfer analogy at the droplet surface is furthermore examined. The heat and mass transfer analogy need to be deliberated when the evaporation is dominated by density differences rather than temperature differences and the numerical results show this transition in detail.

Results show that the application of a local heat transfer boundary condition, when compared to an averaged condition, is important only if the internal velocity of the fluid inside the droplet is small. If the surface tension is high, i.e. if the flow is dominated by Marangoni convection, the surface temperature is instead controlled by the internal mixing rather than the local heat transfer. For the conditions studied here, Marangoni convection is dominating and will enhance the drying rate when compared to the influence of conduction and natural convection. Good agreement between the heat and mass transfer analogy and Fick's law is furthermore shown already at small temperature differences when natural convection is considered.

^a Dep. of Fluid and Experimental Mechanics, Luleå University of Technology, SE- 971 87, Luleå, Sweden

Radially forced parametric oscillations of liquid drops

L. S. Tuckerman^a, A. M. Juric^b, A. Ebo Adou^{a,d}, J. Chergui^d, S. Shin^c & D. Juric^d

We consider the problem of a spherical viscous liquid drop subjected to an oscillating radial acceleration surrounded by a gas or liquid of different density and viscosity. The resulting nonlinear behaviour is of interest to researchers in pattern formation and dynamical systems as well as having practical application over a wide variety of scales from nanodroplets to astroseismology.

Generalizing the Kumar & Tuckerman¹ Floquet solution to a spherical interface, we present a linear stability analysis for the appearance of standing waves. We linearize the governing equations about the state of rest with a poloidal-toroidal decomposition for the internal velocity field, and we decompose deformations of the interface as spherical harmonics $Y_m^\ell(\theta, \phi)$. The stability tongues presented in Fig.1 correspond alternately to subharmonic (SH) and harmonic (H) responses.

We also carry out full three-dimensional numerical simulations using the parallel 3D two-phase flow code, BLUE³, and recover the degree l of the harmonics predicted by the Lamb² dispersion relation for an ideal drop. We are investigating the behaviour in the far nonlinear regime as shown in the snapshot at the bottom of Fig.1.

^a PMMH (UMR 7636 CNRS-ESPCI-UPMC Paris 6-UPD Paris7), 10 rue Vauquelin, 75005 Paris, France

^b Centre National d'Enseignement à Distance

^c Department of Mechanical and System Design Engineering, Hongik University, Seoul, 121-791 Korea

^d LIMSI (UPR 3251 CNRS Univ. Paris Sud Paris XI) BP133, Rue J. von Neumann, 91403 Orsay, France

¹ K. Kumar & L.S. Tuckerman, *J. Fluid Mech.* **279**, 49-68 (1994)

² H. Lamb, *Hydrodynamics*, Cambridge University Press (1932), p.475

³ S. Shin, J. Chergui, D. Juric, A. Farhaoui, L. Kahouadji, L.S. Tuckerman, N. Périnet, in *8th Int. Conf. on Multiphase Flow*, Jeju, Korea (2013).

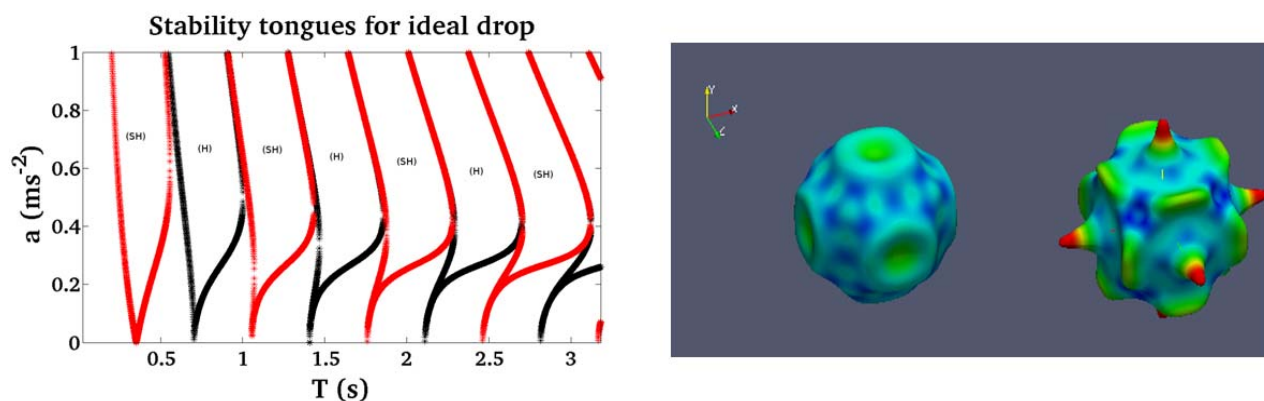


Figure 1: Left: Stability tongues for ideal drop. Right: Two snapshots from a three-dimensional numerical simulation using the code BLUE for $T = 0.06s$ and at a high acceleration of $a=20m/s^2$. The drop surface is colored by the velocity on the interface.

Microfluidics

Transient response of a microcapsule flowing through a sudden expansion

A.-V. Salsac^a, B. Nosengo^a, E. Leclerc^a and D. Barthès-Biesel^a

Microcapsules consisting of a liquid droplet enclosed by a thin polymerized membrane are commonly encountered in nature (cells) or in industrial process (pharmaceutical, cosmetic or food products). When the capsules have a diameter of order a few tens of micrometers, assessing the mechanical properties of the membrane is very difficult. We have designed a novel method¹ based on the measurement of the steady velocity and deformed profile of a capsule flowing in a square section microfluidic tube. The method enables the characterization of the elastic surface shear modulus G_s of the capsule membrane, but does not provide information on eventual viscoelastic properties.

We present a new experiment, where the transient response of a capsule is measured as it flows through a sudden expansion. The initially spherical capsules (mean diameter $d = 60 \mu\text{m}$) have a polymerized ovalbumin membrane and contain glycerol. They are suspended in the same glycerol solution (viscosity $\mu = 0.74 \text{ Pa.s}$) and are forced to flow through a square section microfluidic pore ($50 \times 50 \mu\text{m}$) followed by an expansion ($100 \times 50 \mu\text{m}$), where the depth of the channel is $h = 50 \mu\text{m}$. The successive profiles of a capsule are observed by means of a high-speed video camera mounted on a microscope (Figure 1).

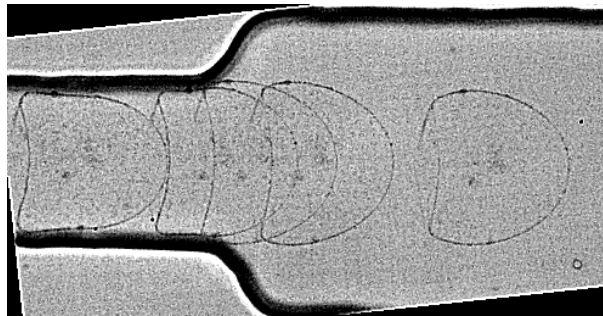


Figure 1: Time-evolution of the shape of a capsule flowing through a sudden expansion.

From the profile in the square channel, we can infer a mean value $G_s = 0.05 \pm 0.005 \text{ N/m}$ following the method described by Hu et al. (2013)¹. We then follow the successive deformations of the capsule as shown in figure 1. When entering the expansion, the capsule slows down and expands laterally, until it reaches a steady state, which is not necessarily spherical if the capsule diameter is larger than the channel height. We find that there are two characteristic times. The first one $\tau_1 = \text{O}(5\text{-}6 \text{ ms})$ corresponds to the capsule exit from the confined square section part. It is of the same order as the relaxation time of a deformed capsule in an unbounded motionless medium. The second time $\tau_2 = \text{O}(7\text{-}15 \text{ ms})$ corresponds to the response time of the capsule to the flow conditions in a rectangular channel, where friction effects with the wall are non negligible.

Using a full numerical model of the flow of a capsule in a square or rectangular channel, we can then relate τ_2 to the intrinsic physical properties of the capsule (size, membrane elastic modulus and internal viscosity).

^a Biomechanics and Bioengineering Laboratory (UMR CNRS 7338), Université de Technologie de Compiègne, BP 60319, 60203 Compiègne, France

¹ Hu et al. *Phys. Rev E*. **87**, 063008 (2013)

Capillary gas rivulets: can increasing viscous forces lead to instability in a capillary flow?

A. Said Mohamed^a, Miguel A. Herrada^a José M. Montanero^b and Alfonso M. Gañán-Calvo^a

A novel microfluidic technique has been recently proposed to produce microbubbles.¹ In this technique, a gaseous stream is injected through a T-junction into a channel transporting a liquid current. The gas adheres to a hydrophobic strip printed on the channel surface. When the gas and liquid flow rates are set appropriately, a gaseous rivulet flows over that strip. The rivulet breaks up downstream due to a capillary pearling instability, which leads to a monodisperse collection of microbubbles. Motivated by this application, we here analyze the instability of a gaseous rivulet coflowing with a liquid current in a quadrangular microfluidic channel. The results essentially differ from those of cylindrical jets because the contact-line-anchorage conditions affect fundamentally the rivulet's instability nature. The temporal stability analysis shows that the rivulet becomes unstable not only for (unperturbed) contact angles larger than $\pi/2$ (as could have been expected) but also for values smaller than that angle. Interestingly enough, the maximum growth factor exhibits a non-monotonic dependence with respect to the Reynolds number (i.e., the viscosities). In fact, there are finite intervals of that parameter where the fluid system becomes unstable, while all the perturbations are damped outside those intervals. The spatio-temporal analysis of the instability region shows the existence of both convective and absolutely unstable behaviors. For sufficiently large contact angles, convective instability appears only if both the Reynolds and Weber numbers (approximately) exceed their corresponding critical values. These values increase with the contact angle. For low contact angles, absolute instability yields convective instability as the Weber number increases, as occurs with cylindrical jets. When viscous stresses dominate inertia, unstable waves are convected downstream.

^a E.S.I, Universidad de Sevilla. Camino de los Descubrimientos s/n 41092, Spain

^b Dep. Ingeniería Mecánica, Energética y de los Materiales, Universidad de Extremadura, E-06071 Badajoz, Spain

¹ Herrada et al. Phys. Rev. E **88**, 033027 (2013)

Rapid emulsification technique using cavitation bubbles in microfluidics

T. Tandiono^a, S. W. Ohl^a, E. Klaseboer^a, D. S. W. Ow^b, A. B. H. Choo^b, F. Li^c, C. D. Ohl^c

Emulsions have been widely used in many applications due to its ability to transport hydrophobic substances in water and vice versa. The applications may include surface treatments, food and cosmetic industries, and drug carriers. The formation of emulsions (emulsification) is basically a shear rupturing mechanism of two immiscible liquids, leading to the fragmentation of one liquid in the other (Leal Calderon et al., 2007). In microfluidics, emulsions can be produced by forcing the dispersed phase into the continuous phase through microchannels. Since in most cases no active force is applied to the fluids to create high shear flow, the droplet size and the production rate depends strongly on geometry of the microchannel, pressures/flowrate, and surface tension of the fluids. Despite its ability to produce monodisperse droplets, the production rate of this method is relatively low. Here, we propose a rapid method to form an emulsion on a nano/microfluidic scale involving the application of ultrasound to a micro-chamber containing two immiscible fluids and a gas. The ultrasound is used to create intense cavitation in a microfluidic channel by driving gas-liquid interfaces into nonlinear oscillation to entrap gas bubbles which later serve as cavitation nuclei (Tandiono et al., 2010). The bubbles oscillate violently, resulting in high shear stress region at the vicinity of the bubbles. Intense mixing and emulsions from two immiscible liquids can then be achieved within a very short duration, as shown in Fig. 1. Several mechanisms for the formation of emulsions are identified using high-speed imaging technique, for example: through (i) the rupture of thin film of dispersed phase due to the built-up shear stress and fast liquid jetting at the interfaces, (ii) fragmentation of large droplets due to the violently oscillating bubbles.

^a Institute of High Performance Computing, 1 Fusionopolis Way 16-16 Connexis, Singapore 138632, SG

^b Bioprocessing Technology Institute, 20 Biopolis Way #06-01 Centros, Singapore 138668, SG

^c Division of Physics and Applied Physics, School of Physical and Mathematical Sciences, Nanyang Technological University, Singapore 637371, SG

¹ Leal Calderon et al., *Emulsion science: basic principles*, Springer (2007).

² Tandiono et al., *Lab Chip* **10**, 1848-1855 (2010).

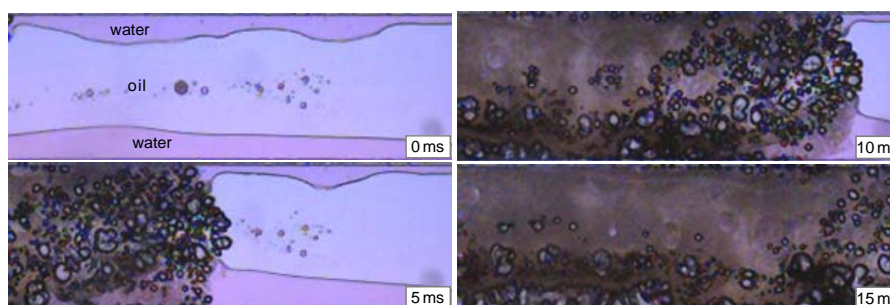


Figure 1: Inertial cavitation bubbles moving along water-oil interfaces in a microchannel forming emulsions.

Electrokinetic microflows at charge selective nano-junctions

A.M. Benneker^a, E. Karatay^a, R.G.H. Lammertink^a and P.A. Tsai^a

We experimentally examine hydrodynamics and ion transport of salt solutions at micro-nanochannel interfaces under a DC electric field. Nanochannels act as a charge selective interface as a result of their miniature sizes, allowing for the overlapping of electric double layers. Due to the charge selective nature of the nano-junctions, counter-ions are depleted at the entrance and enriched on the opposite sides of the junctions, yielding ion concentration polarization (ICP). This ion-selectivity of micro-nano junctions can result in applications of desalination and purification^{1,2,3}. The current research aims at the systematic experimental investigation of microfluidic electrokinetic flows in systems containing nanojunctions acting as the charge selective interface.

Experiments are conducted using glass microchips, shown in Figure 1a. The characteristic dimensions of the microchannel are 30 x 20 μm (in width and height). Ten nanochannels with characteristic dimensions of 2 μm x 10 nm (in width and height) are wet-etched and connected between the main microchannels. Ti/Pt electrodes are equipped for the application of an electric field and I-V characterization. The lower channel is electrically grounded while a potential is applied to the three electrodes in the upper channel. Flow rate (Φ_v) through the microchannels is controlled using a syringe pump. Electrical measurements and I-V characterization is done using a Keithley electrometer controlled by a LabVIEW program. Chronopotentiometry is also used for the characterization of the electrical response at a fixed current. Charged fluorescent dyes are used for visualization of ion concentrations in the microfluidic channels. Hydrodynamic flow is visualized by means of micro-PIV.

The typical I-V response of 1mM NaCl solution in the micro-nano junctions is shown in Figure 1b. The inset shows the corresponding conductance as function of the applied voltage, revealing a transition point towards an over-limiting current. Time-dependence of the electric current was measured at each applied voltage. The time-series data of current show an exponential decay below a certain critical voltage V_c , while a growth above V_c . Our results provide insights into the mechanism and control of ICP for separation and purification in microfluidics.

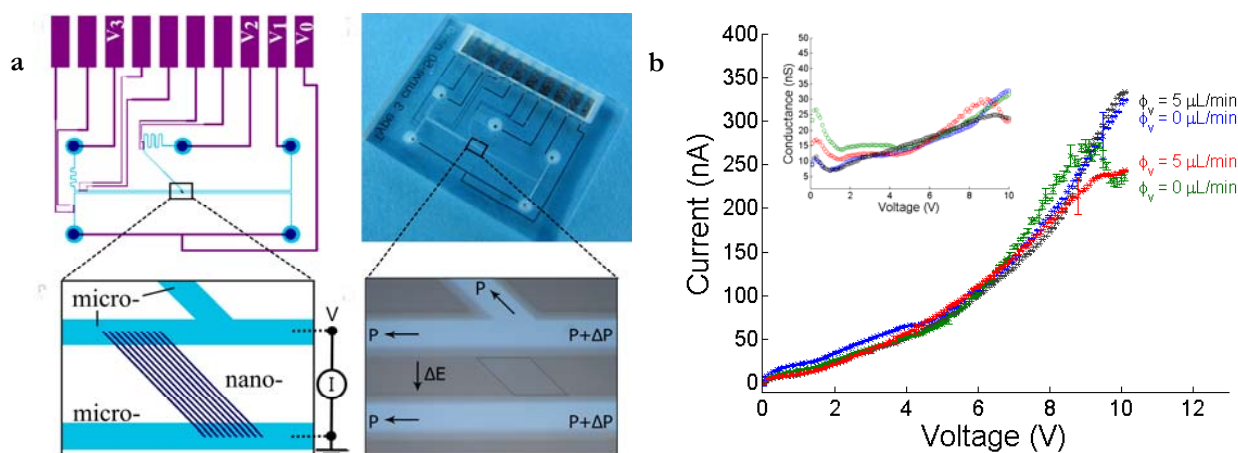


Figure 1 (a) Images of the experimental fluidic chips with micro-nano junctions. (b) Typical I-V response for the microfluidic devices shown in (a) under different applied voltages, with or without a pressure-driven flow, Φ_v .

^a Soft Matter, Fluidics and Interfaces – MESA+ Institute for Nanotechnology, University of Twente, The Netherlands

¹Kim et al., *Nature Nanotechnology* **5**, 297 (2010).

²Nikonenko et al., *Advances in Colloid and Interface Science* **160**, 101 (2010)

³Zangle et al., *Chemical Society Reviews* **39**, 1014 (2010).

Wall shear stress measurements in microfluidic systems

J. Tihon^a, V. Penkavova^a, P. Stanovsky^a, J. Vejrazka^a

The electrodiffusion technique¹ has been mostly used for the near-wall flow diagnostics on large scales. A novel technique for fabrication of plastic microfluidic systems with integrated metal microelectrodes (called technique of sacrificed substrate²) enables us to produce microfluidic devices with precisely shaped sensors for wall shear stress measurements. Several micrometer thick gold sensors built-in into a plastic substrate exhibit good mechanical resistance and smoothness. They can be used for flow investigation in various microfluidic systems (e.g. in complex channel geometries often used as micromixers, in multiphase microfluidic systems dealing with bubbles and drops.)

Proper functioning of prepared microsensors has been first tested in calibration experiments. A chip with an array of 20 gold sensors (160 microns strips separated by 40 microns insulating gaps) serves as a top cover (roof wall) of a microchannel (800 microns in depth). Water with a small addition equimolar potassium ferrocyanide and ferricyanide has been used as a suitable electrochemical system for the electrodiffusion measurements. The polarization curve with a distinct limiting diffusion current plateau, the cubic root dependence between the measured limiting current and applied wall shear stress, and the transient current response following the Cottrell asymptote have been observed. The calibration experiments with well controlled temperature have been carried out to reveal that the diffusion coefficient of active ions is strongly dependent on temperature and the measured data can be fitted by an exponential relationship similar to the Arrhenius equation.

After calibration measurements, the chip with microsensors has been applied in two experiments. First, it has been mounted into a microchannel provided by a step change in its height from 400 (inlet section) to 800 microns (outlet section). The axial profiles of wall shear stresses have been measured for different Re values. The different flow-recirculation zones have been identified downstream the step and high magnitudes of near-wall flow fluctuations observed at reattachment regions. The characteristic frequencies of these pulsations have been provided. Second, the wall shear stress corresponding to the translation of a single air bubble by water flow in a microchannel has been investigated. The typical trace of wall shear stress induced by the bubble movement has been revealed.

^a Institute of Chemical Process Fundamentals, Academy of Sciences of the Czech Republic, Rozvojová 135, 16502 Prague 6, Czech Republic (e-mail: tihon@icpf.cas.cz).

¹ T.J. Hanratty, J.A. Campbell, *Fluid mechanics measurements* (Washington, Hemisphere, 1983).

² W. Schrott, M. Svoboda, Z. Slouka, D. Snita, *Microelectron Eng*, 86, 1340 (2009).).

This work was supported by the Grant Agency of the Czech Republic (Project No. P101/12/0585).

Self-propulsion of autophoretic particles at finite Péclet number

S. Michelin^a, E. Lauga^b and D. Bartolo^c

Autophoretic particles are able to self-propel in low-Reynolds-number flows using short range interactions between their surface and solute molecules. This solute is either produced or consumed by chemical reaction catalyzed at the particle's surface. The resulting motion is a fundamental example of synthetic particles achieving force-free and torque-free propulsion and requiring no external forcing (e.g. magnetic/electric field, chemical/temperature gradient).

In the well-studied diffusive limit, the solute distribution around the particle is completely decoupled from the hydrodynamics problem. When advection is no longer negligible (e.g. for larger or more chemically-active particles), the solute dynamics is fully coupled with the phoretic flows generated by the solute-particle interactions. In this work, we investigate the effect of this advection on the dynamics of a single spherical particle. We show that such advective effects may enhance the propulsion velocity for classical Janus particles that consist of two chemically-different hemispheres (one active and one passive). Also, particles with isotropic surface properties are unable to propel in the diffusive limit. We show here that advective effects and the nonlinear coupling of the solute dynamics to the phoretic flows along the boundary may lead to a symmetry-breaking event and self-propulsion of such systems (Figure 1).

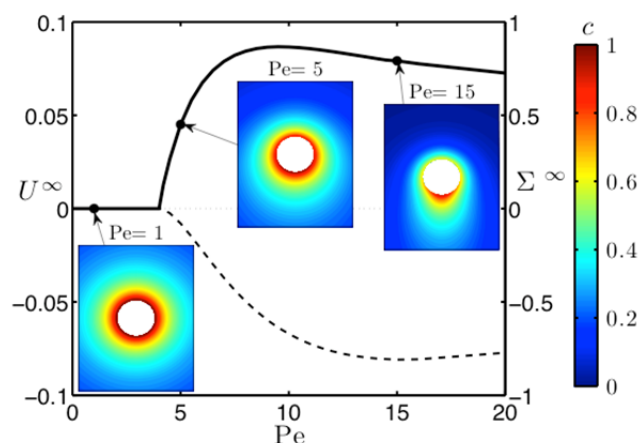


Figure 1: Evolution of the self-propulsion velocity of an isotropically-active phoretic particle with advective effects measured by the Péclet number, Pe . The evolution of the resulting stresslet and solute concentration around the spherical particle is also shown¹.

^a LadHyX - Département de Mécanique, Ecole Polytechnique - CNRS, 91128 Palaiseau Cedex, France

^b Department of Applied Mathematics and Theoretical Physics, University of Cambridge, Cambridge, CB3 0WA, United Kingdom

^c Laboratoire de Physique, Ecole Normale Supérieure de Lyon, Université de Lyon - CNRS, 69007 Lyon, France

¹ Michelin, Lauga & Bartolo, *Phys. Fluids*, **25**, 061701 (2013).

Dynamics of an incompressible fluid film bearing with nano scale gap

N. Bailey^a, S. Hibberd^a and H. Power^b

An incompressible fluid flow model for an axisymmetric fluid-lubricated bearing containing a rigid parallel or coned rotor is derived, using a modified Reynolds equation for the thin-film dynamics in the continuum limit. Mathematical and numerical modelling is applied to the coupled processes of the pressurised fluid flow through the bearing and the axial motion of the rotor and stator. The stator is modelled as a spring–mass–damper system which responds to the forced axial rotor displacement through the film dynamics. The dynamics of a fully coupled, unsteady bearing motion and associated forcing of the rotor with axial periodic oscillations are studied, with the numerical scheme solving for the periodic time dependent face clearance. Results obtained for increasing amplitude of rotor oscillations, show the bearing faces can become very close together but contact does not occur, even when the amplitude is twice that of the equilibrium film thickness².

However for large rotor amplitudes the bearing gap becomes very small, raising concerns that the continuum model may become invalid. Therefore, the model is extended to include nano effects by incorporating a slip length shear condition on the bearing faces, with a modified Reynolds equation derived with nano effects. The fully coupled unsteady bearing motion is studied for a range of slip lengths and configurations, focusing on bearing operation under extreme conditions to examine if face contact is possible for a bearing with a parallel or coned rotor. Results show that incorporating nano effects in a parallel bearing gives no contact for a finite slip length but a coned bearing can have contact between the faces.

Due to the nature of nano flow, the magnitude of slip on the bearing face is not physically quantifiable. An uncertainty quantification approach is adopted to find the probability the bearing gap becomes less than or equal to a given tolerance when the slip length has a fixed value which is not known with certainty. This lack of knowledge is modelled using a subjective interpretation of probability where the slip length is considered as a random variable. Describing the slip length by a suitable probability density function and using the deterministic relationship between the minimum face clearance and slip length, the cumulative density function can be calculated giving the probability a given gap tolerance has been reached.

The amplitude of the forced rotor has in general an uncertain aspect in practical applications. Therefore uncertainty quantification is investigated when both the slip length and rotor amplitude have fixed values which are not known with certainty to find the probability a given gap tolerance is reached.

^a School of Mathematical Sciences, University of Nottingham, Nottingham, NG7 2RD, UK

^b Faculty of Engineering, University of Nottingham, Nottingham, NG7 2RD, UK

¹ Bailey et al., *IMA J. Appl. Math.*, doi: 10.1093/imamat/hxt002 (2013)

Wall nanoconfinement in microchannel

B. Mele^a and R. Tognaccini^a

A great amount of experiments and theoretical analysis concerned the flow of immiscible fluids in circular pipes, typically oil and water mixture. They were performed until the early sixties of the last century in order to classify the flow patterns and characteristics as function of the flow parameters (Reynolds number, capillary and Bond numbers, viscosity and density ratio etc...). These studies were oriented in particular to petroleum industry applications in order to improve the liquid transportation. Following the review of Joseph et al.¹ dedicated to the lubricated flow in an oil core, called core-annular-flow (CAF), there is a kind of "gift of nature in which the water migrates into the region of high shear at the wall of the pipe where it lubricates the flow". The studies of Joseph extended the stability analysis of Hickox² showing that, while the configuration with the less viscous fluid (typically water) at the core is always unstable, the configuration with the more viscous fluid at the core can be stable. He found that the stability of such configuration depends on the ratio of the core radius respect to the radius of the pipe giving the minimum and maximum critical Reynolds number as function of viscosity ratio, surface tension and density ratio.

In the last decade a renewal interest on the subject has grown due to several applications in microfluidic technology. A huge literature concerning two-phase flows in microchannels can be found. Several experimental investigations and analyses of the flow pattern have been devoted to the production of micro droplets, slugs and bubbles in microfluidic device. Such configurations are usually obtained confining the less viscous fluid at the core using the natural tendency of a jet to break-up due to the Rayleigh-Plateau instability. Guillot et al.³ and Colin and Tacogne⁴ studied the stability of bifluid jets in microchannels confirming that the confinement of the less viscous fluid at the core is always unstable.

Therefore a technological problem arises in microfluidic applications when a thin film (50-10 nanometres) is required. A solution that can be derived from the paper of Colin and Tacogne⁴ is to adopt pipe lengths shorter than a critical length related to the more unstable wave. However this solution clearly limits the length of the desired jet.

In this paper we propose, as alternative, to adopt the same gift of nature highlighted by Joseph in petroleum applications. Indeed we present numerical simulations in which the thin confined layer is obtained at the wall instead of the core.

Preliminary numerical simulations of two immiscible fluid in micropipes have been performed first to reproduce the experiments and theoretical analyses known in literature. Then several numerical solutions with different mass flow rate, viscosity and density ratio have been performed to verify the possibility to obtain the desired thickness layer near the wall with feasible conditions in terms of pressure gradient, mass flow rate and viscosity ratio. Analyses of the influence of initial and inflow conditions are also proposed giving interesting information for further experimental investigations.

^a Dipartimento di Ingegneria Industriale, Università di Napoli *Federico II*, Naples, Italy

¹ Joseph et al., *Ann. Rev. Fluid Mech.*, **29**, 1997.

² Hickox, *Phys. Fluids*, **14**, 1971.

³ Guillot et. al., *Phys. Rev. letters*, **99**, 2007.

⁴ Colin and Tacogne, *Eur. J. Mech. B/fluids*, **30**, 2011.

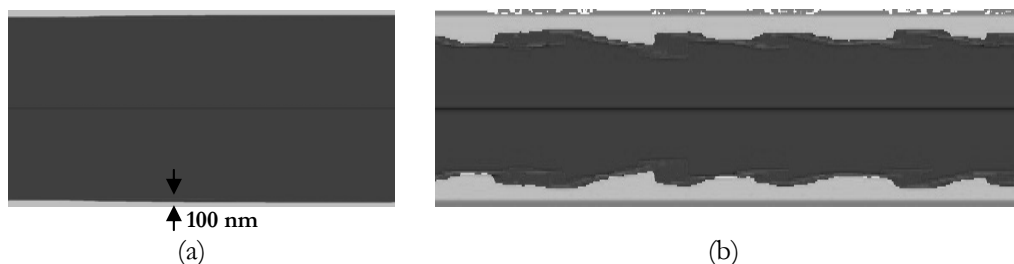


Figure 1: Numerical simulation of two phase flow in a micropipe ($D=500 \mu\text{m}$); black: oil, grey: water. (a): perfect CAF. (b): wavy CAF.

Unsteady regimes in a T-mixer

A. Fani^a, S. Camarri^b, M.V. Salvetti^b

T-shaped micromixers are commonly used in microfluidics to promote mixing between two fluid streams without any external energy supply; in this type of applications, two streams enter from the two opposite pipes (inlet pipes) and the mixture exits from the third pipe (outflow pipe). In this work we consider a T-mixer made by rectangular channels, and the aspect ratio of the inlet and outlet cross sections is equal to $AR_{in} = 0.75$ and $AR_{out} = 1.50$, respectively. The flow in micro T-mixers similar to the one considered here is characterized by several different regimes depending on the Reynolds number (Re , based on the hydraulic diameter of the outflow channel and on the inlet bulk velocity), the mixer geometry and the inflow conditions. At very low values of Re , the flow satisfies the same symmetries of the geometry. As Re exceeds a given critical threshold ($Re \cong 140$ for the considered configuration), the flow becomes steady and asymmetric. This regime, denoted in the literature as the engulfment regime, is characterized by a loss of symmetry in the outflow channel and by fluid elements of one stream reaching the opposite side of the channel. This leads to a considerable mixing efficiency, which motivates the interest in the literature for this particular regime. As Re exceeds a second critical value ($220 < Re < 230$), the flow becomes time-periodic and strongly asymmetric, and this is denoted as unsteady asymmetric regime (UAR). As Re is further increased ($Re \cong 400$), a different time-periodic regime is observed (unsteady symmetric regime, USR), characterized by a continuous and periodic switch from a symmetric configuration to a slightly asymmetric one that resembles the engulfment regime. These two unsteady regimes have only recently been observed in the literature^{1,2} and much less is known about their dynamics and features than for the steady regimes.

In the present work the unsteady flow regimes are investigated through direct numerical simulation (DNS) and by global stability analysis. The UAR and USR found in DNS are in good agreement with the results available in the literature for similar configurations. Their dynamics is characterized in details, for the first time, by analyzing the evolution of the three-dimensional vortical structures forming at the confluence of the two inlet flow streams. An example is shown in Fig. 1 for the UAR: Three-dimensional linear stability analysis is also used to characterize the instability leading to the UAR, which is interesting also for applications due to its high mixing efficiency. The critical Reynolds number and the instability frequency are in very good agreement with those found in DNS. The instability is further characterized by a sensitivity analysis, which allows the identification of the instability core, localized close to the confluence region between the inlet channels. Consistently with the flow dynamics observed in DNS, the core of the instability coincides with the region where the vortical structures typical of the analyzed flow regimes form. This information is useful to design control strategies aimed at promoting or delaying the onset of the UAR. In particular, the sensitivity analysis is specialized here to investigate the effect of a perturbation of the inlet velocity profile.

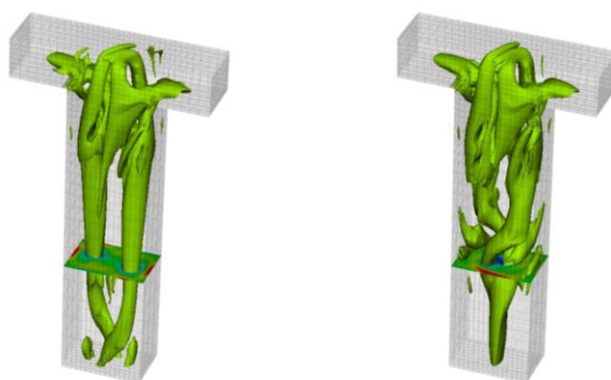


Figure 1: Vortices (λ_2 criterion) and vorticity distribution at two time instants in the UAR.

^a LFMI EPFL, Lausanne, Switzerland

^b Dipartimento di Ingegneria Civile ed Industriale, Università di Pisa, via G. Caruso 8, 56122 Pisa, Italy

¹Thomas et al., *Phys. Fluids* **22**, 013601 (2010).

²Galletti et al., *Chem. Eng. J.* **185**, 300 (2012)

Numerical simulation of a low-Reynolds number flow around a square cylinder controlled by means of plasma actuators

Yosuke Anzai^a, Hiroshi Naito^a and Koji Fukagata^a

Flow separation occurring around a square cylinder causes a pressure drop on the rear surface and vortex shedding in the wake, which eventually causes a drag increase, acoustic emissions and structural vibrations. Various types of flow controls, both passive and active controls, have been studied to remedy such problems.

In the present study, plasma actuators are applied to suppress the vortex shedding behind a square cylinder. The plasma actuator is an active control device, which has many advantages such as low mass and no moving mechanical part; therefore, it can possibly be used in a wide range of applications.

A flow around a square cylinder controlled using plasma actuators is numerically investigated by means of two-dimensional direct numerical simulation. The Reynolds number based on the cylinder diameter and the freestream velocity is set to be 100. Three different locations of plasma actuators on the cylinder surface, as shown in Fig. 1, and two different actuation amplitudes are investigated; the test cases are denoted as Case i-j, where i and j denote the location and the amplitude, respectively, with j = 2 being a stronger actuation.

The mean drag coefficient, C_D , and the root-mean-square of lift fluctuations, $C_{L,rms}$, are shown in Fig. 2. These quantities are found to reduce in some cases, accompanying a suppression of vortex shedding behind the square cylinder. Such an effect is most pronounced in Case 2, where the plasma actuators are installed on the rear surface to induce inward flows. In Case 2, the pressure differences between the front and the rear surfaces are reduced as compared to the uncontrolled case; the pressure fluctuations in the rear surface are also reduced due to the suppression of vortex shedding. The suppression of vortex shedding is observed to be due to a weakened interaction between two shear layers behind the cylinder. The flows induced by two actuators are observed to interact at the mid-section of the rear surface and generate the streamwise jet, which weakens the interaction between two shear layers.

^a Department of Mechanical Engineering, Keio University, Kohoku-ku, Yokohama 223-8522, Japan

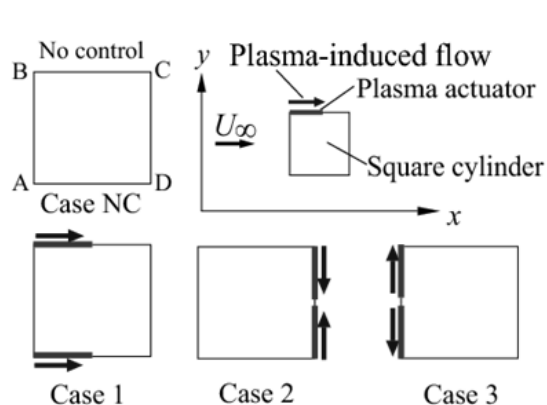


Figure 1: Locations of plasma actuators.

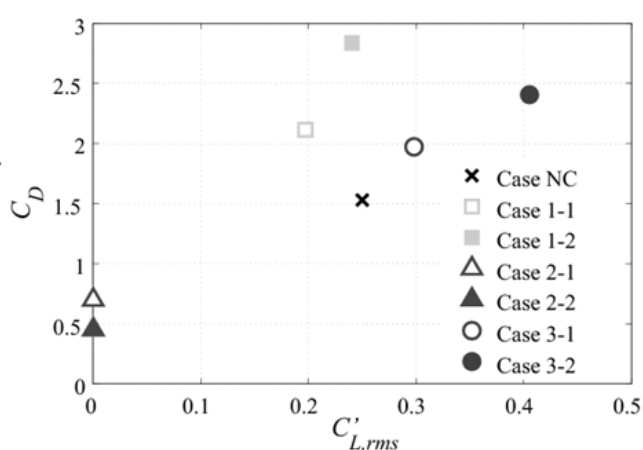


Figure 2: The RMS lift coefficient fluctuations $C_{L,rms}'$ and the drag coefficient C_D .

Acoustics

Asymmetric streaming as a mechanism for acoustic propulsion of small rigid bodies

F. Nadal^a and E. Lauga^b

Recent experiments showed that standing acoustic waves could be exploited to induce self-propulsion of rigid metallic particles in the direction perpendicular to the acoustic wave¹. We propose in this paper a physical mechanism for these observations based on the interplay between inertial forces in the fluid and the geometrical asymmetry of the particle shape. We consider an axisymmetric rigid near-sphere oscillating in a quiescent fluid along a direction perpendicular to its symmetry axis. The kinematics of oscillations can be either prescribed or can result dynamically from the presence of an external oscillating velocity field. Steady streaming in the fluid, the inertial rectification of the time-periodic oscillating flow, generates steady stresses on the particle which, in general, do not average to zero, resulting in a finite propulsion speed along the axis of the symmetry of the particle and perpendicular to the oscillation direction. Our derivation of the propulsion speed is obtained at leading order in the Reynolds number and the deviation of the shape from that of a sphere. The results of our model are consistent with the experimental measurements, and more generally explains how time periodic forcing from an acoustic field can be harnessed to generate autonomous motion.

^a CEA, 15 avenue des sablières CS 60001, 33116 Le Barp Cedex, France

^b Department of Applied Mathematics and Theoretical Physics, University of Cambridge, Center for Mathematical Sciences, Wilberforce Road, Cambridge CB3 0WA, United Kingdom

¹ W. Wang, L.A. Castro, M. Hoyos, and T.E. Mallouk. Autonomous motion of metallic micro-rods propelled by ultrasound. *ACS Nano*, **6** (7): 6122–6132, 2012.

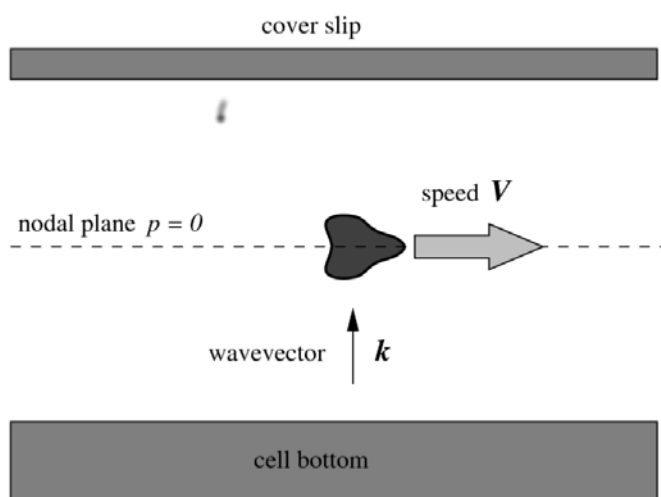


Figure 1: Sketch of the experimental situation. A micro-particle is trapped in the nodal plane (plane of zero pressure) of the first mode of an acoustic resonator. The particle moves in the plane under the effect of the net streaming flow.

Aeroacoustic analysis of the impinging tones in supersonic jets

G. Sinibaldi¹, L. Marino¹, G.P. Romano¹

Noise of impinging jets is one of the most interesting area in Aeroacoustics. This work is focused on the experimental analysis of acoustic and fluid dynamic fields of an under-expanded circular jet impinging on a plate perpendicular to the jet axis. The purpose is to contribute to the study of the discrete component of the noise which characterized these flows, i.e. the impinging tones. The measurements were carried out by means of microphones, Particle Image Velocimetry and pressure tabs. A wide range of nozzle pressure ratios (NPR) and nozzle-to-plate distances (h) was explored to obtain a complete analysis of the impinging tones.

Two sources of the discrete frequency perturbations were observed in the jet-plate configuration^{1,2}. These sources are the stand-off shock oscillation and the vortical instabilities development in the shear layer. Both the two sources are based on acoustic feedback. When the vortical instabilities at the shear layer are involved in noise generation, the acoustic feedback is between the plate and the nozzle lip. This is the same mechanism observed in subsonic impinging jet³. On the other side, when large self-excited stand-off shock oscillations are the source of the discrete tones, the acoustic feedback is between the plate and the shock.

The present investigation highlights different acoustic fields of an under-expanded impinging jet, that are related to modifications of the flow structure and lead to a change in the production of the impinging tones. In particular, by varying the nozzle pressure ratio, three different regions are identified. Figure 1 reports the Power Spectral Density PSD distribution obtained at the nozzle-to-plate distance equal to two nozzle exit diameters, i.e. $h/d=2$, in the three acoustic regions. The middle region, shown in Fig. 1(b), called “region of silence”, is characterized by absence of impinging tones and a significant reduction of the mean sound level. The two ranges of NPR which precede and follow the previous region, shown in Figs 1(a,c), named “pre-silence” and “post-silence” regions, well-defined impinging tones are present. The analysis of the experimental data enables to associate a different generating mechanism of the impinging tones in each of the extreme regions, i.e. the nozzle-plate feedback mechanism in the “pre-silence” region and the shock-plate feedback mechanism in the “post-silence” region. Moreover, the middle range of NPR can be considered as the region of transition where both the two mechanisms are damped.

¹ Dep. Mechanical and Aerospace Engineering, La Sapienza, Via Eudossiana 18, Rome, Italy

¹ Powell, *J. Acoust. Soc. Am.* **83**, 115 (1988).

² Henderson and Powell, *J. Sound Vib.* **168**, 307 (1993).

³ Tam and Ahuja, *J. Fluid Mech.* **214**, 67 (1990).

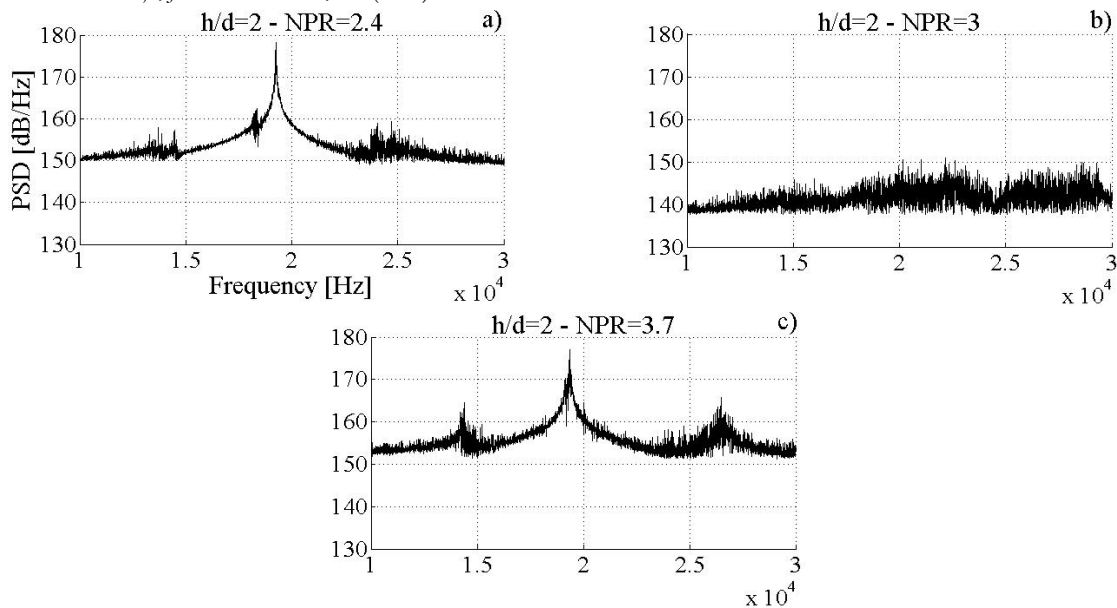


Figure 1: Power Spectral Density PSD distribution at the plate distance $h/d=2$ and at different values of NPR. a) NPR=2.4 (pre-silence region), b) NPR=3 (region of silence), c) NPR=3.7 (post-silence region).

Experimental investigation of transitional acoustic boundary layer in a cylindrical wave guide

I. Reyt^{ab}, H. Baillet^a, J.-Ch. Valière^a

Oscillating flow over a fixed wall is a configuration that occurs in number of fields such as coastal engineering or biomedical science. The boundary layer induced by the harmonic oscillation parallel to a fixed plane wall is usually called the Stokes boundary layer and the corresponding flow field is well described in the laminar case. The study of the transition from laminar to turbulent regime of oscillatory boundary layer has received relatively little attention but is particularly interesting because of its complexity as an unsteady boundary layer. Oscillations can be decomposed in decelerating phases (potentially unstable reverse flow) alternating with accelerating phases (stabilised flow).

In this experimental study, the oscillations are generated by means of acoustics sources coupled to both ends of a smooth cylindrical wave guide filled with air at atmospheric pressure. This allows the production of high acoustic levels at a fixed pulsation. Laser Doppler Velocimetry technique is used to measure particle velocity in the Stokes boundary layer. The evolution of the near wall velocity profile at different phases of the oscillation cycle is studied for increasing Reynolds number $Re_{\delta_v} = U_0 \delta_v / \nu$, with U_0 the amplitude of velocity oscillations in the core of the guide, δ_v the acoustic boundary layer thickness and ν the fluid kinematic viscosity. Results do not show the apparition of turbulent structures when the flow regime departs from laminar as described in the literature^{1,2} but an important change of shape of the velocity profile is observed as Re_{δ_v} is increased. The velocity profile close to the wall is shown by Figure1 for three different Re_{δ_v} at the phase of maximum velocity. This profile distortion is interpreted as the consequence of the development of a turbulent boundary layer whose thickness increases during the laminar to turbulent transition. From such approach a critical Reynolds number value of 245 for transition is estimated.

^a Institut Pprime, CNRS-Université de Poitiers-ENSMA, Dep. Fluids, Thermal and combustion sciences, Bat. B17, 6 rue Marcel Doré, 86073 Poitiers Cedex 9, France

^b Dep. DynFluid, Arts et Métiers ParisTech, 151 Bd. de l'Hôpital, 75013 Paris, France

¹ Merkli and Thomann, *J. Fluid Mech.* **68**, 567 (1975)

² Carstensen et al., *J. Fluid Mech.* **646**, 169 (2010)

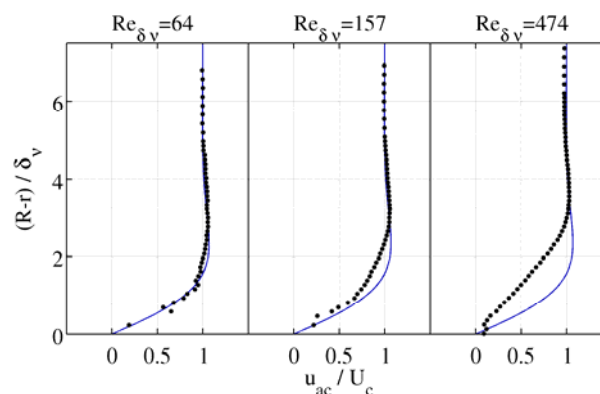


Figure 1: Velocity profiles at phase of maximum velocity for different Re_{δ_v} . (·) Measurements, (—) Laminar Theory.

Bifurcation control of thermoacoustic systems

P. Subramanian¹ and T. M. Schneider^{2,a}

Thermoacoustic systems consist of a source of unsteady heat release enclosed in an acoustic field. Instabilities arise in such thermoacoustic systems due to positive feedback between fluctuations in acoustic pressure and unsteady heat release rate [1]. During such instabilities, thermoacoustic systems display a wide variety of asymptotic dynamical behaviour; from steady states to chaotic trajectories. Thus the ability to control the nature and characteristics of thermoacoustic oscillations is a desired capability to prevent severe oscillations or even failure of parts.

Many thermoacoustic systems display the occurrence of a sub-critical Hopf bifurcation followed by a fold bifurcation. Occurrence of such hysteresis may cause sudden onset of high amplitude instability for the variation of a parameter, e.g. the amount of thermal driving in the system (K). We demonstrate that such a sudden onset can be avoided by changing the criticality of the Hopf bifurcation from sub- to super-critical using feedback control.

The ability to control the nature and characteristics of thermoacoustic oscillations can be achieved by suitably altering the bifurcation behaviour of the uncontrolled system. In order to analyse methods that modify bifurcation behaviour, we choose a well analysed representative thermoacoustic system of a horizontal Rijke tube. Its bifurcation behaviour has been previously documented [2]. Indeed, with suitable choice of linear feedback control, we are able to delay the onset of instability to higher thermal driving values as seen in Figure 1(a).

Suitable choice of feedback control can also be employed to change the nature of the primary instability from being sub-critical to supercritical as seen in Figure 1(b). We will discuss the design of suitable feedback control that can either delay the onset of or modify the nature of the ensuing thermoacoustic instabilities. The methods employed in this work are independent of the model and can therefore be utilized for the modification of bifurcation behaviour of other thermoacoustic systems.

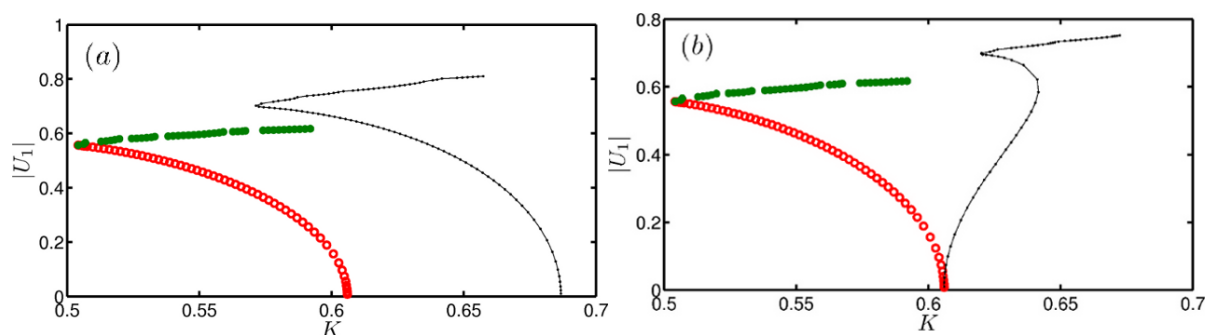


Figure 1: (a) Example of delaying the bifurcation and (b) Example of controlling the criticality of the Hopf bifurcation using feedback control. The amplitude of acoustic velocity oscillations in the fundamental mode is chosen as the measure while the non-dimensional thermal driving K is the chosen system parameter. Hollow/filled circles denote unstable/stable limit cycles of the uncontrolled system. Connected black dots give the modified bifurcation behaviour for the controlled system.

¹ MPRG-ECPS, Max-Planck Institute for Dynamics and Self-Organisation, Göttingen, 37077 Germany

² School of Engineering, Ecole polytechnique fédérale de Lausanne, CH-1015 Switzerland

¹ Rayleigh, *Nature*. **18**, 319-321 (1878).

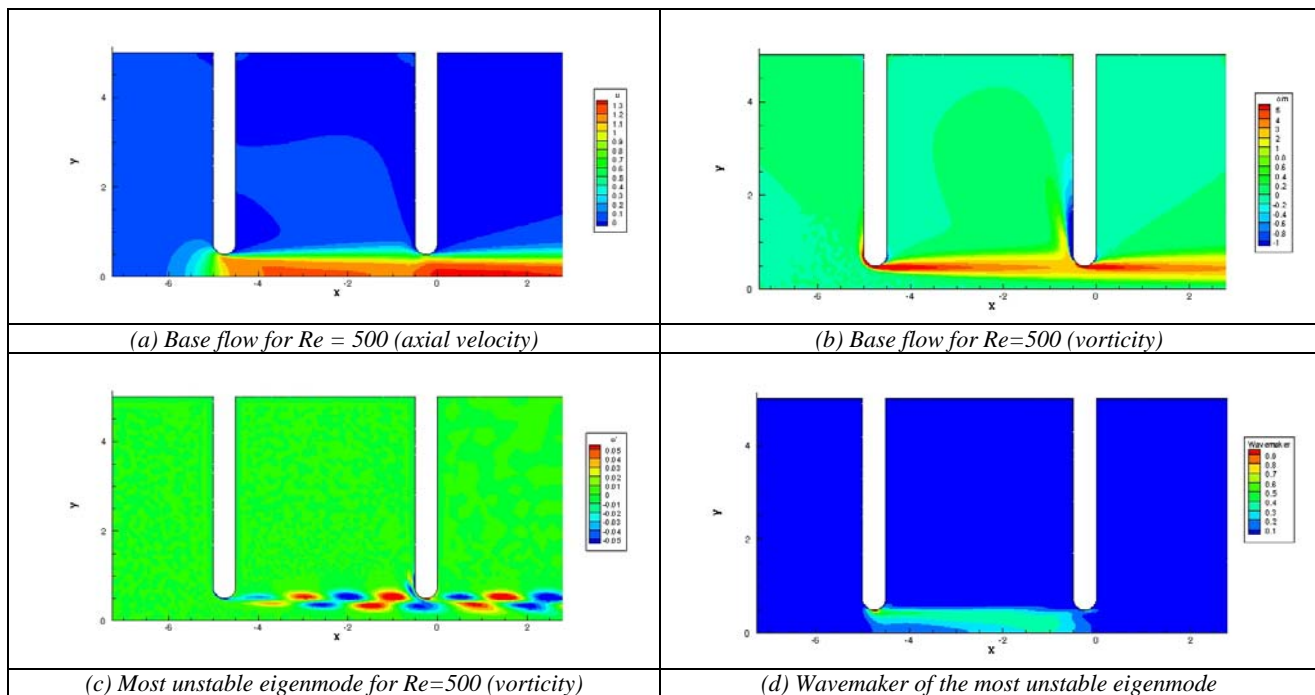
² Subramanian et al., *Intl. J. for Spray and Combustion Dynamics* **2-4**, 325-356 (2010).

Tea kettles, bird calls and whistling jets : Understanding the hole-tone mechanism through a global stability approach

D. Fabre^a, P. Bonnefis^a, P. Luchini^b & F. Giannetti^b

In this work we explore the so-called “hole-tone” phenomenon, namely the sound generated by a flow passing through two successive constrictions. This generic situation is encountered in familiar situations such as the whistle of a steam kettle or the birdcalls used by hunters, as well as in many industrial appliances. Early works by Sondhaus, Rayleigh and Bouasse¹ have explored this situation. Very recently, Henrywood & Agarwal² have conducted detailed experiments and have identified two régimes : at low Reynolds the frequency is constant and selected by the cavity located upstream, while at high Reynolds the frequency is proportional to the velocity, and assumed to be selected by the jet instability. Yet, the respective roles of the jet instability and acoustics remain to be clarified.

The objective of this work is to clarify these issues using a global stability approach³. For this sake, we compute a steady solution of the Navier-Stokes equations in such a geometry (figure (a-b)), and look for exponentially amplified small perturbations in eigenmode form. In an attempt to decouple hydrodynamical effects from acoustic ones, we assume the flow to be incompressible in the jet region and model the upstream and downstream acoustic couplings through convenient impedances. The most amplified eigenmode (figure (c)) is characterized by a Strouhal number in accordance with the experimentally observed one in the high-Reynolds number regime. The structure of this mode and of the associated “wavemaker”⁴ (figure (d)), suggests that, contrary to previous expectations, neither the backward propagation of acoustic waves nor the recirculating flow inside the cavity can explain the positive feedback leading to instability. Based on the results we will propose an alternative explanation based on the spatial stability properties of the jet, involving both an amplified downstream-propagating wave (k^+) and a damped, upstream-propagating wave (k^-).



^a IMFT, University of Toulouse, France

^b DIIN, Università di Salerno, Fisciano, Italy

¹ C. Sondhaus, *Annalen der physik* **167**-1 (1855) ; J. W. S. Rayleigh, *The theory of sound* (1945) ; H. Bouasse, *Instruments à vent, Tome II* (1930)

² R. H. Henrywood and A. Agarwal, *Phys. Fluids* **25**, 107101 (2013)

³ Sipp & Ledev J. *Fluid Mech.* **593**, 333-358, (2007) ; Assemat, Fabre, and Magnaudet. *J. Fluid Mech.* **690**, 173 (2012).

⁴ F. Giannetti and P. Luchini, *J. Fluid Mech.* **581**, 167 (2007).

Experiments on protuberance noise in laminar boundary layer

Masashi KOBAYASHI^a, Masahito ASAI^a and Ayumu INASAWA^a

Understanding the generation mechanism of aerodynamic sound from surface irregularities is of great importance for high-speed vehicle and aircraft design. Sound radiation from step or roughness in turbulent boundary layer has been studied by many researchers. On the other hand, sound generation in laminar boundary layer has been much less studied. In this paper, we present our recent experiment on sound radiation from a two-dimensional protuberance glued on the wall and the related feedback loop mechanism in laminar boundary layer at low Mach numbers.

The experiment was conducted in a low-turbulence and low-noise wind tunnel with square exit cross-section of 500 mm. The test section whose streamwise length of 1.5 m was opened in the anechoic chamber with 4.8 m long, 3.6 m wide and 3.3 m high. A brazed boundary-layer plate with 1000 mm long was installed in the test section. The plate was 5 mm thick and had a sharp leading edge so that the velocity profiles coincided with the Blasius profile immediately downstream of the leading edge. In order to introduce a protuberance, a thin resin tape was attached on the wall parallel to the leading edge. The radiated sound was measured using a microphone set in upstream side 1 m apart from flat plate. A constant-temperature hot-wire anemometer was used to measure mean and fluctuation velocity. The free-stream velocity (U_∞) ranged from 25 to 58 m/s ($M_\infty = 0.07$ to 0.17).

Figure 1 displays spectra of sound pressure level (SPL) for the ratio of the protuberance height to the displacement thickness $h/\delta^* = 3.58$ at $U_\infty = 50$ m/s, measured when protuberance is located at $x = 200$ mm ($R^* = 1423$). Distinct tonal sound is observed around 2390 Hz and its harmonics. This tonal sound had a strong directivity toward upstream side. When the height of protuberance was comparable to the boundary-layer thickness, tonal sound was significantly intensified by a feedback loop mechanism between sound generation at the protuberance and generation of Tollmien-Schlichting (T-S) waves due to a leading-edge receptivity to sound. In such feedback mechanism, occurrence of a separation bubble immediately upstream of the protuberance played an important role in the evolution of instability waves into strong vortices leading to prominent sound generation. Tonal sound frequency was determined by the selective amplification of T-S waves at the linear stage in the upstream boundary layer; therefore, the data lied close to Branch II of the neutral stability curve of Blasius flow as shown in Figure 2. Intensity and frequency of the sound generated was very sensitive to the instability nature of the upstream boundary layer.

^a Dep. Aerospace Engineering, Tokyo Metropolitan University, 6-6 Asahigaoka, Hino, Tokyo 191-0065, Japan

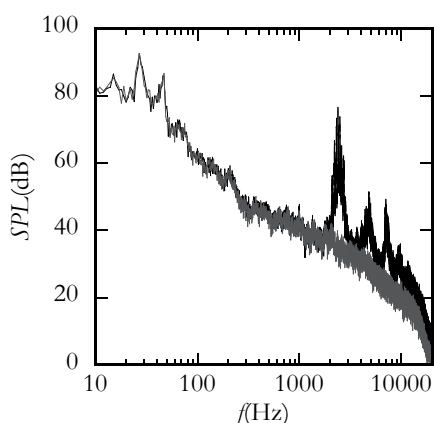


Figure 1: Sound pressure level spectra at $U_\infty = 50$ m/s and displacement-thickness Reynolds number $R^* = 1423$. Gray line displays the background noise.

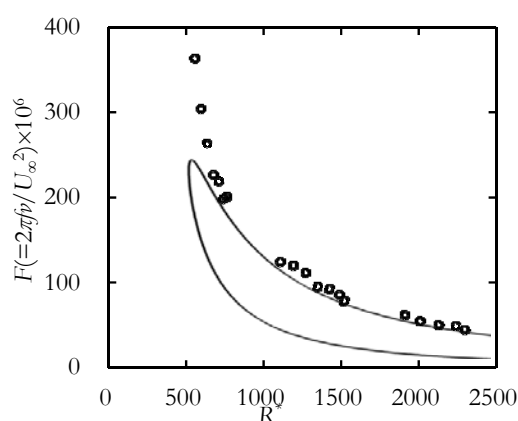


Figure 2: Non-dimensional frequency of tonal sound (F) vs. R^* . Solid curve represents the neutral stability curve of Blasius flow.

Weakly non-linear analysis of azimuthal thermoacoustic modes in annular combustion chambers

D. Laera^a, G. Campa^b, S. M. Camporeale^a

Thermoacoustic combustion instabilities are due to the coupling mechanism between acoustic pressure oscillations and heat release fluctuations. This phenomenon is of great interest since it occurs in lean premixed combustion chambers fueled by natural gas and used in modern gas turbine for power generation. In gas turbine systems with annular combustion chamber, acoustic waves may propagate in the transverse direction. Experiments and previous studies¹ have confirmed a dual nature, either rotating or standing, of acoustic waves.

In this work, the azimuthal modes of a three-dimensional annular combustion chamber are studied by means of a finite element (FEM) code. For each burner, the coupling between heat release fluctuations (q') and the velocity fluctuations (u') is modeled by means of a non-linear analytical Flame Describing Function (FDF) consisting of a third order and fifth order polynomial expression. A delay time between q' and u' is also considered and its influence highlighted. The weakly nonlinear analysis² is performed to determining the bifurcation diagrams for these flame models, considering the interaction index n as the control parameter. At first the heat release is assumed homogeneous along the chamber, subsequently the influence on the bifurcation diagram of spatial inhomogeneities is studied. This approach is used to investigate the nature of the transverse modes once the limit cycle condition is reached.

Preliminarily, the simple combustion chamber geometries examined by *Noiray et al.*³ and *Ghirardo and Juniper*⁴ are analysed. Then a more complex configuration (Fig.1) is analysed as a step forwards more realistic combustion chamber geometries.

^a Dip. di Meccanica, Matematica e Management, Politecnico di Bari, Via Re David 200, 70125, BARI, ITALY

^b Ansaldo Energia spa, Via Nicola Lorenzi 8, 16152, GENOVA, ITALY

¹ Krebs et al., *Combustion Science and Technology*, **174**, 99 (2002).

² Campa and Juniper, *ASME paper*, **GT2012-68241** (2012)

³ Noiray et al., *Combustion Theory and Modelling*, **15**, 585 (2011).

⁴ Ghirardo and Juniper, *Proceedings of the Royal Society A*, **469**, 20130232 (2013).

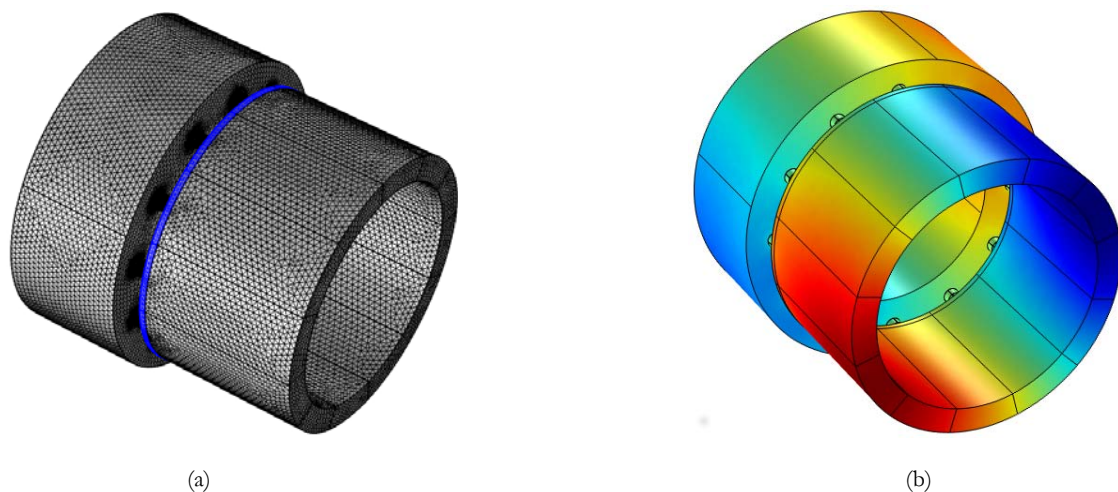


Figure 1: (a) Computational grid and flame zone highlighted. (b) First combustion chamber azimuthal mode.

Numerical investigation of the temperature dependence of acoustic streaming in microchannels

Peter Barkholt Muller^a and Henrik Bruus^a

In many acoustofluidic systems a steady acoustic streaming arises due to the generation of excess stresses in the acoustic boundary layer near rigid walls. The streaming is useful in some applications for mixing, but a hassle in others as it prevents acoustic focusing of small particles, see the review¹. Rednikov and Sadhal² gave an analytical treatment of the thermoviscous effects on the magnitude of the streaming velocity, which were later successfully confirmed experimentally^{3,4}.

Thorough numerical analysis of acoustic streaming in the adiabatic limit have recently been presented by Muller *et al.*⁵ and Lei *et al.*⁶. In this work we go beyond the adiabatic limit and present an improved numerical method based on a direct implementation of the conservation equations for all fields, which takes into account the oscillating temperature field and its influence on the viscosity, especially in the boundary layer. Following Muller *et al.*⁵, we have calculated acoustic streaming using second-order perturbation theory, where the first-order fields for velocity, density, and temperature, act as source fields in the second-order streaming equation.

As shown in Figure 1 the inclusion of thermal effects alters the magnitude of the streaming significantly. The numerical results show good agreement (about 1 %) with the analytical theories in the range from 30 °C to 80 °C, while below 30 °C we find a slight disagreement (about 5 %). The improved computational efficiency of the numerical scheme paves the way for future modeling of acoustic streaming in three dimensions in more complex geometries, as well as modeling of whole-chip systems with the inclusions of fluid-structure interactions.

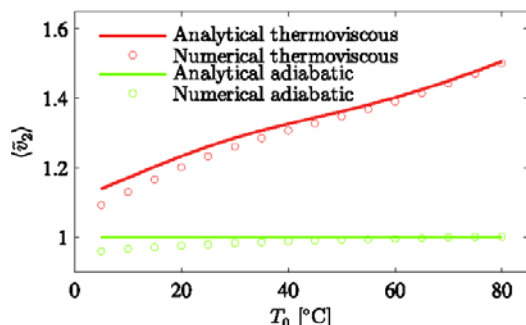


Figure 1. Comparison of the normalized streaming amplitude v_s as function of temperature T_0 from our numerical model and analytical predictions by Rayleigh⁷ (adiabatic) and Rednikov and Sadhal² (thermoviscous).

^aDepartment of Physics, Technical University of Denmark, DK-2800 Kgs Lyngby, Denmark

¹M. Wiklund, R. Green, and M. Ohlin, *Lab Chip* **12**, 2438 (2012).

²A.Y. Rednikov and S.S. Sadhal, *J. Fluid Mech* **667**, 426 (2011).

³R. Barnkob, P. Augustsson, T. Laurell, and H. Bruus, *Phys. Rev. E* **86**, 056307 (2012).

⁴P.B. Muller et al., *Phys. Rev. E* **88**, 023006 (2013).

⁵P.B. Muller, R. Barnkob, M.J.H. Jensen, and H. Bruus, *Lab Chip* **12**, 4617 (2012).

⁶J. Lei, M. Hill, and P. Glynn-Jones, *Lab Chip* **14**, 532 (2014).

⁷Lord Rayleigh, *Philos. Trans. R. Soc. London* **175**, 1 (1884).

Vibration-induced streaming in two-dimensional confinement

Maxime Costalonga^{a,b}, Philippe Brunet^b and Hassan Peerhossaini^{1,† a}

When an acoustic wave propagates in a fluid, it can generate a second order flow which characteristic time is much longer than the period of the wave¹⁻⁴. Within a range of frequency between 1 and several hundred Hz, a relatively simple and versatile way to generate streaming flow is to put a vibrating object in the fluid⁵. The flow patterns and properties have striking similarities with microfluidics flows generated by vibrating bubbles⁶ and sharp edges⁷.

The flow develops vortices in the viscous boundary layer located in the vicinity of the source of vibrations, which in turns leads to an outer irrotational streaming denoted as Rayleigh streaming. Due to that the flow originates from non-linear time-irreversible terms of the Navier-Stokes equation, this phenomenon can be used to move fluids and even to generate efficient mixing at low Reynolds number, for instances in confined geometries. Here we report an experimental study of such streaming flow in a Hele-Shaw cell of 2 millimeters span using long exposure flow visualization and PIV measurements. Our study is especially focused on the effects of acoustic frequency and amplitude on flow dynamics. It is shown that some features of this flow can be predicted by simple scaling arguments, invoking a balance between viscous dissipation in the boundary layer and inertia term, and that acoustic streaming facilitates the generation of vortices.

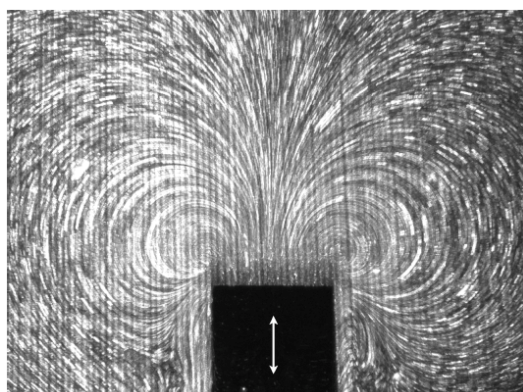


Figure 1. Flow pattern shown by particles trajectories, generated by the vibration of a beam immersed in a Hele-Shaw cell (50 Hz, beam of square shape, 10 mm width, 3.7 s exposure time).

[†] ^aLaboratoire Interdisciplinaire des Energies de Demain (LIED) UMR 8236.

^b Laboratoire Matière et Systèmes Complexes (MSC) UMR CNRS 7057.

Université Paris Diderot, 10 Rue Alice Domon et Léonie Duquet 75013 Paris, FRANCE

¹ J. Lighthill, *Journal of Sound and Vibration* **61**, 391 (1978).

² J. Friend and L. Y. Yeo, *Reviews of Modern Physics* **83**, 647 (2011).

³ S. Boluriaan and P. Morris, *International Journal of Aeroacoustics* **2**, 255 (2003).

⁴ S. S. Sadhal, *Lab on a Chip* **12**, 2292 (2012).

⁵ M. Tatsuno and P. W. Bearman, *Journal of Fluid Mechanics* **211**, 157 (1990).

⁶ Wang, C., S.V. Jalikop, and S. Hilgenfeldt, *Biomechanics* **6**, 012801 (2012).

⁷ P-H. Huang *et al.* *Lab on a Chip* **13**, 3847 (2013).

Turbulent Pipe Flows

Flow dynamics of turbulent flow through ribbed pipes

M.C. Schenker^a, R. Delfos^a, J. Westerweel^a, A. Twerda^{a,b} and E. v Bokhorst^b

Turbulent flow through structured pipes has many applications in a broad range of fields. We focus on a subset of those pipes, called corrugated pipes, where the structure on the pipe walls can be considered as a repeated rib-roughness. Such pipes or hoses are found in, for example, short distance LNG transfer and are used because of their unique combination of flexibility, strength and chemical and thermal endurance.

In many cases, depending on the specific pipe geometry and flow conditions, the ribs can not be considered to behave as a "classical roughness". Hence relevant geometric parameters and new scaling rules need to be defined. It is in this regime that we focus on detailed understanding of the flow dynamics and interaction. For this, we perform an experimental study using static and dynamic pressure measurements and PIV.

The experimental set-up consists of a simplified ribbed structure of a smooth pipe ($D = 50$ mm) with rectangular ribs ($h = 7.5$ mm, $w = 9.5$ mm) inserted orthogonal to the pipe-axis. We vary the pitch of the ribs. Relatively small pitch to rib-height values ($p/h = 1.7$ to 6) were used because of their relevance in most practical applications. Using water as working fluid we measured the pressure loss over a short ribbed section and recorded the dynamic pressure fluctuations using two hydrophones mounted in between the ribs.

The pressure-loss non-dimensionalised with the dynamic pressure, also called K factor, is constant over the largest part of the velocity range, which is considered to be the fully turbulent regime. In this regime K is only a function of the geometry, in this case the rib-pitch; K increases with increasing pitch.

A first step in understanding what causes this dependency, and whether flow regime changes occur, is looking at the power spectra computed from the hydrophone measurements. There are a few distinct peaks visible in the power spectra, of which only one shows a clear dependency on the flow velocity. This isolated peak-frequency versus the bulk velocity and a linear fit through those points is shown in Figure 1 for one of the geometries. The slope of this fit scaled with the rib-pitch is the Strouhal number Sr , shown in Figure 2. Sr shows to be nearly constant within the range of pitches used. Optical measurements (high speed Particle Image Velocimetry) are currently prepared to find the flow mechanisms responsible for this scaling behaviour.

^a Dept. Mech. Engineering, Delft University of Technology, 21 Leeghwaterstraat, Delft, the Netherlands

^b TNO Delft, 1 Stieltjesweg, Delft, the Netherlands

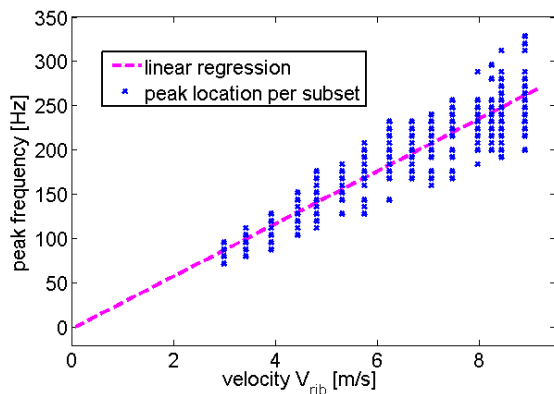


Figure 1: Peak locations and linear fit for $p = 25$ mm.

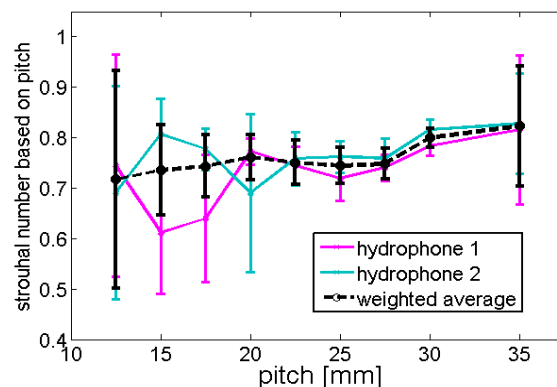


Figure 2: Strouhal number $Sr = fL/U$ based on the slope of the linear regression and rib-pitch.

Coherent vorticity extraction in turbulent channel flow using orthogonal wavelets

T. Sakurai^a, K. Yoshimatsu^a, K. Schneider^b, M. Farge^c, K. Morishita^d and T. Ishihara^e

Turbulent flows exhibit an intrinsic multiscale behaviour owing to a large number of degrees of freedom interacting nonlinearly. Even at large Reynolds number observations show self-organization of the flow into coherent vortices, which is superimposed to a random background flow¹. This motivates to split turbulent flows into these two contributions. The coherent vorticity extraction method, proposed by Farge et al.², decomposes the flow into orthogonal wavelets and applies a thresholding to split the coefficients into two sets. It thus takes into account that both contributions are multiscale and exhibit no scale separation.

In the present work we examine the role of coherent vorticity in turbulent channel flow bounded by two parallel walls. To extract the coherent vorticity, an orthogonal anisotropic wavelet decomposition is applied which accounts for the flow anisotropy by using different scales in the wall-normal direction and in the wall-parallel directions. The orthogonal anisotropic wavelets used here combine periodized Coiflet 30 wavelets, which have ten vanishing moments, in the wall-parallel direction and Cohen-Daubechies-Jawerth-Vial interval wavelets, having three vanishing moments³, in the wall-normal direction.

We analyse direct numerical simulation data⁴ of turbulent channel flow at friction-velocity based Reynolds number $Re_\tau=320$. The flow field, originally computed with 192 Chebyshev grid points in the wall-normal direction, is first interpolated onto 4096 equidistant grid points to ensure that the structures near the walls are sufficiently resolved. The flow vorticity is then decomposed into orthogonal anisotropic wavelets. The coherent vorticity is reconstructed after nonlinearly filtering the wavelet coefficients, namely by retaining only about 0.15% of them that are the most intense. Figure 1 shows that the coherent vorticity retains the vortex tubes of the turbulent flow. The remaining majority of the coefficients corresponds to a structureless, i.e., noise-like incoherent background flow. We will report that the coherent contributions well preserve not only the turbulent statistics, but also the nonlinear dynamics, while the incoherent contributions are noise-like and not dynamically active.

^a Dep. Computational Science and Engineering, Nagoya University, Nagoya, 464-8603, Japan

^b M2P2-CNRS and CMI, Aix-Marseille Université, 38 rue F. Joliot-Curie, 13451 Marseille Cedex 20, France

^c LMD-IPSL-CNRS, Ecole Normale Supérieure, 24 rue Lhomond, 75231 Paris Cedex 05, France

^d Dep. Computational Science, Kobe University, Kobe, 657-0013, Japan

^e Center for Computational Science, Nagoya University, Nagoya, 464-8603, Japan

¹ Brown and Roshko, *J. Fluid Mech.*, **64**, 28 (1974).

² Farge et al., *Phys. Rev. Lett.*, **87**, 45011 (2001).

³ Cohen et al., *C. R. Acad. Sci. Paris Ser. I Math.*, **316**, 417 (1993).

⁴ Morishita et al., *J. Phys.: Conference Series*, **318**, 022016 (2011).

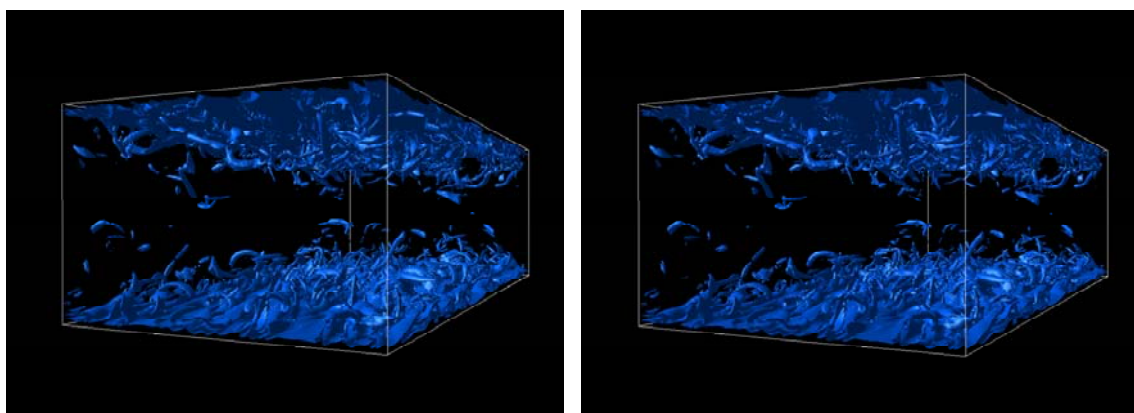


Figure 1: Turbulent channel flow at $Re_\tau=320$. Visualization of isosurfaces ($|\boldsymbol{\omega}| = 10u_\tau^2\nu$) of the modulus of total vorticity (left) and of coherent vorticity (right). Here, u_τ and ν are the wall friction velocity and the kinematic viscosity, respectively.

Turbulent Pipe Flow Investigations at High Reynolds Numbers

E. Öngüner^a, S. Merbold^a, Ch. Egbers^a

For linear stable shear flows, turbulent pipe flow has been investigated for different Re-numbers. Turbulence can be achieved in natural or artificial methods. For transitions some perturbations are needed to trigger turbulence and some structures as puffs and slugs can be observed. In last decades the so called large-scale motions (LSM), which are composed of detached eddies with wide range of azimuthal scales in the outer layer, are identified. Advanced versions of LSM's, the very-large-scale motions (VLSM), have radial scales. The VLSM'S are concentrated around a single azimuthal mode and make a smaller angle with the wall compared to the LSM.

These above mentioned phenomena will be investigated at high Reynolds numbers in the pipe facility Cottbus-Large Pipe at BTU Cottbus-Senftenberg (CoLa-Pipe) which provides a bulk Reynolds number of $Re_m \leq 1,5 \times 10^6$. Zimmer et. al. (2011)₁ and König et. al. (2013)₂ provide an outline for conditions of fully developed turbulent flow state with natural as well as artificial transition. Considering these fully developed flow conditions at CoLa-Pipe, next investigations will be primarily focused on the structures in boundary layer in terms of LSM and VLSM by using hot wire anemometry and PIV. The main aim of this work will be analysing the structure types of high Re-numbers and comparing with those of low Re-numbers regions.

^a Dep. of Aerodynamics and Fluid Mechanics, Brandenburg University of Technology Cottbus-Senftenberg, Siemens-Halske-Ring 14, 03046, Cottbus, Germany

¹ Zimmer et al., *13th European Turbulence Conference ETC*, Sept.12-15, Poland (2011)

² König et al., *4th International Conference on Jets, Wakes and Separated Flows*, Sept.17-21, Japan (2006)

Modulation of turbulent structures by spanwise wall oscillation

Q. Yang^a, Y. M. Chung^a and E. Hurst^a

Turbulent flow control method using spanwise wall oscillation can achieve as much as 40% of drag reduction¹. Effectiveness of this control method has been studied for many years for channel, pipe and boundary layer flows using DNS and LES as well as experiment. Despite extensive efforts over a couple of decades, however, the drag reduction mechanism for spanwise wall oscillation is still not well understood. In this study, direct numerical simulations of turbulent channel flow have been performed to understand the effect of wall oscillation on turbulent near-wall structures and drag reduction. The coherent structures were detected and averaged using the eduction scheme proposed by Jeong et al.², which has previously been used for steady turbulent flows. In this study, this eduction scheme is successfully applied to 3D unsteady turbulent flow.

Figure 1(a) shows the time history of the skin friction coefficient C_f at for three different oscillation periods, *i.e.* $T^+=50$, 100 and 200 (where $T^+=100$ is the optimal oscillation period), with the corresponding drag reductions of 31%, 36% and 22%, respectively. There is a significant amount of fluctuation in C_f values, and the phase-averaged amplitude of C_f fluctuation (shown in the inset) is 0.04% for $T^+=50$, 0.2% for $T^+=100$, and 2% for $T^+=200$. It is found that the amplitude of C_f fluctuation increases with T for all T values considered. Figure 1(b) shows the ensemble-averaged positive and negative structures in the first half of the oscillation period at $T^+=100$. The structure is coloured by the streamwise vorticity fluctuation, with yellow indicating a positive structure while blue for a negative structure. In the first half of the oscillation, a positive structure creates spanwise velocity in the same direction as the wall motion (Case 1 vortex following Littell and Eaton³). The generated Stokes velocity profile is also shown by the pink lines, while the green dashed line indicates the thickness of the Stokes layer. The positive structure appears near the wall at $t/T=1/4$, when C_f has a maximum; then it gradually moves away from the wall with the tilting angle decreasing while C_f decreases to a minimum. At $t/T=1/2$, the positive structure is located further than the Stokes layer. In the second half of the cycle, the variation in C_f is affected mainly by the negative vortex as the wall motion changes the direction while the positive structure slowly moves further away from the wall. This trend continues into the early part of the next cycle, and the positive structure disappears at $t/T=1/8$. The behaviour of the negative structure is similar but with a phase shift of half a period. The modulation of the near wall structures is closely related to the oscillation of C_f shown in Figure 1(a). It is found that wall oscillation modulates the positive and negative structures differently, causing fluctuation in C_f . The role of positive and negative vortices in the drag reduction will be further investigated.

^a School of Engineering and Centre for Scientific Computing, University of Warwick, Coventry CV4 7AL, UK

¹ Jung et al., *Phys.Fluids* **4**, 1605 (1992).

² Jeong et al., *J. Fluid Mech.* **332**, 185 (1997).

³ Littell and Eaton, *J. Fluid Mech.* **266**, 175 (1994).

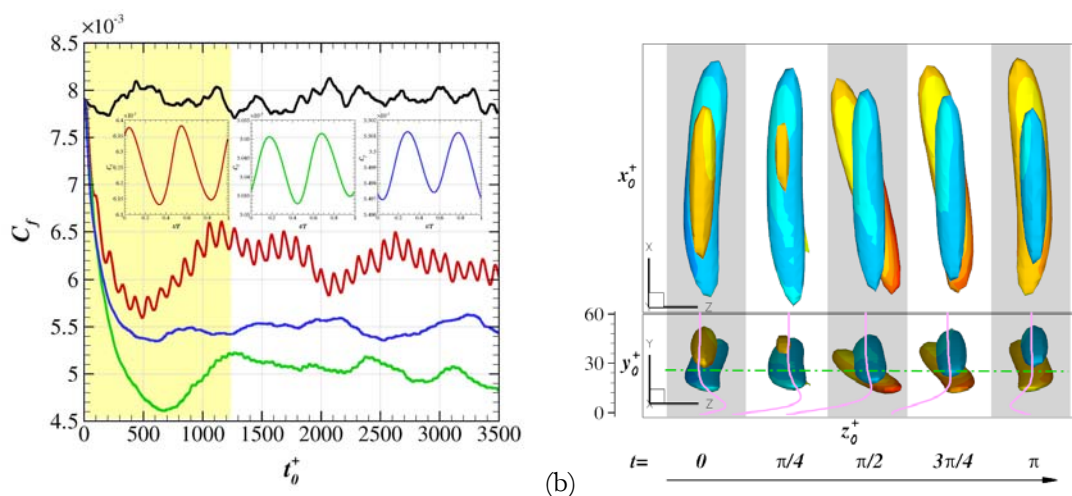


Figure 1: (a) Time history of skin friction coefficient for three oscillation periods: $T^+=50$ (blue), 100 (green) and 200 (red). (b) Variation of positive ($\omega_x > 0$, yellow) and negative ($\omega_x < 0$, blue) structures in the first half of the oscillation period.

Presenters

Presenter name:	Page:	Presenter name:	Page:
Abadie, T.	303	Balusamy, S.	202
Adou, A. Ebo	585	Bangash, Z.A.	260
Agbessi, Y.	141	Barenghi, C.	330
Ahl, S. R.	596	Baskan, Ö.	357
Alam, M.	258	Basse, N. T.	523
Álamo, J.C. del	16, 420	Battista, F.	84
Aleksyuk, A. I.	123	Bauer, K.	102
Alizard, F.	149	Benneker, A.M.	606
Almagro, A. E.	356	Berdowski, T.J.	539
Alméras, E.	358	Bernardini, M.	154
Altmeyer, S.	516	Biancofiore, L.	438
Andersen, A. P.	100	Biferale, L.	575
Andersen, B. O.	519	Billant, P.	396
Andersson, H.I.	319	Biwa, T.	551
Andersson, L. R.	500	Blanco-Rodriguez, F. J.	447
Antoranz, A.	215	Boeck, T.	567
Anufriev, I.S.	522	Bolaños-Jiménez, R.	481
Anzai, Y.	612	Bontozoglou, V.	170
Aslan, Z.	83	Boronin, S.A.	144, 344
Attili, A.	79	Bosco, M.	584
Augier, P.	152	Boujo, E.	349
Babler, M.U.	314	Bourgoin, M.	27
Badas, M.G.	284	Bouwhuis, W.	592
Bahri, C.	375	Brandt, L.	32
Bailey, N.	609	Brauckmann, H. J.	393
Baker, N.	563	Brethouwer, G.	31
Balci, A.	157	Breugem, W.-P.	325

Presenter name:	Page:	Presenter name:	Page:
Brouwer, J.	122	Dam, C.P. van	304
Bublik, O.	64	Danaila, I.	223
Buffat, M.	514	Daniele, E.	188
Burlot, A.	367	Daou, J.	80
Burström, P. E. C.	527	Dedić, A.	471
Busse, A.	230, 248	Delache, A.	576
Callan-Jones, A.	18	Delacroix, J.	562
Candel, S.M.	195, 547	Denier, J.P.	386
Canton, J.	267	Deshmukh, N.	85
Cardesa, J.I.	150	Deusebio, E.	40
Casciola, C.M.	486	Dimopoulos, D.	231
Ceyhan, Ö.	307, 536	Dizés, S. Le	389
Chakravarthy, S. R.	210, 552	Dollet, B.	380
Chavez, L.P.C.	533	Domenichini, F.	409
Chernyshev, S.	364	Douay, C.	348
Chouippe, A.	322	Downs, R. S.	513
Christiansen, C. K.	524	Duchesne, A.	439
Chung, Y.M.	630	Duguet, Y.	63, 509
Citro, V.	132	Ehrenstein, U.	111
Coclite, A.	81	Elhadidi, B.	298
Coenen, W.	280	Eloy, C.	15
Costa, P.	324	Emmert, T.	212
Costalonga, M.	623	Ergin, F. G.	496
Craske, J.	277	Evans, H. B.	26
Creyssels, M.	359	Fabre, D.	619
D'Adamo, J.	583	Fani, A.	256, 611
Daerr, A.	176	Feldman, Y.	337

Presenter name:	Page:	Presenter name:	Page:
Fernandez-Prats, R.	109	Grasso, F.	306
Ferreira, C.S.	540	Griffiths, P.T.	139
Fiebach, A.	58	Grimble, T.A.	459
Filella, A.	183	Grünberg, T.	503
Fomin, V.M.	116	Guerrier, P.	62
Fornarelli, F.	262	Guo, J.	564
Fortini, S.	422	Gupta, A.	143
Frick, P.	402	Guy, R. D.	19
Galiana, F.J. Dura	124	Güttler, A.	136
Gallagher, M.	269	Hai, B.S.M. Ebna	263
Gallardo, J. P.	586	Han, X.	199
García, J.	105	Han, Z.	208
Gaskell, P.H.	175	Harish, N.	276
Gatti, D.	404	Haslavsky, V.	339
Gelfgat, A. Yu.	392	He, X.	229
Gervang, B.	69	Healey, J. J.	352
Ghirardo, G.	197	Heifetz, E.	559
Gillebaart, T.	189	Heijst, G.J.F. van	391
Girfoglio, M.	441	Heil, M.	244
Godoy-Diana, R.	110	Hejlesen, M. M.	449
Gómez, F.	183	Hellström, J. G. I.	381
Gompper, G.	21	Hemchandra, S.	205
Gopalakrishnan, E.A.	207	Hemmingsen, C. S.	526
Gordillo, J.M.	595	Hennekinne, C.	234
Gordillo, L.	435	Henry, D.	232
Gorodkov, A.	424	Hernandez, I.H.	180
Gotoda, H.	206	Hinsberg, M. A. T. van	28

Presenter name:	Page:	Presenter name:	Page:
Hof, B.	374	Johnson, H.	448
Holmstedt, E.	107	Kabardin, I.K.	451
Homeyer, T.	309	Kaiser, R.	236
Hooijdonk, I.G.S. van	37	Kamal, M. M.	209
Hossbach, S.	577	Kamp, L.P.J.	454
Hovad, E.	52	Karapetsas, G.	145
Huang, C.-K.	65	Karlsson, L.	593
Hulin, J.P.	255	Keaveny, E. E.	59
Hwang Y.	98	Kedrinskiy, V.	44
Iaccarino, G.	6	Kerr, O.S.	235
Ibrahim, M.K.	287	Kessar, M.	578
Iglesias, I.	220	Kheradvar, A.	410
Ihme, M.	546	Kidanemariam, A.G.	318
Ingvorsen, K. M.	499	Kidogawa, R.	67
Isaenkov, S.V.	467	Kim, J.	90
Isakova, K.	247	Kim, N. S.	521
Ivanell, S.	191, 535	Kiyama, A.	273
Ivanova, A. A.	226	Kizilova, N.	146, 423
Izard, E.	47	Kjørboe, T.	7
Iungo, G.V.	185	Kobayashi, M.	620
Jabbari, M.	520	Kolosov, G.L.	118
Jackson, M.	331, 333	Kornet, K.	566
Jaensch, S.	548	Kostykin, S. V.	394
Jalikop, S. V.	397	Kotake, A.	126
Jermann, C.	450	Kozlov, V. G.	388
Jiménez-González, J.I.	347	Kozlov, V.V.	508
Jith, J.	245	Kravtsova, A.	343

Presenter name:	Page:	Presenter name:	Page:
Krieg, M.	285	Lohse, D.	475
Kuik, G. van	186	Loiseau, J.-Ch.	101
Kurbatskiy, A. F.	363	Loisy, A.	484
Kurdyumov, V.N.	77	Lopez, D.	33, 257
Laera, D.	621	Lovecchio, S.	97
Larcher, T. von	70	Lucas, A.	162
Larsson, I. A. Sofia	370	Lucchini, M.	82
Layek, G. C.	411	Luginsland, T.	131
Lebedeva, N.A.	66	Machicoane, N.	494
Lebon, L.	587	MacKintosh, F. C.	20
Lemee, T.	316	Madsen, H. Aa.	182
Lerisson, G.	38	Magaletti, F.	477
Lesshafft, L.	340	Magnaudet, J.	151, 482
Levy, B.	491	Magri, L.	545
Li, J.	550	Mamatsashvili, G.R.	565
Li, Y.	369	Mani, A.	323
Li, Z.W.	181	Mantia, M. La	332
Lignarolo, L.	184	Mantic-Lugo, V.	351
Lima, A. C. de	379	Marchioli, C.	326
Limat, L.	440	Marinis, D. De	219
Lin, S. Y.	187	Marner, F.	161
Lin, T. Y.	355	Marquet, O.	345
Linden, P. F.	92	Martinez-Ruiz, D.	76
Liot, O.	237	Massai, T.	254
Litvinenko, M.V.	492	Mehaddi, R.	278
Litvinenko, Yu. A.	75, 581	Mehta, D.	534
Ljung, A.-L.	598	Meliga, P.	133

Presenter name:	Page:	Presenter name:	Page:
Melius, M.S.	300	Naso, A.	372
Meneveau, C.	532	Nepf, H.	3
Merbold, S.	403	Neuhaus, L. K.	537
Merle, M.	342	Noiray, N.	196
Messina, R.	417	Nouat, C.	142
Meyer, K. E.	456	Odier, N.	279
Meyers, J.	192	Okino, S.	272
Michelin, S.	608	Okulov, V.	531
Minier, J.-P.	61	Orchini, A.	204
Miquel, B.	43	Orefice, A. Petrucci	140
Mittal, R.	414	Oresta, P.	469
Mizev, A.	227	Oron, A.	171
Mizeva, I.	497	Oteski, L.	238
Moeck, J. P.	198	Oualli, H.	259
Mogilevskiy, E.	119	Palma, S.	317
Mohamed, A. Said	604	Panina, A.V.	117
Mohseni, K.	302	Paolicchi, L.T.L.C.	115
Molevich, N. E.	560	Paraz, F.	112
Mollicone, J.-P.	571	Parras, L.	291
Moriche, M.	294	Paul, N. H. E.	554
Morzynski, M.	57	Pedri, S.	413
Moudjed, B.	274	Peinke, J.	5
Mukund, V.	515	Pérez, T. S.	502
Muller, P.B.	622	Picano, F.	29
Muralidhar, S. D.	582	Pier, B.	338
Nadal, F.	615	Pierson, J.	430
Nagata, M.	89	Pimponi, D.	95

Presenter name:	Page:	Presenter name:	Page:
Pino, C. del	445	Rybdylova, O.	464
Plesniak, M.W.	412	Rybushkina, G.V.	428
Poelma, C.	421	Saber, A. H.	108
Polin, M.	17	Sakurai, T.	628
Polivanov, P.A.	121	Salin, D.	465
Porfirev, D.	588	Salort, J.	224
Pouliquen, O.	51	Salsac, A.-V.	603
Power, H.	41	Sánchez-Bernabe, F.J.	159
Prosperetti, A.	1	Santoni, C.	190
Quaranta, G.	99	Sasaki, G.	299
Quaranta, H. U.	452	Satoh, A.	313
Rabaud, M.	437	Saurabh, A.	201
Rademaker, H.	104	Sayadi, T.	203
Raibaud, C.	134	Sazhin, S.S.	591
Raynal, F.	321	Scatamacchia, R.	25
Reck, D.	172	Schenker, M.C.	627
Reeuwijk, M. van	574	Schepers, J.G.	179
Reinke, N.	401	Schlatter, P.	30
Reyt, I.	617	Schmidt, L.	320
Riboux, G.	594	Schmitt, S.	463
Rieutord, M.	9	Schmoranzer, D.	228
Risler, T.	22	Schneider, T.M.	91
Robinet, J.-C.	297	Scholle, M.	160
Rodríguez, D. H.	427	Schütz, S.	233
Roszak, R.	295	Schönke, J.	371
Rubio-Rubio, M.	282	Schörner, M.	173
Rusu, I.	167	Scribano, G.	281

Presenter name:	Page:	Presenter name:	Page:
Seifert, A.	301	Sumets, P.	106
Selçuk, C.	453	Suramlishvili, N.	125
Semeraro, O.	270	Sy, N. F.	334
Seminov, N. V.	493	Szewc, K.	478
Sergeev, Y. A.	329	Sørensen, J.N.	541
Shahirpour, A.	457	Sørensen, N.N.	308
Shahriari, N.	511	Tachibana, S.	549
Shakouchi, S.	468	Tagawa, Y.	480
Shakouchi, T.	479	Taguelmimt, N.	153
Shibata, N.	286	Tamai, I.	495
Shin, B. S.	216	Tammisola, O.	553
Shirai, K.	387	Tandiono, T.	605
Shiri, A.	239, 429	Teimurazov, A.	225
Simpson, M.	446	Thalakkottor, J.J.	249
Sinha, A.	271	Thomas, P.J.	315
Sinibaldi, G.	616	Thoraval, M.-J.	597
Slotosch, A.	415	Thoroddsen, S. T.	485
Snoeijer, J.	8	Tihon, J.	607
Sokolovskiy, M.A.	39	Timokha, A.N.	251
Stankiewicz, W.	60	Tognaccini, R.	158
Stepanov, R.	561	Traphan, D.	310
Stepanova, E. V.	360	Traut, A.	243
Stevens, R.J.A.M.	572	Trifonov, Y.	341
Stroh, A.	135	Tsai, P.A.	250
Subramanian, P.	222, 618	Tsamopoulos, J.	174, 470
Succi, S.	4	Tsujimoto, K.	264
Sujith, R.I.	200	Tsyryulnikov, I.S.	120

Presenter name:	Page:	Presenter name:	Page:
Tuckerman, L. S.	599	Wassmer, D.	211
Tullio, N. De	510	Water, W. van de	53
Tunney, A.	507	Weidman, P. D.	385
Tyliszczak, A.	78	Westerberg, L. G.	395, 436
Uchino, K.	218	Wierschem, A.	48
Urban, P.	221	Willis, A. P.	373
Vadri, S.S.	217	Wu, X.	498
Valença, J. C. De	458	Xia, Y.	246
Velden, W.C.P. van der	261	Xu, H.	350
Velte, C.M.	283, 501	Yaqob, B. N.	268
Verzicco, R.	487	Yariv, E.	476
Vesipa, R.	49	Ye, X.	525
Vigdorovich, I. I.	366	Yim, E.	42
Vimmr, J.	419	Young, J.	293
Viola, F.	455	Zammert, S.	512
Viré, A.	71	Zharfa, M.	296
Vita, F. De	418	Zheng, J.G.	127
Volkov, K.N.	305	Zhou, L .	368
Vollant, A.	68	Zhou, W.	253
Voort, D.D. van der	275	Zonta, F.	573
Wacławczyk, T.	376	Zverkov, I.D.	292
Wadhwa, N.	96	Zybin, K. P.	365
Ward, T.	346	Öngüner, E.	629
Warnett, J.M.	50	Özkan, M.	30

Sponsors

The organizing committee would like to thank the following for their contribution to the EFM10 at DTU, Lyngby, Denmark September 2014:



CAMBRIDGE
UNIVERSITY PRESS

